





## **Copyright Notices**

### **Notice 1**

Under the Copyright Act 1968, this thesis must be used only under the normal conditions of scholarly fair dealing. In particular no results or conclusions should be extracted from it, nor should it be copied or closely paraphrased in whole or in part without the written consent of the author. Proper written acknowledgement should be made for any assistance obtained from this thesis.

### **Notice 2**

I certify that I have made all reasonable efforts to secure copyright permissions for third-party content included in this thesis and have not knowingly added copyright content to my work without the owner's permission.

## Declaration for Higher Doctorate submitted work

### General Declaration

I hereby declare that this work contains no material that has been accepted for the award of any other degree or diploma at any university or equivalent institution. I hereby declare that, to the best of my knowledge and belief, this work contains no material previously published or written by another person, except where due reference is made in the text of the work.

The main body of this work includes 20 original papers that have been published in peer reviewed journals. Additionally, within the appendices there are 17 original short-form contributions in the format of editorials and commentaries to demonstrate outreach to the scientific and engineering communities as well as intellectual depth.

The core theme of the work is "Thermal Spray Coatings: Processing, Microstructural Architecture and their Materials Engineering Design".

The principal responsibility of myself, the candidate, working within the discipline of Materials Science and Engineering, for the 20 publications presented in this body of work is detailed in the table below.

In the case of Chapters 1 through to 6 my contribution to the work is listed Table 1.

Table 1. Candidate's Contribution to the 20 Selected Publications.

Chapter and Manuscript Number	Publication title	Publication status	Nature and extent of candidate's contribution
<b>Chapter 1. Processing of Materials</b>			
Manuscript #1.	Characteristics of the Liquid Flame Spray Process', Surf. Coat. Tech., 90 (1997) 210-216.	Peer reviewed and published	8 authors J. Tikkanen, K.A. Gross, <b>C.C. Berndt</b> , V. Pitkanen, J. Keskinen, S. Raghu, M. Rajala and J. Karthikeyan Candidate contribution is 15%
Manuscript #2.	Topographical and microstructural property evolution of air plasma-sprayed zirconia thermal barrier coatings, J. Am. Ceramic Soc., Article first published online: 4 FEB 2014, DOI: 10.1111/jace.12842.	Peer reviewed and published	3 authors M.L. Sesso, <b>C.C. Berndt</b> and Y.C. Wong Candidate contribution is 45%
<b>Chapter 2. Microstructural Evolution and Design</b>			
Manuscript #3.	Microstructural characteristics of cold-sprayed nanostructured WC-Co coatings, Thin Solid Films, 416 (2002) 129-135.	Peer reviewed and published	5 authors R.S. Lima, J. Karthikeyan, C.M. Kay, J. Lindemann and <b>C.C. Berndt</b> Candidate contribution is 35%
Manuscript #4.	Design and manufacture of Nd-Fe-B thick coatings by the thermal spray	Peer reviewed and published	2 authors J.A. Gan and <b>C.C. Berndt</b>

Chapter and Manuscript Number	Publication title	Publication status	Nature and extent of candidate's contribution
	process, Surf. Coat. Tech., 205[19] (2011) p. 4697-4704. DOI: 10.1016/j.surfcoat. 2011.04.034, Published: JUN 25 2011.		Candidate contribution is 50%
Manuscript #5.	Effects of standoff distance on porosity, phase distribution and mechanical properties of plasma sprayed Nd-Fe-B coatings, Surf. Coat. Tech., 216 (2013) p. 127-138. DOI: 10.1016/j.surfcoat.2012.11.040, Published: FEB 15 2013.	Peer reviewed and published	2 authors J.A. Gan and <b>C.C. Berndt</b> Candidate contribution is 50%
Manuscript #6.	Quantification and taxonomy of pores in thermal spray coatings by image analysis and stereology approach, Metall. and Mater. Trans. A, 44A[10] (2013) p. 4844-4858. DOI: 10.1007/s11661-013-1818-4, Published: OCT 2013.	Peer reviewed and published	2 authors J.A. Gan and <b>C.C. Berndt</b> Candidate contribution is 50%
<b>Chapter 3. Mechanical Property Testing</b>			
Manuscript #7.	Measurement of adhesion for thermally sprayed material', J. Adhesion Science and Technology, 7 [12] (1993) 1235-1264.	Peer reviewed and published	2 authors <b>C.C. Berndt</b> and C.K. Lin Candidate contribution is 75%
Manuscript #8.	Contact damage in plasma-sprayed alumina-based coatings, J. Am. Ceram. Soc., 79[7] (1996) 1907-14.	Peer reviewed and published	4 authors A. Pajares, L. Wei, B.R. Lawn and <b>C.C. Berndt</b> Candidate contribution is 25%
Manuscript #9.	Influence of plasma spray parameters on the mechanical properties of yttria stabilized zirconia coatings I: Four point bend test, J. Mater. Engin. and Sci., A284 (2000) 29-40.	Peer reviewed and published	5 authors A. Kucuk, <b>C.C. Berndt</b> , U. Senturk, R.S. Lima and C.R.C. Lima Candidate contribution is 30%
Manuscript #10.	Influence of plasma spray parameters on the mechanical properties of yttria stabilized zirconia coatings II: Acoustic emission response, J. Mater. Engin. and Sci., A284 (2000) 41-50.	Peer reviewed and published	5 authors A. Kucuk, <b>C.C. Berndt</b> , U. Senturk, R S. Lima and C.R.C. Lima Candidate contribution is 30%
Manuscript #11.	Evaluation of microhardness and elastic modulus of thermally sprayed nanostructured zirconia coatings, Surf. Coat. Tech., 135 (2001) 166-172.	Peer reviewed and published	3 authors R.S. Lima, A. Kucuk and <b>C.C. Berndt</b> Candidate contribution is 45%
<b>Chapter 4. Modeling Studies</b>			
Manuscript #12.	Evaluation of off-angle thermal spray, Surf. Coat. Tech., 89 (1997) 213-224.	Peer reviewed and published	2 authors S.H. Leigh and <b>C.C. Berndt</b> Candidate contribution is 50%
Manuscript #13.	Modeling the coverage of splat areas arising from thermal spray processes, J. Am. Ceramic Soc., 95[5] (2012) p. 1572-1580. DOI: 10.1111/j.1551-2916.2012.05113.x Published: MAY	Peer reviewed and published	5 authors A.S.M. Ang, <b>C.C. Berndt</b> , M. Dunn, M.L. Sesso and S.Y. Kim Candidate contribution is



Chapter and Manuscript Number	Publication title	Publication status	Nature and extent of candidate's contribution
	2012.		25%
Manuscript #14.	Thermal spray maps: Material genomics of processing technologies, J. Thermal Spray Tech., 22[7] (2013) p. 1170-1183. DOI: 10.1007/s11666-013-9970-3, Published: OCT 2013.	Peer reviewed and published	5 authors A.S.M. Ang, N. Sanpo N, M.L. Sesso, S.Y. Kim and <b>C.C. Berndt</b> Candidate contribution is 30%
<b>Chapter 5. Applications of Thermal Spray Materials</b>			
Manuscript #15.	Material fundamentals and clinical performance of plasma-sprayed hydroxyapatite coatings: A review, J. Biomedical Materials Research, 58 [5] (2001) 570-592.	Peer reviewed and published	4 authors Limin Sun, <b>C.C. Berndt</b> , K.A. Gross and A. Kucuk Candidate contribution is 45%
Manuscript #16.	Impact of nanoscale roughness of titanium thin film surfaces on bacterial retention, Langmuir, 2010, 26 (3), 1973-1982.	Peer reviewed and published	11 authors E.P. Ivanova, V.K. Truong, J.Y. Wang, <b>C.C. Berndt</b> , R.T. Jones, I.I. Yusuf, I. Peake, H.W. Schmidt, C. Fluke, D. Barnes and R.J. Crawford Candidate contribution is 10%
Manuscript #17.	Transition metal-substituted cobalt ferrite nanoparticles for biomedical applications, Acta Biomaterialia, 9[3] (2013) p. 5830-5837. DOI: 10.1016/j.actbio.2012.10.037, Published: MAR 2013.	Peer reviewed and published	4 authors N. Sanpo, <b>C.C. Berndt</b> , C. Wen and J. Wang Candidate contribution is 45%
Manuscript #18.	Failure during thermal cycling of plasma-sprayed thermal barrier coatings, Thin Solid Films, 108[4] (1983) 427-437.	Peer reviewed and published	2 authors <b>C.C. Berndt</b> and H. Herman Candidate contribution is 50%
Manuscript #19.	Performance Of Thermal Barrier Coatings In High Heat Flux Environments, Thin Solid Films, 119 (1984) 195-202. [also in NASA Tech. Memorandum 83663, April 1984].	Peer reviewed and published	2 authors R.A. Miller and <b>C.C. Berndt</b> Candidate contribution is 50%
<b>Chapter 6. Integration of Processing, Microstructure and Properties</b>			
Manuscript #20.	A review of testing methods for thermal spray coatings, J. Inter. Materials Reviews, 2014, 45 pages, advance on-line article: <a href="http://dx.doi.org/10.1179/1743280414Y.0000000029">http://dx.doi.org/10.1179/1743280414Y.0000000029</a>	Peer reviewed and published	2 authors A.S.M. Ang and <b>C.C. Berndt</b> Candidate contribution is 50%

This application is made on the basis that I am a co-author on the published materials submitted for this degree. Details of my role leading to the publication of the 20 works are provided in Table 2. This self-assessment has been performed to the best of my recollection; keeping in mind that these 20 publications cover 30 years of my research career.

Table 2: Role of the applicant, in terms of authorship status and inputs into (i) the study design, (ii) the generation of data, (iii) the analysis of data, and (iv) writing, for each piece of work. The number assigned to each publication is listed on the previous pages.

Category Description	Description of Input	Publication Number									
		1	2	3	4	5	6	7	8	9	10
Authorship	First author (see Note 1)										
	Senior author (see Note 2)										
	Co-author										
Study design	Not applicable										
	Responsible for whole study										
	Significant input										
	Little / no input										
Generation of data	Not applicable										
	Major role										
	Significant role										
	Some role										
	Little/no role										
Analysis of data	Not applicable										
	Major role										
	Some role										
	Little / no role										
Writing (* with minor input from others)	Wrote submission*										
	Major role										
	Some role										
	Little role										

Category Description	Description of Input	Publication Number									
		11	12	13	14	15	16	17	18	19	20
Authorship	First author (see Note 1)										
	Senior author (see Note 2)										
	Co-author										
Study design	Not applicable										
	Responsible for whole study										
	Significant input										
	Little / no input										
Generation of data	Not applicable										
	Major role										
	Significant role										
	Some role										
	Little/no role										
Analysis of data	Not applicable										
	Major role										
	Some role										
	Little / no role										
Writing (* with minor input from others)	Wrote submission*										
	Major role										
	Some role										
	Little role										

Notes 1 and 2 are stated on the following page.

Note 1: The designation of "First author" has been taken in the literal sense; i.e., the individual who has been listed first for that particular publication. In many instances I could have justified placing myself in the first author position. However, my guiding principal on this topic for the most recent 20 years has been to place the post graduate student or post doctoral fellow in this role so that their career options, via their CVs, are enhanced.

Note 2: The designation of "Senior author" is traditionally the individual who is named last in the author list. I do not follow this tradition and reserve this last position for a junior colleague, a post doctoral fellow or post graduate student so that their career options are enhanced. Thus, I have declared myself as the senior author for those publications where I have played this role, but not necessarily placed myself last in the author list.

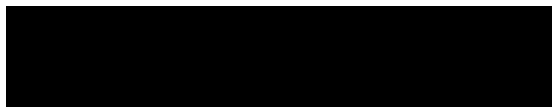
I have not renumbered sections of submitted or published papers. They have been structured into six chapters to generate a consistent presentation within the work.

Table 2 lists the articles that are presented in Appendix 6. Articles numbered 6, 8 and 10 are 50% authored by the candidate, whereas the remaining 14 are 100% authored by the candidate.

Table 2. List of 17 original short-form contributions in the format of editorials and commentaries.

1	1992	C.C. Berndt, "Editorial: 1st Issue of JTST", JTST, 1[1] (1992) 3.
2	1992	C.C. Berndt, "Editorial: Closure of 13th ITSC", JTST, 1[2] (1992) 99.
3	1994	C.C. Berndt, "The Significance of Thermal Spray Awards", JTST (1994) 3[3] 244.
4	1994	C.C. Berndt, "Who's Holding The Gun?", J. Thermal Spray Technology, 4[1] (1994) 331-332.
5	1996	C.C. Berndt, "Standardize And Deliver", JTST, 5[1] (1996) 2-3.
6	1999	R. Seals and C.C. Berndt, "Rationale for a JTST Award for the Best Scientific Paper", JTST, 8[1] (1999) 3-5.
7	2001	C.C. Berndt, "How do we Market JTST", 10 (2001) 3-4.
8	2003	L. Pawlowski and C.C. Berndt, "The Globalization of JTST: A Forum for a World Wide Network", JTST, 12 (2003) 3-4.
9	2006	C.C. Berndt, "State of the Society The Birth of Opportunity", AM&P (2006) 164[5] p94.
10	2006	C.C. Berndt and G. Montavon, "Thermal Spray: Preserving 100 Years Of Technology", J. Thermal Spray Technology, 15[1] (2006) 5-8.
11	2007	C.C. Berndt, "Activism in Thermal Spray: A Call to Arms", Advanced Materials & Processes, 165[8] (2007) 72. Also in JTST, 16[2] (2007) 167.
12	2007	C.C. Berndt, "Commentary. The End of the Beginning; Now Let's Make a Real Effort!", JTST, 16[3] (1992) 320.
13	2007	C.C. Berndt, "One way to pick "Low-hanging fruit" is to chop the tree down!", Journal of Thermal Spray Technology, 16[4] (2007) p. 465. Also 385 AM&P (2007) 165[5] P70.
14	2007	C.C. Berndt, "Thermal Spray: The Best Thing Since Sliced Bread", Advanced Materials & Processes, 165[1] (2007) 100.
15	2008	C.C. Berndt, "'At the end of the day': let-us all take on responsibility for thermal spray", Advanced Materials & Processes, Vol. 166, no. 8 (Aug 2008), p. 58 .
16	2008	C.C. Berndt, "Born again as a technologist", Advanced Materials and Processes, Vol. 166, no. 5 (May 2008), p. 68.
17	2008	C.C. Berndt, "Editorial: will thermal spray ever be the basis for a Nobel Prize?", Advanced Materials & Processes, Vol. 166, no. 11 (Nov 2008), p. 66.

**Signed:**



**Date:**

**August 01, 2014**



**Thermal Spray Coatings:  
Processing, Microstructural Architecture  
and their Materials Engineering Design**

by:

Christopher C. Berndt

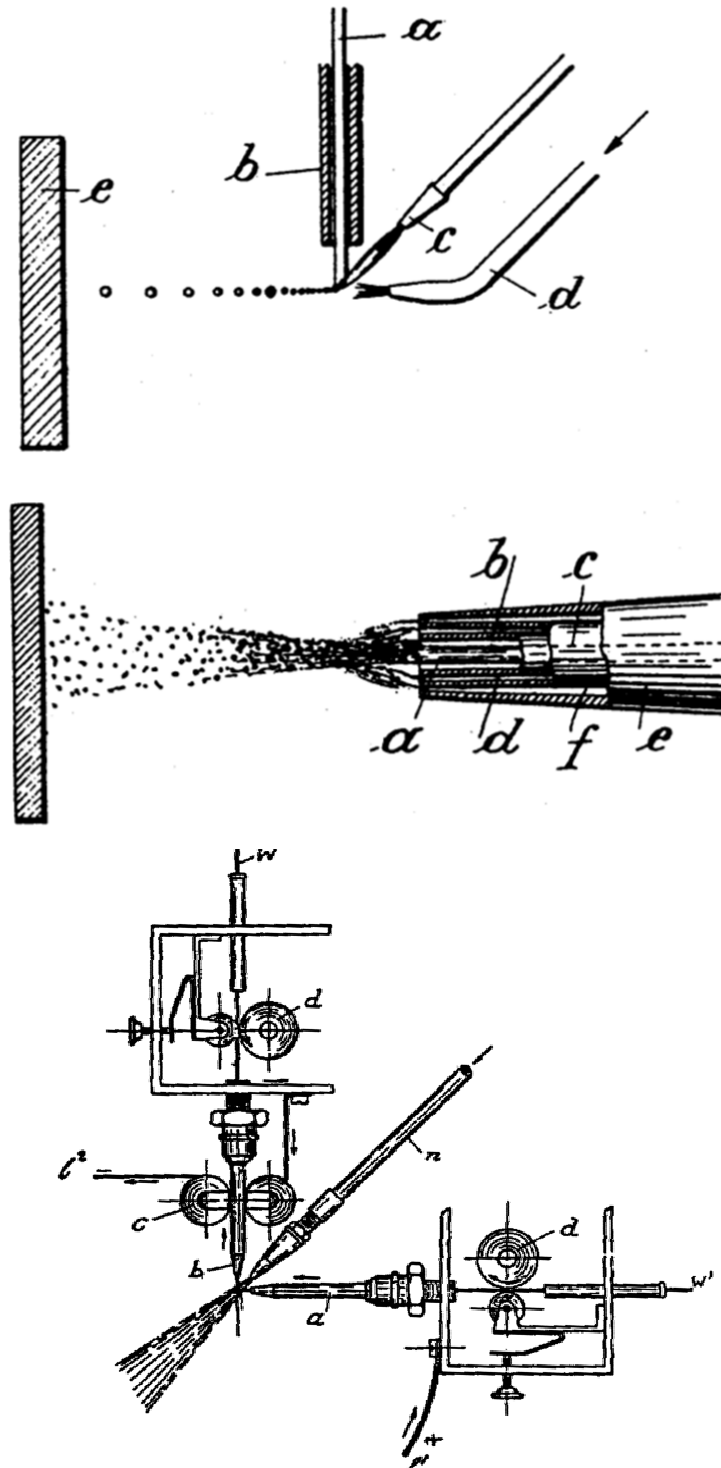
B.App.Sc. (Secondary Metallurgy)

Graduate Diploma (Metallurgy and Materials)

Doctor of Philosophy (Materials Engineering)

Presented for the Degree of:  
Higher Doctorate in Engineering, D.Eng.  
in the  
Faculty of Engineering  
Monash University, Monash, Victoria 3168  
AUSTRALIA

April 2014



Early Forms of Thermal Spray Processes  
 From British Patent 29,001 4<sup>th</sup> December 1912,  
 by E. Morf:

“A Method of Producing Bodies and Coatings of Glass and Other Substances”

Hermann Hesse in the Glass Bead Game describes the young scholar Joseph Knecht who aspires to learn the intricacies of “the Game” from his Music Master. Hesse writes:

*The Game as I conceive it, ‘Knecht once wrote to his former Music Master, ‘encompasses the player after the completion of meditation as the surface of a sphere encompasses its centre, and leaves him with the feeling that he has extracted from the universe of accident and confusion a totally symmetrical and harmonious cosmos, and absorbed it into himself’.*



## Table of Contents

Abstract		v
Summary of Theme of the Work		vi
A Summary of the Development of the Work and Advancement of Knowledge		vii
Declaration		xi
Acknowledgements		xii
Dedication		xiii
<b>Chapter 1. Processing of Materials</b>		
1.1 Introduction		1
1.2 Manuscript #1.	J. Tikkanen, K.A. Gross, C.C. Berndt, V. Pitkanen, J. Keskinen, S. Raghu, M. Rajala and J. Karthikeyan, 'Characteristics of the Liquid Flame Spray Process', Surf. Coat. Tech., 90 (1997) 210-216.	2
1.3 Manuscript #2.	M.L. Sesso, C.C. Berndt and Y.C. Wong, 'Topographical and microstructural property evolution of air plasma-sprayed zirconia thermal barrier coatings, J. Am. Ceramic Soc., Article first published online: 4 FEB 2014, DOI: 10.1111/jace.12842.	9
<b>Chapter 2. Microstructural Evolution and Design</b>		
2.1 Introduction		17
2.2 Manuscript #3.	R.S. Lima, J. Karthikeyan, C.M. Kay, J. Lindemann and C.C. Berndt, 'Microstructural characteristics of cold-sprayed nanostructured WC-Co coatings', Thin Solid Films, 416 (2002) 129-135.	18
2.3 Manuscript #4.	J.A. Gan and C.C. Berndt, 'Design and manufacture of Nd-Fe-B thick coatings by the thermal spray process', Surf. Coat. Tech., 205[19] (2011) p. 4697-4704. DOI: 10.1016/j.surfcoat. 2011.04.034, Published: JUN 25 2011.	25
2.4 Manuscript #5.	J.A. Gan and C.C. Berndt, 'Effects of standoff distance on porosity, phase distribution and mechanical properties of plasma sprayed Nd-Fe-B coatings', Surf. Coat. Tech., 216 (2013) p. 127-138. DOI: 10.1016/j.surfcoat.2012.11.040, Published: FEB 15 2013.	33
2.4 Manuscript #6.	J.A. Gan and C.C. Berndt, 'Quantification and taxonomy of pores in thermal spray coatings by image analysis and stereology approach', Metall. and Mater. Trans. A, 44A[10] (2013) p. 4844-4858. DOI: 10.1007/s11661-013-1818-4, Published: OCT 2013.	45

### Chapter 3. Mechanical Property Testing

3.1 Introduction		61
3.2 Manuscript #7.	C.C. Berndt and C.K. Lin, 'Measurement of adhesion for thermally sprayed materials', J. Adhesion Science and Technology, 7 [12] (1993) 1235-1264.	62
3.3 Manuscript #8.	A. Pajares, L. Wei, B.R. Lawn and C.C. Berndt, 'Contact damage in plasma-sprayed alumina-based coatings', J. Am. Ceram. Soc., 79[7] (1996) 1907-14.	92
3.4 Manuscript #9.	A. Kucuk, C.C. Berndt, U. Senturk, R.S. Lima and C.R.C. Lima, 'Influence of plasma spray parameters on the mechanical properties of yttria stabilized zirconia coatings I: Four point bend test', J. Mater. Engin. and Sci., A284 (2000) 29-40.	100
3.5 Manuscript #10.	A. Kucuk, C.C. Berndt, U. Senturk, R S. Lima and C.R.C. Lima, 'Influence of plasma spray parameters on the mechanical properties of yttria stabilized zirconia coatings II: Acoustic emission response', J. Mater. Engin. and Sci., A284 (2000) 41-50.	112
3.6 Manuscript #11.	R.S. Lima, A. Kucuk and C.C. Berndt, 'Evaluation of microhardness and elastic modulus of thermally sprayed nanostructured zirconia coatings', Surf. Coat. Tech., 135 (2001) 166-172.	122

### Chapter 4. Modeling Studies

4.1 Introduction		129
4.2 Manuscript #12.	S.H. Leigh and C.C. Berndt, 'Evaluation of off-angle thermal spray', Surf. Coat. Tech., 89 (1997) 213-224.	130
4.3 Manuscript #13.	A.S.M. Ang, C.C. Berndt, M. Dunn, M.L. Sesso, S.Y. Kim, 'Modeling the coverage of splat areas arising from thermal spray processes', J. Am. Ceramic Soc., 95[5] (2012) p. 1572-1580. DOI: 10.1111/j.1551-2916.2012.05113.x Published: MAY 2012.	142
4.4 Manuscript #14.	A.S.M. Ang, N. Sanpo N, M.L. Sesso, S.Y. Kim and C.C. Berndt, 'Thermal spray maps: Material genomics of processing technologies', J. Thermal Spray Tech., 22[7] (2013) p. 1170-1183. DOI: 10.1007/s11666-013-9970-3, Published: OCT 2013.	151

## **Chapter 5. Applications of Thermal Spray Materials**

5.1 Introduction		167
5.2 Manuscript #15.	Limin Sun, C.C. Berndt, K.A. Gross and A. Kucuk, 'Material fundamentals and clinical performance of plasma-sprayed hydroxyapatite coatings: A review', J. Biomedical Materials Research, 58 [5] (2001) 570-592.	168
5.3 Manuscript #16.	E.P. Ivanova, V.K. Truong, J.Y. Wang, C.C. Berndt, R.T. Jones, I.I. Yusuf, I. Peake, H.W. Schmidt, C. Fluke, D. Barnes and R.J. Crawford, 'Impact of nanoscale roughness of titanium thin film surfaces on bacterial retention', Langmuir, 2010, 26 (3), 1973-1982.	191
5.4 Manuscript #17.	N. Sanpo, C.C. Berndt, C. Wen and J. Wang, 'Transition metal-substituted cobalt ferrite nanoparticles for biomedical applications', Acta Biomaterialia, 9[3] (2013) p. 5830-5837. DOI: 10.1016/j.actbio.2012.10.037, Published: MAR 2013.	201
5.5 Manuscript #18.	C.C. Berndt and H. Herman, 'Failure during thermal cycling of plasma-sprayed thermal barrier coatings', Thin Solid Films, 108[4] (1983) 427-437.	209
5.6 Manuscript #19.	R.A. Miller and C.C. Berndt, 'Performance Of Thermal Barrier Coatings In High Heat Flux Environments', Thin Solid Films, 119 (1984) 195-202. [also in NASA Tech. Memorandum 83663, April 1984].	220

## **Chapter 6. Advancement of Knowledge**

6.1 Introduction		233
6.2 Manuscript #20.	A.S.M. Ang and C.C. Berndt, 'A review of testing methods for thermal spray coatings', J. Inter. Materials Reviews, 2014, 45 pages, advance on-line article: <a href="http://dx.doi.org/10.1179/1743280414Y.0000000029">http://dx.doi.org/10.1179/1743280414Y.0000000029</a>	234

## **Chapter 7. Summary and Concluding Comments**

7.1 Analysis of Co-Workers and Collaborators	279
7.2 Summary of Publications	282
7.3 Analysis of Publication Content	282
7.4 Analysis of Yearly Output	284
7.5 Concluding Comments	287



## List of Appendices

Appendix 1. Condensed Curriculum Vitae (11 pages).	A3
Appendix 2. Press Release on Christopher C. Berndt: President of ASM International (2 pages).	A15
Appendix 3. Research Portfolio (6 pages).	A17
Appendix 4. Leadership and Engagement Portfolio (6 pages).	A23
Appendix 5. Learning and Teaching Portfolio (6 pages).	A29
Appendix 6. Editorials and Commentaries of Christopher C. Berndt (27 pages).	A35
Appendix 7. List of Publications of Christopher C. Berndt (36 pages).	A63
Appendix 8. Biography of Christopher C. Berndt (1 page).	A98

## **Thermal Spray Coatings: Processing, Microstructural Architecture and their Materials Engineering Design**

---

### **Abstract**

This thesis encompasses the following two major sections. The first section is comprised of twenty (20) manuscripts that are segmented into the 5 areas: viz. (i) the processing of materials, (ii) microstructural evolution and design, (iii) mechanical property testing, (iv) modeling studies, and (iv) applications of thermal spray materials. These manuscripts cover a period from 1983 through to 2013; which is considered the appropriate snapshot in time since the confirmation of the PhD degree in 1981. The selected manuscripts represent an '*original, substantial and distinguished contribution to knowledge*' in the field of thermal spray science, engineering and technology.

The basis of selecting the specific manuscripts lies on three complimentary criteria. (1) Some of the articles have been highly cited. (2) Several review-based articles demonstrate a broad and thorough knowledge of the field of thermal spray. (3) The publications in the past 5-years indicate an integration of knowledge over three decades that leads to new discoveries and expanded knowledge.

The bulk of the thesis exhibits 20 manuscripts that have been down-selected and systematically organized to demonstrate the following content.

- Longevity in the general area of materials science and engineering; and specifically in the area of thermal spray coatings and technology.
- Productivity and focus in several sub-specialties of thermal spray coatings and technology. These areas, although presented as separate entities, are interrelated with themes that cut across several disciplines of science and engineering.
- The continuous development of research subjects that are driven by new methods of analysis; new thermal spray technology; surface science and engineering; and the availability of advanced instrumentation and analytical equipment.

The second section is a compilation of appendices that detail the avenues, many of which are outside the conventional publication route, that the applicant has employed to disseminate knowledge. The appendices provide reviewers and examiners with a more comprehensive perspective of the applicant that cannot be presented by publications alone.

The appendices compliment the body of the thesis in several ways. The appendices present the much bigger view for the development of research by integrating it within (i) a wide-ranging research portfolio, (ii) leadership and engagement within university settings, and (iii) the traditional learning and teaching environment of universities. Therefore, the development of this thesis presents an integrated approach so that examiners can appreciate the deep commitment of the applicant to the development of a comprehensive study in the chosen area.

The appendices include a list of the publications of the applicant. In addition, there is a compilation of editorials and commentaries that are provocative and thoughtful articles that relate to social context issues. These articles have been instrumental in documenting important aspects of thermal spray science, engineering and technology.

## **Summary of Theme of the Work**

Section 3 of the “Higher Doctorate Application” indicates that a summary is required according to the following guidelines: “Please attach a summary of no less than 200 words describing the theme of the work to be assessed.”

### **Thermal Spray Coatings: Processing, Microstructural Architecture and their Materials Engineering Design**

This thesis embodies studies on thermal spray coatings that were initiated in 1977 by the applicant. Publications of the applicant have been selected that segment this work into 5 distinct areas of science and engineering: viz. (i) the processing of materials, (ii) microstructural evolution and design, (iii) mechanical property testing, (iv) modeling studies, and (v) applications of thermal spray materials. These subject areas, although distinct in their own right, are interrelated and it is only by performing a sustained, long term study that they may be integrated into a comprehensive body of work.

The overall theme of this work presents a fundamental understanding of the microstructural evolution of the coating architecture. The processing conditions are extreme in terms of rapid solidification and the kinematic deformation of materials. Microstructural artefacts such as metastable phases, lamellar boundaries, porosity and cracks are typical features observed in thermal spray deposits. These features confer a ‘composite type’ character on the deposit that control the extrinsic properties. Therefore, the extended theme of this work has expanded from that of classical materials science to encompass the processing sciences. In this way the formation conditions of the coating can be examined so that the ‘triumviri of materials science’; i.e., ‘processing-properties-applications’, can be explored.

The advancement of knowledge by the applicant has been developed in many formats. For example:

- The applicant has published extensively in the subject area over 35+ years. Over 450 pieces of work can be attributed to the applicant.
- The applicant was the Foundation Editor, and now Editor Emeritus, of the Journal of Thermal Spray Technology. This is the premier avenue for advancing knowledge on the topic of thermal spray.
- The applicant has been an advocate of thermal spray via professional societies; especially within ASM International (aka ‘the American Society for Materials’) where he attained the position of President. The applicant has advanced knowledge by means of professional talks and management decisions under this responsibility.

The applicant is first and foremost an academician who teaches. His greatest legacy on from the undergraduates he has taught and the post graduates he has trained. These former students and post docs now occupy positions of authority and stature around the globe and this is a testament to the advancement of knowledge instigated by the applicant.



## **A Summary of the Development of the Work and Advancement of Knowledge**

Section 6 of the “Higher Doctorate Application” form indicates that ‘A *summary of the development of the work, of approximately 1000 words*’ is required.

### **Thermal Spray Coatings: Processing, Microstructural Architecture and their Materials Engineering Design**

This body of work has developed along 5 parallel tracks since the applicant completed his PhD in 1981. These tracks might be considered as independent lines of investigation by many researchers; however, the applicant has taken an integrated approach. This methodology has involved exploration of many subjects that have contributed to an in-depth comprehension of thermal spray materials. Hence, the title of this thesis embodies these elements of fundamental research; i.e., materials engineering that is based on microstructural design, but which is also controlled by the extreme processing environment of the thermal spray process. The parallel tracks are described below so that ‘the development of the work’ can be explained with respect to the framework of this thesis.

#### **Processing of Materials**

Chapter 1 (manuscripts #1 and #2) describes selected works under the broad classification of processing.

The study in 1997 built on previous work of the applicant and studied the injection of liquid feedstock into an oxygen-hydrogen flame. The liquid phase was evaporated and subsequent thermochemical reactions produce nanoparticles. This process requires a thorough understanding of the feedstock-flame interactions. The experimental techniques included laser diffraction anemometry for droplet size distribution, laser Doppler velocimetry for particle velocity, pulsed laser Rayleigh backscattering for flame temperature and Schlieren photography for flame structure. The series of manuscripts that evolved from this work laid the foundation for growth in this topical area.

Another approach was taken in 2014 where processing variables were assessed by examination of the spray footprint that developed under a static spray environment where there was no relative movement between torch and substrate. These experimental conditions allowed the important parameters of deposition efficiency and coating roughness to be examined with respect to the stand off distance. Hardness and porosity profiles were mapped to display the effect of process parameters. Dynamic process parameters such as particle trajectory, the evolving impact angle and dwell time were scrutinized in relation to changes in porosity, hardness, and density for different coating profiles.

#### **Microstructural Evolution and Design**

Chapter 2 is composed of 4 manuscripts that, broadly, focus on the microstructural evolution of coatings. The applicant has initiated many studies that formulate schemes to characterize and distinguish microstructures; ranging from an arbitrary classification of morphological features that relate to the density and defect structure, to a quantitative analysis *via* a fractal dimension analysis.

The cold spray study expressed in manuscript #3 examines the difficult-to-process material of WC-Co. It is verified that the optimum microstructure that retains the nanostructure can be achieved. The other three manuscripts pick up on work that was initiated in 1998 (G. Montavon, C. Coddet, C.C. Berndt and S.-H. Leigh, "Microstructural Index To Quantify Thermal Spray Deposit Microstructures Using Image Analysis", J. Thermal Spray Tech., 7[2] (1998) 229-241). These three manuscripts present a detailed description and analysis on the taxonomy of Nd-Fe-B thick coatings. These materials are used in magnetic applications and were difficult to procure. Stereology protocols were used to derive the porosity level, pore size, and shape distributions. The nature of annealing was assessed and did not alter the distribution trend of pore number but influence significantly the distribution of pore volume fractions.

### **Mechanical Property Testing**

The 5 manuscripts in Chapter 3 focus on mechanical properties of thermal spray coatings. This topic was the focus on the applicant's thesis and the studies have been refined since his own submission in 1981. Work has been selected from the 1993-2001 timeframe, with manuscript #7 being a review of the "Measurement of adhesion for thermally sprayed materials". This work also developed into measuring "Contact Damage in plasma-sprayed alumina-based coatings", manuscript #8; and two companion manuscripts on the "Influence of plasma spray parameters on mechanical properties of yttria stabilized zirconia coatings". These manuscripts, #9 and #10, examined the four point bend test and acoustic emission to measure Young's Modulus, a pseudo yield point, and cracking mechanisms.

Hardness measurements have been a favoured technique of the applicant for many years and the unique usefulness, attributes and simplicity of this method is illustrated in manuscript #11 (2001) where the 'Evaluation of microhardness and elastic modulus of thermally sprayed nanostructured zirconia coatings' is explored. This work related hardness to roughness for the series of samples analysed. Likewise, this work was the forerunner to further analysis on the bimodal distribution of hardness tests measured by a Weibull distribution analysis; work that was introduced to the thermal spray community by the applicant in 1988.

### **Modeling Studies**

Chapter 4 presents manuscripts #12, #13 and #14 that characterize contributions for the development of modeling studies. The analysis presented in 1997 on 'Evaluation of off-angle thermal spray' is important since it relates microstructural properties (i.e., the porosity) and physical properties (i.e., roughness) to the spray footprint; which ultimately determines deposition efficiency and the economics of manufacturing. Note that manuscript #2 on 'Topographical and microstructural property evolution of air plasma-sprayed zirconia thermal barrier coatings' approaches the same topic from a different direction.

A more sophisticated development arose in 2013 when Madejski's and McPherson's approaches were considered in 'Modeling the coverage of splat areas arising from thermal spray processes', manuscript #13, where fundamental theory is directly related to the

spray coverage as determined by the spray footprint. These relationships were linked to the deposition efficiency. It is noteworthy that Prof. McPherson was the applicant's PhD advisor.

The final contribution in Chapter 4, manuscript #14, consolidates the known properties of thermal spray materials in 'property-performance maps'. This manuscript, on 'Thermal spray maps: Material genomics of processing technologies', is based on an Ashby approach but is significantly unique since it examines extrinsic properties of thermal spray deposits and manufacturing processes. Manuscript #14 is a review contribution that consolidates much of the known data on alumina and zirconia-based thermal spray coatings. The modeling exercise relates to techniques that enable the assessment of large data sets.

### **Applications of Thermal Spray Materials**

Chapter 5 consists of 5 contributions that encompass applications of thermal spray materials. Specifically, manuscript #15 examines 'Material fundamentals and clinical Performance of plasma-sprayed hydroxyapatite coatings: A review'. This is a highly-cited contribution (more than 530 citations and about 40 citation per year since 2001) that indicates:

'the outlook on using HA coatings on orthopaedic appliances, formed by thermal spray methods, as functional bioactive agents to aid the healing process, is favorable'.

Manuscripts #16 and #17 examine thin coatings, applied *via* thin film technologies, for biomedical applications. The understanding of surface roughness is developed with regard to the ability of the surface to retain microorganisms. Thus, although thermal spray is not directly addressed in these studies; the techniques and understanding gained from prior studies are applied to sol-gel and physical vapour deposition technologies. An extension of this approach has been applied by the applicant so that 'combinatorial coatings' of thermal spray and thin film technologies have been incorporated into a single coating.

Thermal barrier coatings have been a focus of the applicant since his residency at NASA in 1983; leading to many manuscripts of which #18 and #19 are examples; i.e., 'Failure during thermal cycling of plasma-sprayed thermal barrier coatings' and 'Performance of thermal barrier coatings in high heat flux environments'. The development of these early studies has progressed to the present day; for example, manuscripts #2 (2014), #9 (2000), #10 (2000), #12 (1997), and #13 (2012) have evolved from this foundation.

### **Advancement of Knowledge**

Section 6 of the "Higher Doctorate Application" form indicates that 'A statement of the applicant's view of the extent to which the work contributes to the advancement of knowledge' is required.

Chapter 6, titled 'Integration of Processing, Microstructure and Properties', consists of manuscript #20: 'Full critical review: A review of testing methods for thermal spray

coatings', and the following extract summarises the development of the understanding within this body of work.

'An important aspect of this work is to highlight the extrinsic nature of mechanical property measurements with regard to thermal spray coatings. Thermal spray coatings exhibit anisotropic behaviour and microstructural artefacts such as porosity and the splat structure of coatings influence the mechanical characterisation methods. The analysis of coating data variability evolving from the different measurement techniques is of particular relevance to interpret the character of thermal spray deposits.'

Further review articles in this thesis are (i) manuscript #7 on 'Measurement of adhesion for thermally sprayed materials'; (ii) manuscript #14 on 'Thermal spray maps: Material genomics of processing technologies'; and manuscript #15 on 'Material fundamentals and clinical performance of plasma-sprayed hydroxyapatite coatings: A review'. There are a total of 27 review articles listed by the applicant in the introduction to Chapter 6.

Thus, the 'advancement of knowledge' is married to the title of this thesis; i.e., a comprehensive and unified study on 'Thermal Spray Coatings: Processing, Microstructural Architecture and their Materials Engineering Design'.



## **Declaration**

To the best of my knowledge and belief, this higher doctorate thesis is an original compilation of work that has been carried out by the applicant. Collaborators and co-authors are appropriately referenced. It does not contain any material that has been accepted for a higher doctorate in any university

A solid black rectangular box used to redact the signature of Christopher C. Berndt.

Christopher C. Berndt  
April 03, 2014

## **Acknowledgements**

The body of work contained within this higher doctorate thesis could not have been performed without the help of many individuals. The 141 co-authors are listed in Chapter 7. Several sub-groups within this list require special mention. I am particularly indebted to three of my mentors.

Professor Reginald McPherson of Monash University (Melbourne, Australia) guided me from 1977 through to 1981 as my doctoral advisor. He helped me on my return to Monash from 1985 through to 1990. Reg taught me how to perform rigorous experiments and analyze data. Reg passed away on November 02, 1993; yet his legacy lives on.

Professor Herbert Herman of Stony Brook University (NY-USA) was my post doctoral advisor from 1981 to 1983 and then a colleague from 1990 through to 2004. Herb taught me how to write, and also enjoy, the process of documenting research.

Dr Robert A. Miller of NASA Lewis Research Center (Cleveland, OH-USA) was my supervisor from 1983 through to 1985 as well as for an intense summer in 1991. Bob taught me to appreciate criticism as well as to be a critical thinker.

I am fortunate to have supervised post graduate students in Australia and graduate students in the USA who have worked very hard to measure up to demanding research objectives. Likewise, it has been my privilege to work with many excellent post doctoral fellows and university colleagues over more than three decades. To these ladies and gentleman I say: 'Thanks for your help in making discoveries and creating new knowledge.'

It is important that I recognize the support of the many administrators and university managers who oil the cogs of a research and teaching enterprise. I am sincerely grateful for your support. Finally, to the technicians and industrialists who have helped me many times to transform a thought-bubble into a tangible outcome I say 'I am highly appreciative for your input and support'; in some cases over periods of decades. Furthermore: 'I respect your skills and practical knowledge immensely.'

## **Dedication**

To my wife Marita, without whom my life would be less rich.

## Chapter 1. Processing of Materials

### 1.1. Introduction

Chapter 1 (manuscripts #1 and #2) describes selected works under the broad classification of processing.

The study in 1997 built on previous work of the applicant and studied the injection of liquid feedstock into an oxygen-hydrogen flame. The liquid phase was evaporated and subsequent thermochemical reactions produce nanoparticles. This process requires a thorough understanding of the feedstock-flame interactions. The experimental techniques included laser diffraction anemometry for droplet size distribution, laser Doppler velocimetry for particle velocity, pulsed laser Rayleigh backscattering for flame temperature and Schlieren photography for flame structure. The series of manuscripts that evolved from this work laid the foundation for growth in this topical area.

Another approach was taken in 2014 where processing variables were assessed by examination of the spray footprint that developed under a static spray environment where there was no relative movement between torch and substrate. These experimental conditions allowed the important parameters of deposition efficiency and coating roughness to be examined with respect to the stand off distance. Hardness and porosity profiles were mapped to display the effect of process parameters. Dynamic process parameters such as particle trajectory, the evolving impact angle and dwell time were scrutinized in relation to changes in porosity, hardness, and density for different coating profiles.

The 84 publications, with the identification numbers below and listed in Appendix 7, are considered as contributions that focus on this specific subject material. Chapter 7 of this thesis outlines the methodology employed for this analysis.

73	227	353	391	430
113	233	354	399	432
118	245	356	400	437
119	246	357	404	438
141	247	361	405	439
158	254	362	406	440
165	256	366	408	441
174	264	367	409	442
180	266	370	410	443
184	267	373	412	444
185	268	374	414	445
187	270	376	416	451
190	293	378	423	455
202	298	382	424	456
204	329	388	427	457
205	345	389	428	458
212	346	390	429	

## Characteristics of the liquid flame spray process

J. Tikkanen <sup>a,\*</sup>, K.A. Gross <sup>a</sup>, C.C. Berndt <sup>b</sup>, V. Pitkänen <sup>a</sup>, J. Keskinen <sup>a</sup>, S. Raghu <sup>b</sup>,  
M. Rajala <sup>c</sup>, J. Karthikeyan <sup>b</sup>

<sup>a</sup> Tampere University of Technology, Department of Physics, P.O. Box 692, FIN-33101 Tampere, Finland

<sup>b</sup> College of Engineering, SUNY at Stony Brook, Stony Brook, NY 11794, USA

<sup>c</sup> University of Industrial Arts Helsinki, Department of Ceramic and Glass Design, Hämeentie 135 C, FIN 00560 Helsinki, Finland

Received 22 December 1995; accepted 7 November 1996

### Abstract

Liquid flame spraying (LFS) is a new thermal spray process. Liquid feedstock is injected and atomized in an oxygen–hydrogen flame where the liquid phase is evaporated and thermochemical reactions are completed to produce fine particles. Production of nanoparticles requires a thorough understanding of the process. Therefore, various process stages were studied; i.e., the atomization of liquid feedstock, and characterization of the flame and flame–droplet interactions. Experimental techniques included laser diffraction anemometry for droplet size distribution, laser doppler velocimetry for particle velocity, pulsed laser Rayleigh back scattering for flame temperature and Schlieren photography for flame structure.

Atomization is optimized with an organic solvent, such as isopropanol, nebulized with hydrogen gas at a high flow rate. Liquid droplets injected into the flame are subjected to a maximum temperature of 2600°C and are accelerated to about 160 m s<sup>-1</sup>. The flame length can be controlled by flame velocity and the solvent type. Water produces a shorter flame whereas isopropanol extends the flame. Injection of the aerosol produces a “pencil-like” region which does not experience turbulence for most of the flame length. Experimentation with manganese nitrate and aluminium isopropoxide or aluminium nitrate showed conversion to a manganese oxide and alumina, respectively. © 1997 Elsevier Science S.A.

**Keywords:** Liquid flame spraying; Atomization; Vaporization; Nanoparticles; Particle velocity; Flame turbulence

### 1. Introduction

Thermal spraying is an advanced materials processing technique which has found wide acceptance in many high technology industries. In this process, a high temperature-high velocity flame is produced using either chemical or electrical energy to heat, melt and spray material introduced into the flame. Feedstock injected into the flame is more common in the form of powder but can also be in wire or rod form. Molten droplets are thus transported to an object to produce overlay coatings for protection or performance enhancement purposes [1].

In general, thermal spray coatings have a very fine (micron sized) grain structure [1]. However, nano-grained deposits and nanosized particles have superior properties compared to conventional materials [2], and diffusion flames offer a means to produce such materials [3]. The flame spray process has, thus, the potential to

produce nanomaterials at high production rates; yet, no systematic study on flame spray synthesis of nanomaterials has been conducted.

Reduction of the particle size of the thermal spray feedstock improves the homogeneity and properties of coatings [1], however, no successful effort has been reported on using submicron sized feedstock, probably because of (i) high production costs of the small particles, (ii) poor rheological properties of fine particles leads to non-uniform powder transport from the feeder to the spray gun, and (iii) difficulty of particle injection into the core of the spray flame [4].

Preliminary experiments, carried out in our laboratory, indicated that both the above noted goals, viz., nanoparticle synthesis and production of thermal spray coatings with submicron particle feedstock, can be achieved by using atomized liquid droplets as the spray feedstocks. This liquid flame spray (LFS) process [5] is a reactive synthesis technique wherein a precursor is dissolved in a solvent and atomized axially through the combustion flame (Fig. 1). Subsequent thermochemical

\* Corresponding author.

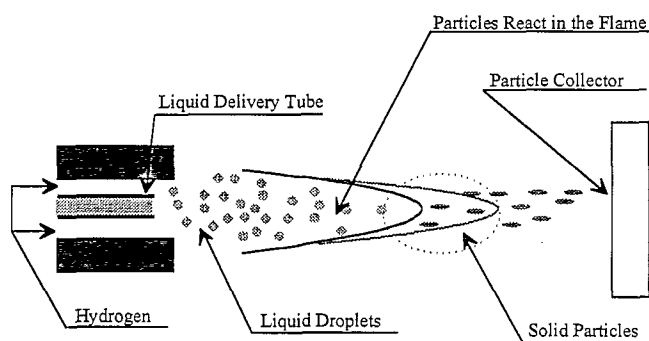


Fig. 1. Operating principle of the LFS process illustrating the atomization, reaction in flame and particle collection stages.

reactions involve the removal of the solvent and production of nanoparticles with high temperature phases. By using the so-produced nanoparticles as “in situ produced fine particle feedstock” it is possible to produce nanograined coatings and nanosized particles of ceramic materials such as alumina, zirconia and others. For example, heating of aluminium nitrate,  $\text{Al}(\text{NO}_3)_3 \cdot 9\text{H}_2\text{O}$ , can produce  $\alpha$ -alumina or granular alumina through a sequence of reactions [6,7], depending upon the heat treatment temperature (Fig. 2). Under non-equilibrium conditions which occur in thermal reactor zones, some reactions may be bypassed and substituted by others.

A combustion flame can be produced by burning any fuel such as hydrogen, acetylene, propylene, propane, etc., with either air or oxygen. The temperature of the flame can be varied by changing the fuel composition, and the flame velocity can be altered by the design of the combustion chamber and combustion nozzle as well as the gas flow rates. A low velocity flame was chosen so that liquid droplets will have a sufficiently long dwell time in the flame, ensuring that all the reactions are driven to completion to result in the formation of fully reacted ceramic particles. Though acetylene can produce a higher temperature flame, this gas was avoided due to

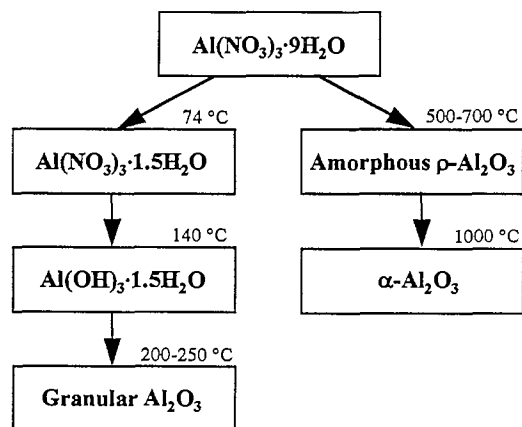


Fig. 2. Reactions for  $\text{Al}(\text{NO}_3)_3 \cdot 9\text{H}_2\text{O}$  upon equilibrium heating [6,7].

the formation of carbides and other impurities in the processed material. Hydrogen was used as the only fuel gas in this work.

The production of nanoparticles requires a clear and thorough understanding of the LFS to help realize its full potential into practical applications. Hence, a systematic study into the atomization of the liquid feedstock, characterization of the spray flame with the liquid feedstocks and flame-droplet interaction was conducted. This article deals with different diagnostic experiments to characterize the LFS process.

## 2. Experimental system and techniques

### 2.1. Liquid flame spray system

The LFS system consists of a custom-made flame spray gun which incorporates an atomizer along the axis of the gun coupled to fuel and oxygen gas flow rate controllers, an infusion pump and associated feed hoses and controls. The gun has a 1-mm diameter liquid feed tube located in the central orifice used for hydrogen gas. A concentric ring delivered oxygen for reaction with the combustion gas. Gas flow rates in the LFS gun are regulated by rotameter flow-meters. Hydrogen and oxygen were delivered in stoichiometric quantities at flows of 40–80 and 20–40  $\text{l min}^{-1}$ , respectively.

Liquid feedstocks can be prepared by dissolving the precursor chemicals in either water (aqueous solutions) or organic solvents such as alcohol, acetone and others. Aqueous solutions allow higher concentrations than organic solvents, are cheaper to produce and are easy and safe to store and handle. A standard infusion pump (Harvard Apparatus, MA, USA) allowed measured quantities of liquid feedstock with exact feed rate control, from 0.0004 to 77  $\text{ml min}^{-1}$ , to be delivered to the two fluid atomizer.

Micron-sized liquid droplets can be produced using various atomizers [8,9], such as an ultrasonic atomizer, centrifugal atomizer, single-fluid atomizer and a two-fluid atomizer. Though the ultrasonic atomizer gives the best performance characteristics with respect to particle size homogeneity [10,11], the two-fluid atomizer is simple to design, build and operate [12]. In this work, a two-fluid atomizer was used to atomize and inject liquid feedstock into the flame. The working principle involves a high velocity hydrogen gas flow exerting a drag force on the slow flowing velocity liquid, thus nebulizing the liquid stream. A high relative gas velocity and atomizing gas density are important parameters for the atomization [13].

The performance characteristics of the atomizer were studied by recording the size distribution of the atomized droplets produced under various operating conditions. Preliminary studies were carried out in air, with water,

isopropyl alcohol and compressed air and helium as the atomized and atomizing fluids respectively. Based on the results of these studies, torch performance involving gun design (atomizer nozzle geometry and dimensions), combustion gas flow and liquid feed rates were optimized.

A parallel plate electrostatic precipitator (consisting of a pair of polished  $100 \times 100 \times 2$ -mm stainless steel plates separated by a 10-mm thick ceramic insulator) with an electric field strength of  $6 \text{ kV cm}^{-1}$  was used to collect the flame synthesized powder. The LFS process was tested by using manganese nitrate, aluminium isopropoxide and aluminium nitrate dissolved in isopropanol and the powder examined with X-ray diffraction.

## 2.2. Diagnostic techniques

Process parameters such as fuel and oxygen flow rates were varied and the flame characteristics recorded to examine the effect of these parameters on the properties of the processing medium. The experimental techniques used for the characterization of the flame, droplets and the particles involved four main methods. These are indicated in Table 1 and will be discussed individually.

### 2.2.1. Laser diffraction anemometry (LDA)

A laser beam is diffracted from particles injected in the path of a laser beam. Diffracted light forms a pattern from which the droplet size distribution is calculated. Measurement is possible for droplets in the range of  $0.7\text{--}875 \mu\text{m}$  with acquisition times of a few seconds up to 120 s. In this study LDA was used to measure the differences in droplet size with different atomizing gases and solutions.

### 2.2.2. Laser doppler velocimetry (LDV)

The “two-beam interference method” was used for recording the velocity profile in a forward scatter mode arrangement (Fig. 3). Two laser beams, generated by a 5-W argon-ion laser ( $514.5 \text{ nm}$  wavelength) are inclined to produce an interference fringe pattern in a test volume of about  $1 \text{ mm}^3$ . The velocity of a particle traversing through this small volume is calculated by analyzing the signal received from the particle traversing through the fringe pattern. A polarizer was used to improve the signal-to-noise ratio in the measurement. The output from the photomultiplier tube was connected to an IFA

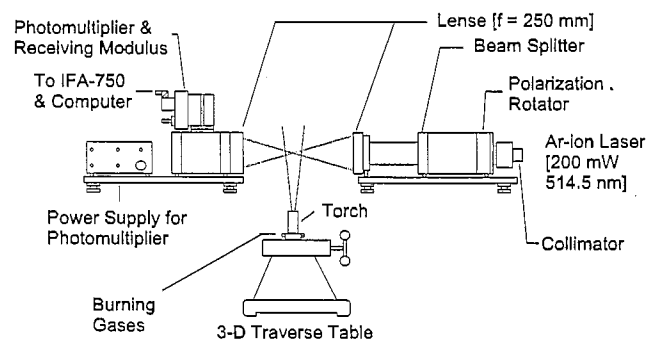


Fig. 3. Typical experimental configuration for flame diagnostics, showing the LDV setup for measuring the velocity profile of the flame.

750 flow analyzer system (TSI Inc.) and the data processed in an IBM-PC computer.

Two torch settings were used to investigate the effect of gas flow rates on the particle velocity. A high flow rate was produced with hydrogen and oxygen flowing at 85 and 48 slpm and a low flow rate used 54 and 29 slpm, respectively. Droplets in the micrometer range were used to measure the velocity.

### 2.2.3. Pulsed laser Rayleigh scattering thermometry

The principle of pulsed laser Rayleigh scattering thermometry (PLRST) technique is to detect the intensity of scattered laser light forming a single spot of  $1 \text{ mm}^3$  in size. The flame was divided into 100 quadrants and the temperature measured along the center axis plane [14]. PLRST directly provides the kinetic gas temperature regardless of non-equilibrium conditions in the flame.

## 2.3. Schlieren photography

The Schlieren technique, based on changes of the gas flow refractive index arising from fluid density variations, was used to visualize the flame and study the structure and turbulence in the flame [15]. It was also employed to qualitatively record the flame–droplet interaction.

The Schlieren system is comprised of a 200-W Xenon light source, two large lenses of 25 cm diameter and 100 cm focal length, a knife-edge and a translucent screen. A parallel beam of light is produced by placing the first lens at the focal length from the aperture of the light source and the second lens is placed approximately 2 m from the first lens. The liquid flame spray (LFS) gun is positioned approximately mid-distance between these two lenses. A knife-edge is placed at the focal point of the second lens so that part of the light can be cut-off by moving the knife-edge.

The Schlieren images indicating the density gradients in the flame were recorded on a CCD camera at a rate of  $30 \text{ frames s}^{-1}$  and then processed using commercially available software. Variation in the flame structure,

Table 1  
Diagnostic techniques used for characterization of particles and flame

Measured property	Experimental technique
Particle size	Laser diffraction anemometry
Particle velocity	laser Doppler velocimetry
Flame temperature	pulsed laser Rayleigh scattering thermometry
Flame structure	Schlieren photography

turbulence and stability of the flame with and without the injection of atomized droplet was recorded to study the effect of droplet injection into the flame.

### 3. Results and discussions

#### 3.1. The atomizer

The droplet size produced by the atomizer will dictate the extent of thermochemical reactions. A smaller droplet size will ensure a higher conversion to the end product for reactions requiring a large heat input. Henceforth, a combination of atomizing conditions were investigated to produce a small droplet size.

The selection of atomizing gas is restricted to either oxygen or hydrogen. The effect of choosing different atomizing gases can be determined theoretically. According to Nukiyama and Tanasawa [13], the Sauter (surface-mean) diameter can be calculated from an empirical formula for small nozzles (max. orifice size of 2 mm) using relative velocity  $U_r$  ( $\text{m s}^{-1}$ ), droplet diameter  $D$  ( $\mu\text{m}$ ), surface tension  $\sigma$  ( $\times 10^{-3} \text{ N m}^{-1}$ ), liquid and gas densities  $\rho_l$  and  $\rho_g$  ( $\text{g cm}^{-3}$ ), liquid viscosity  $\mu_l$  ( $\text{Pa} \cdot \text{s}$ ) and liquid-to-gas mass ratio  $L/G$ . It should be noted that this formula does not include the effect of the atomizing gas density on the particle size. Instead it uses only the liquid to gas volume flow ratio.

$$D_{32} = \frac{585}{U_r} \left( \frac{\sigma}{\rho_l} \right)^{0.50} + 1683 \left( \frac{\mu_l}{\sqrt{\sigma \rho_l}} \right)^{0.45} \left( 1000 \frac{L}{G} \frac{\rho_g}{\rho_l} \right)^{1.5} \quad (1)$$

Calculated  $D_{32}$  values from Eq. (1) for hydrogen and oxygen as an atomizing gas and a stoichiometric fuel composition are plotted as a function of gas flow rate in Fig. 4. The diameter of the droplets produced with hydrogen as the atomizing fluid is always smaller. Based on this result, the LFS gun will operate more effectively with hydrogen as the atomizing gas.

Increasing the atomizing gas velocity by changes in gas flow rate can also lead to a further decrease in droplet size. Results obtained from LDA agree with theoretically predicted changes in droplet sizes (Fig. 5), and indicates that theoretically predicted changes in droplet sizes could be achieved by proper variation of the atomizer parameters.

The experimentally reported droplet size in Fig. 5 was taken from the first peak of the mass distribution data (Fig. 6(a)). The distribution of droplet size varies from several microns to between 50 and 60  $\mu\text{m}$ . In addition to a decrease in droplet size at higher gas flow rates, the population of small droplets increases. This is evident from the increase in the height of the first peak, situated at about 4  $\mu\text{m}$ , in the trimodal distribution. The weighting of the first peak with respect to the total peak area

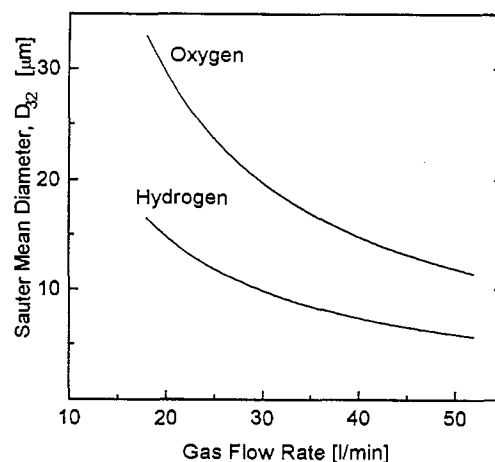


Fig. 4. Droplet diameter as a function of atomizing gas flow rate for hydrogen and oxygen atomizing gases. Water was atomized at a feed rate of  $500 \text{ ml h}^{-1}$  through a  $\varnothing 0.7 \text{ mm}$ . The cross-sectional area of atomizing gas (free volume) is  $0.28 \text{ mm}^2$ .

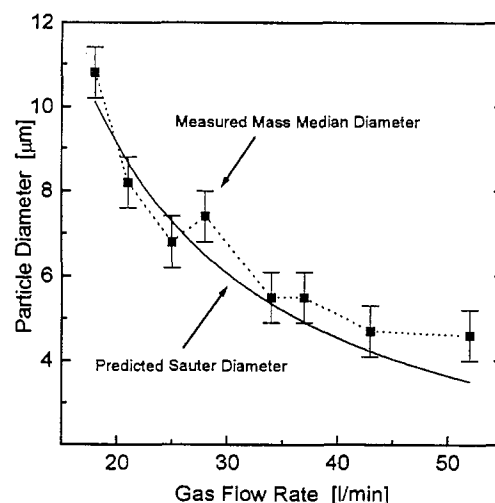
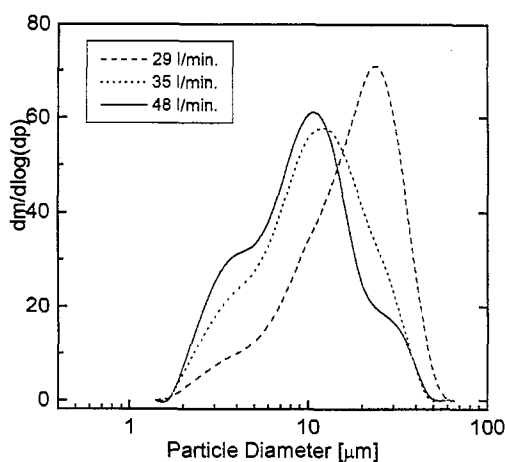


Fig. 5. The effect of atomizing gas flow rate on particle size determined by calculation and experiment. The helium atomizing gas had a free gas volume orifice of  $0.49 \text{ mm}^2$  and liquid feed rate of  $6.2 \text{ cm}^3 \text{ min}^{-1}$  from a  $\varnothing 0.7 \text{ mm}$  nozzle. The predicted particle size has been calculated for the same atomizing parameters.

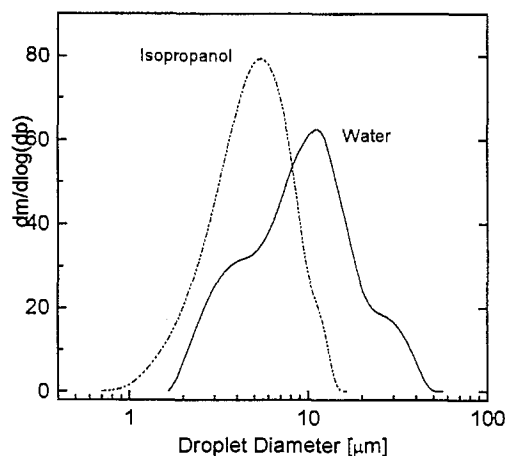
within the droplet size distribution indicates a rise from 8 to 20 and then to 30% of the total population with an increase in gas flow rate (Fig. 6(a)).

Surface tension and liquid viscosity also influence the atomized droplet size. This is illustrated in Fig. 6(b) when the atomizing liquid is changed from water to isopropanol. The mass mean diameter of the droplets produced with the lower viscosity organic fluid (isopropanol) is approximately half the size of water-produced droplets. The surface tension of organic solvents (i.e., isopropanol has  $22 \text{ MN m}^{-1}$ ) is 3.3 times smaller than the surface tension of water at room temperature ( $72 \text{ MN m}^{-1}$ ) [16]. Despite the larger droplet size produced by water it is a better solvation agent allowing





(a)



(b)

Fig. 6. Variation in the droplet size distribution with (a) atomizing gas flow rate and (b) atomizing liquid.

more material to be dissolved; however, isopropanol is preferred when high material delivery rates are not necessary.

### 3.2. The combustion flame

The flame temperature, droplet velocity and flame structure will determine the extent of reaction during liquid flame spraying. These will be examined in turn.

#### 3.2.1. Temperature

The LFS gun performed satisfactorily with a wide range of gas flow rates. Stable flames could be achieved with gas flow rates as high as  $100 \text{ l min}^{-1}$  for hydrogen and  $50 \text{ l min}^{-1}$  for oxygen. Flame temperature measurements showed that even a fast burning oxy-hydrogen flame reached about  $2600^\circ\text{C}$  (Fig. 7). This temperature

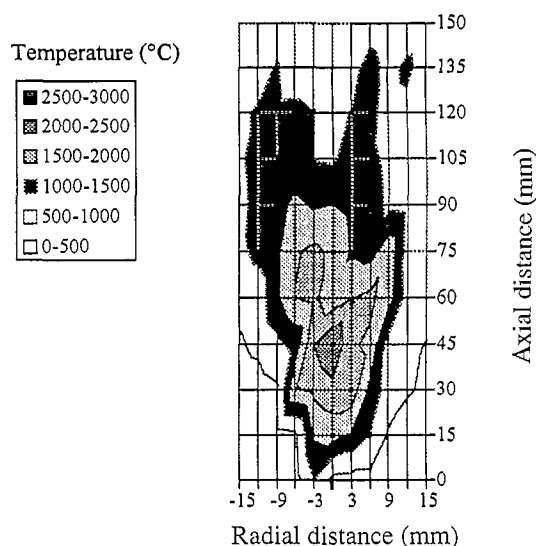


Fig. 7. Flame temperature distribution measured using PLRBS. The spraying parameters are:  $35 \text{ l min}^{-1} \text{ H}_2$ , and  $20 \text{ l min}^{-1} \text{ O}_2$  with no injected liquid.

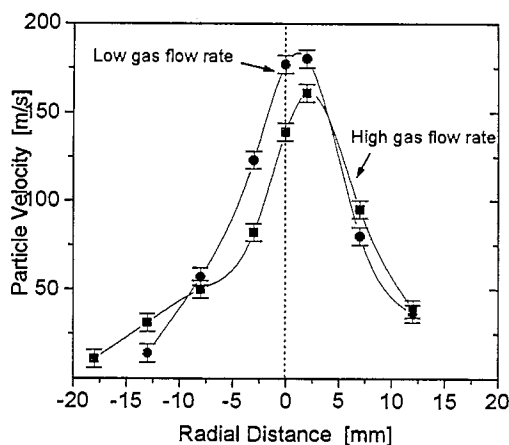
is characteristic of oxy-hydrogen flames with the distribution dependent upon the mixing and turbulence within the flame [17]. The flame temperature increased to a maximum at 45 mm from the nozzle exit. The temperature fall was more gradual, extending out to 130 mm at  $1000^\circ\text{C}$ . Droplets can thus be kept at temperatures above  $1000^\circ\text{C}$  up to 10 cm from the point of injection. It is expected that higher flow rates of the combustion gases will displace these high temperature regions further from the torch exit.

#### 3.2.2. Velocity

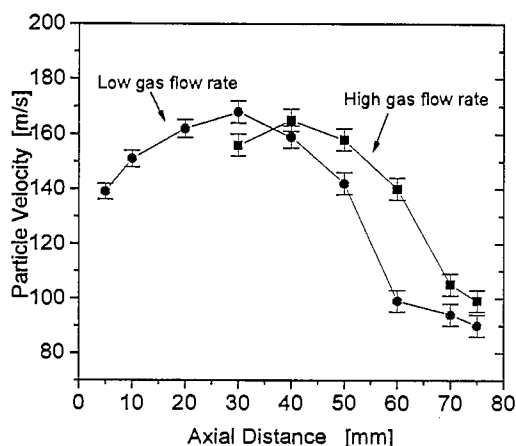
The radial flame velocity distribution, at 60 mm downstream, for a high and low velocity flame, is shown in Fig. 8(a). The high flow rate condition indicates that the flame is broader and particles on the outside of the flame have a higher velocity. The 25-mm broad velocity profile is consistent with Schlieren images where the jet spreads by the same amount (Fig. 9).

The centerline particle velocity is parabolic with respect to the downstream distance (Fig. 8). Particle speed increases rapidly to a maximum velocity and then decreases more slowly further from the torch. The profile for different gas flow rates remains the same but is displaced downstream. For a low gas flow rate, the particles accelerate very rapidly to a velocity of  $140 \text{ m s}^{-1}$  at 5 mm from the exit and reach a maximum of 160 mm at 30 mm. For a higher flow rate the location of maximum particle velocity is offset  $\sim 10 \text{ mm}$  downstream, i.e., it occurs further downstream at  $x=40 \text{ mm}$  but follows a similar phase of acceleration and deceleration.

An initial velocity will be imparted to the droplet from the liquid flow through the atomizer. A greater



(a)

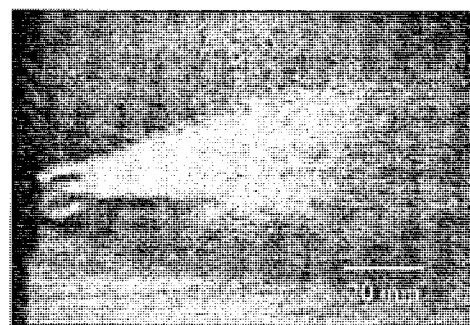


(b)

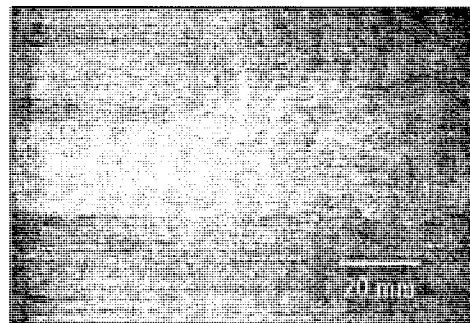
Fig. 8. (a) Radial velocity distribution and (b) axial velocity distribution of the LFS gun flame measured 60 mm from the torch exit.

atomizing gas flow rate will produce smaller droplets, but these attain their maximum velocity further downstream. This delay suggests that droplets in a fast flame have less time to evaporate and thus the large droplet size and higher bulk liquid density (due to more solvent present) prevents the droplet from being accelerated more easily. Use of an aqueous solvent could thus lead to a further decrease in maximum velocity. The lower velocity for particles in the high gas flow rate flame can be seen both in the radial and axial velocity profiles (Fig. 8).

These results indicate that solvent evaporation of the liquid droplets occurs near the exit and the particles maintain the effluent trajectory after achieving their maximum velocity. The particle size measurements using LDA indicates that the size of the particles is less than 10  $\mu\text{m}$ . Thus, the particle velocities are also indicative



(a)



(b)

Fig. 9. Schlieren images of the (a) flame and (b) flame with liquid injection.

of the flow velocities greater than 30–40 mm downstream of the exit. The gas and particle velocities are almost equal in the LFS process. This is not observed in other thermal spray technologies where the injected large particles have velocities which are only a fraction of the flame velocity.

### 3.2.3. Flame structure

Schlieren images illustrate the changes in flame condition, such as turbulence and flame length, upon fluid injection (Fig. 9). High turbulence in the outer region of the flame occurs at the high gas flow rates employed, and is visualized as mixing with the surrounding air. The central “pencil like” unmixed region is seen up to about 4 cm from the nozzle after which it is completely mixed (Fig. 9(a)). This unmixed region is longer upon injection of liquid. The injected liquid delays mixing of the aerosol with the surrounding air. Any thermochemical reaction within this region will thus be dictated by the flame stoichiometry, producing a reducing or oxidizing environment.

The length of the jet is also changed upon liquid injection. Use of isopropanol increases the length and heat content of the flame length due to the exothermic nature of alcohol combustion. By varying the flow rate of the isopropanol liquid, the flame can be extended by as much 10 cm. The opposite effect is obtained with aqueous solutions which cool the flame; hence producing

a shorter flame length (Fig. 9(b)). This shortening of the flame appears as an expansion of the jet. A larger quantity of injected liquid may increase the feed rate of the feedstock but at the cost of reducing the flame length; thus decreasing the amount of heat transfer to the injected liquid and the extent of reaction.

### 3.2.4. Evaluation of LFS process

Various precursors were selected to assess the LFS technique. Manganese nitrate (100 g) dissolved in 500 ml of isopropanol was sprayed with a hydrogen atomizing gas in a stoichiometric flame. X-ray diffraction of the collected powder on the electrostatic precipitator revealed that the thermochemical reactions within the flame produced manganese oxide,  $Mn_2O_3$  with a mean crystal size of 40 nm. This phase has also been reported by Kang et al. with low pressure spray pyrolysis [18]. Aluminium isopropoxide (18 g) dissolved in 350 ml of isopropanol and aluminium nitrate (31 g) in 600 ml of isopropanol produced both  $\delta$ - and  $\gamma$ -alumina after liquid flame spraying. The crystal sizes were approximately the same with  $\delta$ -alumina exhibiting a slightly larger crystal size. Both phases of alumina are typical for highly quenched alumina melts [19]. Present research is addressing the reactions that occur within the flame.

## 4. Conclusions

A new thermal spray process which uses atomized liquid droplets as the spray feedstock has been characterized. Diagnostic experiments have shown that the liquid flame spray gun produces a stable flame under wide ranges of hydrogen and oxygen flow rates. The droplet size distribution can be varied by changing the atomizer parameters such as atomizing gas flow rate, liquid type and liquid feed rate. Micron-sized droplets can be produced both with aqueous and organic feedstock solutions but the latter produces finer size droplets.

Injection of droplets produces a central region where no mixing occurs with the surrounding gases. Flame length is controlled by the gas flow rates and the solvent used to dissolve the precursor material. An organic solvent such as isopropanol extends the flame length.

Droplets show a slightly asymmetric velocity distribution along the torch axis. Acceleration and evaporation of the liquid droplets occur simultaneously. Flame-produced particles then follow the velocity profile of the flame jet.

## Acknowledgement

This research was supported by The Finnish Technology Development Centre and The US National Science Foundation Grants CTS 9312896 and MSS 9311053.

## References

- [1] L. Pawlowski, *The Science and Engineering of Thermal Spray Coatings*, John Wiley & Sons, New York, 1995.
- [2] J.Y. Ying, *J. Aerosol Sci.*, 24(3) (1993) 315–338.
- [3] J.L. Katz and P.F. Miquel, *Nanostructured Mater.*, 4 (1994) 551–557.
- [4] J. Tikkanen, M. Eerola and M. Rajala, *J. Non-Cryst. Solids*, 178 (1994) 220–226.
- [5] J. Tikkanen, V. Pitkanen, M. Eerola and M. Rajala, Finnish patent # 954370, 1995.
- [6] J.W. Mellor, *A Comprehensive Treatise on Inorganic and Theoretical Chemistry*, vol. V, Longmans, London, 1956.
- [7] J.J. Bailar and A.F. Trotman-Dickerson, *Comprehensive Inorganic Chemistry*, Pergamon Press, New York, 1973.
- [8] J.W. Novak and R.F. Browner, *Anal. Chem.*, 52 (1980) 287–290.
- [9] F.R. Gibb, M.J. Utell and P.E. Morrow, *Aerosol Sci. Tech.*, 12 (1990) 376–385.
- [10] R.J., Lang, *J. Acoust. Soc. Am.*, 34(1) (1962) 6–8.
- [11] C. Rodes, T. Smith, R. Crouse and C. Ramachandran, *Aerosol Sci. Tech.*, 13 (1990) 220–229.
- [12] J.M. Goodings, S.M. Graham and W.J. Megaw, *J. Aerosol Sci.*, 14(5) (1983) 679–681.
- [13] R.H. Perry, *Perry's Chemical Engineers Handbook*, 6th edn., McGraw-Hill, New York, 1984.
- [14] J. Larjo, R. Hernberg and J. Vattulainen, *Appl. Phys.*, B 62 (1996) 71–75.
- [15] W. Merzkirch, *Flow Visualization*, Academic Press, New York, 1974.
- [16] CRC, *Handbook of Chemistry and Physics*, CRC Press, Boca Raton, 1980.
- [17] I. Glassman, *Combustion*, Academic Press, New York, 1977.
- [18] Y.C. Kang, S.B. Park and Y.W. Kang, *NanoStructured Mater.*, 5 (1995) 777–792.
- [19] R. McPherson, *J. Mater. Sci.*, 1973, pp. 851–858.

## Permission to publish

J. Tikkanen, K.A. Gross, C.C. Berndt, V. Pitkanen, J. Keskinen, S. Raghu, M. Rajala, J. Karthikeyan, 'Characteristics of the Liquid Flame Spray Process', *Surf. Coat. Tech.*, 90 (1997) 210–216.

As an Elsevier journal author, you retain various rights including Inclusion of the article in a thesis or dissertation whether in part or in toto; see [http://www.elsevier.com/about/policies/author-agreement/lightbox\\_scholarly-purposes](http://www.elsevier.com/about/policies/author-agreement/lightbox_scholarly-purposes) for more information. As this is a retained right, no written permission is necessary. This extends to the online version of your thesis and would include any version of the articles including the final published versions provided that they are not available as individual downloads but only embedded within the thesis itself.

# Topographical and Microstructural Property Evolution of Air Plasma-Sprayed Zirconia Thermal Barrier Coatings

Mitchell L. Sesso,<sup>‡,§,†</sup> Christopher C. Berndt,<sup>‡,§,¶</sup> and Yat C. Wong<sup>‡,§</sup>

<sup>‡</sup>Industrial Research Institute Swinburne (IRIS), Faculty of Science, Engineering and Technology, Swinburne University of Technology, PO Box 218, H38, Hawthorn, Victoria 3122, Australia

<sup>§</sup>Defence Materials Technology Centre, DMTC Ltd., Level 2, 24 Wakefield St, Hawthorn, Victoria, 3122, Australia

<sup>†</sup>Department of Materials Science and Engineering, University of Stony Brook, Stony Brook, New York 11794-2275

The effects of process parameters on thermal barrier coating (TBC) formation and microstructural properties have been studied. Further understanding of the evolution of properties such as porosity and hardness is an important aspect in the design of efficient TBCs. Plasma-sprayed yttria-stabilized zirconia was coated onto mild steel substrates. The torch was held perpendicular to the substrate to form cone-shaped deposits. Standoff distance (SOD) (80, 90, and 120 mm) and time (15, 30, and 60 s) were altered to investigate the microstructural property relationships of the coatings. Shape characteristics of the coatings were measured *via* a coordinate measuring machine, and surface roughness measurements were acquired using a 3D optical profiler. The deposition efficiency and coating roughness were affected by SOD and the evolving contour of the underlying surface. Hardness and porosity profiles were mapped to display the effect of process parameters. Dynamic parameters such as particle trajectory, evolving impact angle and dwell time affected changes in porosity, hardness, and density for each coating profile.

## I. Introduction

THE performance of thermal barrier coatings (TBCs) depends on the process parameters used to form the deposit.<sup>1–5</sup> Many of these variables can be controlled; whether by altering a gas flow rate or power level, or changing to a feedstock with different morphology. Other variables, however, cannot be directly controlled. Thermal spray coating parameters can, therefore, be formed into two different groups: First, those parameters that can be controlled, such as those mentioned previously, which will be referred to as static parameters or variables. The second group of parameters is dynamic, meaning those that are changing over time as the coating is formed. The number of dynamic parameters for any thermal spray coating process will be determined by the shape and nature of the substrate. Parameters related to particle trajectories, temperatures, and velocities will largely fall into the dynamic group. However, as the coating process evolves so too will the number of the static parameters. Moreover, some parameters that would have begun the coating process as static, such as standoff distance (SOD), could move into the dynamic group. This change from static to dynamic could arise either (i) as the coating thickness increases or (ii) as the substrate geometry becomes

more complex and reveals nonsymmetrical changes in SOD within the coating footprint.

Geometry aspects are among the more difficult to control because the spray footprint remains a static variable throughout any single coating process. The size of the geometrical aspect with respect to the spray footprint will cause dynamic parameter changes in velocity, temperature, impact angle, and particle dwell time. These coating variables are known to cause increased porosity due to unmelts.<sup>6</sup> In addition, effects of particles that bounce off the coating surface and shadowing effects due to the deposition angle<sup>7</sup> can also result in increased porosity. Although an increased porosity has been shown to increase thermal shock resistance,<sup>8</sup> the vertically graded porosity within a localized region could become a locus for failure.

The characteristics of a plasma flame depend on static parameters. Review articles published in 1966<sup>9</sup> and 1972<sup>10</sup> outlined the variables involved in plasma spraying and emphasized the sensitivity of the process, especially in terms of spray and deposition efficiency (DE). The effects of altering these static parameters on the performance of the TBC influence their direct relationship between particle temperature and velocity on the coating microstructure.<sup>11</sup> This method of analyzing coating systems was further enhanced with the aid of *in situ* diagnostic equipment that provided the ability to correlate coating microstructures and properties with in-flight particle characteristics.<sup>12</sup> These sensors<sup>13–16</sup> provided important insights into the behavior of in-flight particles; allowing for more robust modeling and refined control of the static process parameters so that more consistent coatings were manufactured.<sup>17,18</sup>

Porosity is an important attribute of TBCs because it is the prime contributing factor to low thermal conductivity and enables higher, more efficient operating temperatures of components.<sup>19,20</sup> Scrivani *et al.*<sup>21</sup> established that gradual increases in porosity of thick TBCs could be achieved by decreasing the plasma torch power, without compromising the integrity of the coating microstructure. A design of experiment using polynomial regression showed that lowering the primary gas flow rate from 50 to 35 L/min and increasing the secondary gas flow rate from 8 to 14 L/min in an argon/hydrogen plasma coating system decreased the porosity of yttria-stabilized zirconia (YSZ) coatings from 21.2% to 8%.<sup>22</sup> The parameter changes within the plasma spray process that lead to increased particle temperatures which are a key contributor to porosity variations.<sup>23</sup>

Regression models<sup>24</sup> have indicated that parameter changes, which lead to increased particle temperatures and velocities, were most influential with respect to creating denser YSZ coatings. Although the technology to measure particle temperature, velocity, and size distribution during the coating operation is becoming increasingly common, the

J. Smialek—contributing editor

angle at which these particles will impact a substrate and form splats adds complexity to the manufacturing operation. Not only do the geometrical attributes of the substrate and torch alignment effect the impact angle, but also the nature in which particles are projected within the plume.<sup>25</sup> An increase in the impact angle has been shown to increase the porosity of a plasma-sprayed coating.<sup>7,26,27</sup> As the impact angle increases, then the likelihood of the splats impacting and taking the form of the underlying contour decreases; thereby leaving large open segments or shadows that cannot be filled by subsequent particles.

A common method of evaluating the performance and mechanical properties of thermal spray coatings employs hardness measurements.<sup>28–31</sup> Although the microhardness of plasma-sprayed ceramic coatings is known to be susceptible to errors,<sup>32</sup> it can be of use as a comparison tool among a group of coatings for a particular experimental matrix. Statistical modeling of the hardness of a two-layer TBC system<sup>33</sup> used a Weibull analysis to show the effect of aging time and temperature on the hardness of the TBC, and displayed the variability in hardness at higher temperatures. Janos *et al.*<sup>31</sup> related the hardness and porosity of plasma-sprayed zirconia to its erosion resistance after periods of thermal aging. This study, along with another,<sup>28</sup> found that coating hardness increased as the porosity was reduced due to sintering effects from thermal aging.

The DE,  $\eta$ , relates the weight of the coating to the weight of the powder that was sprayed. For ceramic TBCs, DEs in the range between 40% and 70% are not uncommon and, as with most microstructural properties, it is closely related to both static and dynamic process parameters<sup>34–36</sup> as well as torch geometry and plasma jet enthalpy.<sup>37</sup>

The importance of understanding the effects of parameter changes is crucial in producing more efficient and performance-designed coatings. There still remains much in terms of understanding and the evaluation of effects that processing parameters confer on the coating microstructures and performance. The aim of this study was to further develop and refine the relationship between surface topography, microstructural characteristics, and plasma spray process parameters; in particular, the classification of parameters into static and dynamic groups and their effect on the coating topographical and microstructural properties. Although a non-conventional method of producing TBCs was used in this study, which resulted in coating buildup and hence thicknesses significantly greater than those used in engine applications, the method allowed for the evaluation of dynamic parameter changes; e.g., particle impact angle, on the microstructural properties during the coating process.

## II. Experimental Procedure

### (1) Materials and Spray Conditions

Ceramic deposits were atmospheric plasma sprayed (APS'ed) onto mild steel plate using a Metco 7 MB plasma torch with a Metco GH nozzle consisting of a 7 mm internal diameter (Sulzer Metco, Westbury, NY). The mild steel plates were 4 mm thick and end milled to 147 mm  $\times$  147 mm with a tolerance of  $\pm 0.01$  mm. Argon was used as the primary gas at a flow rate of 42.1 NL/min or 68.74 g/min at 0.7 MPa. The secondary gas was hydrogen at a flow rate of 6.1 NL/min or 0.503 g/min at 0.34 MPa. The position of the torch was controlled via a six-axis robot (YR-SK16-J00; Motoman Robotics, Miamisburg, OH). Feedstock was yttria-stabilized (8%) zirconia (Metco 204NS, HOSP<sup>TM</sup>)<sup>38</sup> with a particle size range of  $-125 + 11$   $\mu$ m and a morphology that was spherical and hollow. Compared with YSZ feedstock produced via other methods, HOSP<sup>TM</sup> YSZ powders offer advantages when applied as a TBC with APS. The prealloying of the starting materials used to produce the powder ensures the phase stability and homogeneity of the powder. This in turn leads to a coating with the desired cubic-tetragonal structure and com-

**Table I.** Experimental Matrix Used for this Study Where the Values Within the Matrix Represent the Identification Code. That is, “15/80” Represents “15 s at a Standoff Distance of 80 mm”

Time (s)	Standoff distance		
	80 mm	90 mm	120 mm
15	15/80	15/90	15/120
30	30/80	30/90	30/120
60	60/80	60/90	60/120

position resulting in performance benefits during thermal cycling.<sup>39</sup> Furthermore, the spherical morphology and low density of such powders result in improved flowability and uniform melting during the APS process.<sup>38</sup> The powder was fed at 30 g/min with argon as the powder feed gas through a 2-mm-diameter injector nozzle that was placed 8.5 mm from the central torch axis. Time and SOD were altered to form an experimental matrix, Table I. The nonuniform variation in SOD was selected to investigate the effects of large and small SOD fluctuations from an optimum; i.e., 90 mm, on the microstructural properties.

The torch was held stationary while the coatings were created. Once the prescribed time had elapsed two operations were simultaneously performed: (i) the torch was moved away from the target where the shutdown procedure could take place and (ii) the powder feed was terminated. Although this is not a typical procedure used to form a coating, this protocol allowed analysis of dynamic thermal spray variables.

### (2) Shape and Contour Evaluation and DE

Due to the nature of the experiment, the shapes of the coatings obtained are best described as stalagmites, Fig 1. Detailed shape and contour data were achieved with the use of a coordinate measuring machine (CMM - Sheffield Discovery II; Hexagon Metrology Services Ltd, Surrey, UK). The CMM uses a touch sensitive probe attached to a third axis of a gantry-style numerically controlled positioning device. The probe contacts the part or shape being measured, and once a user-defined force is registered at the tip, an XYZ location coordinate is recorded. All XYZ coordinates were referenced with respect to the center point of the end-milled substrates, Fig. 2. The coordinate system origin was located on the surface being coated with the central axis of the torch aligned to this point along the Z axis. The CMM has repeatability no less than 0.48  $\mu$ m and a linear accuracy no less than 4.2  $\mu$ m. The three-dimensional coordinate data were imported into OriginPro 8.5 (OriginLab Corporation, North-

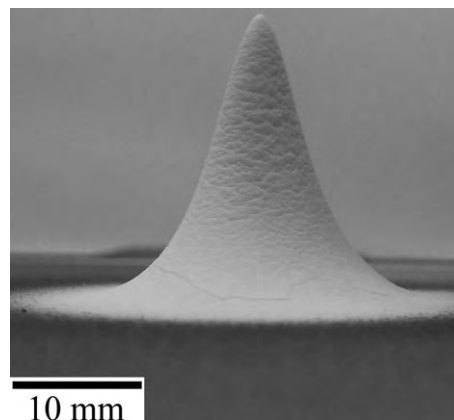


**Fig. 1.** As sprayed stalagmite using a standoff distance of 90 mm and spray duration of 60 s.



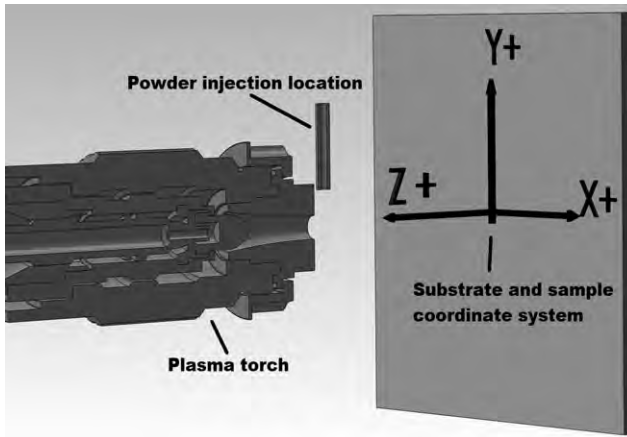


**Fig. 2.** Experimental spray setup showing the XYZ coordinate system used when digitizing the stalagmites. The origin on this coordinate system was located on the surface at the center point of the end-milled substrates. The central axis of the torch was aligned to this point along the Z axis. Powder injection was set parallel to the Y+ axis.

amton, MA), where the shape and contour characteristics were analyzed.

Target DE was calculated by using the relationship of coating weight to weight of powder sprayed. The precision end-milled substrates were weighed before and after each coating operation within an accuracy of 0.01 g. Target DE differs from intrinsic DE in that the former takes into consideration variables such as torch motion and substrate geometry. Intrinsic DE, on the other hand, refers to the maximum possible amount of feedstock deposited for a given set of process parameters.<sup>40</sup> This is particularly important in this study as the evolving shape of the coating continuously affects the DE.

### (3) Surface Topography and Roughness Measurements

The change in surface roughness over the profile of the stalagmites was measured with the Contour GT-1 3D Optical Profiler (Bruker Corporation, Billerica, MA). The plates were aligned on the 3D profiler stage and the highest peak on each stalagmite was located. A  $5 \times 2$  objective scanned  $\sim 1 \text{ mm}^2$  sections of the surface, starting from the peak location. Only certain segments of the stalagmites were recorded. Between 9 and 21 surface profile measurements were taken per sample. The reason for the difference in the number of measurements arises due to a combination of the height of the stalagmites and focal length of the objective. Tilt and curvature were removed from the surface profile data and the roughness was separated from the waviness with the use of a robust Gaussian regression filter as per ASME B46.1<sup>41</sup> using Vision for Profilers 4.20 software (Veeco Instruments Inc., Plainview, NY).

### (4) Porosity and Hardness

All samples were metallography prepared so that porosity and hardness measurements were measured along the Y axis. Samples were first mounted with epoxy resin under vacuum to maintain an intact coating during sectioning along the Y axis. The samples then underwent a second vacuum mounting process to ensure edge retention during the polishing stages. The cross-sectioned samples were divided into seven separate regions where porosity and hardness measurements were taken. These sections consisted of (i) three areas along the base of the coating running parallel to the substrate where the coating thickness was at least  $150 \mu\text{m}$ , denoted bottom left (BL), bottom center (BC), and bottom right (BR); (ii) three areas along the halfway point also running parallel to the substrate denoted middle left (ML), middle

center (MC), and middle right (MR); and (iii) a single area at the tip (TP).

Porosity measurements were performed by image analysis (ImageJ 1.45s; National Institutes of Health, Bethesda, MD). Four to five images under identical conditions were captured at each section under identical conditions; i.e., contrast and brightness, using a Leica MEF4M inverted optical metallographic microscope (Leica Microsystems GmbH, Wetzlar, Germany). Once the characteristics of the coating porosity were established, the images were then subjected to binary thresholding using the Otsu algorithm.<sup>42</sup> This yielded the total porosity of the coating that was then averaged for the particular location.

Vickers microhardness tests (Micromet 2103 Microhardness Tester; Buehler, Lake Bluff, IL) were performed at the same locations with four to five measurements taken at each section. Measurements were conducted so that the two diagonals of the indenter were parallel and perpendicular to the substrate and the distance separating each indent was a minimum of three times the diagonal length. A 300 gf load (2.942N) was applied for 15 s on each test. Average values were then calculated for each section.

## III. Results and Discussion

### (1) Shape and Contour

The contour plots of all coatings within the experimental matrix exhibited similar shape characteristics in the form of an angled ellipse. Figure 3 shows an example of a contour plot for the coating ID 30/120. The elliptical shape has been reported in simulations and is explained by the location of particle injection in terms of the injectors angular location around the plume and particle size distribution within the plasma plume.<sup>43</sup> However, the offset angle experienced in these experimental results could be the result of arc fluctuations during plasma formation within the torch. This relationship between all stalagmites suggests that there is another mechanism outside of the parameters considered, such as that of individual particle trajectory within the plasma flame. The results indicate a link between the particle trajectory and the two parameters altered in this group of experiments.

Figure 4 summarizes the Y axis offset locations (a), peak height (b), and DEs (c) of the stalagmites for the different spray durations and SODs. For SODs of 90 and 120 mm, the stalagmite peak on the Y axis location decreased with increasing time. That is, the stalagmite formed below the central axis of the torch. However, decreasing the SOD to 80 mm caused the Y axis locations of the stalagmite peaks to shift above the central axis of the torch. This decrease in

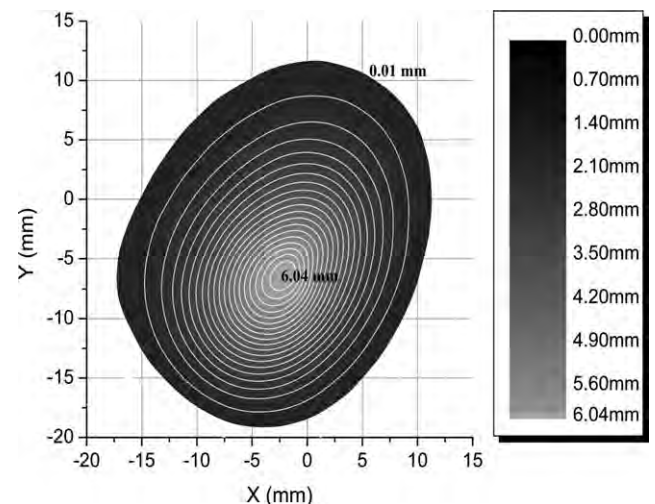


**Fig. 3.** Contour plot of coating ID 30/120 showing the offset angled ellipse of the spray footprint.

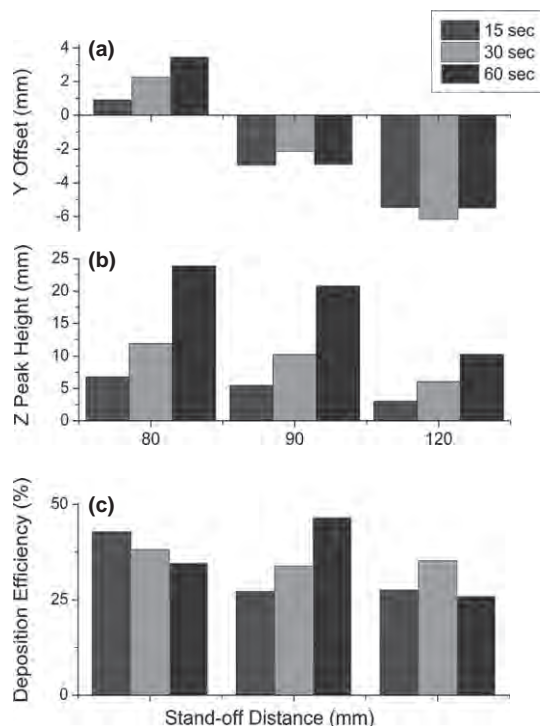


**Fig. 4.** (a) Y axis offset of the stalagmites with respect to the origin of the substrate, (b) Z peak height of the stalagmites, and (c) deposition efficiency. All with respect to standoff distance with the different shades representing the three static times used in the experimental matrix. Refer to Fig. 2 for coordinate system designation.

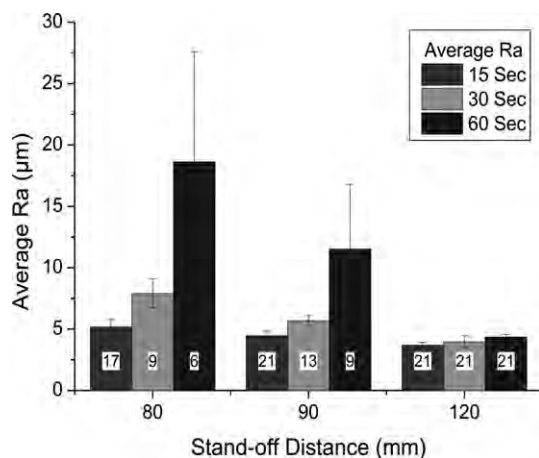


**Fig. 5.** Bar plots showing the average roughness (Ra) for the three different times grouped by standoff distance. The figures inside each bar indicate the number of roughness values used to determine the average ( $n$ ) and the error bars are the standard deviations ( $\sigma$ ).

SOD shortens the dwell time of the particles within the plume, thereby not allowing adequate time for particles to drop through to the central axis of the plasma jet. This causes the stalagmite to form above the central axis of the torch. Maximum stalagmite height and DE are plotted against SOD in Figs. 4(b) and (c), respectively. Trends with respect to peak height, SOD, and time can be distinguished. Coating peak height increases with time and decreases as the SOD lengthens.

## (2) Deposition Efficiency

Deposition efficiency versus SOD is plotted in Fig. 4(c). The DEs over the three times for SODs of 80 and 120 mm show

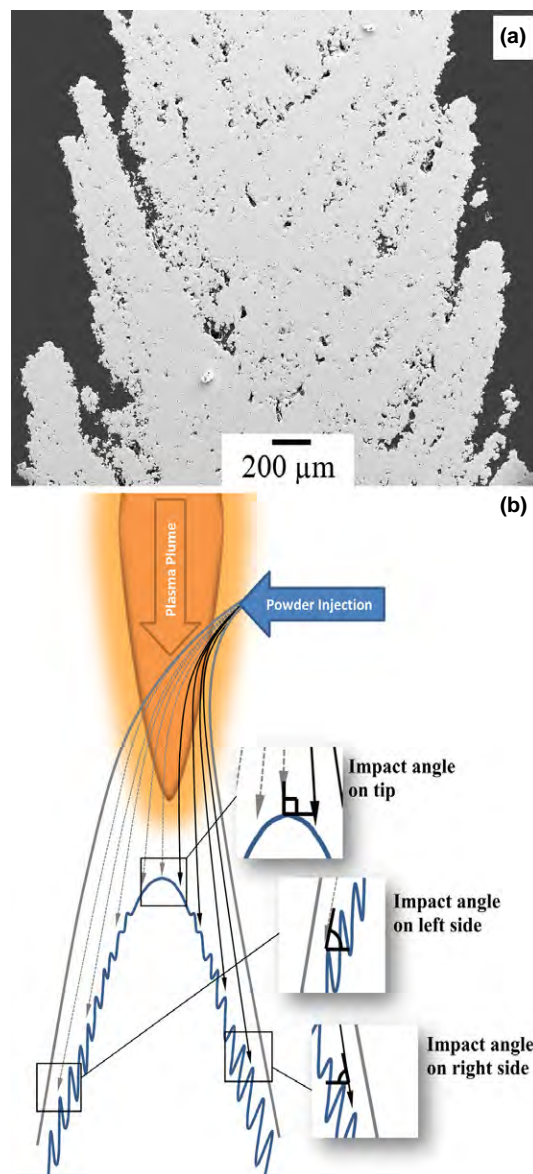


**Fig. 6.** Micrograph of a coating built up over a 60-s period at a standoff distance of 80 mm highlighting the shadowing or Christmas tree effect toward the tip of the stalagmite (a). This was the main cause of the increased roughness during longer dwell times. The schematic highlights the influence of particle trajectories on this Christmas tree effect with respect to impact angle (b).

little variation compared with the 90-mm SOD. The DE for the 80-mm SOD decreases with coating time, from 43% to 35%. This is expected because, as the height of the stalagmite increases, Fig. 4(b), the impact angle within the spray footprint increases resulting in a less than optimum deposition surface. In addition, the dwell time of the particles within the plasma constantly decreases as the stalagmite is formed, allowing less time for the particles to reach an ideal combination of temperature and velocity that would facilitate splat formation. That is, there is a transition from a static to a dynamic variable with regard to the SOD.

The combination of decreasing DE with increasing time in the 80-mm SOD case, and the coating buildup occurring in the positive Y axis location, Figs. 4(c) and (a), respectively, may result from a lesser number of particles reaching locations within the plasma plume that would result in optimum conditions for adhesion. The 90-mm SOD, on the other hand, required more time before the DE began to increase; while the Y offset location, although in the negative region, stabilized at around 3 mm below the origin. The DEs at the



120- and 90-mm SOD, however, depended more on the dynamic parameters of dwell time and travel distance of the particles. The DE for the 90-mm SOD displayed an opposite trend to that of the 80-mm SOD.

Although the optimum flat surface perpendicular to the particle trajectory decreased with time, the recipe of all parameters provided the most favorable temperature and velocity for the particles to adhere to the 90-mm SOD, with DEs of 27%, 34%, and 47% as the time increments increased. A similar analogy can be found when analyzing the DE for a SOD of 120 mm. The coatings at 60 and 15 s displayed the lowest DEs of 25% and 27%, respectively. However, a coating time of 30 s provided conditions that increased the DE to 35%.

### (3) Surface Roughness

The  $R_a$  values of the top 10 mm of each stalagmite are plotted in Fig. 5. The average roughness was observed to decrease with both time and SOD. At 80-mm SOD, the roughness displays the highest variation with values of 5.2, 7.9, and 18.6  $\mu\text{m}$  for 15, 30, and 60 s, respectively. A slightly smaller increase in roughness was observed for the 90-mm SOD that reached a roughness of 11.5  $\mu\text{m}$  after 60 s. For a SOD of 120 mm, however, the variance was relatively small, with all roughness values falling within a 1  $\mu\text{m}$   $R_a$  value of each other; i.e., 3.7, 4.0, and 4.4 for 15, 30, and 60 s, respectively.

The increase in roughness over time is due to a “Christmas tree” effect, or shadowing, that arises as stalagmite peaks increase and widths decrease, Figs. 6(a) and (b). The

Christmas tree effect is pronounced for stalagmites with steep peaks due to the particle flux for the shorter SOD being smaller, resulting in narrower impact angles and hence a larger number of particles depositing onto the forming branches. On the other hand, the longer SODs allow time for the particle impact angle to increase, as well as the particle flux diameter to increase, with the outcome that a broader stalagmite forms with less shadowing or branching.

### (4) Porosity and Hardness

Contour plots depicting the porosity distribution for the experimental matrix can be seen in Fig. 7. All plots have been realigned with the central  $Y$  axis for representation purposes. Both the dwell time and SOD parameters effect the distribution of porosity for each of the stalagmites. All stalagmites display the lowest porosity at the top of the peak, with the denser part of the coating tending to move down the left side of the stalagmite, or below the central axis of the torch. This behavior could indicate that particles passing through the central axis of the plume have acquired sufficient temperature to permit a pore-free solidification process on the underlying surface. It was likely that particles that did not pass through the plume and remained on the outer peripheries were not in the semimolten state adding to the increased porosity in these areas. This is further highlighted by observing the right side of all stalagmites in Fig. 7, which for all cases is above the central axis of the torch and is the location that exhibited the highest percentage of porosity.

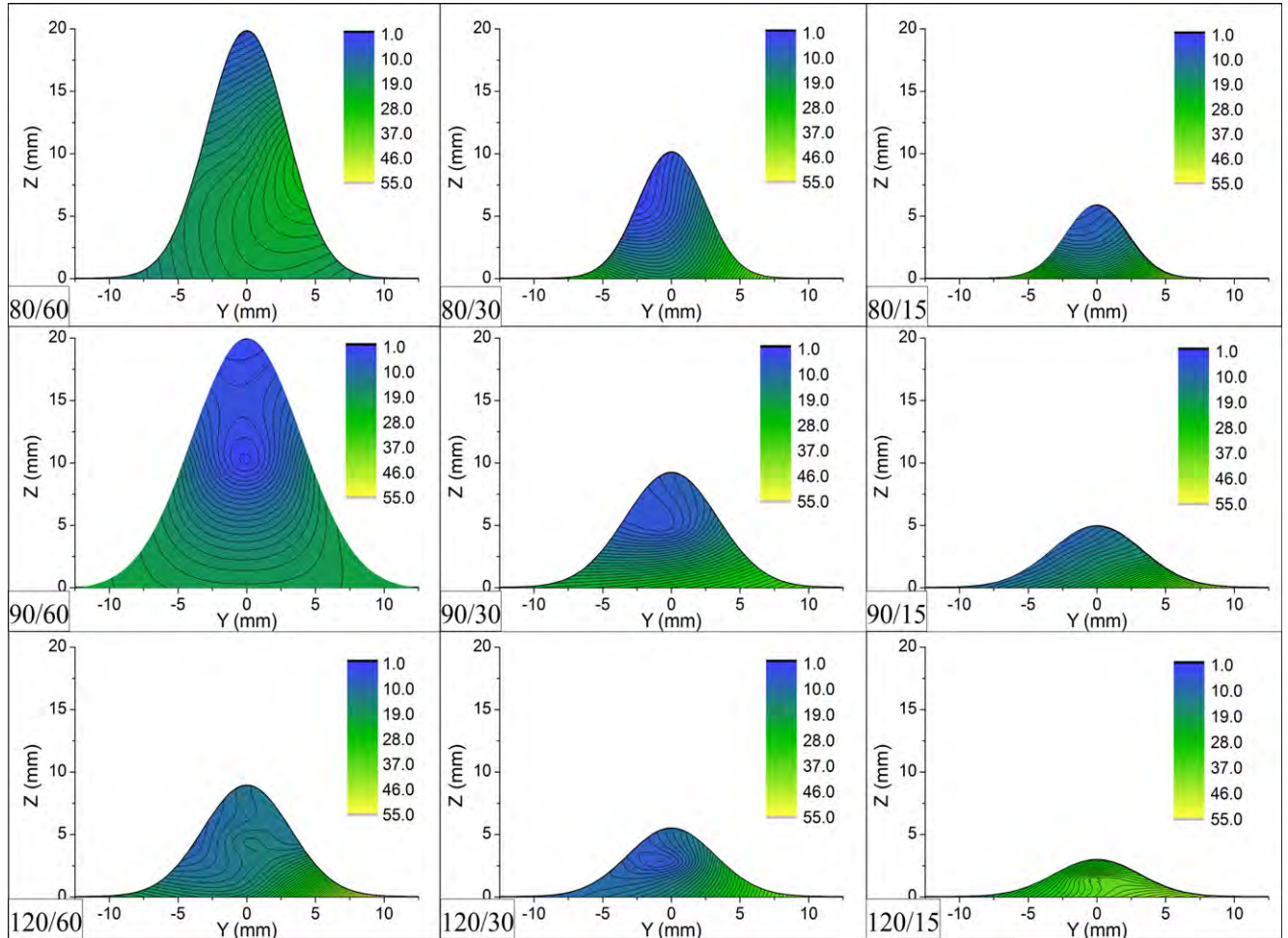


**Fig. 7.** Porosity distribution contour maps of each stalagmite. The section was made down the central  $Y$  axis of the coating. All plots have been realigned with the central  $Y$  axis for representation purposes. The box in the bottom left corner of each plot represents the standoff distance in mm and time in s (SOD/time).



Increasing the SOD provided a more uniform porosity distribution throughout the stalagmite; which is especially evident for coatings formed over 60-s periods. For the SOD of 90 mm, increasing the dwell time caused a decrease in coating porosity at the tips. This trend, however, did not occur for the other SODs of 80 and 120 mm, where in both cases the lowest porosity occurred for a dwell time of 30 s.

The porosity distribution at the tips would arise from several factors. For example, an intense glow was observed at the tips for dwell times of 30 and 60 s and this phenomenon would have attributed to localized sintering of these areas. Although the onset of sintering normally requires a larger number of cycles or hours at temperatures above 1100°C, the microstructural property changes observed are similar to those reported in other studies<sup>8,44</sup> as effects of sintering. The tip region would have also been associated with higher particle temperatures that would result in denser coatings.<sup>23</sup>

The increased porosity at shorter coating times was associated with lower particle temperatures, which give rise to increased substrate temperatures and lower thermal conductivities.<sup>23</sup> The shorter times implied that the stalagmites did not grow to the extent of those formed over longer periods. Therefore, particle temperatures and velocities would have decreased with the increase in dwell time leading to high porosities. For coatings formed over a 15-s period, the porosity at the tips increased from 6.7% to 8.5% to 21% for SODs of 80, 90, and 120 mm, respectively. A similar trend was exhibited for the stalagmites formed over 30-s periods. Comparison of the optical micrographs of microstructures at three different locations, namely, at the tip, middle center, and bottom center of the stalagmites, provided further indication of the possibility of sintering, Fig. 8. This pattern of open porosity distribution for the three locations was observed for all coatings. However, it was more pronounced for coating times of 60 and 30 s.

Contour plots showing the hardness distribution for the experimental matrix can be seen in Fig. 9. As expected, the coating hardness is related to the porosity; with hardness values close to that of dense YSZ at the stalagmite tips. The distribution of the hardness, however, contradicts that of the porosity. The hardness over the contours decreases toward the left of the coatings, or below the central axis of the torch. While an increase in hardness is exhibited on the right side of the stalagmites that is above the central axis of the torch. This could be attributed to local softening of the coating in these regions where higher particle temperatures were present. Moreover, similar decreases in hardness were reported by Portinha *et al.*<sup>30</sup> where their coatings had undergone annealing for 100 h at 1100°C.

Hardness values at the center of the stalagmites were similar to those of dense, as-sprayed coatings.<sup>30,45</sup> The hardness values greater than 900 HV, which are located at the tips of the coatings formed over 60 s and SODs of 80 and 90 mm, are comparable to dense coatings that had undergone 16 h of thermal aging at 1482°C.<sup>31</sup>

The relationship between hardness and porosity at the various locations of the stalagmites is plotted in Fig. 10. The seven individual locations mentioned in Section II(4) are each represented by different shapes on the plot, as shown in the legends. Relationships were established for the left, right, and center locations of the stalagmites as indicated by the solid, dotted, and dashed lines, respectively. Although each of the three sections of the stalagmites displays a decrease in hardness together with decreasing porosity, the range over which the decreases occur, i.e., the slope, demonstrates differences among three locations. The solid linear fit line representing the stalagmite section below the central torch axis shows a steep negative gradient where the porosity varied between 10% and 20%, yet the hardness exhibited a sharp drop from about 820 to 420 HV. The dashed linear fit line that represents the center location of the stalagmites exhibits a slightly broader slope, encompassing a wider range of

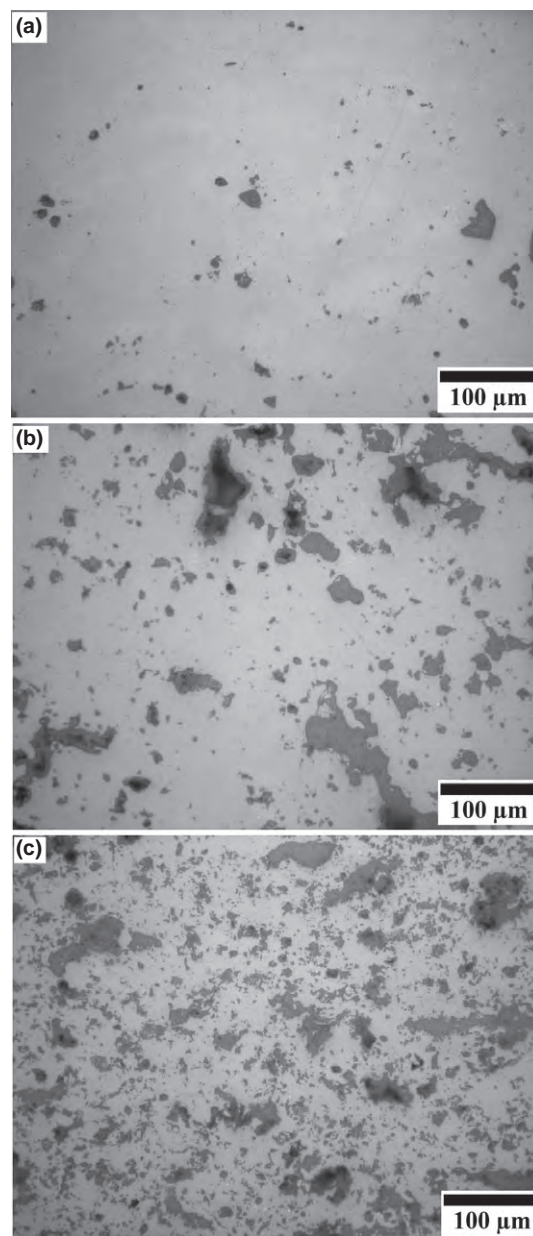


**Fig. 8.** Optical micrographs showing the (a) tip, (b) middle, and (c) base of coating ID 60/80 taken along the central axis sectioned along the *Y* plane.

porosity and hardness. The dotted linear fit line that denotes the stalagmite portion above the central torch axis displays the largest variation in porosity, however, the hardness range matches that of the center location; i.e., 828–604 HV. This behavior not only highlights the relationship of hardness and porosity of TBCs but also the impact of particle trajectories and location on the material properties.

As average values across all SODs and times were used for the plots in Fig. 10, the relationship between the porosity and hardness for the three locations is attributed to impact angle and the location of particle injection. If particle trajectories and injection angles as described in Fig. 6(b) are applied, it can be shown that the negative slope decreases as particles are required to travel further through the plume. Furthermore, the increased particle temperatures and thermal softening experienced on the left side of the stalagmite together with changes in impact angle over small areas within the spray footprint caused only slight variability in the porosity, while the hardness fell from 828 HV to below 300 HV. Particles impinging the right side of the stalagmite

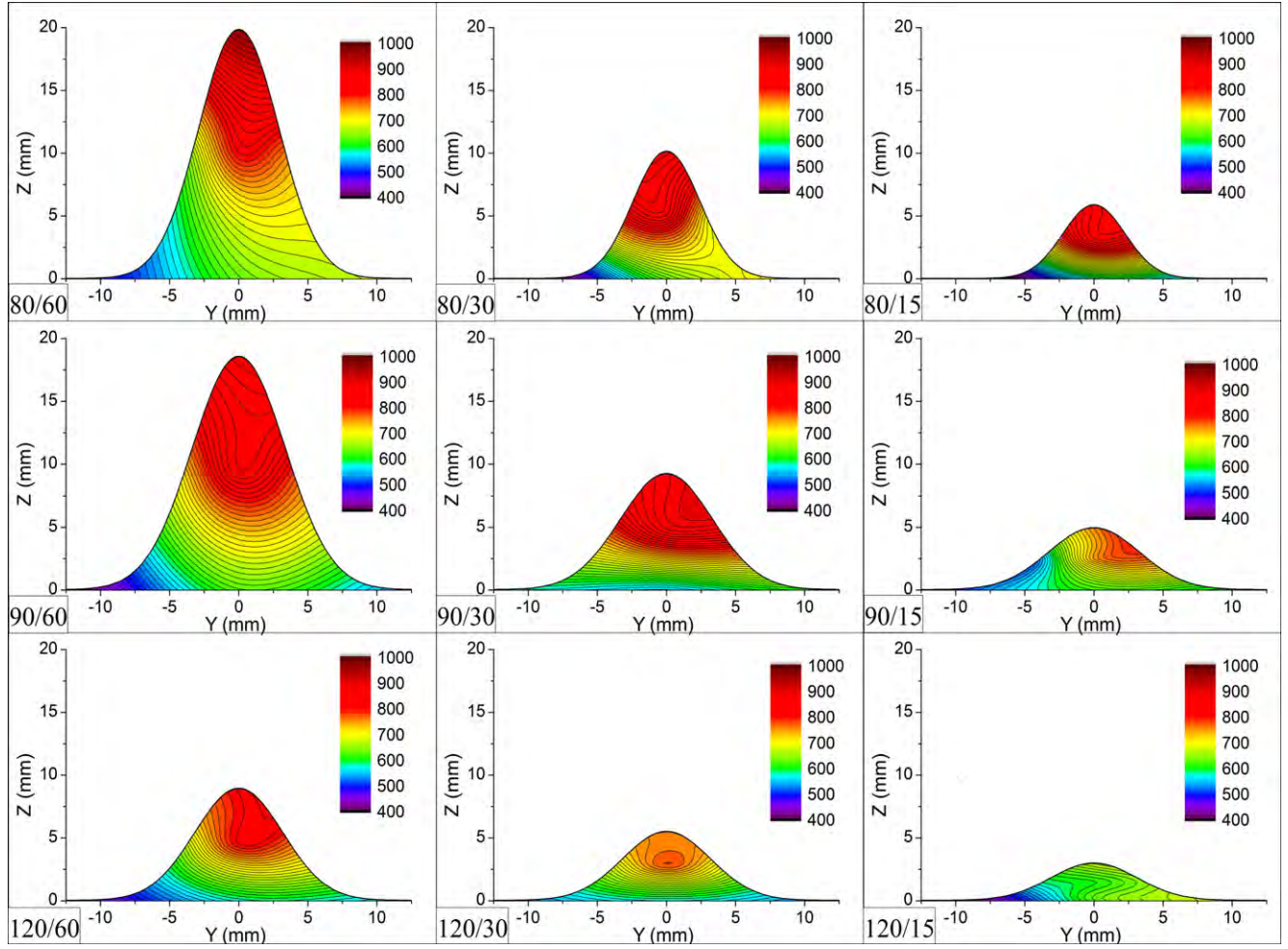


**Fig. 9.** Hardness distribution contour maps of each stalagmite. The section was made down the central  $Y$  axis of the coating. All plots have been realigned with the central  $Y$  axis for representation purposes. The box in the bottom left corner of each plot represents the standoff distance in mm and time in seconds (SOD/time).

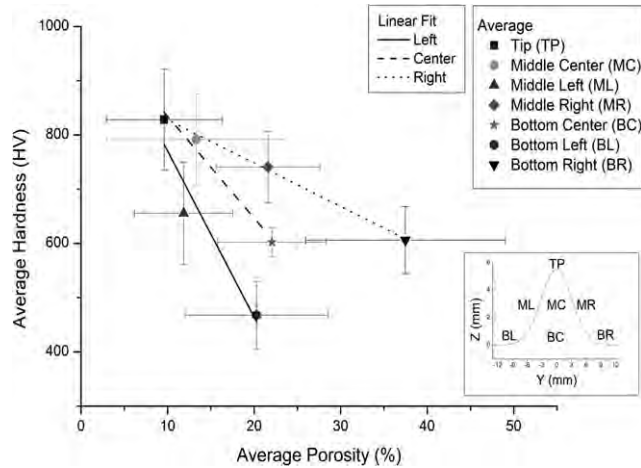


**Fig. 10.** Relationship between the hardness and porosity of the stalagmites. Each marker represents the average hardness–porosity value at the seven different locations were measurements of each property were taken. Linear fits for the left side (solid line), center (dashed line), and right sides (dotted line) are plotted.

with lower temperatures, however, showed a larger variability in porosity while maintaining hardness values between 828 and 600 HV. This relationship between particle behavior and microstructural properties further highlights the effects that a dynamically changing geometry can have on the coating.

#### IV. Concluding Remarks

The effects of static and dynamic process parameters on the topographical and microstructural properties of YSZ TBCs have been studied. The static parameters altered throughout this study, i.e., time and SOD, caused dynamic particle parameters related to the dwell time such as temperature, velocity, and impact angle to change. This resulted in several stalagmite topographies, DEs, and microstructural properties.

The alternating  $Y$  offsets indicate the importance of controlling the powder injection location and SOD. Furthermore, width, peak height, and average roughness are likewise related to SOD. The steep peaks and narrow widths associated with shorter SODs show that the particle flux is confined to a smaller area that broadens as the SOD increases.

DE is seen to be sensitive to both static and dynamic process variables. The closer SOD of 80 mm and short dwell time of 15 s resulted in a DE of 43% that was only matched once the SOD was increased to 90 mm and the coating was allowed to form over 60 s resulting in 48% DE. Therefore, high DEs on complex surfaces can only be achieved with due control of the SOD and dwell time.

There is a close relationship between the microstructural properties of porosity and hardness that is related to the impact angle and injection location. The effects of thermal aging are attributed to the decrease in hardness in the denser zones located below the central torch axis. The increased porosity at the stalagmite base is attributed to the increased impact angle at the edges of the spray footprint along with lower particle temperatures and velocities. The unsymmetrical



behavior of hardness and porosity over the cross section of the stalagmites can be attributed to injection location and, therefore, dynamic particle properties.

The results show the effect of time and SOD on TBC formation and microstructural properties, with a particular emphasis on the dynamic parameters of the plasma spray process. This study shows that small variations during the coating process, whether they be geometric changes in the substrate surface or process parameters that effect particle flight characteristics, influence the microstructural properties of a coating and the DE of the process. Future work will consider particle dynamics within the plume by the use of a diagnostic system and how these can be coupled to coat complex geometries.

### Acknowledgments

The authors thank Dr. Andrew Ang, Mr. Andrew Moore, Mr. Girish Thippurudrappa, and Dr. James Wang for their expert assistance in the plasma coating, substrate pre- and postpreparation, and microscopy. We also acknowledge the support provided by the Defence Materials Technology Centre (DMTC). Swinburne University of Technology has provided financial support by means of an Australian Post Graduate Award.

### References

- <sup>1</sup>S. Stecura, "Effects of Plasma Spray Parameters on Two Layer Thermal Barrier Coating System Life"; NASA Lewis Research Center, Cleveland, OH, National Aeronautics and Space Administration, NASA-TM-81724, March, 1981.
- <sup>2</sup>A. P. Batakis and J. W. Vogan, "Rocket Thrust Chamber Thermal Barrier Coatings"; NASA Lewis Research Center, Cleveland, OH, National Aeronautics and Space Administration, NASA-CR-175022, July, 1985.
- <sup>3</sup>L. Pawlowski, *The Science and Engineering of Thermal Spray Coatings*. Wiley, New York, NY, 1995.
- <sup>4</sup>A. Kucuk, C. C. Berndt, U. Senturk, R. S. Lima, and C. R. C. Lima, "Influence of Plasma Spray Parameters on Mechanical Properties of Yttria Stabilized Zirconia Coatings. I: Four Point Bend Test," *Mater. Sci. Eng. A*, **284** [1–2] 29–40 (2000).
- <sup>5</sup>A. Kucuk, C. C. Berndt, U. Senturk, and R. S. Lima, "Influence of Plasma Spray Parameters on Mechanical Properties of Yttria Stabilized Zirconia Coatings. II: Acoustic Emission Response," *Mater. Sci. Eng. A*, **284** [1–2] 41–50 (2000).
- <sup>6</sup>A. Kulkarni, A. Vaidya, A. Goland, S. Sampath, and H. Herman, "Processing Effects on Porosity-property Correlations in Plasma Sprayed Yttria-stabilized Zirconia Coatings," *Mater. Sci. Eng. A*, **359** [1–2] 100–111 (2003).
- <sup>7</sup>S. H. Leigh and C. C. Berndt, "Evaluation of Off-Angle Thermal Spray," *Surf. Coat. Technol.*, **89** [3] 213–24 (1997).
- <sup>8</sup>C. Giolli, A. Scrivani, G. Rizzi, F. Borgioli, G. Bolelli, and L. Lusvardi, "Failure Mechanism for Thermal Fatigue of Thermal Barrier Coating Systems," *J. Therm. Spray Technol.*, **18** [2] 223–30 (2009).
- <sup>9</sup>J. A. Mock, "Flame Sprayed Coatings," *Mater. Des. Eng.*, **63** [2] 89–104 (1966).
- <sup>10</sup>I. A. Fisher, "Variables Influencing the Characteristics of Plasma-Sprayed Coatings," *Int. Mater. Rev.*, **17** [1] 117–29 (1972).
- <sup>11</sup>R. McPherson, "A Review of Microstructure and Properties of Plasma Sprayed Ceramic Coatings," *Surf. Coat. Technol.*, **39–40** [Part 1] 173–81 (1989).
- <sup>12</sup>P. Fauchais, G. Montavon, M. Vardelle, and J. Cedelle, "Developments in Direct Current Plasma Spraying," *Surf. Coat. Technol.*, **201** [5] 1908–21 (2006).
- <sup>13</sup>C. Moreau, M. Lamontagne, and P. Cielo, "Method and Apparatus for Monitoring the Temperature and Velocity of Plasma Sprayed Particles"; US Patent 5,180,921, January 19, 1993.
- <sup>14</sup>J. R. Fincke, C. L. Jeffery, and S. B. Englert, "In-flight Measurement of Particle Size and Temperature," *J. Phys. E: Sci. Instrum.*, **21** [4] 367–70 (1988).
- <sup>15</sup>C. Moreau, P. Cielo, M. Lamontagne, S. Dallaire, and M. Vardelle, "Impacting Particle Temperature Monitoring During Plasma Spray Deposition," *Meas. Sci. Technol.*, **1** [8] 807–14 (1990).
- <sup>16</sup>J. R. Fincke, W. D. Swank, and C. L. Jeffery, "Simultaneous Measurement of Particle Size, Velocity, and Temperature in Thermal Plasmas," *IEEE Trans. Plasma Sci.*, **18** [6] 948–57 (1990).
- <sup>17</sup>C. Moreau and L. Leblanc, "Optimization and Process Control for High Performance Thermal Spray Coatings," *Key Eng. Mat.*, **197**, 27–57 (2001).
- <sup>18</sup>J. R. Fincke, W. D. Swank, R. L. Bewley, D. C. Haggard, M. Gevelber, and D. Wroblewski, "Diagnostics and Control in the Thermal Spray Process," *Surf. Coat. Technol.*, **146–147**, 537–43 (2001).
- <sup>19</sup>A. G. Evans, D. R. Mumm, J. W. Hutchinson, G. H. Meier, and F. S. Pettit, "Mechanisms Controlling the Durability of Thermal Barrier Coatings," *Prog. Mater. Sci.*, **46** [5] 505–53 (2001).
- <sup>20</sup>R. A. Miller, "Thermal Barrier Coatings for Aircraft Engines: History and Directions," *J. Therm. Spray Technol.*, **6** [1] 35–42 (1997).
- <sup>21</sup>A. Scrivani, G. Rizzi, and C. C. Berndt, "Enhanced Thick Thermal Barrier Coatings That Exhibit Varying Porosity," *Mater. Sci. Eng. A*, **476** [1–2] 1–7 (2008).
- <sup>22</sup>J. F. Li, H. L. Liao, C. X. Ding, and C. Coddet, "Optimizing the Plasma Spray Process Parameters of Yttria Stabilized Zirconia Coatings Using a Uniform Design of Experiments," *J. Mater. Process. Technol.*, **160** [1] 34–42 (2005).
- <sup>23</sup>G. Mauer, R. Vaßen, and D. Stöver, "Atmospheric Plasma Spraying of Yttria-stabilized Zirconia Coatings with Specific Porosity," *Surf. Coat. Technol.*, **204** [1–2] 172–9 (2009).
- <sup>24</sup>M. Friis, C. Persson, and J. Wigren, "Influence of Particle In-flight Characteristics on the Microstructure of Atmospheric Plasma Sprayed Yttria Stabilized ZrO<sub>2</sub>," *Surf. Coat. Technol.*, **141** [2–3] 115–27 (2001).
- <sup>25</sup>M. Vardelle, P. Fauchais, A. Vardelle, K.-I. Li, B. Dussoubs, and N. J. Themelis, "Controlling Particle Injection in Plasma Spraying," *J. Therm. Spray Technol.*, **10** [2] 267–84 (2001).
- <sup>26</sup>A. Hasui, S. Kitahara, and T. Fukushima, "On Relation Between Properties of Coating and Spraying Angle in Plasma Jet Spraying," *Trans. Nat. Res. Inst. Metals*, **12** [1] 9–20 (1970).
- <sup>27</sup>V. V. Sobolev and J. M. Guilemany, "Flattening of Droplets and Formation of Splats in Thermal Spraying: A Review of Recent work—Part 2," *J. Therm. Spray Technol.*, **8** [2] 301–14 (1999).
- <sup>28</sup>B. Siebert, C. Funke, R. Vaßen, and D. Stöver, "Changes in Porosity and Young's Modulus Due to Sintering of Plasma Sprayed Thermal Barrier Coatings," *J. Mater. Process. Technol.*, **92–93**, 217–23 (1999).
- <sup>29</sup>D. Zhu and R. A. Miller, "Thermal Conductivity and Elastic Modulus Evolution of Thermal Barrier Coatings Under High Heat Flux Conditions," *J. Therm. Spray Technol.*, **9** [2] 175–80 (2000).
- <sup>30</sup>A. Portinha, V. Teixeira, J. Carneiro, J. Martins, M. F. Costa, R. Vassen, and D. Stöver, "Characterization of Thermal Barrier Coatings with a Gradient in Porosity," *Surf. Coat. Technol.*, **195** [2–3] 245–51 (2005).
- <sup>31</sup>B. Z. Janos, E. Lugscheider, and P. Remer, "Effect of Thermal Aging on the Erosion Resistance of Air Plasma Sprayed Zirconia Thermal Barrier Coating," *Surf. Coat. Technol.*, **113** [3] 278–85 (1999).
- <sup>32</sup>C. C. Berndt, W. Brindley, A. N. Goland, H. Herman, D. L. Houck, K. Jones, R. A. Miller, R. Neiser, W. Riggs, S. Sampath, M. Smith, and P. Spanne, "Current Problems in Plasma Spray Processing," *J. Therm. Spray Technol.*, **1** [4] 341–56 (1992).
- <sup>33</sup>C. K. Lin and C. C. Berndt, "Statistical Analysis of Microhardness Variations in Thermal Spray Coatings," *J. Mater. Sci.*, **30** [1] 111–7 (1995).
- <sup>34</sup>G. Wuest, S. Keller, A. R. Nicoll, and A. Donnelly, "Plasma Spray Deposition Efficiencies," *J. Vac. Sci. Technol., A*, **3** [6] 2464–8 (1985).
- <sup>35</sup>J. F. Bisson, C. Moreau, M. Dorfman, C. Dambra, and J. Mallon, "Influence of Hydrogen on the Microstructure of Plasma-Sprayed Yttria-Stabilized Zirconia Coatings," *J. Therm. Spray Technol.*, **14** [1] 85–90 (2005).
- <sup>36</sup>B. R. Marple, R. S. Lima, C. Moreau, S. E. Kruger, L. Xie, and M. R. Dorfman, "Yttria-Stabilized Zirconia Thermal Barriers Sprayed Using N<sub>2</sub>-H<sub>2</sub> and Ar-H<sub>2</sub> Plasmas: Influence of Processing and Heat Treatment on Coating Properties," *J. Therm. Spray Technol.*, **16** [5–6] 791–7 (2007).
- <sup>37</sup>H.-D. Steffens and T. Duda, "Enthalpy Measurements of Direct Current Plasma Jets Used for ZrO<sub>2</sub>-Y<sub>2</sub>O<sub>3</sub> Thermal Barrier Coatings," *J. Therm. Spray Technol.*, **9** [2] 235–40 (2000).
- <sup>38</sup>M. R. Dorfman, L. F. Correa, C. G. Dambra, K. Laul, and R. K. Schmid, "Method of Producing a Pre-Alloyed Stabilized Zirconia Powder"; US Patent 6,869,550, March 22, 2005.
- <sup>39</sup>Y. Tan, J. P. Longtin, S. Sampath, and H. Wang, "Effect of the Starting Microstructure on the Thermal Properties of As-Sprayed and Thermally Exposed Plasma-Sprayed YSZ Coatings," *J. Am. Ceram. Soc.*, **92** [3] 710–6 (2009).
- <sup>40</sup>G. Montavon, C. Coddet, S. Sampath, H. Herman, and C. C. Berndt, "Quality Control of the Intrinsic Deposition Efficiency from the Controls of the Splat Morphologies and the Deposit Microstructure," *J. Therm. Spray Technol.*, **6** [2] 153–66 (1997).
- <sup>41</sup>ASME B46.1 2009, *Surface Texture (Surface Roughness, Waviness, and Lay)*. American Society of Mechanical Engineers, New York, NY, 2009.
- <sup>42</sup>N. Otsu, "A Threshold Selection Method from Gray-Level Histograms," *IEEE Trans. Syst. Man Cybern.*, **9** [1] 62–6 (1979).
- <sup>43</sup>K. Remesh, H. W. Ng, and S. C. M. Yu, "Influence of Process Parameters on the Deposition Footprint in Plasma-spray Coating," *J. Therm. Spray Technol.*, **12** [3] 377–92 (2003).
- <sup>44</sup>S. R. Choi, D. Zhu, and R. A. Miller, "Effect of Sintering on Mechanical Properties of Plasma-Sprayed Zirconia-Based Thermal Barrier Coatings," *J. Am. Ceram. Soc.*, **88** [10] 2859–67 (2005).
- <sup>45</sup>M. Kibsey, J. Romualdez, X. Huang, R. Kearsey, and Q. Yang, "Mechanical Properties of Titania-Doped Yttria Stabilized Zirconia (TiYSZ) for Use as Thermal Barrier Coating (TBC)," *J. Eng. Gas Turbines Power*, **133** [12] 122101, 9pp (2011). □

Permission to publish

M.L. Sesso, C.C. Berndt and Y.C. Wong, 'Topographical and microstructural property evolution of air plasma-sprayed zirconia thermal barrier coatings, J. Am. Ceramic Soc., Article first published online: 4 FEB 2014, DOI: 10.1111/jace.12842.

Wiley Publishes Open Access Articles in fully Open Access Journals and in Subscription journals offering Online Open. Although most of the fully Open Access journals publish open access articles under the terms of the Creative Commons Attribution (CC BY) License only, the subscription journals and a few of the Open Access Journals offer a choice of Creative Commons Licenses:: Creative Commons Attribution (CC-BY) license [Creative Commons Attribution Non-Commercial \(CC-BY-NC\) license](#) and [Creative Commons Attribution Non-Commercial-NoDerivs \(CC-BY-NC-ND\) License](#). The license type is clearly identified on the article.

Copyright in any research article in a journal published as Open Access under a Creative Commons License is retained by the author(s). Authors grant Wiley a license to publish the article and identify itself as the original publisher. Authors also grant any third party the right to use the article freely as long as its integrity is maintained and its original authors, citation details and publisher are identified. These details are indicated above. The copyright owner is specified within the particular Journal. Search: <http://onlinelibrary.wiley.com/browse/publications?type=journal> to find the final article.

## Chapter 2. Microstructural Evolution and Design

### 2.1 Introduction

Chapter 2 is composed of 4 manuscripts that, broadly, focus on the microstructural evolution of coatings. The applicant has initiated many studies that formulate schemes to characterize and distinguish microstructures; ranging from an arbitrary classification of morphological features that relate to the density and defect structure, to a quantitative analysis *via* a fractal dimension analysis.

The cold spray study expressed in manuscript 3 examines the difficult-to-process material of WC-Co. It is verified that the optimum microstructure that retains the nanostructure can be achieved. The other three manuscripts pick up on work that was initiated in 1998 (G. Montavon, C. Coddet, C.C. Berndt and S.-H. Leigh, "Microstructural Index To Quantify Thermal Spray Deposit Microstructures Using Image Analysis", J. Thermal Spray Tech., 7[2] (1998) 229-241). These three manuscripts present a detailed description and analysis on the taxonomy of Nd-Fe-B thick coatings. These materials are used in magnetic applications and were difficult to procure. Stereology protocols were used to derive the porosity level, pore size, and shape distributions. The nature of annealing was assessed and found to not alter the distribution trend of pore number but to effect significantly the distribution of pore volume fractions.

The 126 publications with the identification numbers below are considered as contributions that focus on this specific subject material. Chapter 7 of this thesis outlines the methodology employed for this analysis.

1	132	191	232	285	393
2	133	192	235	288	398
18	134	197	238	289	401
21	139	198	241	290	403
22	145	199	242	291	407
26	147	200	248	300	415
68	148	201	249	302	417
70	149	203	252	306	418
74	150	215	253	317	419
84	151	216	255	327	421
88	160	217	257	328	422
91	161	221	258	330	425
92	162	222	265	335	426
96	163	223	274	341	431
97	166	224	275	344	433
98	167	225	276	350	446
99	173	226	278	360	447
111	175	228	279	364	448
117	178	229	280	372	449
126	179	230	283	385	452
128	183	231	284	386	454

# Microstructural characteristics of cold-sprayed nanostructured WC–Co coatings

R.S. Lima<sup>a,1</sup>, J. Karthikeyan<sup>b</sup>, C.M. Kay<sup>b</sup>, J. Lindemann<sup>b</sup>, C.C. Berndt<sup>a,\*</sup>

<sup>a</sup>Department of Materials Science and Engineering, State University of New York at Stony Brook, 306 Old Engineering Building, Stony Brook, NY 11794-2275, USA

<sup>b</sup>ASB Industries, Inc., Barberton, OH 44203-1689, USA

Received 29 November 2000; received in revised form 19 January 2002; accepted 3 July 2002

## Abstract

The cold-spray process was used to prepare nanostructured WC–Co coatings. The coating microstructural characteristics and phase composition were analyzed via optical microscopy, scanning electron microscopy (SEM) and X-ray diffraction (XRD). The morphology and microstructure of the nanostructured WC–Co powder were also analyzed by SEM and XRD. A 10  $\mu\text{m}$  thick coating was achieved. The powder particles and coating microhardness were also evaluated and compared. The results show that there is no degradation of the WC–Co powder during the cold-spray process and well bonded and phase pure WC coating can be produced by the cold-spray process.

© 2002 Elsevier Science B.V. All rights reserved.

**Keywords:** Thermal spray; Cold-spray; Coating; Nanostructured WC–Co; Microstructure

## 1. Introduction

### 1.1. Nanostructured materials

Nanocrystalline materials (also referred to as nanostructures, nanophase materials, or nanometer-sized crystalline solids) have crystal sizes of typically approximately 10–1000 Å (1–100 nm) in at least one dimension. Nanostructured materials come in two general morphologies: (i) nanolayered materials deposited by physical vapour deposition or electrodeposition processes and, (ii) nanograined materials, which are usually consolidated from nanostructured powders [1].

As the grain size becomes smaller, there are an increasing number of atoms associated with grain boundary sites compared to crystal lattice sites. For example, at a grain size of 100 nm, approximately 3% of all

atoms are associated with grain boundaries. As the grain size is reduced to 10 nm, the percentage increases to 30; at 5 nm, approximately 50% of all atoms are associated with the grain boundary sites. The unique properties of nanograined materials are associated with the fineness of structure as well as the enhanced solubility and increasing atomic mobility associated with grain boundaries [1].

### 1.2. Cold-spray processing of nano WC–Co coatings

The cold gas-dynamic process spray method or simply cold-spray is a high-rate material deposition process in which small, unmelted powder particles (typically 1–50  $\mu\text{m}$  in diameter) are accelerated to velocities on the order of 600–1000 m/s in a supersonic jet of compressed gas. Upon impact against a substrate, the solid particles deform and bond together, rapidly building up a layer of deposited material [2–5].

Cold-spray was developed in the former Soviet Union in the mid-1980s. While performing supersonic wind

\*Corresponding author.

E-mail address: [redacted] (C.C. Berndt).

<sup>1</sup> Present address: National Research Council of Canada, 75 De Mortagne Boulevard, Boucherville, Que., Canada J4B 6Y4.

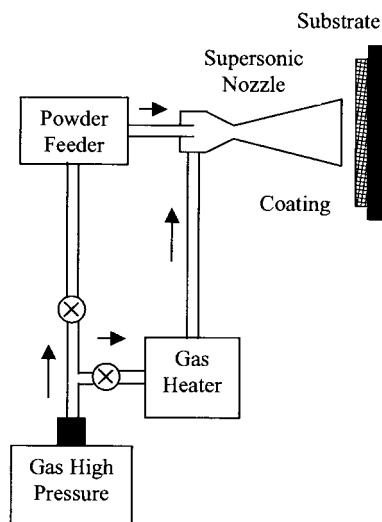


Fig. 1. Schematic of a typical cold-spray system.

tunnel tests with flows containing small tracer particles, scientists observed that above a critical particle velocity (which varies for different materials) there was a transition from particle erosion of a target surface to rapidly increasing deposition [2–4]. Based on these phenomena, a spray system was created and an US patent was issued in 1994 [6].

Fig. 1 shows the schematics of a typical cold-spray system. In cold-spray, a compressed gas, usually He, N<sub>2</sub>, air or their mixtures, at inlet pressures up to 500 psi (3.4 MPa), flows through a converging–diverging nozzle to develop supersonic gas velocities. The powder particles are fed into the gas flow immediately before the converging section of the nozzle and are accelerated by the rapidly expanding gas [2–5].

The compressed gas can be introduced at room temperature, or it can be preheated in order to achieve higher gas flow velocities in the nozzle. Preheat temperatures as high as 600 °C can be used, but the gas rapidly cools as it expands in the diverging section of the nozzle. As a consequence, the dwell time of the particles in contact with hot gas is brief, and the temperatures of the solid particles at impact remain substantially below the initial gas preheat temperature [2].

The mechanisms by which the solid-state particles deform and bond to the substrate or previously deposited layers has not been well characterized. Though it has not yet been demonstrated, plastic deformation may disrupt thin surface films, such as oxides, and provide intimate conformal contact under high local pressure, allowing bonding to occur. This theory would also explain the observed minimum critical velocity necessary to achieve deposition, because sufficient kinetic energy must be available to plastically deform the solid material [2].

Calculations indicate that the particle kinetic energy at impact is typically much less than the energy required to melt the particle [2]. Micrographs of cold-sprayed coatings suggest that the deposition mechanism is primarily a solid-state process [2,3]; i.e. no material melting occurs in this process.

WC–Co coatings are well known for their use in wear resistance applications [7,8]. The hard WC particles form the major wear-resistant constituent of these materials, while the Co binder provides toughness and support [8]. Properties such as the hardness, wear resistance, and strength are influenced primarily by the WC grain size and volume fraction, and in the case of thermal spray coatings, also the porosity, the carbide and binder phase composition [8]. But due to the high temperature characteristics of the traditional thermal spray methods, such as, high velocity oxy-fuel (HVOF), plasma spray, detonation-gun, flame spray and high velocity air-fuel; the WC–Co powder tends to undergo a combination of decarburization, oxidation, reduction by reaction with the H<sub>2</sub> (plasma spray), and dissolution/reaction between the WC and Co during spraying. This behavior results in the formation of hard and brittle phases, such as, W<sub>2</sub>C, W, Co<sub>x</sub>W<sub>y</sub>C<sub>z</sub> (crystalline and amorphous  $\eta$ -phases) and WO<sub>3</sub> [8–12].

Due to its low temperatures, the cold-spray process is a new alternative method for spraying not only WC–Co powders but also nanostructured materials. As an advantage, in cold-spray there is no particle melting and all the nanostructure will be kept intact during the process. In contrary, the traditional thermal spray processes require at least some partial melting of the sprayed material in order to produce adhesion/cohesion of the sprayed particles. Any melting of the nanostructured material will cause the resolidified particles to have the same microstructure as ‘regular’ thermal sprayed particles.

No phase transformation occurs during the cold-spray process since it is a 100% solid-state process; implying no particle melting. Therefore, oxidation, nitriding, decarburizing and any decomposition in general are avoided in this process. The as-sprayed coating phase composition should be the same as the powder phase composition.

But as it was discussed above, WC can be decomposed at temperatures lower than that of its decomposition by the reaction of the WC with the Co binder. The compositional ranges of the  $\eta$ -phases (Co<sub>x</sub>W<sub>y</sub>C<sub>z</sub>) are not fixed and vary with temperature. For example, Co<sub>3</sub>W<sub>3</sub>C exists in the range Co<sub>3.1</sub>W<sub>2.9</sub>C to Co<sub>2.2</sub>W<sub>3.8</sub>C from 1197 to 1427 °C [8]. These temperatures are higher than those experienced during cold-spray, where the maximum gas temperature does not exceed 600 °C [2]. The gas temperature used during this work was 540 °C.

The wettability of WC by most binder metals is better than that of the other carbides and the WC is tougher

Table 1  
Spray parameters

Main gas	N <sub>2</sub>
Main gas temperature at the gun (°C)	540
Gun pressure (psi)	300
Spray distance (mm)	25

than the other carbides. The nanostructural character may improve the mechanical properties of this material. Due to its low temperatures (no WC degradation), the cold-spray process may represent a significant advancement to the spraying of nanostructured carbides.

The objective of this work is to produce nano WC–Co coatings by the cold-spray process and investigate the microstructural characteristics of cold-sprayed WC–Co coatings.

## 2. Experimental procedure

ASB Industries cold-spray system was built according to the design of its Russian inventors [6], and was used for the study reported in this article. The nanostructured WC–12%Co Metco AE7923 feedstock (Sulzer-Metco, Westbury, NY) was cold-sprayed on low carbon steel substrates. The feedstock particle size varies from 10 to 43  $\mu\text{m}$ . The substrates were grit blasted with alumina just before the deposition. The typical coating thickness was 10  $\mu\text{m}$ . The spray parameters applied are listed in Table 1.

The cross-section of the coating was evaluated by using an optical microscope (Nikon-Epiphot 200, Nikon Inc., Melville, NY). The coating and the cross-section of the WC–Co feedstock particles were also analyzed by scanning electron microscopy (SEM).

The Knoop microhardness measurements were performed at 10 g load for 15 s (Tukon, Instron, Canton, MA) on the coating and feedstock particle cross-sections. In order to measure the feedstock microhardness, the particles were vacuum impregnated with epoxy resin and polished. Knoop indentation was chosen because it has a shallow penetration when compared to that of Vickers. Therefore, Knoop indentation seems to be more adequate for performing microhardness measurements in small volumes, such as, powder particles.

X-ray diffraction (XRD) (Model 172a-CuK $\alpha$ , Philips, Almelo, Netherlands) was used to establish the phase composition of the feedstock and coating. XRD was also used to estimate the average grain size of the feedstock and coating [13–16]. The applicability of this method was confirmed by comparing results from transmission electron microscopy (TEM) and XRD techniques [15,16]. The XRD method assumes that the overall broadening of XRD peaks comprises two effects: one arising from the small coherent grain size and one arising from the atomic level microstrain; i.e.  $\Delta d/d$ ,

where  $d$  is the atomic spacing. The peak width resulting from a small grain size effect alone can be described by the Scherrer equation [13,14]:

$$B(2\theta) = \frac{K\lambda}{D\cos\theta} \quad (1)$$

In Eq. (1),  $B(2\theta)$  is the true broadening of the diffraction line measured at half maximum intensity, also known as full-width at half-maximum;  $K$  is a constant (being taken as 0.9);  $\lambda$  is the wavelength of the X-ray radiation;  $D$  is the mean dimension of the grains and  $\theta$  is the Bragg angle. Contributions due to  $K\alpha_1$  and  $K\alpha_2$  were deconvoluted by using the Rachinger correction [13,14], and only the  $K\alpha_1$  peak widths were used for calculation. XRD of a Si specimen was used to measure the instrumental broadening, and the Cauchy correction was used to remove the instrument broadening to obtain the true crystal broadening [14]. According to Ref. [17], results from TEM and XRD of alumina feedstocks showed that the best fit was obtained when the Cauchy correction was applied to remove the instrument broadening factor. The XRD method can provide structural information regarding mean grain size along the entire sample [13–15], and the penetration distance of the X-ray beam into the sample can vary from a few to several micrometers depending on the sample characteristics.

## 3. Results and discussion

### 3.1. Feedstock morphology and phase composition

Figs. 2 and 3 show the typical feedstock particle morphology. The powder particles present the microstructural characteristics representative of agglomerated and sintered particles [8,18]. Individual nanoparticles can not be successfully thermal sprayed because of their

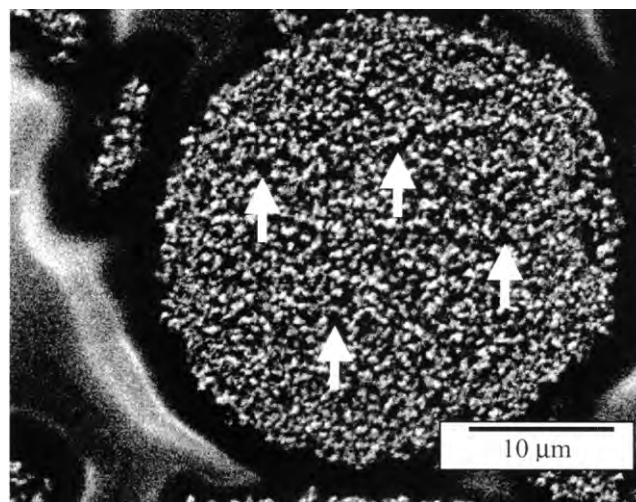


Fig. 2. Typical nanostructured WC–Co particle.



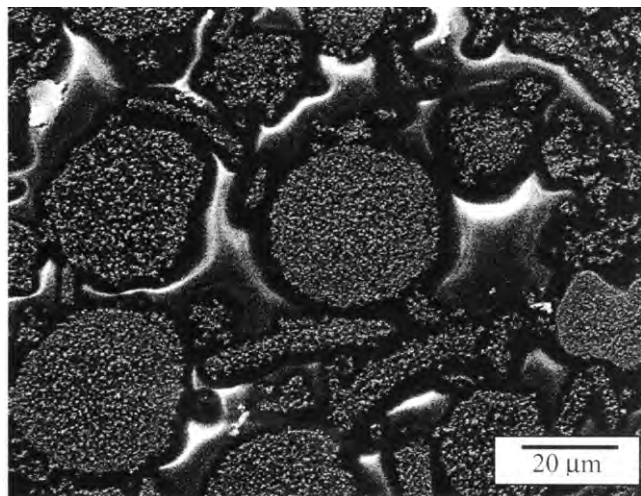


Fig. 3. General morphology of the nanostructured WC–Co particles.

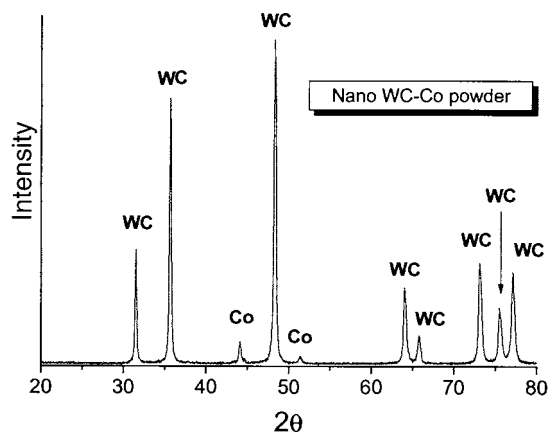


Fig. 4. XRD of the nanostructured WC–12%Co powder.

low mass [19]. Thus, they do not have the inertia required to cross the streamlines in the spray jet and would be segregated to its periphery without deposition on the substrate.

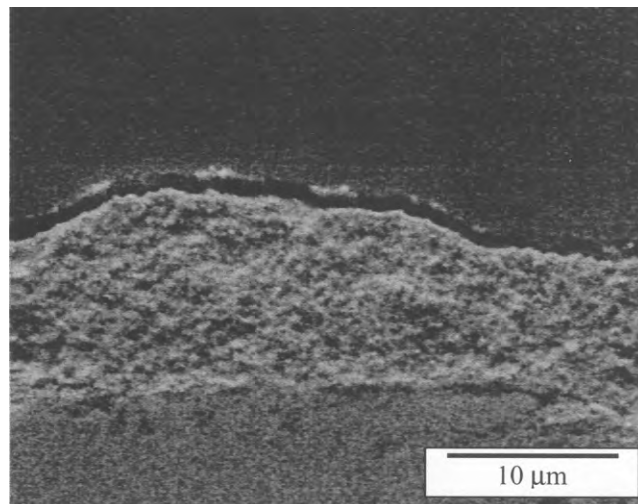


Fig. 6. Cross-section of a nanostructured cold-sprayed WC–12%Co coating (SEM).

To overcome this problem, the feedstock was developed by creating an agglomeration of nanoparticles into large (micron sized) irregular shaped blocks. The agglomeration of nanoparticles into microscopic particles also allows use of existing conventional powder feeders. Each powder particle has two distinct regions. One region is light or white, representing the highly agglomerated nanoparticles of WC. The other region is dark, localized in between the microscopic particles. Some of these typical dark regions indicated in Fig. 2 are expected to be porosity presented in the agglomerated particles. Fig. 3 shows that the particles have a very irregular external morphology, changing from a sphere to a lenticular shape.

The XRD pattern of the nanostructured WC–Co powder is shown in Fig. 4. Only the presence of a well crystalline phase of WC and some amount of Co are noticed.

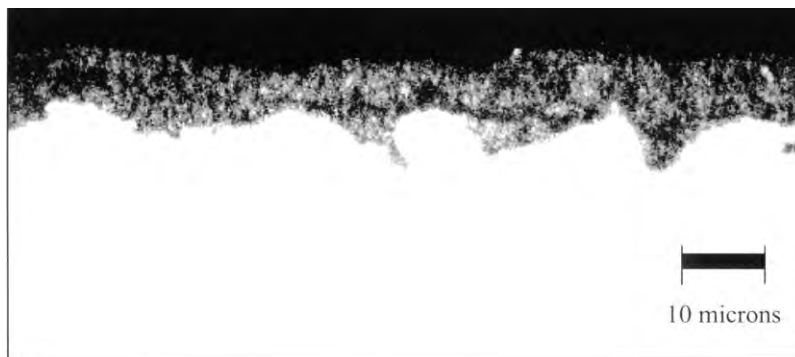


Fig. 5. Cross-section of a nanostructured cold-sprayed WC–12%Co coating (OM).

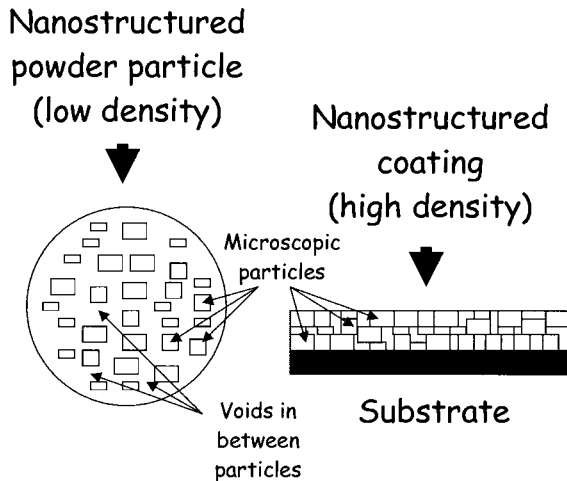


Fig. 7. Schematic of the particle densification upon impact at a high velocity.

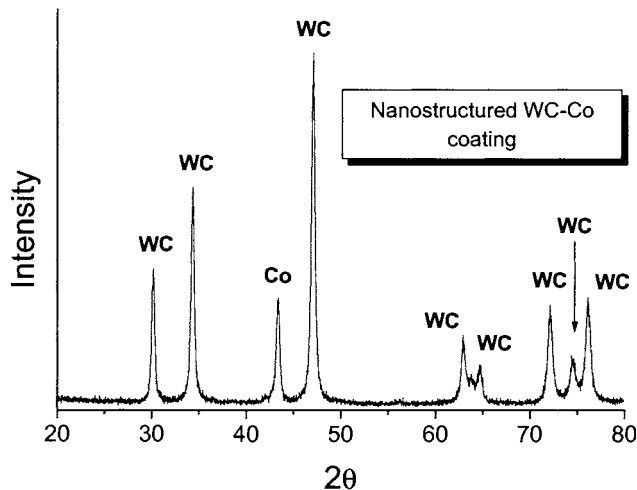


Fig. 8. XRD of the nanostructured WC–12%Co cold-sprayed coating.

### 3.2. Coating cross-section

The cross-section of the nanostructured WC–Co coating analyzed via optical microscopy (OM) and SEM are seen in Figs. 5 and 6, respectively. It is noticed that the coating is very dense, without the presence of porosity. The coating–substrate interface shows no gaps or cracks, which are characteristic feature of ‘good’ adhesion between the coating and the substrate.

Observing the optical micrograph, the substrate surface is very irregular, and exhibits valley and reentrant features. The coating totally fills the reentrant features and follows exactly this very irregular surface. This is probably associated with the supersonic velocities of impact presented by the cold-sprayed particles [4].

Comparing the SEM pictures of the feedstock particle and coating taken with the same magnification of  $1000\times$  (Figs. 2 and 6, respectively), the irregular cross-

section surface, caused by the agglomeration of microscopic particles during manufacturing is noticed. However, the structure of the powder particle is not dense when compared with the structure of the coating. It is possible to observe dark regions in the powder microstructure between adjacent microscopic particles (Fig. 2); as pointed out by arrows. Nevertheless, these dark gaps are not observed in the coating microstructure (Fig. 6); only the irregularities of the cross-section surface created by the microscopic particles are observed.

During the impact at supersonic velocities, and by the fact that the cold-spray is a solid-state process, there should be a densification of the powder particles upon impact, but not any melting. The densification will pack the microscopic particles, eliminating the voids or dark gaps between them. A schematic of the particle structure and its densification upon impact at a high velocity is shown in Fig. 7.

### 3.3. Feedstock and coating microhardness

The Knoop microhardness at 10 g load (number of measurements,  $n=5$ ) for the nanostructured WC–12%Co powder particles is  $42 \pm 7$  kgf/mm<sup>2</sup>. However, the Knoop microhardness at 10 g load (number of measurements,  $n=3$ ) for the nanostructured WC–12%Co cold-sprayed coating is  $1225 \pm 282$  kgf/mm<sup>2</sup>.

These experimental observations agree very well with the densification observed in the microstructures of the powder and coating and with the model described in Fig. 7, supported by the supersonic velocities of impact presented by the cold-sprayed particles [2–4].

Typical Vickers microhardness values for WC–Co coatings HVOF, D-Gun and plasma sprayed are in the range 1000–1400 kgf/mm<sup>2</sup> HV (300 g) [20,21]. At 10-g load the maximum hardness value increases considerably because the indentation impression encloses only a relatively small region of the coating. The indentation sizes are on the order of a single or few splats of the coating. This minimizes the extend of defects, such as, pores, splat boundaries and microcracking enclosed within the indentation [22]. As a consequence, the intrinsic properties of the material are preferentially measured.

However, the hardness values presented by the coating under a low load of 10 g are in the range of those presented at 300 g; considering here that Knoop and Vickers hardnesses have similar characteristics. It may be stated that the significant increase in hardness from feedstock to coating is much more an effect of particle compaction rather than nanostructural characteristics.

### 3.4. Coating phase composition

The XRD pattern of the nanostructured WC–Co coating is shown in Fig. 8. Only the presence of a

Table 2  
Average grain size

Material	Average grain size (nm)
Nanostructured feedstock WC–Co	109
Nanostructured cold-sprayed coating WC–Co	103

crystalline phase of WC and some Co are noticed. None of the phases formed by the degradation of the WC–Co, normally observed in other thermal spray processes [8–12] are present in the cold-sprayed coating. The XRD patterns also agree with the fact that the deposition mechanism is primarily a solid-state process in cold-spray [2,3].

As no phase transformation is noticed, this observation also agrees with the phenomenon described in Fig. 7. The significant increase in microhardness from powder to coating ( $\sim 2800\%$ ) can not be explained on basis of phase transformations. Sintering also can not explain the microhardness increase because of the low gas temperature and dwell time of the particles (fractions of a second) in the spray jet. The impact densification seems to be the most plausible phenomenon.

### 3.5. Feedstock and coating grain size

Table 2 shows the average grain size of the feedstock and coating. According to Ref. [13], the accuracy of a grain size determination depends mainly on the accuracy with which the pure diffraction breadth  $\beta$  can be measured. In Ref. [13] curves of pure diffraction breadth/sample breadth ( $\beta/B$ ) versus instrument broadening/sample breadth ( $b/B$ ) are observed. According to Ref. [13], as the grain size becomes very large (and  $\beta$  very small), the ratio  $b/B$  inevitably increases into the unfavorable range above 0.50, and the ratio  $\beta/B$  decreases in spite of the best possible adjustment of the experimental conditions. As a consequence, one must choose the regions where the high values of  $\beta$  (or  $\beta/B$ ) are found. Thus, based on the above statement, the regions where the ratio  $b/B$  is below 0.50 should be chosen by the observer. For the samples and experimental conditions found in this work, the peak (1 0 1) of the WC (100%) at  $2\theta \sim 48^\circ$  presented optimal characteristics for analysis.

The Scherrer equation was deduced under the assumption that only a small grain size is responsible for peak broadening [13–15]. Strain effects, which may influence the peak broadening are not taken into account [13–15]. In thermal spray, the occurrence of residual stress effects is known [7,23]. However, the residual stresses are normally associated to high temperatures involved in the spray process [7,23]. Since the cold-spray process temperatures much lower than that of the melting point

of the sprayed materials, then the residual stress effects from thermal origin should then be minimized.

In fact, when comparing the results of Table 2, it is noticed that the average grain size of the feedstock particles and the coating are quite similar. This observation collaborates with the issues of the above discussion about residual stress from thermal origin.

However, compressive stresses resulting from the impact of high velocity particles against the substrate surface might be present. As discussed in other section, the impact produces a densification in the WC–Co particles. This densification effect might exhibit similar characteristics to those of ‘shot-peening’; i.e. compressive stresses. Nonetheless, if compressive residual stresses are present, they do not seem to be making a significant effect on average grain size measured by XRD technique (Table 2).

## 4. Conclusions

The nanostructured WC–Co cold-sprayed coating has a high density and microhardness when compared to those of the nanostructured feedstock. The coating microhardness enhancement is much more dependent on the impact velocity than the nanostructured particle microhardness itself. The impact of the particles against the substrate at supersonic velocities, promotes a densification in each nanostructured particle. There is no significant difference between the average grain size of the nanostructured feedstock and coating. It is possible to produce pure and well bonded nanostructured WC–Co coatings via cold-spray processing.

## Acknowledgments

This research program was supported by National Science Foundation grant #: DMI-9903569, STTR Phase I: Nanostructured Protective Coatings for Industrial Applications.

## References

- [1] M. Gell, JOM October (1994) 30.
- [2] R.C. Dykhuizen, M.F. Smith, J. Therm. Spray Tech. 7 (2) (1998) 205.
- [3] R.C. McCune, A.N. Papyrin, J.N. Hall, W.L. Riggs, P.H. Zajchowski, in: C.C. Berndt, S.S. Sampath (Eds.), *Advances in Thermal Spray Science and Technology*, ASM International, Materials Park, OH, 1995, p. 1.
- [4] D.L. Gilmore, R.C. Dykhuizen, R.A. Neiser, T.J. Roemer, M.F. Smith, J. Therm. Spray Tech. 8 (4) (1999) 576.
- [5] J. Karthikeyan, C.M. Kay, J. Lindeman, R.S. Lima, C.C. Berndt, in: C.C. Berndt (Ed.), *Thermal Spray: Surface Engineering via Applied Research*, ASM International, Materials Park, OH, 2000, p. 255.
- [6] A.P. Alkhimov, A.N. Papyrin, V.F. Kosarev, N.I. Nesterovich, M.M. Shuspanov, U.S. Patent No. 5,302,414, April, 1994.
- [7] L. Pawlowski, *The Science and Engineering of Thermal Spray Coatings*, Wiley, Chichester, England, 1995.

- [8] H.L. de Villiers Lovelock, J. Therm. Spray Tech. 7 (3) (1998) 357.
- [9] H.L. de Villiers Lovelock, P.W. Richter, J.M. Benson, P.M. Young, J. Therm. Spray Tech. 7 (1) (1998) 97.
- [10] J.R. Fincke, W.D. Swanck, D.C. Haggard, in: C.C. Berndt, S.S. Sampath (Eds.), *Thermal Spray Industrial Applications*, ASM International, Materials Park, OH, USA, 1994, p. 325.
- [11] K. Korpiola, P. Vuoristo, in: C.C. Berndt (Ed.), *Thermal Spray: Practical Solutions for Engineering Problems*, ASM International, Materials Park, OH, 1996, p. 177.
- [12] C.J. Li, A. Ohmori, Y. Harada, J. Therm. Spray Tech. 5 (1) (1996) 69.
- [13] H.P. Klug, L.E. Alexander, *X-Ray Diffraction Procedures*, second ed., Wiley, NY, USA, 1974.
- [14] B.E. Warren, *X-Ray Diffraction*, Dover Publications, Inc, NY, USA, 1990.
- [15] H.G. Jiang, M. Ruhle, E.J. Lavernia, J. Mater. Res. 14 (2) (1999) 549.
- [16] T. Chraska, Ph.D. Thesis, State University of New York at Stony Brook, NY, USA, 1999.
- [17] T. Ekstrom, C. Chatfield, W. Wruss, M. Maly-Schreiber, J. Mater. Sci. 20 (1985) 1266.
- [18] H.L. de Villiers-Lovelock, S. Luyckx, in: C.C. Berndt (Ed.), *Surface Engineering via Applied Research*, ASM International, Materials Park, OH, 2000, p. 647.
- [19] S. Eidelman, X. Yang, *NanoStructured Mater.* 9 (1997) 79.
- [20] R. Schwetzke, H. Kreye, J. Therm. Spray Tech. 8 (3) (1999) 433.
- [21] R.C. Tucker, J. Vac. Sci. Tech. 11 (4) (1974) 725.
- [22] J.P. Singh, M. Sutaria, M. Ferber, *Ceramic Eng. Sci. Proc.* 18 (4b) (1997) 191.
- [23] S. Kuroda, T. Fukushima, S. Kitahara, *Thin Solid Films* 164 (1988) 157.

#### Permission to publish

R.S. Lima, J. Karthikeyan, C.M. Kay, J. Lindemann and C.C. Berndt, 'Microstructural characteristics of cold-sprayed nanostructured WC-Co coatings', *Thin Solid Films*, 416 (2002) 129-135.

As an Elsevier journal author, you retain various rights including Inclusion of the article in a thesis or dissertation whether in part or in toto; see [http://www.elsevier.com/about/policies/author-agreement/lightbox\\_scholarly-purposes](http://www.elsevier.com/about/policies/author-agreement/lightbox_scholarly-purposes) for more information. As this is a retained right, no written permission is necessary. This extends to the online version of your thesis and would include any version of the articles including the final published versions provided that they are not available as individual downloads but only embedded within the thesis itself.



# Design and manufacture of Nd–Fe–B thick coatings by the thermal spray process

Jo Ann Gan<sup>\*</sup>, Christopher C. Berndt

Industrial Research Institute Swinburne (IRIS), Faculty of Engineering and Industrial Sciences, Swinburne University of Technology, Hawthorn, VIC 3122, Australia

## ARTICLE INFO

### Article history:

Received 12 January 2011

Accepted in revised form 5 April 2011

Available online 13 April 2011

### Keywords:

Rare-earth

Permanent magnet

Magnetic coating

Thermal spray

Microstructure

## ABSTRACT

Permanent magnetic coatings show potential in micro scale applications such as micro motors and micro generators. Nd–Fe–B magnetic coatings of average thickness 50  $\mu\text{m}$  were produced via the flame spray method where the behavior of Nd–Fe–B particles in the thermal spray process was studied through single splat formation. There are generally five types of Nd–Fe–B splat morphology; which correspond to different solidification routes and varying degree of splashing. Microstructures of coating cross sections exhibit features such as cracks and porosity. The microstructural features were related to the physical properties and the brittle nature of the rare-earth alloy feedstock. Cross sections of the coatings also exhibited the presence of two distinct phases: Nd-rich and Fe-rich regions, which have been validated by EDS analysis. Metastable phase formation and decomposition followed by non-equilibrium solidification of the molten droplet prior to impact have been suggested to cause phase separation and were also identified in the formation of single splats. Hardness tests further confirmed the two distinct phases as Nd-rich and Fe-rich areas.

© 2011 Elsevier B.V. All rights reserved.

## 1. Introduction

Nd–Fe–B is a rare-earth permanent magnet that demonstrates strong hard magnet behavior: it has bulk remanent magnetization, coercivity and maximum energy product in the range of 1.0–1.4 T, 9.5–25 kOe and 25–55 MGOe, respectively. Such strong magnetic properties have made Nd–Fe–B increasingly attractive for micro scale applications, such as micro motors [1,2] and micro generators [3,4]. The strong magnetic properties of Nd–Fe–B have allowed miniaturization through the formation of magnetic films via physical processes such as sputter deposition [5,6], evaporation [7,8] and molecular beam epitaxy [9,10] without deterioration of magnetic properties. However, the magnetic films obtained by these means are limited in thickness and involve extended manufacturing schedules. Other deposition methods such as screen printing [11,12], tape casting [13,14], pulsed laser deposition [15,16] and thermal spray [17,18] have been used to overcome these limitations. Fig. 1 shows the intrinsic coercivity of Nd–Fe–B films/coatings as a function of thickness for the various deposition methods.

Thermal spraying is commonly used to deposit coatings of a wide range of materials including polymers, metals and ceramics for thickness up to several millimeters. The high deposition rates of the thermal spray process, together with an ability to deposit materials with a wide range of melting temperature, present a promising route to deposit permanent magnetic coatings for the abovementioned applications. In addition, thermal spray offers advantages such as the

ability to form complex shapes; operate over a wide temperature, velocity and atmospheric environment range; and a simple stream for waste-disposal that can be described as green.

Thermal spray has been used to deposit rare-earth magnetic coatings since late 1970s [19,20]. Optimized spray parameters led to samarium cobalt coatings with thicknesses more than 3 mm and intrinsic coercivity greater than that of its bulk counterparts (3979 kA/m compared to 2785 kA/m). On the other hand, Nd–Fe–B was first sprayed in the mid-1980s using a low pressure plasma spray [21] method. Although bulk Nd–Fe–B has superior magnetic properties compared to that of bulk samarium cobalt, magnetic properties of plasma sprayed Nd–Fe–B coatings have not yet been optimized and the coatings exhibit an intrinsic coercivity that is lower than that of samarium cobalt coatings (867.4 kA/m compared to 3979 kA/m).

The most recent study on plasma spraying of Nd–Fe–B was published by a research group in Dayton, OH–USA [18]. The plasma spray process was carried out in a controlled atmosphere plasma spray (CAPS) chamber, which is expensive to maintain. A controlled atmosphere environment is required since rare-earth and iron elements are prone to oxidation at the high temperatures associated within this process. Another study involves deposition of Nd–Fe–B/Al composite via the cold spray process [22]. Cold spraying of Nd–Fe–B does not require a controlled chamber since the process occurs at a much lower temperature than plasma spray; viz.  $\sim 600^\circ\text{C}$  rather than  $2500^\circ\text{C}$ . However, the considerably lower processing temperature, high velocity of impacting particles and brittle nature of the material all contribute toward particles rebounding from the substrate as well as fracture and fragmentation in the coating. Significant fracture remains even with the blending of a ductile material, such as Al, to retain and trap particles in the coating.

<sup>\*</sup>

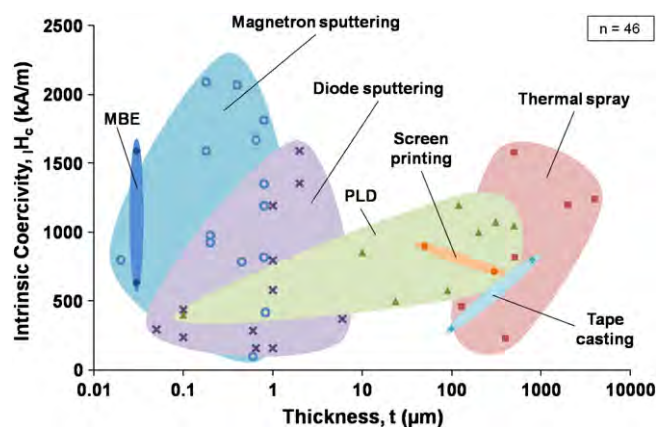


Fig. 1. Intrinsic coercivity of Nd–Fe–B films/coatings deposited by various techniques as a function of film/coating thickness.

The focus within the current work concerns the design and manufacture of a microstructure that is most likely to exhibit appropriate magnetic properties. No magnetic data, per se, are presented since the first step involves the deposition and materials engineering characterization of a coating that is most likely to exhibit functional, extrinsic behavior.

## 2. Experimental methods

The gas atomized Nd–Fe–B powder feedstock was supplied by Magnequench International Inc. (MQP S-11-9). The morphology, composition and particle size of the feedstock were characterized using a ZEISS Supra 40 VP field emission scanning electron microscopy (FESEM) with an in-built energy dispersive X-ray spectroscopy (EDS). Crystallinity of feedstock is characterized using a Bruker AXS D8 Advance X-ray diffractometer (XRD).

As received Nd–Fe–B feedstock was sprayed with a Metco 6 P II oxy-acetylene flame spray torch and Metco 3 MP powder feeder using the spray parameters listed in Table 1. A schematic of the experimental setup is shown in Fig. 2. The prime advantage of this process is that no special precautions were needed to prepare the materials described in this work.

Single splats were collected by spraying a single pass of the feedstock over degreased glass slides and their observation under optical microscopy. Aluminum 5005 alloy was used as the coating's substrate and was grit blasted prior to spraying. The coatings obtained were sectioned using LECO VC-50 equipment and cold mounted using the appropriate procedures and care for thermal spray materials. The cross section of the coatings was polished to a 1 μm finish using a LECO VP-150 polish unit and analyzed by SEM and EDS. Knoop microhardness indentation test was carried out on the polished coating's cross section using a 50 g load for a period of 15 s. The indentations were applied in the center of the Nd-rich and Fe-rich phases. Five indentations were made on each phase.

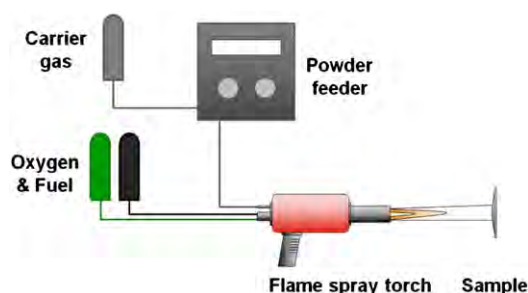


Fig. 2. Schematic of the experimental set up for flame spraying of Nd–Fe–B.

## 3. Results and discussion

### 3.1. Powder feedstock characterization

Morphology of feedstock plays an important role in the flow behavior of the powder into the flame as well as splat and coating formation. Gas-atomized Nd–Fe–B particles exhibit a spherical shape (Fig. 3), with a small portion of ellipsoidal [Fig. 3(a)] and flake-like [Fig. 3(e)] particles. These ellipsoidal and flake-like particles arise from a sequence of liquid stream disintegration during the gas atomization process. Satellites [Fig. 3(b)] are common features of gas atomized powder that result from turbulence near the nozzle during atomization. On the other hand, features such as craters [Fig. 3(c)] and cracks [Fig. 3(d)] may result from collision of smaller particles that re-enter the flight path with accelerated solidified particles.

The particle size exhibited a slight positively skewed distribution with a mean size of 38.9 μm and standard deviation of 11.5 μm; Fig. 4. The particle size ranges from 10 to 68 μm, with more than 90% of the particles in the range of 20 to 60 μm, which is the typical range for thermal spray feedstock.

Composition analysis of the feedstock by EDS shows that the two main elements, Nd and Fe have 19 and 73 wt.% respectively, which are within the range given by the manufacturer; alongside the presence of additives such as zirconium and titanium that made up less than 8 wt.% of the overall composition, Table 2. Boron was not detected due to the limitation of the EDS technique. Elemental mapping by EDS shows that all elements are homogeneous throughout the powder, with Fe having the highest intensity. It can be deduced that the powder is an alloy rather than a mixture of Nd and Fe individual particles. Cross sections of the feedstock particles show no sign of segregation within the particles and the elemental mapping exhibits a similar homogeneous distribution.

XRD analysis (data not shown) reveals that Nd–Fe–B powder is amorphous, which is expected since magnetic powders are typically manufactured as an amorphous phase to reduce oxidation during handling and processing. A post-processing sintering step at temperature between 500 and 700 °C [5] is necessary, with crystallization expected to occur around 550–600 °C [23]. Table 3 shows the magnetic attributes of crystallized feedstock at 25 °C, as supplied by the manufacturer.

### 3.2. Splat formation

Knowledge of splat formation is crucial in understanding and predicting properties of a coating since this is directly related to the deposition efficiency, pore network, and bond strength as well as oxides present in the coating. Real-time observation of particle behavior during spraying; i.e. particle melting, impact and rapid solidification, is difficult since these processes occur in the order of microseconds. As an alternative, observation of both splat size and shape provides insights into splat formation.

Table 1  
Spray parameters for combustion flame spraying of Nd–Fe–B.

Oxygen pressure, kPa	207
Acetylene pressure, kPa	103
Air pressure, kPa	276
Standoff distance, mm	100, 150, and 200
Feed rotation, rpm	0–12
Carrier gas flow, scfh	6–8
Feed rate, g/min	54–120



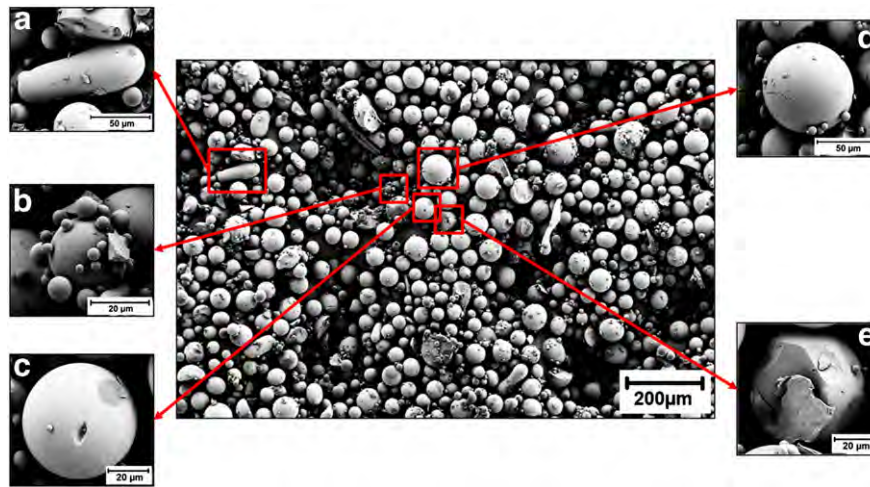


Fig. 3. SEM images highlighting features of Nd-Fe-B powder feedstock (a) ellipsoidal, (b) satellites, (c) crater, (d) cracks and (e) flake-like.

The distribution of splat diameter at various standoff distances is given in Fig. 5. It was observed that the mean splat diameter increases as standoff distance increases. The flattening ratio,  $\xi$ , for splats formed also increases as standoff distance increases, which are 1.8, 2.2 and 2.5 at distances of 100, 150 and 200 mm respectively. This is justified by the fact that as standoff distance increases, the in-flight time becomes longer and hence the final velocity of the particles before impact increases as well (assuming the same initial velocity since the powder is being fed at the same rate). Velocity of the impinging droplet is closely related to the kinetic energy, which is one of the components in the mechanical energy conservation equation that describes flattening of a droplet given by Madejski [24]:

$$\frac{d}{dt}(E_k + E_p + L_f) = 0 \quad (1)$$

where  $E_k$  is the kinetic energy,  $E_p$  is the potential one and  $L_f$  is the work of frictional forces. Derivation of Eq. (1) by Madejski [24] allows determination of the flattening ratio and prediction of splat size by incorporating dimensionless Reynolds, Weber and Péclet numbers. The density of the molten droplet, surface tension and viscosity are accounted for by  $E_k$ ,  $E_p$  and  $L_f$  respectively.

Density, surface tension and viscosity of a droplet are influenced by the degree of melting, which in this case is influenced by the

standoff distance. The melting index is given by the ratio of in-flight time,  $\Delta t_{fly}$  to the time for a particle to be fully melted,  $\Delta t_{melt}$  [25]:

$$M.I. = \frac{\Delta t_{fly}}{\Delta t_{melt}} = \frac{6k_l}{\rho L} \cdot \frac{1}{1 + 2/Bi} \cdot \frac{(T_f T_m) \cdot \Delta t_{fly}}{r_p^2} \quad (2)$$

where  $k_l$  is the thermal conductivity,  $\rho$  is the density,  $L$  is the latent heat of fusion,  $Bi$  is the Biot number ( $hr_p/k_l$ ),  $T_f$  is the flame temperature,  $T_m$  is the melting point,  $r_p$  is the particle radius and  $h$  is the convective heat transfer coefficient. A longer standoff distance results in longer in-flight time and, hence, higher melting index. Better molten particles have lower surface tension and viscosity, and this leads to a higher flattening ratio and wider splats.

However, initial work by Madejski failed to take into account the effects of wettability, thermal contact resistance and solidification rate, all of which are variables that directly influence the splat size and shape. Several other research groups [26–31] have modified the Madejski model by revising variables such as the velocity field, contact angle and the assumed constant,  $\epsilon$ . Validation of the revised models involves the use of large droplets, which means that it may still not be applicable to the small droplets observed in thermal spray deposition since the spreading of small droplets is dominated by surface tension as opposed to viscous dissipation in large droplets.

Another indication of the splat formation process is through observation of the splat shape. Splat geometry is governed by the same factors that have been discussed previously in terms of splat size; thermal contact resistance, wetting, surface tension, viscosity and solidification. Although surface roughness is also an important factor that influences the splat shape, splat studies often involve

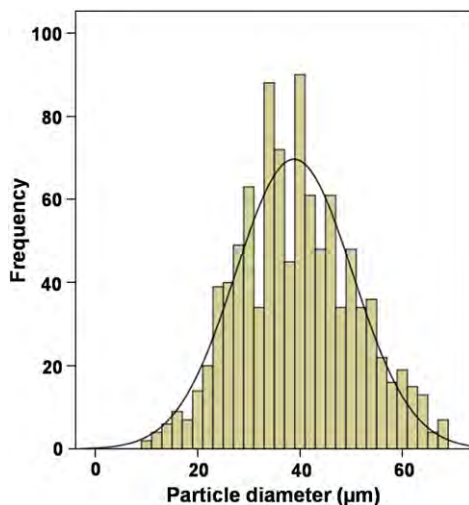


Fig. 4. Particle size distribution of Nd-Fe-B powder by microscopy measurement.

Table 2

Weight percentage of respective elements present in Nd-Fe-B powder.

Element	Weight %	
	Given	Measured
Neodymium	15.0–22.0	19.00
Praseodymium	0.0–5.0	0.00
Boron	0.5–1.8	0.00
Iron	70.0–82.0	73.08
Cobalt	0.0–5.0	0.00
Zirconium	0.0–5.0	5.84
Titanium	0.0–5.0	2.08
Carbon	0.0–1.0	0.00
Copper	0.0–1.0	0.00

**Table 3**  
Magnetic properties of Nd–Fe–B powder.

Remanent magnetization, $B_r$	746 mT
Saturation magnetization, $B_s$	806 mT
Maximum energy product, $(BH)_{\max}$	85 kJ/m <sup>3</sup>
Coercivity, $H_c$	438 kA/m
Intrinsic coercivity, $iH_c$	731 kA/m

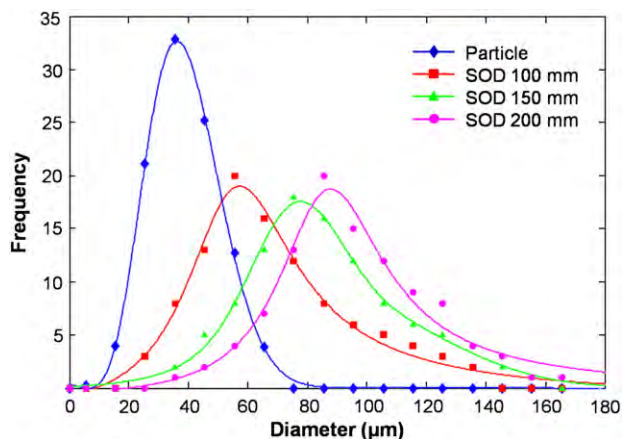


**Fig. 5.** Size distribution for Nd–Fe–B particles and splats formed at standoff distances (SOD) of 100, 150 and 200 mm.

smooth surfaces with roughness,  $R_a$ , of less than 0.2  $\mu\text{m}$  for simplified analysis, as is the case in the current study.

Splat shape can be predicted using the Sommerfeld parameter,  $K = We^{1/2} \cdot Re^{1/4}$ , where  $We$  and  $Re$  are Weber and Reynolds numbers respectively. Deposition occurs for  $3 < K < 58$  while  $K > 58$  represents splashing and for  $K < 3$  the particle simply rebounded from the surface [32]. However, this equation is valid only for an incompressible model where solidification does not occur prior to droplet spreading. In cases where solidification is involved, as is the case in the present work, the splat shape prediction becomes more complex since it depends greatly on the cooling rate.

There are generally five types of splat morphologies identified for Nd–Fe–B, as shown in Fig. 6. Fig. 6(a), (b) and (c) shows disk-type splats with different surface conditions while Fig. 6(d) and (e) shows splash-type splats with finger-like protrusions. All five splat mor-

phologies were observed in samples sprayed at standoff distances of 100, 150 and 200 mm. Fig. 7 shows the fraction of each splat morphology with respect to standoff distance.

Both disk-type and splash-type splats are formed when there is good contact between the splat and the substrate; poor contact leads to fragmented splats. The disk-type splat [Fig. 6(a)] exhibits a greater diameter compared to a splash-type splat [Fig. 6(d)]. An initial analysis of these microstructural artifacts can assume the same flattening ratio for both splats when sprayed at the same standoff distance. In this instance, the disk-type splat with the smaller diameter originates from smaller particles. The impact section of the splat starts solidifying due to good thermal contact with the substrate. At the same time the top part of the splat is still molten and while at a reduced temperature will show an increased viscosity. Therefore, there is insufficient fluidity to freely flow and a disk-type splat evolves. This hypothesized formation mechanism is reinforced by the higher fraction of disk-type splats observed at lower standoff distances, Fig. 7.

On the other hand, splash-type splats are formed when the thermal contact resistance is low, allowing spreading of the impacting particles. As mentioned earlier, splash-type splats have a greater diameter than the disk-type splats. Applying the same assumption on flattening ratio, splash-type splats originate from bigger particles, hence higher impact velocity that results in enhanced radial flow of the molten layer along the substrate surface [33]. In addition, due to the rapid cooling, the molten top layer does not have sufficient time to lose its momentum; thus causing overflow of the molten material beyond the solidified central core boundary [34]. Formation of splash-type splats due to higher impact velocity is evident by the increased fraction of splash-type splats as the standoff distance increases, Fig. 7. The dominating splat type shifted from disk-type to splash-type as the standoff distance increases. This is also supported by the fact that in-flight, or residence, time becomes longer as standoff distance increases, resulting in higher impact velocity.

Dhiman et al. [35] pointed out that there are two types of splash-type splats: (1) freezing-induced splash with long radial fingers and (2) impact-induced fragmented splash with a central core surrounded by a ring of fragments. Only freezing-induced splash behavior was observed in the current study. Thus, solidification of splats upon impact is important in determining the splat morphology of Nd–Fe–B, as was emphasized through modeling of splat formation by Mostaghimi et al. [36]. Dhiman et al. [35] introduced a dimensionless solidification parameter,  $\Theta$ , which can be used to predict splat morphology and the degree of splashing.

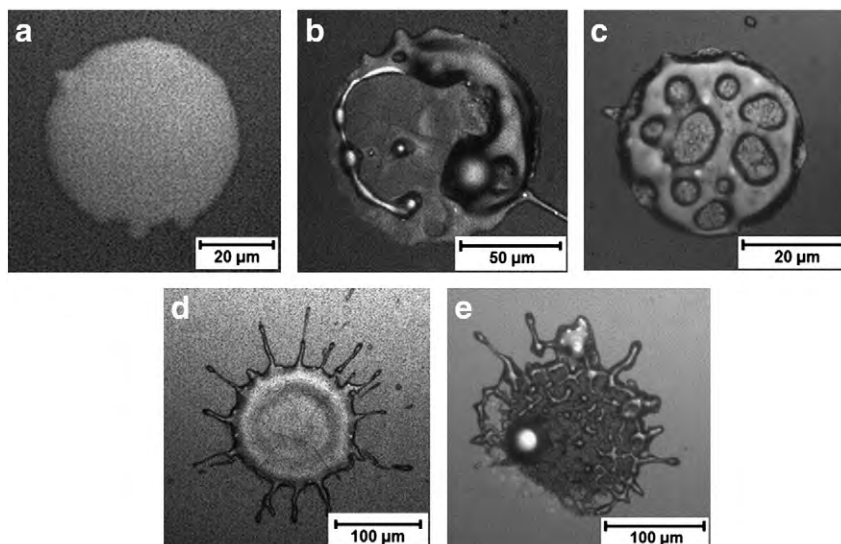


**Fig. 6.** Nd–Fe–B splat morphology: (a) disk-type, (b) disk-type with resolidified Fe, (c) disk-type with pock-like feature, (d) splash-type, and (e) splash-type with resolidified Fe.



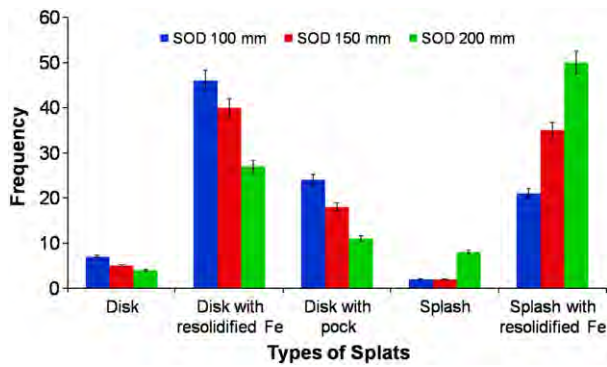


Fig. 7. Percentage of each type of splat morphology at standoff distances 100, 150 and 200 mm.

Splashing can also be caused by the presence of adsorbates and condensates on the substrate surface. Upon contact with hot molten particles, the thin layer of adsorbates and condensates vaporizes rapidly and destabilizes the droplet spreading; thereby resulting in splash-type splats [37]. However, for smaller molten particles, the momentum of the impacting droplet is insufficient to transform droplets into splashes. Instead, vaporization of adsorbates and condensates leads to disk-type splats with pock-like features on the surface, also known as gas escapement holes as shown in Fig. 6(c). The role of impact momentum on the formation of splats with pocks is reinforced by two complementary effects; i.e., (i) the decrease of disk-like splats with pocks is (ii) compensated by an increase in splash-type splats as the standoff distance increases.

Despite the desirability for splats formed from well molten droplets, the majority of splats observed exhibit the morphologies shown in Fig. 6(b) and (e), which contain “bumps” that can be associated with either unmelts or resolidified particles. Similar

morphologies were observed for Nylon-11 splats by Ivosevic et al. [38] and their formation with an unmelted core was attributed to the large radial temperature profile of the polymer particles. In the case of Nd-Fe-B, however, the “bumps” observed were not unmelts, but Fe particles that have been resolidified during in-flight. This phenomenon is attributed to non-equilibrium solidification of the molten droplets and will be discussed further in the next section. More than 65% of the observed splats contain resolidified particles; i.e., disk-type or splash-type with resolidified particles, indicating that the majority of the molten droplets undergo non-equilibrium solidification.

### 3.3. Coating formation

Coatings discussed herein were sprayed at a feed rate of 120 g/min. Samples sprayed at lower feed rates do not have sufficient thickness to be analyzed and the coatings were friable during metallographic preparation, indicating poor mechanical properties and coating integrity. The coatings have an average thickness of 50  $\mu\text{m}$  and failed to build up beyond 50  $\mu\text{m}$ , suggesting poor cohesion.

Topographic views of (i) the substrate after grit blasting and (ii) the coating are depicted in Fig. 8(a) and (b) respectively. Topographic images at 500 $\times$  magnification, Fig. 8(c) and coating cross sections, Fig. 8(d) illustrate typical features of thermal spray coatings such as splats, unmelts and porosity. Occurrence of porosity is often caused by incomplete filling of crevices due to the surface tension of molten droplets [39]. These pores are often small, of less than a few micrometers, depending on the size of the feedstock particles. However, nearly spherical voids as large as 20  $\mu\text{m}$  were observed in the cross sections of Nd-Fe-B coatings. These nearly-spherical voids are resolidified particles that were removed during metallographic preparation due to the brittleness of the material. Thus, within the practical manufacture of a coating there would be no voids present.

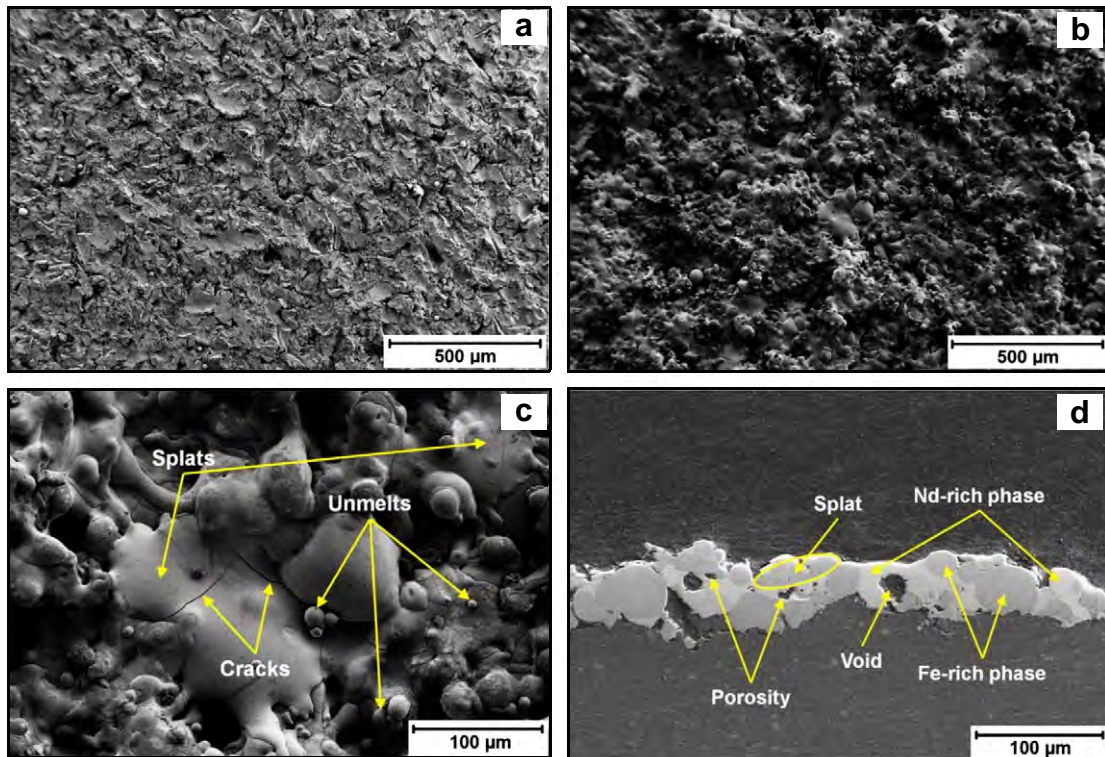
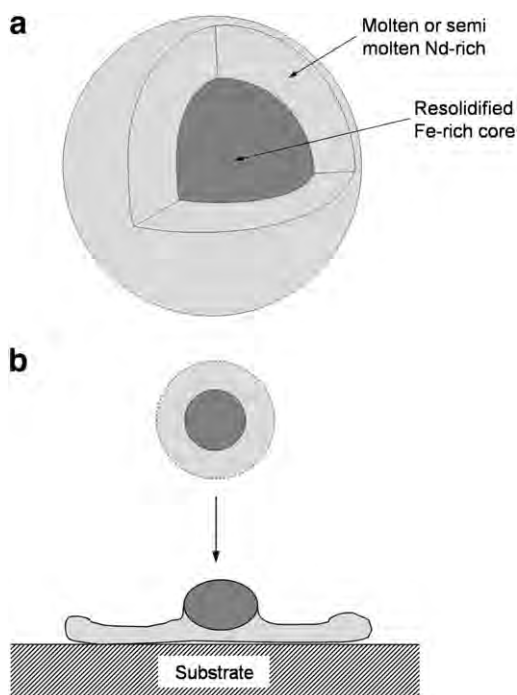


Fig. 8. Topographic view of (a) grit blasted Al 5005 substrate, (b) and (c) Nd-Fe-B coating at 100 $\times$  and 500 $\times$  magnification respectively, and (d) cross sectional view of Nd-Fe-B coating.



**Fig. 9.** Schematic of (a) non-equilibrium solidification of Nd-Fe during in-flight, which results in resolidified Fe-rich core area and molten or semi molten Nd-rich area surrounding the core and (b) formation of splat from resolidified Fe core surrounded by Nd-rich molten droplet.

Two distinct phases were observed in the coatings, the lighter Nd-rich and the darker Fe-rich phase. Similar phase separation was observed in Nd-Fe-B plasma sprayed coatings by Wysocki et al. [40], however the reasoning behind such phase separation was not elaborated further. It was observed that most of the darker Fe-rich areas are near spherical. The shape of these Fe-rich areas indicates that they are either unmelted or have been resolidified during impact with the substrate.

Referring back to the characterization of the feedstock, the feedstock particles are homogeneous alloy particles, and not a mixture of individual Nd and Fe particles. There are also no signs of

segregation within the particles when they are sectioned, which suggests that the near spherical Fe-rich areas are not unmelted, but Fe particles that have been resolidified during in-flight. Such resolidification of Fe from the alloy droplet occurred as a consequence of metastable phase formation and decomposition followed by non-equilibrium solidification.

Heating by flame spray melts the feedstock, which contains 84.5 at.% Fe, to a liquid phase. Upon cooling to below 1180 °C in a stable system,  $\text{Nd}_2\text{Fe}_{14}\text{B}$  ( $\phi$ ) and Fe phases are formed [41]. However, rapid heating and solidification via flame spray lead to metastable behavior where a new phase  $\text{Nd}_2\text{Fe}_{18}\text{B}$  ( $x$ ) forms. Primary crystallization of the  $\phi$  phase is suppressed in favor of Fe phase formation. Decomposition of  $x$  will eventually lead to the formation of  $\phi$  and Fe phases but this did not follow due to the high cooling rate. Instead, the presence of a fourth component, such as oxygen potentially results in the formation of Fe,  $\text{Nd}_2\text{O}_3$  and  $\text{NdB}_4$  phases. Since boron cannot be detected by EDS due to overlapping spectra to carbon, the  $\text{NdB}_4$  phase was detected only as a Nd-rich phase.

Formation of the different phases was accompanied by the occurrence of non-equilibrium solidification. Non-equilibrium solidification leads to non-uniform distribution of elements within an alloy, resulting in segregation within a particle. During non-equilibrium solidification, the element with a higher melting point (which is Fe in this case) will tend to concentrate in the droplet center because this region is the first to solidify. This leaves the lower melting point Nd in a molten or semi molten state, surrounding the Fe-rich core as illustrated in Fig. 9(a). As this semi molten droplet with resolidified Fe core impacts onto the substrate, the resolidified Fe remains in its near spherical shape while Nd deforms onto the substrate to form a splat, as shown in Fig. 9(b).

This type of splat, which contains resolidified Fe, is the dominant splat type as mentioned in the previous section. This explains the failure for a coating to build up and the formation of a non-uniform coating as depicted in Fig. 10(a), since the resolidified Fe core could easily bounce off the surface upon impact, unless there is sufficient adherence between the resolidified Fe and the deformed Nd, or if they are trapped by an incoming semi molten droplet. Another possibility is that the in-flight semi-molten droplet traverses at sufficient velocity (hence high enough impact energy) to deform the resolidified Fe core onto the substrate or existing layer. However, this is not the case in the flame spray process.

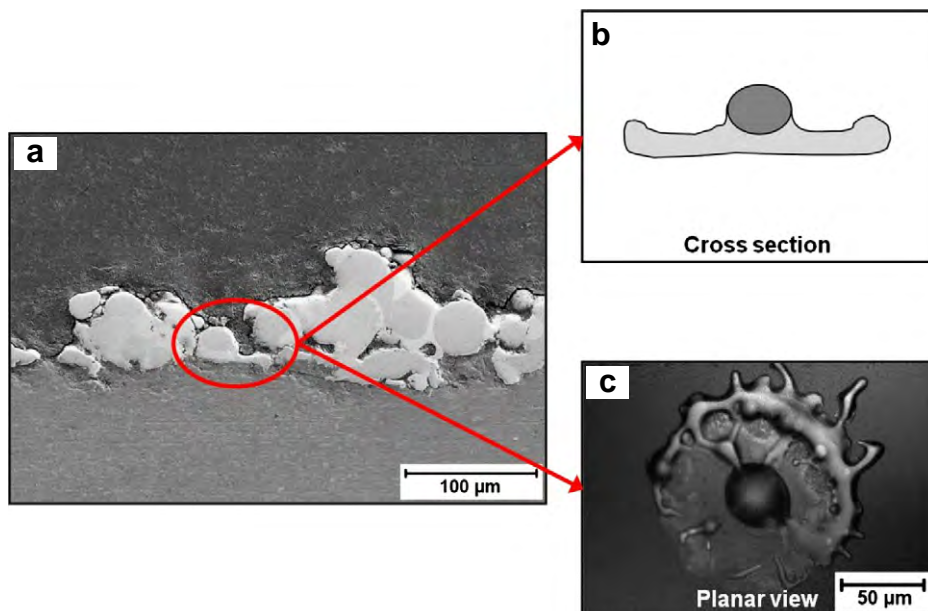


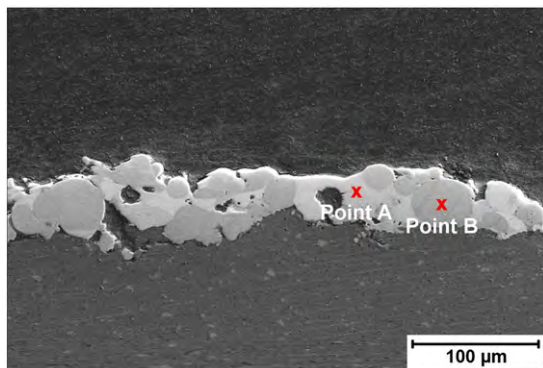
**Fig. 10.** (a) The cross section of the non-uniform coating and the resemblance between a feature in the cross section and a single splat; (b) schematic cross section view and (c) planar view.

**Table 4**  
Composition of Nd–Fe–B feedstock and flame spray coating.

Element	Weight %		
	Feedstock	Point A	Point B
Neodymium	19.00	51.20	0.00
Iron	73.08	1.48	95.89
Oxygen	0.00	29.02	0.00
Titanium	2.08	3.88	0.78
Zirconium	5.84	14.42	0.00
Carbon	0.00	0.00	3.33

The non-uniform coating, Fig. 10, contains more Fe-rich phases (dark area) compared to the more uniform coating, Fig. 8(d), which reinforces the statement that the resolidified Fe causes non-uniformity in the coating. One of the distinct features in the non-uniform coating has been highlighted as a splat with resolidified Fe, as shown in Fig. 10(b) and (c). Table 4 shows the result of elemental analysis that confirms that the lighter area (Point A in Fig. 11) is a Nd-rich area where the weight percent of Nd has increased to 51.20% in the coating compared to only 19.00% in the feedstock; while that of Fe has dropped from 73.07% in the feedstock to 1.48% in the coating. On the other hand, the darker region (Point B in Fig. 11) shows that majority of the area consists of Fe – with a high weight percentage of 95.89%. The remaining area is comprised of Ti additive and C, which may arise due to combustion of the feedstock during particle flight. The presence of oxygen in the Nd-rich area also indicates that this phase is in a molten state during in-flight longer than the Fe-rich area, thus more susceptible to oxidation. This further reinforces the statement that Fe has been resolidified during in flight via non-equilibrium solidification.

The two distinct phases in the coatings were further analyzed by the Knoop microhardness test. The Knoop microhardness test was selected due to the brittleness of the coating material as well as the limited coating's thickness. Only five sets of indentations were made on the uniform coating's cross section due to the limitation in the coating's thickness. The indentations were made at the center of the Nd-rich phase, Fe-rich phase and the substrate respectively using a 50 g load for a period of 15 s. The hardness test reveals that the two distinct phases have different hardness values, as presented in Table 5. For comparative purpose, the Knoop hardness values obtained have been converted to Vickers hardness value, also included in Table 5. Hardness of the Nd-rich area was found to have increased to 542 HV compared to pure Nd (343 HV). The increase in hardness is mainly attributed to the oxidation of the Nd-rich phase. The presence of Ti and Zr additives, which have Vickers hardness of well above 970 and 903 HV respectively could also contribute to the increase in hardness value. On the other hand, the hardness value of

**Fig. 11.** The cross section of Nd–Fe–B coating highlighting lighter Nd-rich phase (Point A) and darker Fe-rich phase (Point B).**Table 5**  
Hardness of the Al 5005 substrate and Nd–Fe–B coating.

Area tested	Knoop hardness, HK 0.05/15		Vickers hardness, HV (converted for comparison purpose)
	Mean	Standard deviation	
Al alloy substrate	60.3	1.4	–
Nd-rich area	570.7	39.4	542
Fe-rich area	676.2	83.4	639

the Fe-rich area is 639 HV, which is fairly close to that of iron (608 HV). This value agrees with the elemental analysis data where there is no oxidation and relatively little Ti additives detected in this region.

#### 4. Conclusions

The Nd–Fe–B feedstock particles have a spherical morphology with a mean size of 38.7 μm. The feedstock powder is amorphous and shows hard magnetic properties with remanent magnetization,  $B_r$  and intrinsic coercivity,  $iH_c$  of 746 mT and 731 kA/m respectively. Single splat studies revealed that there are five types of Nd–Fe–B splat morphology namely, disk-type, disk-type with resolidified Fe, disk-type with pock-like feature, splash-type, and splash-type with resolidified Fe.

Splats with resolidified Fe are the dominant splats (more than 65%) for the spray parameters used, indicating non-equilibrium solidification of the molten droplet prior to impact. Flame sprayed Nd–Fe–B coatings with an average thickness of 50 μm were obtained where there are two distinct phases observed, the lighter and darker phases. Elemental analysis and hardness test verified the two phases to be the Nd-rich and the Fe-rich phase. The occurrence of such phase separation is attributed to metastable phase formation and decomposition followed by non-equilibrium solidification of the molten droplet where the higher melting point Fe concentrates at the center of the droplet and solidifies prior to impacting with the substrate.

#### Acknowledgments

The authors acknowledge the support of a Swinburne University Postgraduate Research Award (SUPRA) for funding this study. The authors would also like to thank Dr. J. Wang and Dr. F. Malherbe for their assistance in operating the FESEM, EDX and XRD.

#### References

- [1] M. Nakano, S. Sato, F. Yamashita, T. Honda, J. Yamasaki, K. Ishiyama, M. Itakura, J. Fidler, T. Yanai, H. Fukunaga, IEEE Trans. Magn. 43 (2007) 2672.
- [2] T. Spiliotis, D. Niarchos, P. Meneroud, G. Magnac, F. Claeysen, J. Pepin, C. Fermon, M. Pannetier, N. Biziere, J. Magn. Magn. Mater. 316 (2007).
- [3] D.P. Arnold, IEEE Trans. Magn. 43 (2007) 3940.
- [4] F. Herrault, C.Y. Ji, M.G. Allen, J. Microelectromech. Syst. 17 (2008) 1376.
- [5] W.F. Liu, S. Suzuki, K. Machida, J. Magn. Magn. Mater. 308 (2007) 126.
- [6] S.L. Chen, W. Liu, Z.D. Zhang, G.H. Gunaratne, J. Appl. Phys. 103 (2008) 023922.
- [7] M. Gasgnier, C. Colliex, T. Manoubi, J. Appl. Phys. 59 (1986) 989.
- [8] L.G. Pereira, S.R. Teixeira, W.H. Schreiner, F.P. Missell, I.J.R. Baumvol, Phys. Status Solidi A 125 (1991) 625.
- [9] D.J. Keavney, E.E. Fullerton, J.E. Pearson, S.D. Bader, J. Appl. Phys. 81 (1997) 4441.
- [10] V. Neu, S. Fähler, A. Singh, A.R. Kwon, A.K. Patra, U. Wolff, K. Häfner, B. Holzapfel, L. Schultz, J. Iron Steel Res. Int. 13 (2006) 102.
- [11] B. Pawlowski, J. Töpfer, J. Mater. Sci. 39 (2004) 1321.
- [12] T. Spiliotis, D. Niarchos, P. Falaras, D. Tsoukleris, J. Pepin, IEEE Trans. Magn. 41 (2005) 3901.
- [13] B. Pawlowski, H. Beer, J. Toepfer, Key Eng. Mater. 132–136 (1997) 1409.
- [14] B. Pawlowski, S. Schwarzer, A. Rahmig, J. Töpfer, J. Magn. Magn. Mater. 265 (2003) 337.
- [15] C. Constantinescu, N. Scarisoreanu, A. Moldovan, M. Dinescu, L. Petrescu, G. Epureanu, Appl. Surf. Sci. 253 (2007) 8192.
- [16] M. Nakano, T. Honda, J. Yamasaki, S. Sato, F. Yamashita, J. Fidler, H. Fukunaga, Sens. Lett. 5 (2007) 48.
- [17] G. Rieger, J. Wecker, W. Rodewald, W. Sattler, F.W. Bach, T. Duda, W. Unterberg, J. Appl. Phys. 87 (2000) 5329.



- [18] M. Willson, S. Bauser, S. Liu, M. Huang, J. Appl. Phys. 93 (2003) 7987.
- [19] K. Kumar, D. Das, Thin Solid Films 54 (1978) 263.
- [20] K. Kumar, D. Das, E. Wettstein, J. Appl. Phys. 49 (1978) 2052.
- [21] R.A. Overfelt, C.D. Anderson, W.F. Flanagan, Appl. Phys. Lett. 49 (1986) 1799.
- [22] P.C. King, S.H. Zahiri, M.Z. Jahedi, J. Therm. Spray Technol. 17 (2008) 221.
- [23] P.G. McCormick, W.F. Miao, P.A.I. Smith, J. Ding, R. Street, J. Appl. Phys. 83 (1998) 6256.
- [24] J. Madejski, Int. J. Heat Mass Transfer 19 (1976) 1009.
- [25] H.B. Xiong, L.L. Zheng, L. Li, A. Vaidya, Int. J. Heat Mass Transfer 48 (2005) 5121.
- [26] A.J. Markworth, J.H. Saunders, Int. J. Heat Mass Transfer 35 (1992) 1836.
- [27] R.H. Rangel, X. Bian, Int. J. Heat Mass Transfer 40 (1997) 2549.
- [28] J.P. Delplanque, R.H. Rangel, Acta Mater. 46 (1998) 4925.
- [29] H. Zhang, Int. J. Heat Mass Transfer 42 (1999) 2499.
- [30] Y.P. Wan, H. Zhang, X.Y. Jiang, S. Sampath, V. Prasad, J. Heat Transfer 123 (2001) 382.
- [31] D. Sivakumar, H. Nishiyama, J. Heat Transfer 126 (2004) 485.
- [32] P. Fauchais, M. Fukumoto, A. Vardelle, M. Vardelle, J. Therm. Spray Technol. 13 (2004) 337.
- [33] C.J. Li, C.X. Li, G.J. Yang, Y.Y. Wang, J. Therm. Spray Technol. 15 (2006) 717.
- [34] K. Sabiruddin, P.P. Bandyopadhyay, G. Bolelli, L. Lusvarghi, J. Mater. Process. Technol. 211 (2011) 450.
- [35] R. Dhiman, A.G. McDonald, S. Chandra, Surf. Coat. Technol. 201 (2007) 7789.
- [36] J. Mostaghimi, M. Pasandideh-Fard, S. Chandra, Plasma Chem. Plasma Process. 22 (2002) 59.
- [37] X. Jiang, Y. Wan, H. Herman, S. Sampath, Thin Solid Films 385 (2001) 132.
- [38] M. Ivosevic, R.A. Cairncross, R. Knight, Int. J. Heat Mass Transfer 49 (2006) 3285.
- [39] M. Xue, S. Chandra, J. Mostaghimi, H.R. Salimijazi, Plasma Chem. Plasma Process. 27 (2007) 647.
- [40] J.J. Wysocki, J. Mater. Sci. 27 (1992) 3777.
- [41] G. Schneider, E.-T. Henig, G. Petzow, H.H. Stadelmaier, Z. Metallkd./Int. J. Mat. Res. 77 (1986) 755.

### Permission to publish

J.A. Gan and C.C. Berndt, 'Design and manufacture of Nd-Fe-B thick coatings by the thermal spray process', Surf. Coat. Tech., 205[19] (2011) p. 4697-4704. DOI: 10.1016/j.surfcoat. 2011.04.034, Published: JUN 25 2011.

As an Elsevier journal author, you retain various rights including Inclusion of the article in a thesis or dissertation whether in part or in toto; see [http://www.elsevier.com/about/policies/author-agreement/lightbox\\_scholarly-purposes](http://www.elsevier.com/about/policies/author-agreement/lightbox_scholarly-purposes) for more information. As this is a retained right, no written permission is necessary. This extends to the online version of your thesis and would include any version of the articles including the final published versions provided that they are not available as individual downloads but only embedded within the thesis itself.



# Effects of standoff distance on porosity, phase distribution and mechanical properties of plasma sprayed Nd–Fe–B coatings

Jo Ann Gan<sup>\*</sup>, Christopher C. Berndt

Industrial Research Institute Swinburne, Faculty of Engineering and Industrial Sciences, Swinburne University of Technology, Hawthorn VIC 3122, Australia

## ARTICLE INFO

### Article history:

Received 12 October 2011

Accepted in revised form 3 November 2012

Available online 23 November 2012

### Keywords:

Plasma spray

Microstructure

Porosity

Phase separation

Bimodal distribution

Weibull distribution

## ABSTRACT

Fabrication of components that require magnetic parts such as in micro motors and micro generators demands an alternative to micro machining processes that are costly and time consuming. In this study, Nd–Fe–B coatings with an average thickness of 200  $\mu\text{m}$  were deposited onto stainless steel substrates by an atmospheric plasma spray technique using amorphous feedstock powder of spherical morphology. The microstructure of the coatings shifted from lamellar to spherical in nature as standoff distance (SOD) increased. The total porosity of the coatings exhibited a minima with respect to SOD and ranged from 1.8 to 8.2%. Two distinct phases; i.e., the Nd-rich and Fe-rich phases, were observed and imply phase separation during the plasma spray process. Occurrence of phase separation was argued to arise due to metastable phase formation and non-equilibrium solidification. The Fe-rich phase increased with increasing SOD due to longer in-flight time allowing non-equilibrium solidification to occur. The presence of two phases results in a bimodal Weibull distribution for Vickers hardness data. However, Weibull plots for Knoop hardness and elastic modulus show monomodal behaviour. The correlation between the degree of data scattering, as reflected by the Weibull modulus, with porosity and phase percentage was determined.

© 2012 Elsevier B.V. All rights reserved.

## 1. Introduction

Neodymium iron boron (Nd–Fe–B) is a rare-earth transition-metal that is used in permanent magnet applications. It has the strongest magnetic properties among other hard magnets including samarium cobalt, alnico and ceramic magnets, which make it a desirable material when the performance and size of the magnet is of prime importance. Increasingly popular use of magnetic parts in minute components such as micro motors [1,2] and micro generators [3,4] has led to studies to improve methods used to fabricate magnetic films or coatings.

Preparation of magnetic films has involved physical processes such as sputtering [5,6], evaporation [7,8] and molecular beam epitaxy [9,10]. Films produced by these techniques have comparable magnetic properties as the bulk material. However, these techniques often produce thin films that do not exceed 5  $\mu\text{m}$  in thickness, and the process involves a long processing time. Other deposition methods including screen printing [11,12], tape casting [13,14], pulsed laser deposition [15,16] and thermal spray [17–19] have overcome these limitations.

Thermal spray has been used to deposit rare-earth magnetic coatings since the late 1970s [20,21]. Its ability to operate over a wide range of temperatures and demonstrate a high deposition rate proves to be effective in overcoming the limitations of other methods. Magnetic properties of samarium cobalt coatings deposited by plasma spray have been reported to be superior to its bulk counterparts, due to its

finer grain size. While Nd–Fe–B has stronger magnetic properties compared to samarium cobalt in its bulk form; the magnetic properties of plasma sprayed Nd–Fe–B coatings have not been optimized. Nd–Fe–B coatings have significantly lower intrinsic coercivity of 867.4 kA/m compared to 3979 kA/m of samarium cobalt coatings. In spite of the successful deposition of thick Nd–Fe–B coatings by controlled atmosphere plasma spray (CAPS) [22] and cold spray [23], the studies either (i) involve relatively expensive environment or (ii) produce coatings that exhibit significant defects.

There have been no reports on a systematic study of thermal spray coatings of Nd–Fe–B in the literature. Existing literature reports on the deposition process and resulting magnetic properties of the coatings neglect to address the effects of the spray parameters on other properties of the coatings; e.g., the mechanical properties. Most reports do not include the spray parameters used in the experiments, which makes it difficult to reproduce the Nd–Fe–B coatings. Important microstructural features of thermal spray coatings that play significant roles in the magnetic properties of a coating, such as porosity, have also not been reported in sufficient detail.

Porosity is considered as a microstructural defect that anchors the Bloch walls of a magnetic structure. Porosity prevents the continuity of magnetic properties throughout the coating and leads to an increase of coercivity. Cherigui and co-workers [24] established that an increase in standoff distance results in increased coercivity due to an increased porosity level, and that the correlation between the standoff distance and porosity is parabolic in nature. It is controversial which outcome, i.e., a low or high coercivity, is considered better performing. Improvement

<sup>\*</sup>

of coercivity values in soft magnetic materials is often associated with a decrease in porosity since the retainment of magnetism after the external magnetic field is removed is undesirable. On the other hand, applications that involve hard magnetic materials; such as those mentioned earlier – motor and generator, usually demand high coercivity for a longer lifetime.

This study is focused in developing suitable process conditions to deposit Nd–Fe–B coatings via atmospheric plasma spray. Variations in microstructural features, especially porosity and phase distribution, and mechanical properties of the coatings as a function of standoff distance are the primary concern of the present work. Magnetic data of the coatings are not presented since the current study is directed towards achieving coatings with a microstructure that are most likely to exhibit functional, extrinsic properties and to understand the behaviour of Nd–Fe–B feedstock that is processed by a thermal spray source. Moreover, the magnetic properties of the as-sprayed coatings are not the primary interest of this paper since they are expected to be improved via subsequent post-deposition heat treatments.

This paper also focuses on the mechanical properties of the Nd–Fe–B coatings since this is an important attribute for a coating that is used in a functional application. The primary potential applications for this coating are micro motor or micro generator, and these applications typically require certain endurance towards torque or force. However, most work in relation to Nd–Fe–B films/coatings primarily focuses only on their magnetic properties and rarely addresses issues concerning the films/coatings' practicality in relation to their mechanical attributes. Mechanical properties of the coatings are a simple and fundamental measure of the coating integrity. In this work, the mechanical properties have been analysed using the Weibull method of distribution analysis to determine the consistency and reliability of the properties throughout the coatings as a function of porosity and phase content.

## 2. Experimental methods

### 2.1. Feedstock material

The feedstock material used was a commercially atomized Nd–Fe–B powder supplied by Magnequench International Inc. (MQP S-11-9). The particle size of the feedstock was determined by a microscopy technique, where the diameters of 1000 particles were measured. The feedstock exhibited a spherical morphology with a mean particle size of 38.9  $\mu\text{m}$ ; more than 90% of the particles are within the range of 20–60  $\mu\text{m}$ , Fig. 1. The feedstock was analysed by an Oxford Instruments Inca X-act energy dispersive X-ray spectroscopy (EDS) and the elemental composition of the feedstock is shown in Table 1. A total of five spectra each were analysed on both the top surface and cross section of the feedstock. The EDS analyses show that the composition of the feedstock at the top surface and cross section is within the same range; as specified in Table 1. Boron was not detected due to limitations of the EDS

technique, however the composition was given as 0.5–1.8% by the manufacturer. Titanium and zirconium are present as additives to enhance the magnetic properties of the material. An X-ray diffraction (XRD) analysis reveals that the as-received feedstock is amorphous, Fig. 2. Most commercial magnetic powders are supplied in an amorphous form since rapidly quenched amorphous powders will provide superior magnetic properties compared to slowly quenched crystalline powders when the powders are subsequently sintered into magnet [25].

### 2.2. Plasma spray process

The as-received feedstock was fed internally to an SG-100 (Praxair Surface Technologies Inc., USA) atmospheric plasma spray torch and sprayed onto austenitic stainless steel 304 substrates (60  $\times$  30  $\times$  3 mm). The substrate was degreased and grit blasted with Black Beauty® abrasives (Burwell Technologies, NSW, AU) to obtain a surface roughness,  $R_a$ , of about 6  $\mu\text{m}$  prior to spraying. Spray parameters are listed in Table 2. All parameters were kept constant except for the standoff distance, which varied between 100 and 300 mm at 50 mm intervals. The coatings were produced by using a varying number of passes at different standoff distances to achieve a coating thickness of 200  $\mu\text{m}$ , due to varying deposition efficiencies at different standoff distances. The coatings were annealed in vacuum (<0.01 Pa) at 650  $^{\circ}\text{C}$  for 30 min.

### 2.3. Characterisation

The coating samples were prepared metallographically by sectioning the coatings in the direction perpendicular to the coating surface and cold mounted using epoxy. Mounted coating cross sections were polished to 1  $\mu\text{m}$  finish. A thin layer of gold film was sputtered-coated on all the samples prior to characterisation. Morphology and microstructure of the feedstock and coatings were observed using a ZEISS Supra 40 VP field emission scanning electron microscope (FESEM) while the chemical compositions were characterized by an in-built energy dispersive X-ray spectroscopy (EDS) unit. The coatings were characterized using the secondary electron (SE) mode of the FESEM; where a high accelerating voltage of 15 kV was used to discriminate phases via their contrast. A Bruker AXS D8 Advance X-ray diffractometer (XRD) with Cu  $K_{\alpha}$  radiation at 40 kV and 40 mA identified the phases present in the feedstock and coatings. The scanning step and sampling time employed were 0.01 $^{\circ}$  and 0.5 s, respectively.

The percentage porosity in the coatings was evaluated using Image Processing and Analysis in Java (ImageJ) software from the National Institutes of Health, Bethesda, MD [26]. The evaluation was carried out in compliance with Test Method B of standard ASTM E 2109 [27]. Twenty fields of random, non-overlapping SEM images at 1000 $\times$  magnification were used to obtain the average total porosity ( $P_t$ ) of the coatings. Critical threshold values were selected by sampling various threshold values and determining the threshold value where the number of

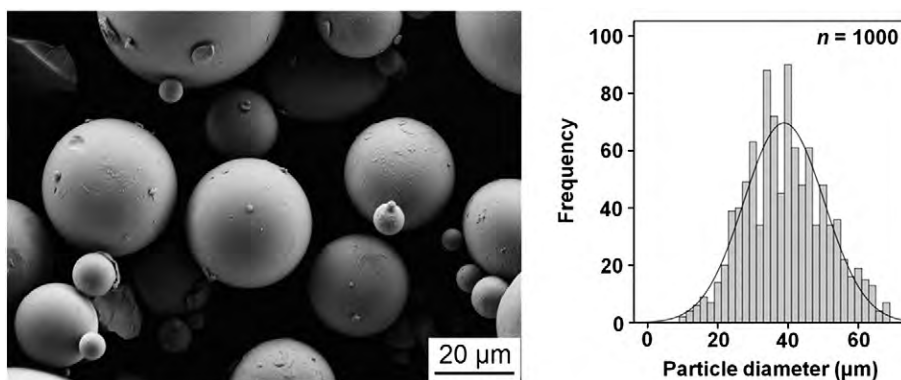


Fig. 1. Morphology and particle size distribution of Nd–Fe–B feedstock powder.

**Table 1**  
Elemental composition of Nd–Fe–B feedstock and plasma sprayed coatings (wt.%).

	Nd	Fe	B	O	Ti	Zr	C	Co	Pr
Feedstock									
As supplied	15.00–22.00	70.00–82.00	0.50–1.80	0.00	0.00–5.00	0.00–5.00	0.00–1.00	0.00–5.00	0.00–5.00
Measured	17.27–19.51	52.79–73.07	0.00	0.00	0.00–2.94	0.00–5.84	0.00–1.70	0.00–3.07	0.00–2.11
Coating									
Fe-rich (dark)	0.00–4.15	77.27–95.14	0.00	0.00–5.52	0.00–2.22	0.00	0.00–5.21	0.00–4.04	0.00–2.79
Nd-rich (light)	42.29–47.89	3.27–7.91	0.00	19.05–26.55	3.87–5.45	0.00–13.13	2.26–2.57	0.00	0.00–5.94
Unmelts	16.22–17.74	65.90–71.57	0.00	0.00	2.10–2.77	0.00	2.77–3.84	0.00	0.00–2.77

isolated bright pixels increased abruptly [28]. Globular pores ( $P_g$ ) were isolated from the crack network ( $P_{cr}$ ) by using the *opening* function; Fig. 3. Phase distribution within the coatings was evaluated using a technique similar to that as for porosity quantification by image analysis.

Vickers hardness values of the coatings were measured using a single load indentation under a 100 g load for 15 s. The indentations were made near the centre line of the coating thickness. A total of 30 measurements were carried out on the polished cross sections of each coating. The elastic modulus of the coatings was measured using the Knoop indentation technique developed by Marshall *et al.* [29]. A total of 30 indentations were made on each coating cross section with the major diagonal perpendicular to the substrate. Statistical analysis on the basis of the Gaussian and Weibull distributions was performed on the hardness and elastic modulus data.

### 3. Results and discussion

#### 3.1. Microstructure

Cross sections of Nd–Fe–B plasma sprayed coatings deposited at various standoff distances (SOD) are shown in Fig. 4(a), (b), (c), (d) and (e). The coatings sprayed at SOD 100, 150, 200, 250 and 300 mm will be referred to as coatings A, B, C, D and E respectively herein. The coatings have an average thickness of 200  $\mu\text{m}$ , which is substantially thicker than previously reported for flame sprayed coatings of the same material [30]. Microstructural features of the coatings, including splats, macro and micro cracks, porosity and unmelts were examined critically as a function of the SOD since they each have vital roles in governing the intrinsic as well as extrinsic properties of the coatings.

The presence of individual pan-cake like splat layers can be observed in the coating cross sections; Fig. 4. The splat layers become less distinct as SOD increases. At lower SOD, a lamellar-type structure as shown in

Fig. 5(a) is mainly observed in the coatings (coatings A and B). This suggests that at SOD 100 and 150 mm the particles are already molten or semi-molten. However, the splat layers in coating A were distinguished to be thicker than those in coating B, indicating that SOD 150 mm provided better melting while particles at SOD 100 mm were only partly molten. As SOD increases beyond 200 mm, the structure of the coatings undergoes a transition from lamellar-type to spherical-type; Fig. 5(b). Such observation indicated that there was coalescence and resolidification of some particles during in-flight at a higher SOD; i.e., from 200 mm onwards. Similar lamellar and spherical structures have been described by Chen *et al.* [6] for the magnetic domain patterns in Nd–Fe–B films as being strip-like and cloud-like, respectively, whereby cloud-like domains correspond to a higher level of disorder and hence harder magnetic properties. Therefore, it is expected that lamellar and spherical structures observed here will follow a similar trend. However, further validation of the relationship between the type of structure and magnetic domain pattern is necessary.

The character of the microstructure allowed a qualitative determination of the coating adhesion and cohesion since the mounting and polishing preparation stages can be quite aggressive. All coatings exhibited microstructures that were indicative of good adhesion and cohesion, with the exception of coating A that demonstrated poor cohesion. Coating A revealed the presence of a continuous horizontal macro crack along the first few layers of splats. Such cracking could form as a consequence of high thermal and quenching stress experienced by coatings deposited at short SOD. The high thermal stress resulted from the high thermal flux [31] at a short standoff distance while quenching stresses developed as a consequence of high thickness per pass [31] at a short standoff distance due to incomplete melting and flattening of splats.

The extent of cracking could also be influenced by the level of porosity and presence of metastable phases in coatings. There is also the possibility of cracking due to post-deposition processing. However, given that the post-processing procedures were identical for all coatings, it is highly unlikely for the crack to be an artefact of post-deposition processes. Regardless, the presence of the continuous crack in coating A but not in the other coatings poses concern because it leads to a cohesion failure issue and eventually delamination of the coating; Fig. 4(f). Fine intersplat micro cracks perpendicular and parallel to the spray directions were also observed in all coatings. These cracks arise probably due to

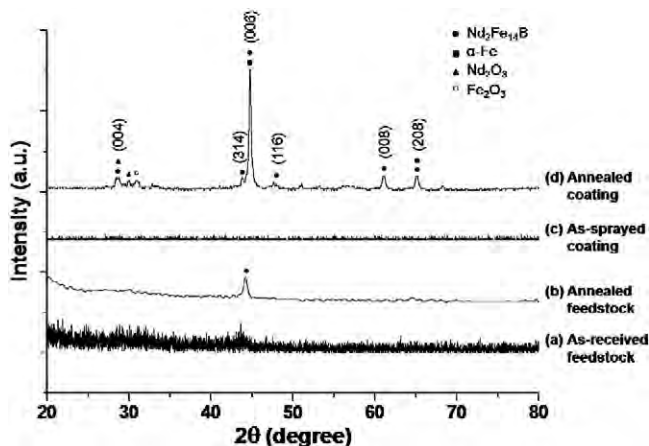


**Fig. 2.** X-ray diffraction (XRD) patterns of (a) as-received feedstock, (b) feedstock annealed at 650 °C, (c) as-sprayed coating and (d) coating annealed at 650 °C.

**Table 2**  
Experimental parameters for plasma spraying of Nd–Fe–B coatings.

Current (A)	750
Voltage (V)	40
Primary gas flow, Ar (slpm)	39
Secondary gas flow, He (slpm)	22
Carrier gas flow, Ar (slpm)	15
Feed rotation (rpm)	3.5
Feed rate (g/min)	30
Standoff distance (mm)	100–300
Torch traverse speed (mm/s)	100
No. of passes	20–50



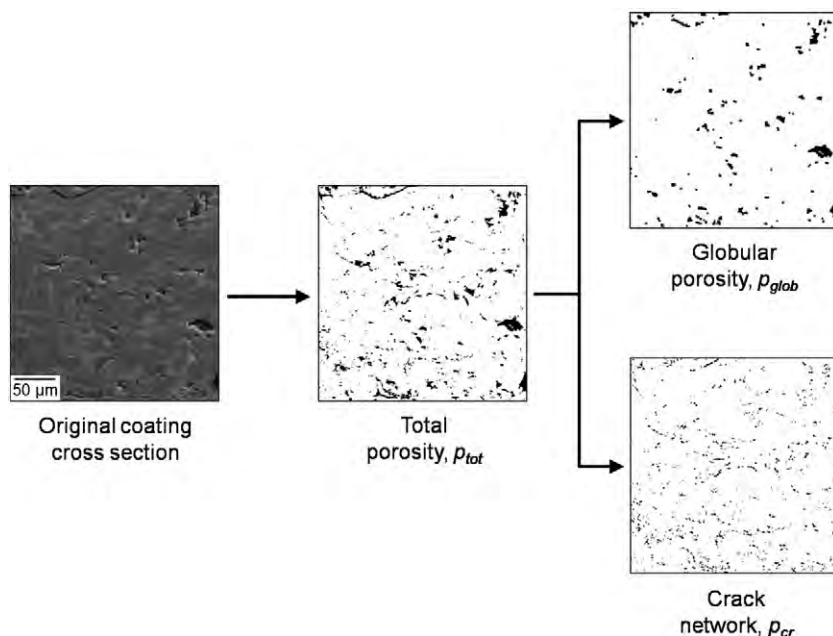


Fig. 3. Isolation of globular pores and crack network from total pores by image analysis.

stress alleviation during cooling or anisotropic thermal expansion among the different phases in the coating, and were accounted for as a part of the porosity and crack network – see Section 3.2.

Spherical inclusions, marked as *U* in Fig. 4, were observed in the coating cross sections. The spherical inclusions were confirmed to be unmelts and not resolidified particles by comparing the cross section of these inclusions with that of the feedstock (not shown). In addition, the EDS analysis on the spherical inclusions revealed that they exhibit the same composition as the feedstock and do not show any presence of oxygen, Table 1. Note that these spherical inclusions identified as unmelts are different than the resolidified particles mentioned earlier in this section. Resolidified particles imply that these particles have been melted during in-flight, and undergo phase separation, which will be discussed in Section 3.3. To put it simply, the resolidified particles will appear to have a distinct phase contrast when observed in the coating cross sections (labelled *R* in Fig. 4).

Large unmelts with diameter greater than 50 µm were observed in coatings C, D and E while unmelts observed in coatings A and B were generally smaller with diameters of ~20 µm. Note that the cross section images of coatings A and B are of different magnifications than the images of coatings C, D and E. Unmelts of ~20 µm in diameter were present in coatings A and B since some of the particles could be travelling at the periphery of the plasma plume instead of the ideal centreline trajectory for particles of this size. The presence of large unmelts in coatings deposited at SOD 200 mm and greater, but not in coatings deposited at shorter SOD contradicts the belief that a longer in-flight time attest to better particle melting. A possible explanation for this observation is that large unmelts are also present at SOD 150 mm and shorter. However, these large unmelts were not found in the cross sections of coatings A and B because these particles were either (i) rebounded off the substrate or previously formed splat layers; or (ii) flattened to what appeared to be partially molten splats (denoted by *M* in Fig. 4) when there was sufficient momentum.

At longer SOD, the spherical shape of the unmelts were retained and the particles were not flattened to form *M* because the particle velocity decreased with the increase of SOD and therefore the particles did not have the sufficient momentum to flatten upon impact. The retention of unmelts at longer SOD was also attributed to the decrease in thermal energy density [32] and the higher heat capacity of larger particles [32,33]. The number of unmelts retained and the decrease of splat

flattening as SOD increased has contributed towards the increase of the porosity level and subsequently deteriorated the mechanical properties of the coatings, which will be discussed in the following sections.

### 3.2. Porosity

The importance of porosity in a magnetic structure has been emphasized in the Introduction section. In thermal spray coatings, pores are typically formed as a result of (i) curling up of splats due to thermal stresses or surface tension of molten splats; (ii) entrapment of gas under impacting particles; or (iii) incomplete filling of crevices or surface irregularities among previously formed layers. Surface irregularities could stem from (i) the rough, grit blasted substrate; (ii) the presence of unmelts; or (iii) solidified satellite droplets that are detached from droplets impacting on the substrate [34].

From the cross sections of the coatings (refer to Fig. 4), it can be observed that coatings A, D and E comprised large globular pores and micro cracks while coatings B and C were relatively dense with the presence of smaller globular pores and a crack network. Total porosity decreased drastically from 7.1% to 1.8% when the SOD increased from 100 to 150 mm. The high level of porosity in coating A can be justified by the lower degree of melting due to a shorter in-flight time compared to coating B. Flattened partially molten splats can be clearly distinguished in Fig. 4(a) where the splats are thicker than the fully molten splats observed in Fig. 4(b). At SOD beyond 150 mm, the molten particles began to resolidify due to the drop in plume temperature at distances further away from the plasma torch, and this results in an increase in the porosity level. The change in the porosity level from SOD 150 to 250 mm is not significant suggesting that the resolidification rate is low within this range. A further increase of SOD to 300 mm resulted in a rise in total porosity to 8.2% since the particles resolidify at a much higher rate; presumably due to a greater drop in plume temperature beyond this point. The presence of large unmelts in coatings C, D and E, as discussed in the previous section, also contributed towards the rise in porosity level.

Sobolev and Guilemany [35] proposed that there are two types of pores: (i) large pores found between flattened particles, referred to as closed or globular pores, which are formed from gas porosity and (ii) smaller pores within the flattened particles, which are referred to as open pores or crack network, that arise from shrinkage porosity. Isolation and quantification of these two types of pores allow the identification of



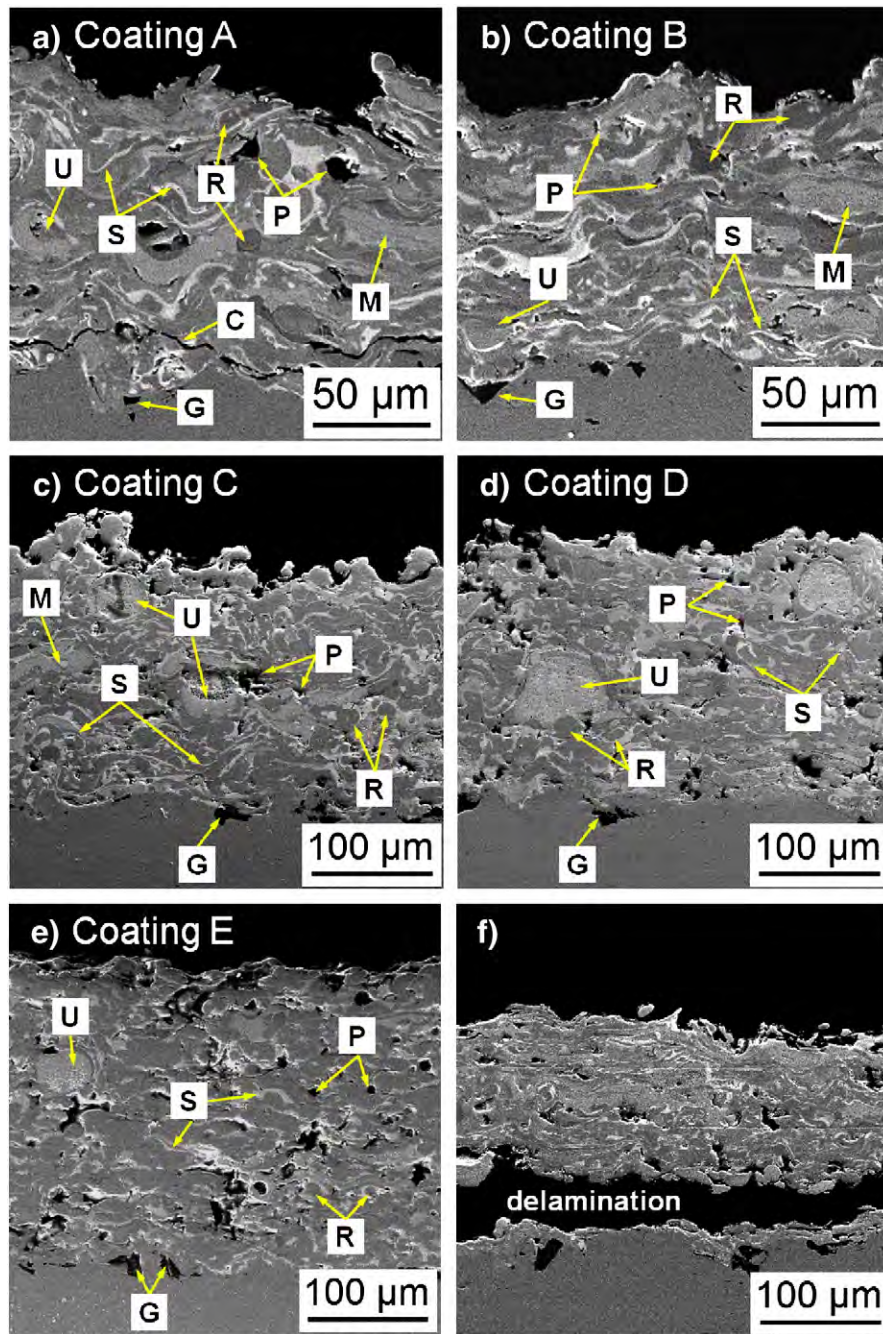


**Fig. 4.** Cross sections of Nd–Fe–B coatings deposited at standoff distances (a) 100 mm, (b) 150 mm, (c) 200 mm, (d) 250 mm, (e) 300 mm and (f) delamination of coating A. C = crack, G = embedded grit, M = partially molten splat, P = pore, R = resolidified particle, S = splat and U = unmelt.

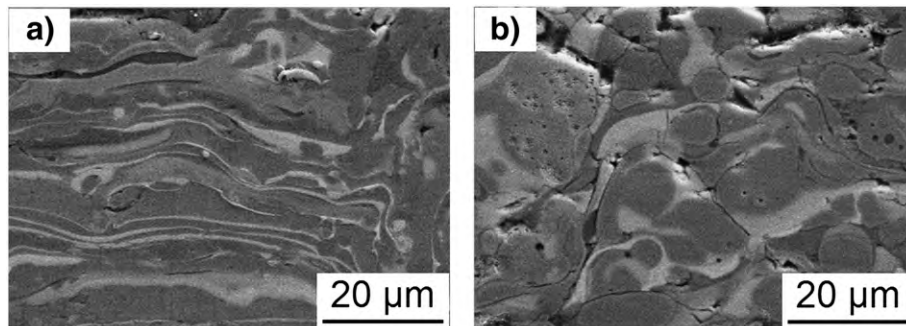


**Fig. 5.** Transition of (a) lamellar-type structure at standoff distance 100 mm to (b) spherical-type structure at standoff distance 300 mm.

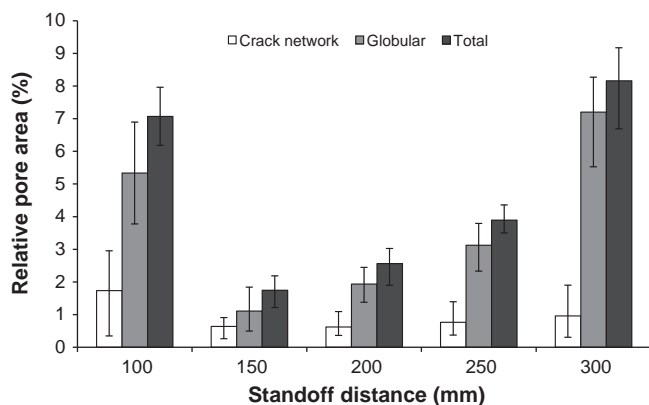


Fig. 6. Variation of percentage pore area with respect to standoff distance.

the pore architecture as well as the dominant mechanisms involved in pore formation associated with that particular set of spray parameters. This information will lead to an understanding of the particle behaviour on impact with the substrate; i.e., spreading, fragmentation and splashing; and ultimately allow the construction of coatings with the desired pore architecture and porosity level.

The procedure to isolate globular pores and crack network (inter- and intralamellar) from total porosity is indicated in Fig. 3. Fig. 6 shows the variation of globular pores, crack network and total porosity with SOD. Changes in both globular pores and crack network with SOD followed the trend of total porosity; a significant decrease from coating A to coating B followed by a gradual increment from coating B to coating D, and then increasing from coating D to coating E.

As mentioned earlier in this section, the decrease of porosity from coating A to coating B arose from the more complete melting of particles with increased SOD; i.e., longer in-flight time. Particles at SOD 100 mm are only partially molten when they impact the substrate and this led to a low degree of flattening and spreading of splats. This resulted in poor filling of surface irregularities and gave rise to globular pores. It can be argued that the low degree of flattening and spreading of splats of coating A led to a higher coating thickness per pass, and therefore yielded a greater quenching stress [31] compared to coating B. In addition, the greater thermal flux at shorter SOD caused a higher thermal stress in coating A due to the greater temperature difference upon impact [31]. Therefore, the greater residual stress; i.e., combination of quenching stress and thermal stress, in coating A consequently promoted the formation of inter- and intralamellar cracks.

Increasing SOD beyond 150 mm brought about a drop in particle temperature that consequently resulted in an increase in the molten particle viscosity and thus a decrease in particle fluidity. Reduced particle fluidity led to poor particle spreading upon impact and, therefore, the inability to

fill surface irregularities on the previously formed layer. This resulted in the formation of stacking defects and increased globular pores. The decrease in particle temperature with SOD also caused the in-flight particles to resolidify and as these resolidified particles impact and subsequent layers are formed, shadow effects developed and contributed towards globular pores. The degree of crack network in coatings B, C and D is comparable, which suggested that the interlamellar contact and quenching stresses within these coatings were similar to each other.

The higher particle temperature at SOD 100 mm compared to 300 mm is anticipated to result in lower surface tension, hence higher particle fragmentation. The higher degree of particle fragmentation in coating A can be observed in the top surface of the coating, Fig. 7. Particle fragmentation tended to reduce shrinkage upon solidification and quenching stresses [36], and therefore coating A was expected to have reduced inter- and intralamellar cracks. However, this was not observed and instead the average percentage of crack network in coating A was higher than in coating E despite the fact that coating E revealed a higher level of total porosity. The implication is that the quenching stress reduction from particle fragmentation was insufficient to compensate for the greater quenching stress and thermal stress in coating A; these effects result from the higher thickness per pass, higher particle temperature and shorter solidification time.

### 3.3. Phase distribution

Cross sections of plasma sprayed Nd–Fe–B coatings, Fig. 4, revealed that the coatings were inhomogeneous, with the presence of two distinct phases. Using EDS analysis, the dark phase was identified as a Fe-rich phase while the lighter phase was an Nd-rich phase. The lighter phase consisted of more than 40 and 19 wt.% of neodymium (Nd) and oxygen, respectively, with traces of iron and additives such as titanium (Ti), zirconium (Zr), cobalt (Co) and praseodymium (Pr). On the other hand, the darker phase contained more than 77 wt.% of iron and only traces of neodymium, oxygen and similar additives; with the exception of zirconium which was not detected in the Fe-rich phase. The unmelts retained the composition of the original feedstock. The compositions of Nd-rich and Fe-rich phases as well as unmelts in the coatings are shown in Table 1. Note that there are limitations for employing EDS for quantitative analysis. In this work EDS analysis was mainly used to distinguish the difference in composition of the main elements, i.e., neodymium and iron, in various regions of the coatings, and was not used to calculate the stoichiometric compositions.

The distribution of the two phases and total porosity in each coating was quantified by varying the threshold level using a technique similar to that for porosity determination and is shown in Fig. 8. The percentage of Nd-rich and Fe-rich phases does not vary significantly with an increase of 50 mm in SOD; i.e., coatings A and B as well as coatings C and D have approximately the same level of Nd-rich and Fe-rich

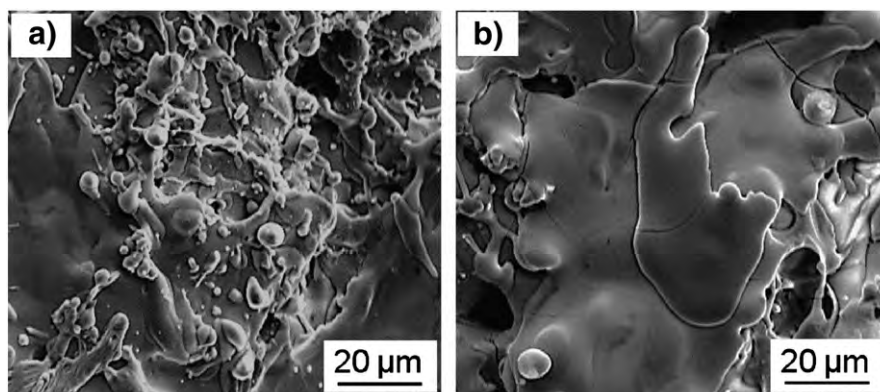


Fig. 7. Top surface view showing particle fragmentation in (a) coating A compared to (b) coating E.



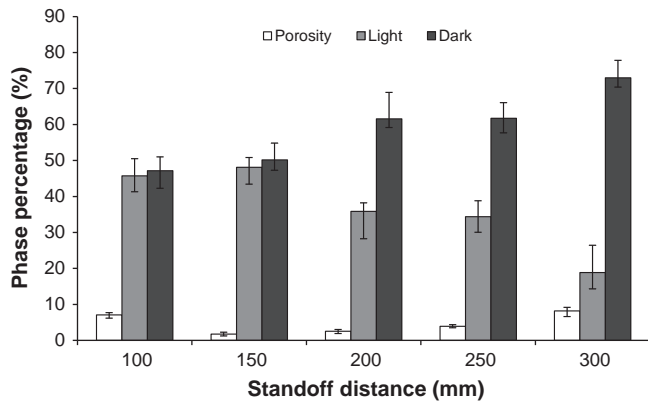


Fig. 8. Relative phase distribution in Nd–Fe–B coatings as a function of standoff distance (SOD).

phases. However, at the 100 mm SOD interval, the dark Fe-rich phase increased by more than 10%, accompanied by a decrease in the light Nd-rich phase. An increase in the Fe-rich phase with SOD was attributed to the increase of the in-flight time; i.e., the molten droplets have more time to undergo phase separation. The increase of the dark phase with SOD can be observed on the coating cross sections (refer to Fig. 4).

The XRD patterns of the as-sprayed and annealed coatings are shown in Fig. 2(c) and (d). There was no distinguishable difference in the XRD patterns for coatings deposited at different SODs, therefore only one spectrum is presented. The phases observed include neodymium iron boron,  $\text{Nd}_2\text{Fe}_{14}\text{B}$ ; alpha iron,  $\alpha\text{-Fe}$ ; neodymium oxide,  $\text{Nd}_2\text{O}_3$  and iron oxide,  $\text{Fe}_2\text{O}_3$ . After annealing, the coatings were crystallized and the primary phase was the tetragonal  $\text{Nd}_2\text{Fe}_{14}\text{B}$ . The major  $\text{Nd}_2\text{Fe}_{14}\text{B}$  peaks that demonstrate the strongest intensity were observed at reflections of the (004), (006) and (008) planes, indicating that the coating crystallography was dominated by the  $\langle 001 \rangle$  texture. In other words, the coatings have the  $c$ -axis aligned in the direction perpendicular to the coating plane. The easy axis of magnetisation for the Nd–Fe–B alloys occurs when the  $c$ -axis is oriented in the direction of the tetragonal structure [37]. Other peaks of the  $\text{Nd}_2\text{Fe}_{14}\text{B}$  phase with weaker intensity that were also observed are the (314), (116) and (208) peaks. In addition to the strong  $\langle 001 \rangle$  texture observed, the absence of the (410) peak, which is the most intense peak in the tetragonal  $\text{Nd}_2\text{Fe}_{14}\text{B}$  phase based on randomly oriented grains [38], further confirmed that the coatings were anisotropic.

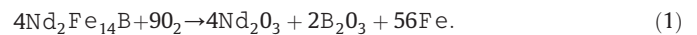
The intensity of the (006) peak was higher than that of the other peaks. This implies that part of the peak could be contributed by the  $\alpha\text{-Fe}$  (110) plane at  $44.7^\circ$ ; i.e., the superposition of the  $\text{Nd}_2\text{Fe}_{14}\text{B}$  (006) and  $\alpha\text{-Fe}$  (110) peaks. This is supported by the presence of the  $\alpha\text{-Fe}$  (200) peak at  $2\theta$   $65.1^\circ$ . The  $\alpha\text{-Fe}$  (110) plane has been known to exhibit high scattering intensity; therefore a small amount of iron can contribute to a large increase in intensity [39]. The presence of the  $\alpha\text{-Fe}$  phase could result from the metastable phase formation and non-equilibrium solidification, where Fe-rich phase has separated from the Nd-rich phase during plasma spray processing.

Such phase separation has been observed in previous works [19,30]. The unique nature of the thermal spray process where deposits are rapidly solidified upon impact with the substrate results in a metastable phase formation, as was the case in the plasma sprayed Nd–Fe–B coatings. Instead of solidifying to the stable  $\text{Nd}_2\text{Fe}_{14}\text{B}$  ( $\varphi$ ) phase, rapid heating and solidification involved in the plasma spray process led to the formation of the metastable phase,  $\text{Nd}_2\text{Fe}_{18}\text{B}$  ( $\chi$ ) [40]. Under normal circumstances; i.e., without the presence of oxygen as it should be in a typical Nd–Fe–B alloying process, this metastable phase that forms (if at all) will eventually decompose to  $\text{Nd}_2\text{Fe}_{14}\text{B}$  ( $\varphi$ ) and Fe since this is the stable phase for Nd–Fe–B. However, in the presence of oxygen under the atmospheric plasma spray process, the oxygen “pulls” Nd from its lattice since Nd is prone to oxidation. The oxidation of Nd led to the formation of

$\text{Nd}_2\text{O}_3$  and left behind Fe and  $\text{NdB}_4$ , thus forming the Nd-rich ( $\text{Nd}_2\text{O}_3$  and  $\text{NdB}_4$ ) and Fe-rich phases. This justification is supported by the fact that only traces of oxygen were detected in the Fe-rich region while the Nd-rich region consisted of more than 19 wt.% of oxygen. In the metastable condition, the remainder of Nd and B formed  $\text{NdB}_4$  [40] and since boron could not be detected by EDS due to the overlapping spectra with carbon, this was designated as an Nd-rich phase. The  $\text{NdB}_4$  phase was not observed in the XRD diffraction patterns because this phase eventually formed the  $\text{Nd}_2\text{Fe}_{14}\text{B}$  phase with Fe upon heat treatment. Trace amounts of Nd in the Fe-rich region and Fe in the Nd-rich region suggested that a ternary Nd–Fe–B phase was present in the coatings. This ternary phase arose from incomplete oxidation of the material prior to impact and therefore was not phase separated. The ternary phase subsequently crystallized into the  $\text{Nd}_2\text{Fe}_{14}\text{B}$  phase upon post-deposition heat treatment, Fig. 2(d).

Rare-earth elements are prone to oxidation. At the high temperatures experienced in the plasma spray process and within an atmospheric environment, the extent of the Nd–Fe–B oxidation observed was low. Low Nd–Fe–B oxidation was observed because of the short in-flight time, in the order of fractions of a millisecond; and rapid solidification, in the order of microseconds. The overall oxygen content within the coatings ranged from less than 6.00 to almost 16.00 wt.%. Oxygen was detected in the Nd-rich phase but not in the Fe-rich phase and suggested that Nd was more susceptible to oxidation than Fe. Although the Nd-rich (oxidation prone) phase decreased with the increase of SOD, the oxygen content did not decrease. Instead, the overall oxygen content was found to increase with SOD as expected, considering the longer in-flight time and hence more exposure to oxygen.

Edgley *et al.* [41] detailed an oxidation process for Nd–Fe–B that was supported by Li *et al.* [42]. Li *et al.* [42] proposed an overall oxidation reaction, Eq. (1). The reaction involved dissociation of Nd–Fe–B followed by the oxidation of Nd and B. Note that Eq. (1) serves as a reference for the oxidation mechanism of  $\text{Nd}_2\text{Fe}_{14}\text{B}$  under stable conditions; i.e., the  $\text{Nd}_2\text{Fe}_{14}\text{B}$  was maintained in solid state at a temperature of less than  $600^\circ\text{C}$  [41,42]. The products of dissociation and oxidation for the solid state oxidation studies differed slightly than that suggested for the metastable phase formation in the present study wherein  $\text{B}_2\text{O}_3$  was formed in the solid state condition instead of  $\text{NdB}_4$ . In the present study, the particles were melted at high temperature in the plasma plume and underwent metastable phase formation and, therefore,  $\text{NdB}_4$  [40] was formed in preference to  $\text{B}_2\text{O}_3$ . Despite the different final products of oxidation, both the equilibrium and metastable phase transformation underwent similar oxidation mechanisms of dissociation followed by oxidation. The absence of oxygen in unmelts (Table 1) indicated that the in-flight time and the duration before the next layer was formed were too short to render oxidation in the unmolten state possible although the processing temperature was sufficiently high.



In addition to the formation of the metastable phases and the oxidation reaction, the difference in melting point of Nd and Fe resulted in non-equilibrium resolidification of the particles during in-flight, which also contributed to the phase separation. In non-equilibrium solidification, elements within an alloy were distributed non-uniformly where the higher melting point element was concentrated in the centre of the droplet since this region was the first to resolidify. In this case, the higher melting point Fe segregated in the centre of the molten droplet forming an Fe-rich core while surrounded by the lower melting point Nd-rich region. Referring back to Fig. 5, the microstructure of the coatings shifted from a lamellar-type to spherical-type as SOD increased. The spherical sections shown in Fig. 5(b) are the dark, Fe-rich regions. This further reinforces the statement that non-equilibrium solidification has occurred in-flight.

At shorter SOD, non-equilibrium solidification initiated. However, before solidification occurred in-flight, the particles that have already

separated into Fe-rich and Nd-rich regions but still remain molten, impacted onto the substrate and solidified, forming a lamellar structure. At higher SOD, the particles with a separated region have more time to solidify during in-flight and by the time the particles impact onto the substrate, the Fe-rich core has already solidified with the surrounding Nd-rich region still remaining molten; hence the spherical structure. A higher degree of melting at high SOD also indicated the possibility of coalescence during in-flight or upon impact onto the substrate; which also contributed towards the spherical-type structure and more well-connected dark phase observed at the coating cross sections.

### 3.4. Mechanical properties and statistical analysis

#### 3.4.1. Bimodal distribution of Vickers microhardness

Thermal spray coatings are generally anisotropic and heterogeneous in nature, thus causing a wide scatter in the hardness values. This microstructural effect will be analysed statistically using Gaussian and Weibull distributions. The statistical analysis of the Vickers microhardness data for each coating is summarized in Table 3.

In spite of the large scatter, a trend in the hardness values with respect to SOD can be observed. The mean Vickers hardness of the coatings increased from 668 to 691 kgf/mm<sup>2</sup> when SOD increased from 100 to 150 mm and then decreased from 150 mm onwards. This trend can be explained by referring to the porosity level of each coating. As porosity level increased, the stiffness of the coating was lowered [43]. Porosities tend to constrain the elastic recovery of the indents, hence resulting in the low hardness value [44]. Coating B (sprayed at SOD 150 mm), which exhibited the lowest total porosity of 1.8%, revealed the highest hardness value of 691 kgf/mm<sup>2</sup>. On the other hand, coating E (sprayed at SOD 300 mm) had the lowest hardness value of 556 kgf/mm<sup>2</sup> corresponding to its high porosity level (8.2%). The hardness range determined is comparable to several values reported for the Nd–Fe–B bulk material [45–47] but is slightly lower than that reported by Ahmed *et al.* [48].

A variation of Fe-rich and Nd-rich phases with SOD also contributed towards the coating hardness. The Fe-rich phase exhibited a higher hardness compared to the Nd-rich phase [30]. Therefore, an increase of the Fe-rich phase in a coating is expected to bring about an increase in the hardness value. Since the percentage of the Fe-rich phase in the coatings increased as SOD increased, it is expected that the hardness value would increase. However, this was not observed. Instead, the increase of hardness occurred concurrently with the increased Nd-rich phase. The effect of porosity level dominated over the role of the Fe-rich phase increment on microhardness.

Coating A exhibited a hardness value slightly higher than coating D (668 compared to 640 kgf/mm<sup>2</sup> respectively) although the total porosity of coating A is higher by 3.2%. This behaviour could be explained by differences in the coating microstructure. Coating A revealed a lamellar microstructure whereas that of coating D shifted more towards a spherical type. In other words, coating A demonstrated better interlamellar contact despite revealing a higher porosity level.

The hardness value reported up to this point is based on the assumption that the data follows a Gaussian distribution. However, the

heterogeneity of thermal spray coatings and the presence of features such as pores and cracks often result in positively skewed distributions [49]. Analyses have shown that the coating microhardness at all SODs do not fit Gaussian distributions. The microhardness data for all coatings were positively skewed while the kurtosis of the data also showed that the microhardness values do not fit Gaussian distribution, for which the kurtosis should ideally be zero, Table 3. Thus, mean and standard deviation alone are insufficient to describe the mechanical properties of thermal spray coatings.

The Weibull distribution (or failure probability function), which is based on the weakest link theory, has been shown to be more appropriate to describe the mechanical properties of thermal spray coatings due to the presence of defects such as pores and cracks that are bound to cause a higher probability of failure [50,51]. The derivation of the Weibull modulus can be used to describe the variability of a material's mechanical properties. A higher Weibull modulus indicates that the material has lower variability in the measured mechanical property. The two-factor Weibull plots for the Vickers microhardness data of plasma sprayed Nd–Fe–B coatings are given in Fig. 9(a), (b), (c), (d) and (e).

The microhardness Weibull plots for each coating revealed bimodal distributions with two unique Weibull moduli. The Weibull moduli ( $m$ ) and characteristic values ( $x_0$ ) of each coating are summarized in Table 3. Although a bimodal distribution could result from the use of a small indentation test load [51], the bimodal behaviour observed here arose from the hardness difference of the two distinguishable phases; i.e., Fe-rich and Nd-rich phases. The hardness value would be higher in the region with a higher concentration of the Fe-rich phase. Such bimodal Weibull distributions have also been observed in nanostructured and multi-modal coatings [52,53], although the bimodal behaviour was more attributed to the mixture of molten and unmolten particles in the coating rather than two distinct phases.

The slopes of the Weibull plots were determined by analysing the coefficient of determination,  $R^2$  values of two linear lines on each  $\ln[1/(1 - P_i)]$  vs.  $\ln(HV)$  plot with ascending  $n_1$  and descending  $n_2$  for all 30 measurements. The point where the largest  $R^2$  values for both lines intercept is the transition point where both data sets are statistically more significant than the other [52]. The Weibull modulus attributed to the Nd-rich phase ( $m_1$ ) generally decreased as the SOD increased, while the Weibull modulus associated with the Fe-rich phase ( $m_2$ ) increased with SOD. The  $m_1$  of coating E is large due to the limitation of the Nd-rich area to be tested where the phase percentage is well below 20%. The correlation between both Weibull moduli with porosity and the phase percentage will be discussed in Section 3.4.3.

#### 3.4.2. Knoop microhardness and elastic modulus

The statistical analysis of the Knoop hardness and elastic modulus of the coatings are summarized in Table 4. Similar to the Vickers hardness, the Knoop hardness also increased from SOD 100 to 150 mm then decreased from 150 mm onwards. As mentioned previously, porosity plays an important role in determining the hardness value. However, the Weibull plot of Knoop hardness, shown in Fig. 10(a), does not reveal a bimodal distribution. This could be attributed to the geometry of the indenter. Since Knoop hardness is determined by measuring its major

**Table 3**  
Statistical analysis for Vickers microhardness values of plasma sprayed Nd–Fe–B coatings.

Sample/SOD (mm)	Gaussian distribution					Weibull distribution					
	$\mu$ (kgf/mm <sup>2</sup> )	$\sigma$ (kgf/mm <sup>2</sup> )	CV (%)	Skewness ( $\pm 0.4^a$ )	Kurtosis ( $\pm 0.8^a$ )	$n_1$	$m_1$	$x_{0(1)}$ (kgf/mm <sup>2</sup> )	$n_2$	$m_2$	$x_{0(2)}$ (kgf/mm <sup>2</sup> )
A – 100	668	80	11.94	0.416	–0.404	8	22.6	626	22	7.4	699
B – 150	691	86	12.51	0.817	–0.106	8	24.3	654	22	6.1	718
C – 200	673	84	12.49	0.616	0.045	8	19.0	643	22	6.7	704
D – 250	640	80	12.49	0.523	0.214	10	16.2	621	20	6.7	669
E – 300	556	53	9.59	0.222	–1.152	5	49.0	509	25	9.4	578

<sup>a</sup> Refers to the standard error.

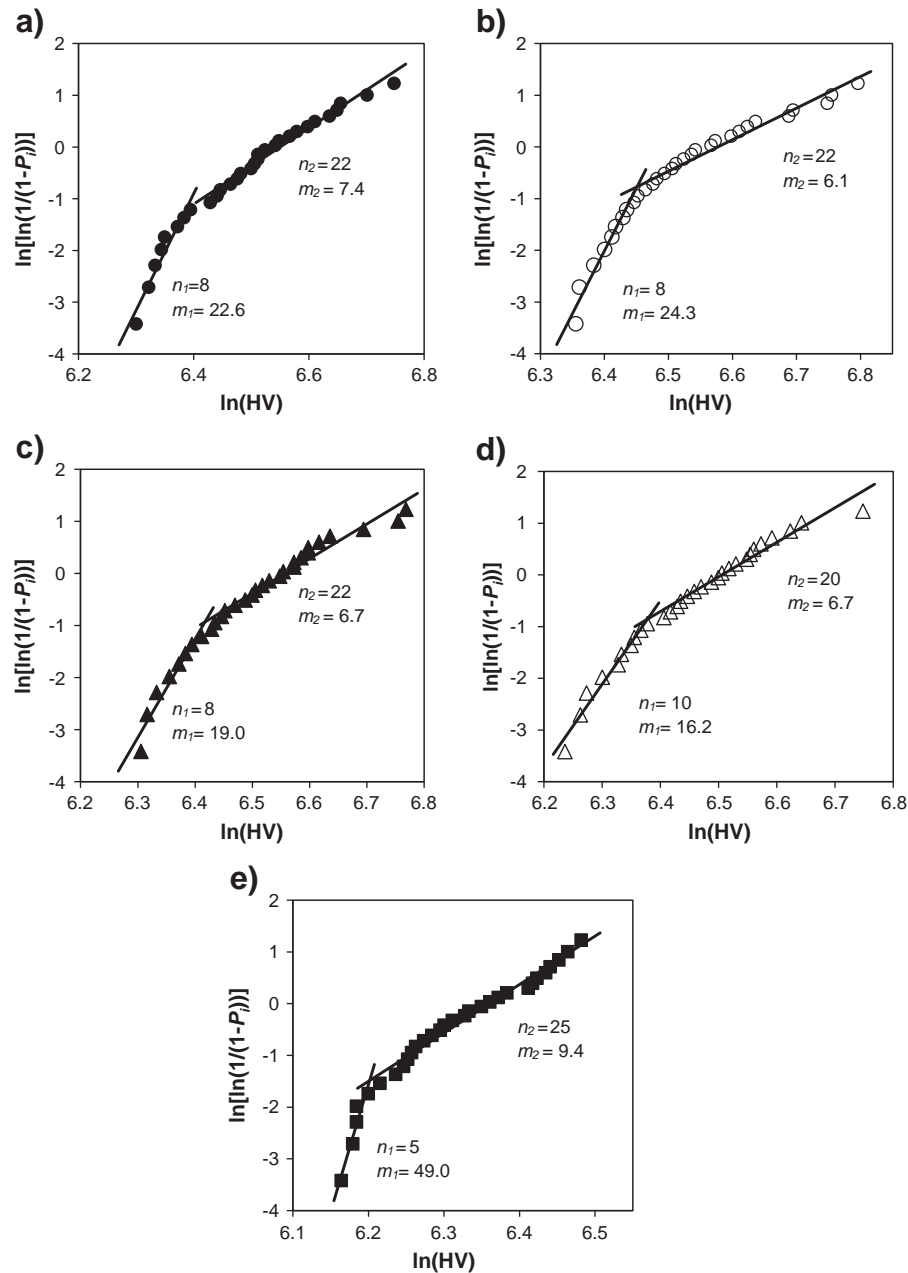


Fig. 9. Weibull plots for Vickers hardness for Nd-Fe-B coatings plasma sprayed at (a) 100 mm, (b) 150 mm, (c) 200 mm, (d) 250 mm and (e) 300 mm.

diagonal, and the indent was made with its major diagonal perpendicular to the substrate, both Fe-rich and Nd-rich phases were measured in a single indent. On the contrary, the geometry of the Vickers indent does not produce as large an areal impression on the coating thickness, but is more localised and hence detects the hardness difference of the two phases.

Studies have shown that the use of Knoop indentation to measure the elastic modulus of the thermal spray coatings revealed different results when measured parallel (cross section direction) and perpendicular (in-plane direction) to the surface due to the anisotropic nature of the coatings [54–57]. The dependency of the coating mechanical properties on the measurement direction was determined by the amount and morphology of pores and cracks in the coatings; i.e., the relative crack density caused by: (i) horizontal interlamellar pores and cracks and (ii) vertical intrasplat cracks [58]. For most thermal spray coatings, the microhardness and elastic modulus measurements on the cross sections

produce higher values than the in-plane direction [54–57]. Such anisotropic behaviour is rendered by the fact that the pores are built up by the in-plane surface while the cracks mainly occur in the cross section direction. Since the pores exhibited a greater total surface area than the cracks, then the mechanical properties were lower in the direction of the in-plane surface [54].

Indents with their major diagonal parallel to the substrate were correlated to the indenter load when measurements were performed parallel to the deposition surface. The resulting elastic modulus was greater than when the indents were located with the major diagonal perpendicular to the substrate. This statement can be explained by sliding phenomenon of the interlamellar boundary. The elastic modulus measured by the Knoop indentation relied on the recovery of the minor diagonal. In the case where the major diagonal is parallel to the substrate and interlamellar boundary, the interlamellar boundary sliding occurred more readily and, therefore, resulted in a shorter minor

**Table 4**  
Statistical analysis for microhardness and elastic modulus values of plasma sprayed Nd–Fe–B coatings from Knoop micro indentation.

Sample/SOD (mm)	Hardness, KHN						Elastic modulus, E (GPa)							
	Gaussian distribution					Weibull distribution	Gaussian distribution					Weibull distribution		
	$\mu$ (kgf/mm <sup>2</sup> )	$\sigma$ (kgf/mm <sup>2</sup> )	CV (%)	Skewness ( $\pm 0.4^a$ )	Kurtosis ( $\pm 0.8^a$ )		$\mu$ (GPa)	$\sigma$ (GPa)	CV (%)	Skewness ( $\pm 0.4^a$ )	Kurtosis ( $\pm 0.8^a$ )	$m$	$x_0$ (GPa)	
A – 100	616	90	14.59	0.235	–0.902	7.5	655	85.6	33.6	39.30	0.468	–0.814	2.7	96
B – 150	653	68	10.44	–0.323	–0.878	10.4	684	142.7	41.5	29.10	0.023	–0.905	3.6	158
C – 200	571	62	10.93	0.496	0.407	10.1	598	142.2	46.8	32.94	0.241	–0.918	3.2	159
D – 250	565	71	12.50	0.294	–0.571	8.9	596	139.5	40.5	29.01	0.044	–1.119	3.6	155
E – 300	550	74	13.44	0.455	–0.624	8.2	582	94.1	34.8	37.01	0.935	0.749	3.1	105

<sup>a</sup> Refers to the standard error.

diagonal compared to the length of a major diagonal [56]. Consequently, the ratio of the minor to the major diagonal was lower and calculates a greater elastic modulus value.

The measurements involving Knoop indentation in this work were performed on the cross sections with the major diagonal perpendicular to the substrate. Therefore, the properties measured represent the attributes of the surface parallel to the deposition surface. The elastic modulus of the coatings followed a trend similar to the hardness values when the SOD was varied. As mentioned previously, the hardness and elasticity of a material were interrelated and were associated with the porosity levels. Coatings with a higher porosity exhibited lower stiffness and hence restrained the ability of an indent to recover elastically; resulting in lower hardness. The mean elastic modulus of the coatings varied from 85.6 to 142.7 GPa, which is slightly lower than that of the corresponding bulk material [59].

The Weibull plot of the elastic modulus of the coatings is shown in Fig. 10(b). The Weibull plot exhibited a monomodal distribution, akin to that of the Weibull plot for the Knoop hardness. The Weibull modulus for both the Knoop hardness and the elastic modulus generally increased then decreased as the SOD increased. The correlation of the Weibull

modulus with the porosity level and phase percentage will be discussed in the next section.

### 3.4.3. Relationship between Weibull moduli with porosity and phase distribution

Both the Weibull moduli for the Vickers microhardness will be referred to as  $m_1$  and  $m_2$  while the moduli for the Knoop hardness and elastic modulus will be referred to as  $m_{HK}$  and  $m_E$ , henceforth. As mentioned previously, the Weibull modulus represents the degree of scatter in a data set. A greater Weibull modulus indicated lower variability in data and does not necessarily coincide with an enhanced (i.e., larger) mechanical property value, although the Weibull modulus generally increased when the mean hardness and elastic modulus increased in this work.

Fig. 11(a) and (b) reveal the correlation between the bimodal Weibull modulus for the Vickers hardness data and porosity as well as the Nd-rich phase percentage. Note that the Nd-rich phase percentage

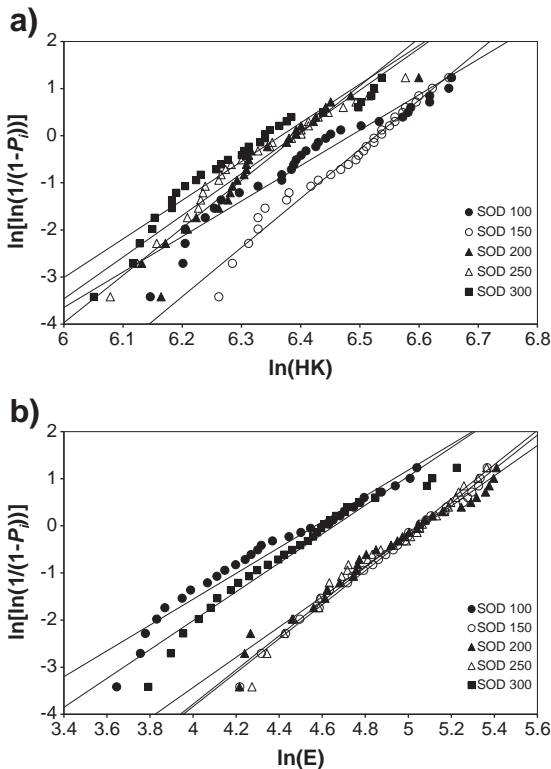


**Fig. 10.** Weibull plots for (a) Knoop hardness and (b) elastic modulus of Nd–Fe–B coatings plasma sprayed at standoff distances (SOD) of 100–300 mm.

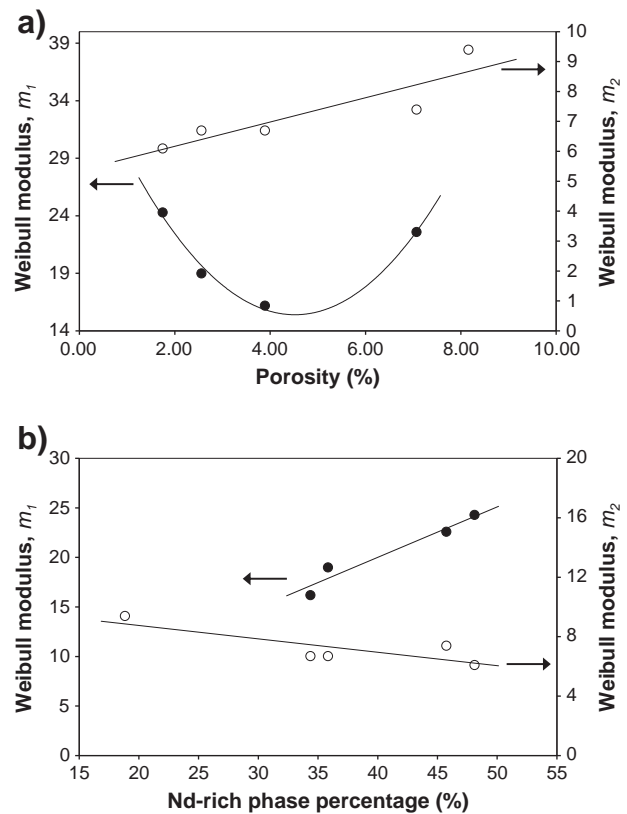


**Fig. 11.** Correlation between Weibull moduli for Vickers hardness ( $m_1$  and  $m_2$ ) and (a) porosity and (b) Nd-rich phase percentage.



and the Fe-rich phase percentage have an inverse relationship; i.e., the Fe-rich phase increases at the expense of the Nd-rich phase. As mentioned in Section 3.3, the  $m_1$  value for coating E is large compared to that of the other coatings. The  $m_1$  value, which is established at the lower hardness values, was associated with the Nd-rich phase. Since the indentations were made randomly across the coating and the Nd-rich phase in coating E is below 20%, the number of indents that were made in relation to the Nd-rich phase is limited:  $n_1$  is five. There are, thus, a limited number of points associated with this modulus value and  $m_1$  for coating E was distinctively large. The authors feel that this is an abnormality of the data set that requires a future investigation and, therefore, this data point has been omitted from the current analysis. It is noted that high Weibull modulus values have been observed in the nanostructured titania-hydroxyapatite coatings where a value of over 60 was attributed to 6 data points [60] for a bimodal distribution. The Weibull moduli for the Vickers microhardness of the other coatings were within the range determined for other thermal spray coatings [51,61], but were higher than that determined for coatings with bimodal distributions [52,53].

From Fig. 11(a),  $m_1$  was found to exhibit a quadratic relationship with porosity while  $m_2$  generally increased with porosity. This finding contradicts the general understanding that porosity increased data variability since the measured values tended to be lower when indentations were made closer to pores. The implication is that the degree of scatter for the hardness data when there are more than one phase present (i.e., bimodal) does not depend on porosity alone. Instead, the phase percentage has a more significant role. Fig. 11(b) shows that  $m_1$  and  $m_2$  increased and decreased respectively when the percentage of the Nd-rich phase increased. This trend is expected since  $m_1$ , which is established at lower hardness values, was associated with the Nd-rich phase while  $m_2$ , found at a higher hardness value, was associated with the Fe-rich phase. As the amount of the respective phase increased in the coating, the hardness values measured that are representative of that phase also became more consistent, hence the increased Weibull modulus.

From Fig. 12, it was established that both  $m_{HK}$  and  $m_E$  decreased when the porosity level increased. The decrease of the Weibull moduli for the Knoop microhardness and the elastic modulus indicated that the variability of mechanical properties in the coatings increased when the porosity level increased. The  $m_{HK}$  and  $m_E$  values were comparable to that of other thermal spray coatings [54]. The  $m_E$  values were generally lower than the other moduli since there was a systematic error introduced to the elastic modulus values when measuring the minor diagonal of the indents, resulting in a more scattered data [56]. On the other hand, there was no distinguishable correlation between the phase percentage with  $m_{HK}$  and  $m_E$ , indicating that the microhardness and elastic modulus values measured by the Knoop indentation were independent of the phase percentage.

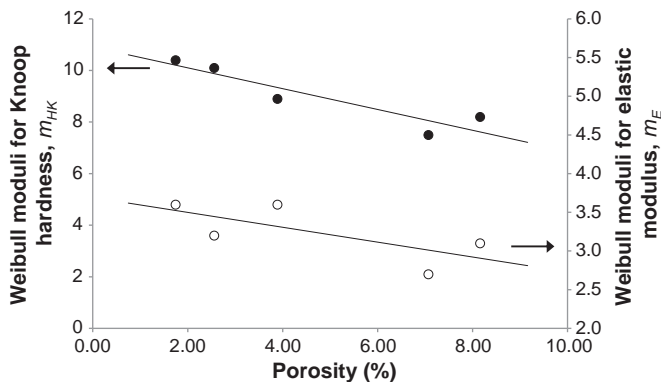


Fig. 12. Correlation between Weibull modulus for Knoop hardness,  $m_{HK}$  and elastic modulus,  $m_E$  with porosity.

The linear relation of  $m_{HK}$  and  $m_E$  values with porosity and their substantial independence of the phase content indicate that the Knoop indentation tests are more representative of the coating microhardness and the elastic modulus values in relation to the microstructural features compared to the Vickers indentation tests when the same load is applied. However, the Vickers indentation test can be representative of the overall properties when a greater load is used, thereby producing larger indents that will measure properties of both phases in a single indent. Due to the restriction of the coating thickness in this work, the Knoop indentation is more suitable to represent the overall coating properties. The relationship established between the Weibull moduli with porosity and the phase content can be used to predict the optimum microstructure that produces coatings with high reliability of mechanical properties; i.e., high Weibull moduli.

#### 4. Conclusion

The microstructures and mechanical properties of plasma sprayed neodymium iron boron (Nd–Fe–B) coatings have been investigated at standoff distances (SOD) of 100–300 mm. The microstructure of the coatings shifted from a lamellar to a spherical type when the SOD increased. The critical SOD was determined to be 150 mm at the given parameters – below which particles were not sufficiently melted and above which particles started to resolidify – both of which contributed to an increased porosity. Phase separation was observed in coatings due to the metastable phase formation and non-equilibrium solidification. The darker Fe-rich phase increased with an increase in SOD at the expense of the lighter Nd-rich phase, with an increment trend at 100 mm SOD intervals.

Increased porosity level results in a decrease of the microhardness and elastic modulus values of the coatings. Mechanical properties were greatest for coating B (SOD 150 mm) with Vickers hardness, Knoop hardness and elastic modulus of 691 kgf/mm<sup>2</sup>, 653 kgf/mm<sup>2</sup> and 142.7 GPa respectively. The Weibull plot for the Vickers hardness data exhibited bimodal behaviour while data acquired through the Knoop microindentation revealed a monomodal distribution. Porosity has a more significant role in determining the degree of data scattering (Weibull modulus) when monomodal behaviour was observed. Where a bimodal distribution was observed, the Weibull moduli were more influenced by the phase percentage of the different phases present. The material properties of Nd–Fe–B coatings can be optimised with respect to the thermal spray process conditions so that an appropriate microstructure can be created for specialised applications.

#### Acknowledgements

The authors would like to thank Dr J. Wang and Dr F. Malherbe for their assistance in operating the FESEM, EDX and XRD. This study is supported by a Swinburne University Postgraduate Research Award (SUPRA).

#### References

- [1] T. Spiliotis, D. Niarchos, P. Meneroud, G. Magnac, F. Claeysen, J. Pepin, C. Fermon, M. Pannetier, N. Biziere, J. Magn. Magn. Mater. 316 (2007) e120.
- [2] J. Töpfer, V. Christopher, Sensors Actuators A 113 (2004) 257.
- [3] D.P. Arnold, IEEE Trans. Magn. 43 (2007) 3940.
- [4] H. Raisigel, O. Cugat, J. Delamare, Sensors Actuators A Phys. 130–131 (2006) 438.
- [5] W.F. Liu, S. Suzuki, K. Machida, J. Magn. Magn. Mater. 308 (2007) 126.
- [6] S.L. Chen, W. Liu, Z.D. Zhang, G.H. Gunaratne, J. Appl. Phys. 103 (2008) 023922.
- [7] M. Gasgnier, C. Colliex, T. Manoubi, J. Appl. Phys. 59 (1986) 989.
- [8] L.G. Pereira, S.R. Teixeira, W.H. Schreiner, F.P. Missell, I.J.R. Baumvol, Phys. Status Solidi A 125 (1991) 625.
- [9] D.J. Keavney, E.E. Fullerton, J.E. Pearson, S.D. Bader, J. Appl. Phys. 81 (1997) 4441.
- [10] V. Neu, S. Föhler, A. Singh, A.R. Kwon, A.K. Patra, U. Wolff, K. Häfner, B. Holzapfel, L. Schultz, J. Iron Steel Res. Int. 13 (2006) 102.
- [11] B. Pawlowski, J. Töpfer, J. Mater. Sci. 39 (2004) 1321.
- [12] T. Spiliotis, D. Niarchos, P. Falaras, D. Tsoukleris, J. Pepin, IEEE Trans. Magn. 41 (2005) 3901.
- [13] B. Pawlowski, H. Beer, J. Töpfer, Key Eng. Mater. 132–136 (1997) 1409.

- [14] B. Pawlowski, S. Schwarzer, A. Rahmig, J. Töpfer, J. Magn. Mater. 265 (2003) 337.
- [15] M. Nakano, T. Honda, J. Yamasaki, S. Sato, F. Yamashita, J. Fidler, H. Fukunaga, Sens. Lett. 5 (2007) 48.
- [16] M. Nakano, R. Kato, S. Hoefinger, J. Fidler, F. Yamashita, H. Fukunaga, J. Alloys Compd. 408–412 (2006) 1422.
- [17] R.A. Overfelt, C.D. Anderson, W.F. Flanagan, Appl. Phys. Lett. 49 (1986) 1799.
- [18] G. Rieger, J. Wecker, W. Rodewald, W. Sattler, F.W. Bach, T. Duda, W. Unterberg, J. Appl. Phys. 87 (2000) 5329.
- [19] J.J. Wysocki, J. Mater. Sci. 27 (1992) 3777.
- [20] K. Kumar, D. Das, Thin Solid Films 54 (1978) 263.
- [21] K. Kumar, D. Das, E. Wettstein, J. Appl. Phys. 49 (1978) 2052.
- [22] M. Willson, S. Bauser, S. Liu, M. Huang, J. Appl. Phys. 93 (2003) 7987.
- [23] P.C. King, S.H. Zahiri, M.Z. Jahedi, J. Therm. Spray Technol. 17 (2008) 221.
- [24] M. Cherigui, S. Guessasma, N. Fenineche, R. Hamzaoui, O. El-Kedim, C. Coddet, Mater. Chem. Phys. 92 (2005) 419.
- [25] J.F. Herbst, R.W. Lee, F.E. Pinkerton, Rare Earth–Iron–Boron Materials: A New Era in Permanent Magnets, Annual Reviews Inc., 1986.
- [26] M.D. Abramoff, P.J. Magalhaes, S.J. Ram, Biophoton. Int. 11 (2004) 36.
- [27] A.S.T.M. International, ASTM E2109: Test Methods for Determining Area Percentage Porosity in Thermal Sprayed Coatings, ASTM International, West Conshohocken, PA, 2007. (2001).
- [28] S. Deshpande, A. Kulkarni, S. Sampath, H. Herman, Surf. Coat. Technol. 187 (2004) 6.
- [29] D.B. Marshall, T. Noma, A.G. Evans, J. Am. Ceram. Soc. 65 (1982) C175.
- [30] J.A. Gan, C.C. Berndt, Surf. Coat. Technol. 205 (2011) 4697.
- [31] J. Matejicek, S. Sampath, D. Gilmore, R. Neiser, Acta Mater. 51 (2003) 873.
- [32] S.W.K. Kweh, K.A. Khor, P. Cheang, Biomaterials 21 (2000) 1223.
- [33] K. Khor, P. Cheang, J. Therm. Spray Technol. 3 (1994) 45.
- [34] M. Xue, S. Chandra, J. Mostaghimi, H.R. Salimijazi, Plasma Chem. Plasma Process. 27 (2007) 647.
- [35] V.V. Sobolev, J.M. Guilemany, Mater. Lett. 18 (1994) 304.
- [36] G. Antou, G. Montavon, F. Hlawka, A. Cornet, C. Coddet, J. Therm. Spray Technol. 15 (2006) 765.
- [37] K. Yamasawa, X. Liu, A. Morisako, J. Appl. Phys. 99 (2006) 08N302.
- [38] S.L. Tang, M.R.J. Gibbs, H.A. Davies, Z.W. Liu, S.C. Lane, N.E. Mateen, Y.W. Du, J. Appl. Phys. 101 (2007) 09K501.
- [39] A. Melsheimer, H. Kronmüller, Physica B 299 (2001) 251.
- [40] G. Schneider, E.-T. Henig, G. Petzow, H.H. Stadelmaier, Z. Metallkd. Int. J. Mater. Res. 77 (1986) 755.
- [41] D.S. Edgley, J.M. Le Breton, S. Steyaert, F.M. Ahmed, I.R. Harris, J. Teillet, J. Magn. Mater. 173 (1997) 29.
- [42] Y. Li, H.E. Evans, I.R. Harris, I.P. Jones, Oxid. Met. 59 (2003) 167.
- [43] R.S. Lima, A. Kucuk, C.C. Berndt, Surf. Coat. Technol. 135 (2001) 166.
- [44] W. Lo, A.M. Campbell, J. Luo, R. Stevens, J. Mater. Res. 10 (1995) 568.
- [45] M. Sagawa, S. Fujimura, N. Togawa, H. Yamamoto, Y. Matsuura, J. Appl. Phys. 55 (1984) 2083.
- [46] Y. Luo, N. Zhang, C.D. Graham Jr., J. Appl. Phys. 61 (1987) 3442.
- [47] H. Wang, A. Li, W. Li, Intermetallics 15 (2007) 985.
- [48] F.M. Ahmed, D.S. Edgley, I.R. Harris, J. Alloys Compd. 224 (1995) 135.
- [49] M. Factor, I. Roman, Surf. Coat. Technol. 132 (2000) 181.
- [50] C.K. Lin, C.C. Berndt, J. Mater. Sci. 30 (1995) 111.
- [51] T. Valente, Surf. Coat. Technol. 90 (1997) 14.
- [52] R.S. Lima, A. Kucuk, C.C. Berndt, Mater. Sci. Eng., A 327 (2002) 224.
- [53] P.K. Aw, B.H. Tan, J. Mater. Process. Technol. 174 (2006) 305.
- [54] S.H. Leigh, C.K. Lin, C.C. Berndt, J. Am. Ceram. Soc. 80 (1997) 2093.
- [55] H.J. Kim, Y.G. Kweon, Thin Solid Films 342 (1999) 201.
- [56] J. Li, C. Ding, Surf. Coat. Technol. 135 (2001) 229.
- [57] J.S. Wallace, J. Ilavsky, J. Therm. Spray Technol. 7 (1998) 521.
- [58] R.S. Lima, S.E. Kruger, B.R. Marple, Surf. Coat. Technol. 202 (2008) 3643.
- [59] W. Rodewald, in: H. Kronmüller, S. Parkin (Eds.), Handbook of Magnetism and Advanced Magnetic Materials, John Wiley & Sons, Ltd, Hoboken, NJ, 2007.
- [60] M. Gaona, R.S. Lima, B.R. Marple, Mater. Sci. Eng., A 458 (2007) 141.
- [61] S.H. Leigh, C.C. Berndt, Surf. Coat. Technol. 89 (1997) 213.

### Permission to publish

J.A. Gan and C.C. Berndt, 'Effects of standoff distance on porosity, phase distribution and mechanical properties of plasma sprayed Nd-Fe-B coatings', Surf. Coat. Tech., 216 (2013) p. 127-138. DOI: 10.1016/j.surfcoat.2012.11.040, Published: FEB 15 2013.

As an Elsevier journal author, you retain various rights including Inclusion of the article in a thesis or dissertation whether in part or in toto; see [http://www.elsevier.com/about/policies/author-agreement/lightbox\\_scholarly-purposes](http://www.elsevier.com/about/policies/author-agreement/lightbox_scholarly-purposes) for more information. As this is a retained right, no written permission is necessary. This extends to the online version of your thesis and would include any version of the articles including the final published versions provided that they are not available as individual downloads but only embedded within the thesis itself.

# Quantification and Taxonomy of Pores in Thermal Spray Coatings by Image Analysis and Stereology Approach

JO ANN GAN and CHRISTOPHER C. BERNDT

Porosity is one of the most important microstructural features in thermal spray coatings and has been actively studied and measured by many methods. Image analysis techniques have become popular techniques in determining porosity in coatings because of simplicity, accessibility, and an ability to measure both open and closed porosities as well as pore characteristics such as size, shape, orientation, and spatial distribution. In the current study, an image analysis technique has been complemented by several stereology procedures to determine the porosity level and characteristics of pores within coatings. Stereology protocols such as Delesse, DeHoff, and Cruz-Orive analyses were used to derive the porosity level, pore size, and shape distributions, and the effectiveness of each stereology protocol was compared. Standoff distance (SOD) and annealing process did not alter the distribution trend of number of pores but influenced the distribution of pore volume fractions significantly. The bivariate size–shape distribution of the pores was used to predict the dominant pore type and fractions of pores that arose from different formation mechanisms. It was found that nearly spherical pores that originated from gas bubbles and entrapped gas pockets dominate at shorter SOD, while the different types of pores become more evenly distributed when the SOD was increased.

DOI: 10.1007/s11661-013-1818-4

© The Minerals, Metals & Materials Society and ASM International 2013

## I. INTRODUCTION

**POROSITY** is perhaps one of the most studied features of thermal spray coatings. Porosity refers to the voids within a body of material usually formed during processing, and is often expressed quantitatively in fraction or percentage. Porosity affects the physical properties of a material distinctively. The dependence of a material's properties on porosity was classified into three categories by Rice:<sup>[1]</sup> (i) properties not dependent on porosity, such as thermal expansion coefficients and melting temperature; (ii) properties dependent only on the porosity level but not on its characteristics, such as heat capacity and dielectric constant; and (iii) properties dependent on both the porosity level and its characteristics, such as mechanical properties and thermal conductivity. Properties of thermal spray coatings that are influenced by porosity level and its characteristics include mechanical properties,<sup>[2]</sup> magnetic properties,<sup>[3]</sup> thermal conductivity,<sup>[4]</sup> and electrical conductivity.<sup>[5]</sup>

Throughout the literature, various types of porosity in thermal spray coatings have been identified, which can be categorized based on its formation mechanism.<sup>[6,7]</sup>

Table I summarizes the types of porosity in thermal spray coatings. Regardless of the formation mechanism, a majority of the pores formed because of the inability of the incoming molten particles to fill the surface irregularities of previously formed layers. These protuberances could be unmelts, fragmented particles, condensates, or the surface architecture of the substrate. Pressure within the incoming molten droplet was often insufficient to break its surface tension; hence, the droplet was unable to penetrate into smaller cavities. This phenomenon depends on factors such as the pressure distribution within the molten droplets, substrate topography, as well as the solidification rate.<sup>[8]</sup> While pores formed of this nature are more irregularly shaped, those arising from gas entrapment are more spherical<sup>[9]</sup> and generally smaller.<sup>[10]</sup>

Porosity could also arise from (i) the shadow effect, (ii) the roof effect, and (iii) the splat-curling effect. The shadow effect occurs when a rough peak-like feature on a previously formed layer blocks incoming particles from depositing on the “shaded area” of the surface. Voids arise from these shaded areas as consecutive layers are formed by the incoming particles, see Figure 1(a). On the other hand, the roof effect is caused by the inability of incoming particles to fill in the concave part of the previously formed layers, thus forming a roof-like-shaped void within the coating, Figure 1(b). The curling effect could be caused by (i) stresses due to thermal expansion coefficient mismatches at interfaces, (ii) surface tension of molten splats, (iii) surface roughness, or (iv) substrate remelting.<sup>[11]</sup> An assumption was made by Xue *et al.*<sup>[11]</sup> that curling occurred entirely because of splat shrinkage upon cooling. The center of the splat was attached to the substrate upon impact while the top surface of the splat

---

JO ANN GAN, Research Engineer, is with the Industrial Research Institute Swinburne, Faculty of Engineering and Industrial Sciences, Swinburne University of Technology, Hawthorn, VIC 3122, Australia. Contact [REDACTED] CHRISTOPHER C. BERNDT, Professor of Surface Science and Interface Engineering, is with the Industrial Research Institute Swinburne, Faculty of Engineering and Industrial Sciences, Swinburne University of Technology, and also Adjunct Professor, with the Department of Materials Science and Engineering, Stony Brook University, Stony Brook, NY 11794.

Manuscript submitted January 7, 2013.

Article published online June 8, 2013

**Table I. Mechanism of Formation for Various Pore Types in Thermal Spray Coatings<sup>6,7</sup>**

	Type	Mechanism of Formation
1	interlamellar	stacking of particles. quantity and size depend directly on particle size and distribution of feedstock.
2	trapped gas pockets	turbulence of gas flow.
3	gas bubbles	dissolution of gas into molten metal and subsequent evaporation upon solidification of the metal.
4	between fragments	disintegration of spray particles at impact.
5	between condensates	condensation of partially evaporated particles; often contains powdery residue.
6	between dendrites	solidification shrinkage of the particles to highly textured dendrites disrupts the coating structure.
7	micro cracks	various (solidification, cooling, external load <i>etc.</i> ).

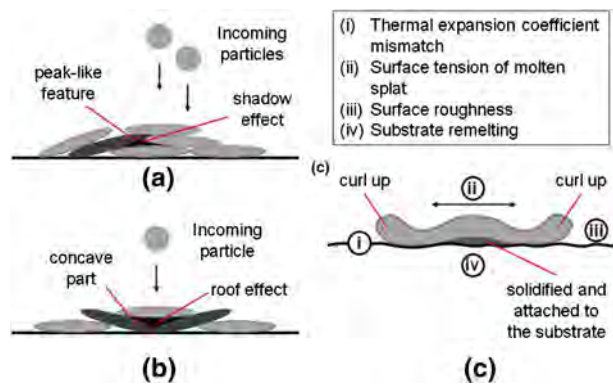


Fig. 1—Schematic of pore formation: (a) shadow effect, (b) roof effect, and (c) splat curling up.

contracted, thus causing the edges to curl up, Figure 1(c). The curl up angle depended on the area of splat bonded to the substrate and the thermal expansion coefficient of the substrate. The microstructural artifact of a curl up is more prone in metallic coatings than in ceramic coatings because of their ductility and higher thermal expansion coefficients. Besides, ceramic coatings are more brittle in character, and stress relief would be reflected by cracking across the splat profile.<sup>[8]</sup>

Measurement techniques to evaluate porosity level in thermal spray coatings include mercury intrusion porosimetry,<sup>[12]</sup> helium pycnometry,<sup>[13]</sup> image analysis,<sup>[14,15]</sup> electrochemical methods,<sup>[16]</sup> and small angle neutron scattering.<sup>[17,18]</sup> Image analysis has become an increasingly popular technique to determine porosity in thermal spray coatings because of its simplicity, convenience, and its capacity to determine various aspects of pores; *i.e.*, open and closed porosity, pore size distribution, and spatial distribution.<sup>[19]</sup> Copper electroplating<sup>[20,21]</sup> has also been used to infiltrate the pores within plasma sprayed coatings and improve visualization of the pores to be analyzed *via* image analysis. However, this technique is applicable to electrically insulating materials only. There is also concern that the electroplating process might alter the microstructure that is being assessed. The appropriate measurement technique must be selected with considerations to the advantages and limitations of each technique.

In the current study, porosity of the coatings was quantified using an image analysis technique that was complemented by a stereology approach. The porosity

level and characteristics, such as size and shape distributions, within thermal spray coatings were examined. The porosity levels quantified by different stereology protocols, as well as the efficiency of each protocol in the quantification of pores in thermal spray coatings were compared. The pores were classified according to their characteristics, and the fractions of each pore type within the coatings were predicted. The significance of these characteristics in terms of the coatings is that it allows for the prediction of the pore origins and therefore, the size and shape of pores within the coatings can be optimized by adjusting the spray parameters to maximize the type of pores desired.

## II. THEORETICAL BACKGROUND

Stereology provides an estimated three-dimensional (3D) space projection based on measurements made on two-dimensional (2D) sections; *i.e.*, the coating's cross section. The estimate is based on geometric probabilities, and the size or shape distribution is expressed instead of the absolute volume of the feature of interest. 3D projection of pore distribution is more accurate than 2D ones in the sense that a 2D distribution often assumes the dominance of elliptical-shaped pores although there is a significant number of spherical pores present.<sup>[22]</sup> Besides, in certain cases, the pore shape is assumed to be spherical, and the pore sizes are given as equivalent diameters. Such assumptions present misleading pore distributions. 3D analysis through a stereology approach offers a more realistic approximation of pore size distributions.

Most features in thermal spray coatings, such as splats and pores, can be approximated to ellipsoids of revolution. There are generally two types of ellipsoids: prolate and oblate ellipsoids which are generated by rotating an ellipse around its major axis ( $M$ ) and minor axis ( $m$ ), respectively. The pore shape in thermal spray coating analysis is assumed to be oblate ellipsoid because of its pancake-like features. Therefore, only the calculations for oblate ellipsoids will be discussed henceforth. There are two protocols for size-shape distributions, which have been applied for thermal spray coating analysis: the DeHoff<sup>[23,24]</sup> and Cruz-Orive<sup>[25,26]</sup> protocols. Both protocols were used to derive the pore size distributions in the current study.



The DeHoff protocol was derived from Saltykov's analysis for spherical particles.<sup>[27,28]</sup> In this analysis, the relative volume of pores was repartitioned in each size class based on its 2D boundaries. However, it should be noted that the distribution given by a DeHoff analysis was a step function and not a continuous one; *i.e.*, it was assumed that the ellipsoids in a given size class were approximately the largest ellipsoid in that particular size class. It was also assumed that the cross sections where the measurements were made represent the average of all possible sections throughout the coating.<sup>[24]</sup>

The 2D ellipses at the coating cross sections were projected into 3D oblate ellipsoids by revolving the ellipses around their minor axis ( $m$ ). The pore size (major axis,  $M$  of the ellipse) was divided into  $k$  size classes of  $\Delta$  size increment, where  $\Delta = M_{\max}/k$ ;  $M_{\max}$  is the longest major axis in the largest size class. The number of ellipsoid particles in each size class per unit volume is given by

$$(N_V)_i = \frac{1}{k(q) \cdot \Delta} \sum_{j=1}^k \beta(i,j) \cdot (N_A)_i \quad [1]$$

where  $k(q)$  is the shape factor for oblate spheroids,  $\Delta$  is the size increment,  $\beta(i,j)$  are the Saltykov coefficients determined from the Saltykov matrix, and  $(N_A)_i$  is the number of ellipses of  $q$  axial ratio per unit area in each size class. The shape factor for oblate particles is expressed as

$$k(q) = \int_0^{\pi/2} \int_0^{\pi/2} \frac{\sqrt{1 + (q^2 - 1) \cdot \cos^2 \varphi}}{\pi/2} \cdot \sin \varphi \cdot d\varphi \cdot d\theta \quad [2]$$

where  $q$  is the average axial ratio of the ellipses,  $\varphi$  is the angle between the normal of the test plane and the  $z$ -axis, while  $\theta$  is the angle between the projection of this normal on the  $xy$  plane and the  $x$ -axis. A plot of shape factor,  $k(q)$  for oblate and prolate ellipsoids of revolution can also be found in the original literature.<sup>[24]</sup>

The volume fraction of the pores per size class,  $(V_V)_i$ , can then be calculated by multiplying  $(N_V)_i$  by the equivalent volume of the ellipsoid,  $V_i$  where  $V_i = \frac{\pi}{6} \cdot (M_{\max-i})^3 \cdot \bar{q}_i$ ;  $M_{\max-i}$  is the maximum major axis at size class  $i$  and  $\bar{q}_i$  is the average axial ratio ( $q = m/M$ ) of size class  $i$ .

On the other hand, Cruz-Orive developed a model that links the size-shape probability density function (pdf) for spheroids with variable size and shape by solving the general spheroid problem.<sup>[25,26]</sup> Again, the systems of particles are considered to consist of either prolate or oblate ellipsoids of revolution generated by ellipses at plane sections. However, this analysis takes into account the shape variations; *i.e.*, random variation about a single type of shape such as ellipsoidal. The shape factor is represented by the eccentricity parameter of  $x^2 = 1 - (b/a)^2$  where  $a$  and  $b$  are the major and minor axes of the spheroids, respectively.

In order to apply this analysis, the phase of interest—pores, must be satisfactorily modeled by spheroids of the same type—must be either prolate or oblate.

Second, the phase of interest must be dilute—the volume occupied by the pores is small in relation to the total volume. The pores are assumed to be non-overlapping, and the orientations of the pores are assumed to be random and isotropic.

Recall that the size variable for oblate spheroids is defined by their major axes. Therefore, the range of pore size is divided into  $k$  classes of  $\Delta = A/k$  where  $A$  is the maximum major axis of the pores in the body of interest. The shape factor,  $x^2$  is also divided into  $s$  classes of size  $1/s$ . Therefore, the population of pores within the body of interest can be described by the bivariate variable  $(a, x^2)$ , which is represented in a  $k \times s$  matrix. Each pore is designated as an  $ij$  spheroid with a certain size of  $i$  and shape  $j$ .

The number of pores per unit volume of sample as a function of pore size and shape is expressed as

$$N_V(i,j) = \Delta^{-1} \sum_{\alpha=i}^s \sum_{\beta=j}^k p^{\alpha} N_A(\alpha, \beta) q^{\beta j} \quad [3]$$

where  $i = 1, 2, 3, \dots, k$  and  $j = 1, 2, 3, \dots, s$ ;  $p^{\alpha}$  and  $q^{\beta j}$  are inverse matrices of  $p_{i\alpha}$  and  $q_{\beta j}$ , respectively; and  $N_A$  is the number of  $ij$  ellipses per unit area.

The volume fractions of the pores for each size class,  $V_V$ , can then be calculated by multiplying the equivalent volume of spheroid  $ij$  by  $N_V$ . Further details on the derivation of Cruz-Orive protocol can be found in the original literature.<sup>[25,26]</sup>

### III. EXPERIMENTAL METHODS

#### A. Feedstock Material and Plasma Spray Process

The feedstock was atomized neodymium iron boron (Nd-Fe-B) powder of grade MQP S-11-9, manufactured by Molycorp Magnequench Inc., Singapore. The feedstock exhibited a dense, spherical morphology with more than 90 pct of the particles between 20 and 60  $\mu\text{m}$ ; Figure 2. The as-received feedstock was deposited *via* a SG-100 (Praxair Surface Technologies Inc., USA) atmospheric plasma spray torch onto stainless steel 304 substrates (60  $\times$  30  $\times$  3 mm<sup>3</sup>). The spray parameters are presented in Table II. All parameters were kept constant, except for the standoff distance (SOD) and number of passes. The SOD was varied to introduce a different range of porosity level and pore characteristics into each coating.<sup>[29–31]</sup> The number of passes was varied to maintain the coating thickness by compensating for the decrease of deposition efficiency as the SOD increased. The sprayed coatings were then annealed in vacuum (<0.01 Pa) at 873 K to 923 K (600 °C to 650 °C) for 30 minutes.

#### B. Image Analysis and Stereology Implementation

The image analysis technique implemented in the current study involved a five-step process: (i) sample preparation (sectioning, mounting, and polishing), (ii) image acquisition *via* scanning electron microscope, (iii) image pre-treatment, (iv) image treatment, and (v) stereology implementation.

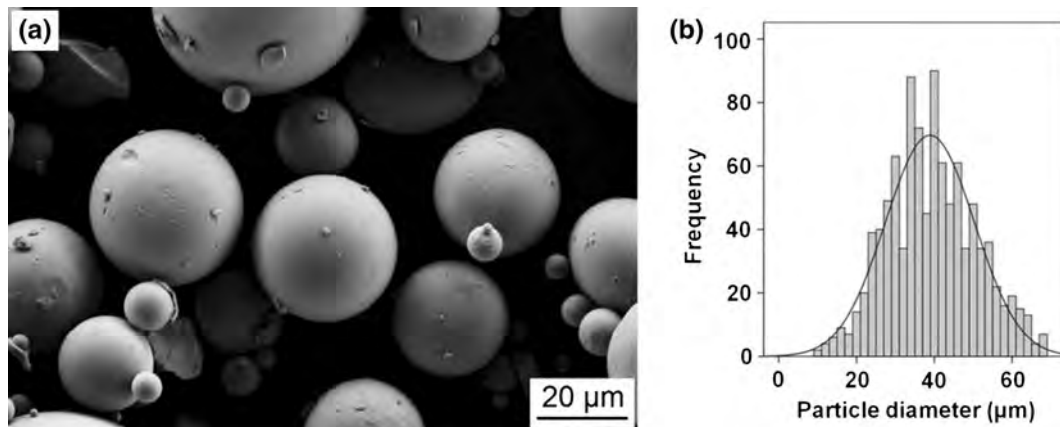


Fig. 2—(a) Morphology and (b) particle size distribution of Nd-Fe-B feedstock powder.

**Table II. Experimental Parameters for Plasma Spraying of Nd-Fe-B Coatings**

Current (A)	750
Voltage (V)	40
Primary Gas Flow, Ar (slpm)	39
Secondary Gas Flow, He (slpm)	22
Carrier Gas Flow, Ar (slpm)	15
Feed Rotation (rpm)	3.5
Feed Rate (kg/s)	$5 \times 10^{-4}$
Standoff Distance, SOD (m)	0.1 to 0.3
No. of Passes	20 to 50

All the samples were sectioned in a direction perpendicular to the coating surface and cold mounted using epoxy. The mounted coatings' cross sections were polished to a  $1 \mu\text{m}$  finish. A thin layer of gold film was sputtered on all the samples before image acquisition using a ZEISS Supra 40 VP field emission scanning electron microscope (FESEM). Electron microscope images provided more accurate results than images taken by optical microscopy because of the former's higher resolution,<sup>[15]</sup> thus all images used in the current study were electron micrographs. Twenty fields of random, non-overlapping SEM images were taken for each sample at 1000 times magnification. All the images were taken using the same acceleration voltage, working distance, resolution, magnification, brightness, and contrast.

The images acquired were processed using Image Processing and Analysis in Java (Image J) software from the National Institutes of Health, Bethesda, MD.<sup>[32]</sup> The evaluation was carried out in compliance with Test Method B of standard ASTM E 2109.<sup>[33]</sup> The pretreatment process of the images refers to the implementation of filters to optimize and reveal the specific structures to be studied; which in this case were the pores. However, this step should be implemented cautiously and not eliminate any of the features to be studied. Four types of filters that are often employed are (i) contrast filters, (ii) arithmetic and logic filters, (iii) spatial filters, and (iv) frequency filters.<sup>[34]</sup> Only a contrast filter was implemented in the current study, since the images obtained in the current study did not contain any apparent noise that required excessive image pre-treatment.

The pre-treated images were further processed by image segmentation and filtering. Image segmentation was performed by thresholding, Figure 3. The critical threshold values were selected by sampling various threshold values and determining the threshold value where the number of isolated bright pixels increased abruptly.<sup>[15]</sup> The *open* filter was used to distinguish between globular porosity and crack network; Figure 3. The *opening* function was executed by consecutive *erosion* and *dilation* operations, where the *erosion* filter removed pixels from the edges of digital objects while the *dilation* filter added pixels to the edges of the objects. The objects were the contiguous black areas in the binary image, while the remaining white area was the background. A pixel was removed by *erosion* filter if four or more of its neighbors were white, and a pixel was added by the *dilation* filter if four or more of its neighbors were black. More than 10,000 voids were analyzed.

The stereology approach was applied to compare the porosity level and pore size distribution derived by 2D image analysis and 3D space projection. The stereology protocols that were implemented include the De-Hoff<sup>[23,24]</sup> and Cruz-Orive protocols.<sup>[25,26]</sup> The theoretical background of these protocols was discussed in Section II. For both protocols, the pore sizes were divided into 15 size classes ( $k$ ) of  $2 \mu\text{m}$  increment ( $\Delta$ ). The shape factor,  $x^2$ , in the Cruz-Orive protocol was divided into  $s$  classes of size  $1/s$  wherein  $s$  was 10.

## IV. RESULTS AND DISCUSSION

### A. Microstructure

The cross sections of the plasma sprayed Nd-Fe-B coatings revealed features that were typical of thermal spray coatings; *i.e.*, splats, porosity, and unmelts, Figure 4. There were two phases that were observed in the coatings—the bright Nd-rich phase, and the dark Fe-rich phase. These two distinct phases result from metastable phase formation and non-equilibrium solidification of Nd-Fe-B during thermal spray processing.<sup>[31,35]</sup>



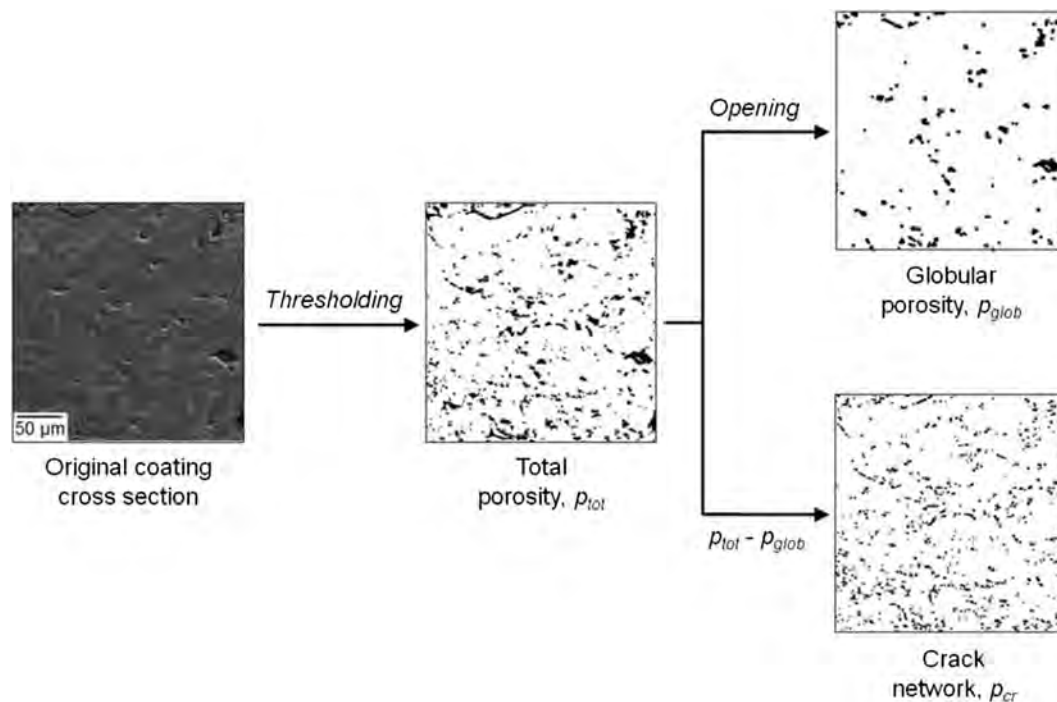


Fig. 3—Implementation of thresholding for image segmentation and *opening* function to distinguish between globular porosity and crack network.

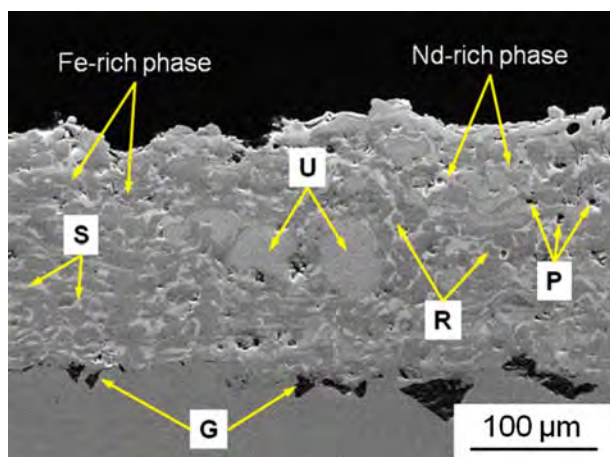


Fig. 4—Cross section of plasma sprayed Nd-Fe-B coating sprayed at 200 mm. G = embedded grit, P = pore, R = resolidified particle, S = splat, and U = unmelt.

The pore types observed in the coatings corresponded to the types listed in Table I and are visualized in Figure 5. Each pore type arose from a different formation mechanism. The size and shape of the pores can be interpreted to predict the origin of the pores and classify them according to their formation mechanisms. This will be discussed further in Section IV-D.

The cross sections of as-sprayed and annealed Nd-Fe-B coatings are shown in Figure 6. It can be observed visually that the porosity level of the coatings has reduced after annealing. Microcracks also evolved as a result of annealing. The quantification of the porosity levels will be discussed in the next section.

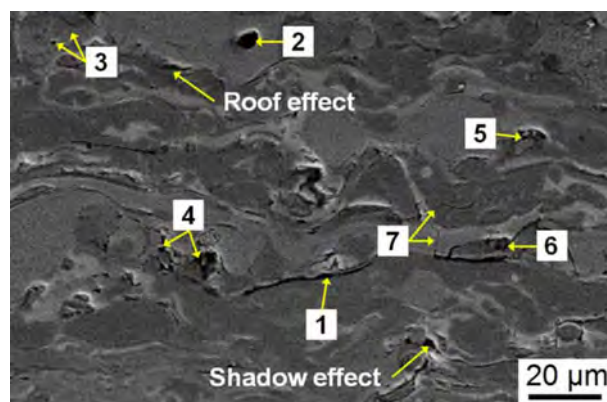


Fig. 5—SEM micrograph showing the various pore types in plasma sprayed Nd-Fe-B coatings. *Note* The numbers correspond to different pore type listed in Table I. 1 = interlamellar, 2 = trapped gas pockets, 3 = gas bubbles, 4 = between fragments, 5 = between condensates, 6 = between dendrites, 7 = micro cracks.

## B. Comparison of Total Porosity

### 1. Delesse vs DeHoff's protocols

The total porosity level of the coatings was quantified using an image analysis technique, implementing two stereology protocols: (i) Delesse<sup>[36]</sup> and (ii) DeHoff.<sup>[23,24]</sup> Delesse's protocol states that for a structure that contains a secondary phase,  $p$ , then the area density,  $A_A$  of phase  $p$  on a random cross section is equal to the volume density,  $V_V$  of that phase in the structure.<sup>[36]</sup> In other words, the total area of a secondary phase  $p$  on random cross sections of a structure is proportional to the total content of phase  $p$  in the whole structure. On the other hand, the DeHoff's protocol functions on the

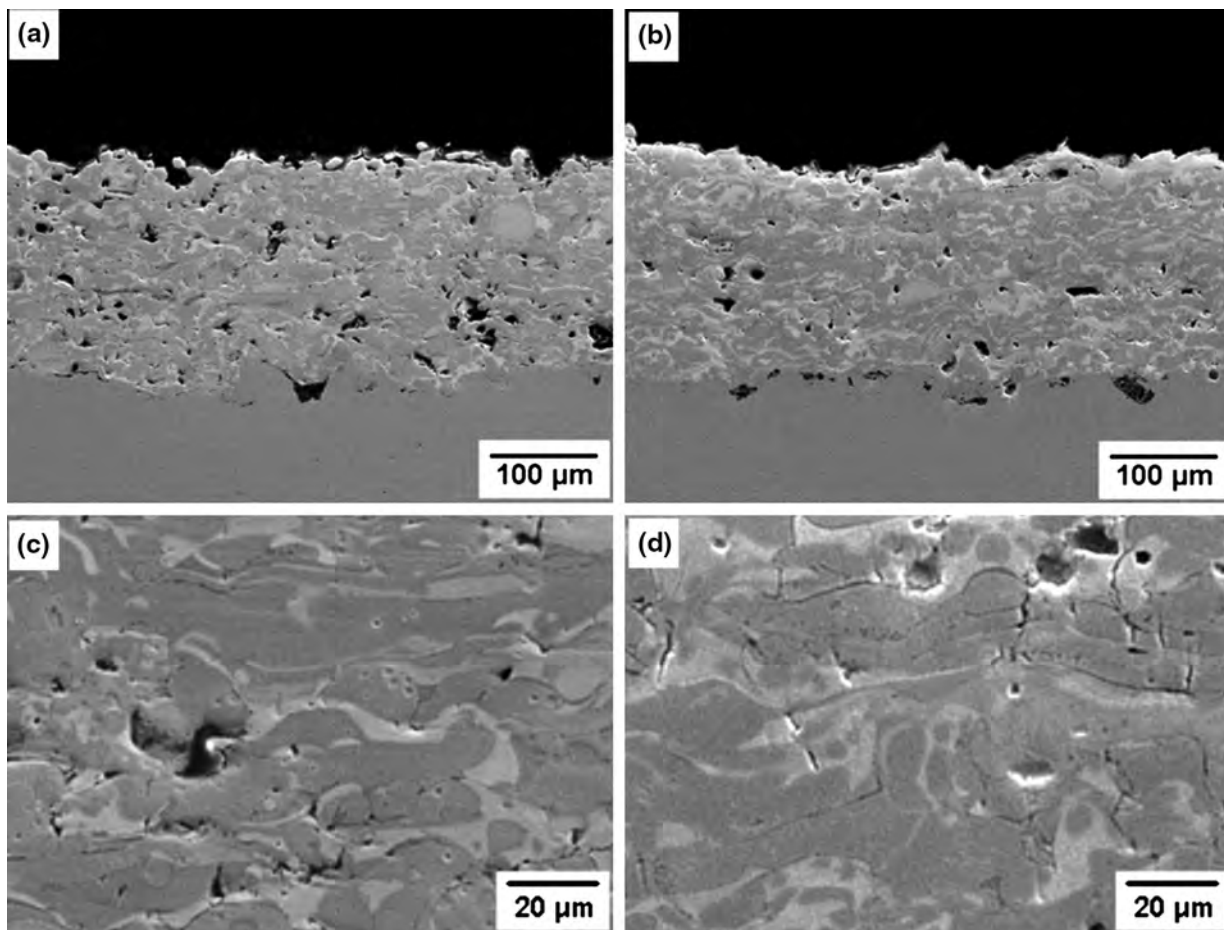


Fig. 6—Cross-sectional views of (a), (c) as-sprayed, and (b), (d) annealed Nd-Fe-B plasma sprayed coatings deposited at 250 mm.

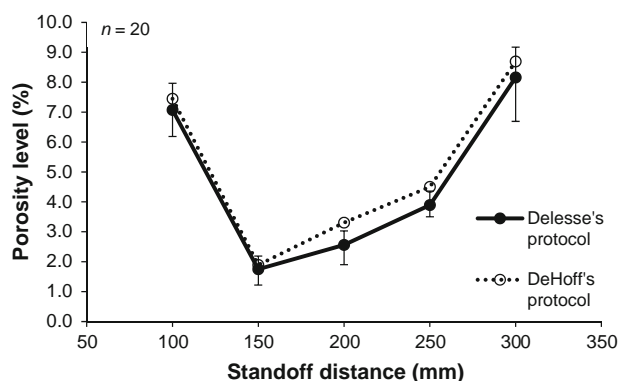


Fig. 7—Comparison of porosity level of plasma sprayed Nd-Fe-B coatings deposited at various standoff distances (SOD) determined using Delesse's and DeHoff's protocols.

concept of repartitioning the projected volume of ellipsoidal pores in each size class based on its 2D boundaries. The theoretical background of DeHoff's protocol has been discussed in Section II.

Figure 7 shows the comparison of porosity level of as-sprayed coatings determined by the two protocols. The Delesse's protocol averaged the porosity determined from 20 different images; thus, the error bars represent

the minimum and maximum porosity determined from the 20 images. There were no error bars for the plot of porosity level derived from DeHoff's protocol because this method integrated the data collected from all 20 images to a single pool of information to generate the size distribution that was used to calculate the average porosity level. The porosity levels determined by Delesse's protocol were close to those determined using DeHoff's protocol, with a difference of less than 0.8 pct. This implied that the porosity level determined by the pore area (Delesse's protocol) was accurate and was a simple method to determine the overall porosity level compared with an ellipsoids of revolution approach (*i.e.*, DeHoff's protocol).

## 2. Effects of standoff distance and annealing

The variation of porosity level in the as-sprayed and annealed coatings determined *via* Delesse's protocol is shown in Figure 8. In general, the total porosity levels for all the coatings decreased after annealing, consistent with micrographic observations. An annealing temperature of 873 K (600 °C) was observed to be more effective in reducing the total porosity level rather than 923 K (650 °C). The higher porosity level of coatings annealed at 923 K (650 °C) may have been caused by the development of microcracks due to relief of residual

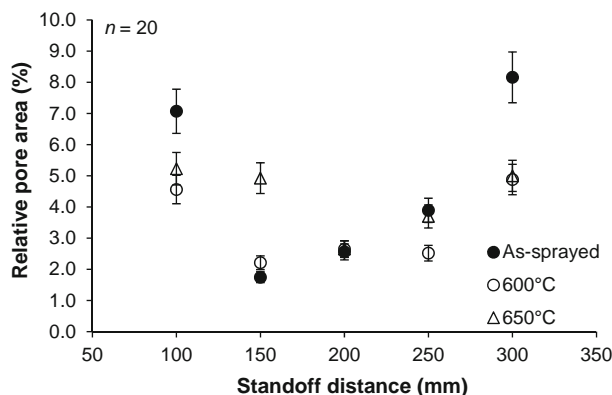


Fig. 8—Variation of porosity level for as-sprayed samples and samples annealed at 873 K and 923 K (600 °C and 650 °C).

stress<sup>[37]</sup> or the coarsening of globular pores through the expansion of entrapped gas.<sup>[18]</sup>

Exceptions in the porosity reduction trend were observed for coatings deposited at SODs of 150 and 200 mm. The porosity level for annealed coatings deposited at 200 mm does not change significantly compared with the as-sprayed coating; however, the porosity level of the coating deposited at 150 mm increased after annealing. This distinct increase of porosity level for the coating deposited at this SOD may have been caused by the increased brittleness of the coating after annealing, thus causing pull-outs during metallographic preparation. Another possibility for the increase of porosity was the expansion of entrapped gas.<sup>[18]</sup>

The refinement of pore structure, and hence the porosity level, in plasma sprayed coatings resulted from the combined actions of phase transformation and sintering.<sup>[38]</sup> Phase transformation altered the bulk density of a structure, which in turn led to a change in the bulk volume of a sample. Through the annealing process, the amorphous Nd-rich phase, formed through rapid solidification endowed by the plasma spray process, transformed into the more stable crystallized Nd<sub>2</sub>Fe<sub>14</sub>B and  $\alpha$ -Fe phase. Densification of the coatings was often compensated by shrinkage of the sample or increased porosity through formation of microcracks.<sup>[38]</sup> On the other hand, sintering altered the porosity level through shrinkage of small pores or coalescence of smaller globular pores to form larger pores.

Figure 9 shows the variation of globular pores and crack network for as-sprayed and annealed coatings. It can be seen that the percentage of globular pores generally decreased after annealing, with the exception of the coatings deposited at SOD 150 mm. This increase in globular pores reinforced an earlier statement that brittleness of the coating after annealing led to more pull-outs during polishing. The increase of globular pores also suggested that the particles at this SOD underwent more gas flow turbulence before deposition, hence more trapped gas pockets that were subjected to expansion during annealing.

On the other hand, the percentage of microcracks for all the coatings increased except for coatings

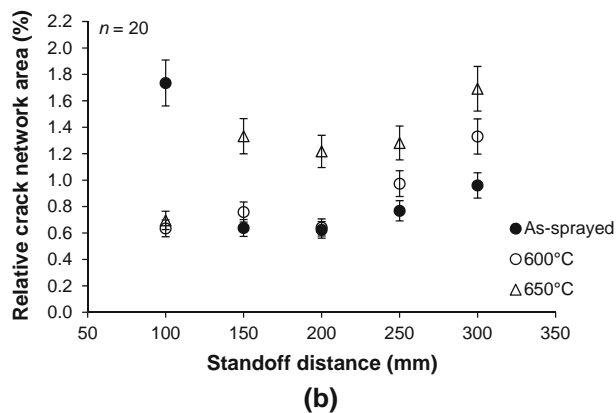
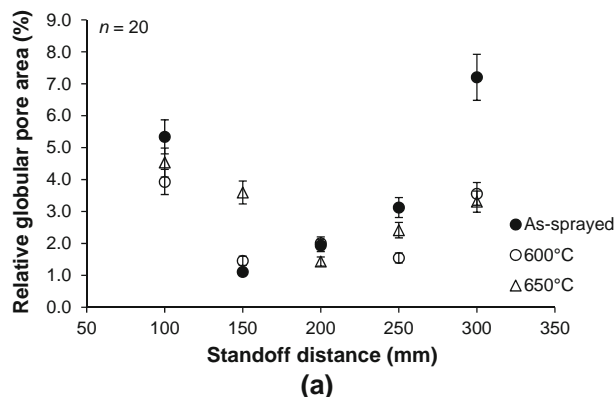


Fig. 9—Variation of (a) globular pores and (b) crack network for as-sprayed coatings and coatings annealed at 873 K and 923 K (600 °C and 650 °C).

deposited at 100 mm. The percentage of microcracks dropped by about 1.1 pct after annealing for coatings deposited at this SOD. Phase transformation for this coating, hence the coating densification through formation of microcracks, might not be so severe as compared with the other coatings since the extent of phase separation during deposition varied for each SOD.<sup>[31]</sup>

Most case histories throughout the literature indicated that microcracks tended to preferentially anneal out even at low temperature.<sup>[18,39]</sup> However, such a trend was not observed for the remainder of the plasma sprayed Nd-Fe-B coatings. Instead, the microcracks developed through coating densification were preserved. Such an increase in microcracks for annealed coatings has also been observed in other plasma sprayed coatings.<sup>[37,40]</sup> In addition to the densification of coatings, the microcracks may have also arisen from the relief of residual stress coupled with the coefficient of thermal expansion mismatch between the coating and substrate.<sup>[37]</sup> It was also observed in Figure 9(b) that the percentage of microcracks for coatings annealed at 923 K (650 °C) was always higher than for coatings annealed at 873 K (600 °C). This observation further reinforced the statement that microcracks were partly caused by residual stresses and coefficient of thermal expansion mismatches.



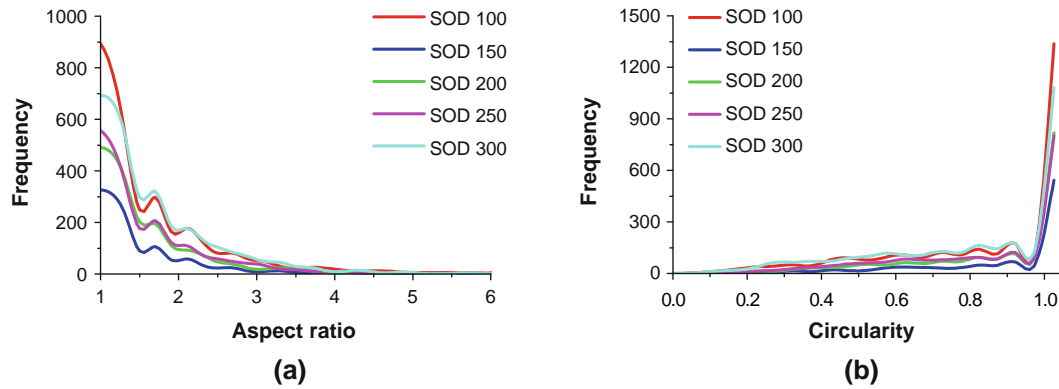


Fig. 10—Distribution of (a) aspect ratio and (b) circularity of the pores in plasma sprayed Nd-Fe-B coatings deposited at various standoff distances.

Table III. Definitions of Various Size and Shape Descriptors Used in Pore Quantification

Descriptor	Symbol	Definition
Aspect Ratio	$AR$	ratio of major axis ( $M$ ) to minor axis ( $m$ )
Circularity	$C$	defined by $4\pi(A/p^2)$ , where $A$ is the area and $p$ is the pore perimeter
Feret's Diameter	$d_F$	the longest distance between any two points along the pore boundary
Major Axis	$M$	the longest diameter of the best fitting ellipse
Shape Factor or Eccentricity Parameter	$x^2$	defined by $x^2 = 1 - (b/a)^2$ , where $a$ and $b$ are the major and minor axes of the spheroids, respectively.

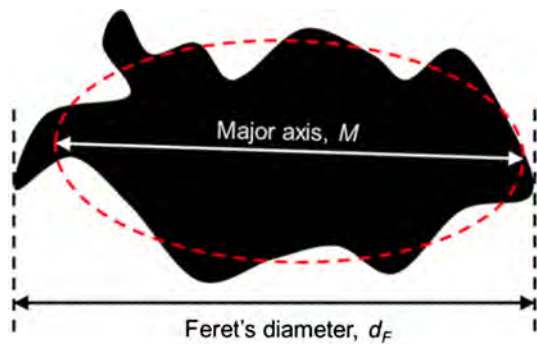


Fig. 11—Schematic illustrating Feret's diameter,  $d_F$  and major axis,  $M$  of a pore.

### C. Pore size and Shape Distribution

#### 1. Two-dimensional (cross section)

The shape of pores within thermal spray coatings depends on their formation mechanism. Certain pores may be spherical, such as those formed by trapped gas pockets or gas bubbles.<sup>[9,41]</sup> However, pores that arose from other mechanisms may not be spherical. To prove this point, the shape descriptors such as aspect ratio and circularity of the pores within the coatings were determined. Aspect ratio,  $AR$ , is defined by the ratio of major axis ( $M$ ) to minor axis ( $m$ ), while circularity,  $C$  is given by  $4\pi(A/p^2)$  where  $A$  is the area, and  $p$  is the pore perimeter. Aspect ratio and circularity approach unity when a pore becomes more spherical. The aspect ratio increases while the circularity decreases, when pores

become more elongated. Figure 10 shows the distribution of aspect ratio and circularity of the pores in plasma sprayed Nd-Fe-B coatings. Although the majority of the pores show an aspect ratio and circularity equivalent to unity, indicating that they were in fact spherical, there were still more than 50 pct of pores within the coatings, which were not spherical.

Therefore, it is inaccurate to represent pore size by equivalent circular diameters. Instead, two other terms known as the Feret's diameter and the major axis have been adopted for the purpose of classifying 2D pore size. Feret's diameter,  $d_F$ , is defined as the longest distance between any two points along the void boundary, while major axis,  $M$ , is defined as the longest diameter of the best-fitting ellipse. A summary of definitions for these shape and size descriptors is provided in Table III. Figure 11 illustrates Feret's diameter and the major axis of a pore. The distributions of major axis and Feret's diameter in the as-sprayed coatings are shown in Figure 12. The shape of the size and shape descriptors' distributions were similar for coatings deposited at all SODs, although they were of varying frequency levels due to the difference in porosity level.

The 2D pore size distributions for all the coatings were positively skewed, with a large portion of the pore Feret's diameters and major axis average ranging from 2 to 4  $\mu\text{m}$ . It can be observed that the increase in total porosity is contributed by both the increase in the number of pores and the pore size. While coatings deposited at SOD 300 mm exhibited the highest porosity level, the coatings deposited at 100 mm revealed a relatively higher number of pores. The coatings deposited at SOD 300 mm showed pores with a wider size

distribution; *i.e.*, Feret's diameter and major axis, see Figure 12. On the other hand, coatings deposited at SOD 150 mm, which showed the lowest porosity level, displayed the lowest number of pores and a narrow pore size distribution compared with all the other coatings.

Figure 13 depicts the bivariate distributions of pore size and shape of coatings deposited at SOD of 100 mm. Coatings deposited at other SODs exhibited the same

trend of bivariate pore size and shape distribution, albeit having different frequencies due to difference in porosity level. It can be seen that the major axis and Feret's diameter of the pores were directly proportional to one another, Figure 13(a). On the other hand, the shape descriptors, aspect ratio and circularity of the pores did not exhibit any apparent trend. However, there was a preference for aspect ratio to decrease as circularity increased. There were many pores that exhibited an

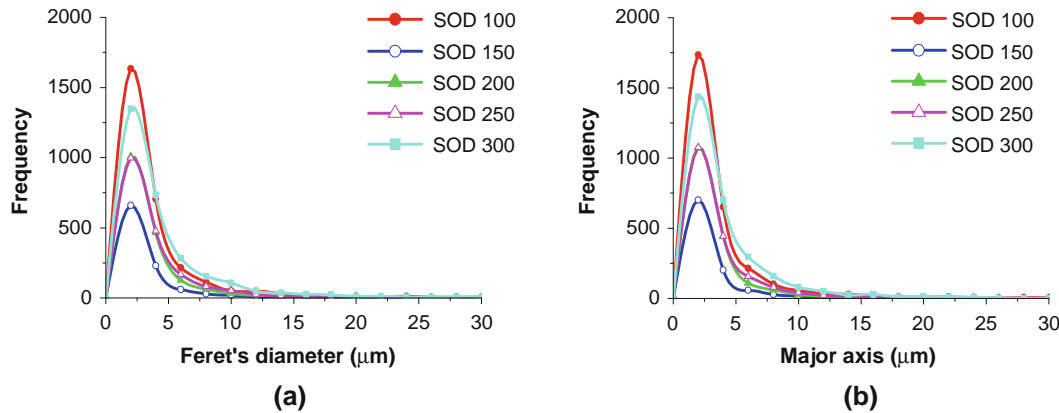


Fig. 12—Distribution of (a) Feret's diameter and (b) major axis of the pores in plasma sprayed Nd-Fe-B coatings deposited at various standoff distances.

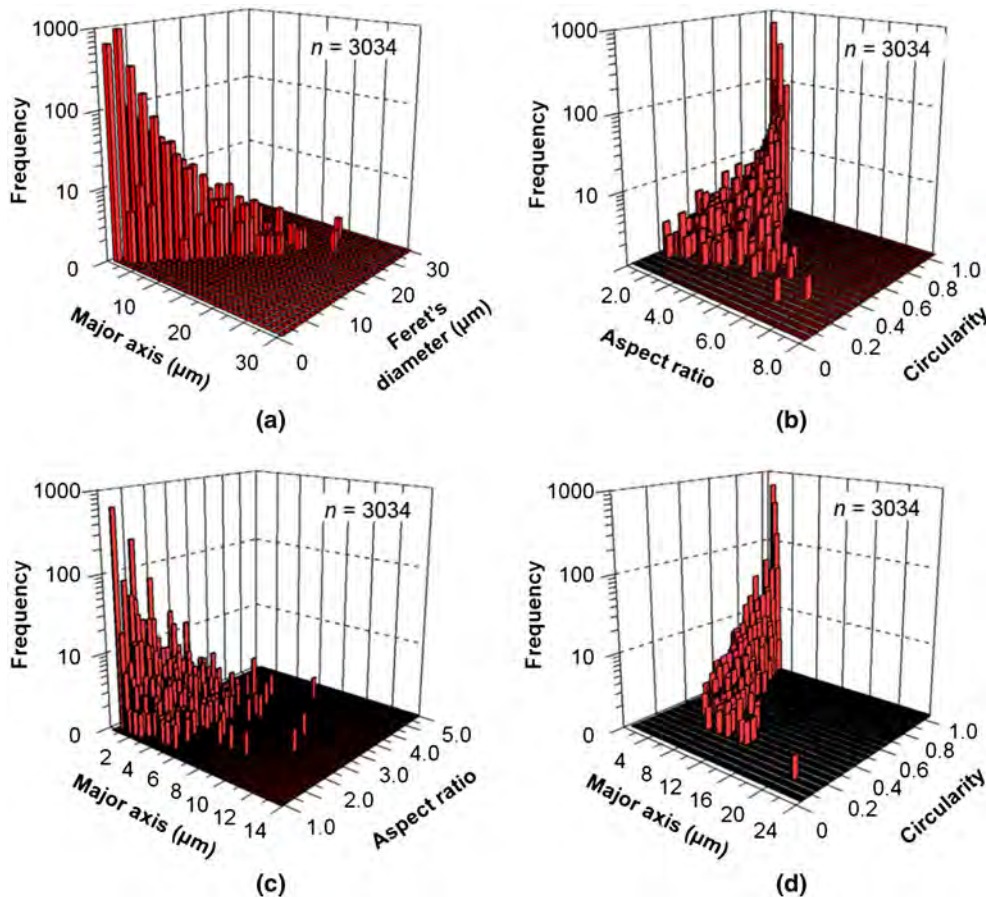


Fig. 13—Bivariate pore size and shape distributions for Nd-Fe-B coating deposited at standoff distance 100 mm: (a) major axis vs Feret's diameter, (b) aspect ratio vs circularity, (c) major axis vs aspect ratio, and (d) major axis vs circularity.

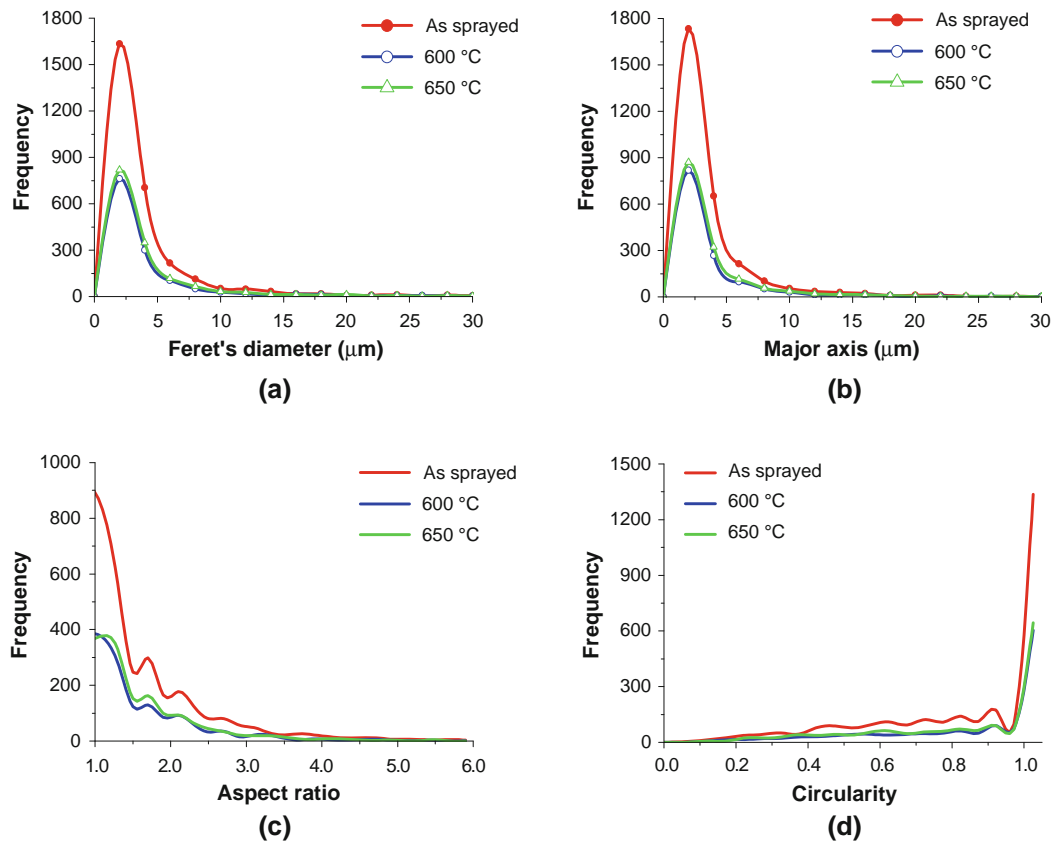


Fig. 14—Effects of annealing on the distribution of (a) Feret's diameter, (b) major axis, (c) aspect ratio, and (d) circularity of the pores in plasma sprayed Nd-Fe-B coatings deposited at standoff distance 100 mm.

aspect ratio equivalent to unity, but with varying circularity values that were less than unity. Again, this demonstrated that even though the pores were not elongated; *i.e.*, since they revealed the same values of major axis and minor axis, they were not necessarily circular.

Plots of major axis and shape descriptor frequency distributions, Figures 13(c) and (d), show that the shape descriptors approach unity; *i.e.*, becomes more spherical, when the pore size is small. These tiny circular pores were small globular pores that were formed from gas bubbles, type 3 pores in Table I, and contributed most toward the number of pores within the coatings, although the cumulative volume of this type of pore was small. Pores that have a high aspect ratio in addition to a large major axis were attributed to microcracks; type 7 pores in Table I.

The effects of annealing on the distribution of the size and shape descriptors of the pores for coatings deposited at SOD 100 mm are depicted in Figure 14. In general, annealing of plasma sprayed Nd-Fe-B coatings in the temperature ranging from 873 K to 923 K (600 °C to 650 °C) did not affect the curve shape of the pore size and shape distributions, but only changed the area under the curve. This is true for coatings deposited at all SODs.

As mentioned earlier in this section, the total porosity level was contributed by both the pore size and the

number of pores. Since these distributions were plotted as a function of frequency, the area under the curve was determined by the number of pores in the coatings instead of the total porosity level. Considering that small globular pores and microcracks contributed most to the number of pores in a given coating, the change in area under the curve for the pore size and shape distributions reflected the changes in the number of these types of pores instead of the total porosity. The broadening of the pore size distribution after annealing above 1273 K (1000 °C), which arose because of conversion of microcracks to globular pores or coarsening of the spherical pores by entrapped gas,<sup>[18]</sup> was not observed here.

The reduction of globular pores and development of microcracks after annealing did not have significant effects on the shape of the pore size and shape distributions for the temperature range studied. However, a significant change in the area under the curve corresponded to the change in total number of pores after annealing was observed. A slight narrowing of the pore size distributions was observed for annealed coatings, caused by the development of microcracks in the annealed coatings.

## 2. Three-dimensional (stereology implementation)

The pore size distributions for coatings deposited at various SODs derived using the DeHoff's protocol are



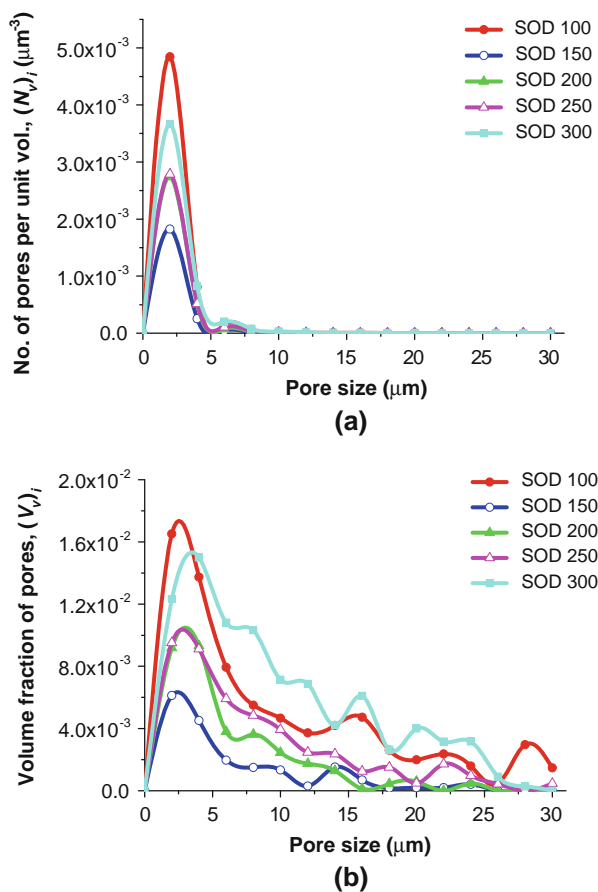


Fig. 15—Pore size distribution of coatings deposited at standoff distances ranging from 100 to 300 mm derived by DeHoff's protocol: (a) number of pores per unit volume,  $(N_V)_i$ ; and (b) volume fraction of pores,  $(V_V)_i$ .

shown in Figure 15. The pore size for all the coatings exhibited multimodal distributions. The first peak ranging from 2 to 4  $\mu\text{m}$  corresponded to microcracks and small globular pores, and was the most intense peak observed for all the coatings. This intense peak for microcracks and small globular pores indicated that these pores contributed to over 90 pct of total porosity by number, Figure 15(a). However, only about 50 pct of the total porosity by volume was composed of these pores, Figure 15(b). This difference in fraction of porosity by number and volume can be explained by the cubic relationship between the pore diameter and its volume.<sup>[13]</sup>

The subsequent peaks for the coatings corresponded to large globular pores, and had considerably lower intensity than the first peak. The peaks for large globular pores ranged from 8 to 28  $\mu\text{m}$ , depending on the SOD. The coatings deposited at 300 mm, which had the highest porosity level, exhibited the most diverse globular pore size among all the coatings where the large globular pores ranged from 8 to 24  $\mu\text{m}$ . On the other hand, the coatings deposited at 150 mm, which revealed the lowest porosity level exhibited the highest relative amount of microcracks and small globular pores, where

these types of pores constituted more than half of its total porosity. Several pores in coatings deposited at 100 and 300 mm showed sizes exceeding 30  $\mu\text{m}$ , which have been treated as outliers and omitted from the analysis. These large pores were presumed to be pull-outs that arose from metallographic preparation because of the brittleness of the coatings. Since all the coatings were prepared using the same metallographic procedure, the presence of pull-outs in these coatings implied that they have poor cohesion compared with coatings deposited at other SODs.

Note that the shape of the distribution for pore size distributions in Section IV-C-1, Figure 12(a) and (b), is similar to the shape for the plot of number of pores per unit volume,  $(N_V)_i$ , Figure 15(a). Unlike the 2D analysis of pore size distributions presented in the previous section where the area under the curve represented the number of pores within each coating, the  $(V_V)_i$  plots, Figure 15(b), represented the total porosity level of the coatings. In other words, the plots of 2D pore size distributions as a function of frequency disclosed the change in number of pores with respect to different coatings while the plot of 3D pore size distribution reflected the change of total porosity level for each coating.

While univariate size distributions, *i.e.*, distributions derived by DeHoff's protocol, are simple, they are suitable only to describe particles with constant shape, which is often unrealistic. The pore size distribution derived using the Cruz-Orive protocol is more suitable to convey information within thermal spray coatings since the pores vary in shape. The bivariate size-shape pore distribution for coatings deposited at SOD 100 mm is depicted in Figure 16. The coatings deposited at other SODs demonstrated similar bivariate pore size-shape distribution trend, with varying  $N_A$ ,  $N_V$ , and  $V_V$  intensity depending on their porosity levels.

Most of the pores observed were within 0 to 10  $\mu\text{m}$ ; Figure 16(a). More than 95 pct per unit volume of the pores were within the range of 2 to 4  $\mu\text{m}$ , Figure 16(b), consistent with the analysis by DeHoff's protocol. The 2 to 4  $\mu\text{m}$  pores existed for the entire range of the shape factor while the pores greater than 4  $\mu\text{m}$  demonstrated a shape factor between 0.2 and 1.0. This trend of pore size-shape distribution held for all the as-sprayed coatings, regardless of the SOD. Note that spherical pores revealed a shape factor or the eccentricity parameter,  $x^2$ , of zero and the value increased to  $\sim 1$  as the pores became sharper and flatter; *i.e.*, there was an increase in the ratio of minor axis to major axis. Although pores with size greater than 4  $\mu\text{m}$  account for less than 5 pct of the number of pores per unit volume, the volume fraction of these pores contributed up to over 50 pct of the total porosity, Figure 16(c), consistent with the DeHoff analysis.

The trend of bivariate size-shape distribution derived using stereology, Figure 16, was notably different from that derived on a 2D basis, Figure 13. This result arose because of the different shape parameters used between these two sections. However, it should be noted that the bivariate pore size-shape factor plots derived on a 2D basis corresponded to the trend observed for  $N_A$  plot, Figure 16(a).

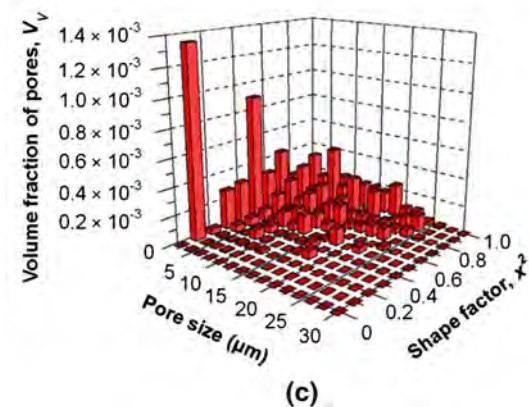
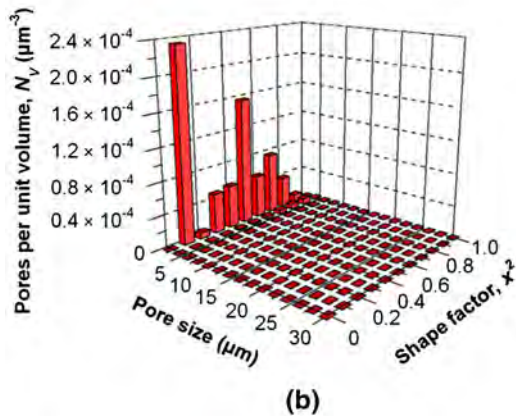
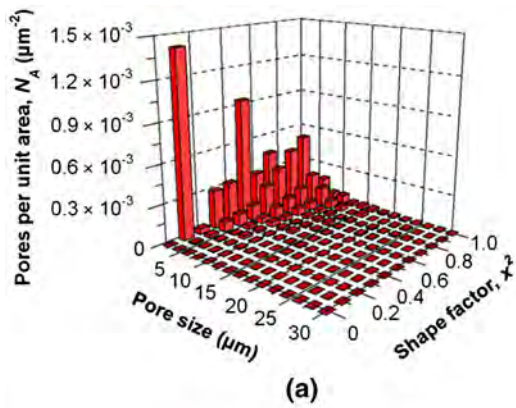


Fig. 16—Bivariate pore size–shape distributions of coating deposited at standoff distance 100 mm: (a) number of pores per unit area,  $N_A$ ; (b) number of pores per unit volume,  $N_V$ ; and (c) volume fraction of pores,  $V_V$ .

#### D. Pore Taxonomy

The pore shapes can be classified into three categories: (i) nearly spherical pores,  $0.1 < x^2 < 0.5$ ; (ii) non-flat spheroidal pores,  $0.5 < x^2 < 0.8$ ; and (iii) sharp disk-shaped pores,  $0.8 < x^2 < 1$ .<sup>[22]</sup> The volume fractions of the three pore types for coatings deposited at SOD ranging from 100 to 300 mm are illustrated in Figure 17. As mentioned earlier, the pores within the range from 2 to 4  $\mu\text{m}$  consisted of small globular pores and micro-cracks and were present in the entire shape factor range. However, it can be seen that regardless of the SOD, the

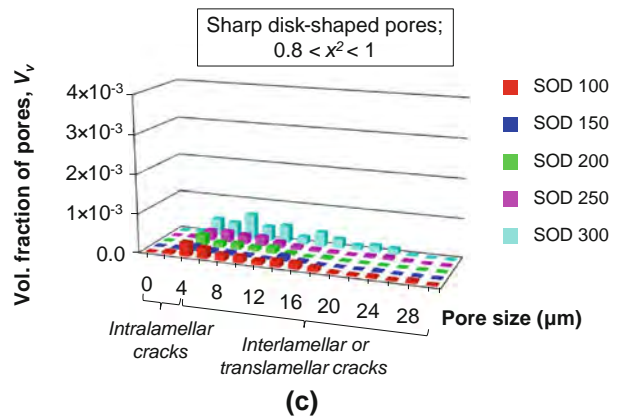
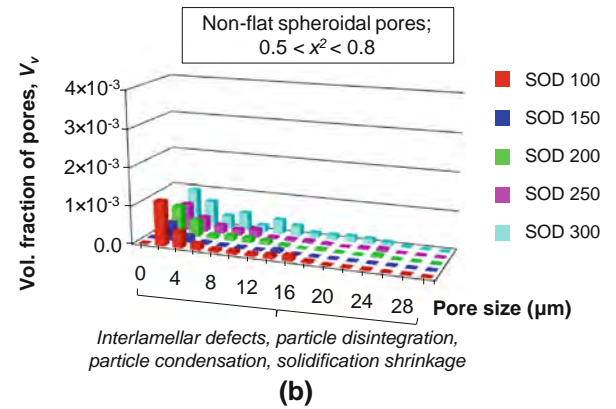
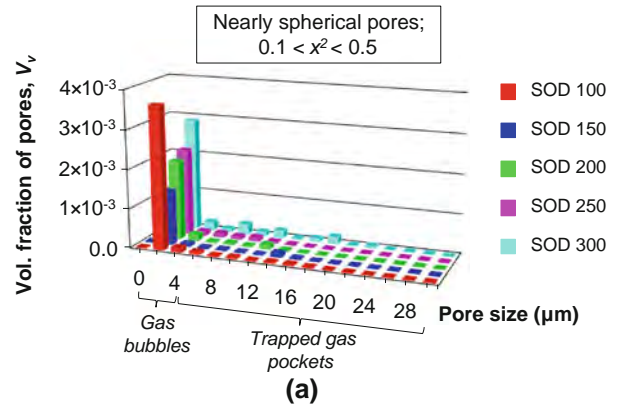


Fig. 17—Volume fraction of pores for coatings deposited at various standoff distance: (a) nearly spherical pores,  $0.1 < x^2 < 0.5$ ; (b) non-flat spheroidal pores,  $0.5 < x^2 < 0.8$ ; and (c) sharp disk-shaped pores,  $0.8 < x^2 < 1$ .

majority of the pores within this size range were small pores that were nearly spherical. On the other hand, pores greater than 4  $\mu\text{m}$  were mostly non-flat spheroidal pores and sharp disk-shaped pores.

Recall that the pores were categorized into globular pores and cracks in Section IV-B. In relation to these two pore types, globular pores were contributed by the pores with a shape factor  $< 1$ ; *i.e.*, nearly spherical and non-flat spheroidal pores. Cracks were contributed by the pores with a shape factor of  $\sim 1$  since cracks are mostly sharp compared with interlamellar pores. Referring back to the mechanism of pore formation discussed in the Introduction, the origin of these globular pores

and cracks can be predicted according to their size and shape.

Small nearly spherical pores with size ranging from 0 to 4  $\mu\text{m}$  were most likely caused by gas bubbles within molten particles that evaporated upon solidification, while near spherical pores larger than 4  $\mu\text{m}$  were caused by trapped gas pockets that result from turbulence of gas flow. Nevertheless, nearly spherical pores can also be formed by other mechanisms such as those for non-flat spheroidal pores; although the likelihood for these pores to be formed by gas bubbles and trapped gas pockets is significantly higher because of their “nearly spherical” shape. Non-flat spheroidal pores, regardless of their size, were formed through a variety of mechanisms including stacking defects, disintegration of particles, condensation of evaporated particles and solidification shrinkage. Sharp pores with shape factors of  $\sim 1$  were associated with microcracks that could result from a variety of mechanisms; *e.g.*, solidification, thermal stresses and external loads. Microcracks within the size range of 0 to 4  $\mu\text{m}$  were allocated as intralamellar cracks while those greater than 4  $\mu\text{m}$  were considered to be interlamellar or translamellar cracks.

The distribution of the three types of pores—(i) nearly spherical, (ii) non-flat spheroidal, and (iii) sharp disk-shaped pores, as a function of SOD—are depicted in Figure 18. The pores formed by gas bubbles and entrapped gas pockets, *i.e.*, type (i), dominated at low SOD. The three types of pores became more evenly distributed when the SOD increased; see Figure 18. This indicated that the dominance of pore-formation mechanism shifted as SOD varied, because of variation of in-flight time, particle velocity, and solidification rate.

It is apparent that the majority of the pores,  $\sim 50$  pct, at lower SOD were formed by gas bubbles and trapped gas pockets. Note that it is possible that globular pores originated from a porous feedstock. However, this was not the case in the current study since cross sections of the as-received feedstock showed a dense and non-porous structure. The gas bubbles arose because of gas dissolution from the molten particles during their

in-flight history; whereas trapped gas pockets were likely to be formed by turbulent gas flow near the plasma spray torch nozzle, refer to Table I. The gas bubbles and trapped gas pockets were subjected to shrinkage and may collapse if the pressure of the molten droplet increased. Thus, collapsed porosity may have also evolved from decompression of dissolved gas during molten droplet impingement on the substrate.<sup>[42]</sup> The release of gas bubbles upon impingement depends on the particle velocity as well as the solidification rate. The globular pores may also be contributed by the evaporation or desorption of gases upon solidification, which dissolved into or adsorbed onto the particles during their in-flight trajectory.<sup>[43]</sup>

Coatings deposited at SOD of 300 mm exhibited a lower volume fraction of small globular pores than those deposited at 100 mm, despite having a higher total porosity. This behavior can be explained by the dynamics of gas bubbles within liquids, where small bubbles tend to coalesce to a larger bubble within the droplet.<sup>[42]</sup> Such a mechanism also explains the significant amount of large globular pores in coatings deposited at SOD of 300 mm since these pores experienced a longer in-flight time and may coalesce. After solidification, some of these trapped gas bubbles have sufficiently large internal pressure that, when released, the formation of microcracks, fragmentation, and residual stresses can evolve.

Figure 19 compares the relative volume fractions of the three types of pores in as-sprayed and annealed coatings. Note that this plot of volume fraction comparison is in relative volume fraction—they are in terms of percentage and the actual volume fractions of pores depends on the total porosity of each coating. It can be seen that the overall percentage of sharp disk-shaped pores generally decreased after annealing and was compensated by the increase of nearly spherical or non-flat spheroidal pores. The data reinforced a mechanism whereby intralamellar cracks were healed or transformed to nearly spherical or non-flat spheroidal pores after annealing.

According to Erk *et al.*,<sup>[44]</sup> there were two mechanisms responsible for microstructural changes during the heat treatment of plasma sprayed coatings: surface diffusion and volume diffusion. Surface diffusion was responsible for the healing of intralamellar cracks and commenced at around 1073 K (800 °C) for ceramic coatings.<sup>[39]</sup> On the other hand, volume diffusion occurred at a higher temperature—well above 1273 K (1000 °C) for ceramic coatings—and accounted for the reduction of porosity through shrinkage of interlamellar pores. However, these temperatures are likely to differ for different materials. Heat treatment was found to decrease the porosity in a copper coating at temperatures as low as 573 K (300 °C).<sup>[5]</sup>

Since all the coatings were heat treated under the same conditions, there was no reason for the difference in sintering behavior to be caused by the annealing process. The different annealing mechanisms were most likely attributed to either the difference in the porosity level or phase content. The coatings deposited at SODs of 100 and 300 mm exhibited an almost similar total porosity level, with a difference of  $\sim 1$  pct. Therefore, the

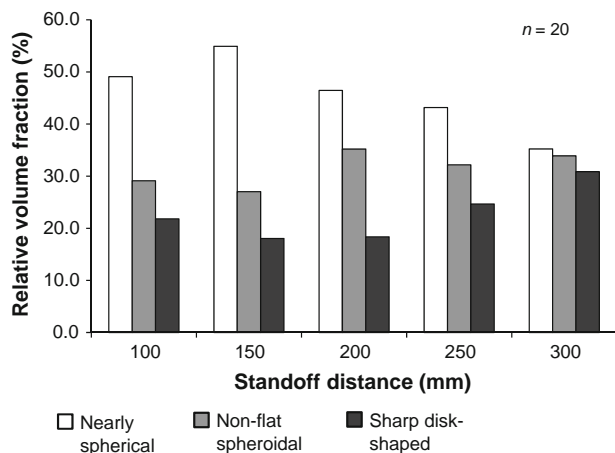


Fig. 18—Distribution of nearly spherical pores, non-flat spheroidal pores, and sharp disk-shaped pores as a function of standoff distance.



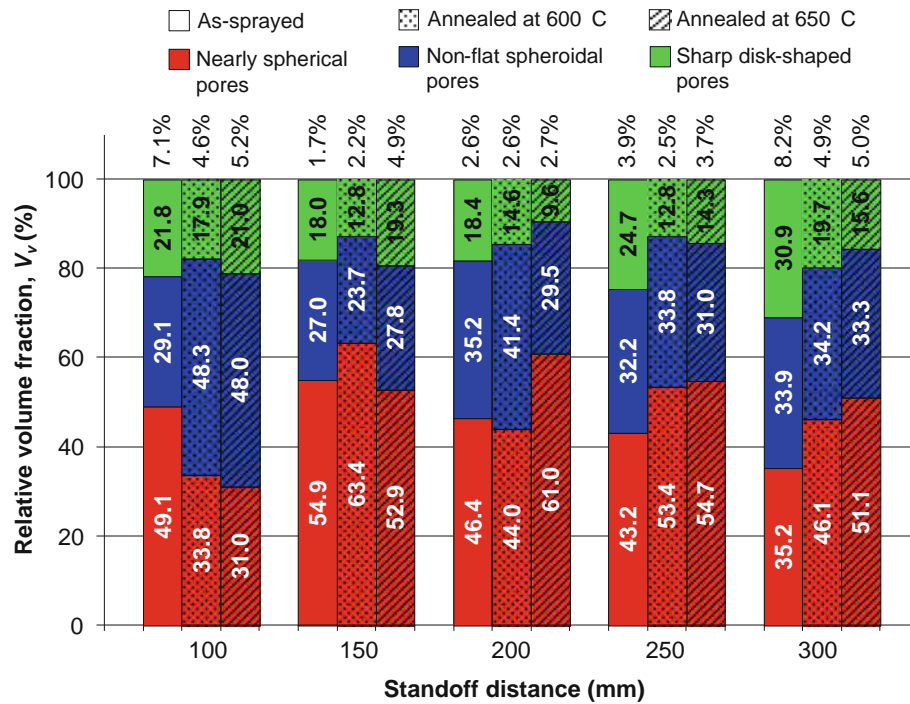


Fig. 19—Effects of annealing on the distribution of nearly spherical pores, non-flat spheroidal pores, and sharp disk-shaped pores as a function of standoff distance. *Note* Each of the three columns for the five SODs represents, from left to right, as-sprayed, annealed at 873 K (600 °C) and annealed at 923 K (650 °C) conditions. The values above each column represent the total porosity of the coatings.

different annealing mechanisms did not contribute to the overall porosity level. Instead, the as-sprayed coatings deposited at SOD of 100 mm showed double the microcrack content of coatings deposited at other SODs. The microcracks that arose from quenching stresses were reformed during the initial stage of annealing into interlamellar pores. The small interlamellar pores subsequently coalesced or coarsened to larger pores.

On the other hand, coatings that were deposited at other SODs experienced a further step of releasing the thermal stresses by developing microcracks during the initial stage of the annealing process—hence, the rise in small globular pores. Since the annealing time was the same for all the coatings; *i.e.*, 30 minutes, the coatings deposited at SODs ranging from 150 to 300 mm only underwent the non-densifying mass transport mechanism where interlamellar cracks transformed into small globular pores, and the annealing process ceased before pore coarsening could take place.

## V. CONCLUSIONS

Cross-sectional studies of plasma sprayed Nd-Fe-B coatings show that coating porosity varies in size and shape, indicating that porosity arose from different formation mechanisms. The pore structure of the coatings also evolved after annealing, where the overall porosity decreased after annealing. The total porosity level determined *via* Delesse's protocol and DeHoff's protocol were comparable, and it was concluded that

the Delesse's protocol offers a simpler and accurate way to determine the total porosity level.

The pore size and shape distribution were determined by comparing the distributions derived on 2D plane and 3D projection (stereology). The SOD did not influence the distribution trend for the number of pores per unit area,  $N_A$  and the number of pores per unit volume  $N_V$ , but significantly affects the volume fraction of pores,  $V_V$ . The area under the curve for the plots of  $N_V$  and of  $V_V$  revealed the total number of pores and total porosity of the coatings, respectively. The pore size distributions derived using DeHoff's and Cruz-Orive analyses were consistent with one another. While DeHoff's protocol was effective in deriving the pore size distribution, Cruz-Orive's protocol can be used to derive bivariate size–shape distributions of the pores.

The bivariate distributions of pore size and shape, where shape factor was represented by the eccentricity parameter,  $x^2$ , allowed for the prediction of dominant pore type in the coatings and the pore fractions that were derived from different origins:

- (i) Nearly spherical ( $0.1 < x^2 < 0.5$ ): gas bubbles (2 to 4  $\mu\text{m}$ ) and trapped gas pockets ( $>4 \mu\text{m}$ ).
- (ii) Non-flat spheroidal ( $0.5 < x^2 < 0.8$ ): interlamellar defects, particle disintegration, particle condensation, and solidification shrinkage.
- (iii) Sharp disk-shaped ( $0.8 < x^2 < 1$ ): intralamellar cracks (2 to 4  $\mu\text{m}$ ) and interlamellar cracks ( $>4 \mu\text{m}$ ).

SOD influenced the pore formation mechanism because of varying in-flight time, particle velocity, and solidification rate. Type (i) pores dominated at short

SOD, while at longer SOD, the three types of pores became more evenly distributed as the entrapped gas were transformed into other forms of pores. Annealing decreased type (iii) pores, while it increased type (i) and (ii) pores, as microcracks were transformed into globular pores.

The means to quantify and classify different types of pores, as well as predict the formation mechanisms for each pore type within thermal spray coatings presented in the current study provide useful insights into controlling the pore size and shape to optimize the preferred porosity level and pore type in the coatings.

## ACKNOWLEDGMENTS

The current study is supported by a Swinburne University Postgraduate Research Award (SUPRA).

## REFERENCES

1. R.W. Rice: *Key Eng. Mater.*, 1996, vol. 115, pp. 1–20.
2. T. Nakamura, G. Qian, and C.C. Berndt: *J. Am. Ceram. Soc.*, 2000, vol. 83, pp. 578–84.
3. M. Cherigui, S. Guessasma, N. Fenineche, R. Hamzaoui, O. El-Kedim, and C. Coddet: *Mater. Chem. Phys.*, 2005, vol. 92, pp. 419–23.
4. Z. Wang, A. Kulkarni, S. Deshpande, T. Nakamura, and H. Herman: *Acta Mater.*, 2003, vol. 51, pp. 5319–34.
5. P. Sudharshan Phani, D. Srinivasa Rao, S.V. Joshi, and G. Sundararajan: *J. Therm. Spray Technol.*, 2007, vol. 16, pp. 425–34.
6. M.P.W. Vreijling. Ph.D. Thesis, TNO Institute of Industrial Technology, The Netherlands, 1998.
7. M.L. Berndt and C.C. Berndt: in *ASM Handbook*, S.D. Cramer and B.S. Covino, Jr., eds., ASM International, Materials Park, OH, 2003, pp. 803–13.
8. M. Xue, S. Chandra, J. Mostaghimi, and H.R. Salimijazi: *Plasma Chem. Plasma Process.*, 2007, vol. 27, pp. 647–57.
9. H. Hu, Z.H. Lee, D.R. White, and E.J. Lavernia: *Metall. Mater. Trans. A*, 2000, vol. 31A, pp. 723–33.
10. R. McPherson and B.V. Shafer: *Thin Solid Films*, 1982, vol. 97, pp. 201–04.
11. M. Xue, S. Chandra, and J. Mostaghimi: *J. Therm. Spray Technol.*, 2006, vol. 15, pp. 531–36.
12. J. Ilavsky, C.C. Berndt, and J. Karthikeyan: *J. Mater. Sci.*, 1997, vol. 32, pp. 3925–32.
13. A. Bacciochini, F. Ben-Ettouil, E. Brousse, J. Ilavsky, G. Montavon, A. Denoirjean, S. Valette, and P. Fauchais: *Surf. Coat. Technol.*, 2010, vol. 205, pp. 683–89.
14. G. Montavon, C. Coddet, C.C. Berndt, and S.H. Leigh: *J. Therm. Spray Technol.*, 1998, vol. 7, pp. 229–41.
15. S. Deshpande, A. Kulkarni, S. Sampath, and H. Herman: *Surf. Coat. Technol.*, 2004, vol. 187, pp. 6–16.
16. G. Antou, G. Montavon, F. Hlawka, A. Cornet, and C. Coddet: *J. Therm. Spray Technol.*, 2006, vol. 15, pp. 765–72.
17. J. Ilavsky, A.J. Allen, G.G. Long, S. Krueger, C.C. Berndt, and H. Herman: *J. Am. Ceram. Soc.*, 1997, vol. 80, pp. 733–42.
18. A.J. Allen, J. Ilavsky, G.G. Long, J.S. Wallace, C.C. Berndt, and H. Herman: *Acta Mater.*, 2001, vol. 49, pp. 1661–75.
19. J.A. Gan, C.C. Berndt, Y.C. Wong, and J. Wang: *J. Therm. Spray Technol.*, 2013, vol. 22, pp. 337–44.
20. A. Ohmori, C.J. Li, and Y. Arata: in *Thermal Spray Coatings: Properties, Processes and Applications*, T.F. Bernecki, ed., ASM International, Pittsburgh, 1991, pp. 105–13.
21. A. Ohmori and C.J. Li: *Thin Solid Films*, 1991, vol. 201, pp. 241–52.
22. S.H. Leigh and C.C. Berndt: *J. Am. Ceram. Soc.*, 1999, vol. 82, pp. 17–21.
23. R.T. DeHoff and F.N. Rhines: *Trans. Metall. Soc. AIME*, 1961, vol. 221, pp. 975–82.
24. R.T. DeHoff: *Trans. Metall. Soc. AIME*, 1962, vol. 224, pp. 474–77.
25. L.M. Cruz Orive: *J. Microsc.*, 1976, vol. 107, pp. 235–53.
26. L.M. Cruz Orive: *J. Microsc.*, 1978, vol. 112, pp. 153–67.
27. SA Saltykov: *Stereometric Metallography*, 2nd ed., Metallurgizdat, Moscow, 1958.
28. S.A. Saltykov: in *Proc. Second Int. Congr. Stereol.*, H. Elias, ed., Springer, Chicago, IL, 1967, pp. 163–73.
29. C.E. Mancini, C.C. Berndt, L. Sun, and A. Kucuk: *J. Mater. Sci.*, 2001, vol. 36, pp. 3891–96.
30. A. Portinha, V. Teixeira, J. Carneiro, J. Martins, M.F. Costa, R. Vassen, and D. Stoeber: *Surf. Coat. Technol.*, 2005, vol. 195, pp. 245–51.
31. J.A. Gan and C.C. Berndt: *Surf. Coat. Technol.*, 2013, vol. 216, pp. 127–38.
32. M.D. Abramoff, P.J. Magalhaes, and S.J. Ram: *Biophotonics Int.*, 2004, vol. 11, pp. 36–42.
33. American Society for Testing and Materials: *Metals—Mechanical Testing; Elevated and Low-Temperature Tests; Metallography*, ASTM International, West Conshohocken, PA, 2007, pp. 1273–80.
34. G. Antou and G. Montavon: *J. Therm. Spray Technol.*, 2007, vol. 16, pp. 168–76.
35. J.A. Gan and C.C. Berndt: *Surf. Coat. Technol.*, 2011, vol. 205, pp. 4697–704.
36. A. Delesse: *Ann. Mines*, 1848, vol. 13, pp. 379–88 (in French).
37. S.W.K. Kweh, K.A. Khor, and P. Cheang: *Biomaterials*, 2000, vol. 21, pp. 1223–34.
38. J. Ilavsky, H. Herman, C.C. Berndt, A. Goland, G. Long, S. Krueger, and A.J. Allen: in *Thermal Spray Industrial Applications*, C.C. Berndt and S. Sampath, eds., ASM International, Boston, MA, 1994, pp. 709–14.
39. J. Ilavsky, G.G. Long, A.J. Allen, and C.C. Berndt: *Mater. Sci. Eng. A*, 1999, vol. 272, pp. 215–21.
40. S.H. Leigh, C.K. Lin, and C.C. Berndt: *J. Am. Ceram. Soc.*, 1997, vol. 80, pp. 2093–99.
41. V.V. Sobolev and J.M. Guilemany: *Surf. Coat. Technol.*, 1994, vol. 70, pp. 57–68.
42. H. Li, K.A. Khor, and P. Cheang: *Biomaterials*, 2004, vol. 25, pp. 3463–71.
43. H. Meyer: *Ber. Dtsch. Keram. Ges.*, 1964, vol. 41, pp. 112–19 (in German).
44. K.A. Erk, C. Deschaseaux, and R.W. Trice: *J. Am. Ceram. Soc.*, 2006, vol. 89, pp. 1673–78.

### Permission to publish

J.A. Gan and C.C. Berndt, 'Quantification and taxonomy of pores in thermal spray coatings by image analysis and stereology approach', *Metall. and Mater. Trans. A*, 44A[10] (2013) p. 4844–4858. DOI: 10.1007/s11661-013-1818-4, Published: OCT 2013.

With kind permission from Springer Science+Business Media. The complete article (text, figures, tables and references) have been kindly reproduced.





## Chapter 3. Mechanical Property Testing

### 3.1 Introduction

The 5 manuscripts in Chapter 3 focus on mechanical properties of thermal spray coatings. This topic was the focus on the applicant's thesis and the studies have been refined since his own submission in 1981. Work has been selected from the 1993-2001 timeframe, with manuscript #7 being a review of the "Measurement of adhesion for thermally sprayed materials". This work also developed into measuring "Contact Damage in plasma-sprayed alumina-based Coatings", manuscript #8; and two companion manuscripts on the "Influence of plasma spray parameters on mechanical properties of yttria stabilized zirconia coatings". These manuscripts, #9 and #10, examined the four point bend test and acoustic emission to measure Young's Modulus, a pseudo yield point, and cracking mechanisms.

Hardness measurements have been a favoured technique of the applicant for many years and the unique usefulness, attributes and simplicity of this method is illustrated in manuscript #11 (2001) where the 'Evaluation of microhardness and elastic modulus of thermally sprayed nanostructured zirconia coatings' is explored. This work related hardness to roughness for the series of samples analysed. Likewise, this work was the forerunner to further analysis on the bimodal distribution of hardness tests measured by a Weibull distribution analysis; work that was introduced to the thermal spray community by the applicant in 1988.

The 144 publications with the identification numbers below are considered as contributions that focus on this specific subject material. Chapter 7 of this thesis outlines the methodology employed for this analysis.

3	33	83	154	234	294	347
4	34	85	159	236	295	349
5	41	87	168	239	296	351
6	42	89	169	240	297	352
7	43	94	170	244	299	358
9	44	100	171	250	303	365
10	55	103	172	251	308	371
11	56	104	176	259	309	377
12	57	105	182	260	310	379
14	58	106	193	261	311	380
15	59	108	194	262	312	381
16	60	112	195	263	313	383
17	62	114	196	269	314	392
23	63	116	206	272	315	394
24	64	127	207	273	316	413
25	67	129	211	277	318	436
28	71	131	213	281	331	453
29	72	136	214	282	332	459
30	76	142	218	286	333	
31	77	143	219	287	338	
32	78	144	220	292	342	

# Measurement of adhesion for thermally sprayed materials

C. C. BERNDT\* and C. K. LIN

*The Thermal Spray Laboratory, Department of Materials Science and Engineering,  
SUNY at Stony Brook, Stony Brook, NY 11794-2275, USA*

Revised version received 21 May 1993

**Abstract**—Thermally sprayed coatings have a distinctive microstructure which can be described as '*a three-dimensional layered structure of discs which are interlaced to form a material of composite nature*'. The coatings are normally greater than 25  $\mu\text{m}$  in thickness and can thus be described as bulk coatings. The minimum microstructural detail would be a single splat (often described as a lamella), which is about 5  $\mu\text{m}$  in thickness and up to 80  $\mu\text{m}$  in diameter. This paper focuses on methods used to define and measure the adhesion of coatings or deposits formed by thermal spray technology. The properties distinguished include those of strength and toughness. Measurements such as the tensile adhesion (according to ASTM C633) and double cantilever beam (DCB) tests will be addressed to illustrate the relevance (if any) of such methods to present industrial practice. Acoustic emission studies have also assessed a function termed as the 'crack density function', i.e. a product of the number of cracks and crack size. Other measuring methods applied to this technology include micro-hardness and scratch testing. The former technique has demonstrated that the material properties of coatings are anisotropic, and the latter method is being considered within the biomedical industry to assess the adhesion of hydroxyapatite to orthopedic prostheses. These techniques, among others, may be used for both fundamental understanding of coating performance (i.e. life prediction and cracking mechanisms) and as tests for quality control.

**Keywords:** Acoustic emission; adhesion; adhesion measurement; coating failure; degradation; double cantilever beam test; fracture mechanics; indentation; lifetime modeling; scratch test; thermally sprayed coatings.

## 1. INTRODUCTION

### 1.1. Formation and structure of thermally sprayed coatings

A variety of thermal spray processes are available to deposit thick coatings for a broad range of applications [1–3]. The processes are essentially similar in that a material is heated up by a gaseous medium and simultaneously accelerated and projected onto the substrate. The family of thermal spray processes includes, among other processes, flame spraying, plasma spraying, vacuum plasma spraying (also called low pressure plasma spraying), high velocity oxygen fuel, arc metallization, and detonation gun spraying. The prime distinctions between these spraying processes are the temperature of the process and the velocity of the thermal source used in the process. These process variables control the nature of the materials that can be sprayed. The techniques also differ with regard to their process economics; that is, factors such as the cost of the equipment, the cost of

---

\*To whom correspondence should be addressed.

the feedstock materials and other consumables such as gases, grit blast media, etc. that may limit the viability of a particular process.

Thermal spray technology is not limited to coating substrates but now also encompasses the manufacture of net shapes [4], which can be considered as very thick coatings [up to, say, 1" (25 mm) in thickness] stripped from the substrate (or 'forming tool') and then used directly as an engineered material [5]. The availability of thermal spray processes enables the production of materials of varying composition and structure—the so-called 'functionally gradient materials'.

Several conferences have been devoted to thermal spray and such proceedings [6–8] cover many of the processing variables associated with this technology. In addition, a quarterly journal called the *Journal of Thermal Spray Technology* is now available that covers the complete engineering and scientific arenas of this technology.

Thermally sprayed coatings consist of a layered structure that is highly anisotropic such that individual splats are oriented parallel to the substrate surface [9]. A microstructural cross-section of a thermally sprayed material is illustrated in Fig. 1, where unmelted particles are embedded within the layered structure and also pores exist either totally inside or between each layer [10]. After formation of the coating, the first property criterion for this coating system is 'How well is the coating adhered to the substrate' and it therefore follows 'How can we evaluate this adhesion strength, especially for coatings which are in service?' The intent of this paper is to describe and then discuss methods of

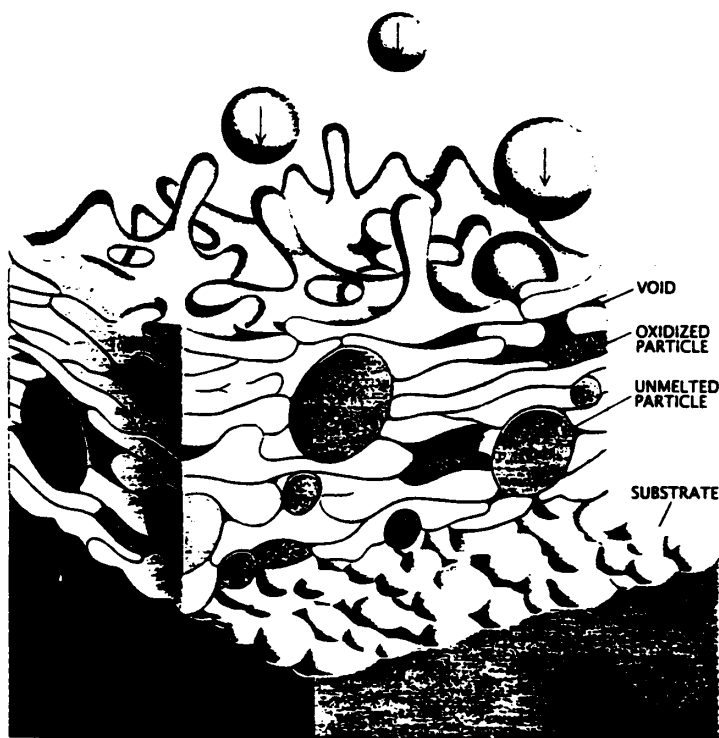


Fig. 1. Microstructure of thermally sprayed coatings [10].

measuring the 'adhesion strength' of thermally sprayed coatings. A strong intent is to always relate such measurements to the ultimate application(s) of the coatings.

### 1.2. Rationale for measuring adhesion

According to Mittal [11], adhesion can be expressed in various ways. For example, 'basic adhesion' signifies the interfacial bond strength and is the summation of all intermolecular or interatomic interactions. The result of an adhesion test is called 'practical adhesion' and is a function of basic adhesion and many factors—all of which represent the work required to detach a film or coating from a substrate. Many theories or mechanisms for adhesion have been proposed [12, 13]; however, none is fulfilled by all situations and there is no adhesion test available which satisfies all requirements. Therefore the best test method often becomes the one that simulates practical stress conditions.

The term 'adhesion' requires special definition for the purposes of thermal spray coatings. For example, the American Society for Testing and Materials (ASTM) [14] states adhesion as '*the state in which two surfaces may consist of valence forces or interlocking forces or both*'. The theories of adhesion between two materials, in general terms, include mechanisms based on diffusion, mechanical interlocking, electrostatic attraction, physical adsorption, chemical bonding, and weak boundary layers [15]. However, the above global definition cannot be universally applied to thermal spray materials since these coatings can be considered as 'composites' at the microstructural level. Thus, bonding mechanisms for forming an integral coating or net shape will also be complex and may involve adhesion processes which are exclusive of those established for classical joining technology. The basic bonding mechanisms that have been defined for thermal spray coatings can be categorized into three major groups [16] (Table 1).

The specific thermal spraying process will influence the microstructure of the coating and, therefore, it can be inferred that the adhesion strength of the deposit will vary. For example, the high velocity oxygen fuel (HVOF) technique produces a very dense microstructure with porosity typically less than 2% compared to the less than 5% porosity, at best, for a flame sprayed or an atmospheric plasma sprayed material. Thus, factors affected by the spray parameters, including the size and distribution of porosity, oxide content, residual stresses, and macro- or micro-cracks, have an important influence on the performance and eventual failure of the coating system.

**Table 1.**  
**The basic bonding mechanisms of thermally sprayed coatings**

<b>Mechanical interlocking (anchoring)</b>
<b>Metallic bonds (metal-metal bonds)</b>
dispersion forces
chemisorption and epitaxy
diffusion
<b>Chemical bonds</b>
intermetallic compounds



The service failure mode(s) can be described as interfacial, cohesive, or of mixed **interfacial/cohesive** failures.\* This service failure mode must also be reflected by any testing method which seeks to perform a meaningful quality control test of coatings. It is thus preferable that any laboratory test induces the observed service failures, otherwise they will be of limited application to engineering design. Useful measurements on adhesion strength and interpretation of the test results to predict the service life of coatings or net shapes are the most challenging problem for thermal spray scientists.

### 1.3. Application of fracture mechanics to adhesion measurement

The adhesion of thermally sprayed coatings is not only an interfacial problem of the individual lamella within a coating, but also concerns examination of the integrity of the interface between the substrate and coating, residual stresses, crack population, and pore size and distribution. Fracture mechanics [17, 18] considers the energy required to initiate or propagate cracks and evaluates the adhesion of the coating system in terms of 'fracture toughness, [19–21]. Four-point bending methods, single-edge notched specimens, double cantilever beam tests, indentation techniques, and other measurements have been employed to assess the adhesion of coating systems [22–24].

The purpose of all these methods is fundamentally the same when they are expressed from the viewpoint of fracture mechanics. The experimental proposition is to establish the equilibrium condition where the elastic energy provided by an external force (as defined by the geometry of the specimen and the applied load) is balanced by the propagation of a stable crack. One form of this energy balance criterion derives the strain-energy release rate,  $G$  (in  $\text{J}/\text{m}^2$ ), and is defined as:

$$G = \frac{\partial (W - U)}{\partial A} \quad (1)$$

where  $W$  is the work done by external forces (in  $\text{J}$ ),  $U$  is the elastic energy stored in the system (in  $\text{J}$ ), and  $A$  is the crack area (in  $\text{m}^2$ ).

It is convenient to write  $G$  as

$$G = \frac{F^2}{2B} \frac{dC}{dL} \quad (2)$$

where  $F$  is the force required to extend a crack (in  $\text{N}$ ),  $L$  is the crack length (in  $\text{m}$ ),  $B$  is the thickness (in  $\text{m}$ ), and  $C$  is the compliance (in  $\text{m}/\text{N}$ ).

The strain-energy release rate can be related to the fracture toughness by

$$K = \sqrt{\frac{EG}{1 - \nu^2}} \quad (3)$$

where  $E$  is the elastic modulus (in  $\text{MPa}$ ) and  $\nu$  is Poisson's ratio (dimensionless).

---

\*Thermal spray engineers should recognize that the term 'interfacial' is used in preference to 'adhesive' to avoid confusion with an 'adhesive' which is used to join materials (i.e. adhesive will be used as a noun rather than as an adjective).

When  $G$  exceeds a critical value,  $G_c$ , crack propagation occurs and failure of the coating system results. The evaluation of  $K$  assumes that both the elastic modulus and Poisson's ratio of the material are known. The physical representation of the above equations is that the change in compliance of the specimen controls the energy input into the creation of new fracture surfaces. Thus, the corollary of this theory is that the crack path and rate of crack growth can be controlled very precisely by appropriate design of the specimen.

Thus, 'mechanical adhesion' can be evaluated in terms of adhesion strength or fracture toughness. Such measurements of coating–substrate adhesion have been reviewed recently and are listed in Table 2 [25–27]. However, test methods for thermally sprayed coatings are restricted. The techniques to be discussed in this paper include the double cantilever beam test, acoustic emission technology, microhardness assessment, and the scratch test. The tensile adhesion test (TAT) is not covered in detail but will be referenced.

Table 2. Methods that can be used to determine coating–substrate adhesion	
Qualitative	Quantitative
<i>Mechanical methods</i>	
Scotch tape test	Direct pull-off method
Abrasion test	Laser spallation test
Bend and scratch test	Indentation test
	Ultracentrifugal test
	Scratch test
<i>Non-mechanical methods</i>	
X-ray diffraction	Thermal method
	Nucleation test
	Capacitance test

2. ADHESION MEASUREMENTS

2.1. Methods

One difficulty with any mechanical property assessment of coatings is how to attach a loading device to the coating without influencing the property that is being measured. Some investigators [28] have approached this problem by manufacturing a pin or disk that could be removed from a mating component (Fig. 2). The surface of this assembly was thermal sprayed and then the pin or disk, depending on the assembly used, removed. The force at fracture was used to find a parameter termed 'the adhesion strength' of the coating. The corresponding shear test is performed by spraying the outside diameter of a cylinder or the head of a pin (Fig. 3) [29]. One potential difficulty with the above test is that the duplex nature of the specimen assembly may influence the coating quality since the heating and cooling behavior of the deposit will be affected by the interface between the two components. Another feature of both the tensile and the shear tests is that the fracture mode is ambiguous since mixed mode failure often occurs.

Other geometries that do not need an adhesive are illustrated in Figs 4 [30] and 5 [31]. These tests have not been widely implemented outside of their

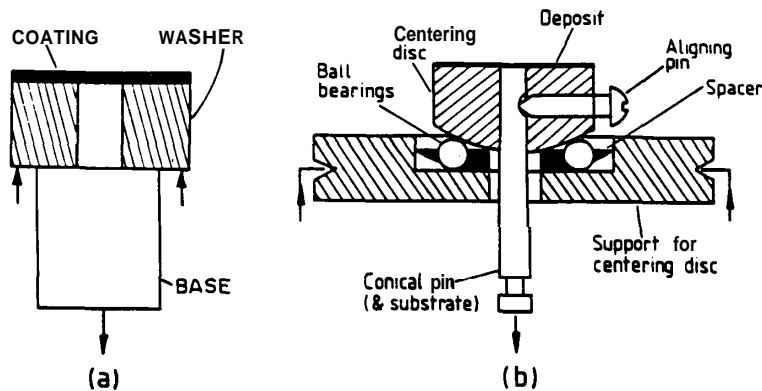


Fig. 2. (a) Specimen for determining adhesion strength; (b) centering device and specimen in cross-section [28].

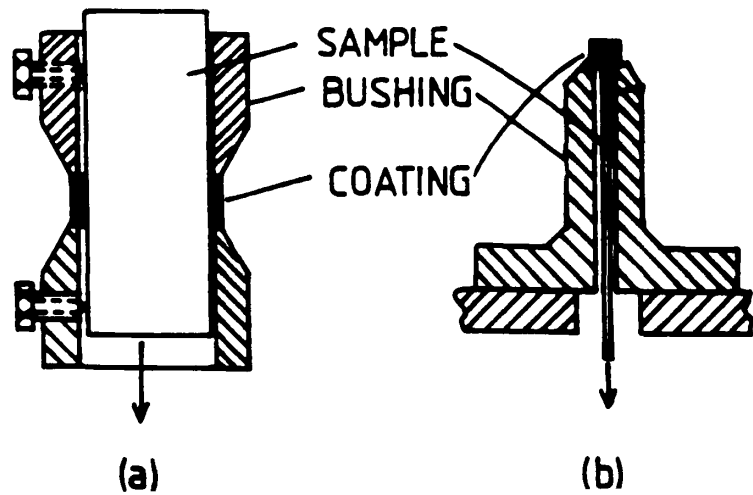


Fig. 3. Shear tests [29].

laboratories of origin. The method of spraying two adjoining conical parts is expected to incorporate a failure which has a large shear component, whereas the other shear test may exhibit either shear failure parallel to the substrate surface or shear failure through the coating thickness.

The adhesion properties of coatings were investigated on the microscopic level [32] by shearing individual particles from the substrate surface (Fig. 6). This study considered that adhesion to the substrate arose from interactions across the particle-substrate interface and a 'strength of growth rate constant' ( $K'$ ) was defined as

$$K' = -\frac{1}{t} \ln \left( 1 - \frac{N(t)}{N_0} \right) \quad (4)$$

where  $t$  is the time,  $N(t)$  is the number of atoms that react during the interaction

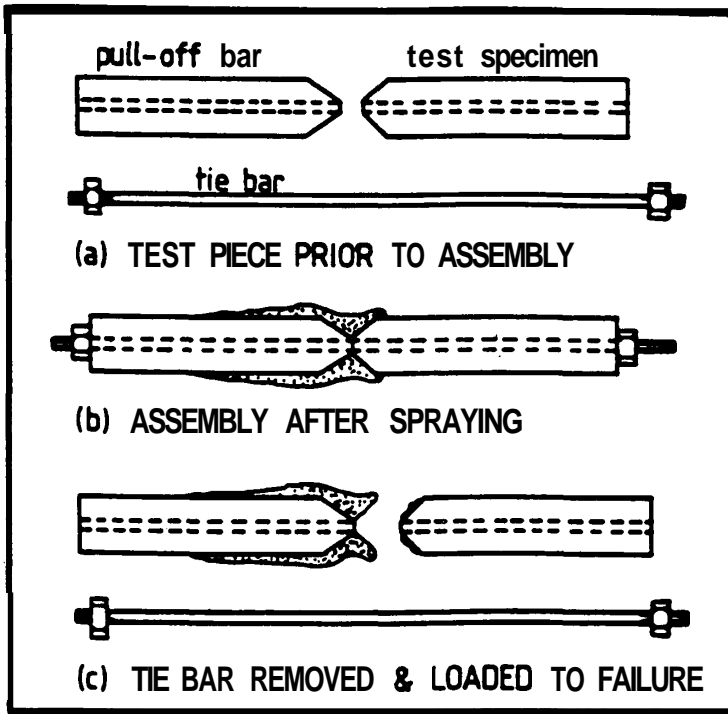


Fig. 4. Adhesion test piece [30].

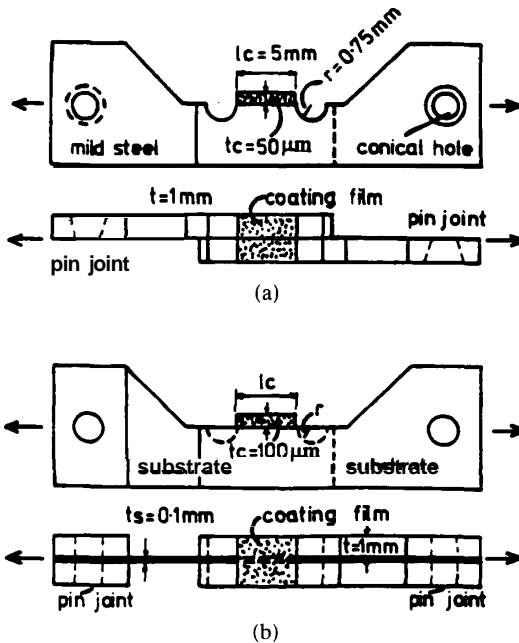


Fig. 5. (a) Shear stress deformation; (b) critical shear stress of adhesion [31].

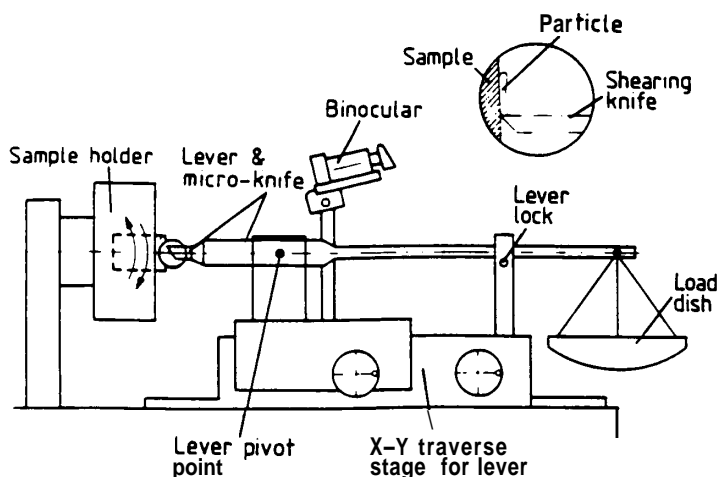


Fig. 6. An instrument for measuring the adhesion strength of the particles [32].

time, and  $N_0$  is the number of atoms in the particle and substrate that are in contact.

The upshot of this analysis was that the strength of the coating at some interaction time of ' $t$ ' was compared with the maximum strength of the coating at the end of the thermal spray process. It was established that the extent of the particle/interface reaction increased with both increasing particle pressure and temperature, and this agreed with the experimental observations that coating adhesion also increased under these conditions. Further theoretical work [33] has treated adhesion as a stochastic process which depends on the formation characteristics of the first monolayer of material. The coating buildup is treated as a statistical process involving input data from the thermal spray processing parameters such as the relative motion between the torch and substrate (i.e. the spray pattern), the velocity and temperature distribution of the thermal source, and the particle size.

## 2.2. Application of adhesion measurements

The reason for performing adhesion measurements can be brought into focus by examining how such experiments are used to ascertain the utility of coatings. For example, bond strength measurements allow optimization of different grit blast media and the angle of grit blasting, as well as establishing the best coating thickness for aluminum coatings (Fig. 7) [34]. Other workers [35] have optimized ceramic compositions and plasma spraying parameters with respect to strength. Thus, the historical basis for these measurements is significant. In recent years, with the adoption of design of experiment methods [36], bond strength measurements along with other physical measurements (roughness, porosity, etc.) have been used to establish specifications to select coatings.

The strength of the specimen may not be the same as the strength of the engineered coating. It can also be difficult to establish how process-induced residual stresses influence the strength measurements. The adhesion measurement is now taken as a control parameter that can be used as a guide to optimize



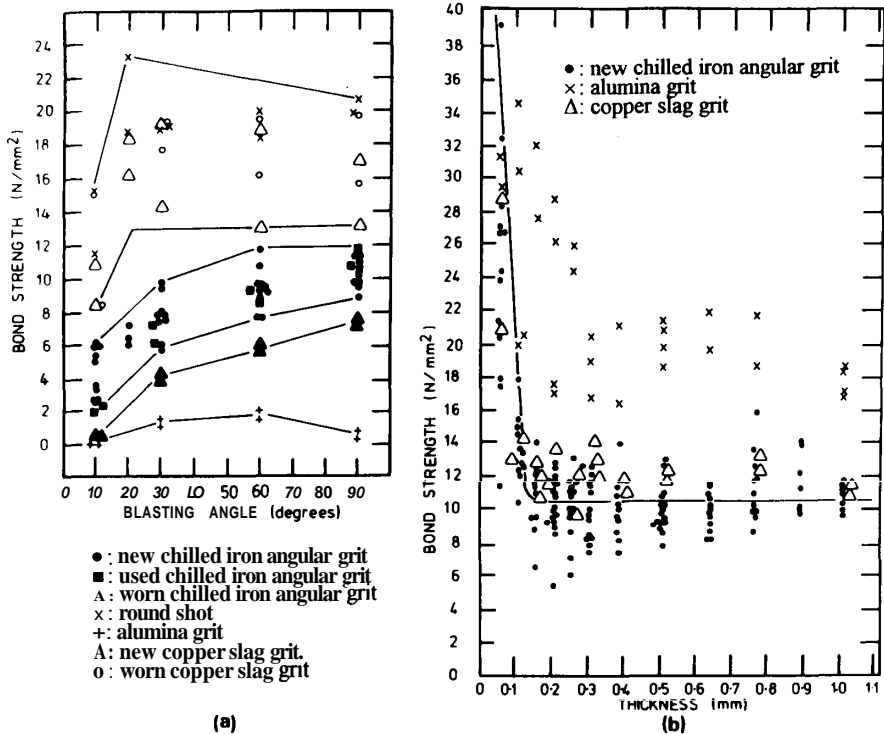


Fig. 7. Variation of the bond strength of aluminum coatings with (a) the blasting angle and (b) the coating thickness [34].

the many process parameters that are involved during thermal spraying. Often the tensile adhesion test is performed as a quality control test and numerous references can be found in thermal spray conference proceedings [6–8].

### 2.3. Fracture mechanics approach

**2.3.1. Overview.** The fracture mechanics approach to evaluate crack propagation is based on defining adhesion in terms of a stress intensity factor  $K$  or strain-energy release rate  $G$ . Methods of measurement include the double cantilever beam (DCB) test; the double torsion test; the bending (three-point or four-point), single-edge notched test; and the compact tension test. Among these, the DCB method allows multiple fracture toughness readings by testing a single specimen and will be discussed in the following section.

The fracture mechanics mode of failure is also a material property that can not only be controlled (to some degree), but must be quantified for engineering design purposes. Thus, a major justification for a fracture mechanics test is that a mode I (tensile) or a mode II (shear) test can be performed and the response of pre-existing flaws ascertained. There is also the possibility of carrying out mixed mode tests that may better replicate a variety of service conditions that the coating may experience throughout its lifetime.

The double torsion test [37, 38] has been applied to thermally sprayed coatings (Fig. 8). The prime advantage of this test is that there is no need to measure the

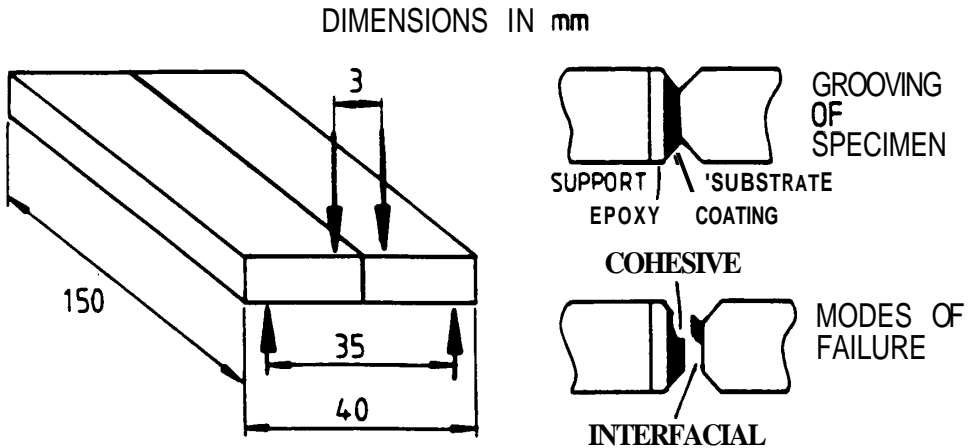


Fig. 8. Double torsion geometry and test configuration.

crack length because cracking occurs at a constant strain-energy release rate or stress intensity factor. Specimen manufacture involves incorporating the coating into an arrangement so that a torque can be applied to the crack front. The shortcomings of the test are that mode I cracking, where the crack front is orthogonal to the crack propagation direction, was never verified despite several attempts. It also appeared that both arms of the double torsion specimen were deflecting at a constant angle along their entire length. Both these conclusions are reflected in the fracture surface morphology as indicated in the inset diagram (on the bottom right) of Fig. 8 where a mixed mode of failure is observed.

The four-point bending test has also been applied to measure the fracture toughness of ceramics joined with metals [39]. The configuration is quite simple and one measurement can be obtained from each test.

**2.3.2. Double cantilever beam (DCB) test.** A major advantage of the DCB test is that it may have wide applicability to the design engineer; however, this ideal comes at the expense of complex specimen preparation and more sophisticated experimental techniques than the quality control departments of thermal spray shops may be prepared to undertake.

Many configurations of this test are available (Fig. 9) and an example of the technique on a thick film conductor of alumina is shown in Fig. 10 [40]. The applied moment method was used in this case since the crack length, a difficult property to measure for these opaque coatings, was not required. These studies are analogous to those on thermal spray coatings (Fig. 11) [41], where interfacial and cohesive modes of failure were distinguished in terms of fracture toughness. Another DCB geometry arrangement is illustrated in Fig. 12 [42], where a single contoured arm was used.

The general nature of the force vs. displacement requirement of a DCB experiment is shown in Fig. 13. The elastic energy of the specimen arms controls the amount of energy which is transferred to the creation of new crack faces within the locus of fracture. Thus, crack growth, as indicated by the dashed line in Fig. 13, will continue until a stable condition is reached and crack propagation

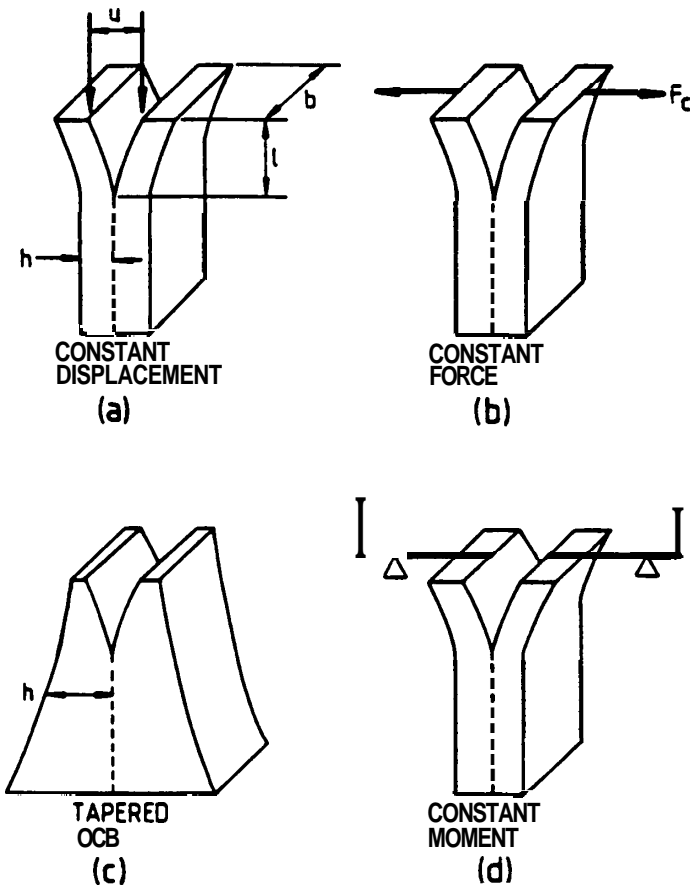


Fig. 9. Double cantilever beam test pieces.

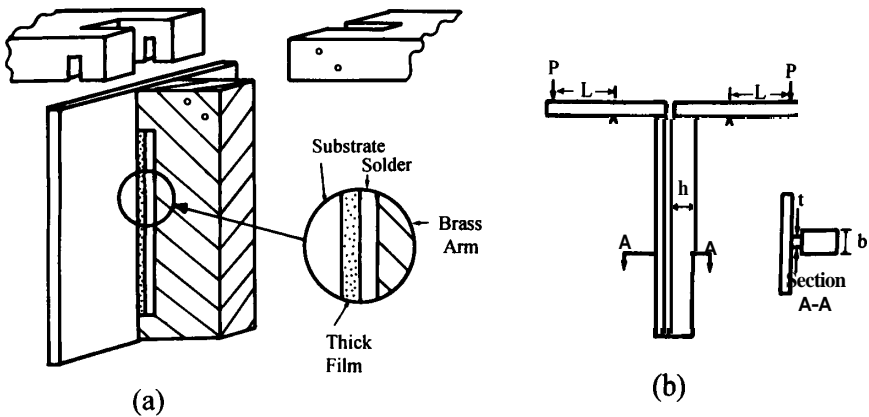
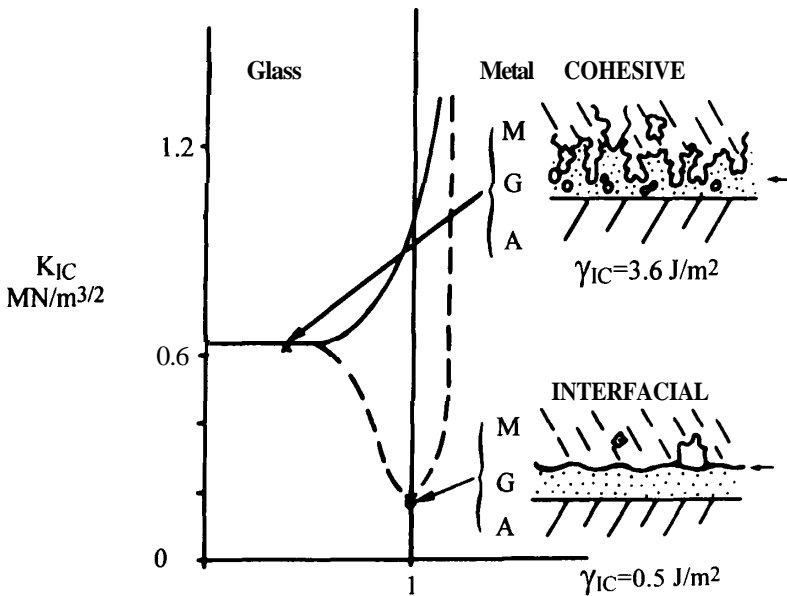
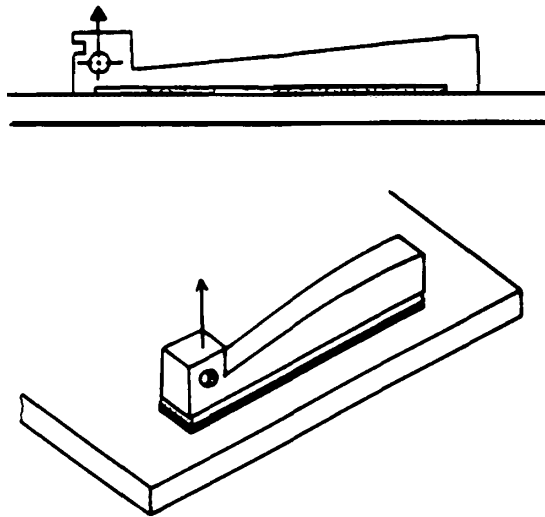


Fig. 10. Applied moment DCB specimen for measuring the adhesion of thick films. (a) Specimen preparation; (b) testing arrangement [40].



**Fig. 11.** Model of stress intensity profile through the film and substrate [41]. (In the detailed figure, M is metal, G is glass, and A is alumina.)



**Fig. 12.** Specimen with DCB geometry in which one arm is contoured [42].

stops at that point. The new slope of the force–displacement curve (i.e. the compliance) indicates the magnitude of the new crack length, and the area enclosed within the force–displacement curve is related to an energy transfer (from the DCB arms to the crack) during crack growth. Thus, the versatility of the DCB method is that the energy input into the coating can be controlled by altering the elastic modulus and/or geometry of the DCB arms.

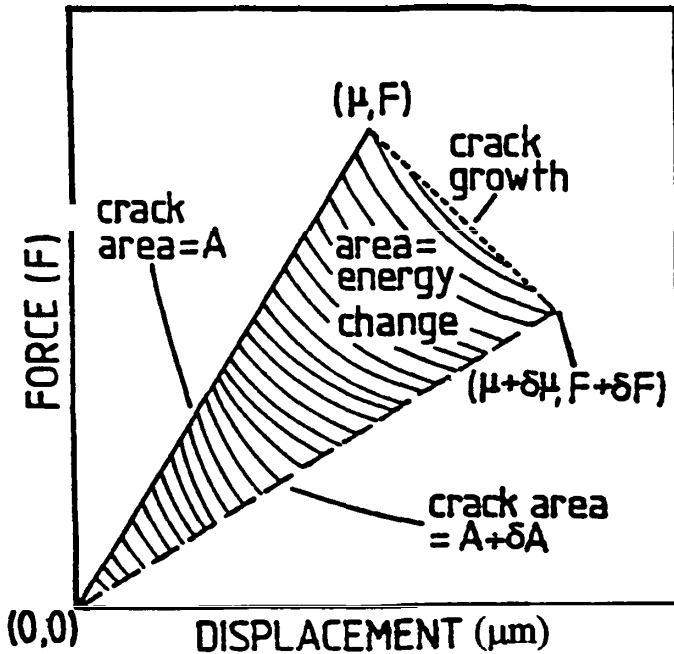


Fig. 13. Energy change when a crack grows.

It is also necessary to verify that the arms of the DCB are indeed bending and that there is no rigid movement of the adherends (Fig. 14a). It was established that true bending of the DCB arms did take place as indicated in Fig. 14c, rather than the ideal situation as depicted in Fig. 14b. The composite DCB geometry which incorporated an adhesive joint does not directly obey the Mostovoy formulation [43] but a modified equation that incorporated displacement at the crack-tip and deformation beyond the crack-tip fitted reasonably well to the theory (Fig. 15).

**2.3.3. DCB test for thermally sprayed materials.** In the basic DCB test on coatings (Fig. 16), a tension force is applied to the specimen assembly and displacement is measured by an extensometer placed on the arms [22]. When cracking initiates, as noticed by load decreasing with extension increasing, the DCB is unloaded. Several loading/unloading sequences are performed until complete failure of the specimen, at which point the morphology can be examined by optical microscopy and scanning electron microscopy (SEM). Either one of the three failure modes, i.e. interfacial, cohesive, and mixed, can be observed and both inter- and trans-lamellar cracking is exhibited. The locus of fracture can be controlled by grooving the edges of the DCB as shown in the inset (right-hand side) of Fig. 16. Another feature of the DCB method is that the method is not limited by the strength of the adhesive, as is the case for tensile adhesion tests but since it is a fracture mechanics test, it is only necessary for the fracture toughness of the adhesive to be greater than that of the coating. This is a relatively easy condition to satisfy.



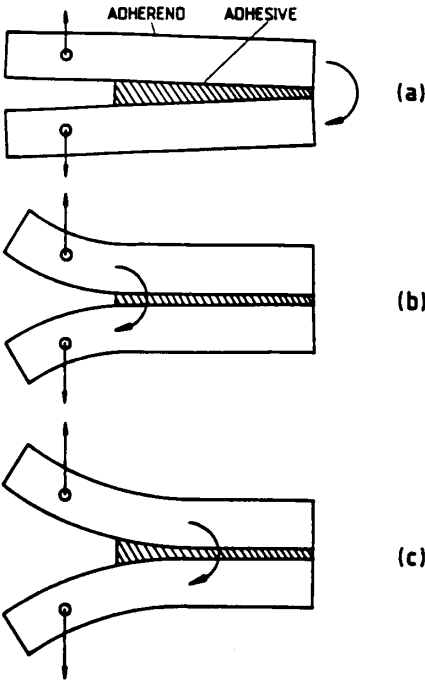


Fig. 14. Bending modes of a DCB specimen. (a) Rigid arms; (b) cantilever beams built in at the crack-tip; (c) rotation of cantilever beams at a point beyond the crack-tip.

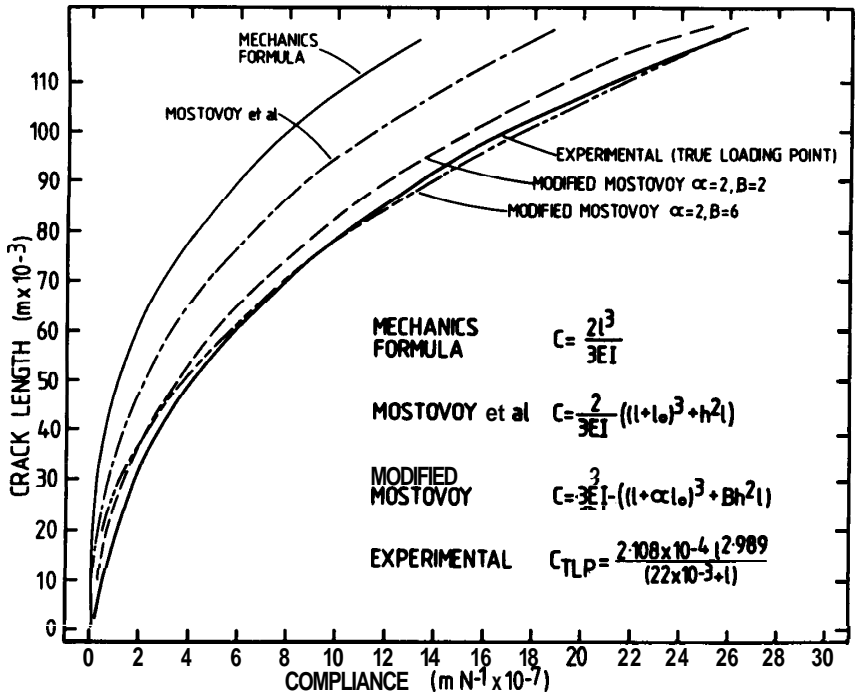


Fig. 15. Experimental compliance-crack length functions compared to various theories.

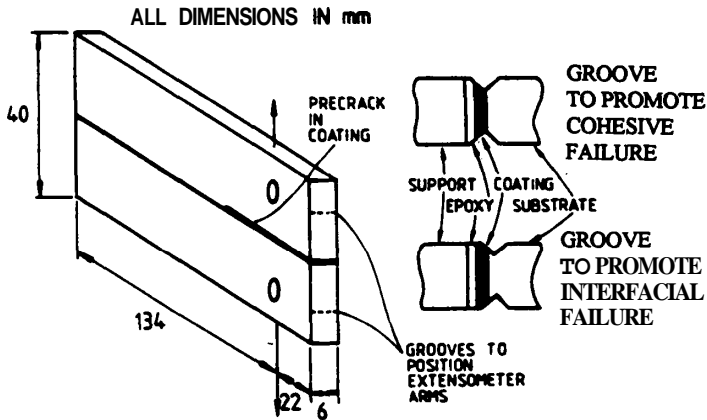


Fig. 16. DCB specimens used for adhesion measurement. The inset shows the grooving procedure to promote either interfacial or cohesive failure.

**2.3.4.  $G_{IC}$  determination.** The critical strain-energy release rate,  $G_{IC}$ , is determined from equation (2). The compliance values,  $dC/dL$ , are determined from the displacement at the loading points ( $C_{LP}$ ), which differs from the values recorded by the extensometer which is termed the crack opening displacement ( $C_{COD}$ ). An experimentally determined calibration curve is necessary to calculate  $dC/dL$  [22, 44]. Several laboratories have used this technique [45, 46] to generate  $G_{IC}$  data. The results are compiled with fracture indentation measurements in Table 3. The mean  $G_{IC}$  values for ceramic coatings exhibit a large range but generally they can be considered to lie below  $\sim 100 \text{ J/m}^2$ , whereas  $G_{IC}$  values for metallic coatings are greater than  $100 \text{ J/m}^2$ .

Table 3a.  
 $G_{IC}$  values (in  $\text{J/m}^2$ ) for thermally sprayed alumina coatings'

Material	Mean	SD	Method	Note	Ref.	Appendix
$\text{Al}_2\text{O}_3$	12	2	DCB	IF	22	Metco 101
$\text{Al}_2\text{O}_3$	16.1	5.3	DCB	CF	23	Metco 105
$\text{Al}_2\text{O}_3$	21	5	DCB	CF	22	Metco 101
$\text{Al}_2\text{O}_3$	31.6	9.3	DCB	CF	23	Sealed
$\text{Al}_2\text{O}_3$	34	9	DT	CF	22	Metco 101
$\text{Al}_2\text{O}_3$	49.8	14.0	DCB	CF	23	PC-WAF
$\text{Al}_2\text{O}_3$	52.7	14.5	DCB	CF	23	As sprayed
$\text{Al}_2\text{O}_3$	58	16	DCB	Int. BC Fail.	22	Metco 101
$\text{Al}_2\text{O}_3$	78	29	DT	IF	22	Metco 101
$\text{Al}_2\text{O}_3$	209	—	Ind.	Load: 47 N	23	—
$\text{Al}_2\text{O}_3$	189	—	Ind.	Load: 98 N	23	—
$\text{Al}_2\text{O}_3$	97.6	—	Ind.	Load: 147 N	23	—
$\text{Al}_2\text{O}_3$ -2.5 wt% $\text{TiO}_2$	15.9	5.6	DCB	CF	23	—
$\text{Al}_2\text{O}_3$ -2.5 wt% $\text{TiO}_2$	218	—	Ind.	Load: 73.5 N	23	—
$\text{Al}_2\text{O}_3$ -2.5 wt% $\text{TiO}_2$	268	—	Ind.	Load: 147 N	23	—
$\text{Al}_2\text{O}_3$ -2.5 wt% $\text{TiO}_2$	301	—	Ind.	Load: 98 N	23	—
$\text{Al}_2\text{O}_3$ -40% $\text{TiO}_2$	48.7	15.8	DCB	IF	23	—

<sup>a</sup> For data given in K, equation (3) is used to convert K into G by assuming  $E = 48 \text{ GPa}$ ;  $\nu = 0.25$ .

SD: standard deviation; IF= interfacial failure; CF= cohesive failure; Int. BC Fail.: interfacial bond coat failure; Ind.: indentation.

**Table 3b.**  
G<sub>IC</sub> values (in J/m<sup>2</sup>) for thermally sprayed zirconia coatings"

Material	Mean	SD	Method	Note	Ref.
ZrO <sub>2</sub> -10 CeO <sub>2</sub>	11.4	3.6	DCB	IF	21
ZrO <sub>2</sub> -15 CeO <sub>2</sub>	74.1	22.9	DCB	IF	21
ZrO <sub>2</sub> -15 CeO <sub>2</sub>	125.4	51.1	DCB	CF	21
ZrO <sub>2</sub> -6 Y <sub>2</sub> O <sub>3</sub>	49.9	16.7	DCB	IF	21
ZrO <sub>2</sub> -6 Y <sub>2</sub> O <sub>3</sub>	95.5	39.4	DCB	CF	21
ZrO <sub>2</sub> -6 Y <sub>2</sub> O <sub>3</sub>	148.3	52.3	DCB	Mixed	21
ZrO <sub>2</sub> -20 Y <sub>2</sub> O <sub>3</sub>	30.0	10.4	DCB	IF	21
ZrO <sub>2</sub> -20 Y <sub>2</sub> O <sub>3</sub>	69.7	31.8	DCB	CF	21
ZrO <sub>2</sub> -20 Y <sub>2</sub> O <sub>3</sub>	43.2	19.6	DCB	Mixed	21
ZrO <sub>2</sub> -8 Y <sub>2</sub> O <sub>3</sub>	11.1	1.3	Ind.	Load: 50 N	68
ZrO <sub>2</sub> -8 Y <sub>2</sub> O <sub>3</sub>	10.4	1.3	Ind.	Load: 100 N	68
ZrO <sub>2</sub> -8 Y <sub>2</sub> O <sub>3</sub>	16.0	1.0	Ind.	Load: 50 N	68
ZrO <sub>2</sub> -8 Y <sub>2</sub> O <sub>3</sub>	21.2	1.2	Ind.	Load: 100 N	68
ZrO <sub>2</sub> -8 Y <sub>2</sub> O <sub>3</sub>	5.7	0.9	Ind.	Load: 50 N	68
ZrO <sub>2</sub> -8 Y <sub>2</sub> O <sub>3</sub>	3.8	0.5	Ind.	Load: 100 N	68
ZrO <sub>2</sub> -8 Y <sub>2</sub> O <sub>3</sub>	5.3	0.5	Ind.	Load: 50 N	68
ZrO <sub>2</sub> -8 Y <sub>2</sub> O <sub>3</sub>	5.8	0.7	Ind.	Load: 100 N	68
YSZ	24.0	6.4	Ind.	Load: 588 N	65

"For data given in K, equation (3) is used to convert K into G by assuming  $\nu = 0.25$ . Mixed: mixed mode failure.

**Table 3c.**  
G<sub>IC</sub> values (in J/m<sup>2</sup>) for thermally sprayed coatings of some metals and ceramics"

Materials	Mean	SD	Method	Note	Ref.
Mild Steel	116	21	DCB	IF	22
Mild Steel	261	71	DCB	CF	22
Ni-Al	319	95	DCB	CF	22
Cr <sub>2</sub> O <sub>3</sub>	43.0	5.2	Ind.	Load: 9.8-98 N	64
Spinel	47.0	12.7	Ind.	Load: 294 N	65
Ti	6.79	0.34	4-P Bending	With stress	39
Ti	2.98	0.19	4-P Bending	Without stress	39
Ni-20% Al	362	16	DCB	CF	23

"For data given in K, equation (3) is used to convert K into G by assuming  $\nu = 0.25$ .

2.4. Acoustic emission

2.4.1. Background. Acoustic emission (AE) is a term describing a class of phenomena whereby transient elastic waves are generated by the rapid release of energy from localized sources within a material.' [47]. The energy usually arises from one or more sources [48], which include phase transformation, plastic deformation, corrosion, and crack initiation and growth [49]. An AE event is detected by a piezoelectric transducer when energy is released from the material. The output is amplified and then features of the AE signal such as the ring down count, rise time, and/or pulse height are subjected to analysis. Often a multi-channel system is used to examine different energy levels and the signal may also be digitized or integrated for an energy analysis.

Special interest lies in formulating crack initiation and growth criteria which

are based on the microstructural design of coatings. This is important because microstructural features can be quantitatively determined [50] by image analysis methods and leads to the conclusion that the microstructure of coatings can be 'controlled' by the thermal spray process. **AE** technology has been combined with fracture mechanics measurements [51–53] or thermal tests [54, 55] to characterize coating properties. **AE** technology has been applied to better understand failure mechanisms and to predict lifetimes [56–58]. It has also been applied to quality control and in-service monitoring.

**2.4.2. Crack density function.** A thermal spray coating has a very rich microstructure, and both macro- and micro-cracking, among other sources, can release energy during coating service. A difficulty is that the **AE** response is overwhelming with regard to acquiring data and this often limits the **AE** method to be a qualitative technique since individual **AE** response-to-coating morphology correlations cannot be made. However, quantitative **AE** analysis may still be possible through a test procedure which is combined with calibration [59, 60]. For example, studies on thermal barrier coatings that were subjected to heat cycling changed from a systematic response to a stochastic response during a certain thermal cycle. This was considered to be indicative of a change in cracking response from micro- to macro-cracking since the change in **AE** response was correlated to the observation of the formation of large cracks (Fig. 17) [61].

The record of **AE** response for coatings will be a combination of all possible noise origins, and a 'crack density function' (CDF) [62] which incorporates both the number of cracks and the size of cracks has been proposed. It is found that macrocracking events tend to occur at low values of the CDF. Figure 18 shows an example of a CDF analysis for two coatings that were prepared to exhibit different behaviors. The essential details are that one sample (indicated by the filled-in parts of the histogram) exhibited a lower frequency of the CDF function and this is indicative of a lower degree of cracking, in terms of both the number of cracks and the size of cracks (since the CDF incorporates these physical characteristics of coatings). At failure and after failure (Figs 18b and 18c), the frequency of these events increased.

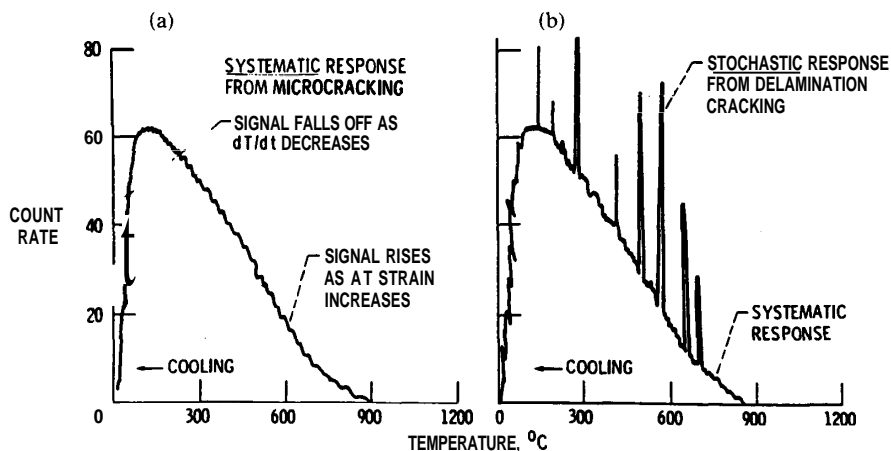


Fig. 17. Schematic diagram of AE effects. (a) Typical cooling cycle; (b) failure during cooling cycle.

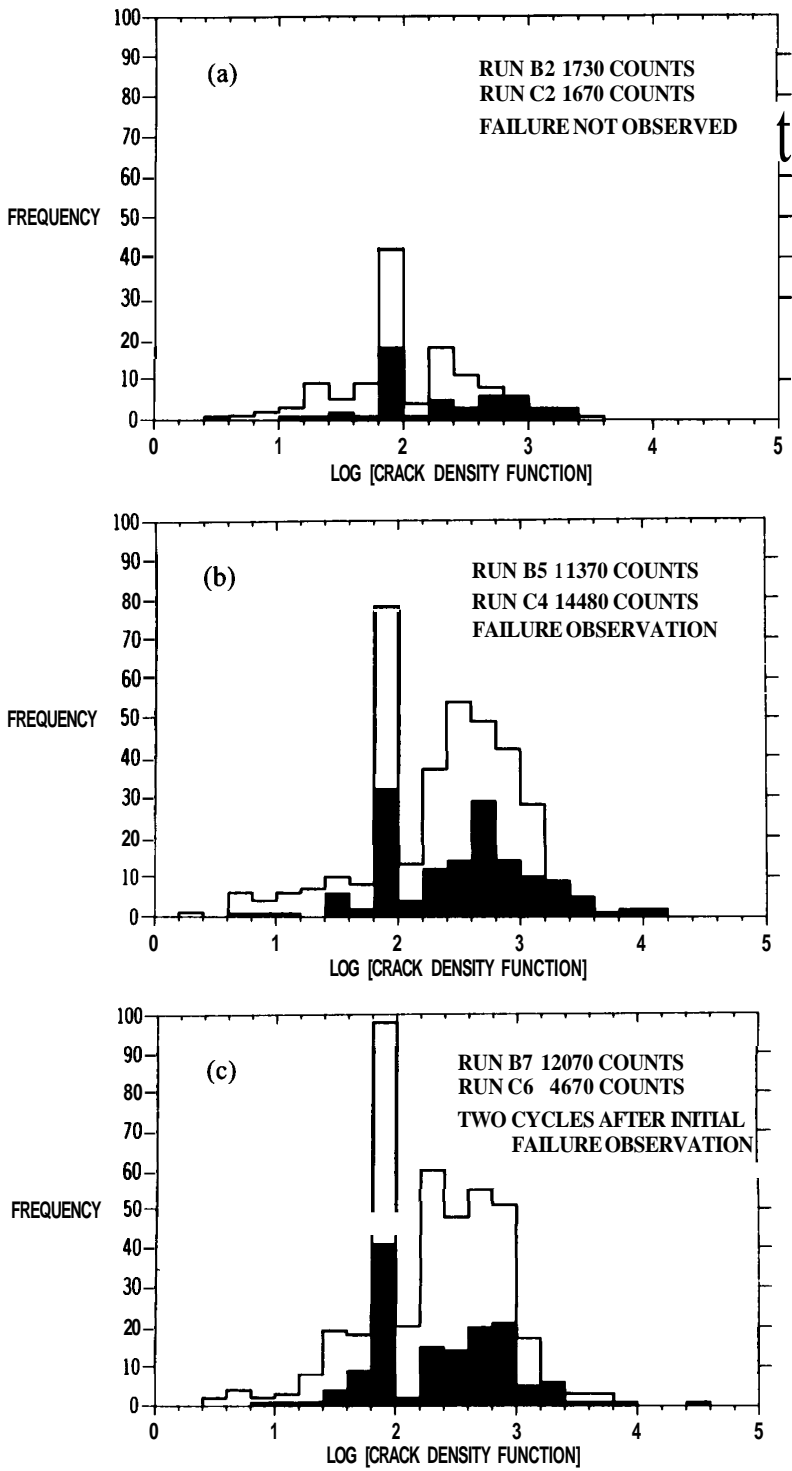


Fig. 18. Crack density function analysis of coatings. (a) First thermal cycle; (b) failure cycle; (c) two cycles after failure.



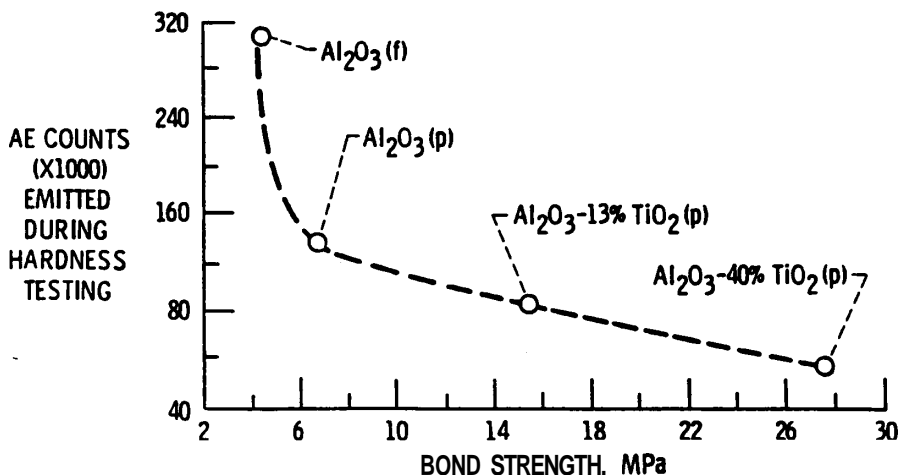


Fig. 19. Bond strength vs. AE emitted during hardness testing.

AE methods have also been used in conjunction with mechanical property measurements. For instance, it has been established that the number of AE counts emitted during a hardness test increases as the density of the material decreases. Figure 19 indicates a number of processes and materials where it is generally understood that flame spraying (indicated by 'f') will produce a less dense deposit than plasma spraying ('p') and also that additions of titania to alumina increase the deposit density. Thus, an intuitive interpretation is that the most dense material exhibits the least cracking behavior and this is reflected in a lower AE response.

Similar correlations have been proposed on the basis of AE measurements performed during tensile adhesion tests (TATs). The AE count accumulated during a TAT is graphed with respect to the so-determined bond strength in Fig. 20. The coatings which incorporate metallic constituents exhibit an activity lower than that of the non-metallic coatings (at equivalent bond strengths). Therefore, a physical interpretation of the mechanical response is that the metallic materials allow more plastic deformation than the ceramic materials. This simple explanation relates well to the general understanding of bulk material behavior, i.e. ceramics are more brittle than metals. However, one caution is that such correlations between bulk material properties and thermally sprayed materials may not be correct since these thick coatings are formed by a rapid solidification process.

The purpose of this discussion is to show that adhesion and cracking mechanisms are symbiotic material properties that can be linked by AE processes. Thus, in a very broad sense, a study and understanding of cracking mechanisms will lead to real improvements in maximizing the adhesion of coatings. For example, consider relating the AE response during a TAT to the cracking and deformation behavior of the specimen assembly. Figure 21 is a schematic diagram which indicates that the strain in the bond coat (the metallic constituent) is always greater than the ceramic strain, although the absolute extension in the ceramic layer is greater than that of the bond coat. The overall view is that cohesive failure occurs by many microcracks throughout the material, whereas interfacial failure has a lower density of cracks. The other implication

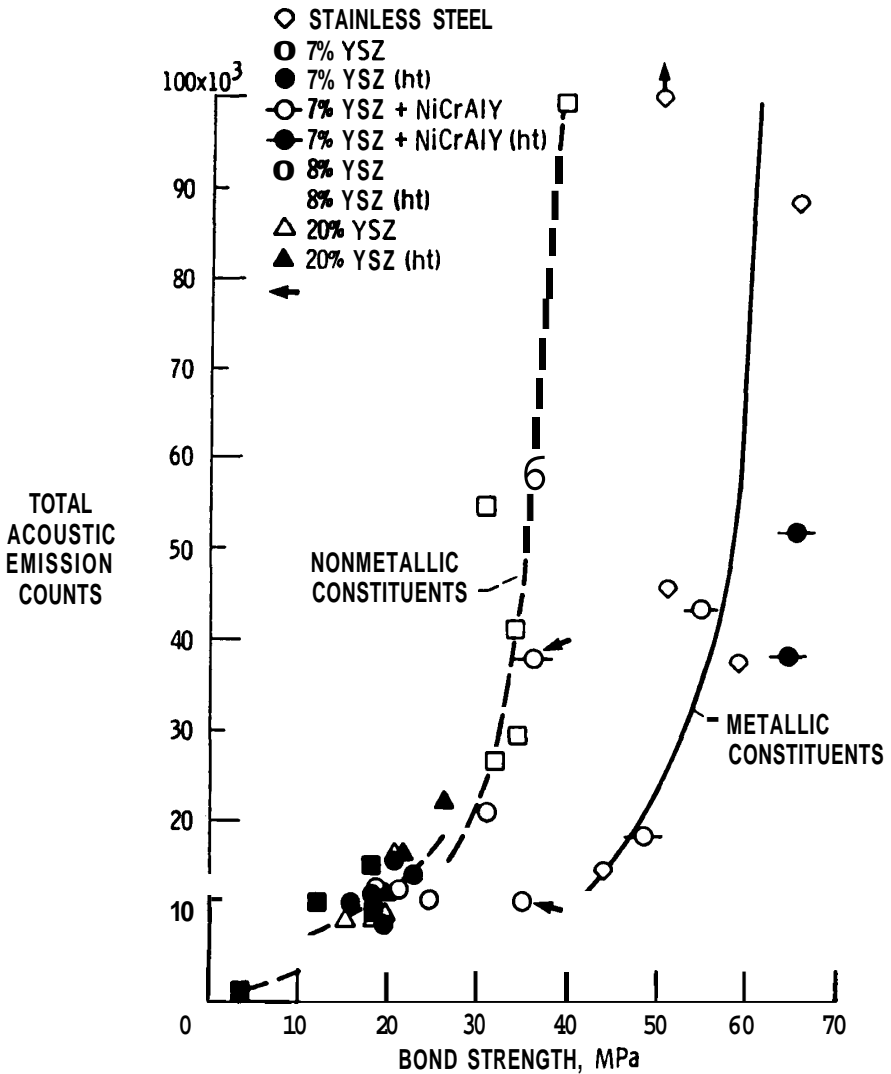


Fig. 20. Bond strength vs. AE emitted during tensile testing.

from Fig. 21 is that cracking during a TAT always begins at the edges of the material and that flaws in this region may dictate the so-determined strength value since they are the weakest link.

2.5. Microhardness assessment

2.5.1. Indentation fracture toughness. Indentation techniques are often used as surface characterization tests. The hardness, implying the resistance of a material to permanent indentation, is measured by a sharp or blunt indenter. Specific crack patterns can be observed [63] in the material at certain loads on the indenter. The indentation method allows the fracture toughness of materials [64–66] and, in particular for thermal spray coatings, the properties of the interface between the

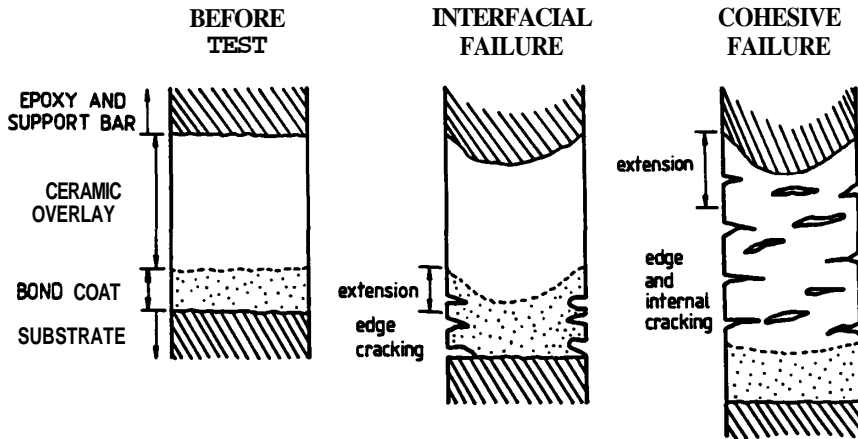


Fig. 21. Schematic diagram to illustrate the coating deformation response during the interfacial and cohesive failure modes.

coating and substrate to be measured. The coating toughness has been measured by the Vickers indentation test [67, 68], where it is necessary to measure the indent diagonals and the crack lengths produced during the test.

The results of several workers have been summarized in Table 3. The indentation fracture toughness measurements tend to be greater than those obtained from DCB tests. Aspects of these measurements that lead to critical discussion are mainly based on the application of the indentation theory to thermal spray coatings since these materials are highly anisotropic. Thus, obtaining a symmetrical crack pattern during any test is never assured, since the coating microstructure has many features that influence their formation and propagation, and therefore the so-determined values are often highly variable. For example, the Weibull modulus of an alumina coating is 0.5 and the modulus of an alumina-titania coating is 0.8. The other main point, as will be discussed in the following section, is that coatings are highly anisotropic throughout their thickness and thus randomly placed indentation fracture mechanics tests would not be expected to have consistent values.

**2.5.2. Anisotropy of thermally sprayed coatings.** The microstructure of thermally sprayed coatings is a mix of lamellae, pores of varying geometry, and oxides, etc. It is recognized that the coating is not homogeneous and microhardness measurements can be used to examine any anisotropy. The mean values of microhardness and the distributions of data sets across the coating thickness change with respect to the test position [69]. Hence, characterizing thermally sprayed coatings by only their hardness is of limited value, since hardness depends on the precise location of the measurement. However, the microhardness measurements can quantify the material property variation in the specimen if the Weibull modulus is determined. In this fashion it was found that the variability of surface properties is greater compared to the properties throughout the specimen cross-section. The morphology of microhardness indents also changes and this feature can be used to study the variation in homogeneity and stress concentration within the specimen.

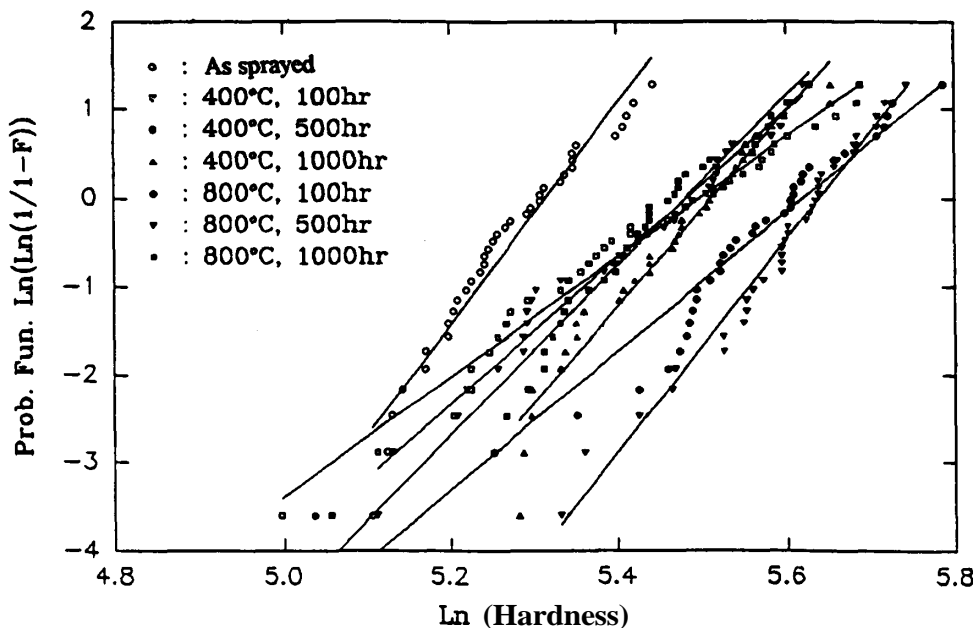


Fig. 22. Weibull plots for microhardness data for as-sprayed and aged samples within the bond coat.

As shown in Fig. 22, the Weibull modulus fluctuates and suggests that the data distributions are a reflection of microstructural changes in the bond coat. For example, the variation in ' $m$ ' may imply the formation and distribution of oxides and crack networks.

**2.5.3. Interpretation to lifetime.** Microhardness measurements have been used to monitor coating behavior after thermal treatments [70]. For example, a series of thermal barrier coatings (a NiCoCrAlY intermetallic bond coat and Ce-stabilized zirconia layer) aged at different times and temperatures (at 400 and 800°C for 100, 500, and 1000 h) were tested for microhardness to assess any material property changes [71]. The major failure mechanisms of thermal barrier coatings are oxidation within the bond coat and cracking due to thermal expansion mismatch within the coating system. This can be reflected by the hardness variation and, in the future, a failure model and lifetime prediction may be based on the analysis of such data.

Temperature effects were noticed in the coating systems. For ceramic coatings, microcracks produced by thermal expansion mismatch may have different sizes and densities. These cracks will be responsible for the variation of mechanical properties. At the same time, the oxide film surrounding the lamellae within the bond coat should have different thicknesses according to the oxidation kinetics at various temperatures. These oxide films, though they may contribute to the increase of microhardness, decrease the adhesion strength of the bond coat. Schematic illustrations of mechanisms that cause coating variation are presented in Fig. 23. Non-monotonic response of hardness and the low Weibull modulus imply complex processes such as stress relaxation, growth of oxides within the bond coat, and phase change.

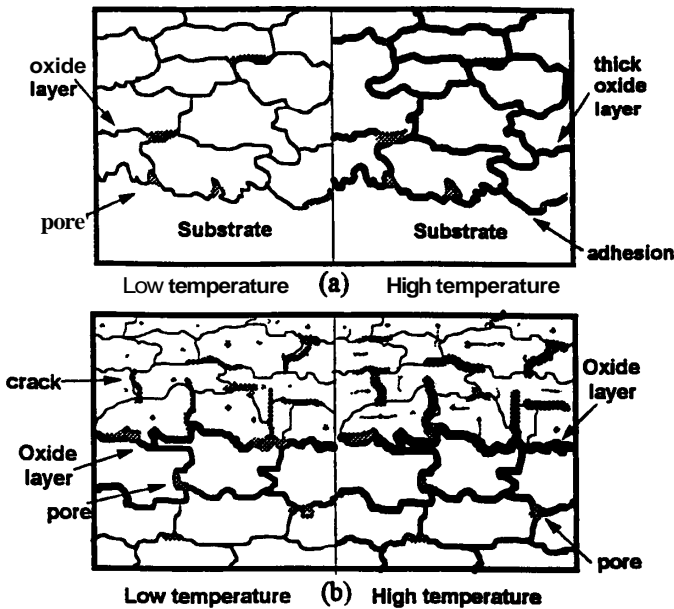


Fig. 23. Physical model of (a) the bond coat-substrate interface and (b) the bond coat-ceramic coating interface.

Thermal cycling of TBCs not only deteriorates the strength of the material at and near the bond coat interface, but also reduces the reliability of the ceramic thermal barrier layer. Microhardness measurements can be used to quantify the material property variation in the specimen. Weibull modulus values obtained in the study show that the reliability of the ceramic coating decreases from 10.5 before cycling to 5.5 after thermal cycling. The wide scatter in the hardness data indicates the variable nature of stress concentration at the test location.

Thus, increasing the reliability of coatings by controlling the variable nature of the material properties requires that the mechanical response throughout coatings be precisely quantified. Microhardness has been selected since this has been used by many authors not only to characterize specific coatings, but also to compare coatings formed from different feedstock materials, spray processes, and process parameters, as well as many other properties.

## 2.6. Other methods

**2.6.1. The scratch test.** The scratch test, originally studied by Benjamin and Weaver [72], is often used to characterize thin hard coatings, such as TiN and TiC [73, 74]. In this test, a loaded Rockwell C diamond stylus is drawn across the coating surface under either constant or gradually increasing load. In one variation of the test, the AE is also monitored during the scratching procedure so that the critical load ' $L_C$ ' for failure can be measured. The failure morphology is examined by optical microscopy or scanning electron microscopy. If interfacial, cohesive, or a mixed failure mode is observed, then  $L_C$  is used as a qualitative value of coating-substrate adhesion.

Three contributions to coating loss have been identified for the scratch

adhesion test [75–78], these being an elastic/plastic indentation (a ploughing component), and internal stress component, and a tangential frictional stress (an adhesion component).

Bull et al. [76] discussed the importance of frictional drag and suggested that under certain limitations the applied load, together with the scratched cross-sectional area, can be a convenient means of predicting the adhesion of thin coatings. Sekler et al. [77] discussed techniques to determine the critical load, and the failure modes in the scratch test were recently reviewed by Bull [78].

The scratch test has been applied in the evaluation of thermally sprayed coatings [52, 79–82]. The major problem for utilization is that all the theories were developed based on thin coatings and may no longer be appropriate for bulk coatings. Das et al. [52], in studying plasma sprayed yttria-stabilized zirconia (YSZ) coatings, proposed a method for the determination of the critical load and discussed the effect of the loading rate  $dL/dt$  and the scratch table speed  $dx/dt$ . Beltzung et al. [81, 82] performed scratch tests on the cross-section of alumina-based coatings. A half-cone-shaped fracture was formed as the indenter approached the free surface. The height of this cone can be related to the cohesive strength or intrinsic fracture toughness of the coating. Interfacial cracking may also occur and can be utilized as a measure of the adhesion strength.

2.6.2. Some tests not covered. There are many other methods that can be employed to evaluate adhesion in the qualitative or quantitative sense. The following are some examples:

- (1) wear tests [83, 84], which are related to the interfacial or cohesive strength of coatings;
- (2) thermal tests [85, 86] during thermal cycling and thermal shock protocols that influence the adhesion strength during heating and cooling processes;
- (3) shear tests [87, 88], which may best reflect the in-service conditions;
- (4) modified short bar [89] and crack-opening displacement methods [90] for fracture toughness tests.

There is still no ideal adhesion test which can satisfy all requirements. Modifications of existing techniques and designing new methods can further improve adhesion tests.

### 3. DEGRADATION AND FAILURE OF THERMALLY SPRAYED COATINGS

#### 3.1. Failure mechanisms

Thermally sprayed coatings have been used widely in applications varying from biomaterials to thermal barrier coatings [91]. Coating failure can occur by one or more mechanisms such as surface damage (e.g. wear or corrosion), elastic or plastic deformation, fracture, etc. The degradation or failure of coatings is fundamentally related to the decrease of adhesion and cohesion strength, both of which cause spallation. Fundamental studies on failure mechanisms, especially for TBCs, have been discussed by NASA [92].

Thermal barrier coatings, usually comprising a metallic bond coat and a ceramic coating, endure detrimental thermal and chemical environments. General failure modes include thermal–mechanical ceramic failure, oxidation bond coat failure, hot corrosion, erosion, and fatigue [93]. The thermal variations and



inelastic strain due to interfacial oxidation, which leads to crack propagation and coating spallation, should exacerbate coating failure. Meanwhile, phase transformation and bond coat plasticity (or pseudo-elasticity) may also contribute to these mechanism(s). It has been suggested that failure is the result of slow crack growth and microcrack link-up within the ceramic which takes place in the ceramic layer close to the bond coat interface.

Chang *et al.* [94] used finite element analysis to calculate the stress field within a hypothetical wavy interface and found that radial stress would promote crack propagation. The stress owing to the thermal expansion mismatch can be estimated as [95]

$$\sigma_{x,y} = \Delta\alpha(T_{\text{cool}} - T_{\text{hot}}) \frac{E_c}{(1 - \nu_c)} \quad (5)$$

where  $\Delta\alpha$  is the difference in thermal expansion coefficients between the substrate and coating,  $T_{\text{cool}}$  is the lower temperature to which a coated specimen cooled,  $T_{\text{hot}}$  is the upper temperature of a stress-free state,  $E_c$  is the elastic modulus of the ceramic, and  $\nu_c$  is Poisson's ratio of the ceramic.

A representation of the thermal-mechanical properties resulting from the coating splat structure is shown in Fig. 24. It has generally been recognized that the coating failure is 'time-at-temperature' dependent, especially for oxidation. Macro- and micro-cracking will decrease the adhesion strength of the system and thus appropriate interpretation of the data obtained from adhesion measurements may be beneficial to improving the reliability and durability of the coatings.

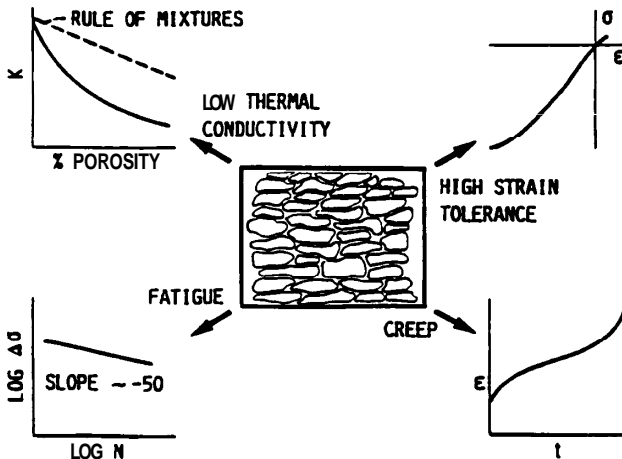


Fig. 24. Schematic representation of thermal-mechanical properties resulting from the coating splat structure of a plasma-sprayed thermal barrier coating. The diagram represents the influence of microstructure on the thermal conductivity, the stress vs. strain response, fatigue, and creep properties [93].

### 3.2. Lifetime modeling

A thermal barrier coating life model was proposed by Miller [95] based on the assumption that oxidation is the 'single most important factor' that limits coating lifetime. An oxidation-based model was used to calculate the cycles to failure as a

function of heating cycle duration. The coating life can be expressed by the oxidative weight gain and oxidation-induced strain as

$$\sum_{N=1}^{N_f} \left[ \left( 1 - \frac{\epsilon_r}{\epsilon_f} \right) \left( \frac{W_N}{W_C} \right)^m + \frac{\epsilon_r}{\epsilon_f} \right]^b = 1 \quad (6)$$

where  $N$  is the number of cycles,  $N_f$  is the number of cycles to failure,  $\epsilon_r$  is the radial strain,  $\epsilon_f$  is the failure strain,  $W_N$  is the oxidative weight gain at cycle  $N$ ,  $W_C$  is the critical weight gain which would lead to failure in a single cycle,  $m$  is the relationship between effective strain and weight gain, and  $b$  is the subcritical crack-growth exponent.

The NASA-sponsored HOST program contributed more effort to model the TBC life [96–98]. Hillery *et al.* [96] used time-dependent, nonlinear finite element analysis to model the stress and strain within the coating system and expressed the life model as

$$\Delta\epsilon_{RZ} + 0.4\Delta\epsilon_R = 0.121 N_f^{-0.486} \quad (7)$$

where  $\Delta\epsilon_{RZ}$  is the shear strain range,  $\Delta\epsilon_R$  is the normal strain range, and  $N_f$  is the number of cycles to failure.

Strangman *et al.* [97] expressed the TBC life as a function of bond coat oxidation, zirconia transformation, and damage due to molten salt deposits. The empirical equation was

$$\text{TBC life} = \frac{(t^{0.25} + 0.181)\text{MTBREF}}{\{\exp[-0.015 T + C_1]\}^{-1} + \{\exp[-0.041 T + C_2]\}^{-1}} \quad (8)$$

where MTBREF is the multi-temperature burner rig experience factor;  $T$  is the temperature (in K);  $t$  is the time; and  $C_1$  and  $C_2$  are constants.

DeMasi *et al.* [98] considered the fatigue performance and expressed the relationship between strain and the oxide layer thickness,  $\delta$ , as

$$\Delta\epsilon_f = \Delta\epsilon_{f0} \left( \frac{1 - \delta}{\delta_c} \right)^c + \Delta\epsilon_i \left( \frac{\delta}{\delta_c} \right)^d \quad (9)$$

where  $\Delta\epsilon_f$  is the strain,  $\Delta\epsilon_{f0}$  is the oxidation strain,  $\Delta\epsilon_i$  is the inelastic strain,  $\delta$  is the oxide thickness at a particular cycle number,  $\delta_c$  is the critical oxide thickness, and  $c$  and  $d$  are constants.

Recently, Meier *et al.* [99] studied TBC deposited by the electron beam PVD fatigue life model and gave

$$N = \left[ \left( \frac{\Delta\epsilon_{ff}}{\Delta\epsilon} \right) \left( 1 - \frac{\delta}{\delta_c} \right)^c + \left( \frac{\delta}{\delta_c} \right)^c \right]^b \quad (10)$$

where  $N$  is the cyclic life,  $\Delta\epsilon_{ff}$  is the furnace failure strain,  $\Delta\epsilon$  is the strain range,  $\delta$  is the oxide thickness at a particular cycle number,  $\delta_c$  is the critical oxide thickness, and  $b$  and  $c$  are constants ( $b = 7.64$ ,  $c = 1.0$ ).

The lifetime modeling of active in-service engineering components is a more complex problem and further effort is in progress.

#### 4. CONCLUDING REMARKS

The measurement of the adhesion of thermally sprayed materials is, at least on the

conceptual level, a routine operation. The tensile adhesion method as detailed in ASTM C633 is simple and often used in industry for ranking different coatings. However, the major shortcoming of this test is that it does not promote any understanding of coating performance, i.e. how coatings can be designed to be more functional. Thus, the present paper has addressed other methods based on fracture mechanics and mechanism-based studies.

The design of experiments with regard to material property optimization of coatings is another area of intense effort. Experimental protocols which are based on Taguchi and response surface methodology allow engineers efficient and viable ways to optimize the process parameters [100, 101]. Such statistical methods are executed to discriminate key parameters which induce the variation of coating properties. The signal-to-noise ratios of the processing parameters are derived from such studies [102]. The Taguchi method does have some shortcomings and limitations [103] but it is a simple and powerful process control procedure.

The coating should be considered as part of the overall component system and therefore current trends are to design the coating as an integral part of the component assembly rather than as an add-on to the substrate. Whereas the property of coating adhesion to the substrate is of principal interest, there is still no single measurement which can satisfy all the requirements for determining material properties. Standardization of measurements, which may be achieved by improving existing experimental techniques or by the combination of two or more techniques, will aid future coating development. Finally, a coating design (i.e. both microstructural and mechanical engineering designs) which is based on lifetime modeling is the critical information that should be forthcoming from any test method. Such designs will increase the knowledge-base and understanding of thermal sprayed materials and coatings so that their reliability and application will grow.

### Acknowledgements

We wish to thank the Alcoa Foundation for supporting parts of this work related to examining failure mechanisms of alumina. We thank Paul S. Fussell and Roger Kaufold as the managers of our program.

### REFERENCES

1. T. N. Rhys Jones, *Surface Coat. Technol.* **43/44**, 402–415 (1990).
2. K. T. Scott and R. Kingswell, in: *Advanced Surface Coatings*, D. S. Rickerby and A. Matthews (Eds), pp. 217–243. Chapman and Hall, New York (1991).
3. J. H. Zatt, *Annu. Rev. Mater. Sci.* **13**, 9–42 (1983).
4. L. E. Weiss, F. B. Prinz, D. A. Adams and D. P. Siewiorek, *J. Thermal Spray Technol.* **1**, 231–237 (1992).
5. K. Neufuss, B. Kolman, J. Dubsky and P. Chraska, *Proc. AustCeram* **92**, Melbourne, 16–21 August pp. 124–129 (1992).
6. C. C. Berndt (Ed.), 1992 International Thermal Spray Conference and Exposition, 28 May–5 June, *Proceedings: Thermal Spray: International Advances in Coatings Technology*, Orlando, FL. ASM International, Materials Park, OH (1992).
7. T. F. Bernecki (Ed.), 1991 National Thermal Spray Conference and Exposition, 4–10 May, *Proceedings: Thermal Spray Coatings: Properties, Processes and Applications*, Pittsburgh, PA. ASM International, Materials Park, OH (1992).

8. S. Blum-Sandmeier, H. Eschnauer, P. Huber and A. R. Nicoll (Eds), *2nd Plasma-Technik-Symposium, Proceedings*, Plasma-Technik AG, Wohlen/Switzerland, Hafliger Druck AG, Wettingen (1991).
9. R. McPherson, *Surface Coat. Technol.* **39/40**, 173–181 (1989).
10. H. Herman, *Sci. Am.* 256, 112–117 (1989).
11. K. L. Mittal (Ed.), in: *Adhesion Measurement of Thin Films, Thick Films, and Bulk Coatings*, ASTM STP640, pp. 5–17. American Society for Testing and Materials, Philadelphia, PA (1978).
12. K. L. Mittal (Ed.), in: *Adhesion Measurement of Thin Films, Thick Films, and Bulk Coatings*, ASTM STP640, American Society for Testing and Materials, Philadelphia PA (1978).
13. R. L. Patrick (Ed.), *Treatise on Adhesion and Adhesive*, Vol. 1. Marcel Dekker, New York (1967).
14. D 907-91b, *Terminology of Adhesives*, American Society for Testing and Materials, Philadelphia, PA (1991).
15. J. Comyn, *Int. J. Adhesion Adhesives* 10, 161–165 (1990).
16. A. Matting and H.-D. Steffens, *Metallwiss. Tech.* 17, 583–593, 905–922, 1213–1230 (1963). Available under Translations Register Index No. 72–14247-13H.
17. M. D. Thouless, *Mater. Res. Soc. Symp. Proc.* **119**, 51–62 (1988).
18. B. R. Lawn and T. R. Wilshaw (Eds), *Fracture of Brittle Solids*. Cambridge University Press, Cambridge (1975).
19. C. C. Berndt and R. McPherson, *Trans. Int. Eng.* **6**, 53–58 (1981).
20. C. C. Berndt, in: *Advances in Fracture Research*, Vol. 4, S. R. Valluri, D. M. R. Taplin, P. Rama Rao, J. F. Knott and R. Dubey (Eds), pp. 2545–2552. Pergamon Press, Oxford (1984).
21. G. N. Heintze and R. McPherson, *Surface Coat. Technol.* **34**, 15–23 (1988).
22. C. C. Berndt, Ph.D. Thesis, Monash University, Australia (1980).
23. P. Ostojic, Ph.D. Thesis, Monash University, Australia (1986).
24. K. L. Mittal, *J. Adhesion Sci. Technol.* 1, 247–259 (1987).
25. D. S. Rickerby, *Surface Coat. Technol.* 36, 541–557 (1988).
26. S. J. Bull and D. S. Rickerby, *Br. Ceram. Trans. J.* 88, 177–183 (1989).
27. P. R. Chalker, S. J. Bull and D. S. Rickerby, *Mater. Sci. Eng.* **A140**, 583–592 (1991).
28. B. A. Lyashenko, V. V. Rishin, V. G. Zil'berberg and S. Yu. Sharivker, *Sov. Powder Metall. Meth. Ceram.* 8, 331–334 (1969).
29. B. M. Zakharov, M. G. Trofimov, L. I. Guseva, Y. I. Golovkin, A. A. Kononov and V. V. Vinokurova, *Sov. Powder Metall. Met. Ceram.* 9, 925–929 (1970).
30. W. E. Stanton, in: *Proc. 7th Int. Metal Spraying Conf.*, 10–14 Sept. 1973. pp. 157–164, 312–314. The Welding Institute, Cambridge (1974).
31. T. Suhara, K. Kitajima and S. Fukada, in: ref. 30, pp. 179–184.
32. N. N. Rykalin, *Pure Appl. Chem.* 48, 179–194 (1976).
33. V. E. Belashchenko and Y. B. Chernyak, in: ref. 6, pp. 433–437.
34. R. L. Apps, *Chem. Eng.* 292, 769–773 (1974).
35. V. Wilms and H. Herman, *Thin Solid Films* 39, 251–262 (1976).
36. T. J. Steeper, D. J. Varacalle, Jr., G. C. Wilson, W. L. Riggs (II), A. J. Rotolico and E. Nerz, in: ref. 6, pp. 415–420.
37. J. O. Outwater and D. J. Gerry, *J. Adhesion* 1, 290–298 (1969).
38. J. A. Kies and A. B. J. Clark, in: *Fracture 1969, Proceedings of the 2nd International Conference*, Brighton, P. L. Platt (Ed.), Chapman and Hall, London (1969).
39. S. J. Howard and T. W. Clyne, *Surface Coat. Technol.* 45, 333–342 (1991).
40. P. F. Becher and W. L. Newell, *J. Mater. Sci.* **12**, 90–96 (1977).
41. P. F. Becher, W. L. Newell and S. A. Halen, in: *Fracture Mechanics of Ceramics*, R. C. Bradt, D. P. H. Hasselman and F. F. Lange (Eds), Vol. III, pp. 463–471. Plenum Press, New York (1978).
42. W. D. Bascom and J. L. Bitner, *J. Mater. Sci.* 12, 1401–1410 (1977).
43. S. Mostovoy, P. B. Crosley and E. J. Ripling, *J. Mater.* 2, 661–681 (1967).
44. G. N. Heintze and R. McPherson, *Surface Coat. Technol.* 36, 125–132 (1988).
45. G. N. Heintze and R. McPherson, in: 1987 National Thermal Spray Conference and Exposition, 14–17 Sept., *Proceedings: Thermal Spray: Advances in Coatings Technology*, Orlando, FL, D. L. Houck (Ed.), pp. 271–275. ASM International Materials Park, OH (1988).
46. P. Ostojic and R. McPherson, *J. Am. Ceram. Soc.* 71, 891–899 (1988).

47. M. J. Noone and R. L. Mehan, in: *Fracture Mechanics of Ceramics*, R. C. Bradt, D. P. H. Hasselman and F. F. Lange (Eds), Vol. 1, pp. 201–229. Plenum Press, New York (1974).
48. *Acoustic Emission*, STP505, American Society for Testing and Materials, Philadelphia PA (1972).
49. J. R. Matthews (Ed.), *Acoustic Emission*, Gordon and Breach, New York (1983).
50. T. C. Nerz, J. E. Nerz, B. A. Kushner, A. J. Rotolico and W. L. Riggs, in: ref. 6, pp. 405–414.
51. L. C. Cox, *Surface Coat. Technol.* **36**, 807–815 (1988).
52. D. K. Das, M. P. Srivastava, S. V. Joshi and R. Sivakumar, *Surface Coat. Technol.* **46**, 331–345 (1991).
53. M. M. Mayuram and R. Krishnamurphy, in: ref. 6, pp. 711–715.
54. N. Iwamoto, M. Kamai and G. Ueno, in: ref. 6, pp. 259–265.
55. H. Nakahira, Y. Harada, N. Mifune, T. Yogoro and H. Yamane, in: ref. 6, pp. 519–524.
56. H. L. Dunegan, *Prevention of Structural Failure*, pp. 86–113, ASM, Materials Park, OH (1975).
57. T. Tsuru, A. Sagara and S. Haruyama, *Corrosion* **43**, 703–707 (1987).
58. F. Bordeaux, C. Moreau and R. G. Saint Jacques, *Surf. Coat. Technol.* **54/55**, 70–76 (1992).
59. C. C. Berndt, *J. Mater. Sci.* **24**, 3511–3520 (1989).
60. I. G. Scott (Ed.), *Basic Acoustic Emission*. Gordon and Breach, New York (1991).
61. C. C. Berndt and R. A. Miller, *Thin Solid Films* **119**, 173–184 (1984).
62. C. C. Berndt, in: *Proc. Thermal Barrier Coatings Workshop*, 21–22 May, pp. 127–137. NASA Lewis Research Center, Cleveland, OH (1985).
63. B. Lawn and R. Wilshaw, *J. Mater. Sci.* **10**, 1049–1081 (1975).
64. C. Richard, J. Lu, J. F. Flavenot, G. Beranger and F. Decomps, in: ref. 6, pp. 11–16.
65. J. G. Binner and R. Stevens, *Trans. Br. Ceram. Soc.* **83**, 168–172 (1984).
66. H. Nayeab-Hashemi and C. A. Tracy, *Exp. Mech.* No. 12, 366–372 (1991).
67. G. K. Beshish, C. W. Florey, F. J. Worzala and W. J. Lenling, *J. Thermal Spray Technol.* **2**(1), 35–38 (1993).
68. R. Dal Maschio, V. M. Sgavo, L. Bertamini and E. Galvanetto, in: ref. 6, pp. 947–951.
69. C. C. Berndt, J. Karthikeyan, R. Ratanaraj and Yang Da Jun, in: ref. 7, pp. 199–203.
70. C. C. Berndt, J. Ilavsky and J. Karthikeyan, in: ref. 6, pp. 941–946.
71. C. K. Lin and C. C. Berndt, in: 1993 National Thermal Spray Conference and Exposition, 7–11 June, *Proceedings: Thermal Spray Coatings: Research, Design and Application*, Anaheim, CA. C. C. Berndt and T. F. Bernecki (Eds.), pp. 561–568. ASM International, Materials Park, OH (1993).
72. P. Benjamin and C. Weaver, *Proc. R. Soc. London, Ser. A* **254**, 163 (1960).
73. A. J. Perry, J. Valli and P. A. Steinmann, *Surface Coat. Technol.* **36**, 559–575 (1988).
74. C. Julia-Schmutz and H. E. Hintermann, *Surface Coat. Technol.* **48**, 1–6 (1991).
75. P. J. Burnett and D. S. Rickerby, *Thin Solid Films* **154**, 403–416 (1987).
76. S. J. Bull, D. S. Rickerby, A. Matthews, A. Leyland, A. R. Pace and J. Valli, *Surface Coat. Technol.* **36**, 503–517 (1988).
77. J. Sekler, P. A. Steinmann and H. E. Hintermann, *Surface Coat. Technol.* **36**, 519–529 (1988).
78. S. J. Bull, *Surface Coat. Technol.* **50**, 25–32 (1991).
79. C. W. Anderson and K. H. Heffner, in: ref. 6, pp. 695–704.
80. M. Gudge, D. S. Rickerby, R. Kingswell and K. T. Scott, in: 1990 National Thermal Spray Conference and Exposition, 20–25 May, *Proceedings: Thermal Spray Research and Application*, Long Beach, CA. T. F. Bernecki (Ed.), pp. 331–337. ASM International, Materials Park, OH (1991).
81. E. Lopez, F. Beltzung and G. Zambelli, *J. Mater. Sci. Lett.* **8**, 346–348 (1989).
82. F. Beltzung, G. Zambelli, E. Lopez and A. R. Nicoll, *Thin Solid Films* **181**, 407–415 (1989).
83. E. Lugscheider, P. Jokiel, G. Purshe, O. Roman and K. Yushchenko, in: ref. 6, pp. 647–651.
84. K. Furukubo, S. Oki and S. Gohda, in: ref. 6, pp. 705–709.
85. R. C. Hendricks and G. McDonald, *Assessment of Variations in Thermal Cycle Life Data of Thermal Barrier Coated Rods*, NASA TM-81743 (1981).
86. H.-D. Steffens and Fischer, *Surface Coat. Technol.* **32**, 327–338 (1987).
87. S. J. Grisaffe, *Analysis of Shear Bond Strength of Plasma-Sprayed Alumina Coatings on Stainless Steel*, NASA TN D3113 (1965).
88. H. Grützner and H. Weiss, *Surface Coat. Technol.* **45**, 317–323 (1991).
89. K. K. Schweitzer, M. H. Zeihl and Ch. Schwaminger, *Surface Coat. Technol.* **48**, 103–111 (1991).

90. M. J. Filaggi and R. M. Pilliar, *J. Mater. Sci.* 26, 5383–5395 (1991).
91. R. A. Miller, *Surface Coat. Technol.* 30, 1–11 (1987).
92. Proc. Thermal Barrier Coatings Workshop, NASA Lewis Research Center, Cleveland, OH, 21–22 May, 1985.
93. R. A. Miller, *J. Eng. Gas Turbines Power* 111, 301–305 (1989).
94. G. C. Chang, W. Phucharoen and R. A. Miller, *Surface Coat. Technol.* 30, 13–28 (1987).
95. R. A. Miller, *J. Am. Ceram. Soc.* 67, 517–521 (1984).
96. R. V. Hillery, B. H. Pilsner, R. L. McKnight, T. S. Cook and M. S. Hartle, *Thermal Barrier Coating Life Prediction Model*, Final Report, NASA CR-180807 (1987).
97. T. E. Strangman, J. Neumann and A. Liu, *Thermal Barrier Coating Life Prediction Model Development*, Final Report, NASA CR-179648 (1987).
98. J. T. DeMasi, M. Ortiz and K. D. Sheffler, *Thermal Barrier Coating Life Prediction Model Development*, Phase I Final Report, NASA CR-182230 (1989).
99. S. M. Meier, D. M. Nissley and K. D. Sheffler, *Thermal Barrier Coating Life Prediction Model Development*, Phase II Final Report, NASA CR-189111 (1991).
100. G. Taguchi and S. Konishi, *Taguchi Methods, Orthogonal Arrays and Linear Groups*, American Supplier Institute, Dearborn, MI (1987).
101. P. Ross, *Taguchi Techniques for Quality Engineering*, McGraw-Hill, New York (1988).
102. G. E. P. Box, *Technometrics* 30, 1–17 (1988)
103. S. Bisgaard, in: ref. 80, pp. 661–667.

### Permission to publish

C.C. Berndt and C.K. Lin, 'Measurement of adhesion for thermally sprayed materials', *J. Adhesion Science and Technology*, 7 [12] (1993) 1235-1264.

Permission is granted for a fee for non exclusive world rights for one edition only. Use beyond this edition requires obtaining another license. This license is granted strictly according to the details of use you specified during the order process and are found in the order details. Entire article electronic reuse is excluded with the exception of eBooks. This license does not cover usage in a Custom Publishing Programme and or database. This license does not cover cases in which Taylor and Francis material consists of more than 20% of your new work. This permission does not cover any third party copyrighted work which may appear in the material requested.

Full acknowledgement must be included showing article title, author, full Journal title, date of publication and publisher, reprinted by permission of the publisher (Taylor & Francis Ltd, <http://www.tandfonline.com>).

Permission is granted by Copyright Clearance Center Inc (CCC) on Taylor and Francis's behalf and by agreeing to the terms and conditions listed above you also agree to (CCC's) additional terms and conditions as the administrators of this licensing service, these terms and conditions are agreed to as a condition of establishing an account and may be seen at <http://myaccount.copyright.com>.



# Contact Damage in Plasma-Sprayed Alumina-Based Coatings

Antonia Pajares,\* Lanhua Wei,<sup>†</sup> and Brian R. Lawn<sup>‡</sup>

Materials Science and Engineering Laboratory, National Institute of Standards and Technology,  
Gaithersburg, Maryland 20899

Christopher C. Berndt<sup>§</sup>

Department of Materials Science and Engineering, State University of New York at Stony Brook,  
Stony Brook, New York 11794

A study of Hertzian contact damage in plasma-sprayed alumina-based ceramic coatings on steel substrates has been made. Presectioned specimens are used to identify subsurface micromechanical damage processes within the coating and substrate layers as a function of increasing contact load, from both postcontact and *in situ* observations. Damage occurs principally by cracking in the ceramic coating and plastic deformation in the metal substrate, along with delamination at the coating/substrate interface. Coating thickness, cycling loading (fatigue), and processing history (coating microstructure) are shown to be important factors in the damage patterns and ensuing modes of failure. Indentation stress-strain curves are used to measure macroscopic mechanical responses, to quantify the maximum sustainable contact stresses and to determine the relative roles of coating and substrate in the net deformation.

## I. Introduction

PLASMA-SPRAYED ceramic coatings up to several hundred micrometers thick are used on metal surfaces to confer wear and erosion resistance, corrosion protection, and thermal or electrical insulation.<sup>1-4</sup> Such coatings have a tendency to be highly defective in their microstructures, with pores, laminar microcracks, and unmolten phases. They consequently are subject to severe mechanical degradation from concentrated mechanical and thermal stresses, especially in repetitive loading. Yet these same coatings are sufficiently damage tolerant that they can attain more than adequate lifetimes in many practical applications.<sup>4</sup>

Despite this practical success, few studies have been aimed at systematic analysis of damage modes in terms of basic materials and geometrical properties. Well-defined materials-evaluation protocols for plasma-spray and other brittle coating systems appear to be desirable. For instance, it is recognized that the lifetimes of coating systems are sensitive to many factors. Among these factors are number of loading cycles, coating thickness, and processing variables such as starting powder composition and deposition history that influence the microstructure. This raises a vital question: what are the best combinations of such factors for optimum resistance to damage accumulation?

Accordingly, in the present paper Hertzian contact damage in plasma-sprayed alumina-based coatings on soft steel substrates

is studied. The Hertzian test uses spherical indenters to introduce damage in a controlled manner. It is simple yet powerful and has direct relevance to damage accumulation and fatigue wear resistance in bearing stress fields. Originally used to analyze cone fractures in ideally homogeneous brittle solids,<sup>5-8</sup> the Hertzian test has recently been applied to the study of subsurface quasi-plastic damage in tough ceramics with heterogeneous microstructures (i.e., weak internal boundaries, large and elongate grains, and high internal stresses).<sup>9-15</sup> Adaptation to ceramic layer systems is even more recent.<sup>16-18</sup> In the present paper this adaptation is extended to the exploration of coating thickness, cyclic loading, and microstructural change as elements in the underlying stress-strain behavior of a model plasma-spray ceramic coating system. For the coating, alumina-titania ( $\text{Al}_2\text{O}_3\text{-TiO}_2$ ) is chosen because it is relatively easy to produce in a uniform state; however, some "pure," but defective, alumina ( $\text{Al}_2\text{O}_3$ ) coatings are also included for comparison. Characterization of the damage in the coating/substrate specimens is achieved primarily by optical microscopy of "bonded-interface" sections using conventional spherical indenters, with ancillary *in situ* tests using cylindrical indenters. Indentation stress-strain curves from the same coating/substrate specimens are used to quantify the damage tolerance and to provide data for future fracture and deformation analyses.

## II. Experimental Procedure

### (1) Materials Selection and Characterization

Alumina-titania ( $\text{Al}_2\text{O}_3\text{-40 wt% TiO}_2$ ) was selected as a model ceramic coating material. Coatings were air-plasma-sprayed onto grit-blasted soft steel substrates ~3 mm thick. No bond coat was used. The coatings were deposited to average thicknesses of 130–200  $\mu\text{m}$  (designated as "thin" coatings) and 350–500  $\mu\text{m}$  ("thick" coatings) onto the substrates and to ~5 mm in free-standing form.

Sections of cut specimens were diamond-polished to a 1  $\mu\text{m}$  finish for characterization. The microstructure of the plasma-sprayed  $\text{Al}_2\text{O}_3\text{-40 wt% TiO}_2$  material is shown in Fig. 1(a). A characteristic lamella splat structure is observed, with compositional variations evident as the wavy texture.<sup>19</sup> Small pores in the structure are associated with processing defects; occasional larger ones are attributed to pull-out of particles during ceramographic preparation. Digital analysis of computer-scanned images indicates a maximum porosity of ~4% in this structure.

Exploratory Vickers tests were performed on polished specimens to obtain a precursory deformation and fracture characterization. Indentation hardness measurements (applied load divided by projected contact area<sup>20</sup>) yielded  $5.0 \pm 0.2$  GPa for the  $\text{Al}_2\text{O}_3\text{-40 wt% TiO}_2$  and  $1.2 \pm 0.1$  GPa for the steel. The coating material is therefore harder than the substrate material but substantially softer than ordinary dense alumina (~18 GPa). Cracks from the indentation corners in free-standing  $\text{Al}_2\text{O}_3\text{-40 wt% TiO}_2$  sections were macroscopically well-

R. H. Dauskardt—contributing editor

Manuscript No. 192304. Received September 25, 1995; approved January 23, 1996. Supported by the U.S. Air Force Office of Scientific Research, the National Science Foundation, and the Ministerio de Educación y Ciencia (DGICYT), Madrid, Spain.

\*Member, American Ceramic Society.

<sup>†</sup>Guest Scientist from Departamento de Física, Universidad de Extremadura, 06071-Badajoz, Spain.

<sup>‡</sup>Guest Scientist on leave from Department of Physics and Astronomy, Wayne State University, Detroit, Michigan 48201.

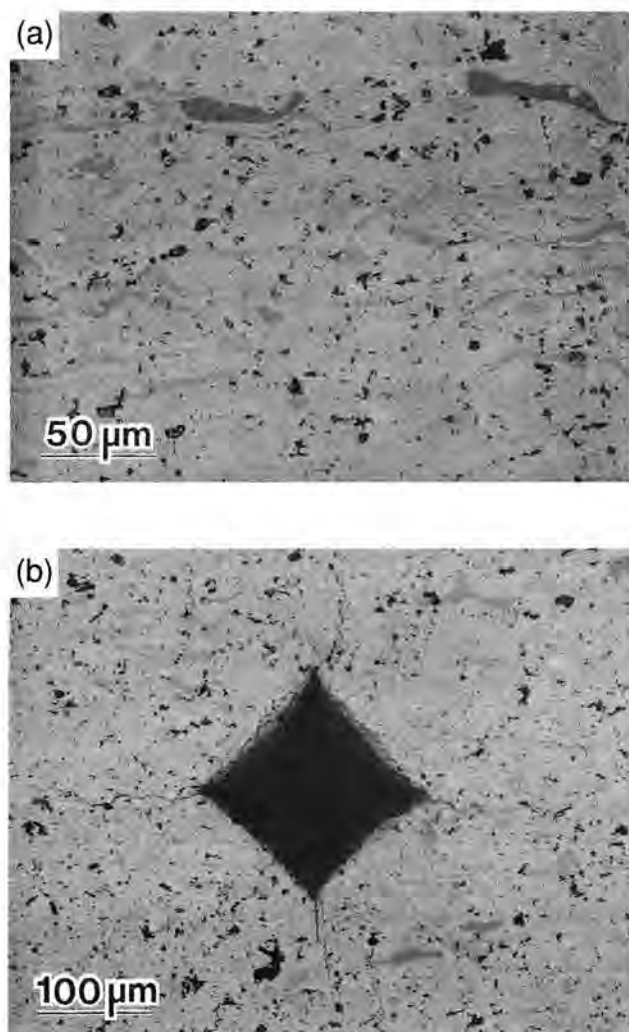


**Fig. 1.** Optical micrographs, showing section through plasma-sprayed  $\text{Al}_2\text{O}_3$ -40 wt%  $\text{TiO}_2$  ceramic, plasma-spray direction vertical: (a) unindented area, (b) indented area with Vickers diamond pyramid at load 100 N. Wavy microstructure indicates  $\text{TiO}_2$  phase. Note porosity. Radial cracks from indentation corners show irregularities at microscopic scale, but are relatively well-formed macroscopically with approximately equal arm lengths.

defined, with radial arms of approximately equal length normal and parallel to the thermal spray direction (Fig. 1(b)). This indicates relative isotropy in the fracture properties, notwithstanding the textured microstructure.

Some pure  $\text{Al}_2\text{O}_3$  specimens from a previous study<sup>18</sup> are also included in the present work, to demonstrate the influence of processing history. These coatings show a similar microstructure, but with defective layers associated with successive, interrupted torch passes and a porosity of ~8%. Such defective layers were meticulously avoided in the processing of the  $\text{Al}_2\text{O}_3$ -40 wt%  $\text{TiO}_2$  specimens.

## (2) Hertzian Indentation Tests

Specimens were first prepared for contact testing and subsequent examination of associated subsurface damage patterns. Bars with surface dimensions 25 mm  $\times$  3.5 mm were cut from the coating/substrate composites and free-standing coatings. Cross sections from adjacent cuts were then polished to a 1  $\mu\text{m}$  finish and bonded together (Fig. 2) by adhesive, in the case of the free coatings,<sup>11,12</sup> and by screws through carefully aligned holes in the metal, in the case of the layer composites.<sup>18</sup> The tops of the bonded specimens then were lightly ground and final polished to a 1  $\mu\text{m}$  flat finish. Previous studies<sup>11,12,21</sup> have confirmed that, provided the opposing specimen halves remain

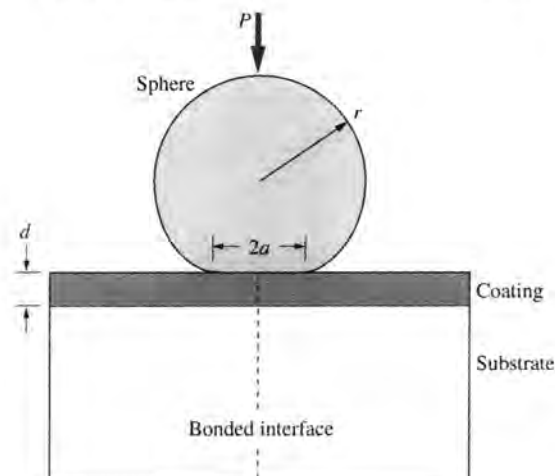


**Fig. 2.** Schematic of Hertzian test. Sphere of radius  $r$  on coating thickness  $d$  produces contact of radius  $a$  at load  $P$ . Some specimens are presectioned to form "bonded interface" for subsurface examination.

in intimate contact during the experiment, potential artifacts in the damage pattern from stress relaxation at the internal interface are easily avoided.

Hertzian tests were then made symmetrically on these top surfaces, along the trace of the bonded interface, in the manner of Fig. 2. The tests were performed in a servohydraulic testing machine (Model 8502, Instron Corp., Canton, MA) using tungsten carbide spheres of radius  $r = 3.18$  mm in air. Sequences of single-cycle contacts were made at peak loads, up to  $P = 1500$  N, with a load/unload time of 0.1 s. Multiple contacts were made at peak loads up to  $P = 500$  N and at a frequency of 10 Hz (to match the contact period in single-cycle loading) under sinusoidal load control, over  $n = 1$ – $10^5$  cycles. After separation, the bars were gold-coated and examined by Nomarski interference microscopy to reveal the subsurface damage.

Some ancillary contact experiments were performed on coating/substrate specimens using a cylinder of radius 1.58 mm in place of the sphere, with the cylinder axis aligned perpendicular to a polished section, to enable *in situ* observation of the damage evolution during a complete load/unload cycle. Results using this configuration were not as definitive as those that were obtained with the spherical indenters, owing to greater difficulty in aligning the indenting cylinder and to a somewhat lower optical resolution. They nevertheless afforded considerable insight into the general sequence of damage events. The specimen cross sections were viewed using a color video camera (Model AS12, Volpi AG, Urdorf/Zürich, Switzerland) with a lens of 50 mm working distance, and the visual images recorded on a video recording machine. These tests were performed slowly on a screw-driven machine (Model 1122, Instron Corp.), in a 5 min load/unload cycle, to follow the damage evolution.

Indentation stress-strain curves<sup>9,12</sup> were measured on polished top surfaces of coating/substrate composite and free-standing coating and substrate specimens. These surfaces were gold-coated prior to contact, to allow subsequent measurement of residual impressions in the deformed thin metal layer (especially at low loads). Indentations were made with tungsten carbide spheres of radius  $r = 1.98$  and 3.18 mm on coating/substrate composites, and  $r = 1.98$ , 3.18, 7.94, and 12.7 mm on free-standing forms (the two larger radii in the latter case to extend the data range to lower strains). Loads up to  $P = 3000$  N were applied using the screw-driven testing machine. The contact radius  $a$  was determined from the residual impression at each indentation<sup>9</sup> to obtain indentation stress ( $P/\pi a^2$ ) as a function of indentation strain ( $a/r$ ).



### III. Results

#### (I) Hertzian Damage Characterization

Sequences of subsurface Hertzian contact damage patterns from bonded-interface specimens are shown in Figs. 3, 4, 6, and 7 for a single sphere radius  $r = 3.18$  mm. These sequences illustrate the effects of coating thickness, contact load, number of contact cycles, and coating microstructure. Arrows at top of the micrographs indicate contact diameters,  $2a$ .

(A) *Effect of Coating Thickness:* Figure 3 shows micrographs of single-cycle contact damage in the  $\text{Al}_2\text{O}_3$ -40 wt%  $\text{TiO}_2$  system, for (a) free-standing coating material, (b) thick coating on steel, and (c) thin coating on steel. These tests have been made at a common peak load  $P = 1000$  N. In the free-standing coating (Fig. 3(a)), a drop-shaped damage zone of depth  $\sim 2a$  is observed in the subsurface region of concentrated shear stress. This drop-shaped damage geometry is characteristic of bulk ceramics with microstructural heterogeneity and high flaw tolerance.<sup>9,11-15</sup> Higher-magnification examinations show the damage to consist of a high density of discrete and constrained microfailures, preferentially along weak boundaries. No trace of classical cone cracks of the type found in homogeneous, ideally brittle solids<sup>8</sup> is evident.

In the coating/substrate layer composites (Figs. 3(b) and (c)), the damage pattern is strongly modified by the substrate, with progressive transfer of the "plasticity" to the soft substrate at diminishing coating thickness  $d$ . The plasticity in the substrate is apparent as an expanding hemispherical zone, and in the coating in Fig. 3(b) as an ever-constrained "caplike" damage zone immediately beneath the contact.<sup>18</sup> A consequence of the progressive transfer of load to the soft substrate is an attendant expansion of the contact diameter and residual coating depression, although the applied load remains the same in all cases in Fig. 3.

The most conspicuous component of the coating damage in Figs. 3(b) and (c) is the fracture pattern, consisting of downward-extending conelike cracks from the top surface and upward-extending transverse cracks from the lower interface. The cone cracks are axisymmetrical,<sup>8</sup> and the upward-extending cracks are shallow, near-circular segments contained in axial planes.<sup>4</sup> These cracks, once initiated, are highly stable: they are well contained in the thick coating in Fig. 3(b), and approach full penetration only in the thinner coating in Fig. 3(c). Any such penetration will inevitably diminish the load support provided by the coating and further transfer this support to the substrate. Delamination at the coating/substrate interfaces also is apparent in Figs. 3(b) and (c), again more so in the thinner coating. (Recall that there is no bond coat in this system, which otherwise might inhibit separation.<sup>18</sup>) Note that the delamination cracks are contained within the diameter of the substrate yield zone.

(B) *Effect of Contact Load:* Figure 4 consists of two series of micrographs, for thick (left) and thin (right)  $\text{Al}_2\text{O}_3$ -40 wt%  $\text{TiO}_2$  coatings on steel, showing the accumulation of single-cycle Hertzian contact damage through loads of  $P = 150, 500$ , and  $1500$  N. The accumulation of damage after the onset of first visible damage is expansive. The location of the first damage is discernible at low load in Figs. 4(a) and (d): in the thick-coating system as subsurface deformation in the coating, immediately beneath the contact; and in the thin-coating system as an incipient plastic zone within the substrate. At intermediate loading (Figs. 4(b) and (e)), damage is observed in the coating and substrate, in both the thick- and thin-coating systems. The first signs of brittle cracking appear, most notably as partially penetrating cone cracks in the thinner coating. Delamination at the coating/substrate interfaces is evident at both thicknesses. At high loading (Figs. 4(c) and (f)), the substrate yield zones extend beyond the contact dimension,

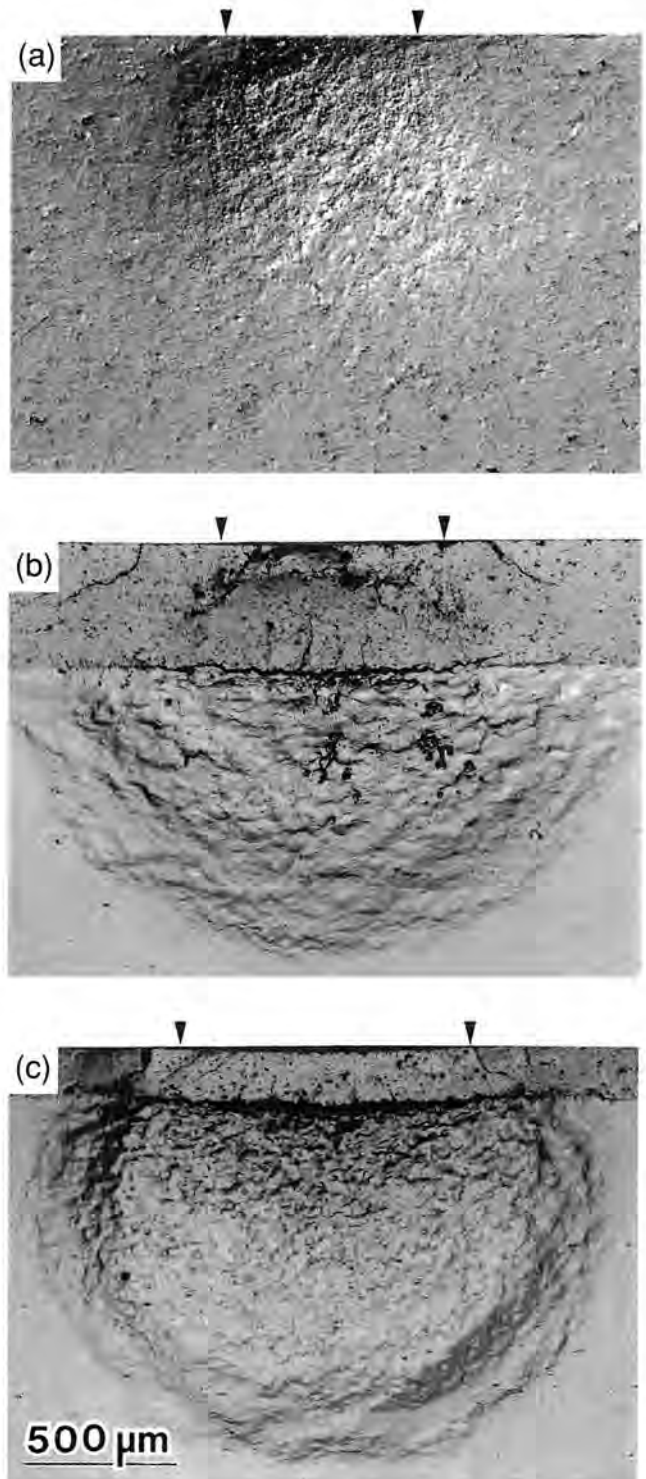
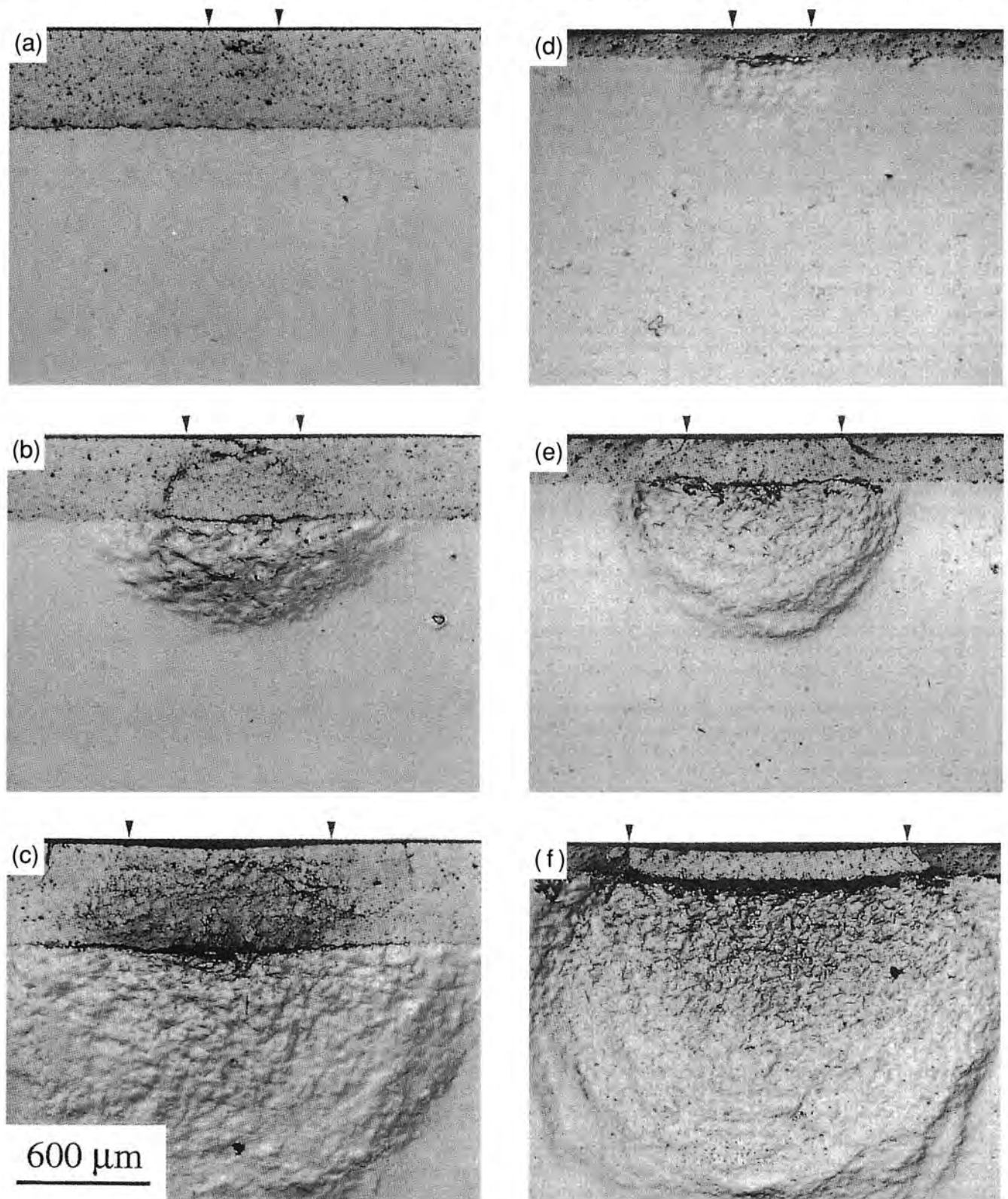


Fig. 3. Optical micrographs (Nomarski illumination) of bonded-interface section of plasma-sprayed  $\text{Al}_2\text{O}_3$ -40 wt%  $\text{TiO}_2$  coatings, showing effect of thickness on Hertzian contact damage: (a) free-standing coating; (b) "thick" coating on steel substrate,  $d = 425$   $\mu\text{m}$ ; and (c) "thin" coating on substrate,  $d = 170$   $\mu\text{m}$ . Single-cycle indentations made at common sphere radius  $r = 3.18$  mm and peak load  $P = 1000$  N. Respective contact diameters indicated by arrows correspond to indentation strains  $a/r = 0.10, 0.11$ , and  $0.15$ , respectively.

approaching a state of full plasticity.<sup>20</sup> The coatings also indicate through-thickness deformation, with resultant permanent bending. At this point, the coating fracture patterns, including delamination, are well developed, to the extent in the thin-coating system that the conelike cracks appear to have penetrated to the substrate, producing a loose (yet still intact) plug

<sup>4</sup>This fact is established from direct optical examination of analogous contact damage patterns in bilayer systems in which the coating layer is made of glass.<sup>17</sup>



**Fig. 4.** Optical micrographs (Nomarski illumination) of bonded-interface section of  $\text{Al}_2\text{O}_3$ -40 wt%  $\text{TiO}_2$  sequences for thick (left) and thin (right) plasma-sprayed coatings on steel, showing effect of loading on single-cycle Hertzian contact damage, at sphere radius  $r = 3.18$  mm: (a) and (d)  $P = 150$  N, (b) and (e)  $P = 500$  N, and (c) and (f)  $P = 1500$  N. Corresponding indentation strains are indicated in Fig. 8. Contact diameters are indicated by arrows. Note slight differences in thickness within each sequence, reflecting point-by-point and specimen-to-specimen variations in coating conditions.

of material, foreshadowing total failure. In this latter case, the substrate is on the verge of assuming the full brunt of the contact load. Ultimately, at even higher loads, the coatings do indeed fail, by spalling.

The sequence of deformation and fracture initiation and development during the load/unload cycle in Fig. 4 has been

established from the *in situ* observations on thick-coating specimens, notwithstanding the configurational differences associated with the cylindrical indenter. A schematic representation of the damage evolution traced from a video sequence during one loading/unloading cycle on a thick coating is given in Fig. 5. Above a critical level in the loading half-cycle

(Fig. 5(a)), plastic deformation is observed to initiate in the substrate. On further loading (Fig. 5(b)), conelike fractures at the outer top surface and upward-extending cracks at the inner coating/substrate interface are seen to pop in and arrest. On proceeding to peak load (Fig. 5(c)), the substrate yield zone continues to expand and the coating cracks to grow. On unloading (Fig. 5(d)), the latter cracks continue to open and even to propagate, albeit in a highly stable manner. Finally, close to full unload (Fig. 5(e)), the delamination cracks open widely.

(C) *Effect of Number of Cycles:* Micrographs of damage from multiple-cycle contact tests on the  $\text{Al}_2\text{O}_3$ -40 wt%  $\text{TiO}_2$ /steel system are presented in Fig. 6 for thin-coating specimens. The tests are conducted at an intermediate load  $P = 500$  N (from Fig. 4(e)), over  $n = (a) 1$ ,  $(b) 10^2$ , and  $(c) 10^5$  cycles. There is a small but systematic increase in the substrate plastic zone size with the cycling, attributable to load/unload yield hysteresis.<sup>22</sup> The fracture damage in the coating also increases, until at  $n = 10^5$  the delamination cracks have opened considerably, and the conelike cracks at the edge of the contact have penetrated to the substrate (cf. damage attained at  $P = 1500$  N in Fig. 4(f)).

Thus, the coatings are subject to significant fatigue. Damage, once initiated, accumulates with each cycle, indicating a finite lifetime. Nevertheless, the coating in Fig. 6(c) has not spalled, and should still provide some protection to the substrate.

(D) *Effect of Processing History and Microstructure:* To demonstrate the importance of processing variables, comparative micrographs for  $\text{Al}_2\text{O}_3$ -40 wt%  $\text{TiO}_2$  and  $\text{Al}_2\text{O}_3$  coating systems are shown in Figs. 7(a) (from Fig. 3(b)) and 7(b), respectively. In these two cases, the tests have been made on thick-coating specimens at a single cycle and a common peak load  $P = 1000$  N. There are some similarities in the damage pattern, notably in the substrate yield zone (although not quite as well developed in the  $\text{Al}_2\text{O}_3$ , consistent with a slightly larger coating thickness), and in the appearance of the caplike distributed deformation in the coating immediately beneath the contact area. This implies some commonality in the yield process in the two  $\text{Al}_2\text{O}_3$ -based coating materials.

However, there also are some striking differences in the damage patterns, most notably in the form of the coating fracture. In the  $\text{Al}_2\text{O}_3$ -40 wt%  $\text{TiO}_2$ , the cracks are predominantly transverse; in the  $\text{Al}_2\text{O}_3$ , they are predominantly (but not exclusively) laminar. From *in situ* tests on the latter specimens, these intracoating laminar cracks were observed to form during loading, as initiation of microcracks along the defective interlayers associated with the four interrupted plasma-spray torch passes. The discrete sources coalesced into the macroscopic laminar cracks during unloading. The operation of this alternative fracture mode in the  $\text{Al}_2\text{O}_3$  appears to have inhibited the development of the transverse fractures. This implies that the mode of coating failure is highly sensitive to the microstructure. Delamination at the coating/substrate interlayer again occurred at the completion of unloading.

## (2) Stress-Strain Curves

Indentation stress-strain curves,  $p_0(a/r)$ , are shown for the  $\text{Al}_2\text{O}_3$ -40 wt%  $\text{TiO}_2$ /steel system in Fig. 8. Data are plotted for free-standing coatings and free-standing substrates, as well as for layer composites of different coating thickness relative to sphere radius,  $d/r$ . Solid curves are empirical fits through the data. For the free-standing coatings and free-standing substrates, the stress-strain curves are universally monotonic, independent of  $r$ . These curves enable evaluation of two key elastic/plastic parameters:<sup>18</sup> Young's modulus,  $E$ , from the initial slopes, in conjunction with the Hertzian elasticity relations, yielding  $70 \pm 5$  GPa ( $\text{Al}_2\text{O}_3$ -40 wt%  $\text{TiO}_2$ ) and  $180 \pm 36$  GPa (steel); and yield stress,  $Y$ , from the contact pressures  $p_0 = 1.1Y$  at the onset of plasticity (most accurately determined from presection observations such as Fig. 3(a), made over a range of loads), yielding  $Y = 1.9$  GPa ( $\text{Al}_2\text{O}_3$ -40 wt%  $\text{TiO}_2$ ) and  $0.42$  GPa (steel). These values of  $E$  and  $Y$  for  $\text{Al}_2\text{O}_3$ -40 wt%  $\text{TiO}_2$

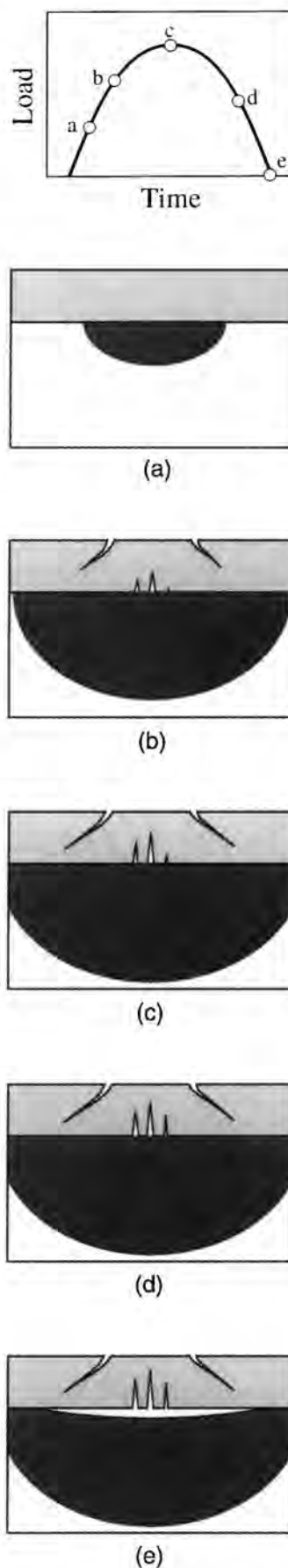
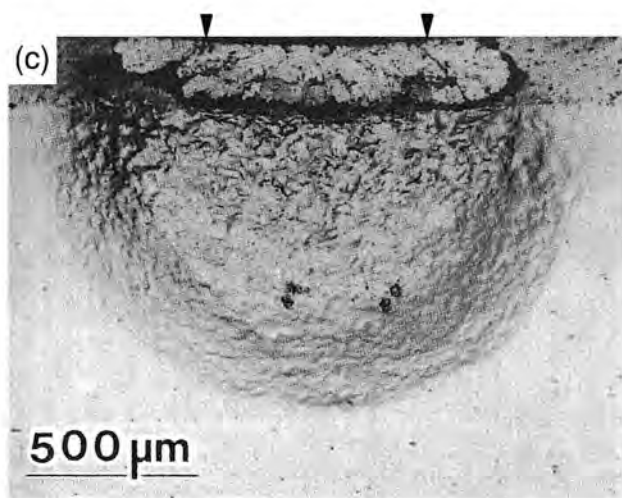
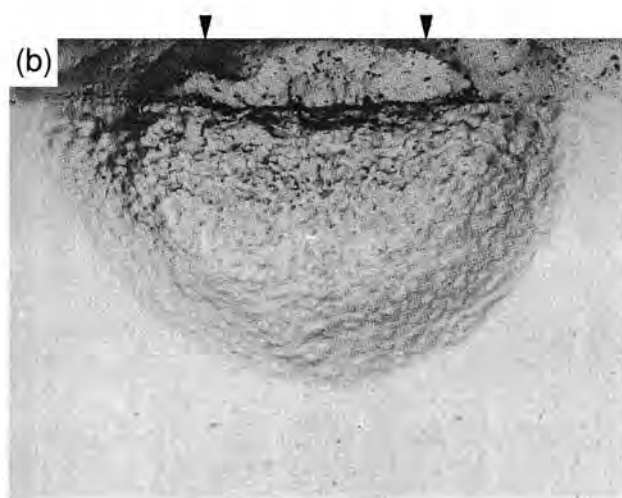
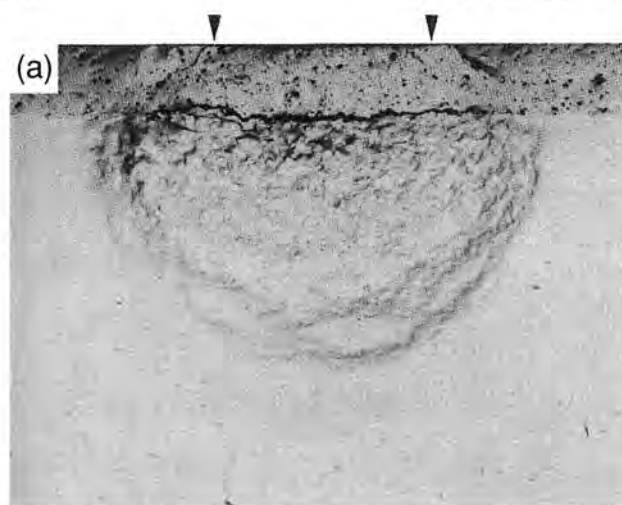


Fig. 5. Evolution of damage in thick plasma-sprayed  $\text{Al}_2\text{O}_3$ -40 wt%  $\text{TiO}_2$  coatings (light shading) on steel. Substrate yield zone (dark shading) and coating fractures traced from *in situ* video recording during load/unload cycle (a)-(e) using cylindrical indenter.





**Fig. 6.** Optical micrographs (Nomarski illumination) of bonded-interface section of  $\text{Al}_2\text{O}_3$ -40 wt%  $\text{TiO}_2$  for thin plasma-sprayed coatings on steel, showing effect of number of cycles on multiple-cycle Hertzian contact damage, at sphere radius  $r = 3.18$  mm and peak load  $P = 500$  N: (a)  $n = 1$  (from Fig. 4(e)), (b)  $n = 10^3$ , and (c)  $n = 10^5$  cycles. Contact diameters are indicated by arrows.

are within 10% of those obtained previously for  $\text{Al}_2\text{O}_3$ ,<sup>18</sup> confirming a relative insensitivity of macroscopic stress-strain parameters to composition and microstructure.

For the composite coating/substrate system,  $p_0(a/r)$  is no longer a universal function but now depends on  $d/r$ , bounded by

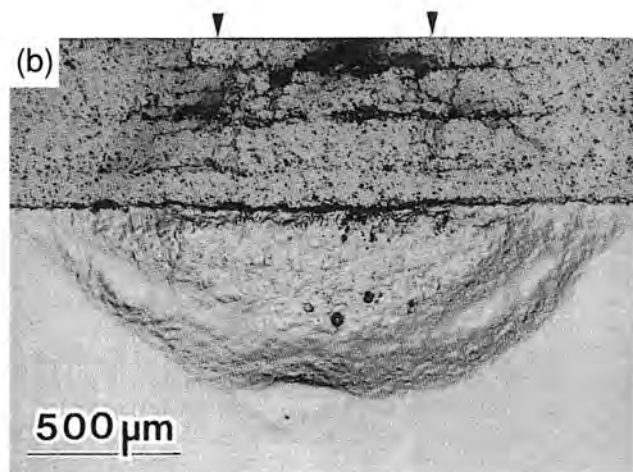
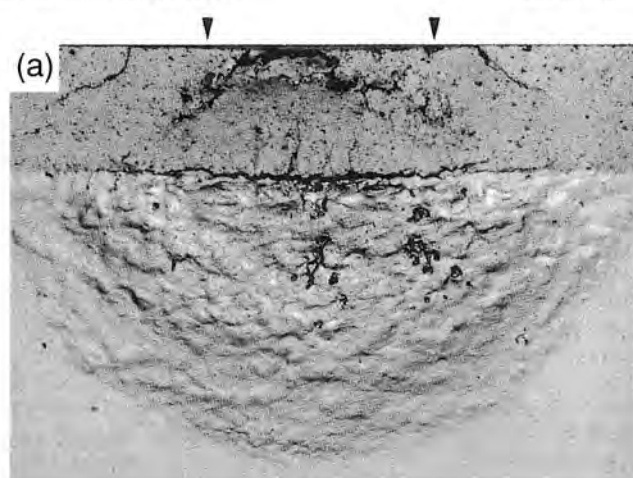


**Fig. 7.** Optical micrographs (Nomarski illumination) of bonded-interface section of thick plasma-sprayed  $\text{Al}_2\text{O}_3$ -based coatings, single-cycle damage at sphere radius  $r = 3.18$  mm and peak load  $P = 1000$  N: (a)  $\text{Al}_2\text{O}_3$ -40 wt%  $\text{TiO}_2$  (from Fig. 3(b)) and (b)  $\text{Al}_2\text{O}_3$ . Contact diameters are indicated by arrows.

the free-standing coating and substrate curves.<sup>18</sup> With increasing contact load, the coating/substrate data for any given value of  $d/r$  initially follow the coating curve closely, but then pass through a maximum,  $p_0 = p_m$  say, and finally approach the substrate curve. The implication is that the load is supported elastically by the coating and plastically by the substrate. In this context, it is interesting to refer to the sequences of micrographs for the thick- and thin-coating series in Fig. 4, and to correlate the onset and development of substrate yield with the points "a," "b," and "c" (thick,  $d/r = 0.15$ ) and "d," "e," and "f" (thin,  $d/r = 0.050$ ) marked on the appropriate curves in Fig. 8. Note the comparatively long tail of the thin-coating material in this comparison, indicating an enhanced capacity to absorb strain energy at a given set of contact loading conditions prior to ultimate failure, characteristic of a more damage-tolerant structure.

The maximum in the stress-strain curve warrants additional consideration, because it implies the existence of a limiting sustainable stress for any given coating and contact configuration. Values of  $p_m$  are plotted as a function of  $d/r$  in Fig. 9, using the determinations for  $\text{Al}_2\text{O}_3$ -40 wt%  $\text{TiO}_2$  from Fig. 8 along with some previous data for  $\text{Al}_2\text{O}_3$ .<sup>18</sup> Hence, the maximum contact pressure in the alumina/steel coating/substrate system in this experiment increases with either increasing coating thickness at fixed sphere radius or decreasing sphere radius at fixed coating thickness, again somewhat insensitively to the alumina microstructure.



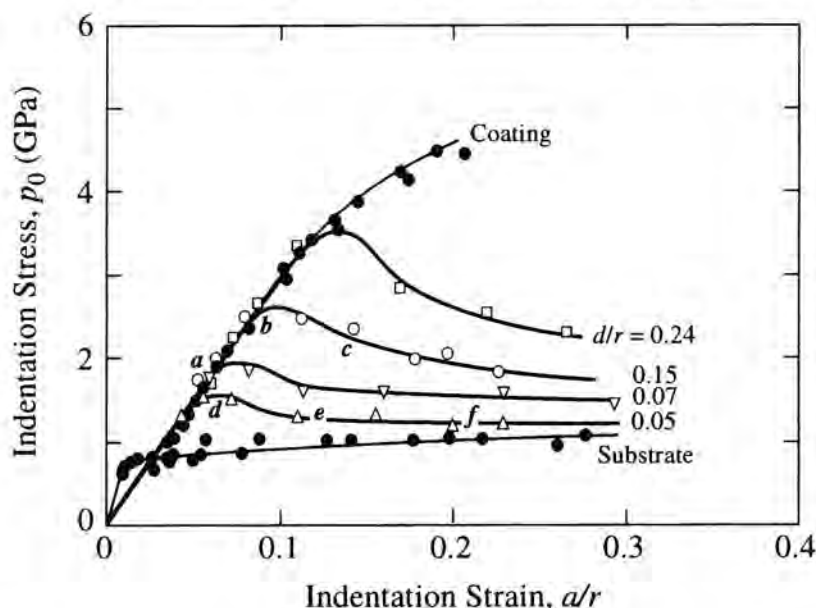


Fig. 8. Indentation stress-strain curves for plasma-sprayed  $\text{Al}_2\text{O}_3$ -40 wt%  $\text{TiO}_2$  coatings on steel. Data for composite coating/substrate systems plotted separately at designated values of coating thickness/sphere radius,  $d/r$ , for thick and thin coatings at  $r = 1.98$  and  $3.18$  mm. Data for free-standing coating and substrate plotted for values of  $r = 1.98$ - $12.7$  mm (not distinguished). Solid curves are empirical fits. Points "a," "b," "c," "d," "e," and "f" respectively correspond to micrographs in Fig. 4. Note maximum in curve for each composite coating/substrate system. Beyond tail regions, coatings fail.

#### IV. Discussion

The results in this study confirm the Hertzian test as a simple but functional means of investigating fracture and deformation modes in ceramic coatings on metal substrates—in this case, plasma-sprayed alumina-based composites on steel—with special relevance to contact problems, bearing stresses, wear and erosion, etc. Specifically, the results confirm the potential of Hertzian testing as a means of evaluating the roles of coating thickness, number of cycles, and microstructural variables in damage accumulation. Even though the Hertzian contact field may not be considered a true representation of many practical stress states (e.g., thermal cycling), it nevertheless constitutes a powerful probe of inherent weaknesses in the structures, without the complexity of simulated rig testing. This kind of macroscopic accumulation of damage in the coating materials is typical of flaw-tolerant ceramics,<sup>9,23-26</sup> although details of the underlying micromechanisms may be superficially different. Conspicuously, the observations reveal the damage tolerance of

the plasma-spray coatings to be high; even where failure appears imminent, at high load or after many cycles, the coatings continue to afford protection to the substrate. Such observations, in combination with an appropriate stress analysis (see below), would appear to offer a basis for ultimate lifetime predictions of brittle coating systems.

Accordingly, the presectioning technique used to obtain the micrographs in Figs. 3, 4, 6, and 7 reveals the distribution of deformation and fracture damage in both coating and substrate beneath spherical contacts. *In situ* observations using contacts with cylinders (Fig. 5) establish the sequence of the individual damage events. Initially, at low loads, the harder alumina-based coating elastically supports the bulk of the load. Beyond a yield point, quasi-plastic deformation sets in. As the contact zone continues to expand, full plasticity develops in the substrate, which assumes an increasing proportion of the load support. Yield also occurs in the coating, but the main damage there appears as transverse fractures, outer downward-extending conelike cracks and inner upward-extending cracks. These cracks pop in during the loading half-cycle, but continue to evolve in a highly stabilized manner during the unloading half-cycle. Interlayer delamination occurs toward the end of unloading. The presence of an intervening bond coat can help alleviate this delamination.<sup>18</sup>

It is instructive to rationalize the damage patterns in terms of combined Hertz and flexure fields. The difference in elastic/plastic properties between the coating and the substrate accounts for the changes in damage mode in Fig. 3 as the coating thickness decreases. Thus, elastic/plastic mismatch redistributes the concentrated shear stresses immediately below the indenter, thereby transferring the yield zone progressively into the soft substrate. The same mismatch redistributes the tensile stresses in the coating during the loading half-cycle, the more so as the coating thickness decreases. The thinner coating layer may be considered to behave more like a constrained flexural plate supported by a still-elastic outer contact boundary and soft plastic underlayer, and less like a purely Hertzian semi-infinite solid. This transition to a greater flexural component inevitably concentrates the tensile coating stresses at the upper free surface shoulders outside the circle of contact and at the coating/substrate interface within the contact, where the transverse cracks develop. At the same time, these flexural stresses

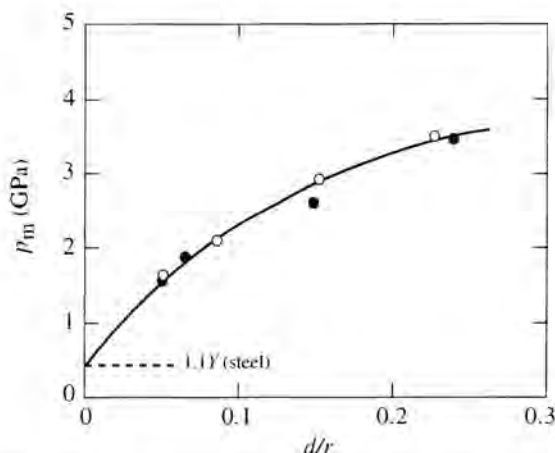


Fig. 9. Plot of maximum stress,  $p_m$ , from Fig. 8 and Ref. 18, as function of  $d/r$ . Yield stress in metal provides lower limit for zero-thickness coatings ((●)  $\text{Al}_2\text{O}_3$ -40 wt%  $\text{TiO}_2$  coatings on steel and (○)  $\text{Al}_2\text{O}_3$  coatings on steel).

must be strongly compressive on the opposing sides of the neutral planes, thus stabilizing the fractures. In making this argument for an increasingly important flexural stress component, the ever-present contribution from the contact field cannot be disregarded, even in the thinnest coatings. The contact field superposes strong elastic compressive stresses onto the transverse cracks, released only when the indenter is withdrawn. Such release explains the continued crack extension during unloading, in the well-documented manner of radial and lateral cracks in residual contact fields beneath Vickers indentations in homogeneous materials,<sup>27,28</sup> and of shear-fault-induced, grain-localized microcracks beneath Hertzian indenters in heterogeneous materials.<sup>29</sup> Perhaps the strongest of all manifestations of elastic/plastic mismatch is the generation of high residual tension at the coating/substrate interface immediately above the substrate plastic zone, where delamination occurs. This extreme mismatch is attributed to a relatively high elastic recovery in the flexed coating layer, again reaching its maximum at complete unload.

To place these observations on a more quantitative footing, and to establish a basis for future fracture-mechanics analysis, a detailed stress analysis is necessary. The invariably complex elastic/plastic fields in the deformed coating structures considered in this paper appear to be beyond analytical solution—numerical evaluation techniques (e.g., finite-element modeling) seem to be necessary. Specifically required are shear-stress distributions in the substrate and coating, to confirm the plastic zone geometry, and tensile stress distributions in the coating, to confirm the fracture geometry. A test of any such stress analysis is self-consistency between the calculated and measured indentation stress-strain curve. The present results establish an environment for such calculations not only by defining the deformation and fracture configurations to be modeled but also by providing essential input parameters, e.g., coating thickness and sphere size, Young's modulus, and yield stress.

The indentation stress-strain curves in Fig. 8 provide a graphical representation of damage evolution in the coating/substrate system. In the present case, where the substrate is considerably softer than the coating, the stress-strain curve exhibits a well-defined maximum,  $p_m$ . Prior to the maximum, the strain is governed principally by the properties of the coating; beyond the maximum, the strain is transferred progressively to the substrate. The value of  $p_m$  is a measure of the maximum sustainable stress in the composite system. Increasing the thickness of the coating relative to the contact diameter increases  $p_m$  (Fig. 9), effectively increasing the hardness of the composite structure. As may be attested by comparison tests on other coating/substrate structures,<sup>18</sup> the very existence of  $p_m$  is contingent on the substrate being softer than the coating—the reverse case leads to an ever-increasing monotonic curve. The long strain-softening tail, most pronounced at the lower values of  $d/r$  in Fig. 8, indicates a damage-tolerant, energy-absorbing structure. Note, for instance, that the point *f* for  $d/r = 0.050$  extends much farther along the tail than the corresponding point *c* for  $d/r = 0.15$  at the same contact load (recall Fig. 4). Hence damage tolerance is gained at the expense of effective structural hardness. Such competing elements, along with the fracture characteristics described above, could be important considerations in the general design of brittle coatings on soft substrates.

Finally, comment may be made on the influence of microstructure based on the brief comparison in this experiment between  $\text{Al}_2\text{O}_3$ -40 wt%  $\text{TiO}_2$  and  $\text{Al}_2\text{O}_3$  coatings. Essentially, the effect of microstructural variation from different processing histories is felt only slightly in the elastic/plastic properties, but is crucial in the fracture properties. For the elastic/plastic properties, recall the similarity of  $E$  and  $Y$  values for these two  $\text{Al}_2\text{O}_3$ -based materials (Section III(2)), indicating an insensitivity of macroscopic stress-strain response to structural details.<sup>18</sup> The fracture properties, on the other hand, are extremely vulnerable to weaknesses in the structures (Fig. 7). Thus in the

$\text{Al}_2\text{O}_3$ , preexistent laminar weaknesses promote intralayer delaminations. These delaminations, by relaxing the stress buildup, most likely suppress the transverse fractures observed in the other, more isotropic  $\text{Al}_2\text{O}_3$ -40 wt%  $\text{TiO}_2$  material. In the context of engineering lifetime, the failure mode and other critical operational properties, such as heat transfer in thermal barrier coatings, may be highly dependent on the microstructural complexion. Interactions between mechanical and thermal properties may constitute a rich area for future study.

**Acknowledgments:** Thanks are due to G. Bancke for assistance in preparing the coatings, E. R. Fuller for the computer evaluations of porosities in the coating materials, and T.-N. Ying for assistance with the *in situ* experiments.

## References

- H. Herman, "Plasma-Sprayed Coatings," *Sci. Am.*, **256** [9] 113–88 (1988).
- H. Herman, "Plasma Spray Deposition Processes," *MRS Bull.*, **13**, 60–67 (1988).
- H. Herman, C. C. Berndt, and H. Wang, "Plasma-Sprayed Ceramic Coatings," pp. 131–88 in *Ceramic Films and Coatings*. Edited by J. B. Wachtman and R. A. Haber. Noyes, Park Ridge, NJ, 1993.
- L. Pawlowski, *The Science and Engineering of Thermal Spray Coatings*. Wiley, New York, 1995.
- H. Hertz, *Hertz's Miscellaneous Papers*; Chs. 5 and 6. Macmillan, London, U.K., 1896.
- F. C. Roesler, "Brittle Fractures Near Equilibrium," *Proc. Phys. Soc., London, Sect. B*, **69**, 981 (1956).
- F. C. Frank and B. R. Lawn, "On the Theory of Hertzian Fracture," *Proc. R. Soc. London, A*, **299** [1458] 291–306 (1967).
- B. R. Lawn and T. R. Wilshaw, "Indentation Fracture: Principles and Applications," *J. Mater. Sci.*, **10** [6] 1049–81 (1975).
- F. Guiberteau, N. P. Padture, H. Cai, and B. R. Lawn, "Indentation Fatigue: A Simple Cyclic Hertzian Test for Measuring Damage Accumulation in Polycrystalline Ceramics," *Philos. Mag. A*, **68** [5] 1003–16 (1993).
- B. R. Lawn, N. P. Padture, H. Cai, and F. Guiberteau, "Making Ceramics 'Ductile,'" *Science*, **263**, 1114–16 (1994).
- F. Guiberteau, N. P. Padture, and B. R. Lawn, "Effect of Grain Size on Hertzian Contact in Alumina," *J. Am. Ceram. Soc.*, **77** [7] 1825–31 (1994).
- H. Cai, M. A. Stevens Kalceff, and B. R. Lawn, "Deformation and Fracture of Mica-Containing Glass-Ceramics in Hertzian Contacts," *J. Mater. Res.*, **9** [3] 762–70 (1994).
- N. P. Padture and B. R. Lawn, "Toughness Properties of a Silicon Carbide with an *In-Situ*-Induced Heterogeneous Grain Structure," *J. Am. Ceram. Soc.*, **77** [10] 2518–22 (1994).
- H. H. K. Xu, L. Wei, N. P. Padture, B. R. Lawn, and R. L. Yeckley, "Effect of Microstructural Coarsening on Hertzian Contact Damage in Silicon Nitride," *J. Mater. Sci.*, **30**, 869–78 (1995).
- A. Pajares, F. Guiberteau, B. R. Lawn, and S. Lathabai, "Hertzian Contact Damage in Magnesia-Partially-Stabilized Zirconia," *J. Am. Ceram. Soc.*, **78** [4] 1083–86 (1995).
- L. An, H. M. Chan, N. P. Padture, and B. R. Lawn, "Damage-Resistant Alumina-Based Layer Composites," *J. Mater. Res.*, **11** [1] 204–10 (1996).
- S. Wuttiphan, B. R. Lawn, and N. P. Padture, "Crack Suppression in Strongly Bonded Homogeneous/Heterogeneous Laminates: A Study on Glass/Glass-Ceramic Bilayers," *J. Am. Ceram. Soc.*, **79** [3] 634–40 (1996).
- A. Pajares, L. Wei, B. R. Lawn, N. P. Padture, and C. C. Berndt, "Mechanical Characterization of Plasma-Sprayed Ceramic Coatings on Metal Substrates by Contact Testing," *Mater. Sci. Eng., A*, **208** [2] 158–65 (1996).
- J. Ilavsky, "Studies of Plasma Sprayed Alumina," Ph.D. Thesis. State University of New York at Stony Brook, Stony Brook, NY, 1994.
- D. Tabor, *Hardness of Metals*. Clarendon, Oxford, U.K., 1951.
- T. O. Mulhearn, "The Deformation of Metals by Vickers-Type Pyramidal Indenters," *J. Mech. Phys. Solids*, **7**, 85–96 (1959).
- S. Suresh, *Fatigue of Materials*. Cambridge University Press, Cambridge, U.K., 1991.
- H. Cai, M. A. S. Kalceff, B. M. Hooks, B. R. Lawn, and K. Chyung, "Cyclic Fatigue of a Mica-Containing Glass-Ceramic at Hertzian Contacts," *J. Mater. Res.*, **9** [10] 2654–61 (1994).
- N. P. Padture and B. R. Lawn, "Contact Fatigue of a Silicon Carbide with a Heterogeneous Grain Structure," *J. Am. Ceram. Soc.*, **78** [6] 1431–38 (1995).
- N. P. Padture and B. R. Lawn, "Fatigue in Ceramics with Interconnecting Weak Interfaces: A Study Using Cyclic Hertzian Contacts," *Acta Metall.*, **43** [4] 1609–17 (1995).
- A. Pajares, L. Wei, B. R. Lawn, and D. B. Marshall, "Damage Accumulation and Cyclic Fatigue in Mg-PSZ at Hertzian Contacts," *J. Mater. Res.*, **10** [10] 2613–25 (1995).
- D. B. Marshall and B. R. Lawn, "Residual Stress Effects in Sharp-Contact Cracking: I. Indentation Fracture Mechanics," *J. Mater. Sci.*, **14** [8] 2001–12 (1979).
- B. R. Lawn, A. G. Evans, and D. B. Marshall, "Elastic/Plastic Indentation Damage in Ceramics: The Median/Radial Crack System," *J. Am. Ceram. Soc.*, **63** [9–10] 574–81 (1980).
- B. R. Lawn, N. P. Padture, F. Guiberteau, and H. Cai, "A Model for Microcrack Initiation and Propagation Beneath Hertzian Contacts in Polycrystalline Ceramics," *Acta Metall.*, **42** [5] 1683–93 (1994).

#### Permission to publish

A. Pajares, L. Wei, B.R. Lawn and C.C. Berndt, 'Contact damage in plasma-sprayed alumina-based coatings', J. Am. Ceram. Soc., 79[7] (1996) 1907-14.

Wiley Publishes Open Access Articles in fully Open Access Journals and in Subscription journals offering Online Open. Although most of the fully Open Access journals publish open access articles under the terms of the Creative Commons Attribution (CC BY) License only, the subscription journals and a few of the Open Access Journals offer a choice of Creative Commons Licenses:: Creative Commons Attribution (CC-BY) license [Creative Commons Attribution Non-Commercial \(CC-BY-NC\) license](#) and [Creative Commons Attribution Non-Commercial-NoDerivs \(CC-BY-NC-ND\) License](#). The license type is clearly identified on the article.

Copyright in any research article in a journal published as Open Access under a Creative Commons License is retained by the author(s). Authors grant Wiley a license to publish the article and identify itself as the original publisher. Authors also grant any third party the right to use the article freely as long as its integrity is maintained and its original authors, citation details and publisher are identified. These details are indicated above. The copyright owner is specified within the particular Journal. Search: <http://onlinelibrary.wiley.com/browse/publications?type=journal> to find the final article.

# Influence of plasma spray parameters on mechanical properties of yttria stabilized zirconia coatings. I: Four point bend test

A. Kucuk <sup>a</sup>, C.C. Berndt <sup>a,\*</sup>, U. Senturk <sup>a,1</sup>, R.S. Lima <sup>a</sup>, C.R.C. Lima <sup>b</sup>

<sup>a</sup> *Department of Materials Science and Engineering, Center for Thermal Spray Research, State University of New York at Stony Brook, 306 Old Engineering, Stony Brook, NY 11794-2275, USA*

<sup>b</sup> *UNIMEP Methodist University of Piracicaba, Technology Center, Rod. Santa Barbara-Iracemapolis, Km 1, Santa Barbara d'Oeste, Sao Paulo 13450-000, Brazil*

Received 12 October 1999; received in revised form 7 February 2000

## Abstract

Yttria (8 wt.%) stabilized zirconia (YSZ) with a NiCrAlY bond coat was atmosphere plasma sprayed on mild steel substrates. The bond coat thickness (100–250  $\mu\text{m}$ ), YSZ coating thickness (300–500  $\mu\text{m}$ ), stand off distance (80–100 mm), and substrate temperature (273–393 K) were changed in a four by 17 experimental design matrix to investigate the influence of each spray parameter on the mechanical properties of coatings. Coatings were tested using a four point bend test arrangement. Coatings sprayed with thinner bond coat on a cold substrate exhibited higher yield strength and stiffness under bending. Change in the stand off distance and the top coat thickness did not statistically influence either yield strength or stiffness of the coatings. © 2000 Elsevier Science S.A. All rights reserved.

**Keywords:** Thermal barrier coatings; Mechanical properties; Plasma spray parameters

## 1. Introduction

Yttria stabilized zirconia (YSZ) plasma sprayed coatings are common thermal barrier coatings (TBCs) for applications such as gas turbines and diesel engines [1]. The TBC system allows conventional metals to be reliably used at high temperatures. At high temperatures, the ceramic layer provides thermal stability to the base metal due to insulation from the heat, while the bond coating (NiCrAlY) provides oxidation resistance [2].

Performance of the coating depends on the composition and characteristics (size and shape) of the feedstock powders [3,4], as well as the spraying condition such as plasma gun type, gun power, plasma gas composition and flow rate, and powder feeding rate [1,3–5]. The performance of TBCs has been determined by

measuring the physical properties such as thermal conductivity [1], thermal shock resistance [6,7], oxidation resistance [2], porosity amount and distribution [4], residual stresses [8–10], and mechanical properties such as tensile adhesion [10,11] and bending strength [12,13], hardness [14], and fatigue [15].

The common practice is to optimize spraying parameters to manufacture coatings with a desired performance. The mechanical performance of YSZ coatings involves brittle fracture by crack initiation and growth. Therefore, it is crucial to understand cracking in ceramic coatings under load. A variety of cracking mechanisms will evolve during loading, and arise from defects such as pores, splat boundaries, secondary phase interfaces, and pre-existing cracks within coatings. Acoustic emission (AE) analysis has also been used to monitor cracking in ceramic coatings during mechanical testing (three point bending [16], four point bending [12,13,17,18], tensile adhesion test [19], and indentation [20]) and during thermal cycling [21].

In the current study, the performance of plasma sprayed YSZ coatings on mild steel substrates with varying bond coat thickness and top coat thickness was

\* Corresponding author.

<sup>1</sup> Present address: PQ Corporation, Research & Development Center, 280 Cedar Grove Rd., Conshohocken, PA 19428-2240, USA.

Table 1  
Samples sprayed according to experimental design

Samples	Bond coat ( $\mu\text{m}$ )	Top coat ( $\mu\text{m}$ )	Substrate temperature (K)	Stand off distance (mm)
G1	100	300	393	80
G2	100	300	393	100
G3	250	300	393	80
G4	250	500	393	100
G5	250	500	393	80
G6	100	500	273	80
G7	100	500	273	100
G8	250	300	273	80
G9	100	500	393	80
G10	100	300	273	80
G11	250	300	393	100
G12	250	300	273	100
G13	250	500	273	80
G14	250	500	273	100
G15	100	300	273	100
G16	100	500	393	100
G17	175	400	333	90

determined using four point bend tests. The influence of substrate temperature and spraying distance on the performance was also investigated. This study aimed to provide further understanding on the mechanical characteristics of thermally sprayed coatings and how the spray processing variables influence these characteristics. It is clear that such information on the mechanical characteristics of the thermally sprayed coatings leads coatings with a better performance.

Senturk et al. [12,13] showed that the in situ monitoring of samples using an AE transducer during a four point bend test could provide further understanding on the deformation of the plasma sprayed YSZ coatings. The same in situ monitoring of the AE activities was also followed during the four point tests in the current study, but will be reported in a separate publication [22].

## 2. Experimental procedure

### 2.1. Sample preparation

YSZ (8 wt.%) was sprayed onto mild-carbon steel substrates ( $90 \times 26.5 \times 2.6 \text{ mm}^3$ ) under spray parameters which were altered with respect to: (i) coating thickness (either 300 or 500  $\mu\text{m}$ ); (ii) the stand off distance (either 80 or 100 mm); and (iii) the substrate temperature (either at 273 or 393 K). The substrate temperature was measured using a hand held infrared temperature detector. The substrates were grit blasted and cleaned with ethyl alcohol before spraying. The average roughness of the grit blasted substrate was measured as  $4.0 \pm 0.5 \mu\text{m}$  using a Hommel T1000 mechanical profilometer (Hommel America, New Britain,

CT). A NiCrAlY bond coating of either 100 or 250  $\mu\text{m}$  thickness was atmospherically plasma sprayed before application of the YSZ top coat. Coatings were sprayed to dimensions of  $30 \times 26.5 \text{ mm}$ , leaving approximately 20 and 40 mm uncoated substrate on both sides since these areas made contact with the bend testing device. Air cooling on the back side of the substrates avoided overheating during the spray process.

A statistical experimental design procedure using StatGraph software (Statistical Graphics, Rockville, MD) was employed to determine the number of samples to be sprayed and the spray parameters necessary to determine relevant correlations. Table 1 lists the samples sprayed in the current study according to this experimental design. Six samples from each group in Table 1 were sprayed (the conditions given in Table 2) using a Metco 3 MB plasma gun (Sulzer-Metco, Westbury, NY) mounted on a six-axis articulated robot (Model S400, GMF Fanuc). Commercially available ceramic (YSZ) (Metco 204NS) and metal (NiCrAlY) (Praxair NI-346-1, Praxair Surface Technologies, Indianapolis, IN) feedstocks were used.

Table 2  
Spraying parameters

	YSZ	NiCrAlY
Gun Type	Metco 3MB	Metco 3MB
Current (A)	600	500
Voltage (V)	70	70
Primary gas, Ar ( $\text{l min}^{-1}$ )	40	40
Secondary gas, $\text{H}_2$ ( $\text{l min}^{-1}$ )	11	8
Powder carrier gas, $\text{N}_2$ ( $\text{l min}^{-1}$ )	3.5	3.65

## 2.2. Four point bend test

An Instron universal test machine (Model 8502, Instron, Canton, MA) was used to perform the four point bend tests at a crosshead displacement rate of  $10 \mu\text{m s}^{-1}$ . The length for inner and outer spans were 20 and 40 mm, respectively, and the samples were tested in a configuration to place the coating in tension. It was determined that six samples from each group would generate a 95% confidence limit. The sides of the samples were polished with 600 mesh abrasive before the tests to minimize artifacts from edge cracking. Six uncoated steel substrates were also tested to establish baseline criteria for the mechanical properties of uncoated samples. Load and displacement were recorded for each measurement. The displacement was corrected for the deformation in the support and the loading beam; i.e. the compliance of the test rig was measured and taken into account. The displacement was calibrated using an external LVDT (Model CD375-500, Macro Sensors, Pennsauken, NJ) that was placed close to the load actuator to enable more exact measurements.

## 3. Results

### 3.1. Four point bend tests

Fig. 1 illustrates the load–displacement curves obtained during the four point bend tests. In the figure, one representative curve is presented although there exists six load–displacement curves for each group. The load–displacement curve could be reproduced with a random 5–20% variation. Bending modulus was calculated from the slope of the load–displacement curve using the following equations:

$$(EI)^* = \frac{2D^3 \Delta P}{3 \Delta y} \quad (1)$$

where

$$(EI)^* = \frac{wE_{St}}{3}[(t_{St} - t_{NA})^3 + t_{NA}^3] + \frac{wE_C}{3}[(t_{St} + t_C - t_{NA})^3 - (t_{St} - t_{NA})^3] \quad (2)$$

where  $E$  is the bending modulus,  $I$  is moment of inertia, and  $t_{NA}$  is the distance of the neutral axis of the bar from the bottom of the substrate (Fig. 2) and is equal to

$$t_{NA} = \frac{E_{St}t_{St}^2 + E_Ct_C^2 + 2E_Ct_{St}t_C}{2(E_{St}t_{St} + E_Ct_C)} \quad (3)$$

where,  $P$  is the applied load,  $D$  is the distance between the loading and support bar (10 mm),  $y$  is the displacement,  $\Delta P/\Delta y$  is the slope of the load–displacement curve,  $w$  is the width of the bar,  $t_{St}$  and  $t_C$  are the

thickness of the substrate and coating layers including both top ( $t_{TC}$ ) and bond ( $t_{BC}$ ) coat layer, respectively. The terms  $E_{St}$  and  $E_C$  are, respectively, the bending modulus of the substrate and coating layer including both top and bond coatings; i.e. top and bond coat was considered as a whole assembly in the calculations. The bending modulus of steel substrate,  $E_{St}$  was calculated from the load–displacement curve for blank steel substrates using the equation:

$$E_{St} = \frac{8D^3 \Delta P}{wt_{St}^3 \Delta y} \quad (4)$$

where thicknesses were measured with an error of  $\pm 0.01$  mm. The bending modulus of the blank mild-steel substrate,  $E_{St}$  was measured as  $200 \pm 14$  GPa which is in agreement with the literature value of 204 GPa [23]. Bending modulus of coatings,  $E_C$  was calculated by solving Eqs. (1)–(3) simultaneously. A graphical solution routine was followed to determinate the  $E_C$  and  $t_{NA}$  from these three equations. In the solution, the bending modulus of the steel ( $E_{St}$ ) substrate was taken as 200 GPa. The bending modulus of some coatings ( $E_C$ ) calculated, such as those for group 14, was slightly negative and indicates a poor physical meaning. The reason for these negative values is that the bending modulus for these coatings are so small that a steel substrate with a coating and a blank steel substrate are indistinguishable in their bending properties within the limits of the experimental errors. One should note that when the  $E_{St}$  was taken as 186 GPa, the calculated  $E_C$  became slightly positive for those groups. The average  $E_C$  values for all the coatings are illustrated in Fig. 3 along with the average yield stress values at the outer surface of the coatings (One should note that stress values change throughout the coating as given in Fig. 2). The yield stress was calculated using the equation:

$$\sigma_{YC} = \frac{P_{YC}D(t_{St} + t_C - t_{NA})}{2(EI)^*} E_C \quad (5)$$

where  $P_{YC}$  is the yielding load and it was taken as the load for 0.01 mm permanent displacement where corresponding strain would be around 0.1%, and  $(EI)^*$  is as given in Eq. (2).

The comparison of bending modulus to yield stress is illustrated in Fig. 4 along with the inset showing yield strain for each group. Yield strain was calculated from Hooke's law by dividing  $\sigma_{YC}$  by  $E_C$ . Yield strain values are similar for the coatings, but it is smaller for the steel substrate.

### 3.2. Statistical analysis

To further understand the significance of the parameters on the properties of the coatings, all the results were statistically analyzed using the Statgraphics Plus 2.0 software.



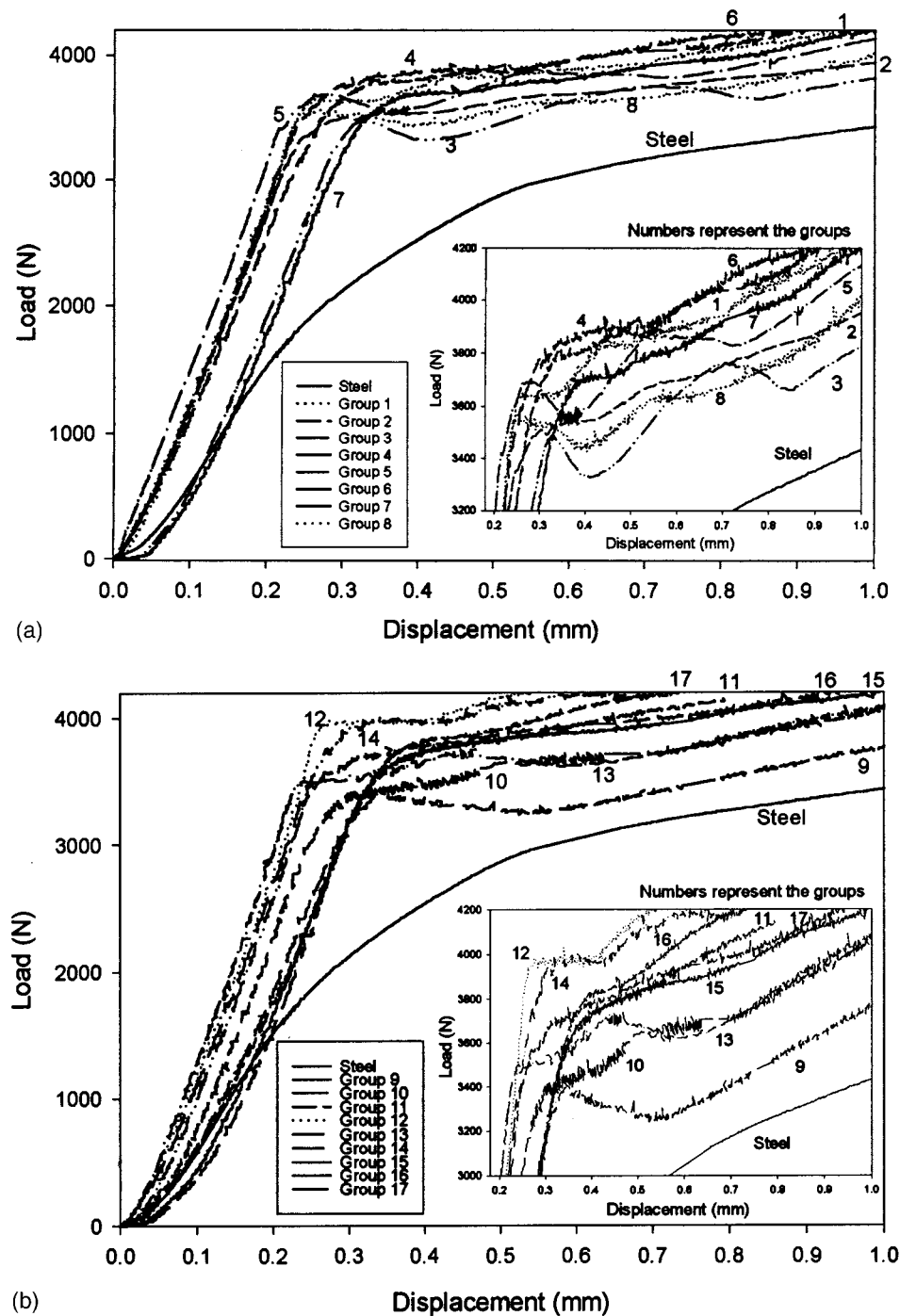


Fig. 1. (a) Load–displacement curves for groups 1–8 along with that of steel substrate. Notice that only one representative curve of six is presented. Inset highlights the yielding load. (b) Load–displacement curves for groups 9–17 along with that of steel substrate. Notice that only one representative curve of six curves is presented. Inset highlights the yielding load.

### 3.2.1. Yield strength of coatings

To understand whether bending yield stresses ( $\sigma_{YC}$ ) significantly differ between the groups, the mean of the yield stress values for each group was compared statistically (Table 3). The numbers in Table 3 were calculated by subtracting the bending stress of the group in the column from the bending stress of the group in the row,

and then normalizing with respect to the bending stress of group in the row (i.e. (row – column)/row). The largest difference in means of the bending yield stress is between group 14 (being lowest) and group 15 (being highest), while many groups have statistically the same mean bending stresses as indicated by an 'N' in Table 3. Although the comparison in Table 3 indicates the dif-

Table 3  
Comparison of the mean of the bending yield stresses of coating layer ( $\sigma_{YC}$ ) for the groups<sup>a</sup>

	G1	G2	G3	G4	G5	G6	G7	G8	G9	G10	G11	G12	G13	G14	G15	G16	G17
G1		0.4	0.7	1	0.3	0.5	N	N	0.8	0.3	0.9	0.8	N	1	−0.5	−0.2	1
G2	−0.6		0.5	0.9	N	N	−0.4	−0.7	0.7	N	0.9	0.6	N	1	−1.3	−0.9	0.9
G3	−2.3	−1.1		0.8	−1.4	−0.7	−1.8	−2.6	N	N	N	0.2	−1.7	1	−3.8	−3	0.9
G4	−21	−13	−5.6		−15	−10	−17	−22	−3.4	−14	N	N	−17	N	−30	−26	N
G5	−0.3	N	0.6	0.9		0.3	N	−0.5	0.7	N	0.9	0.7	N	1	−1	−0.6	1
G6	−0.9	−0.2	0.4	0.9	−0.4		−0.6	−1.1	0.6	N	0.8	0.5	−0.6	1	−1.8	−1.3	0.9
G7	N	0.3	0.6	0.9	N	0.4		−0.3	0.8	N	0.9	0.7	N	1	−0.7	−0.4	1
G8	N	0.4	0.7	1	0.3	0.5	0.2		0.8	0.4	0.9	0.8	0.2	1	−0.3	N	1
G9	−3.9	−2.1	N	0.8	−2.6	−1.6	−3.2	−4.3		−2.3	N	N	−3	N	−6.1	−5	N
G10	−0.5	N	0.6	0.9	−0.1	N	N	−0.6	0.7		0.9	0.6	N	1	−1.1	−0.8	0.9
G11	−10	−6.1	N	N	−7.3	−4.9	−8.6	−11	N	−6.6		N	−8.3	1	−15	−13	N
G12	−3.1	−1.6	N	N	−2.1	−1.2	−2.6	−3.5	N	−1.8	N		−2.4	N	−5	−4.1	N
G13	N	N	0.6	0.9	N	0.4	N	−0.3	0.8	N	0.9	0.7		1	−0.8	−0.5	1
G14	−300	−190	−91	N	−224	−159	−259	−327	N	−205	−26	N	−249		−439	−370	N
G15	0.3	0.6	0.8	1	0.5	0.6	0.4	0.3	0.9	0.5	0.9	0.8	0.4	1		0.2	1
G16	0.2	0.5	0.8	1	0.4	0.6	0.3	N	0.8	0.4	0.9	0.8	0.3	1	−0.2		1
G17	−26	−16	−7.4	N	−20	−13	−23	−29	N	−18	N	N	−22	N	−39	−33	

<sup>a</sup> N means the difference in the bending yield stresses of two groups are not statistically significant. Numbers (unitless) were found by subtracting the bending yield stress value of the group in the column from that of the group in the row, and dividing by that in the row ((row−column)/row).

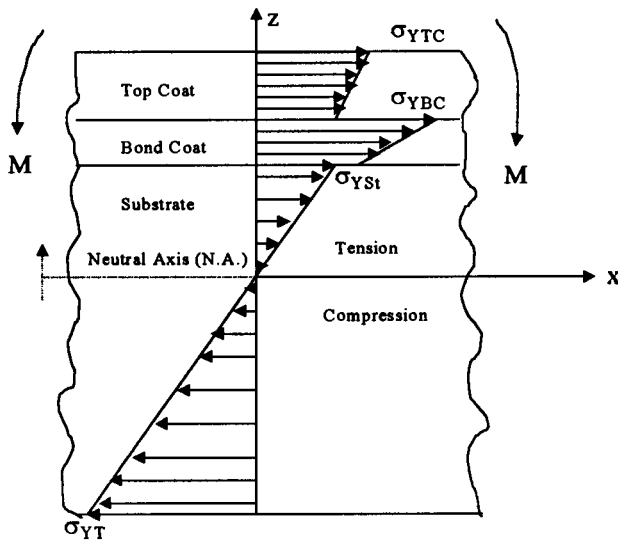


Fig. 2. Schematic illustration of the bending stress in the coating under four point bend test.

ferences for each pair, a more general analysis that might highlight trends was needed. This was achieved by a multi-linear regression analysis on the bending yield stress of coating ( $\sigma_{YC}$ ) values. Table 4 shows the results of fitting a multi-linear regression model to describe the relationship between yield stress and four independent variables (top coat thickness, bond coat thickness, the substrate temperature before coating, and stand off distance). An  $F$ -test<sup>2</sup> shows that there is a

statistically significant relationship between the variables at the 99% confidence interval. A Student  $t$ -test,<sup>3</sup> which was used to determine the significance of each coating parameters, suggests that the bond coat thickness has a statistically significant influence on the bending yield stress ( $\sigma_{YC}$ ) at the 99% confidence interval while the substrate temperature affects the bending yield stress ( $\sigma_{YC}$ ) at the 95% confidence interval (Table 4). On the other hand, the top coat thickness and the stand off distance are not statistically significant parameters for the change in the bending yield stress ( $\sigma_{YC}$ ) of the coatings examined. The following equation from the fitted model indicates that the yield stress depends on the spray parameters; taking caution that this is only valid for the parameter range studied:

$$\sigma_{YC} \text{ (MPa)} = 461 - 0.71 \cdot t_{BC} - 0.47 \cdot T_{St} \quad (6)$$

where  $t_{BC}$  is the thickness of the bond coating (NiCrAlY) in  $\mu\text{m}$ , and  $T_{St}$  is the substrate temperature in K. The average value of residuals (mean absolute error) in the fit is 106 MPa; i.e.  $\sigma_{YC}$  can be calculated from Eq. (6) with a  $\pm 106$  MPa error. It is clear from this analysis that thinner bond coatings, and lower substrate temperature in the investigated interval result in a material with an overall higher yield strength. A 150  $\mu\text{m}$  decrease in bond coating (NiCrAlY) thickness causes a  $\sim 107 \pm 29$  MPa increase in the bending yield stress ( $\sigma_{YCL}$ ), while use of a pre-heated substrate decreases the bending yield stress by about  $56 \pm 28$  MPa

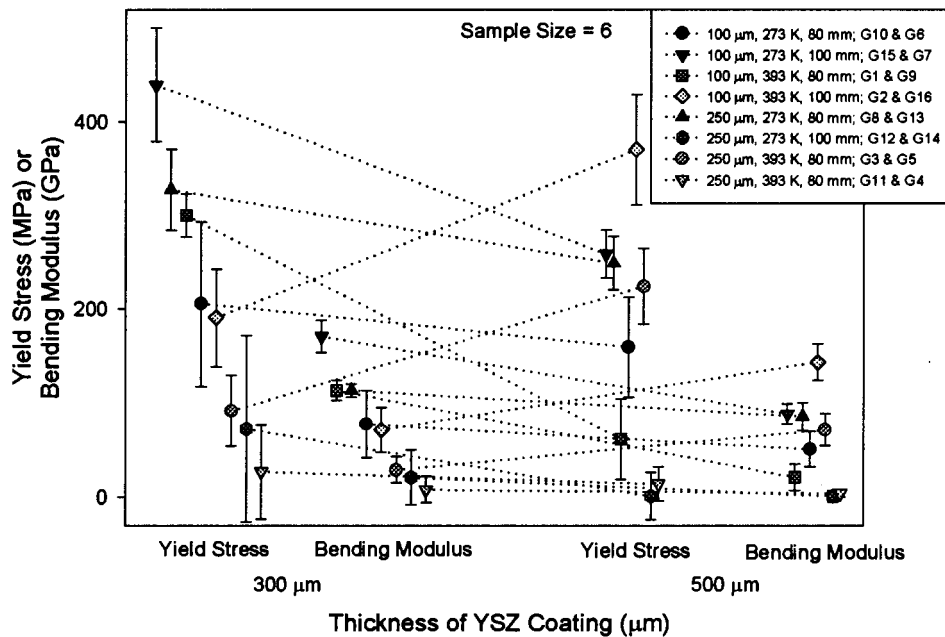


Fig. 3. Change of the bending yield stress ( $\sigma_{YC}$ ) and modulus ( $E_C$ ) of the coatings with spray parameters. The difference between the paired groups is the thickness of the yttria stabilized zirconia (YSZ) layer.

<sup>2</sup>  $F$  test is a statistical test to test the probability of a hypothesis being true. In this case the hypothesis is that there is a statistically significant correlation between the variables and the property.

<sup>3</sup> Student  $t$ -test is statistical test to test the probability of a hypothesis not being true. In this case, the hypothesis is that a variable does not statistically influence the property.

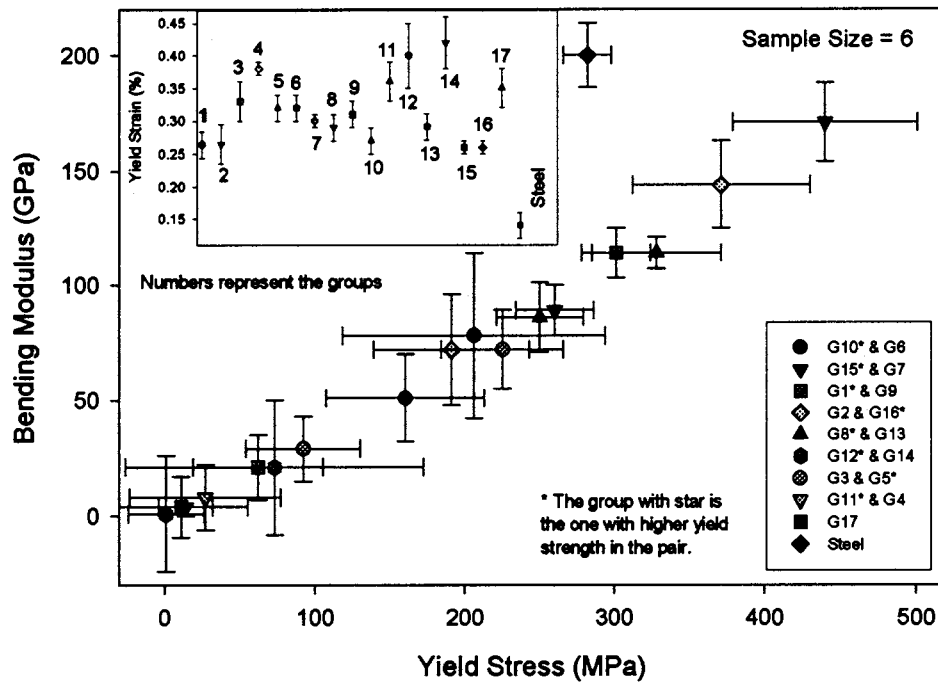


Fig. 4. Comparison of the bending modulus and yield stress for the coatings and the substrate. The yield strain calculated from Hooke's law represented in the inset.

Table 4

Results of the multi-linear regression analysis on the spray parameter dependence of the bending yield stress ( $\sigma_{YC}$ ) and modulus ( $E_C$ ) of the coating layers<sup>a</sup>

	Estimated coefficient		S.E.		<i>t</i> -test probability	
	$\sigma_{YC}$ (MPa)	$E_C$ (GPa)	$\sigma_{YC}$ (MPa)	$E_C$ (GPa)	$\sigma_{YC}$ (MPa)	$E_C$ (GPa)
Constant	461	198	84	37	0.00	0.00
$t_{BC}$ ( $\mu\text{m}$ )	−0.71	−0.31	0.19	0.07	0.00	0.00
$T_{St}$ (K)	−0.47	−0.15	0.23	0.09	0.05	0.09
$t_{TC}$ ( $\mu\text{m}$ )		−0.07		0.05		0.15 (?)
Parameters with no influence						
$t_{TC}$ ( $\mu\text{m}$ )	−0.15		0.14		0.30	
$X_{sod}$ (mm)	−0.61	−0.01	1.4	0.5	0.66	0.98

<sup>a</sup> The *t*-test probability is the probability of each parameter not being statistically significantly influential. Note that *t* values are very high for those that are not statistically significantly influential. ( $t_{BC}$  is the thickness of the bond coating (NiCrAlY),  $t_{TC}$  is the thickness of the top coating (yttria stabilized zirconia, YSZ),  $T_{St}$  is the substrate temperature,  $X_{sod}$  is the stand off distance).

with respect to a cold substrate. Even though the multi-linear regression gave negative coefficients for the influence of top coat thickness and stand off distance on the yield stress indicating higher bending stress for lower top coat thickness and lower stand off distance, it should be cautioned that the statistical confidence according to the Student *t*-test is low (70 and 34%, respectively) as listed in Table 4. Therefore, top coating thickness and stand off distance were excluded as the parameters in Eq. (6).

### 3.2.2. Bending modulus of coatings

A similar comparison procedure was applied for the average bending modulus of each group as given in Table 5. The largest difference in means of the bending modulus is between group 14 (being lowest) and group 15 (being highest), while many groups have statistically the same mean bending modulus as indicated by an 'N' in Table 5. Similar to the bending yield stress analysis, a multi-linear regression procedure was also followed for determining the influence of spray parameters on

Table 5  
Comparison of the mean of the bending modulus of the coating layer ( $E_C$ ) for the groups<sup>a</sup>

	G1	G2	G3	G4	G5	G6	G7	G8	G9	G10	G11	G12	G13	G14	G15	G16	G17
G1		0.4	0.7	1	0.4	0.6	0.2	N	0.8	0.3	0.9	0.8	0.2	1	−0.5	−0.3	1
G2	−0.6		0.6	0.9	N	N	N	−0.6	0.7	N	0.9	0.7	N	1	−1.4	−1	0.9
G3	−2.9	−1.5		0.9	−1.5	−0.8	−2.1	−2.9	N	−1.7	N	N	−2	1	−4.9	−4	0.9
G4	−28	−17	−6.3		−17	−12	−21	−28	N	−19	N	N	−21	N	−42	−35	N
G5	−0.6	N	0.6	0.9		N	N	−0.6	0.7	N	0.9	0.7	N	1	−1.4	−1	0.9
G6	−1.2	N	0.4	0.9	N		−0.7	−1.2	0.6	−0.5	0.8	0.6	−0.7	1	−2.4	−1.8	0.9
G7	−0.3	N	0.7	1	N	0.4		−0.3	0.8	N	0.9	0.8	N	1	−0.9	−0.6	1
G8	N	0.4	0.7	1	0.4	0.6	0.2		0.8	0.3	0.9	0.8	0.2	1	−0.5	−0.3	1
G9	−4.4	−2.4	N	N	−2.4	−1.4	−3.2	−4.4		−2.7	N	N	−3.1	N	−7.1	−5.9	N
G10	−0.5	N	0.6	0.9	N	0.3	N	−0.5	0.7		0.9	0.7	N	1	−1.2	−0.8	0.9
G11	−13	−8	N	N	−8	−5.4	−10	−13	N	−8.8		N	−9.8	N	−20	−17	N
G12	−4.4	−2.4	N	N	−2.4	−1.4	−3.2	−4.4	N	−2.7	N		−3.1	N	−7.1	−5.9	0.8
G13	−0.3	N	0.7	1	N	0.4	N	−0.3	0.8	N	0.9	0.8		1	−1	−0.7	1
G14	−113	−71	−28	N	−71	−50	−88	−113	N	−77	N	N	−85		−170	−143	N
G15	0.3	0.6	0.8	1	0.6	0.7	0.5	0.3	0.9	0.5	1	0.9	0.5	1		0.2	1
G16	0.2	0.5	0.8	1	0.5	0.6	0.4	0.2	0.9	0.5	0.9	0.9	0.4	1	−0.2		1
G17	−28	−17	−6.3	N	−17	−12	−21	−28	N	−19	N	N	−21	N	−42	−35	

<sup>a</sup> N means the difference in the bending modulus of the two groups are not statistically significant. Numbers (unitless) were found by subtracting the modulus value of the group in the column from that of the group in the row, and dividing by that in row ((row−column)/row).

the bending modulus ( $E_C$ ) of the coating layer to have a more complete understanding. An  $F$ -test shows that there is a statistically significant relationship between the variables at the 99% confidence interval. A Student  $t$ -test suggests that the bond coat thickness has a statistically significant influence on the bending modulus ( $E_C$ ) at the 99% confidence interval, while the substrate temperature affects the bending modulus ( $E_C$ ) at the 92% confidence interval (Table 4). The Student  $t$ -test also suggests that top coat thickness is influential on the bending modulus at the 85% confidence interval. On the other hand, the stand off distance does not have any statistically significant influence in the bending modulus of the coatings studied. According to the multi-linear regression analysis, the bending modulus ( $E_C$ ) in the range of parameters studied can be expressed as;

$$E_C \text{ (GPa)} = 198 - 0.31 \cdot t_{BC} - 0.15 \cdot T_{St} - 0.07 \cdot t_{TC} \quad (7)$$

The average value of residuals (mean absolute error) in the fit is 40 GPa, i.e.  $E_C$  can be calculated from Eq. (7) with a  $\pm 40$  GPa error. It is clear from this analysis that thinner bond and top coatings, and lower substrate temperature in the investigated interval result in materials with higher bending modulus. A 150  $\mu\text{m}$  increase in bond coating (NiCrAlY) thickness causes a  $47 \pm 10$  GPa drop in the bending modulus ( $E_C$ ), while use of a pre-heated substrate decreases the bending modulus by about  $19 \pm 11$  GPa with respect to a cold substrate. Similarly, a 200  $\mu\text{m}$  increase in the top coat thickness gives rise to a  $14 \pm 10$  GPa decrease in the bending modulus. The stand off distance as a parameter was excluded in Eq. (7) since the Student  $t$ -test indicated only a 3% confidence for the negative estimated coefficient calculated from the multi-linear regression analysis. One may also consider excluding the influence of

the top coating thickness since the  $t$ -test probability is less than 90%.

## 4. Discussion

### 4.1. Four point bend test

As indicated above, when stress and modulus were calculated from the load–displacement data recorded during the four point bend test, the bond and top coating layers were taken as a single layer since there is only one equation, that allows the determination of only one unknown, from the slope of the load–displacement curve. Therefore, the mechanical properties represented here are rather an average property of the bond and top coatings. One disadvantage of this assumption is that if one of the coating layers has superior properties with respect to the other, then it will not be possible to distinguish the influence of the latter layer on the coating properties.

The values of bending yield stress and elastic modulus for the coatings in the current study exhibit a wide range with a 20–30% average S.D. Table 6 summarizes the elastic modulus and yield strength values for YSZ and NiCrAlY coatings reported in the open literature. Elastic modulus varies from 0.1 to 70 GPa for YSZ coatings, and 100–200 GPa for NiCrAlY coatings, while yield stress is around 20–80 MPa for YSZ coatings, and 1.2 GPa for NiCrAlY coatings. Wallace and Ilavsky [24], for instance, measured the elastic modulus of a 5 mm thick free standing YSZ plasma sprayed coating to be  $29 \pm 1$  GPa on the surface using a Hertzian contact arrangement, while Siemers and Mehan [25] reported that vacuum plasma sprayed NiCrAlY alloy has elastic modulus of 200 GPa, and yield strength of 1.2 GPa under a tensile test. Taka-

Table 6  
Yield strength and elastic modulus of yttria stabilized zirconia (YSZ) and NiCrAlY coating reported in the literature

Yield stress (MPa)	Elastic modulus (GPa)	Method/sample	Ref.
<i>7 wt.% YSZ</i>			
	51	Ultrasonic test on free standing plate, APS	[33]
	45.5	Cantilever beam, coating assembly, APS	[34]
	30–40	Hertzian indentation, free standing plate, APS	[24]
	65	Ultrasonic test, free standing plate, APS	[35]
	$44 \pm 6$	Knoop indentation	[14]
	0.115	Tensile test	[36]
	70	Tensile test	[37]
	40	Uniaxial tension	[34]
<i>NiCrAlY</i>			
	$110 \pm 22$	Knoop indentation, VPS	[14]
1200	200	Tensile test, VPS	[25]
<i>NiCrAlY/YSZ</i>			
27–71		4-point bend test on free standing NiCrAlY/YSZ, APS	[26]
1–440	1–171	4-point bend test on free standing NiCrAlY/YSZ, APS	Current



hashi et al. [26] found that the yield strength of free standing YSZ/NiCrAlY coating depends on the porosity content and varies from 27 to 71 MPa for 18.6–5.0% porosity levels, respectively. Leigh et al. [14] using Knoop indentation measured elastic modulus as  $44 \pm 6$  and  $110 \pm 22$  GPa for YSZ and NiCrAlY coatings, respectively. In general, the variation within the measured properties in the current study is higher than the variation in the values measured using other techniques. The reason for the high deviation in the current study is the presence of a substrate (mild steel) with high elastic modulus and large thickness with respect to the coating layer. The thickness of the substrate is 5–7 times that of the coating layer. For a more accurate determination of bending modulus and yield stress from a four point bend test, it is necessary to produce coatings on a thinner steel substrate.

#### 4.2. Mechanical properties

To understand the observations on the deformation behavior of the coatings, it is necessary to consider the microstructure and the adhesion in coatings. The microstructure of a ceramic coating is rather complex with many cohered splats that consist of a mixture of different phases [1]. As received commercial YSZ powders are mixtures of monoclinic and tetragonal phases [27]. Upon spraying, the majority of the powder melts and forms a metastable tetragonal phase ( $t'$ ) due to rapid solidification, while some of the particles stay unmelted and form monoclinic phase [27]. In addition, micro- and macro-porosities and cracks (dominated by the stresses) exist within and between splats [14]. Stresses in the plasma sprayed coating result from the residual stresses due to tensile quenching stresses in lamella, and due to the cooling stresses (tensile or compressive) caused by the difference in thermal expansion coefficients of the substrate and coating. These residual stresses vary throughout the thickness of the coating [8]. Some of the stresses are released by the formation of micro-cracks in ceramic coatings [8,12,28]. The type and the quantity of the residual stresses also influence the adhesion at the substrate-bond coating, and bond coating-top coating interfaces [10]. It has been shown that the residual stresses in plasma sprayed YSZ coatings on a steel substrate are generally tensile, and increase with the coating thickness [8,9,28,29].

##### 4.2.1. Effect of bond coat thickness

As given in Eqs. (6) and (7), the bending yield stress and modulus of coatings are strongly controlled by the thickness of the bond coat layer. An increase in the bond coat thickness gives rise to a drop in the bending yield strength and bending modulus of the coating system. This is because a thicker bond coat layer introduces more residual stress which weakens both interface

binding strength and the coating body by increasing the amount of flaws in the structure.

##### 4.2.2. Effect of substrate temperature

Eqs. (6) and (7) also indicate that coatings sprayed on a pre-heated substrate exhibit lower bending strength and bending modulus. It has been reported that higher substrate temperature lowers the residual stresses [29]. Therefore, one would expect that coating on a pre-heated substrate should have exhibited higher bending strength. It is believed that adhesion strength between bond coat and substrate is lower for a pre-heated substrate because of weakening in the mechanical adhesion of the bond coat and substrate. It is possible that a locally over-heated area was created when the substrate was preheated. These locally over-heated areas may oxidize easily. It was reported that the oxidation on the substrate surface drastically weakens the adhesion [30]. Therefore, one possibility for the lower strength exhibited in the coatings deposited on pre-heated substrate would be the presence of an oxide layer.

##### 4.2.3. Effect of top coat thickness

As given in Table 6, the mechanical properties of NiCrAlY coatings are superior to that of a YSZ coatings. Therefore, the influence of the change in the top coat (YSZ) thickness on the mechanical properties of a TBC system was suppressed due to the nature of the test. As indicated above, in the calculation procedure the bond and top coat layers were considered as a single layer providing an average property. Nevertheless, as given in Table 4, the increase in top coat thickness decreases the bending modulus and bending yield stress at the 85 and 70% confidence interval, respectively. The confidence limit is lower for the yield stress analysis due to greater variation in this value. It is believed that a more accurate determination (for example using a thinner steel substrate) of the bending modulus would increase the confidence interval.

The reason that a coating with a thicker top coat mechanically weakens is further introduction of residual stresses and defects such as pores and cracks with increasing thickness.

##### 4.2.4. Effect of stand off distance

It was found that the stand off distance has no significant influence on the bending yield strength and bending modulus of the coating layers. The stand off distance mainly controls the cohesion between splats because the temperature and velocity of particles in the plasma flame significantly change with stand off distance [31]. It was reported that the temperature and velocity of particles in the plasma flame may vary by as much as approximately 1000 K, and  $50 \text{ m s}^{-1}$  in a 20 mm change in the stand off distance, respectively [32].

Therefore, better spreading and cohesion would be achieved with shorter spraying distances. However, one should bear in mind that residual stresses introduced are higher for shorter spraying distance since particle temperature is higher [28]. As a result, it is believed that these two competing factors; cohesion strength (positive influence) and residual stresses (negative influence), neutralize each other with respect to their influence on stand off distance and the performance of the coating. Although it was not possible to distinguish the influence of the stand off distance on the deformation characteristics of the plasma sprayed YSZ coatings using the four point bend test due to these two competing factors, the investigation of the AE activities during the four point tests of these samples clearly identified the influence of the stand off distance on the properties of these coatings. The AE studies, whose details will be discussed in the second part of this paper [22], showed that coatings plasma sprayed at shorter stand off distances exhibited higher cracking activities and reflect the presence of a higher amount of residual stresses.

#### 4.2.5. Yield strain

As given in Fig. 4, the yield strains of the coatings are similar, but higher than that of a steel substrate. One would expect that a steel substrate deforms more than a ceramic, however, it is believed that a coating with pores and cracks can deform more than the bulk counterparts before yielding. The yield strains of coatings with thicker bond coat such as coatings from groups 3, 4, 11, 12, and 14 are higher than other coatings. This may be because the coatings in the aforementioned groups have more defects such as pores, voids, and cracks.

## 5. Conclusions

All the coatings prepared with varying spray parameters were tested with four point bending. The bending yield stress and bending modulus were calculated from the load–displacement curves recorded during the bending tests by considering the top–bond coating system as a single assembly. The variation in the bending yield stress and modulus values calculated in the current study were generally higher than the previously reported values determined using other techniques such as Knoop indentation in the open literature.

A multi-linear statistical regression on the bending yield strength and bending modulus of the coating layers showed that coating layers with thinner bond and top coating sprayed on a cold steel substrate yield at higher stresses, and result in higher bending modulus. On the other hand, stand off distance was found to have no statistically significant influence on the bending yield strength and modulus.

## Acknowledgements

The authors would like to thank Dr Raman Singh of the Mechanical Engineering Department in the State University of New York at Stony Brook for his valuable comments and discussion regarding the stress analysis. This work is supported under NSF-MRSEC DMR grant number 9632570.

## Appendix A. Nomenclature

Throughout the text common engineering units of thermal spray field have been used.

$D$	distance between loading and support bar (100 mm)
$E$	bending modulus, GPa
$E_{St}$	bending modulus of steel substrate, GPa
$E_C$	bending modulus of coating system (top and bond coats), GPa
$(EI)^*$	elastic modulus times moment of inertia for the whole system including the substrate, bond coat and top coat layers
$I$	moment of inertia of the test specimen, $wt_c^3/12$ , mm <sup>4</sup>
$P$	load, N
$P_{YC}$	yielding load of the coating system (top and bond coats), N
$t_{St}$	thickness of steel substrate, $\mu\text{m}$
$t_{NA}$	distance between the neutral axis of the test bar and the bottom of the substrate, $\mu\text{m}$
$t_C$	thickness of the coating system (top and bond coats), $\mu\text{m}$
$t_{TC}$	thickness of top coat, $\mu\text{m}$
$t_{BC}$	thickness of bond coat, $\mu\text{m}$
$T_{St}$	temperature of steel substrate, K
$X_{sod}$	stand off distance, mm
$w$	width of the testing bar, mm
$y$	displacement at the cross-head, mm
$\Delta P/\Delta y$	slope of load displacement curve
$\sigma_{YC}$	bending yield stress of the coating system (top and bond coats), MPa

## References

- [1] L. Pawlowski, The Science and Engineering of Thermal Spray Coating, Wiley, New York, 1995.
- [2] R.A. Miller, Surf. Coat. Technol. 30 (1986) 1–11.
- [3] C. Funke, B. Siebert, D. Stover, R. Vassen, in: C.C. Berndt (Ed.), Thermal Spray: A United Forum for Scientific and Technological Advances, ASM International, Materials Park, OH, 1998, pp. 277–284.

- [4] J. Ilavsky, G.G. Long, A.J. Alen, H. Herman, C.C. Berndt, in: C.C. Berndt (Ed.), 9th National Thermal Spray Conference, ASM International, Materials Park, OH, 1996, pp. 725–728.
- [5] P. Boch, P. Fauchais, D. Lombard, B. Rogeaux, M. Vardelle, in: N. Claussen, M. Ruhle, A.H. Heuer (Eds.), *Advances in Ceramics Science and Technology of Zirconia II*, vol. 12, American Ceramic Society, Columbus, OH, 1984, pp. 488–502.
- [6] C.C. Berndt, H. Herman, *Thin Solid Films* 108 (1983) 427–437.
- [7] J. Voyer, F. Gitzhofer, M.I. Boulos, *J. Thermal Spray Technol.* 7 (1998) 181–190.
- [8] J. Matejicek, S. Sampath, J. Dubsky, *J. Thermal Spray Technol.* 7 (1998) 489–496.
- [9] D.J. Greving, E.F. Rybicki, J.R. Shadley, *J. Thermal Spray Technol.* 3 (1994) 379–388.
- [10] D.J. Greving, J.R. Shadley, E.F. Rybicki, *J. Thermal Spray Technol.* 3 (1994) 371–378.
- [11] C.C. Berndt, C.K. Lin, *J. Adhes. Sci. Technol.* 7 (1993) 1235–1264.
- [12] U. Senturk, R.S. Lima, C.C. Berndt, C.K. Lin, C.R.C. Lima, in: E. Lugscheider, P.A. Kammer (Eds.), *United Thermal Spray Conference*, German Welding Society, Dusseldorf, Germany, 1999, pp. 815–819.
- [13] C.K. Lin, U. Senturk, R.S. Lima, C.C. Berndt, J.C. Shieh, P.Y. Lee, in: E. Lugscheider, P.A. Kammer (Eds.), *United Thermal Spray Conference*, German Welding Society, Dusseldorf, Germany, 1999, pp. 809–814.
- [14] S.-H. Leigh, C.-K. Lin, C.C. Berndt, *J. Am. Ceram. Soc.* 80 (1997) 2093–2099.
- [15] A. Ibrahim, Ph. D. Thesis, Department of Materials Sci. Eng. in the State University of New York at Stony Brook, Stony Brook, NY (1998).
- [16] C.C. Berndt, D. Robins, R. Zatorski, H. Herman, Presented at 10th International Thermal Spraying Conference, Essen, Germany, 1983.
- [17] C.K. Lin, C.C. Berndt, S.H. Leigh, K. Murakami, *J. Am. Ceram. Soc.* 80 (1997) 2382–2394.
- [18] C.K. Lin, C.C. Berndt, *Surf. Coat. Technol.* 102 (1998) 1–7.
- [19] C.C. Berndt, *Mater. Sci. Forum* 34–36 (1988) 457–461.
- [20] S. Safai, H. Herman, K. Ono, Presented at 9th International Thermal Spraying Conference, The Hague, Netherlands, 1980.
- [21] C.C. Berndt, *J. Eng. Gas. Turbines Power-Trans. ASME* 107 (1985) 142–146.
- [22] A. Kucuk, C.C. Berndt, U. Senturk, R.S. Lima, *Mater. Sci. Eng. A* 284 (2000) 41–50.
- [23] *Metals Handbook*, vol. 1, ASM International, Materials Park, OH, 1990.
- [24] J.S. Wallace, J. Ilavsky, *J. Thermal Spray Technol.* 7 (1998) 521–526.
- [25] P.A. Siemers, R.L. Mehan, *Ceram. Eng. Sci. Proc.* 4 (1983) 828–840.
- [26] M. Takahashi, M. Saitoh, K. Takaishi, J. Yokohama, T. Kawasaki, J. Sendai, in: E. Lugscheider, P.A. Kammer (Eds.), *United Thermal Spray Conference*, German Welding Society, Dusseldorf, Germany, 1999, pp. 565–570.
- [27] R.S. Lima, U. Senturk, C.C. Berndt, C.R.C. Lima, in: E. Lugscheider, P.A. Kammer (Eds.), *United Thermal Spray Conference*, German Welding Society, Dusseldorf, Germany, 1999, pp. 190–195.
- [28] L. Bianchi, F. Blein, N. Baradel, in: C.C. Berndt (Ed.), *Thermal Spray: A United Forum for Scientific and Technological Advances*, ASM International, Materials Park, OH, 1997, pp. 831–838.
- [29] M. Levit, I. Grimberg, B.Z. Weiss, *Mater. Sci. Eng. A206* (1996) 30–38.
- [30] V.V. Sobolev, J.M. Guilemany, J. Nutting, J.R. Miquel, *Int. Mater. Rev.* 42 (1997) 117–136.
- [31] A. Vardelle, M. Vardelle, R. McPerson, P. Fauchais, Presented at 9th International Thermal Spraying Conference, The Hague, Netherlands, 1980.
- [32] B.M. Cetegen, W. Yu, *J. Thermal Spray Technol.* 8 (1999) 57–67.
- [33] M.C. Sainte-Catherine, J.L. Derop, J.P. Lumet, Presented at 2nd Plasma Technik Symposium, Lucerne, Switzerland, 1991.
- [34] E.F. Rybicki, J.R. Shadley, Y. Xiong, D.J. Greving, *J. Thermal Spray Technol.* 4 (1995) 377–383.
- [35] R. Kawase, K. Tanaka, T. Hamamoto, H. Haraguchi, Presented at 3rd National Thermal Spray Conference, Long Beach, CA, 1990.
- [36] C.C. Berndt, *J. Mater. Eng.* 11 (1989) 274–282.
- [37] H.-D. Steffens, U. Fischer, in: D.L. Houck (Ed.), *Thermal Spray: Advances in Coatings Technology*, ASM International, Materials Park, OH, 1988, pp. 167–173.

#### Permission to publish

A. Kucuk, C.C. Berndt, U. Senturk, R.S. Lima and C.R.C. Lima, 'Influence of plasma spray parameters on the mechanical properties of yttria stabilized zirconia coatings I: Four point bend test', *J. Mater. Engin. and Sci.*, A284 (2000) 29-40.

As an Elsevier journal author, you retain various rights including Inclusion of the article in a thesis or dissertation whether in part or in toto; see [http://www.elsevier.com/about/policies/author-agreement/lightbox\\_scholarly-purposes](http://www.elsevier.com/about/policies/author-agreement/lightbox_scholarly-purposes) for more information. As this is a retained right, no written permission is necessary. This extends to the online version of your thesis and would include any version of the articles including the final published versions provided that they are not available as individual downloads but only embedded within the thesis itself.

# Influence of plasma spray parameters on mechanical properties of yttria stabilized zirconia coatings. II: Acoustic emission response

A. Kucuk, C.C. Berndt \*, U. Senturk <sup>1</sup>, R.S. Lima

*Department of Materials Science and Engineering, Center for Thermal Spray Research, State University of New York at Stony Brook,  
306 Old Engineering, Stony Brook, NY 11794-2275, USA*

Received 12 October 1999; received in revised form 7 February 2000

## Abstract

Yttria (8 wt.%) stabilized zirconia (YSZ) with a NiCrAlY bond coat was atmospherically plasma sprayed on mild steel substrates using various processing parameters including YSZ coating thickness, bond coat thickness, stand off distance, and substrate temperature. The cracking behavior of these coatings under four point bending load was examined using an acoustic emission (AE) recorder. The numbers of AE events exhibited during the elastic and plastic deformation of coatings were analyzed. Using multi-linear regression analysis, the number of AE events was correlated to the spray parameters. This analysis revealed that coatings with thicker YSZ top coat and NiCrAlY bond coat sprayed on a heated substrate at shorter stand off distance exhibited more AE activity and released higher AE energy under the bending. The greater emission activity and higher AE energy were evidence of severe cracking. © 2000 Elsevier Science S.A. All rights reserved.

**Keywords:** Thermal barrier coatings; Acoustic emission; Cracking behavior

## 1. Introduction

Plasma sprayed yttria stabilized zirconia (YSZ) coatings are used as insulative and corrosion resistant layers in high temperature applications such as gas turbine and diesel engines to enable higher working temperatures [1]. Plasma sprayed YSZ coatings, often referred to as thermal barrier coatings (TBCs), with their porous microstructure and ceramic nature provide good heat insulation to the main metal component. A NiCrAlY bond coat layer is applied to enhance adhesion strength between the metal component and YSZ coating. In addition, this NiCrAlY bond coat provides oxidation resistance to the main metal component at high temperatures [2].

Plasma sprayed YSZ coatings are built up from cohered splats that consist of a mixture of different phases. The characteristics of the coating depend pri-

marily on the feedstock powder, spray process parameters such as gun power, gas composition and flow rate, powder feeding rate, and equipment features such as gun type. As-received commercial YSZ feedstocks are generally mixtures of monoclinic and tetragonal phases [3], that may exhibit different size and shape distributions. Upon spraying, the majority of the powder melts and forms a metastable tetragonal phase ( $t'$ ) due to rapid solidification, while some of the particles stay un-melted and form a monoclinic phase [3]. These particles (splats) are randomly deposited and build up the coating. A coating can exhibit voids which are located between splats, due to random deposition and solidification, and within splats, due to solidification. In addition, processing stresses are generated in plasma sprayed coatings from rapid cooling and thermal expansion mismatch between the coating and substrate. These residual stresses vary throughout the thickness of the coating [4]. Some of the stresses are released by the formation of micro-cracks in ceramics [4,5], while residual stress, either compressive or tensile, is preserved in the coating. The type and the quantity of the residual stresses influence the coating performance. For example, it was reported that the adhesion and mechanical

\* [REDACTED]  
[REDACTED]  
<sup>1</sup> Present address: PQ Corporation, Research & Development Center, 280 Cedar Grove Rd., Conshohocken, PA 19428-2240, USA.

Table 1  
Samples sprayed according to experimental design

Samples	Bond coat ( $\mu\text{m}$ )	Top coat ( $\mu\text{m}$ )	Substrate temperature (K)	Stand off distance (mm)
G1	100	300	393	80
G2	100	300	393	100
G3	250	300	393	80
G4	250	500	393	100
G5	250	500	393	80
G6	100	500	273	80
G7	100	500	273	100
G8	250	300	273	80
G9	100	500	393	80
G10	100	300	273	80
G11	250	300	393	100
G12	250	300	273	100
G13	250	500	273	80
G14	250	500	273	100
G15	100	300	273	100
G16	100	500	393	100
G17	175	400	333	90

strength of the coatings directly related to the residual stresses [6]. Optimizing the spray parameters produces coatings with a desired microstructure (i.e. phase distribution, porosity, etc.) which determines coating performance. The deformation in YSZ coatings involves brittle fracture by crack initiation and growth as well as crack propagation from microcracks that evolve due to residual stresses. Therefore, it is crucial to understand cracking in ceramic coatings under load to characterize the deformation behavior of coatings. Cracks initiate and propagate during loading from defects such as pores, splat boundaries, secondary phase interfaces, and pre-existing cracks within coatings. A valuable tool in the analysis of cracks is to monitor acoustic emission (AE) response of deformation activities [7–10]. *AE is a term describing a class of phenomena whereby transient elastic waves are generated by the rapid release of energy from localized sources within a material* [11]. AE analysis has been successfully used to monitor cracking in ceramic coatings during mechanical testing (three point bending [12], four point bending [9,13], tensile adhesion test [14,15], and indentation [16]) and thermal cycling [8].

In the first part of this study [17], the influence of spray parameters such as top and bond coat thickness, stand off distance and substrate temperature on the mechanical properties of plasma sprayed YSZ coating were examined using a four point bend test. It was found that coatings with a thin bond coat sprayed on a cold substrate exhibited higher bending yield strength and bending modulus. However, stand off distance and top coat thickness were not found to have a statistically significant influence on the strength and stiffness of the coatings [17].

In the current work, the AE response of YSZ coatings under four point bend tests was investigated to further understand the cracking behavior of thermally sprayed YSZ coatings.

## 2. Experimental procedure

### 2.1. Sample preparation

Ytria (8 wt.%) stabilized zirconia (YSZ) was sprayed onto mild-carbon steel substrates under various process parameters including coating thickness (either 300 or 500  $\mu\text{m}$ ), stand off distance (either 80 or 100 mm) and substrate temperature (either at 273 or 393 K). In addition, the thickness of the atmospherically plasma sprayed bond coat, NiCrAlY, was varied as either 100 or 250  $\mu\text{m}$ .

The substrates were grit blasted with alumina grit and cleaned with ethyl alcohol before spraying. The average roughness of the grit blasted substrate was  $4.0 \pm 0.5 \mu\text{m}$  as measured with a Hommelwerke T1000 mechanical profilometer (Hommel America, New Britain, CT). Some of the substrates were pre-heated before spraying by using the plasma flame. The temperature of the substrates was measured using a hand held infrared temperature detector.

A statistical experimental design procedure using StatGraphics Plus 2.0 software (Statistical Graphics, Rockville, MD) was employed to determine the appropriate number of samples and spray parameters for relevant correlations. Table 1 gives the list of the samples sprayed in the current study according to this experimental design. Six samples from each group in Table 1 were sprayed with the conditions given in Table

2, using a Metco 3MB plasma gun (Sulzer-Metco, Westbury, NY). Further details of sample preparation have been presented elsewhere [17].

## 2.2. Four point bend test and in situ AE

The four point bend tests were performed using an Instron universal test machine (Model 8502, Instron, Canton, MA). The details of the four point bend test were previously given [17]. During the bend test, AE activities were monitored using an IBM compatible PC controlled MITRAS 2001 AE system (Physical Acoustics, Princeton, NJ). AE signals were received using a transducer of 22.5 mm diameter (model AC175L, Hartford Steam Boiler Inspection Technologies, Hartford, CT) placed on the steel substrate (in a non-coated location), and pre-amplified with a 2/4/6-AST model preamplifier (Physical Acoustics, Lawrenceville, NJ), and filtered with a 100H model preamplifier filter (Physical Acoustics). Details of AE data analysis were given elsewhere [18].

Six samples from each group were loaded under the four point bend conditions to generate results with a 95% confidence limit. To minimize artifacts from edge

cracking, the sides of the samples were polished with 600 mesh abrasive before the tests.

## 3. Results

### 3.1. Four point bend test

The bending yield stress and modulus, calculated from the load–displacement out put of the four point bend test, were reported previously [17]. The data are summarized in Table 3.

### 3.2. AE

Samples from each group exhibited different AE activity during four point bend tests (Fig. 1). Fig. 1 graphs the total AE events and sub-set of those generated only during the elastic regime. The activities were separated according to those generated during the elastic deformation and those generated after yield point. The influences of spray parameters on the numbers of AE activities in the elastic region are illustrated along with the total number of AE activities in Fig. 1. The trend in the number of AE response of the coatings sprayed with different parameters is similar in elastic and total deformation (Fig. 1). The order of groups according to the number of AE events in the elastic region and the total number, for example, is similar. Thus, the number of AE activities increases from  $G15 < G1 < G12 < G11 < G2 < G8 < G10$  to  $G3$  for the top coat thickness of 300  $\mu\text{m}$ . As seen in Fig. 1, five out of eight coatings revealed higher AE response under the four point test for increasing top and bond coat thickness while six out of eight coatings exhibited increasing AE activity for higher substrate temperature or shorter stand off distance. Further analysis of the effect of each spray parameter is given in Section 3.3.

Fig. 2 illustrates the comparison of total number of AE events with the number of AE activities in the elastic region. (The general trend is that samples with higher number of AE response in the elastic region, also exhibited higher total AE response). The samples in the groups can be separated into three categories according to AE response; i.e. high, medium, and low AE response. According to the number of AE events in the elastic region (i.e. the square boundaries in Fig. 2), groups 1, 12, 15, 16, and 17 are in the low response, and groups 2, 4, 6, 7, 8, 9, 10, 11, and 14 are in the medium response categories while groups 3, 5, and 13 are in the high response category. On the other hand, according to total number of AE activities (i.e. the ellipses in Fig. 2), the low response category includes groups 1, 11, 12, 15, and 16, while the medium response category consists of groups 2, 6, 7, 8, 10, 14, and 17, and the high response category includes groups 3, 4, 5,

Table 2  
Spraying parameters

	YSZ	NiCrAlY
Gun Type	Metco 3MB	Metco 3MB
Current (A)	600	500
Voltage (V)	70	70
Primary gas, Ar ( $\text{l min}^{-1}$ )	40	40
Secondary gas, $\text{H}_2$ ( $\text{l min}^{-1}$ )	11	8
Powder carrier gas, $\text{N}_2$ ( $\text{l min}^{-1}$ )	3.5	3.65

Table 3  
Summary of the mechanical properties of the coatings in this study [17]

Groups	Bending yield strength (MPa)	Bending modulus (GPa)
1	$301 \pm 23$	$114 \pm 11$
2	$191 \pm 52$	$72 \pm 24$
3	$92 \pm 38$	$29 \pm 14$
4	$14 \pm 18$	$4 \pm 4$
5	$225 \pm 41$	$72 \pm 17$
6	$160 \pm 53$	$51 \pm 19$
7	$260 \pm 26$	$89 \pm 11$
8	$328 \pm 43$	$114 \pm 7$
9	$62 \pm 43$	$21 \pm 14$
10	$206 \pm 88$	$78 \pm 36$
11	$27 \pm 50$	$8 \pm 14$
12	$73 \pm 99$	$21 \pm 29$
13	$250 \pm 30$	$86 \pm 15$
14	$1 \pm 25$	$1 \pm 6$
15	$440 \pm 61$	$171 \pm 17$
16	$371 \pm 59$	$144 \pm 19$
17	$11 \pm 44$	$4 \pm 13$



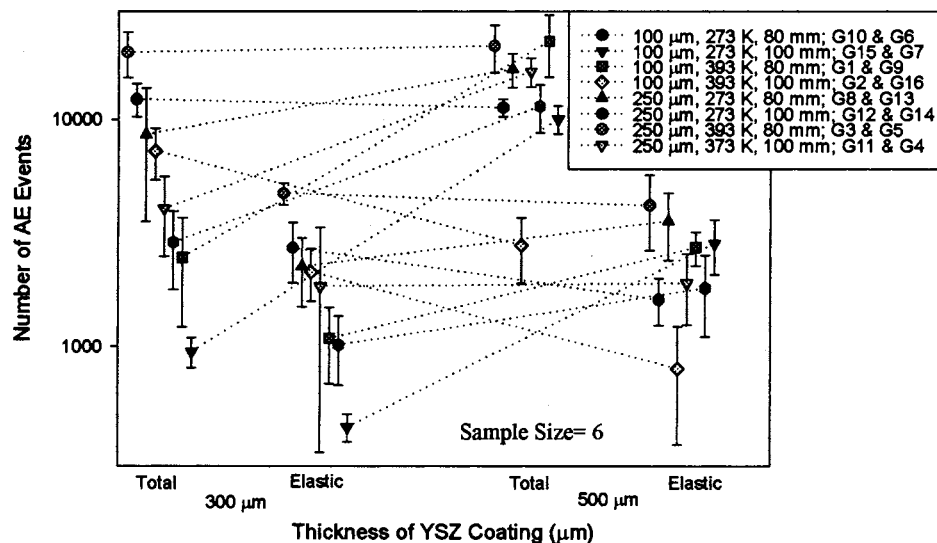


Fig. 1. Change in the numbers of acoustic emission (AE) activities under elastic and total deformation with spray parameters. The difference between the paired groups is the thickness of the yttria stabilized zirconia (YSZ) layer.

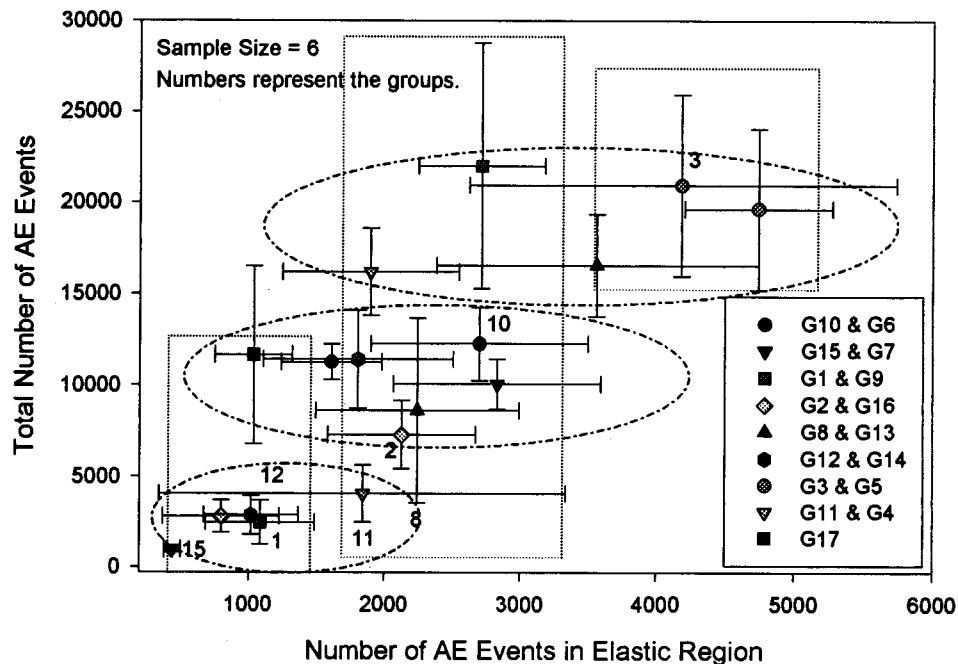


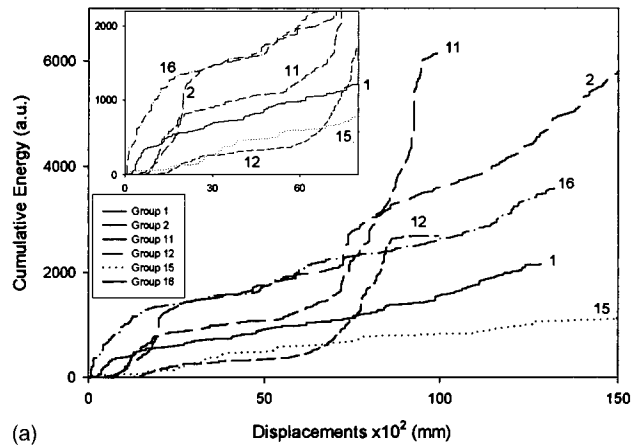
Fig. 2. Comparison of acoustic emission (AE) response of coatings under elastic and total deformation. Rectangles are for the categories according to AE response under elastic deformation while ellipsoids are for the categories according to acoustic response under total deformation.

9, and 13. There is no simple correlation between these categories and the spray parameters.

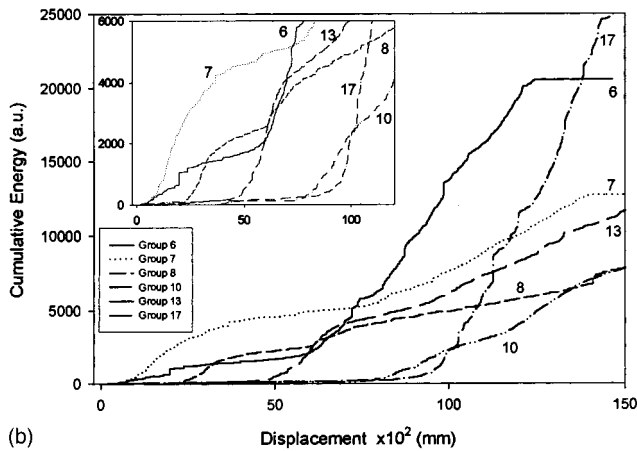
Since the energy of AE response is as important as the number of the AE response in understanding the deformation characteristic of coatings under load, the cumulative energy of the AE activities was calculated for each sample. Fig. 3 illustrates the change of cumulative energy with cross-head displacement in the four bend test. One should notice that only one representative curve out of six curves for each group is presented

in Fig. 3. The variation in cumulative energy of AE varied as high as 50% within a group. In Fig. 3 the cumulative energy value for AE activity in the elastic region is presented as an enlarged portion. As shown, a significant change in the cumulative energy of AE can be seen upon transition from an elastic to plastic deformation region. A similar change in the number of AE events was also observed upon the elastic–plastic deformation transition (Fig. 2). The same categorization proposed according to the number of AE events was

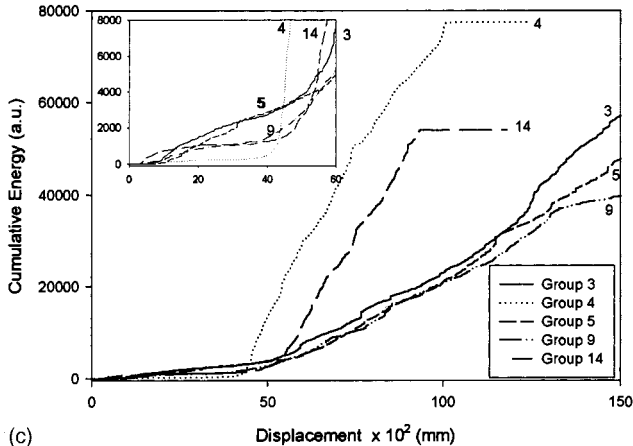
valid for the cumulative energy of AE activities (Fig. 3): Samples in groups 1, 2, 11, 12, 15, and 16 exhibited AE activities with low amounts of cumulative energy, samples in groups 6, 7, 8, 10, 13, 17 released medium amounts of cumulative energy, while samples in groups



(a)



(b)



(c)

Fig. 3. (a) Change in cumulative acoustic emission (AE) energy of coatings with deformation. Inset illustrates the cumulative AE energy under elastic deformation. (b) Change in cumulative AE energy of coatings with deformation. Inset illustrates the cumulative AE energy under elastic deformation. (c) Change in cumulative AE energy of coatings with deformation. Inset illustrates the cumulative AE energy under elastic deformation.

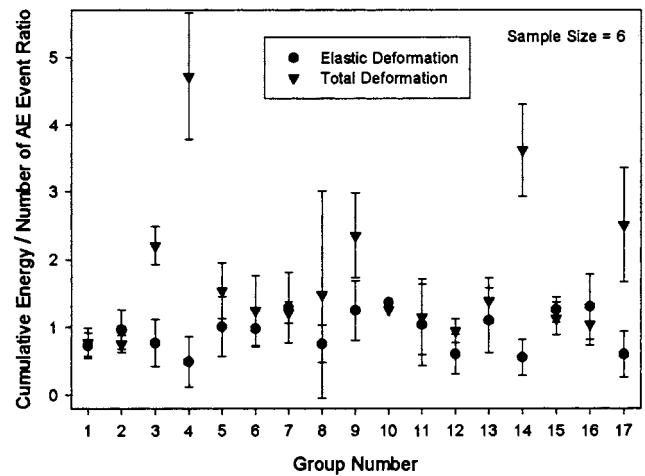


Fig. 4. Ratio of the cumulative acoustic emission (AE) energy to the number of AE events under elastic and total deformation.

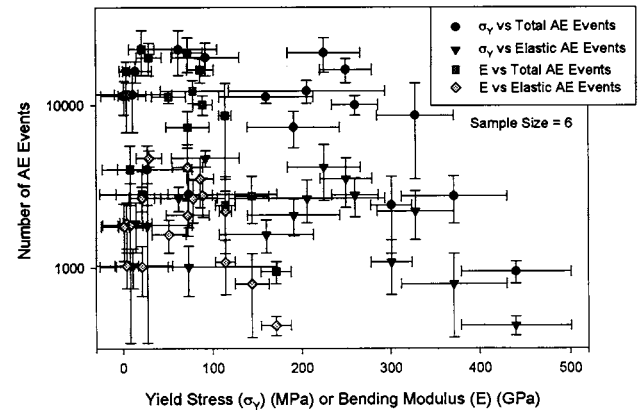


Fig. 5. Comparison of the number of acoustic emission (AE) activities with the mechanical properties of the coating measured in a previous study [17].

3, 4, 5, 9, 14 generated high amounts of AE cumulative energy.

The ratio of the cumulative energy to number of AE events for both elastic and total deformation is presented in Fig. 4. The ratios are similar except those for 3, 4, 9, 14, and 17.

In Fig. 5, the AE response of samples were compared with the mechanical properties of the coatings; bending yield strength and modulus measured in the previous study [17]. There is no simple correlation between the number of AE activities and the mechanical strength of the coatings.

### 3.3. Statistical analysis on results

To further understand the significance of each parameter on the AE response of the coatings, all the results were statistically analyzed using multi-linear regression.

Table 4

Results of the multiple linear regression analysis on the spray parameter dependence of the number of acoustic emission (AE) activities during elastic and total deformation under four point bending of the coatings<sup>a</sup>

	Estimated coefficient		S.E.		<i>t</i> -test probability	
	Elastic	Total	Elastic	Total	Elastic	Total
Constant	4520.5	8291.6	1673.5	7224.3	0.007	0.255
$t_{BC}$ (μm)	5.9	28.2	1.7	7.7	0.001	0.001
$t_{TC}$ (μm)	2.2	39.0	1.3	5.8	0.094	0.000
$T_{St}$ (K)	4.1	25.9	2.2	9.7	0.065	0.009
$X_{sod}$ (mm)	−62.7	−303.4	13.0	57.7	0.000	0.000

<sup>a</sup> The *t*-test probability is the probability of each parameter not being statistically significantly influential. ( $t_{BC}$  is the thickness of bond coating (NiCrAlY) in μm,  $t_{TC}$  is the thickness of the top coating (YSZ) in μm, and  $T_{St}$  is the substrate temperature in K,  $X_{sod}$  is the stand off distance in mm.)

Table 5

The predicted changes in the number of the elastic and total acoustic emission (AE) response of the coatings during four point bend test<sup>a</sup>

	Change in parameter	Change in elastic AE response	Change in total AE response
$t_{BC}$ (μm)	+150	+888 ± 216	+4234 ± 1156
$t_{TC}$ (μm)	+200	+438 ± 256	+7791 ± 1156
$T_{St}$ (K)	+120	+487 ± 259	+3106 ± 1159
$X_{sod}$ (mm)	+20	−1254 ± 260	−6068 ± 1155

<sup>a</sup> Plus (+) and minus (−) signs indicate increase and decrease in the quantity, respectively. ( $t_{BC}$  is the thickness of bond coating (NiCrAlY) in μm,  $t_{TC}$  is the thickness of the top coating (YSZ) in μm, and  $T_{St}$  is the substrate temperature in K,  $X_{sod}$  is the stand off distance in mm).

### 3.3.1. Number of AE events in elastic region

A multi-linear regression analysis was applied to the results on the number of AE events monitored in the elastic region to examine the influence of the spray parameters using the Statgraphics Plus 2.0 software. An *F*-test validated the significance of a relationship between the four independent variables (bond coat thickness, top coat thickness, substrate temperature and stand off distance) and the number of AE activities in the elastic region at the 99% confidence interval. A Student *t*-test proved that bond coat thickness and stand off distance are significantly influential on the number of AE activities observed in the elastic region at the 99% confidence interval (Table 4) while top coat thickness and substrate temperature have significant influence on the number of AE activities at more than 90% confidence interval. The following equation from the fitted model relates the number of AE events in the elastic region,  $N_{AE}(\text{elastic})$  to the spray parameters in the studied interval:

$$N_{AE}(\text{elastic}) = 4520.6 + 5.92 \cdot t_{BC} + 2.19 \cdot t_{TC} + 4.06 \cdot T_{St} - 62.72 \cdot X_{sod} \quad (1)$$

where  $t_{BC}$  is the thickness of bond coating (NiCrAlY) in μm,  $t_{TC}$  is the thickness of the top coating (YSZ) in μm,  $T_{St}$  is the substrate temperature in K, and  $X_{sod}$  is the stand off distance in mm. The average value of residuals (mean absolute error) in the fit is 906.

While coatings with longer stand off distance exhibit smaller number of AE events, an increase in the bond or top coating thickness, and substrate temperature results in larger number of AE activities. An increase in bond coat thickness by 150 μm, or in top coat thickness by 200 μm causes  $888 \pm 261$  or  $438 \pm 256$  additional AE activities, respectively, while moving stand off distance from 80 to 100 mm results in a decrease in AE activities by  $1254 \pm 260$ . The number of AE activities in the elastic region are higher by  $487 \pm 259$  for the coatings on pre-heated (393 K) substrates with respect to that on cold substrates (Table 5). As seen, the most influential parameter on the number of AE activities monitored in elastic region is the stand off distance. No such dependence could be detected from the classical bend test measurements.

### 3.3.2. Number of total AE events

A similar multi-linear regression analysis was applied on the total number of AE events to determine the effects of each spray parameter. An *F*-test shows that there is a statistically significance correlation between the four independent variables (bond coat thickness, top coat thickness, substrate temperature and stand off distance) and the total number of AE activities at the 99% confidence interval. The Student *t*-test proved that all the spray parameters are significantly influential on the total number of AE activities at the 99% confidence interval (Table 4). The dependence of the total number

of AE events on the spray parameters,  $N_{AE}(\text{total})$  can be expressed by the formula:

$$N_{AE}(\text{total}) = 8291.6 + 28.2 \cdot t_{BC} + 39.0 \cdot t_{TC} + 25.9 \cdot T_s - 303.4 \cdot X_{sod} \quad (2)$$

where  $t_{BC}$ ,  $t_{TC}$ ,  $T_s$ , and  $X_{sod}$  are as described above. The average value of residuals (mean absolute error) in the fit is 3750. It is clear from this analysis that a sample with thinner bond and top coat sprayed on a cold substrate at longer stand off distance releases a lower total number of AE activities under four point bending. A 150  $\mu\text{m}$  decrease in bond coat thickness lowers the total number AE events by  $4234 \pm 1156$  while a 200  $\mu\text{m}$  decrease in top coating thickness results in  $7791 \pm 1156$  drop in the total number of AE activities. Similarly, a 120° increase in the substrate temperature or a 20 mm decrease in the stand off distance causes  $3106 \pm 1159$ , or  $6068 \pm 1155$  increase in the total number of AE events, respectively (Table 5).

#### 4. Discussion

The analysis of the AE data requires correlation of the AE response of coatings under load with the microstructure. The plasma sprayed YSZ coating microstructure includes splats (lamellae), porosity, voids, microcracks, and un-melted particles [1]. Splats can be a mixture of different phases such as metastable tetragonal ( $t'$ ) and monoclinic [3]. Porosity can be inter-lamellar or within lamellar. Inter-lamellae pores mostly form from the random built-up of splats. In addition, the volume change during solidification results in pores between and within lamellae pores. Microcracks in the ceramic layer form from the processing stresses. Rapid solidification and mismatch between the thermal expansion coefficient of the substrate and coating are the sources of the processing stresses. Bianchi et al. [19] reported that tensile solidification stresses and compressive stresses from thermal expansion coefficient mismatch in YSZ coatings yield tensile residual stresses. Greving et al. [20] found that residual stresses vary throughout the TBC with a 254  $\mu\text{m}$  YSZ top coat and a 76  $\mu\text{m}$  NiCrAlY bond coat layers on a Hastelloy Alloy X substrate: 30 MPa tensile stress on the surface of the top coating decreases to 10 MPa compressive stress in the middle of top coat, and then it increases back to 30 MPa tensile stress at the top coat bond coat interface. It reaches 60 MPa tensile stress in the bond coat, and drops to 5 MPa compressive stresses at the bond coat/substrate interface. The stresses in the substrate are 150 MPa compressive near the interface. Matejcek et al. [4] measured residual stresses in a 200  $\mu\text{m}$  NiCrAlY and a 200  $\mu\text{m}$  YSZ on a steel substrate as  $99 \pm 15$  MPa tensile and  $15 \pm 10$  tensile respectively using X-ray diffraction.

#### 4.1. Effect of stand off distance

As given in Eqs. (1) and (2), a change in stand off distance has the most significant influence on the number of AE events during the four point bend test. It has been reported that stand off distance does not influence the bending yield strength and modulus of plasma sprayed TBCs [17,21]. Ilavsky et al. [22] reported that percent porosity in plasma sprayed YSZ coating produced using plasma-spherodized powders increases from 10 to 14 vol.% with a change in the spray distance from 65 to 145 mm; while the crack surface area decreases by half with the same change in the spray distance. The decrease in the crack surface area implies that the residual stresses in a YSZ coating decreases with increasing spray distance. When temperature and particle velocity in the plasma plume are taken into consideration, it is reasonable to have higher stresses for shorter spray distances. Both the temperature and velocity of particles decreases with increasing distance from the plasma source. For example, the temperature and velocity of the particles in the plasma flame may vary as much as 1000 K, and 100  $\text{m s}^{-1}$  in a 20 mm change in the stand off distance. Higher particle temperatures result in a higher amount of quenching (solidification) residual stresses. In addition, the density and viscosity of particles are lower for higher temperatures. Therefore, particles spread better according to the Madejski equation [1]. Higher particle temperatures also provide more effective packing of splats, and better cohesion between splats. The decrease in percentage porosity and roughness, and increase in hardness is an indication of this more effective packing and cohesion between splats. Therefore, one would think that a coating with more effective packing and better cohesion would exhibit a lower AE response under load, i.e. coatings sprayed at lower spray distance would be expected to exhibit less AE activity. However, the converse is experimentally observed whereby an increase in spray distance decreases the number of AE activities recorded during a four point bend test. This arises because one should also consider changes in residual stresses with stand off distance because any tensile residual stresses present in the coating will be relieved by crack formation. For example, a 10 MPa tensile residual stress can be relieved by formation of  $0.1 \text{ m}^2 \text{ m}^{-3}$  fracture surface; i.e. crack formation. The crack surface was calculated by taking the fracture surface energy of YSZ as  $50 \text{ J m}^{-2}$  [23]. Wigren et al. [24] reported that when spray distance change from 'short' to 'long'<sup>2</sup> in spraying of a 420  $\mu\text{m}$  YSZ, residual stresses measured by the modified layer-removal method dropped by 40–50%. The decrease in AE activity ob-

<sup>2</sup> The exact spray distance in the mentioned study was not given, but just referred as 'short' and 'long'.

served by increasing spray distance implies that the effect of residual stresses on AE response of the coatings are the more dominant of effects from two parameters; residual stresses, and packing and cohesion efficiency.

The influence of processing stresses on AE response of coatings are 2-fold: (i) higher amount of processing stresses generate higher amount of microcracks which weaken the mechanical strength of coatings; and (ii) higher residual stresses from greater processing stresses promote cracking during loading. The microcracks formed during the release of processing stresses propagate under the load and generate AE energy. Therefore, AE analysis is a powerful tool to characterize the influences of processing and residual stresses. As given in Eqs. (1) and (2), the coefficient for stand off distance, estimated from multi-linear regression analysis, is high with respect to other parameters. The effect of stand off distance on the number of AE activities is more pronounced in the elastic region than the total deformation. It is believed that the more pronounced effect of stand off distance on the AE activities can be related to residual stresses. The load applied during the four point bend test promotes the relief of residual stresses by cracking. One should note that residual stress can not cause cracking unless they overcome the threshold value which is the minimum energy required to create a fracture surface. Lin et al. [25] carried out four point bend tests with varying loads on a YSZ TBC which yielded at a 3000 N bending load. They monitored AE response of a coating during the four point bend test under subsequent loads. They found that the number of AE activities changes as 460, 436, 186, 203, and 42 525 under the applied loads of 250, 1000, 1500, 2500, and 4800 N, respectively. As seen, the majority of the AE energy in the elastic region was released during the initial two loadings. This can be interpreted as an evidence for the relief of residual stresses by cracking during the first two loadings. Therefore, the more pronounced effect of stand off distance, which is driven by the amount of stresses, on the AE activity in the elastic region is reasonable.

#### 4.2. Effect of top coat thickness

As given in Eqs. (1) and (2), coatings with a thicker YSZ top coat generate more AE events in the four point bend test. One obvious reason for such AE response is the size effect. Since the volume of the thicker top coating is greater than that of a thinner coating, the number of cracks present after the spray process and generated during loading is higher for a larger volume. However, an increase in the AE activity with increasing top coat thickness can not be rationalized only by the size effect because otherwise the coefficients (2.18 and 38.96) for elastic and total deformation

would have been the same. In addition to a slight contribution from the size effect, the change in residual stresses due to thickness plays a significant role in the AE response of coatings. It was reported that residual stresses increased with the coating thickness [4].

The contribution of the top coat thickness with respect to the AE response of coating drastically increases after the yield point. As seen in Eqs. (1) and (2), the top coat thickness coefficient jumps from 2.19 to 38.89 for elastic and total deformation, respectively. Part of the reason for this observation is the nature of the test. In the four point bend test, the arrangement is such that the coating is under tension. The bending strain increases with respect to the distance from the neutral axis, and it is the highest on the outer layer of the coating. Therefore, the top coat undergoes the greatest amount of deformation, and the difference in the strain of the layer gets larger upon an increase in cross-head displacement during the four point bend test. As a result, a large contribution is observed with regard to the influence of top coat thickness on AE activity after the yield point. One other reason for a large change in the number of AE events after the yield point could be the delamination. After a certain amount of deformation, layers separate because of shear forces originating from the bending load. The AE energy emitted from such events (delamination) is much higher than the energy rising from vertical cracks. As given in Fig. 4 the cumulative energy increases after the yield point.

#### 4.3. Effect of bond coat thickness

The number of AE events increases with increasing bond coat thickness for both elastic and total deformation as given in Eqs. (1) and (2). Similar to the rational for the influence of top coat on the AE response, residual stresses play a significant role. One should notice that the residual stresses are much higher in the metallic bond coat than in the ceramic top coat since the bond coat is ductile with respect to brittle ceramic coating; i.e. residual stresses in the ceramic can be relieved by cracking processes. The effect of bond coat thickness on AE activity is more pronounced in the elastic and this might indicate relief of residual stresses upon initial loading.

#### 4.4. Effect of substrate temperature

Coatings sprayed on a pre-heated substrate exhibited more AE events as given in Eqs. (1) and (2). It has been reported that higher substrate temperature generally lowers the residual stresses in the coating layers [5]. Therefore, one would expect that coating on a pre-heated substrate should have given a lower number of AE activities. However, one should also consider other contributions such as oxidation and surface roughness.

Even though the temperature of the pre-heated substrate is reported as 393 K in the current study, it is believed that the local temperatures could be far more than the measured values. These local high temperature areas in the steel substrate give rise to oxidation of the substrate that lowers adhesion between the substrate and the bond coat. In addition, it also affects the deposition built-up such a way that packing could change.

#### 4.5. Energy of events

Although it is difficult to directly correlate the nature of cracking and the AE energy, it was attempted to determine the average energy per cracking. The ratio of cumulative energy to the number of AE events is given in Fig. 4. One is cautioned that rather than an average energy per cracking, a distribution of energy and cracking is more close to reality. Nevertheless, it is believed that the ratios represented in Fig. 4 present useful information. Strikingly, the ratios for elastic and total deformation and for different coating are of the same magnitude within the errors except coatings from groups 3, 4, 9, 14, and 17. At this point, no clear understanding on this observation was developed.

### 5. Conclusions

The cracking behavior of plasma sprayed TBCs under a four point bend loading was monitored using an in situ AE analysis. Depending on the spray parameters, the coatings exhibited different AE responses that were characteristic different amounts of AE energy. AE response of the coating during elastic and plastic deformation were differentiated, and analyzed separately. The number of AE events and AE energy released increased significantly after the yield point. However, the ratio of cumulative AE energy to the number of AE events under elastic and plastic deformation was similar for the coatings sprayed using different spray parameters except for coatings from groups 3, 4, 9, 14, and 17. For those exceptional groups, the ratio under total deformation was much higher than the ratio under elastic deformation.

A multi-linear regression analysis, applied on the AE activity monitored during elastic and plastic deformation of coatings, revealed that coatings with thinner bond and top coats sprayed on cold substrate at longer stand off distance exhibited a lower degree of cracking. The stand off distance within these four parameters was the most influential parameter on the AE response of coatings. It is believed that cracking behavior of coatings under four point bend loading is strongly controlled by the stresses created during processing due to rapid cooling and thermal expansion mismatch between

the coating layers and the substrate. Some of the processing stresses release by cracking in the coating. These cracks behave as sites for further cracking and crack propagation during loading. In addition, the tensile residual stresses in the coating promote cracking during loading.

The bending yield strength and modulus of coatings calculated in a previous work [17] was compared with the AE response of coatings. At the current stage of the work, no simple correlation between the bending strength and the AE response of coatings has been developed, however, further studies are being carried out.

### Acknowledgements

The authors would like to thank Dr Carlos R.C. Lima of University of Piracicaba, Brazil for his help with sample preparation during his sabbatical stay in SUNY at Stony Brook. This work was sponsored under NSF-MRSEC DMR grant number 9632570.

### References

- [1] L. Pawlowski, *The Science and Engineering of Thermal Spray Coating*, Wiley, New York, 1995.
- [2] R.A. Miller, *Surf. Coat. Technol.* 30 (1986) 1–11.
- [3] R.S. Lima, U. Senturk, C.C. Berndt, C.R.C. Lima, in: E. Lugscheider, P.A. Kammer (Eds.), *United Thermal Spray Conference*, German Welding Society, Dusseldorf, Germany, 1999, pp. 190–195.
- [4] J. Matejcek, S. Sampath, J. Dubsky, *J. Thermal Spray Technol.* 7 (1998) 489–496.
- [5] M. Levit, I. Grimberg, B.Z. Weiss, *Mater. Sci. Eng. A206* (1996) 30–38.
- [6] D.J. Greving, J.R. Shadley, E.F. Rybicki, *J. Thermal Spray Technol.* 3 (1994) 371–378.
- [7] C.C. Berndt, *J. Eng. Gas. Turbines Power-Trans. ASME* 107 (1985) 142–146.
- [8] J. Voyer, F. Gitzhofer, M.I. Boulos, *J. Thermal Spray Technol.* 7 (1998) 181–190.
- [9] U. Senturk, R.S. Lima, C.C. Berndt, C.K. Lin, C.R.C. Lima, in: E. Lugscheider, P.A. Kammer (Eds.), *United Thermal Spray Conference*, German Welding Society, Dusseldorf, Germany, 1999, pp. 815–819.
- [10] C.K. Lin, C.C. Berndt, *Surf. Coat. Technol.* 102 (1998) 1–7.
- [11] M.J. Noone, R.L. Mehan, in: R.C. Bradt, D.P.H. Hasselman, F.F. Lange (Eds.), *Fracture Mechanics of Ceramics*, Plenum Press, New York, 1974, pp. 201–229.
- [12] C.C. Berndt, D. Robins, R. Zatorski, H. Herman, Presented at 10th International Thermal Spraying Conference, Essen, Germany, 1983.
- [13] C.K. Lin, C.C. Berndt, S.H. Leigh, K. Murakami, *J. Am. Ceram. Soc.* 80 (1997) 2382–2394.
- [14] C.C. Berndt, *Mech. Eng.* 106 (1984) 85–85.
- [15] C.C. Berndt, *Mater. Sci. Forum* 34–36 (1988) 457–461.
- [16] S. Safai, H. Herman, K. Ono, Presented at 9th International Thermal Spraying Conference, Hague, Netherlands, 1980.
- [17] A. Kucuk, C.C. Berndt, U. Senturk, R.S. Lima, C.R.C. Lima, *Mater. Sci. Eng. A* 284 (2000) 29–40.



- [18] C.K. Lin, S.H. Leigh, C.C. Berndt, *Thin Solid Films* 310 (1997) 108–114.
- [19] L. Bianchi, F. Blein, N. Baradel, in: C.C. Berndt (Ed.), *Thermal Spray: A United Forum for Scientific and Technological Advances*, ASM International, Materials Park, OH, 1997, pp. 831–838.
- [20] D.J. Greving, E.F. Rybicki, J.R. Shadley, *J. Thermal Spray Technol.* 3 (1994) 379–388.
- [21] P. Boch, P. Fauchais, D. Lombard, B. Rogeaux, M. Vardelle, in: N. Claussen, M. Ruhle, A.H. Heuer (Eds.), *Advances in Ceramics Science and Technology of Zirconia II*, vol. 12, American Ceramic Society, Columbus, OH, 1984, pp. 488–502.
- [22] J. Ilavsky, G.G. Long, A.J. Alen, H. Herman, C.C. Berndt, in: C.C. Berndt (Ed.), *9th National Thermal Spray Conference*, ASM International, Materials Park, OH, 1996, pp. 725–728.
- [23] W.D. Kingery, H.K. Bowen, D.R. Uhlmann, *Introduction to Ceramics*, 2nd edition, Wiley, New York, 1976.
- [24] J. Wigren, L. Pejryd, B. Gudmundsson, R.T.R. McGrann, D.J. Greving, E.F. Rybicki, J.R. Shadley, in: C.C. Berndt (Ed.), *9th National Thermal Spray Conference*, ASM International, Materials Park, OH, 1996, pp. 847–854.
- [25] C.K. Lin, U. Senturk, R.S. Lima, C.C. Berndt, J.C. Shieh, P.Y. Lee, in: E. Lugscheider, P.A. Kammer (Eds.), *United Thermal Spray Conference*, German Welding Society, Dusseldorf, Germany, 1999, pp. 809–814.

#### Permission to publish

A. Kucuk, C.C. Berndt, U. Senturk, R S. Lima and C.R.C. Lima, 'Influence of plasma spray parameters on the mechanical properties of yttria stabilized zirconia coatings II: Acoustic emission response', *J. Mater. Engin. and Sci.*, A284 (2000) 41-50.

As an Elsevier journal author, you retain various rights including Inclusion of the article in a thesis or dissertation whether in part or in toto; see [http://www.elsevier.com/about/policies/author-agreement/lightbox\\_scholarly-purposes](http://www.elsevier.com/about/policies/author-agreement/lightbox_scholarly-purposes) for more information. As this is a retained right, no written permission is necessary. This extends to the online version of your thesis and would include any version of the articles including the final published versions provided that they are not available as individual downloads but only embedded within the thesis itself.

# Evaluation of microhardness and elastic modulus of thermally sprayed nanostructured zirconia coatings

R.S. Lima, A. Kucuk, C.C. Berndt\*

*Department of Materials Science and Engineering, State University of New York at Stony Brook, 306 Old Engineering Building,  
Stony Brook, NY 11794-2275, USA*

Received 8 February 2000; accepted in revised form 2 August 2000

## Abstract

Results concerning microhardness and roughness ( $R_a$ ) of plasma sprayed coatings fabricated from nanostructured partially stabilized zirconia (PSZ) feedstock are presented. Nanostructured zirconia particles were plasma sprayed ( $\text{Ar}/\text{H}_2$ ) at three power levels, with two argon flow rates at two spray distances. The results indicate that the microhardness, elastic modulus and roughness of the nanostructured zirconia coatings exhibit the following trends: the smoother the roughness, the higher the microhardness and elastic modulus. It was found that roughness is an indicator of the coating state that reflects the intrinsic microstructure of the coatings. It was ascertained that a surface profilometer could be used to determine the level of microhardness and elastic modulus as a non-destructive and in situ test by simple comparison with standard samples. © 2001 Elsevier Science B.V. All rights reserved.

**Keywords:** Thermal spray; Microhardness; Elastic modulus; Roughness; Nanostructured zirconia-yttria; Thermal barrier coatings

## 1. Introduction

Nanocrystalline materials (also referred to as nanostructures, nanophase materials, or nanometer-sized crystalline solids) are single-phase or multi-phase polycrystals. The crystal size is typically approximately 1–100 nm in at least one dimension [1,2]. Nanostructured materials come in two general morphologies: (i) nanolayered materials deposited by physical vapour deposition or electrodeposition processes and; (ii) nanograined materials, which are usually consolidated from nanostructured powders [1,2]. As the grain size

becomes smaller, there are an increasing number of atoms associated with grain boundary sites compared to crystal lattice sites. The unique properties of nanograined materials are associated with the fineness of structure as well as the enhanced solubility and increasing atomic mobility associated with grain boundaries [1,2]. It has also been demonstrated that nanostructured ceramics can be sintered at relatively low temperatures, exhibit improved ductility, and even potential superplasticity, in the nanocrystalline state [1].

Thermal barrier coatings (TBCs) consist of a bond coat and a zirconia coating overlay. They are primarily used for aerospace applications. TBCs, due to their low thermal conductivity and thermal diffusivity combined with proper chemical stability at high temperatures, provide a means for (i) raising the operating tempera-

ture of hot part sections (e.g. turbine blades, nozzles and combustion chambers) or (ii) they enable the underlying material to operate at lower temperatures due to a temperature drop through the ceramic coating. TBCs can also increase engine efficiency either by increasing the working temperature whilst maintaining a constant component temperature, or by decreasing the use of cooling systems in components [3,4].

Individual nanoparticles cannot be successfully thermal sprayed because of their low mass. They do not have enough inertia required to cross the streamlines in the spray jet, being projected to its periphery without depositing on the substrate. To overcome this problem, the feedstock was developed by creating a dispersion of nanosized particles into a colloidal suspension, followed by the addition of a binder and subsequent spray drying into granules, followed by sintering.

The final powder structured consists of agglomerated micron-sized particles (spherical shape) [5] formed from the coalescence of many nanosized particles. This powder can be fed by conventional mechanical powder feeders [5]. Since the particles are porous, the plasma gas could penetrate into the inner part of the particles; thereby melting its surface. The air which is trapped inside the particle heats up; thereby exploding the previously agglomerated particles into several tiny particles during their residence time in the plasma [5]. The unmelted cores of these particles will keep the powder nanostructure intact in the coating [5]. As a consequence, the presence of non-molten particles in the coatings is very important.

In the current work, the influence of different spray parameters on the microhardness, elastic modulus and roughness of nanostructured coatings is investigated as a continuing study to better understand the microstructural characteristics [6–9] of this new class of sprayed material.

It is important to comment that the thermal spray industry does not have simple effective methods to evaluate the coating quality because the traditional methods are destructive. In this work, a surface profilometer was used to determine the quality of a coat-

ing in situ. These roughness measurements were correlated to microhardness and elastic modulus.

## 2. Experimental procedure

The nanostructured PSZ ( $\text{ZrO}_2$ -7 wt.%  $\text{Y}_2\text{O}_3$ ) experimental powder Nanox 4007 (Inframat Corp., North Haven, CT, USA) was plasma sprayed under different parameters in air on mild steel substrates with a 40-kW, standard SG100 plasma torch (Praxair, Appleton, WI, USA). The substrates were grit-blasted with alumina just before thermal spraying ( $R_a = 4.1 \pm 0.3 \mu\text{m}$ ). The substrates were not pre-heated. Typical coating thickness was 0.9–1.1 mm. The spray parameters applied are listed in Table 1.

The Vickers microhardness measurements were performed at 500 and 1000 g loads for 15 s (Buehler Micromet II, Buehler Ltd., Lake Bluff, IL, USA) on the top-surface and the cross-section of coatings. The Knoop microhardness measurements were performed at 1000 g load for 15 s (Tukon, Instron, Canton, MA, USA) on the cross-section of coatings. The cross-sections of the samples were polished before the indentations. For the cross-sections, the indentations were applied near the center line of the coating thickness. The distance between the indentations was at least three times the diagonal to prevent stress-field effects from nearby indentations for both the top-surface and cross-section studies [10].

The arithmetic mean roughness value ( $R_a$ ) of the coatings was determined by a mechanical profilometer T1000 (Hommel America Inc, New Britain, CT, USA) performed along two orthogonal directions on the as-sprayed coating surfaces, with the following specifications; type of roughness filter: M1 (DIN 4777), tracing length: 4.8 mm, cut-off length: 0.8 mm and tracing speed: 0.5 mm/s. Roughness measurements near the coating edges were avoided. A total of 10 measurements were taken for each test condition of hardness, elastic modulus and roughness.

Table 1  
The spraying parameters used for the PSZ coatings

Parameters	Set 1	Set 2	Set 3	Set 4	Set 5	Set 6
Power (kW)	40	40	40	40	32	24
Current (A)	800	800	800	800	800	600
Voltage (V)	50	50	50	50	40	40
Ar flow-plasma (slpm)	48	38	48	38	48	48
H <sub>2</sub> flow-plasma (slpm)	≈ 5	≈ 5	≈ 5	≈ 5	≈ 4	≈ 4
Ar flow-carrier gas (slpm)	5	5	5	5	5	5
RPM-Hopper (%)	30	30	30	30	30	30
Spray distance (cm)	6	6	8	8	8	8

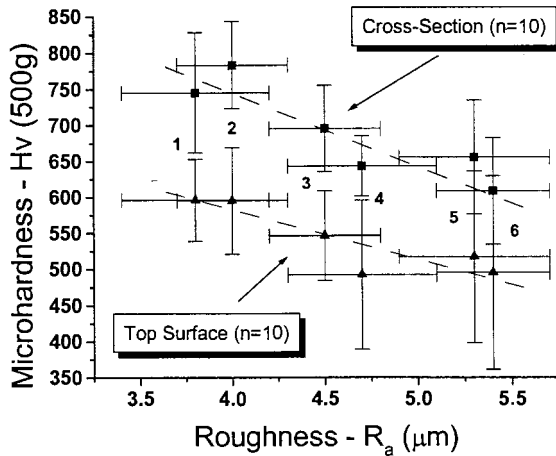


Fig. 1. Vickers microhardness–roughness relationship (500 g load) for different sets of spray parameters (Table 1).

### 3. Results and discussion

#### 3.1. Roughness

The arithmetic mean roughness value ( $R_a$ ) is the average deviation of a surface profile from the centerline over the measuring length, defined by Eq. (1);

$$R_a = \frac{1}{L} \int_{x=0}^{x=L} |y(x)| dx \quad (1)$$

where  $y$  is the deviation of the surface profile from the centerline.

The average roughness varied significantly with change in spray conditions (Figs. 1–4). The  $R_a$  increased with increasing spray distance (set 1 vs. set 3 and set 2 vs. set 4). Similarly, increase in torch power resulted in decrease in roughness of the coatings (set 6, set 5 and set 3). However, change in  $H_2/Ar$  ratio made a slight difference in the  $R_a$  of the coatings.

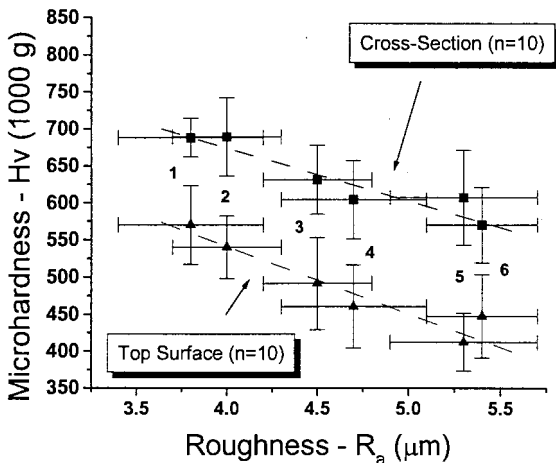


Fig. 2. Vickers microhardness–roughness relationship (1000 g load) for different sets of spray parameters (Table 1).

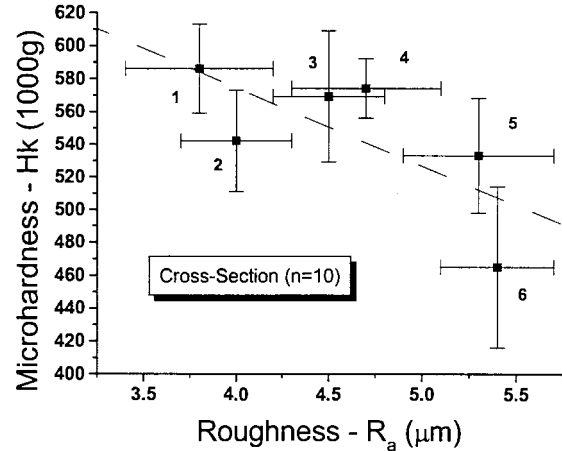


Fig. 3. Knoop microhardness–roughness relationship (1000 g load) for different sets of spray parameters (Table 1).

#### 3.2. Microhardness–roughness

Figs. 1 and 2 show a trend whereby the roughness decreases as the hardness increases. A dashed line was placed in Figs. 1 and 3 as a ‘guideline for eye’ to show this trend. The data points on these figures indicate plasma spray parameter sets where the plasma power decreases and the spray distance increases from set 1 through set 6. It is speculated that these responses are also a manifestation of the physical principles that are implicit in the Madejski equation [11]. Madejski formulated a theoretical model on the impact of a molten droplet with a solid substrate by making a relationship between the splat diameter ( $D$ ) and the diameter of the initial droplet ( $d$ );

$$\frac{D}{d} = 1.2941 \left( \frac{\rho v_d d}{\mu} \right)^{0.2} = 1.2941 (Re)^{0.2} \quad (2)$$

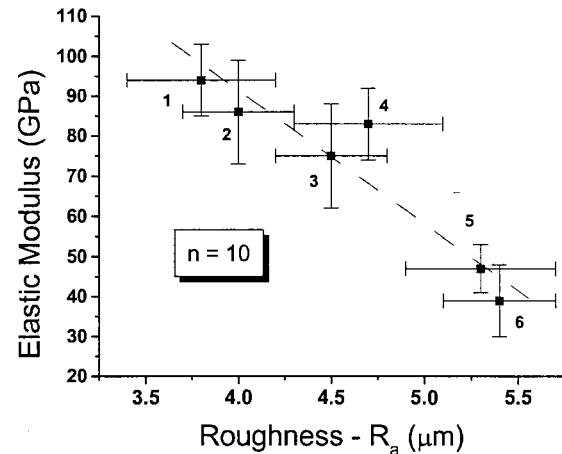


Fig. 4. Elastic modulus–roughness relationship for different sets of spray parameters (Table 1).

where  $\rho$ ,  $\mu$  and  $v_d$  are the density, viscosity and the impact velocity, respectively, of the particle. The Reynolds number is represented as  $Re$ . According to Eq. (2), when the velocity of the particles is increased and/or the viscosity is decreased then particle spreading tends to increase. It becomes apparent that highly flattened particles will form a coating with low roughness, while low flattened particles will form a coating with high roughness. According to Vardelle et al. [12], when particle velocity and temperature increase, the flattening degree increases in a linear trend. The particles sprayed with parameter set 1 should exhibit the highest velocity and the lowest viscosity, since they are processed under conditions of the highest power and shortest spray distance. The opposite effect is demonstrated by particles sprayed with parameter set 6; i.e. these particles will have the lowest velocity and highest viscosity since they are sprayed at the lowest power and with the shortest spray distance. Experimental observations of splat formation and solidification of zirconia APS particles show that the Reynolds number also influences the flattening degree in an almost linear trend [12]. But according to theoretical works [13,14] the flattening degree increases non-uniformly with the increase of Reynolds number, in the regions of small values of Reynolds number.

Other physical relationships can be ascertained from the observations the spray parameters. Thus, increasing argon flow will increase the particle velocity because the velocity of the plasma gas flame is proportional to the working gas mass flow rate [15]. Also, increasing the plasma gas flow will increase the length of the plasma flame [16,17], extending the high temperature zone and, thereby, preventing resolidification (decreasing of viscosity) of the sprayed particles. At the same time, increasing plasma power increases the temperature and the extent of temperature and velocity isocontours [17]. Clearly, increasing the plasma gas temperature causes enhanced conditions for particle melting and, thereby, lowering particle viscosity.

Vardelle et al. [18] deals with the plasma phenomena exhibited when the spray distance is decreased. For an  $Ar/H_2$  plasma, alumina particle temperatures and velocities were measured as a function of spray distance for the same plasma gas flow. A change in spray distance from 8 to 6 cm, increases average particle velocity by  $\sim 60$  m/s, while the gain in temperature was  $\sim 1000$  K [18]. This difference of 60 m/s in 2 cm may be reflected in the particle flattening behavior, because the maximum plasma gas velocity for regular air plasma spray systems is approximately 300–400 m/s [15]. The difference of 1000 K in 2 cm is sufficient to cause a drop in the viscosity, thereby preventing partial or total resolidification of the sprayed particles prior impact against the substrate. This effect can be more pronounced with the nanostructured powder after it

defragments within the plasma stream. Vardelle et al. [12] and Pawloski [15] detail results of particle flattening calculations as a function of the impact temperature at the impact. It was found that the flattening degree is enhanced for higher impact temperatures. The dual effects of particle velocity and temperature can be linked and also show that the particle temperature increases at the moment of impact due to the transformation of the kinetic energy into heat and thereby contributing to a higher flattening degree.

It has been suggested that the microstructure of plasma-sprayed ceramic coatings consists of regions of perfect contact separated by thin regions of no contact. The regions of imperfect contact arise from gas entrapped beneath spreading liquid droplets during coating formation and is aided by factors such as low viscosity and low velocity. These thin regions of poor contact are, physically, very narrow pores (approx. 0.01–0.1  $\mu m$ ) [9,19–21] with a real area of contact splat–splat is in fact approximately 20% [9]. The influence of microstructural factors on the mechanical properties of coatings has led to the suggestion that the mechanical behavior of a coating is limited by the degree of contact between splats within the coating, or between the splat and substrate, rather than the nature of the bond in regions of good contact [9,19–21].

The elastic modulus of coatings is much lower than that of the bulk material. For example, the elastic modulus of plasma sprayed alumina is approximately 20% that of a sintered ceramic [9,21]. This is a much larger reduction than can be explained on the basis of randomly distributed spherical pores but is consistent with the concept of narrow planar pores between splats with a low ‘true contact’ area [9,19–21].

Large changes in the elastic modulus of plasma sprayed ceramic coatings have also been observed after heating [22]. This effect can be explained by changes in the shape of the intersplat pores from an essentially continuous thin gap, containing small regions of true contact, to more rounded pores and a considerable increase in the area of true contact. This could occur with negligible change in the total porosity of the coating [9,21]. The interfaces between splats or between splats and the substrate must be regarded as the ‘weak links’ with respect to mechanical properties and, therefore, improvement of the mechanical behavior of coatings must be aimed at enhancing interfacial bonding [9].

The mechanical properties of the coatings, will be ruled by how effectively the sprayed particles can be compacted during spraying, among other influences. On the basis of this discussion and the experimental results with respect to roughness, it is apparent that low roughness coatings will exhibit splats that are well-packed compared to coatings with a high  $R_a$ . Hardness is usually defined as resistance to penetration, defor-

mation, scratching and erosion [23], and can be considered to reflect the splat-to-splat cohesion of thermal spray coatings; i.e. a higher hardness coating implies a greater degree of splat-to-splat cohesion.

Vickers microhardness measured on cross-section and top surface for 500 and 1000 g are shown in Figs. 1 and 2, respectively. The values measured at top surface have slightly lower values than those measured at cross-section. Microhardness measurements in thermal spray coatings with respect to the planar or cross-sectional aspects of individual splats will correspond area measurements on circles or ellipses [10]. These two testing orientations would be reflective of anisotropic modes of deformation, which do not produce identical hardness values. The planar hardness values were normalized with respect to the cross-section hardness values for indenting loads of 500 and 1000 g. These ratios were  $\sim 0.78 \pm 0.13$  and demonstrate the relative anisotropic degrees of splat packing with respect to the two testing directions.

Knoop microhardness values measured using 1000 g on the cross-sectional area are given in Fig. 3. The Knoop values are lower than the Vickers values at the same load. In addition, the variation in Knoop values is higher than that in Vickers. Both phenomena are probably related to the difference in geometry of the two indenters, which provide different force fields in the coatings.

Observing Figs. 1–3, the following trend is noticed. Following the  $R_a$  axis from left to right, starting at spray parameter 1 throughout 6, the torch power is decreasing and the spray distance is increasing. When the plasma torch power is decreased, particle temperature and velocity will tend to drop, which will impede a larger spreading of the sprayed droplet, as discussed above. Also, when the spray distance is increased, the particle temperature and velocity will drop due to their interaction with the air. This also will impede a larger particle spreading and its effects on mechanical properties as already discussed.

When the plasma power decreases, the number of non-molten particles should increase. The presence of non-molten particles will also increase the roughness of the coating, and it will lower the values of hardness due to low particle cohesion. This also should increase the porosity of the coatings. An increase in porosity will lower the coating stiffness, producing a decrease in the values of hardness.

### 3.3. Elastic modulus-roughness

References in literature propose and use indentation techniques for measurement of elastic modulus [10,24–26]. The elastic modulus of the coatings was determined via Knoop microhardness tests [10,24]. The

elastic modulus is determined by measuring the major and minor diagonals of a Knoop indenter (2a and 2b, respectively).

The orientation of the indenter main diagonal was parallel to deposition surface, i.e. the main diagonal was at  $90^\circ$  with respect to the splashing direction of the droplets. As the microstructure of thermal spray coatings is anisotropic, the mechanical properties will have different values for different orientations, as experimentally observed in the preceding section for hardness. The elastic modulus determination technique developed by [24] is based on the measurement of elastic recovery of the in-surface dimensions of Knoop indentations, i.e. the length of the major and minor diagonals of the indentation after the unloading is measured. The elastic recovery reduces the length of the minor diagonal as well as the residual indentation depth, whereas the length change in major diagonal is negligible. As the measurement of the elastic modulus is based on the minor diagonal, the elastic modulus values obtained in this work represent the in-plane orientation of the coating.

The advantage of this type of test is that the values of elastic modulus and Knoop microhardness can be obtained simultaneously and a small specimen can be used for a large number of tests [10]. The Knoop indentation test enables elastic modulus values of thermal spray coatings to be obtained in a simple fashion and has a potential to be used as a quality-control tool in industry and laboratories [10]. The values of elastic modulus and their relationship with roughness are shown in Fig. 4.

Again a same trend is observed: the smoother the coating, the higher the Knoop microhardness and elastic modulus. A dashed line was placed in Figs. 3 and 4 as a ‘guideline for eye’ to show this trend. The elastic modulus slightly changes from spray parameters 1 to 4, where the same plasma power was applied for different  $H_2/Ar$  ratios and a difference in spray distance of 2 cm. This experimental observation agrees with the elastic modulus measurements of PSZ coatings via four-point bending method [27], which the PSZ coatings did not present a significant change in elastic modulus values varying the spray distance in 2 cm keeping the same plasma power. But when the plasma power was decreased (spray parameters 5 and 6), the drop in the elastic modulus values is clearly noticed.

Specifically for the elastic modulus, when the splats are highly flattened (low roughness) they have a large area of contact and as a consequence they have high cohesion. High splat cohesion will imply high stiffness which is measured as elastic modulus. The opposite behavior takes place for the splats which are not high flattened.



### 3.4. Other influence factors

This method used to evaluate the microhardness and elastic modulus by relating them with roughness for the nanostructured coatings may be also applied to other coatings. Each group feedstock and thermal spray process combination will demonstrate their own characteristics. Also factors such as substrate roughness, preheating and substrate temperature [28,29], spray angle [30], bond coat and coating thickness may have an influence on the final roughness. Therefore, there would be the necessity to calibrate each system prior to employing this simple method for evaluating mechanical properties. Modern surface profilometers are able to distinguish between roughness and waviness. Thus, even non-flat surfaces can be tested and analyzed.

Bianchi et al. [29] corroborates with way of thinking discussed in this work. Preheating the substrate prior to spraying always induces higher values of coating adhesion regardless of particle size and plasma parameters [29]. When the substrate is preheated to temperatures greater than 300°C before spraying, contact of splats to the substrate or previously deposited layers is improved, probably due to increased wettability of the ceramic droplets [29], which lead to better spreading. The same phenomenon was observed for hardness [29]. Also the influence of particle velocity on splat contact with hot substrates was noted. A corresponding improvement of coating adhesion on preheated substrates also occurs when sprayed with a mean particle velocity of approximately 250 m/s compared to a velocity of 130 m/s [29]. Again, the same phenomenon was observed for hardness [29].

Beyond splat–splat cohesion, microcracking can also play a role in the elastic modulus of zirconia APS coatings. Microcracking changes the load vs. displacement curves during four-point bend tests of TBCs [27,31–33]. These results were also studied with acoustic emission [31–33]. Extensive microcracking along the coating changes the behavior of stress vs. displacement curves, lowering the stiffness of the coating, decreasing the value of the yielding load of the system substrate + TBC.

A new reference [34] characterized the microstructure of APS PSZ coatings by the measurement of surface roughness and Vickers microhardness. The authors observed that the Vickers hardness decreases with an increase in roughness. Yasuda et al. [34] state that the surface roughness of the APS PSZ coatings reflected the state of piling up of the melted powder particles. Yasuda et al. [34] also discuss the possibility that the greater the surface roughness of the zirconia coatings, the lower the elastic modulus; a factor which was proven during this work.

### 4. Conclusions

The experimental observations of this work conclude the following:

- The microhardness–roughness relationship has the following trend; smoother the coating, higher the microhardness; in all cases.
- The elastic modulus–roughness relationship has the following trend; smoother the coating, higher the elastic modulus; in all cases.
- When the roughness is smooth, the splats present a high degree of flattening, creating more points of contact or anchors between splats at a microscopic level, increasing the cohesion of the coating. The enhancement of cohesion will increase the microhardness and the elastic modulus of the coating.
- A surface profilometer can be used to evaluate the microhardness and the elastic modulus of a coating in situ without destroying it by simple comparison based on a standard sample.
- The ratio between top-surface and cross-section of the Vickers microhardness at both loads (500 or 1000 g) is  $0.78 \pm 0.13$ .

### Acknowledgements

This work was supported by the US Navy-Office of Naval Research under grant number N00014-97-0843 and the Center of Thermal Spray Research under NSF-MRSEC DMR grant number 9632570.

### References

- [1] C. Suryanarayana, F.H. Froes, *Metal. Trans. A* 23A (1992) 1071.
- [2] M. Gell, *J. Metals*, October (1994) 30.
- [3] J.A. Nesbitt, *Surf. Coat. Technol.* 43/44 (1990) 458.
- [4] T.M. Yonushonis, *J. Thermal Spray Technol.* 6 (1997) 50.
- [5] R.S. Lima, U. Senturk, C.C. Berndt, C.R. C. Lima, *Conference Proceedings of the United Thermal Spray Conference*, in: E. Lugscheider, P.A. Krammer (Eds.), Verlag fur Schweissen und verwandte Verfahren DVS – Verlag GmbH, Dusseldorf, Germany (1999) 190.
- [6] K. Muraleedharan, J. Subrahmanyam, S.B. Bhaduri, *J. Am. Ceram. Soc.* C 71 (1988) 226.
- [7] R. Chaim, M. Ruhle, A.H. Heuer, *J. Am. Ceram. Soc.* 68 (1985) 427.
- [8] R.A. Miller, R.G. Garlick, J.L. Smialek, *Am. Ceram. Soc. Bull.* 62 (12) (1983) 1355.
- [9] R. McPherson, *Surf. Coat. Technol.* 39/40 (1989) 173.
- [10] S-H. Leigh, C-K. Lin, C.C. Berndt, *J. Am. Ceram. Soc.* 8 (8) (1997) 2093.
- [11] J. Madejski, *Int. J. Heat Mass Transfer* 19 (1976) 1009.
- [12] M. Vardelle, A. Vardelle, A.C. Leger, P. Fauchais, D. Gobin, *J. Thermal Spray Technol.* 4 (1994) 50.
- [13] V.V. Sobolev, J.M. Guilemany, A.J. Martin, *Mater. Lett.* 29 (1996) 185.

- [14] V.V. Sobolev, J.M. Guilemany, A.J. Martin, *Surf. Coat. Technol.* 89 (1997) 82.
- [15] L. Pawlowski, *The Science and Engineering of Thermal Spray Coatings*, John Wiley & Sons Ltd, 1995.
- [16] A.V. Donskoi, V.M. Goldfarb, V.S. Klubnikin, *Physics and technology of low-temperature plasmas*, in: S.V. Dresvin (Ed.), 1972 (T. Cheron, Trans. and H.U. Eckert (Ed.), Iowa State University Press, 1977 (cited by E. Pfender, M. Boulos, P. Fauchais, *Methods and Principles of Plasma Generation. Plasma Technology in Metallurgical Processing*, in: J. Feinman (Ed.), Warrendale: Iron & Steel Society, 1987, pp. 27–47).
- [17] P. Eichert, M. Imbert, C. Coddet, *J. Thermal Spray Technol.* 7 (4) (1998) 505.
- [18] M. Vardelle, A. Vardelle, P. Fauchais, M.I. Boulos, *AIChEJ* 29 (1983) 236 ((cited by M. Boulos, E. Pfender, P. Fauchais, *Fundamentals of Plasma-Particle Momentum and Heat Transfer. Plasma Technology in Metallurgical Processing*, in: J. Feinman (Ed.), Warrendale: Iron & Steel Society, 1987, pp. 49–63)).
- [19] R. McPherson, *Thin Solid Films* 83 (1981) 297.
- [20] R. McPherson, B.V. Schaffer, *Thin Solid Films* 97 (1982) 201.
- [21] R. McPherson, *Thin Solid Films* 112 (1984) 89.
- [22] P. Boch, D. Fargeot, C. Gault, F. Platon, *Rev. int. hautes Temper. Refract.* 18 (1981) 85.
- [23] K.M. Amin, Toughness, hardness, and wear. *Engineered materials handbook*, in: S.J. Schneider (Ed.), *Ceramic and Glasses*, 4, ASM International, 1991, pp. 599–609.
- [24] D.B. Marshall, T. Noma, A.G. Evans, *J. Am. Ceram. Soc.* C 65 (10) (1982) 175.
- [25] J.P. Singh, M. Sutaria, M. Ferber, *Ceram. Eng. Sci. Proc.* 18 (4B) (1997) 191.
- [26] J.C. Conway, Jr., *J. Mater. Sci.* 21 (1986) 2525.
- [27] A. Kucuk, C.C. Berndt, U. Senturk, R.S. Lima, C.R.C. Lima, *Mater. Sci. Eng. A* 284 (2000) 29.
- [28] M. Mellali, P. Fauchais, A. Grimaud, *Surf. Coat. Technol.* 81 (1996) 275.
- [29] L. Bianchi, A. Grimaud, F. Blein, P. Lucchese, P. Fauchais, *J. Thermal Spray Technol.* 4 (1995) 59.
- [30] S.H. Leigh, C.C. Berndt, *Surf. Coat. Technol.* 89 (1997) 213.
- [31] A. Kucuk, C.C. Berndt, U. Senturk, R.S. Lima, *Mater. Sci. Eng. A* 284 (2000) 41–50.
- [32] U. Senturk, R.S. Lima, C.C. Berndt, C.K. Lin, C.R.C. Lima, *Conference Proceedings of the United Thermal Spray Conference*, in: E. Lugscheider, P.A. Krammer (Eds.), *Verlag fur Schweissen und verwandte Verfahren DVS – Verlag GmbH, Dusseldorf, Germany* (1999) 815.
- [33] U. Senturk, R.S. Lima, C.R.C. Lima, C.C. Berndt, *J. Eng. Gas Turbines Power* (accepted for publication).
- [34] K. Yasuda, S. Suenaga, H. Inagaki, Y. Goto, H. Takeda, K. Wada, *J. Mater. Sci.* 35 (2000) 317.

#### Permission to publish

R.S. Lima, A. Kucuk and C.C. Berndt, 'Evaluation of microhardness and elastic modulus of thermally sprayed nanostructured zirconia coatings', *Surf. Coat. Tech.*, 135 (2001) 166–172.

As an Elsevier journal author, you retain various rights including Inclusion of the article in a thesis or dissertation whether in part or in toto; see [http://www.elsevier.com/about/policies/author-agreement/lightbox\\_scholarly-purposes](http://www.elsevier.com/about/policies/author-agreement/lightbox_scholarly-purposes) for more information. As this is a retained right, no written permission is necessary. This extends to the online version of your thesis and would include any version of the articles including the final published versions provided that they are not available as individual downloads but only embedded within the thesis itself.

## Chapter 4. Modeling Studies

### 4.1 Introduction

Chapter 4 presents manuscripts #12, #13 and #14 that characterize contributions for the development of modeling studies. The analysis presented in 1997 on ‘Evaluation of off-angle thermal spray’ is important since it relates microstructural properties (i.e., the porosity) and physical properties (i.e., roughness) to the spray footprint; which ultimately determines deposition efficiency and the economics of manufacturing. Note that manuscript #2 on ‘Topographical and microstructural property evolution of air plasma-sprayed zirconia thermal barrier coatings’ approaches the same topic from a different direction.

A more sophisticated development arose in 2013 when Madejski’s and McPherson’s approaches were considered in ‘Modeling the coverage of splat areas arising from thermal spray processes’, manuscript #13, where fundamental theory is directly related to the spray coverage as determined by the spray footprint. These relationships were linked to the deposition efficiency. It is noteworthy that Prof. McPherson was the applicant’s PhD advisor.

The final contribution in Chapter 4, manuscript #14, consolidates the known properties of thermal spray materials in ‘property-performance maps’. This manuscript, on ‘Thermal spray maps: Material genomics of processing technologies’, is based on an Ashby approach but is significantly unique since it examines extrinsic properties of thermal spray deposits and manufacturing processes. Manuscript #14 is a review contribution that consolidates much of the known data on alumina and zirconia-based thermal spray coatings. The modeling exercise relates to the implementation of techniques that enables the assessment of large volumes of data.

The 36 publications with the identification numbers below are considered as contributions that focus on this specific subject material. Chapter 7 of this thesis outlines the methodology employed for this analysis.

8
13
19
35
36
37
38
45
61
75
82
93

115
140
155
156
164
243
301
304
305
319
323
326

334
339
348
363
368
369
402
411
420
434
435
450

# Evaluation of off-angle thermal spray

S.H. Leigh, C.C. Berndt \*

*Thermal Spray Laboratory, Department of Materials Science and Engineering, State University of New York at Stony Brook,  
Stony Brook, NY 11794-2275, USA*

Received 16 May 1995; accepted 19 January 1996

## Abstract

The effect of spray angle on the properties of plasma spray deposits has been investigated. Two different materials, NiAl and  $\text{Cr}_3\text{C}_2\text{-NiCr}$ , were sprayed at angles from 50 to 90° with respect to the substrate. The spray angle influenced the microstructure and the properties of the deposits. The porosity increased as the spray angle decreased, i.e. as the angle was shifted away from the perpendicular position. The surface roughness of the  $\text{Cr}_3\text{C}_2\text{-NiCr}$  deposit was not sensitive to the spray angle, whereas NiAl exhibited an increase as the spray angle decreased. Microhardness, tensile adhesion strength, and interfacial fracture toughness decreased with spray angle. The change of these properties with spray angle is attributed to (1) the morphology of the splats, (2) the change of the local spray angle, and (3) the change of momentum of particles impacting on the substrate or previously deposited particles. The mechanical-property variations arise from porosity changes which occur from the spray angle variations. © 1997 Elsevier Science S.A.

**Keywords:** Mechanical properties; Porosity; Splat morphology; Spray angle; Spray pattern; Thermal spray

## Nomenclature

$P(x)$	Gaussian probability distribution function
$\sigma$	standard deviation
$\mu$	mean
$\alpha$	spray angle (degrees)
$P'(x, \alpha)$	probability distribution function with spray angle $\alpha$
$\sigma_{90}$	standard deviation at a 90° spray angle
$d$	spray distance (mm)
$\mu_3$	skewness
$P_x$	spreading momentum
$P_y$	impacting momentum
$m$	Weibull modulus
$X_0$	characteristic strength
$\mathcal{G}_c$	critical strain energy release rate ( $\text{J m}^{-2}$ )
$K_{IC}$	fracture toughness ( $\text{N m}^{-3/2}$ )
$P_c$	fracture force (N)
$D$	outside diameter of the circumferentially notched bar (m)
$d$	inside diameter of the circumferentially notched bar (m)

## 1. Introduction

The thermal spraying process is controlled by numerous parameters which have a direct influence on the properties of the deposit. The sprayed deposits are often not reproducible between laboratories or factories

because it is difficult to maintain all of the processing parameters which are related to the properties of deposits. In addition, there are factors which are often ignored; for example, the spray angle is usually assumed to be 90° to the substrate.

The evaluation of thermally sprayed deposits is mostly carried out using coupons sprayed at 90°<sup>1</sup>. The engineering component, however, sometimes requires spraying at angles other than 90°. This aspect would be notable when no automation was used during the spray process, since it is not easy to maintain a torch at right angles to a three-dimensional substrate. The property of “off-angle spraying” is becoming an important aspect as the demand of spraying complex-shaped parts increases, especially in the thermal spray forming area. Moreover, Fasching et al. [1] recently reported that asymmetries of spray distribution can be corrected by tilting the spray torch so that uniformly thick deposits can be built up. Such off-angle spraying may also change the structure and properties of coatings.

Hasui et al. [2] studied the effect of spray angles

<sup>1</sup>The reference angle of 90° denotes an arbitrary reference where the torch axis is perpendicular to the substrate. Angles less than 90° will align the torch axis parallel to the substrate such that at 0° virtually no particles impact the substrate.

\* Corresponding author.

ranging from 90 to 45° on the properties of molybdenum and alumina coatings. The porosity and surface roughness increased with the decrease of the spray angle, although only a slight change in porosity was reported. The adhesion and cohesion strengths were found to increase as the spray angle decreased, and deposition efficiency decreased with a decrease in spray angle. The morphology of splats was observed to vary with spray angle, i.e. the deposit splats tended to orient on the plane perpendicular to the spray direction. The properties of coatings sprayed at the angles down to 45° were not inferior to coatings sprayed at 90°.

Tucker and Price [3] also reported data dealing with the influence of spray angles on the mechanical properties of tungsten carbide–cobalt-based materials. They also observed similar microstructural changes with spray angle and found that there was no significant change in wear properties with spray angle.

In the current research, tests have been performed to characterize the properties of off-angle sprayed deposits, as well as a mathematical modeling of spray patterns which may be employed to optimize spraying processes in the spray-forming of complex-shaped parts.

## 2. Model of off-angle spraying

### 2.1. Macroscopic analysis

Materials deposited by thermal-spray processing exhibit a mass distribution across the substrate. This distribution, in the first instance, can be approximated by a Gaussian distribution. Fig. 1 depicts a typical configuration of a thermal spray system which shows the gun, spray jet, powder feeder, target and particle trajectory. It is assumed that the spray pattern is conical and symmetrical with the centerline of the torch. When the spray gun is tilted, the distribution of deposited materials would deviate from the Gaussian distribution.

The Gaussian probability distribution function [ $P(x)$ ]

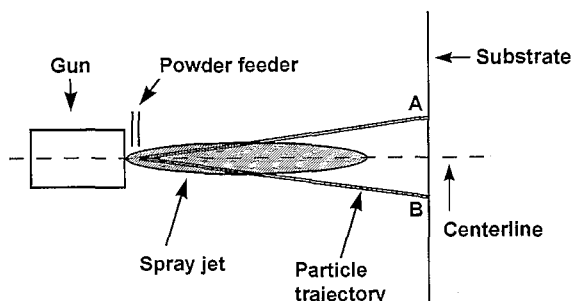


Fig. 1. Typical configuration of thermal spraying.

is expressed as:

$$P(x) = \frac{1}{\sqrt{\pi}\sigma} \exp \left[ -\frac{(x-\mu)^2}{2\sigma^2} \right], \quad -\infty < x < \infty \quad (1)$$

where  $\sigma$  is the standard deviation and  $\mu$  is the mean. In the case of spraying at 90° it is convenient to set  $\mu$  to zero.

Fig. 2 shows the geometry of the spray process with a spray torch tilted by an angle  $\alpha$ . For a certain spray angle  $\alpha$ , the above equation can be transformed into a general form as a function of  $x$  and  $\alpha$  (see Appendix A):

$$P'(x, \alpha) = \frac{1}{\sqrt{2\pi}\sigma_{90}} d^2 \frac{\cos(90-\alpha)}{[d-x\sin(90-\alpha)]^2} e^{-\frac{\left[ \frac{dx \cos(90-\alpha)}{d-x\sin(90-\alpha)} \right]^2}{2\sigma_{90}^2}} \quad (2)$$

where  $\alpha$  is the spray angle,  $\sigma_{90}$  is the standard deviation at a 90° spray angle, and  $d$  is the spray distance. Fig. 3 shows simulated distributions of spray deposits for spray angles from 90 to 30° when the stand-off distance ( $d$ ) was 240 mm and the diameter of the perpendicular section through the cone at the substrate (line AB in Fig. 2) was 60 mm. This analysis assumed that the deposition efficiency was not influenced by the angle of particle impact, i.e. the area under each curve was unity. As will be shown later, these distributions would not exhibit equal areas at non-orthogonal angles. Thus, the cone angle can be determined as 14° and the standard deviation of the deposit pattern (or “spray print”) at a 90° spray angle is 30.6 mm (see Appendix A).

In practical situations, these parameters vary with gun types and spray parameters. Furthermore, the particle trajectory centerline does not necessarily coincide with the torch centerline but shifts to either side [1,4]

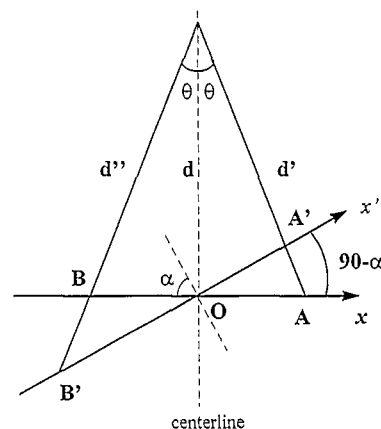


Fig. 2. Schematic of spray geometry. The torch is aligned along the dashed centerline, while the substrate orientation varies from AB to A'B' at angles  $\alpha$  with respect to the normal orientation.

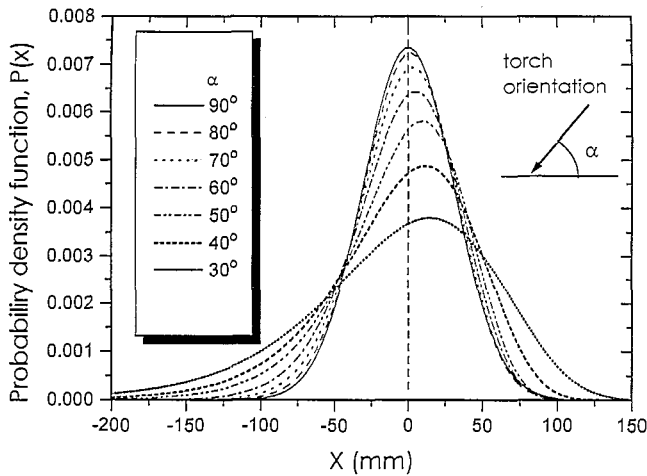


Fig. 3. Probability distribution of spray pattern for seven spray angles.

and the mass flux at the edge of the spray pattern would be diminished since the unmelted/resolidified particles would tend to rebound from the substrate. The deposit patterns at less than a 90° spray angle showed an asymmetry which increased as the spray angle decreased. The mean ( $\mu$ ) and the skewness ( $\mu_3$ ) are defined as:

$$\mu = \int_{-\infty}^{\infty} xP'(x, \alpha) dx \quad (3)$$

$$\mu_3 = \frac{\int_{-\infty}^{\infty} (x - \mu)^3 P'(x, \alpha) dx}{\sigma^3} \quad (4)$$

The mean value varied with the spray angle (Fig. 4), i.e. the centroid of the mass of the deposit pattern deviated from the centerline of the torch as the spray angle decreased. The skewness, which describes the symmetry of the mass distribution (see Fig. 3), of 90° deposit pattern was 0 and decreased with the spray angle (Fig. 5).

The spray distance is a critical spray parameter in

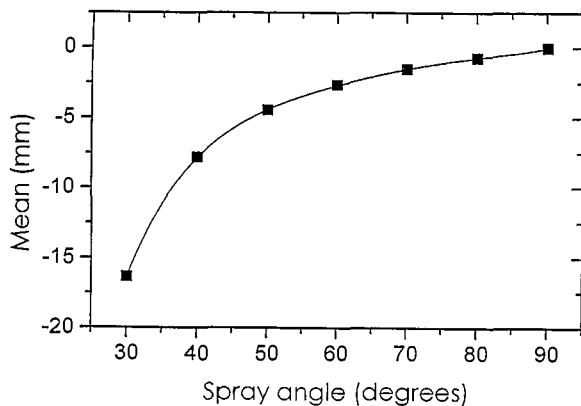


Fig. 4. Mean values of spray pattern distribution for different spray angles (90° is the optimum spray angle).

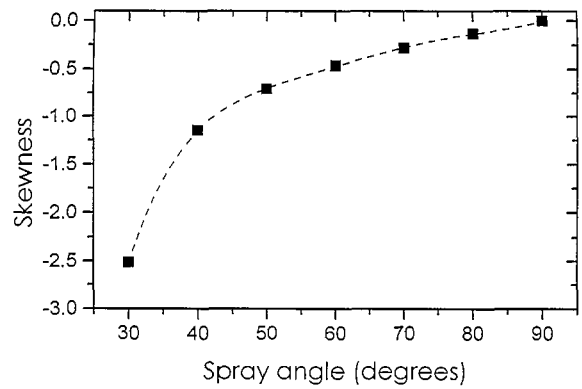


Fig. 5. Skewness of spray pattern distribution for different spray angles (90° is the optimum spray angle).

determining the property of sprayed deposits. The “local spray distance” gradually decreases from point B' to A' (on vector  $x'$  of Fig. 2) and the difference of the spray distance between the two points became larger as the spray angle ( $\alpha$ ) decreased. In Fig. 6 the local spray distance arising from off-angle spraying is normalized with respect to the torch centerline distance. This simple calculation indicated a -15 to +23% change in the optimum spray distance for the  $\pm 30.6$  mm spray print of the 50° torch–substrate orientation. Thus, the smaller spray angle would yield a more inhomogeneous deposit. This effect can be neglected at high spray angles (say, from 90 to 80°) because the conical spray jet produces a slight variance of spray distance from point A to B or A' to B'.

## 2.2. Microscopic analysis

The morphology of splats changes with respect to spray angle. [5,6] An example is illustrated in Fig. 7, where a molten particle impacts the substrate at an

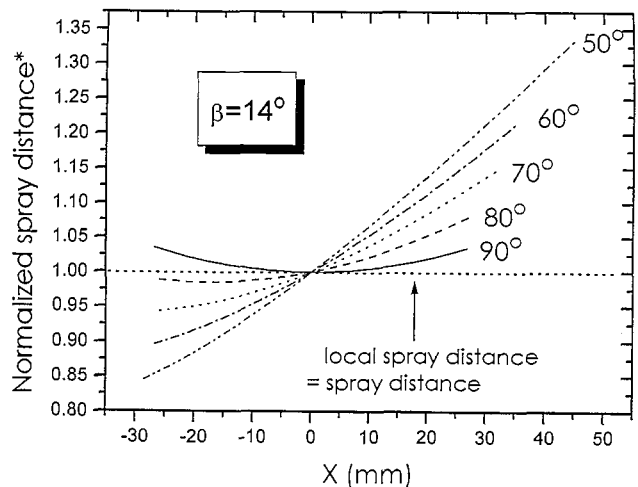


Fig. 6. Variation of local spray distance with different spray angles. \*Normalized spray distance = local spray distance/spray distance.



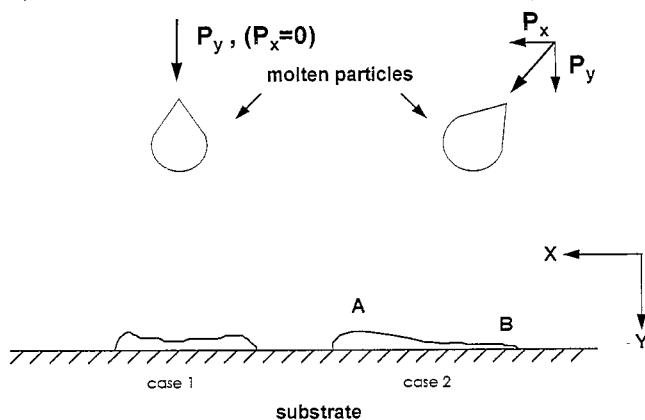


Fig. 7. Splat formation model.

angle other than  $90^\circ$ , i.e. if Cartesian coordinates are introduced, the particle impacts the substrate with  $x$  and  $y$  components of momentum  $P_x$  and  $P_y$ , respectively, whereas the particle traveling perpendicular to the substrate has a zero  $x$  component, i.e.  $P_x=0$ . The  $P_x$  component promotes particle spreading over the substrate rather than impacting on the substrate, and thus a thin and flat splat is created, i.e.  $P_x$  can be identified as a “spreading” momentum and  $P_y$  as an “impacting” momentum. The  $P_y$  component is smaller than that of a  $90^\circ$  impacting particle because the overall energy is divided into two components rather than one. Therefore, the deposit porosity would be expected to change with respect to spray angle (see Section 4.1 because the particles of low  $P_y$  do not impact the substrate with a sufficiently high momentum to consolidate the thermal spray coating structure. An asymmetric splat morphology is expected to occur because  $P_x$  contributes to the spreading of unsolidified materials toward point A (Fig. 7) during the solidification process. This phenomenon is dependent on material properties such as substrate surface roughness, substrate temperature, heat conductivity of substrate and solidification kinetics. [2,7–9] A rough substrate, for example, would prevent particles from spreading, and ceramic materials with high melting points would spread less than metals before solidification.

### 3. Experimental procedure

#### 3.1. Materials and sample preparation<sup>2</sup>

Two materials, NiAl (Metco 450NS) and  $\text{Cr}_3\text{C}_2$ -NiCr (Metco 81VFNS), were sprayed onto steel substrates to determine the influence of the spray angles on characteristics of the thermal spray coatings. The NiAl was prepared at subsonic and  $\text{Cr}_3\text{C}_2$ -NiCr at supersonic

(Mach 2) velocity. The spray equipment was a Miller Thermal SG-100<sup>®</sup> plasma gun and model 3620 control console. The chemical compositions of the feedstock materials are given in Table 1. The particle size distribution was measured using MicroTrac<sup>®</sup> equipment (Fig. 8).

Ten samples were sprayed onto disk-shaped substrates (25.4 mm (1 in) diameter and 6.4 mm (0.25 in) thick) for tensile adhesion tests (TATs) and on 25.4 mm (1 in)  $\times$  31.8 mm (1.25 in) panels for surface roughness, hardness, and metallography at angles of 50, 60, 70, 80 and  $90^\circ$  for both NiAl and  $\text{Cr}_3\text{C}_2$ -NiCr.

#### 3.2. Surface roughness test

The arithmetical average [10] of the coatings was measured using a SurfTest III<sup>®</sup> profilometer (Mitutoyo

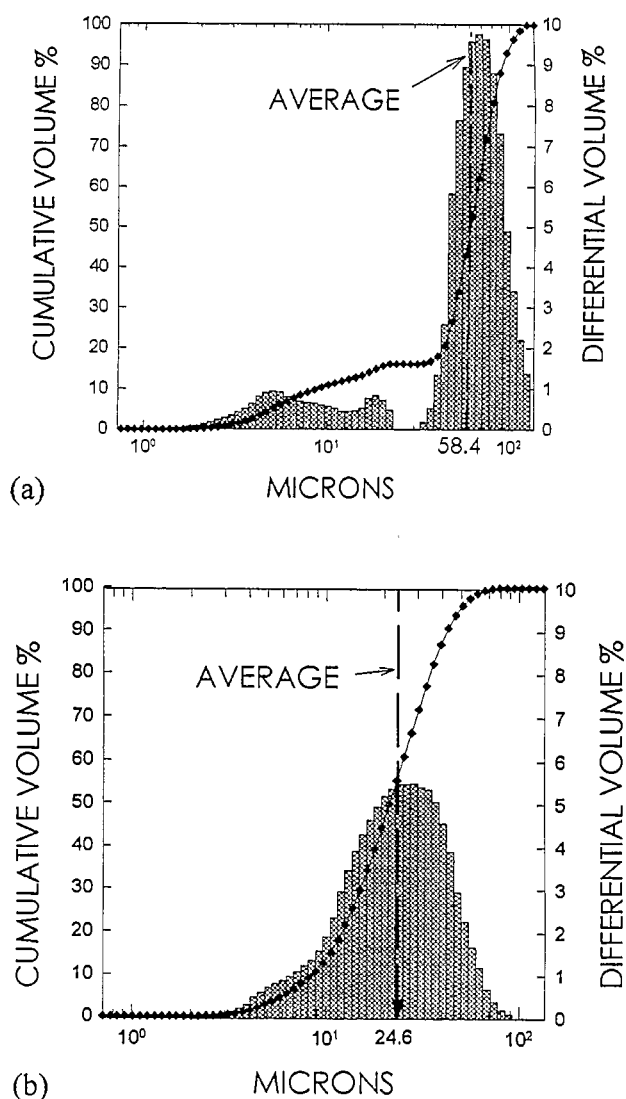


Fig. 8. Particle size distribution of (a) NiAl and (b)  $\text{Cr}_3\text{C}_2$ -NiCr powders (the bimodal distribution for the NiAl composite powder arises from de-adhesion of the aluminum particles from the nickel core).

<sup>2</sup>This study was conducted on materials supplied by Metco, Inc. This company is now known as Sulzer-Metco, Inc.

Table 1

	Components	Content (w.%)	Minimum (%)	Maximum (%)
NiAl Powder	Aluminum	4.320	4.000	5.500
	Nickel	93.430	93.000	0.000
	Organic solids	2.200	0.000	2.500
	Others total	0.050	0.000	1.000
Cr <sub>3</sub> C <sub>2</sub> –NiCr powder				
Chromium carbide powder (75%)	Carbon	13.1	12.5	
	Silicon	0.08		0.10
	Chromium	86.14	85.50	
	Iron	0.23		0.70
Nickel chromium alloy (25%)	Carbon	0.01		0.25
	Manganese	0.88		2.50
	Silicon	1.00		1.50
	Chromium	20.09	18.00	22.50
	Nickel	77.89	76.00	80.00
	Iron	0.13		1.00

MFG. Co. Ltd.). The cut-off value and stylus transverse speed were 0.8 mm and 6 mm s<sup>-1</sup>, respectively. The measurement range was 30 µm for NiAl coatings and 10 µm for Cr<sub>3</sub>C<sub>2</sub>–NiCr coatings.

### 3.3. Tensile adhesion test (TAT)

#### 3.3.1. Test fixture

The tensile adhesion test (TAT) was based on ASTM C 633. [11] The disk-shaped coupons were glued to the usual TAT fixtures so that a tensile force could be applied to the coating. The configuration of the test was similar to that specified by ASTM C 633, except that the pull-off bar had an 8 mm (5/16 in) diameter hole through which a dowel pin passed instead of a tapped hole as specified by ASTM C633. Another distinction is that the pull-off bar is slightly longer (30.48 mm (1.2 in)) than that recommended by the ASTM standard (25.4 mm (1 in)). This pull-off bar would produce different test results (by ~20% higher) from ASTM C 633 because of the different stress distribution near the testing area. [12,13] However, the test results are still valid for relative comparisons.

#### 3.3.2. Specimen assembly

The test coupon was placed between the two pull-off bars and attached using an adhesive. The surfaces of the pull-off bars and the test coupons (except the coating) were grit-blasted to enhance the adhesion of the epoxy. After curing, excess epoxy was removed using emery paper. Table 2 summarizes the test conditions.

Good alignment of the test assembly (two pull-off bars and the test coupon) was achieved by using a self-aligning jig during epoxy curing.

### 3.4. Microhardness test

Microhardness tests were performed using a Micromet II® (Buehler Ltd., Lake Bluff, Illinois) hardness tester. The measurement was made on the cross-section with one diagonal of the indenter parallel to the interface. The samples were polished using an Automet®2/Ecomet®3 automated polishing machine under the conditions shown in Table 3. The indenter load for the NiAl coating was 300 and 500 gf for the Cr<sub>3</sub>C<sub>2</sub>–NiCr coating. The duration of loading was 15 s for both materials. The indentations were applied near the center line of the coating thickness, and the distance between the indentations was at least three times the diagonal to prevent stress-field effects from nearby indentations.

### 3.5. Interfacial fracture toughness

An indentation technique was used to measure the interfacial critical strain energy release rate of the coatings. The applied load was 1 kgf and other test conditions and the sample preparations were the same as the microhardness test. The indentation was applied to the interface of the coating and the substrate with an indenter diagonal aligned with the interface.

### 3.6. Porosity

Optical image analysis (Omnimet®1, Buehler Ltd., Lake Bluff, Illinois) was used to measure the porosity of the coatings. The cross-sections of samples were polished with the conditions presented in Table 3. Ten frames were measured and then averaged for each sample.

Table 2

Test instrument and model no.	Hydraulic Instron (Instron Corp., Canton, MA), AW2414-1
Load cell capacity	200 kN
Crosshead speed	0.013 mm s <sup>-1</sup> (0.030 in min <sup>-1</sup> )
Diameter of pull-off bar	25.4 mm (1 in)
Length of pull-off bar	30.5 mm (1.2 in)
Adhesive bonding agent	Liquid epoxy (Master Bond EP15, Hackensack, NJ)
Adhesive curing temperature	170 ± 6°C (340 ± 10°F)
Adhesive curing time	60 min, under pressure (about 0.3 MPa)

Table 3

Grinding	Time (min) <sup>a</sup>	Force, N sample <sup>-1</sup> (lb sample <sup>-1</sup> )	rad s <sup>-1</sup> (rpm)
240 grit SiC paper	3 [3]	13.3 (3)	25.1 (240)
45 µm diamond	3 [5]	22.2 (5)	25.1 (240)
9 µm diamond	5 [10]	22.2 (5)	8.4 (80)
3 µm diamond	6 [10]	22.2 (5)	12.6 (120)
0.05 µm alumina	3 [5]	22.2 (5)	12.6 (120)

<sup>a</sup>The bracketed numbers are for Cr<sub>3</sub>C<sub>2</sub>-NiCr coatings, and the unbracketed data are for NiAl.

## 4. Results and discussion

### 4.1. Porosity

The porosity increased from 2.1 to 4.5% for Cr<sub>3</sub>C<sub>2</sub>-NiCr and from 2.5 to 4.2% for NiAl when the spray angle changed from 90 to 50° (Fig. 9). The porosity of Cr<sub>3</sub>C<sub>2</sub>-NiCr coatings was more sensitive to the spray angle, with significant changes occurring at 70° compared to a lower angle of 60° for the NiAl feedstock porosity. The decrease in porosity was partly because the *Y* component of particle momentum (Fig. 7), as explained in Section 2, decreased with spray angle, i.e. higher impacting momentum of molten particles produced a denser deposit. In addition, when the

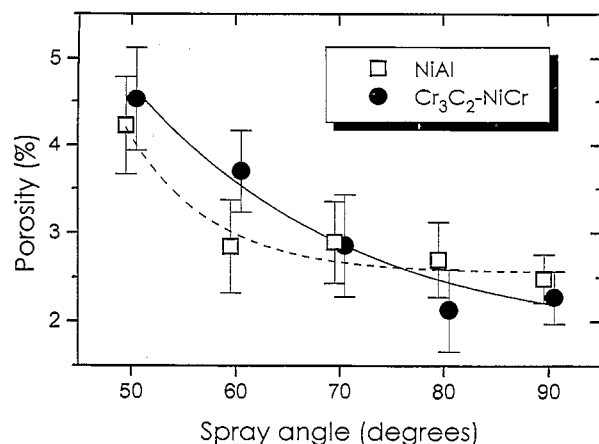
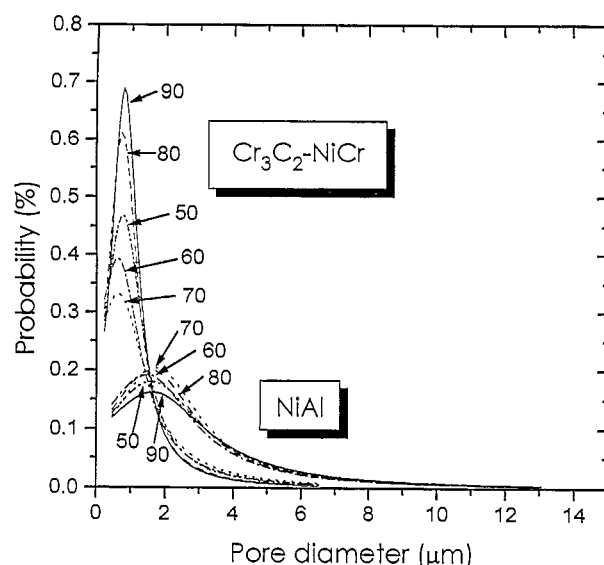


Fig. 9. Variation of porosity with spray angles.

particles impinge on the substrate at smaller angles the particles would not effectively cover the roughened surface of the substrate or previously deposited splats (i.e. a shadow effect). On the other hand, particles sprayed at 90° to the substrate covered the irregular contours more effectively.

Pore-size distributions were obtained using the Schwartz-Saltykov method [14,15]. Fig. 10 represents the pore size distribution of the two materials at five different spray angles. For Cr<sub>3</sub>C<sub>2</sub>-NiCr coatings, most of pores were within the range 0–2 µm, and for NiAl coatings 0–4 µm. The spray angle changed the pore size distribution of the Cr<sub>3</sub>C<sub>2</sub>-NiCr coating, i.e. spray angles less than 80° produced larger pores. The “shadow effect” accounts for the change in pore size distribution, i.e. it increases as the spray angle decreases, and therefore contributes to the larger pore size. The pore size increase is also attributed to the deviation of the local spray distance from the optimum condition, which leads to improper melting of particles and a smaller flattening degree of the impacting particles. NiAl coatings did not show notable changes in pore size distributions with spray angle.

Fig. 10. Pore size distribution of Cr<sub>3</sub>C<sub>2</sub>-NiCr and NiAl for different spray angles.

#### 4.2. Surface roughness

Fig. 11 shows the surface roughness of NiAl and  $\text{Cr}_3\text{C}_2\text{-NiCr}$  coatings sprayed at various angles. The surface roughness was strongly dependent on the particle size of the sprayed powder (see Fig. 8), and was related to the porosity level. The surface roughness values of NiAl coatings tended to decrease as the spray angle increased. On the other hand,  $\text{Cr}_3\text{C}_2\text{-NiCr}$  coatings showed no such trend with respect to spray angle.

#### 4.3. Microhardness test

Fig. 12 illustrates the results of the microhardness tests of NiAl and  $\text{Cr}_3\text{C}_2\text{-NiCr}$  coatings at five different spray angles. The  $\text{Cr}_3\text{C}_2\text{-NiCr}$  coatings exhibited hardness values between 600 and 700 VHN, and the NiAl data were between 130 and 150 VHN. The mean value of hardness data of both coatings decreased slightly (9% decrease for  $\text{Cr}_3\text{C}_2\text{-NiCr}$  and 8% for NiAl) when spray-

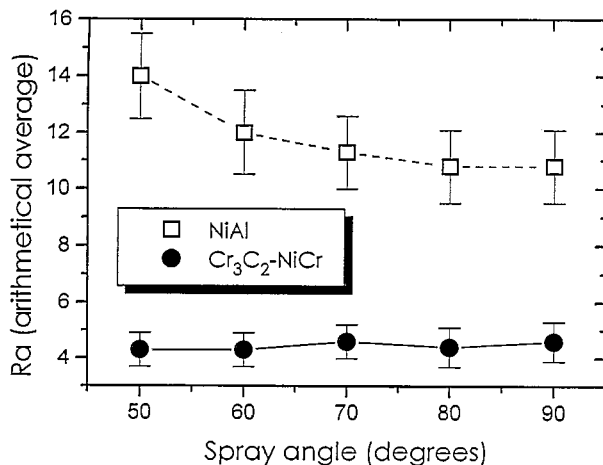


Fig. 11. Surface roughness of  $\text{Cr}_3\text{C}_2\text{-NiCr}$  and NiAl coatings ( $\mu\text{m}$ ).

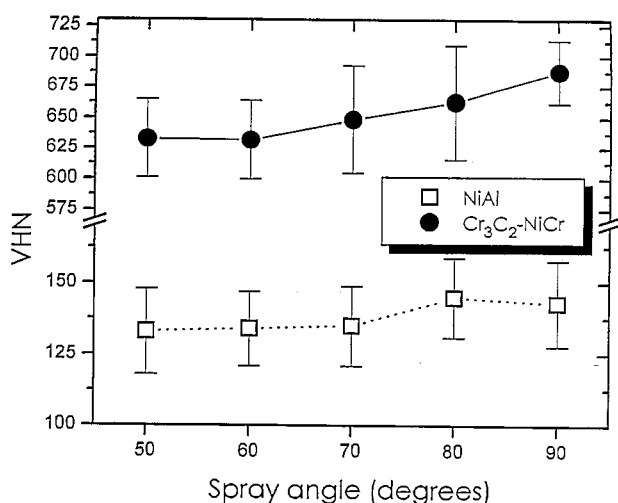


Fig. 12. Microhardness of  $\text{Cr}_3\text{C}_2\text{-NiCr}$  and NiAl coatings.

ing at angles of less than  $90^\circ$ . The data points of NiAl were more widely distributed than those of  $\text{Cr}_3\text{C}_2\text{-NiCr}$  and the standard deviations of data did not show any dependence on spray angle (Table 4).

A Weibull analysis is a method of finding a parameter to assess the variability of the data and to index the reliability of materials. Fig. 13 compares Weibull plots of the two coatings with different spray angles. The Weibull moduli and the characteristic values for the two materials are listed in Table 4. The Weibull moduli exhibited no trends of change with spray angles and the values existed in quite narrow ranges.

The Weibull modulus ( $m$ ), and the characteristic strength ( $X_0$ ) can also be obtained using the maximum likelihood method; [16] and the values obtained are quite similar to the graphical method determined from the Weibull plot. The 90 and 95% confidence intervals of the Weibull moduli [15] are constructed in Fig. 14 and show that the Weibull moduli were essentially independent of spray angle. The Weibull modulus of 6–18 for NiAl coatings can be compared to 6.8–12.5 for a NiCoCrAlY bond coat [15]. The  $\text{Cr}_3\text{C}_2\text{-NiCr}$  coatings exhibited high Weibull moduli; this was attributed to the hypersonic spraying process, whereas ceramic deposits normally exhibit values in the range of 4–6. The higher Weibull modulus of  $\text{Cr}_3\text{C}_2\text{-NiCr}$  coatings compared to NiAl can be also inferred by the pore size distribution. Thus, the  $\text{Cr}_3\text{C}_2\text{-NiCr}$  coating had a large number of smaller pores, whereas NiAl exhibited larger pores with a wider size distribution. The small area of the microhardness test (35–40  $\mu\text{m}$  diagonal for  $\text{Cr}_3\text{C}_2\text{-NiCr}$  and 60–70  $\mu\text{m}$  diagonal for NiAl under the conditions used in the current study) examined only the properties of a limited area. Therefore, the more homogeneous  $\text{Cr}_3\text{C}_2\text{-NiCr}$  coating resulted in higher Weibull modulus values.

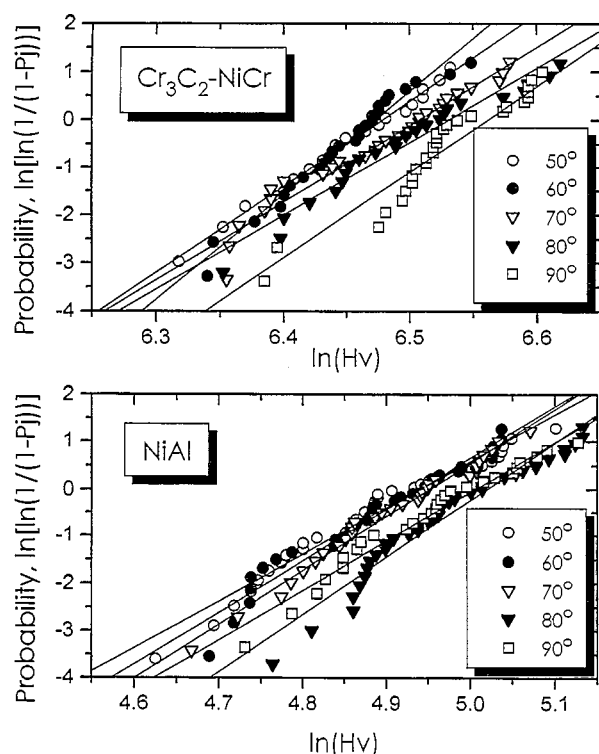
#### 4.4. Interfacial critical strain energy release rate

The experimental results of interfacial critical strain energy release rate ( $\mathcal{G}_c$ ) for NiAl and  $\text{Cr}_3\text{C}_2\text{-NiCr}$  coatings on steel substrates are presented in Fig. 15. The  $\mathcal{G}_c$  values increased slightly with spray angle for both coatings, with the exception of the  $\text{Cr}_3\text{C}_2\text{-NiCr}$  materials sprayed at  $90^\circ$ .

Weibull plots of interfacial fracture toughness for the two materials are presented in Fig. 16. NiAl coatings had slightly higher Weibull moduli than  $\text{Cr}_3\text{C}_2\text{-NiCr}$  coatings. Spray angle did not influence the Weibull moduli, and high variance in data (up to 49%) was measured for both coatings (Table 5). Both materials exhibited low Weibull modulus values: 2.3–3.9 for  $\text{Cr}_3\text{C}_2\text{-NiCr}$  coatings and 2.8–3.2 for NiAl coatings. The low Weibull moduli were attributed to the following causes. The contour of the interface between the coating and the substrates was irregular due to the grit-blasting prior to spraying, and it is difficult to align the indenter

Table 4

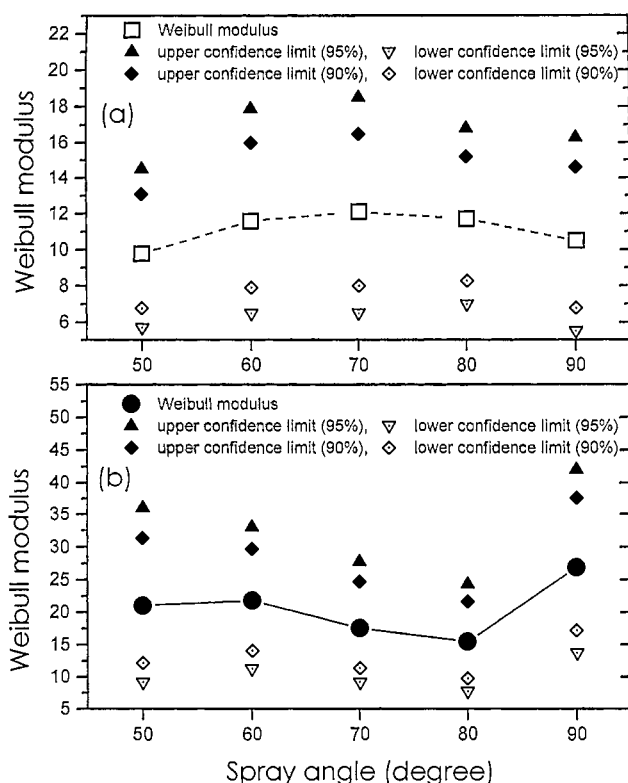
Material	Spray angle (°)	Number of tests	Mean (VHN)	Std. dev. (VHN)	Coefficient of variance (%)	Weibull modulus	Characteristic value (VHN)
Cr <sub>3</sub> C <sub>2</sub> -NiCr	50	19	633	32	5	18.0	650
	60	26	632	32	5	21.8	647
	70	28	649	44	7	16.2	669
	80	24	663	47	7	16.2	685
	90	29	687	41	6	18.0	706
NiAl	50	36	133	15	11	9.9	140
	60	34	134	13	10	11.0	140
	70	30	135	14	10	11.4	141
	80	40	145	14	10	12.1	151
	90	28	143	15	10	10.4	149

Fig. 13. Weibull plot of microhardness for Cr<sub>3</sub>C<sub>2</sub>-NiCr and NiAl coatings.

precisely to the interface because of the nature of the interface. In addition to the cracks at the interface originating from the indentation tip, many other cracks were observed near the indentation, which made interpretation difficult. Another distinction was that there are three types of crack path: (1) at the interface, (2) in the first or second layer of splats, or (3) both (1) and (2), which can be substantial factors in lowering the Weibull modulus.

#### 4.5. Tensile adhesion test (TAT)

Fig. 17 shows the experimental results of TATs performed on NiAl and Cr<sub>3</sub>C<sub>2</sub>-NiCr coatings. The adhesion

Fig. 14. Confidence interval of Weibull moduli for (a) NiAl and (b) Cr<sub>3</sub>C<sub>2</sub>-NiCr coatings. Lines indicate the trend in the average Weibull modulus.

strength increased with spray angle: NiAl sprayed at 90° exhibited approximately 5% higher values than NiAl sprayed at 50°, and Cr<sub>3</sub>C<sub>2</sub>-NiCr at 90° was about 20% higher.

The mean fracture toughness from a TAT was converted to critical strain energy release rate ( $\mathcal{G}_{IC}$ ) (Fig. 18). The  $\mathcal{G}_{IC}$  values ranged from 15.8 to 17.6 J m<sup>-2</sup> for NiAl coatings and from 16.8 to 23.7 J m<sup>-2</sup> for Cr<sub>3</sub>C<sub>2</sub>-NiCr and can be compared to those obtained from indentation tests (see Section 4.4,

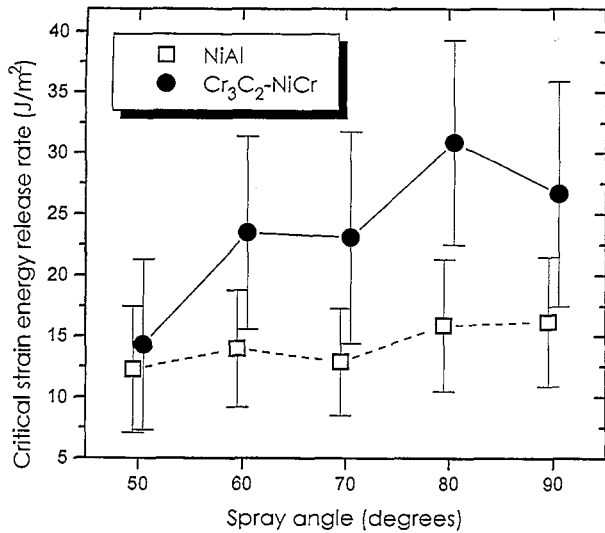


Fig. 15. Interfacial critical strain-energy release rate of Cr<sub>3</sub>C<sub>2</sub>-NiCr and NiAl coatings.

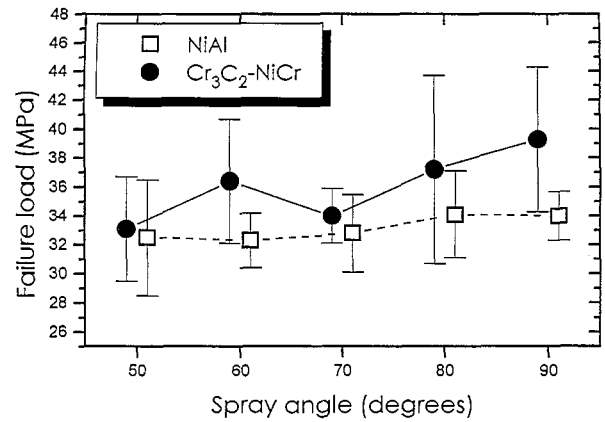


Fig. 17. TAT results of Cr<sub>3</sub>C<sub>2</sub>-NiCr and NiAl coatings.

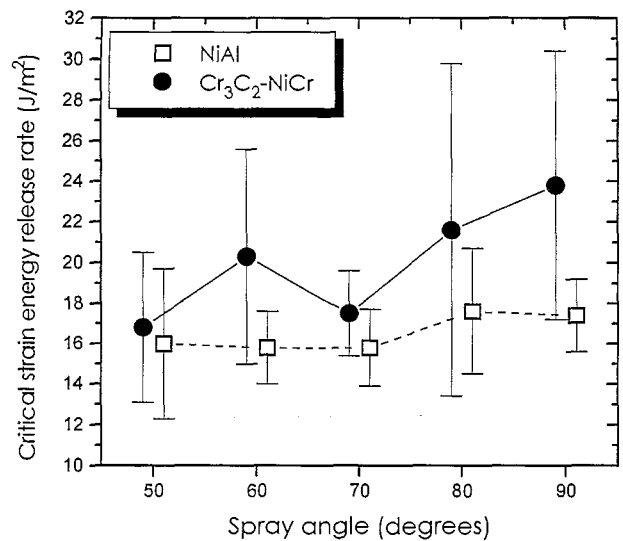


Fig. 18. Critical strain-energy release rate calculated from TAT data of Cr<sub>3</sub>C<sub>2</sub>-NiCr and NiAl coatings.

decreased with decreasing spray angles. By spraying at 90° denser structures with enhanced mechanical properties were achieved.

The influence of spray angle on the properties of deposits was attributed to the change in the local spray distance, and the impacting momentum. The local spray distance deviated from the optimum spray distance and this phenomenon became more pre-eminent as the spray angle decreased. The impacting momentum of the particle decreased with decreasing spray angle, which resulted in higher porosity and weaker bonding between lamellae (or between lamella and substrate).

## 5. Concluding remarks

The effects of spray angle on the thermal spraying process and the properties of thermal spray deposits of NiAl and Cr<sub>3</sub>C<sub>2</sub>-NiCr have been investigated. A simple

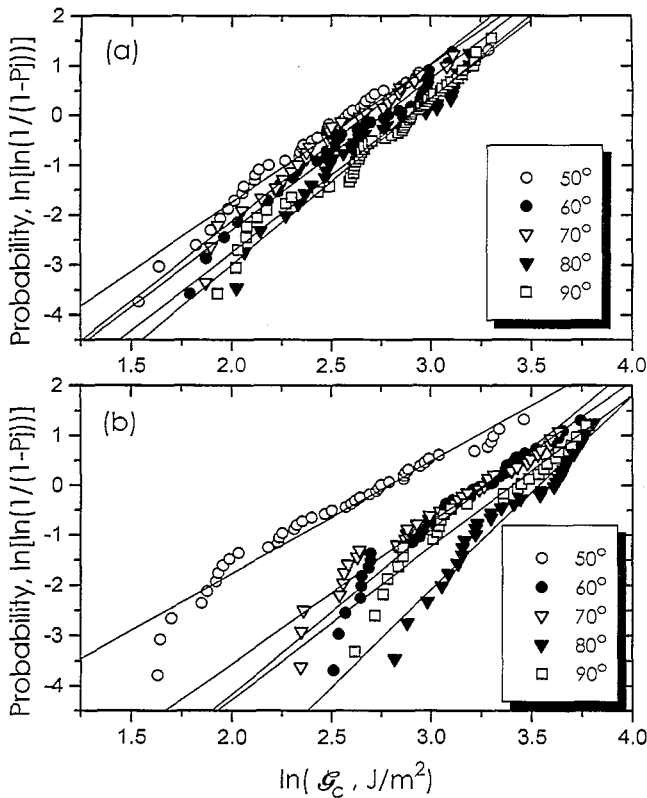


Fig. 16. Weibull plot of interfacial critical strain-energy release rate for (a) NiAl and (b) Cr<sub>3</sub>C<sub>2</sub>-NiCr coatings.

12.3–16.2 J m<sup>-2</sup> for NiAl and 14.3–30.9 J m<sup>-2</sup> for Cr<sub>3</sub>C<sub>2</sub>-NiCr.

The properties of thermal spray coatings are determined by several spray conditions. Spray angle has an influence on the mechanical properties: microhardness, adhesion strength and interfacial fracture toughness



Table 5

Material	Spray angle (°)	Number of tests	Mean (J m <sup>-2</sup> )	Std. dev. (J m <sup>-2</sup> )	Coefficient of variance (%)	Weibull modulus	Characteristic value (J m <sup>-2</sup> )
Cr <sub>3</sub> C <sub>2</sub> -NiCr	50	43	14.3	7.0	49	2.3	16.1
	60	39	23.5	7.9	34	3.3	26.3
	70	37	23.1	8.7	38	2.8	26.0
	80	31	30.9	8.4	27	3.9	34.2
	90	27	26.7	9.2	34	3.0	30.0
NiAl	50	41	12.3	5.2	42	2.8	13.8
	60	35	14.0	4.8	34	3.1	15.7
	70	28	12.9	4.4	34	3.2	14.4
	80	31	15.9	5.4	34	3.1	17.9
	90	54	16.2	5.3	33	3.1	18.1

mathematical model of deposit patterns at various spray angles has been formulated. The deposit pattern at a 90° spray angle was assumed to exhibit a Gaussian distribution. The deposit pattern deviated from the Gaussian distribution and the centroid of mass shifted to either side of the distribution as the spray angle decreased.

The porosity decreased with the spray angle for both materials. The surface roughness of NiAl was sensitive to spray angle, whereas Cr<sub>3</sub>C<sub>2</sub>-NiCr was not. The high porosity at low spray angles was attributed to the lower impacting momentum of particles as well as the low incident angle of particles impinging on the substrate. This phenomenon promoted conditions where the forming coating was less effective in covering the rough surface of the substrate or previously deposited particles.

The mechanical properties such as microhardness, adhesion strength and interfacial fracture toughness are altered by changes in the spray angle.

### Acknowledgement

The authors would like to thank R. West and B. Palmieri (Howmet Corporation, 30 Corporate Drive North Haven, CT 06473) for sample preparation. The authors also wish to acknowledge S.M. Yi (Department of Mathematics, SUNY at Stony Brook) for his contribution to mathematical modeling of the spray print.

### Appendix A

#### Derivation of general equation of distribution for spray angle $\alpha$

The equation of a Gaussian distribution is:

$$P(x) = \frac{1}{\sqrt{\pi}\sigma} \exp\left[-\frac{(x-\mu)^2}{2\sigma^2}\right], \quad -\infty < x < \infty$$

In order to obtain a distribution equation on the  $x$  axis,

$x$  should be transformed to  $x'$ :

$$\frac{x}{x'} = \frac{\sin[90-(\alpha-\theta)]}{\sin(90-\theta)} \quad (\text{A1})$$

Since  $(90-X) = \cos X$  and  $\cos(X-Y) = \cos X \cos Y + \sin X \sin Y$ :

$$\begin{aligned} \frac{x}{x'} &= \frac{\cos(\alpha-\theta)}{\cos\theta} = \frac{\cos\alpha \cos\theta + \sin\alpha \sin\theta}{\cos\theta} \\ &= \cos\alpha + \sin\alpha \tan\theta \end{aligned} \quad (\text{A2})$$

Therefore, if  $\tan\theta$  is replaced by  $x/d$  and then (Eq. (A2)) is arranged for  $x$ :

$$x = \frac{dx' \cos\alpha}{d - x' \sin\alpha} \quad (\text{A3})$$

Substituting (Eq. (A3)) into (Eq. (1)) and setting  $\mu=0$ :

$$P(x, \alpha) = \frac{1}{\sqrt{2\pi}\sigma} e^{-\frac{\left[\frac{dx \cos(90-\alpha)}{d - x \sin(90-\alpha)}\right]^2}{2\sigma^2}} \quad (\text{A4})$$

The function  $P$  is a probability function, and thus the integration of function  $P$  from  $-\infty$  to  $+\infty$  with regard to  $x$  should be 1, i.e.:

$$\int_{-\infty}^{\infty} P(x) dx = \int_{-\infty}^{\infty} P(x', \alpha) \frac{dx}{dx'} dx' = 1 \quad (\text{A5})$$

Meanwhile, the integration of  $P(x', \alpha)$  with regard to  $x'$  is larger than 1. Therefore, a general equation for a certain spray angle  $P'(x', \alpha)$  is obtained:

$$P'(x', \alpha) = P(x', \alpha) \frac{dx}{dx'} \quad (\text{A6})$$

After a simple calculation of  $\frac{dx}{dx'}$ , (Eq. (A6)) turns out

to be:

$$P'(x', \alpha) = \frac{1}{\sqrt{2\pi}\sigma} d^2 \times \frac{\cos(90-\alpha)}{[d-x' \sin(\alpha)]^2} e^{-\frac{\left[\frac{dx' \cos(90-\alpha)}{d-x' \sin(90-\alpha)}\right]^2}{2\sigma^2}} \quad (\text{A7})$$

#### 7.0.1. Calculation of standard deviation

To estimate the standard deviation of the Gaussian distribution, the concept of tolerance limit can be used. An interval covers a fixed portion of the population distribution with a specified confidence, and the end point of such intervals are called tolerance limits. Tolerance intervals are of the form:

$$\bar{X} \pm C_{T,P}(n)s \quad (\text{A8})$$

where  $C_{T,P}(n)$  is a constant which is determined so that the interval covers a certain percentage such as 90%, 95%, or 99% of the population with confidence  $\gamma$ ,  $s$  is a standard deviation, and  $\bar{X}$  is a mean. In this case  $\bar{X}$  is zero and the confidence limit can be considered as the perpendicular section of the cone at the substrate (line AB in Fig. 2), and thus the standard deviation can be calculated.

## Appendix B

### Background to interfacial fracture toughness measurement

Numerous techniques exist to obtain the fracture toughness or critical strain-energy release rate of materials [17–19]. The indentation test evaluates the interfacial fracture toughness of thermal spray coatings [20–22]. The Vickers indenter introduces a mechanically stable crack into the interface of the coating and the substrate. The resistance of crack propagation along the interface is considered to be a measure of adhesion, and is expressed as a fracture mechanics parameter such as critical strain-energy release rate or critical stress intensity factor. A Vickers indenter was directly applied to the interface of the coating and the substrate. The crack length was then measured to determine the critical strain energy release rate,  $\mathcal{G}_c$ . Special care was taken to place the indenter tip exactly on the interface and to align the indenter diagonal with the interface. According to Willis [23] the critical strain energy release rate  $\mathcal{G}_c$  is given by:

$$\mathcal{G}_c = \alpha \Phi(G_1, G_2, \nu_1, \nu_2) \Psi(E_1, E_2, H_1, H_2) \frac{a^4}{c^3} \quad (\text{A9})$$

with

$$\Phi(G_1, G_2, \nu_1, \nu_2) = \frac{b^2 - d^2}{b} (1 + 4k^2)$$

$$b = \frac{1 - \nu}{2\pi G_1} + \frac{1 - \nu_2}{2\pi G_2}$$

$$d = \frac{1 - G\nu_1}{4\pi G_1} - \frac{1 - 2\nu_2}{4\pi G_2}$$

$$k = \frac{1}{2\pi} \ln \left[ \frac{b+d}{b-d} \right]$$

$$\Psi(E_1, E_2, H_1, H_2) = \frac{1}{\left[ \frac{1}{E_1} + \frac{1}{E_2} \right]^2} \frac{1}{\left[ \sqrt{\frac{E_1}{H_1}} + \sqrt{\frac{E_2}{H_2}} \right]^2}$$

where  $H_1$  and  $H_2$  are hardness,  $G_1$  and  $G_2$  are the shear elastic moduli,  $\nu_1$  and  $\nu_2$  are the Poisson's ratios of the two materials,  $E_1$  and  $E_2$  are the Young's moduli of the coating,  $a$  and  $c$  are indentation impression and crack length, respectively,  $\alpha$  is a constant independent of the system indenter and specimen. In this case  $\alpha$  is 0.0197.

## Appendix C

### Background to fracture toughness calculation from TAT data

TAT data can be used to calculate the fracture toughness of thermal spray coatings. The specimen configuration of the TAT is regarded as a circumferentially cracked bar and the results can be analyzed in a same way as a fracture toughness test. The stress analysis from this type of specimen was conducted by Bueckner [24] and the fracture toughness is given by:

$$K_{IC} = P_c \times [-1.27 + 1.72(D/d)] \times D^{-3/2}$$

and

$$0.4 \leq d/D \leq 0.9$$

where  $K_{IC}$  is the fracture toughness ( $\text{N m}^{-3/2}$ ),  $P_c$  is the fracture force (N),  $D$  is the outside diameter of the bar ( $2.54 \times 10^{-2}$  m), an  $d$  is the inside diameter in the circumferentially notched bar (m).

## References

- [1] M.M. Fasching, F.B. Prinz and L.E. Weiss, *J. Thermal Spray Technol.*, 2 (1993) 45.
- [2] A. Hasui, S. Kitahara and T. Fukushima, *Trans. Nat. Res. Inst. Metals*, 12 (1970) 9.
- [3] R.C. Tucker, Jr. and M.O. Price, *Proc. Int. Symp. on Advanced Thermal Technology and Allied Deposits (ATTAC)*, Osaka, Japan, 13–15 May, 1988, p. 61.

- [4] W.D. Swank, J.R. Fincke and D.C. Haggard, *Proc. 5th National Thermal Spray Conference*, ASM International, Anaheim, CA, 7–11 June, 1993, p. 25.
- [5] G. Montavon, C. Coddet, S. Sampath, H. Herman and C.C. Berndt, *Proc. 7th National Thermal Spray Conference*, ASM International, Boston, MA, 20–24 June, 1994, p. 469.
- [6] M.F. Smith, R.A. Neiser and R.C. Dykhuizen, *Proc. 7th National Thermal Spray Conference*, ASM International, Boston, MA, 20–24 June, 1994, p. 603.
- [7] L. Bianchi, A. Geimaud, F. Blein, P. Lucchese and P. Fauchais, *J. Therm. Spray Technol.*, 4 (1995) 59.
- [8] S.J. Yankee and B.J. Pletka, *J. Therm. Spray Technol.*, 2 (1993) 271.
- [9] M. Vardelle, A. Vardelle, P. Fauchais and M.I. Boulos, *AIChE J.*, 29 (1983) 236.
- [10] ANSI B46.1-1978, *Surface Texture*, The American Society of Mechanical Engineers, New York, 1978.
- [11] ASTM C633-79, *Standard Test Method for Adhesion or Cohesion Strength of Flame Sprayed Coatings*, American Society for Testing and Materials, Warrendale, PA, 1992.
- [12] S.H. Leigh and C.C. Berndt, *J. Thermal Spray Technol.*, 3 (1994) 184.
- [13] W. Han, E.F. Rybicki and J.R. Shadley, *Proc. 13th International Thermal Spray Conference*, ASM International, Orlando, FL, 28 May – 5 June, 1992, p. 911.
- [14] E.E. Underwood, in R.T. DeHoff and F.N. Rhines (Eds.), *Quantitative Microscopy*, McGraw-Hill, New York, 1968, p. 149.
- [15] E.E. Underwood, *Quantitative Stereology*, Addison-Wesley, Reading, MA, p. 119.
- [16] C.K. Lin and C.C. Berndt, *J. Mater. Sci.*, 30 (1995) 111.
- [17] G.R. Anstis, P. Chantikul, B.R. Lawn and D.B. Marshall, *J. Am. Ceram. Soc.*, 64 (1981) 533.
- [18] S.D. Brown, B.A. Chapman and G.P. Wirtz, *Proc. 2nd National Thermal Spray Conference*, ASM International, Cincinnati, OH, 24–28 October, 1988, p. 147.
- [19] C.C. Berndt, in S.R. Valluri, D.M.R. Taplin, P. Rama Rao, J.F. Knott and S. Dubey (Eds.), *Advances in Fracture Research*, Vol. 4, Pergamon, Oxford, 1984, p. 2545.
- [20] D. Choulier, P. Fluzin and C. Coddet, *Proc. 6th International Conference on Heat Treatment of Metals*, ASM International, Chicago, IL, 28–30 September, 1988, p. 75.
- [21] D. Choulier and C. Coddet, *Proc. 12th International Conference on Thermal Spraying*, London, 4–9 June, 1989, Paper No. 45.
- [22] R. Dal Maschio, V.M. Sgavo, F. Rigoni, L. Beramini and E. Galvanetto, *Proc. 13th International Thermal Spray Conference*, ASM International, Orlando, FL, 28 May – 5 June, 1992, p. 947.
- [23] J.R. Willis, *J. Mech. Phys. Solids*, 19 (1971) 353.
- [24] H.F. Bueckner, *Fracture Toughness Testing and Its Applications*, ASTM STP 381, American Society for Testing and materials, Philadelphia, PA, 1965, p. 85.

#### Permission to publish

S.H. Leigh and C.C. Berndt, 'Evaluation of off-angle thermal spray', *Surf. Coat. Tech.*, 89 (1997) 213–224.

As an Elsevier journal author, you retain various rights including Inclusion of the article in a thesis or dissertation whether in part or in toto; see [http://www.elsevier.com/about/policies/author-agreement/lightbox\\_scholarly-purposes](http://www.elsevier.com/about/policies/author-agreement/lightbox_scholarly-purposes) for more information. As this is a retained right, no written permission is necessary. This extends to the online version of your thesis and would include any version of the articles including the final published versions provided that they are not available as individual downloads but only embedded within the thesis itself.

# Modeling the Coverage of Splat Areas Arising from Thermal Spray Processes

Andrew Siao Ming Ang,<sup>†,‡,§</sup> Christopher C. Berndt,<sup>‡,§</sup> Michelle Dunn,<sup>‡,§</sup> Mitchell L. Sesso,<sup>‡,§</sup>  
and Sun Yung Kim<sup>‡,§</sup>

<sup>‡</sup>Industrial Research Institute Swinburne, Swinburne University of Technology, Melbourne, Australia

<sup>§</sup>Swinburne University of Technology, H66, P.O. Box 218, Hawthorn 3122, Victoria, Australia

The coverage of a deposited material that arises from the integration of discrete splat areas is an essential parameter that needs to be understood during thermal spray processes. However, there is absence of a theoretical method to predict and estimate the area coverage per pass by a thermal spray torch; for example by the plasma spray process. In this study, a model is presented that calculates the splat area coverage for a thermal spray process of ceramic materials. A focused survey of the published literature takes into consideration experimental observations that are related to this work. The model accounts for physical events in thermal spray processes, such as the use of a mono-modal feedstock and size of spray stream. The model predictions for the area coverage of plasma sprayed yttria-stabilized zirconia (YSZ) ranged between 12% and 18% depending on the value assumed for the maximum flattening ratio. The results for the model were demonstrated via wipe studies where microscope glass slides were spray coated with YSZ and image analysis conducted. The average coverage calculated was approximately 13% for the sprayed images. The experiment verifies that the simulation results from the model predict adequately the splat area coverage of a thermal spray process.

## I. Introduction

COATING formation in a thermal spray process involves the rapid solidification and stacking of millions of micrometer sized splats that are created by impinging molten droplets. The coating properties depend on the formation processes of a lamellar structure that consists of thin lenticular splats. A large number of factors, such as spray parameters and spray materials, influence this structure and can be summarized by the spatial interaction of three physical distributions; i.e., the particle size, the high energy temperature field, and the velocity field.<sup>1,2</sup> Researchers have engaged in understanding thermal spray processes via the study of splats.<sup>2–5</sup> The nature of this research encompasses finite solid particles that are transformed by an energy source into molten or semimolten particles that are then subjected to spreading kinetics on impact against a substrate. Splats of a rich morphological character with different shape diameters and thicknesses are formed.

Much of the reported work on the flattening process of splats can be classified according to (i) experimental observations,<sup>2,6–13</sup> (ii) numerical simulation,<sup>14–19</sup> and (iii) theoretical methods.<sup>3,4,19–24</sup> Metrological studies of splats have identified key factors that affect the splat diameter, thickness, circularity, and degree of fragmentation. Jones *et al.*<sup>3</sup> and Madejski

*et al.*<sup>4</sup> proposes a mathematical quantity,  $\zeta$  (“Xi”) that is defined as either the “degree of flattening” or “flattening ratio.” This value, shown in Eq. (1), relates the diameter of the splat  $d_s$  to the diameter of the initial particle  $D_p$  and would be expected to be greater than unity.

$$\zeta = \frac{d_s}{D_p} \quad (1)$$

The flattening ratio relates the energy interaction that occurs between the injected particle and the superheated plasma gas stream to the dynamics of splat impingement on the substrate.

For experimental splat studies researchers use a wipe test, also called a line scan test,<sup>25</sup> to collect splats and to determine whether the material or thermal spray parameters are suitable. Past experimental studies<sup>10</sup> reported the coverage area of plasma sprayed yttria-stabilized zirconia (YSZ) deposited onto glass substrates. The area coverage was between 50% and 90% with deposition efficiencies (DEs) from 7% to 25%. In addition, the average flattening ratio was from 4.8 to 6.2 and the splat thickness  $\sim 1.0 \mu\text{m}$ ; with all of these values based on the Madejski splat model.<sup>4</sup> Besides splat geometries, the primary purpose of a wipe test, from the applicator’s point of view, is to determine the area coverage achieved per pass.

Area coverage is an essential parameter that controls the mechanics of a thermal spray process. Other than a scientific need to understand the rate of coverage of a substrate, this parameter has significant technological importance as it determines the minimum number of spray passes to achieve complete coverage. However, these parameters are rarely measured and often not presented with the usual “spray tables” for a material. Often the term of “thickness per pass” is quoted as being a major spray characteristic; however, the assumption of 100% coverage per pass is highly misleading.

Thus, the primary motivation of this study is to formulate a method to predict and estimate the area coverage per pass by a thermal spray torch, such as by the plasma spray process. This involves surveying the published literature and takes into consideration any associated experimental observations. A critical review of this literature then allows calculation of the coverage area per pass. Graphical representations of this method are plotted using MATLAB (MathWorks Inc., Natick, MA) for further analysis. Finally, these model results are compared and validated against physical observations of plasma sprayed YSZ coatings on smooth glass slides.

## II. Formulation of the Model

### (1) Founding Principals of Madejski

The work assumes an incompressible model for the impact process, which is a reasonable boundary condition when the physics of the thermal spray process is considered as there is a transition from a liquid to a solid state. This founding

T. Troczynski—contributing editor

principle permits calculation of the splat diameter and thickness on the basis of volume conservation.

A simplified model for the impingement-flattening stage of molten droplets onto a solid substrate by Jones<sup>3</sup> indicated that the flattening ratio was related to the decay of kinetic energy via viscous dissipation. However, this study<sup>3</sup> ignored the effects of surface tension and solidification during the flattening process. These intrinsic properties were incorporated by Madejski *et al.*<sup>4</sup> and have been the cornerstone for modeling the spreading and solidification of molten droplets.

Madejski *et al.*<sup>4</sup> explained how splats flattened by taking into account (i) viscosity, (ii) surface tension, and (iii) solidification behavior; thereby creating a differential equation based on mathematics and physical properties. The above terms are each expressed as a function of three dimensionless parameters; viz. (i) the Reynolds number ( $Re$ ) that relates inertia and viscous effects that depend on impact velocity and fluid dynamic instabilities; (ii) the Weber number ( $We$ ) that accounts for the transformation of impact kinetic energy to surface energy; and (iii) the modified Peclet number ( $Pe$ ) that considers solidification rates.

## (2) Literature Survey of Flattening Ratio Equations

Models developed for analysing splat formation in thermal spray applications describe an ideal case of a molten droplet that impacts a planar, smooth substrate and continuously deforms till complete solidification.<sup>2,26</sup> Table I summarizes thermo-physical variables and related equations that have been compiled from the literature. Most solutions, however, neglect one or more of the three dimensionless parameters and as a consequence do not accurately predict thermal spray practice. Literature concerning millimeter-sized impact

particles has not been included in this review as there is ambiguity whether scaling laws can be employed.<sup>27,28</sup>

The Madejski model does not take into account interface factors between the particle and the substrate; for example the substrate temperature and the desorption of adsorbates on the substrate surface that influence the thermal contact resistance,  $R_{th}$ , between the substrate and droplet. The effect of thermal contact resistance manifests itself in morphologies that range from splash-like to disk-like splats. Splash-like splats usually cause splat fragmentation that is destructive and promotes the formation of coating defects, such as porosity, micro cracks, and voids. The degree of fragmentation depends on the deposition temperature, droplet velocity, substrate roughness, and desorption of adsorbates from the substrate surface.<sup>12</sup> Experimental studies<sup>8,26</sup> suggest that splat splashing is primarily due to local solidification. The splashing phenomena is promoted when substrate/particle and particle/particle conditions exhibit low wettability or a high thermal contact resistance. Other studies<sup>11,21</sup> also indicate the effect of wave propagation after impact within the molten liquid; which induces so-called “impact splashing”.<sup>29</sup> Impact splashing is dissimilar from flattening splashing as this gives rise to different solidification behavior.

Fukamoto *et al.* have reported on a substrate transition temperature,  $T_t$ , at which the splat morphology changes from a splash to a disk splat.<sup>12,30</sup> Splashing in this case can be predicted by a modified Sommerfeld number<sup>11</sup>  $K_f = 0.5a^{1.25} Re^{-0.3} K$ ; where  $a$ , corresponds to the ratio of the flattening velocity,  $V_f$ , to the impact velocity,  $v$ , of the particle and  $K$  is the Sommerfeld number. The equation was formulated on the basis of in-flight data of the particle and the substrate temperature. Researchers<sup>13,31</sup> have also reported on the effects of reducing surface contaminants, adsorbates, condensates, and

**Table I. Flattening Equations from Various Open Literature**

Viscous dissipation	Surface tension	Solidification effects	Governing equations			Remarks	Ref.
✓	×	×	$\zeta_m = a Re^b$	a	b		
				1.16	0.125	Splat freezing velocity slower than impact velocity. Surface energy neglected	3
				1.29	0.2	For $Re > 100$ and $We^{-1} = 0$	4
				1.0	0.2	Simulation at isothermal conditions. $We = 200-2000$ , $Re > 10^2$	14
				0.83	0.2	Simulation at isothermal conditions. 30–100 $\mu m$ particle	16
				1.04	0.2	Navier-Stokes numerical simulation	17
				0.93	0.2	Numerical simulation together with solidification effects	18
				1.00	0.22	Experiment data fit	9
				1.06	0.167	Analysis of kinetic energy to viscous dissipation only	23
				1.16	0.2	Modified Madejski model. $Re > 140$ and $We^{-1} = 0$	24
			$\frac{3\zeta_m^2}{We} + \frac{1}{Re} \left( \frac{\zeta_m}{1.29} \right)^5 = 1$			Neglect contact resistance. No solidification	4
✓	✓	×	$\frac{3[(1-\cos\theta)\zeta_m^2-4]}{We} + \frac{1}{Re} \left( \frac{\zeta_m}{1.29} \right)^5 = 1$			Considering wetting angles	32
			$\frac{3[(1-\cos\theta)\zeta_m^2-4]}{We} + \frac{1}{Re} \left( \frac{\zeta_m}{1.16} \right)^5 = 1$			For $We > 670$ and $Re > 140$	24
✓	✓	✓	$\frac{1}{Re} \left( \frac{\zeta_m}{1.18} \right)^5 + \frac{3(1-\cos\theta)(\zeta_m-1)}{We} + S \left( \frac{\zeta_m}{1.15} \right)^{2.5} = 1$			Solution accounts for thermal contact resistance. $S = 0.001-0.005$	19
✓	×	✓	$\left( \frac{\zeta_m}{1.18} \right)^{2.5} = \sqrt{Re} \left( \sqrt{\left( \frac{S}{2} \sqrt{Re} \right)^2 + 1} - \frac{S}{2} \sqrt{Re} \right)$			Effect of surface tension and wetting angle was neglected	22
×	×	✓	$\zeta_m = 0.82 \left( \frac{Pe}{U^2} \right)^{0.25}$			Simplified single solidified layer. $Re^{-1} = We^{-1} = 0$	27
×	✓	×	$\zeta_m = \sqrt{\frac{We}{3}}$			$Re^{-1} = 0$ , $We > 100$	4

✓ – work considers the effect.

×



oxide layers to achieve disk-like splats: factors that can be integrated into a thermal contact resistance effect.

Figure 1 depicts factors that influence splat formation. None of these cases predict splashing. As a result, it is assumed in the presented model that spherical particles are transformed into disk-like shapes.

The majority of most models for splat-substrate interactions are based on Case (1) that considers the importance of  $Re$  that is based on viscous dissipation effects. The effects of  $We$ , which is based on surface tension behavior, is significant during the initial freezing stage at the splat edges and toward the termination stage of solidification when  $Re$  is low.<sup>14</sup> Simulations have demonstrated that the two processes of (i) heat transfer and solidification; and (ii) flattening and solidification are decoupled processes. The flattening time is approximately 0.14–1.08  $\mu$ s and the freezing time is an order of magnitude greater at 4–20  $\mu$ s.<sup>18</sup>

Analysis of the Reynolds and Weber numbers have indicated that the flattening process, flattening diameter, and flattening time are not affected by surface tension. Liu *et al.*<sup>17</sup> reported that (i) when the impact velocity and droplet diameter remain constant, and (ii) when  $We$  was varied; then the effect of surface tension remains similar. These droplets solidify after deformation<sup>16,17</sup> and are in perfect physical contact and thus conditions exist for ideal heat transfer. Under this condition the splat edge did not exhibit a smooth convex front and indicated that the effect of inertia force is greater than the surface tension.

Surface tension effects are considered in Case (2). Bennett *et al.*<sup>32</sup> developed a modified solution using the Young–Dupre equation<sup>33</sup> to breakdown the surface tension into components of solid-gas, solid-liquid, and gas-liquid interfacial surface tensions with the wetting contact angle,  $\theta_s$ . Pasanideh-Fard<sup>34</sup> and Aziz<sup>21</sup> demonstrated experimentally that the changes in the equilibrium contact angle influence the spread factor. However, it is worthwhile to note that their observations were for millimeter-sized droplets. Delplanque<sup>35</sup> proposed an improved Madejski model featuring a more appropriate velocity field that satisfies the no-shear boundary condition at the free surface, and an accurate derivation of the dissipation term from the mechanical energy equation.

A governing equation by Zhang<sup>19</sup> considers all the individual contributions of viscous, surface tension and solidification effects is presented as Case (3). It was predicted that a molten droplet would form a recoiled splat; i.e., splat with thicker edges, as the wetting contact angle increases and at a

slow solidification rate. The model also revealed that thermal contact resistance delays solidification and, accordingly, decreases the solidification rate.

However, further experimental work<sup>22</sup> of Zhang *et al.* resolved the flattening dependence relationship with that of  $Re$  and  $S$  (the “solidification coefficient”), ignoring the surface tension effects. The dominating components for splat flattening were viscous dissipation and solidification as seen in Case (4). The findings showed that surface tension and the wetting contact angle, were insignificant for spreading of typical thermal spray droplets (i.e., 10–90  $\mu$ m) and that droplets with high velocity (i.e., >100 m/s) form disk-like splats.

The foregoing discussion concerning the particle/substrate interface and associated factors leads to the following conditions that are needed to achieve fully disk-like splats that show no fragmentation or the splat recoil effect.

1. A smooth substrate surface is used that allows almost perfect splat contact and ideal cooling conditions; i.e., surface roughness,  $R_a = 0.1 \mu$ m.
2. There is an absence of surface contaminants, adsorbates, condensates, and oxide layers as these influence the heat transfer coefficient.
3. The wetting angle is ideal to allow perfect wetting with the substrate and prevent recoil; i.e.,  $0^\circ$ .
4. The substrate transition temperature  $T_i$  is exceeded and the modified Sommerfeld number  $K_f$  is less than the critical requirements for splashing to occur; i.e.,  $T_i > 600$  K and  $K_f < 7$ .
5. A low thermal contact resistance<sup>7</sup> corresponding to ideal contact between the splat and substrate; i.e.,  $R_{th} = 10^{-8}$  K m<sup>2</sup> W<sup>-1</sup>.

### III. Method to Calculate Surface Coverage

A method of estimating the area coverage to account for practical situations in the thermal spray process will be briefly covered in this section. Inputs to the model include; (i) use of a monomodal feedstock distribution in a thermal spray torch, (ii) considerations to the particle temperature-velocity envelope in the plasma spray plume, and (iii) effects of key dominant mechanisms, such as viscous dissipation, surface tension or solidification effects, in the flattening process. The methodology provides an approximation to the deposition phenomenon and can be represented in Fig. 2. In addition to the earlier assumptions on the ideal contact and heat transfer, the following assumptions are made.

1. The angle between the torch centerline axis and the tangent to the surface of the substrate (i.e., spray angle) is  $90^\circ$  and all molten droplets impact normally onto the substrate.
2. There is no particle deformation or evaporation of the particle before impingement.

#### (1) Monomodal Feedstock

Feedstock that is used in a thermal spray process can be estimated to exhibit a Gaussian distribution with respect to particle size. For spherical YSZ feedstock (Metco 204NS; Sulzer Metco, Westbury, NY), the distribution is between +16 ( $d_{10}$ )–125  $\mu$ m ( $d_{90}$ ). The average particle size is 72  $\mu$ m and standard deviation,  $\sigma$ , 21.3  $\mu$ m. This data can be transformed into a probability density function using the following relationship:

$$F(x) = \begin{cases} \frac{1}{\sqrt{2\pi}\sigma^2} e^{-\frac{(x-\bar{x})^2}{2\sigma^2}}, & 16 < x < 125 \\ 0, & \text{all other } x \end{cases} \quad (2)$$

The function  $F(x)$  is coded into the MATLAB model to return a distribution of particles for a given DE. In the model, particles are assumed to be distributed evenly from

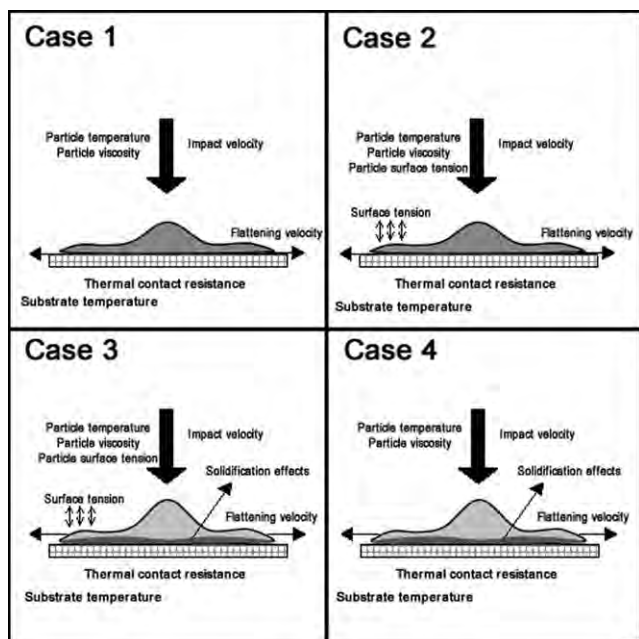


Fig. 1. Various possible factors affecting splat formation.

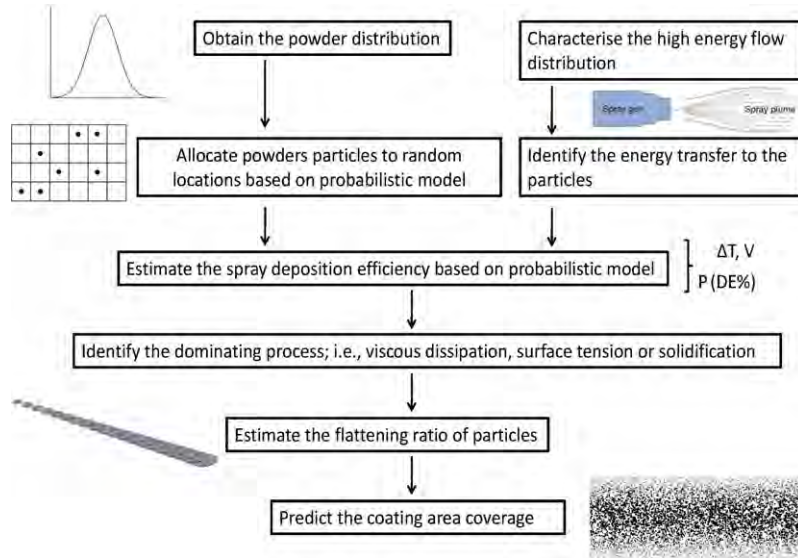


Fig. 2. Schematic of MATLAB model.

the torch during the plasma spray process. Consequently, the locations of the particles impacting the surface have been modeled as being an evenly distributed grid on the surface, with the centers of the splats located at the intersections of the grid. Although these assumptions may not be strictly acceptable, they can be considered as a first level approximation so that boundary conditions can be determined.

The number of particles per second impacting the surface is equivalent to the spray rate,  $M$ , divided by the mass of a single particle, Eq. (3). The mass of a single particle can be calculated using the density,  $\rho$ , and the diameter,  $d$ , of the particle. The distance between particles, also referred to as the *grid spacing*, is a function of the area covered by the spray footprint and the number of particles per second impacting the surface. This relationship is shown in Eq. (4).

$$\begin{aligned} \text{no. of particles per second, } \frac{dN}{dt} &= \frac{\text{spray rate}}{\text{mass of single particle}} \\ &= \frac{d}{dt} \left( \frac{M}{\frac{1}{6}\pi\rho d^3} \right) \end{aligned} \quad (3)$$

$$\text{grid spacing} = \sqrt{\frac{\text{area covered by spray footprint per second}}{\text{number of particles per second}}} \quad (4)$$

For this work, the feedstock is YSZ with density of 6.0 g/cm<sup>3</sup> and the spray rate is 30 g/min, which is a typical spray rate for this material. The number of particles that are evenly distributed on the grid will be  $4.3 \times 10^5$  YSZ particles per second. The plasma torch transverse speed was assumed to be 1 m/s and the width of spray footprint taken to be 25 mm. This corresponds to a 4167 by 105 grid consisting of square with spacing of 240  $\mu\text{m}$ .

## (2) Flattening Behavior of Splats in Plasma Spray Stream

The flattening ratio of YSZ splats are direct representations of the energy transfer (both momentum and heat) from the plasma source to the YSZ feedstock. These energy interactions that result in an increase in particles' thermal and kinetic energies begin when particles enter into the plasma spray plume until they impact onto the substrate. The volume of

space in which particles and superheated plasma gases interact can be termed the particle spray stream. Consequently, the projected particle spray stream forms the spray footprint on the substrate. In earlier work<sup>36</sup>, it was assumed that the flattening ratio within a particle spray stream is a constant value. This implies that the plasma spray plume is isothermal with equal thermal and kinetic energy and this would be rarely achieved.<sup>37</sup>

On the other hand, the energy flux of a plasma spray plume varies and influences the degree of splat flattening with respect to the particle location in the spray stream. The centerline of a plasma spray plume possesses the highest enthalpy and momentum fields and particles passing through this part of the plume would achieve the maximum flattening ratio as they will acquire a low viscosity (due to a higher temperature) and a high momentum upon impact. Subsequently, there is a decrease in energy flux toward the edge of the spray footprint, as observed in experiments,<sup>10</sup> as unmelted or re-solidified particles rebound and are not deposited onto the substrate.

The dimension of the spray footprint must also be considered to better predict the physical flattening behavior of feedstock. In practical situations, the size of the particle spray stream is influenced by the divergence of the exiting plasma gases. Thus, particle spray stream and spray footprint can be affected by the distance of the torch to the substrate (i.e., standoff distance) and also the operating conditions of the plasma torch. In this work, the plasma spray torch generates a conical plasma stream into which feedstock particles are injected symmetrically with respect to the centerline. The distribution of the deposited material can be approximated by a Gaussian distribution.<sup>38</sup>

The Gaussian probability distribution  $P(y)$  of the plasma energy flux distribution, with  $y$  denoting the function of distance from centerline of torch is:

$$P(y) = \begin{cases} \frac{1}{\sqrt{2\pi}\sigma^2} e^{-\frac{(x-\bar{x})^2}{2\sigma^2}}, & -\text{distance} < y < \text{distance from} \\ \text{center line of torch } 0, \text{ all other } y \end{cases} \quad (5)$$

The shape of the curve is controlled by the standard deviation,  $\sigma$ , which measures the width of the particle spray stream, Fig. 3. For a narrow (20 mm wide) particle spray stream, the total area of the spray footprint is small whereas the average plasma energy flux is high. These conditions result in a high population density of particles entering the



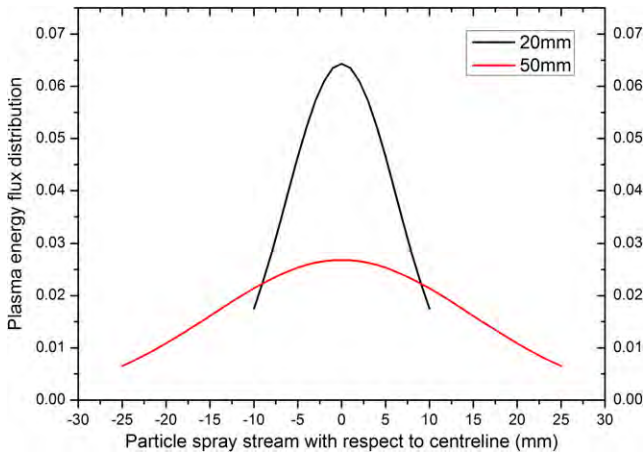


Fig. 3. PDF distribution of energy flux with respect to different particle spray stream width.

“ideal” zone for optimum energy transfer and that these particles undergo high flattening ratios. On the other hand, when the spray pattern is wide (50 mm) a low population density of particles; as reflected by a broad grid distribution of particles, forms the spray stream. However, due to the lower average plasma energy flux, only some particles can be melted and deposited as splats that exhibit a low flattening ratio. Particles that are not melted or do not enter the spray stream can be assumed to bounce off the substrate surface and are not deposited. The width of the particle spray pattern was varied from 20 to 30 mm.

### (3) Selecting Equations for Flattening

Four cases of flattening, summarized by Fig. 1, are considered to address the dominant forces affecting splat formation. Table II presents the governing equation for each case and the physical conditions with regards to  $Re$ ,  $We$ ,  $S$ , and  $\theta_s$  that are assumed. These equations are then graphed to estimate the maximum flattening ratio of the feedstock for a given set of thermal spray conditions.

The influence of the thermal spray processing conditions that give rise to a maximum flattening ratio can be expressed as a transfer function,  $\phi$ , that can be applied to  $P(y)$ . That is:

$$\phi = \frac{\zeta_{max}}{\max(P(y))} \quad (6)$$

then,

$$D(y) = \phi * P(y) \quad (7)$$

where  $\zeta_{max}$  is the maximum achievable flattening ratio and  $\max(P(y))$  is the probability density function at centerline of

the plume.  $D(y)$  can be viewed as a comprehensive representation of the splat flattening behavior with respect to a particle spray stream that follows a Gaussian distribution.

### (4) Deposition Efficiency

The deposition efficiency (DE) that represents a typical YSZ plasma sprayed footprint in industrial processes varies from 20% to 65%.<sup>10</sup> There are many process variables that influence deposition efficiency and therefore it is important to differentiate between the terms of “intrinsic DE” and “target DE”.<sup>39</sup> Intrinsic DE refers to the maximum yield of material deposition under ideal conditions for the given feedstock where the plasma spray process parameters and the substrate condition have been optimized. Intrinsic DE is the parameter that is quoted within suppliers’ data sheets and is used only as a guideline for practical application. Intrinsic DE is the parameter of relevance to this work. Target DE refers to the deposition yield of a material that deposits onto a practical engineering job. The target DE is less than the intrinsic DE as it takes into account practical operational characteristics, such as the torch motion and geometry of the substrate.

In the present model, the intrinsic deposition efficiency is selected to be between 20% and 30% and represents a typical DE on a smooth substrate<sup>10</sup>, such as the glass slides used in this work. The intrinsic deposition efficiency is not constant over the entire coating thickness. It can be quite low (i. e., DE = 20%) for the first few layers and reaches then its nominal value.

A MATLAB program was written for matrix calculations and used to generate individual grids with various DEs. The program generates a “particle matrix” that consists of either 1 or 0 depending on the spray deposition efficiency and particle spray footprint specified. If the value is 1 then the particle stays in the cell and will be subsequently deposited as a splat. Conversely, if a null value is returned, then the physical interpretation is that the particle is not deposited.

## IV. Results from the Model

### (1) Flattening Ratio Graphs

Figs. 4–7 are graphs of flattening equations. In general,  $Re$  is plotted from 140 to 1500 and  $We$  is varied from 670 to 1500. The range of wetting angle considered is from 0° to 90°, which represents the transition from ideal splat/substrate contact to wettability conditions with weak splat/substrate interactions.

Viscous dissipation is the only factor considered in Fig. 4 (Case 1) and it can be seen that the flattening ratio increases with  $Re$ . Particles that are accelerated to high velocities or melted to high dynamic viscosities should have a large  $Re$  and hence are likely to experience a large degree of flattening. The graph predicts that for most plasma spray operations, the flattening ratio ranges between 2.2 and 3.6. The maximum achievable flattening is approximately 3.6 when  $Re = 1500$ .

Table II. Summary of Flattening Cases and Related Equations Used for Constructing the Second Model

Governing equations		Remarks	Ref.
Case 1	$\zeta_m=0.83Re^{0.2}$	For $Re > 140$ and $We-1 = 0$	16
Case 2	$\frac{3(1-\cos\theta)\zeta_m^2-4]}{We} + \frac{1}{Re} \left(\frac{\zeta_m}{1.16}\right)^5 = 1$	For $\theta = 0^\circ-90^\circ$ . For $We > 670$ and $Re > 140$	24
Case 3	$\frac{1}{Re} \left(\frac{\zeta_m}{1.18}\right)^5 + \frac{3(1-\cos\theta)(\zeta_m-1)}{We} + S\left(\frac{\zeta_m}{1.15}\right)^{2.5} = 1$	Solution accounts for thermal contact resistance. $S = 0.001-0.005$	19
Case 4	$\left(\frac{\zeta_m}{1.18}\right)^{2.5} = \sqrt{Re}\left(\sqrt{\left(\frac{S}{2}\sqrt{Re}\right)^2+1} - \frac{S}{2}\sqrt{Re}\right)$	Effect of surface tension and wetting angle was neglected	22

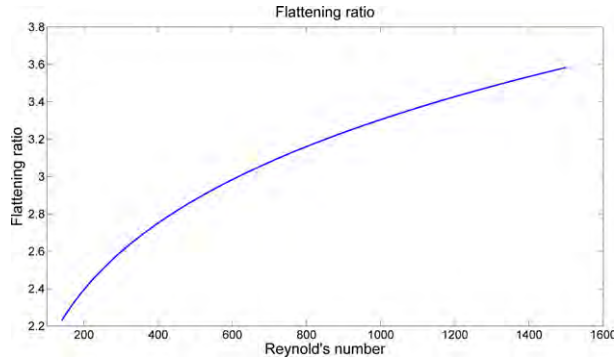


Fig. 4. Graph for flattening ratio when viscous dissipation is the dominant force (Case 1).

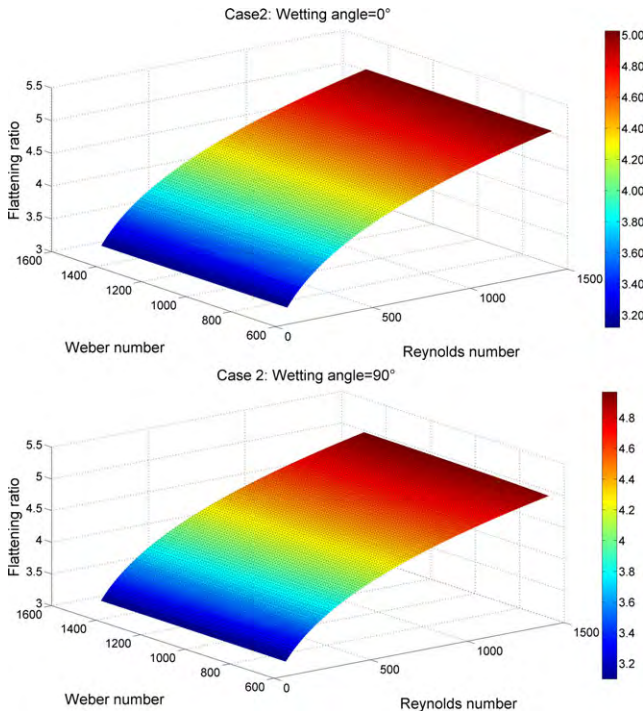


Fig. 5. 3D plot for flattening ratio when viscous dissipation and surface tension are the dominant forces (Case 2).

Viscous dissipation and surface tension are considered for Case 2. The effects of  $Re$ ,  $We$ , and  $\theta_s$  on the flattening ratios are shown in Fig. 5. The three dimensional plot shows that the flattening ratio does not vary greatly with increasing  $We$ . When surface tension was evaluated from  $We = 670$  to 1500 for an ideal wetting condition (i.e.,  $\theta_s = 0$ ), the maximum flattening ratio decreased from 5.02 to 5.01. The wetting angle is also studied from  $0^\circ$  to  $90^\circ$ , but indicates a minimal difference of 0.05 on the maximum achievable flattening ratio. This analysis shows that even at low wetting angle, the surface tension on the molten splats could be too small to promote splat spreading. Nevertheless, the predicted flattening ratio ranges from 3.1 to 5.0 for all conditions specified.

Case 3 includes the solidification effect on splat formation. Zhang's equation<sup>19</sup> is plotted in Fig. 6. The splat geometry can be determined by the interaction of viscous and surface tension dissipation of the inertial energy and the arrest of liquid flow by solidification. The solidification factor,  $S$ , influences the flattening ratio. The red surface plot, representing a low solidification factor of  $S = 0.001$  is higher when compared with the blue surface plot where  $S = 0.005$ . A low solidification factor suggests that the splats have sufficient

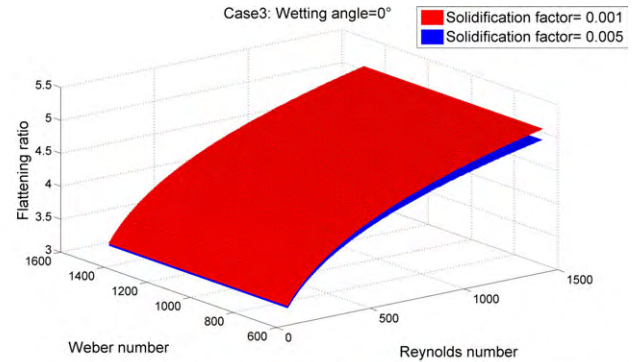


Fig. 6. 3D plot for flattening ratio when viscous dissipation, surface tension and solidification are the dominant forces (Case 3).

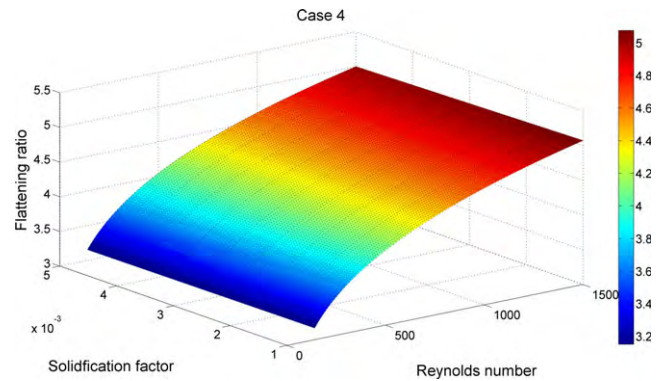


Fig. 7. 3D plot for flattening ratio when viscous dissipation and solidification are the dominant forces (Case 4).

time to spread out before the solidification starts and arrests the molten liquid front. Again, the surface tension and the wetting angle have negligible influence on the final flattening ratio. The graph postulates that the flattening ratio for high solidification rates is 3.1–4.9 and for low solidification rate the range is 3.2–5.1.

Figure 7 assumes that the surface tension and the wetting angle have been ignored; i.e., Case 4. The plot shows that change in flattening ratio is from 3.2 to 5.1.

All four cases show that the graph trends are all influenced by increasing  $Re$ . Thus, it is evident that the most critical parameter for flattening ratio predictions, as first predicted by the Madejski model, is viscous dissipation forces that are manifested in the value of Reynolds number. Most importantly, these graphs aid in the completion of the model and account for the different scenarios during particle impingement and splat formation.

## (2) Splat Flattening within the Particle Spray Stream

In the current study, the maximum flattening ratio for YSZ particles is assumed to be between the range 3.5–4.5, which



agrees with the graphical data. As the plasma spray stream expands outward, the flattening ratio decreases due to the reduction in energy flux available for flattening. It is realistic to accept that only a flattening ratio greater than a value = 1 should be included in the transfer function  $P(y)$  as splat fragmentation is not included in the current model. Therefore, the model is programmed to reject flattening values less than 1 in the simulations.

(3) Simulation of Model

Simulation of area coverage per pass of a plasma spray torch was conducted using the model with the deposition efficiency set at 20%. The results of the simulation are presented in Fig. 8 with 5 mm wide spray sections displayed at the constant SOD of 100 mm. Measurements of the coverage area per pass are 12.3% when the maximum allowable splat flattening is 3.5 and reaches a maximum coverage area of 18.7% for a flattening ratio of 4.5. The majority of overlapping splats occur in the centerline of the spray footprint and, logically and numerically, become more pronounced when the splat flattening ratio increases. The results of the simulation shows that when a low flattening ratio is selected, which could represent a plasma spray plume with low average energy flux, then the particles at the periphery of the spray footprint are not deposited. To verify the simulation, plasma sprayed YSZ glass slides were collected and image analysis was carried out. The next section presents these experimental details.

V. Experimental Setup

(1) Plasma Spraying of Glass Slides

To assess the results of the model, microscope glass slides (75 mm by 25 mm) were coated with commercially available YSZ (Metco 204NS) using a conventional air plasma spray system (Metco 7MB, Sulzer Metco). In these experiments, operating conditions were selected to correspond to typical coating parameter settings. Argon was used as the primary plasma operating gas and hydrogen was used as the auxiliary gas. The primary gas flow was fixed at 42.1 NL/min at 0.7 MPa and the flow of the auxiliary gas was 6.10 NL/min at 0.34 MPa. Argon was used as the powder feeding gas and the powder feed-rate was 30 g/min. Plasma arc current and volt-

age were set at 35 kW (500 A and 70 V). The plasma torch was mounted on a robotic arm (YR-SK16-J00, Motoman Robotics, Miamisburg, OH) that was programed to transverse a single pass at 1 m/s across the mounted glass slides. All slides were at a constant stand off distance of 100 mm.

(2) Imaging of Plasma Sprayed YSZ Coatings

The glass slides were painted with black paint on the non-coated side to provide good contrast for the cream-colored YSZ splats. All slides were then photographed using a 10.2 mega-pixel sensor camera (Lumix DMC-LX5, Panasonic Corporation, Osaka, Japan) set to the macro mode. The camera aperture was set to F8.0 and the shutter speed was 8.0 s. The camera focus distance was set to 10 mm. The slides were illuminated using low-flicker fluorescent lights mounted using a diffuser. A side lighting configuration was used to prevent specular reflection from the mirror-like surface of the painted slide. Other reflections were avoided by masking surrounding surfaces, such as the camera body, black and blocking out all ambient lighting.

The resulting images were analysed using the MATLAB image processing toolbox. First, the images were converted into grayscale, then normalized to avoid any overall brightness changes that resulted from image sensor variability. Next, grayscale histograms were then developed for each image and Otsu’s method<sup>40</sup> used to find the threshold level; the threshold level varied by 3.5% across the entire range of images. An example of a thresholded image is depicted in Fig. 9. The coverage of the slides was then calculated by counting the number of white pixels in the thresholded image and dividing by the total number of pixels. Note that this experimental method was not designed to count the number of splats as the desired data could be gathered without such a determination. Thus, spat density calculations were outside the scope of this study that focussed on deposition efficiency and coverage. A total of six slides were image processed and the coverage values are shown in Table III. The low coeffi-

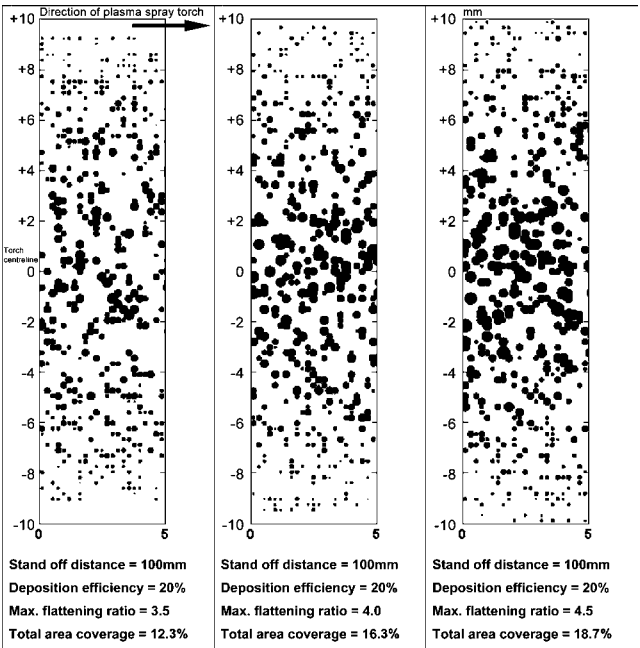


Fig. 8. Various sections of spray path when flattening ratio is varied and DE is 20%.



Fig. 9. Threshold applied to the sample image for analysis.

Table III. Image Analysis Results of Plasma Sprayed YSZ on Glass Slides	
Slide	Coverage calculated (%)
100 mm_S1	15.8
100 mm_S2	12.3
100 mm_S3	14.3
100 mm_S4	16.4
100 mm_S5	9.3
100 mm_S6	12.3
Average	13.4
SD	2.7

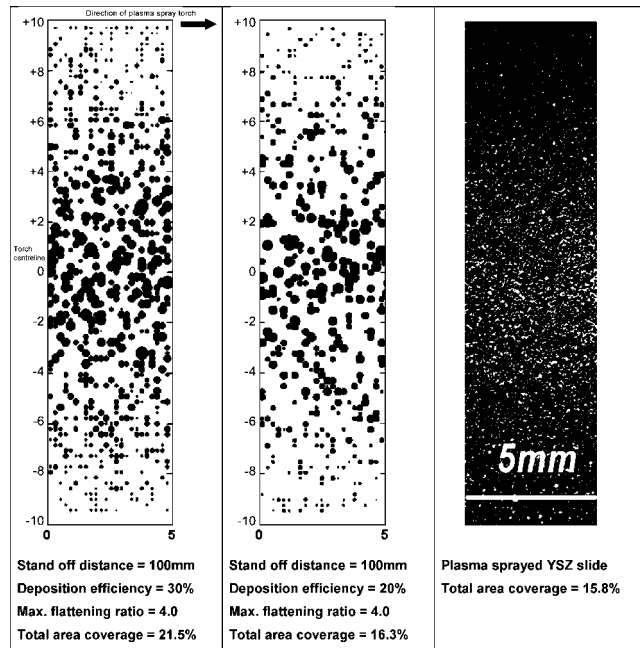


Fig. 10. Comparison of models with plasma sprayed YSZ slide.

cient of variance of 0.2 indicates that this data set was sufficient for this study.

## VI. Discussion

The experimental results show that the coverage area of plasma sprayed YSZ on glass slides is 13.4%. The variability in coverage values between individual slides can be explained by factors relating to the plasma spray process, which can include instabilities of the plasma arc jet and intervals during powder feeding. In addition, the results indicate that the coverage area in this current study is lower than the reported literature values of between 50% and 90%.<sup>10</sup> However, this difference can be attributed to the dissimilar experimental parameters used and the unique method of image analysis conducted on the collected glass slides.

When comparisons are made between the experimental and proposed model, it is found that the model adequately predicts the percentage of area coverage with simulation results of 16.3% and experimental results of 13.4%. The simulated spray model agrees well with the slides collected from the plasma spray experiments. The size of the spray footprint from the samples was approximately 20 mm, which coincides with the model prediction that only particles within 10 mm proximity of the plume centerline will be deposited as splats. The implication is that the various assumptions about the plasma spray process and feedstock made in the modeling process are valid.

However, it can be seen from the glass slides (Figs. 9 and 10) that the splats collected are not necessarily circular as asymmetric and fragmented splats can be observed. The future model, thus, should account for such irregularities to map out these splats within the simulations. Nevertheless, this work indicates that it is possible to model and predict the coverage area of plasma sprayed ceramic materials.

## VII. Conclusion

A model to calculate the coverage area for a thermal spray process of ceramic materials has been presented. The model is based on a critical review of splat literature, which identified four cases of splat flattening mechanisms that can be applied to thermal spray processing of ceramics. Splat flattening

mechanisms can be attributed to those forces that dominate during the process: these being viscous dissipation, surface tension, and solidification effects. It was found that the flattening process is most influenced by effects of viscous dissipation and, correspondingly, a *Re*-based model is sufficient to predict the coverage area of most thermal spray ceramic materials. In addition, all modeling steps assume that the final splats are disk-like with no occurrence of splat fragmentation.

This model has accounted for physical events in the thermal spray process. It employs statistical data collected from a sample of YSZ feedstock and the spray stream energy flux is modeled with respect to its centerline. The maximum flattening ratio achieved by particles is therefore represented at the spray footprint centerline. Results from the model have been displayed in simulated spray sections and yield predictions from 12% to 18% depending on the maximum flattening ratio.

Validation of the model was performed using glass slide samples of plasma sprayed YSZ that were collected and analysed via imaging techniques. The average splat coverage area per pass was measured to be 13.4% for the thresholded images, which verifies the simulation results from the model. These results show that the current model can adequately predict the spray area coverage per pass for thermal sprayed ceramic materials and is able to account for many of the prime thermal spray variables. Future models will address the formation of noncircular splats, splat fragmentation, and extend into nonceramic materials.

## Acknowledgment

The authors thank Mr Andrew Moore for expert assistance in the preparation and plasma spray procurement of samples. This work is supported under a Swinburne University Postgraduate Research Award. We also acknowledge support from the Defence Materials Technology Centre (DMTC).

## Appendix

### Nomenclature

Symbol	
$D$	Splat diameter
$d$	Droplet diameter
$Re$	Reynolds number ( $\rho v d / \mu$ )
$We$	Weber number ( $\rho v^2 d / \gamma$ )
$Pe$	Peclet number ( $v d / \alpha_s$ )
$S$	Solidification coefficient
$v$	Impact velocity (m/s)
$V_f$	Flattening velocity (m/s)
$K$	Impact Sommerfeld number ( $K = We^{0.5} Re^{0.25}$ )
$t$	Time (s)
$a$	Constant ( $V_f / v$ )
$dM/dt$	Thermal spray feedrate (kg/s)
$m$	Mass of single particle
$dN/dt$	Particle per second
Greek Symbols	
$\zeta$	Flattening ratio ( $D/d$ )
$\mu$	Droplet viscosity ( $m^2/s$ )
$\gamma$	Surface tension (N/m)
$\alpha$	Thermal diffusivity
$\rho$	Density ( $kg/m^3$ )
$\theta$	Wetting contact angle
Subscripts	
$s$	Splat
$p$	Powder particle
$m$	Maximum

## References

1. McPherson, "The Relationship Between the Mechanism of Formation, Microstructure and Properties of Plasma-Sprayed Coatings," *Thin Solid Films*, **83** [3] 297–310 (1981).

- <sup>2</sup>S. Fantassi, M. Vardelle, A. Vardelle, and P. Fauchais, "Influence of the Velocity of Plasma-Sprayed Particles on Splat Formation," *J. Therm. Spray Technol.*, **2** [4] 379–84 (1993).
- <sup>3</sup>H. Jones, "Cooling, Freezing and Substrate Impact of Droplets Formed by Rotary Atomization," *J. Phys. D Appl. Phys.*, **4** [11] 1657–60 (1971).
- <sup>4</sup>J. Madejski, "Solidification of Droplets on a Cold Surface," *Int. J. Heat Mass Transf.*, **19** [9] 1009–13 (1976).
- <sup>5</sup>C. Moreau, P. Cielo, and M. Lamontagne, "Flattening and Solidification of Thermally Sprayed Particles," *J. Therm. Spray Technol.*, **1** [4] 317–23 (1992).
- <sup>6</sup>C. J. Li, H. L. Liao, P. Gougeon, G. Montavon, and C. Coddet, "Experimental Determination of the Relationship Between Flattening Degree and Reynolds Number for Spray Molten Droplets," *Surf. Coat. Technol.*, **191** [2–3] 375–83 (2005).
- <sup>7</sup>M. Vardelle, A. Vardelle, A. C. Leger, P. Fauchais, and D. Gobin, "Influence of Particle Parameters at Impact on Splat Formation and Solidification in Plasma Spraying Processes," *J. Therm. Spray Technol.*, **4** [1] 50–8 (1995).
- <sup>8</sup>L. Bianchi, A. C. Leger, M. Vardelle, A. Vardelle, and P. Fauchais, "Splat Formation and Cooling of Plasma-Sprayed Zirconia," *Thin Solid Films*, **305** [1–2] 35–47 (1997).
- <sup>9</sup>C. W. Kang and H. W. Ng, "Splat Morphology and Spreading Behavior Due to Oblique Impact of Droplets Onto Substrates in Plasma Spray Coating Process," *Surf. Coat. Technol.*, **200** [18–19] 5462–77 (2006).
- <sup>10</sup>A. Kucuk, R. S. Lima, and C. C. Berndt, "Influence of Plasma Spray Parameters on Formation and Morphology of  $ZrO_2$ -8 wt%  $Y_2O_3$  Deposits," *J. Am. Ceram. Soc.*, **84** [4] 693–700 (2001).
- <sup>11</sup>M. Fukumoto, E. Nishioka, and T. Nishiyama, "The Criterion for Splashing in Flattening of Thermal Sprayed Particles Onto Flat Substrate Surface," *Surf. Coat. Technol.*, **161** [2–3] 103–10 (2002).
- <sup>12</sup>M. Fukumoto, M. Shiiba, H. Kaji, and T. Yasui, "Three-Dimensional Transition Map of Flattening Behavior in the Thermal Spray Process," *Pure Appl. Chem.*, **77** [2] 429–42 (2005).
- <sup>13</sup>S. Costil, H. Liao, A. Gammoudi, and C. Coddet, "Influence of Surface Laser Cleaning Combined with Substrate Preheating on the Splat Morphology," *J. Therm. Spray Technol.*, **14** [1] 31–8 (2005).
- <sup>14</sup>G. Trapaga and J. Szekely, "Mathematical Modeling of the Isothermal Impingement of Liquid Droplets in Spraying Processes," *Metall. and Materi. Trans. B*, **22** [6] 901–14 (1991).
- <sup>15</sup>H. Zhang, X. Y. Wang, L. L. Zheng, and X. Y. Jiang, "Studies of Splat Morphology and Rapid Solidification During Thermal Spraying," *Int. J. Heat Mass Transf.*, **44** [24] 4579–92 (2001).
- <sup>16</sup>T. Yoshida, T. Okada, H. Hamatani, and H. Kumaoka, "Integrated Fabrication Process for Solid Oxide Fuel Cells Using Novel Plasma Spraying," *Plasma Sources Sci. and Technol.*, **1** [3] 195–201 (1992).
- <sup>17</sup>H. Liu, E. Lavernia, and R. Rangel, "Numerical Simulation of Impingement of Molten Ti, Ni, and W Droplets on a Flat Substrate," *J. Therm. Spray Technol.*, **2** [4] 369–78 (1993).
- <sup>18</sup>M. Bertagnolli, M. Marchese, and G. Jacucci, "Modeling of Particles Impacting on a Rigid Substrate Under Plasma Spraying Conditions," *J. Therm. Spray Technol.*, **4** [1] 41–9 (1995).
- <sup>19</sup>H. Zhang, "Theoretical Analysis of Spreading and Solidification of Molten Droplet During Thermal Spray Deposition," *Int. J. Heat Mass Transf.*, **42** [14] 2499–508 (1999).
- <sup>20</sup>L. Li, A. Vaidya, S. Sampath, H. Xiong, and L. Zheng, "Particle Characterization and Splat Formation of Plasma Sprayed Zirconia," *J. Therm. Spray Technol.*, **15** [1] 97–105 (2006).
- <sup>21</sup>S. D. Aziz and S. Chandra, "Impact, Recoil and Splashing of Molten Metal Droplets," *Int. J. Heat Mass Transf.*, **43** [16] 2841–57 (2000).
- <sup>22</sup>Y. P. Wan, H. Zhang, X. Y. Jiang, S. Sampath, and V. Prasad, "Role of Solidification, Substrate Temperature and Reynolds Number of Droplet Spreading in Thermal Spray Deposition: Measurements and Modeling," *J. Heat Transfer*, **123** [2] 382–9 (2001).
- <sup>23</sup>H. Fukunuma, "Porosity Formation and Flattening Model of an Impinging Molten Particle in Thermal Spray Coatings," *J. Therm. Spray Technol.*, **3** [1] 33–44 (1994).
- <sup>24</sup>J. P. Delplanque and R. H. Rangel, "An Improved Model for Droplet Solidification on a Flat Surface," *J. Mater. Sci.*, **32** [6] 1519–30 (1997).
- <sup>25</sup>K. A. Roberts and T. W. Clyne, "A Simple Procedure for the Characterization of Spray Deposition Processes - The Linescan Test," *Surface and Coatings Technology*, **41** [1] 103–15 (1990).
- <sup>26</sup>C. Moreau, P. Gougeon, and M. Lamontagne, "Influence of Substrate Preparation on the Flattening and Cooling of Plasma-Sprayed Particles," *J. Therm. Spray Technol.*, **4** [1] 25–33 (1995).
- <sup>27</sup>R. C. Dykhuizen, "Review of Impact and Solidification of Molten Thermal Spray Droplets," *J. Therm. Spray Technol.*, **3** [4] 351–61 (1994).
- <sup>28</sup>J. Fukai, Z. Zhao, D. Poulikakos, C. M. Megaridis, and O. Miyatake, "Modeling of the Deformation of a Liquid Droplet Impinging Upon a Flat Surface," *Phys. Fluids A*, **5** [11] 2588–99 (1992).
- <sup>29</sup>S. Chandra, and P. Fauchais, "Formation of Solid Splats During Thermal Spray Deposition," *J. Therm. Spray Technol.*, **18** [2] 148–80 (2009).
- <sup>30</sup>M. Fukumoto, E. Nishioka, and T. Matsubara, "Flattening and Solidification Behavior of a Metal Droplet on a Flat Substrate Surface Held at Various Temperatures," *Surf. Coat. Technol.*, **120–121** 131–7 (1999).
- <sup>31</sup>H. Li, S. Costil, H. L. Liao, C. J. Li, M. Planche, and C. Coddet, "Effects of Surface Conditions on the Flattening Behavior of Plasma Sprayed Cu Splats," *Surf. Coat. Technol.*, **200** [18–19] 5435–46 (2006).
- <sup>32</sup>T. Bennett and D. Poulikakos, "Splat-Quench Solidification: Estimating the Maximum Spreading of a Droplet Impacting a Solid Surface," *J. Mater. Sci.*, **28** [4] 963–70 (1993).
- <sup>33</sup>T. Young, "An Essay on the Cohesion of Fluids," *Philos. Trans. R. Soc. London*, **95** 65–87 (1805).
- <sup>34</sup>M. Pasandideh-Fard, Y. M. Qiao, S. Chandra, and J. Mostaghimi, "Capillary Effects During Droplet Impact on a Solid Surface," *Phys. Fluids*, **8** [3] 650–9 (1996).
- <sup>35</sup>J. P. Delplanque and R. H. Rangel, "A Comparison of Models, Numerical Simulation, and Experimental Results in Droplet Deposition Processes," *Acta Mater.*, **46** [14] 4925–33 (1998).
- <sup>36</sup>G. Montavon, S. Sampath, C. C. Berndt, H. Herman, and C. Coddet, "Effects of the Spray Angle on Splat Morphology During Thermal Spraying," *Surf. Coat. Technol.*, **91** [1–2] 107–15 (1997).
- <sup>37</sup>A. Vardelle, M. Vardelle, R. McPherson, and P. Fauchais, "Study of the Influence of Particle Temperature and Velocity Distribution Within a Plasma Jet Coating Formation," pp. 155–61 *Proceedings of the General Aspects of Thermal Spraying*, May 19–23, Edited by J. H. Zaai. Nederlands Inst voor Lastechiek, The Hague, The Netherlands, (1980).
- <sup>38</sup>S. H. Leigh and C. C. Berndt, "Evaluation of off-Angle Thermal Spray," *Surf. Coat. Technol.*, **89** [3] 213–24 (1997).
- <sup>39</sup>G. Montavon, C. Coddet, S. Sampath, H. Herman, and C. Berndt, "Quality Control of the Intrinsic Deposition Efficiency From the Controls of the Splat Morphologies and the Deposit Microstructure," *J. Therm. Spray Technol.*, **6** [2] 153–66 (1997).
- <sup>40</sup>N. Otsu, "Threshold Selection Method From Gray-Level Histograms," *IEEE Trans Syst. Man Cybern.*, **SMC-9** [1] 62–6 (1979). □

## Permission to publish

A.S.M. Ang, C.C. Berndt, M. Dunn, M.L. Sesso, S.Y. Kim, 'Modeling the coverage of splat areas arising from thermal spray processes', *J. Am. Ceramic Soc.*, 95[5] (2012) p. 1572-1580. DOI: 10.1111/j.1551-2916.2012.05113.x Published: MAY 2012.

Wiley Publishes Open Access Articles in fully Open Access Journals and in Subscription journals

offering Online Open. Although most of the fully Open Access journals publish open access articles under the terms of the Creative Commons Attribution (CC BY) License only, the subscription journals and a few of the Open Access Journals offer a choice of Creative Commons Licenses: Creative Commons Attribution (CC-BY) license [Creative Commons Attribution Non-Commercial \(CC-BY-NC\) license](#) and [Creative Commons Attribution Non-Commercial-NoDerivs \(CC-BY-NC-ND\) License](#). The license type is clearly identified on the article.

Copyright in any research article in a journal published as Open Access under a Creative Commons License is retained by the author(s). Authors grant Wiley a license to publish the article and identify itself as the original publisher. Authors also grant any third party the right to use the article freely as long as its integrity is maintained and its original authors, citation details and publisher are identified. These details are indicated above. The copyright owner is specified within the particular Journal.

Search: <http://onlinelibrary.wiley.com/browse/publications?type=journal> to find the final article.



# *Thermal Spray Maps: Material Genomics of Processing Technologies*

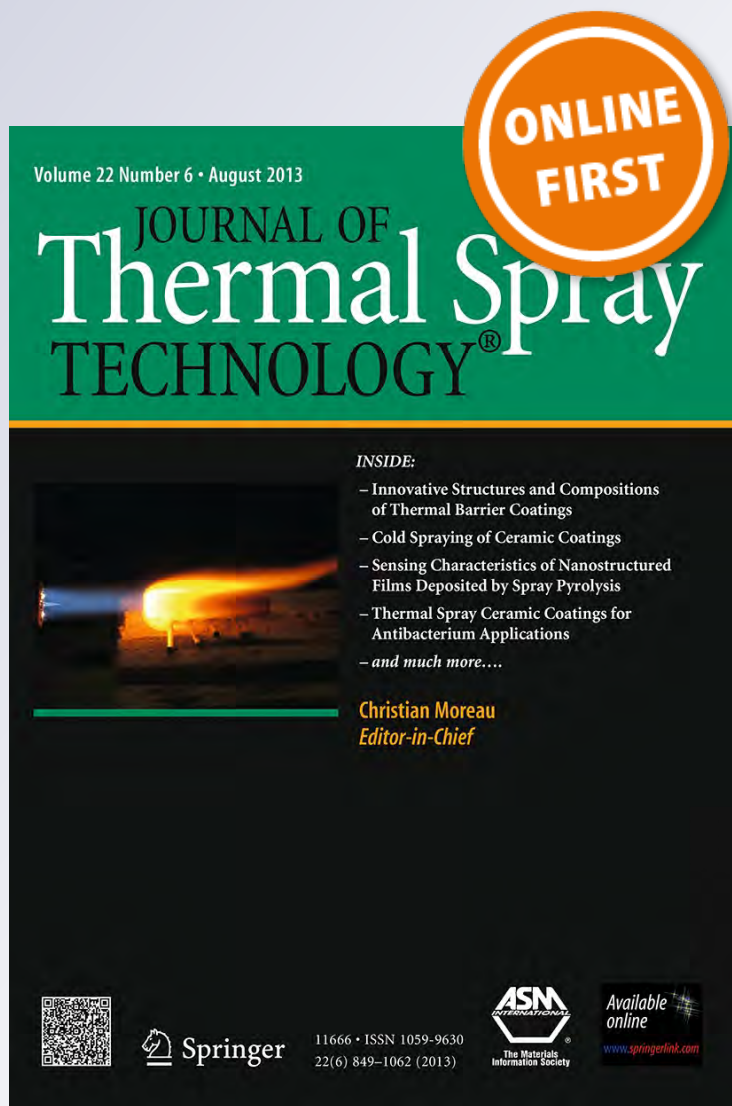
**Andrew Siao Ming Ang, Noppakun Sanpo, Mitchell L. Sesso, Sun Yung Kim & Christopher C. Berndt**

**Journal of Thermal Spray Technology**

ISSN 1059-9630

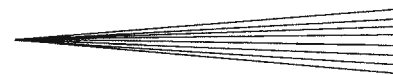
J Therm Spray Tech

DOI 10.1007/s11666-013-9970-3





**Your article is protected by copyright and all rights are held exclusively by ASM International. This e-offprint is for personal use only and shall not be self-archived in electronic repositories. If you wish to self-archive your article, please use the accepted manuscript version for posting on your own website. You may further deposit the accepted manuscript version in any repository, provided it is only made publicly available 12 months after official publication or later and provided acknowledgement is given to the original source of publication and a link is inserted to the published article on Springer's website. The link must be accompanied by the following text: "The final publication is available at [link.springer.com](http://link.springer.com)".**



# Thermal Spray Maps: Material Genomics of Processing Technologies

Andrew Siao Ming Ang, Noppakun Sanpo, Mitchell L. Sesso, Sun Yung Kim, and Christopher C. Berndt

(Submitted January 31, 2013; in revised form June 16, 2013)

There is currently no method whereby material properties of thermal spray coatings may be predicted from fundamental processing inputs such as temperature-velocity correlations. The first step in such an important understanding would involve establishing a foundation that consolidates the thermal spray literature so that known relationships could be documented and any trends identified. This paper presents a method to classify and reorder thermal spray data so that relationships and correlations between competing processes and materials can be identified. Extensive data mining of published experimental work was performed to create thermal spray property-performance maps, known as “TS maps” in this work. Six TS maps will be presented. The maps are based on coating characteristics of major importance; i.e., porosity, microhardness, adhesion strength, and the elastic modulus of thermal spray coatings.

**Keywords** adhesion, data mining, elastic modulus, genomic analysis, hardness, property map, sliding wear, spray parameters, thermal spray

## 1. Introduction

In the field of surface engineering, thermal spray is a generic term for a group of processes in which liquid droplets, semi-molten or solid particles impact and are then deposited onto a substrate as morphological features that are known as “splats” (Ref 1). A coating can be generated if the accelerated droplets or particles can (i) plastically deform or rapidly cool into thin lamellae on impact, (ii) adhere to the surface, and (iii) overlap and interlock into a consolidated coating during the solidification process. The coating is usually generated in multiple passes from 5 to 100 depending on the thickness required. The coating material may be metal based, a ceramic oxide or carbide, a polymer, or a composite; all of which may be in the morphology of a powder, wire, or rod (Ref 2).

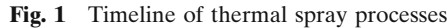
There are two important variables for any thermal spray process, flame jet temperature and particle velocity, which together are known as “TV relationships” (Ref 3, 4). This refers to the direct spatial interaction of

three physical distributions, i.e., the feedstock characteristics, the high energy temperature field, and the gas jet velocity field, that influence directly the spreading of the molten particle during splat formation. The splats or solidified molten particles, along with other important artifacts such as oxides, voids, and cracks, are the fundamental building blocks of a thermal spray coating.

### Abbreviations

APS	Atmospheric plasma spray
ASTM	American Society for Testing and Materials
CAPS	Controlled atmosphere plasma spray
CS	Cold spray
D-Gun®	Detonation gun spray
FS	Flame spray
HA	Hydroxapapite
HRC	Rockwell hardness C-scale
HVOF	High-velocity oxygen fuel spray
HVSFS	High-velocity suspension flame spray
LPPS	Low pressure plasma spray
PTWA	Plasma-transferred wire arc spray
RF	Radio frequency
SOD	Standoff distance
SPS	Suspension plasma spray
SPPS	Solution precursor plasma spray
TAT	Tensile adhesion test
TBC	Thermal barrier coating
TS	Thermal spray
TV	Flame temperature and particle velocity
TWA	Twin Wire Arc
VPS	Vacuum plasma spray
WC	Tungsten monocarbide
WC-Co	Tungsten carbide-cobalt
WSP	Water-stabilized plasma spray
YSZ	Yttria-stabilized zirconia

**Andrew Siao Ming Ang, Noppakun Sanpo, Mitchell L. Sesso, SunYung Kim, and Christopher C. Berndt**, Industrial Research Institute Swinburne, Swinburne University of Technology, H66, P.O. Box 218, Hawthorn, VIC 3122, Australia; **Andrew Siao Ming Ang, Noppakun Sanpo, Mitchell L. Sesso, and Christopher C. Berndt**, Defence Materials Technology Centre (DMTC), Swinburne University of Technology, P.O. Box 218, Hawthorn VIC 3122, Australia; and **Christopher C. Berndt**, Department of Materials Science and Engineering, Stony Brook University, Stony Brook, NY 11794. Contact [REDACTED]



Although there is a vast amount of literature documenting the development of new coating materials or processes, the thermal spray field lacks a systematic method that integrates materials' chemistry, processing, structure, property, and performance. On the other hand, there has been a paradigm shift in materials research and

Another way to understand thermal spray processes is by mapping the coating formation process that influenced the particle temperature and velocity, Fig. 2. Along with Table 2, which was compiled from references (Ref 1, 2).



**Table 1** List of references for timeline of TS development (as shown in Fig. 1)

Year	Application	Lead inventor/Company	Reference details
1911	Flame spray	M.U. Schoop	M.U. Schoop, "Improvements in or connected with the coating of surfaces with metal, applicable also for Soldering or Uniting Metals and other Materials." United Kingdom Patent No. A.D 5,712 U. K. P. Office, 1911
1912	Flame spray	M.U. Schoop	M.U. Schoop, "An Improved Process of Applying Deposits of Metal or Metallic Compounds to Surfaces." United Kingdom Patent No. A.D.21066. U. K. P. Office, 1912
1915	Electric wire arc spray	M.U. Schoop	M.U. Schoop, "Apparatus for Spraying Molten Metal and Other Fusible Substances." USA Patent No. 1,133,507. U. S. P. Office, 1915
1925	Flame spray/Pistol	F. Schori,	F. Schori, "Improved Process of and Apparatus for Atomizing." United Kingdom Patent No. 221,828. U. K. P. Office, 1925
1930	Thermal spray companies founded	Metco/MONGUL/Metallisation	"JTSA History." International Thermal Spray Association, <a href="http://www.thermalspray.org/index.php?option=com_content&amp;task=view&amp;id=58&amp;Itemid=92">http://www.thermalspray.org/index.php?option=com_content&amp;task=view&amp;id=58&amp;Itemid=92</a>
1937	Colomony's spray and fuse	N.W. Cole.	N.W. Cole and W. H. Edmonds, "Hardening material resistant to heat, acid, corrosion, and abrasion, and method of producing the same." USA Patent No. 2088838. U. S. P. Office, 1937
1938	Flame spray/Type E torch	Metco	"History: Over 75 years of Sustainable Surface Solutions," Sulzer Metco, <a href="http://www.sulzer.com/en/About-us/Our-Businesses/Sulzer-Metco/History">http://www.sulzer.com/en/About-us/Our-Businesses/Sulzer-Metco/History</a>
1939	Plasma spray	Reinecke	J.R. Davis, <i>Handbook of Thermal Spray Technology</i> , ASM International, Materials Park, OH, USA, 2004
1950	ThermoSpray Powder Gun	Metco	"History: Over 75 years of Sustainable Surface Solutions," Sulzer Metco, <a href="http://www.sulzer.com/en/About-us/Our-Businesses/Sulzer-Metco/History">http://www.sulzer.com/en/About-us/Our-Businesses/Sulzer-Metco/History</a>
1955	D-Gun®	R.M. Poorman/Union Carbide	R.M. Poorman, H. B. Sargent, and L. Headlee, "Method and apparatus utilizing detonation waves for spraying and other purposes." USA Patent No. 2714563. U. S. P. Office, 1955
1957	Flame spray/Rokide® ceramic coating	Norton Company	C.W. Cheape, <i>Family Firm to Modern Multinational: Norton Company, A New England enterprise</i> , Harvard University Press, 1985
1957	Plasma spray/Argon plasma torch	R.M. Gage/Union Carbide	R.M. Gage, "Arc torch and process." United States of America Patent No. 2806124. U. S. P. Office, 1957
1960	Plasma spray/SG-1 torch	G.M. Giannini/Plasmadyne Corporation	G.M. Giannini and A.C. Ducati, "Plasma Stream Apparatus and Methods." USA Patent No. 2,922,869. U. S. P. Office, 1960
1967	RF Plasma	T.B. Reed/Massachusetts Institute of Technology	T.B. Reed, "Induction plasma torch with means for recirculating the plasma." United States of America Patent No. 3324334. U. S. P. Office, 1967
1960	Plasma spray/MB series torches	Metco Inc.	"History: Over 75 years of Sustainable Surface Solutions," Sulzer Metco, <a href="http://www.sulzer.com/en/About-us/Our-Businesses/Sulzer-Metco/History">http://www.sulzer.com/en/About-us/Our-Businesses/Sulzer-Metco/History</a>
1960	Twin wire arc/torch improvements	Various authors	D.M. Yenni, W.C. McGill, and J.W. Lyle, "Electric arc spraying." USA Patent No. 2982845. U. S. P. Office, 1961
1973	Plasma spray/LPPS	E. Muehlberger/Electro-Plasma Inc.	G.A. Jensen, "Device for coating substrates." USA Patent No. 3140380. U. S. P. Office, 1964 I. Kiyoshi, "Method of and apparatus for the electric spray-coating of substrates." USA Patent No. 3358114. U. S. P. Office, 1967 E. Muehlberger and P. Meyer, LPPS—Thin Film Processes: Overview of Origin and Future Possibilities, <i>Proceedings of the International Thermal Spray Conference 2009</i> , B.R. Marple, M.M. Hyland, Y.-C. Lau, C.-J. Li, R.S. Lima, and G. Montavon, Ed., 4-7 May 2009 (Las Vegas, NV, USA), ASM International, 2009, p 737-740.
1975	Plasma spray/SG100 torch	Plasmadyne Corporation	"Plasma Equipment Solutions," Praxair Surface Technologies Inc., Praxair Technology, Inc., USA, 2012
1979	Plasma spray/Gatorgard	L.S. Sokol/United Technologies Corporation	L.S. Sokol, C.C. McComas, and E.M. Hanna, "Plasma spray method and apparatus." USA Patent No. 4256779. U. S. P. Office, 1981.
1970	Plasma spray/F4 torch	Metco Inc.	"History: Over 75 years of Sustainable Surface Solutions," Sulzer Metco, <a href="http://www.sulzer.com/en/About-us/Our-Businesses/Sulzer-Metco/History">http://www.sulzer.com/en/About-us/Our-Businesses/Sulzer-Metco/History</a>
1982	HVOF/JetKote®	J.A. Browning	J. A. Browning, "Ignition method and system for internal burner type ultra-high velocity flame jet apparatus." USA Patent No. 4342551. U. S. P. Office, 1982
1988	Plasma spray/APG torch	Metco Inc.	"History: Over 75 years of Sustainable Surface Solutions," Sulzer Metco, <a href="http://www.sulzer.com/en/About-us/Our-Businesses/Sulzer-Metco/History">http://www.sulzer.com/en/About-us/Our-Businesses/Sulzer-Metco/History</a>



Table 1 continued

Year	Application	Lead inventor/Company	Reference details
1989	HVOF/second Generation	Various suppliers	F. Gärtner, H. Kreye and H. J. Richter, HVOF spraying with powder and wire, <i>7th Colloquium HVOF Spraying</i> C. Penszior and P. Heinrich, Ed., 9-10 November 2006, (Unterschleißheim, Germany), GTS e.V., 2006
1990	Super D-Gun®	Union Carbide Coatings Service Corporation	B. J. Gill, <i>Super D-Gun</i> , Aircraft Engineering and Aerospace Technology, 62, MCB UP Ltd., 1990, p 10-33
1980	Cold Spray	A. Papyrin	A. Papyrin, Cold spray technology. <i>Advanced Materials and Processes</i> , 2001, 159(9), p 49-51
1980	TWA/Equipment improvements	Various suppliers	L. Pawlowski, <i>The Science and Engineering of Thermal Spray Coatings</i> , Wiley, Chichester, 2008
1992	Plasma spray/PlazJet 170kW torch	Praxair	K. E. Schneider, V. Belashchenko, M. Dratwinski, S. Siegmann, and A. Zagorski, <i>Practical Experience Today</i> , Thermal Spraying for Power Generation Components, Wiley-VCH Verlag GmbH & Co. KGaA, 2006, p 17-104
1992	HVOF/third Generation	Various suppliers	F. Gärtner, H. Kreye, and H.J. Richter, HVOF spraying with powder and wire, <i>7th Colloquium HVOF Spraying</i> C. Penszior and P. Heinrich, Ed., 9-10 November 2006, (Unterschleißheim, Germany), GTS e.V., 2006
1992	RF Plasma/1 MW torch	M.I. Boulos/Tekna	M. I. Boulos and J. Jurewicz, "High performance induction plasma torch with a water-cooled ceramic confinement tube," USA Patent No. 5200595; U. S. P. Office, 1993
1990	Water-stabilized plasma spray	M. Hrabovský/Institute of Plasma Physics ASCR	M. Hrabovský, Water-stabilized plasma generators. <i>Pure and Applied Chemistry</i> , 1998, 70(6), p 1157-1162
1990	Plasma spray/Triplex 24kW torch	Sulzer Metco	"History: Over 75 years of Sustainable Surface Solutions," Sulzer Metco, <a href="http://www.sulzer.com/en/About-us/Our-Businesses/Sulzer-Metco/History">http://www.sulzer.com/en/About-us/Our-Businesses/Sulzer-Metco/History</a>
1994	Plasma spray/Axial III torch	Northwest Mettech Corp.	"About Us: Northwest Mettech," Northwest Mettech Corp. <a href="http://www.mettech.com/company/corporate/about-us.html">http://www.mettech.com/company/corporate/about-us.html</a>
1995	DPV 2000/Particle diagnostics	Tecnar Ltd.	"TECNAR Spray Diagnostics Products: Online Characterization Of Particles During Thermal /Cold Spraying," Tecnar Ltd., <a href="http://www.tecnar.com/index.php/products/spray-diagnostics">http://www.tecnar.com/index.php/products/spray-diagnostics</a>
1998	Plasma spray/Triplex II 55kW torch	Sulzer Metco	"History: Over 75 years of Sustainable Surface Solutions," Sulzer Metco, <a href="http://www.sulzer.com/en/About-us/Our-Businesses/Sulzer-Metco/History">http://www.sulzer.com/en/About-us/Our-Businesses/Sulzer-Metco/History</a>
1998	Plasma-transferred wire arc spray	D.R. Marantz/Ford Global Technologies, Inc.	D.R. Marantz, K. A. Kowalsky, J. R. Baughman and D. J. Cook, "Plasma transferred wire arc thermal spray apparatus and method," USA Patent No. 5808270, U. S. P. Office, 1998
1999	SprayWatch/Particle diagnostics	Oseir Ltd.	"Company Info: Oseir Ltd.," Oseir Ltd., <a href="http://www.oseir.com/">http://www.oseir.com/</a>
2001	Plasma spray/100HE 105kW torch	Progressive Technologies	"Improving the Economics of Plasma Spray: 100HE Sixteen Hour Durability Run," Progressive Technologies, <a href="http://www.progressivesurface.com/downloads/casestudies/100HE_16hour_run.pdf">http://www.progressivesurface.com/downloads/casestudies/100HE_16hour_run.pdf</a> , 2003.
2000	Cold Spray/Kinetics family torches	CGT GmbH.	"Linde launches cold spray technology," <a href="http://www.gasworld.com/linde-launches-cold-spray-technology/1702.article">http://www.gasworld.com/linde-launches-cold-spray-technology/1702.article</a> , 2007
2006	Warm Spray	J. Kawakita/NIMS	J. Kawakita, S. Kuroda, S. Krebs and H. Katanoda, In-situ densification of Ti coatings by the warm spray (two-stage HVOF) process. <i>Materials Transactions</i> , 2006, 47(7), p 1631-1637
2008	Nano-ceramic coatings	Northwest Mettech Corp.	J. Oberste Berghaus, J. G. Legoux, C. Moreau, R. Hui, C. Decès-Petit, W. Ou, S. Yick, Z. Wang, R. Maric and D. Ghosh, Suspension HVOF spraying of reduced temperature solid oxide fuel cell electrolytes. <i>Journal of Thermal Spray Technology</i> , 2008, 17(5-6), p 700-707
2009	Plasma spray/PlazJet II 220kW torch	Praxair TAFE	"Plasma Equipment Solutions," Praxair Surface Technologies Inc., Praxair Technology, Inc., USA, 2012

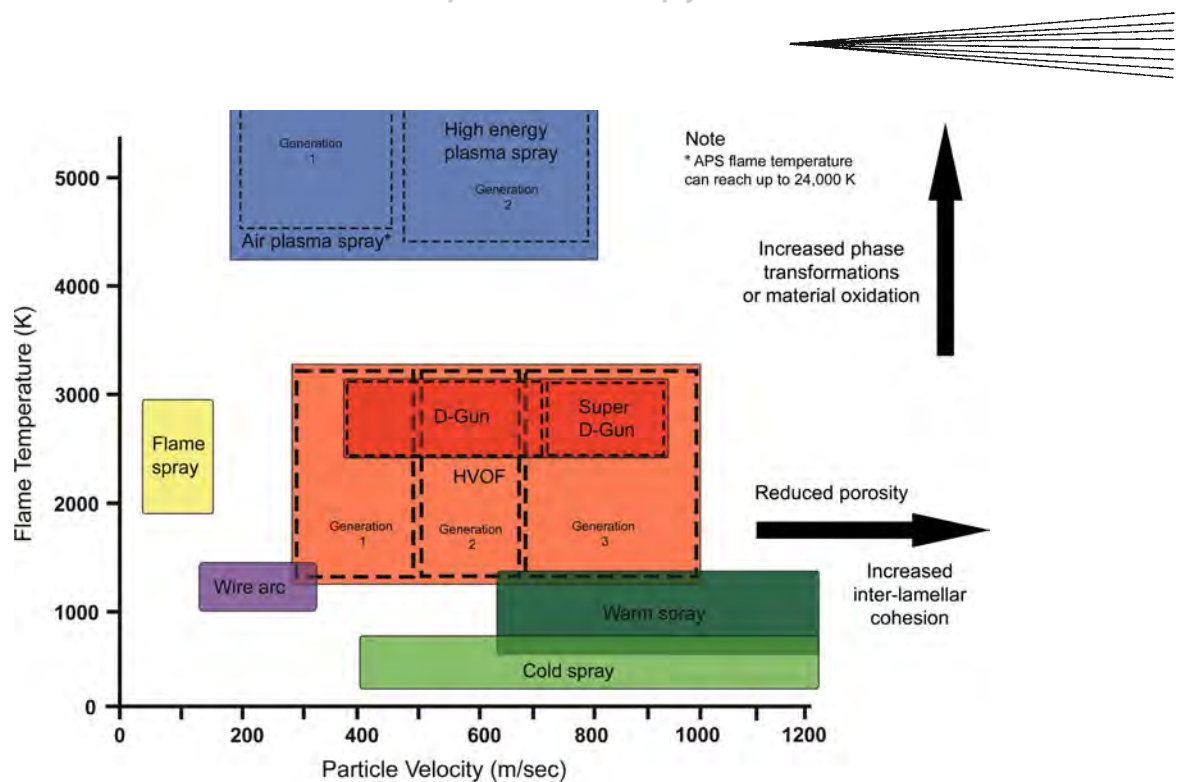


**Fig. 2** Classification of thermal spray processes with accordance to particle velocity and flame temperature

**Table 2** Comparison of typical process variables in thermal spray technology

Spray process	Flame temperature, K	Particle velocity, m/s	SOD, mm	Width of spray footprint, mm
FS	3000	150	120-250	50
TWA	6000	240	50-170	40
D-Gun®	4500	750	100	<25
APS	10000	350	60-130	20-40
LPPS	15000	600	300-400	50-60
HVOF	3400	650	150-300	<20
CS	1000	800	10-50	<5

Fig. 1 and 2 illustrate that advances in thermal spray technology are a direct consequence of altering the temperature-velocity characteristics of the spray devices. Therefore, the TS maps that will be presented later may be cross-indexed onto Fig. 2 so that a concordance approach evolves. The cross correlation of distribution analyses involving (i) the TV characteristics and (ii) the property-process relationships is beyond the scope of this review.

The third critical factor in thermal spray processing revolves around the feedstock. Depending on the thermal spray operation considered, an appropriate combination between the feedstock material and size must be considered. Table 3 compiles a list of commercially available powder feedstocks and the associated thermal spray method that is typically employed (Ref 13–16). Correct selection of feedstock is critical since this decision relates to the deposition efficiency of the process and, therefore, the overall manufacturing economics.

### 3. Material Genomic Approach for Thermal Spray

Although thermal coatings have been produced for certain applications, there are certain material properties that are mutually dependent. These properties include (i) porosity, (ii) hardness, (iii) adhesion, (iv) elastic modulus, (v) fracture toughness, and (vi) the Poisson's ratio of thermal spray coatings. A scoping study for relevant data from the literature revealed that this was a complex task. For example, it was necessary to consolidate and standardize the property data of different coatings that had been manufactured with a variety of equipment under diverse reporting standards.

The issue of reporting standards and lapses in documentation in the open literature focussed the current study toward classes of materials and processes that can be considered of widespread popularity. For instance, WC-Co coatings are extensively used as wear-resistant



**Table 3** Compilation of commercially available powders produced via the various production methods

Classification	Material constituents	Possible production method								
		Gas atomized	Water atomized	Fused and crushed	Sintered and crushed	Agglomerated and sintered	Dense coated	Plasma densified	Blend	Application method
Metal/metallic alloy	Al, Al-Si	X								APS, CS, FS
	Cu, Cu-Ni, Cu-Al	X								HVOF, APS, CS, FS
	Ti, Ta	X								VPS, CS
	FeCr, FeCrNiMo, FeCr based	X	X				X			APS, FS
	MCrAlY (M=Co, Ni, Fe)	X								APS, HVOF,VPS
Metallic composite	Mo, Mo based				X	X		X		APS
	Ni, Ni-Cr, Ni-Al, Ni based,	X	X				X			APS, FS, CS, HVOF, VPS
	Al-Si-based abrasibles CoNi-based abrasibles Ni-based abrasibles Cu-Al-Bronze						X		X	APS, FS APS FS HVOF, APS
Intermetallic	CoCrNiWC, CoCr based	X	X							HVOF, APS
	NiCrSiB, NiCrSiB-based, self-fluxing alloys	X	X							FS, HVOF
Cermet	Mo-Mo <sub>2</sub> C					X				APS
	CrC-NiCr, CrC-Ni based				X	X	X		X	APS HVOF FS
Ceramic	WC-Co, WC-Ni, WC based				X	X	X	X		APS HVOF FS
	Al <sub>2</sub> O <sub>3</sub> , Al <sub>2</sub> O <sub>3</sub> - TiO <sub>2</sub>			X					X	APS, FS
	Cr <sub>2</sub> O <sub>3</sub> , Cr <sub>2</sub> O <sub>3</sub> -TiO <sub>2</sub> , Cr <sub>2</sub> O <sub>3</sub> -TiO <sub>2</sub> -SiO <sub>2</sub>			X	X	X			X	APS APS, FS
	TiO <sub>2</sub> ZrO <sub>2</sub> -Y <sub>2</sub> O <sub>3</sub> , ZrO <sub>2</sub> -MgO			X		X				APS

FS: Flame spray. APS: Atmospheric plasma spray. VPS: Vacuum plasma spray. HVOF: High-velocity oxygen fuel spray. CS: cold spray

FS: Flame spray. APS: Atmospheric plasma spray. VPS: Vacuum plasma spray. HVOF: High-velocity oxygen fuel spray. CS: cold spray



coatings and alumina-based coatings represent a large proportion of the market for thermal spray as anti-wear and corrosion-resistant coatings. Although there is an emphasis on these materials, it can be pointed out that they can be sprayed by many processes, the maps of which are very informative as will be presented later.

The material-property measurements of thermal spray coatings are related to the lamellar microstructure. Analyzing the literature on thermal spray coatings is challenging due to the many types of feedstock, spray systems, spray parameters, and other variables that influence the coating final structure. The lack of an overall framework for the presentation of properties has also arisen because researchers have focused on the properties and performance of specific coatings or processes rather than relationships among the entire family.

Relationships among the feedstock materials, thermal spray methods, and spray parameters have been drawn by compiling the mechanical properties into a single database. This material genomic approach is depicted in a flow chart, Fig. 3. The database structure was constructed and then populated by reviewing the available literature so that trends could be discerned. In this manner, the broader relationships of thermal spray coatings were explored by constructing plots that summarized data to show the interactions between processes and materials. These so-determined scatter plots were inspired, in part, by the material selection plots formulated by Prof. M. Ashby of Cambridge University in the United Kingdom (Ref 10). The Ashby scatter plots displayed two or more properties of many materials or classes of materials. Similarly, the “thermal spray property-performance maps” (termed as “TS maps”) created in the current work have incubated a fresh perspective that has allowed a balanced comparison of results across different laboratories.

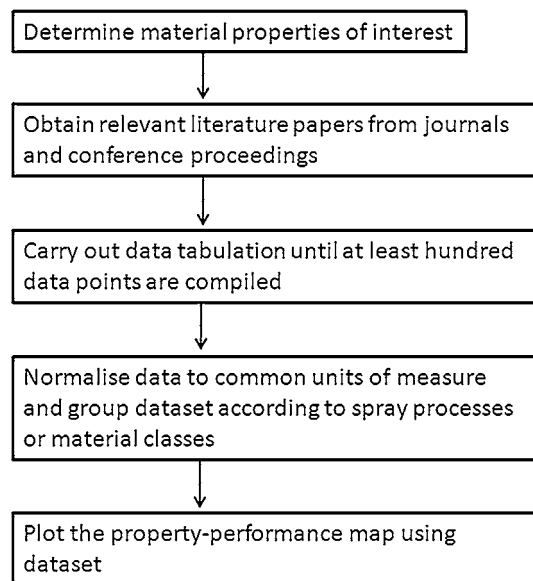


**Fig. 3** Flow chart to describe TS PPM construction process

It must be noted that the TS maps are conceptually different from process maps in thermal spray technology (Ref 17, 18) which are used to assess coating reliability. Process maps have been yielded from the in situ monitoring of the temperature and velocity spray profile of the powder particles and splats. These process maps are constructed on the basis of experimental work and are specific for a defined feedstock. Hence, it can be recognized that TS maps provide an overview of the different processes and feedstocks available, while “process maps” relate specifically to the variability in a particular spray-feedstock system.

The following section compiled test data of commonly investigated thermal spray coating properties from the published literature. There is a natural, intrinsic cause and effect relationship among the temperature-velocity conditions, the feedstock materials, and their particle size distribution. Thus, analysis of these datasets was expected to yield observable trends and comparisons with regard to the thermal spray processes. Such a retrospective analysis and review has not been reported previously.

## 4. Review of Thermal Spray Coating Property Data

Five frequently investigated coating properties will be presented in this work. The TS maps are focussed on porosity, hardness, coating adhesion, elastic modulus, and sliding wear performance of thermal spray coatings. It is important to emphasize that this study was intended as a broad survey of coating properties. All of the experimental details are presented in the original manuscripts and the properties determined by these original investigators were applied to studies within their own context.

The first step to construct TS maps was to assemble data from the literature and standardize the units of measure. The complexity of data collection laid in dealing with the different reporting formats and in some cases interpreting and estimating the reported values. These data were then plotted onto scatter graphs with common axes.

The TS maps presented in this study were plotted from approximately 100 individual data points. Figure 3 is a flow chart that describes the TS map construction procedure. Six TS maps are reviewed in this study and these can be considered as typical of the information that can be revealed by careful analysis.

### 4.1 Map 1: Hardness-Porosity of Thermal Sprayed WC-Co Coatings

The scatter plot of hardness and porosity of tungsten carbide-cobalt (WC-Co) composite coatings is presented in Fig. 4. Four thermal spray methods are represented in the plot: atmospheric plasma spray (APS), high-velocity oxygen fuel (HVOF) spray, detonation gun (D-Gun<sup>®</sup>) spray, and cold spray (CS). These deposition techniques are typically used for WC-Co coatings. The units of hardness have

been normalized to GPa and only cross-sectional microhardness test values considered. The differences in the test method, i.e., Vickers and Knoop tests, have been assumed to be negligible. The authors appreciate that these hardness techniques sample different volumes of materials under dissimilar stress conditions; however, pooling such data allows a more comprehensive database to be created without compromising data quality to a large degree. The coating porosity data can be quantified by many methods (Ref 19, 20) and the data across techniques are presumed indifferent for the purposes of this current study.

The assumptions stated above can be disputed. However, this current study is aimed at setting a foundation for future data-mining exercises where limitations that depend on reporting and testing protocols can be more rigorously resolved. In other words, one of the outcomes of this review is that all investigators need to report testing methods and protocols more meticulously so that data-mining exercises may be prescribed in the future.

Figure 4 reveals a large degree of variance of coating hardness across the four spray methods. A clustering of data points for each individual spray method can be identified. Thermal spray techniques, such as CS and D-Gun<sup>®</sup>, which use high particle kinetic energy for coating formation, lead to a low coating porosity and high coating hardness. The high thermal input of APS coating deposition produced coatings with large numerical variations in porosity and hardness. The thermal spray footprint, or spray envelope, of the APS process is significantly larger and more flat than those of HVOF, D-gun<sup>®</sup>, and CS, refer to Table 2 and Fig. 2. Thus, the TV processing zone is more variable and this leads to material characteristics that are highly dispersed. It can also be observed for the HVOF and D-gun<sup>®</sup> processes, where there are statistically significant data, that low porosity materials revealed hardness data that were clustered. That is, processes that

lead to high-density coatings will also give rise to the most reliable material characteristics.

The APS process also leads to decarburization of WC to W<sub>2</sub>C, which can occur at high temperature. This phase transformation creates formation of a brittle phase that increased the overall coating hardness (Ref 21) and which has contributed to the data scatter. Another reason for the data scatter arose due to differences in feedstock and spray parameters. For instance, there can be changes in the coating composition between the ratio of ceramic WC and metallic cobalt feedstock. Different laboratory or research groups may also choose to experiment with (i) a unique blend of WC-Co, (ii) different feedstock size, or (iii) spray parameters.

Nevertheless, the general trend is that the microstructural porosity decreases with increasing coating hardness. In other words, a dense coating would have a higher coating hardness compared to a porous coating. Although this conclusion might be as expected on the basis of a fundamental understanding of material-property relationships, the TS map allows visualization of (i) relationships among different TS processes, (ii) a broad ranking of the TS processes with respect to porosity and hardness, (iii) aim values for specific hardness and porosity combinations, and (iv) the reliability of obtaining specific properties on the basis of process reproducibility.

#### 4.2 Map 2: Hardness-Porosity of Thermal Sprayed Alumina Coatings

Alumina (Al<sub>2</sub>O<sub>3</sub>) and alumina-based (i.e., Al<sub>2</sub>O<sub>3</sub>-TiO<sub>2</sub>) coatings have significant industrial applications and, thus, these coatings have been data mined in greater detail. The TS map for alumina is plotted using the same methods and assumptions from the WC-Co map. In addition to the four earlier mentioned thermal spray techniques, other methods such as low pressure plasma spray (LPPS), solution precursor plasma spray (SPPS), and high-velocity suspension fuel spray (HVSFS) have been included on the map. Eight thermal spray processes are represented in Fig. 5.

It can be noted that the common spray techniques were identifiable by highlighted clusters. Pure alumina coatings exhibited higher hardness; however, the coatings were also brittle. Thus, 2 to 4 wt% of titania is usually blended with the alumina feedstock to increase the toughness of the thermal spray coating. Coatings produced from materials with increasingly higher percentages of titania, commonly 13 or 40 wt.% TiO<sub>2</sub>, exhibited lower hardness (Ref 22, 23). Coatings produced via CS must include a metallic binder that would have lowered the average hardness values.

Alumina also exhibited several phases, the most stable being the alpha phase. Almost all sintered alumina products are available in the hexagonal close-packed structures of the alpha phase. On the other hand, due to the rapid melting and quenching rates of thermal spray processes, gamma phase alumina was prevalent within a thermal spray coating (Ref 24, 25). The gamma phase is a fine-grained alumina that exhibits the cubic spinel structure. In the case of thermal spray alumina coatings, the phase

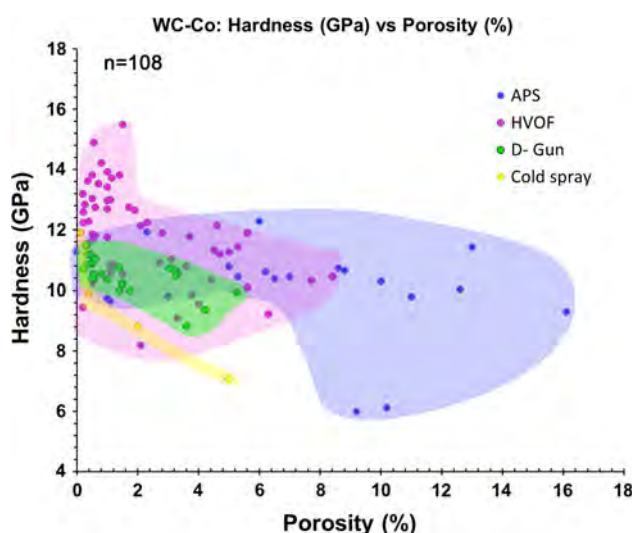


**Fig. 4** Hardness-porosity map of thermal spray tungsten carbide-cobalt coatings ( $n=108$  data points)

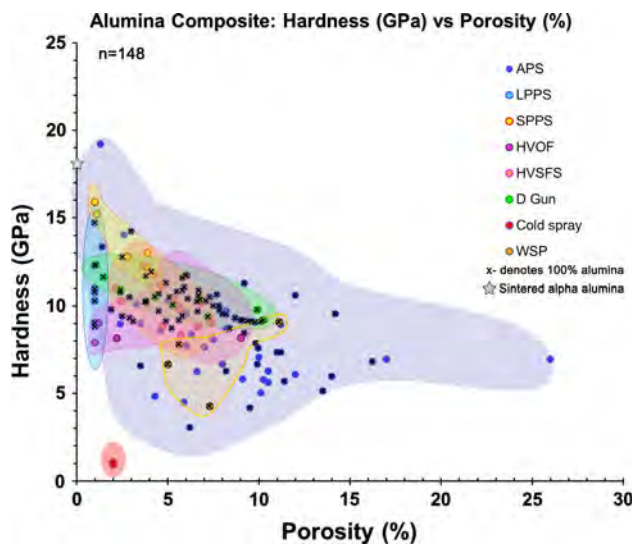


**Fig. 5** Hardness-positivity map of thermal spray alumina composite coatings ( $n=148$  data points). Note: “x” overlay symbol represents pure alumina coatings

changes did not influence the hardness values as markedly as the decarburization of WC-Co phase. Gamma alumina has a lower hardness compared to the alpha phase that exhibits a hardness of approximately 16–20 GPa. It can be seen from the microhardness axis of Fig. 5 that, due to the presence of gamma alumina within the spray coating microstructure, coating hardness is lower than for sintered alpha alumina ceramics.

It should be noted that some of the compiled data consisted of thermal spray coatings that were heat treated. The gamma phase converts to the alpha phase at sintering temperatures above 1000 °C (Ref 24, 26). These heat-treated coatings exhibited increased hardness and reduced porosity due to grain coarsening. By comparison, the gamma structure exhibited a higher specific surface area compared to the alpha phase. Therefore, during transformation from gamma to alpha alumina, densification of the coating microstructure occurred (Ref 24).

The general trend within Fig. 5 is similar to the previous TS map; hardness decreases with increasing coating porosity. Coatings with near to zero porosity can be achieved with thermal spray processes such as the LPPS, SPPS, and HVSFS. Although, not displayed in Fig. 2, SPPS and HVSFS are emerging thermal spray methods that allow the deposition of nanostructured alumina coatings using a liquid-based feedstock. APS offered the most flexible thermal spray process to achieve coatings with a wide-ranging porosity level.

#### 4.3 Map 3: Porosity-Bond Strength of Thermal Spray Coating

The two TS hardness-positivity maps presented previously establish the trend that hardness decreases with increasing porosity. The next TS map explores the effects of coating porosity on bond strength. Collation of tensile adhesion test data (TAT) of thermal spray coatings

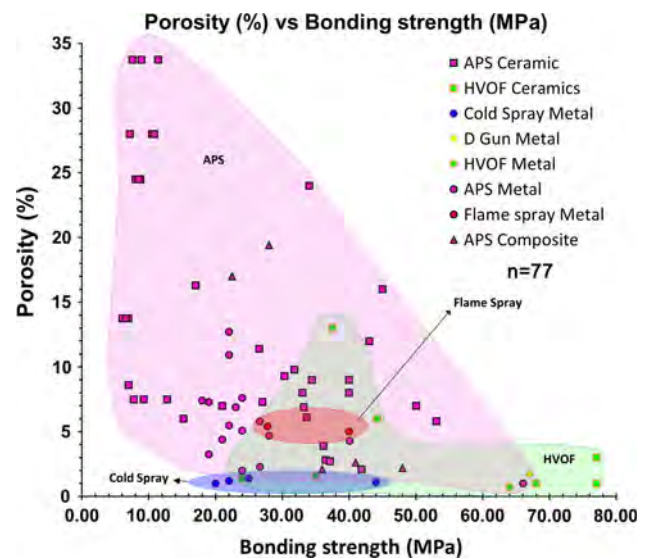


**Fig. 6** Porosity-bond strength map of thermal spray coatings from different processes ( $n=77$  data points). The coating classes are distinguishable by the plot shape; metallic coatings are plotted as circles, ceramic coatings are plotted as squares, and composites are shaped as triangles

performed using the ASTM C633 standard (Ref 27) or its equivalent was carried out. The reported TAT data have been normalized to MPa by taking the ratio of the failure load to the test area of the coating. In cases when a range of values for a particular coating system was quoted within the research work, an average value was calculated. The corresponding porosity levels were also gathered and plotted collectively to form the porosity-bond strength TS map seen in Fig. 6.

Five thermal spray processes are represented in the TS map and have been outlined by different color shades. The graph legend displays the different combinations of process and materials' classes. The thermal spray processes are APS (pink), HVOF (green), CS (blue), flame spray (red), and D-Gun® (yellow). Coating details such as feedstock type and spray parameters have not been included within this TS map to maintain clarity. Although this generalization simplifies the scatter plot for user interpretation, there is a loss of information such as the mode of failure for individual data points. In addition, the original data points have not been classified with regard to experiment conditions such as the type of adhesive, the specimen geometry, or coating thickness. As mentioned earlier, each data point has been treated as unique information since the original authors were seeking specific data for their own study.

It can be ascertained from the scatter plot that bond strength increased with decreasing porosity. The TS map also affirms that thermal spray deposition methods such as HVOF and D-Gun® were associated with coatings of high bond strength and low porosity. The APS method revealed a large variance on measured bond strength that probably depended on the coating application. Coatings for biomedical applications (i.e., hydroxyapatite) and



thermal barrier protection (i.e., yttria-stabilized zirconia) required intentional porosity within the microstructure. The APS method offered the most flexible deposition option in these instances. However, the large void content acted as stress concentrators or failure sites for crack growth and gave rise to low bond strength (Ref 28).

#### 4.4 Map 4: Hardness-Bond Strength of Thermal Spray Coating

The relationship of coating bond strength among material classes was investigated on a TS map that was based on coating hardness. The reasoning was that thermal spray ceramic coatings would present higher coating hardness values than metallic ones. The fourth TS map is, therefore, presented in Fig. 7 and exhibits the microhardness vs. bond strength for several thermal spray coatings. The three classes of material are color shaded: ceramics (red), metals (green), and composites (yellow).

Figure 7 indicates that metallic thermal spray coatings exhibited greater bond strengths than ceramic coatings. Coated ceramics revealed high microhardness, but relatively more data points of low tensile bond strength. Metallic coatings have high bond strength, but low microhardness values. The minimum failure stress was also comparatively higher for metallic thermal spray coatings. The reasons for the difference in bond strengths are probably related to the effective intersplat contact, coating residual stress, and failure mechanism (Ref 29, 30). These factors are not reflected in this particular TS map and insufficient data exist to document additional TS maps.

The failure strength of thermal spray composite coatings, for example, WC-Co, exhibited properties that overlapped its parent material classes, i.e., metals and ceramics, and the properties depended on the relative coating composition and spray method. Within the same material class, the HVOF and VPS methods exhibited the

highest bond strength, which was associated with their dense coating microstructure.

#### 4.5 Map 5: Porosity-Elastic Modulus of Thermal Spray Coating

The consolidation of the elastic modulus data for thermal spray coatings would reveal any dissimilarity in this mechanical property compared to bulk materials. The elastic moduli for common bulk engineering materials were compiled from references (Ref 31, 32), Table 4. The differences arise due to the unique microstructure of a thermal spray coating since they exhibit intersplat, pseudo-ductile behavior. There are many methods, as well as several prime specimen orientation directions, to measure coating elastic modulus, all of which make data normalization challenging. Firstly, both tension and compression testing data are considered, with the majority of available data reported in the compression mode.

**Table 4** The bulk elastic modulus properties of common engineering materials

	Material	Elastic modulus ( $E$ ), GPa
Metals	Al	67
	Cu	128
	Fe	208
	Zn	69-138
	Ni	207
	Ti	120
Ceramics	TiO <sub>2</sub> (rutile)	283
	Al <sub>2</sub> O <sub>3</sub> (alpha)	380
	Cr <sub>2</sub> O <sub>3</sub>	> 103
	Partially stabilized ZrO <sub>2</sub>	205
	Fully stabilized ZrO <sub>2</sub> (cubic)	97-207
	Cr <sub>3</sub> C <sub>2</sub>	373
	Cemented carbides	96-654

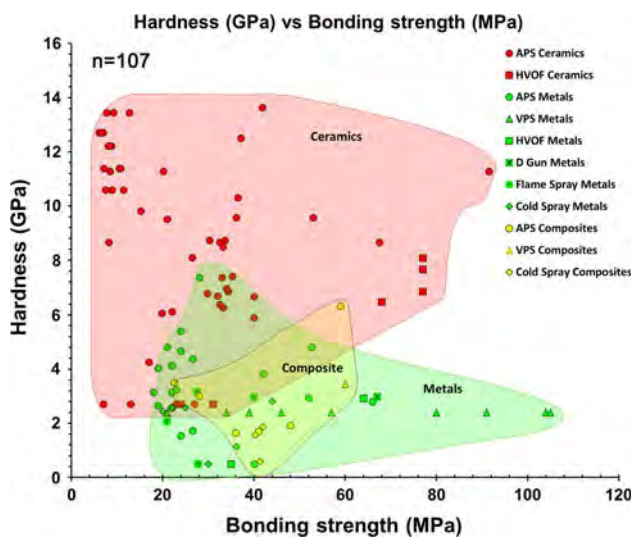


**Fig. 7** Hardness-bond strength map of thermal spray coatings from different material classes ( $n = 107$  data points). The shape of the data points represents the spray technique

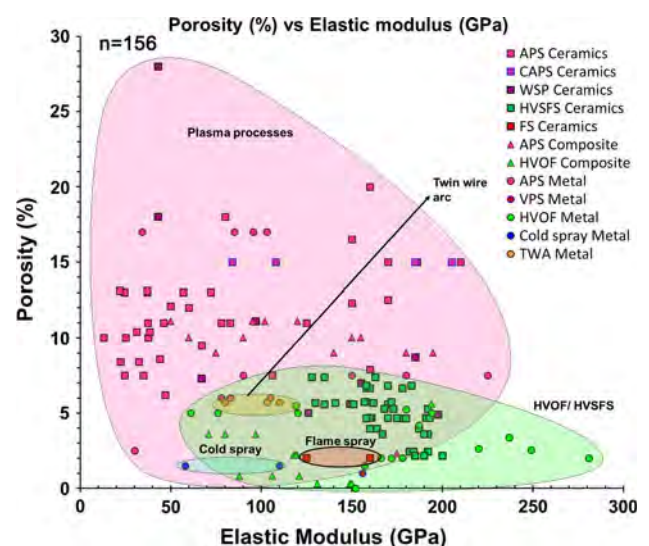


**Fig. 8** Porosity-elastic modulus map of thermal spray coatings from different processes ( $n = 156$  data points)

In addition, the porosity-elastic modulus data consist of both in-plane and cross-sectional elastic modulus for thermal spray coatings. All of the available data are presented for completeness so that appropriate comparisons to the bulk material can evolve, although it has been mentioned earlier that the coating elastic moduli are interrelated with specimen orientation. Finally, the units for elastic modulus were standardized to GPa. Therefore, after data normalization, the fifth TS map is presented in Fig. 8. The style of the plot is consistent with the earlier TS maps; that is, the five individual thermal spray processes are color shaded and the legend indicates the three different material classes.

Two observations can be made concerning the range of coating elastic moduli. Firstly, the values for ceramic thermal spray coatings were significantly lower than for the corresponding bulk sintered ceramic values. In-plane coating elastic modulus was expected to be higher than the cross-sectional values due to the anisotropic lamellar microstructure that offers limited pseudo-ductility in that direction. However, from Fig. 8, it is evident that a majority of the thermal spray ceramic coatings (square-shaped data) do not exceed an elastic modulus of 200 GPa. For instance, some values of sintered ceramics (Ref 33) are as follows: alumina is 380 GPa; titania is 283 GPa; and partially stabilized zirconia is 205 GPa. Therefore, the effects of intersplat sliding within the porous microstructure of the coating reduced the effective stiffness. In other words, the stiffness values of thermal spray ceramic coatings will be significantly lower compared to bulk ceramics, especially in instances where coating porosity increases.

The second observation relates to the higher values of elastic modulus for metal thermal spray coatings, depicted as circles in Fig. 8. This unexpected effect arose probably due to the oxidation of metallic splats during the thermal spray process. The formation and entrapment of metal oxides within the coating microstructure would have caused an increase in the overall coating modulus.

Figure 8 demonstrates that thermal spray coatings deviate considerably from the conventional elastic properties of the corresponding bulk material. The general trend exhibited is that the coating elastic modulus decreased with increasing porosity. A physical interpretation is that there would be a greater tendency of lamellae sliding due to regions of poor intersplat contact (Ref 34, 35). Plasma-based thermal spray processes revealed the largest data variation among the spray methods. The properties depended on the porosity levels as well as phase transformations that occurred during the spray process. High kinetic energy spray processes, such as HVOF, HVSFS, and CS techniques, exhibited less scatter in these data since the porosity levels were low and the coating properties would be affected only by phase transformations.

#### 4.6 Map 6: Hardness-Elastic Modulus of Thermal Spray Coating

It would be expected that the elastic modulus of ceramics be greater than that of metals. Therefore, using

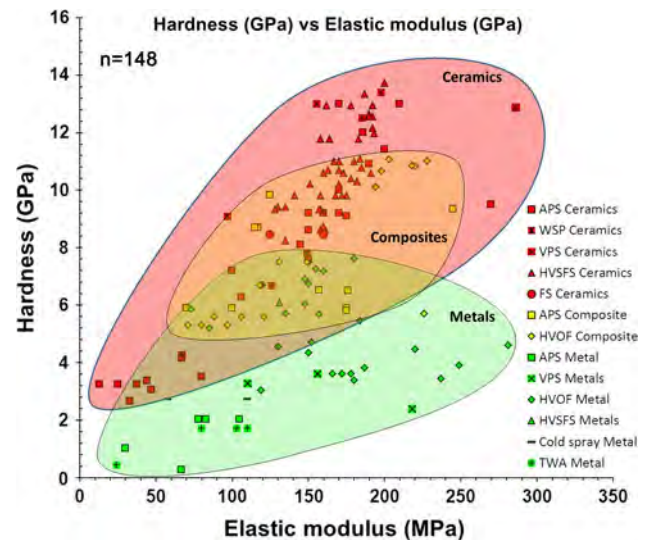


Fig. 9 Hardness-elastic modulus map of thermal spray coatings from different processes ( $n = 148$  data points)

the same concept as in TS Map 4, coating hardness data were used to discriminate the various material classes. The coating elastic modulus was plotted against the microhardness data to determine whether the expected trend could be validated. The three types of material classifications were identified by the same color scheme adopted for TS Map 4. The results, Fig. 9, show that metal coatings appear on the lower region compared to ceramic coatings, which is consistent with fundamental material-property behavior.

The general trend is that the elastic modulus increases with coating microhardness, which follows the expected trend that modulus and hardness are positively correlated. It must be noted that only the corresponding cross-sectional elastic moduli values of coatings were taken into consideration to be consistent with the coating cross-sectional microhardness values.

Plasma-based processes are widely used methods for deposition of ceramic coatings, whereas HVOF techniques are more common for metal-based coatings. Both methods are able to produce the greatest coating elastic modulus and hardness readings among their respective material class.

The six property-performance TS maps constructed in this work allow a systematic analysis for the material properties of thermal spray coatings with respect to thermal spray processes. The scatter plots consisted of more than 80 data points across many variants of deposition techniques and feedstocks from different researchers and laboratories. The nature in which these data were collected involved an unbiased representation so that no specific research group or publication paper could be favored.

The new approach taken in this work is more significant than a conventional literature review. The property-performance TS maps have indicated an ability to interrelate all data within the field of thermal spray and provide a



holistic explanation to coating properties. The TS map approach was different from that of TS processing map methods, which suggested that particle velocity and flame temperature play a critical role in coating microstructure as depicted in Fig. 2.

The TS processing map proposition is that increasing particle velocity, such as conferred by high kinetic energy processes, decreased the porosity and increased the intersplat cohesion. There was increased thermal phase transformation for high thermal input processes. The effects of porosity, intersplat cohesion, and thermal phase transformation are all represented within the trends of the TS maps in this study.

A summary of the trends and TS map details is presented in Table 5. Thus, TS maps lend unbiased and strong evidence to suggest that combinations of spray processes, spray parameter tables, and feedstocks yield variations to the coating properties in a systematic and ordered fashion.

#### 4.7 Other Possible TS Mapping Techniques/Combinations

A similar data-consolidating procedure can be employed to map out the application-specific performance of thermal spray coatings and provide an overview of

**Table 5** Summary of TS map trends and details

Map number	Trend	Number of data points	Year earliest reference	Year latest reference
1: Hardness-porosity (WC-Co)	Porosity decreases with increasing coating hardness	108	1997	2010
2: Hardness-porosity (alumina)	Porosity decreases with increasing coating hardness	148	1997	2010
3: Porosity-bond strength	Bond strength increases with decreasing porosity	77	2001	2011
4: Hardness-bond strength	Metal-based thermal spray coatings show better bond strengths than their ceramics counterparts	107	2001	2011
5: Porosity-elastic modulus	Coating elastic modulus decreases as porosity increases	156	1997	2010
6: Hardness-elastic modulus	Elastic moduli of ceramics coatings are greater than that of metallic coatings. Increasing microhardness with increases in the elastic modulus	148	1997	2010

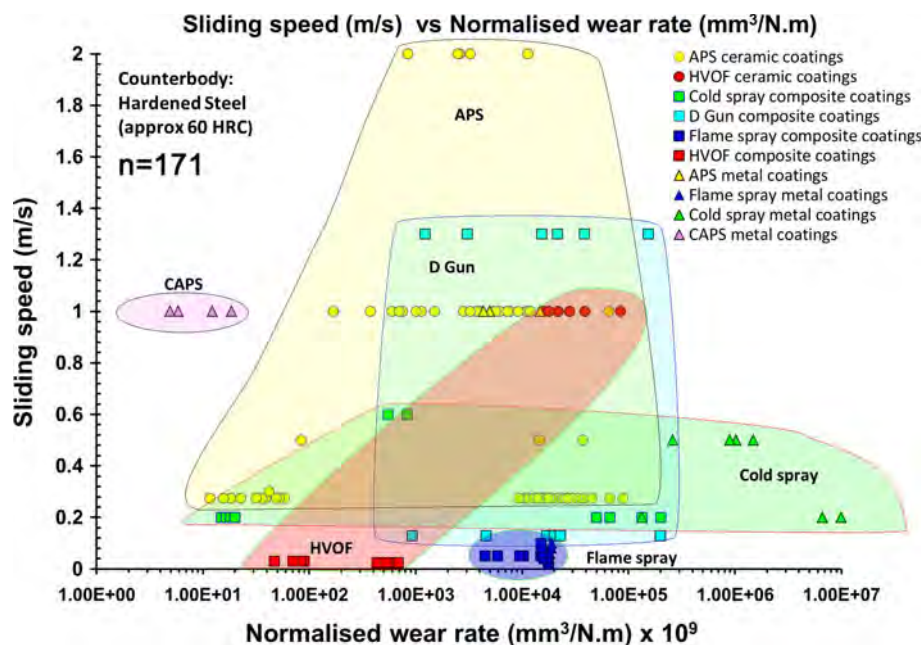


**Fig. 10** Sliding wear rate of various thermal spray coating plotted against sliding speed ( $n = 171$  data points)

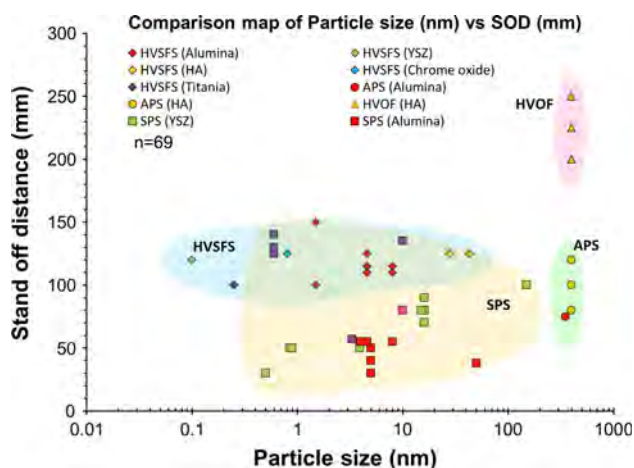


**Fig. 11** Map to suggest required standoff distance for various starting feedstock sizes ( $n = 69$  data points)

potential coating solutions. An example of a wear application map is presented in Fig. 10. It must be pointed out that this wear application map is compiled based on reported experiments and shows wear rate at a specific sliding speed, which depended on the researcher. This map also reveals the conundrum with sliding wear testing for thermal spray materials, i.e., there were no standardized test speeds. Figure 10 highlights this gap in knowledge. Also, this map indicates that APS ceramic coatings should be a possible solution for applications that require high sliding speeds.

Alternatively, process evaluation TS maps can be constructed. Figure 11, for example, provides an estimate of the required standoff distance for different feedstock sizes. This TS map provides a useful teaching tool to explain the fundamental relationships between feedstock and standoff distance with regard to the need for different spray distances for different processes. It can be said that as the particle size decreases for each of the thermal spray families (i.e., plasma or combustion energy source), the standoff distance also decreases.

Hence, such TS maps can be a tool to aid the design of a new generation of thermal spray coatings by highlighting existing gaps and frontiers in the current technology.

## 5. Conclusions

Thermal spray coatings are identified by a lamellar microstructure formed from the rapid solidification of molten droplets and cohesion among splats. This structure gave rise to the anisotropic mechanical behavior of coatings produced via different thermal spray methods since a distinctive splat structure and associated void system was created.

A comprehensive literature survey was conducted to compile relevant thermal spray coating property vs. performance data. The six property-performance TS maps constructed in this work showed the ability to interrelate

all data within the field of thermal spray and provided a holistic explanation to coating properties. TS maps have been created with respect to porosity, hardness, coating adhesion, and elastic modulus. The effects of porosity, intersplat cohesion, and thermal phase transformation are all represented within the trends of the TS maps. This understanding agreed with the notion that particle velocity and flame temperature play a critical role in creating the coating microstructure.

## Acknowledgments

This work was supported under a Swinburne University Postgraduate Research Award. We also acknowledge support from the Defence Materials Technology Centre (DMTC).

## References

1. J.R. Davis, *Handbook of Thermal Spray Technology*, ASM International, Materials Park, OH, 2004
2. L. Pawlowski, *The Science and Engineering of Thermal Spray Coatings*, Wiley, Chichester, 2008
3. R. McPherson, The Relationship Between the Mechanism of Formation, Microstructure and Properties of Plasma-Sprayed Coatings, *Thin Solid Films*, 1981, **83**(3), p 297-310
4. S. Fantassi, M. Vardelle, A. Vardelle, and P. Fauchais, Influence of the Velocity of Plasma-Sprayed Particles on Splat Formation, *J. Therm. Spray Technol.*, 1993, **2**(4), p 379-384
5. M. Vardelle, A. Vardelle, and P. Fauchais, Spray Parameters and Particle Behavior Relationships During Plasma Spraying, *J. Therm. Spray Technol.*, 1993, **2**(1), p 79-91
6. P. Fauchais and G. Montavon, Plasma Spraying: From Plasma Generation to Coating Structure, *Advances in Heat Transfer*, vol. 40, Elsevier, Amsterdam, 2007, p 205-344
7. M.U. Schoop, An Improved Process of Applying Deposits of Metal or Metallic Compounds to Surfaces, U.K. Patent A.D. 21066, U. K. P. Office, 1912
8. Z.-K. Liu, and D.L. McDowell, Center for Computational Materials Design (CCMD) and Its Education Vision, *Materials Science and Technology (MS&T) 2006: Fundamentals and Characterization*, B. Fahrenholtz, A. Kimel, and P.E. Cantonwine, Eds., Cincinnati, OH, 2006, p 111-118
9. G.B. Olson, Computational Design of Hierarchically Structured Materials, *Science*, 1997, **277**(5330), p 1237-1242
10. M.F. Ashby, Chapter 4—Material Property Charts, *Materials Selection in Mechanical Design*, 4th ed., Butterworth-Heinemann, Oxford, 2011, p 57-96
11. S. Saber-Samandari and C.C. Berndt, IFTHSE Global 21: Heat Treatment and Surface Engineering in the Twenty-First Century: Part 10—Thermal Spray Coatings: A Technology Review, *Int. Heat Treat. Surf. Eng.*, 2010, **4**(1), p 7-13
12. A. Papyrin, Cold Spray Technology, *Adv. Mater. Process.*, 2001, **159**(9), p 49-51
13. Sulzer Metco, *Thermal Spray Materials Guide*, Sulzer Metco (US) Inc., Westbury, NY, 2012
14. Praxair Surface Technologies Inc., *Powder Solution Catalog: Praxair and TAFE Thermal Spray Powders*, Praxair Technology, Inc., USA, 2009
15. Amperit® Thermal Spray Powders, *Surface Technology*, H.C. Starck, Ed., H.C. Starck GmbH, Goslar, 2010
16. Flame Spray Technologies b.v., *Flame Spray Technologies: Powders*, Flame Spray Technologies b.v., Netherlands, 2008
17. M. Friis and C. Persson, Control of Thermal Spray Processes by Means of Process Maps and Process Windows, *J. Therm. Spray Technol.*, 2003, **12**(1), p 44-52

18. G. Dwivedi, T. Wentz, S. Sampath, and T. Nakamura, Assessing Process and Coating Reliability Through Monitoring of Process and Design Relevant Coating Properties, *J. Therm. Spray Technol.*, 2010, **19**(4), p 695-712
19. J. Ilavsky, G.G. Long, A.J. Allen, H. Herman, and C.C. Berndt, Use of Small-Angle Neutron Scattering for the Characterization of Anisotropic Structures Produced by Thermal Spraying, *Ceramics—Silikaty*, 1998, **42**(3), p 81-89
20. J. Matějček, B. Kolman, J. Dubský, K. Neufuss, N. Hopkins, and J. Zwick, Alternative Methods for Determination of Composition and Porosity in Abradable Materials, *Mater. Charact.*, 2006, **57**(1), p 17-29
21. H.L. De Villiers Lovelock, Powder/Processing/Structure Relationships in WC-Co Thermal Spray Coatings: A Review of the Published Literature, *J. Therm. Spray Technol.*, 1998, **7**(3), p 357-373
22. A.A. Abdel-Samad, A.M.M. El-Bahloul, E. Lugscheider, and S.A. Rassoul, Comparative Study on Thermally Sprayed Alumina Based Ceramic Coatings, *J. Mater. Sci.*, 2000, **35**(12), p 3127-3130
23. M. Wang and L.L. Shaw, Effects of the Powder Manufacturing Method on Microstructure and Wear Performance of Plasma Sprayed Alumina-Titania Coatings, *Surf. Coat. Technol.*, 2007, **202**(1), p 34-44
24. R. McPherson, On the Formation of Thermally Sprayed Alumina Coatings, *J. Mater. Sci.*, 1980, **15**(12), p 3141-3149
25. P. Chráska, J. Dubsky, K. Neufuss, and J. Písacka, Alumina-Base Plasma-Sprayed Materials Part I: Phase Stability of Alumina and Alumina-Chromia, *J. Therm. Spray Technol.*, 1997, **6**(3), p 320-326
26. J. Ilavsky, C.C. Berndt, H. Herman, P. Chraska, and J. Dubsky, Alumina-Base Plasma-Sprayed Materials—Part II: Phase Transformations in Aluminas, *J. Therm. Spray Technol.*, 1997, **6**(4), p 439-444
27. ASTM C633-01(2008), *Standard Test Method for Adhesion or Cohesion Strength of Thermal Spray Coatings*, ASTM International, West Conshohocken, PA, 2008
28. K.A. Khor, C.S. Yip, and P. Cheang, Ti-6Al-4V/Hydroxyapatite Composite Coatings Prepared by Thermal Spray Techniques, *J. Therm. Spray Technol.*, 1997, **6**(1), p 109-115
29. R.C. Tucker, Jr., Structure Property Relationships in Deposits Produced by Plasma Spray and Detonation Gun Techniques, *J. Vac. Sci. Technol.*, 1974, **11**(4), p 725-734
30. H.D. Steffens, B. Wielage, and J. Drozak, Interface Phenomena and Bonding Mechanism of Thermally-Sprayed Metal and Ceramic Composites, *Surf. Coat. Technol.*, 1991, **45**(1-3), p 299-308
31. H. Baker, Properties of Metals, *Metals Handbook*, J.R. Davis, Ed., ASM International, Materials Park, OH, 1998
32. R.L. Lehman, Overview of Ceramic Design and Process Engineering, *Engineered Materials Handbook, 4, Ceramics and Glasses*, ASM International, Materials Park, OH, 1991, p 30
33. A.F. Liu, *Mechanics and Mechanisms of Fracture: An Introduction*, ASM International, Materials Park, OH, 2005
34. C. Li, A. Ohmori, and R. McPherson, The Relationship Between Microstructure and Young's Modulus of Thermally Sprayed Ceramic Coatings, *J. Mater. Sci.*, 1997, **32**(4), p 997-1004
35. S.H. Leigh, C.K. Lin, and C.C. Berndt, Elastic Response of Thermal Spray Deposits Under Indentation Tests, *J. Am. Ceram. Soc.*, 1997, **80**(8), p 2093-2099

#### Permission to publish

A.S.M. Ang, N. Sanpo N, M.L. Sesso, S.Y. Kim and C.C. Berndt, 'Thermal spray maps: Material genomics of processing technologies', *J. Thermal Spray Tech.*, 22[7] (2013) p. 1170-1183. DOI: 10.1007/s11666-013-9970-3, Published: OCT 2013.

With kind permission from Springer Science+Business Media. The complete article (text, figures, tables and references) have been kindly reproduced.

## Chapter 5. Applications of Thermal Spray Materials

### 5.1 Introduction

Chapter 5 consists of 5 contributions that encompass applications of thermal spray materials. Specifically, manuscript #15 examines ‘Material fundamentals and clinical Performance of plasma-sprayed hydroxyapatite coatings: A review’. This is a highly-cited contribution (more than 530 citations and about 40 citations per year since 2001) that indicates:

‘the outlook on using HA coatings on orthopaedic appliances, formed by thermal spray methods, as functional bioactive agents to aid the healing process, is favorable’.

Manuscripts #16 and #17 examine thin coatings, applied *via* thin film technologies, for biomedical applications. The understanding of surface roughness is developed with regard to the ability of the surface to retain microorganisms. Thus, although thermal spray is not directly addressed in these studies; the techniques and understanding gained from prior studies are applied to sol-gel and physical vapour deposition technologies. An extension of this approach has been applied by the applicant so that ‘combinatorial coatings’ of thermal spray and thin film technologies have been incorporated into a single coating.

Thermal barrier coatings have been a focus of the applicant since his residency at NASA in 1983; leading to many manuscripts of which #18 and #19 are examples; i.e., ‘Failure during thermal cycling of plasma-sprayed thermal barrier coatings’ and ‘Performance of thermal barrier coatings in high heat flux environments’. The development of these early studies has progressed to the present day; for example, manuscripts #2 (2014), #9 (2000), #10 (2000), #12 (1997), and #13 (2012) have evolved from this foundation.

The 26 publications with the identification numbers below are considered as contributions that focus on this specific subject material. Chapter 7 of this thesis outlines the methodology employed for this analysis.

20
27
69
86
95
101
102
107
135

146
152
153
177
181
186
189
208
237

307
320
321
322
336
355
375
387

# Material Fundamentals and Clinical Performance of Plasma-Sprayed Hydroxyapatite Coatings: A Review

Limin Sun,<sup>1</sup> Christopher C. Berndt,<sup>1</sup> Karlis A. Gross,<sup>2</sup> Ahmet Kucuk<sup>3</sup>

<sup>1</sup> Center for Thermal Spray Research, State University of New York at Stony Brook, Stony Brook, New York 11794-2275

<sup>2</sup> Department of Materials Engineering, Monash University, Victoria 3800, Australia

<sup>3</sup> Karl Storz Endovision, Inc., Charlton, Massachusetts

Received 27 November 2000; revised 2 May 2001; accepted 3 May 2001

**Abstract:** The clinical use of plasma-sprayed hydroxyapatite (HA) coatings on metal implants has aroused as many controversies as interests over the last decade. Although faster and stronger fixation and more bone growth have been revealed, the performance of HA-coated implants has been doubted. This article will initially address the fundamentals of the material selection, design, and processing of the HA coating and show how the coating microstructure and properties can be a good predictor of the expected behavior in the body. Further discussion will clarify the major concerns with the clinical use of HA coatings and introduce a comprehensive review concerning the outcomes experienced with respect to clinical practice over the past 5 years. A reflection on the results indicates that HA coatings can promote earlier and stronger fixation but exhibit a durability that can be related to the coating quality. Specific relationships between coating quality and clinical performance are being established as characterization methods disclose more information about the coating. © 2001 John Wiley & Sons, Inc. *J Biomed Mater Res (Appl Biomater)* 58: 570–592, 2001

**Keywords:** plasma spray, hydroxyapatite coating, orthopedic implant, implant fixation, bone growth, resorption, wear

## INTRODUCTION

Plasma-sprayed hydroxyapatite (HA) coatings have been used as surface coatings on metallic implants in dentistry and orthopedics since the mid 1980s.<sup>1,2</sup> The advantages that are sought in this application include (i) more rapid fixation and stronger bonding between the host bone and the implant, and (ii) increased uniform bone ingrowth and/or ongrowth at the bone-implant interface.<sup>3–5</sup> Although little clinical advantage was found in some trials with HA-coated implants,<sup>6–8</sup> most clinical experience with either weight-bearing or non-weight-bearing models have shown promising results shortly after the implantation and continued fixation for up to 10 years.<sup>9–13</sup> What is more inspiring is that an HA coating can enhance bone growth across a gap of 1 mm between the bone and the implant in both stable and unstable mechanical conditions, and it is capable of limiting the formation of any fibrous membrane and converting a motion-induced fibrous mem-

brane into a bony anchorage.<sup>14–16</sup> HA coatings have also suggested to have good sealing effects against the migration of polyethylene particles along the bone-implant interface, which may reduce the incidence of osteolysis and the subsequent implant failure.<sup>17,18</sup>

However, there are still many concerns about the use of HA coatings, especially with regard to long-term stability. One important concern is the resorption and degradability of HA coatings in a biological environment, which could lead to disintegration of the coating, resulting in the loss of both the coating-substrate bond strength and the implant fixation. There is also the threat of coating delamination and disintegration with the formation of particulate debris.<sup>19,20</sup> Another concern is that HA may lead to increased polyethylene wear or third-body wear, and thus result in an increased incidence of osteolysis.<sup>21–23</sup> Also, hydroxyapatite coatings have been said to occlude the porous implant surface, and this may compromise any advantage in the long term.

The most important concern, however, is the quality of the HA coating, which has been found to affect the major factors for both implant fixation and its long-term stability, such as the coating resorption, bone ingrowth, and mechanical fixation.<sup>24</sup> The factors that influence the performance of the HA coating include its compositional, physical, and mechanical

Correspondence to: Christopher C. Berndt, Ph.D., Department of Materials Science and Engineering, SUNY at Stony Brook, 306 Old Engineering, Stony Brook, NY 11794

Contract grant sponsor: National Science Foundation; contract grant numbers: MRSECDMR 9632570 and INT 9513462.

© 2001 John Wiley & Sons, Inc.



issues.<sup>18</sup> The implant can be controlled by choosing suitable metals and surface texture, and all other factors can be optimally controlled by varying the processing condition.

This review will relate these material fundamentals of the HA coating with the clinical outcomes of HA-coated implants, with the aim to investigate the optimal HA coating for clinical use and deal with some clinical concerns from material aspects. Most of the clinical performances of HA-coated implants cited in this review have been based on the clinical and radiographic outcome with hip implants obtained within the past five years (1996–2000).

## MATERIAL FUNDAMENTALS OF HA COATINGS

Bone consists of three major components: collagen, which is flexible and very tough; bone mineral, which is the reinforcing phase of the composites; and bone matrix or ground substance, which performs various cellular support functions.<sup>25</sup> The mineral phase, which is around 60–70 wt% of the bone,<sup>26,27</sup> can be described as a calcium phosphate with an apatitic structure and a composition close to hydroxyapatite [ $\text{Ca}_{10}(\text{PO}_4)_6(\text{OH})_2$ , HA, Ca/P = 1.67]. About 2 kg of HA is present in an average-sized person and the stoichiometry of the HA varies with its location in the human body. Biological apatites are known to be calcium-deficient ( $\text{Ca}_{(10-x)}(\text{HPO}_4)_x(\text{OH})_{2-x}$ ) with a Ca/P ratio as low as 1.5. Bone apatites contain carbonate, whereas dental enamel contains substantial amounts of fluoride.<sup>28</sup> Hydroxyapatite is biocompatible and bioactive in the human body. It is compatible with various tissue types and can adhere directly to osseous, soft, and muscular tissue without an intermediate layer of modified tissue.<sup>29–32</sup> It also displays an osteoconductivity: a property of a material to encourage bone already being formed, to lie closely to, or adhere to, its surface.<sup>32</sup> This is especially useful for an implant where fast healing is required. Despite its excellent properties as a biomaterial, the inherent mechanical properties of HA—specifically, brittleness, poor tensile strength, and poor impact resistance—have restricted its application in many load-bearing situations.<sup>33</sup> Therefore, the concept of applying HA onto metallic implants as a surface coating was developed, and the HA-coated implant combined the good strength and ductility of the metal with the excellent biocompatibility and bioactivity of the HA.<sup>34,35</sup>

Hydroxyapatite coatings were first introduced in the mid-1980s for improved fixation between bone and the implant.<sup>36,37</sup> Various methods have been used to deposit HA coatings, such as dip coating–sintering,<sup>38,39</sup> immersion coating,<sup>40,41</sup> electrophoretic deposition,<sup>41,42</sup> hot isostatic pressing (HIP),<sup>38,41</sup> solution deposition,<sup>43</sup> ion-beam sputter coating<sup>44</sup> and dynamic mixing,<sup>45</sup> thermal spraying techniques such as plasma spraying,<sup>35,46,47</sup> flame spraying,<sup>48</sup> and high-velocity oxy-fuel (HVOF) combustion spraying.<sup>49</sup> Detailed descriptions of these methods have been given by Lacefield<sup>38</sup> and Berndt, Haddad, Farmer, and Gross.<sup>35</sup> A comparison of these methods has been described by Jaffe and Scott,<sup>43</sup> and is summarized in Table I. So far, thermal spraying, especially

the conventional atmospherical plasma-spray method, appears to be the most favorable and, thus, most commonly used for clinical application. This review will concentrate on plasma-sprayed HA coatings; hereafter, the term *HA coating* refers to a plasma-sprayed HA coating unless specifically stated.

Plasma-sprayed hydroxyapatite coatings are able to bond directly to bone,<sup>3</sup> promote earlier and greater fixation,<sup>50,51</sup> enhance bone ingrowth,<sup>52</sup> and protect the surrounding bone against metal-ion release from the metallic implant.<sup>53</sup> However, plasma spraying involves the acceleration of the feedstock<sup>1</sup> HA powders to a high velocity and temperature (as high as 30,000 K) and a subsequent rapid cooling when the HA adheres to the metallic substrate. The composition and the structure of the HA is significantly modified from the feedstock powders. Therefore, from a materials-science perspective, the physiological response of the coating need not necessarily reflect the exact characteristics of the feedstock. When different spray parameters are employed, such as gas combination and flow rate, spray power, and stand-off distance, this modification will be different, as shown in Figure 1. Even before it is sprayed, the HA powder can be varied in terms of particle morphology, size distribution, microstructure, density, and hydroxyl content, given that fully crystalline HA powders are used. The metallic implant type and surface texture is another variable that influences the formation and performance of the HA coating. Therefore, the overall quality of the HA coating is a combined outcome of feedstock powders, implant metals, and spray parameters.

Critical quality specifications for HA coatings include purity (phase composition), crystallinity, Ca/P ratio, microstructure, porosity, surface roughness, thickness, and implant type and surface texture, which also lead to different mechanical properties, such as cohesive and bond strength, tensile strength, shear strength, Young's modulus, residual stress, and fatigue life.<sup>18</sup> All these variables can lead to different bioactivity and durability of the coating. The different coating designs and especially process methods to achieve these characteristics remain as company intellectual property. It has been suggested that an ideal HA coating for orthopedic implants would be one with low porosity, strong cohesive strength, good adhesion to the substrate, a high degree of crystallinity, and high chemical and phase stability.<sup>34</sup> Other documents,<sup>54,55</sup> however, indicate that an amorphous coating may be more beneficial for early bone ingrowth than a coating with high crystallinity. As well, some properties need to be reconciled with each other because of the nature of the manufacturing process.

### Purity and Crystallinity

The typical feedstock for HA coatings is a fully crystalline pure HA powder. It is commonly manufactured by chemical precipitation from a mixture of a calcium-ion-containing so-

<sup>1</sup> Refers to the sprayable material in the thermal spray industry and includes powders, wires, or liquids.



**TABLE I. Comparison of Different Methods for Depositing HA Coatings**

Method	Characteristics	Comments/References
Dip coating/sintering	The high-temperature sintering ( $>1000^{\circ}$ ) can degrade mechanical properties of metal implants and lead to low bond strength and impurity of HA.	Not applicable to orthopedic implants References 38–42
Electrophoretic deposition	Same problems as dip coating/sintering, also leads to nonuniform thickness of HA.	
Immersion coating	The high-temperature-process ( $>1500^{\circ}$ ) results in a coating of non-HA compound mixture and very poor adherence.	
Hot isostatic pressing	The encapsulating materials react to the HA coating. Difficult to seal borders on implants with complex shapes.	
Solution deposition	A low-temperature precipitation process resulting in a pure, highly crystalline, firmly adherent HA coating. Good for coating evenly for porous and beaded surfaces. Maximum thickness of 20 $\mu\text{m}$ limits its use as a primary mode of fixation.	Marketed in Europe, but not approved in US Reference 43
Sputter coating	Too slow and has a low deposition rate. Ca/P ratio of the coating is higher than that of synthetic HA if RF magnetron sputtering is used.	References 44 and 45
Thermal spraying	High deposition rate. Good chemical and microstructure control, biocorrosion resistance, and substrate fatigue resistance of the coating. Can obtain various coating thickness and be used for complex shapes.	References 35, 46 and 47

lution and a phosphate-containing solution followed by calcination.<sup>56–58</sup> After plasma spraying has occurred, both the purity<sup>2</sup> and the crystallinity<sup>3</sup> of the HA decrease because of the decomposition of HA at high temperature and the rapid cooling rate. The new phases that most commonly appear in the HA coating include an amorphous phase, tricalcium phosphate [ $\text{Ca}_3(\text{PO}_4)_2$ ; i.e.,  $\alpha$ -TCP and/or  $\beta$ -TCP], tetracalcium phosphate ( $\text{Ca}_4\text{P}_2\text{O}_9$ ; i.e., TTCP) and calcium oxide ( $\text{CaO}$ ).<sup>34,59,60</sup> A solid solution of oxyapatite [ $\text{Ca}_{10}(\text{PO}_4)_6\text{O}$ , i.e., OAp] in HA, that is, oxyhydroxyapatite [ $\text{Ca}_{10}(\text{PO}_4)_6(\text{OH})_{2-2x}(\text{O})_x(\square)_x$ , OHA, where  $\square$  represents a vacancy] could also form in the HA coating because of the dehydroxylation of the HA.<sup>61,62</sup> Hydroxyapatite is very stable in the body fluid, but the dissolution rates of other phases formed during spraying are much higher than HA, which is in the order of  $\text{ACP} \gg \text{TTCP} > \alpha\text{-TCP} > \text{OHA} > \beta > \text{-TCP} \gg \text{HA}$ .<sup>61,63</sup> Calcium oxide has no biocompatibility and dissolves significantly faster than TCP,<sup>64</sup> thus it is a detrimental phase that should be avoided. Table II lists these calcium-phosphate phases, their crystal structure information,<sup>62,65–68</sup> and their solubility product.<sup>69</sup> The dissolution of a material is dictated by its free energy and can be evaluated by its solubility product; a lower free energy corresponds to a lower solubility product.

<sup>2</sup> Refers to the percentage of HA in terms of phase composition.

<sup>3</sup> Generally refers to the percentage of crystalline HA with regard to a total of crystalline HA and amorphous phase.

The phase composition of HA coatings depends on the selection of production parameters and is a deciding factor for the dissolution of HA coatings in the physiological environment. The faster dissolution produces a supersaturated environment, which allows physiologically produced HA to precipitate on the coating and enhance the bone ingrowth, but it also leads to the resorption or degradation of the coating.<sup>69–72</sup> Therefore, to obtain HA coatings with predictable properties, both the purity and the crystallinity of the HA should be effectively designed. To achieve this, both the spray parameters and the quality of the original feedstock HA powders should be strictly controlled.

Currently, there is a general agreement that the chemical purity of HA should be as high as possible ( $\geq 90\%$ ) with a Ca/P ratio of 1.67.<sup>73</sup> This is followed by most manufacturers to ensure predictable implant performance. However, there is no agreement on the crystallinity, which can be varied from 50% to 90% (usually around 70%). The crystalline HA phase may include both the unmolten core of a particle and the new, recrystallized HA phase. The measurement of the crystallinity has been mainly performed with x-ray diffraction and supplemented with infrared spectroscopy, where both the lower crystal perfection caused by cooling from high temperatures and an amorphous phase are considered. Some standards<sup>74</sup> have been suggested for this measurement, but none have been generally approved. It has been found that the amorphous phase has a higher tendency to form at the coat-

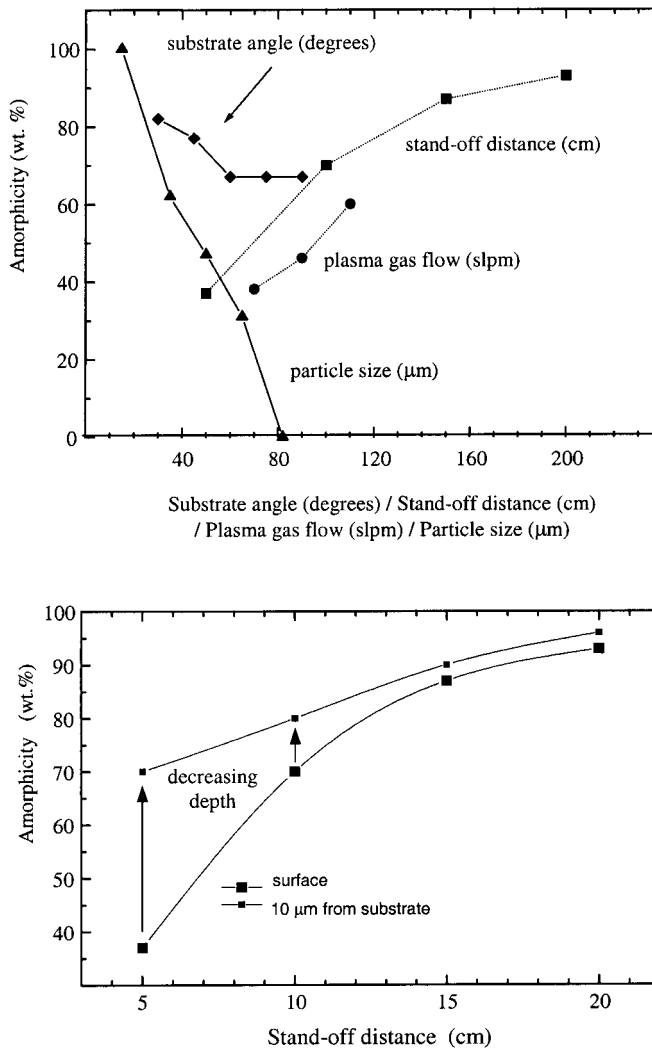


Figure 1. Phase formation and distribution in plasma-sprayed HA coatings.<sup>74</sup>

ing-metal interface than in the coating, as shown in Figure 1, but little information is available on the size of the crystalline areas and their distribution throughout the coating.

Bone growth occurs at a faster rate when the coating has a higher content of amorphous phase because of more rapid initial dissolution. Bone grows toward the implant, and collagen incorporates the HA crystals in the body to produce a strong interface. Faster fixation is especially favorable in hip-implant recipients where the hip is partially weight bearing within approximately a week from the operation. However, the fast resorption of the HA coating may lead to the loss of the fixation and coating bonding (i.e., implant loosening) as well as the production of particle debris in the long term. The trend, therefore, to produce crystalline coatings was supported because of the above concern. It was found that the early biological fixation could also be achieved with a high-crystalline, high-purity HA coating, which is probably because of the existence of residual stress, pores, and the small crystal size of the thermal spray coating. Nonetheless, HA coatings with high crystallinity usually contain more unmelted or partially melted particles, which could also lead to lower bonding and cohesive strength as well as particle debris. Although the crystallinity could be increased by post-heat treatment, such a process is generally accompanied by cracking, and thus is not advised.

#### Microstructure, Porosity, and Roughness

Microstructure and porosity is another important coating characteristic that influences its performance. The porosity of a commercially available HA coating may vary from 1% to 10%,<sup>6,13,142,182</sup> and sometimes up to 50%,<sup>136</sup> but generally, little information is provided by the manufacturer regarding the microstructure. When different feedstock powders and spray parameters are employed, the original particles can become well-flattened splats, accumulated splats, spheroidized particles, partially melted particles, or remain unmelted, as shown in Figure 2. These microstructural features lead to different forms of porosity in the coating. In extreme situations, for example, in cases of fine feedstock powders and very high spray power level, microcracks are more likely to appear in the splats. The nature of the porosity is very

TABLE II. Calcium Phosphate Phases in HA Coatings

Phase	Chemical Formula	Abbreviation	Solubility Constant Ks at 25°C <sup>69</sup>	Crystal Structure/References	JCPDS No.
Hydroxyapatite	$\text{Ca}_{10}(\text{PO}_4)_6(\text{OH})_2$	HA	$6.62 \times 10^{-126}$	Hexagonal P6 <sub>3</sub> /65	9-432
Amorphous phase	N/A	ACP	N/A	Irregular	N/A
Alpha tricalcium phosphate	$\alpha\text{-Ca}_3(\text{PO}_4)_2$	$\alpha\text{-TCP}$	$8.46 \times 10^{-32}$	Monoclinic P2 <sub>1</sub> /a/66	9-348
Beta tricalcium phosphate	$\beta\text{-Ca}_3(\text{PO}_4)_2$	$\beta\text{-TCP}$	$2.07 \times 10^{-33}$	Rhombohedral R3c/67	9-169
Tetracalcium phosphate	$\text{Ca}_4\text{P}_2\text{O}_9$	TTCP	N/A	Monoclinic P2 <sub>1</sub> /68	25-1137
Oxyhydroxyapatite	$\text{Ca}_{10}(\text{PO}_4)_6(\text{OH})_{2-2x}(\text{O})_x(\square)_x$	OHA	$\sim 10^{-69}$ (oxyapatite)	Hexagonal/62 P6 <sub>3</sub> /62	9-432

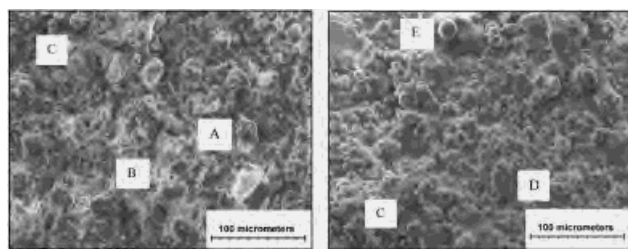


**Figure 2.** Surface morphology of plasma-sprayed HA coatings. (a) partially melted large particle, (b) partially melted fine particle, (c) flattened splat, (d) accumulated splats, (e) spheroidized particle.

important, because this controls the specific area in contact with the physiological medium and, therefore, influences physiochemical interactions at the implant–host interface.<sup>34</sup>

Hydroxyapatite coatings may fail by delamination<sup>75–77</sup> or release of coating segments.<sup>78</sup> The possibility is increased for coatings of high crystallinity, because, as has been stated before, there are more unmelted or partially melted particles and higher porosity in such coatings, which leads to poor cohesive and bonding strength. If the coating segments or particle debris remain in the vicinity of the implant and are too large, the body is not able to dissolve them by phagocytosis<sup>19,79</sup> and lowers the local physiological pH in an attempt to dissolve the particle. This lower pH could lead to coating destruction and could modify the bone-formation process around the implant. If coating segments are removed from the coating and are mobile, they may then be transported to another site, such as the bearing surface of the hip joint and, thereafter, produce third body wear and increase the incidence of osteolysis.

Surface roughness of the HA coating also affects its dissolution and the bone apposition on the coating or bone ingrowth, because the coating surface, once implanted, is directly in contact with the bone and body fluid. High surface roughness will increase the coating and body-fluid interface, and thus increase the dissolution rate and apatite precipitation. Roughness can also be controlled by using different feedstock powders and spray parameters.<sup>34,80</sup>

### Thickness

The thickness of the HA coating affects both its resorption and mechanical properties. Thicker coatings usually exhibit poorer mechanical properties. De Groot and co-workers<sup>81,82</sup> determined that an optimum thickness of 50  $\mu\text{m}$  would avoid fatigue failure, which commonly occurred in coatings thicker than 100  $\mu\text{m}$ , but still provide reasonable coating bioresorption and consistent bone growth.

Wang, Lee, Chang, and Yang have evaluated the effects of the coating thickness on the shear strength at the bone–implant interface and failure mode of HA coatings using both a transcortical implant model<sup>83</sup> and an intramedullary implant model.<sup>84</sup> It was found that in both cases, a 50  $\mu\text{m}$  coating exhibits significantly higher shear strength than a 200  $\mu\text{m}$  coating. In addition, although it has similar histological be-

havior, the 50  $\mu\text{m}$  coating only fractured at the implant–bone interface, whereas the 200  $\mu\text{m}$  coating also fractured within the coating in a cohesive manner or at the coating–implant interface in an adhesive mode. These different failure locations indicated that the residual stress in the thick coating is possibly responsible for a decrease in the mechanical properties of the coating.

A thickness of 50–75  $\mu\text{m}$  has been followed by most manufacturers for commercially used orthopedic implants. The value, however, is completely dependent upon the location of implantation, cellular environment, cleanliness of implant, and coating characteristics; for example, the thickness of the HA coating for dental implants can be several hundred micrometers.

### Mechanical Properties

Mechanical properties are important for the long-term performance of the HA-coated implants and is related to the characteristics of the HA coating that have been discussed above. A comparison of the tensile strength and Young's modulus of the main current implant materials with those of bone is shown in Table III.<sup>85,86</sup> According to the proposed standards, the shear strength should be 22–29 MPa, and the minimum tensile strength should be 51 MPa for the HA coating.<sup>87,88</sup> No criterion has been suggested on the Young's modulus. The HA coating was found to commonly fail at the coating and substrate interface rather than within the coating during the tensile adhesion testing (TAT), which is the standard adhesion testing technique for thermal spray coatings.<sup>89</sup> Other researchers<sup>90,91</sup> also showed that failure mainly occurs at this interface in their *in vivo* studies, and the failure probability at this interface increased with the period of implantation, because the strength of the coating–bone interface tends to increase with time during the initial postoperative recovery. The bond strength of the HA coating is, in addition to the coating characteristics, also related to the thickness of the coating as well as the type and design of the implant, as will be discussed below.

The understanding of other important mechanical properties, such as Young's modulus, thermal stress, fracture tough-

**TABLE III.** Comparison of Mechanical Properties between Implant Materials and Bone<sup>85,86</sup>

Material	Young's Modulus (GPa)	Tensile Strength (MPa)
Alumina	365	6–55
Sintered HA	70–90	50–110
HA coating	0.5–5.3 <sup>34</sup>	>51 <sup>87,88</sup>
316L stainless steel	193	540
Co-Cr alloys	230	900–1540
Ti-6Al-4V, wt %	106	900
PMMA bone cement	3.5	70
HDPE	1	30
Cortical bone	7–30	50–150
Cancellous bone	0.1–1	1.5–3

ness, and fatigue life, is still incomplete. An appropriate Young's modulus for the implant is crucial in order to avoid stress shielding and bone resorption, and it also determines the fatigue behavior of the coating under cyclic loading. It is well known that the Young's modulus of a plasma-sprayed coating is usually much lower than its bulk counterpart. Eberhardt, Zhou, and Rigney<sup>92</sup> indicated that only a Young's modulus with a value of  $\sim 5.5$  GPa would enable a reasonable prediction of the residual stresses for HA coatings. Tsui, Doyle, and Clyne<sup>34</sup> agreed with this prediction and obtained some values of  $\sim 0.5$ – $5.3$  GPa using a cantilever-beam test. Using this Young's modulus, together with an *in situ* curvature monitoring technique and a numerical model, they also predicted that residual stresses in the air-plasma-sprayed HA coatings on a Ti-6Al-4V substrate are also relatively low ( $\sim 20$ – $40$  MPa) and should always be tensile unless the substrate is held below room temperature during spraying. Brown, Turner, and Reiter,<sup>93</sup> however, reported a much higher residual stress level of greater than 200 MPa for air-plasma-sprayed HA.

Sergo, Sbaizero, and Clarke<sup>94</sup> determined with Raman piezospectroscopy that the residual stresses of HA coatings were tensile ( $\sim 100$  MPa) when deposited in air and compressive ( $\sim 60$  MPa) when deposited in a vacuum. They concluded that the existence of residual stress in HA coatings can alter the concentration of supernatant species in solution, tensile stresses enhancing dissolution, and compressive stresses impeding dissolution. The great variability among the residual stresses obtained by different authors probably arises from different coating characteristics as well as different measurement techniques.

The interfacial fracture toughness of the HA/Ti-6Al-4V system obtained from two types of Mode I tests has been reported. Filliaggi, Coombs, and Pilar<sup>95</sup> used a short bar chevron notch test and obtained values of  $K_{Ic}$  equal to  $0.60$ – $1.41$  MPa/m<sup>1/2</sup>. Gross<sup>96</sup> and Tsui et al.<sup>34</sup> obtained some similar values of  $K_{Ic}$  of  $\sim 0.28$ – $1.1$  MPa/m<sup>1/2</sup> using a single-edge, notch-bend test. However, the interfacial fracture toughness of the system under mixed-mode conditions still needs to be investigated, because this is most relevant to its in-service condition.

### Metallic Implants

The metallic materials commonly used as implants are cobalt–chromium (Co-Cr) alloy and titanium (Ti) and its alloy, Ti-6Al-4V, as these provide good corrosion resistance and reasonable fatigue life. These alloys are much stiffer than cortical bone, as shown in Table III, whereas the titanium alloys result in less potential proximal stress shielding and bone resorption because of the lower Young's modulus.<sup>97,98</sup> Titanium alloy also demonstrated a 33% percent increase in bonding strength to the HA coating *in vitro* compared to Co-Cr alloy. It was suggested that this increase arose because of the formation of a chemical bond between Ti and HA in addition to the expected mechanical locking.<sup>3,99–101</sup> This interfacial diffusion or reaction, however, was not observed

in all work,<sup>102</sup> which is probably because of the different plasma spray parameters, used such as the nature of the secondary gas employed.

The coefficient of thermal expansion is another important factor to consider, and again, there is more of an agreement between titanium ( $9$ – $10 \times 10^{-6}$  /°C) and HA ( $12 \times 10^{-6}$  /°C) as opposed to Co-Cr alloy ( $16 \times 10^{-6}$  /°C) and HA. A smaller difference in thermal expansion is important to minimize the residual stresses within the coating. The added advantage of a Ti alloy is the low density and good bone bonding capacity.<sup>103</sup>

Before plasma spraying takes place, the surface of the metallic implant can be textured into microstructured, macrostructured, or porous morphologies.<sup>43</sup> The microstructuring can be grit blasting or beading. Grit blasting is a surface-preparation method used prior to the application of plasma-sprayed coatings; it alters the smoothness of the metal surface to produce a roughness of around several micrometers ( $R_a \approx 3$ – $6$   $\mu$ m). This method has proved successful for implant fixation and is currently the major method for implants in clinical use. Macrostructuring can be in the form of grooves, threads, meshes, or a deposited metal coating. Improved fixation has been demonstrated with grooved-surface implants *in vivo* both in the initial period and 1 year after implantation.<sup>104</sup> The purpose of macrostructuring is to increase the shear strength between the substrate and the coating, and this could result in improved long-term fixation between the implant and the bone if biodegradation of the coating occurs.<sup>105–107</sup>

The use of porous coatings is another method for implant surface treatment, and such structures have been shown to be of more benefit than a grit-blasted surface.<sup>108</sup> The porous coating itself can promote biological fixation between the implant and the bone, but many clinical retrieval studies of porous implants have revealed fibrous fixation rather than bone ingrowth.<sup>109,110</sup> Some strict operative techniques (such as the use of autogenous-graft bone chips at the time of operation) and implant design could promote consistent bone growth into a porous-coated implant. However, a layer of fibrous tissue still could be seen in the regions where the gaps were not filled with autogenous-graft bone chips. Also, the amount of bone that can grow into the porous coating is determined by and can be no more than the amount of host bone, which may not be sufficient for bone-implant fixation at some anatomical sites.<sup>111</sup> The fibrous membrane is a sign of incomplete osseointegration of the implant; but with HA this condition could be changed. Although grit blasting and the HA coating could occlude some pores and decrease the surface roughness of the porous coating, the addition of the HA coating improved the osseointegration of the implant. The presence of HA was found to limit the formation of fibrous membranes and induce their conversion to bone, and even to be capable of overcoming a 1-mm gap between the implant and the bone.<sup>14,15,112,113</sup> This osteoconductive effect is not limited to immobilized implants, but has been reported to be prolonged under loaded conditions, so that the move-



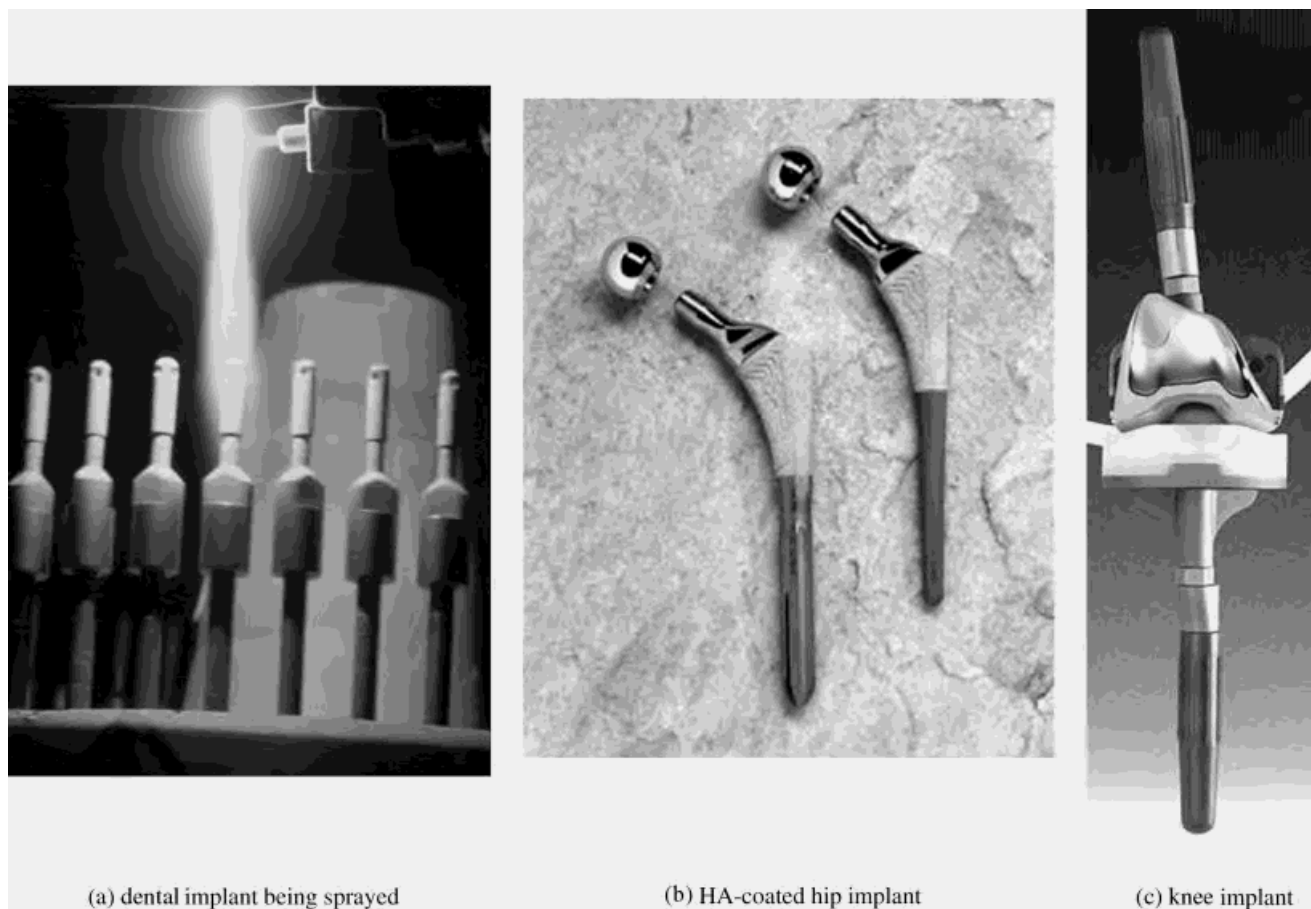


**Figure 3.** Typical (a) dental, (b) hip, and (c) knee implants (www.sulzermetco.com and www.osteonics.com).

ment-induced fibrocartilagenous tissue is replaced by bone when it is immobilized.<sup>16</sup>

The osteoconductiveness is important when preparing the bone bed for insertion of the implant. An uncoated titanium prosthesis cannot tolerate a gap with the bone and will not undergo successful integration if the gap separation is larger than 0.1 mm. Hydroxyapatite has been employed as a coating because its presence can lead to bone formation and successful fixation at a gap distance of 1 mm.<sup>113</sup> The bone density will initially be lower as a result of more rapid ingrowth in spaces, but is modified by further bone remodeling as a response to the load environment.<sup>16,104</sup>

### CLINICAL PERFORMANCE OF HA COATINGS

The first reported clinical trials of HA coatings were with femoral stems by Furlong and Osborn<sup>1</sup> in 1985 and by Geesink<sup>2</sup> in 1986. Since then, hydroxyapatite coatings have been extensively used in both dental and orthopedic prostheses, such as hip and knee implants, and in screws and pins used in bone plates for fixing bone fractures; here the coating is in close contact with bone. Most of these clinical practices and studies, however, are still with femoral stems of hip

implants, therefore this is the focus of this review. Hydroxyapatite coatings have been found to promote fast fixation and enhance fixation strength, but the long-term stability of the fixation is still in controversy. Another main controversy in this clinical application is the possibility that HA coatings increase polyethylene wear or third-body wear and osteolysis.

### Dental and Orthopedic Implants

Dental implants include subperiosteal, transosteal, and endosseous implants. It is the endosseous form that is most commonly used. Endosseous implants can take the form of plate or root, with the majority of implants in the root form. A root form implant consists of a post, an abutment and a crown. Hydroxyapatite is usually coated to the surface of dental posts [Figure 3(a)]. Tooth implants that fit closely to the bone can enable bone attachment. After careful preparation of the implant site, the post is placed into the maxilla or mandible. The gingiva covers the implant and a 3-month healing phase enables new bone to form close to the immobile implant. The implant site is then opened, and the crown is mounted with an abutment so that the post can be exposed to masticatory forces. For the next 18 months, the newly formed bone

remodels according to the magnitude, direction, and frequency of the applied force.

Orthopedic prostheses include both temporary devices such as bone plates, screws, pins, and intramedullary nails, and permanent devices such as hip, knee, elbow, and ankle implants. Hydroxyapatite has been coated to bone screws and pins, and hip and knee implants for faster and stronger fixation. Bone screws and pins, although not the prime application, are important because, unlike the permanent prostheses, they require fast initial fixation and have an implantation time of 3 months.<sup>114</sup> The removal torque of HA-coated screws was significantly greater than uncoated titanium screws,<sup>115</sup> and the adhesion between the coating and the screw remained unaffected.

The replacement of a hip or knee is usually conducted because of osteoarthritis, osteoporosis, or some form of injury. Chances of successful fixation are reduced in the former two cases. Orthopedic implants have a more complex geometry than dental implants and have accordingly, more sophisticated tooling to prepare the bone bed. Primary fixation depends on the prosthesis geometry and this is supplemented by a secondary mechanism—tissue bonding to HA. However, there is inevitably a space between the implant and surrounding bone in some locations. This will affect the bone growth and, hence, attachment to the implant. The orthopedic implant can bear partial weight 1 week after surgery; that is, there is no resting stage for the bone regeneration as with dental implants; therefore the requirements for good bonding are more stringent.

A hip prosthesis [so-called total hip arthroplasty (THA), Figure 3(b)] consists of an acetabular cup implanted into the hip and a femoral stem placed into the femur. Acetabular reconstruction is used for relief of pain, the restoration of joint function, the preservation of bone stock, and the maintenance of implant stability. Various designs exist with geometries that maximize the stress transfer from the femoral stem to the surrounding bone. Otherwise, bone will resorb and the implant will become loose, causing aseptic loosening and pain, which are indications for revision surgery. Hydroxyapatite is usually coated to the surface of the femoral stem, and the outer face of the acetabular cup. The application of a HA coating can be over the entire stem (or cup) or proximally, whereas the interface stress transfer is more uniform in the latter proximally coated stem. In case of infection a partly coated stem (or cup) is easier to remove than a fully coated stem (or cup). The mechanical and biological environments for hip implants are also more complex compared to dental implants, and vary with the implantation site. For example, the femoral stem placed laterally into the bone is in contact with the cortical bone in the proximal region and the trabecular bone at the distal end of the stem. A coating on a femoral stem and a acetabular cup will experience shear stresses as well as normal direct stresses (tension or compression). The magnitude of each stress component, however, depends on the particular loading characteristics, the shape of the component, the surrounding structures such as trabecular and cortical bone, the elastic properties of implant materials,

and the bonding characteristics of the interface, which may be fully coated or proximally coated.<sup>116,117</sup>

A knee prosthesis [so-called total knee arthroplasty (TKA), Figure 3(c)] consists of a femoral component and a tibial component. Hydroxyapatite coatings have been applied to the tibial component to enhance its fixation because loosening of the tibial component is far more common than loosening of the femoral components in knee prostheses.<sup>118</sup> The tibial component is subject to great torque and shear forces, which is different from the load condition on hip prostheses. In a similar fashion to the development of the total knee prostheses, which was started many years later than the total hip prostheses, the application of HA coatings for knee implants is relatively recent.<sup>8,119,120</sup> Therefore, the benefits of HA coatings on the fixation of the tibial component are still not well documented in the open literature.

### Fixation Mechanisms

A prerequisite for any orthopedic arthroplasty or dental implant is permanent fixation to the surrounding environment with no intervening soft tissue. A successful fixation should be fast and strong initially and exhibit lifelong stability. Fixation takes place by osseointegration, which was first described by Brånemark<sup>121</sup> as the intimate contact between a titanium implant surface and the surrounding bone. The currently accepted definition for osseointegration is “contact established between normal and remodeled bone and an implant surface without the interposition of non-bone or connective tissue, at the light microscopic level.”<sup>122</sup>

Prostheses have been implanted into the human body by either cemented or cementless fixation methods. Although the traditional cemented fixation using polymethylmethacrylate (PMMA) can obtain immediate fixation between the implant and bone, this type of prosthesis is not suitable for young (< 50 years) active patients where more stable fixation and bone growth are needed. Problems of cell necrosis from the exothermic reaction, cement failure, or monomer release and loss of endosteal bone are still a concern with the cement fixation method.<sup>123,124</sup> Thus, cementless fixation, primarily by biological means whereby press-fit insertion is followed by bone growth into a porous surface, has been developed. However, there is little histological evidence of sufficient bone ingrowth in retrieved uncemented porous-coated prostheses<sup>125,126</sup> and it has been shown that bone must be within 50  $\mu\text{m}$  of the porous coating for ingrowth to occur.<sup>127</sup> Meanwhile, fibrous rather than bony ingrowth into porous surfaces has been found, and the loss of endosteal bone still exists. Although consistent bone growth into the porous coating has been reported to be possible if strict operative techniques (such as the use of autogenous-graft bone chips at the time of operation) and implant design are used, a layer of fibrous tissue still could be seen in the regions where the gaps were not filled with autogenous-graft bone chips.<sup>111</sup>

Bioactive materials such as HA and bioactive glass can stimulate a direct bond to form between the implant and the surrounding bone and improve osseointegration. This bone-



implant bonding is one of the most important factors for implant fixation and function. HA coatings have been shown to achieve a very strong bond with living bone, in a relatively short period, even under loaded conditions and with the presence of a gap.<sup>14–16</sup>

The process has been suggested to be initiated with the dissolution of the coating soon after the implantation and can be described as follows: (a) partial dissolution of HA coating where calcium and phosphate ions are released from the coating, which will cause a rise of the calcium and phosphate ion concentration in the local environment around the coating; (b) precipitation of crystals on HA coating and ion exchange with surrounding tissues; (c) formation of a carbonated calcium phosphate layer of microcrystals and macrocrystals with the incorporation of a collagenous matrix and bone growth toward the implant; (d) bone remodeling in area of stress transfer: osteoclasts resorb normal bone by actively secreting hydrogen ions into the extracellular space, creating a local pH of approximately 4.8, and leading to fast resorption of both carbonated HA in bone mineral and the HA coating; and (v) the bone-implant interface is subjected to further bone ingrowth and remodeling, and a biological fixation can be achieved through the bidirectional growth of a bonding layer. A diagram that schematically models this process is shown in Figure 4.

Mechanical loading is usually found to accelerate coating resorption, bone remodeling, and growth processes. Faster dissolution/resorption is likely to result in faster and stronger fixation in the initial period of implantation, but could also lead to disintegration of the coating, with rapid loss of the bonding strength and mechanical fixation, delamination, and the production of particles, which has been cited as a potential complication. By contrast, slow controlled resorption may allow the surrounding bone the opportunity to replace resorbed coating and maintain long-term stability. The actual establishment of bonding, however, is complex and involves many factors, including implant-related factors, such as material, shape, topography and surface chemistry, mechanical loading, surgical technique and procedure, and bone bed preparation, and patient variables, such as bone quality and quantity.<sup>128</sup>

### Clinical Performance

After more than a decade's clinical practice with HA-coated prostheses, there is general agreement that the originally pursued benefits of HA coatings, that is, earlier fixation and stability with more bone ingrowth or ongrowth, can be achieved. Most components became stabilized within 3 months with bone apposition. It was suggested that migration of the femoral component within the first 2 years is related to the final outcome.<sup>129,130</sup> A large group of clinical trials with HA coatings have also shown continued fixation for longer periods (2–10 years), but doubts still exist concerning the durability of the fixation. A main concern is the degradability of the HA coating and the disintegrated HA granules, which are claimed to accelerate the polyethylene wear or cause

third-body wear. Any HA degradation will lead to increased osteolysis, and there is the potential that the degradation products will enter the joint space and damage the articulating surfaces.<sup>131</sup>

In summary, the following section will review the clinical performance of various HA-coated implants, femoral stems, acetabular cups, knees, pins, and teeth, with respect to their initial fixation and stability and long-term performance. It will then address two major concerns with their clinical use: resorption and wear.

### Fixation and Durability

**(1) Application in Femoral Stem** Most clinical practice with HA coatings has been with total hip arthroplasty, mainly on the femoral component. Fixation of a hip prosthesis can be assessed by two ways: by failure rate<sup>11,132</sup> or by radiographic features,<sup>132,133</sup> as shown in Table IV, with the latter used most often. Bone remodeling is generally characterized by calcar resorption, distal cortical hypertrophy, and cancellous condensation. This progressive bone remodeling and new bone formation phenomenon occurred around the implant. It is different from normal bone remodeling, which happens in bones all the time through a balanced two-phase process—resorption and formation, without net loss of bone. Cancellous condensation and cortical hypertrophy occurs around the stem in the femur as a result of the adaptation of bone to the stresses that act upon it. The insertion of an endoprosthesis into a femur changes the stress distribution within the femur, which is a combination of axial, bending, and torsional stresses,<sup>116,117</sup> and this causes the bone to remodel according to the stress transfer from the stem. Cancellous condensation is defined as new bone formation between the implant and endosteal surface of the femur, as indicated by so-called spot welding.<sup>7</sup> Many studies have described the radiographic features of bone remodeling and osseointegration around HA-coated femoral stems and/or estimated their failure rate, which showed a promising outcome with the use of HA coatings. Information on the corresponding HA-coating specification is shown in Table V. However, the clinical performance of HA-coated implants can not be easily related to the coating specification since many variables are involved in the whole implant system and during implantation.

D'Lima, Walker, and Colwell<sup>134</sup> followed up an Omni-fit-HA titanium alloy stem with a proximal third circumferential HA coating in 60 THAs in 56 patients for 2–5 years. Both the clinical and radiographic outcome were excellent, with absence of nonprogressive subsidence after 1 year and stable bony ingrowth around the proximal third (HA-coated portion) of the stem as well as absence of distal endosteal lysis.

In a multicenter study of 316 hips (282 patients, average age of 50 years) with a proximally HA-coated titanium stem and either a HA- or porous-coated pure titanium cup (all manufactured by Osteonics, Allendale, NJ), Capello, Antonio, Manley, and Feinberg<sup>135</sup> confirmed that HA-coated hip components do enhance ingrowth or ongrowth with no dete-

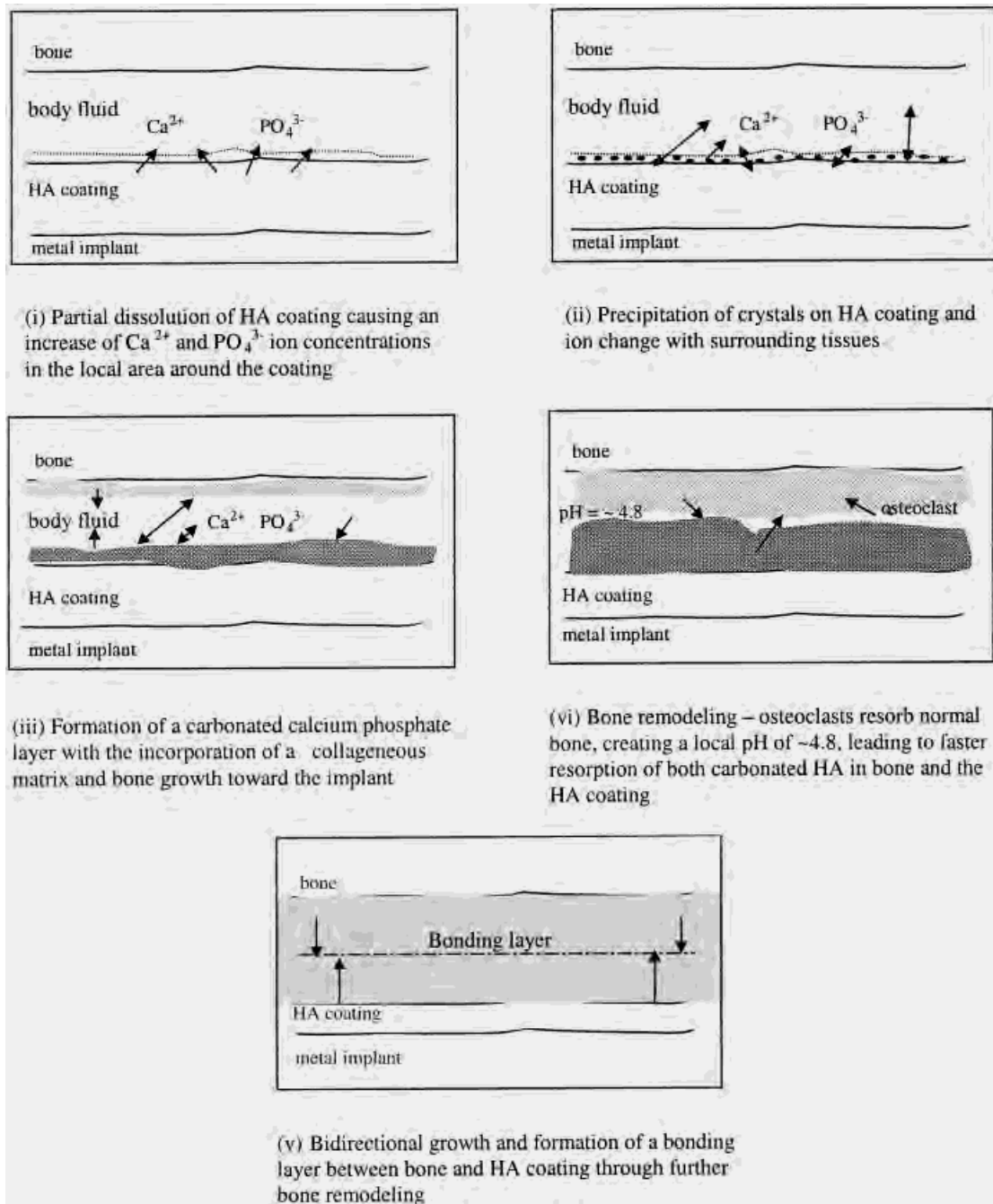


**Figure 4.** Schematic diagram of the establishment of bone-implant bonding. (a) Partial dissolution of HA coating causing an increase of  $\text{Ca}^{2+}$  and  $\text{PO}_4^{3-}$  ion concentrations in the local area around the coating. (b) Precipitation of crystals on HA coating and ion change with surrounding tissues. (c) Formation of a carbonated calcium phosphate layer with the incorporation of a collagenous matrix and bone growth toward the implant. (d) Bone remodeling—osteoclasts resorb normal bone, creating a local pH of  $\approx 4.8$ , leading to faster resorption of both carbonated HA in bone and the HA coating. (e) Bidirectional growth and formation of a bonding layer between bone and HA coating through further bone remodeling.

rioration of femoral component fixation for an average of 8.1 years. Radiographic analysis of the HA-coated stems suggests enhanced bone ongrowth as shown by progressive modeling (cancellous condensation and cortical hypertrophy) of the femur around the middle and distal portions of the stem.

Røkkum et al.<sup>136</sup> followed 100 consecutive entirely HA-coated Ti-6Al-4V hip arthroplasties for 7–9 years. The HA coating was applied over the whole stem and has a mean thickness of  $155 \pm 3.5 \mu\text{m}$ . The clinical results were excellent, and bony incorporation was extensive in all components.

**TABLE IV. Methods of Assessing Fixation of Hip Implants**

Method 1—By Failure Rate <sup>11,132</sup>	Method 2—By Radiographic Features <sup>132,133</sup>
<ul style="list-style-type: none"> <li>Mechanical failure rate: due to aseptic loosening or radiographic loosening</li> <li>Clinical failure rate: due to osteolysis or pain or activity-limited pain with well-fixed stems</li> <li>Combined failure rate: the sum of the former two</li> </ul>	<ul style="list-style-type: none"> <li>Presence of radiolucent lines (RLL)</li> <li>Level of migration or subsidence</li> <li>Appearance of bone</li> <li>Degree of cancellous condensation and cortical hypertrophy</li> <li>Incidence of endosteal lysis</li> <li>Level of pain</li> </ul>

No stem loosened or subsided, which is more satisfactory compared to other cementless fixation.

D'Antonio, Capello, Manley, and Franklin<sup>132</sup> specifically addressed the remodeling of bone around HA-coated femoral stems and presented a detailed description about the progressive remodeling process. They followed 224 THAs with a proximally HA-coated femoral component in 201 patients for a mean duration of 71 months. Of the 224 THAs, 208 (93%, 190 patients) yielded a good or excellent clinical result, 4 patients (2%) reported mild-to-moderate activity-related pain in the thigh, and 2 (1%) experienced aseptic loosening. The radiographs showed progressive new-bone formation (cortical hypertrophy and cancellous condensation) throughout the zones adjacent to the middle and distal portions of the stem.

Bone remodeling began early, with extensive proximal fixation of the implant. The distal stress transfer through the implant was predictable and progressed through the follow-up period, as shown in Figure 5. Cortical hypertrophy about the middle and distal portions of the stem occurred predominantly in the mediolateral plane (47% compared with 6% in the anteroposterior plane), and it was more common in patients who had poorer bone quality preoperatively. Intramedullary osteolysis was present in one femur (0.4%) at 5 years, and the osteolytic area was less than 5 mm in its largest dimension and had not progressed at the time of the 6-year follow-up evaluation.

Capello, D'Antonio, Feinberg, and Manley<sup>11</sup> also found excellent clinical and radiographic results with HA-coated total hip femoral components in patients younger than 50 after 5–8 years of follow-up of 152 hips in 143 patients (16–49 years old, average 39). Radiographic changes consistent with bone remodeling (cancellous condensation and cortical hypertrophy) typically were seen around the midpart of the shaft of the prostheses, and all stems were radiographically osseointegrated. A review of serial radiographs (Figure 6) showed mechanically stable implants with osseous ingrowth, evidence of stress transfer at the middle part of the stem, and minimum endosteal osteolysis. This promising result in young patients is important because cemented stems do not exceed the life expectancy of young patients, and because of some other inherent problems with cemented fixation, such as cell necrosis and loss of endosteal bone.<sup>123</sup>

**TABLE V. Specifications of HA Coatings in Some Clinical Studies With Femoral Stems**

Author	Thickness (T)/Porosity (P)/Density (D)	Crystallinity (C)/Purity (P)	Tensile Bond Strength (T)/Shear Strength (S)/Fatigue Life (F)	Others
Capello and co-workers <sup>11,135</sup>	$T = 50 \mu\text{m}$	N/A	N/A	N/A
D'Antonio et al. <sup>132</sup>	$T = 50 \mu\text{m}$	$P > 90 \text{ wt } \%$	N/A	N/A
D'Lima et al. <sup>134</sup>	$T = 50 \mu\text{m}$ Dense	$C = 70\%$ $P = 95 \text{ wt } \%$	$T > 65 \text{ MPa}$ $F > 107 \text{ cycles at } 8.3 \text{ MPa}$	Implanted with a 4% press fit
Donnelly et al. <sup>138</sup>	$T = 50\text{--}90 \mu\text{m}$	$C > 70\text{--}90\%$ $P = 97\text{--}98 \text{ wt } \%$	$S > 25 \text{ MPa}$	$Ra = 6\text{--}16 \mu\text{m}$
Dorr et al. <sup>142</sup>	$T = 55 \pm 5 \mu\text{m}$ $D = 3.02 \text{ g/cm}^3$	$C > 72\%$ $P > 94 \text{ wt } \%$	$S = 34\text{--}38 \text{ MPa}$ $T = 45\text{--}48 \text{ MPa}$	Porous Ti alloy stem (pore size = $750 \mu\text{m}$ and $490 \pm 30 \mu\text{m}$ before/after HA coating; Ca/P = 1.75)
Onsten et al. <sup>137</sup>	$T = 50 \mu\text{m}$	N/A	N/A	N/A
Røkkum et al. <sup>136</sup>	$T = 155 \pm 3.5 \mu\text{m}$ $D = 1.2\text{--}1.6 \text{ g/cm}^3$	$C = 50\text{--}70\%$ $P > 98 \text{ wt } \%$	$T = 20\text{--}30 \text{ MPa}$	Thick coating; $Ra = 10 \mu\text{m}$
Rothman et al. <sup>6</sup>	$T = 50\text{--}70 \mu\text{m}$ $D = 3.135 \text{ g/cm}^3$	$C > 62\%$ $P > 95 \text{ wt } \%$	N/A	Porous Ti stem
Tonino et al. <sup>182</sup>	$P < 10\%$	$C > 75\%$ $P > 90 \text{ wt } \%$	$T = 62\text{--}65 \text{ MPa}$	Vacuum sprayed, with a Ti bond coat; Ca/P = 1.67
Yee et al. <sup>140</sup>	$T = 50\text{--}70 \mu\text{m}$ $D = 3.135 \text{ g/cm}^3$	$C > 62\%$ $P > 95 \text{ wt } \%$	N/A	N/A

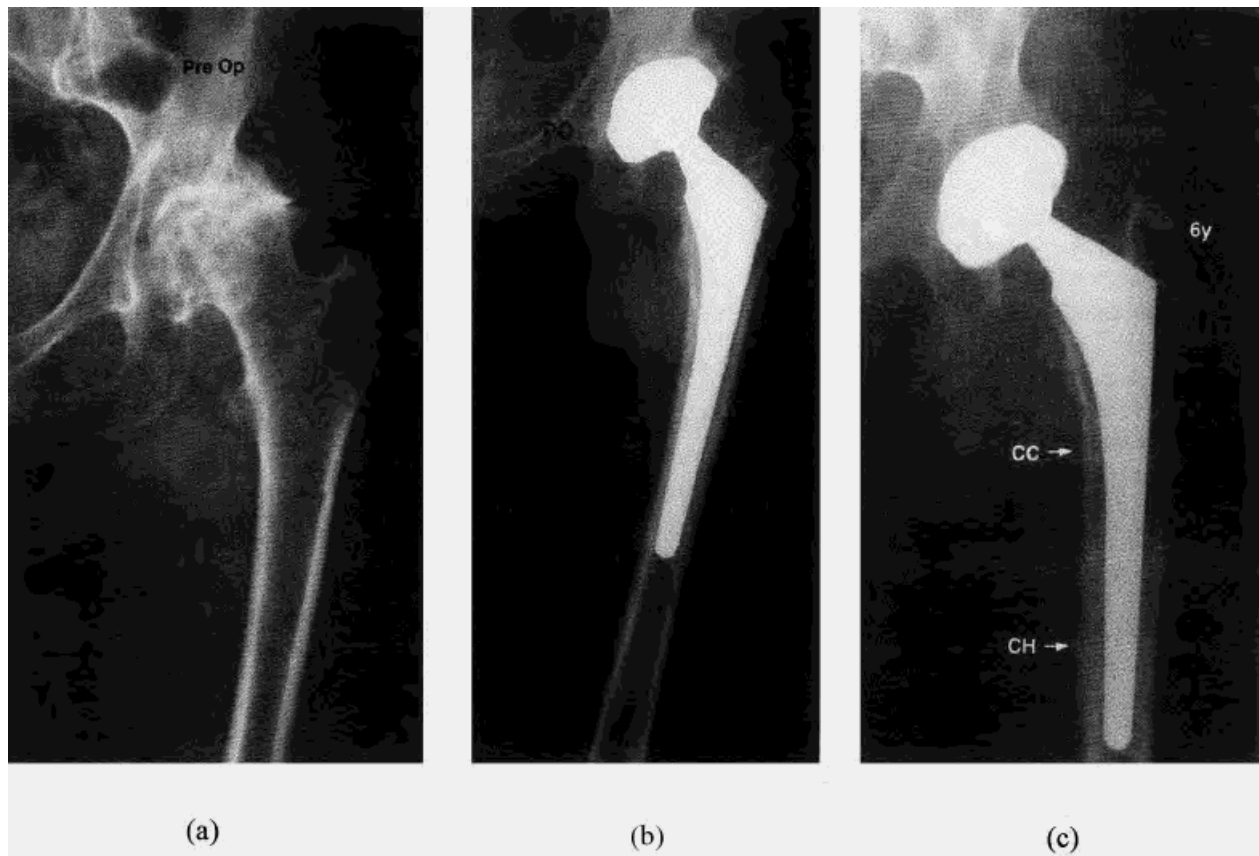


**Figure 5.** Radiographs of a 54-year-old woman who had osteoarthritis and type-C bone. (Courtesy of D'Antonio et al.<sup>145</sup>) (a) Preoperative radiograph. The joint space is obliterated, with partial collapse of the femoral head and periarticular osteophyte formation. (b) Anteroposterior radiograph made 6 weeks postoperatively. (c) Anteroposterior radiograph made 6 years postoperatively, showing the full extent of the cancellous condensation adjacent to the middle and distal portions, and cortical hypertrophy in Zones 2, 3, and 5.

*HA-Coated vs. Cemented Fixation* Some authors specifically compared the fixation of the HA-coated stem with that of the cemented stem and found comparable and even preferable results with the use of the HA-coated stem. Onsten, Carlsson, Sanzen, and Besjakov<sup>137</sup> followed up a consecutive series of 30 total hip replacements with proximally HA-coated stems for 2 years. It was found that the micromotion of these prostheses were comparable to that of the cemented Charnley prostheses, which have been used as controls, with respect to migration and wear.

Donnelly et al.<sup>138</sup> compared the radiological results and survival of four types of fixation of femoral stems with one design, including (a) a press-fit, shot-blasted, smooth Ti-Al-V stem; (b) a press-fit, shot-blasted, proximally ridged stem; (c) a proximally HA-coated stem, and (d) a cemented stem. They followed up 538 replaced hips for 5–10 years. Survival analysis at 5–6 years showed better results for HA-coated and cemented stems (100% survival rate) and a lower mean rate of migration. More radiolucent lines and osteolytic lesions were observed in the press-fit groups, with a trend for a lower incidence in the HA compared with the cemented group. Proximal osteopenia increased in the press-fit and cemented prosthesis with time, but did not occur in the HA group.

There was also a higher incidence of femoral neck resorption with time in the cemented group than the other three.

The results with the HA-coated stems in this study is particularly surprising, because the stems were used in the more demanding younger group (< 60 years). This compares to the slightly less satisfactory survival rates and increased incidence of radiolucent lines and lytic lesions in cemented prostheses used in the older patients (> 60 years). The apparent absence of proximal osteopenia in the HA group seems to be a further advantage in the longer term, which is presumably because only this group of prostheses secured reliable proximal, but not distal, fixation. Therefore, although HA and cemented interfaces both provide secure fixation, there is a trend in favor of HA in terms of fewer radiolucent lines, fewer lytic lesions, and less proximal osteopenia, and longer survival.

*HA-Coated vs. Porous Fixation* Before the adoption of HA coatings, the femoral stem with a porous surface was once the most preferred in cementless fixation, with the aim being to increase bone growth into the pore structure of the implant. However, some clinical retrieval studies have exhibited fibrous, rather than bony, ingrowth into porous surfaces,<sup>109</sup> so the addition of HA may improve osseointegration. Animal



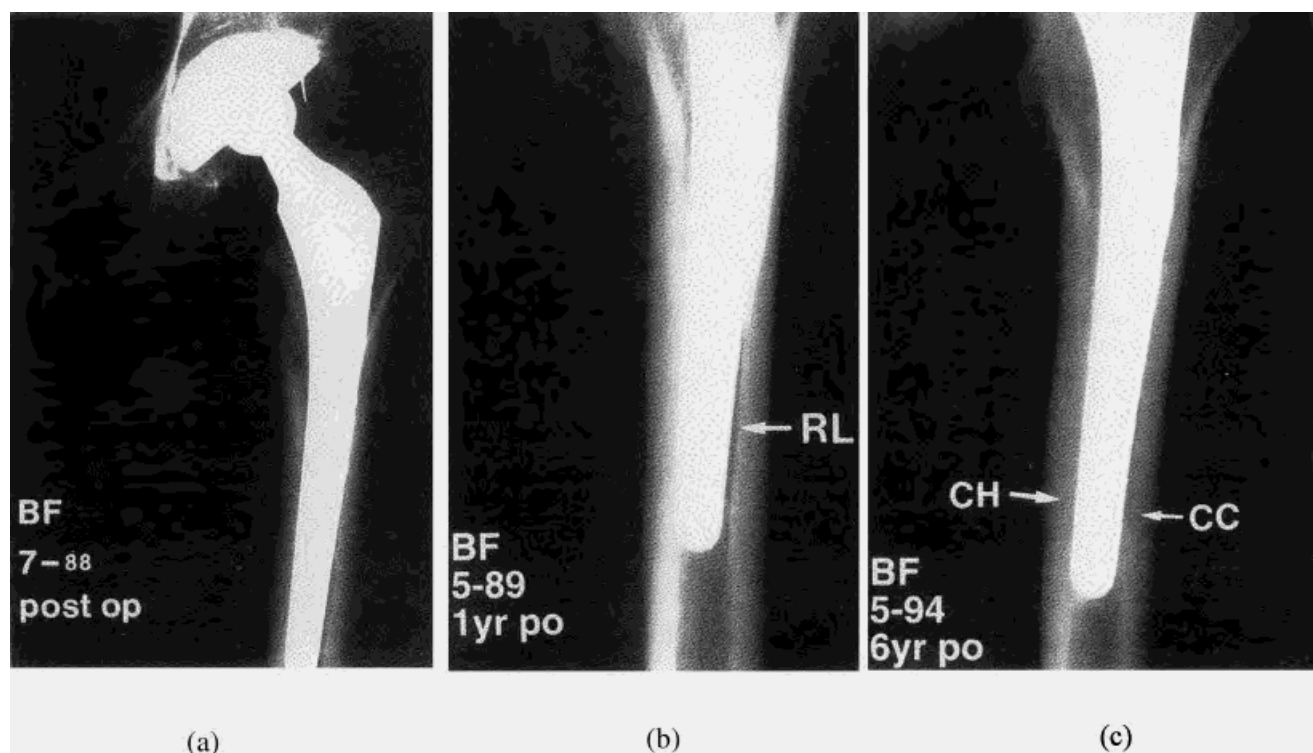


**Figure 6.** Radiographs of a 25-year-old man who had avascular necrosis of the left hip. (Courtesy of Capello et al.<sup>11</sup>) (a) Early postoperative anteroposterior radiograph. (b) Close-up radiograph, made 1 year postoperatively, showing evidence of a radiolucent line around the distal part. (c) Close-up radiograph, made 6 years postoperatively, showing areas of cancellous condensation and cortical hypertrophy, but no evidence of radiolucent line around the distal part.

models have supported the belief that, unlike uncoated porous titanium implants, HA-coated ones may limit the extent of the fibrous membrane formed and can even overcome a 1-mm gap between the implant and bone.<sup>14,15,139</sup>

Many clinical trials have compared the clinical performance of these two types of fixation. Rothman, Hozack, Ranawat, and Moriarty<sup>6</sup> found no clinical or radiographic advantage with the use of HA in primary total hip arthroplasties. This was a retrospective, matched-pair analysis after following up for an average of 2.2 years, where a HA-coated porous titanium femoral stem and its non-coated counterpart were implanted in 52 pairs of patients. McPherson, Dorr, Gruen, and Saberi<sup>7</sup> found better bone remodeling but no clinical differences in a 3-year, matched-pair comparison of porous-coated stems with proximally sprayed HA and porous-coated stems. In a prospective, randomized trial, 62 total hip arthroplasties with either HA-coated or non-coated femoral prostheses were implanted by one surgeon in 55 patients.<sup>140</sup> The dual tapered femoral stem, with a Ti-6Al-4V porous coating at the proximal third of the stem (some prostheses also included an HA coating); a roughened, grit-blasted textured surface on the middle third of the prostheses; and a smooth surface at the distal third. No femoral prostheses failed, and migration or subsidence was not observed after an average of 4.6 years. Although the Harris hip score<sup>141</sup> and femoral stem survivorship in this study do not indicate a significant clinical advantage with the use of HA-coated

femoral prostheses, the HA-coated stems showed trends toward increased distal stem related cortical hypertrophy, increased cancellous condensation and less endosteal cavitation.

Dorr, Wan, Song, and Ranawat<sup>142</sup> suggested that the use of HA coating did provide improved fixation and the possibility of improved durability. They followed up 15 patients who have bilateral hip replacement with the same porous titanium alloy stem design where only one of the stems incorporated an HA coating, for an average of 6.5 years. Despite the small number of patients, compared to the above two comparative methods, this method allowed the complete control of bone type and metabolism, immunology, activity, weight, age and emotional response of the patients. The radiographic measurements revealed fewer radiolucent lines ( $P = 0.013$ ) in the fixation with HA-coated stems and improved bone modeling as measured by proximal cancellous hypertrophy, and this was prolonged to the final follow-up. In addition, the occlusion of pores with the HA coating in this study did not change the improved radiographic fixation.

**(2) Application in Acetabular Component** Despite the encouraging clinical results in femoral prostheses, the use of the HA coating on the acetabular component does not seem as successful as in femoral components. Moilanen et al.<sup>143</sup> compared the HA-coated (71 same size) and noncoated (40 sample size) press-fit Co-Cr alloy acetabular cups in total hip replacements after 2–3 years of implantation. It was found

that HA coatings enhanced the stability of acetabular components, with a reduced rate of proximal migration and a significant reduction in rotational migration and the number of radiolucent lines.

Manley et al.<sup>144</sup> evaluated 377 patients (428 hips) with a porous-coated, press-fit acetabular cup, an HA-coated threaded screw-in cup, or one of two similar designs of HA-coated press-fit cups after an average of 7.9 years of follow-up. All cups were made of commercial pure titanium and the same Osteonics femoral components were used in all cases. Radiographic evaluation of the 383 acetabular cups that were *in situ* at the time of the most recent follow-up showed that (a) 123 (99%) of the 124 HA-coated threaded cups, (b) 101 (98%) of the 103 porous-coated cups, and (c) 139 (89%) of the 156 HA-coated press-fit cups were stable with osseous ingrowth, as indicated by the absence of radiolucent line at the interface and the absence of migration within the acetabulum. The probability of revision due to aseptic loosening was significantly greater for the HA-coated press-fit cups than for the HA-coated threaded cups or the porous-coated, press-fit cups ( $p < .001$  for both comparisons.) The HA-coated threaded cups and the porous-coated press-fit cups continued to perform well more than 5 years after the operation. In the multicenter study by Capello et al.,<sup>135</sup> the HA-coated femoral stem showed enhanced bone ingrowth and fixation for as many as 10 years with only one (0.3%) stem exhibiting aseptic loosening. However, 3 (2.7%) porous-coated cups, 24 (14%) HA-coated press fit cups, and one (2.6%) HA-coated threaded cup were revised for aseptic loosening.

The unsatisfactory results on the acetabular component suggest that in the specific biomechanical environment of the acetabulum, physical interlocking between the cup and the supporting bone beneath it may be a prerequisite for long-term stability; thus cup design is very critical for its performance. Therefore, despite the good short term (2–3 years) results with the HA-coated cups, fatigue failure between the metal surface and the HA coating, arising in response to prolonged distraction stress medially imposed by the patients' activity, was thought to be responsible for the separation of the socket from the bone in the case of press-fit cups in the long term.<sup>136</sup>

Similarly, the HA-coated femoral stem in the Røkkum et al. study<sup>136</sup> also demonstrated excellent clinical results with no stem loosening or subsidence. However, five cups (5%) in this study were revised because of loosening after having functioned painlessly for 3.8–5.5 years with radiological ingrowth exhibited, and this is higher compared to other studies.<sup>145,146</sup> This late occurrence of acetabular loosening contrasts with the porous-coated cups, for which a high incidence of early lucent lines suggesting poorer bonding has been reported.<sup>147,148</sup> In addition to the inherent problems with the acetabular cups described above, the loosening of cups may be attributed to the use of thick coatings ( $155 \pm 3.5 \mu\text{m}$ ) in this study (the commonly used HA coatings are  $50 \mu\text{m}$  thick<sup>81,82</sup>), because thicker coatings may have poor mechanical properties, and the HA-to-metal interface is thought to be

the weak point.<sup>83,131,149</sup> This difference may also explain the fact that loose cups in this study had almost completely lost their HA coating.

**(3) Application in Knee Prostheses** New methods are constantly being developed to improve the fixation of tibial components, especially for young active patients. Since the development of the knee arthroplasty and the promising clinical results with noncoated cementless fixation are relatively recent, studies on the use of HA coatings for knee prostheses are rare. Nilsson, Cajander, and Karrholm<sup>8</sup> have described subsidence as much as 1 cm and delamination of the coating in one type of knee prosthesis with a thick coating. Nelissen, Valstar, and Rozing<sup>119</sup> performed a prospective, randomized, double-blind study to evaluate three different means of fixing tibial components, 11 cemented, 11 HA-coated, and 10 non-coated. After 2 years of follow-up, it was found that micromotion of the HA-coated components was similar to that of the cemented components. Both HA-coated prostheses exhibited far less micromotion along the longitudinal axis (subsidence) and less translation along the transverse axis and sagittal axis throughout the follow-up period than the non-coated components. This result indicates that the HA coating may be used as a biological mediator, which is necessary for adequate fixation of tibial components when cement is not used. In the randomized studies of Toksvig-Larsen, Jørn, Ryd, and Linderstrand<sup>120</sup> on 62 tibial prosthetic fixations, the HA coating was found to have a strong positive effect on the tibial component fixation after a 1–2 year follow-up. The HA-coated groups had far less micromotion compared to the porous-coated groups and no prosthesis in this group showed continuous migration.

**(4) Application in Pin/Screw Components** The bone-to-pin/screw interface is the site of major complications in external fixations: bone-pin loosening and pin-track infection.<sup>150–152</sup> Due to excellent advantages exhibited in hip prostheses, HA coatings were also proposed for use in external fixation with the aim to improve the pin osseointegration and fixation stability.<sup>153,154</sup> Moroni and co-workers<sup>155,156</sup> showed enhancement of bone-to-pin osseointegration and interfacial strength in HA-coated pins compared with uncoated or titanium coated pins in two animal studies under loaded conditions. They further proved this in their clinical studies with three groups of seven patients, who had external fixation of mid-diaphyseal tibial fractures using, respectively, uncoated pins, uncoated bicylindrical pins, and HA-coated bicylindrical pins.<sup>157</sup> They found that both types of uncoated stainless-steel pins showed a lower extraction torque than insertion torque in all cases, whereas the mean extraction torque of the HA-coated pins was unchanged. Seven of the 14 patients receiving uncoated pins revealed pin-track infection, compared with none of the patients with HA-coated pins. Thus, HA-coated external pins did increase stability and, thereby, reduce the risk for pin-track infection and mechanical failure of fracture fixation. The authors<sup>157</sup> also indicated that although pin removal was more painful with HA-coated pin extraction than with the uncoated pins, the pain was of



short duration and should not be the reason for not placing such pins into clinical use.

In another clinical study by Magyar, Toksvig-Larsen, and Moroni,<sup>13</sup> the HA coating was also found to increase threaded pin fixation. The torque forces for the extraction of the standard screws were much lower than that for the HA-coated pins. All 18 of the metaphyseal standard screws were loose at extraction, but only one of the HA-coated screws in the metaphysis was loose. The standard screws in the distal femur lost around 40% of their fixation compared to the HA-coated screws, which retained full fixation strength. No adverse effect has been found in using the HA-coated screw in this study.

**(5) Application in Dentistry** As in hip implants, HA coatings have been used clinically in root-form endosseous implants for over a decade. The short-term survival rates of HA-coated implants have been found comparable to those of titanium implants.<sup>158–160</sup> The main concern with the clinical use of HA-coated dental implants is their long-term survival, with the longest-running studies of 6 or 7 years compared to the good survival rate of titanium implants for over a 25-year period.<sup>161</sup> Biesbrock and Edgerton<sup>161</sup> have reviewed clinical use of HA-coated dental implants and concluded that HA-coated implants are as predictable as titanium implants in short-term periods. They also suggested that HA-coated implants may be useful treatment modalities in a variety of clinical situations, such as in type-IV bone (cancellous bone), in shorter implants (implant size less than or equal to 10 mm), in fresh extraction sites (immediate implants), and in graft-augmented maxillary and nasal sinuses.

Another concern with the use of HA-coated dental implants is the increased incidence of infection. *In vitro* studies by Wolinsky, deCamargo, Erard, and Newman<sup>162</sup> have demonstrated that specific bacteria (e.g., *Streptococcus sanguis* and *Actinomyces viscosus*) can more easily adhere to HA powder and/or beads than titanium powder and/or beads. Johnson<sup>163</sup> suggested that HA coatings are more susceptible to bacterial colonization than titanium implants or natural teeth because of the surface roughness and hydrophilicity of HA. He even proposed that putative periodontal pathogens, such as *Fusobacterium* species and *Peptostreptococcus prevotii*, might preferentially adhere to HA surfaces, predisposing peri-implantitis. However, many clinical microbiologic studies do not seem to support this concern. Gatewood, Cobb, and Killoy<sup>164</sup> examined the maturation of subgingival dental plaque on titanium, HA, and cementum surfaces and found the sequence and composition of microbial morphotypes in the maturation process were similar regardless of the surface. Rams et al.<sup>165</sup> compared the microbial colonization of 30 HA-coated implants and 10 titanium implants in a 10-month clinical study and found no significant difference in the development of microflora.

In a prospective study, Roynesdal, Ambjornsen, Stovne, and Haanas<sup>166</sup> investigated the clinical outcome and marginal bone resorption of three different endosseous implants placed in the anterior mandibles of 15 elderly patients. The results of 3-year follow-up indicated that, compared to titanium plas-

ma-sprayed cylinder implants, the titanium screw-shaped and the HA-coated cylinder implants were significantly better in terms of bone resorption. They also concluded that an overdenture in the mandible supported by a few implants with ball attachments is a predictable, simple, and economic treatment method that can be used in most patients with expected favorable prognoses. The long-term stability of HA-coated implants has been questioned by the possibility of the existence of HA detachment and resorption.

Piattelli, Scarano, Alberti, and Piattelli<sup>167</sup> retrieved two HA-coated implants after 12 months of loading because of an abutment fracture and found close contact between the bone and the coating with no gap or connective tissue capsule at the interface under light microscopy, as shown in Figure 7(a). A reduction in the coating thickness was also found, just in one area, along with the presence of some detached HA particles embedded in the newly formed bone [Figures 7(b) and 7(c)]. This suggests that the resorption or the detached HA particles would not cause any adverse problem for the long-term survival of the implant.

**Coating Resorption and Bone Growth.** In HA-coated implants, one of the most important events occurring at the bone-implant interface is the resorption of the HA coating, also called degradation or coating loss, sometimes with the presence of HA particles. Although it is essential for the establishment of bone-implant bonding, this has been one of the main concerns for the durability of the HA-coated implants. Some studies have shown resorption of HA coatings up to 2 years after implantation,<sup>168–170</sup> and a complete loss of a 60- $\mu\text{m}$ -thick HA coating after 4 years.<sup>171</sup> Based on the observation of animal studies and human retrievals, Bauer<sup>172</sup> hypothesized and described four mechanisms whereby HA coating can be lost from the implant surface: (a) dissolution at neutral pH, (b) osteoclastic resorption of the coating as part of normal bone remodeling, (c) delamination due to bond failure, and (d) abrasion from lack of primary fixation. This has been supplemented by Gross, Ray, and Røkkum<sup>173</sup> with two more mechanisms: (e) lamellae cracking from the release of residual stress on the coating surface; and (f) preferential amorphous phase dissolution producing free crystalline debris.

The HA particles can be resorbed by macrophages if their size is sufficiently small compared to the macrophages (approximately 30  $\mu\text{m}$ ).<sup>174,175</sup> HA particles in the macrophage will persist as a cellular irritant. When a macrophage phagocytizes the particles, the cells release cytokines, prostaglandins, and collagenases almost immediately. It has been reported that release of these factors begins immediately after HA ingestion and that maximal release occurs between 12 and 24 h.<sup>176</sup> If the particles do not dissolve within the lifespan of the macrophage, more macrophages will accumulate at the site in response to the release of cytokines to digest the dead macrophages and undissolved HA particulates. As well, particles larger than a macrophage ( $> 30 \mu\text{m}$ ) will not be digested by macrophages and will probably become engulfed by a giant cell. The excessive cellular reaction to HA particulates and the stimulation of a foreign-body response could

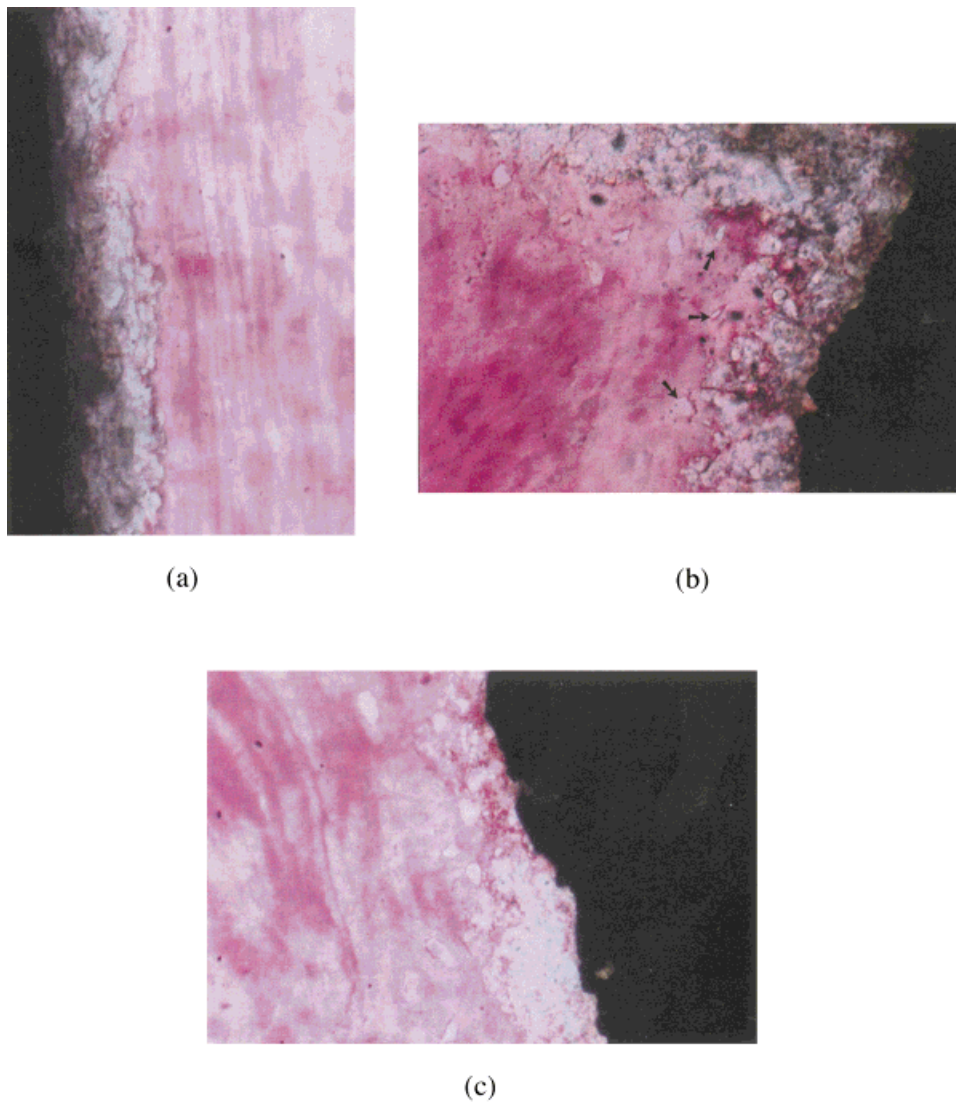


**Figure 7.** Interface between a HA-coated dental implant and bone. (a) Implant in intimate contact with mature lamellar bone. (b) Resorption of the HA coating in some portions of the interface, with some detached HA embedded in the newly formed bone (arrow) and biological material inside the coating. (c) A reduction of coating thickness in some portions of the interface (basic fuchsin and toluidine blue, original magnification  $\times 400$ ). [From Piattelli et al., *Int J Oral Maxillofac Implants*, 14, 233–238, 1998, Quintessence Publishing Co., Inc, reproduced with permission.]

lead to a decrease in local pH, which disrupts the bone remodeling process, causing the resorption of both HA and bone. Additional problems could arise if particulate debris travels to the hip bearing surface, producing third-body wear and component loosening.<sup>177</sup> Although described as a significant theoretical problem, coating delamination has only been identified in some animal studies, probably because of the small thickness and low crystallinity of the HA coating in clinical use.<sup>178</sup> Delaminated HA particles, if present, were found to act more like a bone graft substitute; that is, they were commonly surrounded by bone and not associated with a foreign-body giant cell reaction, histiocytic proliferation, fibrosis or osteolysis, so they cannot be a significant cause of bone resorption or implant abrasion.<sup>172</sup> The HA-coating abrasion is more of a theoretical problem. The latter two mech-

anisms (e) and (f) still need further investigation. So generally there is only concern for the former two (a) and (b) resorption mechanisms.

Partial dissolution of the HA coating is essential to trigger bone growth. Less crystalline coatings usually promote earlier bone growth and stronger fixation, as was discussed in Section 3.1. Meanwhile, bone remodeling proceeds; that is, osteoclasts resorb normal bone by actively secreting hydrogen ions into the extracellular space, creating a local pH of approximately 4.8. Although the highly crystalline HA coating may be very stable at neutral pH, it is more soluble at these acidic local environments, and the low-crystallinity coating shows even more rapid dissolution. So both the low-crystalline carbonated HA in bone mineral and the HA coating can be focally dissolved by osteoclasts at pH 4.8. This

resorption of the coating as part of normal bone remodeling is probably the main coating loss mechanism in the long run and has been shown in many time-related studies on histological specimens.<sup>179–181</sup> The coating can disappear with time as a response to this bone remodeling process, but the absence of coating was usually replaced with the presence of new bone, especially in some areas with load transfer, suggesting the acceleration of coating resorption and bone remodeling with mechanical loading.<sup>19,168</sup>

Tonino, Therin, and Doyle<sup>182</sup> retrieved five total hip arthroplasties with vacuum plasma sprayed HA-coated Ti-6Al-4V stems after 3.3–6.2 years of implantation. They proved that the resorption of the HA coating is cell-mediated and dependent on bone-remodeling processes. This conclusion was based on the fact that most HA resorption takes place at the most proximal level of the metaphysis with less at the more distal sections. All the stems were fixed in the femur and showed osseointegration of both the proximal (HA-coated) and distal (uncoated) parts, as evidenced by the radiological extension of new endosteal or periosteal bone apposition. The appearance of the coating was nonuniform, as shown in Figure 8. In areas covered by bone it was thick and regular, but in those covered by bone marrow it was thin and fully absorbed or irregular; an intermediate stage (50% of HA loss or 50% of the original thickness) was seldom observed. Bone marrow was observed directly in contact with the metal or coating surface without any fibrous interface, illustrating the quality of the osseointegration and the absence of micromovement. In areas where bone resorption was focally increased, the resorption of HA was also increased, and some osteoclasts were observed. When bone marrow was adjacent to the stem, HA granules were sometimes seen with active signs of phagocytosis. The almost complete loss of HA, as seen in one case, did not seem to jeopardize fixation or osseointegration, and the amount of bone-implant contact in this case did not change substantially in the proximal-stem region and was similar to the other osseointegration. There is no coating delamination, which, according to the authors,<sup>182</sup> may be attributed to the excellent homogeneity and bonding strength of the coating obtained by vacuum plasma spraying.

An interesting observation in the Røkkum et al. study<sup>136</sup> is that their histological studies of HA-coated prostheses retrieved from patients have shown no resorption of HA coating up to 9 months after implantation. The crystallinity of the coating used in this study is 50–70%, which would be more soluble even in neutral pH environments. However, the clinical results of their study are still excellent, with extensive bony incorporation in all components. The reasons for this are not clear, but the coating they used is quite thick and it is applied to the entire femoral stem.

**Wear and Osteolysis.** Another concern about the clinical use of HA coating is that it will lead to increased polyethylene wear or third-body wear, and, thus, result in increased incidence of osteolysis. Harris<sup>183</sup> stated that osteolysis, but not the fixation method, is the leading issue in contemporary total hip arthroplasty. Osteolysis was described as any focal

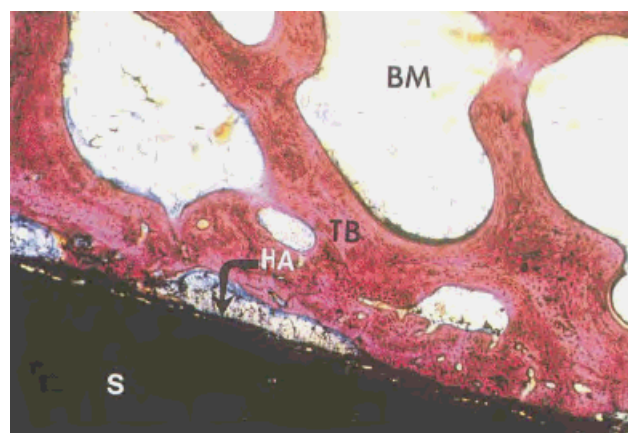


**Figure 8.** Details of the anterior side of the Gruen zone 1A to 7A of a HA-coated femoral stem (Courtesy of Tonino et al.<sup>182</sup>). HA coating is thicker and more regular in areas covered with trabecular bone (TB) than in areas in contact with bone marrow (BM). The mature TB is spread on the implant (S) surface ( $\times 20$ ).

area of bone loss adjacent to the prosthesis, which is believed to be caused by the biological response to wear debris, mainly polyethylene particles, but also including metallic and HA particles.<sup>22,184</sup> Osteolysis of the femoral cortex has often been found with both cemented and porous-coated stems,<sup>185–188</sup> and it most often appeared around cementless acetabular components in hips with abundant polyethylene particles.<sup>189–191</sup> Metallosis in hips with incomplete polyethylene wear implies third-body wear.

Critics of HA argue that the most probable third bodies are particles of HA that may detach during insertion, especially from the threads of a screw cup, as well as HA evolving from resorption of the coating.<sup>22,169</sup> Bloebaum and co-workers<sup>22,184</sup> anticipated that HA would increase wear and osteolysis based on experience with implant retrievals obtained at revisions. Buma and Gardeniers<sup>171</sup> expressed similar concerns of fragmentation and loss of HA coating, as observed from a single stem revised for thigh pain. HA lost from surfaces uncovered by bone could more easily enter the joint and damage the articulating surfaces.<sup>131</sup> However, no fragmentation has been observed in some other implant retrievals.<sup>19,192</sup> D'Antonio, Capello, and Jaffe<sup>145</sup> and Geesink<sup>193</sup> have not observed osteolysis with the HA Omnifit stem. Thus, HA resorption and, probably, fragmentation most likely do occur but do not seem to promote increased wear and osteolysis in the absence of loose implant.<sup>11,194</sup> HA particles, if present, would not cause any adverse problems; small particles can be resorbed by macrophages,<sup>174</sup> and the large ones usually act like a bone graft surrounded by new bone.<sup>172</sup>

On the other hand, proponents of HA coating suggest that, because of its biocompatibility and potential circumferential bone apposition, HA coatings may prevent polyethylene and metal debris from migrating along the bone-implant interface and, thus, reduce the incidence of osteolysis and the failure of implants. Moilanen et al.<sup>143</sup> found no increased wear with the use of HA-coated implants, and their results on the fixation with HA-coated acetabular components revealed few radiolu-



cent lines and migration compared with press-fit acetabular components. In the multicenter study of 316 hip implants by Capello et al.,<sup>135</sup> there are no cases of distal endosteal femoral osteolysis (intramedullary osteolysis), whereas proximal femoral osteolysis and polyethylene wear was no greater than that seen with other cementless or cemented components. This suggests that a circumferential HA coating may prevent the distal egress of wear debris effectively.

In the Dorr et al. bilateral total hip arthroplasty study,<sup>142</sup> the overall wear in the hips was high, with an average of 0.136 mm linear wear<sup>4</sup> per year, but the wear and osteolysis were not increased in porous-coated stems hips with HA coatings. The D'Lima et al. study with an Omnifit-HA stem<sup>134</sup> also showed an absence of distal endosteal lysis, along with correlation of calcar erosion to polyethylene wear, suggesting that early circumferential bony ingrowth afforded by the HA coating prevents distal endosteal access to polyethylene debris at short term follow-up. Donnelly et al.<sup>138</sup> also found the absence of lytic lesions in their study with 538 HA-coated hips for 5–10 years, implying that an HA coating impedes the access of polyethylene debris to the interface.

Røkkum et al.<sup>136</sup> specifically addressed the problem of polyethylene wear, osteolysis, and acetabular loosening in their study with 100 consecutive extensively HA-coated hip arthroplasties. The polyethylene wear and osteolysis in their study was worse than general cemented and cementless studies. Eighteen hips with excessive polyethylene wear required surgery and six needed revisions. Osteolysis was found in 66 hips, including all those reoperated on for excessive polyethylene wear. They also found that both calcium phosphate and metal particles were embedded within the polyethylene surface, as has been reported by others.<sup>22,184</sup> It is unclear whether these particles have arisen from the coating or are simply bone fragments. The poor mechanical properties of these thick coatings may have enhanced HA abrasion and provided a source of HA particles. The largest lesion was in the cancellous bone. The gap often seen lateral to the proximal part of the stem could be a route for the transport of particles into the greater trochanter; whereas the hole in the metal backing could have provided access to the acetabular bone. The complete absence of femoral endosteal cortical osteolysis in spite of the abundance of particles is assuring, which may be explained by the fact that the extensive HA coating of the stem seals the whole interface and blocks the passage of particles.

In the histological and histomorphometric examination of five HA-coated hip implants, Tonino et al.<sup>182</sup> found metal particles with little inflammatory response in nearly all metaphyseal sections; mostly in combination with some HA granules in areas where there was resorption of the HA coating. Hydroxyapatite debris, when present, was only seen adjacent to the metaphyseal part of the stem and never distal to the level of the coating, so did not cause any adverse or

inflammatory reaction. Osteoclasts or macrophages were sometimes seen phagocytosing the HA granules. They also confirmed the absence of polyethylene particles at the interface, because it was closed proximally by circumferential osseointegration.

## SUMMARY AND FUTURE DEVELOPMENT

Plasma-sprayed HA coatings have demonstrated advantages in promoting faster and stronger fixation and bone growth both *in vivo* and clinically, and shown promising short-term and medium-term clinical results in femoral stems, knee prostheses, pins/screws, and dental implants. Its application in acetabular components, however, is more dependent on the design of the acetabular cup. HA coatings allow direct bonding to living tissues compared to a loosely adherent layer of fibrous tissue at the implant interface in other cementless fixation, which is especially beneficial for young active patients.

The wear and osteolysis problem did not exhibit any obvious increase in HA-coated implants compared to other cemented and cementless fixation methods. The HA coating even seemed to be able to seal the polyethylene and metal debris from entering the bone-implant interface and reduce wear and osteolysis.

Resorption of the HA coating did occur in most clinical cases, mainly cell-mediated as the result of normal bone remodeling. The initial resorption generally relies on the dissolution rate of the coating, and faster dissolution is preferred to initiate quicker and stronger fixation. The loss of the coating is usually followed by the growth of new bone. Thus, if the resorption rate can be optimally controlled so that the new bone can grow immediately to replace the resorbed coating, the durability of the bone-implant fixation should not be affected. Both the initial dissolution and the resorption for the HA coating are a direct influence of the phase composition, microstructure and coating defects (i.e., cracks, pores), and surface characteristics. Therefore, the feedstock HA powders, coating design, and manufacturing technique are very important. The overall implant performance, however, cannot be well connected with the HA coating, because it depends on a combination of factors such as coating manufacture, implant material and design, bone bed preparation, bone quality and quantity, and surgical technique.

As to future development, the knowledge bases regarding for example, amorphous and impurity phases and their distribution throughout the coating; mechanical properties, residual stress control, and their influences on the resorption and wear of the coating, are still incomplete. These materials-science aspects still need further investigation. Meanwhile, the characterization and testing methods vary from person to person, and standards need to be established to ensure better quality control. Besides these points, some other material-design methods, such as gradient structures, surface treatment, and composite coatings, have also been developed. The concept of gradient structures is to have a very amorphous

<sup>4</sup> Wear is measured as smallest radius from the center of femoral head to outer border of the acetabular cup.

coating surface with high initial dissolution and gradually increase the crystallinity to a higher level at the coating-implant interface to improve coating durability. This method, however, is not easy to control in manufacturing.

An alternative method is to use a composite of HA with a calcium phosphate with higher solubility, such as  $\beta$ -TCP. The surface layer can be  $\beta$ -TCP, and the HA/ $\beta$ -TCP ratio increases with the gradient of the coating. The base of the coating should be a pure and highly crystalline HA.<sup>34</sup> The concept of surface treatment is to alter a thin surface layer of the crystalline HA coating to become more amorphous for a more rapid initial dissolution rate while still keeping the crystalline structure for the underlying coating. The design of HA/ZrO<sub>2</sub> composite coatings is based on the high strength of ZrO<sub>2</sub> and its special stress-induced transformation toughening or toughening caused by crack-particle interaction to increase the toughness of the coating.<sup>195-197</sup> A final design concerning the use of HA/polymer coating aims to obtain a composite with a Young's modulus close to cortical bone, superior toughness, and considerable bioactivity.<sup>198,199</sup>

In summary, the outlook on using HA coatings on orthopedic appliances, formed by thermal spray methods, as functional bioactive agents to aid the healing process, is favorable. Future developments that revolve around process control in order to predetermine the precise coating chemistry and exact thickness of the HA or HA-composite coating will assure agreeable clinical results.

## REFERENCES

1. Furlong RJ, Osborn JF. Fixation of hip prostheses by hydroxyapatite ceramic coatings. *J Bone Joint Surg* 1991;73B:741-745.
2. Geesink RGT. Experimental and clinical experience with hydroxyapatite-coated hip implants. *Orthopedics* 1989;12:1239-1242.
3. Geesink RGT, de Groot K, Klein CP. Bonding of bone to apatite-coated implants. *J Bone Joint Surg* 1988;70B:17-22.
4. Cook SD, Thomas KA, Dalton JF, Volkman TK, Whitecloud TS III, Kay JF. Hydroxyapatite coating of porous implants improves bone ingrowth and interface face attachment strength. *J Biomed Mater Res* 1992;26:989-1001.
5. Stephenson PK, Freeman MA, Revell PA, Germain J, Tuke M, Pirie CJ. The effect of hydroxyapatite coating on ingrowth of bone into cavities in an implant. *J Arthroplasty* 1991;6:51-58.
6. Rothman RH, Hozack WJ, Ranawat A, Moriarty LRN. Hydroxyapatite-coated femoral stems. A matched-pair analysis of coated and uncoated implants. *J Bone Joint Surg* 1996;78A:319-324.
7. McPherson EJ, Dorr LD, Gruen TA, Saberi MT. Hydroxyapatite-coated proximal ingrowth femoral stems. A matched pair control study. *Clin Orthop* 1995;315:223-330.
8. Nilsson KG, Cajander S, Karrholm J. Early failure of hydroxyapatite coating in total knee arthroplasty. *Acta Orthop Scand* 1994;65:212-214.
9. Roynesdal AK, Ambjornsen E, Stovne S, Haanas HR. A comparative clinical study of three different endosseous implants in edentulous mandibles. *Int J Oral Maxillofac Implants* 1998;13:500-505.
10. Donnelly WJ, Kobayashi A, Chin TW, Freeman MAR, Yeo H, West M, Scott G. Radiological and survival comparison of four fixation of a proximal femoral stem. *J Bone Joint Surg* 1997;79B:351-360.
11. Capello WD, D'Antonio JA, Feinberg JR, Manley MT. Hydroxyapatite-coated total hip femoral components in patients less than fifty years old. Clinical and radiographic results after five to eight years of follow-up. *J Bone Joint Surg* 1997;79A:1023-1029.
12. Nelissen, RGHH, Valstar ER, Rozing PM. The effect of hydroxyapatite on the micromotion of total knee prostheses. A prospective, randomized, double-blind study. *J Bone Joint Surg* 1998;80A:1665-1672.
13. Magyar G, Toksvig-Larsen S, Moroni A. Hydroxyapatite coating of threaded pins enhances fixation. *J Bone Joint Surg* 1997;79B:487-489.
14. Soballe K et al. Gap healing enhanced by hydroxyapatite coatings in dogs. *Clin Orthop* 1991;272:300-307.
15. Soballe K, Hansen ES, Rasmussen HB, Bunger C. Tissue ingrowth into titanium and hydroxyapatite coated implants during stable and unstable mechanical conditions. *J Orthop Res* 1992;10:285-299.
16. Soballe K, Hansen ES, Rasmussen HB, Bunger C. Hydroxyapatite coating converts fibrous tissue to bone around loaded implants. *J Bone Joint Surg* 1993;75B:270-288.
17. Rahbek O, Overgaard S, Soballe K, Bunger C. Hydroxyapatite coating might prevent peri-implant particle migration: A pilot study in dogs. *Acta Orthop Scand* 1996;67(Suppl 267):58-59.
18. Soballe K, Overgaard S. The current status of hydroxyapatite coating of prostheses. *J Bone Joint Surg* 1996;78B:689-690.
19. Bauer TW, Geesink RCT, Zimmerman R, McMahon JT. Hydroxyapatite-coated femoral stems. Histological analysis of components retrieved at autopsy. *J Bone Joint Surg* 1991;73A:1439-1452.
20. Collier JP, Surprenant VA, Mayor MB, Wrona M, Jensen RE, Surprenant HP. Loss of hydroxyapatite coating on retrieved, total hip components. *J Arthroplasty* 1993;8:389-393.
21. Morscher EW, Hefti A, Aebi U. Severe osteolysis after third-body wear due to hydroxyapatite particles from acetabular cup coating. *J Bone Joint Surg (Br)* 1998;80B:267-272.
22. Bloebaum RD, Dupont JA. Osteolysis from a press-fit hydroxyapatite-coated implant. A case study. *J Arthroplasty* 1995;8:195-202.
23. Rothman RH, Hozack WJ, Ranawat A, Moriarty L. Hydroxyapatite-coated femoral stem. A matched-pair analysis of coated and uncoated implants. *J Bone Joint Surg* 1996;78A:319-324.
24. Dalton JE, Cook SD. *In vivo* mechanical and histological characteristics of HA-coated implants vary with coating vendor. *J Biomed Mater Res* 1995;29:239-245.
25. Hench LL, Wilson J. An introduction to bioceramics. Singapore: World Scientific; 1993.
26. Grynaps M. Age and disease-related changes in the mineral of bone. *Calcif Tissue Int* 1993;53(Suppl 1):S57-S64.
27. Bloebaum RD, Skedros JG, Vajda EG, Bachus KN, Constantz BR. Determining mineral content variations in bone using backscattered electron imaging. *Bone* 1997;20:485-490.
28. Ben-Nissan B, Chai C, Evans L. Crystallographic and spectroscopic characterization of morphology of biogenic and synthetic apatites. Part B. In: Wise DL, editor. *Encyclopedic handbook of biomaterials and bioengineering*. New York: Marcel Dekker; 1995. p 196.
29. De Lange G, De Putter C. Structure of the bone interface to dental implants *in vivo*. *J Oral Implantol* 1993;19:123-135.
30. Jasen JA, van der Waerden JP, de Groot K. Development of a new percutaneous access device for implantation in soft tissue. *J Biomed Mater Res* 1991;25:1535-1545.
31. Denissen HW, de Groot K, Makkes PC, van den Hooff A, Kloppe PJ. Tissue response to sense apatite implants in rats. *J Biomed Mater Res* 1980;14:713-721.

32. Black J. Biological performance of materials (3rd ed.). New York: Marcel Dekker; 1999. p 444.
33. Jarcho M. Calcium phosphate ceramics as hard tissue prosthetics. *Clin Orthop* 1981;157:259–278.
34. Tsui YC, Doyle C, Clyne TW. Plasma sprayed hydroxyapatite coatings on titanium substrates. Part 1: Mechanical properties and residual stress levels. *Biomaterials* 1998;19:2015–2029.
35. Berndt CC, Haddad GN, Farmer AJD, Gross KA. Thermal spraying for bioceramic applications. *Mater Forum* 1990;14:161–173.
36. M, Mornacho R, Constant G. Spraying technique for apatite coatings. *Coches Minces Vide* 1985;40:305–308.
37. De Groot K, Geesink R, Klein CP, Serekian P. Plasma sprayed coatings of hydroxylapatite. *J Biomed Mater Res* 1987;21:1375–1381.
38. Laceyfield WR. Hydroxyapatite coatings. In: Ducheyne P, Lemons JE, editors. *Bioceramics: Material characteristics versus in vivo behavior*. Ann NY Acad Sci 1988;523:72–80.
39. Li TT, Lee JH, Kobayashi T, Aoki H. Hydroxyapatite coating by dipping method, and bone bonding strength. *J Mater Sci Mater Med* 1996;7:355–357.
40. Locardi B, Pazzaglia UE, Gabbi C, Profilo B. Thermal behavior of hydroxyapatite intended for medical applications. *Biomaterials* 1993;14:437–441.
41. Yankee SJ, Platka BJ, Luckey HA, Johnson WA. Process for fabricating HA coatings for biomedical applications, thermal spray research and applications. In: *Proceedings of the Third Annual Thermal Spray Conference*, Long Beach, California; May 20–25, 1990. p 433–438.
42. Raemdonck WV, Ducheyne P, Meester PD. Auger electron spectroscopic analysis of hydroxyapatite coating on titanium. *J Am Ceram Soc* 1986;63:381–384.
43. Jaffe WL, Scott DF. Total hip arthroplasty with hydroxyapatite-coated prostheses. *J Bone Joint Surg* 1996;78A:1918–1934.
44. Ong JL, Lucas LC. Post-deposition heat treatments for ion beam sputter deposited calcium phosphate coatings. *Biomaterials* 1994;15:337–341.
45. Yoshinari N, Ohtsuka Y, Derand T. Thin hydroxyapatite coating produced by the ion beam dynamic mixing method. *Biomaterials* 1994;15:529–535.
46. Lin JHC, Liu ML, Ju CP. Structure and properties of hydroxyapatite-bioactive glass composites plasma sprayed on Ti-6Al-4V. *J Mater Sci Mater Med* 1994;5:279–283.
47. Brossa F, Cigada A, Chiesa R, Paracchini L, Consonni C. Adhesion properties of plasma sprayed hydroxyapatite coatings for orthopaedic prostheses. *Biomed Mater Eng* 1993;3:127–136.
48. Bortz SA, Onesto EJ. Flame-sprayed bioceramics. *Am Ceram Soc Bull* 1975;52:898.
49. Haman JD, Lucas LC; Crawmer D. Characterization of high velocity oxy-fuel combustion sprayed hydroxyapatite. *Biomaterials* 1995;16:226–237.
50. Oonishi H, Yamamoto M, Ishimaru H, Tsuji E, Kushitani S, Aono M, Ukon Y. The effect of hydroxyapatite coating on bone growth into porous titanium alloy implants. *J Bone Joint Surg* 1989;71B:213–216.
51. Dalton JE, Cook SD. In vivo mechanical and histological characteristics of HA-coated implants vary with coating vendors. *J Biomed Mater Res* 1995;29:239–245.
52. Ducheyne P, Hench LL, Kagan A, Martens M, Burssens A, Mulier JC. The effect of hydroxyapatite impregnation on skeletal bonding of porous coated implants. *J Biomed Mater Res* 1994;28:225–237.
53. Ducheyne P, Healy K. The effect of plasma sprayed calcium phosphate ceramic coatings on the metal ion release from porous titanium and cobalt chromium alloys. *J Biomed Mater Res* 1988;2:1137–1163.
54. Maxian SH, Zawadsky JP, Dunn MG. Mechanical and histological evaluation of amorphous calcium phosphate and poorly crystallized hydroxyapatite coatings on titanium implants. *J Biomed Mater Res* 1993;27:17–28.
55. De Bruijn JD, Bovell YP, van Blitterswijk CA. Structural arrangements at the interface between plasma sprayed calcium phosphates and bone. *Biomaterials* 1994;15:543–550.
56. Akao M, Aoki H, Kato K. Mechanical properties of sintered hydroxyapatite for prosthetic applications. *J Mater Sci* 1981;16:809–812.
57. Luo P, Nieh TG. Preparing hydroxyapatite powders with controlled morphology. *Biomaterials* 1996;17:1959–1964.
58. Kweh SWK, Khor KA, Cheang P. Production and characterization of hydroxyapatite (HA) powders. *J Mater Process Technol* 1999;89-90:373–377.
59. Wang BC, Chang E, Lee TM, Yang CY. Changes in phases and crystallinity of plasma-sprayed hydroxyapatite coatings under heat treatment: A quantitative study. *J Biomed Mater Res* 1995;29:1483–1492.
60. Gross KA, Berndt CC. Optimization of spraying parameters for hydroxyapatite. In: Blum-Sandmeier S, Eschnauer E, Huber P, editors. *Proc 2nd Plasma-Technik Symposium*, Wohlen, Switzerland: Plasma-Technik AG; 1991. vol 3, p 159–170.
61. Radin SR, Ducheyne P. Plasma spraying induced changes of calcium phosphate ceramic characteristics and the effect on in vitro stability. *J Mater Sci Mater Med* 1992;3:33–42.
62. Trombe JC, Montel G. Some features of the incorporation of oxygen in different oxidation states in apatite lattice. *J Inorg Nucl Chem* 1978;40:15–21.
63. LeGeros RZ. Biodegradation and bioresorption of calcium phosphate ceramics. *Clin Mater* 1993;14: 65–68.
64. Lide DR, editor. *Handbook of chemistry and physics* 71st ed.). Boca Raton, FL: CRC Press; 1990. p 8–39.
65. Kay MI, Young RA. Crystal structure of hydroxyapatite. *Nature*, 1964;204:1050–1052.
66. Mathew M, Schroeder LW, Dickens B, Brown WE. The crystal structure of  $\alpha$ -Ca<sub>3</sub>(PO<sub>4</sub>)<sub>2</sub>. *Acta Crystallogr* 1977;B33:1325–1333.
67. Dickens B, Schroeder LW, Brown WE. Crystallographic studies of the role of Mg as a stabilizing impurity in  $\beta$ -Ca<sub>3</sub>(PO<sub>4</sub>)<sub>2</sub>. I. The crystal structure of pure  $\beta$ -Ca<sub>3</sub>(PO<sub>4</sub>)<sub>2</sub>. *J Solid State Chem* 1974;10:232–248.
68. Dickens B, Brown WE, Kruger GJ, Stewart JM. Ca<sub>4</sub>(PO<sub>4</sub>)<sub>2</sub>O, Tetracalcium diphosphate monoxide. Crystal structure and relationships to Ca<sub>5</sub>(PO<sub>4</sub>)<sub>3</sub>OH and K<sub>3</sub>Na(SO<sub>4</sub>)<sub>2</sub>. *Acta Crystallogr* 1973;B29: 2046–2056.
69. Elloit JC. Structure and chemistry of the apatites and other calcium orthophosphates. Amsterdam: Elsevier; 1994. p 6.
70. Ducheyne P, Radin S, King L. The effect of calcium phosphate ceramic composition and structure on in vitro behavior. I. Dissolution. *J Biomed Mater Res* 1993;27:25–34.
71. Gross KA, Berndt CC, Goldschlag DD, Iacono VJ. In vitro changes of hydroxyapatite coatings. *Int J Oral & Maxillofac Implants* 1997;12:589–597.
72. Weng J, Liu Q, Wolke JGC, Zhang X, de Groot K. Formation and characteristics of the apatite layer on plasma-sprayed hydroxyapatite coatings in simulated body fluid. *Biomaterials* 1997;18:1027–1035.
73. ASTM. Standard specification for composition of ceramic hydroxyapatite for surgical implants. ASTM; 1988, F1185-88, 415.
74. Gross KA, Berndt CC, Herman H. Formation of the amorphous phase in hydroxyapatite coatings. *J Biomed Mater Res* 1998;39:407–417.
75. Misch CE, Dietsh F. Bone-grafting materials in implant dentistry. *Implant Dent* 1993;2:158–167.



76. Debissen HW, Kalk W, de Nieuport HM, Maltha JC, van de Hooff A. Mandibular bone response to plasma sprayed coatings of hydroxyapatite. *Int J Prosthodont* 1990;3:53–58.
77. David A, Eitenmueller J, Muhr G, Pommer A, Baer HF, Ostermann PAW, Schildhauer TA. Mechanical and histological evaluation of hydroxyapatite-coated, titanium-coated and grit blasted surfaces under weight-bearing conditions. *Arch Orthop Trauma Surg* 1995;114:112–118.
78. Friedman RJ, Black J, Gustke KA, Braunohler WM, Guyer WD, Savory C. Four to six year results of hydroxyapatite total hip arthroplasty. In 20th Ann. Meeting of The Society of Biomaterials; 1994. p 37.
79. Wang JS, Goodman S, Aspenberg P. Bone formation in the presence of phagocytosable hydroxyapatite particles. *Clin Orthop Relat Res* 1994;304:272–279.
80. Lima RS, Kucuk A, Berndt CC. Evaluation of microhardness and elastic modulus of thermally sprayed nanostructured zirconia coatings. *Surface Coating Technol* 2001;135:166–172.
81. De Groot K. HA coatings for implants in surgery. In: Vincenzini P, editor. *High tech ceramics*. Amsterdam: Elsevier; 1987. p 381–386.
82. Geesink RGT, de Groot, K, Klein CPAT. Chemical implant fixation using hydroxyl-apatite coatings. The development of a human total hip prosthesis for chemical fixation to bone using hydroxyl-apatite coatings on titanium substrates. *Clin Orthop* 1987;225:147–170.
83. Wang BC, Lee TM, Chang E, Yang CY. The shear strength and the failure mode of plasma-sprayed hydroxyapatite coating to bone: the effect of coating thickness. *J Biomed Mater Res* 1993;27:1315–1327.
84. Yang CY, Wang BC, Lee TM, Chang E, Chang GL. Intramedullary implant of plasma-sprayed hydroxyapatite coating: An interface study. *J Biomed Mater Res* 1997;36:39–48.
85. Bonfield W.I In: Paipetis SA, editor. *Engineering applications of new composites*. Oxford: Omega Scientific; 1988. p 17–21.
86. Thompson ID, Hench LL. Mechanical properties of bioactive glasses, glass-ceramics and composites. *Proc Inst Mech Eng Pt H: J Eng Med* 1998;212:127–136.
87. FDA. Calcium phosphate (Ca-P) coating draft guidance for preparation of FDA submissions for orthopedic and dental endosseous implants. Washington, DC: Food and Drug Administration; 1992. p 1–14.
88. ISO. Implants for surgery: Coating for hydroxyapatite ceramics. ISO; 1996. p 1–8.
89. ASTM standard C633-79 (reapproved 1993). Standard test method for adhesion or cohesive strength of flame-sprayed coatings. Philadelphia, PA: ASTM; 1979. p 652–656.
90. Inadome T, Hayashi K, Nakashima Y, Tsumura H, Sugioka Y. Comparison of bone-implant interface shear strength of hydroxyapatite-coated and alumina-coated metal implants. *J Biomed Mater Res* 1995;29:19–24.
91. Hayashi K, Inadome T, Tsumura H, Nakashima Y, Sugioka Y. Effect of surface roughness of hydroxyapatite-coated titanium on the bone-implant interface shear strength. *Biomaterials* 1994;15:1187–1191.
92. Eberhardt AW, Zhou C, Rigney ED. Bending and thermal stresses in a fatigue experiment of hydroxyapatite coated titanium rods. In: Berndt CC, Sampath S, editors. *Proc 7th National Thermal Spray Conf ASM Int*; 1994. p 165–169.
93. Brown SR, Turner IG, Reiter H. Residual stress measurement in thermal sprayed HA coating. *J Mater Sci Mater Med* 1994; 5:756–759.
94. Sergio V, Sbaizero O, Clarke DR. Mechanical and chemical consequences of the residual stresses in plasma sprayed hydroxyapatite coatings. *Biomaterials* 1997;18:477–482.
95. Filiaggi MJ, Coombs NA, Pillar RM. Characterization of the interface in the plasma-sprayed HA coating/Ti-6Al-4V implant system. *J Biomed Mater Res* 1991;25:1211–1229.
96. Gross KA. Surface modification of prostheses. Master's thesis, Monash University, Victoria, Australia; 1990. p 144.
97. Wolke JGC, de Groot K, Kraak TG. The characterization of HA coatings sprayed with VPS, APS and DJ system. In: *Thermal spray coatings: Properties, processes and applications*. Materials Park, OH: ASM International; 1991. p 81–90.
98. Mears DC. *Materials and orthopedic surgery*. Baltimore: Williams & Wilkins; 1979.
99. Filiaggi MJ, Coombs NA, Pilliar RM. Characterization of the interface in the plasma-sprayed HA coating/Ti-6Al-4V implant system. *J Biomed Mater Res* 1991;25:1211–1229.
100. Ducheyne P, Healy KE. The effect of plasma-sprayed calcium phosphate ceramic coatings on the metal ion release from porous titanium and cobalt-chromium alloys. *J Biomed Mater Res* 1988;22:1137–1163.
101. Ji H, Ponton CB, Marquis PM. Microstructural characterization of hydroxyapatite coating on titanium. *J Mater Sci Mater Med* 1992;3:183–187.
102. Park E, Condrate RA, Hoelzer DT, Fischman GS. Interfacial characterization of plasma-spray coated calcium phosphate on Ti-Al-4V. *J Mater Sci Mater Med* 1998;9:643–649.
103. Semlitsch M. Titanium alloys for hip joint replacements. *Clin Mater* 1987;2:1–13.
104. Stephenson PK, Freeman MA, Revell PA, Germain J, Tuke M, Pirie CJ. The effect of hydroxyapatite coating on ingrowth of bone into cavities in an implant. *J Arthroplasty* 1991;6:51–58.
105. Jaffe WL, Scott DF. Total hip arthroplasty with hydroxyapatite-coated prostheses. *J Bone Joint Surg* 1996;78A:1918–1934.
106. Butler CA, Jones LC, Hungerford DS. Initial implant stability of porous coated total hip femoral components: A mechanical study of micromovement. *Trans Orthop Res Soc* 1988;13:549.
107. Kay JF. A new concept for noncemented fixation of orthopedic device. *Tech Orthop* 1987;2: 1.
108. Overgaard S, Lind M, Dalstra M, Bunger C, Soballe K. Improved fixation of porous versus blasted surface texture of hydroxyapatite coated implants. *Trans ORS* 1996;42:513.
109. Bobyn JD, Engh CA, Glassman AH. Histological analysis of a retrieved microporous-coated femoral prosthesis. A seven-year case report. *Clin Orthop* 1987;224:303–310.
110. Collier JP, Mayor MB, Chae JC, Surprenant VA, Surprenant HP. Macroscopic and microscopic evidence of prosthetic fixation with porous-coated materials. *Clin Orthop* 1988;235: 173–180.
111. Bloebaum RD, Bachus KN, Jensen JW, Scott DF, Hofmann AA. Porous coated metal backed patellar components in total knee replacement. *J Bone Joint Surg* 1998;80A:518–528.
112. Cook SD, Thomas KA, Delton JE, Volkman T, Kay JF. Enhancement of bone ingrowth and fixation strength by hydroxyapatite coating porous implants. *Trans Orthop Res Soc* 1991;16:550.
113. Dalton JE, Cook SD, Thomas KA, Kay JF. The effects of operative fit and hydroxyapatite coating on the mechanical and biological response to porous implants. *J Bone Joint Surg* 1995;77-A:97–110.
114. Augat P, Claes L, Hanselmann KL, Suger G, Flieschmann W. Increase of stability in external fracture fixation by hydroxyapatite-coated bone screw. *J Appl Biomater* 1995;6:99–104.
115. David A, Eitenmueller J, Muhr G, Pommer A, Baer HF, Ostermann PAW, Schildhauer TA. Mechanical and histological evaluation of hydroxyapatite-coated, titanium-coated and grit-blasted surfaces under weight-bearing conditions. *Arch Orthop Trauma Surg* 1995;114:112–118.
116. Huiskes R, Weinans H, Dalstra M. Adaptive bone remodeling and biomechanical design considerations for noncemented total hip arthroplasty. *Orthopedics* 1989;12:1255–1267.
117. Huiskes R. The various stress patterns of press-fit, ingrown, and cemented femoral stems. *Clin Orthop* 1990;261:27–38.

118. Insall JN, Windsor RE, Scott WN, Kelly MA, Aglietti P. *Surgery of the knee* (2nd ed.). New York: Churchill Livingstone; 1993.
119. Nelissen RGHH, Valstar ER, Rozing PM. The effect of hydroxyapatite on the micromotion of total knee prostheses. A prospective, randomized, double-blind study. *J Bone Joint Surg* 1998;80-A:1665-1672.
120. Toksvig-Larsen S, Jørn LP, Ryd L, Linderstrand A. Hydroxyapatite-enhanced tibial prosthetic fixation. Hydroxyapatite-enhanced tibial prosthetic fixation. *Clin Orthop Relat Res* 2000;379:192-200.
121. Brånemark PI. Osseointegration and its experimental background. *J Prosthet Dent* 1983;50:399-410.
122. Mentag PJ. American Academy of Implant Dentistry. Glossary of terms. *J Oral Implantol* 1986;12:284-292.
123. Galante JO, Jacobs J. Clinical performance of ingrowth surfaces. *Clin Orthop* 1992;276:41-49.
124. Hulbert SF, Cook SD. The case of a composite hip prosthesis. In: Vincenzini P, editor. *Ceramics in substitutive and reconstructive surgery*. Amsterdam: Elsevier; 1991. p 545-565.
125. Bloebaum RD, Mihalopoulos NL, Jensen JW, Dorr LD. Post-mortem analysis of bone growth into porous-coated acetabular components. *J Bone Joint Surg* 1997;79-A:1013-1022.
126. Pidhorz LE, Urban RM, Jacobs JJ, Sumner DR, Galante JO. A quantitative study of bone and soft tissues in cementless porous-coated acetabular components retrieved at autopsy. *J Arthroplasty* 1993;8:213-225.
127. Bloebaum RD, Bachus KN, Momberger NG, Hofmann AA. Mineral apposition rates of human cancellous bone at the interface of porous coated implants. *J Biomed Mater Res* 1994;28:537-544.
128. Puleo DA, Nanci A. Understanding and controlling the bone-implant interface. *Biomaterials* 1999;20:2311-2321.
129. Freeman MAR, Plante-Bordeneuve P. Early migration and late aseptic failure of proximal femoral prostheses. *J Bone Joint Surg* 1994;76-B:432-438.
130. Karrholm J, Borssen B, Lowenhielm G, Snorrason F. Does early micromotion of femoral stem prostheses matter? 4-7 steroradiographic follow-up of 84 cemented prostheses. *J Bone Joint Surg* 1994;76-B:912-917.
131. Morscher E. Editorial. Hydroxyapatite coating of prostheses. *J Bone Joint Surg* 1991;73-B:705-706.
132. D'Antonio JA, Capello WN, Manley MT, Franklin L. Remodeling of bone around hydroxyapatite-coated femoral stems. *J Bone Joint Surg* 1996;78A:1226-1234.
133. Geesink RGT, Hoefnagels NHM. Six year results of hydroxyapatite-coated total hip replacement. *J Bone Joint Surg* 1995;77-B:534-547.
134. D'Lima DD, Walker RH, Colwell, Jr. CW. Omnifit-HA stem in total hip arthroplasty. *Clin Orthop Relat Res* 1999;363:163-169.
135. Capello WN, Antonio JAD, Manley MT, Feinberg JR. Hydroxyapatite in total hip arthroplasty. *Clin Orthop Relat Res* 1998;355:200-211.
136. Røkkum M, Brandt M, Rye K, Hetland KR, Waage S, Reigstad A. Polyethylene wear, osteolysis and acetabular loosening with a HA-coated hip prosthesis. *J Bone Joint Surg* 1999;81-B:582-589.
137. Onsten I, Carlsson AS, Sanzen L, Besjakov J. Migration and wear of a hydroxyapatite-coated hip prostheses a controlled roentgen stereophotogrammetric study. *J Bone Joint Surg* 1996;78B:85-91.
138. Donnelly WJ, Kobayashi A, Freeman MAR, Chin TW, Yeo H, West M, Scott G. Radiological and survival comparison of four fixation of a proximal femoral stem. *J Bone Joint Surg* 1997;79B:351-360.
139. Soballe K, Brockstedt-Rasmussen H, Hansen ES, Burger C. Hydroxyapatite coating modifies implant membrane formation. Controlled micromotion studied in dogs. *Acta Orthop Scand* 1992;63:128-140.
140. Yee AJM, Kreder HK, Bookman I, Davey JR. A randomized trial of hydroxyapatite coated prostheses in total hip arthroplasty. *Clin Orthop Relat Res* 1999;366:120-132.
141. Harris WH. Traumatic arthritis of the hip after dislocation and acetabular fractures: Treatment by mold arthroplasty. *J Bone Joint Surg* 1969;51-A:737-755.
142. Dorr LD, Wan Z, Song M, Ranawat A. Bilateral total hip arthroplasty comparing hydroxyapatite coating to porous-coated fixation. *J Arthroplasty* 1998;13:729-736.
143. Moilanen T, Stocks GW, Freeman MA, Scott G, Goodier WD, Evans SJW. Hydroxyapatite coating of an acetabular prosthesis effect on stability. *J Bone Joint Surg* 1996;78-B:200-205.
144. Manley MT, Capello WN, D'Antonio JA, Edidin A, Geesink RGT. Fixation of acetabular cups without cement in total hip arthroplasty. A comparison of three different implant surface at a minimum duration of follow-up of five years. *J Bone Joint Surg* 1998;80A:1175-1185.
145. D'Antonio JA, Capello WN, Jaffe WL. Hydroxyapatite-coated hip implants: multicenter three-year clinical and roentgenographic results. *Clin Orthop Relat Res* 1992;285:102-115.
146. Geesink RGT, Hoefnagels NHM. Six year results of hydroxyapatite-coated total hip replacement. *J Bone Joint Surg* 1995;77-B:534-547.
147. Haddad RJ, Cook SD, Brinker MR. A comparison of three varieties of noncemented porous-coated hip replacement. *J Bone Joint Surg* 1990;72-B:2-8.
148. Callaghan JJ, Dysart SH, Savory CG. The uncemented porous-coated anatomic total hip prosthesis: Two year results of a prospective consecutive series. *J Bone Joint Surg* 1988;70-A:337-346.
149. Ducheyne P, Cuckler JM. Bioactive ceramic prosthetic coatings. *Clin Orthop* 1992;276:102-114.
150. Aro HT, Markel DM, Chao EYS. Cortical bone reactions at the interface of external fixation half-pins under different loading conditions. *J Trauma* 1993;35:776-785.
151. Pettine KA, Chao EYS, Kelly PJ. Analysis of the external fixation pin-bone interface. *Clin Orthop* 1993;293:18-27.
152. Green SA, Ripley MS. Chronic osteomyelitis in pin tracts. *J Bone Joint Surg* 1984;66A:1092-1098.
153. Moroni A, Caja VL, Stea S et al. Improvement of the bone external fixation pin interface by hydroxyapatite coating. Abstracts of the 41st Annual Meeting, Orthopaedic Research Society, Orlando, FL; 1995. p 253.
154. Caja V, Moroni A. Hydroxyapatite coated external fixation pins. *Clin Orthop* 1996;325:269-275.
155. Morini A, Orienti L, Stea S, Visentin M. Improvement of the bone pin interface with hydroxyapatite coating, An in vivo long term experimental study. *J Orthop Trauma* 1996;10:236-242.
156. Moroni A, Toksvig-Larsen S, Maltarello, MC, Orienti L, Stea S, Giannini S. A comparison of hydroxyapatite-coated, and titanium-coated, and uncoated tapered external-fixation pins. An in vivo study in sheep. *J Bone Joint Surg* 1998;80A:547-554.
157. Moroni A, Aspenberg P, Toksvig-Larsen S, Falzarano G, Giannini S. Enhanced fixation with hydroxyapatite-coated pin. *Clin Orthop* 1998;346:171-177.
158. Saadoun AP, LeGall ML. Clinical results and guidelines on Steri-Oss endosseous implants, *Int J Periodont Rest Dent* 1992;12:487-499.
159. Kent JN, Block MS, Finger IM, Guerra L, Larsen H, Misiek DJ. Biointegrated hydroxyapatite-coated dental implants: 5-year clinical observations. *J Am Dent Assoc* 1990;121:138-144.
160. Block MS, Kent JN. Prospective review of integral implants. *Dent Clin North Am* 1992;36:27-37.

161. Biesbrock AR, Edgerton M. Evaluation of the clinical predictability of hydroxyapatite-coated endosseous dental implants: A review of the literature. *J Oral Maxillofac Implants* 1995; 10:712–720.
162. Wolinsky L, deCamargo P, Erard J, Newman M. A study of in vitro attachment of *Streptococcus sanguis* and *Actinomyces viscosus* to saliva treated titanium. *Int J Oral Maxillofac Implants* 1989;4:27–31.
163. Johnson BW. Ha-o/coated dental implants: long-term consequences. *J Calif Dent Assoc* 1992;20:33–41.
164. Gatewood RR, Cobb CM, Killoy WJ. Microbial colonization on natural tooth structure compared with smooth and plasma-sprayed dental implant surfaces. *Clin Oral Implants Res* 1993; 4:53–64.
165. Rams TE, Roberts TW, Feik D, Molzan AK, Slots J. Clinical and microbiological finds on newly inserted hydroxyapatite-coated and pure titanium human dental implants. *Clin Oral Implants Res* 1991;2:121–127.
166. Roynesdal AK, Ambjornsen E, Stovne S, Haanas HR. A comparative clinical study of three different endosseous implants in edentulous mandibles. *Int J Oral Maxillofac Implants* 1998;13:500–505.
167. Piattelli A, Scarano A, Alberti LD, Piattelli M. Bone-hydroxyapatite interface in retrieved hydroxyapatite-coated titanium implants: A clinical and histologic report. *Int J Oral Maxillofac Implants* 1998;14:233–238.
168. Bauer TW, Stulberg BN, Jiang M, Geesink RGT. Uncemented acetabular components, histologic analysis of retrieved hydroxyapatite coated and porous implants. *J Arthroplasty* 1993; 8:167–177.
169. Collier JP et al. Loss of hydroxyapatite coating on retrieved, total hip components. *J Arthroplasty* 1993;8:389–393.
170. Hardy DCR, et al. Two-year outcome of hydroxyapatite-coated prostheses: two femoral prostheses retrieved at autopsy. *Acta Orthop Scand* 1994;65:253–257.
171. Buma P, Gardeniers JW. Tissue reactions around a hydroxyapatite-coated hip prostheses: case report of a retrieved specimen. *J Arthroplasty* 1995;10:389–395.
172. Bauer TW. Hydroxyapatite: Coating controversies. *Orthopedics*, 1995;18:885–888.
173. Gross KA, Ray N, Røkkum M. The contribution of coating microstructure to degradation and particle release in hydroxyapatite coated prostheses. *J Appl Biomater*, submitted for publication 2001.
174. Evans EJ. Toxicity of hydroxyapatite in vitro: The effect of particle size. *Biomaterials* 1991;12:574–576.
175. Bloebaum RD, Lundeen GA, Bachus KN, Ison I, Hofmann AA. Dissolution of particulate hydroxyapatite in a macrophage organelle model. *J Biomed Mater Res* 1998;40:104–114.
176. Harada Y, Wang JT, Doppalapudi VA, Willis AA, Jasty M, Harris WH, Nagase M, Goldring SR. Differential effects of different forms of hydroxyapatite and hydroxyapatite/tricalcium phosphate particulates on human monocyte/macrophages in vitro. *J Biomed Mater Res* 1996;31:19–26.
177. Friedman RJ, Black J, Galante JO, Jacobs JJ, Skinner HB. Orthopedic biomaterials and implant fixation. *J Bone Joint Surg* 1993;77A:1086–1109.
178. Capello WN, Bauer TW. Hydroxyapatite in orthopedic surgery. In: Cameron HU, editor. *Bone implant interface*. St. Louis: CV Mosby; 1994. p 191–202.
179. Hardy SCR, Frayssinet P, Guilhem A, Lafontaine MA, Delince PF. Bonding of hydroxyapatite-coated femoral prostheses: histopathology of specimens from four cases. *J Bone Joint Surg* 1991;73-B:732–740.
180. Frayssinet P, et al. Histological analysis of the bone-prosthesis interface in man after implantation of a hip: coated with plasma-sprayed hydroxyapatite. *Rev Chir Orthop Reparatrice Appar Mot* 1993;79:177–184.
181. Dhert WJ, Klein CP, Jansen JA, van der Velde EA, Vriesde RC, Rozing PM, de Groot K. A histological and histomorphometrical investigation of fluorapatite, magnesium whitlockite, and hydroxyapatite plasma-sprayed coatings in goats. *J Biomed Mater Res* 1993;27:127–138.
182. Tonino AJ, Therin M, Doyle C. Hydroxyapatite-coated femoral stems: Histology and histomorphometry around five components retrieved at post mortem. *J Bone Joint Surg* 1999;81-B:148–154.
183. Harris WH. The problem is osteolysis. *Clin Orthop* 1995;311: 46–53.
184. Bloebaum RD, Beeks D, Dorr LD, Savory CG, DuPont JA, Hofmann AA. Complications with hydroxyapatite particulate separation in total hip arthroplasty. *Clin Orthop* 1994;298:19–26.
185. Jasty MJ, Floyd WE, Schiller AI, Goldring SR, Harris WH. Localized osteolysis in stable non-septic total hip replacement. *J Bone Joint Surg* 1986;68-A:912–919.
186. Tanzer M, Maloney WJ, Jasty M, Harris WH. The progression of femoral cortical osteolysis in association with total hip arthroplasty without cement. *J Bone Joint Surg* 1992;74-A: 404–410.
187. Maloney WJ, Woolson ST. Increasing incidence of femoral osteolysis in association with uncemented Harris-Galante total hip arthroplasty: A follow-up report. *J Arthroplasty* 1996;11: 130–134.
188. Owen TD, Moran CG, Smith SR, Pinder IM. Results of uncemented porous-coated anatomic total hip replacement. *J Bone Joint Surg* 1994;76-B:258–262.
189. Zicat B, Engh CA, Gokcen E. Patterns of osteolysis around total hip components inserted with and without cement. *J Bone Joint Surg* 1995;77-A:432–439.
190. Kim YH, Kim VEM. Uncemented porous-coated anatomic total hip replacement. *J Bone Joint Surg* 1993;75-B:6–13.
191. Berry DJ, Barnes CL, Scott RD, Cabanela ME, Poss R. Catastrophic failure of the polyethylene liner of uncemented acetabular components. *J Bone Joint Surg* 1994;76-B:575–578.
192. Lintner F, Bohm G, Huber M, Scholz R. Histology of tissue adjacent to an HAC-coated femoral prosthesis: A case report. *J Bone Joint Surg* 1994;76-B:824–830.
193. Geesink RGT. Hydroxyapatite-coated total hip prostheses: 2 years clinical and roentgenographic results of 100 cases. *Clin Orthop* 1990;261:39.
194. Bauer TW, Taylor SK, Jaing M, Medendorp SV. An indirect comparison of third-body wear in retrieved hydroxyapatite-coated, porous, and cemented femoral components. *Clin Orthop* 1994;298:11–18.
195. Hannink RHJ, Kelly PM, Muddle BC. Transformation toughening in zirconia-containing ceramics. (Review). *J Amer Cer Soc* 2000;83:461–487.
196. Chang E, Chang WJ, Wang BC, Yang CY. Plasma spraying of zirconia-reinforced hydroxyapatite composite coatings on titanium: Part I. Phase, microstructure and bonding strength. *J Mater Mater Med* 1997;8:193–200.
197. Chang E, Chang WJ, Wang BC, Yang CY. Plasma spraying of zirconia-reinforced hydroxyapatite composite coatings on titanium: Part II. Dissolution behavior in simulated body fluid and bonding degradation. *J Mater Mater Med* 1997;8:201–211.
198. Bonfield W, Grynblas MD, Tully AE, Bowman J, Abram J. Hydroxyapatite reinforced polyethylene – a mechanically compatible implant material for bone replacement. *Biomaterials* 1981;2:185–186.
199. Brogan JA, Gross KA, Chen Z, Berndt CC, Herman H. Investigation of combustion sprayed hydroxyapatite/polymer composite coatings. In: *Proceedings of 7th National Thermal Spray Conference*, Boston, MA; June 20–24, 1994. p 159–164.

#### Permission to publish

Limin Sun, C.C. Berndt, K.A. Gross and A. Kucuk, 'Material fundamentals and clinical performance of plasma-sprayed hydroxyapatite coatings: A review', J. Biomedical Materials Research, 58 [5] (2001) 570-592.

Wiley Publishes Open Access Articles in fully Open Access Journals and in Subscription journals offering Online Open. Although most of the fully Open Access journals publish open access articles under the terms of the Creative Commons Attribution (CC BY) License only, the subscription journals and a few of the Open Access Journals offer a choice of Creative Commons Licenses:: Creative Commons Attribution (CC-BY) license [Creative Commons Attribution Non-Commercial \(CC-BY-NC\) license](#) and [Creative Commons Attribution Non-Commercial-NoDerivs \(CC-BY-NC-ND\) License](#). The license type is clearly identified on the article.

Copyright in any research article in a journal published as Open Access under a Creative Commons License is retained by the author(s). Authors grant Wiley a license to publish the article and identify itself as the original publisher. Authors also grant any third party the right to use the article freely as long as its integrity is maintained and its original authors, citation details and publisher are identified. These details are indicated above. The copyright owner is specified within the particular Journal. Search: <http://onlinelibrary.wiley.com/browse/publications?type=journal> to find the final article.



## Impact of Nanoscale Roughness of Titanium Thin Film Surfaces on Bacterial Retention

Elena P. Ivanova,<sup>\*,†</sup> Vi Khanh Truong,<sup>†</sup> James Y. Wang,<sup>‡</sup> Christopher C. Berndt,<sup>‡,§</sup>  
Robert T. Jones,<sup>||</sup> Iman I. Yusuf,<sup>⊥</sup> Ian Peake,<sup>⊥</sup> Heinrich W. Schmidt,<sup>⊥</sup> Christopher Fluke,<sup>#</sup>  
David Barnes,<sup>#</sup> and Russell J. Crawford<sup>†</sup>

<sup>†</sup>Faculty Life and Social Sciences and <sup>‡</sup>Faculty of Engineering and Industrial Sciences, IRIS, Swinburne University of Technology, P.O. Box 218, Hawthorn, Victoria, 3122, Australia, <sup>§</sup>State University of New York at Stony Brook, Stony Brook, New York 11794, <sup>||</sup>Centre for Materials and Surface Science, Department of Physics, La Trobe University, Victoria 3086, Australia, <sup>⊥</sup>School of Computer Science and Information Technology, RMIT University, GPO Box 2476 V, Melbourne, Victoria 3001, Australia, and <sup>#</sup>Centre for Astrophysics and Supercomputing, Swinburne University of Technology, P.O. Box 218, Hawthorn, Victoria, 3122 Australia

Received July 17, 2009. Revised Manuscript Received August 31, 2009

Two human pathogenic bacteria, *Staphylococcus aureus* CIP 68.5 and *Pseudomonas aeruginosa* ATCC 9025, were adsorbed onto surfaces containing Ti thin films of varying thickness to determine the extent to which nanoscale surface roughness influences the extent of bacterial attachment. A magnetron sputter thin film system was used to deposit titanium films with thicknesses of 3, 12, and 150 nm on glass substrata with corresponding surface roughness parameters of  $R_q$  1.6, 1.2, and 0.7 nm (on a  $4\ \mu\text{m} \times 4\ \mu\text{m}$  scanning area). The chemical composition, wettability, and surface architecture of titanium thin films were characterized using X-ray photoelectron spectroscopy, contact angle measurements, atomic force microscopy, three-dimensional interactive visualization, and statistical approximation of the topographic profiles. Investigation of the dynamic evolution of the Ti thin film topographic parameters indicated that three commonly used parameters,  $R_a$ ,  $R_q$ , and  $R_{\text{max}}$ , were insufficient to effectively characterize the nanoscale rough/smooth surfaces. Two additional parameters,  $R_{\text{skw}}$  and  $R_{\text{kur}}$ , which describe the statistical distributions of roughness character, were found to be useful for evaluating the surface architecture. Analysis of bacterial retention profiles indicated that bacteria responded differently to the surfaces on a scale of less than 1 nm change in the  $R_a$  and  $R_q$  Ti thin film surface roughness parameters by (i) an increased number of retained cells by a factor of 2–3, and (ii) an elevated level of secretion of extracellular polymeric substances.

### Introduction

Titanium, in different forms, is commonly used in indwelling devices including orthopedic and dental prostheses and cardiac valves, maxillofacial surgery and vascular stents, because of its high biocompatibility, low toxicity and high corrosion resistance.<sup>1,2</sup> The use of these implants is diversifying and increasing, as is research into the use of titanium that has been subjected to surface modification to increase biocompatibility.<sup>3</sup>

It is well-documented that biofilm formation by human pathogenic bacteria on medical implants can be dramatic, leading to failure of the device, often resulting in the necessity to surgically remove the implant. This can be associated with systemic infection, loss of organ or limb function, amputation, or death.<sup>3–5</sup> It has been determined that some bacteria residing in biofilms have a reduced susceptibility to antimicrobial agents compared to planktonic bacteria of the same species, measured by comparing the minimum biofilm eradication concentration (MBEC) with the

minimum inhibitory concentration (MIC).<sup>6,7</sup> Biofilm removal from indwelling devices is an issue of concern. An estimate by the Centre for Disease Control and Prevention (CDCP) indicated that 65% of human bacterial infections involve biofilm formation.<sup>8</sup> For example, Troodle et al., showed biofilm formation by *Staphylococcus aureus*, *Escherichia coli*, and *Pseudomonas aeruginosa* on all samples collected from catheters removed from patients.<sup>9</sup> *S. aureus* strains in particular are reported to be significant contributors to infections associated with orthopedic implants.<sup>8</sup> Therefore, understanding the retention of human pathogens on host tissues and inanimate surfaces is an important step in efforts to reduce infection.

There has been a number of conflicting research results published concerning the influence of substratum surface roughness on bacterial attachment, and whether the roughness has a positive, negative, or neutral impact on bacterial adhesion. In addition, there has been little work reported that directly links the surface architecture of the substrate to the extent of bacterial attachment.<sup>7,10,11</sup> The aim of this study was to investigate whether

\*Corresponding author. Address: Swinburne University of Technology, P.O. Box 218, Hawthorn, Victoria 3122, Australia. ■■■■■

(1) Whitehead, K. A.; Verran, J. *Int. Biodeterior. Biodegrad.* **2007**, *60*, 74–80.  
(2) Jeyachandran, Y. L.; Karunakaran, B.; Narayandass, S. K.; Mangalaraj, D.; Jenkins, T. E.; Martin, P. J. *Mater. Sci. Eng., A* **2006**, *431*, 277–284.  
(3) Hudson, M. C.; Ramp, W. K.; Frankenburg, K. P. *FEMS Microbiol. Lett.* **1999**, *173*, 279–284.  
(4) Ong, Y. L.; Razatos, A.; Georgiou, G.; Sharma, M. M. *Langmuir* **1999**, *15*, 2719–2725.  
(5) Diaz, C.; Cortizo, M. C.; Schilardi, P. L.; de Saravia, S. G. G.; de Mele, M. A. *F. L. Mater. Res.* **2007**, *10*, 11–14.

(6) Donlan, R. M. *Clin. Infect. Dis.* **2001**, *33*, 1387–1392.  
(7) An, Y. H.; Friedman, R. J.; Draughn, R. A.; Smith, E. A.; Nicholson, J. H.; John, J. F. *J. Microbiol. Methods* **1995**, *24*, 29–40.  
(8) Tortora, G. J.; Funke, B. R.; Case, C. L. *Microbiology: An Introduction*, 8th ed.; Pearson Education, Inc., Benjamin Cummings: San Francisco, CA, 2004.  
(9) Troodle, L.; Finkelstein, F. *Ann. Clin. Microbiol. Antimicrob.* **2006**, *5*, 1–7.  
(10) Whitehead, K. A.; Colligon, J.; Verran, J. *Colloids Surf., B: Biointerfaces* **2005**, *41*, 129–138.  
(11) Mitik-Dineva, N.; Wang, J.; Truong, V. K.; Stoddart, P.; Malherbe, F.; Crawford, R. J.; Ivanova, E. P. *Curr. Microbiol.* **2008**, *58*, 268–273.

nanoscale roughness of titanium thin film surfaces affects the nonspecific attachment and subsequent retention of two bacterial species, *P. aeruginosa* and *S. aureus*.

## Experimental Section

**Titanium Thin Film Preparation.** The titanium thin films of 3, 12, or 150 nm thickness (henceforth referred to as 3, 12, or 150 nm films) were prepared onto precleaned plain microscope slide substrates (Biolab Scientific, Ltd.) using a Kurt J Lesker CMS-18 magnetron sputtering thin film deposition system in direct current mode at an argon gas pressure of 4 mTorr and a power of 150 kW. The base pressure of the system is below  $5 \times 10^{-8}$  Torr. Glass slides were cleaned using 0.25% potassium hydroxide (KOH), flushed with distilled water, soaked in 5 M HNO<sub>3</sub> for 10 min, flushed with distilled water, soaked in 5 M KOH for 10 min, flushed with water, and finally blow-dried using 99.99% purity nitrogen gas. Commercial-grade 99.99% pure titanium (ASTM grade-2 titanium) was used to deposit titanium thin films of 3, 12, and 150 nm thickness. The deposition conditions used were as described elsewhere,<sup>12</sup> and the thickness of the film was controlled by the period of sputtering, calculated from the calibrated deposition rate.<sup>12</sup>

**Contact Angle Measurements.** The contact angles of different solvents on titanium disks were measured using the sessile drop method.<sup>13–15</sup> Three solvents, Milli-Q water, formamide (Sigma), and diiodomethane (Sigma) were used. An FTA1000 (First Ten Angstroms, Inc.) instrument was used to measure the contact angles at room temperature (ca. 23 °C) in air. An average of at least five measurements was taken for each solvent and titanium surface. Each measurement of a particular contact angle was recorded in 50 images in 2 s with a Pelco model PCHM 575-4 camera, and the contact angle was determined as a result of images analyzed using the FTA Windows Mode 4 software. The average contact angle for each of the three solvents on each surface was used to calculate the surface free energy and its components, based on the Lewis acid/base method.<sup>13–15</sup>

Statistical data processing was performed using the SPSS 16.0 program (SPSS, Inc., Chicago, IL). Single independent group *t*-tests were performed to evaluate the consistency of surface roughness parameters.

**Titanium Thin Film Surface Characterization.** A scanning probe microscope (SPM) (Solver P7LS, NT-MDT) was used to obtain images of the surface morphology and to quantitatively measure and analyze the surface roughness of metallic surfaces on the nanometer scale. The analysis was performed in the semicontact mode, which reduces the interaction between the tip and sample, thus avoiding the destructive action of lateral forces present in the contact mode. Carbon “whisker” type silicon cantilevers (NSC05, NT-MDT) with a spring constant of 11 N/m, tip radius of curvature of 10 nm, aspect ratio of 10:1, and resonance frequency of 150 kHz were used to obtain topographic resolution. Scanning was performed perpendicular to the axis of the cantilever at a rate of typically 1 Hz. Image processing of the raw topographical data was performed with first-order horizontal and vertical leveling, and the topography and surface profile of the samples were obtained simultaneously (as shown in Figures 1 and 2). In this way, the surface features of the samples were measured with a resolution of a fraction of a nanometer, and the surface roughness of the investigated areas could be statistically analyzed using standard instrument software (LS7-SPM v.8.58).

For extended nanosurface characterization beyond algorithms built in to the atomic force microscopy (AFM) package, the image analysis software package *Nano-SPAce Topography* (NSPAT)

was developed. Around this package the following experiment workflow was carried out: (i) acquisition of nanosurface AFM data together with metadata characterizing sputter density, film thickness, nanoscale grid resolution, and other parameters required either for the analysis itself or for the visualization and interpretation of results; (ii) export of the raw data acquired in the AFM experiments; (iii) reformatting and storage of the raw data with the metadata in a distributed file system; (iv) data analysis using the NSPAT package and native XGrid functionality on a parallel server cluster; and (v) visualization of the results.

NSPAT has been implemented to run on a parallel Apple Mac OS 10.5 server cluster dedicated to biomedical image processing and visualization. Six high-end eight-core servers are available directly, and several hundred Macs in student laboratories can be accessed seamlessly in addition through the native Apple Xgrid protocol. The cluster is also connected through Globus<sup>16</sup> to the broader worldwide grid computing infrastructure to serve other advanced medical image analysis. While the parallelization was not critical for the few data sets analyzed in this paper, it is significant in our project for processing and visualizing very large amounts of raw data meaningfully and, more importantly, refining our algorithms iteratively and repeatedly running them on an ever growing collection of data sets within a very short period of time.

The main functions of NSPAT are these:

**Mean Plane.** For all topographic parameters, the profile is calculated relative to the *mean plane*. The mean plane is defined as the statistical mean of the data grid.

**Maximum Height and Depth.** *Maximum height* and *depth* (relative to the mean plane) are parameters used in several other functions. In addition, some of the functions work relative to a *band* defined around the mean plane.

**Skewness  $R_{skw}$ .** Skewness is a measure of the symmetry of the height probability density function and can distinguish between wide valleys with narrow sharp peaks versus high plateaus with sharp deep valleys. For example, a Gaussian surface, having a symmetrical shape for the height distribution has a skewness of zero; a plateau honed surface with predominant plateau and sharp deep valleys would tend to have a negative skew, whereas a surface composed of a disproportionate number of sharp steep peaks will have positive skew.<sup>17</sup>

**Kurtosis  $R_{kur}$ .** Kurtosis represents a key feature in the probability density function of the height profile, the “peakedness” of the profile. A Gaussian surface has a kurtosis value of 3; a surface that is centrally distributed has a kurtosis value greater than 3; a surface that has a well spread out distribution has a kurtosis value of less than 3.<sup>17</sup>

**Peak Count  $R_p$  and Valley Count  $R_v$ .** The *peak and valley count* is the number of discernible peaks (or valleys, respectively) relative to a narrow band around the base plane. Data above the band counts toward definite peaks (high), data below counts as definite valleys (low), and data within the band counts as uncertain. The band chosen depends on the properties of the experiment such film thickness. This means valleys and peaks entirely contained within the band are ignored in the peak count as height variations that are “too small to count”. A scanning trajectory of points entirely contained in the band and connecting a low point (definite valley) to a high point (definite peak) indicates an *ascent* to a peak; one that connects from a high to a low point is a *descent* from a peak. While the rough peak count may be sufficient for characterizing some aspects of the topography, it ignores, for example, spiral connectivity, where a single peak and a single valley may curl around each other and where unidirectional scans in any two orthogonal directions will recognize this topography as multiple peaks. An *exact 3D peak count* is

(12) Wang, J. Y.; Ghantasala, M. K.; McLean, R. J. *Thin Solid Films* **2008**, 517, 656–660.

(13) Van Oss, C. J.; Good, R. J.; Chaudhury, M. K. *J. Colloid Interface Sci.* **1985**, 111, 378–390.

(14) Van Oss, C. J.; Good, R. J.; Chaudhury, M. K. *Langmuir* **1988**, 4, 884–891.

(15) Öner, D.; McCarthy, T. J. *Langmuir* **2000**, 16, 7777–7782.

(16) Foster, I.; Kesselman, C., *The GRID: Blueprint for a New Computing Infrastructure*; Morgan Kaufmann: San Francisco, CA, 1999.

(17) Gadellmawla, E. S.; Koura, M. M.; Maksoud, T. M. A.; Elewa, I. M.; Soliman, H. H. *J. Mater. Process. Technol.* **2002**, 123, 133–145.



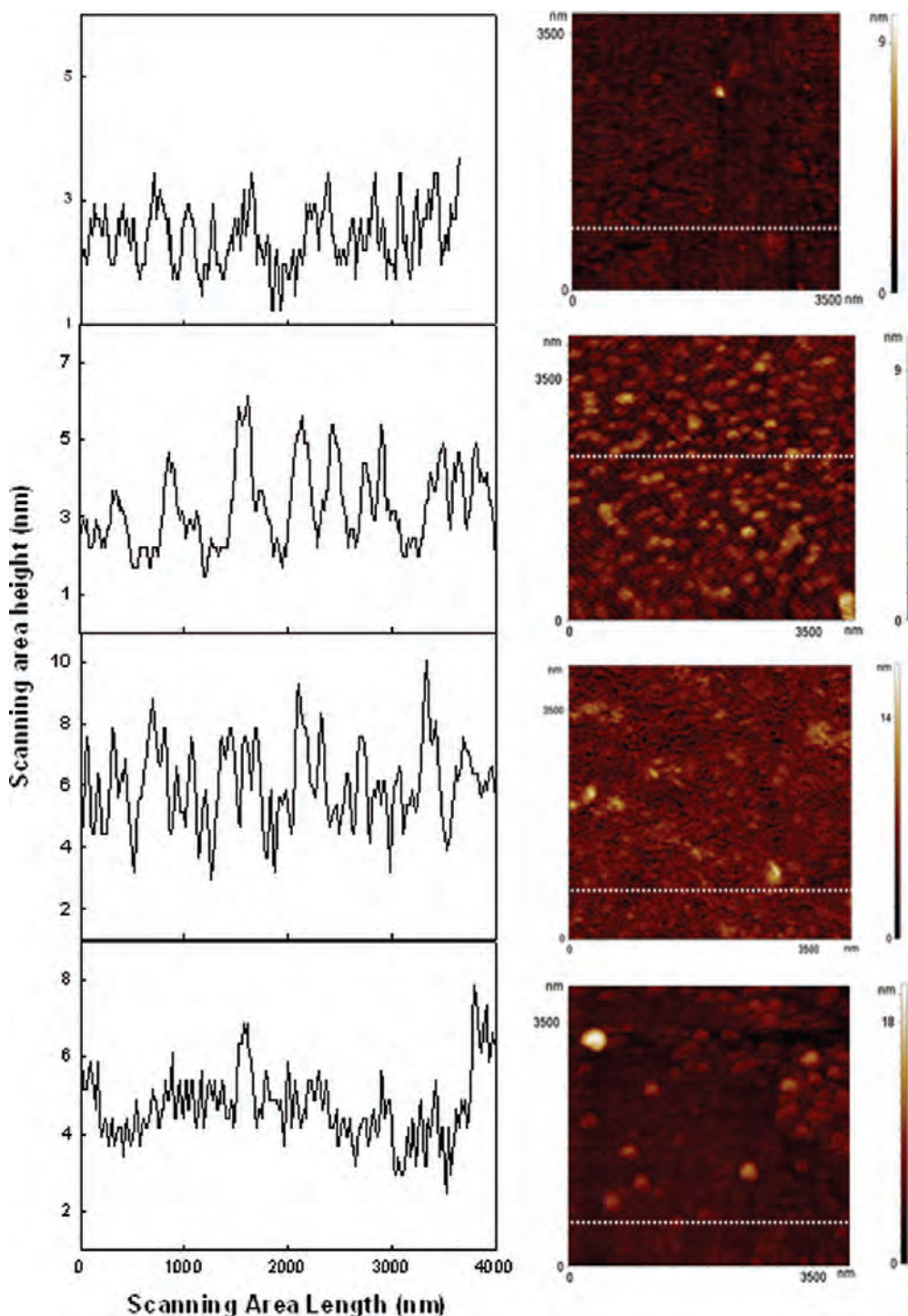


**Figure 1.** Typical two-dimensional (2D) AFM images and surface profiles of glass substrata and titanium thin film surfaces from approximately  $4\ \mu\text{m} \times 4\ \mu\text{m}$  scanned areas.

implemented using a parallel variant of the well-known and efficient maze flooding algorithm, treating inside-band data as maze wall points, distinguishing parallel flooding peaks above and valleys below by different colors (positive and negative numbers), and counting the corresponding number of colors needed.

**X-ray Photoelectron Spectroscopy (XPS) Analysis.** The surface compositions of the titanium-coated glass slides were determined from X-ray photoelectron spectra using a Kratos Axis Ultra DLD spectrometer (Kratos Analytical Ltd., U.K.). The energy scale of the instrument was calibrated by measuring the Au  $4f_{7/2}$  ( $E_b = 84.0\ \text{eV}$ ), Ag  $3d_{5/2}$  ( $E_b = 368.3\ \text{eV}$ ), and Cu  $2p_{3/2}$  ( $E_b = 932.7\ \text{eV}$ ) binding energies for pure metal foils.

Spectra were recorded while irradiating the samples with a monochromated Al  $K\alpha$  source ( $h\nu = 1486.6\ \text{eV}$ ) operating at 150 W. The analysis area was approximately  $300 \times 700\ \mu\text{m}^2$ .

Elements present on the surface of each sample were identified from survey spectra recorded over the energy range 0–1400 eV at intervals of 1 eV and a pass energy of 160 eV. High-resolution spectra were recorded for selected photoelectron peaks (C 1s, O 1s, N 1s, Ti 2p, and Si 2p) at intervals of 0.1 eV and a pass energy of 20 eV.

**Bacterial Strains.** The bacteria used in this study were *S. aureus* CIP 68.5 and *P. aeruginosa* ATCC 9025. Bacterial strains were obtained from American Type Culture Collection

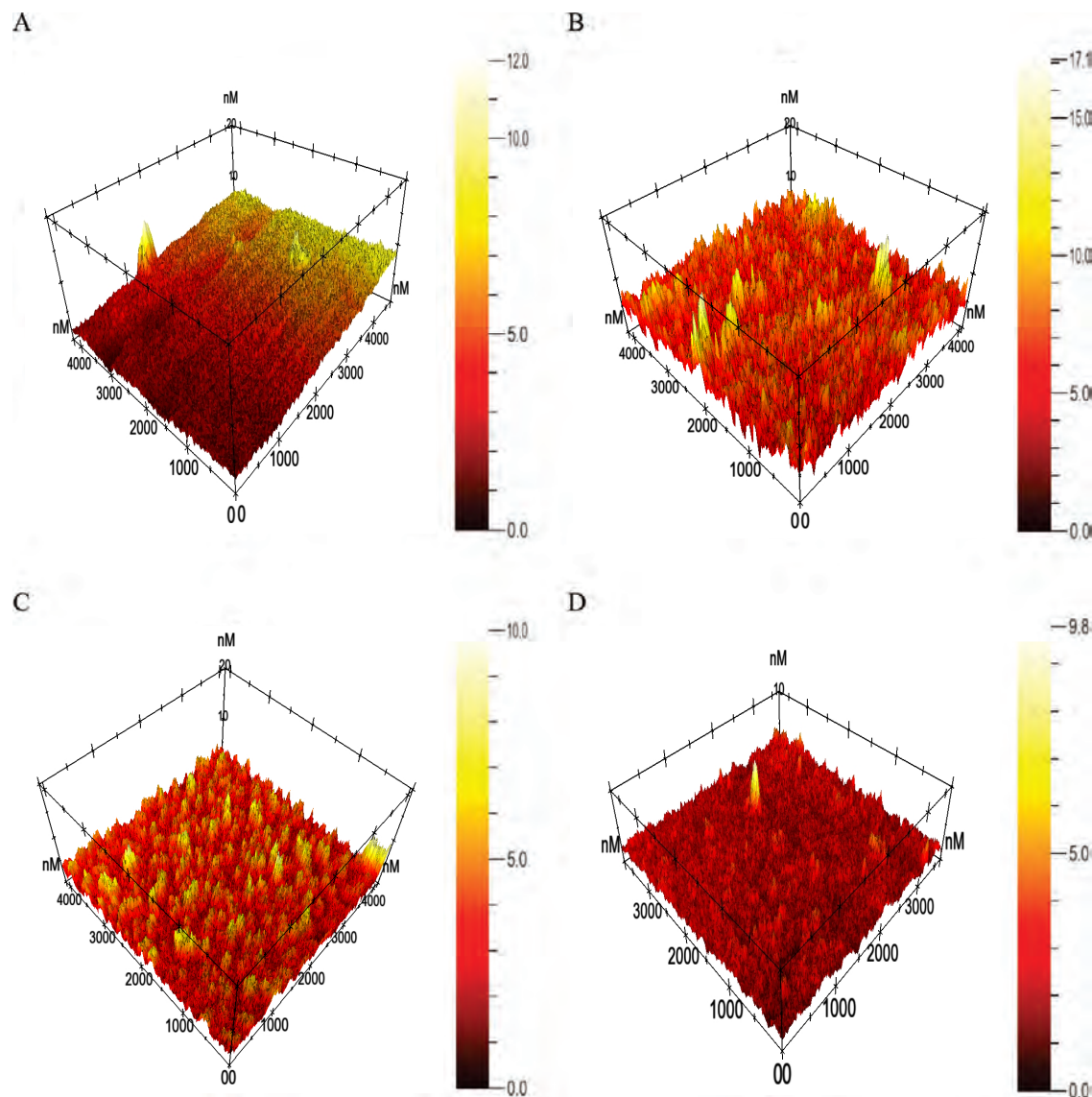


**Figure 2.** Three-dimensional (3D) projections of typical AFM images and surface profiles of glass substrata and titanium thin film surfaces from approximately  $4\ \mu\text{m} \times 4\ \mu\text{m}$  (bottom) scanned areas. Readers using version 8.0 or higher of Acrobat Reader can enable interactive, 3D views of the data by clicking on the figure panels. Once enabled, 3D mode allows the reader to rotate and zoom the view using the mouse.

(ATCC, USA) and Culture Collection of the Institute Pasteur (CIP, France). Bacterial strain stocks were prepared in 20% glycerol nutrient broth (Merck) and stored at  $-80\ ^\circ\text{C}$ . Both strains were cultured on nutrient agar (Oxoid) and nutrient broth (Oxoid) at room temperature (ca.  $22\ ^\circ\text{C}$ ).

**Cellular Surface Charge Measurements.** Bacterial cell surface hydrophobicity was evaluated from contact angle measurements on lawns of bacteria using the sessile drop method as described elsewhere.<sup>18</sup> In brief, bacterial cells in a buffer ( $\text{OD}_{600} = 0.3$ ) were deposited on cellulose acetate membrane filters (Sartorius,  $0.2\ \mu\text{m}$ ). The wet filters were air-dried at ambient temperature (ca.  $22\ ^\circ\text{C}$ ) for approximately 30–40 min to attain a “plateau state”.

Zeta potential measurements of both strains were obtained by measuring the electrophoretic mobility (EPM) using a standard protocol described elsewhere.<sup>19</sup> The EPM was measured as a function of ionic strength by microelectrophoresis using a zeta potential analyzer (ZetaPALS, Brookhaven Instruments Corp, Holtsville, NY). The bacterial cell suspension was freshly

prepared before the measurement. All measurements were executed in triplicate, and for each sample the final EPM quoted represented the average of five successive ZetaPALS readings, each of which consisted of 14 cycles per run. All data were processed using software that employed the Smoluchowski equation.<sup>19,20</sup>

**Bacterial Growth and Sample Preparation.** Prior to each experiment, a fresh bacterial suspension was prepared for each of the strains grown overnight in 100 mL of nutrient broth (Oxoid) (in 0.5 L Erlenmeyer flasks) at  $37\ ^\circ\text{C}$  with shaking (120 rpm). Bacterial cells were collected at the logarithmic stage of growth as confirmed by growth curves (data not shown). As cell densities may vary, the cell density of each strain was adjusted to  $\text{OD}_{600} = 0.3$  to obtain samples that possessed a similar number of cells in each sample. A hemocytometer was used to quantify cell numbers in the adjusted bacterial suspensions before attachment experiments according to the method described by Mather and Roberts.<sup>21</sup> An aliquot of 5 mL of bacterial suspension was added

(18) Mitik-Dineva, N.; Wang, J.; Mocanu, R. C.; Stoddart, P. R.; Crawford, R. J.; Ivanova, E. P. *Biotech J* **2008**, *3*, 536–544.

(19) de Kerchove, A. J.; Elimelech, M. *Langmuir* **2005**, *21*, 6462–6472.

(20) Eboigbodin, K. E.; Newton, J. R. A.; Routh, A. F.; Biggs, C. A. *Langmuir* **2005**, *21*, 12315–12319.

(21) Mather, J.; Roberts, P. *Introduction to Cell and Tissue Culture: Theory and Technique*; Plenum Press: New York, 1998.



in a sterile Petri dish with samples of glass slides that had been coated with titanium thin films. These were incubated for 18 h at room temperature (ca. 22 °C). Sterile nutrient broth (5 mL) was used as a negative control. Samples were handled under sterile conditions until just prior to imaging. After incubation, glass slides with titanium thin films were gently washed with copious amounts of sterilized nanopure H<sub>2</sub>O (18.2 M  $\Omega$  cm<sup>-1</sup>) to remove nonattached cells and left to dry at room temperature for 45 min at 55% humidity. This procedure allowed the bacterial cells to maintain at least a semihydrated state, as confirmed by their morphological appearance, and allowed all imaging experiments to be performed under identical conditions.

**Visualization and Quantification of Viable Cells and Extracellular Polymeric Substances (EPSs).** Two dyes were used simultaneously; the first to monitor the level of production of extracellular substances, and the second to enable the visualization of viable bacterial cells retained on the surfaces. An aliquot of Concanavalin Alexa Fluor 488 (Molecular Probes Inc.) dye was added to the suspension, and incubated for 30 min to allow the dye to diffuse thoroughly throughout the sample. This dye selectively binds to  $\alpha$ -mannopyranosyl and  $\alpha$ -glucopyranosyl residues in EPSs.<sup>22</sup> The dye stock solution was prepared by dissolving 5 mg in 5 mL of 0.1 M sodium bicarbonate at pH 8.3 and stored at 20 °C. A ratio of 20  $\mu$ L dye to 100  $\mu$ L suspension was used to stain any EPS produced. After the initial 30 min incubation period, a Vybrant CFDA SE Cell Tracer Kit (Molecular Probe, Inc.) was used to stain viable cells. Working solutions were prepared by diluting 1  $\mu$ L of a 10 mM stock solution to 1000  $\mu$ L in 10 mM phosphate-buffered saline (PBS) solution (pH 7), followed by warming to 37 °C. A volume of 20  $\mu$ L working solution was then added to 100  $\mu$ L of suspension and incubated at 37 °C for 15 min. This dye concentration was found to be sufficient to visualize labeled cells. After incubation, the samples were resuspended in fresh medium at 37 °C for 30 min. The samples were then washed with sterilized nanopure H<sub>2</sub>O (18.2 M  $\Omega$  cm<sup>-1</sup>), left to dry for a few hours at room temperature (ca. 22 °C, humidity 55%) without additional fixation to prevent the deformation of the cells and analyzed using confocal scanning laser microscopy (CSLM). The CSLM used was an Olympus FluoView FV1000 Spectroscopic Confocal System, which includes an inverted Microscope System OLYMPUS IX81 (20 $\times$ , 40 $\times$  (oil), 100 $\times$  (oil) UIS objectives) and operates using multi Ar and HeNe lasers (458, 488, 515, 543, and 633 nm). The system is equipped with a transmitted light differential interference contrast attachment and a charge-coupled device (CCD) camera (Cool View FDI).

Digital image analysis of the CSLM optical images was performed to quantify the volume of presumed EPS and viable cells. FV10-ASW 1.6 software was used to measure and analyze the intensity integration (counts per second, cps) of a fluorescent dye to determine the amount of each substance present.<sup>23,24</sup> The total intensity of a biofilm was considered to be the total intensity of the EPS and viable cells. All samples were scanned at four locations of 126.72  $\mu$ m  $\times$  126.72  $\mu$ m area each.

**Scanning Electron Microscopy (SEM).** In all SEM experiments, titanium discs with adsorbed bacteria were initially sputter-coated with 20 nm gold thin films using a Dynavac CS300 according to a procedure developed previously.<sup>25,26</sup> High-resolution images of titanium thin films with the retained bacterial cells were taken using a field-emission SEM (FESEM; ZEISS SUPRA 40 VP) at 3 kV at 1000 $\times$ , 5000 $\times$  and 20000 $\times$  magnification.

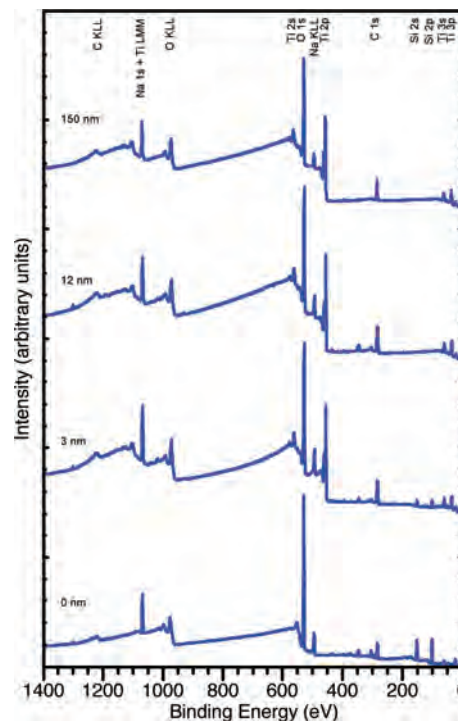


**Figure 3.** XPS wide spectra of titanium thin film surfaces of 150, 12, and 3 nm and glass substratum, 0 nm.

Images at 1000 $\times$  and 5000 $\times$  magnification were used to calculate the number of bacteria adhering to the titanium surfaces. The results were statistically analyzed.

**Reconstruction of Interactive 3D Images.** Interactive 3D visualization of the titanium surfaces was undertaken with a custom C-code and the S2PLOT graphics library.<sup>27,28</sup> The input data files were in NT-MDT format and were read into the viewing tool (mdtview) using a modification of the nt-mdt module of Gwyddion by David Necas and Petr Klapetek (<http://gwyddion.net/>, version 2.12). NT-MDT files were converted into a 3D surface, colored according to height, and displayed with the S2PLOT s2surpa function. Visualizations were exported from mdtview to an intermediate VRML format, with textures for axis labels in TGA format. Textures were converted to PNG format, and the VRML model was imported into Adobe Acrobat 3D version 8 to create an interactive figure, using the approach described by Barnes & Fluke.<sup>27</sup> JavaScript commands were used to provide additional functionality. If viewing this paper in electronic format, the interactive Figure 2 can be viewed by mouse clicking on the four panels, provided Adobe Reader Version 8.0 or higher is being used. This opens a window where the surface can be examined interactively using the mouse to control the camera orientation and zoom level.

## Results

**Titanium Surface Characterization.** The XPS and AFM analyses and contact angle measurements were performed for Ti thin film surfaces to evaluate elemental composition, surface topography, and the surface wettability of the Ti thin films. The XPS elemental analysis was carried out for both Ti thin films and glass substrata to assess the surface elemental composition, chemical functionality, and Ti coverage. The XPS elemental analysis showed that titanium and oxygen were the most abundant elements, hence indicating that Ti was present as TiO<sub>2</sub>

(22) Goldstein, I. J.; Hollerman, C. E.; Smith, E. E. *Biochemistry* **1964**, *4*, 876–883.

(23) Feller, B. E.; Kellis, J. T., Jr.; Cascão-Pereira, L. G.; Knoll, W.; Robertson, C. R.; Frank, C. W. *Langmuir* **2008**, *24*, 12303–12311.

(24) Neu, T. R.; Lawrence, J. R. *FEMS Microbiol. Ecol.* **1997**, *24*, 11–25.

(25) Mitik-Dineva, N.; Wang, J.; Truong, V. K.; Stoddart, P.; Malherbe, F.; Crawford, R. J.; Ivanova, E. P. *Curr. Microbiol.* **2009**, *58*, 268–273.

(26) Truong, V. K.; Rundell, S.; Lapovok, R.; Estrin, Y.; Wang, J. Y.; Berndt, C. C.; Barnes, D. G.; Fluke, C. J.; Crawford, R. J.; Ivanova, E. P. *Appl. Microbiol. Biotechnol.* **2009**, *83*, 925–937.

(27) Barnes, D.; Fluke, C. *New Astron.* **2008**, *13*, 599–605.

(28) Barnes, D.; Fluke, C.; Bourke, P.; Parry, O. *Publ. Astron. Soc. Aust.* **2006**, *23*, 82–93.

**Table 1. Atomic Fractions<sup>a</sup> of Elements<sup>b</sup> Detected on the Surface of Each Sample by XPS**

Ti film thickness [nm]	Mg	Zn	Na	O	Ti	Ca	N	K	C	Si	Al
0	0.3	<dl <sup>c</sup>	5.9	55.5	<dl	1.3	0.5	0.7	17.8	17.0	0.8
3	0.3	0.1	<dl	53.9	13.6	<dl	0.5	<dl	26.9	4.0	<dl
12	0.5	<dl	<dl	51.3	14.1	1.2	0.7	<dl	32.0	<dl	<dl
150	<dl	<dl	<dl	51.2	19.3	<dl	0.8	<dl	28.7	<dl	<dl

<sup>a</sup> It is conventional to list surface compositions obtained from XPS analyses as atomic fractions (or concentrations), rather than as mass fractions.

<sup>b</sup> The uncertainty in the elemental atomic fractions in each value is at best 5%, so only the first decimal place is retained. <sup>c</sup> <dl, less than the detection limit (ca. 0.1 at. %)

**Table 2. Titanium Thin Film Surfaces Contact Angle and Surface Free Energy Values**

Ti film thickness [nm]	contact angle $\theta$ (°) <sup>a</sup>			surface free energy [mN m <sup>-1</sup> ] <sup>b</sup>				
	$\theta_W$	$\theta_F$	$\theta_{Di}$	interfacial tension (IFT) $\gamma^{TOT}$	dispersive $\gamma^{LW}$	polar $\gamma^{AB}$	acid $\gamma^+$	base $\gamma^-$
0	4.7 ± 0.6	21.5 ± 1.5	43.4 ± 1.6	52.2 ± 6.7	37.90	14.40	0.90	60.50
3	76.3 ± 0.9	46.1 ± 2.1	42.0 ± 0.7	43.5 ± 2.5	38.57	4.66	1.34	4.04
12	74.6 ± 1.3	48.0 ± 3.8	38.5 ± 1.4	44.3 ± 3.5	40.35	3.92	0.63	6.04
150	81.4 ± 0.8	51.9 ± 3.6	39.9 ± 1.4	42.3 ± 2.9	39.66	2.66	0.64	2.76

<sup>a</sup>  $\theta_W$ ,  $\theta_F$ , and  $\theta_{Di}$ : water, formamide, and diiodomethane contact angles, respectively. <sup>b</sup> Surface free energies components: Lifshitz–van der Waals ( $\gamma^{LW}$ ), acid/base ( $\gamma^{AB}$ ), electron acceptor ( $\gamma^+$ ), and electron donor ( $\gamma^-$ ) components.

(Supporting Information, Figure S1; Figure 3 and Table 1). Peak-fitting treatment of high resolution XPS spectra yielded dominant doublet peaks (BE peaks ~458.0 eV and ~463 eV) for titanium surfaces, attributable to TiO<sub>2</sub>. The Ti 2p<sub>3/2</sub> binding-energy ranges reported in the NIST database are 453.7–454.3 eV for elemental Ti, 454.6–455.9 eV for TiO, 456.8–457.8 eV for Ti<sub>2</sub>O<sub>3</sub>, 458.3–459.2 eV for TiO<sub>2</sub>, and 457.9–458.9 eV for the titanate ion (Ti<sub>2</sub>O<sub>3</sub>).

The low atomic fraction of Ti on the 3 nm film surfaces is likely to be due to the heterogeneity of the Ti films as a consequence of the nanoroughness of the glass surface, to the extent that some regions are thin enough for some of the underlying substrate to fall within the depth of analysis. In these instances, the Ti filled the deep “valleys” in the surface, but only just covered some of the higher “peaks”. The depth of XPS analysis varies with the nature of the surface, but is nominally around 5 to 10 nm. Thus, for a perfectly flat interface between the glass and Ti, one would expect the Si/Ti ratio to progressively decrease until the depth of the Ti layer becomes greater than the depth of analysis, which is indeed shown in this case. It appeared that XPS results are consistent for two Ti layers of the 12 and 150 nm thicknesses.

The XPS survey spectrum demonstrated some carbon contamination on the titanium surface, which is typical for adventitious, unavoidable hydrocarbon contamination, adsorbing spontaneously from ambient air onto the surface.<sup>29–31</sup> Three peaks were fitted and assigned as follows: the main carbon peak at 285.0 eV was assigned to hydrocarbon species (C–H/C–C); the other two fitted peaks were attributed to C–O (i.e., alcohol and ether) species at 286.6 eV and C=O (i.e., carbonyl) species at 288.5 eV, respectively (Figure 3).

The contact angle and surface free energy components for each titanium film are shown in Table 2. The 150 nm films were found to be moderately hydrophobic (a contact angle of approximately 81°), while the 3 or 12 nm films were found to be less hydrophobic (contact angles of approximately 76–75°). The difference in contact angles is regarded as statistically significant ( $t = 0.03$ ,  $p < 0.05$ ). The glass substrates exhibited electron donor components due to the presence of hydroxyl groups (–OH) on the glass

surface.<sup>32</sup> The 3, 12, and 150 nm films exhibited electron donor components rather than electron acceptor components so that negative charges are formed on a titanium surface as a result of the presence of a TiO<sub>2</sub> layer.<sup>31</sup> The total surface free energy values of the 150 nm films were found to be slightly lower than those of the 3 or 12 nm films (Table 2). However, a statistical analysis showed that no statistically significant difference existed between the total surface free energies of these films ( $p > 0.05$ ).

**Titanium Surface Topography and Architecture.** A comparative AFM analysis of the titanium thin films indicated that the sputtered titanium exhibited a heterogeneous surface architecture and fine topographical alteration in the decrease of the surface roughness parameters at the nanoscale as the thickness of the Ti layer increased (Figures 1 and 2).

An analysis of the surface roughness parameters was performed for two different scan areas (10  $\mu\text{m} \times 10$  and 4  $\mu\text{m} \times 4$   $\mu\text{m}$ ) for each of the Ti film samples and the uncoated glass substrate, the results of which are presented in Table 3. It can be seen that, for both scan areas, the average roughness ( $R_a$ ) of the substrate increased slightly when coated with a 3 nm thick film; however, as the thickness of the film increased, the average roughness decreased to a point where the 150 nm thick film exhibited an average roughness that was approximately half that of the original (uncoated) substrate. The root-mean-square (rms) roughness ( $R_q$ ) was seen to decrease as the film thickness increased in the case of the 4  $\mu\text{m} \times 4$   $\mu\text{m}$  scanning area, whereas a similar decrease was observed as the film thickness was increased from 3 to 150 nm for the 10  $\mu\text{m} \times 10$   $\mu\text{m}$  scanning area data, following the slight increase that occurred as the 3 nm film was added to the uncoated substrate. A similar trend was also seen for the maximum peak height ( $R_{\text{max}}$ ), with the exception that an increase in maximum peak height was observed for the 4  $\mu\text{m} \times 4$   $\mu\text{m}$  scan area as the thickness of the film increased from 12 to 150 nm. A statistical analysis of the  $R_a$  and  $R_q$  data obtained for the 10  $\mu\text{m} \times 10$   $\mu\text{m}$  scan areas highlighted that there is a significant difference between the roughness of the 3, 12, and 150 nm films ( $p < 0.05$ ). However, no significant difference was seen for the 4  $\mu\text{m} \times 4$   $\mu\text{m}$  scan areas ( $t = 0.14$  and  $0.09$  for  $R_a$  and  $R_q$ , respectively;  $p > 0.05$ ).

A statistical analysis of the  $R_{\text{max}}$  data obtained for the 10  $\mu\text{m} \times 10$   $\mu\text{m}$  scan areas highlighted that there was no significant difference in the maximum height for the 12 and 150 nm films ( $t = 0.22$ ,  $p > 0.05$ ); however, a significant difference in  $R_{\text{max}}$  was confirmed for the 3 and 12 nm films in the 4  $\mu\text{m} \times 4$   $\mu\text{m}$  scan areas

(29) Cai, K.; Muller, M.; Bossert, J.; Rechtenbach, A.; Jandt, K. D. *Appl. Surf. Sci.* **2005**, *250*, 252–267.

(30) Bertóti, I.; Mohai, M.; Sullivan, J.; Saied, S. *Appl. Surf. Sci.* **1995**, *84*, 357–371.

(31) Liu, X.; Chu, P. K.; Ding, C. *Mater. Sci. Eng. R: Rep.* **2004**, *47*, 49–121.

(32) Gu, Y.; Li, D. *J. Colloid Interface Sci.* **2000**, *226*, 328–339.

Table 3. AFM Surface Roughness Analysis of Ti Thin Film Surfaces on Two Scanning Areas

	Ti film thickness (nm)	average roughness (nm) $R_a$	rms (nm) $R_q$	maximum height (nm) $R_{max}$	maximum profile peak height (nm) $R_p$	maximum profile valley depth (nm) $R_v$	maximum peak to valley height (nm) $R_t$	skewness $R_{skw}$	kurtosis $R_{kur}$
$10 \times 10$	0	$1.23 \pm 0.04$	$2.02 \pm 0.09$	$24.78 \pm 1.43$	$20.93 \pm 1.19$	$3.01 \pm 0.17$	$23.94 \pm 1.39$	$3.2 \pm 0.1$	$18.8 \pm 0.6$
	3	$1.47 \pm 0.21$	$2.25 \pm 0.05$	$37.90 \pm 1.97$	$26.75 \pm 1.39$	$10.69 \pm 0.55$	$37.44 \pm 1.91$	$1.2 \pm 0.2$	$9.2 \pm 1.3$
	12	$0.95 \pm 0.01$	$1.21 \pm 0.01$	$15.86 \pm 2.52$	$11.38 \pm 1.80$	$3.30 \pm 0.52$	$14.68 \pm 2.32$	$1.0 \pm 0.1$	$5.6 \pm 0.1$
$4 \times 4$	150	$0.64 \pm 0.02$	$0.87 \pm 0.04$	$13.28 \pm 1.981$	$9.21 \pm 1.37$	$2.67 \pm 0.40$	$11.88 \pm 1.78$	$2.3 \pm 0.1$	$36.7 \pm 1.1$
	0	$1.01 \pm 0.03$	$1.66 \pm 0.12$	$18.47 \pm 2.88$	$15.30 \pm 2.39$	$3.05 \pm 0.48$	$18.35 \pm 2.86$	$3.4 \pm 0.1$	$19.5 \pm 0.6$
	3	$1.22 \pm 0.27$	$1.61 \pm 0.34$	$17.37 \pm 3.84$	$11.14 \pm 2.46$	$5.99 \pm 1.32$	$17.13 \pm 3.79$	$0.6 \pm 0.1$	$5.4 \pm 1.2$
	12	$0.92 \pm 0.06$	$1.16 \pm 0.06$	$9.05 \pm 0.53$	$5.72 \pm 0.39$	$3.31 \pm 0.19$	$9.03 \pm 0.53$	$0.8 \pm 0.1$	$3.8 \pm 0.2$
	150	$0.58 \pm 0.08$	$0.73 \pm 0.14$	$12.35 \pm 1.87$	$9.66 \pm 1.46$	$2.57 \pm 0.40$	$12.23 \pm 1.91$	$1.5 \pm 0.2$	$16.1 \pm 2.2$

( $t = 0.02$ ,  $p < 0.05$ ). Further statistical analyses confirmed that, for the  $10 \mu\text{m} \times 10 \mu\text{m}$  scanning areas,  $R_q$  and  $R_{max}$  for the 3 nm films were different from those of the uncoated glass substrate ( $t = 0.01$  and  $0.00$  ( $p < 0.05$ ), respectively). However, for the smaller scan areas, e.g.,  $4 \mu\text{m} \times 4 \mu\text{m}$ , the difference in  $R_a$ ,  $R_q$ , and  $R_{max}$  for the 3 nm films and uncoated glass substrate was not found to be statistically significant ( $t = 0.23$ ,  $0.84$ , and  $0.63$ ;  $p > 0.05$ ), whereas the  $R_a$ ,  $R_q$ , and  $R_{max}$  values for the 12 and 150 nm films were found to be significantly different from those of the uncoated glass substrate for both scan areas ( $p < 0.05$ ).

Since three commonly used surface roughness parameters (the average roughness ( $R_a$ ), the rms roughness ( $R_q$ ), and the maximum roughness ( $R_{max}$ )) were found to be insufficient to comprehensively characterize the surfaces, we developed a software package written in Java to enable an extended surface roughness parameter analysis. This package acquires the AFM raw data and derives key topographic features from these data including the mean plane, maximum height and depth (relative to the mean plane), skewness  $R_{skw}$ , and kurtosis  $R_{ku}$  (Table 3).

To better understand the surface topography, the peak-to-valley height parameter,  $R_t$ , was also used to describe the distance between the highest peak and lowest valley on the surface. A statistical consideration of the  $R_t$  data revealed that only the 3 nm films exhibited a significant difference in  $R_t$  compared to that of the uncoated glass surface for both scan areas ( $t = 0.02$ ,  $p < 0.05$ ).

All of the surfaces studied exhibited a  $R_{skw}$  greater than 0 and  $R_{kur}$  greater than 3, i.e., the  $R_{skw}$  values indicate that these surfaces are composed of a disproportionate number of peaks; the  $R_{kur}$  values indicate that these surfaces exhibit a considerable number of sharp peaks and low valleys.<sup>17,33</sup> In each case, the uncoated glass substrate surfaces exhibited a higher  $R_{skw}$  and  $R_{kur}$  than that of the 3 nm films, i.e., most peaks were found to be more uniformly distributed over the uncoated glass substrate surface than on the 3 nm films. The  $R_{skw}$  and  $R_{kur}$  on the 3 nm films were higher than those of the 12 nm films for the  $10 \mu\text{m} \times 10 \mu\text{m}$  scan areas, and the  $R_{skw}$  and  $R_{kur}$  of the 3 nm films were lower than those of the 12 nm films for the  $4 \mu\text{m} \times 4 \mu\text{m}$  scan areas. No significant difference was found, however, between the  $R_{skw}$  and  $R_{kur}$  values for the 3 and 12 nm films ( $t = 0.22$ ,  $p > 0.05$ ), while the  $R_{skw}$  and  $R_{kur}$  of the 150 nm films were higher than those of the 3 and 12 nm films. Thus, these roughness parameters highlighted the fact that 150 nm films exhibited small steep peaks in a somewhat homogeneous manner. 3D visualization of the topographic profiles of titanium surfaces (Figure 2) offers further insight into the surface architecture.

**Bacterial Cell Surface Characteristics and Retention Patterns.** *P. aeruginosa* cells were found to be moderately

hydrophilic ( $\theta = 43^\circ$ ), and *S. aureus* cells exhibited more hydrophobic characteristics ( $\theta = 72^\circ$ ) (Table 4). The hydrophobic nature of *S. aureus* cells can be attributed to the presence of highly negatively charged and hydrophobic teichoic and lipoteichoic acid sites, which are some of the main constituents of *S. aureus* cell walls.<sup>34</sup> The zeta potentials of these cells were measured in order to characterize their electrokinetic surface properties.<sup>19,20,35,36</sup>

The observed cellular surface charge of *P. aeruginosa* and *S. aureus* are shown in Table 4. The values reported here agree with previously published data.<sup>37,38</sup> The least electronegative species was *P. aeruginosa* with an EPM of  $-1.12 \mu\text{s}^{-1} \text{V cm}^{-1}$ , followed by *S. aureus* with a mobility of  $-2.8 \mu\text{s}^{-1} \text{V cm}^{-1}$ .

The analysis of SEM (Supporting Information, Figure S2) and CSLM images (Figure 4) indicated that *P. aeruginosa* and *S. aureus* exhibited varying attachment responses when grown on the studied titanium surfaces. CSLM images of *P. aeruginosa* showed that retained cells typically gathered in areas of moderate cell density (Figure 4). Presumed EPS (green colored) is visible in several locations, predominantly in areas of high cell density. Both strains appeared to be relatively evenly distributed at the low cell density across the 3 nm films while attached in large clusters and were retained in greater number on the nano-smoother 12 and 150 nm films. The surfaces included in the 3D images in Figure 4 show typical retention profiles of the successfully attached viable *S. aureus* cells. It can be seen that the greatest quantities of EPS are present in areas where cells are within close proximity of one another. EPS quantification data confirmed visual observation of the confocal images (Figure 4). A statistical analysis showed that a statistically significant increase in the extent of biofilm formation occurred on the 150 nm films ( $p < 0.05$ ). It is noteworthy, however, that the amount of *P. aeruginosa* biofilm formed on the 12 nm films was not significantly different from that formed on the 150 nm film ( $p > 0.05$ ). As the smoothness of the film increased, so did the presence of both viable *P. aeruginosa* and *S. aureus* cells ( $p < 0.05$ ). *S. aureus*, however, appeared to be the more efficient colonizer of the 150 nm films.

## Discussion

The progression of the surface roughness parameters and change in surface morphology is best seen in the images presented in Figures 1 and 2, and in the data presented in Table 3. The degree of roughness associated with the glass substrate was

(34) Gross, M.; Cramton, S. E.; Gotz, F.; Peschel, A. *Infect. Immun.* **2001**, *69*, 3423–3426.

(35) Eboigbodin, K. E.; Newton, J. R. A.; Routh, A. F.; Biggs, C. A. *Appl. Microb. Cell Physiol.* **2006**, *73*, 669–675.

(36) Tsuneda, S.; Jung, J.; Hayashi, H.; Aikawa, H.; Hirata, A.; Sasaki, H. *Colloids Surf., B: Biointerfaces* **2003**, *29*, 181–188.

(37) van der Mei, H. C.; Busscher, H. J. *Appl. Environ. Microbiol.* **2001**, *67*, 491–494.

(38) Busscher, H. J.; Norde, W. J. *Biomed. Mater. Res.* **2000**, *50*, 463–464.

(33) Lamolle, S. F.; Monjo, M.; Rubert, M.; Haugen, H. J.; Lyngstadaas, S. P.; Ellingsen, J. E. *Biomaterials* **2009**, *30*, 736–742.



Table 4. Bacterial Cell Surface Characteristics and Numbers of Retained Cells on Titanium Surfaces

bacterial strain	water contact angle $\theta$ [°]	EPM [ $\mu\text{s}^{-1}$ V $\text{cm}^{-1}$ ]	zeta potential $\zeta$ [mV]	initial cell density $\times 10^6$ [number of cells per $\text{mm}^2$ ]	percentage of attached cells [%] retained cells <sup>a</sup> $\times 10^5$ [number of cells per $\text{mm}^2$ ]					
					Ti film thickness [nm]					
					3	12	150	3	12	150
<i>P. aeruginosa</i>	43.3 $\pm$ 8	−1.1 $\pm$ 0.1	−14.4 $\pm$ 0.7	13.0 $\pm$ 1.5	0.5 $\pm$ 0.2	0.7 $\pm$ 0.3	1.4 $\pm$ 0.3	0.8 $\pm$ 0.1	1.0 $\pm$ 0.2	1.8 $\pm$ 0.4
<i>S. aureus</i>	72.2 $\pm$ 8	−2.8 $\pm$ 0.8	−35.2 $\pm$ 1.0	20.8 $\pm$ 1.7	1.1 $\pm$ 0.2	2.9 $\pm$ 0.3	5.8 $\pm$ 0.2	2.3 $\pm$ 0.3	6.0 $\pm$ 1.1	12.0 $\pm$ 1.7

<sup>a</sup> Cell densities have estimated errors of approximately 15–20% due to local variability in the surface coverage.

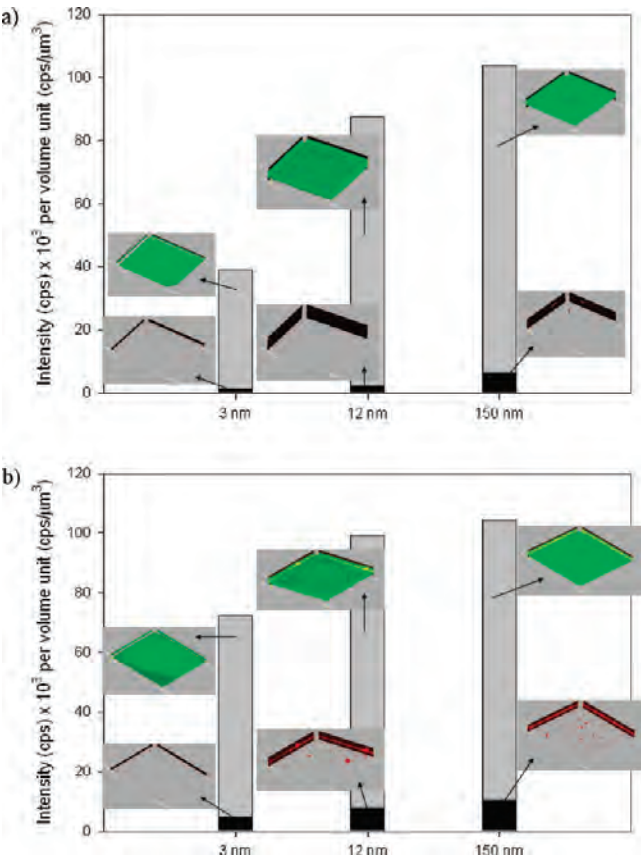


Figure 4. 3D visualization (projections of CSLM images) of representative *P. aeruginosa* (A) and *S. aureus* (B) specimens on the titanium thin film surfaces of 3, 12, and 150 nm thickness after 18 h incubation and corresponding quantification of the volume of the biofilm and viable cells (colored red) retained on the surfaces.

accentuated by the titanium sputtering: a 3 nm film of titanium produced high peaks (up to 18–20 nm) at low density and low valleys, giving the surface a striped appearance and larger  $R_q$  value than the glass substratum. This initial increase in surface roughness is likely to be the result of the shadow effect associated with the sputtering process.<sup>2,39</sup> The commonly used surface roughness parameters, e.g.,  $R_a$  and  $R_q$ , do not adequately characterize surface profiles where the surface smoothness reaches dimensions of approximately 1 nm and less; i.e., particularly for the 12 and 150 nm films. Two additional parameters, the skewness and kurtosis parameters ( $R_{skw}$  and  $R_{kur}$ ) appeared useful for characterizing the surface architecture. While the  $R_a$  and  $R_q$  parameters for the 12 and 150 nm films are very similar and therefore afford little insight into the dissimilar bacterial

attachment propensities, the  $R_{skw}$  and  $R_{kur}$  parameters for these same surfaces are considerably different; hence indicating a different surface architecture in terms of morphology of peaks and valleys.

Generally speaking, the degree of surface hydrophobicity of the Ti films was found to be negatively correlated to the degree of surface roughness, with the smoother 150 nm film surface exhibiting the highest degree of surface hydrophobicity (a contact angle of approximately 81°). This result is in agreement with previously reported results, suggesting that the ‘roughness factor’ could predict the effect of the surface topography on the contact angle/surface hydrophobicity.<sup>15,40</sup> Wenzel’s equation accounts for the fact that the contact angle measured on a rough surface is different from the intrinsic contact angle that would be measured on a smooth, chemically identical surface:

$$\cos \theta_e^r = f \cos \theta_e^s$$

where  $f$  is the Wenzel roughness factor;  $\theta_e^s$  and  $\theta_e^r$  are the equilibrium contact angles measured on the smooth and rough surfaces, respectively.

$\cos \theta_e^s$  is related to the surface and interfacial tensions acting on the three phase line of contact as described by Young’s equation:<sup>15,40</sup>

$$\cos \theta_e^s = \frac{\gamma_{SV} - \gamma_{SL}}{\gamma_{LV}}$$

Due to the surface topography and architectural differences, the 12 nm films were found to be slightly less hydrophobic than the 3 nm films (which is consistent with previous observations<sup>15</sup>) and less hydrophobic than the 150 nm films. The calculated surface free energy values presented in Table 2 for each of the films studied, however, were not significantly different from each other, ranging between 42 and 44 ( $p > 0.05$ ). Surface free energy values correspond to a measure of the interfacial attractive forces existing between the solid surface and a liquid, and they provide an insight into the extent of interaction between the phases, giving an indication of the “wettability” of a surface<sup>41</sup> as a “predictive index of cytocompatibility”.<sup>42</sup> It has been shown that there is a direct correlation between the wettability of a surface and the rate of bacterial attachment: the higher wettability of a surface, the higher its interaction with liquids, which results in a higher level of cell attachment and subsequent spreading rates.<sup>42</sup> Our data suggest that surface architecture is also a significant factor that influences the level of surface wettability, and is therefore a major factor in the regulation of bacterial attachment.

(39) Karunasiri, R. P. U.; Bruinsma, R.; Rudnick, J. *Phys. Rev. Lett.* **1989**, 62, 788–791.

(40) Furstner, R.; Barthlott, W.; Neinhuis, C.; Walzel, P. *Langmuir* **2005**, 21, 956–961.

(41) Ponsonnet, L.; Reybier, K.; Jaffrezic, N.; Comte, V.; Lagneau, C.; Lissac, M.; Martelet, C. *Mater. Sci. Eng., C* **2003**, 23, 551–560.

(42) Lim, Y. J.; Oshida, Y. *Bio-Med. Mater. Eng.* **2001**, 11, 325–341.

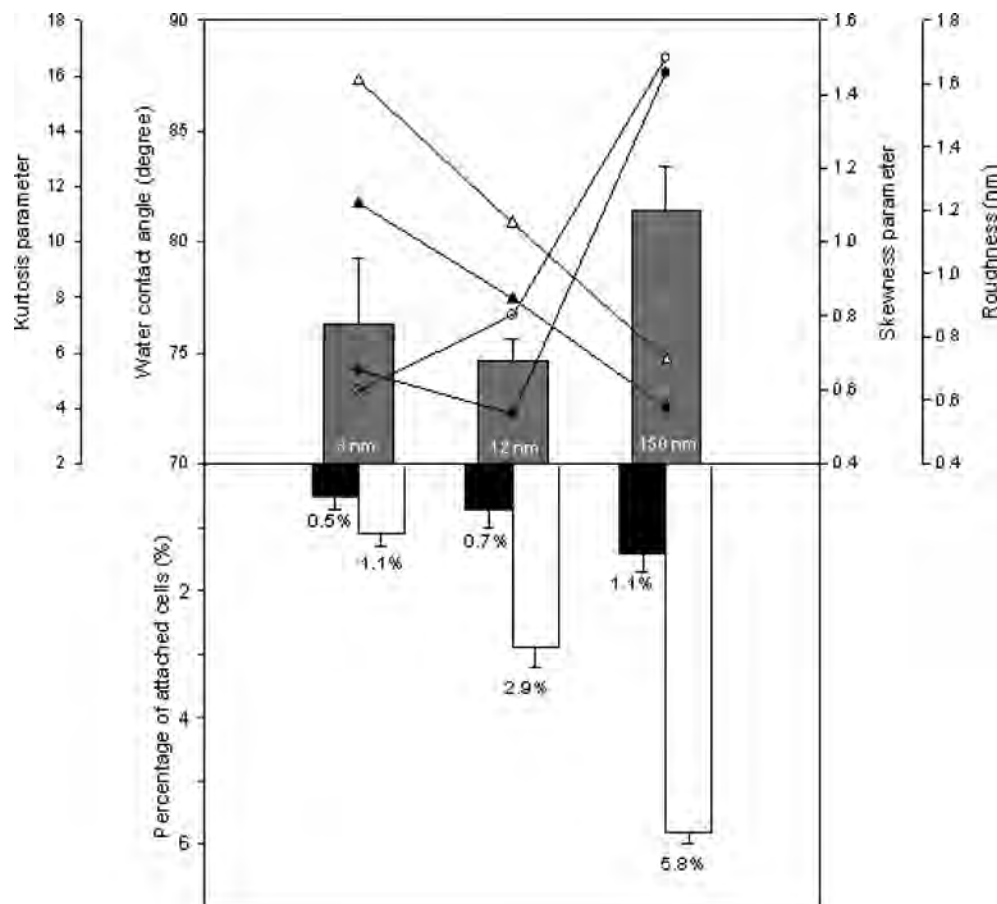


**Figure 5.** The correlation between Ti thin film thicknesses and wettability (gray bar) inferred from the water contact angle measurements, surface topography parameters ( $R_a$  (▲),  $R_q$  (△), Kurtosis (●) and Skewness (○)) are shown on the top, and corresponding bacterial cell retention (percentage of attached cells) of *P. aeruginosa* (black bar) and *S. aureus* (white bar) are shown on the bottom.

**Bacterial Response on Titanium Surfaces of Various Degrees of Nanoroughness.** The attachment responses (cell attachment density and EPS production) of two species of bacteria suggest that they were able to differentiate between titanium surfaces possessing different morphology and nanoroughness. The extent of *S. aureus* cell attachment increased as the surface became smoother (Table 4). The *P. aeruginosa* cell attachment pattern was similar to that of *S. aureus*; however, the extent of attachment of *P. aeruginosa* occurred to a greater extent (Figure 5).

Previously published results have shown that the topography of microrough titanium surfaces can influence the extent of attachment and growth of *Pseudomonas fluorescens* and *S. aureus*.<sup>5,43</sup> In these studies, it was shown that the cells grew along the trenches in long rows (known as contact guidance); however, they attached unevenly to smooth surfaces.<sup>5,44</sup> Some studies reported that bacteria displayed no preference for adhesion to surface scratches or grooves and regarded surface roughness as a “minor factor” in the attachment mechanism.<sup>45</sup> Studies of bacterial adhesions as a function of surface roughness, using 120, 240, 400, 600, or 1200 grit silicon carbide metallographic paper to create degrees of roughness ranging from 0.44 to 1.25 nm ( $R_a$ ), showed that no significant correlation could be identified in

the adherence of *Staphylococcus epidermidis* to titanium.<sup>7</sup> Our recent investigation of the possible impact of ultrafine bulk crystallinity and the associated surface morphology of equal channel angular pressing (ECAP) modified titanium surfaces on the attachment patterns of medically significant bacteria indicated that titanium surface micro- and nanomorphology appeared to be the most influential factor controlling the attachment of *P. aeruginosa*, *S. aureus*, and *E. coli*.<sup>39</sup> Some studies demonstrated relationships between the surface roughness and the propensity for attachment of *P. aeruginosa* onto contact lenses made from polymethyl methacrylate (PMMA), stating that surfaces with values ranging between 4 and 14 nm appeared to have little effect on the extent of attachment, whereas higher  $R_q$  values tended to increase the extent of microorganism attachment.<sup>10</sup> Notably, however, these surface roughness characteristics are on a larger scale than those investigated in this study.

The extent of production of EPS by the two strains of bacteria used in this study was also shown to be related to the pattern of surface roughness. For example, the EPS produced by *S. aureus* cells was found to be greater on the 12 and 150 nm films, rather than on the 3 nm films (Figure 4). Other studies regarding the level of EPS production by bacteria when adsorbing onto surfaces of various roughness have shown that, for some microorganisms, surface roughness on a scale comparable to that of the colonizing microorganism can profoundly affect the extent of attachment, the attachment morphology, and level of EPS production.<sup>5,25,26</sup> For example, *P. fluorescens* has been shown to initially attach in the trenches of

(43) Harris, L. G.; Tosatti, S.; Wieland, M.; Textor, M.; Richards, R. G. *Biomaterials* **2004**, 25, 4135–4148.

(44) Scheuerman, T. R.; Camper, A. K.; Hamilton, M. A. *J. Colloid Interface Sci.* **1998**, 208, 23–33.

(45) Bos, R.; Van Der Mei, H. C.; Busscher, H. J. *FEMS Microbiol. Rev.* **1999**, 23, 179–229.

a nanopatterned gold surfaces, did not produce large quantities of EPS, and were smaller in size than those attached to non-nanopatterned surfaces.<sup>5</sup> The data reported here are also in agreement with our recently reported studies on the bacterial response to changes in glass and polymer surface nanotopography, thus confirming the hypothesis that the surface morphology and topography could strongly influence the degree of bacterial attachment to surfaces.<sup>18,25,46</sup>

### Conclusions

The controlled deposition of titanium onto glass substrata resulted in the fabrication of surfaces with differing morphology and nanoroughnesses, which controlled the overall surface architecture. Remarkably, the extent of attachment of two strains of bacteria indicated that they had the ability to differentiate between surfaces with very small differences in surface roughness, of the order of about 0.3–0.5 nm in the  $R_a$  and  $R_q$  parameters.

(46) Ivanova, E. P.; Mitik-Dineva, N.; Wang, J.; Pham, D. K.; Wright, J. P.; Nicolau, D. V.; Mocanu, R. C.; Crawford, R. J. *Micron* **2008**, 39, 1197–1204.

The attachment of *P. aeruginosa* and particularly *S. aureus* to titanium is of great relevance to the fabrication of medical implants. Thus, a better understanding of the role that surface topographical characteristics play in controlling the attachment of bacteria is of considerable importance.

**Acknowledgment.** This study was supported in part by the Australian Research Council (ARC) and Advanced Manufacturing Co-operative Research Centre (AMCRC). V.K.T. is a recipient of a Swinburne University Postgraduate Research Award.

**Supporting Information Available:** Figure S1: Typical XPS spectra of glass and Ti2p and O1s onto titanium thin film surfaces of 3 nm, 12 and 150 nm thickness after 18 h incubation. Figure S2: Typical SEM images of *P. aeruginosa* (I) and *S. aureus* (II) retention patterns onto titanium thin film surfaces of 3, 12, and 150 nm thickness after 18 h incubation. This material is available free of charge via the Internet at <http://pubs.acs.org>.

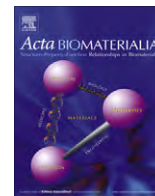
### Permission to publish

E.P. Ivanova, V.K. Truong, J.Y. Wang, C.C. Berndt, R.T. Jones, I.I. Yusuf, I. Peake, H.W. Schmidt, C. Fluke, D. Barnes and R.J. Crawford, 'Impact of nanoscale roughness of titanium thin film surfaces on bacterial retention', *Langmuir*, 2010, 26 (3), 1973–1982.

### PERMISSION/LICENSE IS GRANTED FOR YOUR ORDER AT NO CHARGE

This type of permission/license, instead of the standard Terms & Conditions, is sent to you because no fee is being charged for your order. Please note the following:

- Permission is granted for your request in both print and electronic formats, and translations.
- If figures and/or tables were requested, they may be adapted or used in part.
- Please print this page for your records and send a copy of it to your publisher/graduate school.
- Appropriate credit for the requested material should be given as follows: "Reprinted (adapted) with permission from (COMPLETE REFERENCE CITATION). Copyright (YEAR) American Chemical Society." Insert appropriate information in place of the capitalized words.
- One-time permission is granted only for the use specified in your request. No additional uses are granted (such as derivative works or other editions). For any other uses, please submit a new request.



# Transition metal-substituted cobalt ferrite nanoparticles for biomedical applications

Noppakun Sanpo, Christopher C. Berndt, Cuie Wen, James Wang\*

Industrial Research Institute Swinburne (IRIS), Faculty of Engineering and Industrial Sciences, Swinburne University of Technology, Hawthorn, VIC 3122, Australia

## ARTICLE INFO

### Article history:

Received 5 September 2012

Received in revised form 26 October 2012

Accepted 29 October 2012

Available online 5 November 2012

### Keywords:

Sol gel

Cobalt ferrite

Antibacterial properties

Transition metals

Citric acid

## ABSTRACT

Transition metals of copper, zinc, chromium and nickel were substituted into cobalt ferrite nanoparticles via a sol-gel route using citric acid as a chelating agent. The microstructure and elemental composition were characterized using scanning electron microscopy combined with energy-dispersive X-ray spectroscopy. Phase analysis of transition metal-substituted cobalt ferrite nanoparticles was performed via X-ray diffraction. Surface wettability was measured using the water contact angle technique. The surface roughness of all nanoparticles was measured using profilometry. Moreover, thermogravimetric analysis and differential scanning calorimetry were performed to determine the temperature at which the decomposition and oxidation of the chelating agents took place. Results indicated that the substitution of transition metals influences strongly the microstructure, crystal structure and antibacterial property of the cobalt ferrite nanoparticles.

© 2012 Acta Materialia Inc. Published by Elsevier Ltd. All rights reserved.

## 1. Introduction

Metal-oxide nanoparticles are of interest because of their unique optical, electronic and magnetic properties. Cobalt ferrite ( $\text{CoFe}_2\text{O}_4$ ) nanoparticles have high permeability, good saturation magnetization and no preferred direction of magnetization. Moreover, they exhibit a high coercivity of more than 5 kOe; a moderate saturation magnetisation of about  $80 \text{ emu g}^{-1}$ ; excellent chemical stability and mechanical hardness; a large magneto-optic effect; a high Curie temperature; and high electromagnetic performance [1,2]. Therefore, cobalt ferrite is a promising candidate material for high-density magnetic recording [3], ferrofluids technology [4], biomedical drug delivery [5], magnetic resonance imaging [6], biocompatible magnetic nanoparticles for cancer treatment [7] and magneto-optical devices [8]. The substitution of the  $\text{Co}^{2+}$  ion that is present in cobalt ferrite with, for example,  $\text{Zn}^{2+}$ ,  $\text{Ni}^{2+}$ ,  $\text{Cr}^{2+}$  and  $\text{Cu}^{2+}$  allows variations in their properties that can be tuned to specific applications.

Vaidyanathan and Sendhilnathan [9] demonstrated that, when  $\text{Co}^{2+}$  was substituted with  $\text{Zn}^{2+}$  in  $\text{CoFe}_2\text{O}_4$ , the new  $\text{Co}_x\text{Zn}_{(1-x)}\text{Fe}_2\text{O}_4$  nanoparticles exhibited enhanced properties – e.g. excellent chemical stability, high corrosion resistivity, magneto-crystalline anisotropy, magnetostriction and magneto-optical characteristics. Singhal et al. [10] studied nickel-substituted cobalt ferrite nanoparticles produced by an aerosol route. The results showed that the lattice parameter of nanoparticles decreased linearly with an increase in nickel concentration, which could be attributed to the

smaller ionic radius of  $\text{Ni}^{2+}$  compared to  $\text{Co}^{2+}$ . Moreover, the increase in nickel concentration decreased the saturation magnetization because the relatively high orbital contribution of the  $\text{Ni}^{2+}$  to the magnetic moment of  $\text{Co}^{2+}$  induces large anisotropy.

The magnetic nanoparticles need modification to increase the biocompatibility and bacterial activity before implementation for drug delivery applications. For example, coating a thin silver film onto  $\text{Fe}_3\text{O}_4$  nanoparticles can improve bacterial activity, as well as benefiting the paramagnetic properties of the nanostructures so that they can be recovered and recycled from the site of action by means of an external magnetic field [11]. Moreover, oleic acid was used as a surfactant coating for  $\text{Fe}_3\text{O}_4$  nanoparticles, followed by an adsorption coating with four different antibiotics (cephalosporins) [12]. The bacterial activity was tested on two organisms: *Escherichia coli* and *Staphylococcus aureus*. It was observed that, for the same time interval, the inhibition zone diameters for cephalosporins were greater than those for the cephalosporin nanofluid. The nanofluid only acts as a carrier for the antibiotic. Moreover, the small size of the magnetic nanoparticles allows delivery of an antibiotic when targeting certain organs such as the brain and kidney.

On the other hand, most of the transition metal-substituted cobalt ferrite nanoparticles have been studied only for their magnetic property, with few having been applied for biomedical applications. The special properties of magnetic nanoparticles required for biomedical applications demand precise control of particle size, shape, dispersion and conditions that influence these properties. In principle, it is necessary to stabilize the magnetic nanoparticle dispersion in the aqueous environment. Thus, coating the magnetic nanoparticles with a polymer shell, including organic (polyethylene glycol, dextran, chitosan, polyethyleneimine and phospholipids) or

\*



inorganic (silica) materials, is usually the first step that leads to highly dispersed and high-quality nanoparticles with good biocompatibility [13].

Techniques reported for synthesizing cobalt ferrite nanoparticles include solid-state reaction [14], microemulsion [15], combustion [16], the redox process [17], chemical co-precipitation [18], the hydrothermal method [19] and microwave synthesis [20]. However, sol–gel techniques offer enhanced control over homogeneity, elemental composition and powder morphology. In addition, uniform nanosized metal clusters can be achieved, which are crucial for enhancing the properties of the nanoparticles. These advantages favour the sol–gel route over other conventional preparation methods of ceramic oxide composites [21].

Therefore, the objective of this study is to develop novel multifunctional magnetic iron-based nanoparticles that also exhibit antibacterial properties to fulfil the requirements of a drug delivery system so that the antibiotic concentration could be minimized. For this purpose, we have synthesized transition metal-substituted cobalt ferrite nanoparticles ( $\text{Co}_{0.5}\text{X}_{0.5}\text{Fe}_2\text{O}_4$  with  $\text{X} = \text{Cu}, \text{Zn}, \text{Mn}$  and  $\text{Ni}$ ) by the sol–gel process using citric acid (CA) as the chelating agent. We have investigated the effect of substitution of these transition metals on surface morphology, size distribution and antibacterial properties of the synthesized transition metal-substituted cobalt ferrite nanoparticles.

## 2. Methods and procedures

### 2.1. Sample preparation

The chelating agent, CA gel, was prepared by dissolving CA powders in distilled water (5% w/v) at 70 °C. The chelating agent solutions were kept at 70 °C for 5 h or until the solution became clear. Cobalt nitrate ( $\text{Co}(\text{NO}_3)_2 \cdot 6\text{H}_2\text{O}$ ), iron nitrate ( $\text{Fe}(\text{NO}_3)_3 \cdot 9\text{H}_2\text{O}$ ), copper nitrate ( $\text{Cu}(\text{NO}_3)_2 \cdot 6\text{H}_2\text{O}$ ), nickel nitrate ( $\text{Ni}(\text{NO}_3)_2 \cdot 6\text{H}_2\text{O}$ ), manganese nitrate ( $\text{Mn}(\text{NO}_3)_2 \cdot 4\text{H}_2\text{O}$ ) and zinc nitrate ( $\text{Zn}(\text{NO}_3)_2 \cdot 6\text{H}_2\text{O}$ ) powders with Fe:Co:(Zn, Cu, Ni, Mn) molar ratios of 2:0.5:0.5 were dissolved into the chelating agent solution under magnetic stirring. The sol–gel reaction was continued for 3 h and then the temperature increased to 80 °C for 10 h or until the gel dried into powder form. Finally, all samples were sintered at 800 °C for 4 h and then ground using a mortar and pestle to form a nanoparticle.

### 2.2. Characterization

Elemental composition analyses of the transition metal-substituted cobalt ferrite nanoparticles were performed using energy-dispersive X-ray spectroscopy (EDX) and phase analyses were carried out using X-ray diffraction (XRD). Thermogravimetric analysis (TGA) and differential scanning calorimetry (DSC) were conducted in air to determine the temperature for the decomposition and oxidation of the chelating agent. Surface wettability, an indicator of the surface interaction of the metal oxide with a given solvent and a measure for biomedical applications, was measured using the water contact angle technique (WCA-FTA200). The surface roughness of all nanoparticles was measured using an AlphaStep-D-120 Stylus Profiler (KLA-Tencor Instruments). The morphology of the nanoparticles was observed using field emission scanning electron microscopy (FESEM; ZEISS SUPRA 40 VP).

The antimicrobial activity of transition metal-substituted cobalt ferrite nanoparticles was tested against the Gram-negative bacterium *E. coli* and the Gram-positive bacterium *S. aureus*. Both types of bacterial strain were obtained from the American Type Culture Collection (ATCC), USA. The bacteriological test series were carried out according to the modified ASTM E2180-07 (Standard Test Method for Determining the Activity of Incorporated Antimicrobial

Agent(s) in Polymeric or Hydrophilic Materials). All tests were performed on solid agar plates with different transition metal-substituted cobalt ferrite nanoparticles. *E. coli* and *S. aureus* were grown aerobically at 37 °C overnight with shaking (200 rpm) in an ordinary broth medium. The optical density (OD) of the overnight culture (OVN culture) was measured at 600 nm with an ultraviolet spectrometer and diluted with lysogeny broth (LB) to achieve an OD of 0.1. The diluted OVN culture was then seeded into 20 ml of LB (in a 50 ml Falcon tube) and incubated at 37 °C on the shaker for 2 h to obtain an OD of 0.3. At OD = 0.3, the diluted OVN culture and transition metal-substituted cobalt ferrite nanoparticles were further incubated for 24 h and 100  $\mu\text{l}$  of these mixtures were spread on an agar plate using an L-shaped spreader.

The inoculated plates were incubated at 37 °C and the number of colonies on the Petri dishes were counted after 24 h. The colony-forming units were calculated by multiplying the number of colonies by the dilution factor. The survival percentage was used to evaluate the antimicrobial effect of particles, which is defined by the formula [22]:

$$\text{Survival \%} = \frac{\text{Colony number of treated bacteria}}{\text{Colony number of control bacteria}} \times 100 \quad (1)$$

For the modified Kirby–Bauer method [23], an equal amount of transition metal-substituted cobalt ferrite nanoparticles obtained from CA were coated on filter papers. All samples were placed on the *E. coli* growth LB agar plate and incubated overnight at 37 °C. The zone of inhibition was measured.

Prior to each bacterial attachment experiment, a fresh bacterial suspension of OD = 0.2 was prepared from *E. coli* and *S. aureus* cells grown in LB at room temperature ( $\sim 22$  °C) for 24 h. All nanoparticles were attached to the glass slides using double sided tape. A 3–5 ml aliquot of bacterial suspension was poured into sterile Petri dishes, where the glass slides (one per Petri dish) were completely immersed and left to incubate for 12 h at room temperature ( $\sim 22$  °C). After incubation all of the slides were washed with deionized water and left to dry in air. This experimental approach allowed bacterial attachment to be performed under identical conditions for each microscope slide. A FESEM–ZEISS SUPRA 40VP was used to obtain high-resolution images of the bacterial cells. Just before imaging, all slides were gold coated to achieve better conductivity.

## 3. Results and discussion

### 3.1. Differential scanning calorimetry and thermogravimetric analyses

DSC and TGA curves of synthesized transition metal-substituted cobalt ferrite nanoparticles ((a)  $\text{Co}_{0.5}\text{Cu}_{0.5}\text{Fe}_2\text{O}_4$ , (b)  $\text{Co}_{0.5}\text{Zn}_{0.5}\text{Fe}_2\text{O}_4$ , (c)  $\text{Co}_{0.5}\text{Mn}_{0.5}\text{Fe}_2\text{O}_4$  and (d)  $\text{Co}_{0.5}\text{Ni}_{0.5}\text{Fe}_2\text{O}_4$ ) obtained from CA as a chelating agent are shown in Fig. 1. The TGA curve exhibits two distinct weight loss steps and the DSC curve presents one exothermic and one endothermic peak over 25–500 °C. The first weight loss step in the range of 25–150 °C, which was accompanied by an endothermic broad peak around 150 °C in the DSC curve, arises due to the loss of residual moisture in the powder. The second weight loss step in the range of 200 °C and the sharp exothermic peak around 200 °C are associated with the combustion of nitrates and the oxidation of carbon from the CA to form carbon dioxide. No weight loss was observed above 300 °C, implying the presence of transition metal-substituted cobalt ferrite nanoparticles in this temperature range.

### 3.2. FESEM/EDX analyses

SEM micrographs were analysed to investigate the grain structure of the nanoparticles and assist in understanding the



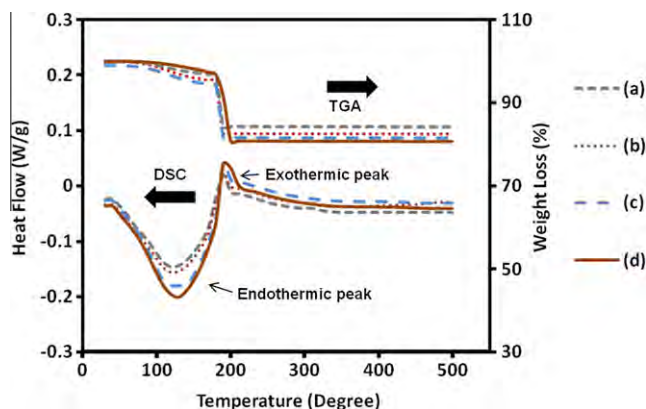


**Fig. 1.** DSC/TGA curves of synthesized transition metal-substituted cobalt ferrite nanoparticles: (a)  $\text{Co}_{0.5}\text{Cu}_{0.5}\text{Fe}_2\text{O}_4$ , (b)  $\text{Co}_{0.5}\text{Zn}_{0.5}\text{Fe}_2\text{O}_4$ , (c)  $\text{Co}_{0.5}\text{Mn}_{0.5}\text{Fe}_2\text{O}_4$  and (d)  $\text{Co}_{0.5}\text{Ni}_{0.5}\text{Fe}_2\text{O}_4$ .

development of the grain sizes. Fig. 2 shows the SEM images of the synthesized cobalt ferrite and transition metal-substituted cobalt ferrite nanoparticles ((a)  $\text{CoFe}_2\text{O}_4$ , (b)  $\text{Co}_{0.5}\text{Cu}_{0.5}\text{Fe}_2\text{O}_4$ , (c)  $\text{Co}_{0.5}\text{Zn}_{0.5}\text{Fe}_2\text{O}_4$ , (d)  $\text{Co}_{0.5}\text{Mn}_{0.5}\text{Fe}_2\text{O}_4$ , and (e)  $\text{Co}_{0.5}\text{Ni}_{0.5}\text{Fe}_2\text{O}_4$ ). The  $\text{CoFe}_2\text{O}_4$  nanoparticles (Fig. 2a) exhibit an angular morphology. The nanoparticles synthesized with transition metal doping in Fig. 2b–e present particles with irregular shapes and agglomeration where some particles form large clusters. The average sizes

of 30 grains, measured by ImageJ manufactured from NIH Image Company, for  $\text{CoFe}_2\text{O}_4$ ,  $\text{Co}_{0.5}\text{Cu}_{0.5}\text{Fe}_2\text{O}_4$ ,  $\text{Co}_{0.5}\text{Zn}_{0.5}\text{Fe}_2\text{O}_4$ ,  $\text{Co}_{0.5}\text{Mn}_{0.5}\text{Fe}_2\text{O}_4$  and  $\text{Co}_{0.5}\text{Ni}_{0.5}\text{Fe}_2\text{O}_4$  are  $42.97 \pm 0.5$ ,  $40.14 \pm 0.4$ ,  $44.18 \pm 0.6$ ,  $40.26 \pm 0.2$  and  $41.01 \pm 0.5$  nm, respectively.

The elemental compositions of synthesized cobalt ferrite and transition metal-substituted cobalt ferrite nanoparticles ( $\text{Co}_{0.5}\text{X}_{0.5}\text{Fe}_2\text{O}_4$ , with  $\text{X} = \text{Cu, Zn, Mn and Ni}$ ) are listed in Table 1. These results indicate that the ratio of Co/transition metal/Fe for all of the synthesized nanoparticles is almost the same as that of the ideal transition metal-substituted cobalt ferrite ( $\text{Co}_{0.5}\text{X}_{0.5}\text{Fe}_2\text{O}_4$ , with  $\text{X} = \text{Cu, Zn, Mn and Ni}$ ) structure, which could confirm that no organic chelating agents remained in the system.

### 3.3. XRD analyses

X-ray diffraction patterns of synthesized cobalt ferrite and transition metal-substituted cobalt ferrite nanoparticles ((a)  $\text{CoFe}_2\text{O}_4$ , (b)  $\text{Co}_{0.5}\text{Cu}_{0.5}\text{Fe}_2\text{O}_4$ , (c)  $\text{Co}_{0.5}\text{Zn}_{0.5}\text{Fe}_2\text{O}_4$ , (d)  $\text{Co}_{0.5}\text{Mn}_{0.5}\text{Fe}_2\text{O}_4$  and (e)  $\text{Co}_{0.5}\text{Ni}_{0.5}\text{Fe}_2\text{O}_4$ ) obtained from sol–gel methods using CA as chelating agent and calcined at  $800^\circ\text{C}$  for 4 h are shown in Fig. 3.

The peaks at  $30.12^\circ$ ,  $35.54^\circ$ ,  $37.12^\circ$ ,  $43.13^\circ$ ,  $53.41^\circ$ ,  $56.89^\circ$  and  $62.62^\circ$  are indexed as the reflection planes of (220), (311), (222), (400), (422), (511) and (440), respectively. Analysis of the XRD patterns of all samples confirmed the formation of the cubic spinel structure [24] as the main characteristic peak. Moreover, no XRD peaks corresponding to the other phases such as  $\alpha\text{-Fe}_2\text{O}_3$ , CoO, ZnO, NiO,  $\text{MnO}_2$ ,  $\text{Co}_2\text{O}_3$  or  $\text{Co}_3\text{O}_4$  were detected, which indicates that

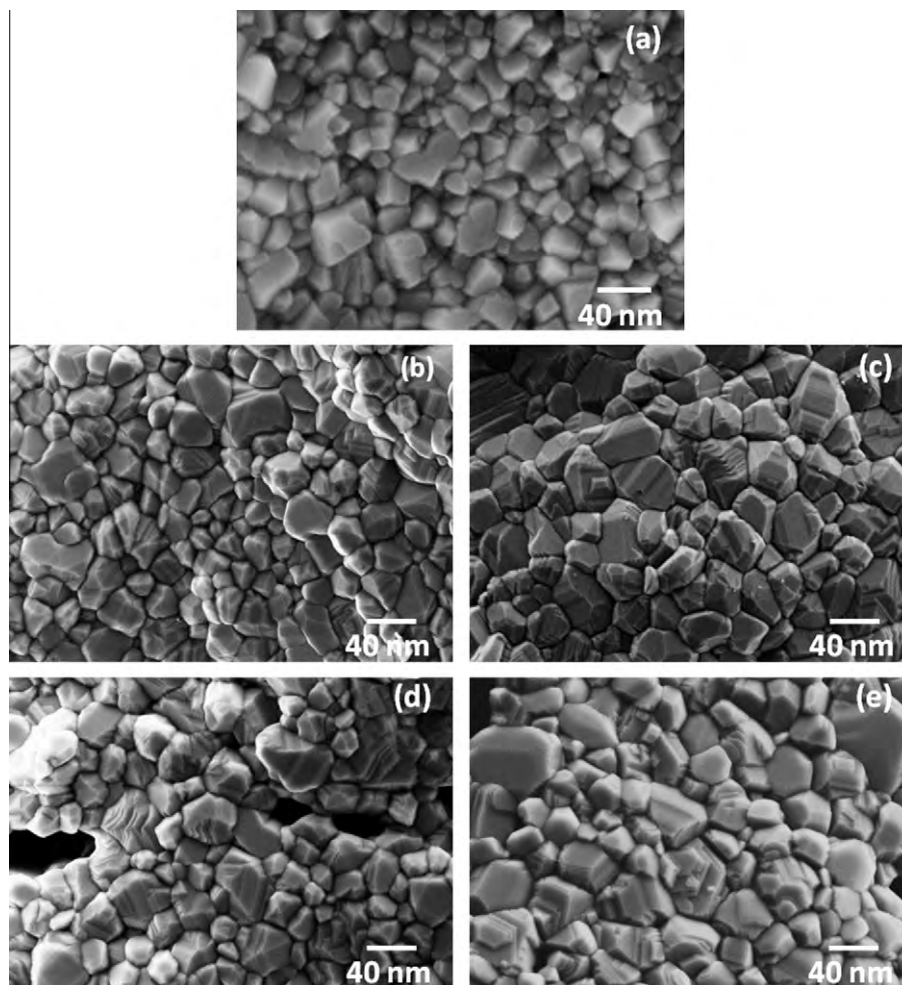


**Fig. 2.** SEM images of synthesized transition metal-substituted cobalt ferrite nanoparticles: (a)  $\text{CoFe}_2\text{O}_4$ , (b)  $\text{Co}_{0.5}\text{Cu}_{0.5}\text{Fe}_2\text{O}_4$ , (c)  $\text{Co}_{0.5}\text{Zn}_{0.5}\text{Fe}_2\text{O}_4$ , (d)  $\text{Co}_{0.5}\text{Mn}_{0.5}\text{Fe}_2\text{O}_4$  and (e)  $\text{Co}_{0.5}\text{Ni}_{0.5}\text{Fe}_2\text{O}_4$ .

**Table 1**

The elemental composition of synthesized cobalt ferrite and transition metal-substituted cobalt ferrite nanoparticles.

Ferrite composition	at. %						
	Co	Cu	Zn	Mn	Ni	Fe	O
CoFe <sub>2</sub> O <sub>4</sub>	14.49	–	–	–	–	28.54	56.97
Co <sub>0.5</sub> Cu <sub>0.5</sub> Fe <sub>2</sub> O <sub>4</sub>	7.38	7.43	–	–	–	28.31	56.88
Co <sub>0.5</sub> Zn <sub>0.5</sub> Fe <sub>2</sub> O <sub>4</sub>	7.36	–	7.40	–	–	28.46	56.78
Co <sub>0.5</sub> Mn <sub>0.5</sub> Fe <sub>2</sub> O <sub>4</sub>	7.32	–	–	7.51	–	28.35	56.82
Co <sub>0.5</sub> Ni <sub>0.5</sub> Fe <sub>2</sub> O <sub>4</sub>	7.34	–	–	–	7.48	28.37	56.81

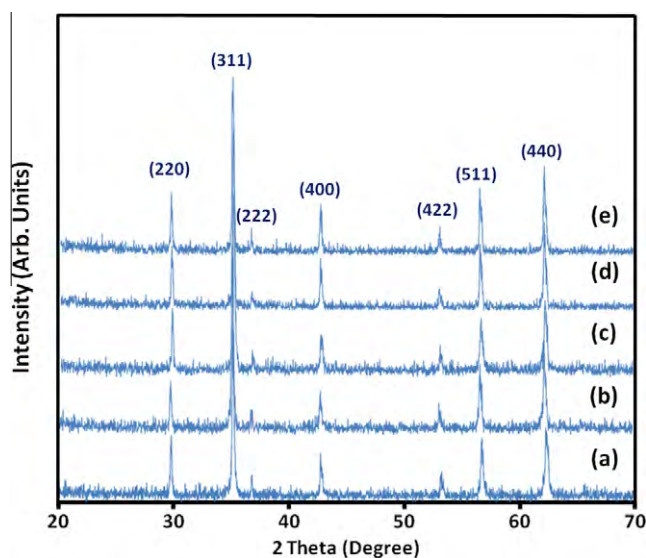


**Fig. 3.** X-ray diffraction patterns of synthesized transition metal-substituted cobalt ferrite nanoparticles: (a) CoFe<sub>2</sub>O<sub>4</sub>, (b) Co<sub>0.5</sub>Cu<sub>0.5</sub>Fe<sub>2</sub>O<sub>4</sub>, (c) Co<sub>0.5</sub>Zn<sub>0.5</sub>Fe<sub>2</sub>O<sub>4</sub>, (d) Co<sub>0.5</sub>Mn<sub>0.5</sub>Fe<sub>2</sub>O<sub>4</sub> and (e) Co<sub>0.5</sub>Ni<sub>0.5</sub>Fe<sub>2</sub>O<sub>4</sub>.

transition metals were completely substituted into the cobalt ferrite lattice synthesized by calcination of the precursor and chelating agent derived from the sol–gel process. These results are in good agreement with Zi et al. [25].

The crystallite size  $D$  was calculated according to the Scherrer equation [26]:

$$D = \frac{0.9 \lambda}{\beta \cos \theta} \quad (2)$$

where  $\lambda$  is the wavelength of the radiation,  $\theta$  is the diffraction angle and  $\beta$  is the full width at half maximum (FWHM) of the diffraction peak. The lattice parameter was calculated according to the formula:

$$a = d_{hkl} \sqrt{h^2 + k^2 + l^2} \quad (3)$$

The reflection plan (311) was used to calculate the crystallite size and lattice constant since this crystallographic plane exhibited the maximum diffraction intensity. The crystallite size and lattice constant of the cobalt ferrite and transition metal-substituted cobalt ferrite nanoparticles (Co<sub>0.5</sub>X<sub>0.5</sub>Fe<sub>2</sub>O<sub>4</sub> with X = Cu, Zn, Mn and Ni) have been summarized in Table 2. The calculated lattice constant  $a$  (using the  $d$  value and respective  $hkl$  (311) parameters) increased from 8.385 to 8.401 Å for the samples calcined at 800 °C with zinc substitution. Meanwhile, the lattice constant decreased to 8.361, 8.309 and 8.356 Å with copper, manganese and nickel substitution, respectively. The relationship between transition metals substitution and lattice parameter can be explained by Vegard's law [27]. This law implies the formation of solid solutions

**Table 2**

The crystallite size and lattice constant of the synthesized cobalt ferrite and transition metal-substituted cobalt ferrite nanoparticles.

Ferrites composition	Lattice parameter (Å)	Crystallite size (nm)
CoFe <sub>2</sub> O <sub>4</sub>	8.385	42.97
Co <sub>0.5</sub> Cu <sub>0.5</sub> Fe <sub>2</sub> O <sub>4</sub>	8.361	40.14
Co <sub>0.5</sub> Zn <sub>0.5</sub> Fe <sub>2</sub> O <sub>4</sub>	8.401	44.18
Co <sub>0.5</sub> Mn <sub>0.5</sub> Fe <sub>2</sub> O <sub>4</sub>	8.309	40.26
Co <sub>0.5</sub> Ni <sub>0.5</sub> Fe <sub>2</sub> O <sub>4</sub>	8.356	40.01

of homogeneous transition metal-substituted cobalt ferrite nanoparticles (Co<sub>0.5</sub>X<sub>0.5</sub>Fe<sub>2</sub>O<sub>4</sub>, with X = Cu, Zn, Mn and Ni). The increase in the lattice parameter results from the difference in the Zn<sup>2+</sup> (0.74 Å) and Co<sup>2+</sup> (0.72 Å) ionic radii [28]. On the other hand, a decrease in the lattice parameter results from the smaller ionic radii of Cu<sup>2+</sup>, Mn<sup>2+</sup> and Ni<sup>2+</sup> compared with Co<sup>2+</sup>. Moreover, the crystallite size of cobalt ferrite and transition metal-substituted cobalt ferrite nanoparticles determined by taking the FWHM of the (311) peak was found to lie in the range of 40–50 nm; the values agree well with those measured from ImageJ.

### 3.4. Contact angle measurement and roughness parameters

The hydrophilicity and surface roughness are presented in Table 3. The surface of cobalt ferrite and transition metal-substituted cobalt ferrite nanoparticles were hydrophilic since the water contact angle was less than 90°. The results indicate that cobalt ferrite nanoparticles are marginally more hydrophilic than those derived from transition metal-substituted cobalt ferrite nanoparticles. Significant differences in the type of substitution transition metal ions have been noticed with respect to the contact angles of the transition metal-substituted cobalt ferrite nanoparticles. The water contact angles increase with the substitution of zinc, manganese, copper and nickel, respectively. In term of the surface roughness of nanoparticles, nickel-substituted cobalt ferrite presents the smoothest surface following by copper, manganese, pure cobalt ferrite and zinc, respectively. These results are in good agreement with the previous XRD results in Table 2, which revealed that nickel-substituted cobalt ferrite has the smallest crystallite nanoparticles size.

### 3.5. Antibacterial activities of the samples

#### 3.5.1. Contact biocidal studies

The contact biocidal property of all ferrite nanoparticles obtained was investigated using a modified Kirby–Bauer technique [23]. Filter papers are partially covered with and without ferrite nanoparticles and placed on a lawn of *E. coli* in an agar plate. The contact antibacterial property can be measured by the clear zone of inhibition around the filter papers after a 24 h incubation (Fig. 4). The diameter of the zone of inhibition for the copper-substituted cobalt ferrite nanoparticles (Fig. 4c) is the largest, followed by zinc-substituted cobalt ferrite (Fig. 4d), nickel-substituted cobalt ferrite (Fig. 4f), pure cobalt ferrite (Fig. 4b) and manganese-substituted cobalt ferrite (Fig. 4e), in decreasing order. The results are in

**Table 3**

Surface wettability and roughness parameters for synthesized cobalt ferrite and transition metal-substituted cobalt ferrite nanoparticles.

Samples	Water contact angle (degree)	Surface roughness Ra (μm)
CoFe <sub>2</sub> O <sub>4</sub>	61 ± 0.2	3.54
Co <sub>0.5</sub> Cu <sub>0.5</sub> Fe <sub>2</sub> O <sub>4</sub>	65 ± 0.3	2.97
Co <sub>0.5</sub> Zn <sub>0.5</sub> Fe <sub>2</sub> O <sub>4</sub>	64 ± 0.3	3.95
Co <sub>0.5</sub> Mn <sub>0.5</sub> Fe <sub>2</sub> O <sub>4</sub>	65 ± 0.1	3.28
Co <sub>0.5</sub> Ni <sub>0.5</sub> Fe <sub>2</sub> O <sub>4</sub>	66 ± 0.2	2.58

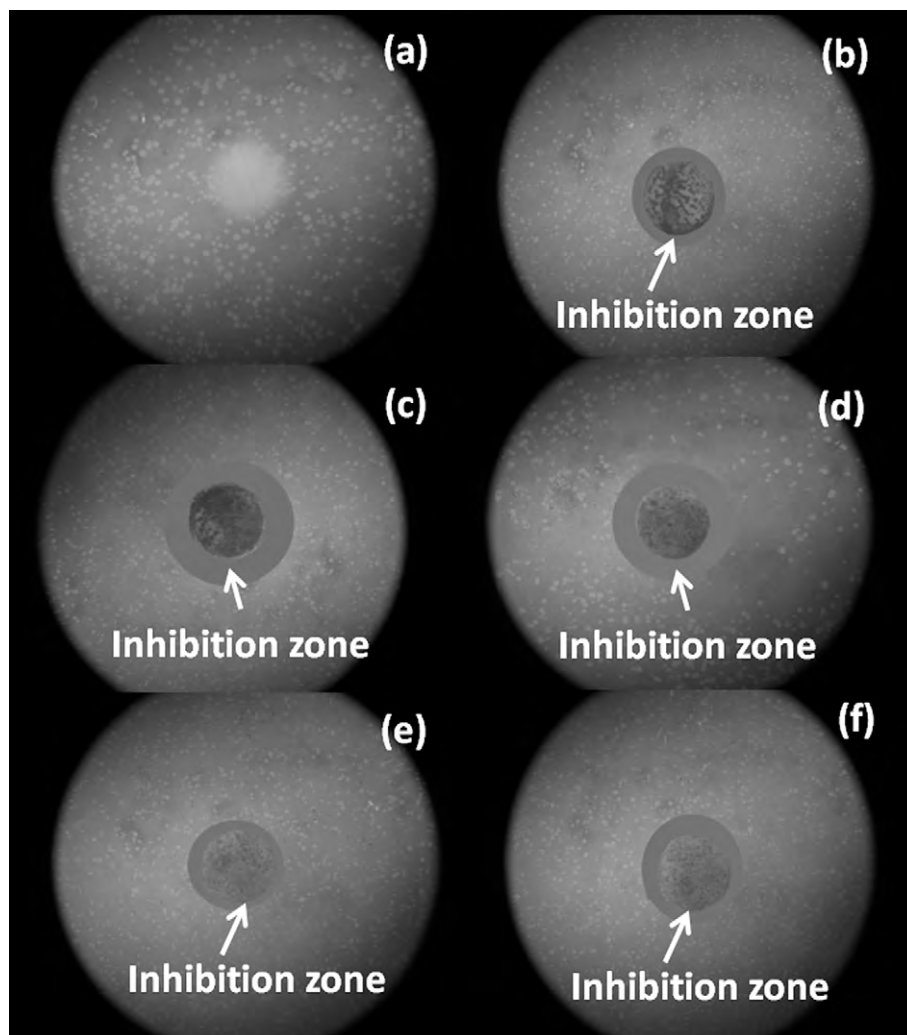


**Fig. 4.** Image of *E. coli* incubated for 24 h at 37 °C together with filter paper: (a) without cobalt ferrite nanoparticles, (b)  $\text{CoFe}_2\text{O}_4$ , (c)  $\text{Co}_{0.5}\text{Cu}_{0.5}\text{Fe}_2\text{O}_4$ , (d)  $\text{Co}_{0.5}\text{Zn}_{0.5}\text{Fe}_2\text{O}_4$ , (e)  $\text{Co}_{0.5}\text{Mn}_{0.5}\text{Fe}_2\text{O}_4$  and (f)  $\text{Co}_{0.5}\text{Ni}_{0.5}\text{Fe}_2\text{O}_4$ .

good agreement with the quantitative bacterial tests which indicated that the copper-substituted cobalt ferrite nanoparticles have the most effective antibacterial property against *E. coli* among all of the nanoparticles.

### 3.5.2. Bacteria attachment studies

The potential for adhesion between a bacterial cell and a substratum surface is governed by several factors, including the physico-chemical properties of the bacterium, the physico-chemical properties of the substratum and the environmental conditions under which the attachment takes place [29]. With all other parameters being equal, any differences in the degree of attachment of a given bacterium on two different substrata under the same conditions will be due to the different surface properties of the materials. While a substantial amount of research has been conducted to investigate the effects of substratum surface chemistry on bacterial adhesion, the recent trend has focused on the role that surface topography plays in the bacterial attachment process [30,31]. Typical SEM images in Fig. 5 indicated that the morphology of the *S. aureus* attached to the glass surface was similar to those attached to the transition metal-substituted cobalt ferrite nanoparticles. The number of the attached cells on the glass surfaces decreased considerably compared to transition metal-substituted cobalt ferrite nanoparticles. The number of the attached cells on the

nanoparticles surface decreased in the order of  $\text{Co}_{0.5}\text{Zn}_{0.5}\text{Fe}_2\text{O}_4 < \text{Co}_{0.5}\text{Cu}_{0.5}\text{Fe}_2\text{O}_4 < \text{Co}_{0.5}\text{Mn}_{0.5}\text{Fe}_2\text{O}_4 < \text{CoFe}_2\text{O}_4 < \text{Co}_{0.5}\text{Ni}_{0.5}\text{Fe}_2\text{O}_4$ . This could be attributed to the difference in chemical composition, surface architecture and roughness of the nanoparticles, as previously discussed.

The typical SEM images representing the attached *E. coli* on synthesized transition metal-substituted cobalt ferrite nanoparticles are presented in Fig. 6. Both the morphology and number of bacteria attached to the glass surface were significantly different from those attached to the synthesized transition metal-substituted cobalt ferrite nanoparticles. Biofilms were also noticed on the surface of transition metal-substituted cobalt ferrite nanoparticles. Biofilms are the most common mode of bacterial growth in nature and are highly resistant to antibiotics. This form of microbial growth has been studied in a wide range of scientific disciplines, including biomedicine, water engineering and evolutionary biology [32,33]. The intensity of biofilms covered on the nanoparticles surface increased in the order  $\text{Co}_{0.5}\text{Ni}_{0.5}\text{Fe}_2\text{O}_4 > \text{CoFe}_2\text{O}_4 > \text{Co}_{0.5}\text{Mn}_{0.5}\text{Fe}_2\text{O}_4 > \text{Co}_{0.5}\text{Zn}_{0.5}\text{Fe}_2\text{O}_4 > \text{Co}_{0.5}\text{Cu}_{0.5}\text{Fe}_2\text{O}_4$ .

### 3.5.3. Bacterial quantitative studies

The antibacterial activities of the transition metal-substituted cobalt ferrite nanoparticles against *E. coli* and *S. aureus* are shown in Fig. 7. All tests were repeated 10 times for statistical studies



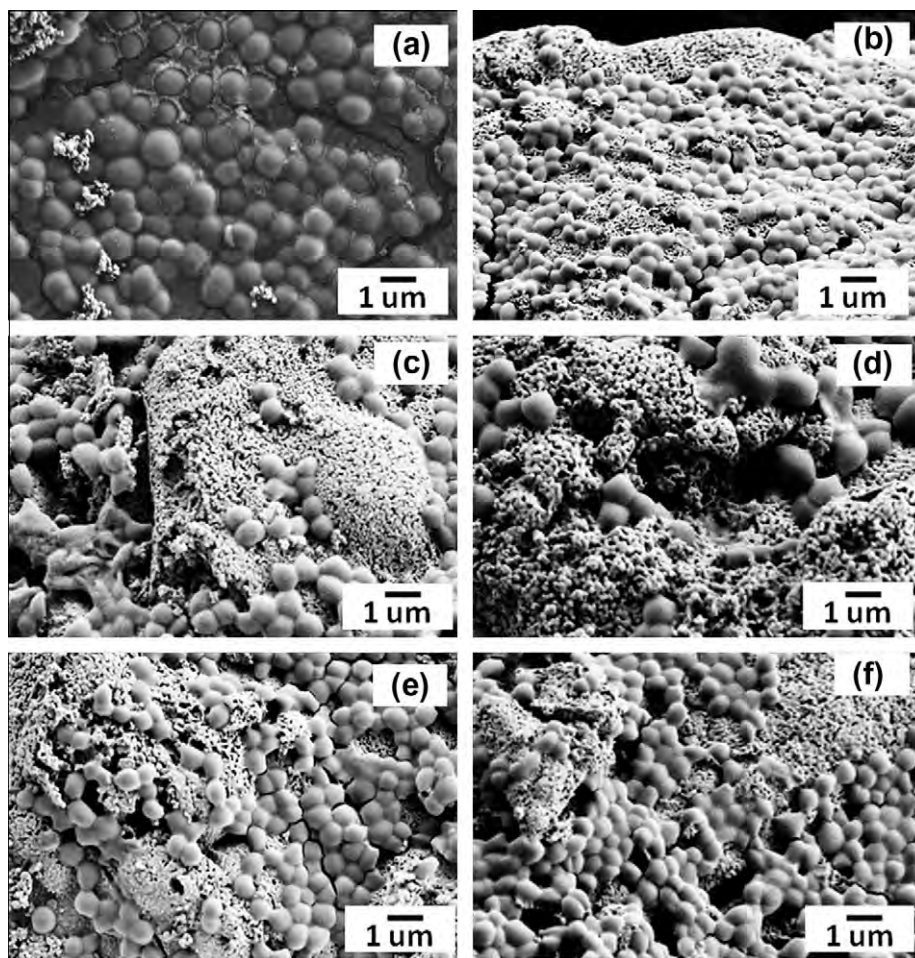


**Fig. 5.** Typical SEM images representing the attached *S. aureus* on synthesized transition metal-substituted cobalt ferrite nanoparticles: (a) without cobalt ferrite nanoparticles, (b)  $\text{CoFe}_2\text{O}_4$ , (c)  $\text{Co}_{0.5}\text{Cu}_{0.5}\text{Fe}_2\text{O}_4$ , (d)  $\text{Co}_{0.5}\text{Zn}_{0.5}\text{Fe}_2\text{O}_4$ , (e)  $\text{Co}_{0.5}\text{Mn}_{0.5}\text{Fe}_2\text{O}_4$  and (f)  $\text{Co}_{0.5}\text{Ni}_{0.5}\text{Fe}_2\text{O}_4$  after 12 h incubation.

after culture incubation at 37 °C overnight. The concentration of cobalt ferrite nanoparticles was fixed at  $1 \text{ g l}^{-1}$ . Compared to the control (the sample of bacteria solution without adding nanoparticles), cobalt ferrite and transition metal-substituted cobalt ferrite nanoparticles inhibit the growth of both *E. coli* and *S. aureus*, and the *E. coli* killing rate of all ferrite composite nanoparticles is higher than the *S. aureus* killing rate. The antibacterial properties of manganese and nickel-substituted cobalt ferrite nanoparticles are lower than the pure cobalt ferrite nanoparticles. However, their antibacterial abilities became more dominant when copper and zinc were substituted into the cobalt ferrite nanoparticles.

There are several possible mechanisms for the antibacterial action of zinc and copper ceramic nanoparticles. Studies have suggested that, when *E. coli* is treated with copper nanoparticles, changes take place in its cell membrane morphology. These nanoparticles adhere to the bacterial cell wall and penetrate through the cell membrane [34]. Copper ions cause destruction of the bacterial cell wall, degradation and lysis of the cytoplasm, leading to cell death. Moreover, high concentrations of copper nanoparticles demonstrate complete cytotoxicity against *E. coli* [35]. As nanoparticles have a large surface area, their bactericidal efficacy is enhanced compared to large sized particles; hence, they are believed to impart cytotoxicity to microorganisms. Copper nanoparticles have a large surface-to-volume ratio, which enhances their bioactivity and makes them effective bactericidal agents [36]. For the zinc nanoparticles system, studies showed that zinc binds to the membranes of microorganisms, similar to mammalian cells, prolonging the lag phase of the growth cycle and increasing

the generation time of the organisms so that it takes each organism more time to complete cell division [37].

Another proposition maintained that the main chemical species contributing to the occurrence of the antibacterial activity were assumed to be active oxides; for example, hydrogen peroxide ( $\text{H}_2\text{O}_2$ ) and super-oxide ( $\text{O}_2^-$ ), generated from the surface of the zinc ceramics [38]. These active oxides readily penetrate the cell wall of bacteria and cause cell destruction [39]. The penetration rate of active oxides through the bacteria cell wall plays an important role in the killing rate of zinc ceramic nanoparticles against bacteria. Furthermore, the structure and chemical composition of the cell walls are quite different between *E. coli* and *S. aureus*. The *E. coli* cell wall consists of lipid A, lipopolysaccharide and peptidoglycan, whereas that of *S. aureus* consists mainly of peptidoglycan. The results indicate that active oxides generated from transition metal-substituted cobalt ferrite have more capability to penetrate the cell wall and decrease the cell division of *E. coli* rather than *S. aureus*. However, the precise mechanism of interaction between bacteria (*E. coli* and *S. aureus*) and transition metal-substituted cobalt ferrite nanoparticles needs to be investigated further.

#### 4. Conclusions

A sol-gel technique for synthesizing transition metal-substituted cobalt ferrite nanoparticles that employs citric acid as a chelating agent was developed. Transition metal-substituted cobalt ferrite nanoparticles formed a cubic spinel structure and exhibited

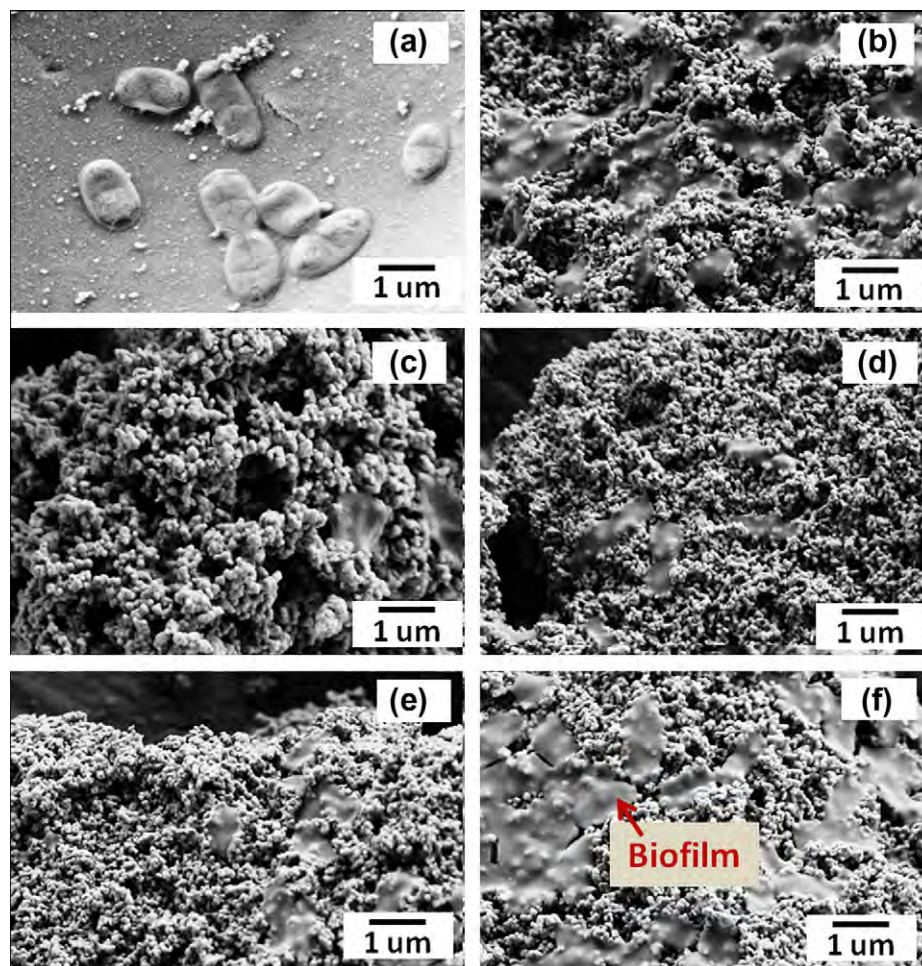


**Fig. 6.** Typical SEM images representing the attached *E. coli* on synthesized transition metal-substituted cobalt ferrite nanoparticles: (a) without cobalt ferrite nanoparticles, (b)  $\text{CoFe}_2\text{O}_4$ , (c)  $\text{Co}_{0.5}\text{Cu}_{0.5}\text{Fe}_2\text{O}_4$ , (d)  $\text{Co}_{0.5}\text{Zn}_{0.5}\text{Fe}_2\text{O}_4$ , (e)  $\text{Co}_{0.5}\text{Mn}_{0.5}\text{Fe}_2\text{O}_4$  and (f)  $\text{Co}_{0.5}\text{Ni}_{0.5}\text{Fe}_2\text{O}_4$  after 12 h incubation.

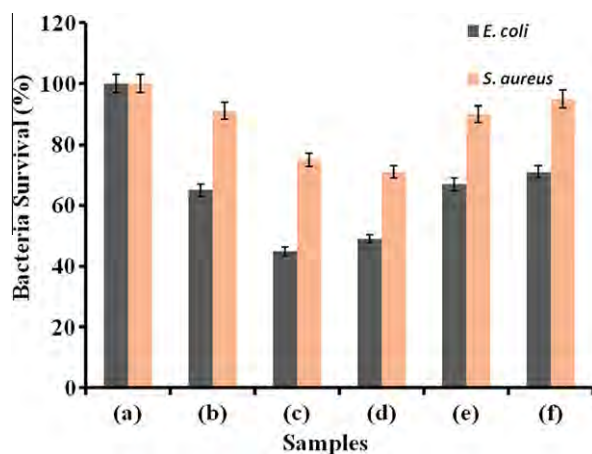


**Fig. 7.** Antibacterial activities against *E. coli* and *S. aureus* of synthesized transition metal-substituted cobalt ferrite nanoparticles: (a) without cobalt ferrite nanoparticles, (b)  $\text{CoFe}_2\text{O}_4$ , (c)  $\text{Co}_{0.5}\text{Cu}_{0.5}\text{Fe}_2\text{O}_4$ , (d)  $\text{Co}_{0.5}\text{Zn}_{0.5}\text{Fe}_2\text{O}_4$ , (e)  $\text{Co}_{0.5}\text{Mn}_{0.5}\text{Fe}_2\text{O}_4$  and (f)  $\text{Co}_{0.5}\text{Ni}_{0.5}\text{Fe}_2\text{O}_4$ .

irregular morphology with a crystallite size in the range of 40–50 nm. The substitution of zinc and copper in cobalt ferrite nanoparticles significantly improved antibacterial activity against *E. coli* and *S. aureus*. Copper-substituted cobalt ferrite nanoparticles have the most effective contact biocidal property among all of the nanoparticles.

The antibacterial activity of transition metal-substituted cobalt ferrite nanoparticles against *E. coli* was higher than *S. aureus*. Zinc- and copper-substituted cobalt ferrite nanoparticles could be used in drug delivery systems as well as in other biomedical and biotechnology applications.

#### Acknowledgement

C.W. acknowledges the financial support from the Australian Research Council (ARC) through the ARC Discovery Project DP110101974.

#### Appendix A. Figures with essential colour discrimination

Certain figures in this article, particularly Figs. 1, 3, 6 and 7, are difficult to interpret in black and white. The full colour images can be found in the on-line version, at <http://dx.doi.org/10.1016/j.actbio.2012.10.037>.

#### References

- [1] Meng X, Li H, Chen J, Mei L, Wang K, Li X. Mössbauer study of cobalt ferrite nanocrystals substituted with rare-earth  $\text{Y}^{3+}$  ions. *J Magn Magn Mater* 2009;321:1155–8.
- [2] Phua LX, Xu F, Ma YG, Ong CK. Structure and magnetic characterizations of cobalt ferrite films prepared by spray pyrolysis. *Thin Solid Films* 2009;517:5858–61.



- [3] Sugimoto M. The past, present, and future of ferrites. *J Am Ceram Soc* 1999;82:269–79.
- [4] Pileni MP. Magnetic fluids: fabrication, magnetic properties, and organization of nanocrystals. *Adv Funct Mater* 2001;11:323–36.
- [5] Liu C, Zou B, Rondinone AJ, Zhang ZJ. Reverse micelle synthesis and characterization of superparamagnetic  $\text{MnFe}_2\text{O}_4$  spinel ferrite nanocrystallites. *J Phys Chem B* 2000;104:1141–5.
- [6] Zhen L, He K, Xu CY, Shao WZ. Synthesis and characterization of single-crystalline  $\text{MnFe}_2\text{O}_4$  nanorods via a surfactant-free hydrothermal route. *J Magn Mater* 2008;320:2672–5.
- [7] Kim D-H, Nikles DE, Johnson DT, Brazel CS. Heat generation of aqueously dispersed  $\text{CoFe}_2\text{O}_4$  nanoparticles as heating agents for magnetically activated drug delivery and hyperthermia. *J Magn Magn Mater* 2008;320:2390–6.
- [8] Jamon D, Donatini F, Siblini A, Royer F, Perzynski R, Cabuil V, et al. Experimental investigation on the magneto-optic effects of ferrofluids via dynamic measurements. *J Magn Magn Mater* 2009;321:1148–54.
- [9] Vaidyanathan G, Sendhilnathan S. Characterization of  $\text{Co}_{1-x}\text{Zn}_x\text{Fe}_2\text{O}_4$  nanoparticles synthesized by co-precipitation method. *Phys B Condens Matter* 2008;403:2157–67.
- [10] Singhal S, Singh J, Barthwal SK, Chandra K. Preparation and characterization of nanosize nickel-substituted cobalt ferrites ( $\text{Co}_{1-x}\text{Ni}_x\text{Fe}_2\text{O}_4$ ). *Solid State Chem* 2005;178:3183–9.
- [11] Sun S, Zeng H, Robinson DB, Raoux S, Rice PM, Wang SX, et al. Monodisperse  $\text{MFe}_2\text{O}_4$  (M = Fe, Co, Mn) nanoparticles. *J Am Ceram Soc* 2004;126:273–9.
- [12] Buteică AS, Mihaiescu DE, Grumezescu AM, Vasile BŞ, Popescu A, Mihaiescu OM, et al. The anti-bacterial activity of magnetic nanofluid:  $\text{Fe}_3\text{O}_4$ /oleic acid/cephalosporins core/shell/adsorption-shell proved on *S. aureus* and *E. coli* and possible applications as drug delivery systems. *Dig J Nanometer Bios* 2010;5:927–32.
- [13] Byrappa K, Ohara S, Adschiri T. Nanoparticles synthesis using supercritical fluid technology – towards biomedical applications. *Adv Drug Deliv Rev* 2008;60:299–327.
- [14] Rafferty A, Prescott T, Brabazon D. Sintering behaviour of cobalt ferrite ceramic. *Ceram Int* 2008;34:15–21.
- [15] Choi EJ, Ahn Y, Kim S, An DH, Kang KU, Lee BG, et al. Superparamagnetic relaxation in  $\text{CoFe}_2\text{O}_4$  nanoparticles. *J Magn Magn Mater* 2003;262:L198–202.
- [16] Yan CH, Xu ZG, Cheng FX, Wang ZM, Sun LD, Liao CS, et al. Nanophased  $\text{CoFe}_2\text{O}_4$  prepared by combustion method. *Solid State Commun* 1999;111:287–91.
- [17] Rajendran M, Pullar RC, Bhattacharya AK, Das D, Chintalapudi SN, Majumdar CK. Magnetic properties of nanocrystalline  $\text{CoFe}_2\text{O}_4$  powders prepared at room temperature: variation with crystallite size. *J Magn Magn Mater* 2001;232:71–83.
- [18] Pannaparayil T, Komarneni S. Synthesis and characterization of ultrafine cobalt ferrites. *Magn IEEE Trans* 1989;25:4233–5.
- [19] Daou TJ, Pourroy G, Bégin-Colin S, Grenèche JM, Ulhaq-Bouillet C, Legaré P, et al. Hydrothermal synthesis of monodisperse magnetite nanoparticles. *Chem Mater* 2006;18:4399–404.
- [20] Bensebaa F, Zavaliche F, L'Ecyer P, Cochrane RW, Veres T. Microwave synthesis and characterization of Co-ferrite nanoparticles. *J Colloid Interf Sci* 2004;277:104–10.
- [21] De G, Mattei G, Mazzoldi P, Sada C, Battaglin G, Quaranta A. Au–Cu alloy nanocluster doped  $\text{SiO}_2$  films by sol–gel processing. *Chem Mater* 2000;12:2157–60.
- [22] Lu Z, Li CM, Bao H, Qiao Y, Toh Y, Yang X. Mechanism of antimicrobial activity of CdTe quantum dots. *Langmuir* 2008;24:5445–52.
- [23] Wikins TD, Holdeman LV, Abramson IJ, Moore WE. Standardized single-disc method for antibiotic susceptibility testing of anaerobic bacteria. *Antimicrob Agents Chemother* 1972;1:451–9.
- [24] Sickafus KE, Wills JM, Grimes NW. Structure of spinel. *J Am Ceram Soc* 1999;82:3279–92.
- [25] Zi Z, Sun Y, Zhu X, Yang Z, Dai J, Song W. Synthesis and magnetic properties of  $\text{CoFe}_2\text{O}_4$  ferrite nanoparticles. *J Magn Magn Mater* 2009;321:1251–5.
- [26] Robertson J. Elements of X-ray diffraction by B.D. Cullity. *Acta Crystallogr A* 1979;35:350.
- [27] Parkin IP. Basic solid state chemistry. *Appl Organomet Chem* 2000;14:227–8.
- [28] Köseoğlu Y, Baykal A, Toprak MS, Gözüak F, Başaran AC, Aktaş B. Synthesis and characterization of  $\text{ZnFe}_2\text{O}_4$  magnetic nanoparticles via a PEG-assisted route. *J Alloys Compd* 2008;462:209–13.
- [29] An YH, Friedman RJ. Concise review of mechanisms of bacterial adhesion to biomaterial surfaces. *J Biomed Mater Res* 1998;43:338–48.
- [30] Bos R, Van Der Mei HC, Busscher HJ. Physico-chemistry of initial microbial adhesive interactions – its mechanisms and methods for study. *FEMS Microbiol Rev* 1999;23:179–229.
- [31] Katsikogianni MG, Missirlis YF. Bacterial adhesion onto materials with specific surface chemistries under flow conditions. *J Mater Sci Mater Med* 2010;21:963–8.
- [32] Austin JW, Bergeron G. Development of bacterial biofilms in dairy processing lines. *J Dairy Res* 1995;62:509–19.
- [33] Carr JH, Anderson RL, Favero MS. Comparison of chemical dehydration and critical point drying for the stabilization and visualization of aging biofilm present on interior surfaces of PVC distribution pipe. *J Appl Bacteriol* 1996;80:225–32.
- [34] Hu C-H, Xia M-S. Adsorption and antibacterial effect of copper-exchanged montmorillonite on *Escherichia coli* K88. *Appl Clay Sci* 2006;31:180–4.
- [35] Raffi M, Mehrwan S, Bhatti TM, Akhter JI, Hameed A, Yawar W, et al. Investigations into the antibacterial behavior of copper nanoparticles against *Escherichia coli*. *Ann Microbiol* 2010;60:75–80.
- [36] Stoimenov PK, Klinger RL, Marchin GL, Klabunde KJ. Metal oxide nanoparticles as bactericidal agents. *Langmuir* 2002;18:6679–86.
- [37] Radke LL, Hahn BL, Wagner DK, Sohnle PG. Effect of abscess fluid supernatants on the kinetics of *Candida albicans* growth. *Clin Immunol Immunopathol* 1994;73:344–9.
- [38] Yamamoto O, Sawai J. Preparation and characterization of novel activated carbons with antibacterial function. *Bull Chem Soc Jpn* 2001;74:1761–5.
- [39] Sawai J, Shoji S, Igarashi H, Hashimoto A, Kokugan T, Shimizu M, et al. Hydrogen peroxide as an antibacterial factor in zinc oxide powder slurry. *J Ferment Bioeng* 1998;86:521–2.

### Permission to publish

N. Sanpo, C.C. Berndt, C. Wen and J. Wang, 'Transition metal-substituted cobalt ferrite nanoparticles for biomedical applications', *Acta Biomaterialia*, 9[3] (2013) p. 5830-5837. DOI: 10.1016/j.actbio.2012.10.037, Published: MAR 2013.

As an Elsevier journal author, you retain various rights including Inclusion of the article in a thesis or dissertation whether in part or in toto; see [http://www.elsevier.com/about/policies/author-agreement/lightbox\\_scholarly-purposes](http://www.elsevier.com/about/policies/author-agreement/lightbox_scholarly-purposes) for more information. As this is a retained right, no written permission is necessary. This extends to the online version of your thesis and would include any version of the articles including the final published versions provided that they are not available as individual downloads but only embedded within the thesis itself.

## FAILURE DURING THERMAL CYCLING OF PLASMA-SPRAYED THERMAL BARRIER COATINGS\*

CHRISTOPHER C. BERNDT† AND H. HERMAN

*Department of Materials Science and Engineering, State University of New York at Stony Brook, Stony Brook, NY 11794 (U.S.A.)*

(Received April 18, 1983; accepted April 21, 1983)

The thermal cycling behavior of plasma-sprayed  $\text{ZrO}_2$ -12wt.% $\text{Y}_2\text{O}_3$  coatings was studied. Coatings were produced with and without bond coats of Ni-Cr-Al-Zr and in some cases the substrates were heated to above the optimum temperature prior to spraying. The coatings (attached to the substrate) were thermal cycled to 1200°C and their cracking behavior was followed by acoustic emission (AE) techniques. It was possible to examine the failure mechanisms by statistical analysis of the AE data and to evaluate the influence of preheating and bond coating. It is shown that the AE spectrum changes when a bond coat is used because of the presence of microcracks which, in turn, dissipate energy and improve the coating integrity. The preheating effect is reflected by a decrease in the peak count rate and an increase in the temperature at which AE activity is initiated.

### 1. INTRODUCTION

Early studies of plasma-sprayed coatings stressed microstructural features<sup>1,2</sup> and mechanical properties<sup>3,4</sup> in order to characterize coating performance. More recently, the focus of mechanical properties has turned to fracture mechanics<sup>5</sup>, statistical analysis<sup>6</sup> and failure mechanisms<sup>6,7</sup>.

A major problem in the development of thermal barrier coatings is establishing their material properties and correlating these properties with the fracture behavior. Coating failure is often classified as adhesive or cohesive, there generally being little indication of the specific failure mechanism, *i.e.* the description of fracture morphology does not *per se* indicate the mechanism(s) of failure. Mechanistic studies of coating failure will aid in an understanding of coating integrity and thus are expected to lead to improvements in future thermal barrier coating systems.

Acoustic emission experiments carried out during the thermal cycling of plasma-sprayed coatings are described in this paper. In this way the progressive failure of coatings was ascertained.

\* Paper presented at the International Conference on Metallurgical Coatings, San Diego, CA, U.S.A., April 18-22, 1983.

† Present address: NASA-Lewis Research Center, Surface Protection Section, MS 105-1, Cleveland, OH 44135, U.S.A.

*In situ* evaluation during mechanical and thermal tests was carried out by analyzing acoustic emission (AE) spectra (*i.e.* count rate data as a function of time). The mechanical studies were based on tensile adhesion tests<sup>8</sup> and showed that coatings which fail at high tensile stress also exhibit a high AE count. More detailed analysis<sup>9</sup> was employed to relate the time dependence of count rate distribution to the fracture morphology.

In another AE study carried out during thermal cycling of coatings<sup>10</sup> it was found that the total AE count changed with respect to specimen temperature and that these trends could be correlated with coating integrity. However, in that study edge effects in the planar sample geometry may have masked failure processes for the bulk of the coating. Also, the mild steel substrate was not a typical high temperature alloy and thus the temperature limit of the tests was 650 °C; otherwise oxidation-related effects of the substrate would have generated high AE activity. More importantly, it is considered that the count rate distribution (rather than total counts) is more indicative of failure phenomena, since analysis of these distributions has proven valuable in interpreting AE events resulting from tensile adhesion tests<sup>9,11</sup>.

## 2. EXPERIMENTAL DETAILS

Coatings were prepared in a manner that maximized differences in their AE behavior. For example, substrates which are overheated prior to plasma spraying are known to produce coatings with short lifetimes compared with the "optimally" processed substrate. Also, it is well known that bond coating greatly enhances coating lifetime. In this manner coatings of yttria-stabilized zirconia (YSZ) ( $\text{ZrO}_2$ -12wt.% $\text{Y}_2\text{O}_3$  0.04 cm thick) were deposited onto the grit-blasted substrate with and without a bond coat (Ni-Cr-Al-Zr 0.01 mm thick) such that "good" and "bad" coatings could be produced. The Udimet-700 substrate rod was 35.6 cm long and 1.25 cm in diameter and both ends were paper ground to a smooth finish. Coatings 2.5 cm wide were plasma sprayed 7.5 cm from one end of the bar which was supported in a cantilever fashion from the opposite end. The AE transducer was attached using a suitable high temperature couplant and spring arrangement. A 20 kW tubular furnace was employed together with a programmed temperature controller which allowed a nominal heating and cooling rate of 5.5 °C min<sup>-1</sup>. The specimen was normally cycled (for up to seven times) to 1200 °C and the trends in the AE count rate and the total AE counts were measured. The AE arrangement incorporated a Dunegan-Endevco modular system (3000 series) to amplify the signal from a 0.1-0.5 MHz transducer for a total system gain of 96 dB. The AE count rate data were subsequently digitized and computer processed. A schematic representation of the experimental arrangement is shown in Fig. 1.

## 3. EXPERIMENTAL RESULTS

The AE was generated on cooling, the count rate being measured over 1 min intervals with respect to time (and thus temperature). The gain of the AE instrumentation was adjusted so that no counts were generated during the thermal cycling of the uncoated substrate. Thus the AE activity arose from processes which

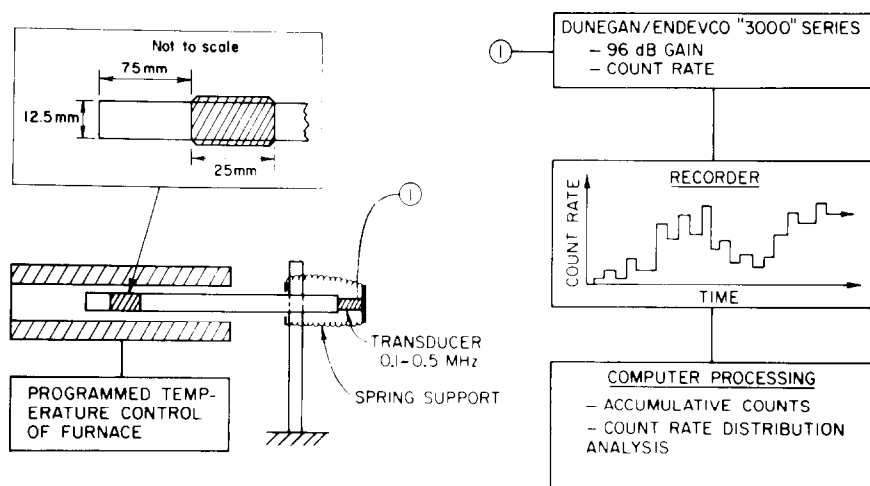


Fig. 1. Experimental arrangement.

depended only on the coating behavior. It should be emphasized that these data were manipulated in several analyses to discern different trends.

The AE spectra of specimens prepared in exactly the same manner showed the same trends; however, the detailed shapes of the response curves were not identical. It should be noted that the specimens showed significant AE activity only on cooling (Fig. 2).

### 3.1. Cumulative acoustic emission data

#### 3.1.1. Effect of pretreating the substrate

Preheating the substrate resulted in high AE activity during the initial cooling period for all the coatings (Figs. 2(b) and 2(d)). For example, the bond-coated samples exhibited AE activity immediately upon the start of cooling (*i.e.* at 1200 °C) only when the substrates were preheated. However, the "optimally" sprayed bond-coated specimens showed activity only at temperatures below 320–420 °C (Fig. 2(c)).

The samples with no bond coat showed similar behavior, except that AE activity was recorded immediately on the cooling portion of the cycle for both previous heat treatment conditions (Figs. 2(a) and 2(b)). The preheated substrate exhibited more counts in the early part of the cooling cycle (above 440 °C), however, and both samples, as in the case of the preheated sample with a bond coat, showed a distinct rise in activity at approximately 440 °C.

#### 3.1.2. Effect of the bond coat

The incorporation of the bond coat decreased the total number of AE counts, regardless of the previous treatment of the substrate. Bond coating also delayed failure, as measured by AE activity, of the coating which was optimally sprayed (Fig. 2(c)).

#### 3.1.3. Influence of thermal cycling on the acoustic emission spectrum

The shape of the AE spectrum was retained on cycling. Small differences in the displacements of the spectrum were associated with a change in the count rate data; these are best seen in the following analysis.

### 3.2. Analysis of count rate data

The count rate is a more sensitive measurement than are the cumulative counts (as in Fig. 2), since it can be employed to identify the cracking mechanism. For example, additional work has shown that high count rates are usually associated with cracking around fine topographic features on the surfaces of individual particles, while low count rates can be related to interlamellar failure. Therefore the raw count rate data were arranged in ascending order and classified into count rate intervals of  $5 \times 10^2$ . The original time (and therefore temperature) sequence of each count rate datum point could be recalled from the original data file. The distribution of any particular count rate interval was thus evaluated in terms of a mean time value, the standard deviation of time, the skewness parameter (the third moment) and the kurtosis parameter (the fourth moment). The last two parameters give an indication of the distribution shape with respect to a normal distribution.

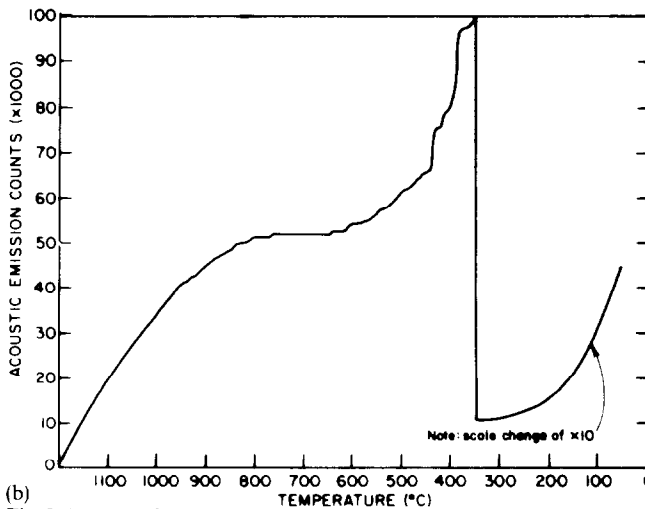
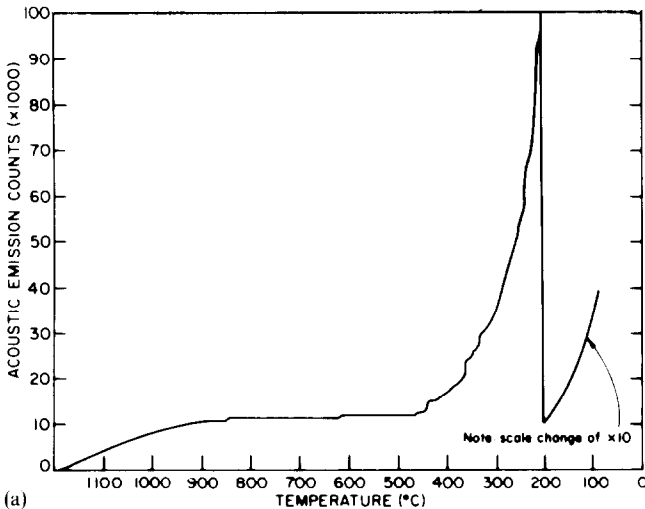


Fig. 2 (continued).



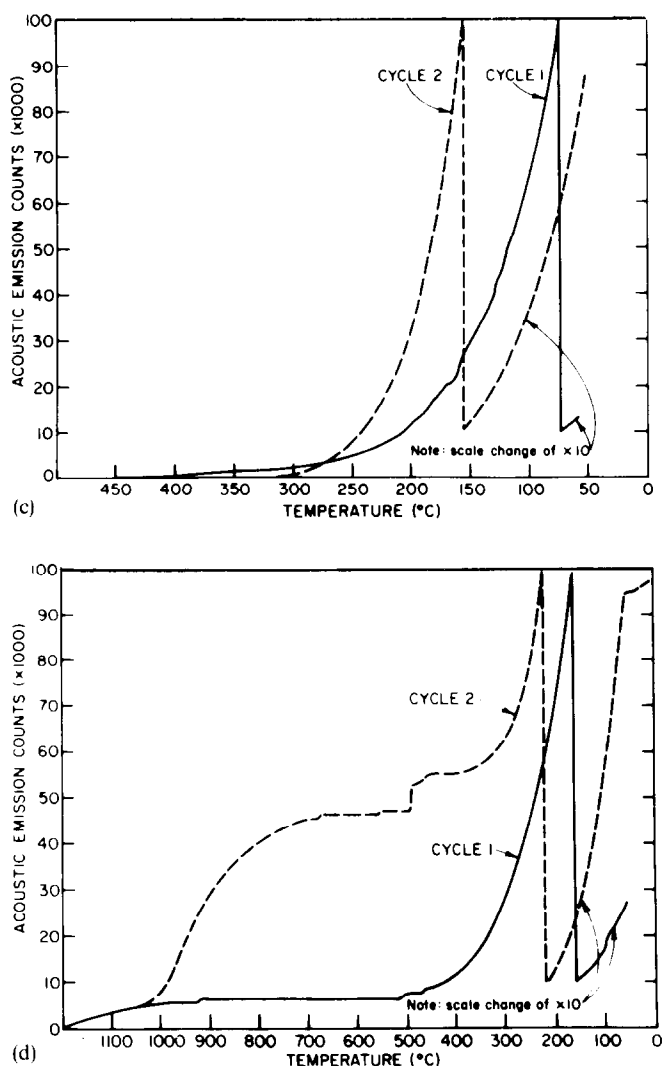


Fig. 2. Cumulative AE data: (a) specimen 21 (YSZ coated); (b) specimen 22 (preheated and YSZ coated); (c) specimen 18 (bond coated and YSZ coated); (d) specimen 20 (preheated, bond coated and YSZ coated).

The results of such an analysis are shown in Fig. 3 and are summarized in Table I. The total number of counts for a specific count rate interval are plotted with respect to the count rate interval. In this way it is possible to ascertain which *specific* count rate makes a significant contribution to the overall cracking process. The graphs also show the average temperature of the count rate interval and Table I includes the coefficient of variance (defined as  $100 \times \text{standard deviation}/\text{mean}$ ). A high coefficient of variance indicates that the counts did not occur within a narrow temperature range.

### 3.2.1. Effect of preheating the substrate

Preheating of the substrate increased the temperature where maximum counts

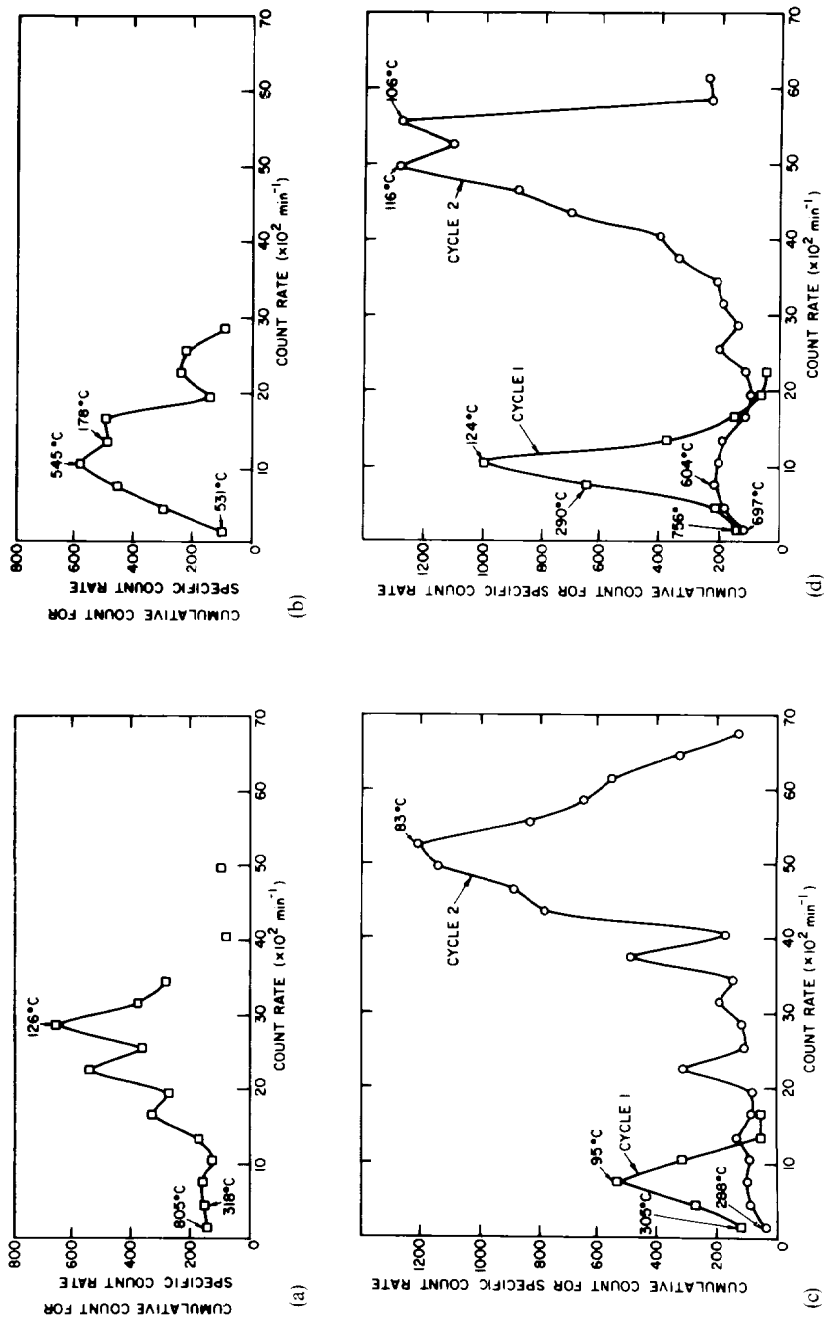


Fig. 3. Count-rate analysis of the AE data: (a) specimen 21 (YSZ coated); (b) specimen 22 (preheated and YSZ coated); (c) specimen 18 (bond coated and YSZ coated); (d) specimen 20 (preheated, bond coated and YSZ coated).

TABLE I  
SUMMARY OF ACOUSTIC EMISSION DATA ANALYSIS FOR THERMALLY CYCLED  $ZrO_2$ -12wt.% $Y_2O_3$  COATINGS

Substrate treatment and coating	Thermal cycles	Specimen <sup>a</sup>	Initial AE activity		Peak counts		Maximum count rate		Number of counts	TP/TC <sup>c</sup> (%)
			Temperature (°C)	CV <sup>b</sup> (%)	Temperature (°C)	CV <sup>b</sup> (%)	Median count rate	Temperature (°C)		
YSZ	2	15(1)	328	8	92	23	37.5	88	26	21
	1	21(1)	805	39	126	19	28.5	98	11	17
Preheat + YSZ	1	19(1)	708	44	156	26	19.5	308	36	11
	1	22(1)	531	32	545	83	10.5	156	28	13
Bond coat + YSZ	7	16(1)	406	18	139	34	10.5	135	28	38
		16(2)	361	17	74	25	76.5	82	2	11
	7	18(1)	305	79	95	40	7.5	116	30	40
		18(2)	288	6	83	19	52.5	78	9	14
Preheat + bond coat + YSZ	7	17(1)	338	22	119	155	19.5	120	1	17
		17(2)	571	42	88	36	52.5	119	25	12
	2	20(1)	756	45	124	48	10.5	95	1	37
		20(2)	697	48	116	66	49.5	105	13	13

<sup>a</sup> The number in parentheses is the run number.

<sup>b</sup> CV, coefficient of variance.

<sup>c</sup> TP, total peak counts; TC, total number of counts.

<sup>d</sup> Isolated value of 79.5 counts min<sup>-1</sup> at 1153 °C.

occurred. For example, maximum AE activity of the YSZ coating was observed at 126 °C (Fig. 3(a)) as compared with 545 °C for the preheated substrate (Fig. 3(b)). The YSZ/bond coat samples exhibited a maximum activity at 95 °C (Fig. 3(c)) as compared with 124 °C for the preheated substrates (Fig. 3(d)). It is also important to note that the preheated samples displayed a larger coefficient of variance, this being a mitigating factor in generalizing these AE trends for all of the specimens. The data show that the count rate increases during the cooling period and, for most coatings, preheating results in a low count rate which is initiated at a high temperature.

### 3.2.2. *Effect of the bond coat*

The incorporation of a bond coat decreases the peak count rate (*i.e.* the interval where most counts occur) as well as the maximum count rate. This is true for both optimally prepared and preheated substrates during the first thermal cycle. For the optimally prepared coatings the temperature range for the peak count rate is approximately the same for coatings with (95–139 °C) and without (92–126 °C) bond coats. However, preheating the substrate increased the temperature range of the peak count rate from 119–124 °C to 156–545 °C for the optimally sprayed YSZ.

### 3.2.3. *Influence of thermal cycling on acoustic emission spectra*

The second and subsequent thermal cycles of the bond-coated specimens exhibited (i) a significantly higher peak count rate at a lower temperature and (ii) a greater maximum count rate at a lower temperature. A major distinction between the optimally prepared and the preheated substrates was that the former exhibited a lower temperature for the onset of AE activity on the second thermal cycle. The preheated samples, however, started cracking at a higher temperature on cooling during the second cycle.

## 4. DISCUSSION

The central aspect of this study was to gain an understanding of how the AE phenomena are related to physical processes within the coating. The “extent of cracking” (or crack distribution and growth) is directly related to coating durability. The “cracking mechanism”, however, is a process which identifies whether failure occurs through a lamellar or translamellar cracking mechanism or through interactions between the bond coat and the substrate. The present AE analysis cannot directly be used to identify cracking mechanisms. However, the effects can be studied by correlating the results for different coatings. Thus it is certain that any specific count rate value, in itself, is the total for many different cracking events, each of which may have their own AE generation characteristics. However, since the count rates do not appear in a completely random manner, but are related to some narrow temperature range, it is our view that it is justifiable to associate a particular count rate with a specific cracking mechanism.

The effect of substrate preheating is to increase the number of cracking events immediately upon cooling (Fig. 2). The character of this *extra* activity varies for samples with and without bond coats, as shown in Fig. 3. The specimens with no bond coat which were optimally prepared (Fig. 3(a)) displayed a larger peak count rate than did samples which were preheated (Fig. 3(b)). Thus any conditioning of the substrate causes macrocracking rather than microcracking. In the case of specimens without a bond coat, these microcracks occur at a higher temperature, thus implying

pre-existing defects. This phenomenon arises from high residual stresses that are established by depositing the ceramic coating directly onto an overheated substrate. The use of a ceramic coating alone is impractical; however, the preheating effect with this specimen was used to discern a change in the cracking mechanism. It should also be remembered that both of these spraying conditions result in catastrophic coating failure upon the first thermal cycle. Therefore neither spraying procedure (*i.e.* YSZ or YSZ and preheating) should be interpreted as providing less susceptibility to coating failure.

All of the bond-coated specimens (Fig. 3) exhibited cumulative count rate peak positions at almost identical count rates for the same thermal cycle number, the only differences being that the preheated specimens exhibited more cracking on the first cycle (*i.e.* higher count value at the peak count rate) and that this occurred at higher temperatures. The AE spectra of the second cycle were almost identical, as shown in Figs. 3(c) and 3(d), but it should be remembered that these are actually displaced with respect to temperature. If this fact is taken into account, it can then be observed that the optimally prepared coating was far more crack resistant since cracking is activated by thermal stress and thus by temperature. The bond-coated specimens had the same peak count rate value as the preheated YSZ samples for the first thermal cycle. However, the temperature where this maximum AE activity occurs is much less for the bond-coated specimens, indicating more resistance to cracking. It is not straightforward to relate the peak count rates of the duplex and single coating systems because of their different cracking mechanisms.

It is interesting to notice that the peak count rate for the bond-coated specimens is the same as that for the preheated specimens without a bond coat. This leads to one of two inferences with regard to cracking mechanism. If cracks occur only within the ceramic coating, the bond coat reduces the extent of cracking (on the first cycle) since the peak in Fig. 3(c) is narrower than that in Fig. 3(b). However, if this were the only possibility then bond coating and preheating (Fig. 3(d)) have an adverse effect relative to coating integrity. However, experience does not support this conclusion. The more probable mechanism is that cracking occurs within both the bond coat and the ceramic coating. In this case the AE from both types of cracking gives rise to the peak count rate. The contribution from each type of event cannot be deconvoluted, but it is clear that the major event is bond-coat cracking. Thus if ceramic failure gives rise to a broad spectrum (Fig. 3(b)), the bond-coat effect must be significant in order for this spectrum range to decrease. Cracking within the ductile bond coat is more tolerable and preferable than failure within the brittle ceramic and thus coating integrity is improved. The shape of the AE spectrum changes significantly on further cycling because the coating structure has a high density of cracks.

Statistical techniques were used to analyze the AE spectra. Therefore it is important to appreciate the errors and the dependence (if any) of the results on the methods used. For example, count rate intervals of 100, 200, 300 and 500 showed identical results. In all the analyses, the kurtosis and the skewness parameters were approximately from +2.0 to +4.0 and from -2.0 to +2.0 respectively. The kurtosis parameter is more statistically significant since the inference is that the distributions are "highly peaked" compared with the normal distribution. Thus,  $\pm 1$  standard deviation (which is used as the error range) would incorporate more than 68% of the



observations. A major problem in interpreting AE data is the difficulty in ascertaining whether exactly the same failure phenomenon occurs within duplicate specimens. For example, equivalent specimens display up to a 55% difference in cumulative counts. However, upon normalizing the peak count with respect to the total count it is seen that the duplicates follow the same trends.

## 5. CONCLUSION

The failure mechanisms of plasma-sprayed thermal barrier coatings are a complex function of imperfections contained within the oxide coating and at the interfacial region, and the means by which these imperfections respond to thermal cycling. Cracking mechanisms, both initiation and propagation, generate significant acoustic energy which, we believe, can be used to probe these mechanisms.

Details on the statistical evaluation of acoustic emission spectra associated with the failure processes of thermal barrier coatings are presented in this paper. It is emphasized that great care must be exercised in interpretations of these results. In fact, it is our ultimate goal in this program to develop rather more straightforward correlations among AE behavior and the wide range of microstructural features which are available for study.

Several plasma spray coating parameters were varied and the changes in cracking response were analyzed. The degree of preheating and the incorporation of a bond coat significantly affects the cracking behavior as determined by AE response. The AE data can be analyzed in terms of cumulative counts or peak count rate.

It was established that preheating of the substrate gives rise to cracking of the coating during the early stages of cooling. These effects were observed whether or not a bond coat was used. The incorporation of a bond coat had a similar effect in reducing the temperature at which cracking occurred.

The cracking susceptibility, or AE count, is a measure of the coating integrity and is directly related to its performance in thermal barrier applications. Further study is clearly suggested, both of detailing the pertinent frequency spectra of the AE and of correlating such information with microscopy.

## ACKNOWLEDGMENTS

The authors wish to acknowledge the support of National Aeronautics and Space Administration (NASA) Lewis Research Center, Surface Protection Section, for support under Contract NAG3-164. The experimental work was carried out during a NASA-Case Western Reserve University Summer (1982) Faculty Fellowship.

Appreciation is extended to Robert Miller and to David Hull of NASA for their assistance and consideration.

## REFERENCES

- 1 F. J. Koubek, Microstructures of melt sprayed oxide ceramic coatings as observed by scanning electron microscope, *Proc. 3rd Annual Scanning Electron Microscopy Symp.*, April 28-30, 1970, ITT Research Institute, Chicago, IL, 1970, pp. 393-400.

- 2 F. N. Longo, Metallurgy of flame-sprayed nickel aluminide coatings, *Met. Constr. Br. Weld. J.*, **45** (1966) 66S–69S.
- 3 R. L. Apps, The influence of surface preparation on the bond strength of flame-sprayed aluminum coatings on mild steel, *J. Vac. Sci. Technol.*, **11** (1974) 741–746.
- 4 J. A. Catherall and K. E. Kortegas, Measurement of bond strength of flame-sprayed deposits, *Met. Constr. Br. Weld. J.*, **4** (1972) 11–13.
- 5 C. C. Berndt and R. McPherson, The adhesion of plasma-sprayed ceramic coatings to metals, *Mater. Sci. Res.*, **14** (1981) 619–628.
- 6 R. C. Hendricks and G. McDonald, Assessment of variations in thermal cycle life data of thermal barrier coated rods, *NASA Tech. Memo. TM81743*, April 1981 (National Aeronautics and Space Administration).
- 7 R. A. Miller and C. E. Lowell, Failure mechanisms of thermal barrier coatings exposed to elevated temperatures, *Thin Solid Films*, **92** (1982) 265–274.
- 8 N. R. Shankar, C. C. Berndt and H. Herman, Characterization of the mechanical properties of plasma-sprayed coatings, *Mater. Sci. Res.*, **15** (1983).
- 9 N. R. Shankar, C. C. Berndt and H. Herman, Failure and acoustic emission response of plasma-sprayed  $\text{ZrO}_2$ -8wt.% $\text{Y}_2\text{O}_3$  coatings, *Proc. 6th Annu. Conf. on Composites and Advanced Ceramic Materials*, in *Ceram. Eng. Sci. Proc.*, **3** (9–10) (1982) 772–792.
- 10 N. R. Shankar, C. C. Berndt, H. Herman and S. Rangaswamy, Acoustic emission from thermally-cycled plasma-sprayed oxides, *Am. Ceram. Soc., Bull.*, **62** (5) (1983) 614–619.
- 11 C. C. Berndt, Behavior of plasma-sprayed coatings, in L. L. Hench and D. R. Ulrich (eds.), *Proc. Int. Conf. on Ultrastructure Processing of Ceramics, Glasses and Composites*, Gainesville, FL, February 13–18, 1983, Wiley, New York, to be published.

#### Permission to publish

C.C. Berndt and H. Herman, 'Failure during thermal cycling of plasma-sprayed thermal barrier coatings', *Thin Solid Films*, **108**[4] (1983) 427–437.

As an Elsevier journal author, you retain various rights including Inclusion of the article in a thesis or dissertation whether in part or in toto; see [http://www.elsevier.com/about/policies/author-agreement/lightbox\\_scholarly-purposes](http://www.elsevier.com/about/policies/author-agreement/lightbox_scholarly-purposes) for more information. As this is a retained right, no written permission is necessary. This extends to the online version of your thesis and would include any version of the articles including the final published versions provided that they are not available as individual downloads but only embedded within the thesis itself.

## PERFORMANCE OF THERMAL BARRIER COATINGS IN HIGH HEAT FLUX ENVIRONMENTS\*

ROBERT A. MILLER AND CHRISTOPHER C. BERNDT

*Lewis Research Center, National Aeronautics and Space Administration, Cleveland, OH 44135 (U.S.A.)*

(Received March 19, 1984; accepted April 9, 1984)

Thermal barrier coatings were exposed to the high temperature and high heat flux produced by a 30 kW plasma torch. Analysis of the specimen heating rates indicates that the temperature drop across the thickness of the 0.038 cm ceramic layer was about 1100°C after 0.5 s in the flame. An as-sprayed  $\text{ZrO}_2$ -8wt.% $\text{Y}_2\text{O}_3$  specimen survived 3000 of the 0.5 s cycles without failing. Surface spalling was observed when 2.5 s cycles were employed but this was attributed to uneven heating caused by surface roughness. This surface spalling was prevented by smoothing the surface with silicon carbide paper or by laser glazing. A coated specimen with no surface modification but which was heat treated in argon also did not surface spall. Heat treatment in air led to spalling in as early as one cycle from heating stresses. Failures at edges were investigated and shown to be a minor source of concern. Ceramic coatings formed from  $\text{ZrO}_2$ -12wt.% $\text{Y}_2\text{O}_3$  or  $\text{ZrO}_2$ -20wt.% $\text{Y}_2\text{O}_3$  were shown to be unsuited for use under the high heat flux conditions of this study.

## 1. INTRODUCTION

A thermal barrier coating system with sufficient durability to survive on airfoil surfaces in a research gas turbine engine with moderately high heat fluxes and moderately high temperatures was first reported in the mid-1970s<sup>1,2</sup>. However, this early thermal barrier coating system, which consisted of a layer of air-plasma-sprayed  $\text{ZrO}_2$ -12wt.% $\text{Y}_2\text{O}_3$  applied directly over a layer of air-plasma-sprayed Ni-Cr-Al-Y bond coat, was unable to survive in an advanced research gas turbine engine<sup>3</sup>. Thermal barrier coatings have now been improved to the extent that they are used in revenue service on vane platforms in advanced commercial gas turbine engines<sup>4</sup>. Among the more significant advances responsible for this current success is the discovery that a  $\text{ZrO}_2$ -8wt.% $\text{Y}_2\text{O}_3$  coating is much more durable than the earlier  $\text{ZrO}_2$ -12wt.% $\text{Y}_2\text{O}_3$  version<sup>5</sup>. Possible reasons for this have been discussed by Miller *et al.*<sup>6</sup>

In the future, advanced engines operating at heat fluxes greater than those

\* Paper presented at the International Conference on Metallurgical Coatings, San Diego, CA, U.S.A., April 9-13, 1984.

characteristic of current engines will require thermal barrier coatings for protecting airfoil surfaces. The testing which has led to advances in coating performance has been conducted in the low to moderate heat flux environment of furnaces and burner rigs. The initiation of coating failure in such rigs is associated with thermal expansion mismatch strain encountered on cooling and with time-at-temperature effects such as bond coat oxidation and plastic deformation<sup>7</sup>. Strains encountered on heating in such rigs are not severe enough to initiate coating failure<sup>7</sup>. It is not yet known whether strains encountered on heating in a gas turbine engine are severe enough to contribute to failure initiation.

Therefore testing procedures must be devised that allow determination of when the thermal loads developed on rapid heating become severe enough to initiate coating failure. This information may then be used to guide the processing of coatings for improved tolerance to such loads. In this study, a commercial plasma torch has been used as a high heat flux source. Various plasma-sprayed  $\text{ZrO}_2\text{-Y}_2\text{O}_3$  thermal barrier coating systems were exposed in this rig and the response of these coatings to the high heat flux environment generated was characterized.

The plasma torch rig used for this study is intended to serve as an interim rig until a high pressure burner rig and a rocket engine test rig dedicated to materials research are available at the Lewis Research Center. Precedents for this type of test exist<sup>8,9</sup>. The torch is relatively simple and inexpensive to operate. Possible disadvantages of this rig include the small flame diameter and the extremely high gas temperature attained.

## 2. EXPERIMENTAL DETAILS

A schematic diagram of the test rig is shown in Fig. 1. The plasma torch shown is operated at a power level of 30 kW. The nitrogen arc gas flow rate was  $2800 \text{ l h}^{-1}$ . The distance from the exit nozzle of the torch to the specimen is 4.4 cm. Specimens are held in the flame for cycles of length 0.5, 2.5 or 5.0 s followed by 30, 75 or 120 s of forced air cooling. An additional 0.50 s is required for the specimen to move between the cooling position and the heating position, and specimen heating begins before the specimens are fully in the heating position. Therefore effective heating times may be taken as 0.1 s longer than the nominal times.

Test specimens were solid superalloy rods 1.3 cm in diameter. Usually the alloy

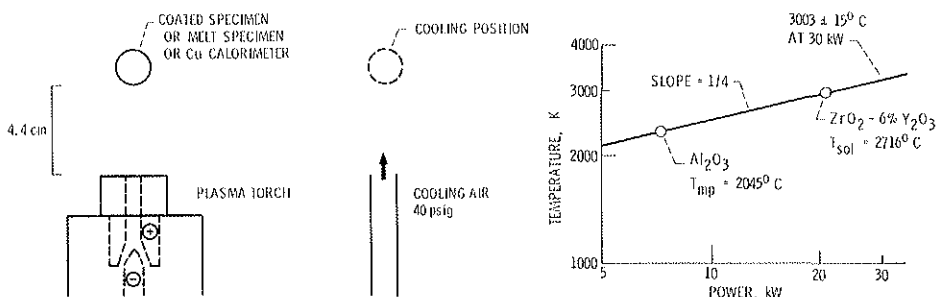


Fig. 1. Schematic diagram of a plasma torch test rig.

Fig. 2. Plasma torch arc power vs. apparent gas temperature.

was René 41. The thermal barrier coatings consisted of 0.013 cm of bond coat which was usually Ni-14wt.%Cr-14wt.%Al-0.1wt.%Zr under a 0.038 cm layer of plasma-sprayed  $\text{ZrO}_2\text{-Y}_2\text{O}_3$  ceramic. The  $\text{Y}_2\text{O}_3$  level was usually 8 wt.%; 12 and 20 wt.%  $\text{Y}_2\text{O}_3$  ceramics were also investigated. Sintered starting powders were used for the 8 and 12 wt.%  $\text{Y}_2\text{O}_3$  compositions while a non-reacted composite powder was used for the 20 wt.%  $\text{Y}_2\text{O}_3$  composition.

Specimens were tested in the as-sprayed condition, after heat treating in air or in argon, and after surface treatment by smoothing with silicon carbide paper or laser glazing. The laser-glazed specimens were only available as hollow cylindrical specimens.

### 3. RESULTS AND DISCUSSION

#### 3.1. Characterization of the plasma flame and of specimen heating rates

The apparent gas temperature of a 30 kW nitrogen plasma at a distance of 4.4 cm from the nozzle was determined through measurement of the power required to melt small samples of  $\text{Al}_2\text{O}_3$  or  $\text{ZrO}_2\text{-6wt.\%Y}_2\text{O}_3$ . A plot of the logarithm of the known melting (or solidus) points *versus* the logarithm of the power required to melt the samples gives a line of slope 0.25 as shown in Fig. 2. This slope arises from the Stefan-Boltzmann relationship and is consistent with the assumption that heat is transferred from the cathode of the plasma torch to the plasma by radiation<sup>10</sup> and from the gas to the samples by convection and conduction<sup>11</sup>.

Extrapolation of the line in Fig. 2 to 30 kW yields an apparent flame temperature of 3000 °C. The actual gas temperature may differ somewhat since heat will be lost from the sample by radiation or gained by aerodynamic heating.

The coefficient of heat transfer from the gas to the sample was measured to be  $0.2 \text{ W cm}^{-2} \text{ }^\circ\text{C}^{-1}$ . A button calorimeter similar to those described in refs. 9 and 12 but of simplified design was used for this determination. The heat transfer coefficient and the apparent gas temperature were used to calculate the temperature distributions in the coated specimens as a function of time. A one-dimensional finite difference model was used for this calculation. The computer code employed was taken from ref. 13 (the reader is cautioned that there are several errors in the FORTRAN listing given in ref. 13). Values for the thermal conductivities and heat capacities of the bond coat and ceramic were taken from ref. 14. Values pertaining to 500 °C were used.

The calculated heating rates at the ceramic surface and at the interface with the bond coat are presented in Fig. 3. An initial response at 0.1 s was assumed as explained in the experimental section. Temperatures measured with a thermocouple centered 0.076 cm below the interface are also shown on the plot. These temperatures appear to be consistent with the calculated interface temperatures. The time at which the surface of the specimen was observed to be fully glowing in a 1/8000 s photograph is also indicated on the plot. This time corresponds to a calculated surface temperature of about 1100 °C, and the observation of glowing at this temperature seems plausible in view of the very short exposure time.

A very large  $\Delta T$  between the surface and the interface has been achieved in this test. At 0.5 s this difference is almost 1100 °C. As shown in the figure this is much greater than the  $\Delta T$  calculated for a 0.018 cm ceramic coating in a research gas



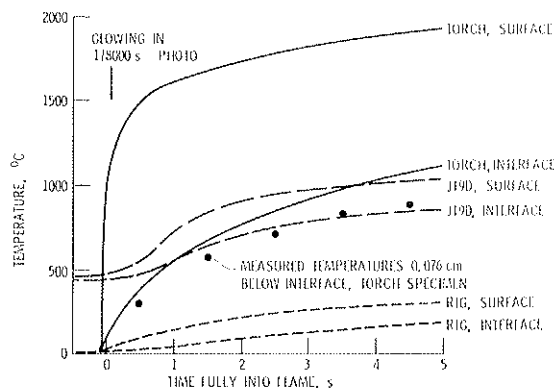


Fig. 3. Calculated heating rates at the ceramic layer surface and the interface with the bond coat for a 0.038 cm ceramic coating in the plasma torch (—) or Mach 0.3 burner rig (···) or a 0.018 cm ceramic coating in a research gas turbine engine (---).

turbine engine during the take-off portion of the cycle<sup>3</sup> and is greater still than the  $\Delta T$  for a 0.038 cm coating in a Mach 0.3 burner rig<sup>15</sup>.

One can calculate the compressive thermal strain at the surface of the ceramic relative to the mean thermal strain in the ceramic from the expression<sup>16</sup>

$$\varepsilon = \alpha(\bar{T} - T_{\text{surf}}) \quad (1)$$

where  $\alpha$  is the thermal expansion coefficient of the ceramic—about  $10^{-5}$  (ref. 17)—and  $\bar{T}$  is the mean temperature in the ceramic layer. The values of the relative strain calculated from eqn. (1) are  $-0.57\%$ ,  $-0.48\%$  and  $-0.42\%$  at 0.5 s, 2.5 s and 5.0 s respectively. It may be noted that surface compressive strains are larger after 0.5 s than after 2.5 or 5.0 s. A complete calculation of strain would include ceramic-metal thermal expansion mismatch strains and residual stress.

From the above analysis it is apparent that the thermal loads imposed on coated specimens in this plasma torch rig are much more severe than those to be expected in a gas turbine engine.

### 3.2. Response of thermal barrier coating to high heat flux

The results of this investigation are displayed in Fig. 4. In this figure the composition of the ceramic, the pretreatment given to the specimen, the duration of the heat cycle and the type of failure observed (if any) are given. The total number of cycles is represented by the length of the bar. A pointed arrow indicates no failure. The test was terminated if no failure was observed after 1000 cycles of 0.5 s or after 100 cycles of 2.5 s. An exception was case A which ran for 3000 cycles before removal from the test.

Case A pertains to as-sprayed  $\text{ZrO}_2\text{-}8\text{wt.}\% \text{Y}_2\text{O}_3$  ceramic and the lack of failure after 3000 cycles is quite encouraging. When the cycle duration was increased to 2.5 s or 5.0 s (cases B and C respectively) then surface spalling was observed after 15 cycles. This surface spalling was observed even though the relative surface strains at the end of the 0.5 s cycles exceeded those at the end of the 2.5 s cycles. A photograph of the surface of the specimen from case B is shown in Fig. 5. In case C the surface spalling was accompanied by surface melting even though the calculated

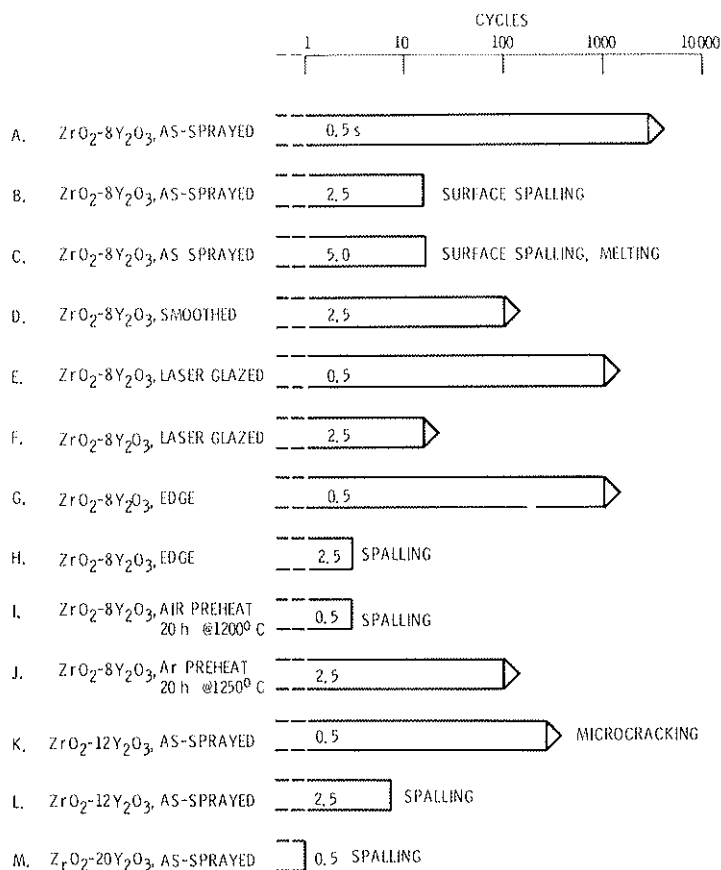


Fig. 4. Response of 0.038 cm ZrO<sub>2</sub>-Y<sub>2</sub>O<sub>3</sub> coatings to 0.5, 2.5 and 5.0 s exposure cycles in a 30 kW (3000 °C) plasma flame.

temperature after 5 s (see Fig. 3) was about 800 °C lower than the melting point of the ceramic. This indicates that there must be local hot spots on the rough surface. High speed photography indicated that some regions of the rough specimen began to glow almost 0.1 s before the surface came to a full glow. This local glowing occurs even before the specimen comes fully into position. Therefore it can be expected that there will be areas of severe local stress concentration at the rough surface of a specimen exposed to these very high temperatures.

Smoothing the coating surface with silicon carbide paper (case D and Fig. 6) prevents surface spalling. This smoothing reduced the measured roughness (arithmetic average) from about 10 µm to about 4 µm. A laser-glazed specimen did not surface spall after 15 2.5 s cycles (case F). The results for the laser-glazed specimen must be considered preliminary because the only specimens available at the time of this study were on hollow substrates which had previously been tested to failure in the hot zone region in a burner rig test. Regions away from the failure area were exposed in the plasma torch rig. The specimen in case F actually spalled after 20 cycles. However, at the present time it is not known whether this may have been due

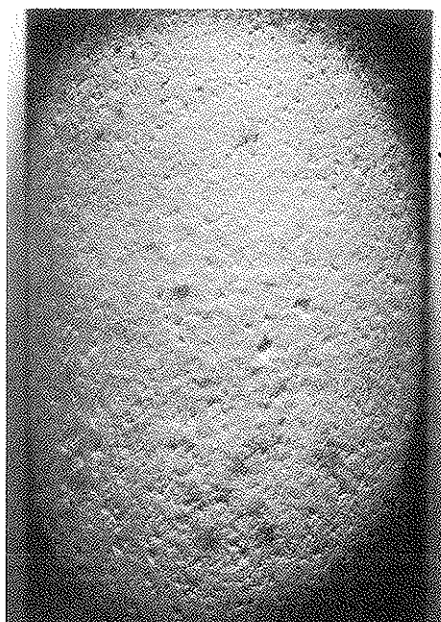


Fig. 5. As-sprayed  $\text{ZrO}_2$ -8wt.% $\text{Y}_2\text{O}_3$  specimen after 15 cycles of 2.5 s (case B) in a 30 kW plasma flame.

Fig. 6. Smoothed  $\text{ZrO}_2$ -8wt.% $\text{Y}_2\text{O}_3$  specimen after 100 cycles of 2.5 s (case D) in a 30 kW plasma flame.

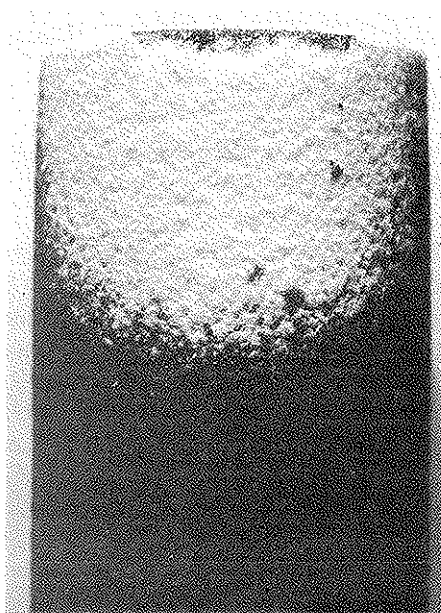
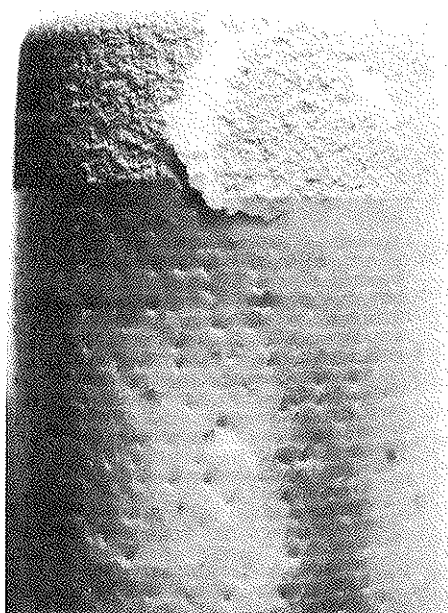


Fig. 7. Laser-glazed  $\text{ZrO}_2$ -8wt.% $\text{Y}_2\text{O}_3$  specimen after the first 25 of a total of 1000 cycles of 0.5 s (case E) in a 30 kW plasma flame. The hot zone is near the bottom. Edge effect cracking of the coating occurs on the hollow specimen in the unglazed region near the top.

Fig. 8. Edge of a  $\text{ZrO}_2$ -8wt.% $\text{Y}_2\text{O}_3$  specimen after three cycles (case H) in a 30 kW plasma flame.

to some factor such as overheating of the hollow specimen. The laser-glazed specimen in case E survived 1000 cycles of 0.5 s but it cracked and eventually spalled in the unglazed region near the upper edge as shown in Fig. 7. It should be noted that the cracks emanating from the unglazed areas dissipate once they reach the mudcracked laser-glazed region. Thus, even though the results on laser-glazed specimens are preliminary, this process (which has been discussed by Zaplatynsky<sup>18</sup>) is promising for high heat flux applications.

Since spalling had been observed at the edge of the hollow specimen in case E, the response of a solid specimen to heating at an edge was investigated. No edge effect spalling was observed after 1000 cycles of 0.5 s (case G). However, a minor amount of edge spalling was observed after three of the 2.5 s cycles (case H and Fig. 8).

Case I indicates that there is a strong correlation between oxidation and spalling on heating. A specimen which had received a relatively severe oxidative heat treatment—20 h at 1200 °C in air—spalled in the first cycle in one test (Fig. 9) and in the third cycle in another test. Presumably the ceramic had been weakened near the interface with the bond coat as a result of strains induced by the formation of an oxide layer at the interface combined with thermal expansion mismatch strains encountered on cooling. A specimen heated for 20 h at 1250 °C in an inert environment (case J and Fig. 10) did not spall and did not even surface spall after 100 cycles of 2.5 s.

A specimen coated with  $\text{ZrO}_2$ -12wt.% $\text{Y}_2\text{O}_3$  was severely microcracked after



Fig. 9. Preoxidized  $\text{ZrO}_2$ -8wt.% $\text{Y}_2\text{O}_3$  specimen (20 h at 1200 °C main) after one 0.5 s cycle (case I) in a 30 kW plasma flame.

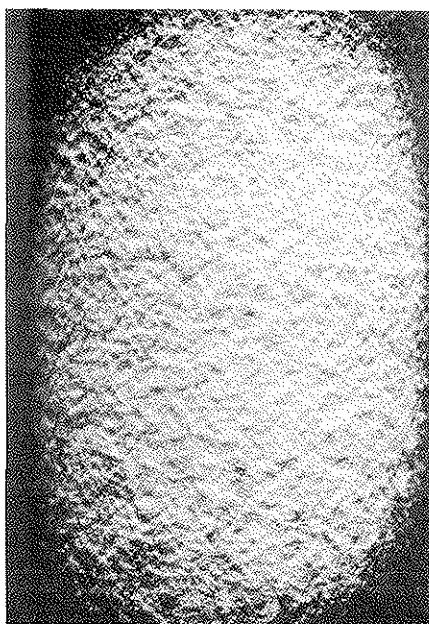


Fig. 10.  $\text{ZrO}_2$ -8wt.% $\text{Y}_2\text{O}_3$  specimen (heat treated in argon for 20 h at 1250 °C) after 100 cycles of 2.5 s (case J) in a 30 kW plasma.

250 cycles of 0.5 s (case K). This specimen was subsequently destroyed when it became stuck in the heating position. Another  $\text{ZrO}_2$ -12wt.% $\text{Y}_2\text{O}_3$  specimen began to spall after seven 2.5 s cycles (case L). Three  $\text{ZrO}_2$ -20wt.% $\text{Y}_2\text{O}_3$  specimens (case M) spalled during the first cycle.

#### 4. CONCLUSION

The above results show that thermal barrier coatings with a ceramic layer based on  $\text{ZrO}_2$ -8wt.% $\text{Y}_2\text{O}_3$  can withstand thermal strains greatly in excess of those expected in a gas turbine engine. Surface spalling associated with extremely high gas temperatures was encountered but this could be prevented by smoothing the surface with silicon carbide paper. Heat treatment in an inert environment may also prevent surface spalling. Results on laser-glazed specimens are preliminary, but it appears that glazed specimens also withstand heating stresses quite well.

Oxidation appears to induce spalling on heating. Thus oxidation has been implicated as a key factor in coating failure both in the heating mode in high heat flux plasma torch tests and in the cooling mode in moderate heat flux burner rig tests. This observation is cause for concern regarding the use of coatings for long periods of time in a high heat flux environment. Therefore the effects of oxidation require further investigation. Spalling at an edge may be a minor concern. Coatings formed from  $\text{ZrO}_2$ -12wt.% $\text{Y}_2\text{O}_3$  or  $\text{ZrO}_2$ -20wt.% $\text{Y}_2\text{O}_3$  were unsuitable for use at the high heat flux generated by the plasma torch.

#### REFERENCES

- 1 S. Stecura, *NASA Tech. Memo. TM X-3425*, 1976 (National Aeronautics and Space Administration).
- 2 C. H. Liebert, R. E. Jacobs, S. Stecura and C. R. Morse, *NASA Tech. Memo. TM X-3410*, 1976 (National Aeronautics and Space Administration).
- 3 W. R. Sevcik and B. L. Stoner, *NASA Contract. Rep. CR-135360*, 1978 (National Aeronautics and Space Administration; Pratt and Whitney Aircraft).
- 4 K. D. Sheffler, R. A. Graziani and G. C. Sinko, *NASA Contract. Rep. CR-167964*, 1982 (National Aeronautics and Space Administration; Pratt and Whitney Aircraft).
- 5 S. Stecura, *NASA Tech. Memo. TM-78976*, 1979 (National Aeronautics and Space Administration).
- 6 R. A. Miller, R. G. Garlick and J. L. Smialek, *Am. Ceram. Soc., Bull.*, 62 (1983) 1355.
- 7 R. A. Miller and C. E. Lowell, *Thin Solid Films*, 95 (1982) 265.
- 8 A. N. Curren, S. J. Grisaffe and K. C. Wycoff, *NASA Tech. Memo. TM X-2461*, 1972 (National Aeronautics and Space Administration).
- 9 H. E. Smith and J. C. Wurst, *Rep. ASD-TDR-623-655*, 1962 (Wright-Patterson Air Force Base).
- 10 C. W. Change and J. Szekely, *J. Met.*, 34 (1982) 57.
- 11 M. Usheo, J. Szekely and C. W. Chang, *Ironmak. Steelmak.*, (1981) 279.
- 12 J. Hummik, Jr., *High Temperature Inorganic Coatings*, Reinhold, New York, 1963, pp. 197-198.
- 13 H. Schenk, Jr., *FORTTRAN Methods in Heat Flow*, Ronald Press, New York, 1959, pp. 93-106.
- 14 P. A. Siemers and W. B. Hillig, *NASA Contract. Rep. CR-165351*, 1981 (National Aeronautics and Space Administration; General Electric Company).
- 15 G. McDonald and R. C. Hendricks, *Thin Solid Films*, 73 (1980) 491.
- 16 S. S. Manson, *Thermal Stress and Low-Cycle Fatigue*, McGraw-Hill, New York, 1966, p. 277.
- 17 C. C. Berndt and H. Herman, *Ceram. Eng. Sci. Proc.*, 3 (1982) 792.
- 18 I. Zaplatynsky, *Thin Solid Films*, 95 (1982) 275.



# Performance of Thermal Barrier Coatings in High Heat Flux Environments

**Robert A. Miller**  
*Lewis Research Center*  
*Cleveland, Ohio*

and

**Christopher C. Berndt**  
*Cleveland State University*  
*Cleveland, Ohio*

Permission to publish

R.A. Miller and C.C. Berndt, 'Performance Of Thermal Barrier Coatings In High Heat Flux Environments', *Thin Solid Films*, 119 (1984) 195-202. [also in NASA Tech. Memorandum 83663, April 1984].

As an Elsevier journal author, you retain various rights including Inclusion of the article in a thesis or dissertation whether in part or in toto; see [http://www.elsevier.com/about/policies/author-agreement/lightbox\\_scholarly-purposes](http://www.elsevier.com/about/policies/author-agreement/lightbox_scholarly-purposes) for more information. As this is a retained right, no written permission is necessary. This extends to the online version of your thesis and would include any version of the articles including the final published versions provided that they are not available as individual downloads but only embedded within the thesis itself.

Note: The previous publication arose from and is identical to NASA TM 83663.

Prepared for the  
International Conference on Metallurgical Coatings  
sponsored by the American Vacuum Society  
San Diego, California, April 9-13, 1984

## Chapter 6. Advancement of Knowledge

### 6.1 Introduction

Section 6 of the “Higher Doctorate Application” form indicates that ‘A statement of the applicant’s view of the extent to which the work contributes to the advancement of knowledge’ is required.

Chapter 6 consists of manuscript #20, ‘Full critical review: A review of testing methods for thermal spray coatings’, and the following extract summarises the development of the understanding within this body of work.

‘An important aspect of this work is to highlight the extrinsic nature of mechanical property measurements with regard to thermal spray coatings. Thermal spray coatings exhibit anisotropic behaviour and microstructural artefacts such as porosity and the splat structure of coatings influence the mechanical characterisation methods. The analysis of coating data variability evolving from the different measurement techniques is of particular relevance to interpret the character of thermal spray deposits.’

Further review articles in this thesis are (i) manuscript #7 on ‘Measurement of adhesion for thermally sprayed materials’; (ii) manuscript #14 on ‘Thermal Spray Maps: Material Genomics of Processing Technologies’; and manuscript #15 on ‘Material fundamentals and clinical performance of plasma-sprayed hydroxyapatite coatings: A review’.

There are a total of 27 review and summary articles presented by the applicant in Appendix 7 and these are listed below.

4
12
88
105
106
107
108
118
119

136
142
199
208
265
302
308
321
322

323
335
336
346
399
412
447
451
459

# A review of testing methods for thermal spray coatings

Andrew Siao Ming Ang<sup>1</sup> and Christopher C. Berndt<sup>1,2\*</sup>

The primary focus of this review concerns the test methods used to evaluate thermal spray coatings. Techniques to measure coating intrinsic properties such as (i) porosity and (ii) residual stress state; as well as extrinsic mechanical properties that include (iii) hardness, (iv) adhesion, (v) elastic modulus, (vi) fracture toughness, and (vi) the Poisson's ratio of thermal spray coatings are presented. This review also encompasses the feedstock and thermal spray method since process variants create a specific microstructure. An important aspect of this work is to highlight the extrinsic nature of mechanical property measurements with regard to thermal spray coatings. Thermal spray coatings exhibit anisotropic behaviour and microstructural artefacts such as porosity and the splat structure of coatings influence the mechanical characterisation methods. The analysis of coating data variability evolving from the different measurement techniques is of particular relevance to interpret the character of thermal spray deposits. Many materials can be thermal sprayed but this review focuses on alumina and partially stabilised zirconia since (i) these materials have many proven applications, and (ii) there is a wealth of information that has been reported on these ceramics.

**Keywords:** Tensile adhesion testing, Porosity, Microhardness, Elastic modulus, Fracture toughness, Poisson's ratio, Thermal spray coatings, Residual stress, Anisotropic, Microstructure–property relationships

## Introduction

The rapid solidification and stacking of molten metal or ceramic splats by multiple passes of the spray torch form the fundamental building blocks of a thermal spray coating.<sup>1,2</sup> The so-formed splat anatomy is the result of the spatial interaction of three inputs; i.e., the feedstock distribution and associated physical characteristics, the temperature–velocity field of the heat source, and the temperature–velocity fields of the particles.<sup>3,4</sup> In practical terms, the spreading of the molten particles during splat formation,<sup>5</sup> along with other important artefacts such as oxides and voids can be controlled by the feedstock and thermal spray processes employed. The term ‘voids’ is inclusive of cracks and porosity.

The thermal spray process selected by the operator dictates the flame jet temperature and particle velocity, which together are known as the TV relationships.<sup>6,7</sup> It is important to note that the modern (post year 2000) interpretation of TV relationships pertains to the properties of the in-flight particle, which includes information concerning the particle size distribution.<sup>8,9</sup> The flame jet temperature provides the operator with a reference point concerning the degree of melting of the sprayed material.

Particle velocity refers to the value before impact with the substrate and is imparted by an inert carrier gas and the velocity field of the flame jet. The combination of feedstock material and size must be considered with regard to the thermal spray process; that is, different feedstocks present microstructural differences that reflect on physical property measurements. Therefore, a retrospective review of commercial feedstocks and thermal spray methods is relevant.

The coating architecture and associated microstructural properties are also examined; including the porosity and cracking behaviour, as well as its residual stress state. In addition, although thermal spray coatings have been produced for specific applications, certain mutual mechanical properties exist. These mechanical properties are often used to determine the structural integrity of the component. This review presents a focussed critique on measurement techniques that enables an improved understanding of performance–property relationships.

## Thermal spray feedstock

Feedstock is a generic term that is applied to materials that are fed into a thermal spray device. Feedstock materials for a thermal spray device can be classified into three categories: (i) powders, (ii) rods and wires, and (iii) solutions and suspensions. The following discussion refers largely to powder feedstock, unless otherwise stated, since this is the prime product for the thermal spray market.

<sup>1</sup>Industrial Research Institute Swinburne, Swinburne University of Technology, H66, PO Box 218, Hawthorn, VIC 3122, Australia

<sup>2</sup>Department of Materials Science and Engineering, Stony Brook University, Stony Brook, NY 11794, USA

\*Corresponding author, [REDACTED]

A key prerequisite for a feedstock is its transportation to the thermal spray device in a regular and consistent flow; and this is termed as the ‘flowability of the feedstock’. Powders are fed *via* polymer tubes with an internal diameter of  $\sim 3$  mm for distances of up to 5 m. Table 1 lists commercial powder feedstocks and the associated thermal spray method that is typically used. The particulate morphology will manifest itself in the coating architecture; therefore, an understanding of this feature is critical when interpreting material properties.

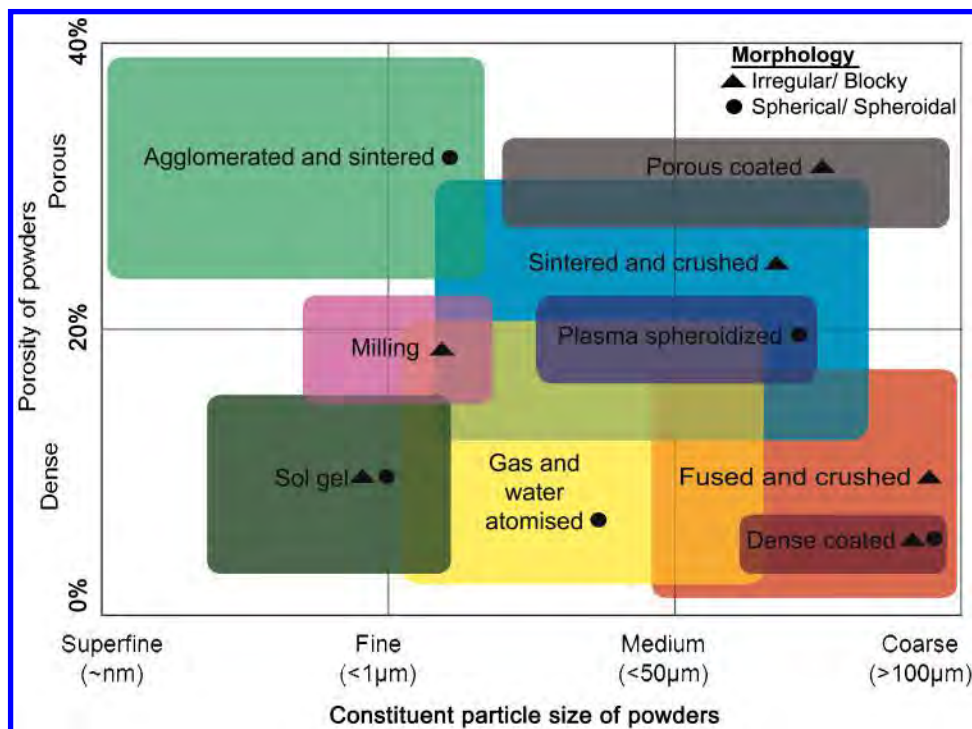
The principal characteristics of all feedstocks are linked to their manufacturing process.<sup>10–14</sup> In essence, the feedstock that is injected into the torch is transformed into a highly oriented coating structure with lamellae that lie approximately parallel to the substrate surface. This unique microstructure determines the properties of the thermal spray coating because the individual splats can be viewed as the fundamental building blocks of the coating. It is widely recognised that no thermal spray process or post-coating procedure can

**Table 1** Compilation of commercially available powders sorted by application method

Coating type	Material constituents	Application method <sup>+</sup>	Typical particle size*	Approximate melting point
Metal/metallic alloy	Al, Al–Si	APS	–90+45 $\mu\text{m}$ [–170+325 mesh]	660°C [1220 F]
		CS	–45 $\mu\text{m}$ [–325 mesh]	
		FS	–90+45 $\mu\text{m}$ [–170+325 mesh]	
	Cu, Cu–Ni, Cu–Al	HVOF	–88+31 $\mu\text{m}$ [–170 mesh+31 $\mu\text{m}$ ]	Cu: 1083°C [1981 F] Cu–Al: 1040°C [1904 F] Cu–Ni: 1205°C [2201 F]
		APS	–75+45 $\mu\text{m}$ [–200+325 mesh]	
		CS	–35+15 $\mu\text{m}$ [–400 mesh+15 $\mu\text{m}$ ]	
		FS	–75+45 $\mu\text{m}$ [–200+325 mesh]	
		VPS	–90+22 $\mu\text{m}$ [–170 mesh+22 $\mu\text{m}$ ]	
	Ti, Ta	CS	–63 $\mu\text{m}$ [–230 mesh]	Ti: 1665°C [3029 F]
		APS	–106+45 $\mu\text{m}$ [–140+325 mesh]	
	FeCr, FeCrNiMo, FeCr-based	HVOF	–45+5.5 $\mu\text{m}$ [–325 mesh+5.5 $\mu\text{m}$ ]	815–1200°C [1499–2192 F]
		FS	–125+45 $\mu\text{m}$ [–120+325 mesh]	
		APS	–38+5 $\mu\text{m}$ [–400 mesh+5 $\mu\text{m}$ ]	>1120°C [>2048 F]
	MCrAlY (M=Co, Ni, Fe)	HVOF	–45+22 $\mu\text{m}$ [–325 mesh+22 $\mu\text{m}$ ]	
		VPS	–38+5 $\mu\text{m}$ [–400 mesh+5 $\mu\text{m}$ ]	
	Mo, Mo-based Ni, Ni–Cr, Ni–Al, Ni-based	APS	–90+38 $\mu\text{m}$ [–170+400 mesh]	2620°C [4748 F] 1232–1453°C [2250–2647 F]
		APS	–106+45 $\mu\text{m}$ [–140+325 mesh]	
		FS	–125+45 $\mu\text{m}$ [–120+325 mesh]	
		CS	–30+10 $\mu\text{m}$	
		HVOF	–45+11 $\mu\text{m}$ [–325 mesh+11 $\mu\text{m}$ ]	
		VPS	–37 $\mu\text{m}$ [–400 mesh]	
		APS	–150+7.8 $\mu\text{m}$ [–100 mesh+7.8 $\mu\text{m}$ ]	
		FS	–125+5 $\mu\text{m}$ [–120 mesh+5 $\mu\text{m}$ ]	
Metallic composite	Al–Si-based abrasives	APS	–176+11 $\mu\text{m}$ [–80 mesh+11 $\mu\text{m}$ ]	577°C [1071 F] ~1140°C [2084 F] 1453°C [2647 F] 1040°C [1904 F]
	CoNi-based abrasives	FS	–90+30 $\mu\text{m}$ [–170 mesh+30 $\mu\text{m}$ ]	
	Ni-based abrasives	HVOF	–45+15 $\mu\text{m}$ [–325 mesh+15 $\mu\text{m}$ ]	
	Cu–Al–Bronze-based	APS	–125+11 $\mu\text{m}$ [–120 mesh+11 $\mu\text{m}$ ]	
		FS	–106+45 $\mu\text{m}$ [–140+325 mesh]	
		HVOF	–45+11 $\mu\text{m}$ [–325 mesh+11 $\mu\text{m}$ ]	
Intermetallic	CoCrNiWC, CoCr-based	APS	–45+15 $\mu\text{m}$ [–325 mesh+15 $\mu\text{m}$ ]	1230–1600°C [2246–2912 F]
		FS	–75+45 $\mu\text{m}$ [–200+325 mesh]	
		FS	–106+45 $\mu\text{m}$ [–140+325 mesh]	
		HVOF	–45+11 $\mu\text{m}$ [–325 mesh+11 $\mu\text{m}$ ]	
Cermets	NiCrSiB, NiCrSiB-based, self-fluxing alloys	APS	–90+45 $\mu\text{m}$ [–170+325 mesh]	2620°C [4748 F] 1930°C [3506 F]
		APS	–53+11 $\mu\text{m}$ [–270 mesh+11 $\mu\text{m}$ ]	
		HVOF	–38+10 $\mu\text{m}$ [–400 mesh+10 $\mu\text{m}$ ]	
	Mo–Mo <sub>2</sub> C CrC–NiCr, CrC–Ni-based	FS	–53+11 $\mu\text{m}$ [–270 mesh+11 $\mu\text{m}$ ]	
		APS	–53+11 $\mu\text{m}$ [–270 mesh+11 $\mu\text{m}$ ]	
		HVOF	–45+11 $\mu\text{m}$ [–325 mesh+11 $\mu\text{m}$ ]	
Ceramic	WC–Co, WC–Ni, WC-based	APS	–53+11 $\mu\text{m}$ [–270 mesh+11 $\mu\text{m}$ ]	1250–1480°C [2282–2696 F]
		FS	–90+45 $\mu\text{m}$ [–170+325 mesh]	
		HVOF	–45+11 $\mu\text{m}$ [–325 mesh+11 $\mu\text{m}$ ]	
	Al <sub>2</sub> O <sub>3</sub> , Al <sub>2</sub> O <sub>3</sub> –TiO <sub>2</sub>	FS	–90+45 $\mu\text{m}$ [–170+325 mesh]	2054°C [3729 F] 3 wt% TiO <sub>2</sub> : 2040°C [3704 F] 13 wt% TiO <sub>2</sub> : 2000°C [3632 F] 40 wt% TiO <sub>2</sub> : 1840°C [3344 F]
		APS	–45+5 $\mu\text{m}$ [–325 mesh+5 $\mu\text{m}$ ]	
		FS	–45+5 $\mu\text{m}$ [–325 mesh+5 $\mu\text{m}$ ]	
	Cr <sub>2</sub> O <sub>3</sub> , Cr <sub>2</sub> O <sub>3</sub> –TiO <sub>2</sub> , Cr <sub>2</sub> O <sub>3</sub> –TiO <sub>2</sub> –SiO <sub>2</sub> , TiO <sub>2</sub>	APS	–106+30 $\mu\text{m}$ [–140 mesh+30 $\mu\text{m}$ ]	2435°C [4415 F] 1843°C [3349 F]
		FS	–125+7.8 $\mu\text{m}$ [–120 mesh+7.8 $\mu\text{m}$ ]	
		APS	–88+7.8 $\mu\text{m}$ [–170 mesh+7.8 $\mu\text{m}$ ]	
	ZrO <sub>2</sub> –Y <sub>2</sub> O <sub>3</sub> , ZrO <sub>2</sub> –MgO, ZrO <sub>2</sub> -based	FS	–88+7.8 $\mu\text{m}$ [–170 mesh+7.8 $\mu\text{m}$ ]	CaO: 2565°C [4649 F] MgO: 2140°C [3884 F] TiO <sub>2</sub> : 2535°C [4595 F] 20 wt% Y <sub>2</sub> O <sub>3</sub> : 2480°C [4496 F] 8 wt% Y <sub>2</sub> O <sub>3</sub> : 2800°C [5072 F]
		APS	–125+11 $\mu\text{m}$ [–170 mesh+11 $\mu\text{m}$ ]	
		APS	–125+11 $\mu\text{m}$ [–170 mesh+11 $\mu\text{m}$ ]	

+ FS: flame spray; APS: atmospheric plasma spray; VPS: vacuum plasma spray; HVOF: high velocity oxygen fuel spray; CS: cold spray.

\* All particle sizes have been presented in absolute terms. ‘–90+45  $\mu\text{m}$ ’ indicates that the particle size lies between 45 and 90  $\mu\text{m}$ . US mesh sizes have been presented where appropriate.



Note: 50 µm is about mesh 270 and 100 µm is about mesh 140

# 1 Powder production methods and their classification with respect to powder porosity and grain size

compensate for a poor quality feedstock; that is, the oxide content in coatings can never be lower than that of the sprayed feedstock.<sup>15,16</sup> It is vital that the feedstock be of high quality to obtain correspondingly high-quality coatings.

The important characteristics for thermal spray feedstock, other than the starting chemical composition, include the particle size distribution, bulk density, morphology, and grain size.<sup>17</sup> Similar materials with identical chemical composition, for instance alumina or tungsten carbide, can have distinctive characteristics that depend on the powder manufacturing process. Figure 1 presents a map that summarises the manufacturing routes and relates them to the porosity and grain fineness. In general terms, more dense particles are likely to form dense coatings that exhibit mechanical properties more akin to the bulk material.

The typical powder size ranges for feedstock used in thermal spray are from 15 to 45 µm [mesh–325 + 15 µm] (termed as ‘a fine cut’) and 45 to 106 µm [mesh–140 + 325] (termed as ‘a coarse cut’)<sup>\*1</sup>. Other size permutations, such as a narrow cut from 5 to 22 µm [mesh–500 + 5 µm], can be specified and it is generally accepted that a narrow powder size distribution will produce more homogenous coating properties.<sup>18,19</sup> In general terms, particle size ranges of 20–60 µm [mesh–230 + 632] are preferred to form coatings of high integrity. However, the more recent sol gel technologies are also capable of forming fine grained, dense coatings that exhibit good mechanical properties.<sup>20,21</sup>

In any spray torch setup, regardless of axial or radial particle injection, the average particle speed at the injector exit port is independent<sup>22</sup> of the particle size

distribution for a given feed condition. In other words, for a specified carrier gas flow and injector port diameter, the friction and collision among particles results in similar injected particle velocities. However, the individual particle momentums would be diverse due to their different specific masses and, thus, the distribution of particle trajectories within the spray jet often exhibits a large spread. Consequently, the final impact velocities and temperatures imparted from the energetic spray jet to the feedstock particles will be affected and cause coating property variations.<sup>23</sup>

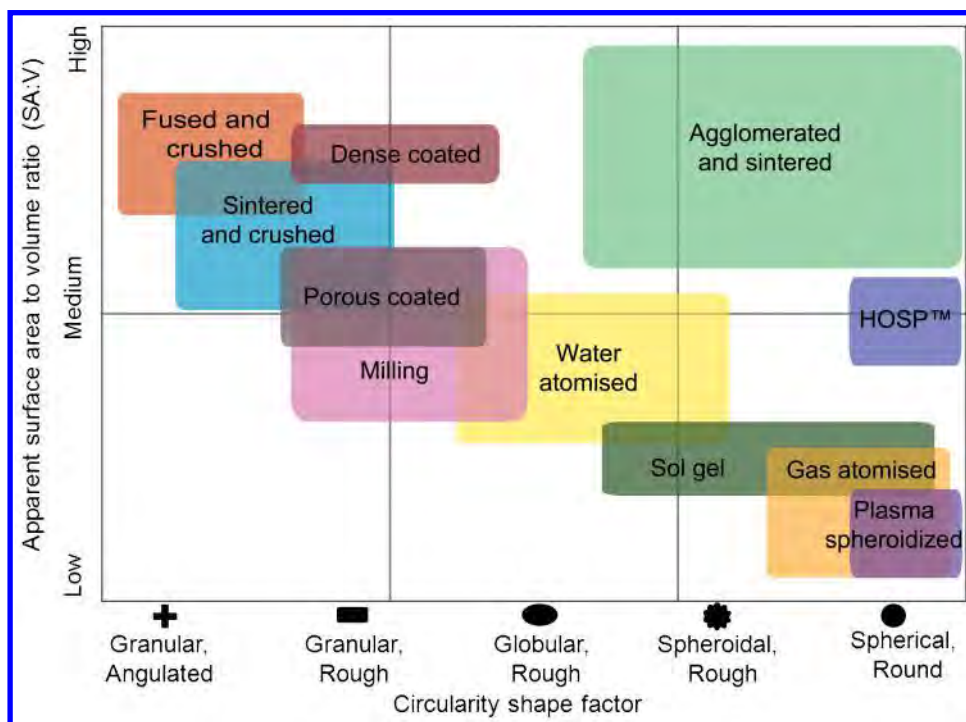
Another variable that influences the particle impingement velocity and temperature is the particle morphology and porosity content. Feedstocks of different morphology but of similar chemical composition require an optimisation process to achieve a coating with comparable properties.<sup>24</sup> For instance, hollow spherical powders<sup>25,26</sup> (HOSP<sup>TM</sup>)\*<sup>2</sup> exhibit excellent flow properties and their low mass allows consistent melting in the high temperature plasma spray jet.<sup>27</sup> With reference to Fig. 1, it can be seen that feedstock porosity level varies with respect to the production methods. The intrinsic grain size of the powder particles and morphology can also be altered by the production method, which suggests different surface area to volume ratios (SA : V). Also, the morphologies of feedstocks can be described by the circularity shape factor, measured by two-dimensional image analysis (IA)<sup>28</sup> and defined as

$$\text{Circularity shape factor} = \frac{4\pi A_p}{P_f^2} \quad (1)$$

\*<sup>1</sup>Absolute particle sizes are presented from the smallest to the largest particle size. However, relative sizes, such as mesh values, are presented in the reverse order; i.e., from the largest to the smallest particle size. As well, a common abbreviation for ‘mesh’ is ‘#’.

\*<sup>2</sup>The expansion of the acronym ‘HOSP’ is ambiguous in the literature’. For example, ‘hot oven spherical particles’, ‘hollow oxide spherical particles’, and ‘homogeneous special particles’ have been reported. The indicated reference from the patent literature unambiguously indicates that the correct expansion is ‘hollow spherical particles’.





2 Classification of powder surface to volume ratio with respect to shape factor. The circularity shape factor varies from 0.16 for a granular and angulated feedstock to 1.00 for a spherical particle

where  $A_p$  is based on the projected area of the feedstock particle and  $P_f$  is the perimeter of the feedstock.

A classification of SA : V and circularity shape factor of powders manufactured *via* different production routes is shown in Fig. 2. It can be noted that for particles of similar size, spherical particles will exhibit the least SA:V compared to blocky feedstock. In addition, porous or agglomerated powders reveal a greater surface area compared to dense, spherical powders. This finding relates to the heat transfer and melting of powders during thermal spraying, which ultimately controls the coating mechanical properties. Materials with large SA : V (i.e. very porous or blocky in morphology) are heated more rapidly because the increase in surface area benefits heat transfer processes.

There is also the potential for irregular pulsing during spray torch operation. Irregular powder flow can arise from either (i) insufficient carrier gas flow, or (ii) overloading of the feeding system with a too-high powder delivery rate. In both of these instances the irregular feeding is manifested by spasmodic powder flow that is technically known as 'saltation'.<sup>1</sup> This observation is indicative of sequential powder clogging and discharging within the feed tube because of pressure fluctuations in the powder delivery equipment. This processing condition will be reflected in the formation of a heterogeneous microstructure with clumping of unmelts or porous features; all of which influence mechanical properties.

With regard to the powder grain sizes, there has been interest in the production of nanostructured coatings, similar to ceramic nano-composites proposed by Niihara,<sup>29</sup> in which nano-sized particles are either dispersed within the matrix grains or at the grain boundaries of the matrix (see Fig. 3). However, one constraint of thermal spraying is the formation of nanostructured coatings from nano-sized primary particles. First, conventional powder feeding techniques

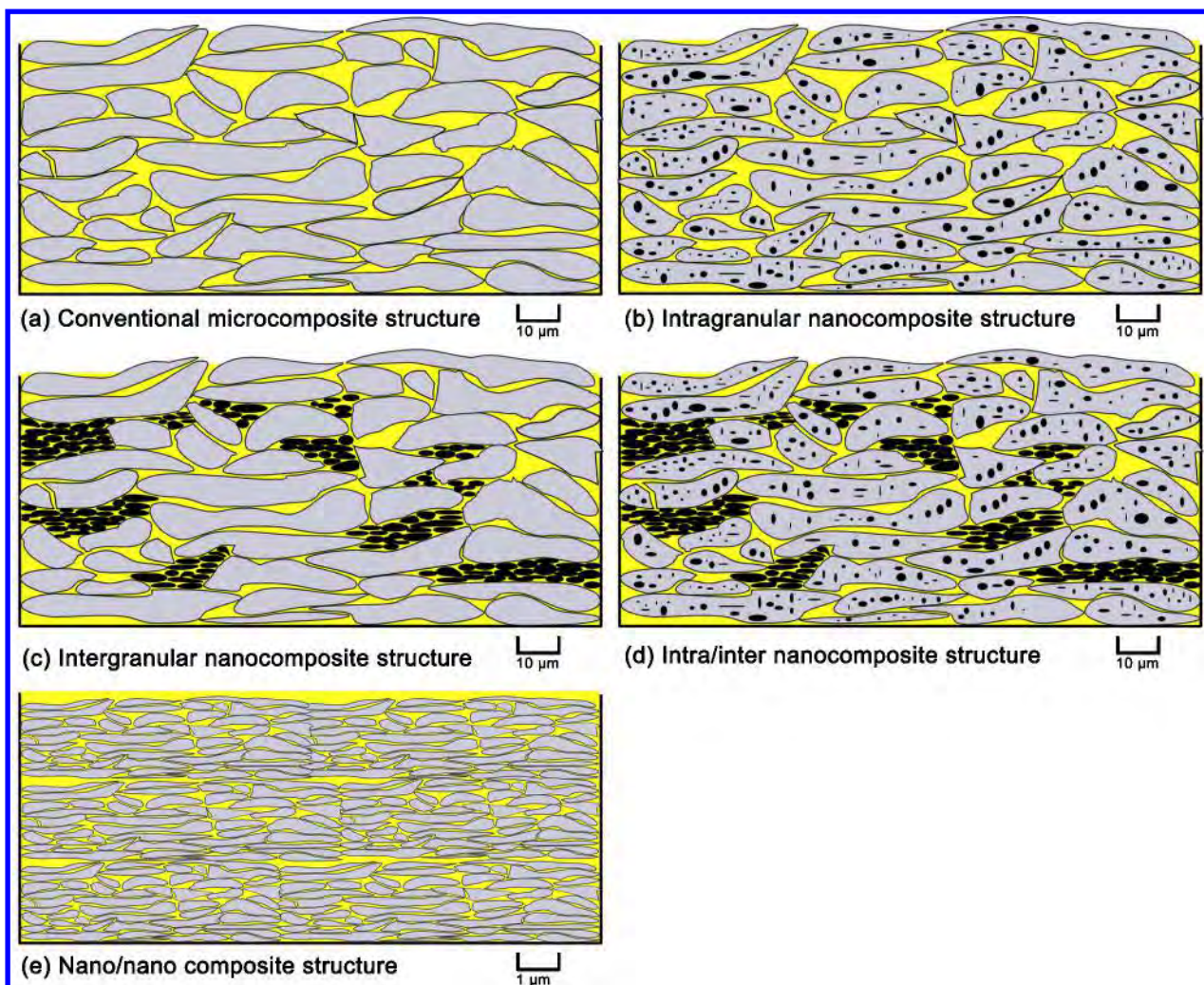
and equipment cannot deal with feedstock sizes below 10  $\mu\text{m}$ . Second, strong agglomeration of the nano-scaled powder prevents good flowability.<sup>30,31</sup> Third, potential health hazards exist because the nano-particles may be distributed into the atmosphere and absorbed by human skin or into the respiratory system.<sup>32,33</sup>

The approach to overcome these issues is to pre-agglomerate the primary nano-particles into micro-metre-sized feedstock.<sup>34,35</sup> However, it has been reported that agglomerated particles may either lose their nanostructure<sup>36–38</sup> or undergo undesirable chemical changes owing to melting and solidification.<sup>39</sup> With reference to the current work that focuses on mechanical properties; certain types of nano-composite coatings demonstrate significant advantages in terms of mechanical strength and fracture resistance when reducing the splat grain size.<sup>40,41</sup>

Another approach taken to achieve nanostructured coatings is *via* sol-gel or suspension plasma spraying.<sup>42–45</sup> Much research has been undertaken by Fauchais and coworkers<sup>12</sup> to understand the challenges encountered in this novel process. The as-sprayed coatings of suspension plasma sprayed alumina, yttria stabilised zirconia (YSZ) and metal oxides have been reported<sup>42–45</sup> to surpass the performance of conventional plasma spray deposits.

## Thermal spray processes

Thermal spray processes can be classified into three broad families: (i) the use of combustion heat sources; namely the flame, detonation gun and high velocity oxygen fuel spray (HVOF) processes; (ii) another uses electrical energy; either in the form of plasma or as an arc, and (iii) the third is a recent extension to the thermal spray family<sup>46</sup> and is known as cold spray, kinetic spray or hypersonic spray, which uses the energy that evolves from gas expansion. Figure 4 shows the relationship



**3 Classification of nanocomposite structures in thermal spray coatings. Note that the typical scale for a type (e) structure is more refined**

among the achievable particle velocity, particle temperature and the typical feedstock size.<sup>13</sup> This process map is different from the conventional TV map in three respects: (i) the temperature and velocity are represented in terms of the optimised particles rather than the effluent environment, (ii) there is an overlay for material class on the right hand side, and (iii) a logarithm scale for the feedstock particle size is used.

### Fuel gas processes

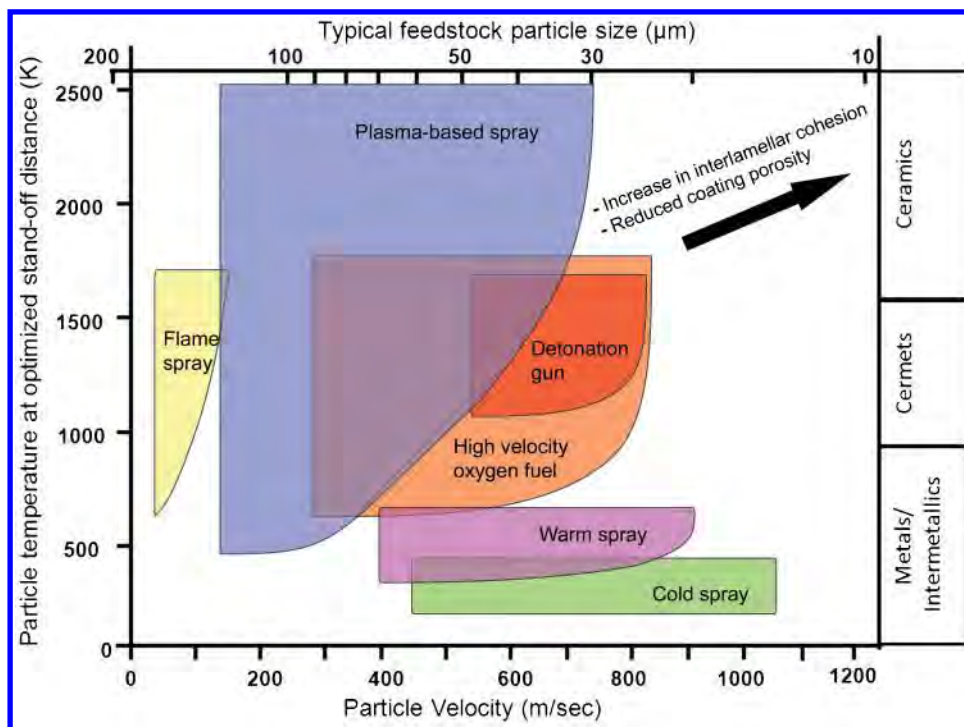
The flame spray (FS) process was first described by M.U. Schoop's patent in 1912<sup>47</sup> and represented the rudimentary form of the combustion process; which now accounts for 30–45% of the worldwide thermal spray coating business.<sup>48,49</sup> In conventional FS torches, a stream of fuel and oxygen is combusted externally at the nozzle tip while powders are introduced axially into the flame *via* an inert carrier gas such as argon or nitrogen. The feedstock can also be in the form of wires or rods, in which a carrier gas is not needed. This process yields the lowest particle acceleration ( $>200 \text{ m s}^{-1}$ ) because the fuel gases are supplied at low pressure and combustion occurs at atmospheric pressure outside the torch; that is: FS employs an open, non-confined flame. Flame jet temperatures in excess of 2900 K may be obtained depending on the type of fuel gas and the oxygen/fuel gas ratio, Table 2.<sup>50</sup> Propane provides the lowest flame

temperature while acetylene will generate the highest temperature. Figure 5 shows the relationship of flame jet temperature with respect to the oxygen/fuel ratio of different fuel gases.<sup>51</sup>

The detonation gun, D-Gun®, process is a proprietary process developed by Union Carbide Inc.<sup>52</sup> in the 1950s. Coating services are now offered under Praxair Surface Technologies Inc., the company that evolved from Union Carbide Inc. Russian researchers have also developed a similar patented process.<sup>53</sup> The working principle of the torch is based on generating a high energy pressure wave through repeated ignition of an explosive mixture, usually acetylene and oxygen, within a long, constricted tube. The thermal output and detonation pressure waves, operating at 3–15 Hz, are intense and represent the TV source that heats and accelerates the powder particles towards the substrate. D-Gun® coatings have achieved dense coatings with high bond strength<sup>54,55</sup> and they have been compared to plasma spray coatings under conditions of abrasion and erosion wear resistance.<sup>56</sup> In general, D-Gun® coatings outperform plasma spray coatings in niche markets but they are not as versatile as other thermal spray coatings with regard to materials selection, equipment availability and engineering design of the component.

The high velocity oxygen fuel spray process, developed and marketed in the early 1980s by Browning and





4 Classification of thermal spray processes in accordance with particle velocity, particle temperature and average feedstock size. The right hand scale indicates the range of materials that correspond, approximately, to each spray process

coworkers, uses high kinetic energy and controlled thermal output to produce dense, low porosity coatings.<sup>57</sup> Unlike the exclusive D-Gun® process, variants of HVOF systems are regularly being introduced by equipment manufacturers. The operating characteristics are based on a continuous combustion of the fuel gas mixture supplied at high volumetric flow to the burning chamber of the torch. Process gas selections include propylene, propane, hydrogen or natural gas used in gas-fuelled systems and kerosene in liquid-fuelled systems.<sup>58</sup>

Table 3 shows the HVOF torches that use these fuels and their typical oxygen-to-fuel ratio for combustion. The torches in Table 3 have been ranked in accordance to their chronological development. The increase in combustion rate of the DJ series torches over the JetKote™ is evident while the use of liquid fuel, i.e., kerosene, provides increased particle acceleration.<sup>59</sup> Recent developments of HVOF spray systems have aimed predominantly at optimising the combustion, minimising fuel consumption, and increasing the particle acceleration.

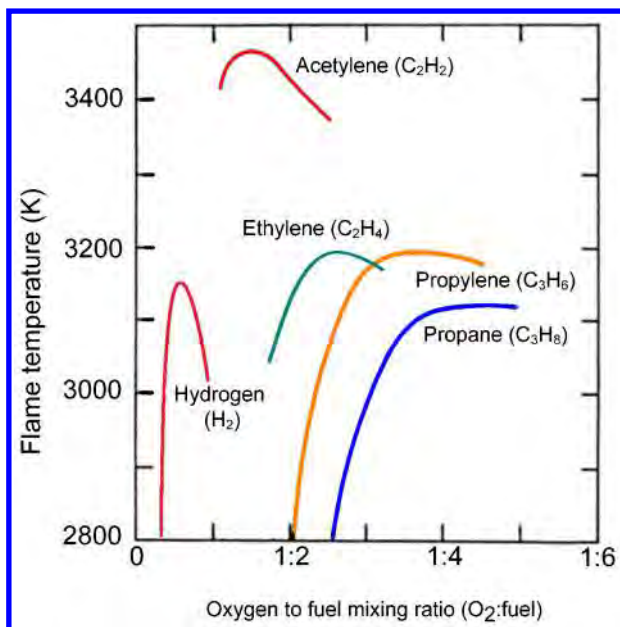
Depending on the fuel gas used and torch design, the combustion jet temperatures reach 4000 K and the energies are in the order of 288–1000 MJ h<sup>-1</sup> (80–278 kW). After passing the nozzle, the gas velocities are

in excess of 1800 m s<sup>-1</sup>, resulting in the formation of a 'shock' diamond pattern within the exiting flame jet. The feedstock, in powdered form, is usually axially fed through the torch using an inert carrier gas such as nitrogen. The ignited gases surround and heat the powdered spray material as it exits the torch and particle velocities may reach 800 m s<sup>-1</sup>.<sup>60,61</sup> As a result of the high kinetic energy transferred to the particles through the HVOF process, the coating material generally does not need to be fully molten.<sup>61,62</sup> Instead, the powder particles can be in a semi molten state so that they flatten plastically on impact against the work piece.

High velocity oxygen fuel spray coatings often exhibit densities of >95% and adhesion values greater than 10000 lb in<sup>-2</sup> (69 MPa).<sup>1,63</sup> High velocity oxygen fuel spray coatings demonstrate lower residual internal stresses<sup>64,65</sup> compared to air plasma spray coatings because the coating deposition temperatures are significantly lower; and hence reduce the tensile quenching stresses experienced by the splats as they cool and solidify. In addition, peening stresses are generated when particles impact at high velocity. These stresses induce compressive stresses that superimpose and reduce the prior-formed tensile quenching stresses.<sup>66</sup> Therefore, dense HVOF coatings of up to 2 mm can be deposited.<sup>67,68</sup> The feedstock undergoes a short flame residence time,

Table 2 Properties of typical fuel gas for flame spraying arranged in the order of ascending flame temperature<sup>50</sup>

Fuel gas	Chemical formula	Maximum flame temperature/K/[F]	Calorific value/MJ m <sup>-3</sup> /[Btu ft <sup>-3</sup> ]	Required oxygen to fuel ratio for:	
				Maximum surface temperature	Stoichiometry
Propane	C <sub>3</sub> H <sub>8</sub>	3101 [5122]	93.2 [2501]	4.5	5.0
Hydrogen	H <sub>2</sub>	3129 [5173]	10.8 [290]	0.42	0.5
Propylene	C <sub>3</sub> H <sub>6</sub>	3169 [5245]	27.6 [741]	3.7	4.5
Ethylene	C <sub>2</sub> H <sub>4</sub>	3197 [5295]	59.5 [1597]	2.4	3.0
Acetylene	C <sub>2</sub> H <sub>2</sub>	3433 [5720]	56.4 [1513]	1.5	2.5



5 Common process gases used for the flame spray (FS) process

measured in milliseconds,<sup>69</sup> that minimises excessive metal oxidation, decarburisation or phase changes.<sup>70,71</sup>

### Plasma processes

Energy sources for the thermal plasmas used in spray equipment are usually the DC electric arc or RF discharge that create arc energies of 72–720 MJ h<sup>-1</sup> (20–200 kW).<sup>1</sup> Plasma temperatures in the heating region range from 6000 to 15 000 K; significantly above the melting point of any known material.<sup>72,73</sup> In the field of thermal spray, thermal plasmas are employed in atmospheric plasma spray (APS), vacuum plasma spray (VPS; and also called low pressure plasma spray, LPPS<sup>TM</sup>), and controlled atmospheric plasma spray (CAPS) processes. Atmospheric plasma spray is extensively discussed in the following sections because it is a common coating method that can serve as a model for typical thermal spray processes.

The plasma jet flow influences the trajectories of feedstock owing to the relative amount of momentum imparted to the in-flight particles.<sup>74–76</sup> There is a large temperature drop of several thousand degrees centigrade over a few millimetres from the jet core to the boundary

between the nozzle and the environment, and the velocity also decays rapidly as the jet exits from the nozzle.<sup>72</sup> Thus, depending on the design of the plasma torch,<sup>77,78</sup> there will be variations to the kinetic energy<sup>76</sup> imparted to the feedstock that influence the final coating microstructure.<sup>79,80</sup> In addition, the feeding position of the feedstock is usually in the radial direction. Axial injection, such as employed for the Mettech Axial III<sup>TM</sup> DC plasma torch, has claimed attributes in terms of improved heat transfer to the particles.<sup>73,81</sup>

Another important point to discuss in DC plasma spraying concerns arc root fluctuations for stick type plasma torches.<sup>82,83</sup> These fluctuations arise because of (i) the movement induced by the drag force of the gas flowing in the cold boundary layer, and (ii) the magneto hydrodynamic forces that result from arc short circuits. The corresponding transient voltage can exhibit a restrike, take-over or mixed mode that leads to voltage fluctuations of  $\pm 35\%$ .<sup>84</sup> The frequency of voltage fluctuations, ranging between 3 and 8 kHz, depends strongly on the condition of the torch anode and its operating parameters.<sup>83</sup> A peak frequency at around 4 kHz is usually observed<sup>85,86</sup> for stick type plasma torches. Such fluctuations influence the plasma jet velocity and, subsequently, the melting of feedstock for coating formation.<sup>83,87,88</sup>

The feedstock particle temperature and velocity during plasma spraying is also sensitive to torch parameters such as input power, arc gas flow, carrier gas, spray distance and type of plasma arc gases used. A summary of plasma spray process parameters has been compiled by Gerdeman and Hecht;<sup>89</sup> which are depicted in Fig. 6. Many parameter settings have been studied extensively<sup>90–92</sup> and, for instance, Mash *et al.*<sup>90</sup> have schematically illustrated the effects of some process variables on the coating deposition efficiency in Fig. 7.

### Wire arc spray process

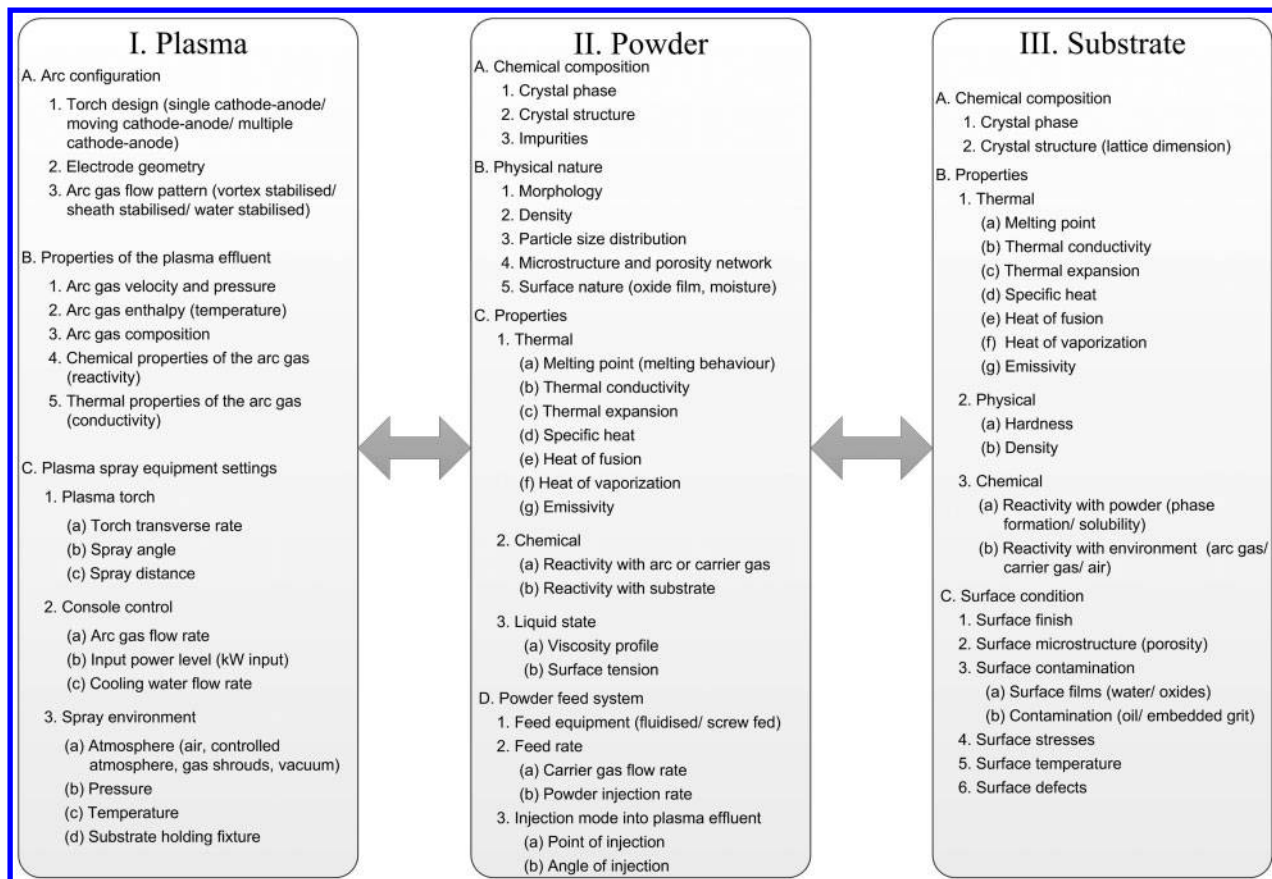
The twin wire arc (TWA) spray process originated from a patent of M.U. Schoop in 1910.<sup>93</sup> It is a reliable, economical and commonly used method for depositing metal coatings for, mainly, corrosion protection applications. The principal technical details are simple: a direct current electric arc is formed between two consumable electrode wires and a high velocity gas jet propels the molten material towards the substrate. The temperature within the arc jet ( $\sim 7000$  K) is sufficient to

Table 3 Properties of typical high velocity oxygen fuel spray (HVOF) fuels and torch combinations\*

Torch (year)	Fuel gas option	Fuel flow/L min <sup>-1</sup>	Oxygen flow/L min <sup>-1</sup>	Air flow/L min <sup>-1</sup>	Oxygen to fuel ratio <sup>†</sup>
JetKote®, Deloro Stellite (1982)	Hydrogen	432	302	–	0.7
	Propane	50	350	–	7.0
	Ethylene	80	337	–	4.2
Top Gun, UTP (1989)	Hydrogen	432	217	–	0.5
	Propane	50	250	–	5.0
	Ethylene	80	240	–	3.0
DJ2600, Sulzer Metco (1989)	Hydrogen	613	214	344	0.47
DJ2700, Sulzer Metco (1994)	Propane	189	278	391	1.90
	Ethylene	111	247	360	2.91
	Propane	68	240	375	4.67
JP-5000®, Praxair (1992)	Kerosene	0.379	876	–	2314
WokaStar <sup>TM</sup> , Sulzer Metco (2004)	Kerosene	0.379	876	–	2314
GTV K2, GTV (2005)	Kerosene	0.372	820	–	2204

\* Compiled from (i) equipment manufacturers published technical data and (ii) typical spray tables provided from feedstock suppliers.

† The values for the liquid feed processes are high since the liquid flow rates are comparatively low.



Adapted from Ref. 89

## 6 Summary of plasma spray process parameters

melt the consumable electrodes, which are atomised into particles, accelerated and deposited onto the substrate. Thus, the thermal efficiency of the wire arc spray is greater than other thermal spray processes because the particles are in a fully molten state when they enter the spray jet. Deposition efficiencies of up to 99.5% have been reported but typical spray efficiencies lie in the range of 58%\*<sup>3</sup> due to practical application limitations.<sup>94</sup>

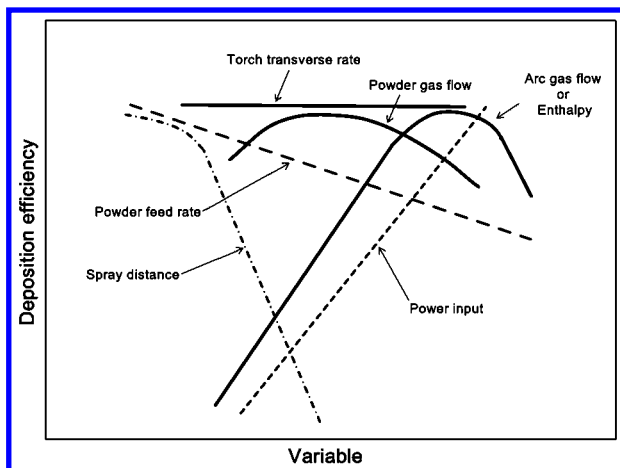
The molten particles start cooling immediately after leaving the arc zone. Therefore, coating properties such as porosity and adhesion can be affected. Developments of this process, such as high velocity nozzle caps, have opened up new applications with particle velocities

similar to those experienced for HVOF processes. Wire arc spraying is not limited to metal wires; for instance, cored wires consist of powdered materials such as carbides or amorphous alloys that are contained within a nickel or iron-based metal sheath.

## Cold spray process

The cold spray process of thermal spray was discovered during the mid-1980s.<sup>95</sup> It was established that when a particle-laden supersonic gas jet impinged onto a solid surface, above a particular minimum particle velocity, then the abrasion caused by the metal particles transitioned to adhesion of the particles.<sup>96</sup> The relatively small and unmelted particles, ranging in size from approximately 1–50 µm in diameter, deformed and subsequently a coating deposited onto an appropriate substrate. The phenomenon of 'cold spray' was coined. It was further found that the coating effect was enhanced by an increase in gas temperature.<sup>46,97</sup>

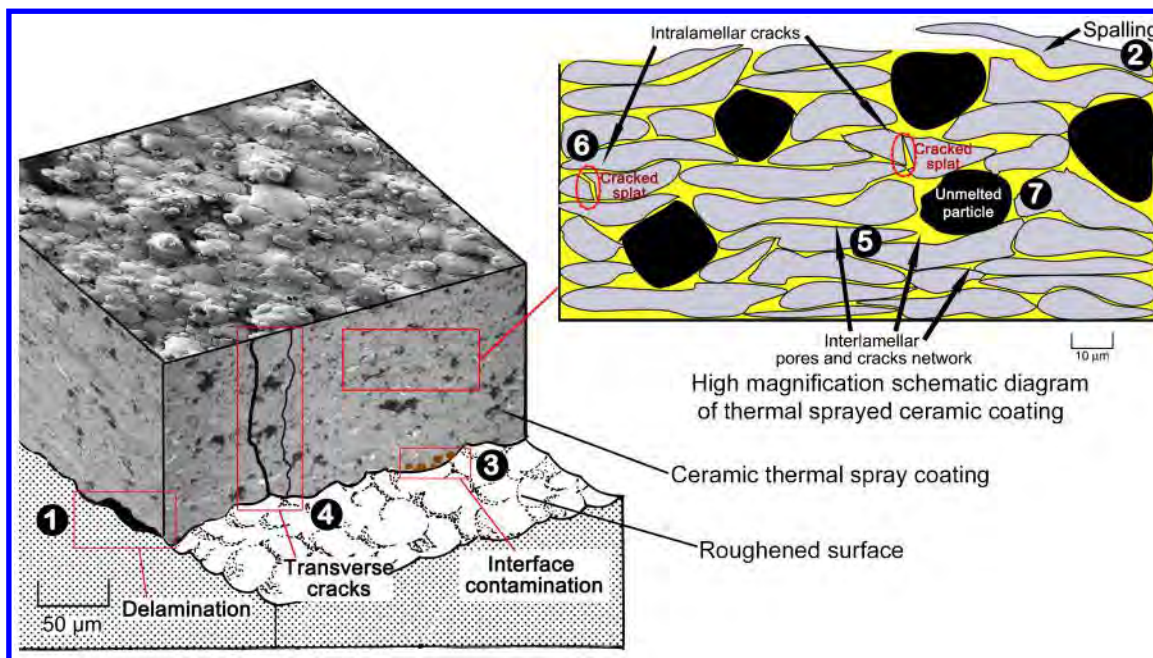
The most distinguishing feature of the cold spray process is an ability to produce coatings with preheated gas temperatures in the range of 0–800°C, a range that is lower than the melting temperature of the feedstock.<sup>98</sup> Consequently, the deleterious effects of high temperature oxidation, decarburisation, melting, residual stress, de-bonding, gas release, and other concerns associated with high temperature thermal spray processes are

The figure has been redrawn from the original paper<sup>90</sup>

## 7 Effect of plasma spray parameters on deposition efficiency

\*<sup>3</sup>The 'deposition efficiency' is determined from spray experiments on a flat or round test coupon that is most likely to be unrepresentative of the practical job. The 'spray efficiency', however, relates to the engineering component that is likely to have a complex, 3-D geometry. Thus, the spray efficiency is always less than the deposition efficiency.





The numbered features are keyed to Table 4. Feature 8 is not indicated since this is an artefact arising from the metallographic preparation technique

#### 8 Illustration of a ceramic thermal spray coating microstructure

reduced.<sup>1,46,99</sup> The size distribution of the powder is also important and powder cuts between 10 and 40 µm are favoured to obtain dense cold spray coatings.<sup>100</sup>

The mechanism by which the solid state particles deform and bond, both to the substrate and to each other, is not well understood. However, modelling<sup>101</sup> of cold spray processes shows a change in almost all key parameters near the particle interface with the beginning of unstable adiabatic shear at the interface. The shear instability is characteristically associated with high strain rate deformation. Experimental, theoretical, and computational investigations have also documented the formation of 'surface scrubbing' jets; that is, high interfacial pressures that disrupt the oxide films on the particle and substrate surfaces. The atomic structures of the impacting materials are placed into intimate contact, there are large extents of plastic deformation in the interfacial region, and temperatures are increased during impact.<sup>102,103</sup> Most recent studies have recommended that the adhesive bonding to a dissimilar metal substrate arose from the mechanical interlocking of the deformed particles onto the substrate and discrete local atomic bonding.<sup>104</sup>

### Anisotropic nature of thermal spray coating architecture

The fundamental feature of any thermal spray coating is its lamellar microstructure formed by the rapid solidification of impinging molten droplets and cohesion among splats. Formation of this lamellar microstructure is a stochastic process and is associated with confounded processing variables such as the feedstock size, feedstock material, flame jet temperature, and particle velocity. The flattening ratio may be derived from the splat dimensions and depend on the spray method; as compiled in previous work.<sup>5</sup> An illustration of a typical ceramic thermal spray microstructure is depicted in Fig. 8. As a result of the cumulative interactions of

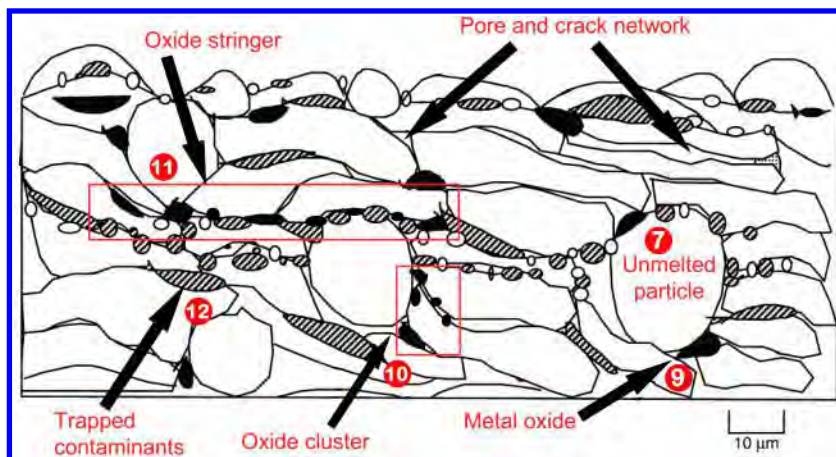
variables within the spray stream, discriminating features such as splat dimensions, pore sizes, crack density, inter-splat coalescence, and associated artefacts can be determined.

A schematic for a metal-based thermal spray coating is presented in Fig. 9.<sup>1</sup> The key difference is that spraying metal particles under a normal atmosphere is likely to create oxides during the time of flight or during spreading and solidification. Metal oxides will be trapped within the coating and influence the mechanical properties and other performance characteristics of the coating.

The terminology of thermal spray microstructural elements can be found in Table 4. The lamellar splat structure also gives rise to the highly anisotropic mechanical properties of thermal spray coatings. Thus, the coating material properties depend on the direction measured as opposed to an isotropic bulk material. The anisotropic nature of a thermal spray microstructure has been specifically defined as transversely isotropic because the architecture has two orthogonal planes of symmetry: i.e., (i) a microstructural texture that follows the spray direction, and (ii) a cross-section orientation, perpendicular to the spray direction (Fig. 8) that reflects the cross-sections of splats.

In addition, there is an overall reduction of mechanical properties due to the pore and crack network, which together are termed as the void network, within a thermal spray deposit.<sup>105</sup> The void microstructure formed in a thermal spray coating is dominated by two morphologies: inter-lamellar pores and intra-lamellar cracks.

The formation of the dominant void system varies with the spray technique and material. Ilavsky and coworkers<sup>106</sup> showed that alumina deposits, manufactured by a high-power water-stabilised plasma spray system, consisted of a microstructure dominated by intra-lamellar cracks. The same material deposited by a standard lower-power, gas-stabilised, plasma spray



Adapted from Ref. 1. The numbered features are keyed to Table 4

#### 9 Schematic of a metal thermal spray coating

system exhibited equal surface areas for the intra-lamellar cracks and inter-lamellar pores. However, in the case of zirconia, the microstructure was always dominated by inter-lamellar pores.

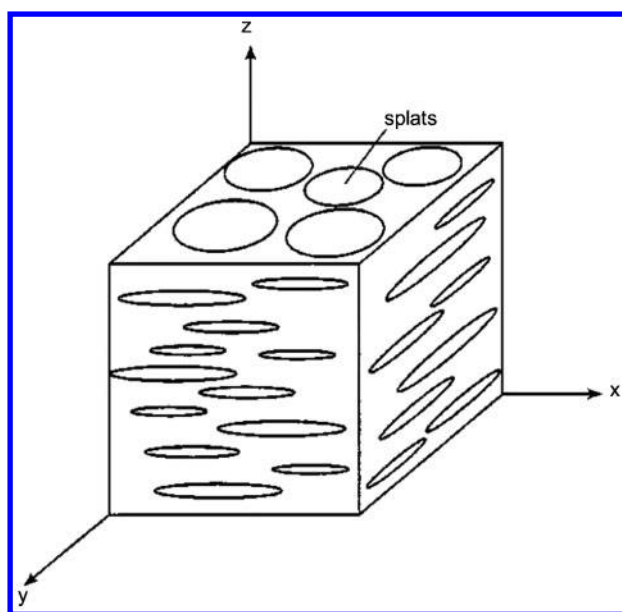
The influence of the dominant void system also affected the elastic and fracture behaviour of a thermal spray coating.<sup>107</sup> This was due to the fact that intra-lamellar cracks, which were perpendicular or normal to the substrate, reduced the coating mechanical properties in that direction. Inter-lamellar pores were manifested in a scattered orientation and their effect imparted a condition that can be described as 'inverse anisotropy' on the coating mechanical strength.<sup>108</sup> That is, the strength in the direction normal to the substrate was improved.

The third distinctive feature of a thermal spray coating lies within the two similar orthogonal planes or cross-section views of the coating as shown in Fig. 10. The 'XZ' and 'YZ' planes representing a cross-sectioned coating are essentially similar. Both planes exhibit a lamellar microstructure due to the flattening of splats as represented by the splats being elliptical-shaped (see Fig. 10). The

microstructural characteristics of these planes will be controlled by the spray protocol; primarily the spray beam diameter and the degree of overlap during the coating manufacture. The microstructure would be expected to exhibit differences of material properties when measured across axes in the (i)  $z$  direction, or (ii) the  $x$  and  $y$  directions. This cross-sectioned anisotropic behaviour has been highlighted by Ostojic and McPherson<sup>109</sup> when carrying out fracture toughness tests along the different cross-sectional axes. Therefore, the anisotropic mechanical behaviour of coatings produced *via* different thermal spray methods is related to a distinctive splat structure and their associated void systems.

In many practical cases of thermal spraying ceramics, the incorporation of a bond coat is required and this increases the complexity of the manufacturing process. The coating system of the substrate, bond coat and ceramic overlay may be treated as a three-dimensional, interlaced, tile structure that is composite-like in character. This complex material system alters the deformation mechanism, which reflects on the mechanical property value. A metal-based bond coat is applied before the deposition of a ceramic top layer for several reasons: (i) to reduce thermal mismatch between the substrate and ceramic coating; especially for high temperature applications, (ii) to provide a surface architecture that enables keying in of the ceramic overlay, and (iii) to protect the substrate from environmental effects such as high temperature corrosion.

The success of the two-layered thermal barrier coatings (TBCs) found in modern gas turbine engines can be attributed to the use of a nickel-based (NiCrAlY) bond coat.<sup>110,111</sup> NiCrAlY bond coats have been extensively used in TBCs for two reasons; first to help accommodate differences in coefficient of thermal expansion (CTE) between ceramic topcoats and metal substrates. This compliant layer partially accommodates thermal stresses in the TBCs during the cyclic thermal operating conditions. The second reason for using bond coats was to seal the underlying substrate from corrosive mediums; especially since the ceramic YSZ top coat was porous. Strong bonding between the oxide ceramic and metal substrate was achieved even after being subjected to a high temperature oxidation environment. Bond coat thicknesses for most cases should be between 150 and 200  $\mu\text{m}$ . Other selections of bond coats are indicated in Fig. 11.<sup>112</sup>



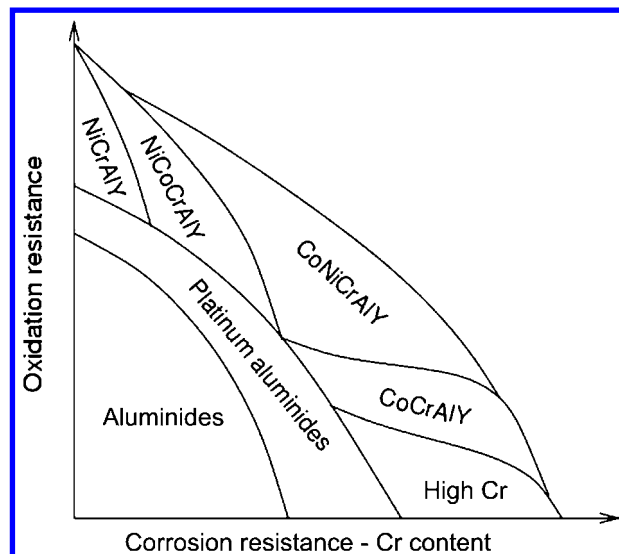
10 Schematic representation of splat microstructure with respect to the principal axes

Table 4 Microstructural characteristics of a thermal spray coating

Classification	Definitions	Anisotropic effect?	Feature ID**
Voids	A generic description of defects that includes porosity and cracks.	-	-
Porosity	Holes or pores within a coating. A microstructural feature containing no matter.	-	-
Delamination	Cracking or separation within a coating or between the coating–base metal interface.	No	1
Spalling	Detachment or flaking of particles/layers from a surface.	No	2
Interface contamination	Embedded foreign particles, contamination, or voids observed at the interface between the base metal and the coating.	No	3
Transverse cracks	Cracks perpendicular to the substrate.	Yes	4
Inter-lamellar pores	The unfilled volume along inter-splat boundaries due to incomplete splat stacking or relaxation of vertical stresses.	Yes	5
Intra-lamellar cracks	Cracking within the splat microstructure, usually in the vertical direction that is perpendicular to substrate.	Yes	6
Unmelted particles	Unreacted powder particles. Spherical, non-flattened or partially flattened with an aspect ratio (width to height) of less than 3:2.	No	7
Pull-outs	Artificially induced porosity resulting from unsatisfactory materialographic preparation.	N/A	-
*Oxides	Particles or linear striations that result from the metal powder combining with oxygen during the spray process.	Yes	9
*Oxide cluster	Oxide artefacts grouped closely together.	Yes	10
*Oxide stringer	Continuous linear oxide striations running parallel to the coating–base metal interface.	Yes	11
*Metallic inclusion	Presence of metal particles in the coating.	No	12

\*Defects that occur only in metal-based thermal spray coatings.

\*\* The feature identification (ID) can be found in Figs. 8 and 9.



Reproduced from Ref. 112

#### 11 Selection map for coating composition in relation to oxidation and hot-corrosion resistance

Other unique coating architectures are formed in nanostructured thermal spray coatings or in bimodal-structured thermal spray coatings.<sup>40,113</sup> The intention of such coating architectures was to modify the anisotropic behaviour of the coating by introducing micro- and nano-structures that act as crack arresters; thereby enhancing the as-sprayed coating toughness.<sup>40</sup>

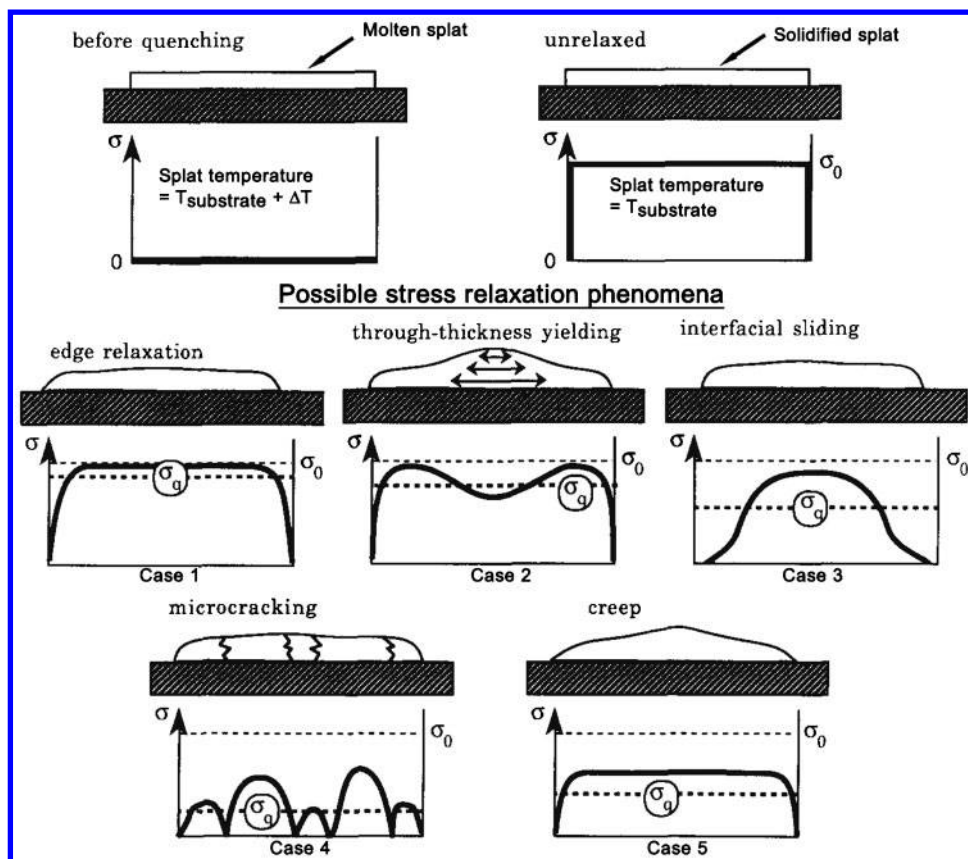
## Residual stresses of thermal spray coatings

Apart from the complex porosity and crack networks, the thermal spray process also generates residual stresses. These were initially referred to as ‘internal stresses’ in coatings by Fisher,<sup>114</sup> Ballard<sup>115</sup> and Marynowski.<sup>116</sup> The generation of ‘transient and residual stress’ suggested by Tucker<sup>54</sup> was used to describe the generation of coating stress states. The term ‘residual stress’ was used in the 1990s<sup>117,118</sup> to refer to the collective summation of stresses imposed onto the surface during the different stages of thermal spraying. The compressive or tensile residual stresses will influence the mechanical properties of thermal spray coatings.<sup>54,118</sup>

The review on the origins of residual stress by Clyne *et al.*<sup>118</sup> proposed two main contributors to residual stresses: (i) quenching stresses, and (ii) differential thermal contraction stresses. The quenching or intrinsic stresses arise due to the hindered shrinkage of individual molten splats as they undergo rapid solidification;<sup>117</sup> refer to Fig. 12. Therefore, quenching stresses relate to micro stresses since they arise at the splat level.<sup>119</sup> The existence of quenching stresses has been suggested by McPherson<sup>3</sup> and measurements of these stresses were executed by Kuroda *et al.*<sup>120</sup> The quenching stresses were found to be always tensile in splats;<sup>119</sup> however, the values in many cases are less than 100 MPa<sup>117</sup> due to stress relaxation.

The substrate is usually maintained at an elevated temperature during coating deposition. Consequently when the coated system is allowed to cool, any differences between the thermal expansion of the deposit and the substrate will generate a second type of residual stress that is termed as the differential thermal contraction





Reproduced from Ref. 117

12 Schematic illustration of the quenching stress distribution within a splat before and after stress relaxation phenomena

stress. Depending on the sign of the expansion mismatch,  $\Delta\epsilon_{th}$ , the macro type stresses can be tensile or compressive.<sup>118</sup> That is

$$\Delta\epsilon_{th} = \Delta\alpha\Delta T \quad (2)$$

$$\sigma_{thermal} T = \Delta\epsilon_{th} E_d T \quad (3)$$

where  $\Delta\alpha$  is the difference in the coefficients of thermal expansion between the coating and substrate materials.  $\Delta T$  is the temperature drop after the spray process.  $\sigma_{thermal}(T)$  and  $E_d(T)$  are the differential thermal contraction stress and Young's modulus of the coating at specific temperatures, respectively. Intuitively, the magnitude of the coating's differential thermal contraction stress increases with the temperature difference between the spray temperature and room temperature. The stress level is also influenced by the dissimilar thermal expansion coefficients, the thermal conductivities, Table 5, and Young's moduli of the abutting materials. The thermal contraction stresses between

thermal spray ceramic coatings and the substrate, which can result in delamination, can be reduced by employing a bond coat.<sup>1</sup>

In addition, when considering high particle velocity spray systems such as HVOF and cold spray, the semi-molten or solid particles impinging on the substrate or underlying sprayed layer cause a release of kinetic energy similar to the shot peening process.<sup>66,119</sup> The micro stresses that evolve are known as peening stresses. These stresses are compressive and can be considered to occur at the splat level; i.e., within microstructural elements in the order of tens of micrometres. It has been proposed that peening stresses are created within cold sprayed coatings.<sup>122</sup> For processes such as HVOF or D-Gun®, plastic deformation of the underlying surface will only arise when the impacting particles are partially solidified and possess sufficient momentum. The surface layer of the coating will still exhibit quenching stresses<sup>66</sup> due to solidification of the splats.

Apart from the coating process, the compressive stress state of the substrate surface could also be induced *via*

Table 5 Coefficients of thermal expansion and thermal conductivity for some substrates and coating materials<sup>121</sup>

	Mild steel	Al	Ni alloy (Hastelloy X)	NiCrAlY Alloy	YSZ	Al <sub>2</sub> O <sub>3</sub>	Cr <sub>2</sub> O <sub>3</sub>
Material	Substrate	Substrate	Substrate	Bond coat material	Top coat material	Top coat material	Top coat material
Coefficient of thermal expansion (10 <sup>-6</sup> K <sup>-1</sup> )	13	22.2	13.3	12	8.6	5.4	8.7
Thermal conductivity (W m <sup>-1</sup> K <sup>-1</sup> )	43	205	13.4	12.5	1.8	3.6	1.2

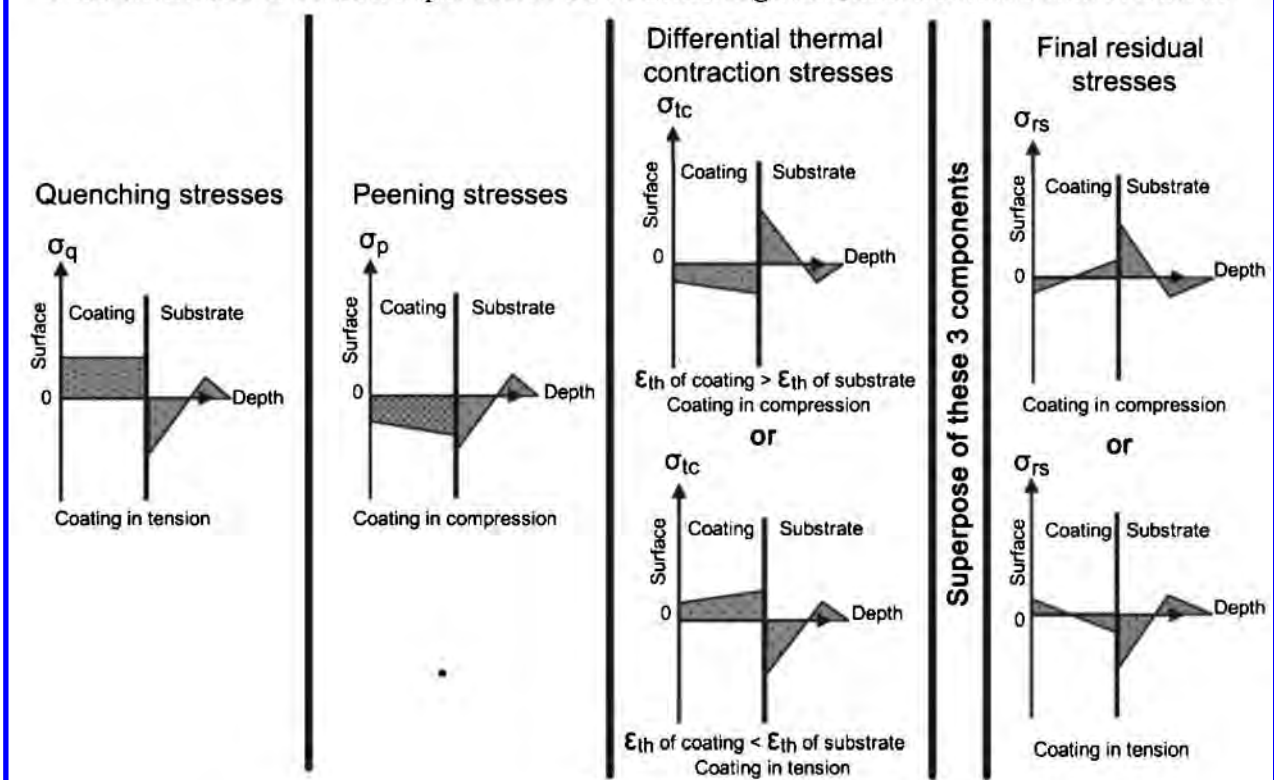
Spray type	Coating	Substrate	Quenching stresses <sup>1</sup>	Peening stresses <sup>2</sup>	Thermal stresses
Flame spray/ Plasma spray/ Wire arc spray	Metal	Metal	Y	N	Tensile or compressive <sup>3</sup>
	Ceramic/cermet	Metal	Y	N	Tensile
	Ceramic/cermet	Ceramic	Y	N	Tensile or compressive <sup>3</sup>
	Metal	Ceramic	Y	N	Compressive
HVOF/ D-Gun®	Metal	Metal	Y	Y	Tensile or compressive <sup>3</sup>
	Ceramic/cermet	Metal	Y	Y	Tensile
Cold spray	Metal/Cermet	Metal	N	Y	N

Note:

<sup>1</sup> Quenching stresses are always in tension.

<sup>2</sup> Peening stresses are always in compression.

<sup>3</sup> If the coefficient of thermal expansion of the substrate is greater, then the stresses are in tension.



Based on Ref. 68

### 13 Schematic representation of the final residual stress distribution with the coating/substrate system for thermal spray methods

the grit blasting operation. However, these stresses are partially relaxed if the preheat temperature is near the recovery temperature. These sources of stress within the coating and substrate will interact and superimpose to establish the residual stress state of the coating/substrate system. Figure 13 indicates that different thermal spray

methods will produce dissimilar outcomes of the residual stress state.

The final residual stress state evolves from a complex balance of stresses generated within the coating and substrate system. There are two essential considerations during practical spray process. First, the thickness per



pass should be less than 50  $\mu\text{m}$  and be tuned with regard to the traverse speed of the spray torch. It has been shown that a rapid rate of coating build up per pass can be detrimental to the coating mechanical properties<sup>123</sup> due to the discontinuity of the splat architecture. The slow torch traverse speed leads to an unbalanced distribution of coating residual stresses,<sup>118</sup> in particularly splat quenching stresses,<sup>117</sup> which can result in micro-cracking and delamination between the coating layers. Conversely, a low thickness build-up rate; i.e., less than 5  $\mu\text{m}$  per pass, would lead to longer spray times that are not practical from the production and manufacturing efficiency viewpoints.

The second consideration relates to the heat flux input from the thermal spray process to the coated work piece. There are merits and disadvantages of thermal spraying a work piece at an elevated temperature. With most thermal spray processes (except cold spray), the impacting molten particles and hot gas stream imparts heat to the coated surface during deposition. Auxiliary cooling accessories, such as compressed air nozzles attached alongside the spray torch or stationary cooling air hoses, are employed to reduce the temperature of the work piece. The heating rate of the entire work piece is directly proportional to the traverse speed of the spray torch across its surface. The shape, size and mass of the substrate, along with thermal conductivity and influence of any auxiliary cooling processes, affect the net temperature of the work piece during coating. Thus, control over the substrate spray temperature requires a balance between (i) the traverse speed of the spray torch, which imparts large heat fluxes into the substrate, and (ii) the removal of excess heat with cooling accessories. The cooling jets should provide active cooling during spraying without interfering with the stream of the molten particles.

The heat flux input from the thermal spray torch traverse motion should not be confounded with the procedure of preheating substrates with a propane torch. Preheating before grit-blasting and coating deposition is intended to remove condensates and adsorbates from the substrate surface.<sup>124,125</sup>

Maintaining the sprayed substrate at an elevated temperature during the thermal spray process has been shown by Sampath *et al.*<sup>126</sup> to lower porosity, improve coating mechanical strength and increase the coating thermal conductivity. These effects can be attributed to the crack structure within the coating because intrinsic splat quenching stresses are lower when impacting molten particles flatten onto a heated surface.<sup>127,128</sup> The molten splats experience longer solidification time and splat-to-splat contact is promoted. Columnar grain growth through splats occurs, further improving the interlayer bonding strength that aids to reduce the density of both vertical and horizontal cracks within the coating microstructure. As previously discussed, micro-cracking of the deposit is related to the evolution of the splat quenching stresses.<sup>117</sup>

However, thermal spray operations at substrate temperatures above 400°C magnify other sources of residual stress; especially the differential thermal contraction stresses that arise between the substrate and coating. Table 5 shows that the values are larger for metal substrate and bond coat materials compared to the ceramics. Consequently, when spraying at high

temperature, large misfit strain can arise when the coated specimen cools to room temperature and inelastic release of thermal contraction stress occurs. A thermal spray ceramic deposit undergoes extensive micro-cracking at high substrate temperatures; whereas metal deposits are prone to plastic yielding or creep. It is, therefore, not feasible to thermal spray at high substrate temperatures; although there are exceptions under VPS conditions.

## Thermal spray coating testing methods

### Porosity of coatings

Porosity is a key microstructural feature of thermal spray coatings. The pore and crack network originate during the chaotic processes of flattening and solidification of impacting molten droplets. Splat breakup and cracking due to rapid solidification, splat shrinkage upon cooling, and trapped unmelted particles are some of the traditional explanations for porosity formation.<sup>1</sup> Controlling the quantity and size of pores and cracks is essential for reliable coating performance. For instance, a coated bearing surface would require a dense coating with minimal porosity<sup>1</sup> while a medical implant coating requires 8–12% porosity of 50–100  $\mu\text{m}$  in dimensions to allow bone ingrowth during the healing process.<sup>129</sup>

The strain tolerance of APS YSZ coatings for thermal barrier applications has also been attributed to the numerous pores, gaps, microcracks and interfaces<sup>130</sup> that form the microstructure of these complex coatings. However, the high permeability of oxygen requires a dense bond coat that reduces the oxidation rate in a severe corrosion environment and such coating barriers can be applied by HVOF or VPS processes. A comprehensive review of thermal barrier coating compositions and technical approaches has been discussed by Darolia *et al.*<sup>131</sup>

It is necessary to classify void morphologies to discriminate among the many pore morphologies and types of micro-cracks. The three prime void morphologies, following the outline in Table 4, are: (i) inter-lamellar pores, (ii) intra-lamellar cracks, and (iii) delamination features. It is also possible to distinguish the void network of the coating in terms of its connectivity. There can be two types of void connectivity within a thermal spray coating microstructure; (i) a closed void network, and (ii) an open void network. A closed void network describes voids that are not connected and confined within the interior microstructure of the coating. An open void network accounts for all the pores and cracks that are connected to the coating surface.

Other key interests in porosity characterisation are the total porosity content, also known as global void content, and the void size distribution. Common measuring techniques used to quantify porosity have been reviewed by Fauchais *et al.*<sup>132</sup> and Table 6 presents a compilation of these techniques with respect to the measurement capabilities. Many measurement devices are available to characterise porosity and cracks. Nonetheless, most of these techniques are highly specialised to measure a certain variable; such as the open void network content, and are unable to provide other concurrent measurements. Thus, a complete

Table 6 Compilation of methods to quantify porosity

Porosity measurement techniques	Working principle	Void morphology				Void connectivity		Reference
		Total porosity	Void distribution	Pores	Cracks	Delamination	Closed void network	Opened void network
Mercury intrusion porosimetry (MIP)	Non-wetting liquid volume of mercury is measured as a function of the applied impregnation pressure on sprayed sample.	x						x
Gas pycnometry (Helium pycnometry)	Sample volume is calculated from the observed pressure changes between a chamber cell containing the sample.							x
Water absorption/immersion (Archimedes method)	Determine the water mass that fill the pores after immersion. Used to quantify the closed void content by measuring the 'dry' weight and the 'wet' weight of the sample.						x	
Electrochemical test	Based on the infiltration of an electrolyte through the connected pores in a coating and corrosion of the metallic substrate. The more connected the porosity, the higher the measured corrosion current.							x
Image analysis (IA)	Imaging of a polished sample to determining the ratio between area of void and the total area of sample analysed. Different void morphologies are distinguished.	x	x	x	x			
Small angle neutron scattering (SANS) and multiple small angle neutron scanning (MSANS)	Scattering of a monochromatic and collimated beam of cold neutrons with known wavelength. Porod scattering measurements enable the determination of compositional and structural non-homogeneities, such as void surfaces.	x	x	x	x			
Ultra-small angle X-ray scattering (USAXS)	Similar to SANS and is a non-destructive characterisation technique recording elastic scattering of X-rays induced by compositional and structural inhomogeneities.	x	x					
X-ray computed microtomography* (CMT)	A non-destructive technique in which an image is constructed by point-to-point linear attenuation coefficients (LAC) in a slice. The LAC depends on the physical density of the material, its effective atomic number and the X-ray beam energy. Density maps are obtained by reconstructing the sequential cross-sectional slices.	x	x	x	x	x		
Ultra sound	Using the relationship between density and porosity content, the ultrasonic velocity may be used to estimate porosity. Ultrasonic velocity in porous ceramics and plasma sprayed coatings is linearly dependent on their porosity level.	x						

\*Emerging technique and is still limited by sensor spatial resolution.

analysis of void morphologies and connectivity requires a combination of methods.

Many researchers have quantified porosity *via* IA due to its ease of implementation and ability to distinguish void morphologies, distribution and content. The IA method is described in Ref. 145. The procedure involves cross-sectioning the coating sample, then polishing and obtaining suitable images for stereographic protocols. This method, although suffering from the disadvantage of being destructive, provides an indication of porosity. The reliability of the results is influenced by factors that include (i) metallographic preparation,<sup>138,146</sup> (ii) the sample imaging technique,<sup>139</sup> and (iii) post processing techniques of the image such as thresholding procedures and other technical details.

Image digitisation of a cross-sectioned sample requires the proper combination of camera resolution, lighting and magnification. The minimum sensor resolution of the camera should be at least 3  $\mu\text{m}$  per pixel when capturing a thermal spray coating with porosity artefacts of approximately 10  $\mu\text{m}^2$  in area. The photographic configuration should employ near monochromatic<sup>147</sup> lighting. The sensor size and lens magnification also must allow an image dimension to be between 10 and 15 times larger than the objects of interest and account for the representative elementary volume (REV) of the structure.<sup>148</sup> For these reasons, images taken *via* the scanning electron microscope (SEM) that has a higher resolution than a conventional optical microscope are preferred. It has been claimed that SEM images allow the detection of finer globular and inter-lamellar pores; and finer micro-cracks also become visible. In addition, the higher depth-of-field allows the identification and elimination of pullouts and the crack network that is associated with sample preparation procedures.<sup>139</sup>

The REV size requirement is governed by the magnification of the microscope images because the image resolution is determined by a fixed number of pixels on the charge coupled device (CCD) camera. While high magnification and high image resolution allow the fine details of the structure, such as micro-cracks, to be photographed, the resulting REV may be too small. The optimal REV must be large enough to capture the complete material structure and may, therefore, require a low magnification that sacrifices the image resolution. Consequently, a compromise between a high resolution and a low magnification must be made, which should be representative of the structure and independent of its location within the sample.

Post-processing of the image involves converting it into an 8-bit greyscale image format with 256 possible grey scale levels or 'bins'. Once the image is in a grey scale format, it is converted into a black and white image by using a thresholding method. The value of the threshold impacts the output thresholded image and, as a result, can be adjusted to suit the needs of the investigator. To avoid any biasing of the results, it is recommended to use a standardised method of threshold selection such as Otsu's method.<sup>149</sup> The porosity is calculated by dividing the number of black pixels by the total number of pixels in the image. In addition to this, multiple images of the sectioned sample should be taken in different locations and a consistent image processing method used. Sufficient images taken at random locations are required to ensure that the calculated average

porosity is a true representation of the coating porosity distribution.

Antou and Montavon *et al.*<sup>148</sup> suggested that filters be applied on the digitised image to calculate the different void morphologies in thermal spray coatings. Filtering techniques can be divided into two categories: (i) convolution filters that are linear in nature, and (ii) non-convolution filters that are non-linear. Both techniques accomplish their results by examining and processing an image in small regions, called pixel neighbourhoods. A neighbourhood is a square region of image pixels (i.e., 3 by 3 in size). The commonly used filters are:

1. Non-convolutional erosion filter to remove pixels from the edges of the objects, where contiguous black areas in the image are considered objects and the background is assumed to be white. This is a morphological filter that erodes (i.e., reduces) the boundaries of bright objects in an image and enlarges the boundaries of dark ones. It is often used to reduce, or eliminate, small bright objects. A pixel will be removed (i.e., set to white) if four or more of its eight neighbours, depending on the selected option, are white. The erosion filter separates objects that are touching and removes isolated pixels.
2. The 'dilation' filter has an opposite effect compared to the 'erosion' filter. It adds pixels to the edges of the objects. A pixel is added (i.e., set to black) if four or more of its eight neighbours, depending on the selected option, are black. Dilation connects discontinuous objects and fills in holes. The filter changes the shape of objects by enlarging the boundaries of bright objects, and reducing the boundaries of dark ones. The dilation filter can be used to increase the size of small bright objects.
3. The 'open' filter successively executes the 'erosion' and 'dilation' filters. It smoothens the outline of the digital object and removes isolated pixels.
4. The 'close' filter has an opposite effect compared to the 'open' filter. It sequentially performs the 'dilation' and 'erosion' filters. It smoothens the outline of the digital object and fills in isolated holes within objects that can correspond to artefacts.

Appropriate applications of image manipulation methods allow isolation of the distinctive morphological features in an image. Subsequently, the calculation of relevant void content can be carried out.

A compilation of measured coating porosity levels using the different methods is presented in Table 7. Note that there are large variations in reported levels, even for coatings of similar feedstock and spray method. First, coating porosity levels calculated from IA *via* conventional optical light microscopy tend to register higher results compared to those gathered from SEM. Second, the limitations of these techniques become apparent. Particularly, IA tends to overestimate<sup>139</sup> and MIP provides underestimated readings compared to other techniques. X-ray computed microtomography may be used to obtain a three-dimensional representation of the porosity architecture.

### Measurement of residual stresses in thermal spray coatings

Residual stress measurement techniques for thermal spray coatings can be generally classified as (i)

**Table 7** Compilation of reported porosity levels for thermal spray coatings

TS method	Material	Porosity <sup>a</sup> /%	Measurement method	Remark <sup>+</sup>	Ref
APS	WC-17 wt-% Co	10.2	IA (Optical)	Agglomerated and sintered, 11–53 µm	150
APS	WC-17 wt-% Co	1–1.1	IA (Optical)	Agglomerated and sintered, <63 µm	151
HVOF	WC-17 wt-% Co	2.21	IA (Optical)	HV2000, crushed and sintered, 15–45 µm	152
HVOF	WC-18 wt-% Co	5.7–6	IA (Optical)	JetKote, nanostructured, 10–50 µm	153
D-Gun	WC-17 wt-% Co	0.6	IA (Optical)	Agglomerated and sintered, 11–45 µm	151
VPS	WC-17 wt-% Co	3	IA (Optical)	Agglomerated and sintered, <63 µm	151
APS	WC-12 wt-% Co	6	IA (SEM)	Axial III, crushed and agglomerated, 15–45 µm	154
APS	WC-10 wt-% Co-4 wt-% Cr	5.3–16.1	IA (SEM)	Axial III, crushed and agglomerated, 15–45 µm	155
HVOF	WC-10 wt-% Co-4 wt-% Cr	3.7–8.4	IA (SEM)	DJ2700, crushed and agglomerated, 15–45 µm	155
HVOF	WC-10 wt-% Co-4 wt-% Cr	0.6	IA (SEM)	JP5000ST, crushed and agglomerated, 15–45 µm	155
HVOF	WC-10 wt-% Co-4 wt-% Cr	2.1–3.1	IA (SEM)	JP5000, crushed and agglomerated, 15–45 µm	155
HVOF	WC-12 wt-% Co	1	IA (SEM)	JP5000, agglomerated and sintered, 15–45 µm	154
HVOF	WC-12 wt-% Co	0.38	IA (SEM)	Agglomerated and sintered, 11–45 µm	156
Cold Spray	WC-17 wt-% Co	0.11–0.38	IA (SEM)	Nanostructured, 11–45 µm	157
D-Gun	WC-12 wt-% Co	0.3–5.25	IA (SEM)	Agglomerated, 10–60 µm	158
APS	Al <sub>2</sub> O <sub>3</sub> -13 wt-% TiO <sub>2</sub>	2.3	IA (Optical)	High energy plasma, blend, 23–45 µm	159
APS	Al <sub>2</sub> O <sub>3</sub> -13 wt-% TiO <sub>2</sub>	2.8	IA (Optical)	Blend, 23–45 µm	159
APS	Al <sub>2</sub> O <sub>3</sub> -13 wt-% TiO <sub>2</sub>	5–6	IA (SEM)	Mechanically clad, 15–53 µm	160
APS	Al <sub>2</sub> O <sub>3</sub> -13 wt-% TiO <sub>2</sub>	7.5–10.5	IA (SEM)	Agglomerated, nanostructured, 40–70 µm	160
APS	Al <sub>2</sub> O <sub>3</sub> -13 wt-% TiO <sub>2</sub>	2.6–4.4	IA (SEM)	Agglomerated, nanostructured, 14–62 µm	161
APS	Al <sub>2</sub> O <sub>3</sub> -13 wt-% TiO <sub>2</sub>	1.9–4.7	IA (SEM)	Cladded of fused and crushed alumina, 15–53 µm	161
HVOF	Al <sub>2</sub> O <sub>3</sub> -13 wt-% TiO <sub>2</sub>	1	IA (SEM)	Agglomerated, nanostructured, 2–24 µm	161
HVOF	Al <sub>2</sub> O <sub>3</sub> -13 wt-% TiO <sub>2</sub>	2.2	IA (SEM)	Fused and crush, 5–22 µm	161
APS	Al <sub>2</sub> O <sub>3</sub>	3	IA (Optical)	High energy plasma, fused, 5–20 µm	159
APS	Al <sub>2</sub> O <sub>3</sub>	3.7	IA (Optical)	Fused, 23–45 µm	159
D-Gun	Al <sub>2</sub> O <sub>3</sub>	1.02	IA (Optical)	Fused and crushed alumina, 5–25 µm	162
APS	Al <sub>2</sub> O <sub>3</sub>	1.4–10.1	IA (SEM)	Fused and crush, range of feedstock sizes.	163
APS	Al <sub>2</sub> O <sub>3</sub>	12.2	IA (SEM)	Sol-gel, 15–50 µm	139
HVOF	Al <sub>2</sub> O <sub>3</sub>	11	IA (SEM)	Sintered, 5–22 µm	139
APS	Al <sub>2</sub> O <sub>3</sub>	11.2	SANS	Sol-gel, 15–50 µm	139
HVOF	Al <sub>2</sub> O <sub>3</sub>	10	SANS	Sintered, 5–22 µm	139
APS	Al <sub>2</sub> O <sub>3</sub>	6.2	WIP	-	164
WSP	Al <sub>2</sub> O <sub>3</sub>	5–11.1	MIP	-	164
APS	Al <sub>2</sub> O <sub>3</sub>	7.9	MIP	Sol-gel, 15–50 µm	142
APS	Al <sub>2</sub> O <sub>3</sub>	25	MIP	Fused and crushed, 45–90 µm	142
HVOF	Al <sub>2</sub> O <sub>3</sub>	3.9	MIP	Sintered, 5–22 µm	142
APS	Al <sub>2</sub> O <sub>3</sub>	8.4	CMT	Sol-gel, 15–50 µm	142
APS	Al <sub>2</sub> O <sub>3</sub>	23.8	CMT	Fused and crushed, 45–90 µm	142
HVOF	Al <sub>2</sub> O <sub>3</sub>	4.4	CMT	Sintered, 5–22 µm	142
APS	YSZ	21	IA (Optical)	HOSP™ 27–95 µm	165
APS	YSZ	25	IA (Optical)	Agglomerated and sintered, 27–97 µm	165
APS	YSZ	20	IA (Optical)	Fused and crushed, 31–97 µm	165
APS	YSZ	17	IA (Optical)	Fused and crushed, 10–60 µm	139
APS	YSZ	27	IA (Optical)	Sol-gel, 5–50 µm	139
APS	YSZ	14.5	IA (Optical)	HOSP™, 20–55 µm	139
APS	YSZ	9.5	IA (SEM)	Fused and crushed, 10–60 µm	139
APS	YSZ	14	IA (SEM)	Sol-gel, 5–50 µm	139
APS	YSZ	7.9	IA (SEM)	HOSP™, 20–55 µm	139
APS	YSZ	8	SANS	Fused and crushed, 10–60 µm	139
APS	YSZ	13.5	SANS	Sol-gel, 5–50 µm	139
APS	YSZ	6	SANS	HOSP™, 20–55 µm	139
APS	YSZ	9	SANS	As sprayed	166
APS	YSZ	11.1	SANS	Thermally cycled	166
APS	YSZ	15	SANS	Agglomerated and sintered, 20–70 µm	167
APS	YSZ	12.2	SANS	HOSP™, 20–120 µm	167
APS	YSZ	10.2–12.7	MSANS	Fused and crushed, 40–115 µm	168
APS	YSZ	14.6–17.1	MSANS	HOSP™, 25–95 µm	168
APS	YSZ	6.2	MIP	HOSP™, 20–45 µm	169
APS	YSZ	7.5–8.5	MIP	HOSP™, 53–75 µm	169
APS	YSZ	9.1–9.2	MIP	HOSP™, 90–120 µm	169
APS	YSZ	7.9–9	MIP	HOSP™, 20–125 µm	169
APS	YSZ	13	MIP	Nanostructured	170
APS	YSZ	14.5	MIP	Agglomerated and sintered, 20–70 µm	167

Table 7 Continued

TS method	Material	Porosity*/%	Measurement method	Remark <sup>+</sup>	Ref
APS	YSZ	10	MIP	HOSP, 20–120 $\mu\text{m}$	167
APS	YSZ	10.5	MIP	As sprayed	166
APS	YSZ	9	MIP	Thermally cycled	166
APS	YSZ	7.5–8.6	MIP	-	164
APS	YSZ	1.9–4.1	Helium pycnometry	Nanostructured, 30–290 nm	140
APS	YSZ	12.9–19.3	USAXS	Nanostructured, 30–290 nm	140
APS	YSZ	7.67–11.06	USAXS	Fused and crush, 31–97 $\mu\text{m}$	171
APS	YSZ	10.21	USAXS	Fused and crush, 31–97 $\mu\text{m}$	171
APS	YSZ	12.36	USAXS	HOSP, 61–95 $\mu\text{m}$	171
APS	YSZ	10.32	USAXS	Agglomerated and sintered, 59–97 $\mu\text{m}$	171

\* The number of measurements for porosity varies over a large range.

+ Details concerning the thermal spray process, feedstock morphology, and feedstock particle size are presented.

APS: atmospheric plasma spray; VPS: vacuum plasma spray; HVOF: high velocity oxygen fuel spray; CS: cold spray; IA: image analysis; SANS: Small angle neutron scattering; MSANS: multiple small angle neutron scanning; USAXS: ultra-small angle X-ray scattering; CMT: X-ray computed microtomography; MIP: mercury intrusion porosimetry; HOSP<sup>TM</sup>: hollow spherical powders; YSZ: yttria stabilised zirconia.

non-destructive, and (ii) destructive. These methods can be further subdivided on the basis of the measurement principles to detect the residual stress states, Table 8.

#### Non-destructive methods

Non-destructive methods can be grouped into two categories. The first category employs electromagnetic radiation directed towards a coating in the form of X-ray diffraction,<sup>172,173</sup> neutron diffraction<sup>174,175</sup> or laser beam excitation spectroscopy.<sup>176</sup> Diffraction methods are based on the measurement of the lattice plane spacing and are capable of determining the stress state of specific coating phases. The laser beam excitation spectroscopy method explores the shifts in the Raman bands<sup>177</sup> or  $\text{Cr}^{3+}$  luminescence peaks.<sup>176</sup> Electromagnetic radiation methods are often adopted due to the simple experimental setup, but care needs to be taken with respect to the specimen thickness requirement and the detection depth limitations, Table 9.

The use of laboratory X-ray diffraction (XRD) methods employs the reflection-based  $\sin^2\psi$  technique. Changes in crystal lattice plane  $d$ -spacing are measured with respect to the coating surface. Shifts in  $d$ -spacing from the original diffraction peaks and the specimen tilt angle,  $\psi$ , are correlated with internal strains in the coating. Thus, coating stress can be calculated with the use of appropriate elastic constants.<sup>173</sup>

The conventional laboratory XRD method is limited due to the shallow penetration of the X-ray beams, typically in the several micrometres range. It is possible to determine a coating's through-thickness residual stress profile by performing XRD measurements that require progressive mechanical or chemical layer removal.<sup>68</sup> However, this procedure compromises the non-destructive character of the XRD method; the details of which are provided in the next section.

Synchrotron or high energy X-rays offer 20–300 keV photons that are over a thousand times more penetrating than laboratory X-rays. Among the synchrotron techniques, transmission high energy X-rays have been used to determine localised phase composition and strains in plasma sprayed coatings.<sup>180</sup> This method is also based on the  $\sin^2\psi$  concept, but allows for diffraction of discrete volumes of coating material through the coating thickness and uses an area detector to capture the full Debye

diffraction cone from polycrystalline coatings.<sup>181</sup> The transmission technique requires cross-sectional samples with limited thickness but does not require material removal for discrete measurements throughout the entire thickness of the coating.

The neutron diffraction methods are capable of providing a through-thickness stress profile analysis up to centimetres, without the need of successive layer removal or cross-sectioning. This method uses a pulsed polychromatic neutron beam to measure Bragg reflections at fixed scattering angles and the time of flight of each diffracted neutron defines its wavelength. Two apertures, one before and one after the specimen, define the size of incident and diffracted beams.<sup>178</sup> Their intersection defines the 'gauge volume' and is the volume being probed by the neutrons. From a set of lattice spacings in different orientations, and a stress-free lattice spacing, an elastic strain tensor can be found. Subsequently, using Hooke's law, the stress tensor component can be established. At least six measurements in different orientations are required for the determination of the six independent stress tensor components.<sup>182</sup>

While neutron diffraction is not limited by penetration depth, the low spatial resolution ( $\sim 0.3$  mm) necessitates long scanning times<sup>178,185</sup> of about tens of minutes per measurement point. Neutron-based depth profiling near the interface is usually not representative of the coating.<sup>186,187</sup> Also, the surface 'vertical scan' arrangement is preferred, in which the coated specimen is moved up or down in the 'z' direction for the depth profiling of strain in the coating and substrate material.<sup>188</sup> In this arrangement there is no change in diffraction angle and, hence, no pseudo-strains generated since the gauge volume is consistently referenced with respect to the surface. A comparison of these methods<sup>178,179,181</sup> is presented in Table 9.

The second category of non-destructive methods to measure residual stress involves substrate curvature monitoring by optical or mechanical means. The residual stresses can be calculated by comparing the curvature of strip-shaped samples before and after spraying.<sup>189</sup> The *in-situ* curvature monitoring method, proposed by Kuroda *et al.*,<sup>117,120</sup> can provide information of (i) intrinsic quenching stresses during coating deposition and (ii) the

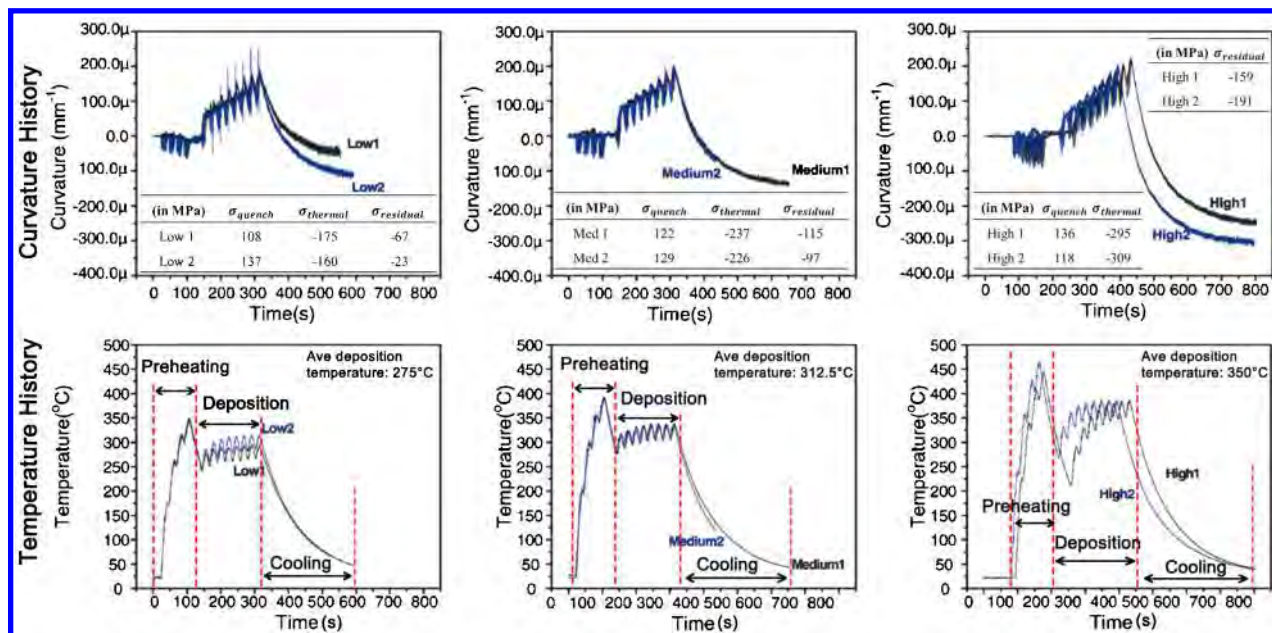


**Table 8 Classification of methods to measure residual stresses in thermal spray coatings based on the measurement principle**

Measurement principle		Profile measured	Local/phase stress or average stress	Ability to distinguish between quenching stresses and thermal stresses
Non-destructive	Electromagnetic radiation	X-ray diffraction Neutron diffraction	Phase distinctive stress Phase distinctive stress	Yes Yes
	Curvature measurement <i>In-situ</i> curvature monitoring Strain gauge	Laser excitation  Hole drill Modified layer removal	Local stress Average stress Average stress Average stress	No No Yes No
Destructive	Electromagnetic radiation	X-ray Synchrotron (high energy X-ray) diffraction Laser excitation	Average stress Phase distinctive stress Phase distinctive stress	No Yes Yes
	Displacement	Indentation Focus ion beam	Local stress Average stress Average stress	No No No

**Table 9 Comparison of electromagnetic radiation methods of measuring residual stresses in thermal spray coatings**

Working principle	Spatial resolution <sup>178</sup>	Accuracy <sup>178</sup>	Ability to measure through thickness	Limitations	Ref
X-ray diffraction	20 µm in depth; 1 mm lateral	± 20 MPa	Yes. Have to apply material layer removal.	Cannot measure depth > 20 µm	173, 179
Synchrotron (high energy X-ray) diffraction	20 µm lateral; 1 mm in depth	± 50 µε	Yes. But have to cross-section sample.	Difficult for X-ray transmission if thickness > 2.5 mm	180, 181
Neutron diffraction	0.3-0.5 mm	± 10 µε	Yes. Up to centimetres.	Scan orientation required to account for pseudo-strains	175, 182, 183
Laser excitation	< 1 µm	< 1 µm	Yes. But have to cross-section sample.	Small scan area ~ 4 µm in diameter	176, 177, 184



Reproduced from Ref. 195

**14 Change of temperature and deflection of plasma sprayed molybdenum with respect to processing history. The average deposition temperature influences the residual stress state of the coating**

differential thermal contraction stresses created during the cooling process. Variations of this method have been implemented across laboratories<sup>190,191</sup> to monitor the residual stress build-up during the deposition and cooling stages.

Quenching stresses are determined from knowledge of the coating thickness and the gradient of curvature response during deposition. The quenching stress,  $\sigma_q$ , can be determined by using Brenner and Senderoff's formula<sup>192</sup>

$$\sigma_q = \frac{E'_s t_s (t_s + \beta^{1/25} \Delta t_D)}{6 \Delta R \Delta t_D} \quad (4)$$

where  $\Delta R$  is the change in radius of curvature caused by quenching stresses in a deposited layer of thickness  $\Delta t_D$ ;  $E'_s$  and  $E'_D$  are the effective Young's moduli of the substrate and deposit respectively;  $\beta$  is the ratio of  $E'_D/E'_s$  and  $t_s$  is the substrate thickness. Tsui and Cyne<sup>193</sup> developed models to predict the quenching stress for several geometric shapes. The models assume a layer-by-layer coating build up process such that the misfit strain was accommodated after each additional layer. Since curvature changes after each torch pass can be monitored, the quenching stress can be inversely deduced.<sup>193,194</sup>

After the deposition process, the differential thermal contraction stresses can be evaluated<sup>190</sup> from equation (3). An example of temperature–curvature data of a plasma sprayed molybdenum coating is shown in Fig. 14.<sup>195</sup> The different sub-processes such as preheating, deposition and cooling can be identified. Furthermore, the effect of the deposition condition is observed to influence the evolution of the coating stress states.

#### Destructive methods

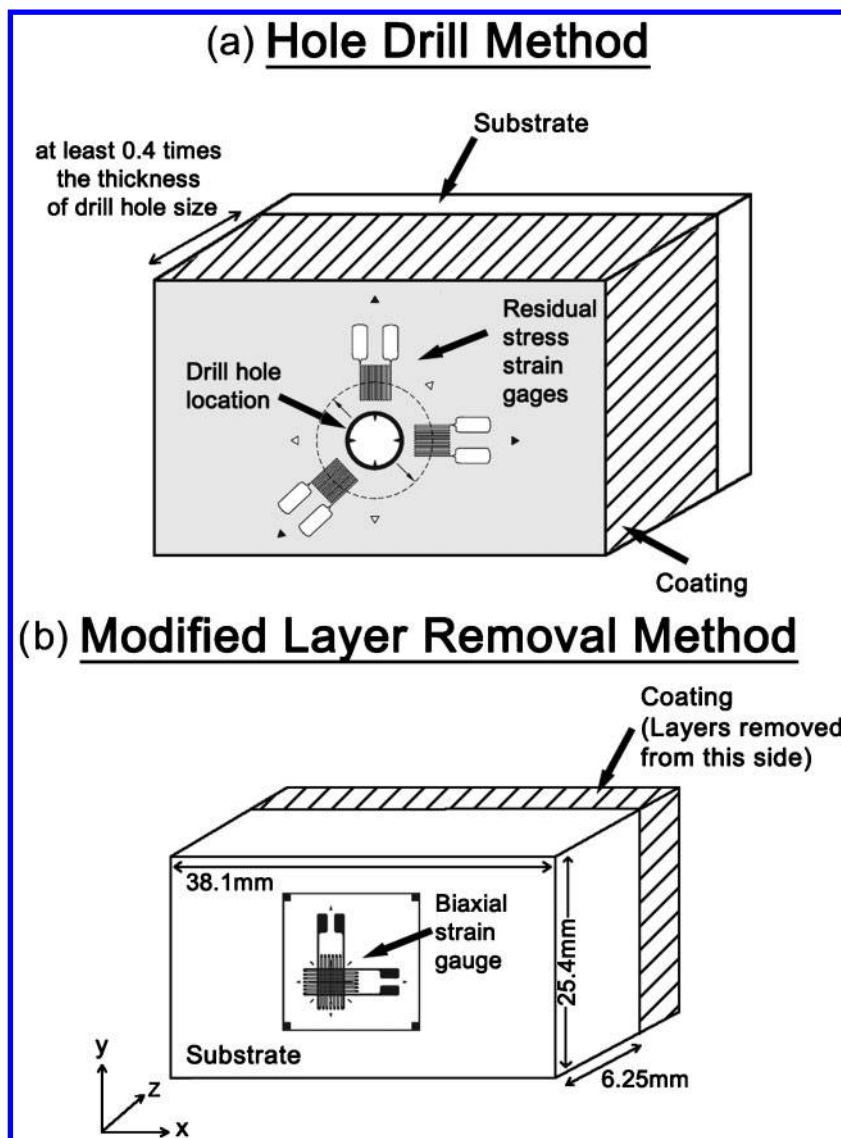
In destructive tests, the thermal spray coating is subjected to strain release as a result of material removal. The measurement of change in the stressed coating microstructure can be performed by means of (i) conventional, physically attached strain gauges,<sup>196,197</sup> (ii) XRD,<sup>68</sup> or (iii) optical displacement measurements.<sup>198,199</sup> The

destructive techniques are unable to differentiate the source of the induced stress. In addition, challenges exist in removing the material in a controlled manner. Plastic deformation or damage of the coating microstructure, especially ceramic coatings, implies that the assumption of a linear elastic change in the through-thickness stress state is invalid.

The hole drilling method that employs a strain gauge rosette is based on Mathar's observation<sup>200</sup> that the shape of a circular hole drilled into a stressed structure will change. It is the most common practical technique for determining residual stresses in bulk materials.<sup>201</sup> Reference 202 details its execution. The hole drilling procedure, shown in Fig. 15a, involves two stages (i) removal of the stressed material by drilling a small hole into the surface of the body at the centre of a special strain gauge rosette, and (ii) measurement of the relaxation strain occurring around the hole location. It is possible to calculate the strain state by means of an analytical model.<sup>197</sup>

However, since thermal spray coatings display non-uniform through-thickness residual stresses, it is recommended to measure the stress profile through the coating. Therefore, the technique can be modified to perform incremental hole drilling. This method involves drilling a series of small steps of about 20–40  $\mu\text{m}$  in depth<sup>203,204</sup> that produce measurable strain relaxation. Analytical evaluation of the detected strain data using an 'integral method' is considered to be the most suitable<sup>204,205</sup> data analysis method. It considers simultaneously the contribution of the measured strain relaxation of the stresses at all depths and also provides a separate evaluation of the residual stresses with each depth increment.

An alternate method was proposed by Greving *et al.*<sup>196,206</sup> that involves the controlled removal of the coating *via* either electropolishing or wet polishing and monitoring the changes in strain on the substrate side (see Fig. 15b). The method is based on the concept that the removed layer from the surface of a stressed plate or



15 Schematic representation of strain gauge methods to measure thermal spray residual stress; *a* hole drill method,<sup>197</sup> and *b* modified layer removal method<sup>196</sup>

beam will release a force and moment acting on the remaining sample. The removed layer has to be insignificantly small so that (i) sufficient depth resolution is achieved, and (ii) the material removal process does not induce strain artefacts. Accordingly, the recorded strain data and thickness changes are used as inputs to calculate the residual stresses.<sup>196</sup>

Although low energy XRD methods offer high spatial resolution, there is a 10–50  $\mu\text{m}$  depth detection limitation owing to the effective penetration of the radiation source wavelength and coating material.<sup>179</sup> Thus, the strain measured on an as-sprayed coating relates to (i) a depth of no greater than its surface roughness, and (ii) is within a region subjected to substantial stress relaxation.<sup>118</sup> Methods that combine the residual stress measurements from coatings of varying thicknesses are not an accurate representation of the through-thickness stress profile.

Therefore, to allow the residual stress depth profile analysis of a single thermal spray coating sample, controlled removal of the coating layers using electro-polishing for metals or cermets and wet polishing for ceramics has been combined with a reflective-based X-ray technique.<sup>68,207</sup> Transmission high energy X-rays

also can be applied to cross-sectioned samples for residual stress measurements.<sup>208</sup> This technique allows diffraction from discrete volumes of coating material through the coating thickness and uses an area detector to capture the full Debye diffraction cone from a polycrystalline coating.<sup>181</sup>

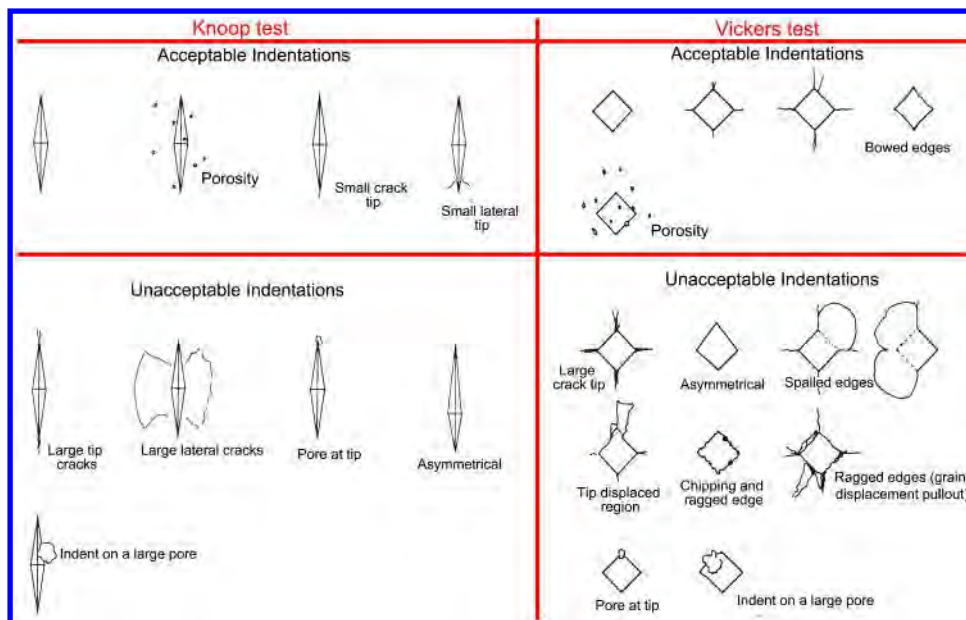
Other residual stress measurement methods that have been applied include Moiré interferometry with cutting relaxation,<sup>198</sup> probing surfaces with an indenter<sup>209</sup> and digital image correlation with focussed ion beam milling techniques.<sup>198</sup>

## The hardness of thermal spray coatings

### Types of hardness test for thermal spray coatings

Indentation tests<sup>210</sup> have been used widely for thermal spray coatings to quantitatively measure their resistance to deformation under an applied load. Mechanical properties such as hardness,<sup>211–213</sup> elastic modulus,<sup>164,214</sup> fracture toughness,<sup>109,215</sup> and interfacial adhesion or cohesion strength<sup>216,217</sup> can be determined by performing variations of the indentation test method.

Reference 218 describes hardness test methods for most materials. Both of these indentation methods are



16 Guidelines for acceptance of indentations for Knoop (left) and Vickers (right) microhardness tests<sup>219,220</sup>

commonly used for thermal spray coating characterisation. Essentially, the type of indenter (i.e., Knoop or Vickers) yields the associated hardness number. Specifically, for the indentation testing of advanced ceramics, there are five unique standards as shown in Table 10.

These standards highlight that ceramic materials have a tendency to develop cracks during testing as opposed to metal materials. Therefore, indentation at a small test load (typically less than 1000 gf) or microindentation hardness testing is recommended for ceramic materials. It is also necessary to allow sufficient spacing in between successive indents and implement a procedure to reject indents that develop excessive cracking. These details are covered within ASTM standards C1326<sup>219</sup> and C1327<sup>220</sup> and are also represented in Fig. 16.

Another reason to avoid macroindentation hardness tests, which use loads between 1 and 100 kg, on thermal spray coatings concerns the size of the indent imprint. Typical thermal spray coatings have thicknesses less than

\*<sup>4</sup>The discussion refers to the imprint diagonal to height ratio of 5 for the Vickers microhardness test and 30 for Knoop microhardness test. This should not be confused with the requirements for a macroindentation test. As well, the acronyms of 'VPN' and 'HV' are used to describe the hardness value determined by a Vickers hardness test.

1 mm; thus macroindentation hardness tests on the coating top surface cannot be applied because the depth ratio of the imprint to coating thickness must be at least<sup>\*4</sup> 10.<sup>219,220</sup> Similarly, if the macroindentation hardness tests were performed on cross-sectioned coating samples, the imprint diagonal lengths will most likely exceed the dimension of the coating surface under examination. Under a load of 1 kg (i.e. 9.81 N) the Vickers indent diagonal length for materials of 300–800 HV is between 78 and 48  $\mu\text{m}$ . The depth of imprints on cross-sectioned coatings should preferably not be greater than the splat geometry since the deformation response of the underlying layer cannot be resolved. On the other hand, microindentation hardness tests have the attribute of a small indent imprint; therefore specific phases or constituents and regions can be evaluated. Such information would be lost if a macroindentation test was performed.

#### Vickers and Knoop hardness tests

The Vickers indentation test uses a square-based, pyramidal-shaped diamond indenter with an included angle between opposite faces of  $136^\circ$ . Indentation is carried out at a predetermined load onto the surface of the polished coating. The Vickers hardness, HV in units of GPa, is determined from using the following relationship

Table 10 Test standards for the indentation microhardness test

ID	Knoop indentation test	ID	Vickers indentation test
1.	ASTM C1326-08 (USA)	5.	ASTM C1327-08 (USA)
2.	CEN ENV 843-4 (European)*	2.	CEN ENV 843-4 (European)*
3.	JIS R1610 (Japan)*	3.	JIS R1610 (Japan)*
4.	ISO 4516 (International)*	4.	ISO 4516 (International)*

\*Standard includes both Knoop and Vickers indentation tests.

1. ASTM C1326-08: 'Standard test method for Knoop indentation hardness of advanced ceramics'.

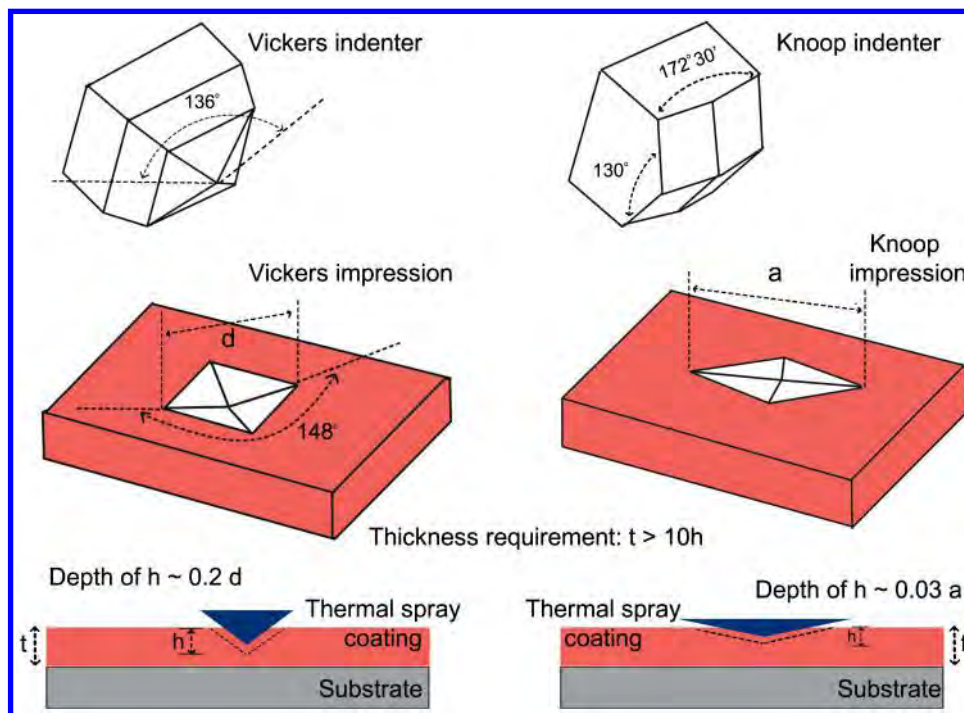
2. CEN ENV 843-4: 'Advanced technical ceramics – Monolithic ceramics – Mechanical properties at room temperature, Part 4: Vickers, Knoop and Rockwell superficial hardness tests'.

3. JIS R1610: 'Test methods for hardness of fine ceramics'.

4. ISO 4516-2002: 'Metallic and other inorganic coatings – Vickers and Knoop microhardness tests'.

5. ASTM C1327-08: 'Standard test method for Vickers indentation hardness of advanced ceramics'.





' $t$ ' is the coating thickness; ' $h$ ' is the penetration depth of the indentation; ' $d$ ' and ' $a$ ' are the diagonal impression lengths for the Vickers and Knoop microhardness tests, respectively

#### 17 Indenter geometries used for hardness characterisation of thermal spray coatings

$$HV = \frac{2P \sin \theta}{d^2} = 0.0018544 \frac{P}{d^2} \quad (5)$$

where  $P$  is the test load (in newtons),  $\theta$  is the included angle between opposite indenter faces ( $136^\circ$ ), and  $d$  is the average length (in millimetres) of the two diagonals of the indentation measured. It is meaningful to point out that the use of SI units, GPa, is consistent with the reporting format of scientific papers; although the use of the Vickers hardness scale is a more familiar format for engineers. A similar Knoop hardness scale also exists.

The SI unit of GPa is similar to that of pressure, tensile strength or elastic moduli and suggests that hardness may be correlated with the intrinsic material properties.<sup>210,221</sup> There is such a correlation between the hardness values and elastic modulus.<sup>222,223</sup> However, hardness is a more complex property than elasticity since it involves plastic deformation and brittle failure.<sup>221</sup> Therefore, interpretation of a hardness value without relating this number to the microstructure may lead to a poor understanding of structure–property relationships.

A Knoop indentation test involves using a calibrated machine to force a pointed rhombic-based, pyramidal-shaped diamond indenter with specified face angles, under a predetermined load into the coating surface. Figure 17 illustrates the geometrical dimensions of the Vickers and Knoop indenters and sketches their indentation impressions. Unlike a Vickers hardness test, Knoop indentations only require the measurement of the long diagonal of the resulting impression.

Another difference in comparison to the Vickers test concerns the calculation of Knoop hardness, which is the ratio of the applied test load to the projected area on the indented surface. The Knoop calculation assumes that the elastic recovery of the narrow diagonal is negligible. The mathematical relationship of Knoop hardness, in GPa, is given as

$$HK = \frac{P}{A_p} \times 10^{-3} = 0.014229 \frac{P}{a^2} \quad (6)$$

where  $P$  is the test load (in newtons),  $A_p$  is the projected area of the indentation (in square millimetres),  $a$  is the length of the major diagonal of the indentation measured (in millimetres).

The diagonal lengths of a Vickers indent are approximately 2.8 times shorter than the major diagonal of a Knoop indent for the same specimen at a similar test load. The indentation depth of the Vickers indent is approximately 1.5 times more deep than the Knoop indent.<sup>220</sup>

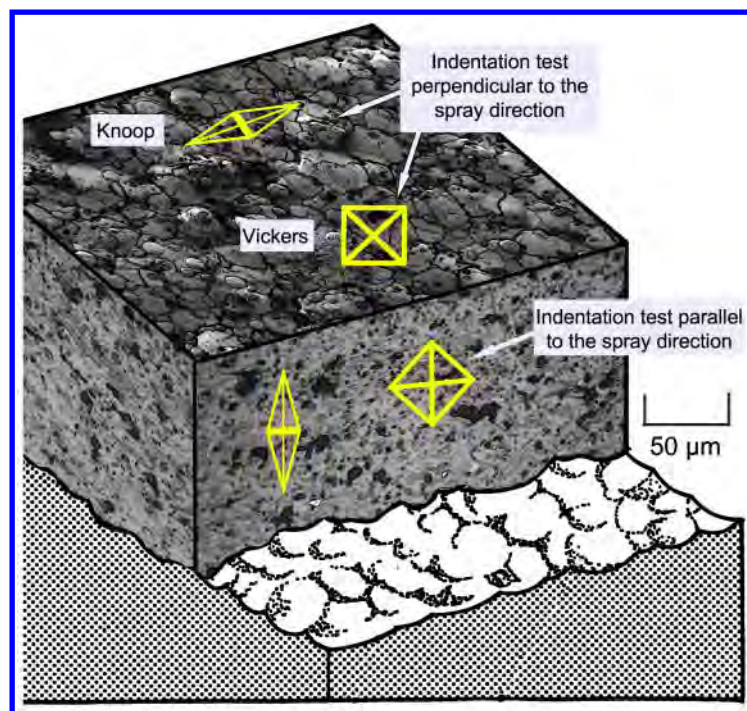
The deeper Vickers indents are, therefore, more likely to cause cracks in ceramics than Knoop indentations. The cracks may influence the measured hardness by fundamentally altering the deformation process that contributed to the formation of the impression. Generally, the cracks impair the measurement of the diagonal length because of distortion at the indent tip and edges. On the other hand, the long slender tip edge of the Knoop indentation is more difficult to discern precisely; especially for thermal spray coatings that have revealed multiple phases.

The Vickers and Knoop hardness measurements exhibit dissimilar indenter geometries and, thus, different impressions on the coating surface. Thus, forming relationships between these hardness scales is not recommended. In other words, there is no numerical equivalency between the Knoop and Vickers hardness scales and empirical conversions between these scales have no basis in scientific rigour.

#### Microstructural relationships in hardness testing.

The hardness values should be independent of the test load since the impressions made by the indenter are geometrically similar. However, it has been reported<sup>224,225</sup>





18 Indentation test perpendicular to spray direction (coating top section) and parallel to spray direction (cross-section)

that lower test loads are more affected by localised microstructural variations than higher test loads. The ensuing hardness-load dependence was also found for microhardness testing of bulk ceramics and is known as the indentation size effect (aka 'ISE').<sup>226</sup> The ISE states that hardness will usually decrease with increasing indentation test load until it reaches a constant,<sup>227</sup> assuming that there are no substrate-induced effects. The phenomenon has been associated with factors such as the lamellar microstructure, surface energy and indenter shape. The ISE was more pronounced during hardness testing of thermal spray coatings due to the heterogeneous microstructure. The scatter experienced with the void systems, as well as the different phases of solidified splat layers, influenced the elastic response of the indent.

Therefore, the test load should be reported with the hardness value. The recommended choice of test load for both indentation methods should be sufficiently large to allow good indent observations but not cause excessive cracking at the surface. Typical microhardness test loads used for thermal spray coatings are 1 N (100 gf), 3 N (300 gf) and 5 N (500 gf). Lower test loads should not be used unless accompanied with suitable microstructural evaluation and the ISE should be taken into account during the reporting of such data.

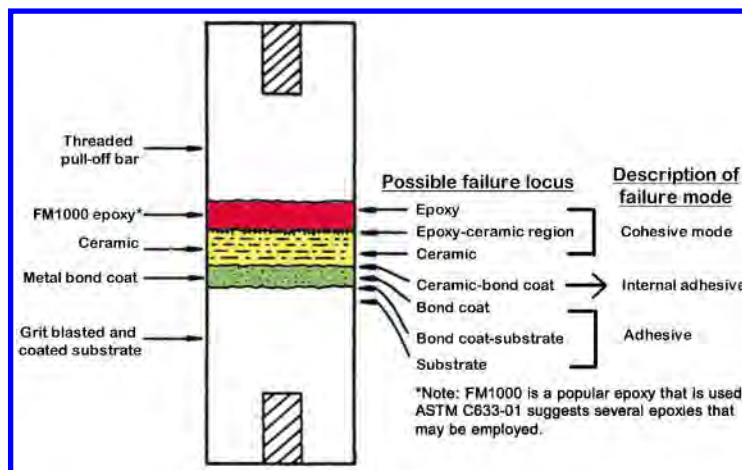
The materialographic preparation before testing can influence the hardness results. In most cases, measurements were made with the test indent on the cross-section of the lamella structure. Thus, similar to porosity measurements by IA, the accuracy of the hardness test depended on the surface roughness that arises from the grinding and polishing procedures. An appropriate method of sample preparation for thermal spray coatings is described by Ref. 228.

Berndt and Leigh<sup>105</sup> have shown that the Knoop hardness in the plane of the coating surface was about 1.5 times higher than indents made perpendicular to the substrate; i.e., on the coating cross-section. This can be explained by the anisotropic architecture of thermal

spray coatings on the two orthogonal planes of symmetry. Thus, as illustrated in Fig. 18, indentations carried out (i) parallel to the spray direction, and (ii) perpendicular to the spray direction, should yield different values due to the splat piling orientations. The distinct void network and the volume of material under indentation loading account for the relative differences in hardness values.

The most common orientation for an indentation test is on the cross-section of the thermal spray coating. However, the literature makes little mention of the indenter orientation with respect to the thermal spray lamellar microstructure. Thus, the indenter alignment can exhibit two prime orientations where the pyramid axes are rotated by 90°. It can be appreciated that the indent orientation may influence the test results; for instance, the axis of the indenter can be aligned (i) along the lamellar layers, or (ii) across the lamellar layers. Therefore, under such testing conditions the coating cross-section might reflect anisotropic behaviour.

It was expected that there would be scatter in the hardness data for a thermal spray coating because the random distribution of the pore and crack network influences the indent hardness values. Subsequently, the reliability of the entire data depends on the number of indentations performed. Ten indentations are recommended by the ASTM standards for Vickers and Knoop hardness tests. However, the heterogeneous nature of thermal spray coatings indicates that more indents are necessary. The associated coefficient of variance; i.e., standard deviation divided by the mean, should also be reported with the calculated mean.<sup>227</sup> Berndt *et al.*<sup>211</sup> and Valente *et al.*<sup>212</sup> further suggested that the hardness data could be assessed by using statistical tools such as the Student's test and Weibull distribution analysis. The data scatter can be reduced by performing tests on carefully selected regions that appear to have no void defects. However, it must be cautioned that preferentially choosing dense areas within the coating for



The coating system is not drawn to scale but exaggerated for clarity of potential coating failure modes

#### 19 Nomenclature of failure loci and mode for the TAT samples

indentation will bias the data to high values and is not recommended.

Another indent technique uses a spherical indenter<sup>229</sup> that is intended to reduce coating damage during indentation. The stress field under such a blunt Hertzian indenter is quite different from that generated under a sharp indenter.<sup>230,231</sup> Thus, comparisons of data generated by these two different test methods are not valid. A similar argument can be made concerning Rockwell hardness tests that employ a brale, 120° diamond cone, indenter.

Individual splats and lamellae can be characterised by using nanoindentation techniques that employ a 3-sided pyramid-shaped Berkovich tip.<sup>232</sup> Nanoindentation is highly sensitive to the material phases and structural defects within the splat and is, thus, defect sensitive. The nanoindentation technique has also measured the material properties of singular nano-sized splats in coatings.<sup>233–235</sup> In these tests, the nano-sized indents lie entirely within a single lamellar and it is expected that the indent depth is less than 1/7 of the lamellar thickness. Thus, these indent tests measure intrinsic material properties and represent the maximum value in coating characteristics. The influence of crack and pore networks that are micrometre-sized are not measurable by nanoindentation methods.

### Bond strength of thermal spray coatings

The unique microstructure of thermal spray coatings contributes to several bonding mechanisms within the layers. The possible bonding mechanisms present in a typical thermal spray coating can be categorised into five major types: (i) mechanical keying, (ii) physical adhesion by dispersion forces, (iii) chemisorption and epitaxy, (iv) diffusion, and (v) chemical reaction.<sup>236,237</sup> The dominating bonding mechanisms vary with specific coatings and are sensitive to factors such as surface roughness; thermal stresses at the interface; and particle velocity and temperature before impingement. These aspects can be categorised with respect to process parameter controls. For instance, coating procedures such as parameters for grit blasting can influence the degree of mechanical keying, which will reflect on the coating adhesion strength.

It is difficult to measure accurately the magnitude of each type of interfacial bonding mechanism. Thus,

laboratory tests have focussed on a holistic approach for measuring the bond strength that relates to the entire coating structure. Measuring the 'adhesion bond strength' of the coating not only addresses the interfacial problem of the lamellar character of a coating but also involves the integrity of the interfaces between the substrate and coating, residual stress, crack population, pore size, and pore distribution. Techniques suitable to study the adhesion bond strength of coatings have been presented.<sup>217,237–239</sup> Some of the quantitative methods used to measure the bond strength of coatings can be found in Table 11.

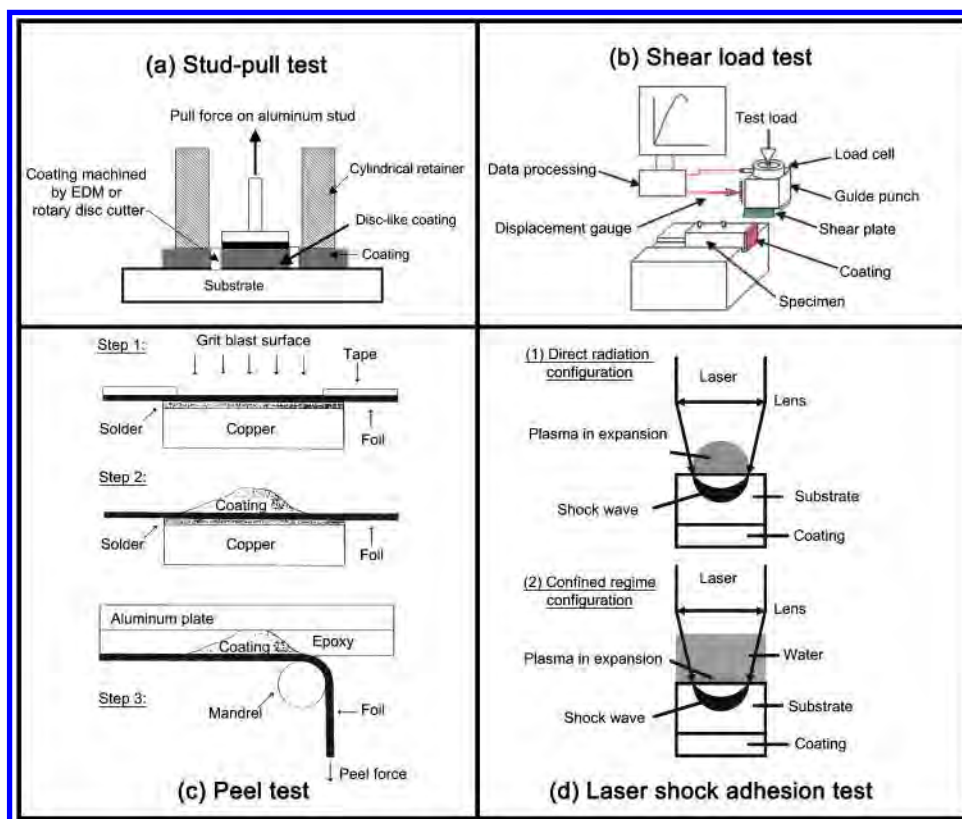
The most common method to measure coating adhesive bond strength follows the tensile adhesion test (TAT) method.<sup>243</sup> There are industrial and national standards that provide guidelines to performing TATs; e.g., described in Ref. 240. The TAT method is comprised of a thermal spray coated disk of a known diameter that is attached with epoxy to a complimentary uncoated plug. A tensile force is then applied to the coating assembly using a uniaxial tensile loading device. The ultimate stress at failure is known as the coating system's minimum tensile adhesion or cohesion bond strength, depending on the interpretation of the failure locus as shown in Fig. 19. Attention should be taken in interpreting the results, especially for multi-component coatings, since the TAT value is a measure for failure at the weakest plane that may occur in a combination of locations.

It is important to note that the description of the 'failure mode' is not to be confused with 'failure mechanism'. The failure mode refers to the physical description of the failure location determined from Fig. 19. This description provides only limited insights into the fracture process; that is, how and where micro-cracks initiate, grow in size, coalesce with each other, and interact to form macro-cracks; causing eventual coating failure. Such understanding of the fracture process relates to the failure mechanism. Coating failure mechanism studies can be carried out using acoustic emission or ultrasound to qualitatively assess the thermal spray coating behaviour.<sup>261–263</sup>

It is also pointed out that the tensile adhesion strength for a test is calculated by dividing the maximum load by the tested cross-sectional area. However, this may not always be a true reflection of the adhesion strength. In

**Table 11 Methods to quantify thermal spray coating bond strength on the basis of the measurement principles**

Measurement technique	Working principle	Can distinguish and measure			Test standards	References
		Adhesion strength	Cohesive strength			
Tensile adhesion test	The test consists of a thermal sprayed coating on one face of a cylindrical substrate fixture bonded to the face of a loading fixture using epoxy glue. This assembly of coatings and fixtures is subjected to a tensile load normal to the plane of the coating with the failure load and failure location noted.	x	x		ASTM C633-01(2008) <sup>240</sup> , ISO 14916:1999 <sup>241</sup> , JIS H8302:2010 <sup>242</sup>	243,244
Stud-pull test	This method uses a loading fixture or 'stud' mounted with an epoxy coating onto a flat coating surface. Machining is then performed, either by electro-discharge or a rotary disc cutter, to form a disc-like structure in the coating to which a stud is mounted. The stud is then pulled off at a controlled rate with the breaking force and failure location recorded.	x	x		ASTM D4541-09 <sup>245</sup>	246
Pin and ring test	A cylindrical pin and coaxial ring made from similar material is aligned within the same plane before a thermal spray coating is deposited. The gap between the pin and the ring is typically 40 µm but the coating stiffness will prevent any movement of the assembly. No epoxy glue is required in this technique. The cylindrical pin is then pulled off the coaxial ring with the breaking force and failure location noted.	x	x		-	239
Shear load test	A wedge-shaped shear plate made of conventional tungsten carbide cutting tool is aligned parallel to the interface of the coating and substrate. A uniform loading is applied to the upper face of the sample and monitored by a high precision load cell. Different failure modes can be deduced from the force-displacement curves and coating failures.	x	x		DIN EN 15340 <sup>247</sup>	239,248
Peel test	A thin metal foil is coated and subsequently the top coat is glued onto an aluminium plate using epoxy. The assembly is then mounted to a jig and the foil peeled away from the coating at a constant rate. From the load displacement curve, the peel strength as a function of the crack position is calculated. This test is adapted from ASTM D3167-10: 'Standard Test Method for Floating Roller Peel Resistance of Adhesives'.	x			-	249,250
Laser shock adhesion test (LASAT)	The test is based on a spallation technique, which allows generation of normal tensile stresses at the coating-substrate interface. The laser shock is generated by irradiating the substrate side using a high powered laser. The incident compressive stress wave is reflected backward into a tensile stress wave that may delaminate the coating. The LASAT threshold is determined by incrementing input laser power density until delamination occurs. Thus, the strength of the interface may be determined.	x			-	251-253
Scratch test	An indenter such as a Rockwell diamond is used to scratch a path on cross-sections of the coatings. As the stylus slides from the substrate towards the coating, the normal, friction and critical forces; the coefficient of friction; and the penetration and residual depth of the stylus are measured.	x	x		ASTM C1624-05(2010) <sup>254</sup> , ISO/DIS 27307 (working draft) <sup>255</sup>	256-258
Interfacial indentation test	Apparent coating interfacial toughness is calculated based on a measurement of the crack length initiated along the coating-substrate interface. The calculated value, $K_{CA}$ , can be correlated to the adhesion bond strength of the coating.	x			-	259,260



a stud-pull test, b shear load test, c peel test, and d laser shock adhesion test

## 20 Schematic representation of alternative methods to measure the bond strength of thermal spray coatings

the case of partial failure, a region of a coating that did not detach or fail and may remain on the substrate after the test. The measurement of the effective failure area is, therefore, uncertain. Possible data normalisation could be achieved by either testing the remaining coating or accounting for the reduction in failure area in the calculation of adhesion strength.<sup>264</sup> The ASTM standard and similar standards from other organisations does not allow for such a normalisation procedure; nor has such a procedure been reported in the literature.

The TAT test results often display large variability in the failure stress and, thus, the minimum number of tests required to obtain reliable results is often questioned.<sup>243</sup> The ASTM standard recommends testing five sprayed samples and averaging the adhesion strength. This method may serve as an effective tool for industrial quality control but is insufficient for quantitative research in which the variability in strength is of interest. Thus, experiments must be conducted to a coefficient of variance of about 30% to determine a valid statistical representation of the failure bond strength for a specific coating. A low coefficient of variance is an indication of good repeatability within a data set.

The statistical analysis can be further extended by fitting the data set to an appropriate distribution function; i.e., either a Normal or Weibull distribution, to allow the study of failure probabilities and ascertain estimations for the coating strength. The Weibull distribution is an effective representation of brittle materials such as ceramic thermal spray coatings.<sup>243</sup> The underlying hypothesis of the Weibull distribution<sup>265</sup> is that failure of a structure initiates within the microstructure, which causes macroscopic crack growth. A material structure can be segregated to small representative elements or volumes.

These elements will interact in the same way as the links of a chain. Therefore, cracking from one representative element will cause the whole structure to fail. The application of the Weibull model to thermal spray coatings is valid since the likelihood of failure would be caused by the initiation of micro-cracks and crack growth within the lamellae in an analogous fashion to the failure of a chain.

The TAT stress and strain properties of samples are not usually reported or used to distinguish the mechanical properties of different coatings. As stress and sample extension measurements are variables recorded during a test run, analysis of these measurements could be performed. Berndt *et al.*<sup>244</sup> demonstrated that the stress v. extension plot was useful in identifying coating failure modes. The stress and strain properties also related to (i) the mechanism(s) of lamellae sliding over each other, (ii) the coating porosity level, and (iii) the elastic modulus of the coating.

Tensile adhesion test procedures have shifted to using a heat activated, film adhesive instead of the traditional two part liquid mix that has the potential of excessive penetration into the coating.<sup>266</sup> In a round robin test conducted using liquid and film epoxies, it was found that liquid epoxies resulted in a higher tensile strength and greater scatter in data.<sup>267</sup> Other criteria pertinent to TAT methods include (i) a coated specimen area between 452 and 531 mm<sup>2</sup> (i.e., about 1 inch in diameter) that was normalised with respect to the maximum failure force, and (ii) the tensile test machine crosshead rate of between 0.010 and 0.021 mm s<sup>-1</sup> to simulate quasi static loading conditions.

The stud pull test, see Fig. 20a, proposed by Elmoursi *et al.*<sup>246</sup> is similar to the TAT described earlier. It can be



applied to coatings deposited on any geometrically flat sample and employs a simple, portable pull-off tester. However, it also requires machining around the circumference of the bonded stud-coating boundary. The machining can be performed either using EDM or a slurry fed rotary-disc cutter. Both of these methods can introduce sectioning or thermal stresses; as well as being difficult machining processes for ceramic or cermet coatings.

Another method that does not require the use of an epoxy is the shear load test; Fig. 20b, which probes the coating's resistance against shear stress and is claimed to be akin to loading conditions of coatings in practice.<sup>248</sup> The DIN EN 15340<sup>247</sup> standard describes the execution steps for testing. Three failure types can be determined, (i) cohesive, (ii) adhesive and (iii) a mixed adhesive/cohesive.

Other techniques to measure the bond strength of coatings include the peel test<sup>249</sup> (Fig. 20c), a laser shock adhesion test<sup>251</sup> (Fig. 20d), the pin and ring test,<sup>239</sup> the scratch test,<sup>256</sup> and the indentation test.<sup>259</sup>

### Stiffness of thermal spray coatings

The elastic moduli,  $E_c$ , or coating stiffness of thermal spray coatings usually differ from the corresponding bulk material, especially for ceramic and composite coatings.<sup>268,269</sup> The coating elastic modulus can be viewed as an indication of the following intrinsic microstructural properties:<sup>164,270,271</sup> (i) inter-lamellar splat cohesion, (ii) porosity or the void and crack network, (iii) chemical phases and their proportions within a coating, and (iv) the residual stress state.

#### Elastic modulus measurements

The elastic modulus is traditionally evaluated from the slope of the initial linear portion of the stress-strain curve. Beyond the elastic limit, the sample undergoes plastic deformation, yielding and finally fracture. For bulk ceramic materials, the associated elastic limit, elastic modulus and fracture strength is a well-defined value.

However, for thermal spray ceramics or composite coatings, the elastic modulus is influenced by factors such as cohesion of the lamellae as well as the distribution of void and crack networks. The inhomogeneous architecture of a coating is likely to cause pseudo ductility because the lamellae may slide over each other.<sup>268</sup> In response to the external loading, the elastic energy dissipation will be governed by crack growth and fracture. Therefore, the determination of the precise elastic limit, as well as estimating the linear portion of the stress-strain curve can be a challenge. Consequently, there is a wide range of values for  $E_c$  for similar coating compositions deposited by an identical thermal spray method. These values can differ significantly from the equivalent bulk material.<sup>269,271</sup>

The stiffness result is sensitive to the test direction due to the anisotropic nature<sup>164</sup> of the coating. In other words, it is important to remember the relative orientation of mechanical testing since the elastic moduli of thermal spray coatings are different in a direction parallel to the coating surface compared to the perpendicular direction.

The  $E_c$  measurement for thermal spray ceramics is difficult to execute because of the limited coating thickness and the brittle nature of the coating. There are different methods to measure the coating stiffness

and most relate to the coating stiffness parallel to the substrate. Elastic modulus in thermal spray coatings can be categorised into destructive and non-destructive test methods, Table 12.

The two common techniques used by researchers to obtain elastic modulus values of thermal spray coatings are by the indentation<sup>164</sup> and flexural bend tests,<sup>276</sup> which are the first two methods presented in Table 12. These techniques are used due to the simple specimen preparation procedures as well as the ease of executing the experiments and calculations. Another notable test that provides *in-situ* measurement values is the cantilever beam test<sup>117,190</sup> that tracks the curvature profile of a thin substrate during the thermal spray process.

#### Indentation methods to measure modulus

The indentation test of thermal spray coatings undergoes the same procedure as a conventional indentation hardness test. The fundamental principle is based on the resistance of a solid material against the penetration of the indenter under load. An elastic-plastic field develops during the indentation process and the deformed coating is comprised of reversible, or elastic; and irreversible, or plastic, behaviour.

The Marshall *et al.*<sup>223</sup> method to calculate modulus assumes elastic recovery of the in-surface dimension of a Knoop indentation. Elastic modulus was hence determined by measuring the major and minor diagonals of the Knoop indent on the sample. In the fully loaded state, the ratio of the diagonal dimensions,  $a$  (major) and  $b$  (minor) of the Knoop contact area was defined by the indenter geometry,  $a/b=7.11$ . Elastic recovery during the unloading cycle reduced the length of the diagonals and indentation depth. The reduction in length was evident for the minor diagonal,  $b'$ , while the major diagonal change,  $a'$ , was negligible. Therefore, on modelling the Knoop indent as an elliptical hole subjected to uniaxial stress, the relationship of the displacement can be summarised as follows

$$\frac{b'}{a'} \approx \frac{b'}{a} = \frac{b}{a} - \frac{\alpha H_k}{E} \quad (7)$$

The elastic modulus,  $E$ , is derived by rearrangement of equation (7).

$$E = \frac{\alpha a H_k}{b - b'} \quad (8)$$

where  $H_k$  is the Knoop hardness (in GPa) and  $\alpha$  is a constant determined by Marshall *et al.*<sup>223</sup> to be 0.45. Since the measurement depends on the elastic recovery of the minor diagonal,  $b'$ , its alignment with respect to the coating microstructure can be used to measure anisotropic behaviour. The extent of recovery depended on the hardness to modulus ratio and the ratio of  $a/b'$  was always greater than 7.11. Although, the Knoop indenter caused less damage among other sharp indenter geometries, it was critical to select the most appropriate test load. For example, an excessive indentation load may cause extensive cracking around the indent impression. However, crack-free measurements require low load indentation. The observation of small indent dimensions may require the use of SEM.

The alternative to the Marshall method is the Oliver and Pharr method<sup>222</sup> that used depth sensing indentation measurements. In this method, the applied load  $P$ , and



Table 12 Compilation of coating stiffness measurement techniques

$E_c$ measurement technique	Working principle	Measurement direction with respect to substrate		References
		Parallel	Perpendicular	
Micro-indentation test	A polished coating section is indented with an indenter of known geometry. The test method should allow for either the measurement of indent geometries or analysis of the indentation load/penetration-depth curve.	x	x	164,229,272–275
3-point/4-point flexure test	Flexure tests are based on the principle that the applied force induces an elastic displacement. The stiffness of the coating is deduced from the deflection of the specimens under bending; measuring either the longitudinal strain or the midsection displacement. Complex quadratic equations are then solved on the basis of a linear elastic model.	x	x	272,276–282
Compression or tensile test	The stiffness and strength is found by measuring the applied load and the resulting deflection on a free standing, as-sprayed coating. There are many specimen configurations that can be used but usually they take on the shape of a rod or bar. The strain of the coating specimen can be recorded, by using strain gauges, under tensile or compression loading. The gradient of the resulting constitutive relations (i.e., stress–strain relationship) is the elastic modulus of the free standing coating.	x	x	277,283,284
Cantilever beam test	During coating deposition, a thin substrate will adopt a curvature due to the changes in through-thickness stress gradients and the inelastic stress relaxation. Continuous curvature monitoring allows the calculation of elastic modulus based on the balance of forces and moments between the substrate and the coating. The curvature displacement can be monitored via contact probes or a non-contact scanning laser extensometer and video recording. Alternatively, post-coating testing can also be used. This involves thicker substrates with strain gauges located on the coating and substrate surfaces. A series of increasing loads is applied to the end of the cantilever beam and the moment at the gauged section is calculated. Using laminated plate bending theory, the Young's modulus and Poisson's ratio are inferred on the basis of a least squares fit of the equilibrium equations.	x		118,190,285–287
Laser ultrasonic method or laser acoustic test	The first technique employs two lasers: a generating laser and a detection laser to modulate the detection light into an interferometer. The alternate method uses acoustic surface waves with frequencies up to 200 MHz, which are also induced by short laser pulses and detected with a piezoelectric transducer. The ultrasonic waves are usually generated by a Nd:YAG laser pulse. The surface wave signals are processed by cross-correlation and Fourier transformation to determine a dispersion spectrum with optimal signal-to-noise ratio. The theoretical curve is fitted to the measured dispersion spectrum to derive film parameters such as Young's modulus, density and/or film thickness. This test involves the study of the mechanical resonance of solids in terms of the frequency spectrum, which is a source of information on the elastic and damping properties of materials. Ultrasonic wave velocity measurements are carried out by attaching a pair of identical broadband ultrasonic transducers on opposite sides of the specimen. One transducer is used to transmit a continuous, harmonic elastic wave into the specimen; the other one receives the signal transmitted through the specimen. While sweeping at the frequency from 100 kHz upwards, the phase shift between the incident and transmitted waves are measured continuously. Depending on the geometry, density and assumed elastic symmetry of the samples, the elastic stiffness tensor can be calculated from the free body resonance frequencies identified among the peaks in the spectra.	x	x	275,288
Resonant ultrasound spectroscopy test	This test is based on the fundamental resonant frequency of specimens when excited mechanically by a singular elastic strike from an impulse tool; i.e., a hammer. Specimen supports, impulse locations, and signal pick-up points are selected to induce and measure specific modes of the transient vibrations. A transducer senses the resulting mechanical vibrations of the specimen. The appropriate fundamental resonant frequencies, dimensions, and mass of the specimen are used to calculate dynamic Young's modulus, dynamic shear modulus, and Poisson's ratio.	x		289,290
Impulse excitation test		x	X	277

penetration depth,  $h_i$ , curve are recorded simultaneously for the complete loading and unloading cycle. Different sharp indenter tips (i.e., Vickers and Berkovich geometries) and spherical indenters can be used and the apparent elastic modulus of the indenter specimen system (also known as reduced modulus,  $E^*$ ) can be defined as

$$E^* = \frac{1}{c^* \bar{A}} \frac{dP}{dh_i} \quad (9)$$

where  $\bar{A}$  is the contact area of the indenter,  $dP/dh_i$  is the slope of the  $P$ - $h_i$  curve of the initial stage of unloading from  $P_{\max}$ . The constant  $c^*=1.142$  for the Vickers, 1.167 for the Berkovich, and 1.128 for circular conical indenters.<sup>291</sup> The contact area at peak load was determined by the geometry of the indenter and the depth of the contact. Subsequently, the elastic modulus of the coating was determined by accounting for the elastic effects of the non-rigid indenter. Mathematically,

$$\frac{1}{E^*} = \frac{1-\nu^2}{E} + \frac{1-\nu_{in}^2}{E_{in}} \quad (10)$$

Rearranging for elastic modulus,  $E$

$$E = \frac{1-\nu^2}{\frac{1}{E^*} - \frac{1-\nu_{in}^2}{E_{in}}} \quad (11)$$

The characteristic material properties of the indenter,  $E_{in}$  and  $\nu_{in}$ , can be obtained from the equipment manufacturer. The use of the Oliver and Pharr method<sup>222</sup> requires knowledge of Poisson's ratio for the thermal spray coating. However, Poisson's ratio values have not been determined widely for thermal spray materials and are often assumed to follow those of bulk dense materials that range between 0.20 and 0.30. Poisson's ratio values for thermal spray materials are discussed further in 'Poisson's ratio of thermal spray coatings' section.

The size of the indent relates to the difference in measuring the elastic properties of the consolidated coating microstructure or the individual splats. Nano-sized indentations are most likely related to the local splat properties of the sprayed coating since the indents are sufficiently small to probe the individual splat. Local material phases and their elastic properties within a splat can be measured but the effects of micrometre-sized pores and cracks are not measured.

Thermal spray coatings are more appropriately measured with the use of micrometre-sized indents. Conventional microindentation will result in impressions that span across several splat layers, various void morphologies and the crack network. An appropriate indentation load must be selected that does not cause excessive cracking or localised densification of the coating.<sup>277</sup> The resulting micrometre-sized indent is, therefore, considered a more direct representation of the elastic and plastic mechanical responses of a thermal spray coating. It is cautioned that the interaction of indenter geometry with the microstructure under investigation must be considered when interpreting or comparing nanoindentation and microindentation results.

#### Bending test methods to measure modulus

The flexural test method can be used for either coated substrates or free standing coatings, in either the tension

or compression modes. Producing free standing coatings can be arduous and the following discussion applies to flexural testing on a coating that has been sprayed onto a substrate.

The major difference between three-point and four-point flexural tests is the location of the bending moment. While three-point bending can be performed, the disadvantage is that there is a linear variation of the bending moment from a maximum at the loading point to zero at the two supports. This load pattern predetermines the failure location in the tested thermal spray coating; i.e., the failure locus is positioned under the loading nose.

The four-point bending method allows for uniform bending moment distribution between the two inner loading noses. In this case, the thermal spray coating fails at its weakest point within a large volume of the sample. In other words, four-point bending is able to measure the structural weaknesses within the coating loaded between the inner load noses and is a preferred test method for measuring thermal spray coating strength.

Nonetheless, the elastic modulus *via* the flexural method is determined from the measurement of applied force and sample deflection curves. There are mechanics of materials approaches that can be used for calculations. For three-point bending, the flexural elastic modulus of a beam under loading is related to the deflection  $w$  measured

$$E_{\text{beam}} = \frac{PL^3}{4bh^3} \times \frac{1}{w} = \frac{L^3 \nabla}{4bh^3} \quad (12)$$

where  $P$  is the force applied,  $L$  is the length of the outer supports (or 'noses'),  $b$  is the specimen width and  $h$  is the beam thickness. The slope of the load versus deflection curve,  $\nabla$ , can also be used to calculate the flexural elastic modulus of the beam.

The formula for the flexural elastic modulus of a beam under four-point bending requires calculations that depend on the location of the loading span. There are 2 commonly adopted configurations, (i) the loading span is 1/3 of the support span (i.e.,  $a=b$ ), or (ii) the loading span is 1/2 of the support span (i.e.,  $2a=b$ ). The deflection is related to two loads acting simultaneously and  $E_{\text{beam}}$  can be calculated by applying the principle of superposition

$$E_{\text{beam}} = \frac{P(3aL^2 - 4a^3)}{4bh^3} \times \frac{1}{w} = \frac{(3aL^2 - 4a^3) \nabla}{4bh^3} \quad (13)$$

The calculation for the 1/3 support span configuration is

$$E_{\text{beam}} = 0.21 \frac{L^3 \nabla}{bh^3} \quad (14)$$

The calculation for the 1/2 support span configuration is

$$E_{\text{beam}} = 0.17 \frac{L^3 \nabla}{bh^3} \quad (15)$$

The coating modulus is deconvoluted from the beam modulus by applying the rule of mixtures between the thermal spray coating and substrate. The elastic modulus of the thermal spray coating can be calculated

**Table 13** Compilation of elastic modulus values of thermal spray coatings

TS method	Material	Elastic modulus (GPa)	Measurement method	Ref
APS	Al <sub>2</sub> O <sub>3</sub> –13 wt-% TiO <sub>2</sub>	270	Indentation	233
APS	ZrO <sub>2</sub> –8 wt-% Y <sub>2</sub> O <sub>3</sub>	100–200	Indentation	293
APS	ZrO <sub>2</sub> –8 wt-% Y <sub>2</sub> O <sub>3</sub>	44–106	Indentation	164
APS	Al <sub>2</sub> O <sub>3</sub>	33–67	Indentation	164
APS	ZrO <sub>2</sub> –8 wt-% Y <sub>2</sub> O <sub>3</sub>	36–39	Ultrasonic	277
APS	ZrO <sub>2</sub> –8 wt-% Y <sub>2</sub> O <sub>3</sub>	25	Uniaxial compression	277
APS	ZrO <sub>2</sub> –8 wt-% Y <sub>2</sub> O <sub>3</sub>	13	Uniaxial tension	277
FS	TiO <sub>2</sub>	125–160	Indentation	275
WSP	TiO <sub>2</sub>	155–210	Indentation	232
WSP	Al <sub>2</sub> O <sub>3</sub>	67–149	Indentation	164
APS	Ni–5 wt-% Al	78	Four-point bending	186
APS	Ni–5 wt-% Al	83–105	Indentation	186
CS	Ni–5 wt-% Al	58–110	Indentation	186
HVOF	Ni–5 wt-% Al	172–178	Indentation	186
HVOF	Ni–5 wt-% Al	166	Four-point bending	186
TWA	Ni–5 wt-% Al	80–110	Indentation	186
TWA	Ni–5 wt-% Al	103	Four-point bending	186
HVOF	WC–17 wt-% Co	179–95	Cantilever beam method	287
APS	ZrO <sub>2</sub> –8 wt-% Y <sub>2</sub> O <sub>3</sub>	45–51	Cantilever beam method	287

APS: atmospheric plasma spray; HVOF: high velocity oxygen fuel spray; CS: cold spray; FS: flame spray; TWA: twin wire arc.

from the following equation

$$E_{\text{coating}} = E_{\text{beam}} \times \frac{h_{\text{coating}}}{h_{\text{coating}} + h_{\text{substrate}}} \quad (16)$$

The use of equation (16) is valid for both modes of flexural bending and has provided estimates for the coating elastic modulus.<sup>281</sup>

A second method is derived from a mathematical relation of the bending mechanics of a bi-material beam. For flexural testing, the entire coated specimen bending modulus,  $E_{\text{beam}}$ , is expressed by

$$E_{\text{beam}} = \frac{1}{3} \left( E_c^* h_c^3 + E_s^* h_t^3 - h_c^3 - \frac{E_c^* h_c^2 + E_s^* h_t^2 - h_c^2}{4 E_c^* h_c + E_s^* h_s} \right) \quad (17)$$

where  $h_t$  is the entire specimen thickness and subscripts 'c' and 's' denote coating and substrate, respectively. The apparent elastic modulus,  $E^*$ , includes both bending deflection and shear deflection while the true modulus includes only the bending deflection. Their relationships are

$$E_s^* = \frac{E_s}{1 - \nu_s^2} \quad (18)$$

$$E_c^* = \frac{E_c}{1 - \nu_c^2} \quad (19)$$

The elastic modulus of the substrate,  $E_s$ , can be predetermined by conducting a bending test on an uncoated calibration coupon. The apparent modulus  $E_c^*$  can be solved by relating the relevant equation, (12) or (13) with equation (17). Finally, the coating elastic modulus can be found by relating the apparent elastic modulus to the true elastic modulus.

The methods presented above are generally employed in cases for the flexural testing of a thermal spray coating–substrate system. Different variants of the test orientation<sup>278,292</sup> and calculation methods exist but are not covered here.

The elastic moduli of thermal spray coatings depend on the concentration, shape, continuity, and the spatial

distribution of the different phases in a composite or multi-phase coating. Consider the simple case of a composite comprised of two elastically isotropic phases, wherein the applied load causes equal strains in each of the phases at all times. In the case of a two phase structure, the overall composite stress is the sum of the stresses carried by each phase. The composite modulus is the weighted average of the moduli of two constituents<sup>280</sup>

$$E_c = \text{vol}_1 E_1 + 1 - \text{vol}_2 E_2 \quad (20)$$

The subscripts represent the elastic modulus of the particular phase and *vol* is the volume fraction of that phase. Equation (20) is applicable to thermal spray coatings in which multi phases often exist within a coating microstructure due to the rapid melting and quenching of splats. This physical effect accounts for the differences in elastic moduli of coatings with similar chemical composition but processed by distinct thermal spray parameters that could alter the proportion of metastable phases.

Reported literature elastic modulus values for thermal spray coatings are presented in Table 13. A comparison of these values reveals that although indentation methods were often employed, these tend to exhibit higher elastic modulus readings compared to other methods. This is probably attributed to indents that are most likely placed in dense regions of the coating to enable a well-defined deformation for measuring purposes. Subsequently, the coating stiffness values will appear high since the test is measuring a sample region where the void content is low. This example highlights the subjective nature of the indentation technique that may present large errors if applied inappropriately.

In addition, thermal spray coatings also perform differently with respect to the load direction; coating stiffness in compression is usually higher than that measured in tension.<sup>277</sup> Under compressive stresses, the elastic closing of the pore and crack network tends to cause a gradual decrease of the microcrack density or increase in coating density. However, under tensile stresses, there is a coalescence of these microcracks;

and such inelastic processes reduce the effective coating elastic modulus.<sup>294</sup>

### Models to calculate modulus

The methods to calculate the elastic modulus of the coating are derived, mostly, from the literature on dense sintered materials. Prior knowledge of structural features such as splat dimensions, degree of inter-lamellar bonding, porosity type and distribution are required for their application to thermal spray coatings.

For instance, porous materials can be considered as two phase structures, whereby the second phase is the void network; i.e.  $E=0$ . The elastic modulus of this microstructure was found to conform to an empirical relationship such as

$$E = E_o e^{-k\rho} \quad (21)$$

where  $E_o$  was the modulus of the dense material,  $\rho$  the volume fraction of porosity, and  $k$  a material constant. This relationship relates the volume fraction of voids to the coating microstructure and has ignored the influence of void morphology; that is, the effect of cracks contrasted to pores on the overall elastic modulus.<sup>271</sup> The following expression has been used<sup>164</sup> on the basis of pores and cracks that interact

$$E = E_o \left( 1 - \frac{5a}{4c} + \frac{3}{4} P_s \right) \quad (22)$$

where, ' $c$ ' is the axis parallel to the stress direction and ' $a$ ' is the plane perpendicular to ' $c$ '.  $P_s$  is the porosity. The model was used to explain the effects of oriented spheroidal-shaped pores on the thermal spray coating. Coatings with orientated spheroidal pores underwent a larger decrease in overall elastic modulus perpendicular to the major axis of the spheroidal pores. However, the model; i.e., equation (22), cannot be applied to practical situations.

Appropriate models encompassing the effects of the orientation and shape of voids on the elastic value of thermal spray coatings have been discussed by Nakamura *et al.*<sup>231</sup> and Sevostianov *et al.*<sup>108</sup> These models were effective in describing the anisotropic character of thermal spray coatings. By adapting these models, Kroupa *et al.*<sup>294</sup> modelled coating properties as a function of (i) globular pores, (ii) inter-splat horizontal pores/cracks, and (iii) intra-splat vertical cracks.

For instance, within a representative volume element  $V$  of a thermal spray coating there are  $N$  randomly distributed spherical pores of radii  $R_k$  and the coating porosity  $P_s$  is given by

$$P_s = \frac{1}{V} \sum_{k=1}^N \frac{4}{3} \pi R_k^3 \quad (23)$$

According to this model, cracks contribute to porosity  $P$ . The family of horizontal cracks and vertical cracks each have unique representative functions.<sup>295</sup> For a family of approximately  $N_3$  circular and randomly distributed horizontal micro-cracks of radii  $r_{3k}$  their scalar crack density  $p_3$  is

$$p_3 = \frac{1}{V} \sum_{k=1}^{N_3} r_{3k}^3 \quad (24)$$

The  $p_3$  function can be used to represent the crack network parallel to the substrate surface, which mimics imperfect bonding between splats along the interface. Similarly, for a family of approximately  $N_1$  circular and randomly distributed vertical micro-cracks of radii  $r_{1k}$  the scalar crack density  $p_1$  is

$$p_1 = \frac{1}{V} \sum_{k=1}^{N_1} r_{1k}^3 \quad (25)$$

The microstructural characteristics of thermal spray coatings with respect to anisotropy of the elastic moduli in the in-plane  $E_{ip}$  and through thickness  $E_{tt}$  directions are expressed as

$$E_{ip} = \frac{E_o}{1 + (c_1) \left( \frac{P_s}{1 - P_s} \right) + (a_1) \left( \frac{p_1}{1 - P_s} \right)} \quad (26)$$

$$E_{tt} = \frac{E_o}{1 + (c_3) \left( \frac{P_s}{1 - P_s} \right) + (a_3) \left( \frac{p_3}{1 - P_s} \right)} \quad (27)$$

where the positive constants  $c_1$ ,  $a_1$ ,  $c_3$  and  $a_3$  depend on the Poisson's ratio,  $\nu_o$ .

$$c_1 = c_3 = \frac{3(1 - \nu_o)(9 + 5\nu_o)}{[2(7 - 5\nu_o)]} \quad (28)$$

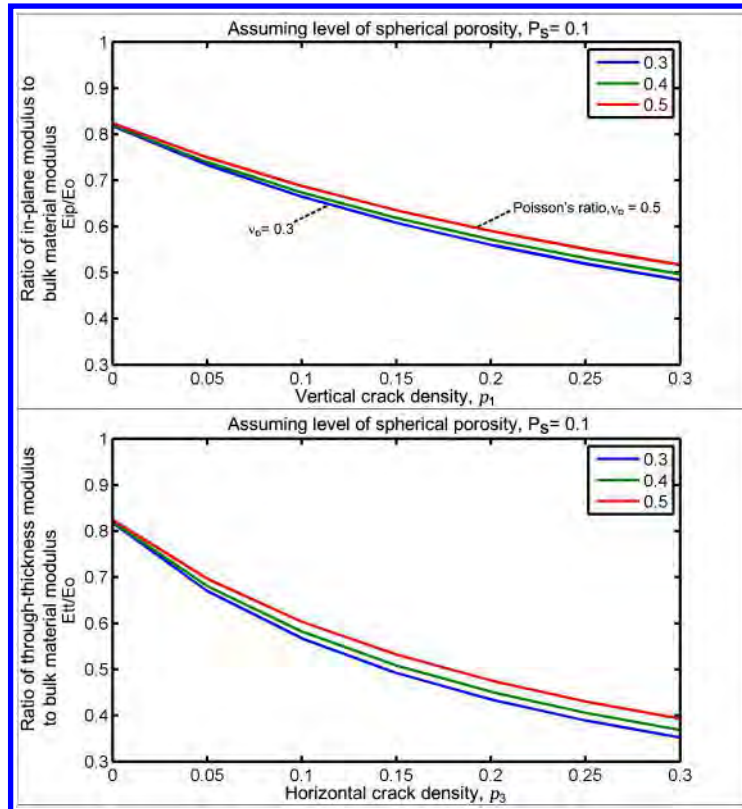
$$a_1 = \frac{8(1 - \nu_o^2)(1 - 3\nu_o/8)}{[3(1 - \nu_o/2)]} \quad (29)$$

$$a_3 = \frac{16(1 - \nu_o^2)}{3} \quad (30)$$

It can be deduced from these equations that coatings with the same porosity levels ( $P_s$ ) and scalar crack density values (i.e.,  $p_1=p_3$ ) may exhibit anisotropic behaviour with respect to the two-dimensional elastic moduli, as shown in Fig. 21. The net effects of void size and shape dependencies are reflected in the ratios of its elastic moduli  $E_{ip}/E_o$  on  $p_1$  and  $E_{tt}/E_o$  on  $p_3$ .

Another theoretical model of the relationship between the coating elastic modulus and structural parameters was proposed by Li *et al.* and McPherson *et al.*<sup>271,296</sup> It was assumed that when a load was applied perpendicular to the deposit plane, then the stress would be transferred from one lamella to the other through the bonded interface area. Under such loading conditions, lamellae would experience tension at the bonded interface area and bending at the non-bonded regions. Thus, neglecting the effects of vertical cracks, this analysis showed that the elastic modulus of an idealised thermal spray coating perpendicular to the coating plane consisted of two components. These being:

1. The localised elastic deformation at bonded regions between lamellae, which was directly proportional to the bonding ratio or fractional contact area between lamellae.
2. The bending of lamellae between bonded regions, which became significant for a bonding ratio of less than 40% and depended strongly on the ratio of the mean dimension of the individual contact regions to the mean lamellar thickness.



21 Graphic plots of equations (26) and (27) to show the ratio of coating modulus with respect to the intrinsic modulus. A constant volume of spherical pores of 0.1 is assumed. The levels of vertical and horizontal cracks are plotted on the x-axis. The variation in Poisson's ratio is represented by each individual line

Using circular plate theory for an idealised microstructure consisting of the stacking of micrometre-sized lamellae; the Young's modulus in the through thickness direction,  $E_{tt}$ , can be determined as

$$\frac{E_{tt}}{E_0} = \alpha \left[ 1 + 2\pi \left( \frac{a}{\delta} \right)^4 \beta^2 f(\beta) \right]^{-1} \quad (31)$$

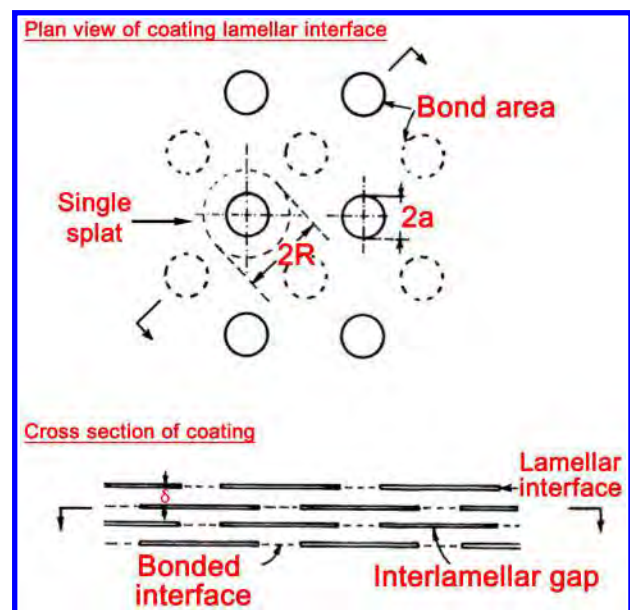
$$\beta = \frac{R}{a} = \sqrt{\frac{\pi}{8\alpha}} \quad (32)$$

Where  $2R$  is the diameter of the single splat,  $2a$  is the size of the bonded region,  $\delta$  is the mean lamellar thickness and  $\alpha$  is the bonding ratio between lamellae. The term  $f(\beta)$  is a function of the interface bonding ratio. There are two components of elastic strain for the coating under tensile stress; one arising from localised elastic strain at regions of 'true' contact between lamellae and the other arising from elastic bending of the lamellae between the contact regions.

The modelling of micro-cracks as a distribution of flat hollow rotational ellipsoids as shown in Fig. 22 should not be interpreted as the actual micro-crack distribution. Physically, the inter-splat boundary structure exhibited regions of good bonding, surrounded by interconnected non-bonded regions of complex shapes. Similarly, ignoring micro-crack formation to achieve an idealised thermal spray microstructure is not experimentally possible. Nevertheless, the models developed can be considered as useful theoretical treatments, to explain the low values of Young's moduli and elastic anisotropy of thermal spray deposits.

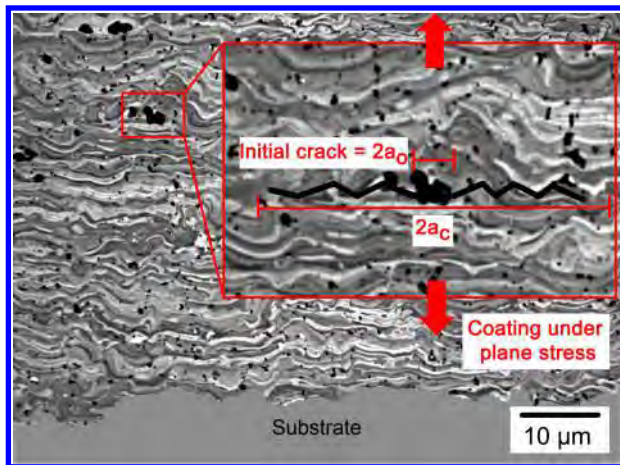
### Fracture toughness of thermal spray coatings

Fracture toughness measurements indicate the stress required to propagate a pre-existing flaw. Thermal spray coatings have pre-existing cracks and pores that can individually or collectively serve as crack initiation zones and stress concentrators. Fractographic analysis of thermal spray coatings<sup>297</sup> has found that the prime mechanisms of crack propagation are by intra-splat



22 Theoretical model of the idealised microstructure in relation to Li's model<sup>271</sup>





23 Illustration showing crack growing from an initial crack length to a critical crack length. An inter-splat boundary has been overlaid onto this image to indicate potential fracture initiation sites

cracking and inter-splat de-cohesion. These were followed by interlinking of pores and cracks, splat sliding and pore compaction. Formation of secondary cracks and crack bifurcation led to a significant increase in fracture surface area. Therefore, the fracture toughness of a thermal spray coating is a measure of the residual strength of a microstructure under the influence of its void network. The importance of fracture toughness on the durability of APS YSZ coatings has been highlighted by Darolia *et al.*<sup>131</sup>

### The Griffith concept

The fracture mechanics approach for assessing thermal spray coatings is based on linear elastic fracture mechanics (LEFM) that was pioneered by Griffith.<sup>298</sup> The Griffith theory indicates that the fracture work per unit crack extension at the onset of unstable fracture is balanced by the strain energy release rate from the surrounding elastically strained material. In other words, the fracture zone absorbs a large amount of additional energy and this must be balanced by the energy required to create a new fracture surface.<sup>237,299,300</sup>

In particular, the 'strain energy release rate concept' will be introduced to further clarify the quantity of energy released from a fracture. Two terms need to be defined:

1. The strain energy release rate,  $G$ , is the quantity of stored elastic strain energy released due to the extension of a crack advancing by a unit area.
2. The critical strain energy release rate,  $G_c$ , is the component of work irreversibly absorbed in local plastic flow and cleavage to create a unit of fracture.

The condition for spontaneous fracture is reached when the strain energy release rate,  $G$  equals  $G_c$ . The mathematical relationship relating the strain energy release rate for the crack tip is

$$G_c = \frac{\sigma_c^2 \pi a_c}{E} \quad (33)$$

where  $\sigma_c$  is the stress level and  $2a_c$  is the crack length at fracture.  $E$  is the elastic modulus of the material.

The problem can also be formulated in terms of the concept known as 'stress intensity', leading to the terms of (i) stress intensity factor,  $K$ , (i.e.,  $K_I$  for plane stress) and (ii) critical stress intensity factor,  $K_c$ , (i.e.,  $K_{Ic}$ ). The

quantities such as  $K_c$  and  $K_{Ic}$  are commonly referred to as the material fracture toughness. Linear-elastic fracture toughness of a material in plane stress or plane strain,  $K_{Ic}$ , is related to  $G_{Ic}$  and the material Poisson's ratio,  $\nu$

$$K_{Ic} = \begin{cases} \sqrt{G_{Ic} E} & \text{plane stress} \\ \dots & \dots \\ \sqrt{\frac{G_{Ic} E}{1 - \nu^2}} & \text{plane strain} \end{cases} \quad (34)$$

The equations (33) and (34) can be rewritten to describe the tensile stress that corresponds to initiating a crack of length  $a_c$

$$\sigma_c = \begin{cases} \frac{K_{Ic}}{\sqrt{\pi a_c}} & \text{plane stress} \\ \dots & \dots \\ \sqrt{\frac{K_{Ic}^2 (1 - \nu^2)}{\pi a_c}} & \text{plane strain} \end{cases} \quad (35)$$

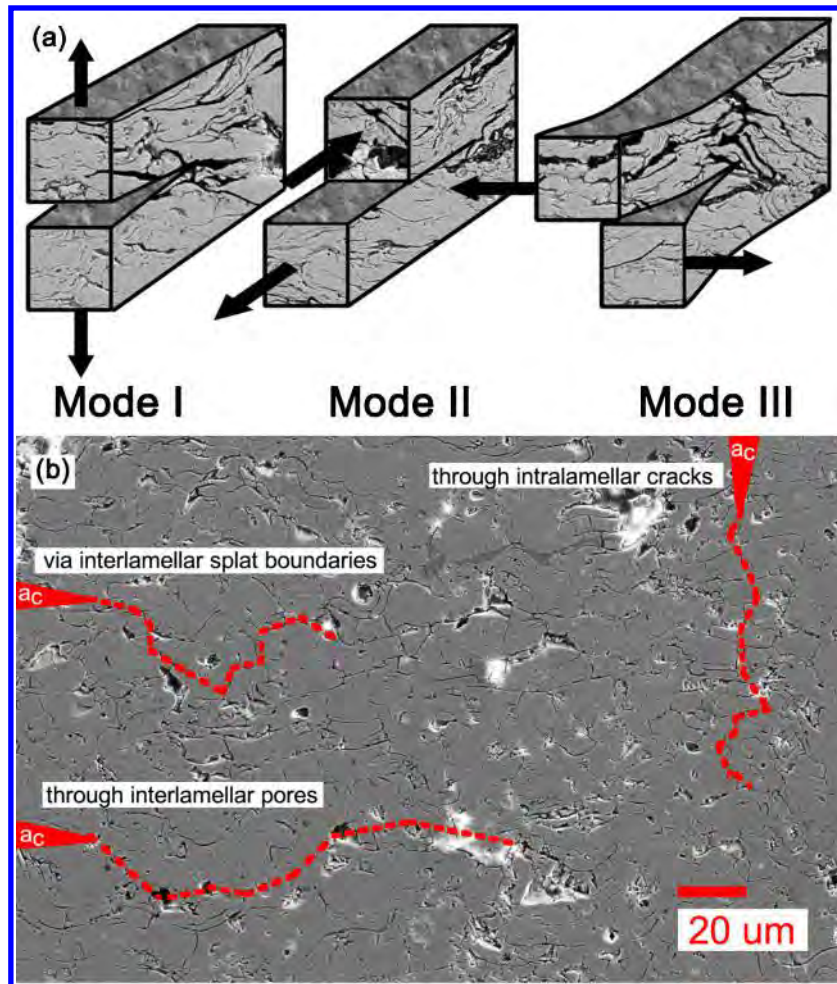
### Application to thermal spray coatings

For thermal spray coatings, the  $\sigma_c$  from the above equation relates to the strength of the microstructure of the sprayed material under the influence of the pore and crack network.<sup>268</sup> It is shown in Fig. 23 that the initial crack  $a_0$  grows to the critical crack length  $a_c$  for coating failure. The coating elastic modulus,  $E$ , depends on the porosity and contact between the lamellae. Therefore,  $G_{Ic}$  would also depend on these microstructural features because a crack can propagate between areas of weak contact within the splats. In other words, the fracture strength of a coating is related to its microstructure by  $E$  and  $G_{Ic}$ . The largest pores or micro-cracks produced during spraying would be expected to act as fracture initiating defects<sup>268</sup> and, thus, influence strength through  $a_c$ .

The focus of discussion on fracture toughness has been on plane stress loading or fracture in 'mode I'. The subscript 'Ic' denotes 'mode I' crack opening under a normal tensile stress perpendicular to the crack. Other modes of fracture, Fig 24a, include the shear (mode II) or the tearing (mode III). However, thermal spray ceramic coatings typically exhibit a much higher compressive strength than tensile strength; therefore, they do not fail in shear modes under loading normal to the coating surface. That is  $K_{IIc}$  and  $K_{IIIc}$  are much higher than  $K_{Ic}$ .<sup>299</sup> For this reason, the testing of thermal spray coating fracture toughness has been limited mostly to 'mode I' or determining  $K_{Ic}$  or  $G_{Ic}$ ,<sup>238</sup> although 'mode 2' fracture studies have been performed.<sup>301</sup> The complex splat interactions also dictate the crack path. As depicted in Fig. 24b, the initial crack,  $a_0$ , can propagate through defects within the coating.

The methods to determine fracture toughness has been detailed by Lin and Berndt<sup>237,238</sup> and include (i) the double cantilever beam (DCB) test, (ii) the double torsion test, (iii) a flexural bending test, (iv) the scratch test, (v) the indentation test method, and (vi) the tensile test. Table 14 compiles several of these methods and identifies the related quantity of measure,  $K_{Ic}$  or  $G_{Ic}$ .

The locality of measurement is determined by the fracture path of the specimen. By controlling the locus of fracture, it is possible to carry out fracture toughness tests for either the coating-substrate interface or within the coating structure itself. One example is the DCB test, in which carefully orientated grooved edges are machined



**24 a** Possible fracture modes for thermal spray coatings. **b** ‘ $a_c$ ’ represents the initiation cracks. Three potential cracking mechanisms are suggested

during the specimen assembly.<sup>237</sup> The DCB testing of plasma sprayed alumina coatings measured values of  $G_{Ic}=10\text{--}15\text{ J m}^{-2}$  for adhesive and  $G_{Ic}=16\text{--}25\text{ J m}^{-2}$  for cohesive failures.<sup>237</sup> The preference for fracture at the coating–substrate interface during four-point bend methods implies that fracture toughness values reflect the microstructure’s interface strength. Modified four-point bend measurements on APS YSZ coatings have shown that the interfacial fracture toughness<sup>304,306</sup> is about  $G_{Ic}=17\text{--}50\text{ J m}^{-2}$  but can increase to about  $\sim 120\text{ J m}^{-2}$  after accounting for sintering effects after high temperature exposure.<sup>306</sup> Similar values for DCB testing of APS YSZ coatings,  $G_{Ic}=20\text{--}80\text{ J m}^{-2}$ , have been obtained by Heintze and McPherson.<sup>309</sup>

The TAT data are a measure of coating fracture; hence it is possible to correlate the TAT results to the fracture toughness of thermal spray coatings. The TAT geometry can be considered as a bar with circumferential cracks;

therefore, permitting a fracture mechanics interpretation of the adhesive/cohesive strength of the coating. Berndt<sup>243</sup> proposed that the tensile strength can be transformed into fracture toughness by the relationship<sup>310</sup>

$$K_{Ic} = P \left[ -1.27 + 1.72 \left( \frac{D}{d} \right) \right] D^{-1.5} \quad (36)$$

where  $P$  is the TAT specimen failure force,  $D$  is the outside diameter of the bar and  $d_i$  is the inside diameter in the circumferentially notched bar. It was assumed that the notch in the bar was conferred by pre-existing defects such as splat boundaries and other defects.

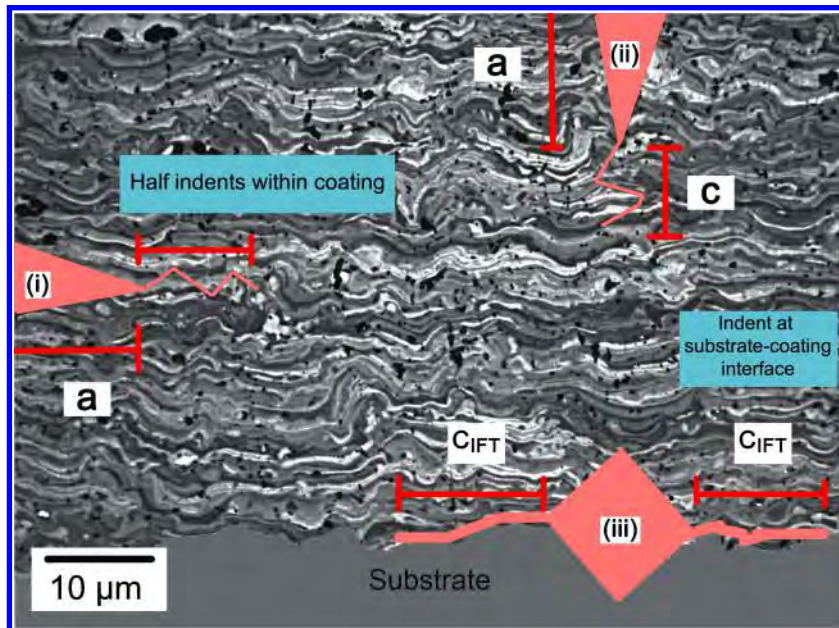
#### Indentation methods

Fracture toughness measurements for thermal spray coatings can be performed by the indentation method. However, it must be pointed out that the location of the indent determines the region of the microstructure that

**Table 14** Compilation of fracture toughness testing methods for thermal spray coating

Method	Locality of measurement		Initial quantity measured	Application reference
	Interface (adhesive)	Coating (cohesive)		
Double cantilever beam test	x	x	$G_{Ic}$	3,237
Four-point bend test (standard)	x		$K_{Ic}$	277,302,303
Four-point bend test (modified)	x		$G_{Ic}$	304–306
Indentation	x	x	$K_{Ic}$	109,216,307,308
Uniaxial tension	x	x	$K_{Ic}$	243,303





'a' refers to the diagonal length and 'c' is the total crack length; (i) Parallel cracks within the coating lamellae; (ii) perpendicular cracks within the coating lamellae; (iii) crack along the coating-substrate interface

## 25 Effects of indenter location and test orientation

is measured. Importantly, the coating fracture toughness should not be confused with its interface fracture toughness. Thus, the interface fracture toughness refers to indentation along the coating-substrate interface.<sup>216</sup> On the other hand, an overload indentation test measures an average fracture toughness of the coating that is not localised to a specific microstructural feature.

Failure is most likely to occur along the interface between the bond coat and substrate interface for the majority of fracture toughness measuring techniques. If a particular feature of a coating microstructural volume is the artefact of interest, then crack propagation must be deliberately controlled to cause the specified fracture mode. For the DCB test,<sup>311</sup> a groove can be placed within the coating to promote cohesive failure. Similarly, Vickers indents<sup>109</sup> may be placed within the microstructural volume of the coating to obtain the fracture toughness of this specified element without the influence of the substrate.

The difference in interface fracture toughness and coating fracture toughness is highlighted in Fig. 25. The indentation fracture toughness of a thermal spray coating microstructure can be calculated by several methods. The methods of (i) Lawn *et al.*,<sup>109,312</sup> and (ii) Niihara *et al.*<sup>307,313</sup> are listed below:

$$\text{Lawn Method : } K_{Ic} = 0.025 E_c^{0.5} P^{0.5} c^{-1.5} \quad (37)$$

$$\text{Niihara Method : } K_{Ic} = 0.103 a^{0.8} E_c^{0.4} P^{0.6} c^{-1.5} \quad (38)$$

where  $a$  is the diagonal length of the indent,  $E_c$  is the elastic modulus of the sprayed coating,  $P$  is the indenter load,  $c$  is the total crack length, and  $H_v$  is the measured Vickers hardness value. In both methods, a median crack type<sup>312</sup> is assumed; and  $cla \geq 2.5$ . It should be emphasised that Lawn *et al.* intended this method to be employed for dense ceramics and never applied this relationship to sprayed coatings. However, the method has been adopted by scientists and engineers in the thermal spray community.

Chicot and coworkers<sup>216</sup> have investigated the interface fracture toughness. They found that for a given coating and substrate couple, there exists a load that is independent of the coating thickness and which corresponds to the cracking ability of the interface. The Vickers indent was deliberately placed along the axis of the substrate-coating interface, inducing semi-circular shaped cracks localised along this interface. The measurement of the crack formation was proportional to the substrate-coating interface fracture toughness values

$$K_{IFT} = 0.015 \frac{P_c}{C_{IFT}^{1.5}} \left( \frac{E_a}{H_a} \right)^{0.5} \quad (39)$$

where  $P_c$  was the critical indenter load and was considered to be representative of the adhesive properties of the coating on its substrate. The term  $H_a$  was the apparent hardness at that indenter load,  $E_a$  was the apparent elastic modulus and  $C_{IFT}$  was the length of crack induced along the interface. The interfacial fracture toughness of flame sprayed alumina coatings on steel substrate<sup>217</sup> was found to be between 0.7 and 1.9 MPa m<sup>0.5</sup>.

The cracking behaviour of a coating is influenced strongly by its anisotropic microstructure. Therefore, the orientation and placement of indents must be appropriately considered for the indentation fracture toughness testing of thermal spray coatings.

It was mentioned that the elastic modulus of thermal spray coatings was lower than that of the bulk material because of its porosity network and diminished contact area that results from splat overlays. Similarly, the effective fracture surface energy,  $(G_c)_{eff}$ , would be lower than that of the bulk material  $G_c$  since a crack would pass from one region of good contact to another.

McPherson *et al.*<sup>268</sup> proposed a simple model to describe the effective strain energy release rate in a typical thermal spray microstructure. Since  $(G_c)_{eff}$  was related to the bonding ratio between the neighbouring

splats, fracture would not be expected to occur by propagation of a single crack in a coating. The mathematical relation is:

$$(G_{Ic})_{eff} = 2m_c \alpha G_{Ic\_dense} \quad (40)$$

where  $\alpha$  is the bonding ratio between lamellae; that is the fraction of the lamellae surfaces in contact with other lamellae, and  $m_c$  is a factor describing the multiplication of crack branching that would increase the crack surface area.  $G_{Ic\_dense}$  is the fracture surface energy of a dense material.

### Poisson's ratio of thermal spray coatings

Compression of material in one direction leads to expansion in the other two orthogonal directions. Conversely, tensile loading leads to contraction in the orthogonal directions. The ratio of the relative contraction/transverse strain under loading is known as Poisson's ratio ( $\nu$ ).

It has been noted that the evaluation of coating bond strength, crack growth rates, and coating stresses during in-service loading requires accurate values of the coating Poisson's ratio. In addition, Poisson's ratio of a thermal spray coating depends on its unique lamellar microstructure and, therefore, can vary greatly with spray parameters. The range of Poisson's ratio that has been assumed for most thermal spray coatings lies between 0.20 and 0.30.<sup>302,305</sup> Measurements of Poisson's ratio for thermal spray coatings are rarely conducted; thereby bringing these assumptions into question.

The lack of Poisson's ratio data in the field of thermal spray arises because these coatings are thin and bonded to the substrate. Consequently, it is experimentally difficult to remove the coating and apply conventional uniaxial testing procedures. Substrate removal techniques such as physical sectioning,<sup>283</sup> and chemical etching or high temperature combustion<sup>277</sup> have been employed. Yet, it is quite likely that these post processing steps would damage the coating microstructure. Nonetheless, after the coatings were removed, the specimens were machined to the required specimen sizes and Poisson's ratio determined; usually by a uniaxial compression or tension test. The compression method has been a preferred test mode since thermal spray coatings exhibit a low tensile strength. The stress-strain curve was fitted by a linear relation through the least-squares fit method, and the slope of the fitted line was equal to the elastic modulus. Correspondingly, the slope of the fitted line with the curve of transverse strain and longitudinal strain was the measured Poisson's ratio. The measurements of transverse and longitudinal strain were accomplished with strain gauges mounted on the coating.<sup>283</sup>

The reported Poisson's ratio associated with 'coating-only' experiments for plasma spray YSZ ceramic coatings range from  $\nu=0.04$  (as sprayed) to 0.2 (annealed at 1316°C for 500 h).<sup>277</sup> Plasma sprayed nickel (45 wt-%) chromium coatings averaged a Poisson's ratio of around  $\nu=0.15$ .<sup>283</sup> These reported values suggest that the commonly used estimate of  $\nu=0.20$ –0.30 was inaccurate to describe the influence of spray parameters and post-treatment processes on the Poisson's ratio thermal spray coatings.

Another method to determine *in-situ* values of thin films with substrates employed a cantilever beam test

that was instrumented with strain gauges.<sup>287</sup> The test consisted of a beam that was clamped at one end and weights applied to the other end. Strain gauges were pre-placed on the coating and substrate surfaces. Readings were taken as the weights were applied. The elastic modulus and Poisson's ratio of the coating were calculated from the strain gauge data, the dimensions of the specimen, the mechanical properties of the substrate, and the applied bending moment. The analysis method used the equations of equilibrium for bending moments and forces at the gauged section. The Poisson's ratio for HVOF sprayed tungsten carbide coatings<sup>287</sup> was about 0.33, while for plasma spray YSZ coatings<sup>287</sup> it was around 0.181. However, this method has not been universally adopted by researchers.

There has been little experimental work to understand the unique transversely isotropic microstructure on Poisson's ratio measurements. The measured Poisson's ratios relate specifically to the test orientation in the prior discussion. That is, uniaxial compression or tension loading was applied on the plane section of the coating while the coating cross-sections were measured for transverse and longitudinal strain. The above test orientation would be appropriate for the majority of thermal spray applications. However, if the test orientation was altered then the strain measurements would likely be dissimilar; thereby implying that the Poisson's ratio is an anisotropic material property.

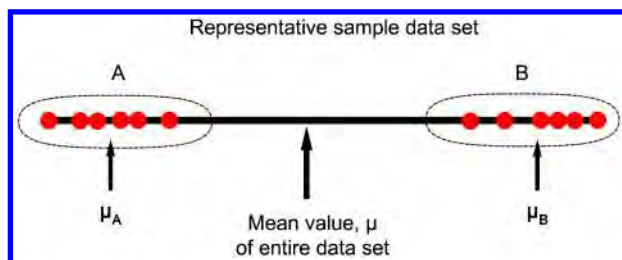
### Reporting statistical concepts for thermal spray coating testing

Robust calibration and well-planned experiments have allowed high accuracy in the measurement of the mechanical properties of thermal spray coatings. Yet, data variability within the experimental results gathered from the mechanical tests used to assess thermal spray coatings is not uncommon. The following section examines the importance of using statistical methods to analyse data variability.

#### The numerical average and coefficient of variation

A customary practice to account for variability is to present the data as a statistical mean ( $\mu$ ) along with the standard deviation ( $\sigma$ ) of the mean. This statistical treatment accounted for the random error, which was related to the uncertainty due to small errors in the assayed values as well as specimen batch-to-batch variability; i.e., the random uncertainty in the experimental process.

Accordingly, the ratio of standard deviation to the arithmetic mean is used to indicate whether the measurement was repeatable; commonly expressed as the coefficient of variation (COV). In probability theory and statistics the COV represents the normalised measure of dispersion of a probability distribution. Distributions with a low COV demonstrate data with low variance. For example, the COV for the TAT data of a typical thermal spray coating, manufactured by a flame or plasma spray process, is 0.23–0.31.<sup>243,314</sup> For microhardness data, the COV of plasma sprayed coatings can range from 0.05 to 0.27<sup>211,212,314</sup> while coatings produced *via* D-gun® and HVOF have a COV ranging from 0.11 to 0.18.<sup>212,227</sup> Also, as the sample size increases, the COV value decreases.



26 Hypothetical experiment with possible data scattering

There is a concern when the COV is large with a sample size greater than 20. Such a data set indicates fluctuations within the microstructure. In fact, it is not possible to obtain a low COV for coatings that exhibit multiple phase compositions randomly distributed throughout the microstructure. The representation of this possible data variability is illustrated in Fig. 26. Random uncertainty was not the root cause for data scatter in this case study. Instead, the expected COV will be high because the data is bimodal. The points were skewed into two separate regions of A and B, which might specify instances such as differences in porosity or phase composition. Moreover, the arithmetic mean of the data set did not reflect this segmentation of data points. Bimodal coating properties have been reported by various authors.<sup>212,315–317</sup>

Nonetheless, the concept of a singular mean value to describe material properties is deeply entrenched in science and engineering and is necessary for modelling exercises. The relevance of the reported arithmetic mean only becomes statistically significant if there is a method to identify data variability caused by the intrinsic coating microstructure or random uncertainties. Since data scatter could be indicative of anisotropic and heterogeneous behaviour in coating microstructure, it is essential to interpret such information with respect to micrographs that illustrate the porosity and phase composition. That is, a standard statistical presentation of measured values might be misinterpreted, especially when the COV was high.

### Probabilistic aspect of ceramic thermal spray coating properties

The study of thermal spray ceramics has been approached statistically and follows the concept of statistical distributions originating from data analysis of brittle fracture in ceramic components.<sup>318</sup> With regard to fracture experiments on ceramic specimens, it indicates that the size of the specimens influences the probability of failure. Similarly, the probabilistic aspect of analysing the mechanical properties of thermal spray coatings can be adopted. The approach was applicable to thermal spray ceramic coatings because fracture also generally initiated from small flaws that are discontinuities in the microstructure. For simplicity, the flaws can be assumed to be small cracks that are distributed in the surface or volume. Thus, strength depends on the size of the largest defect in a specimen, which varies among coatings.

The strength-size effect cannot be explained in a deterministic way using the model of a single crack in an elastic body. Instead, interpretation requires understanding the behaviour of cracks distributed throughout a material. Consequently, it was assumed that many

flaws, which behave like cracks, are stochastically distributed in a ceramic material. It was further assumed that cracks do not interact; that is, their separation was large enough for their stress fields not to overlap. This assumption is essential for the following argument and is equivalent to the weakest link hypothesis: i.e., failure of a specimen was triggered by the weakest volume element or by the largest flaw.

A single number cannot describe the strength of a thermal spray ceramic coating adequately. A strength distribution function is necessary and a large number of specimens are required to characterise mechanical properties. By assessing coating mechanical strength data to a known statistical distribution, such as Weibull or Normal distributions, the coating has a certain probability of failure or survival. Researchers have proposed and applied the Weibull theory to the mechanical behaviour of thermal spray coatings.<sup>212,227,311,315</sup>

In Weibull theory, the size effect on the nominal strength arises from the fact that large structures have a greater probability of revealing a material element of a critically small strength. The principles of this statistical size effect were proposed by Prof. Waloddi Weibull.<sup>265</sup> He concluded that the tail distribution of low strength values in a large data set, i.e. those data that have a low probability, cannot be represented by any of the previously known distributions. The underlying hypothesis is based on the inception that macroscopic crack growth in one small element of the structure causes failure. Therefore, small representative volumes of the material in the structure interact in the same way as the links of a chain, that is, in a series coupling.

According to Weibull theory, the cumulative probability,  $P_i$ , that a sample will yield at a particular random property value  $x_i$  is given by

$$P_i = 1 - \exp\left[-\left(\frac{x_i - x_u}{x_0}\right)^m\right] \quad (41)$$

The equation may be presented in the following linear form

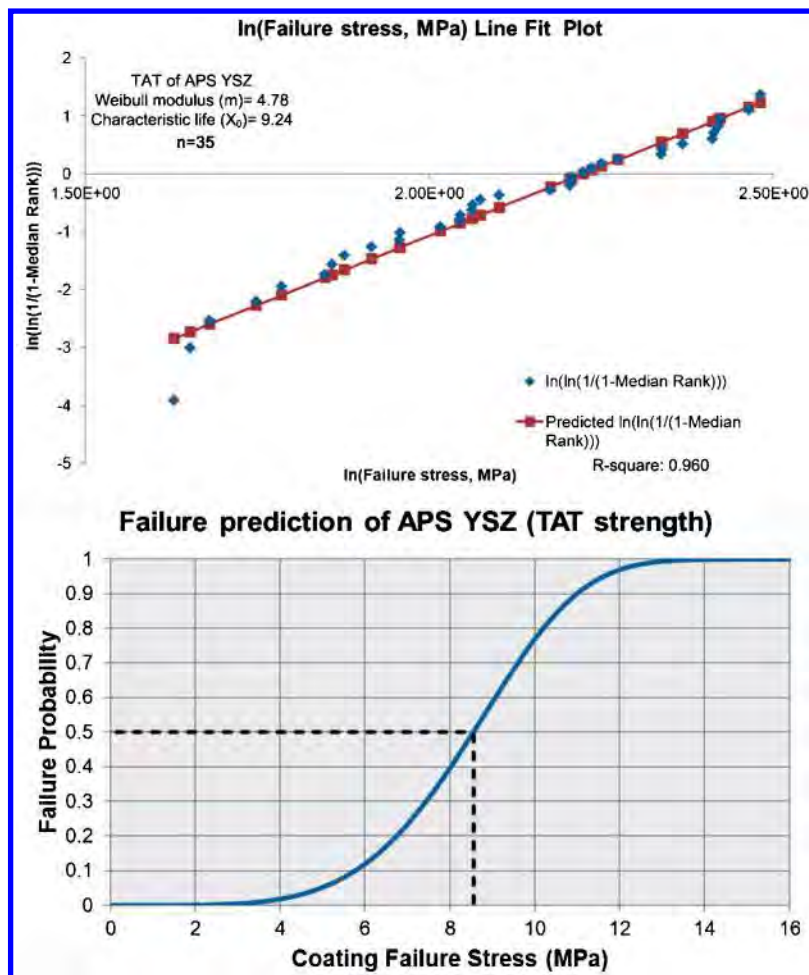
$$\ln\left[\ln\left(\frac{1}{1-P_i}\right)\right] = m \ln(x_i - x_u) - m \ln x_0 \quad (42)$$

where  $x_0$  is the Weibull central location parameter and defined as the value that represents 63.2% of the data points.  $x_u$  is the threshold parameter.  $m$  is the Weibull modulus and is an indication of the spread of the data.

Consequently, two-parameter or three-parameter formulations are available for the Weibull distribution. The three-factor formulation requires knowledge of the threshold parameter. This can be calculated by linear regression of the data set to determine the offset value that provides the best coefficient of determination.<sup>227</sup> However, the two-parameter Weibull formulation usually leads to a more conservative estimate for the component probability of failure and the mathematical treatment is less complex. The two-parameter Weibull formulation is adopted in this work and the calculation method is shown below.

The threshold parameter is set to zero (i.e.,  $x_u = 0$ ) in the two-parameter Weibull method. To construct the plot, the data is ranked and the value that represents the 63.2% probability is assumed to be  $x_0$ . The two-factor Weibull fit is graphed by plotting  $\ln\left[\ln\left(\frac{1}{1-P_i}\right)\right]$  against





27 Coating reliability chart based on Weibull analysis of tensile adhesion strength data of plasma sprayed YSZ coatings.<sup>314</sup> An example for 0.5 level of significance is indicated to show a coating failure stress of 8.55 MPa

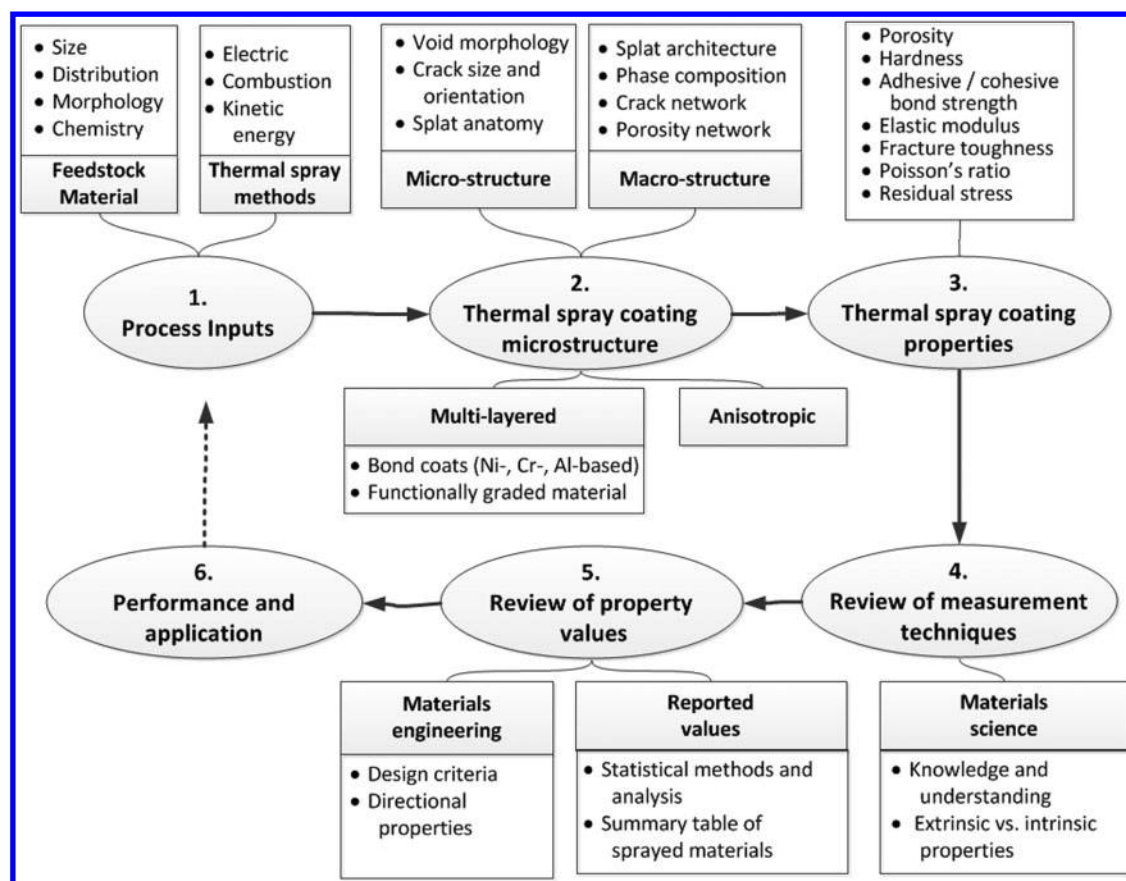
$\ln x_i$ . Equation (43) displays the simplified linear form of the Weibull distribution.

$$\ln\left[\ln\left(\frac{1}{1-P_i}\right)\right] = m \ln x_i - m \ln x_0 \quad (43)$$

The Weibull modulus ( $m$ ) can be used to approximate other distributions. For instance, if  $m=3.6$ , then the Weibull distribution approximates the normal distribution.<sup>265</sup> It has been argued that the assumption of setting the threshold value to zero and employing two-parameter Weibull formulation might result in an inaccurate determination of the Weibull modulus.<sup>227</sup> However, the use of Weibull statistics is often constrained to quantitative assessment of data variability and its relation to the microstructure. The Weibull modulus becomes a measure of the distribution of flaws and, hence, describes the variability in mechanical properties of ceramic materials. If the measurements show little variation, then the calculated Weibull modulus will be high and it may be concluded that the physical flaws are distributed uniformly throughout the material. If the measurements show high variation, the calculated Weibull modulus will be low. This result reveals that flaws are clustered inconsistently and the measured data will be generally variable. Accordingly, the reported confidence interval should be calculated from the Weibull distribution parameters instead of the standard  $t$ -distribution.

The use of the Weibull distribution over the Gaussian distribution in microhardness testing for thermal spray coatings has been shown to provide detailed information concerning the variability within coating system.<sup>211</sup> The coating microhardness data was highly skewed or broadly distributed and the Weibull distribution has the merit of being a simple way to describe the data. In addition, Lima *et al.*<sup>315</sup> showed that YSZ coatings of the same composition could exhibit similar values of microhardness (i.e., average and standard deviation) but significantly different Weibull modulus values. The bimodal Weibull distribution found in the microhardness data of the nanostructured YSZ coating suggests the presence of two distinct constituents within the microstructure.

Further work<sup>212,319</sup> also showed that the Weibull moduli of different thermal spray coatings tend to increase with indentation load. This effect arises when a low indentation load is used since there is an increased likelihood of sampling 'low defect' regions; whereas using a large indentation load relates to achieving a representative test volume. In other words, as the volume under scrutiny increases, the scatter in the measurement reduces and is reflected in the higher Weibull modulus; although the mean value will be lower. Therefore, it is also relevant to note that the Weibull values of hardness of two or more coatings should be compared only if the coatings were indented at the same load.



28 The mutual relationship between thermal spray process inputs, the anisotropic microstructure and mechanical properties

Apart from microhardness data, Weibull theory has been applied to other types of mechanical test results such as (i) porosity where  $m=2.6-6.2$ ,<sup>320</sup> (ii) tensile adhesion strength where  $m=2.4-5.9$ ,<sup>314,321</sup> (iii) elastic modulus where  $m=2.3-12.6$ ,<sup>164,273</sup> and (iv) fracture toughness where  $m=0.5-0.8$ .<sup>109</sup>

A useful application of the Weibull distribution on thermal spray data is to construct reliability charts that allow prediction of the coating properties at a chosen level of significance, Fig. 27. In this specific exemplar, the YSZ coating adhesion strength, at a 0.5 level of significance, should be approximately 8.55 MPa.

Other important statistical analysis tools for thermal spray data relate to the ability to compare and identify competing data sets that have similar average values.<sup>212</sup> If there are only two unique data sets, a Student's *t* test can be used to assess the statistical significance.<sup>211</sup> If more than two means are compared, then the analysis of variance method (ANOVA) should be employed to account for the variance between observations.<sup>227</sup>

## Conclusions

The relationships among the topics covered in this review are summarised in Fig. 28. Thermal spray coatings and their mechanical properties are influenced by the fundamental factors of (i) jet temperature, (ii) particle velocity, and (iii) characteristics of the feedstock.

In the selection of powdered feedstock, the starting chemistry is only one of the many criteria. The particle size distribution, flow, bulk density, morphology, and grain size must also be considered. These feedstock

characteristics are differentiated by the manufacturing method and have been categorised into charts in this review.

The retrospective review of thermal spray methods suggests that there is a trend of innovation to increase the jet temperature and/or particle velocity. Nonetheless, thermal spray methods can be classified into three broad families: (i) the use of combustion heat sources, (ii) the use of electrical energy, and (iii) the use of gas decompression. Each method has its own merits; but it is common that the spray parameters influence the temperature-velocity distribution of the particles.

Thermal spray coatings are identified by a lamellar microstructure formed from the rapid solidification of impinging molten droplets and cohesion among splats. This structure gives rise to the anisotropic mechanical behaviour of coatings produced *via* different thermal spray methods since a distinctive splat structure and associated void system is created. This anisotropic characteristic must be noted when applying measurement techniques on the thermal spray coating.

A focussed critique is presented on the respective measurement techniques after critically reviewing the literature. The measurement techniques compiled included (i) porosity, (ii) residual stresses (iii) hardness, (iv) adhesion, (v) elastic modulus, (vi) fracture toughness, and (vii) the Poisson's ratio of thermal spray coatings.

The measurement of porosity levels in thermal spray coatings have advanced in the past two decades with the adoption of neutron beam, X-ray source and ultrasound-based methods. These traditional methods have been lent from the field of characterising bulk materials.

Nonetheless, traditional IA still remains popular but must be applied in accordance to recommended standards, such as ASTM E2109-01.<sup>145</sup>

Concurrently, advanced neutron beam, X-ray and laser beam sources have been employed to study the residual stresses in thermal spray coatings. These non-destructive testing techniques often require specific coating dimensions as well as complex mathematical models to resolve the measured results. Adoption of these advanced characterisation techniques for the thermal spray job shop is a steep learning curve. Nevertheless, the understanding of quenching, peening and thermal contraction stresses introduced or built-up during the coating process is critical; especially for a thermal spray coating that bears load. Differentiating between the stress components that contribute to a coating's overall residual stress can be achieved by using the *in-situ* curvature monitoring or equivalent methods.

It was found that there is an emerging demand for standardisation within the field of hardness and bond strength testing of thermal spray coatings. An increasing number of national and international test standards for characterisation of thermal spray coatings are available or under development. In particular, the microhardness testing of thermal spray coatings is widely used as a quality control tool in the industry. However, due to the anisotropic architecture of the coating, an indenter's alignment (i) along the lamellar layers, or (ii) across the lamellar layers can lead to different microhardness results.

In the area of coating bond strength testing, while the standard TAT method and the similar method of stud pull test remain popular, numerous test methods are now available to evaluate the coating bond strength without the use of an epoxy. Methods like the shear load test, the pin and ring test, the scratch test and the laser shock adhesion test remove the ambiguity of epoxy penetration into a porous coating. However, some of these test methods require complex equipment setup as well as empirical modelling relationships to calculate the coating adhesion bond strength. Again, these could be barriers for adoption by the typical coating job shop.

Important properties of thermal spray coatings such as the elastic modulus, fracture toughness and Poisson's ratio are required by design engineers and researchers to evaluate the integrity of the entire structure or system. It can be difficult to measure such stress-strain relationships in thermal spray coatings due to the inhomogeneous microstructure of the coating and the influence of the void and crack networks. Nonetheless, indentation and bending methods modified from the measurement of bulk material properties have been applied effectively.

The lack of an overall framework for the presentation of mechanical properties highlights a misconception: that is, researchers have focussed on the properties and performance of specific coatings or processes rather than relationships among the entire family of thermal spray coatings. Thus, although there is a vast amount of literature documenting the development of coating materials or processes, the thermal spray field lacks a systematic method that integrates materials chemistry, processing, structure, property and performance. A materials genomic approach, which systematically correlates different properties among all thermal spray processes, has addressed this critical need.<sup>322</sup>

## Acknowledgement

This work has been supported under a Swinburne University Postgraduate Research Award. The authors acknowledge the support and encouragement of Messieurs Andrew Moore and Brian Dempster.

Dedication: This body of work is dedicated to Mr Richard Moore, a practitioner of thermal spray, who passed away suddenly on 30 June 2013. May he rest in peace.

## References

1. J. R. Davis: 'Handbook of Thermal Spray Technology'; 2004, Materials Park, OH, USA, ASM International.
2. S. Saber-Samandari and C. C. Berndt: *Int. Heat Treat. Surf. Eng.*, 2010, **4**, (1), 7–13.
3. R. McPherson: *Thin Solid Films*, 1981, **83**, (3), 297–310.
4. S. Fantassi, M. Vardelle, A. Vardelle and P. Fauchais: *J. Therm. Spray Technol.*, 1993, **2**, (4), 379–384.
5. A. S. M. Ang, C. C. Berndt, M. Dunn, M. L. Sesso and S. Y. Kim: *J. Am. Ceram. Soc.*, 2012, **95**, (5), 1572–1580.
6. P. Fauchais and A. Vardelle: *Int. J. Therm. Sci.*, 2000, **39**, (9–11), 852–870.
7. S. Sampath, V. Srinivasan, A. Valarezo, A. Vaidya and T. Streibl: *J. Therm. Spray Technol.*, 2009, **18**, (2), 243–255.
8. M. Friis and C. Persson: *J. Therm. Spray Technol.*, 2003, **12**, (1), 44–52.
9. J. F. Bisson, M. Lamontagne, C. Moreau, L. Pouliot, J. Blain and F. Nadeau: 'Ensemble in-flight particle diagnostics under thermal spray conditions', Proc. Int. Thermal Spray Conf., Singapore, 2001, Materials Park, OH, USA, ASM International, 705–714.
10. C. C. Berndt: 'Feedstock material considerations', in 'Handbook of thermal spray technology', (ed. J. R. Davis), 137–141; 2004, Materials Park, OH, USA, ASM International.
11. P. Fauchais, G. Montavon and G. Bertrand: *J. Therm. Spray Technol.*, 2010, **19**, (1–2), 56–80.
12. P. Fauchais, R. Etchart-Salas, V. Rat, J. F. Coudert, N. Caron and K. Wittmann-Ténèze: *J. Therm. Spray Technol.*, 2008, **17**, (1), 31–59.
13. L. Pawlowski: 'The science and engineering of thermal spray coatings', xxx, 656 p.; ill.; 624 cm; 2008, Chichester, UK, John Wiley & Sons.
14. L. Pawlowski: *Surf. Coat. Technol.*, 2008, **202**, (18), 4318–4328.
15. T. H. Van Steenkiste, J. R. Smith and R. E. Teets: *Surf. Coat. Technol.*, 2002, **154**, (2–3), 237–252.
16. S. Sampath and S. F. Wayne: *J. Therm. Spray Technol.*, 1994, **3**, (3), 282–288.
17. H. L. De Villiers Lovelock: *J. Therm. Spray Technol.*, 1998, **7**, (3), 357–373.
18. P. Suresh Babu, D. S. Rao, G. V. N. Rao and G. Sundararajan: *J. Therm. Spray Technol.*, 2007, **16**, (2), 281–290.
19. P. Cheang and K. A. Khor: *J. Therm. Spray Technol.*, 1996, **5**, (3), 310–316.
20. S. Jiansirisomboon, K. J. D. MacKenzie, S. G. Roberts and P. S. Grant: *J. Eur. Ceram. Soc.*, 2003, **23**, (6), 961–976.
21. J. Wang, E. Jordan and M. Gell: *J. Therm. Spray Technol.*, 2010, **19**, (5), 873–878.
22. P. Fauchais and G. Montavon: *Adv. Heat Transfer*, 2007, **40**, 205–344.
23. M. Vardelle, A. Vardelle, P. Fauchais, K. I. Li, B. Dussoubs and N. J. Themelis: *J. Therm. Spray Technol.*, 2001, **10**, (2), 267–284.
24. P. Cheang and K. A. Khor: *J. Mater. Process. Technol.*, 1995, **48**, (1–4), 429–436.
25. F. N. Longo, N. F. Bader and M. R. Dorfman: 'Hollow sphere ceramic particles for abradable coatings', US Patent, 445,018,4 A, 1984.
26. M. R. Dorfman, L. F. Correa, C. G. Dambra, K. Laul and R. K. Schmid: 'Method of producing a pre-alloyed stabilized zirconia powder', US Patent, 6,869,550 B2, 2005.
27. A. Vaidya, T. Streibl, S. Sampath and H. Zhang: 'A comparative diagnostic analysis of morphologically different YSZ powders', Proc. Int. Thermal Spray Conf., Osaka, Japan, 10–12 May 2004, 400–406; 2004, Duesseldorf, Germany DVS-Verlag GmbH.
28. A. M. Bouwman, J. C. Bosma, P. Vonk, J. A. Wesselingh and H. W. Frijlink: *Powder Technol.*, 2004, **146**, (1–2), 66–72.

29. K. Niihara: Nippon Seramikkusu Kyokai Gakujutsu Ronbunshi/ J. Ceram. Soc. Jpn, 1991, **99**, (1154), 974–982.
30. A. Singhal, G. Skandan, A. Wang, N. Glumac, B. H. Kear and R. D. Hunt: *Nanostruct. Mater.*, 1999, **11**, (4), 545–552.
31. I. S. Altman, I. E. Agranovski and M. Choi: *Appl. Phys. Lett.*, 2005, **87**, (5), ID: 053104.
32. V. Stone, H. Johnston and M. J. D. Clift: *IEEE Trans. Nanobiosci.*, 2007, **6**, (4), 331–340.
33. C. M. Sayes, K. L. Reed and D. B. Warheit: *Toxicol. Sci.*, 2007, **97**, (1), 163–180.
34. B. H. Kear and G. Skandan: *Nanostruct. Mater.*, 1997, **8**, (6), 765–769.
35. P. Luo and T. G. Nieh: *Biomaterials*, 1996, **17**, (20), 1959–1964.
36. R. S. Lima, A. Kucuk and C. C. Berndt: *Mater. Sci. Eng. A*, 2001, **313**, (1–2), 75–82.
37. Y. Qiao, T. E. Fischer and A. Dent: *Surf. Coat. Technol.*, 2003, **172**, (1), 24–41.
38. L. L. Shaw, D. Goberman, R. Ren, M. Gell, S. Jiang, Y. Wang, T. D. Xiao and P. R. Strutt: *Surf. Coat. Technol.*, 2000, **130**, (1), 1–8.
39. Z. Ying Chun, D. Chuan Xian, K. Yukimura, T. Danny Xiao and P. R. Strutt: *Ceram. Int.*, 2001, **27**, (6), 669–674.
40. R. S. Lima and B. R. Marple: *Mater. Sci. Eng. A*, 2005, **395**, (1–2), 269–280.
41. H. Chen, Y. Zhang and C. Ding: *Wear*, 2002, **253**, (7–8), 885–893.
42. J. Karthikeyan, C. C. Berndt, J. Tikkanen, S. Reddy and H. Herman: *Mater. Sci. Eng. A*, 1997, **238**, (2), 275–286.
43. E. Bouyer, F. Gitzhofer and M. I. Boulos: *IEEE Trans. Plasma Sci.*, 1997, **25**, (5), 1066–1072.
44. J. Tikkanen, K. A. Gross, C. C. Berndt, V. Pitkänen, J. Keskinen, S. Raghu, M. Rajala and J. Karthikeyan: *Surf. Coat. Technol.*, 1997, **90**, (3), 210–216.
45. J. Karthikeyan, C. C. Berndt, S. Reddy, J. Y. Wang, A. H. King and H. Herman: *J. Am. Ceram. Soc.*, 1998, **81**, (1), 121–128.
46. A. Papyrin: *Adv. Mat. Process.*, 2001, **159**, (9), 49–51.
47. M. U. Schoop: ‘An improved process of applying deposits of metal or metallic compounds to surfaces’, UK Patent, A.D.21,066, 1912.
48. M. Ducos and J. P. Durand: ‘Thermal coatings in Europe: a business prospective’, Proc. Int. Thermal Spray Conf., Singapore, 28–30 May 2001, 1267–1271; 2001, Materials Park, OH, USA, ASM International.
49. M. Fukumoto: *J. Therm. Spray Technol.*, 2008, **17**, (1), 5–13.
50. Anon: ‘LINDOFLAMM® flame solutions, in Linde Gases Division, Linde AG’, 2013, Pullach, Germany.
51. R. F. Bunshah: ‘Handbook of hard coatings’, 2001, Park Ridge, NJ, USA, William Andrew Publishing/Noyes.
52. R. M. Poorman, H. B. Sargent and H. Lamprey: ‘Method and apparatus utilizing detonation waves for spraying and other purposes’, US Patent, 2,714,563, 1955.
53. A. I. Zverev, A. S. Bondarenko, M. A. Pudzinsky, V. M. Sopryazhinsky and N. A. Yakshin: ‘Apparatus for detonating application of coatings’, US Patent, 4,004,735, 1977.
54. R. C. Tucker Jr.: *J. Vac. Sci. Technol.* 1974, **11**, (4), 725–734.
55. G. Sundararajan, K. U. M. Prasad, D. S. Rao and S. V. Joshi: *J. Mater. Eng. Perform.*, 1998, **7**, (3), 343–351.
56. K. Niemi, P. Vuoristo and T. Mäntylä: *J. Therm. Spray Technol.*, 1994, **3**, (2), 199–203.
57. M. L. Thorpe and H. J. Richter: *J. Therm. Spray Technol.*, 1992, **1**, (2), 161–170.
58. S. Kamnis and S. Gu: *Chem. Eng. Sci.*, 2006, **61**, (16), 5427–5439.
59. W. Rusch: ‘Comparison of operating characteristics for gas and liquid fuel HVOF torches’, Proc. Int. Thermal Spray Conf., Beijing, China, 14–16 May 2007, 572–576; 2007, Materials Park, OH, USA, ASM International.
60. E. Dongmo, M. Wenzelburger and R. Gadow: *Surf. Coat. Technol.*, 2008, **202**, (18), 4470–4478.
61. M. Li and P. D. Christofides: *Chem. Eng. Sci.*, 2006, **61**, (19), 6540–6552.
62. S. V. Joshi and R. Sivakumar: *Surf. Coat. Technol.*, 1991, **50**, (1), 67–74.
63. C. J. Li and Y. Y. Wang: *J. Therm. Spray Technol.*, 2002, **11**, (4), 523–529.
64. G. Bolelli, L. Lusvardi, T. Varis, E. Turunen, M. Leoni, P. Scardi, C.-L. Azanza-Ricardo and M. Barletta: *Surf. Coat. Technol.*, 2008, **202**, (19), 4810–4819.
65. J. Lesage and D. Chicot: *Thin Solid Films*, 2002, **415**, (1–2), 143–150.
66. S. Kuroda, Y. Tashiro, H. Yumoto, S. Taira, H. Fukunuma and S. Tobe: *J. Therm. Spray Technol.*, 2001, **10**, (2), 367–374.
67. J. Stokes and L. Looney: *Surf. Coat. Technol.*, 2004, **177–178**, 18–23.
68. J. Pina, A. Dias and J. L. Lebrun: *Mater. Sci. Eng. A*, 2003, **347**, (1–2), 21–31.
69. L. Zhao, M. Maurer, F. Fischer, R. Dicks and E. Lugscheider: *Wear*, 2004, **257**, (1–2), 41–46.
70. B. H. Kear, G. Skandan and R. K. Sadangi: *Scr. Mater.*, 2001, **44**, (8–9), 1703–1707.
71. R. S. Lima and B. R. Marple: *Surf. Coat. Technol.*, 2006, **200**, (11), 3428–3437.
72. E. Pfender: *Thin Solid Films*, 1994, **238**, (2), 228–241.
73. M. P. Planche, J. F. Coudert and P. Fauchais: *Plasma Chem. Plasma Process.*, 1998, **18**, (2), 263–283.
74. B. M. Cetegen and W. Yu: *J. Therm. Spray Technol.*, 1999, **8**, (1), 57–67.
75. K. Remesh, S. C. M. Yu, H. W. Ng and C. C. Berndt: *J. Therm. Spray Technol.*, 2003, **12**, (4), 508–522.
76. D. K. Das and R. Sivakumar: *Acta Metall. Mater.*, 1990, **38**, (11), 2193–2198.
77. P. Fauchais: *J. Phys. D Appl. Phys.*, 2004, **37**, (9), 86–108.
78. M. Cao, F. Gitzhofer, D. V. Gravelle, R. Henne and M. I. Boulos: *Plasma Sources Sci. Technol.*, 1997, **6**, (1), 39–45.
79. S. Zhu and B. Xu: *Key Eng. Mater.*, 2005, **280–283**, (II), 1203–1206.
80. H. Tahara and Y. Ando: *Vacuum*, 2008, **83**, (1), 98–101.
81. A. Scrivani, U. Bardi, L. Carrafiello, A. Lavacchi, F. Nicolai and G. Rizzi: *J. Therm. Spray Technol.*, 2003, **12**, (4), 504–507.
82. J. F. Coudert and P. Fauchais: *Ann. N. Y. Acad. Sci.*, 1999, **891**, 382–390.
83. P. Fauchais, J. F. Coudert and M. Vardelle: *J. De Phys.*, 1997, **7**, (4), 187–198.
84. A. Vardelle, P. Fauchais, M. Vardelle and G. Mariaux: *Adv. Eng. Mater.*, 2006, **8**, (7), 599–610.
85. J. L. Dorier, C. Hollenstein, A. Salito, M. Loch and G. Barbezat: *High Temp. Mater. Processes*, 2001, **5**, (4), 477–489.
86. M. Vysokliid and J. Heberlein: ‘Investigation of arc voltage fluctuations in a plasma torch SG-100 operated with Ar/H<sub>2</sub>’, Proc. Int. Thermal Spray Conf., Osaka, Japan, 10–12 May 2004, 998–1003; 2004, DVS-Verlag GmbH.
87. B. Dussoubs, G. Mariaux, A. Vardelle, M. Vardelle and P. Fauchais: *High Temp. Mater. Processes*, 1999, **3**, (2–3), 235–254.
88. S. Goutier, E. Noguès-Delbos, M. Vardelle and P. Fauchais: *J. Therm. Spray Technol.*, 2008, **17**, (5–6), 895–901.
89. D. A. Gerdeman and N. L. Hecht: ‘Arc plasma technology in materials science’, 206; 1972, New York, Springer-Verlag.
90. D. R. Mash, N. E. Weare and D. L. Walker: *J. Metals*, 1961, **13**, 473–478.
91. J. Cizek, K. A. Khor and Z. Prochazka: *Mater. Sci. Eng. C*, 2007, **27**, (2), 340–344.
92. P. Fauchais, A. Vardelle and B. Dussoubs: *J. Therm. Spray Technol.*, 2001, **10**, (1), 44–66.
93. M. U. Schoop: ‘Apparatus for spraying molten metal and other fusible substances’, USA Patent, 1,133,507, 1915.
94. D. J. Varacalle, G. C. Wilson, R. W. Johnson, T. J. Steeper, G. Irons, W. R. Kratochvil and W. L. Riggs: *J. Therm. Spray Technol.*, 1994, **3**, (1), 69–74.
95. A. P. Alkhimov, A. N. Papyrin, V. F. Kosarev, N. I. Nesterovich and M. M. Shushpanov: ‘Gas-dynamic spray method for applying a coating’, US Patent, 5,302,414, 1994.
96. R. C. Dykhuizen and M. F. Smith: *J. Therm. Spray Technol.*, 1998, **7**, (2), 205–212.
97. T. Stoltenhoff, H. Kreye and H. J. Richter: *J. Therm. Spray Technol.*, 2002, **11**, (4), 542–550.
98. R. C. Dykhuizen, M. F. Smith, D. L. Gilmore, R. A. Neiser, X. Jiang and S. Sampath: *J. Therm. Spray Technol.*, 1999, **8**, (4), 559–564.
99. T. H. Van Steenkiste, J. R. Smith, R. E. Teets, J. J. Moleski, D. W. Gorkiewicz, R. P. Tison, D. R. Marantz, K. A. Kowalsky, W. L. Riggs II, P. H. Zajchowski, B. Pilsner, R. C. McCune and K. J. Barnett: *Surf. Coat. Technol.*, 1999, **111**, (1), 62–71.
100. T. Schmidt, F. Gärtner, H. Assadi and H. Kreye: *Acta Mater.*, 2006, **54**, (3), 729–742.
101. H. Assadi, F. Gärtner, T. Stoltenhoff and H. Kreye: *Acta Mater.*, 2003, **51**, (15), 4379–4394.
102. M. Grujicic, C. L. Zhao, W. S. DeRosset and D. Helfrich: *Mater. Des.*, 2004, **25**, (8), 681–688.
103. M. Grujicic, J. R. Saylor, D. E. Beasley, W. S. DeRosset and D. Helfrich: *Appl. Surf. Sci.*, 2003, **219**, (3–4), 211–227.
104. T. Hussain, D. G. McCartney, P. H. Shipway and D. Zhang: *J. Therm. Spray Technol.*, 2009, 1–16.

105. S. H. Leigh and C. C. Berndt: *Acta Mater.*, 1999, **47**, (5), 1575–1586.
106. J. Ilavsky, G. G. Long, A. J. Allen, H. Herman and C. C. Berndt: *Ceram. Silik.*, 1998, **42**, (3), 81–89.
107. A. J. Allen, G. G. Long, H. Boukari, J. Ilavsky, A. Kulkarni, S. Sampath, H. Herman and A. N. Goland: *Surf. Coat. Technol.*, 2001, **146–147**, 544–552.
108. I. Sevostianov and M. Kachanov: *Mater. Sci. Eng.: A*, 2001, **297**, (1), 235–243.
109. P. Ostojic and R. McPherson: *Mater. Forum*, 1987, **10**, (4), 247–255.
110. S. Stecura: 'Advanced thermal barrier system bond coatings for use on Ni, Co- and Fe-base alloy substrates', NASA-TM-87062, E-2437, NAS 1-15:87062, NASA, Lewis Research Center, Cleveland, OH, USA, 1985.
111. S. Stecura: 'Thermal barrier coating system', US Patent, 4,485,151, 1984.
112. M. Schütze: 'Fundamentals of high temperature corrosion', in Eds: RW Cahn, P Haasen, EJ Krame, 'Materials science and technology: a comprehensive treatment', 67–130; 2008, Weinheim, Germany, Wiley-VCH Verlag GmbH.
113. J. M. Guilemany, S. Dosta and J. R. Miguel: *Surf. Coat. Technol.*, 2006, **201**, (3–4), 1180–1190.
114. I. A. Fisher: *Int. Mater. Rev.*, 1972, **17**, (1), 117–129.
115. W. E. Ballard and T. H. Turner: 'Metal spraying and the flame deposition of ceramics and plastics'; 1963, London, UK, Griffin.
116. C. W. Marynowski, F. A. Halden and E. P. Farley: *J. Electrochem. Soc.*, 1965, **3**, 109–115.
117. S. Kuroda and T. W. Clyne: *Thin Solid Films*, 1991, **200**, (1), 49–66.
118. T. W. Clyne and S. C. Gill: *J. Therm. Spray Technol.*, 1996, **5**, (4), 401–418.
119. J. Matějček and S. Sampath: *Acta Mater.*, 2001, **49**, (11), 1993–1999.
120. S. Kuroda, T. Fukushima and S. Kitahara: *J. Therm. Spray Technol.*, 1992, **1**, (4), 325–332.
121. V. Teixeira, M. Andritschky, W. Fischer, H. P. Buchkremer and D. Stöver: *Surf. Coat. Technol.*, 1999, **120–121**, 103–111.
122. R. C. McCune, W. T. Donlon, O. O. Popoola and E. L. Cartwright: *J. Therm. Spray Technol.*, 2000, **9**, (1), 73–82.
123. J. A. Ellor, W. T. Young and J. Repp: 'Thermally sprayed metal coatings to protect steel pilings: final report and guide', 0309088011 9780309088015, Transportation Research Board, Washington, DC, USA, 2004.
124. X. Jiang, Y. Wan, H. Herman and S. Sampath: *Thin Solid Films*, 2001, **385**, (1–2), 132–141.
125. M. Fukumoto, M. Shiiba, H. Kaji and T. Yasui: *Pure Appl. Chem.*, 2005, **77**, (2), 429–442.
126. S. Sampath, X. Y. Jiang, J. Matějček, A. C. Leger and A. Vardelle: *Mater. Sci. Eng. A*, 1999, **272**, (1), 181–188.
127. P. Bengtsson and C. Persson: *Surf. Coat. Technol.*, 1997, **92**, (1–2), 78–86.
128. P. Bengtsson and T. Johansson: *J. Therm. Spray Technol.*, 1995, **4**, (3), 245–251.
129. L. Sun, C. C. Berndt and C. P. Grey: *Mater. Sci. Eng. A*, 2003, **360**, (1–2), 70–84.
130. R. Miller: *J. Therm. Spray Technol.*, 1997, **6**, (1), 35–42.
131. R. Darolia: *Int. Mater. Rev.*, 2013, **58**, (6), 315–348.
132. P. Fauchais, G. Montavon, R. S. Lima and B. R. Marple: *J. Phys. D Appl. Phys.*, 2011, **44**, (9), 1–53.
133. J. Ilavsky, C. C. Berndt and J. Karthikeyan: *J. Mater. Sci.*, 1997, **32**, (15), 3925–3932.
134. J. Matějček, B. Kolman, J. Dubský, K. Neufuss, N. Hopkins and J. Zwick: *Mater. Charact.*, 2006, **57**, (1), 17–29.
135. A. Bacciocchini, G. Montavon, J. Ilavsky, A. Denoirjean and P. Fauchais: *J. Therm. Spray Technol.*, 2010, **19**, (1–2), 198–206.
136. Y. Arata, A. Ohmori and C.-J. Li: *Thin Solid Films*, 1988, **156**, (2), 315–326.
137. S. Kuroda, T. Dendo and S. Kitahara: *J. Therm. Spray Technol.*, 1995, **4**, (1), 75–84.
138. D. B. Fowler, W. Riggs and J. C. Russ: 'Image analysis applied to thermal sprayed coatings', Proc. 3rd National Spray Conf., Long Beach, CA, USA, 20–25 May 1990, 303–319; 1990, Materials Park, OH, USA, ASM International.
139. S. Deshpande, A. Kulkarni, S. Sampath and H. Herman: *Surf. Coat. Technol.*, 2004, **187**, (1), 6–16.
140. A. Bacciocchini, J. Ilavsky, G. Montavon, A. Denoirjean, F. Benettouil, S. Valette, P. Fauchais and K. Wittmann-Teneze: *Mater. Sci. Eng. A*, 2010, **528**, (1), 91–102.
141. A. Kulkarni, J. Gutleber, S. Sampath, A. Goland, W. B. Lindquist, H. Herman, A. J. Allen and B. Dowd: *Mater. Sci. Eng. A*, 2004, **369**, (1–2), 124–137.
142. A. Kulkarni, S. Sampath, A. Goland, H. Herman and B. Dowd: *Scr. Mater.*, 2000, **43**, (5), 471–476.
143. B. Rogé, A. Fahr, J. S. R. Giguère and K. I. McRae: *J. Therm. Spray Technol.*, 2003, **12**, (4), 530–535.
144. S. Parthasarathi, B. Tittmann and E. Onesto: *J. Therm. Spray Technol.*, 1997, **6**, (4), 486–488.
145. Anon: 'ASTM E2109 – 01, Test methods for determining area percentage porosity in thermal sprayed coatings'; 2007, West Conshohocken, PA, ASTM International.
146. J. P. Sauer: *J. Therm. Spray Technol.*, 2005, **14**, (3), 313–314.
147. J. B. Pawley: 'Points, pixels and gray levels: digitizing image data', in 'Handbook of biological confocal microscopy', (ed. J. B. Pawley), 3rd edn, 59–79; 2006, New York, USA, Springer-Verlag.
148. G. Antou and G. Montavon: *J. Therm. Spray Technol.*, 2007, **16**, (2), 168–176.
149. N. Otsu: *IEEE Trans. Syst. Man. Cybern.*, 1979, **SMC-9**, (1), 62–66.
150. J. Mateos, J. M. Cuetos, E. Fernández and R. Vijande: *Wear*, 2000, **239**, (2), 274–281.
151. H. Liao, B. Normand and C. Coddet: *Surf. Coat. Technol.*, 2000, **124**, (2–3), 235–242.
152. P. K. Aw, A. L. K. Tan, T. P. Tan and J. Qiu: *Thin Solid Films*, 2008, **516**, (16), 5710–5715.
153. Z. G. Ban and L. L. Shaw: *J. Therm. Spray Technol.*, 2003, **12**, (1), 112–119.
154. J. Voyer and B. R. Marple: *Wear*, 1999, **225–229**, (I), 135–145.
155. J. G. Legoux, B. Arsenault, L. Leblanc, V. Bouyer and C. Moreau: *J. Therm. Spray Technol.*, 2002, **11**, (1), 86–94.
156. T. Sahraoui, N. E. Fenineche, G. Montavon and C. Coddet: *J. Mater. Process. Technol.*, 2004, **152**, (1), 43–55.
157. A. S. M. Ang, C. C. Berndt and P. Cheang: *Surf. Coat. Technol.*, 2011, **205**, (10), 3260–3267.
158. H. Du, W. Hua, J. Liu, J. Gong, C. Sun and L. Wen: *Mater. Sci. Eng. A*, 2005, **408**, (1–2), 202–210.
159. A. A. Abdel-Samad, A. M. M. El-Bahloul, E. Lugscheider and S. A. Rassoul: *J. Mater. Sci.*, 2000, **35**, (12), 3127–3130.
160. E. H. Jordan, M. Gell, Y. H. Sohn, D. Goberman, L. Shaw, S. Jiang, M. Wang, T. D. Xiao, Y. Wang and P. Strutt: *Mater. Sci. Eng. A*, 2001, **301**, (1), 80–89.
161. R. Lima, C. Moreau and B. Marple: *J. Therm. Spray Technol.*, 2007, **16**, (5), 866–872.
162. P. Saravanan, V. Selvarajan, S. V. Joshi and G. Sundararajan: *J. Phys. D Appl. Phys.*, 2001, **34**, (1), 131–140.
163. R. Westergård, L. C. Erickson, N. Axén, H. M. Hawthorne and S. Hogmark: *Tribol. Int.*, 1998, **31**, (5), 271–279.
164. S. H. Leigh, C. K. Lin and C. C. Berndt: *J. Am. Ceram. Soc.*, 1997, **80**, (8), 2093–2099.
165. W. Chi, S. Sampath and H. Wang: *J. Therm. Spray Technol.*, 2006, **15**, (4), 773–778.
166. A. Kulkarni, A. Goland, H. Herman, A. J. Allen, J. Ilavsky, G. G. Long and F. Carlo: *J. Therm. Spray Technol.*, 2005, **14**, (2), 239–250.
167. A. Kulkarni, Z. Wang, T. Nakamura, S. Sampath, A. Goland, H. Herman, J. Allen, J. Ilavsky, G. Long, J. Frahm and R. W. Steinbrech: *Acta Mater.*, 2003, **51**, (9), 2457–2475.
168. A. J. Allen, J. Ilavsky, G. G. Long, J. S. Wallace, C. C. Berndt and H. Herman: *Acta Mater.*, 2001, **49**, (9), 1661–1675.
169. H. B. Guo, H. Murakami and S. Kuroda: *J. Am. Ceram. Soc.*, 2006, **89**, (12), 3797–3804.
170. H. Zhou, F. Li, J. Wang and B.-D. Sun: *J. Coat. Technol. Res.*, 2009, **6**, (3), 383–390.
171. Y. Li, W. Chi, S. Sampath, A. Goland, H. Herman, A. J. Allen and J. Ilavsky: *J. Am. Ceram. Soc.*, 2009, **92**, (2), 491–500.
172. P. Scardi, M. Leoni and L. Bertamini: *Surf. Coat. Technol.*, 1995, **76–77**, (1–3 Pt. 1), 106–112.
173. J. Matějček, S. Sampath and J. Dubsky: *J. Therm. Spray Technol.*, 1998, **7**, (4), 489–496.
174. J. Matějček, S. Sampath, T. Gnaeupel-Herold and H. J. Prask: *Appl. Phys. A Mater. Sci. Process.*, 2002, **74**, (Suppl. II), 1692–1694.
175. P. Scardi, M. Leoni, L. Bertini, L. Bertamini and F. Cernuschi: *Surf. Coat. Technol.*, 1998, **108–109**, (1–3), 93–98.
176. K. W. Schlichting, K. Vaidyanathan, Y. H. Sohn, E. H. Jordan, M. Gell and N. P. Padture: *Mater. Sci. Eng. A*, 2000, **291**, (1–2), 68–77.
177. M. Tanaka, M. Hasegawa, A. F. Dericioglu and Y. Kagawa: *Mater. Sci. Eng. A*, 2006, **419**, (1–2), 262–268.



178. P. J. Withers and H. K. D. H. Bhadeshia: *Mater. Sci. Technol.*, 2001, **17**, (4), 355–365.
179. O. Kesler, J. Matejček, S. Sampath, S. Suresh, T. Gnaeupel-Herold, P. C. Brand and H. J. Prask: *Mater. Sci. Eng. A*, 1998, **257**, (2), 215–224.
180. J. Thornton, S. Slater and J. Almer: *J. Am. Ceram. Soc.*, 2005, **88**, (10), 2817–2825.
181. C. M. Weyant, J. Almer and K. T. Faber: *Acta Mater.*, 2010, **58**, (3), 943–951.
182. J. Matějček, S. Sampath, P. C. Brand and H. J. Prask: *Acta Mater.*, 1999, **47**, (2), 607–617.
183. R. Ahmed, H. Yu, S. Stewart, L. Edwards and J. R. Santisteban: *J. Tribol.*, 2007, **129**, (2), 411–418.
184. A. Portinha, V. Teixeira, J. Carneiro, M. G. Beghi, C. E. Bottani, N. Franco, R. Vassen, D. Stoeber and A. D. Sequeira: *Surf. Coat. Technol.*, 2004, **188–189**, (1–3 Spec. ISS.), 120–128.
185. V. Luzin, K. Spencer and M. X. Zhang: *Acta Mater.*, 2011, **59**, (3), 1259–1270.
186. S. Sampath, X. Y. Jiang, J. Matejček, L. Prchlik, A. Kulkarni and A. Vaidya: *Mater. Sci. Eng. A*, 2004, **364**, (1–2), 216–231.
187. R. Ahmed, M. E. Fitzpatrick and N. H. Faisal: *Surf. Coat. Technol.*, 2012, **206**, (19–20), 4180–4185.
188. R. Ahmed, H. Yu, V. Stoica, L. Edwards and J. R. Santisteban: *Mater. Sci. Eng. A*, 2008, **498**, (1–2), 191–202.
189. G. Marot, P. Démarécaux, J. Lesage, M. Hadad, S. Siegmans and M. H. Staia: *Surf. Coat. Technol.*, 2008, **202**, (18), 4411–4416.
190. J. Matějček and S. Sampath: *Acta Mater.*, 2003, **51**, (3), 863–872.
191. Y. Itoh, M. Saitoh and M. Tamura: *J. Eng. Gas Turbines Power*, 1999, **122**, (1), 43–49.
192. A. Brenner and S. Senderoff: *J. Res. Natl. Bur. Stand.*, 1949, **42**, 105–123.
193. Y. C. Tsui and T. W. Clyne: *Thin Solid Films*, 1997, **306**, (1), 23–33.
194. X. Zhang, M. Watanabe and S. Kuroda: *Acta Mater.*, 2013, **61**, (4), 1037–1047.
195. A. Vaidya, T. Streibl, L. Li, S. Sampath, O. Kovarik and R. Greenlaw: *Mater. Sci. Eng. A*, 2005, **403**, (1–2), 191–204.
196. D. J. Greving, E. F. Rybicki and J. R. Shadley: *J. Therm. Spray Technol.*, 1994, **3**, (4), 379–388.
197. M. S. J. Hashmi, C. Pappalettere and F. Ventola: *J. Mater. Process. Technol.*, 1998, **75**, (1–3), 81–86.
198. J. Zhu, H. Xie, Z. Hu, P. Chen and Q. Zhang: *J. Therm. Spray Technol.*, 2012, **21**, (5), 810–817.
199. J. G. Zhu, H. M. Xie, Y. J. Li, Z. X. Hu, Q. Luo and C. Z. Gu: *Exp. Mech.*, 2012, 1–10.
200. J. Mathar: *Trans ASME*, 1934, **59**, 249–254.
201. N. J. Rendler and I. Vigness: *Exp. Mech.*, 1966, **6**, (12), 577–586.
202. Anon: 'ASTM E837-08e2 standard test method for determining residual stresses by the Hole-Drilling Strain-Gage Method'; 2008, West Conshohocken, PA, ASTM International.
203. G. Montay, A. Cherouat, J. Lu, N. Baradel and L. Bianchi: *Surf. Coat. Technol.*, 2002, **155**, (2–3), 152–160.
204. T. Valente, C. Bartuli, M. Sebastiani and A. Loreto: *J. Therm. Spray Technol.*, 2005, **14**, (4), 462–470.
205. Y. Y. Santana, J. G. La Barbera-Sosa, M. H. Staia, J. Lesage, E. S. Puchi-Cabrera, D. Chicot and E. Bemporad: *Surf. Coat. Technol.*, 2006, **201**, (5), 2092–2098.
206. D. J. Greving, J. R. Shadley and E. F. Rybicki: *J. Therm. Spray Technol.*, 1994, **3**, (4), 371–378.
207. H. Gassot, T. Junquera, V. Ji, M. Jeandin, V. Guipont, C. Coddet, C. Verdy and L. Grandsire: *Surf. Eng.*, 2001, **17**, (4), 317–322.
208. V. Luzin, A. Valarezo and S. Sampath: *Mater. Sci. Forum*, 2008, **571–572**, 315–320.
209. S. Suresh and A. E. Giannakopoulos: *Acta Mater.*, 1998, **46**, (16), 5755–5767.
210. S. M. Walley: *Mater. Sci. Technol.*, 2012, **28**, (9–10), 1028–1044.
211. C. K. Lin and C. C. Berndt: *J. Mater. Sci.*, 1995, **30**, (1), 111–117.
212. T. Valente: *Surf. Coat. Technol.*, 1997, **90**, (1–2), 14–20.
213. M. Factor and I. Roman: *Surf. Coat. Technol.*, 2000, **132**, (1), 65–75.
214. D. Chicot, I. Hage, P. Démarécaux and J. Lesage: *Surf. Coat. Technol.*, 1996, **81**, (2–3), 269–274.
215. E. López Cantera and B. G. Mellor: *Mater. Lett.*, 1998, **37**, (4–5), 201–210.
216. D. Chicot, P. Demarecaux and J. Lesage: *Thin Solid Films*, 1996, **283**, (1–2), 151–157.
217. M. Hadad, G. Marot, P. Demarecaux, D. Chicot, J. Lesage, L. Rohr and S. Siegmans: *Surf. Eng.*, 2007, **23**, (4), 279–283.
218. Anon: 'ASTM E384 – 11e1 Standard Test Method for Knoop and Vickers Hardness of Materials'; 2011, West Conshohocken, PA, ASTM International.
219. Anon: 'ASTM C1326 – 08 Standard Test Method for Knoop Indentation Hardness of Advanced Ceramics'; 2008, West Conshohocken, PA, ASTM International.
220. Anon: 'ASTM C1327 – 08 Standard Test Method for Vickers Indentation Hardness of Advanced Ceramics'; 2008, West Conshohocken, PA, ASTM International.
221. A. R. Oganov and A. O. Lyakhov: *J. Superhard Mater.*, 2010, **32**, (3), 143–147.
222. W. C. Oliver and G. M. Pharr: *J. Mater. Res.*, 1992, **7**, (6), 1564–1580.
223. D. B. Marshall, T. Noma and A. G. Evans: *J. Am. Ceram. Soc.*, 1982, **65**, (10), c175–c176.
224. S. W. K. Kweh, K. A. Khor and P. Cheang: *Biomaterials*, 2000, **21**, (12), 1223–1234.
225. C. J. Villalobos-Gutiérrez, G. E. Gedler-Chacón, J. G. La Barbera-Sosa, A. Piñero, M. H. Staia, J. Lesage, D. Chicot, G. Mesmacque and E. S. Puchi-Cabrera: *Surf. Coat. Technol.*, 2008, **202**, (18), 4572–4577.
226. M. Sakai: *J. Mater. Res.*, 1999, **14**, (9), 3630–3639.
227. M. Factor and I. Roman: *Surf. Coat. Technol.*, 2000, **132**, (2–3), 181–193.
228. Anon: 'ASTM E1920 – 03(2008) standard guide for metallographic preparation of thermal sprayed coatings'; 2008, West Conshohocken, PA, ASTM International.
229. J. Alcalá, F. Gaudette, S. Suresh and S. Sampath: *Mater. Sci. Eng. A*, 2001, **316**, (1–2), 1–10.
230. B. R. Lawn: *J. Am. Ceram. Soc.*, 1998, **81**, (8), 1977–1994.
231. T. Nakamura, G. Qian and C. C. Berndt: *J. Am. Ceram. Soc.*, 2000, **83**, (3), 578–584.
232. P. Čtřibor, P. Boháč, M. Stranyánek and R. Čtvrtlík: *J. Eur. Ceram. Soc.*, 2006, **26**, (16), 3509–3514.
233. J. Rodríguez, A. Rico, E. Otero and W. M. Rainforth: *Acta Mater.*, 2009, **57**, (11), 3148–3156.
234. S. Saber-Samandari and K. A. Gross: *Surf. Coat. Technol.*, 2009, **203**, (12), 1660–1664.
235. S. Saber-Samandari, C. C. Berndt and K. A. Gross: *Acta Biomater.*, 2011, **7**, (2), 874–881.
236. H. A. Matting and H. D. Steffens: *Prog. Appl. Mater. Res.*, 1967, **7**, 91–133.
237. C. C. Berndt: 'The adhesion of flame and plasma sprayed coatings', PhD thesis, Monash University, Clayton, VIC, Australia, 1980.
238. C. K. Lin and C. C. Berndt: *J. Therm. Spray Technol.*, 1994, **3**, (1), 75–104.
239. R. Mušálek, V. Pejchal, M. Vilémová and J. Matějček: *J. Therm. Spray Technol.*, 2013, **22**, (2–3), 221–232.
240. Anon: 'ASTM C633-01(2008) Standard Test Method for Adhesion or Cohesion Strength of Thermal Spray Coatings'; 2008, West Conshohocken, PA, ASTM International.
241. Anon: 'ISO 14916:1999 thermal spraying – determination of tensile adhesive strength'; 1999, Geneva, Switzerland, International Organization for Standardization.
242. Anon: 'JIS H 8302:2010 Build-up Thermal Spraying'; 2010, Tokyo, Japan, Japanese Standards Association.
243. C. C. Berndt: *J. Mater. Eng.*, 1990, **12**, (2), 151–158.
244. C. C. Berndt: *J. Mater. Eng.*, 1989, **11**, (4), 275–282.
245. Anon: 'ASTM D4541 – 09e1 Standard Test Method for Pull-Off Strength of Coatings Using Portable Adhesion Testers'; 2009, West Conshohocken, PA, ASTM International.
246. A. A. Elmoursi and N. Patel: *J. Adhes. Sci. Technol.*, 2004, **18**, (5), 597–606.
247. Anon: 'DIN EN 15340 thermal spraying – determination of shear load resistance of thermally sprayed coatings'; 2007, Berlin, Germany, Deutsches Institut für Normung.
248. S. Siegmans, M. Dvorak, H. Gruetzner, K. Nassenstein and A. Walter: 'Shear testing for characterizing the adhesive and cohesive coating strength without the need of adhesives', *Proc. Int. Therm. Spray Conf.*, 2005, 823–829.
249. M. Sexsmith and T. Troczynski: *J. Therm. Spray Technol.*, 1994, **3**, (4), 404–411.
250. H. Kurzweg, R. B. Heimann, T. Troczynski and M. L. Wayman: *Biomaterials*, 1998, **19**, (16), 1507–1511.
251. S. Barradas, R. Molins, M. Jeandin, M. Arrigoni, M. Boustie, C. Bolis, L. Berthe and M. Ducos: *Surf. Coat. Technol.*, 2005, **197**, (1), 18–27.
252. C. Bolis, L. Berthe, M. Boustie, M. Arrigoni, S. Barradas and M. Jeandin: *J. Phys. D Appl. Phys.*, 2007, **40**, (10), 3155–3163.

253. L. Berthe, M. Arrigoni, M. Boustie, J. P. Cuq-Lelandais, C. Broussillou, G. Fabre, M. Jeandin, V. Guipont and M. Nivard: *Nondestr. Test. Eval.*, 2011, **26**, (3–4), 303–317.
254. Anon: 'ASTM C1624 – 05(2010) standard test method for adhesion strength and mechanical failure modes of ceramic coatings by quantitative single point scratch testing'; 2010, West Conshohocken, PA, ASTM International.
255. Anon: 'ISO/DIS 27307 evaluation of adhesion/cohesion of plasma sprayed ceramic coatings by scratch testing'; Under development, Geneva, Switzerland, International Organization for Standardization.
256. A. Vencel, S. Arostegui, G. Favaro, F. Zivic, M. Mrdak, S. Mitrovic and V. Popovic: *Tribol. Int.*, 2011, **44**, (11), 1281–1288.
257. D. K. Das, M. P. Srivastava, S. V. Joshi and R. Sivakumar: *Surf. Coat. Technol.*, 1991, **46**, (3), 331–345.
258. E. Lopez, F. Beltzung and G. Zambelli: *J. Mater. Sci. Lett.*, 1989, **8**, (3), 346–348.
259. D. Chicot, P. Araujo, N. Horny, A. Tricoteaux and J. Lesage: *Surf. Coat. Technol.*, 2005, **200**, (1–4 SPEC. ISS.), 174–177.
260. G. Marot, J. Lesage, P. Démarécaux, M. Hadad, S. Siegmans and M. H. Staia: *Surf. Coat. Technol.*, 2006, **201**, (5), 2080–2085.
261. C.-K. Lin, S.-H. Leigh and C. C. Berndt: *Thin Solid Films*, 1997, **310**, (1–2), 108–114.
262. G. Goch, B. Schmitz, B. Karpuschewski, J. Geerkens, M. Reigl, P. Sprongl and R. Ritter: *Precis. Eng.*, 1999, **23**, (1), 9–33.
263. D. P. Almond, P. M. Patel, I. M. Pickup and H. Reither: *J. Mater. Energy Syst.*, 1985, **6**, (4), 287–292.
264. M. H. Staia, E. Ramos, A. Carrasquero, A. Roman, J. Lesage, D. Chicot and G. Mesmacque: *Thin Solid Films*, 2000, **377–378**, (1–2), 657–664.
265. W. Weibull: *J. Appl. Mech.*, 1951, **18**, 293–297.
266. J. P. Sauer and S. Ruoff: 'Epoxies used in tensile testing: films vs. liquid-why is there a difference?', Proc. Int. Thermal Spray Conf., Orlando, FL, USA, 5–8 May 2003, 1447–1453; 2003, Materials Park, OH, USA, ASM International.
267. K. A. Evans: 'Tensile bond strength variance of thermally sprayed coatings with respect to adhesive type', Proc. 9th Natl. Thermal Spray Conf., Cincinnati, OH, 7–11 October 1996, 803–806; 1996, Materials Park, OH, USA, ASM International.
268. R. McPherson: *Surf. Coat. Technol.*, 1989, **39–40**, (C), 173–181.
269. H.-J. Kim and Y.-G. Kweon: *Thin Solid Films*, 1999, **342**, (1–2), 201–206.
270. J. Matějček, S. Sampath, D. Gilmore and R. Neiser: *Acta Mater.*, 2003, **51**, (3), 873–885.
271. C. Li, A. Ohmori and R. McPherson: *J. Mater. Sci.*, 1997, **32**, (4), 997–1004.
272. R. Musalek, J. Matejcek, M. Vilemova and O. Kovarik: *J. Therm. Spray Technol.*, 2010, **19**, (1–2), 422–428.
273. J. Li and C. Ding: *Surf. Coat. Technol.*, 2001, **135**, (2–3), 229–237.
274. Q. Hongyu, Y. Xiaoguang and W. Yamei: *Int. J. Fract.*, 2009, **157**, (1–2), 71–80.
275. R. S. Lima, S. E. Kruger and B. R. Marple: *Surf. Coat. Technol.*, 2008, **202**, (15), 3643–3652.
276. A. Kucuk, C. C. Berndt, U. Senturk, R. S. Lima and C. R. C. Lima: *Mater. Sci. Eng. A*, 2000, **284**, (1–2), 29–40.
277. S. R. Choi, D. Zhu and R. A. Miller: *Int. J. Appl. Ceram. Technol.*, 2004, **1**, (4), 330–342.
278. M. Beghini, G. Benamati, L. Bertini and F. Frendo: *Exp. Mech.*, 2001, **41**, (4), 305–311.
279. O. Kovářik, J. Siegl, J. Nohava and P. Chráska: *J. Therm. Spray Technol.*, 2005, **14**, (2), 231–238.
280. K. A. Khor, Y. W. Gu and Z. L. Dong: *Surf. Coat. Technol.*, 2001, **139**, (2–3), 200–206.
281. J. H. You, T. Hoschen and S. Lindig: *J. Nucl. Mater.*, 2006, **348**, (1–2), 94–101.
282. D. Schwingel, R. Taylor, T. Haubold, J. Wigren and C. Gualco: *Surf. Coat. Technol.*, 1998, **108–109**, (1–3), 99–106.
283. W. Z. Wang, C. J. Li and Y. Y. Wang: *Mater. Trans.*, 2006, **47**, (7), 1643–1648.
284. E. H. Lutz: *J. Am. Ceram. Soc.*, 1994, **77**, (5), 1274–1280.
285. S. Kuroda, T. Fukushima and S. Kitahara: *Thin Solid Films*, 1988, **164**, (0), 157–163.
286. J. A. Thompson and T. W. Clyne: *Acta Mater.*, 2001, **49**, (9), 1565–1575.
287. E. Rybicki, J. Shadley, Y. Xiong and D. J. Greving: *J. Therm. Spray Technol.*, 1995, **4**, (4), 377–383.
288. M. Buchmann, M. Escibano, R. Gadow, G. Bürkle, M. Mahlich and H. J. Fecht: 'On the elastic mechanical properties of thermally sprayed coatings', Thermal Spray 2002: International Thermal Spray Conference, Essen, Germany, 4–6 March 2002, 598–605; 2002, Duesseldorf, Germany, DVS, Deutscher Verband für Schweißen.
289. R. J. Damani and A. Wanner: *J. Mater. Sci.*, 2000, **35**, (17), 4307–4318.
290. Y. Tan, A. Shyam, W. B. Choi, E. Lara-Curzio and S. Sampath: *Acta Mater.*, 2010, **58**, (16), 5305–5315.
291. A. E. Giannakopoulos and S. Suresh: *Scr. Mater.*, 1999, **40**, (10), 1191–1198.
292. V. Harok and K. Neufuss: *J. Therm. Spray Technol.*, 2001, **10**, (1), 126–132.
293. A. Rico, J. Gómez-García, C. J. Múnez, P. Poza and V. Utrilla: *Surf. Coat. Technol.*, 2009, **203**, (16), 2307–2314.
294. F. Kroupa: *J. Therm. Spray Technol.*, 2007, **16**, (1), 84–95.
295. J. R. Bristow: *Br. J. Appl. Phys.*, 1960, **11**, (2), 81.
296. R. McPherson and B. V. Shafer: *Thin Solid Films*, 1982, **97**, (3), 201–204.
297. R. Musálek, O. Kovárik and J. Matejček: *Surf. Coat. Technol.*, 2010, **205**, (7), 1807–1811.
298. A. A. Griffith: *Philos. Trans. R. Soc. Lond. A*, 1921, **221**, (582–593), 163–198.
299. A. F. Liu: 'Mechanics and mechanisms of fracture: an introduction', 458; 2005, Materials Park, OH, USA, ASM International.
300. D. Z. Guo and L. J. Wang: *Surf. Coat. Technol.*, 1992, **56**, (1), 19–25.
301. P. J. Callus and C. C. Berndt: *Surf. Coat. Technol.*, 1999, **114**, (2–3), 114–128.
302. M. Watanabe, A. Owada, S. Kuroda and Y. Gotoh: *Surf. Coat. Technol.*, 2006, **201**, (3–4), 619–627.
303. Y. C. Zhou, T. Tonomori, A. Yoshida, L. Liu, G. Bignall and T. Hashida: *Surf. Coat. Technol.*, 2002, **157**, (2–3), 118–127.
304. P. F. Zhao, C. A. Sun, X. Y. Zhu, F. L. Shang and C. J. Li: *Surf. Coat. Technol.*, 2010, **204**, (24), 4066–4074.
305. Y. Yamazaki, A. Schmidt and A. Scholz: *Surf. Coat. Technol.*, 2006, **201**, (3–4), 744–754.
306. Y. Zhao, A. Shinmi, X. Zhao, P. J. Withers, S. Van Boxel, N. Markocsan, P. Nylen and P. Xiao: *Surf. Coat. Technol.*, 2012, **206**, (23), 4922–4929.
307. M. M. Lima, C. Godoy, P. J. Modenesi, J. C. Avelar-Batista, A. Davison and A. Matthews: *Surf. Coat. Technol.*, 2004, **177–178**, 489–496.
308. A. K. Ray: *Bull. Mater. Sci.*, 1999, **22**, (1), 25–32.
309. G. N. Heintze and R. McPherson: *Surf. Coat. Technol.*, 1988, **34**, (1), 15–23.
310. W. F. Brown and J. E. Srawley: 'Plane strain crack toughness testing of high strength metallic materials', 129; 1966, Materials Park, OH, USA, ASTM International.
311. C. C. Berndt and C. K. Lin: *J. Adhes. Sci. Technol.*, 1993, **7**, (12 Pt. 2), 1235–1264.
312. B. R. Lawn, A. G. Evans and D. B. Marshall: *J. Am. Ceram. Soc.*, 1980, **63**, (9–10), 574–581.
313. K. Nihara, R. Morena and D. P. H. Hasselman: *J. Mater. Sci. Lett.*, 1982, **1**, (1), 13–16.
314. A. S. M. Ang and C. C. Berndt: 'Mechanical properties of plasma sprayed YSZ coatings measured using TAT and TCT test', Int. Thermal Spray Conf. 2013: innovative coating solutions for the global economy, Busan, Korea, May 13–15, 2013; 2013, Materials Park, OH, USA, ASM International.
315. R. S. Lima, A. Kucuk and C. C. Berndt: *Mater. Sci. Eng. A*, 2002, **327**, (2), 224–232.
316. P. K. Aw and B. H. Tan: *J. Mater. Process. Technol.*, 2006, **174**, (1–3), 305–311.
317. L. Wang, Y. Wang, X. G. Sun, J. Q. He, Z. Y. Pan and C. H. Wang: *Vacuum*, 2012, **86**, (8), 1174–1185.
318. R. Danzer, T. Lube, P. Supancic and R. Damani: *Adv. Eng. Mater.*, 2008, **10**, (4), 275–298.
319. R. S. Lima and B. R. Marple: *J. Therm. Spray Technol.*, 2003, **12**, (2), 240–249.
320. J. F. Li and C. X. Ding: *J. Mater. Sci. Lett.*, 1999, **18**, (19), 1591–1593.
321. P. Ostojic and C. C. Berndt: *Surf. Coat. Technol.*, 1988, **34**, (1), 43–50.
322. A. S. M. Ang, N. Sanpo, M. L. Sessa, S. Y. Kim and C. C. Berndt: *J. Therm. Spray Technol.*, 2013, **22**, (7), 1170–1183.

Permission to publish: A.S.M. Ang and C.C. Berndt, "A review of testing methods for thermal spray coatings" J. Inter. Materials Reviews, 2014, 45 pages, advance on-line article:

Permission is given subject to the proper acknowledgement of the publisher and copyright holder. Permission is also subject to acknowledgement of the original place of publication of the material listed above, in your forthcoming publication. Finally, permission is given on the condition that components of the thesis aren't indexed individually in any catalogue, only the thesis as a whole. See: <http://www.manevonline.com/doi/abs/10.1179/1743280414Y.0000000029>.

## Chapter 7. Summary and Concluding Comments

This chapter indicates (i) the collaborators of the applicant, (ii) the prime topics that the applicant investigated over his career, and (iii) his annual output.

### 7.1 Analysis of Co-Workers and Collaborators

A listing of the 141 co-authors associated with the applicant is provided in the table below. The relationship to the applicant is indicated. It is logical that the majority of the co-authors would be in the categories of (i) Advisor/Mentor, (ii) University Colleague, and (iii) Post Graduate Students of the applicant.

Co-Author	# Papers	Relationship
Herman H.	76	Advisor / Mentor
McPherson R.	13	Advisor / Mentor
Miller R.A.	6	Advisor / Mentor
Coddet C.	16	University Collaborator
Khor K.A.	5	University Collaborator
Vardelle M.	5	University Collaborator
Fauchais P.	4	University Collaborator
Vardelle A.	4	University Collaborator
Heberlein J.V.R.	4	University Collaborator
Lugscheider E.	3	University Collaborator
Ng H.W.	3	University Collaborator
Planche M.P.	3	University Collaborator
Remesh K.	3	University Collaborator
Yan F.Y.	3	University Collaborator
Yu S.C.M.	3	University Collaborator
Bernard D.	2	University Collaborator
Bonfield W.	2	University Collaborator
Chen Z.	2	University Collaborator
Dinnebier R.	2	University Collaborator
Hewitt D.	2	University Collaborator
Knowles J.C.	2	University Collaborator
Lam Y.C.	2	University Collaborator
Leger A.C.	2	University Collaborator
Lins V.F.C.	2	University Collaborator
Mook W.	2	University Collaborator
Wiener M.	2	University Collaborator
Yokota O.	2	University Collaborator
Lindemann J.	4	Industry
Kay C.M.	3	Industry
Rizzi G.	3	Industry
Roberts G.	3	Industry
Scrivani A.	3	Industry
Abbate A.	2	Industry
Kotidis P.	2	Industry
Russell W.	2	Industry

Co-Author	# Papers	Relationship
Zimmerman F.	1	Industry
Truong V.K.	7	Joint Post Graduate
Shankar N.R.	6	Joint Post Graduate
Chraska T.	5	Joint Post Graduate
Gansert R.	4	Joint Post Graduate
Minagar S.	4	Joint Post Graduate
Qian G.	4	Joint Post Graduate
Benary R.	3	Joint Post Graduate
Gansert R.V.	3	Joint Post Graduate
Goldschlag D.	3	Joint Post Graduate
Kanta A.F.	3	Joint Post Graduate
Campbell G.R.	2	Joint Post Graduate
Easton C.D.	2	Joint Post Graduate
Guessasma S.	2	Joint Post Graduate
Guru D.N.	2	Joint Post Graduate
Usmani S.	2	Joint Post Graduate
Vcelka M.	2	Joint Post Graduate
Vetter W.M.	2	Joint Post Graduate
Montavon G.	16	Long Term Lab Visitor
Branco J.R.T.	4	Long Term Lab Visitor
Claudon A.	4	Long Term Lab Visitor
Tikkanen J.	4	Long Term Lab Visitor
Murakami K.	3	Long Term Lab Visitor
Long G.G.	13	National Lab Collaborator
Allen A.J.	12	National Lab Collaborator
Allan M.L.	5	National Lab Collaborator
Haddad G.N.	5	National Lab Collaborator
Chraska P.J.	4	National Lab Collaborator
Goland A.N.	3	National Lab Collaborator
Krueger S.	3	National Lab Collaborator
Lawn B.R.	3	National Lab Collaborator
Pajares A.	3	National Lab Collaborator
Wallace J.	3	National Lab Collaborator
Boukari H.	2	National Lab Collaborator
Curro R.	2	National Lab Collaborator
Dubsky J.	2	National Lab Collaborator
Kim S.Y.	2	National Lab Collaborator
Lee W.Y.	2	National Lab Collaborator
Marple B.R.	2	National Lab Collaborator
Wei L.	2	National Lab Collaborator
Kucuk A.	21	Post Doc
Karthikeyan J.	18	Post Doc
Senturk U.	16	Post Doc
Saber-Samandari S.	6	Post Doc
Morks M.F.	3	Post Doc
Ostojic P.	3	Post Doc

Co-Author	# Papers	Relationship
Gross K.A.	40	Post Grad Student
Lima R.S.	28	Post Grad Student
Leigh S-H.	24	Post Grad Student
Ilavsky J.	20	Post Grad Student
Lin C.K.	20	Post Grad Student
Brogan J.A.	16	Post Grad Student
Ibrahim A.	11	Post Grad Student
Sun L.	11	Post Grad Student
Gan J.A.	10	Post Grad Student
Sanpo N.	9	Post Grad Student
Ang A.S.M.	8	Post Grad Student
Callus P.J.	6	Post Grad Student
Yi J.H.	6	Post Grad Student
Gross K.	5	Post Grad Student
Mediaswanti K.	5	Post Grad Student
Racek O.	5	Post Grad Student
Hasan M.F.	5	Post Grad Student
Michlik P.	4	Post Grad Student
Reddy S.	4	Post Grad Student
Wang D.	4	Post Grad Student
Alamara K.	3	Post Grad Student
Choudhury T.A.	3	Post Grad Student
Otterson D.	3	Post Grad Student
Sesso M.L.	3	Post Grad Student
Xie W.	3	Post Grad Student
Cheang P.	2	Post Grad Student
Dambra C.G.	2	Post Grad Student
Mansur M.R.	2	Post Grad Student
Bancke G.A.	3	Research Engineer
Durandet Y.	3	Research Engineer
Zatorski R.A.	3	Research Engineer
Dunn M.	2	Research Engineer
Jewett T.J.	2	Research Engineer
Mair R.H.	2	Research Engineer
Ratnaraj R.	2	Research Engineer
Shu L.	2	Research Engineer
Collinson D.	3	Under Graduate
Mancini C.E.	2	Under Graduate
Wang J.	37	University Colleague
Sampath S.	29	University Colleague
Ivanova E.P.	12	University Colleague
Wen C.	9	University Colleague
King A.H.	8	University Colleague
Lima C.R.C.	7	Post Grad Student
Iacono V.J.	6	University Colleague
Simon G.P.	6	University Colleague



Co-Author	# Papers	Relationship
Crawford R.J.	5	University Colleague
Malherbe F.	5	University Colleague
Nakamura T.	5	University Colleague
Wong Y.C.	5	University Colleague
Hodzic A.	3	University Colleague
Jacob M.V.	3	University Colleague
Lima C.R.C.	7	Post Grad Student
Leong Y.K.	3	University Colleague
Raghu S.	3	University Colleague
Stephens P.	3	University Colleague
Breslin V.T.	2	University Colleague
Chan D.	2	University Colleague
Dudley M.	2	University Colleague
Hosseinzadeh N.	2	University Colleague
Woods G.S.	2	University Colleague

## 7.2 Summary of Publications

Each publication listed in Appendix 7 was assigned a ‘Type’ according to the classification system indicated in the Table below. In this way the relative contributions according to the publication descriptor was determined.

Table 2: Analysis of publication descriptors.

Type	Descriptor	Total	%
1	Books (Theses, CD's & Edited Conference Proceedings)	17	4
2	Reviewed Chapters in Books	147	32
3	Journals	192	42
4	Conference Articles accepted after soft review	60	13
5	Other	43	9
	TOTAL Publication Count	459	100
	C.C. Berndt as first author (includes all publications)		147 (32%)
	Publications with a significant review content		27
	Percent hard reviewed (excludes Type 4 and 5 publications)		78%

## 7.3 Analysis of Publication Content

The thesis is organized in chapters according to subject content that is broadly defined as (i) processing, (ii) microstructure, (iii) mechanical properties, (iv) modeling, and (v) applications. Thus, it is appropriate to systematically assess each of the hard-reviewed contributions (416 publications) according to these five categories. Each publication was assigned an order of priority with respect to the 5 subject content indicators.

For example, consider publication #435: A.S.M. Ang, C.C. Berndt, M. Dunn, M.L. Sesso, S.Y. Kim, ‘Modeling the Coverage of Splat Areas Arising from Thermal Spray Processes’, J. Am. Ceramic Soc., 95[5] (2012) p. 1572-1580. DOI: 10.1111/j.1551-2916.2012.05113.x Published: May 2012. This publication was assigned the following priorities #1= modeling, #2 = processing, #3 = microstructure, #4 = applications, and #5 = mechanical properties. Note that there is some judgment required in making the individual assessments on each publications. However, this consistent approach enables a semi-quantitative valuation of this body of work.

Table 3 is a summary of the 5 priority areas over all of the publications that were considered. This analysis indicates a strong focus of the thesis on ‘processing – structure – property’ relationships. Modeling and applications, however, are still robust contributors to the overall theme of the presented work and are core components for the integrated study.

Table 3: Analysis of publication content.

Priority	Processing	Micro-structure	Mechanical props	Modeling	Applications
#1	84	126	144	36	26
#2	150	152	37	56	21
#3	107	104	43	55	107
#4	56	26	102	66	166
#5	19	8	90	203	96
checksum	416	416	416	416	416

The 416 entries were also examined to assess chronological trends in the general content of the publications from 1983 through to 2014. Thus, the top 3 priority areas (i.e., 3 out of (i) modeling, (ii) processing, (iii) microstructure, (iv) applications, and (v) mechanical properties) for each publication were weighted in the ratio of 50:30:20. The contributions from each year were normalized. In this way the general trends of these priority areas was assessed, Figure 1.

Figure 1 indicates the development of the research and activity themes of the applicant. The general trends exhibited by Fig. 1 are:

- The theme of processing has increased over the past 37 years.
- The themes of mechanical properties and modeling were strong in the mid-80s, which is as expected since these topics were primary ones of the applicant’s thesis.
- The theme of microstructure has been consistently high, which gels with the undergraduate and post graduate training/education of the applicant.
- The theme of applications has been a consistent contribution to the outputs of the applicant with some localized importance in 1990 and 2009. The peaks reflect the importance and focus on specific projects in the preceding 2-3 years; i.e., there is often a lag of several years between the research activity and the publishing schedule.

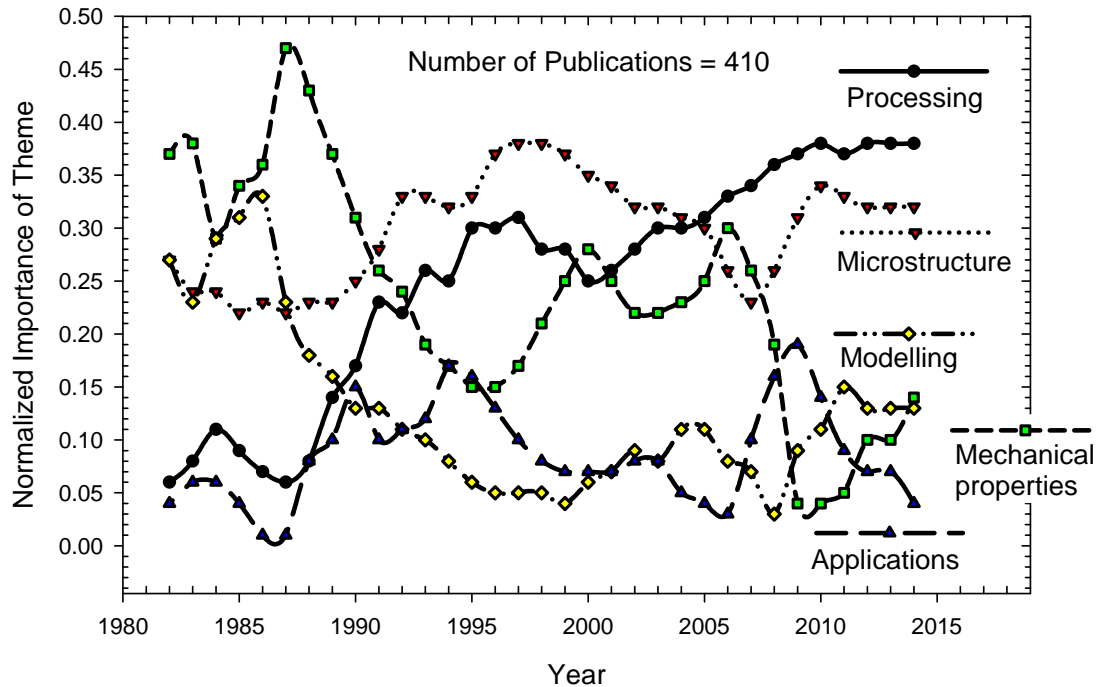


Figure 1. A chronological view of publication themes.

#### 7.4 Analysis of Yearly Output

The raw data of publications per year is highly variable. Thus, a moving 3-year average was employed to reduce data fluctuations, Figure 2. The average output of reviewed publications is about 11-12 per year over the 37-year of the applicant.

This data can be interpreted with respect to the development of the work based on research maturity and opportunity. For example, major transitions to Monash in 1985 and to James Cook University in 2004 correspond to local minima in Figure 2. This might be expected when significant changes occur within a career. There was a period of several years before laboratory infrastructure was built up; after which research and publication output increased.

A summary of the Journals where the applicant has published is presented in Table 4. Data is not available for every journal presented. The impact factors are either 1-year or 5-year values depending on the data available. A reasonable impact factor for a materials science and engineering journal is between 1 and 2. However, it is also important to report research outputs in a variety of mainstream journals that may not lend themselves to citations; but which reach out to more disciplines of engineering communities.

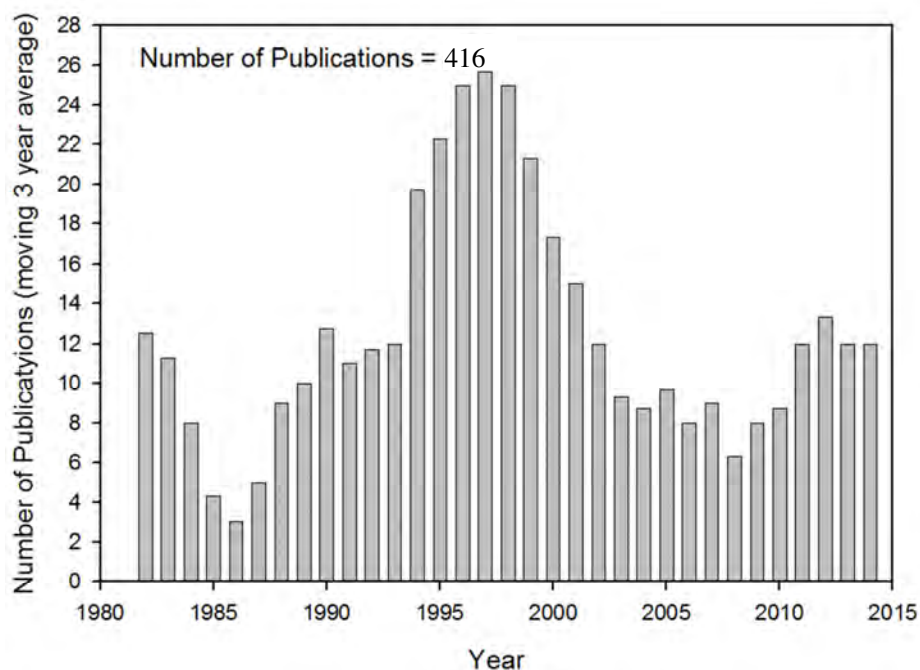


Figure 2. Yearly publication rate.

Table 4. Journals that have accepted the applicant's submissions.

Title of Journal	Number of Contributions	Impact Factor
Acta Biomaterialia	3	5.093
Acta Materialia	2	3.941
Advanced Engineering Materials	3	1.608
American Ceramic Society Bulletin	3	0.32
Applied Microbiology Biotechnology	1	3.689
Applied Surface Science	3	2.112
Australian Welding Research	2	NA
Biomacromolecules	1	5.371
Biomaterials	1	8.496
Brookhaven National Laboratory Report	1	NA
Ceramic Engineering Science Proceedings	2	NA
Chemical Engineering Science	1	2.386
Coatings	1	NA
Expert Systems with Applications	1	1.854
Geotechnical and Geological Engineering	1	NA
Geothermal Resources Council Transactions	1	NA
Industrial and Engineering Chemistry Research	1	2.206
International Journal of Fracture	1	1.25
International Journal of Oral and Maxillofacial Implants	2	1.521
International Journal Turbo and Jet Engines	1	0.261
Journal of Adhesion Science & Technology	1	0.857
Journal of Applied Physics	1	2.21

<b>Title of Journal</b>	<b>Number of Contributions</b>	<b>Impact Factor</b>
Journal of Applied Polymer Science	1	1.395
Journal of Biobased Materials and Bioenergy	1	0.826
Journal of Biomaterials Science	1	1.7
Journal of Biomedical Materials Research	5	2.834
Journal of Dental Research Special Issue	1	3.826
Journal of Engineering for Gas Turbines and Power	1	0.93
Journal of International Materials Reviews	1	7.48
Journal of Materials Chemistry B	1	6.101
Journal of Materials Engineering and Performance	3	0.915
Journal of Materials Research	1	1.713
Journal of Materials Science	7	2.163
Journal of Materials Science – Materials in Medicine	2	2.325
Journal of Materials Science Letters	1	2.163
Journal of Nano Research	1	0.341
Journal of Practical Failure Analysis	1	1.21
Journal of the American Ceramic Society	15	2.107
Journal of the Australian Ceramic Society	1	0.164
Journal of the Materials Research Society	1	1.713
Journal of Thermal Spray Technology	25	1.481
Key Engineering Materials	3	NA
Langmuir	1	4.187
Macromolecules	1	5.521
Materials and Manufacturing Processes	1	1.39
Materials Science and Engineering A	13	2.349
Materials Science Forum	4	NA
Materials Science Research	5	NA
Mechanics of Materials	1	1.936
Metallurgia Italiana	1	0.123
Metallurgy and Materials Transactions	1	1.627
Nanostructured Materials	2	NA
NASA Technical Memorandum	1	NA
Plasma Chemistry and Plasma Processes	1	1.728
Polymer Engineering and Science	2	1.243
Powder Technology	1	2.024
Progress in Organic Coatings	1	1.848
Resources, Conservation and Recycling	1	2.319
Silikáty	1	0.418
Surface and Coatings Technology	21	1.941
Surface Journal International	1	NA
The Finishing Line	1	NA
Thin Solid Films	9	1.604
Transactions ASME Engineering Gas Turbines	1	0.82
Transactions Institution Engineers Australia	1	NA
Wear	1	1.262



### **7.5 Concluding Comments**

This chapter provides metrics concerning (i) the collaborators of the applicant, (ii) the prime topics that the applicant has worked in over his career, and (iii) the annual output. Methods have been developed by the applicant to visualize these interactions in a semi-quantitative fashion.

This chapter also presents data concerning ‘the advancement of knowledge’ *via* (i) training of students and post doctoral fellows, (ii) working with co-authors and colleagues from around the globe, and (iii) dissemination of knowledge by means of published outputs.

-- END --

## List of Appendices

Appendix 1.	Condensed Curriculum Vitae (11-pages). Note: There is cross-referencing to other documents within the appendices.	A3
Appendix 2.	Press Release on Christopher C. Berndt: President of ASM International (2-pages). This personalised article was distributed to the 36,000 members of ASM International when Chris Berndt was appointed as the President of this society.	A15
Appendix 3.	Research Portfolio (6 pages).	A17
Appendix 4.	Leadership and Engagement Portfolio (6 pages).	A23
Appendix 5.	Learning and Teaching Portfolio (6 pages).	A29
Appendix 6.	Editorials and Commentaries of Christopher C. Berndt (27 pages). A compilation of Editorials and Commentaries that have been published in journals is contained within this appendix.	A35
Appendix 7.	List of Publications of Christopher C. Berndt (35 pages). The list is current as of late February 2014. Several other publications have come to pass since this documentation.	A63
Appendix 8.	Biography of Christopher C. Berndt (1-page). This short biography is used for publication relations purposes when there is this need.	A98

## Curriculum Vitae of Christopher Charles BERNDT

Address: Swinburne University of Technology  
Faculty of Science, Engineering and Technology  
Bldg. ATC, Rm. 818, Mail Stop H66  
John Street  
Hawthorn, VIC 3122

WWW: <http://www.swinburne.edu.au/engineering/staff/Christopher-Berndt-286>

Current Academic Positions: Professor of Surface Science and Interface Engineering

Adjunct Professor; Stony Brook University, NY-USA

Personal Details: DOB is 2<sup>nd</sup> September 1953, Married to Marita, No children.

### TABLE OF CONTENTS

<b>1</b>	<b>Tertiary Education .....</b>	<b>1</b>
<b>2</b>	<b>Appointments.....</b>	<b>1</b>
<b>3</b>	<b>Research Interests .....</b>	<b>2</b>
<b>4</b>	<b>Awards and Honors .....</b>	<b>2</b>
<b>5</b>	<b>Professional Membership .....</b>	<b>4</b>
<b>6</b>	<b>Professional Activities.....</b>	<b>5</b>
	6.1 Publications	5
	6.2 Patent Activities	6
	6.3 Miscellaneous	6
<b>7</b>	<b>Grant Proposals and Reports .....</b>	<b>8</b>
<b>8</b>	<b>Academic Responsibilities.....</b>	<b>8</b>
<b>9</b>	<b>Academic Conferences / Grant Reviewer .....</b>	<b>8</b>
	9.1 Administrative Duties and University Service	8
	9.2 Educational and University Committees	9
	9.3 Teaching	10
<b>10</b>	<b>Publications.....</b>	<b>10</b>

Note: An informal introduction to Chris has been published in the open literature as ‘Christopher C. Berndt: 2011-2012 President of ASM International’, authored by R. Knight, Advanced Materials and Processes, January 2012, pp. 34-35. This article appears within the Appendix material. As well, more detail on specific areas is contained within the 3 attached portfolios on ‘research’, ‘leadership and engagement’, and ‘learning and teaching’.

### 1 Tertiary Education

1977-1980	Ph.D., Monash University, Dept. Materials Engineering, Melbourne, Australia. Thesis supervisor: Assoc. Prof. R. McPherson. Title: ‘The Adhesion Of Flame And Plasma Sprayed Coatings’. PhD accepted/conferred June 05, 1981.
1976	Graduate Diploma in Metallurgy and Materials (Honors Class II) from the South Australian Institute of Technology, School of Metallurgy, Adelaide. (Now ‘The University of South Australia’.) Thesis supervisor: Dr. P.W. Slattery. Title: ‘The Stress Corrosion Cracking Of Magnesium-Aluminium Alloys’
1971-1975	B.App.Sci. in Secondary Metallurgy from the South Australian Institute of Technology, School of Metallurgy, Adelaide.

### 2 Appointments

October 2012+	Professor, Professor of Surface Science and Interface Engineering, IRIS, Swinburne University of Technology, Victoria, Australia
April 2008 – Oct 2011	Director, IRIS: ‘manufacturing research at Swinburne’, Swinburne University of Technology, Victoria, Australia

Dec.2007 +	Professor of Surface Science and Interface Engineering, Swinburne University of Technology, Victoria, Australia
January 2006 +	Adjunct Professor, the Department of Materials Science and Engineering, Stony Brook University, NY-USA.
Nov.2004 2007	Professor and Research Leader in Surface Science and Interface Engineering, James Cook University, Queensland, Australia
2001 - 2004	Associate Dean for Undergraduate Studies, College of Engineering and Applied Sciences, Stony Brook University, NY-USA.
1991	Associate Professor, then Professor (September 1994), in the Department of Materials Science and Engineering, Stony Brook University, NY-USA. <ul style="list-style-type: none"> <li>• Adjunct Professor of Orthopedics, Stony Brook University, 1997.</li> <li>• Research Collaborator, Dept. of App. Sci. Brookhaven National Lab., NY-USA, 1992.</li> <li>• Research Collaborator at the High Temperature Materials Laboratory of Oak Ridge National Laboratory, TN-USA, 1994-95.</li> </ul>
July-Sept. 1991	NASA Lewis Summer Faculty Fellow, Cleveland, OH-USA.
1989	Snr. Lecturer in the Department of Materials Engineering, Monash University, Australia.
1986	Lecturer in the Department of Materials Engineering, Monash University, Australia.
1985	Snr. Research Fellow, Dept. of Materials Engineering, Monash University, Australia.
1983	Senior Research Associate with Cleveland State Uni., working full time at NASA Lewis Research Center. <ul style="list-style-type: none"> <li>• Principal Investigator of NASA cooperative agreement NCC 327.</li> <li>• Fellow of the Joint Institute for Aerospace Propulsion and Power.</li> </ul>
1981	Post Doctoral Research Associate 1981, Stony Brook University, Dept. Materials Science and Engineering, Stony Brook, NY-USA. <ul style="list-style-type: none"> <li>• Co-Principal Investigator for NASA Contract NAG3164, 'A microstructural study of plasma sprayed thermal barrier coatings'; ONR N 000 1480 C0824, 'Thermal barrier coatings for shipboard protection'.</li> <li>• NASA Lewis Summer Faculty Fellow July-Sept. 1982.</li> <li>• Lecturer for ESM 510 Spring 1983, 'Kinetic processes in solids'.</li> </ul>
1977	<ul style="list-style-type: none"> <li>• Monash University, Dept. of Materials Engineering, Melbourne, Victoria, Australia. Duties included: Doctoral Thesis, Part time tutor, Research assistant (for 4 months) for Dr. H. Brown on 'The impact toughness of polycarbonate'.</li> <li>• Royal Melbourne Institute of Technology, Melbourne, Victoria. Part time tutor in the Mining and Metallurgy Department.</li> </ul>
1975	The South Australian Institute of Technology, School of Metallurgy, Adelaide, South Australia. Completion of Metallurgy and Honors degrees.
1971	The Broken Hill Proprietary Co. Ltd., Whyalla, South Australia. Metallurgy cadet in an integrated steel works and ship yard. (4-years part time study)

### **3 Research Interests**

#### **Thermally Sprayed Coatings**

Experiments and analysis of thermal expansion coefficients.  
Fracture toughness and mechanical property measurements.  
Acoustic emission studies.  
Fiber reinforced coatings.  
Nano-materials and thermal spray.

#### **Biomaterials**

Biocompatible coatings of hydroxyapatite.  
Bioceramic orthopaedic plates and appliances.

### **4 Awards and Honors**

---

#### 4 Awards and Honors

2013	Elected to Fellow of the American Ceramic Society. One of 3 representatives from Australia.
2013	Elected as Vice-President of the Australian Ceramics Society
2012	Various honors accepted on behalf of ASM International while President of the society.
2011	President of ASM International. (A 1-year appointment as Chair of the Board of Trustees)
2011	Elected to Fellow of ASMu (Alpha Sigma Mu, the honor society for materials science and engineering)
2009	President of the Australian Ceramics Society (a 2-year appointment)
2007	Elected to the ASM-Thermal Spray Society 'Hall of Fame'. One of 2 representatives from the Southern Hemisphere. (Thirty-three people have been elected to this honor.)
2007	Chair of the Townsville Regional Group of Engineers Australia
2006	Appointed to the Editorial Board of 'Materials Science and Engineering A'.
2006	James Cook University Inaugural Professorial Lecture on 'Nanotechnology: Science Fiction or Science Fact!'.
2006	Elected to the Award of the 'Order of the Engineer' by the National Institute of Ceramic Engineering.
2006	Vice Chair of the Townsville Regional Group of Engineers Australia
2005	Invited to join the Federal Council of the Australian Ceramic Society
2005	Appointed to the Editorial Boards of (i) Journal of International Materials Reviews (ii) Journal of Phase Equilibria and Diffusion (iii) Journal of Materials Engineering and Performance.
2005	Recognition Award as the Foundation Editor of the Journal of Thermal Spray Technology; 13-years of service.
2005	Member of the Board of ASM International (2005-2008)
2005	Initiated as an 'Eminent Engineer' of the 'Tau Beta Pi Engineering Society' after being nominated by students.
2004	Editor Emeritus of the Journal of Thermal Spray Technology. (Founding Editor for the Journal of Thermal Spray Technology, 1991-2004.)
2004	Chairman of the Editorial Board of the Journal of Thermal Spray Technology
2002	President of the Thermal Spray Society (2002-2004)
2002	ASM International 'Allan Ray Putnam Service Award'.
2001	Admitted to the 'Academy of Teachers-Scholars' of Stony Brook University
2001	University of Minnesota, Mechanical Engineering Distinguished Lecture Series on 'Biomaterials'
2001	ASM MEI (Materials Engineering Institute) Instructor of Merit Award
2000	Best Paper Award for the Journal of Thermal Spray Technology, Volume 8
2000	Award for ASM 'Fellows Speaker Program'
2000	Plenary talk at the Annual Meeting of the Center for Plasma-Aided Manufacturing, Madison, WI. June 14. 'Plasma Spraying of Biocompatible Coatings'.
1997	Keynote and Distinguished Lecturer, 'Fourth International Conference on Composites Engineering', July 6-12, 1997, Hawaii.



#### 4 Awards and Honors

1997	Teaching Award, Stony Brook University
1996	Inaugural President's Award from the Thermal Spray Society of ASM International for 'Exemplary and Unselfish Service'.
1994	Honorable Mention for 'Spray Forming of Graded Polymer Composite Components' in 'The DuPont Plunkett Student Awards for Innovation with Teflon®'
1994	ASM International, Thermal Spray Society, Service Award for NTSC'94 Proceedings Co-Editor.
1994	Third Annual University at Stony Brook Faculty Achievement Dinner.
1994	Inclusion into the American Men & Women of Science.
1993	Acceptance into The Institution of Engineers, Australia; Foundation Member of the College of Biomedical Engineers.
1993	First Prize in 'Color Category' of the American Powder Metallurgy Institute, Metallography Competition'. Poster by John Z. Chen, C. Perdikaris, H. Herman, C.C. Berndt, and C.C. Huang, title of poster 'Composite Powders with Shell Structure Formed by Mechanofusion'.
1993	Award of Honor from College of Engineering and Applied Sciences - Stony Brook for 'Excellence in Teaching' in the MSE Department.
1993	Certificate of Merit from ASM International for a best paper in the National Thermal Spray Conference, Anaheim. Paper by C.C. Berndt, J. Ilavsky, H. Herman, and M.B. Beardsley, title of paper 'Thermal Expansion of Metallic and Cermet Coatings'.
1993	Alcoa Foundation Fellowship.
1992	Plaque of appreciation from ASM International for 'commitment to quality' as the Proceedings Editor for The 13th International Thermal Spray Conference.
1992	Alcoa Foundation Fellowship
1992	Award from the Department of Dentistry, University Hospital, Stony Brook University for contributions as a guest speaker.
1991	Visiting Summer Faculty Program at NASA - Lewis Research Center (Materials Division)
1991	ASM International Award to attend the 4th National Thermal Spraying Conference, Pittsburgh, May 1991.
1990	Medal Presentation by 'Societe Francaise De Metallurgie' for invited presentation and session Chairing at the 3rd International Conference on Surface Modification (November, 1990).
1990	Certificate of Appreciation from the Thermal Spray Division of the ASM as an Invited Speaker at the NTSC-90.
1990	J.A. Edgerton Award for the best paper published by a Victorian Member of The Australian Institute of Metals.
1986	Travel Award from the Ian Potter Foundation to attend the 11th. International Thermal Spraying Conference.
1983	Award to attend the NATO Advanced Study Institute on Surface Engineering.
1982	NASA Lewis Summer Faculty Fellow.

#### 5 Professional Membership

- Professional Member of the Institute of Metals and Materials Australasia (1976-85)
- The Australian Ceramic Society. (1979+)
- Chartered Professional Engineer - Australia. (1981+)
- The American Ceramic Society - USA (1981+)

## 5 Professional Membership

- National Institute of Ceramic Engineers - USA (1981+)
- IOM3, Chartered Engineer - UK (1983+), **Fellow 1995**
- Member of the Institution of Engineers - Australia (1985+), **Fellow 1995**, Foundation Member of the College of Biomedical Engineers - Australia (1994+), Member of the Mechanical Engineering College 2001
- ASM International - USA - Thermal Spray Society (1988+), **Fellow 1996**
- New York Academy of Sciences (1992-2004)
- American Society for Testing and Materials - USA (1992-2011)
- Steel Structures Painting Council - USA (1993-2013)
- Society of Manufacturing Engineers - Senior Member. Senior Member of Composites Manufacturing Association - USA (1994+)
- American Society for Engineering Education (1995-2006)
- National Association of Corrosion Engineers - USA (1994+)
- American Welding Society - USA (1995+)
- The Biomaterials Society - USA (1996-2004)
- The American Society for Mechanical Engineers (1997+)

## 6 Professional Activities

### 6.1 Publications

- Special Editor for 'Surface Coatings and Technology' and 'Journal of Thermal Spray Technology'. Appointments for 2013-2014 while special journal issues are being compiled.
- Appointed to the Editorial Boards of (i) Journal of International Materials Reviews, (ii) Journal of Phase Equilibria and Diffusion, and (iii) Journal of Materials Engineering and Performance.
- Member of the Journal of Materials Engineering & Performance Committee, 2001-2006 (two 3-year terms).
- 'Excellent Reviewer' for Metallurgical and Materials Transactions, 2001.
- Proceedings Editor for the International Thermal Spray Conference, May 2001, Singapore.
- Foundation Editor for the Journal of Thermal Spray Technology, 1991 to present.
- Co-Chairman of the United Engineering Foundation Conference on 'Novel Synthesis and Processing of Nanostructured Coatings for Protection Against Degradation', August 12-17, 2001, Davos, Switzerland.
- Chairman of the United Engineering Foundation Conference on 'Thermal Spray Processing of Nanoscale Materials II', August 1999, Quebec City, Canada.
- Member of Journal of Materials Engineering and Performance Editorial Committee, Fall 2000.
- Proceedings Editor for the International Thermal Spray Conference, May 2000, Montreal, Quebec, Canada; Co-Editor for the International Thermal Spray Conference, May 2001, Singapore.
- Member of the 'Action in Education Team' of ASM International, Fall 1999.
- Reviewer of numerous technical articles for the Journal of Thin Solid Films, Acta Materialia / Scripta Materialia, Journal of the American Ceramic Society, Journal of Materials Research, Materials Science and Engineering A, Journal of Materials Engineering and Performance, Journal of Applied Biomaterials
- Proceedings Editor for the National Thermal Spray Conference, September 1996, Cincinnati, OH, USA; September 1995, Houston, TX, USA; June 1994, Boston, MA, USA; July 1993, Anaheim, CA, USA.
- International Editorial Board of 'TecAd: Technology Advances' (Pub. SCI & INST Canada, 1993).
- Proceedings Editor for the International Thermal Spray Conference, May-June 1992, Orlando, FL, USA.
- Contributor to 'Spraytime'; the broad sheet of The International Thermal Spray Association (1992+).
- Foundation Editor of the Journal of Thermal Spray Technology, Pub. ASM International (1991+).
- Book reviewer for the Institute of Metals and Materials, Australasia; The American Ceramic Society; Materials and Science Engineering; John Wiley & Sons, etc.
- Reviewer of numerous technical articles for the Journal of Thin Solid Films, Acta Materialia / Scripta Materialia, Journal of the American Ceramic Society, Journal of Materials Research, Materials Science and Engineering A, Journal of Materials Engineering and Performance, Journal of Applied Biomaterials, J. Surface Coatings and Technology, J. Thin Solid Films.

- Reviewer of document titled 'Perspectives in biomaterials bioceramics', prepared by the Department of Industry, Technology and Commerce; March 1988.
- 6.2 Patent Activities**
- M.R. Gold and C.C. Berndt, 'A Multifunctional, High-Sensitivity, Scratch Tester', June 2001.
  - C.C. Berndt and R.L. Lima, 'Microstructural Engineering and Processing for TBCs', April 2001.
  - C.C. Berndt, R.S. Lima and A. Kukuk, 'Tailored Microstructures for Predictable Coating Properties', February, 2001.
  - R.Benary, R.Gansert, C.C.Berndt and H.Herman, 'Automated Thermal Spray System (ATSS)', R-7099. Disclosed February 21, 1995.
  - J.Brogan, S.Reddy, C.C.Berndt, H.Herman and S.Sampath, 'Spray Forming of Graded Polymer Composite Components', S-7056. Disclosed April 5, 1994.
  - J.Brogan, C.C.Berndt, R.Lampo, K.A.Gross, S.Sampath and H.Herman, 'Thermal Spraying of Recycled and Post-Consumer Commingled Polymer Material', S-7088. Disclosed November 17, 1994.
  - S.Sampath, H.Herman and C.C.Berndt, 'Graded Metal Reinforced Ceramic Free Standing Forms', S-7060. Disclosed April 20, 1994.
  - C.C. Berndt, H. Herman and S. Sampath, 'Bar Coding of Powder Lots to Improve Process Efficiency During Thermal Spraying'. R-7103.
  - C.C. Berndt, H. Herman and S. Sampath, 'Method for Processing Layered and Gradient Structures through Thermal Spray Forming'. R-7091.
  - C.C. Berndt, H. Herman and S. Sampath, 'Silicide Based Graded Bond Coats for High Temperature Thermal Barrier Coatings'. R-7090.
  - C.C.Berndt, 'Graded Hydroxyapatite / Polymer Materials for Biomaterials Applications', R-861. Disclosed May 23, 1991.
- 6.3 Miscellaneous**
- Reviewer for the US Nuclear Authority in 2012 and 2013.
  - External Assessor of Promotion file for James Cook University, Australia.
  - Reviewer for the Small Business Industrial Research (SBIR) proposals of the Environmental Protection Agency (EPA) on Nanomaterials, 2003.
  - Reviewer of the Foundation for Research Science and Technology (FRST) of the New Economy Research Fund (NERF) for New Zealand, 2003.
  - Reviewer of the NSERC (Natural Sciences and Engineering Research Council of Canada) Discovery Grants 2003.
  - Member of the NSERC Site Visit Committee responsible for the review of 'Plasma Quebec', University of Montreal, May 2003, Government of Canada.
  - Member of the NSERC Site Visit Committee responsible for the review a Collaborative Research and Development Grants on 'Manufacturing Near Net-Shape Parts by Vacuum Plasma Spray Forming', November 14, 2002; Government of Canada.
  - President of the Thermal Spray Society of ASM International, Fall 2002 - 2004.
  - Delegate of ASM International to the TMS ABET Accreditation Committee, 2000, 2001, 2002, 2003.
  - Member of ASM International 'Strategic Planning Committee', 2002, 2003.
  - Member of ASM International 'ASM Surface Engineering Task Force', 2002, 2003.
  - Panel Member to the SBIR Phase I, 2003 RFP on 'Nanomaterials & Clean Technology' issued by the USA EPA. September 17-19, 2003. Washington DC-USA.
  - 'Advisory Committee' to the Canadian Plasma Technology Network, Spring 2002.
  - Successful nomination of Richard Knight to the position of Fellow of ASM International, Fall 2003.
  - Successful nomination of R.C. Tucker, Jr. to the Vice Presidency of ASM International, Spring 2002.
  - Successful nomination of Richard Sisson to the position of Trustee of ASM International, Spring 2002.
  - Successful nomination of Jockel Heberlein to the position of Fellow of ASM International, Fall 2001.
  - Instructor for the ASM 3-day course in 'Thermal Spray'. Rosemont, Chicago, IL-USA. October 1998. Course also held in 1999, 2000, 2001, 2002.
  - Vice President of the Thermal Spray Society of ASM International, Fall 2000 - 2002.
  - Reviewer of Australian Research Council Proposals, 1995-2001.
  - Reviewer of Cooperative Grants Program of the US Civilian Research and Development Foundation (CRDF), 2001.
  - Chairman of the ASTM sub-committee to provide a major revision of ASTM C633. Task completed in June 2001 after 8 years of review and discussion.

- Member of Journal of Materials Engineering and Performance Editorial Committee, Fall 2000.
- Member of the 'Action in Education Team' of ASM International, Fall 1999 to present.
- Panel Member for the 21<sup>st</sup> Century Fund of the State of Indiana responsible for disbursing \$20M, 1999, 2001.
- Member of the Scientific Committee for the 2000 International Thermal Spray Conference, May, Montreal, Canada.
- Member of review for distinguished professorial appointments for the University of Minnesota, 1999.
- Member of review for professorial appointments for the University of Cambridge, UK, 1999.
- Member of the Scientific Committee for the 1998 United Thermal Spray Conference, March, Dusseldorf, Germany.
- Member of the Scientific Board for ITSC'98 (Nice, France).
- Presidium Member of the International Conference on Advanced Manufacturing Technology (ICAMT99), Xian, PRC, June 1999.
- Voted to be a Member of the Thermal Spray Society Board for a second term, 1998.
- Listed in the Speakers Directory of the ASM Thermal Spray Society outreach program, 1998.
- Proposal Reviewer for the Natural Sciences and Engineering Research Council of Canada (1998)
- Proposal Reviewer for the National Science Foundation (1998), SBIR Proposal Reviewer for the National Science Foundation (1998, 1999, 2000)
- External Reviewer for the FCAR (Canada) Government research programs, 1997.
- External reviewer for DOE SBIR Phase II Awards, 1997.
- Contributor to 'Ask the Experts' at ASM annual event in 1997 on the subject of thermal spray.
- Review Member of the NSF Engineering Research Center for Plasma-Aided Manufacturing, 1996.
- Member of Peer Review Panel for DOE Fossil Energy Advanced Research Program Panel 16 - Alloys/Coatings. March 1995.
- Member of the Steering Committee of the Thermal Spray Society, 1994.
- Member of the Scientific Advisory Board of White Eagle International Technologies, Chairman of the Advanced Materials efforts (1994+)
- Foundation Member of the Executive Board of the Thermal Spray Society of ASM International (1994+)
- Member of NACE Committee T-6H-45 on 'Thermal Spray Coatings' (1994+)
- Member of The International Advisory Committee of ITSC'95, Kobe, Japan (1993+)
- Chairman of ASTM Committee B08.14 for 'Thermal Spray Coatings' (1993+)
- Member of AWS Committee C2.2 Subcommittee on 'Zn TSC on Reinforced Concrete' (1993+)
- Faculty Mentor for the Fall House program of Stony Brook University (1993)
- Reviewer for NSF and DOE SBIR grant applications (1993).
- Reviewer for the 'Australian Research Council' and the 'National Health and Medical Council' in the areas of Research proposals, Postdoctoral Fellowships, and Queen Elizabeth II Fellowships
- Invited by NSF to be a 'Site Panel Member' for the Engineering Research Center on Plasma-Aided Manufacturing.
- Research Council (Australia) from 1991-1992.
- International Advisory Committee for the International Symposium and Exhibition on Advances in Materials & Processes, 16-19 February 1992, Bombay, India.
- Chairman of the 'Awards Committee' of ASM International for 1992, 1993, 1994.
- Chairman of the Proceedings Committee of the Thermal Spray Division of ASM International since 1992+.
- Co-organizer of 'Workshop on Plasma Spray Forming', Stony Brook, March 16, 1993.
- Member of ASM International Thermal Spray Division National Conference Organizing Committee for 1991 to 1993.
- Member of ASM International Thermal Spray Division Executive Committee since 1991.
- Committee member of 'Standards Association of Australia', 1990-1991.
- Invited to join Subcommittee WD/2/4 (Hard Facing Consumables) of the Standards Association of Australia (April, 1990). Corresponding member since 1991.
- International Advisory Committee of the Satellite Symposium I High Performance Ceramic Coatings, of the 7th. CIMTEC World Ceramics Congress, Montecatini Terme, Italy, 3 June, 1990.

- Invited to join Panel 8 (Surfacing and Hardfacing) of the Australian Welding Research Association, March 1989. Corresponding member of the Welding Technology Institute of Australia, Panel on Hardfacing.
- Convener of 'Special seminar on thermally sprayed coatings', 13th. November, 1986, Monash University.
- Invited to panel discussion on 'Corrosion Control', sponsored by Pugh-Roberts Associates, September 28, 1985, Houston, Texas, USA. Submitted a document titled 'Literature search with regard to using thermal sprayed coatings for corrosion protection'.

## **7 Grant Proposals and Reports**

### Refer to Research Portfolio

- Chris Berndt has been the point of contact for the Defence Materials Technology Centre (DMTC) and the Advanced Manufacturing Cooperative Research Centre (AMCRC) since 2008. He was also a lead research in the AutoCRC. In these capacities he has been responsible for managing approximately 5-7 projects per year on behalf of SUT. The total funding level per year (until 2013) has averaged out to ~\$500,000. He has been directly responsible for procuring funding for colleagues; e.g., Prof. McArthur, Dr. Wade, Prof. Nagarajah, Assoc. Prof. Sbarski, Dr. Dong, Dr. Wong, and Dr. Durand.
- Chris Berndt, in his prior role as Director of IRIS from 2008 to 2011, was responsible for procuring resources for new staff who joined IRIS; i.e., Prof. McArthur, Prof. Wen, Prof. Kingschott, Dr. Wade, and Assoc. Prof. Stoddart. The startup funds were significant in terms of lab resources and equipment. For example, he procured \$300,000 for Prof. Wen and \$750,000 for Prof. Kingschott so that their labs could be populated with modern equipment. In an alike fashion the labs of Prof. McArthur, Assoc. Prof. Stoddart and Dr. Wade were refurbished and into modern working environments.

## **8 Academic Responsibilities**

### Refer to Teaching Portfolio

## **9 Academic Conferences / Grant Reviewer**

- NSF Panel Reviewer for National Science Foundation's National Science, Course Curriculum and Laboratory Instruction (CCLI), Washington, DC, July 14-17, 2003.
- NSF Panel Reviewer for National Science Foundation's National Science, Technology, Engineering, and Mathematics Education Digital Library (NSDL), Washington, DC, May 19-21, 2003.
- NSF Panel Reviewer for Small Business Industrial Research proposals on the topic of 'Phase I Electronics Panel concerning Semiconductor and Other Materials/Plasma Engineering', July 16, 2003.
- NSF Panel Reviewer, Special Invitation for 'Unsolicited Proposals on Engineering Education', March 27-28, 2003.
- NSF Panel Reviewer for Course, Curriculum, and Laboratory Improvement (CCLI) program, Adaptation and Implementation (A&I), Washington, DC, January 22-25, 2003.
- NSF Panel Reviewer for 'ATE', Advanced Technological Education (ATE) program, Washington, DC, December 5-7, 2002.
- Stony Brook University Team Member for the SENCER Summer Institute, August 1-5, 2003, Santa Clara University.
- NSF Panel Reviewer for 'STEP', Washington, DC, July 1-2, 2002.
- NSF Panel Reviewer for Computer, Science, Engineering, and Mathematics Scholarships 'CSEMS', Washington, DC, March 1-2, 2002.
- NSF Engineering & Computing Education Grantees Conference, Washington, DC, September 30-October 1, 2002.
- Building Science, Mathematics, Engineering and Technology (SMET) Research and Teaching Capacity at Minority Institutions, Washington, DC, February 22-23, 2002.
- Integrating Research and Education at NSF Materials Research Centers, UCSB, October 21-23, 1998.
- ASEE Spring Regional ABET meeting, March 1998, Binghamton.
- Rose-Hulman Institute of Technology, 'Best Assessment Processes in Engineering Education II', October 16-17, 1998, Terre Haute, Indiana.
- ASEE Spring Regional Conference, April 1998, New Jersey.
- ASEE Fall Regional Conference, November 1, 1997, DuPont, Delaware.
- Participated in 'National Educators Workshop', November 12-14, 1991, Oak Ridge, TN, USA.

### **9.1 Administrative Duties and University Service**

- Leader of the State University of New York coalition on 'e-Learning', a coalition of Electrical Engineers from Stony Brook, Buffalo and Binghamton Universities.



- Occasional Member of the Provost's Advisory Group throughout 2002-2003 representing the College of Engineering and Applied Science.
- Member of the University 'Assessment Committee', 2003+.
- Member of the University Senate as Senator for Materials Science and Engineering 2003+.
- Instructor for new 'ITS101' (Information Technology Studies) section on 'Biomaterials'.
- Member of the University 'CUE', Committee for Undergraduate Education, 2001, 2002, 2003.
- Member of the Stony Brook University 'Middle States Accreditation' Steering Committee, 2002, 2003.
- Participation in the 'Women for Women', W:W, program (Mentor for Christienne Mancini), 2001, 2002, 2003
- Chairman and organizer of the State University of New York Workshop on 'Ethics in the Engineering Discipline', April 2002.
- Chairman and organizer of the College of Engineering and Applied Sciences 'Distinguished Speaker' committee.
- Membership of the 'School of Professional Development Council', Fall 2001
- Member of Stony Brook University Team to participate in the Invited Conference, 'Institute on Campus Leadership for Sustainable Innovation', July 2001.
- College of Engineering and Applied Sciences faculty representative for the following Stony Brook University committees: URECA Committee, Simons Fellowships, Undergraduate Program Directors.
- Appointment as the 'Director of Assessment' for the College of Engineering and Applied Sciences, Fall 1997.
- Participation in the WISE 'Introduction to Research' introductory sessions. 1998-1999.
- Materials Science and Engineering representative on CTPC.
- Materials Science and Engineering representative on the Academic Dishonesty Committee. Chairman from 1997-1998.
- Materials Science and Engineering representative on Open Day.
- Volunteer for the Stony Brook University 'Discover Stony Brook' activity.
- Mentor to Sapna Shah who won a GT Equipment Technologies Scholarship, 1997
- Participation in the 1997 Student Research Support Program.
- Advising of students for the NSF-supported State University of New York Alliance for Minority Participation Program (1997 academic year)
- Undergraduate Program Director - Mid-Spring 1995+
- Member of the Stony Brook University Bioengineering Committee - 1994+
- College of Engineering and Applied Sciences Committee Representative for the 'Bioengineering Symposium Series', 1994-2004.
- Undergraduate Laboratory Chairman, 1994-2004.
- Deputy Chairman for Fall 1993-2004
- Library committee – 1993-2004.
- Organizer of President Marburger's Visit to MSE 1993
- University Contact / coordinator for 3 ARPA-TRP proposals in June 1993. These 3 proposals involved 10 Universities, 20 Companies and 3 Professional Societies for requested funds of ~ \$9.5 M.
- Faculty committee to examine the College's interests in 'Manufacturing Engineering'.
- Chairman of a University Search Committee to employ a Senior Research Specialist (November - December 1993).
- Mentor to two '1993 Summer Research Institute Students'.
- Mentor for State University of New York Alliance for Minority Participation, 1995.
- Instructor for Materials Science and Engineering Day, November 12, 1995.
- Marshal for Convocation 1996, May 12, 1996.
- Materials Science and Engineering representative during Summer Advisement.

## **9.2 Educational and University Committees**

- External Reviewer for Promotions for The Ames Laboratory, IA-USA, 2003.
- Member of the Advisory Committee for the 'Strategic Network in Science and Advanced Applications of Plasmas, Plasma-Québec' of Canada, 2002-2003.
- External Reviewer for Promotions for Université de Technologie de Belfort – Montbéliard, France, 2002.
- External Reviewer for Promotions for Nanyang Technological University Faculty, Singapore, 2002.
- External Reviewer for Promotions for Tampere University of Technology Faculty, Finland, 2002.
- External Reviewer for Merit Promotions and Raises for University of Cambridge Faculty, UK, 2000 and 2001.

- Invited External Reviewer for the Mechanical and Production Engineering Program at Nanyang Technological University, Singapore, 1998-2004 (a three term appointment).
- ABET External visitor to the University of Pittsburgh, 2001.
- ABET External visitor to the Johns Hopkins University, 1999.
- Faculty mentor to the Tau Beta Pi society.
- Participation in Stony Brook University AGEF, 'The Alliance for Graduate Engineers in the Professoriate', program.
- Participation in the 'Center for Excellence in Learning and Teaching', CELT.
- Participation in The Alliance for Inclusive Graduate Education and the Professoriate Program', AGEF (mentor for Dominic Vasquez)
- Director of Assessment for the College of Engineering and Applied Sciences from Spring 1998.
- Representative for ASM as the 'Liaison to the TMS/ABET Accreditation Commission'.
- Undergraduate Program Director for Engineering Science from 1994
- Simons Fellowship Program (for High School students). Mentor to >15 students since 1997.
- URECA Committee for undergraduate scholarships.
- Outreach Coordinator for the MRSEC on Thermal Spray.

### 9.3 Teaching

Refer to Teaching Portfolio

### 10 Publications

Please note that these records are not 100% complete on this topic. A quick data base search under 'Berndt, C.C.' finds the majority of publications. A summary is provided below. A separate document that lists these publications is available.

- Editor of 17 Books: i.e., Theses, DVDs, and Edited Conference Proceedings
- 390+ Peer-Reviewed Papers, Book Chapters, and Conference Proceeding Papers.
- 51 Miscellaneous Publications (Book Reviews, Poster Presentations, Editorials etc.)
- In excess of 450 publications
- The screen capture below indicates the results from a search of the 'Swinburne Research Bank'.

Search Swinburne Research Bank

berndt

Limit search by

Popular Authors

- › Berndt, C. C. (371)
- › Herman, Herbert (33)
- › Wang, James (30)
- › Gross, Karlis A. (28)
- › Lima, Rogerio S. (20)
- › Herman, H. (18)
- › Kucuk, Ahmet (18)
- › Leigh, Sang Ha (14)
- › Sanpo, Noppakun (14)
- › Ivanova, Elena P. (13)

Show More

Popular Subjects

- › Plasma spraying (65)
- › Microstructure (43)

Home > List of Titles

Showing Results 1 - 15 of 403.

First Previous 1 2 3 4 5 6 7 8 9 10 Next

Sort: T

**Fabrication and characterization of TiO<sub>2</sub>-ZrO<sub>2</sub>-ZrT manufactured via anodization**  
 Author: Minagar, Sepideh | Berndt, C. C. | Gengenbach  
 Publication year: 2014  
 Publication type: Journal article  
 Peer reviewed: ✓

**Behavior of CFRC/Al foam composite sandwich be**  
 Author: Vcelka, Martin | Dunn, Michelle | Durandet, Yv  
 Publication year: 2014 (in press)  
 Publication type: Journal article

END

March 2014

# Christopher C. Berndt

## 2011-12 President of ASM International

► **Richard Knight,**  
**Ph.D., FASM**  
Drexel University  
Philadelphia, Pa.

I am both proud and honored to introduce ASM International's 2011-12 president, Dr. Christopher C. Berndt, HoF, FASM. It is important that the members of ASM know something about the person behind the very impressive CV – what he's like to work with, his style, and his vision.

### Service to the Materials Community and ASM

I have been fortunate to have worked closely alongside Chris in various ASM-related activities for more than 15 years now, so I have a pretty good understanding of his style and his mettle. Chris and I go back a long way—from the early days of the ASM Thermal Spray Society, born out of the former Thermal Spray Division (whose last chair was none other than 2010-11 ASM president Mark Smith), where we both served as members of various committees, then on the TSS Board of Directors and ultimately both as TSS President. Chris was the founding Editor in Chief of ASM's *Journal of Thermal Spray Technology*, the world's first peer-reviewed journal dedicated to the field of thermal spray. Those of you who follow the careers of ASM presidents may spot a theme here: 2010-11 ASM President Mark Smith also has a background in thermal spray and “came up through the ranks” of TSS; clearly something is working very well there.

More recently, Chris returned to the ASM Board of Trustees as president-elect, where again I had the chance to work alongside him on strategic planning activities, defining the visions, strategies, and tactics that will guide the society through the next few years. I also had the pleasure of co-teaching ASM's Thermal Spray Technology 3-day course with Chris on almost a dozen occasions around the world, from Columbus, Ohio to Beijing, to Essen, Germany—so many places, we should have had t-shirts printed. Chris's service to the field of materials in general, and to ASM in particular, has earned him the recognition of his peers as evidenced by the numerous awards he has received, including the ASM Allan Ray Putnam Service Award (2002).

### Education and Training

Chris's background is a traditional “heat it and beat it” metallurgist, the traditional core of



Christopher C. Berndt

ASM, earning his Bachelor of Applied Science from the South Australian Institute of Technology, School of Metallurgy, Adelaide, in 1975. Yet, today he is much more than that, since during his career he has worked in industry, at a national laboratory, and in academia. Chris developed a thorough grasp of the entire field of materials, from metals to ceramics; from nanomaterials to biomaterials; to corrosion (Chris's wife Marita is a corrosion engineer); through his own Ph.D. studies in thermal spray at Monash University in Melbourne Australia (completed in 1980), his time as a post-doc at SUNY Stony Brook (1981), as a research fellow and lecturer back at Monash, as a Fellow of the Joint Institute for Propulsion and Power at NASA Lewis (now Glenn Research Center, Cleveland, Ohio) from 1983-85; as a summer faculty fellow at NASA Glenn Research Center (1991), as an associate and then full professor back at SUNY (1991-2004) and simultaneously as Associate Dean for Undergraduate Studies, and more recently in universities (James Cook University and Swinburne University of Technology) back in his native Australia. Through-

out his career, he always had an eye on understanding materials processing, structure, and properties and ultimately their application, this completing the holy grail of materials science and engineering. With around 400 journal and conference publications and presentations to his name, combined with membership in more than a dozen professional societies in the U.S., Australia, and the UK, Chris truly puts the “International” in ASM International, and is only the second president from outside the U.S., Dr. Hans Portisch from Austria being the first in 1998-99.

### Style and Personality

Chris has a unique, infectious style (perhaps that’s due to his Scottish family origins?), but don’t be misled by his sometime use of funky fonts (Comic Sans anyone?) in his lectures and his use of metaphors to make a point; he cares passionately about everything he does, be it in the classroom or representing ASM. Chris has always been a “can do” person; many a time at an International Thermal Spray Conference event, when there has been a no-show, Chris has inevitably stepped up to fill in the gap by giving a talk. Chris has selflessly volunteered his time, his intellect, and his passion time and time again in the name of TSS and of ASM. Anyone who meets Chris will not fail to be inspired by his enthusiasm and dedication to all things ASM.

Like all good engineers, Chris is data-driven, and he brings this trait to the leadership of ASM. Underlying whatever is being discussed or worked on is the same fundamental question: How does this benefit the members of ASM? In the end, that is what it’s all about; being a member of the ASM Board of Trustees, vice-president, and now president is an honor, and Chris recognizes that this is a very important responsibility; involving stewardship and being entrusted to serve the interests and needs of the members of ASM. A key tenet of the current evolution of ASM’s strategic plan has been consideration of “a day in the life of the customer” as ASM adapts itself to the ever-changing materials information world and the ways in which *Life-long Learning and Education*, *Content is “Everything Material,”* *Emerging Technology*, and *Volunteerism*, the core elements of ASM today, dovetail together to enable things to happen. Chris will lead by example, will not be afraid to ask the tough questions, and will make the decisions necessary for ASM to move ahead.



Chris and his wife Marita.

### Vision

Chris developed his vision for his presidency of ASM, and has shared it with the ASM membership at the ASM Annual Meeting and will undoubtedly share it with members of the society during his busy chapter visit schedule, and his travel and teaching schedule. Thematically, it is to keep the ship on a steady course while maintaining momentum and while defining metrics so success can be documented, with minor tweaks to the strategic plan where necessary to ensure that the Value Proposition is delivered to the customer focus groups representing the members of ASM. Key to Chris’s vision is the need to focus. ASM’s strategic planning activities have generated a long list of ideas for products and services which *could* be developed, but in a time of finite resources, it is necessary to prioritize and focus, so ASM’s resources, of which society volunteers are perhaps the most important component, are deployed wisely to realize near- and medium-term SMART (specific, measurable, achievable, relevant and time-bound) objectives.

One obvious question asked of Chris was “Can you really do the job when you are so far away in Australia?” This was a defining question that Chris asked *himself* when deciding whether or not he was willing to be nominated as vice-president, and unequivocally the answer was yes! In all the years I have known Chris, I have never seen him agree to do something and then not do it. If Chris commits to something, then he will do whatever it takes to see it through to a conclusion; he is a professional leader, with the vision and integrity befitting the president of ASM International. As more of you get to know him during his tenure, you will find him to be a true friend, the kind one can agree to disagree about something with, then at the end of the day get together and socialize; in short, a consummate professional, dedicated to ASM, who will serve the society well as its 2011-12 president. ○

### 3. Research Portfolio

This portfolio represents a high level summary of the approach, metrics and outcomes for my research since I started on this path in 1977 as a PhD student.

#### Table of Contents

<b>3. Research Portfolio</b>	<b>1</b>
3.1. Statement concerning my research approach	1
3.2. Publications of Chris Berndt	1
3.3. Research Interests	2
3.4. Professional Activities that Focus on Publishing	2
3.5. Patent Disclosures	2
3.6. Grant Proposals and Reports since 2000	3
3.7. Post Graduate Courses and PhD students	4
3.8. The BIG Picture	5

#### 3.1. Statement concerning my research approach

I have been an active researcher since 1977. At one stage I thought I knew it all: I was wrong! It may seem strange for me to say that ‘The more I know, the less I understand and the more I need to know.’ This is, however, a lesson that I transmit to UGs and PGs so that they are enthused to reach for greater heights. In other words, I am continually striving to understand the fundamental principles of the new science that I am exploring. I feel that I am challenging the conventional barriers of science in this continual quest.

My metrics concerning research; i.e., publications, PhD graduations, citations and research programs, are important but not the complete picture. Thus, I have a commitment to scientific rigor and producing substantial research outcomes that look into the future. Examples would include (i) measurement of mechanical properties of coatings, (ii) the first to demonstrate solution plasma spray and similar techniques, (iii) integrating a knowledge base that follows materials genomic principles, and (iv) transmitting my materials-related knowledge via international workshops. The accompanying figure, aka the ‘BIG research integration picture’ visualizes my research activities.

My outlook can be presented in a bulleted format.

1. Provide an environment and opportunities for research exploration.
2. Engender a research culture that reaches across academic boundaries. This is an exciting space to explore and where significant discoveries are being uncovered.
3. Provide a strong example to colleagues so that they see me ‘walking the walk’ and not just talking.
4. Leverage my many global contacts in industry, government and academia to present intrinsic research opportunities. This is no easy task; however, I am credible as an honest broker and when the value proposition is identified then these opportunities can be realized.
5. I have a personal passion about integrating research into the UG curriculum. This is a partly selfish need to recruit students who can slot directly into post graduate programs. However, there is also a great deal of satisfaction to see young people captured by their own imagination.
6. Working with industry to deliver productivity and economic gain for their manufacturing processes.

There are many R&D opportunities of historical significance in the world of materials; i.e., fiber reinforced composites, nanostructured materials, superconducting materials, CNTs, etc.; and there are emerging initiatives; i.e., genomic materials databases, additive manufacturing, MAX phases, high entropy alloys etc. The future challenge (or opportunity) is, thus, many fold. My research agenda is to pursue, with vigor and focus, opportunities as they arise and as they are created. There is still the need to mentor, encourage and promote the next generation of researchers. I am unselfish in this aspect and this attitude will continue throughout my professional career and beyond.

In summary: I have credentials of being a research leader for many years. This will continue into the future because ‘research is in my veins’. Research is a continuous process that requires patience and persistence with a great deal of passion. I have had success in conveying that passion to my PGs, UGs and colleagues around the globe.

#### 3.2. Publications of Chris Berndt

The table below presents a summary of publications within the defined categories. A conservative estimation of the peer-reviewed publications (books, book chapters and journals) is > 63% of his output;



taking note that the additional category of ‘Conference Articles’ has many contributions that were ‘soft-reviewed’ for format and technical content.

Descriptor	Total	Relative (%)
Books (Theses, CD's & Edited Conference Proceedings)	17	4
Reviewed Chapters in Books	147	32
Journals	192	42
Conference Articles	60	13
Other	43	9
TOTAL Publication Count	459	100

### 3.3. Research Interests

A short listing of Chris’s research interests would include ‘thermal spray coatings’ with a focus on experiments and analysis of thermal expansion coefficients; fracture toughness and mechanical property measurements; processing sciences and fiber reinforced coatings; nano-materials; and modelling and simulation. .

Chris also has strong credentials in ‘biomaterials’ with a specialization on biocompatible coatings of hydroxyapatite and bioceramics.

### 3.4. Professional Activities that Focus on Publishing

- Chris is the Foundation Editor of the Journal of Thermal Spray Technology that is published by ASM International. He held this position from 1991 to 2004 and then became Editor Emeritus. He was responsible for appointing the original Editorial Board, the Editorial Committee and designing and implementing the scope of this Journal.
- Chris is a current Guest Editor for special issues in two journals (i) ‘Surface Coatings and Technology’ and (ii) the ‘Journal of Thermal Spray Technology’ in 2013-2014.
- Chris has held appointments on the Editorial Boards of (i) Journal of International Materials Reviews, (ii) Journal of Phase Equilibria and Diffusion, and (iii) Journal of Materials Engineering and Performance from 1999 through to 2012.
- Chris is a reviewer of numerous technical articles for the Journal of Thin Solid Films, Acta Materialia / Scripta Materialia, Journal of the American Ceramic Society, Journal of Materials Research, Materials Science and Engineering A, Journal of Materials Engineering and Performance, Journal of Applied Biomaterials, etc. He reviews about 35-45 manuscripts per year. He was recommended as an ‘Excellent Reviewer’ for Metallurgical and Materials Transactions in 2001.
- Chris, in his capacity as Chair or co-Chairman of the United Engineering Foundation Conference on ‘Novel Synthesis and Processing of Nanostructured Coatings for Protection Against Degradation’ was responsible for the conference proceedings that evolved from the 2001 meeting in Davos, Switzerland, and the 1999 meeting in Quebec City, Canada. The later proceedings is available in the Swinburne Research Bank.
- Chris was the Proceedings Editor for the International Thermal Spray Conferences in (i) Singapore in 2001; and Montreal, Canada, in 2000. He was also the Proceedings Editor or co-Editor for the National Thermal Spray Conferences in (i) Cincinnati in 1996; (ii) Houston in 1995; (iii) Boston in 1994; (iv) Anaheim in 1993; and (v) Orlando in 1992.
- Chris has been a strong contributor to ‘Spraytime’; the news bulletin of the International Thermal Spray Association since 1992. Chris was also the Editor for 2 years of iTSSe (International Thermal Spray and Surface Engineering) newsletter that was published by ASM International.
- Chris has been a book reviewer for the Institute of Metals and Materials, Australasia, The American Ceramic Society, Journal of Materials and Science Engineering, John Wiley & Sons, and others. For example, in 1988 he reviewed a document titled ‘Perspectives in biomaterials bioceramics’, prepared by the Department of Industry, Technology and Commerce.

In Summary: Chris has an extensive history of (i) editorial duties for peer-reviewed journals, (ii) editorial and writing duties for trade journals, (iii) as a reviewer of technical articles, and (iv) as an editor of conference proceedings.

### 3.5. Patent Disclosures

Chris has patent disclosures that have evolved from his fundamental R&D activities. These are listed below.

- M.R. Gold and C.C. Berndt, ‘A Multifunctional, High-Sensitivity, Scratch Tester’, June 2001.
- C.C. Berndt and R.L. Lima, ‘Microstructural Engineering and Processing for TBCs’, April 2001.

- C.C. Berndt, R.S. Lima and A. Kukuk, 'Tailored Microstructures for Predictable Coating Properties', February, 2001.
- R.Benary, R.Gansert, C.C.Berndt and H.Herman, 'Automated Thermal Spray System (ATSS)', R-7099. Disclosed February 21, 1995.
- J.Brogan, S.Reddy, C.C.Berndt, H.Herman and S.Sampath, 'Spray Forming of Graded Polymer Composite Components', S-7056. Disclosed April 5, 1994.
- J.Brogan, C.C.Berndt, R.Lampo,K.A.Gross, S.Sampath and H.Herman, 'Thermal Spraying of Recycled and Post-Consumer Commingled Polymer Material', S-7088. Disclosed November 17, 1994.
- S.Sampath, H.Herman and C.C.Berndt, 'Graded Metal Reinforced Ceramic Free Standing Forms', S-7060. Disclosed April 20, 1994.
- C.C. Berndt, H. Herman and S. Sampath, 'Bar Coding of Powder Lots to Improve Process Efficiency During Thermal Spraying'. R-7103.
- C.C. Berndt, H. Herman and S. Sampath, 'Method for Processing Layered and Gradient Structures through Thermal Spray Forming'. R-7091.
- C.C. Berndt, H. Herman and S. Sampath, 'Silicide Based Graded Bond Coats for High Temperature Thermal Barrier Coatings'. R-7090.
- C.C.Berndt, 'Graded Hydroxyapatite / Polymer Materials for Biomaterials Applications', R-861. Disclosed May 23, 1991.

In Summary: Chris has worked closely with his students and colleagues to transform lab-based R&D into commercial products.

### **3.6. Grant Proposals and Reports since 2000**

Chris has worked extensively over his career to attract research funding. Much of this effort has been performed within a team environment and the listing below shows the major activities since year 2000.

- 2013, 'Thermal Spray Project with United Surface Technologies (under Technology Voucher Program)', Victorian Department of Innovation, Industry and Regional Development, Berndt is the lead investigator, \$49,572.
- 2013, 'Cold Spray project with Rosebank Engineering (under Business R&D Voucher Program)', Victorian Department of Innovation, Industry and Regional Development, Berndt is the lead investigator, \$49,755.
- 2012, 'Magnetron sputtering of nanolaminates with materials designed and engineered properties', Australia-India Strategic Research Fund, Wen is the lead investigator. \$440,000.00.
- 2011, 'DMTC Project Activities 2010-11 Support funding: cross-program technical services support', Defence Materials Technology Centre (DMTC), Berndt is the lead investigator. \$75,000.
- 2010, 'Molecular spectroscopic 2D and 3D Imaging Systems at Sub-Micron Spatial Resolution', ARC Linkage Infrastructure and Equipment, Stoddart was the lead investigator. \$350,000.
- 2009-2013, 'DMTC Project 4.2 Development and Manufacture of a Combustor', Defence Materials Technology Centre (DMTC), Berndt was the lead investigator. ~\$300,000.
- 2009-2013, 'Development of polymer concrete material for bases of grinding tool machines (Advanced Manufacturing CRC Polymer Concrete Systems 1)' with A/P Sbarski; Advanced Manufacturing CRC Polymer Concrete Systems 1. \$251,353.
- 2006-2008, LP0668222, Dr JD Ginger; CC Berndt; W Karunasena; C Healy; S Gowripalan, James Cook University, 'Failure Mechanisms of Roof Cladding under Fluctuating Wind Loads'. \$90,450.
- 2007, LE0775614, Dr MV Jacob, CC Berndt, ME Tobar, JE Mazierska, RD White, ML Heron, Y Ho, JG Hartnett, GS Woods, CJ Kikkert, V Jegatheesan, and J Krupka. 'National Electromagnetic Characterization Facility for Advanced Electronic and Biomaterials', \$150,000
- 2006, LE0668506, Prof MJ Percy; RW Crawford; CC Berndt; Q Li; JM Bell, Queensland University of Technology and James Cook University, 'A Multi-Axis Biomaterials Testing Facility', \$150,000.
- 2005-2007, Sugar Research Development Council, JCU025, 'Thermoformable biodegradable composite material from sugar cane bagasse fibre', Berndt is the lead investigator, \$189,788.
- 2005, Support to develop and launch an 'ALN B.S. degree in Electrical Engineering' (2005-6-14) Project Director: Dr. David Porush Grant Amount: \$300,000.00 Institution: Research Foundation of State University of New York Fiscal Year: 2005 Note: This project was awarded after Berndt left the USA; but he was responsible for bringing forming the team that brought it to fruition.
- 2004, C.C. Berndt et al., NSF 'Making the Connection: Linking Stony Brook and Community Colleges via CSEMS', \$398,693.
- 2004-2006, R Kamoua, A Pacelli, CC Berndt and KK Likharev, 'NUE: Introducing Nanoscale System Design into the Undergraduate Electrical and Computer Engineering Curriculum', \$99,762.

- 2002-2003, CC Berndt et al., NSF ‘Inquiry-Based, Interdisciplinary Curricula within an Engineering Research Culture’, \$100,000.
- 2003-2005, S. Judex (co-PI C.C. Berndt), ‘High Resolution Micro-Computed Tomography Scanning of Biological Tissues’, NSF-Major Research Instrumentation, \$397,000.
- 2002-2005, CC Berndt, NASA, ‘Revolutionary Thermal Barrier Coatings’, \$643,000.
- 2001-2002, CC Berndt, State University of New York, ‘Ethics within the Engineering Profession: A Workshop for faculty’, \$15,000.
- 1999-2000, CC Berndt, DOE / BNL, ‘Materials for Geothermal Environments’, \$24,964.
- 1997-2001, CC Berndt, ONR, ‘Advanced Coatings Technology Development’, \$147,462.

In Summary: Chris has had continuous funding since he entered academia in 1981 as a Post Doc at Stony Brook University. This funding has provided a means to build labs and support post graduate students.

### **3.7. Post Graduate Courses and PhD students**

A listing of Chris’s Post Graduate lecture courses is provided below and detailed in the Learning and Teaching portfolio. As well, Chris has graduated 24 PhD students and details are provided. Further details concerning Masters post grads are provided in the Learning and Teaching portfolio.

- Stony Brook University: ESM 506 Mechanical Properties of Engineering Materials
- Stony Brook University: ESM 696 Seminar in Thermal Spray Science and Technology
- Swinburne University of technology: ADM80007 Surface Engineering

#### Monash University (1986-1991)

1. Mr. Jung Hyuk Yi on ‘Methods for strengthening thermally sprayed coatings’; 1992: Currently a Manager at GE in Korea.
2. Mr. Michael Cohn on ‘A totally synthetic prosthetic ligament’ (withdrew, 1991).
3. Mr. Paul Callus on ‘Deformation mechanism studies on thermally sprayed coatings’; 1993: Currently a Senior Scientist/Engineer at the Defence Scientific Technology Organization.
4. Mr. Duo Wang on ‘Low expansion thermally sprayed coatings’; 1992: Current position is unknown.
5. Mr. Phillip Hong Ning Cheang on ‘The microstructure and mechanical properties of plasma sprayed coatings’; Graduated in 1989: Currently an Engineering Dean at UniSIM, Singapore.

#### Stony Brook University (1991 to 2005)

6. Mr. Ondrej Racek on ‘Microstructure and mechanical properties of ceramic and metallic thermal spray coatings’; 2005: Currently with BTG Duroblade in Elclepens, Switzerland.
7. Mr. Petr Michlik on ‘Development and application of a microstructure level FEM Simulation tool for thermal barrier coatings’; 2005: Currently a Manager at Caterpillar Inc., IL-USA.
8. Ms. Limin Sun on ‘Characteristics and dissolution of plasma sprayed hydroxyapatite coatings’; 2002: Currently a General Engineer at Food and Drug Administration, DC-USA.
9. Mr. Rogerio Lima on ‘Relationships between physical properties and spray variables for thermal spray coatings’; 2001: Currently a Senior Research Scientist at National Research Council, Canada. Graduate Council Commendation as ‘Distinguished Doctoral Student’ of the State University of New York at Stony Brook.
10. Mr. Ahmed Ibrahim on ‘Fatigue testing of HVOF sprayed aluminum and tool steels’, 2001: Currently a Professor at SUNY at Farmingdale, NY-USA.
11. Mr. Sang-Ha Leigh, ‘Stereological investigations on structure / property relationships of plasma spray deposits’, 1996: Currently Managing Director of EPITAX Pte Ltd., Singapore/Korea.
12. Mr. Jeffrey Brogan, ‘Thermal spraying of polymers’, 1996: Currently President of Mesoscribe Inc., Stony Brook, NY-USA.
13. Mr. Chung-Kwei Lin on ‘Statistical Approaches to Study Variations in Thermal Spray Coatings’, 1995: Currently Professor at Taipei Medical University, Taiwan.
14. Mr. Karlis Gross on ‘The Amorphous Phases in Hydroxyapatite Coatings’, 1995: Leader of Biomaterials Research Laboratory at Riga Technical University.
15. Mr. Jan Ilavsky, on ‘Porosity of deposits processed by the water stabilized plasma’, 1994: Currently Senior Researcher, Argonne National Lab., IL-USA.

#### Swinburne (from 2004 to 2014)

16. Mr. Kadim Al Amara on ‘Optimization of polypropylene Splats Using the Flame Spray Process’, 2012: Current position is unknown.
17. Vi Khanh Truong on ‘Investigation of Bacterial Attachment Patterns on Micro- and Nano-restricted Surface Topographies’ (Committee member), 2012: Currently a Post Doc at Swinburne.
18. Mr. Wei Xie on ‘Thermal Spray Processing of Ethylene Methacrylic Acid and Polymer-Ceramic Composites’, 2013: Currently a Post Doc in Washington, USA.

19. Ms. Jo Ann Gan on 'Preparation and Characterization of Thermal Sprayed Neodymium Iron Boron Magnetic Coatings', 2013: Currently a casual tutor at Swinburne.
20. Mr. Andrew Ang on 'Mechanical Properties of Ceramic Thermal Sprayed Coatings', 2013: Currently a Post Doc at Swinburne.
21. Mr. Noppan Sanpo on 'Fabrication and Characterisation of Cobalt Ferrite Nanoparticles and SPDS-Deposited Cobalt Ferrite Splats Prepared by Sol-Gel Methods', 2013: Currently looking for a position.
22. Mr. Tanveer A. Choudhury on 'Artificial Neural Networks Applied to Plasma Spray Manufacturing', 2013: Currently a casual tutor at Swinburne.
23. Mr. Rakib on 'Deposition and Characterization of a Coating from Calcium Phosphate and Titanium Alloy on Austenitic Stainless Steel', Under examination and to graduate in 2014.
24. Mr. Fahad on 'Microstructure and Properties of Plasma Sprayed and Sol-Gel Modified Hydroxyapatite Coatings', Under examination and to graduate in 2014.

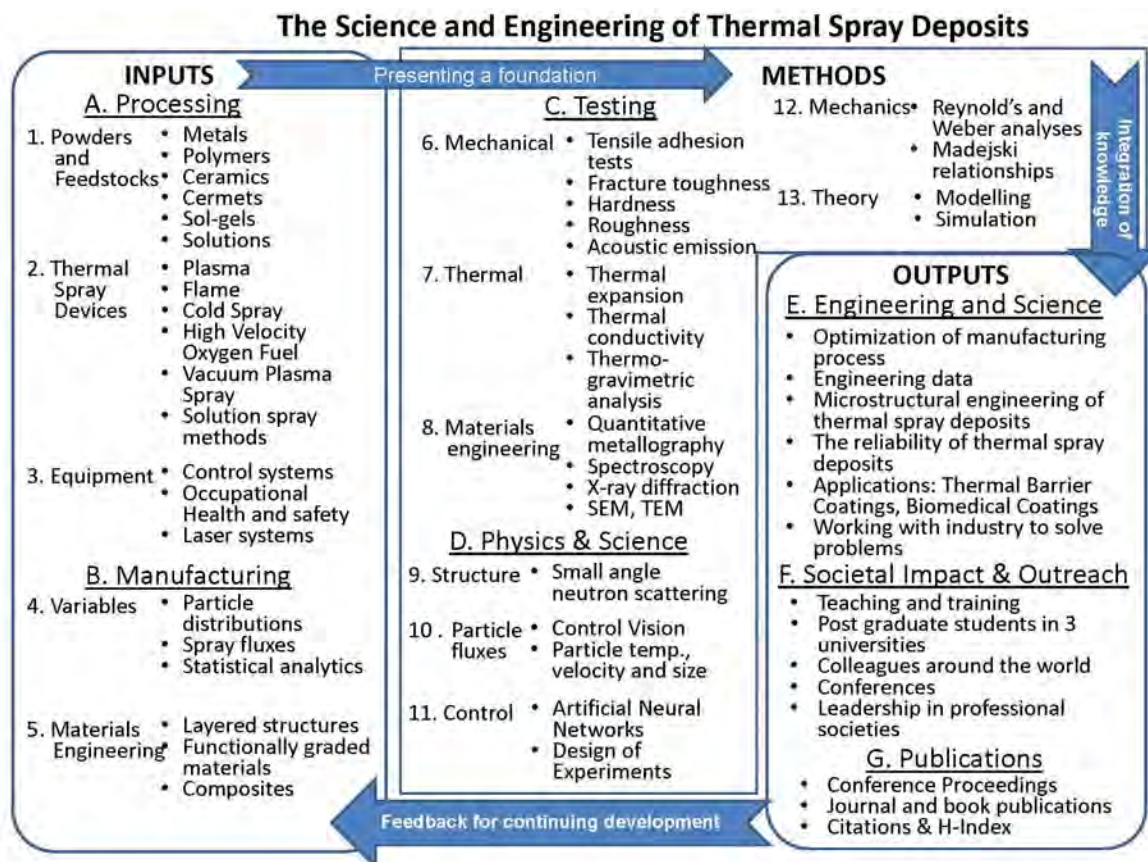
Chris has also been an examiner of theses from: (i) Nanyang Technological University, Singapore; (ii) Université des Sciences et Technologies de Lille, France; (iii) University of Limoges, France; (iv) Université de Franche-Comté (UFC), France; (v) Université de Sherbrooke, Canada; (vi) University of South Australia; (vii) the University of British Columbia, Canada; and (viii) Monash University, Australia. In addition, he has been a committee member for 29 PhD candidates.

In Summary: Chris has wide-ranging experience in the supervision of post graduates as well as formal teaching credentials.

### 3.8. The BIG Picture

A comprehensive picture of Chris's approach in the exploration of thermal spray deposits is presented in the BIG picture for 'The Science and Engineering of Thermal Spray Deposits'. All of the sub-topics in this picture have been addressed within the research career of Chris. This figure also demonstrates the integration of the 3 topics that are broadly described as 'research', 'leadership and engagement' and 'learning teaching'. That is, these subject areas are intermingled and inter-related.

In Closure: Chris Berndt has demonstrated (i) a high level of publishing outputs in journals and books, (ii) editorial and reviewing duties, (iii) procurement of funding for colleagues and himself to perform research, and (iv) teaching and training of post graduate students. Chris is especially proud of his undergraduate and post graduate students who find positions of authority in society.



#### 4. Leadership and Engagement Portfolio

Chris has made significant contributions to leadership across many areas of engagement; for example, to professional societies; to the publishing fields as an author, editor and reviewer; to the global thermal spray community; and to committee structures within academic settings.

Chris has published several of his opinions on topical points of interest in the form of formal speeches, commentaries and editorials. Several of these have been collated and appear in an Appendix that is attached to his complete file.

---

#### Table of Contents

<b>4. Leadership and Engagement Portfolio</b>	<b>1</b>
4.1. Leadership and Engagement of Professional Societies	1
4.2. Leadership and Engagement within the Context of Publications and Outreach	2
4.3. Leadership and Engagement within the Global Community of Thermal Spray	2
4.4. Leadership and Engagement within the Academic Community	3
4.5. Leadership and Engagement across Many Disciplines as a Peer Reviewer	4
4.6. Leadership and Engagement in Educational and University Committees	4

---

The 'leadership and engagement' activities of Chris Berndt have taken on various formats. Highlights of these accomplishments and recognition are presented in a bulleted and condensed format. There may be some slight duplication across other portfolios.

##### 4.1. Leadership and Engagement of Professional Societies

- Fellow in 5 professional engineering societies. Notably he is the only 3<sup>rd</sup> member of the American Ceramic Society to be resident in Australia.
- Inducted into the Thermal Spray Hall of Fame. Notably he is the second member, and only living member, from the Southern hemisphere.
- Recognized by students and peers by elevation in two honor societies as (i) an 'An Eminent Engineer' in Alpha Beta Tau, and (ii) a 'Fellow in Alpha Sigma Mu'. Chris has also been presented with the 'Order of the Engineer' that was conferred by the National Institute of Ceramic Engineers.
- Recognized by ASM International in 2002 with the 'Allan Ray Putnam Service Award'. This is the highest award that can be conferred on a member for service to the society.
- 2012: Elected as Vice-President of the Australian Ceramic Society (ACS). Chris was also President of ACS on 2008-09. Thus, his re-election 4-years later represents the regard that is bestowed on his leadership of this society.
- 2011: President of ASM International. This appointment was for 1-year just after a global financial crisis. Strong and authoritative leadership was necessary. The term within the Presidential track is 7 years; i.e., 3.5 years as a Trustee (i.e., a Director) and then 3.5 years in the VP, President, and Past Presidential positions. In the case of Chris there was an interval of 2-years between the Trustee position and being nominated as Vice President of the Society. Therefore, Chris was associated within the Leadership Group of ASM International for 7-9 years.
- In his ASM International Presidential year (2010-2011), Chris participated in 72 engagements that can be broken down as follows: (i) 14 visits to ASM Chapters in the USA and India; (ii) 15 Executive Committee meetings with Chapter Committees; (iii) 23 visits to industry and companies within the manufacturing sector; (iv) 12 University visits where technical and professional presentations were delivered; (v) and 5 thermal spray courses of one half to one day in length. Another 3 miscellaneous activities were requested to accommodate special needs of the local host.
- 2005: Vice Chair and then Chair of the Townsville Regional Group of Engineers Australia (EA). The major outcome for this 2-year appointment was an EA conference for the Northern Chapters of the society.
- Member of high level ASM International committees; e.g. 'Strategic Planning Committee', 2002 and 2003. Participated in this committee throughout his term as an officer. Chris Chaired this



committee when he was VP in 2010. Also, Chris was a member of the 'ASM International Surface Engineering Task Force' in 2002 and 2003.

- Chris is a Director of the ASM MEF (ASM Materials Educational Foundation). This is a not-for-profit Foundation that, through an endowment of \$18 mill. is able to support many students and educational activities.
- Chris has participated in the National Association of Corrosion Engineers (NACE) as a member of Committee T-6H-45 on 'Thermal Spray Coatings' from 1994 onwards. He was the Chairman of ASTM Committee B08.14 for 'Thermal Spray Coatings' from 1993 to 2001. This resulted in a revision of the standard ASTM C633-01. He is a member of the American Welding Society (AWS) Committee C2.2 Subcommittee on 'Zn TSC on Reinforced Concrete' from 1993 onwards.

In summary: Chris has demonstrated leadership and engagement within many national and international professional societies. He has led at a high level in some of these societies as the President or as a member or chairman within committee structures.

#### **4.2. Leadership and Engagement within the Context of Publications and Outreach**

- Chris was the Founding Editor for the Journal of Thermal Spray Technology and served in this capacity from 1991-2004. He was responsible for jump-starting this journal and bringing it from an unknown to its current status of authority and prestige. In 2004 Chris was recognized for these contributions by being appointed as 'Editor Emeritus of the Journal of Thermal Spray Technology'. Chris was the Chairman of the Editorial Board of the Journal of Thermal Spray Technology in 2004 through to 2006.
- Chris has received several awards for his contributions to the technical literature. For example; (i) in 2000 for the Best Paper in the Journal of Thermal Spray Technology; and (ii) Certificate of Merit from ASM International for a best paper in the National Thermal Spray Conference, Anaheim.
- Chris is a reviewer of numerous technical articles for the Journal of Thin Solid Films, Acta Materialia, Scripta Materialia, Journal of the American Ceramic Society, Journal of Materials Research, Materials Science and Engineering A, Journal of Materials Engineering and Performance, Journal of Applied Biomaterials, J. Surface Coatings and Technology, J. Thin Solid Films, etc.. He reviews about 1 manuscript per week for peer-reviewed journals.
- Chris has participated in leadership roles for many conferences. He has been on the organizing committee of the International Thermal Spray Conference (ITSC) series (and its predecessor series, NTSC and UTSC) since 1990. He was the conference Chair for the 2004 ITSC in Orlando. As well, Chris has been on the International Advisory Committee of the Satellite Symposium I High Performance Ceramic Coatings, of the 7th. CIMTEC World Ceramics Congress, Montecatini Terme, Italy in 1990. He is a symposium Chair for the CIMTEC meeting in 2014, which will also be held in Montecatini Terme, Italy. Chris was the co-chair of 3 United Engineering Foundation meetings on the 'Thermal Spray Processing of Nanomaterials'. This series of meetings was convened in Davos, Switzerland in 1997 and 2001, and in Quebec City, Canada, in 1999.

In summary: Not only does Chris have a high publication record, he also has led many activities in this subject area. It is important to recognize that he has created the only peer review journal in the topical area of thermal spray. He has been a high level participant in many conference organizations as well as the General Chair in 4 international meetings.

#### **4.3. Leadership and Engagement within the Global Community of Thermal Spray**

- Chris was recognized by the Thermal Spray Society in 1996 with the Inaugural President's Award for 'Exemplary and Unselfish Service'. Chris also has been recognized for leadership by the ASM MEI (Materials Engineering Institute) in 1991 as an Instructor of Merit. In 1994 he received the ASM International Thermal Spray Society Service Award for being the Co-Editor of the National Thermal Spray Conference Proceedings.
- Chris received an Honorable Mention for 'Spray Forming of Graded Polymer Composite Components' in 'The DuPont Plunkett Student Awards for Innovation with Teflon®' in 1994. The student who Chris mentored was Mr (now Dr) Jeffery Brogan.
- Chris was the President of the Thermal Spray Society from 2000 to 2002. The Presidential track is a 6-year appointment since it also includes stints as VP and Past President.

- Chris has led numerous nominations for ASM awards. A short list of successful nominations includes: Richard Knight to the position of Fellow of ASM International, 2003; R.C. Tucker, Jr. to the Vice Presidency of ASM International, 2002; Richard Sisson to the position of Trustee of ASM International, 2002; Jockel Heberlein to the position of Fellow of ASM International, 2001; and many others. Chris leads and prepares nomination files for an average of about 2-3 individuals per year.

In summary: Chris has led thermal spray in many ways and formats: from being the President of the Thermal Spray Society to being a champion to ensure that well-deserving people are recognized.

#### **4.4. Leadership and Engagement within the Academic Community**

- In 2001 Chris was admitted to the “Academy of Teachers-Scholars” of Stony Brook University (SBU). At the time of this appointment, Chris was the only Engineer at SBU accorded this privilege and honor.
- Chris has been strongly engaged in ABET, the Accreditation Board for Engineering and Technology; which, is equivalent to the engineering accreditation mechanism of Engineers Australia (EA). Admission to becoming an ABET Visitor involved 12-months of training and a peer review trial period. Chris participated in ABET Training Sessions from 1999 through to 2004. Chris was also the ASM Liaison representative to the TMS/ABET Accreditation Committee, 1999 – 2004. Chris participated as an ABET evaluator of (i) the Illinois Institute of Technology in 2002; (ii) Johns Hopkins University in 2000; and (iii) the University of Pittsburgh 2001.
- Chris has participated in EA accreditation committees; e.g., (i) Flinders University in 2011, (ii) Auckland University of Technology in 2011, (iii) the University of Wollongong in 2010, and (iv) the University of Western Australia in 2009. He was Chair and Team Leader of the visit to Flinders University.
- Chris has been called upon, as well as volunteered, to present to the university community on a variety of topics; which have included (i) ‘Welcome to Stony Brook University: A Research University’, Introduction talk to Freshman engineers, 2001; (ii) ‘The Importance of Investing Time in Excellent Teaching’, Plenary talk to the incoming graduate students of 2000; and (iii) ‘How to Prepare and Make Presentations’, March 2000 for the Stony Brook University Center for Excellence in Learning and Teaching Program.
- Chris has represented his university in outreach programs to industry; e.g., (i) ‘Technology Transfer - A Case History of Collaboration between Industry and Academia’, ASEE Fall Regional Conference, November 1, 1997, DuPont, Delaware; and (ii) ‘An Integrated Plan of Outreach to Schools’, ASEE Fall Regional Conference, November 1, 1997, DuPont, Delaware.
- Chris has been an External Reviewer for Promotions for (i) the Ames Laboratory, IA-USA, 2003; (ii) Université de Technologie de Belfort – Montbéliard, France, 2002; (iii) Nanyang Technological University Faculty, Singapore, 2002; (iv) Tampere University of Technology Faculty, Finland, 2002; and (v) Promotions and Raises for University of Cambridge Faculty, UK, 2000 and 2001. Chris also played a role as a Member of Review for distinguished professorial appointments at the University of Minnesota, 1999.
- In 2001 Chris visited the University of Minnesota, Mechanical Engineering Department to deliver a Distinguished Lecture Series on ‘Biomaterials’. This was a 5-day, 8-hours per day engagement to a class of professors and post graduate students.
- Chris has had extensive leadership and engagement roles in Canada. For example: he was (i) a member of the Advisory Committee for the ‘Strategic Network in Science and Advanced Applications of Plasmas, Plasma-Québec’ of Canada in 2002-2003; (ii) a reviewer of the NSERC (Natural Sciences and Engineering Research Council of Canada) Discovery Grants in 2003; (iii) on the Site Visit Committee responsible for the review of ‘Plasma Quebec’ at the University of Montreal in 2003; (iv) on the Site Visit Committee responsible for the review a Collaborative Research and Development Grants on ‘Manufacturing Near Net-Shape Parts by Vacuum Plasma Spray Forming’ in 2002; (v) on the Government of Canada Advisory Committee to the Canadian Plasma Technology Network in 2002; (vi) a Proposal Reviewer for the Natural Sciences and Engineering Research Council of Canada in 1998; and (vii) an External Reviewer for the FCAR (Canada) Government research programs in 1997.

- Chris Berndt, in his role as Director of IRIS from 2007 to 2011, engaged strongly in mentoring roles for colleagues. For example, Chris was directly responsible for procuring resources for new staff who joined IRIS; i.e., Prof. McArthur, Prof. Wen, Prof. Kingshott, Dr. Wade, and Assoc. Prof. Stoddart. The startup funds were significant in terms of lab resources and equipment. He procured \$300,000 for Prof. Wen and \$750,000 for Prof. Kingshott so that their labs could be populated with modern equipment. In an alike fashion the labs of Prof. McArthur, Assoc. Prof. Stoddart and Dr. Wade were refurbished and into modern working environments.
- Chris was the Leader and Point-of-Contact for the Defence Materials Technology Centre (DMTC) and the Advanced Manufacturing Cooperative Research Centre (AMCRC) from their inception in 2008 to 2013. He was also a lead researcher in the AutoCRC. In these capacities he has been responsible for managing approximately 5-7 projects per year on behalf of SUT. The total funding level per year (until 2013) has averaged out to ~\$500,000. He has been directly responsible for procuring funding for colleagues; e.g., Prof. McArthur, Dr. Wade, Prof. Nagarajah, Assoc. Prof. Sbarski, Dr. Dong, Dr. Wong, and Dr. Durandet.
- Chris proposed that the DMTC and the AMCRC be established and headquartered at Swinburne. He wrote the two proposals on behalf of the university. Both of these proposals were successful with the positive outcome that two CRCs have become embedded within the Swinburne physical infrastructure. In other words, many people and organizations have come to know of Swinburne because they visit the university for CRC business.

In summary: Chris has reached out and been called upon from organizations and institutes around the globe to participate in a large variety of professional activities; e.g., accreditation committees, internal review processes and outreach programs. In many instances he has led or chaired these activities. Within the university environments he has mentored and supported colleagues in an unselfish and nurturing manner.

#### **4.5. Leadership and Engagement across Many Disciplines as a Peer Reviewer**

- Chris has had extensive engagements as a peer reviewer for many agencies; for example (i) the US Nuclear Authority in 2012 and 2013; (ii) the Small Business Industrial Research (SBIR) proposals of the Environmental Protection Agency (EPA) on Nanomaterials in 2003; (iii) the Foundation for Research Science and Technology (FRST) of the New Economy Research Fund (NERF) for New Zealand in 2003; (iv) Cooperative Grants Program of the US Civilian Research and Development Foundation (CRDF) in 2001; (v) the NSF Engineering Research Center for Plasma-Aided Manufacturing from 1996 to 2001; (vi) SBIR Phase I RFP on 'Nanomaterials & Clean Technology' issued by the USA EPA in 2003; (vii) Member for the 21<sup>st</sup> Century Fund of the State of Indiana responsible for disbursing \$20M in 1999 and 2001; (viii) Reviewer for the National Science Foundation from 1998 through to 2004; and (ix) reviewer for DOE SBIR Phase II Awards in 1997.
- Chris was a Member of a Peer Review Panel for DOE Fossil Energy Advanced Research Program Panel 16 - Alloys/Coatings in 1995.
- Chris was invited to join Subcommittee WD/2/4 (Hard Facing Consumables) of the Standards Association of Australia from 1990 through to 1995. He was invited to join Panel 8 (Surfacing and Hardfacing) of the Australian Welding Research Association, March 1989 through to 1995. He discontinued activity in these committees on his relocation to the US.
- Chris was invited to be a proposal reviewer for the Irish Research Council in 2005 and 2013. Both of these engagements required travel to Ireland for face-to-face meetings.

In summary: Chris has engaged with many agencies, institutes and authorities as a peer reviewer. His opinions concerning many aspects of science and technology have been sought after and are highly respected. He is considered a leader in several fields by many external organizations. As well, he is appreciated as a person of integrity and honesty who delivers quality reports and assessments on time.

#### **4.6. Leadership and Engagement in Educational and University Committees**

- Chris was the Undergraduate Program Director for Engineering Science from 1994 through to 2004. He was responsible for implementing program changes that improved and updated the subject sequence that undergraduates followed throughout their studies. Part of this activity

involved membership on several university committees; i.e., a curriculum committee and an academic discipline committee. Chris, eventually, chaired these committees for several terms.

- Chris was appointed as the Director of Assessment for the College of Engineering and Applied Sciences from 1998 to 2004. In this position he instituted processes and mechanisms that allowed the College to formalize, with rigor, the manner in which we had internal controls that met external standards. This position transformed into that of Associate Dean for Undergraduate Studies in 1999 through to 2004.
- Chris was invited as the External Reviewer for the Mechanical and Production Engineering Program at Nanyang Technological University, Singapore, from 1998 through to 2004. This position involved 2 visits to Singapore for face-to-face meetings with academic staff, educational program Directors, Deans, and the University President.
- Chris has participated in several university scholarship programs; for example, (i) AGEF, 'The Alliance for Inclusive Graduate Education and the Professoriate Program' where he mentored Mr. Dominic Vasquez; (ii) the 'Center for Excellence in Learning and Teaching', CELT; (iii) the Simons Fellowship Program (for High School students) where he mentored more than 15 students over 8 years; and (iv) the Undergraduate Research Experience and Creative Activity (URECA) Committee for undergraduate scholarships.
- Chris has participated in many review panels for the National Science Foundation; for example (i) Course Curriculum and Laboratory Instruction (CCLI) in 2003; (ii) National Science, Technology, Engineering, and Mathematics Education Digital Library (NSDL) in 2003; (iii) Small Business Industrial Research proposals on the topic of 'Phase I Electronics Panel concerning Semiconductor and Other Materials/Plasma Engineering' in 2003; (iv) Special Invitation for 'Unsolicited Proposals on Engineering Education' in 2003; (v) Course, Curriculum, and Laboratory Improvement (CCLI) program, Adaptation and Implementation (A&I) in 2003; (vi) Advanced Technological Education (ATE) program in 2002; (vii) the 'STEP' program in 2002; and (viii) Computer, Science, Engineering, and Mathematics Scholarships 'CSEMS' in 2002.
- Chris has been an attendee and active participant in educational meetings, special seminars and conferences; for example (i) NSF Engineering & Computing Education Grantees Conference in 2002; (ii) Stony Brook University Team Member for the SENCER Summer Institute in 2003; (iii) Building Science, Mathematics, Engineering and Technology (SMET) Research and Teaching Capacity at Minority Institutions in 2002; (iv) Integrating Research and Education at NSF Materials Research Centers in 1998; (v) the ASEE Spring Regional ABET meeting in 1998; (vi), 'Best Assessment Processes in Engineering Education II' convened at the Rose-Hulman Institute of Technology in 1998; (vii) ASEE Regional Conferences in 1998 and 1997; and (viii) The 'National Educators Workshop' in 1991.
- Chris was the convener and chair of a State University of New York wide symposium on 'Ethics in Engineering'. A 2-day workshop of invited presentations was held at the Stony Brook campus in 2002. He sought and received funding from the central office of SUNY to engage 4 nationally-renown authorities to present at this symposium that was attended by 60 colleagues from within the SUNY system.

In summary: Chris has contributed to the undergraduate mission through representation and participation within many forums. For example: as a reviewer of educational initiatives, supporter of undergraduate programs and attending conferences that focus on the pedagogy of education.

Final comment of this portfolio: This portfolio represents a snap shot of activities across a broad spectrum of activities in the subject area of 'leadership and engagement'. Chris Berndt's overall approach has been to lead by example and demonstrate to peers, managers and less-experienced colleagues that 'all things are possible' if you are creative and hardworking. He is keen to participate in all manner of activities and contributes to positive outcomes. He is equally as happy to support projects, as a valued team member, in whatever manner is logical and reasonable with respect to his skill-base.

## 5. Learning and Teaching

There are many interrelated components that are associated with the topics of Learning and Teaching (L&T). Learning and Teaching is more than delivering lectures and then walking away. Comprehensive L&T also involves those aspects that are listed in the Table of Contents of this portfolio. Thus, the integrated approach has aspects such as funding mechanisms; outreach to external constituencies; undergraduate and postgraduate supervision; mentoring of students and colleagues; and unit and program accreditation.

### Table of Contents

<b>5. Learning and Teaching</b>	<b>1</b>
5.1. Teaching and Learning Statement	1
5.2. Teaching of Undergraduate and Post Graduate Students	2
5.3. Mentoring Honours and Awards by Students	2
5.4. Presentations and Accreditation Activities	3
5.5. Funding for Teaching and Learning	3
5.6. Administrative Duties and University Service	4
5.7. Final Comment of L&T Portfolio	5

#### 5.1. Teaching and Learning Statement

Reviewers reading this statement can, without a doubt, remember those instructors and professors who impacted their lives. I still remember quite vividly those academics who have positively, and in some cases negatively, influenced my own learning experiences. It is these interactions that I recall when I deliver lectures and presentations: whether they be to undergraduates, graduates or professionals at meetings. Thus, I have a strong opinion that teaching and transferring knowledge is the most important part of an academician's job. We directly influence lives on a day-to-day basis.

Thus, let me state some basic principles that I have followed over my career; some of which are quite obvious but which should be listed for completeness.

1. Preparation on a continuous basis. Lecture material should be updated every year.
2. Use of technology must be appropriate. That is, teaching is not a parade of videos and Power Points. Teaching is imparting a lifelong learning experience.
3. Attending local or national workshops to keep abreast of trends and current pedagogy in my field.
4. Requesting critical feedback from students *via* formal and informal means so that improvements can be instituted.
5. Providing a nurturing and safe environment for undergraduate and post graduate excellence.
6. Integrating my course with those of others that are within the academic program of the students.

As a senior member of the academic community there is another list of requirements; for example:

1. Mentoring staff so that they develop over their careers.
2. Being a cheer-leader and advocate for the University, as well as for the profession.
3. Maintaining a positive outlook and steady composure under difficult circumstances; for example under university restructures and funding issues.
4. Finding resources for laboratory development and exploratory programs.
5. Recognizing and rewarding, where appropriate and if possible, the achievements of our faculty and alumni.

Learning cannot be separated from teaching. Thus, a prime objective in my teaching method is to help students 'learn how they can learn'. This is part of the continuous professional learning that is embedded within our national curriculum. In other words, students should gain the confidence, from exposure in the classroom, to explore areas of interest that are outside their core curriculum.

In an alike fashion, I consider that my role is to set a high standard of achievement by example. Thus, I am also continually learning from students, colleagues and the literature. I have the experience and confidence to impart professional lessons to students that will stead them well into their own careers.

In Summary: Teaching is a passionate topic for me since it is fundamental to the future of the nation and the benefit of our society. Learning must be fully integrated into teaching so that students, either undergraduates or post graduates, evolve as good citizens for their chosen profession. This brief



statement can touch only the highlights of my total commitment to deliver strong courses, subjects and programs that will be judged as the best in the country.

## **5.2. Teaching of Undergraduate and Post Graduate Students**

Chris has developed and delivered many courses throughout his career. These are listed below. Some of these courses have been challenging. For instance teaching large classes of 400+ students in two, replicated lecture theatres due to a space issue. In other cases, the classes have been time-tabled at either 7:30 AM or 8:30 PM to accommodate the work schedule of mature age students.

### Monash University Courses

151	Mechanical Properties of Materials (class size of up to 450 students)
3503	Introduction to Materials Processing
3507	Ceramics I
3510	Surfaces I
4523	Project
4537	Ceramics II
4539	Biomaterials

### Stony Brook University Courses:

ESG 201	Engineering Responses to Society
ESM 216	Materials in Art, Design, and Technology
ESG 310	Research Methods
ESM 332	Biomaterials
ESM 335	Mechanical Properties of Materials
ESM 353	Biomaterials
ESM 441	Senior Design
ESM 450	Phase Changes & Mechanical Properties of Materials
ESM 488	Coop in Industrial Practice
ESM 499	Research in Materials Science
ESC 499	Research in Mechanics
ESM 506	Mechanical Properties of Engineering Materials (graduate course)
ESM 696	Seminar in Thermal Spray Science and Technology (graduate course)

### Swinburne University of Technology Units

HES 2281	Materials and Manufacturing
ADM80007	Surface Engineering (post graduate course)
Various ad hoc guest lectures to undergraduate classes on the subject of research.	

Chris considers that supervising post graduate students is also a strong component of Learning and Teaching. A summary of these student-related activities is listed below.

### Monash University (1986-1991)

- Ph.D. advisor to 6 students with 5 completions.
- M.Eng.Sc. advisor to 4 students with 4 completions.

### Stony Brook University (1991 to 2005)

- Ph.D. advisor to: 10 students
- M.S. advisor to: 6 students
- Committee member for 30 Ph.D. defences. Several of these involved travel to France and external examination of candidates from other universities.
- Committee member for 11 MS examinations.

### Swinburne University of Technology (2005-2014)

- Ph.D. advisor to 9 of which 7 have been awarded the degree to date.

In Summary: Chris has delivered thousands of formal lectures to tens of thousands of students. Chris has been recognized with several teaching awards over his career.

## **5.3. Mentoring Honours and Awards by Students**

Chris has mentored many students on a one-on-one basis. Many of these students have won awards and scholarships on the basis of their R&D projects. For example, several undergraduates include:

- i. Christienne Mancini and Soo-Hyun Tark won Undergraduate Recognition Awards in 2003.
- ii. Christienne Mancini and John Soehengen won URECA awards to help manufacture a wheel chair for disabled children in 2003.

- iii. Christienne Mancini received an Undergraduate Recognition Award in 2002 for her work on 'Porosity Determinations on Thermally Sprayed Hydroxyapatite Coatings'.
- iv. Christienne Mancini, received an ITSA Undergraduate Scholarship, January 2000.
- v. Dominic Vasquez was a minority student who Chris mentored for 2.5 years. Dominic was married with 4 children and Chris was able to assist in the provision of a 'MARC Scholarship' to him for 2.5 years on the basis of his strong academic record..
- vi. Dominic Vasquez and Christopher Dambra won URECA 2000 Summer Fellowships.
- vii. Jooyeon M. Lee and Dominic Vasquez were awarded Weinig Foundation Scholarships in 2000.
- viii. Christine Borello received an 'Anne Sayre Award to an Outstanding WISE Woman' in 1999 and an International Thermal Spray Award in 1999.

Some of these undergraduates students have remained in occasional contact with Chris; for example, Christienne Mancini went on to work for several defence companies before moving to Cambridge University and gaining a PhD. Chris Dambra is a Senior Engineer with a major thermal spray company on Long Island and Dominic Vasquez moved to New Mexico where he completed a Masters degree before accepting a job with a manufacturing company.

Chris has invited selected high school students into his lab for summer and intern research experiences. They were presented with quite complex and challenging problems of a fundamental nature. Several of these students won awards of recognition for their studies; e.g.,

- i. Shira Billet and Dora Sosnowik were high school students who were Gold Medal national winners on the topic 'A Viscometer for Ultra Thin Films' for the Siemens 2001 competition. (Note: also supervised by Prof. M. Rafailovich).
- ii. Michele Nudelman was an Intel semifinalist in 2001. As well, as a High School student, she worked with Chris and his Post Doc on the topic of 'Computer Analysis and Simulation of Thermal Spray Processes to Optimize Efficiency and Coverage Simulation of the Thermal Spray Process'. Michele won a US Army Award at the 2000 Long Island Science and Engineering Fair. She was one of three students to represent Long Island (from 250 entries) at the State level Long Island Science Congress run by the Science Teachers Association of NYS.
- iii. Mark Gebel, (Smithtown High School) carried out a research project on the 'Analysis of Material Failures' in May 2001. Note that Mark Gebel and Michele Nudelman also received 1999 Simons-NSF Thermal Spray Center Summer Research Fellowships.
- iv. Laura Cava, Glen Behrend and Ajai Ajitanand were High School Seniors who received 2000 Bright Lights Scholarships to enter the Engineering Science Program at Stony Brook University. Chris was the gateway by which these students entered engineering.

In Summary: Chris believes that it is never too early to promote education to the younger generations. Thus, he has actively supported UGs and high school students within his local Learning and Teaching environments so that they gain hands-on experience with respect to a deep university experience. These students have prospered from this interaction; often by financial means so that they were burdened less by the cost of a quality education. More importantly, they have also gained a foothold into the profession of engineering and science.

#### **5.4. Presentations and Accreditation Activities**

- Chris has participated in learning and teaching activities that focussed on undergraduates. These have been detailed in the portfolio on Leadership and Engagement.
- Chris has engaged as a reviewer of educational-based funding opportunities. These have been included in the portfolio on Leadership and Engagement.

In Summary: Chris has contributed extensively to Learning and Teaching in terms of accreditation activities as well as the peer review process of funding. These interactions have enabled an improved environment for Learning and Teaching.

#### **5.5. Funding for Teaching and Learning**

- Chris has secured funding to realize educational objectives; for example:
  - i. C.C. Berndt et al., NSF 'Making the Connection: Linking Stony Brook and Community Colleges via CSEMS'. [\$398,693].

- ii. R. Kamoua, A. Pacelli, C.C. Berndt and K.K. Likharev, 'NUE: Introducing Nanoscale System Design into the Undergraduate Electrical and Computer Engineering Curriculum', June 01 2004 to May 31, 2006. [\$99,762].
- iii. Support to develop and launch an 'ALN B.S. degree in Electrical Engineering' (2005-6-14) Project Director: David Porush, Grant Amount: \$300,000.00 Institution: Research Foundation of State University of New York Fiscal Year: 2005. Note: This project was awarded after Chris left the USA; but he was responsible as a strong contributor to the team that brought it to fruition.
- iv. C.C. Berndt et al., NSF 'Inquiry-Based, Interdisciplinary Curricula within an Engineering Research Culture', October 01, 2002 to September 31 2003, [\$100,000].
- v. C.C. Berndt, State University of New York, 'Ethics within the Engineering Profession: A Workshop for faculty', 05/01/01 to 04/30/02, [Total budget ~\$15,000].
- vi. C.C. Berndt, 'National Educators Workshop', 11/01/98. [\$3,095].
- Chris lead the Educational Outreach activity of a 'Materials Research Science and Engineering Center' from 1996 through to 2002 that was sponsored by NSF [\$3,800,000 for the whole Center]. H.Herman was the lead investigator. Summer programs were held for high school students and undergraduates under the auspices of this MRSEC. Selected UGs were also awarded stipends during the teaching year in order to be laboratory assistants. Many of the students who undertook MRSEC activities were, subsequently, engaged by the university to continue their UG and PG aspirations.
- Chris, with Clint Rubin as the lead investigator, was part of a university-wide team that successfully attracted funding from the Whitaker Foundation to commence a Biomedical Engineering program at the university. May 1996 - April 1999. [\$996,906].
- Chris lead a team to procure funding for a 'US- Australia Cooperative Research: Thermal Spray Processing of Polymers' activity sponsored by NSF, 06/01/96 to 05/31/99. [\$22,560]. This funding permitted 3 Post Graduates from the USA to visit Monash over 3 consecutive years for periods of 2-3 months each. This constituted a wonderful, life-long experience for these future scientists and engineers.
- Chris was able to supplement a basic science proposal on 'Plasma-based ultrafine particle synthesis' with Research Experiences for Undergraduate (REU) funding from NSF. March 1994 to June 2 1999. [an increase in the budget of \$8,500 on \$290,000 base].

In Summary: Chris has procured extensive resources so that Learning and Teaching has been enabled. Many students at the UG and PG capability have benefitted from these opportunities.

## **5.6. Administrative Duties and University Service**

Chris has recognised that Learning and Teaching happens under an appropriate administrative umbrella; which should be transparent to a large degree to the student. The administration aspect cannot be ignored since this provides the framework for educational reform by, for example, setting policy and standards. Chris has played a large role in Learning and Teaching from this aspect and several key points are listed below.

- Chris has represented engineering in many university committees; and in several instances been the leader and chair of specialised projects.
  - i. Leader of the State University of New York coalition on 'e-Learning', a coalition of Electrical Engineers from Stony Brook, Buffalo and Binghamton Universities.
  - ii. Member of the University 'Assessment Committee', 2003-2004.
  - iii. Member of the Stony Brook University 'Middle States Accreditation' Steering Committee, 2002, 2003.
  - iv. Occasional Member of the Provost's Advisory Group throughout 2002-2003 representing the College of Engineering and Applied Science.
  - v. Member of the University Senate as Senator for Materials Science and Engineering 2003-2004.
  - vi. Member of the University 'CUE', Committee for Undergraduate Education, 2001, 2002, 2003.
  - vii. Membership of the 'School of Professional Development Council' in 2001

- viii. College of Engineering and Applied Sciences faculty representative for the following Stony Brook University committees: URECA Committee, Simons Fellowships, Undergraduate Program Directors.
  - ix. Representative for Materials Science and Engineering on the curriculum committee as well as the Academic Dishonesty Committee. Chairman from 1997-1998.
  - x. Appointment as the 'Director of Assessment' for the College of Engineering and Applied Sciences from 1998-2004.
  - xi. Undergraduate Program Director from 1995-2004. Deputy Chairman of MSE from 1993-2004. Undergraduate Laboratory Chairman from 1994-2004.
  - xii. University Contact / coordinator for 3 ARPA-TRP proposals in 1993. These 3 proposals involved 10 Universities, 20 Companies and 3 Professional Societies for requested funds of ~\$9.5 M. These proposals were aimed at 'retraining the defence workforce'.
  - xiii. Chairman in 1993 of a University Search Committee to employ a Senior Research Specialist. This appointment was for an individual who sat directly under the VP for Research.
- Chris has participated in and Chaired specialized conferences and workshops that have focussed on the curriculum and Learning and Teaching.
    - i. Chairman and organizer of the State University of New York Workshop on 'Ethics in the Engineering Discipline', April 2002.
    - ii. Chairman and organizer of the College of Engineering and Applied Sciences 'Distinguished Speaker' committee.
    - iii. Member of Stony Brook University Team to participate in the Invited Conference, 'Institute on Campus Leadership for Sustainable Innovation' in 2001.
  - Chris has a passion for certain mainstream Learning and Teaching topics; i.e., biomaterials and manufacturing. He was responsible for growing these areas of interest into the undergraduate and post graduate curricula and several administrative roles that he played in this role are listed.
    - i. Instructor for new 'ITS101' (Information Technology Studies) section on 'Biomaterials'.
    - ii. Member of the Stony Brook University Bioengineering Committee - 1994+
    - iii. Faculty committee to examine the College's interests in 'Manufacturing Engineering'.
  - Chris took active participation on minority-based programs; several of which are documented below.
    - i. Participation in the 'Women for Women', W:W, program (Mentor for Christienne Mancini), 2001, 2002, 2003
    - ii. Participation in the WISE 'Introduction to Research' introductory sessions. 1998-1999.
    - iii. Advising of students for the NSF-supported State University of New York Alliance for Minority Participation Program (1997 academic year)
    - iv. Mentor for State University of New York Alliance for Minority Participation, 1995.

In Summary: Chris has taken on administrative duties and many related tasks in his commitment to provide input and impact towards an integrated approach for Learning and Teaching. The prime beneficiaries of these duties have been 'the students'; both undergraduates and post-graduates, for whom the university exists.

### **5.7. Final Comment of L&T Portfolio**

This portfolio of Chris Berndt lists those areas of professional activities that fall under the umbrella of 'Learning and Teaching'. However, this listing is somewhat 'dry' since it does not convey the passion and energy that Chris inputs into Learning and Teaching from many perspectives.

Chris considers Learning and Teaching as one of the most important aspects of his professional duties. Chris's short 1-page CV, in its closing sentence, indicates this in another way by stating: *'He is especially proud of his students and post docs who have achieved professional prominence and earned good lives over the past 30 years.'*

# STATE OF THE SOCIETY

## THE BIRTH OF OPPORTUNITY



**T**he intent of International Thermal Spray and Surface Engineering; aka "iTSSe" and pronounced as "itsy," is market discriminated from existing publications in several ways. First and foremost, although the acronym TSS occupies the central part of iTSSe, this publication is much more than thermal spray. The coverage extends to all surface engineering processes and technologies. Secondly, iTSSe is a rapid-response publication that presents technology when it is first invented or deployed to the general public. Therefore, iTSSe can be considered as the radar for surface engineering.

Since this is my first contribution as the Editor of iTSSe, then let me paint the landscape that has given rise to its birth. This industrially oriented publication has been a glimmer in my eyes for over five years. It seemed to be the natural extension of the *Journal of Thermal Spray Technology*, which in itself has been an extremely successful technical journal. It then took some courage and certain amount of opportunism within the Thermal Spray Society to take advantage of an environment that was receptive to a quick-response, industrially related publication that would serve the needs of ASM members. iTSSe has now arrived!

The vision is that all surfacing technologies and related activities, such as testing, processing, and applications, will have a home in iTSSe. Surface engineering will be promoted and marketed by means of short, to-the-point articles that respect the time of busy people. This will be a publication that will be found next to the coffee pot in the back room of an engineering company, or equally, on the coffee table of an executive; as a resource for all who need to keep abreast of current developments in surface engineering and science.

iTSSe presents you with opportunities to market your products and applications, to showcase your recent work, and to let the world know that you and your company are on the map! I encourage and exhort you to contact me if you want to take advantage of these opportunities.

A single e-mail may change your impact on the world of surface coatings and engineering! Make an effort to contribute.

### Permission to publish

C.C. Berndt, "State of the Society The Birth of Opportunity", *Advanced Materials & Processes*, (2006) 164[5] p94.

With kind permission from Springer Science+Business Media. The complete article (text, figures, tables and references) have been kindly reproduced.

**Chris Berndt, FASM, Editor**  
Editor Emeritus: *The Journal of Thermal Spray Technology*

### Permission to publish

C.C. Berndt, "State of the Society The Birth of Opportunity", *Advanced Materials & Processes*, (2006) 164[5] p94.

The above article is made available as an electronic reprint with the permission of ASM International. One print or electronic copy may be made for personal use only. Systematic or multiple reproduction, distribution to multiple locations via electronic or other means, duplications of any material in this article for a fee or for commercial purposes, or modification of the content of this article is prohibited.

ASM International Board of Trustees.

**Mr. Peter Hanneforth**, President, SpaCom LLC, Huntington, New York, becomes President for 2006-2008. He previously served on the Board as a member and most recently as Vice President. **Dr. Richard Knight**, FASM, Auxiliary Professor and CPPM Director, Drexel University, Philadelphia, Pennsylvania, remains on the Board for two years as Immediate Past President.

The following members were elected in 2006.

**Mr. Mitchell R. Dorfman**, Director of Ceramics, Materials Development, Sulzer Metco (US) Inc., Westbury, New York, has been elected Vice President for two years, and will automatically progress to President. Mitch has served on the Board since 2004. He has over 27 years of thermal spray material-development experience and has been an active member in the thermal spray community for more than 18 years, serving as chairman of the ASM/TSS Information and Development Committee; participating in thermal spray-related conferences as program organizer, session chair, and workshop instructor; and serving as reviewer of technical papers for *JTST*. He has au-

thored new membership, and to continue to develop strong technical conference programs.

**Mr. Raymond J. Sinatra**, Senior Engineer, Rolls-Royce Corp., Indianapolis, Indiana. Ray has worked in the field of thermal spray coatings for 36 years, and has been an active participant in the ASM TSS during the past ten years, serving on the TSS Board since 2003, and serving on the TSS Strategic Recognition Committee and Accepted Practices Committee on Metallography, as well as on the ASM Surface Engineering Congress Organizing Committee. Ray also has been re-elected to a second term on the TSS Board from 2006-2009. Ray believes the ASM Thermal Spray Society needs to be a strong resource for technical information required to support the ever-growing global business of coatings; that the information TSS develops and supplies to its members must be accurate, timely, and represent the latest advances in coating technology; and that training in all aspects of thermal spray will continue to be a strong member driven need that TSS must address by developing the appropriate resources.

The following are newly elected Board members for 2006-2009:



## Thermal Spray: The Best Thing Since Sliced Bread?

**H**ow many times have you been placed in the position of (a) having to describe what thermal spray (TS) is all about, (b) defending the physical attributes of a thermal spray coating with respect to another product or process, or (c) arguing the attributes of thermal spray on the basis of life cycle costs? And sometimes all of these topics might be discussed within a single business exchange.

There are many pragmatic answers to these questions. There are many resources that discuss the TS process including conferences, web sites, peer-reviewed literature, patents, private databases, and professional societies.

In some cases, the honest answer is "Yes, I fully understand where you are coming from. Thermal spray may not be the specific solution that your company needs for this particular application." In such instances, your expertise in understanding the entire array of surfacing solutions can be brought to bear. The outcome is that the customer may very well be satisfied with the alternative solution and your own credibility as an expert will be reinforced. Thus, this person will feel comfortable in coming back to you, even though TS was not the solution for that particular application.

A more difficult circumstance is where you are placed in the position of defending the microstructure of TS coatings. Remember viewing your own coating under the microscope where the eyes focused on a structure of pores, inclusions, and cracks. It is not hard to see then that persons trained as engineers, scientists, and technologists would find it difficult to understand how such structures can function as coatings under actual engineering conditions. It's easy to foresee the many questions that might arise about coating strength vs. fully dense materials, the effects of surface roughness, and mechanical properties including yield and ultimate tensile strengths, fatigue strength, and modulus.

As practitioners, we know that TS coatings do in fact perform more than satisfactorily in many adverse mechanical and corrosive environments. So we are able to defend the microstructure largely through the many successful case histories and extensive industrial practices that are available.

Finally, the cost of TS coatings apparently is favorable since a global market of several billion dollars exists for thermal spray. I see the important numbers as the cost of people and compliance to environmental regulations. The high capital equipment cost can be amortized over 5 to 10 years, so the major cost is people—engineers who can specify coatings and skilled operators who can program manufacturing cells and/or hand spray complex geometries.

Is thermal spray the best thing since sliced bread? I have had experiences where thermal spray has been over-sold, leaving the client cautious about repeating a negative experience. However, in the past decade, the database of successful examples of thermal spray and other coating technologies has increased significantly to build a high confidence level that the coatings will perform in accordance to the required specification.

Thermal spray is a competitive technology for many applications. Whether TS is better than sliced bread should not be based on what we are told to believe, but on the basis of solid engineering results and hard data. There is a strong need for unbiased results and data, and many people are striving to fill this need.



Chris Berndt, FASM, Editor  
Editor Emeritus: *The Journal of Thermal  
Spray Technology*

## Activism in Thermal Spray: A Call to Arms!

**F**ree rides and free lunches come back to haunt you. What a way to start a commentary that aims to ask you to commit to the ASM Thermal Spray Society (TSS).

The TSS has over 1,000 members worldwide who have paid to be recognized as having an affiliation with thermal spraying. This is a conscious decision on their part, which implies they see tangible benefits in belonging to TSS. The benefits of being a TSS member are numerous and can be segmented into soft and hard categories. The soft benefits include criteria such as "TSS is in your area of interest; thus you should belong to this Society." These emotive arguments are important ones; however, many people also need to look at the so-called bottom line.

Therefore, TSS has worked very closely with staff at ASM International to create hard products that can be offered to TSS members at a discounted price. For example, ITSC conference fees, JTST subscription rates, TSS Workshops (there is a Cold Spray Workshop in October, 2007), and many other tangible products are priced in such a way that the cost reflects on your bottom line. Both of these types of benefits have a direct impact on how TSS members perceive *value in belonging*.

So where does the title of this commentary "Activism in Thermal Spray" come from? It is as simple as this: volunteer members of TSS drove the creation of these benefits so that EVERY MEMBER could realize commercial (viz. hard) and philosophical (viz. soft) opportunities. These volunteers constitute the grass-roots activism that has been the hallmark of ASM and, especially, TSS. The volunteers include the TSS Board of Directors, the various committees, and people who help out at events as Session Chairs; as well as the speakers themselves.

The committee structure of TSS incorporates probably about 60 to 80 people who dedicate their time and energy to make things happen. These are the people who work behind the scenes to create the framework for the ITSCs, to publish in JTST, and to formulate standards and best practices guidelines for the TS industry. All of these products are driven by active TS'ers who are not only concerned with important parts of the industry; but who also can see that they need to be part of this action.

So, where does the "free lunch" come in and why can't I just sit around and let others do the work? This is a quite common response because we are all busy people and we may not have the time or inclination to jump in and volunteer. Yet, as professionals we all know that you only get back what you put in. And often the more you invest, then the more you will reap in terms of positive outcomes. My argument here is that individuals must be active so that their personal needs are best suited. Therefore, if an individual has a burning need or desire for certain products, then it is imperative for that person to stand up and be counted as a contributing volunteer. You will find that you will be welcomed with open arms and that you will harvest so much more than what you put in via networking contacts, knowledge, and respect from like-minded colleagues.

An excellent example of where volunteer activism by TSS members has led to a tangible product is the new TSS web portal that has been created over the past 18 months. The project planning for this commenced in mid-2005 will be rolled out in mid-2007. A working group of TSS volunteers and ASM professional staff has been prototyping a silent web site since September 2006. The new web portal that has been produced is magnificent. The functionalities of the new TSS web portal will outstrip any other professional society development that is available. The value of TSS membership has just increased enormously.

My call to arms is "Volunteer: The TSS Needs You!"



Chris Berndt, FASM  
Editor  
Editor Emeritus: *The Journal of Thermal Spray Technology*

## Will Thermal Spray Ever Be the Basis for A Nobel Prize?

will answer this question later. The more fundamental questions should be "Who cares and why do they care?"

First: Who cares? Naturally, research scientists care since the Nobel Award represents the pinnacle of achievement and carries the dual hallmarks of success and long-term security with regard to funding. The currency of a Nobel Prize can translate into the best labs, the best post docs, the most prestigious invitations, and much more. There is an afterglow effect to everyone and every organization associated with the award.

Second: Why do they care? The recognition that a Nobel Award carries positions the topic under discussion into a place where it can be taken as a field or research that has serious credibility. In other words, to paraphrase the comedian Rodney Dangerfield "The topic gets respect!" Therefore, we should all care that thermal spray science is considered worthy of a Nobel Award since the associated benefits and reflected glory are of quite substantial monetary and emotional value.

Please don't read too much into the benefits of such a distinction for the job shop that is spraying tool steel to rehab worn shafts. Their profits are not going to change overnight with the advent of an individual being awarded a prize on the basis of a major scientific discovery. In the short term, these job shops will still need to spray massive amounts of tool steel to stay in business. It is the far and distant horizon that will be influenced by the Nobel Prize.

Now we can address the question: Will thermal spray ever be the basis for a Nobel Prize? And if it is, then in what area will it be awarded? In my opinion, the greatest science will lie in the discovery and modification of functional, advanced materials. Thermal spray, or devices that can be traced back to currently used equipment, will be used as the process zones that enable the creation of new materials. Thus, I predict that thermal spray will be elevated to a great science that not only reaches page one of your national newspapers, but also becomes a household word.

There would be few disagreements about how wonderful it would be for thermal spray to be associated with a Nobel Award. Yet we should also keep in perspective that such accomplishments do not occur in isolation or by dreaming that they will happen. Thus, a paramount need is to enthuse young scientists and engineers about the satisfaction gained from the joined processes of discovery and creation. The future generations need to inherit this legacy of excitement so they identify that thermal spray, or materials modification in general, can play a major part in their lives.

I assure you that a Nobel Award in thermal spray is just around the corner waiting to be awarded!



Chris Berndt, FASM, Editor  
Editor Emeritus: The Journal of Thermal Spray Technology  
IRIS, Faculty of Engineering and Industrial Sciences  
Swinburne University of Technology  
Mail 66 PO Box 218  
Hawthorn, Victoria 3122 AUSTRALIA

## Born Again as a Technologist

**W**e all make transitions in life, which allow revitalization and growth to occur. While such opportunities arise in our personal environments, how does growth occur for a technology? What are tipping points for the advancement of surfacing technologies such as thermal spray, hardfacing, PVD, etc., and how can individuals play a role that suits their personal career goals?

Is technology the driver or engine for innovation? The answer is no. The real drivers are people who dedicate their careers to make the impossible possible, responding to an intrinsic curiosity to do what is considered by their peers as undoable and the need to solve specific engineering applications challenges.

Has thermal spray reached its technological limit? This often seems the case on a year-to-year basis when new developments appear to progress at glacial speed. Yet a literature and the state-of-the-art search in 5- or 10-year increments reveals that people who appear within relatively old conference proceedings are still publishing, which suggests that thermal spray provides a sustainable long-term career. There also is a steady progression of people passing through the field of thermal spray technology, growing at an annual rate of about 15-20%. Furthermore, there is growth in the number and diversity of companies involved in both publishing and exhibiting at conferences, which indicates a healthy prospect for thermal spray with new players and new associated technologies contributing to synergistic growth.

Is there is a limited need for specialists in coatings technology? To survive as a relevant technology, it is not enough to maintain (for example) a \$3-billion annual global market. This will not lead to sustainability, and thermal spray will devolve to essentially a boutique technology for special applications rather than the household word that denotes true acceptance. New basic and applied R&D programs are needed to achieve the above goal. Furthermore, technology-savvy people are desirable to start, manage, and implement these programs. Where will these people come from and what incentives are there for a young professional to enter the surface engineering field? The answers to these questions are disappointing. Many young people find science and engineering "too hard," and surface engineering technologies are suffering. On the positive side, professional societies including TSS, ITSA, DVS, GTS, and many others are playing a significant role in specialized education and training for technologists of all types.

The born-again technologist is a person who meshes the three themes presented so next-generation products can be developed. This technologist, by keeping an open mind, holds the key to the leap-frog technology that surface engineering continues to create.



Chris Berndt, FASM, Editor  
Editor Emeritus: The Journal of Thermal Spray Technology  
IRIS, Faculty of Engineering and Industrial Sciences  
Swinburne University of Technology  
Mail 66 PO Box 218  
Hawthorn, Victoria 3122 AUSTRALIA

## 'At the End of the Day': Let Us All Take on Responsibility for Thermal Spray

**H**ow many times have we heard this phrase and actually considered what this management cliché means? The physical reaction may be a cringe or a wiry smile that belays discontent. Or it could be a mental somersault that questions the intent of the comment in the first place. As a first point of reference, a web source defines "at the end of the day" as "something that you say before you say what you believe to be the most important fact of a situation." That is, according to this particular source, the phrase is intended to summarize discussion so a decision can be formulated. I would like to pose a different explanation as well as comment on the authenticity of such a statement.

The principle of moving the discussion forward is pragmatic in that it might allow a certain box on a management chart to be ticked, but at what cost does this occur? I propose that what really happens at the end of the day is that a large degree of information is lost, or even ignored, during such a decision making process and the final result may be seriously flawed. There is also a moral leap of faith that assumes the preceding discussion was legitimate, which again can not be validated if a follow-up conversation has not been held.

For example, you may have noticed in your own dealings that the expression "at the end of the day" is voiced when (1) strongly divergent opinions have been raised, (2) there seems to be a temporary lull in the to-and-throe of argument and (3) there is indecisiveness within the meeting and someone is trying to wrap it up in the form of a forced decision.

So, at the end of the day, what are we missing? The first thing would be direction; that is, the notion that a discussion can be neatly parcelled up by a nonsequitur. Next, there is the question whether a decision should be forced at that particular moment of time. It is often perfectly acceptable to delay a decision until people have thought about or politicked outcomes. Therefore, the time frame could very well be at the end of the week or at the end of the month, and there would be no adverse outcomes concerning the question at hand. Thus, the finality of the statement "at the end of the day" demands serious consideration on whether it should be taken at face value or just ignored.

Let's not miss the main point of this editorial. We need to be quite cautious when the cliché is used in the same train of thought as thermal spray, since the implicit assumption could be that thermal spray is limited in scope and application. I would like to think that at the end of the day, there is no end for thermal spray. This is an admittedly tortured way of saying thermal spray and, in fact, all surface engineering methods do not have an end point. As engineers, scientists, and technologists, we are continually reinventing thermal spray so there is always a new beginning and a solid foundation for a sustainable future.

In summary, at the end of the day does not exist for thermal spray. What does exist is continual rebirth and growth of a technology that is undergoing change. This is an opportunity that can not be ignored, dare I say, at the end of the day.



Chris Berndt, FASM  
Editor  
Editor Emeritus: The Journal of Thermal Spray Technology  
IRIS, Faculty of Engineering and Industrial Sciences  
Swinburne University of Technology  
Mail 66 PO Box 218  
Hawthorn, Victoria 3122 AUSTRALIA



# Editorial



This editorial coincides with the closure of the 13th International Thermal Spray Conference; thus, it is appropriate to open some discussion concerning this important meeting. In terms of absolute numbers: ITSC'92 attracted more exhibitors (70) and provided the largest Conference Proceedings (161 papers and 1070 pages) of any prior conference and exhibition that has addressed solely the area of thermal spray technology. There was also a very successful educational and workshop series of four different activities that commenced four days before the main conference. The delegates were certainly kept busy running between three concurrent sessions as well as participating in a quite active "standing room only" exhibition and many social events!

There seems to be no doubt that the Conference was a financial success as well as extremely well-organized, but possibly the more appropriate question to ask is, "Was ITSC'92 technically and professionally rewarding for the majority of delegates?" This question should be answered by ITSC'92 attendees since it is only by offering constructive and frank criticism that true development of thermal spray activity can advance throughout the world. Of course the answer to this question will vary from person-to-person, but the important point is to pass on your comments and ideas, whether they be those aspects of the meeting that need improvement or those that were accomplished, to the appropriate person. The Editor suggests that you call or write the Chairman of the Thermal Spray Division at ASM International, Materials Park, Ohio 44073 USA.

Expectations may have been realized or there may have been some disappointment. For instance, another less impressive statistic (depending on your viewpoint!) is that there were probably more committee meetings during the Conference than at any previous ITSC. The result is that those who may have had much to contribute to the discussion of thermal spray were by necessity removed from the general body of the Conference at times. This conflict may be insolvable, since, realistically, it is only at these conferences that the committee members assemble.

Another question is—"Are the young thermal sprayers being nurtured within the industry?"—since it is only by attracting and retaining *new* viewpoints and ideas that the future of the industry can be secured. There is clearly room for broadening the horizons, in this area and the Editor would be happy to use *JTST* as a forum to explore this question. One example of stimulating undergraduates to enter the thermal spray community has been the establishment of substantial scholarships by the International Thermal Spraying Association to graduate students who have embarked on a career in thermal spray. No doubt other creative ideas abound, and your input is welcome.

The theme of this commentary has been to open a discussion about several issues that affect the thermal spray community. Thus, with this thought in mind, a final point concerns this *Journal*. The first issue of Volume 1 has been circulated for several months and has been internally critiqued by its Editorial Committee during ITSC'92. The general feeling is quite positive. However, the Committee is very aggressively soliciting feedback from all subscribers and extends to you a sincere invitation to let us know your thoughts and ideas, so that the *Journal* can best suit your needs and concerns and those of your industry!

**Christopher Berndt**  
Editor

Permission to publish

C.C. Berndt, "Editorial: Closure of 13th ITSC", *JTST*, 1[2] (1992) 99. With kind permission from Springer Science +Business Media. The complete article (text, figures, tables and references) have been kindly reproduced.

# Editorial

## The significance of THERMAL SPRAY AWARDS



The Thermal Spray Society (previously the Thermal Spray Division) of ASM International has, since its inception, appointed an Awards Committee so that excellent work of thermal sprayers could be acknowledged. Prior to the International meeting in Orlando (May - June 1992) the awards were based on the oral presentation at the NTSC's and judged according to the audience response to standard session questionnaires.

From 1992, for the three most recent conferences, the judging has been based on only the written submission for the conference proceedings. The judging of the papers in every year has been performed by 30 panelists from the North American thermal spray community. The awards process would not exist but for the unselfish efforts of these panelists and they certainly deserve recognition for the high credibility of the awards.

Each panelist was forwarded a package of about 10 to 15 papers which were of similar subject content. Each paper was submitted to 3 panelists so that some averaging procedure could be implemented. (Of course, no author who may also have been on the judging panel, voted on their own paper.) The Chairman of the awards committee, who did not judge any papers, performed various normalizing procedures to account for statistical variations among judges and therefore eliminate any potential bias. The papers at this stage were referenced by a number to de-person-

alize the mechanism of establishing a ranking for conferring awards.

The judges were asked to rank their group of papers in order of merit. The guidelines for this ranking were to consider; (i) the novelty and originality of the subject, (ii) the presentation format and attention to details such as figures and referencing, (iii) the scientific and engineering merit of the work (i.e., does this work open up new applications or enable better understanding of thermal spray processes and coatings?); and (iv) a discretionary component to account for any of the judge's special interests.

In 1994 some 6% of the papers were judged as deserving special merit. The four "NTSC'94 Best Paper Awards" are considered as premier contributions to thermal spray technology and are listed below.

- T. Eckardt, W. Mallener, and D. Stover, "Reactive Plasma Spraying of Silicon in Controlled Nitrogen Atmosphere."
- J-G. Legoux and S. Dallaire, "Copper-Ceramic Composite Coatings for Steel Strip Casting."
- V. Kadyrov, Y. Evdokimenko and V. Kise, "Calculation of the Limiting Parameters for Oxide Ceramic Particles During HVOF Spraying."
- R.A. Miller, W.J. Brindley, J.G. Goedjen, R. Tiwari, D. Mess, "The Effect of Silica on the Cyclic Life of a Zirconia-Yttria Thermal Barrier Coating."

"Certificates of Merit" for outstanding work were presented to:

- D.J. Greving, E.F. Rybicki, and J.R. Shadley, "Residual Stress Evaluations of Thermal Spray Coatings by a Modified Layer Removal Method."
- S.E. Hartfield-Wunsch and S.C. Tung, "The Effect of Microstructure on the Wear Behavior of Thermal Spray Coatings."
- X.L. Jiang, R. Tiwari, F. Gizhofer, and M.I. Boulos, "Induction Plasma Reactive Deposition of Tungsten and Titanium Carbide."
- M. Vardelle, A. Vardelle, A.C. Leger, and P. Fauchais, "Dynamics of Splat Formation and Solidification in Thermal Spraying Processes."
- 

Each year the Journal of Thermal Spray Technology recognizes the best paper published during the year. The **1993 Best Paper Award for JTST** was presented to M. Vardelle, A. Vardelle, and P. Fauchais for their paper entitled "Spray Parameters and Particle Behavior Relationships During Plasma Spraying."

The **Thermal Spray Hall of Fame** was established in 1993 by the Thermal Spray Division of ASM International. Induction into the Hall of Fame is a means of recognizing and honoring outstanding leaders who have made significant achievements and contri-

butions to the science, technology, practice, education, management, and advancement of thermal spraying. Again, a panel of 6 eminent thermal sprayers, representing practitioners, engineers, scientists, and managers in the thermal spray arena were asked to evaluate the nominating files of candidates. The first class of inductees, presented at NTSC'94 in Boston, include:

- William E. Ballard (deceased), "For pioneering and unparalleled efforts in cataloging the development, growth and commercialization of the thermal spray industry in his anthology Metal Spraying and the Flame Deposition of Ceramics and Plastics."
- Max Ulrich Schoop (deceased), "For landmark contributions as the inventor of the thermal spray process and the subsequent refinement and expansion of thermal spray technology to provide the foundation for the modern thermal spray industry."
- Herbert Herman, Leading Professor, State University of New York at Stony Brook, Stony Brook, New York. "For outstanding contributions in thermal spray education, expanding the thermal spray technology science base and developing and advancing coating characterization techniques."
- Daniel R. Marantz, President, Flame-Spray Industries, Inc., Stony Brook, New York. "For pioneering work in the development of thermal spray devices including the single wire plasma gun, and playing a central role in introducing thermal spray technology to industry."
- Merle L. Thorpe, President, Thorpe Thermal Technologies Inc., Concord, New Hampshire. "For pioneering contributions to the successful commercialization of important thermal spray process and materials technologies; development of new applications and markets; and a strong entrepreneurial spirit which has contributed significantly to the growth of the thermal spray industry."

The question that begs to be asked is "Are there too many awards?" The facts are that the total number of thermal spray awards has decreased every year over the past 4 years; for example there were 16 awards in 1993 compared with 9 in 1994 in the same two categories in an expanded field of potential contributions. Thus, it is becoming quite prestigious to be honored in this fashion! The purpose of these awards is to not only confer "official peer-reviewed honor" upon the awardee; but to nurture and encourage truly excellent contributions to the world of thermal spray. It is also important to note that acknowledgment, *per se*, is often quite valuable from the perspective of the professional career of the awardees since unbiased peer review, outside their own organization, lends support to their research and engineering accomplishments.

The Chairman of the Awards Committee (C.C.Berndt, Stony Brook) of the Thermal Spray Society (TSS) recognizes that there is further room for improvement. For example, is it possible (or even desirable) for the TSS to replicate in some fashion or form the **Student Scholarships** that have been instituted by the International Thermal Spray Association; or is there a need to have a **Met-allographic Competition** as there has been occasionally in the past?

The Awards Committee of the TSS is very open to any suggestions or comments concerning their rationale or procedures and invite such contributions to be sent to C.C.Berndt of Stony Brook for discussion.

#### C.C. Berndt

The Thermal Spray Laboratory  
Department of Materials Science and Engineering  
SUNY at Stony Brook  
Stony Brook, NY 11794-2275

Permission to publish

C.C.Berndt, "The Significance of Thermal Spray Awards", JTST (1994) 3[3] 244.

With kind permission from Springer Science+Business Media. The complete article (text, figures, tables and references) have been kindly reproduced.



# Commentary

## Conferences and Meetings - Who's Holding the Gun?



More about the title of this commentary later on - but first some background.

Twenty years ago it was reasonably straight forward for a scientist or engineer to decide THE meeting to attend if their interests lay in thermal spray - it was the International Metal Spraying Conference that was held every 3 or 4 years. The last International Metal Spraying Conference, the 7th, was convened in 1973 in London. This conference then underwent a name change so that the series of ITSC's (International Thermal Spray Conferences) kicked off in 1976 as the 8th ITSC in Miami. Of course, a parallel series of meetings, the International Symposium on Plasma Chemistry (ISPC), also have an extended history of fundamental science which is related to thermal sprayers.

Other conferences evolved in the 1970's, such as the International Conference on Metallurgical Coatings (ICMC), organized by the Vacuum Metallurgy Division of The American Vacuum Society (AVS). These meetings were co-sponsored by what was then known as The American Society for Metals; the forerunner of ASM International. The National Thermal Spray Conferences (NTSC's) evolved in 1981, initially under the umbrella of the American Welding Society but since 1984 under the sponsorship of ASM International. And in parallel there are "international/national" meetings in Germany (sponsored by the DVS) and Switzerland (sponsored

by Plasma Technik) every 3 or so years. Then, there are seminars (for instance, the Gorham meetings), conference sessions (for instance, at Materials Week, the National Association for Corrosion Engineers meetings, and the Cocoa Beach American Ceramic Society meeting), industrial meetings (for example, The International Thermal Spraying Association convention) and workshops (at the National Institute for Standards and Technology and Brookhaven National Laboratory).

The list of meetings that could be attended in areas that address thermal spray is quite large - conservatively 3 or 4 meetings per year rather than the once per 3 years are several decades ago. Of course this plethora of conventions is good news not only for the professional societies that rely on the income to provide member services and benefits; for also, more importantly, the industry and microcosm of thermal spray. Thermal spray has clearly emerged as an enabling technology for the manufacturing sector, for the transportation industry, and infrastructure, chemical processing, biomedical and many other applied engineering fields.

So, the aspect of "conferences and meetings" has been addressed but "who's holding the gun?" refers to a fundamental boundary condition which relates publishing, presenting, travel budgets and new information; i.e., it is difficult for personnel to attend every meeting; yet generate new data. Thus, scientists and engineers must differentiate and prioritize (as well as justify to their upper management) the meetings that they attend. It is clear that the NTSC's have developed a niche market in North America by being held every year. Likewise other conferences will be attractive due to their locality and convenience or by being held in conjunction with related subjects; for example, by being part of a ceramics, biomedical or coatings meeting.

So the point of this commentary is not to lament the choices that need to be made each year concerning "What meeting to attend?" since no such opportunities existed in the not so recent past, but to consider the wide range of available conferences as an indicator of the burgeoning field of thermal spray.

To add to this choice of meetings this commentary announces a "NASA/NIST/DOE THERMAL BARRIER COATINGS WORKSHOP" to be held March 28-29, 1995 in Cleveland, Ohio.

Thermal Barrier Coatings (TBC) have been the target of intense interest as one of few viable near term means to fill the gap between current metallic and future ceramic components. The objectives of the two day workshop are to assess the state of TBC knowledge, the goals for TBC performance for current and next generation engines and also to identify critical gaps in the knowledge that must be addressed to reach desired TBC performance levels. To achieve these objectives, the following topics will be addressed for the application areas of aircraft turbines, land and marine based turbines and diesel engines:

- Rationale for TBC use, a design perspective
- Current NASA/NIST/DOE Program Areas
- Engine Experience and Failure Modes for current TBC applications
- Current and alternate processing
- TBC Properties: Thermal, Physical and Mechanical properties of all constituents of the TBC
- Modeling: Life Prediction, Mechanical and Thermal Modeling
- Characterization and Standards:

including NDE and possible test standards for TBC's • TBC Effects on Component Durability: Creep, Oxidation, Fatigue. The workshop will include discussion periods for each session.

A detailed agenda and registration form will be mailed at a later date. The tentative registration fee for the workshop is approximately \$80. Since it is inevitable that interested people have been missed on the mailing list, please pass this information along to others that may be interested.

The 1995 Thermal Barrier Coatings Workshop Organizing Committee consists of Bill Brindley, John Goedjen (both of NASA Lewis Research Center), Sandy Dapkunas (NIST) and Woo Lee (Oak Ridge National Laboratory). For more information contact: Bill Brindley (NASA-Lewis MS 24-1, Cleveland, OH 44135) John Goedjen

**Christopher C. Berndt**  
The Thermal Spray Laboratory  
Department of Materials Science and Engineering  
SUNY at Stony Brook  
Stony Brook, NY 11794-2275

Permission to publish

C.C. Berndt, "Who's Holding The Gun?", J. Thermal Spray Technology, 4[1] (1994) 331-332.

With kind permission from Springer Science+Business Media. The complete article (text, figures, tables and references) have been kindly reproduced.



# Editorial



## **“Standardize and Deliver”**

This headline appeared recently in the press. Can you imagine a popular global newspaper paying any attention to the subject of “standards”, at least in the sense that it concerns engineering and manufacturing? Read on. This is becoming the hot topic, especially for thermal spray and the commercial sector.

“The whole point of standards is that you should not have to think about them. Such considerations as credit cards being of the uniform shape, size and numbering convention to allow them to be used anywhere in the world should be taken care of by somebody else. And, fortunately, somebody else has done so.” So writes Claire Gooding in the Survey section of the *Financial Times* (October, Friday 13, 1995, page 1).

### **Specifications versus Standards**

But first it is important to point out that “c” are not standards. A specification will, for example, state that the elastic modulus for a particular material will be of such a value or lie between some well defined limits under certain conditions. A standard (at least as how it is defined within this article) will state the method by which the measurement was obtained, for example, by using a tensometer that has been calibrated with respect to load and displacement to within certain accuracy. Thus, it is probably more logical to refer to “standard methods”.

### **The Advocacy for Standards**

So what do standard methods mean with regard to the thermal spray community? To quote the *Financial Times* again: “Standards are more important than they have ever been, in a world economy that increasingly promotes the idea of consumer choice. Choice is included in the concept of consumer power, but so is the principle that the choice should be a safe one.” Therefore, standard methods will allow a common lexicon to develop so that specifications can be clearly stated with, presumably, no ambiguity. For instance, a customer will be able to specify that a material have a defined hardness, measured according to a certain standard test method, and be assured that the material, regardless of where it was manufactured, meets his requirements.

### **The Prosecution Against Standards**

The writer of this editorial is not so certain of arguments against test methods. But some could be:

- “This will add cost to the product that I sell since I now need to use new test methods.”
- “It is unreasonable to subject my company to these new test methods since we have been very satisfied with our present techniques for many years.”
- “These new test methods impose yet another regulation upon my company.”
- and others—(Readers: Please let the author know of any other points that you would like to raise!)

The above arguments of “additional cost!”, “my customers and I are already happy with our present test methods” and “what—more regulation?!” are non-trivial and can often be argued forcibly on pragmatic terms (rather than on the basis of emotive arguments). For example, consider the conversion of the USA to the metric system. Every reader probably agrees that this has been a dismal failure.

## What are the Important Standards and Who “Carries the Torch”?

A list of standards that need to be developed for thermal spray materials includes the following as a bare minimum:

- Bond strength testing
- Hardness testing
- Thermal expansion testing
- Measurement of roughness
- Measurement of porosity

The organizations presently involved in this type of activity for thermal spray materials include, but are not restricted to, ASM International, the American Society for Testing Materials (ASTM), the American Welding Society (AWS), the International Standards Organization (ISO), the National Association of Corrosion Engineers (NACE) and the National Institute for Standards and Technology (NIST). As well, the larger companies, in their quest to maintain rigid tolerances on their products, often have internal standard test methods which eventually pervade the job shops.

It quickly becomes apparent that no single organization can or should champion the cause of “standards” or “standard methods” for the thermal spray community. There is just so much work needed. What really is needed is a “call to arms” of all the interested parties; i.e., industry, national labs, and universities, so that a concerted and unified approach can be made. After all, the formulation of such essential engineering needs will benefit all of the thermal spray society. Please write to the Editor if you would like to join in an activity that addresses the subject content of this editorial.

**Christopher C. Berndt**  
SUNY at Stony Brook

**Editor**  
*Journal of Thermal Spray Technology*

Permission to publish

C.C. Berndt, "Standardize And Deliver", JTST, 5[1] (1996) 2-3.

With kind permission from Springer Science+Business Media. The complete article (text, figures, tables and references) have been kindly reproduced.

# Commentary



Roland D. Seals



Christopher C. Berndt

## The Rationale for a *JTST* Award for the Best Scientific Paper\*

From its very inception in 1991, *JTST* has striven to be a leader. Of course, the prime mission of *JTST* is to attract the best peer-reviewed papers and the most up-to-date thermal spray news from around the world. However, another very important aspect of *JTST* is to promote thermal spray and provide a feedback mechanism to potential *JTST* authors that lets them know that their contributions are valued. Thus, the Editorial Committee of *JTST* instituted a "Best Paper Award" in 1992. The intent has been to honor those authors who contribute their time and energies into making *JTST* a success. An important by-product of this process is that peer recognition can be a professional boost to the recipient(s) as well as acknowledgment of their institutions and to their funding agencies. Thus, a *JTST* Best Paper Award can make a substantial difference.

However, behind the scenes of the *JTST* Best Paper Award lies a strict and rigorous process that takes several months of effort by a dedicated Panel of Judges. The intent of this Commentary is to inform *JTST* readers of this process so that they can understand the effort that is needed to institutionalize this Award.

The entire judging process of Volume 1 of *JTST* was administered by the Editor of *JTST*. However, it became apparent that this was an untenable position for the Editor. Thereafter, Dr. Richard Nieser (Sandia National Laboratories) volunteered to chair the *JTST* Best Paper Award Committee, and after a stint of four years (1993-1996) he was succeeded by Dr. Roland Seals (Oak Ridge National Laboratory). The Chairman of this Committee has the job of selecting a balanced team of judges from segments of academia, industry, and government laboratories. The *JTST* Awards Chairman acts autonomously from any other *JTST* and ASM-TSS committees in order to preserve absolute confidentiality of the process.

The box below details some of the broad aspects of the 1997 awards process and the responsibilities of the Panel of Judges. This protocol was formulated, refined, and fine-tuned by C.C. Berndt, R.A. Nieser (see *JTST*, Vol 6 (No. 4), 1997, p 408 for further comments), and R.D. Seals over the last seven years. In passing, it can be noted that this process incorporates elements that have been instituted for the NTSC, ITSC, and UTSC conferences that are organized by ASM International.

### The *JTST* Awards Process and Guidelines for Judges

**Objective:** The Panel will judge the best articles that have been published in Volume 6 (1997) of *JTST*. It is expected that one, or perhaps two, papers of the 42 will receive awards. The award(s) will be presented at ITSC '98 in Nice, France, in May 1998.

**Duties:** The judging will be conducted in two phases. In the first phase, the Judges will be asked to review the articles in one of four groups of papers in Volume 6. The Judges will select the three best papers and rank them in descending order (with 1 being the best). Once the Phase I results have been collated and assessed by the *JTST* Awards Chairman, between four and eight articles will be chosen for the Phase II review. In Phase II, the Judges will be asked to review these four to eight articles, rank them in descending order, and return the results to the Chairman. The Panel consists of 10 judges and, thus, the awards will be the consensus of a committee decision.

**Guidelines for Judges:** You may choose what you believe to be the top three papers in the issue assigned to you by any means you choose; however, the following approach has been used previously for award determinations and has proven to be quite helpful. Under this approach, each paper is considered by itself on the following merits:

1. *Scientific and Engineering Merit.* What is your evaluation of the merit of the work? Are the experiments well-thought out; is the discussion detailed; are the conclusions correct and detailed? Are the experiments logical and complete? How much impact does the work have on our current understanding and practices?
2. *Originality.* Assess the originality of the work. Is this the first time you have seen the reporting of the work; is this an original interpretation of the data; do the results and discussion represent new ideas?
3. *Presentation Style.* Is the paper clearly written (grammar and format), are the figures and tables well presented; is the referencing correct? Is there a clear statement of objectives; and does the paper fulfill these?
4. *Discretionary.* If you think that any of the above aspects deserve extra credit, then allot further points as you see fit. Or your own category can be added.

\*Also see the Editorial of *JTST*, Vol 3 (No. 3), 1994

The 42 reviewed papers in Volume 6 were divided among four subcommittee groups, judged, and evaluated on the above merits. From these 42 papers, the best 12 papers were selected for a Phase II evaluation. The following five papers (presented in alphabetical order) were evaluated as the top papers: Brindley, p 85; Dallaire, p 456; Jones, p 77; Korpiola, p 469; and Tamura, p 463. The Best Paper Award for the 1997 Volume 6 of *JTST* was that of W.J. Brindley et al., NASA Research Center, Cleveland, OH, for his paper entitled, "Properties of Plasma-Sprayed Bond Coats." Some of the judges' comments on these papers are listed below.

*Comments on Brindley's paper:*

- "Excellent comparison of real, industrial coatings. This paper adds insight to understanding how these complex TBC systems behave in use."
- "A review of fundamental work on determining critical system parameters for TBC life."
- "My reason for selecting Brindley's paper is that he did an excellent job of describing the background and history of thermal barriers, the issues involved in the SYSTEM of a thermal barrier coating, and provided convincing experimental data to support the behavior of current thermal barrier coatings."
- "Good presentation and approach, good test sequence, and very useful conclusions and relationships."
- "Addressed an overlooked issue in TBC. He gave us a new direction for bond coat development."

*Comments on Dallaire's paper:*

- "This is a new finding with good metallurgy that allows understanding to make systematic future improvements. It is important to see this kind of careful materials science applied to a mature technology like arc spray, and I feel it is one of the missions of the *Journal* to promote rigorous science and technology of thermal spray."
- "Very thorough analysis that can lead to new coating materials."

*Comments on Jones' paper:*

- "The figures and chemical equations are a great help in the understanding of TBC degradation. I think much emphasis is placed on the heat and thermal shock that cause spallation, when the chemical degradation of these materials is also very important."
- "The paper by Jones was quite good also. Here he presented an educational background of ceramic science pertaining to the stabilized zirconia systems. Moreover, he provided a clear, succinct description of causes and problems of hot corrosion in TBC's and offered several good suggestions for mitigating this problem."
- "Excellent research on the chemistry of an important thermal spray application area."
- "Jones did an excellent job of researching other peoples works and tying them together with his own findings. He also wrote in a way that was easy to follow his logic."

*Comments on Korpiola's paper:*

- "Korpiola has expanded the basic fundamentals of HVOF spraying. He applied simple equations to validate his assumptions."

*Comments on Tamura's paper:*

- "Innovative, fresh ideas, nice presentation."
- "Great new innovative approach to coating application. Great to see people looking outside the box."

A general comment on these papers was that "In my opinion, these papers represent, in depth, critical studies of important phenomena. Their results help further the science and technology of thermal spraying."

The recipients of this prestigious award since its inception are listed below. Note that in the first year there were four awards presented, but then this was cut back to a single award per year.

***JTST*, Vol 1, 1992 Plaques of Excellence**

"Diagnostics of Thermal Spraying Plasma Jets," P. Fauchais, J.F. Coudert, M. Vardelle, A. Vardelle, and A. Denoirjean" (Laboratoire de Ceramique Nouvelles, University of Limoges, France)

"Structure/Property Relationships of Sintered and Thermally Sprayed WC-Co," S.F. Wayne (GTE Laboratories Inc.) and S. Sampath (Osram Sylvania Inc.)

***JTST*, Vol 1, 1992 Certificates of Merit**

"Significance of Quenching Stress in the Cohesion and Adhesion of Thermally Sprayed Coatings," S. Kuroda, T. Fukushima, and K. Kitahara (National Research Institute for Metals, Japan)

"Thermal Spray Shape Deposition," L.E. Weiss, F.B. Pronz, D.A. Adams, and D.P. Siewiorek (Carnegie Mellon University)

"Flattening and Solidification of Thermally Sprayed Particles," C. Moreau, P. Cielo, and M. Lamotagne (National Research Council of Canada)



**JTST, Vol 2, 1993 Best Paper Award**

"Spray Parameters and Particle Behavior Relationships During Plasma Spraying," M. Vardelle, A. Vardelle, and P. Fauchais (Laboratoire de Ceramique Nouvelles, University of Limoges, France)

**JTST, Vol 3, 1994 Best Paper Award** (for a set of two papers published by the same authors)

"Effects of Coating Thickness and Residual Stresses on the Bond Strength of ASTM C633-79 Thermal Spray Coating Test Specimens," and "Through-Thickness Residual Stress Evaluations for Several Industrial Thermal Spray Coatings Using a Modified Layer-Removal Method," D.J. Greving, E.F. Rybicki, and J.R. Shadley (The University of Tulsa)

**JTST, Vol 4, 1995 Best Paper Award**

"Microstructure Evolution During Reactive Plasma Spraying of MoSi<sub>2</sub> with Methane," X. Liang, E.J. Lavernia, and J. Wolfenstine (University of California at Irvine ) and A. Sickinger (Sulzer-Metco)

**JTST, Vol 5, 1996 Best Paper Award**

"Residual Stresses in Thermal Spray Coatings and Their Effect on Interfacial Adhesion," T.W. Clyne and S. Gill (Cambridge University, U.K.)

**JTST, Vol 6, 1997 Best Paper Award**

"Properties of Plasma-Sprayed Bond Coats," W.J. Brindley (NASA-Lewis Research Center)

**Roland D. Seals**

Oak Ridge National Laboratory

**Christopher C. Berndt**

SUNY at Stony Brook

Permission to publish

R. Seals and C.C. Berndt, "Rationale for a JTST Award for the Best Scientific Paper", JTST, 8[1] (1999) 3-5.

With kind permission from Springer Science+Business Media. The complete article (text, figures, tables and references) have been kindly reproduced.



# Commentary

## How Do We Market JTST 10[1]

### Introduction

Depending on their perspective and background, some might say that JTST is not marketed very well at all! This comment can be contrasted with that of a pure scientist who might say that there is no room for marketing of a journal or within a journal. Clearly, there is some stance between these extremes that would benefit the majority of JTST subscribers.

Let's first look at the facts concerning JTST. This volume marks 10 years of production. Each year comprises about 550 pages of thermal spray science and engineering. There are about 50 peer-reviewed articles published per year, as well as thermal spray news and many miscellaneous features. Special "guest columns" have been added over time. As the Editor, I feel that we have a complete and technically diverse journal that encompasses all aspects of thermal spray.

The journal has grown with the technology and will continue to so. A number of volunteers help me with several sections of JTST, and their assistance and reliability is extremely valuable in enabling me to focus on other, more developmental aspects of the journal. I also want to remind readers that there are several key players at ASM International (Materials Park, Ohio) who have very professionally executed the production process of JTST.

Any journal with vitality requires a continuous influx of manuscripts and such a very healthy flow has been maintained over the lifetime of the journal. There are strong reasons to expect that the journal will continue to flourish in the future. I would encourage any potential author to consider JTST as the place to publish his or her work. Authors receive a thorough review and timely publication. I am also always looking for reviewers, and if you can commit to this task, then please let me know immediately. Over the past 3 months the editorial office has instituted a system whereby manuscripts can be received via e-mail attachments. This journal address is [REDACTED]. This site has already proven very convenient for authors, and, in the longer term, it will also be of immense value to the Editor.

The subscription base for JTST lies at about 500 and herein lies the opportunity addressed by the title of this editorial. JTST still needs to grow with respect to our subscription base to maintain financial viability. I am often amazed at how the growth of the global thermal spray arena has *not* also been reflected in a proportionate growth of JTST! Please keep this thought in mind and try to be an active protagonist in attracting new subscriptions. Encourage your colleagues to subscribe, ensure that your libraries have subscriptions to JTST, and consider giving JTST subscriptions to your customers as an indication of your respect.

### The JTST Marketing Committee

Over the years the Editorial Committee, under the leadership of its chairman, has actively discussed how to grow the journal. The current chairman, Prof. Heberlein, has proactively recruited a group of industrialists to explore avenues whereby JTST can open new doors. Professor Heberlein has formulated a "JTST Marketing Committee" and he has crafted the following Mission Statement: "To establish a roadmap for making JTST financially self-supporting as well as contribute to the financial support of ASM."

Two prime tasks have been identified.

*Task 1: Determine ways to increase subscriptions.*

- (a) Identify market segments that are underrepresented in the subscriber list (i.e., among hardware and consumable suppliers, spray shops, major industrial laboratories, national laboratories, academic laboratories).
- (b) Identify geographical areas that are underrepresented in the subscriber list.
- (c) Identify reasons for the lack of subscriptions in the identified market segments. For example, consider:



The members of the JTST Marketing Committee are Mr. Peter Hanneforth, Vice President Marketing, Sulzer; Mr. Richard P. Mason, Vice President, Sales and Marketing, Ametek; and Mr. William J. Lenling, Materials Engineer, VP, Thermal Spray Technologies Inc.

- (1) Lack of awareness of the journal.
- (2) Imbalanced content, that i.e., are the different subject areas such as calendar, various front matter items, patent information, reviewed papers, abstracts appropriately proportioned within the journal?
- (d) Devise a promotional approach for increasing awareness of journal.
- (e) Recommend changes in content that are likely to lead to increased subscriptions.

*Task 2: Evaluate additional sources of revenue*

- (a) Find companies willing to advertise and find ways to make advertising attractive.

**In Summary:** The *Journal of Thermal Spray Technology* is technically sufficient yet I feel the need to caution subscribers that JTST needs your assistance with regard to the "big financial picture." Any help that you can provide with increasing our subscription base will help secure our long-term future. Give this editorial some very serious thought and see how "you can help JTST." If you have any ideas or wish to discuss any particular aspects of JTST, then have no hesitation in contacting me. Thus, we need to get on top of any potential problems that might influence JTST before they actually arrive. Help me do this so that we have a healthy, vibrant, and successful journal.

If you have any new ideas or wish to comment on old ones for JTST, please contact the editor (C.C. Berndt), the chairman of the JTST Editorial Committee (J.V. Heberlein), or the members of the JTST Marketing Committee who are listed below. I will always endeavor to respond to your requests and concepts quickly. The three members of the blue-ribbon JTST Marketing Committee are:

- Mr. William J. Lenling, Materials Engineer, VP, Thermal Spray Technologies Inc.; [REDACTED]
- Mr. Richard P. Mason, Vice President, Sales and Marketing, Ametek, Specialty Metal Products Division; [REDACTED]
- Mr. Peter Hanneforth, Vice President Marketing, Sulzer Metco (US) Inc.; [REDACTED]

**Christopher C. Berndt, Ph.D.**  
Professor / Editor  
SUNY at Stony Brook  
Department of Materials Science and Engineering  
306 Old Engineering  
Stony Brook, NY 11794-2275

[REDACTED]  
<http://DOL1.eng.sunysb.edu/tsl/berndt1.html>

Permission to publish

C.C. Berndt, "How do we Market JTST", JTST, 10 (2001) 3-4.

With kind permission from Springer Science+Business Media. The complete article (text, figures, tables and references) have been kindly reproduced.



# Commentary

## A Message From The President of TSS

### Join Us In Orlando As We Bring Thermal Spray Into the 21<sup>st</sup> Century

*"ITSC 2003 will be the biggest event in the history of thermal spray. Do not miss it!"*

We are pleased to invite you, the thermal spray experts, engineers and scientists, as well as those people who are new to thermal spray, to our first event of the new millennium in the Americas. Experienced as well as novice practitioners will gather to learn the latest information and what is on the near horizon with respect to this dynamic technology.

We anticipate more than 2000 delegates representing over 30 countries around the world to join us in wonderful Orlando, Fla., the recreation capital of the world. This event is jointly sponsored by the ASM Thermal Spray Society (TSS), the German Welding Society (DVS), and the International Institute of Welding (IIW).

There will be in excess of 370 presentations. These will be led by an exceptional Plenary Session comprised of (1) Dr. Bruno Walser, president, Markets and Technology, Sulzer Ltd., Switzerland; (2) Prof. Teruo Kishi, president, National Institute for Materials Science, Japan; and Dr. Ann Stevens, vice president, North American Operations, Ford Motor Company, USA.

Of course, the Exhibition of thermal spray products is a mainstay for this important series of ITSCs. The conference success is closely associated with an exposition in which more than 45 companies from 15 countries will participate. There is no doubt that this highly successful ITSC forum is oriented towards the practical needs of participants since it is highly supported by companies within the thermal spray economy. It also provides attendees with up-to-date information about current developments in the field of thermal spray and related technology.

Within the conference there will be seven highly focused symposia: (1) Corrosion and Wear Protective Coatings, (2) Thermal Spraying of Polymers, (3) Sensors and Controls, (4) Thermal Barrier and Environmental Barrier Coatings, (5) High Velocity Oxygen Fuel Processes, (6) Cold Spray Technology, and (7) Gas Turbine Repair. Additional symposia, designed for the generalist yet appropriate for the expert, will focus on (1) Feedstocks and Novel Materials, (2) Science and Applications of Thermal Spray, and (3) Equipment and Processes. These ten symposia will coexist within the framework of four parallel sessions; thus, there will be ample opportunity for attendees to "do it all" over the four-day period of the meeting. We will also have several poster sessions where attendees can speak one-on-one with authors, make important business connections, and network with experts. And finally, there will be several pre-conference workshops and short courses on thermal spray, as well as industrial tours.

There are not only numerous authors of presentations and poster sessions who will contribute to ITSC-2003, but also the experts who make themselves available as the chairmen of discussions. ASM-TSS, DVS, and IIW also extend an invitation to experts from all over the world to take part in ITSC 2003. You will have the opportunity to network and exchange your experience and knowledge so that thermal spray can flourish over the next century with additional new market segments and commercial opportunities.

ITSC 2003 is an opportunity not to be missed. The Program Committee and organizers are proud to have worked extremely hard in developing an outstanding program that is a full four-day event.

*Join us for the biggest TS event in history that will allow you to prosper!*

**Christopher C. Berndt**  
Stony Brook University, NY-USA  
President, ASM Thermal Spray Society



Permission to publish

C.C. Berndt, "Editorial: Join us in Orlando as we bring Thermal Spray into the 21st Century", JTST (2002) 11[4] 431.

With kind permission from Springer Science+Business Media. The complete article (text, figures, tables and references) have been kindly reproduced.

# Editorial

## The Globalization of JTST: A Forum for a World Wide Network

It is worthwhile occasionally to be introspective and, with this thoughtful process in mind, let us ask a fundamental question: "Whose interests does JTST serve?"

A partial answer is found on the inside front cover of every issue of JTST and appears as its mission statement:

*"The Journal of Thermal Spray Technology publishes contributions on all aspects — fundamental and practical — of thermal spray science including processes, feedstock manufacture, testing, and characterization. As the primary vehicle for thermal spray information transfer, its mission is to synergize the rapidly advancing thermal spray industry and related industries by presenting research and development efforts leading to advancements in implementable engineering applications of the technology".*

This mission statement is reconsidered every year by the Editorial Committee and often tweaked and adjusted to reflect the changing times.

Another conversation can also take place and address the community that JTST may benefit; keeping in mind that this is a symbiotic, active relationship with JTST also playing a major role in the community. Thus, JTST is published in the USA, yet, just like thermal spray technology, it is international in scope and stature. Various business studies have estimated that the total annual worldwide market for thermal spray is \$2.5 billion US dollars with the market share being roughly equally divided between North America, the PacRim region, and Europe. This line of reasoning also parlays into an economic dimension for JTST as well as its important scientific/technical ones.

From the economic point of view it is obvious (we trust!) that those who invest into any venture have a decisive voice in determining the policy of that venture; whether it be an industrial product or a peer-reviewed journal. Therefore, if the thermal spray community wants to have a decisive voice in the journal, it is reasonable to request financial input, for instance, a small contribution while paying the TSS yearly fee. In the same frame of mind, it is reasonable to ask authors who publish in JTST to also contribute financially since they benefit significantly from the peer review and publishing process. The editorial in JTST 10(4) detailed the rationale for this JTST policy.

Other than authors, ASM International, and TSS, let us ask again: "Whose interests does JTST serve?" The answer boils down fundamentally to a truly international thermal spray community. Taking the recent ITSC 2002 in Essen as a reference point, we note that there were participants from virtually every continent. Therefore, JTST serves a vast community of engineers, scientists, and technologists due to this globalization of thermal spray. A basic set of rules may be formalized, such as, for example (and this list is not intended to be exhaustive):

- applications of thermal spray technology.
- JTST will promote international exchange of ideas and scientific/technical knowledge JTST will promote thermal spray technology around the world.
- JTST will promote new in the area of thermal spray.
- JTST will elevate the understanding of thermal spray processes.
- JTST will be a vehicle that facilitates thermal spray networks to grow.

One way to promote the globalization of thermal spray is to encourage news from various regions, for example:

- News from Africa, South America, and Australia/New Zealand
- News from Asia
- News from Europe
- News from North America

The proposal is that each of these Regional News contributions would have up to three pages in every volume of JTST. Thus, JTST would now have the opportunity of figuratively and practically covering the whole world over the course of the four annual issues. This



Lech Pawlowski



Christopher C. Berndt

format and plan not only allows the newsworthy items to surface, but also does not place the corresponding contributor under stress in meeting multiple deadlines per year.

And now — the bottom line — do you want to volunteer yourself or a colleague to commit to be the champion for your part of the world as a JTST Corresponding Contributor? Do you want to have the opportunity to help “globalize thermal spray”? If so, then please contact either the editor or associate editor of JTST whose contact details appear below.

**Lech Pawlowski**  
Associate Editor, JTST

**Christopher C. Berndt**  
Editor, JTST

Permission to publish

C.C. Berndt, "L. Pawlowski and C.C. Berndt, "The Globalization of JTST: A Forum for a World Wide Network", JTST, 12 (2003) 3-4.

With kind permission from Springer Science+Business Media. The complete article (text, figures, tables and references) have been kindly reproduced.



# Commentary

## Thermal Spray: Preserving 100 Years Of Technology

### Why Choose 2006 As The First 100 Years?

The Schoop Patent that concerns the origins of thermal spray (TS) can be traced back to 1912 (for example: "Metal Plating with the Air Brush," *Scientific American*, Vol 1, 1913, p 346). A tradition exists where chronological anniversaries are recognized by an appropriate public observance. Such an observance recognizes an important historical event and allows a retrospective account of that event. In many instances no specific date is selected, but rather a time frame that may span several days, a few months, or an entire year, since the magnitude of the event is such that its anniversary needs to be placed into the context of its evolution.

The observance of the first 100 years of thermal spray falls under a very broad time frame because the early history of this technology is clouded by lack of referred documentation. The early practitioners and inventors of thermal spray were probably unaware that their efforts would spawn multimillion dollar industries across many technological sectors. It is probably safe to assume that these early workers were more interested in preserving jobs rather than history. As well, a certain amount of secrecy would have given these early technologists a commercial edge.

It is certainly reasonable to question why the year 2006 could be selected as the first century of TS, and the following arguments are posed to justify this assertion. It is documented that Schoop (the proclaimed "father of TS" according to the book by Ballard) was publishing on that topic in 1910. It is fair to comment that the precursor work that led to this patent commenced from 6 to 10 years before being issued. Thus, it is suggested that Schoop was working on the ideas and concepts associated with TS in about 1906. Regardless of the exact date and timing of Schoop's efforts, there is a convincing argument that the time frame of 2006-2010 can be declared as the period during which "The First Century of Thermal Spray" can be celebrated.

It can be further noted that an 1882 German Patent (number 24,460) illustrates the elementary principles of thermal spray

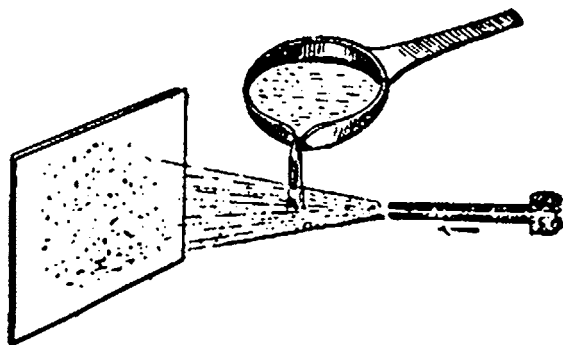


**Fig. 1** The basic principles of thermal spray. Taken from Ref 1, p 1 and, in turn, attributed to an 1882 German patent



**Christopher C. Berndt**



**Ghislain Montavon**

(Fig. 1). Therefore, the statement concerning "The First Century of Thermal Spray," although used with some reserve and caution, is an appropriate date that can serve the purpose of promoting thermal spray within a global context.

### Time Capsules: Their Meaning and Purpose

The First Century of Thermal Spray is an important historical event that is worthy of recognition. For example, this present document is a vehicle that intends to promote discussion concerning a long-term plan for recording important historical events that relate directly to TS. Another aspect of this effort is that such an introspective account can lead to a prospective foretelling of future events; that is, there is the opportunity for an analysis of important future events that will steer TS in the near (10 to 15 years in the future) and long (more than 20 years) terms.

The discussion concerning "time capsules" is important because it helps formulation of a course of action that not only recognizes the past, but can be used to promote technology. The discussion below, cleaved primarily from the literature (Ref 2), is used as the backdrop for future actions.

### What is a Time Capsule?

According to Ref 2:

A time capsule is a historic cache of goods and/or information, usually intended as a method of communication with people in the future. Time capsules are sometimes created and buried with much hoopla during celebrations such as a World Fair, cornerstone laying for a building or other events. They can also be unintended caches such as at Pompeii. The term "time capsule" has been in use since about 1937, but the idea is as old as the earliest human civilizations in Mesopotamia.

They can generally be classified into four types. Intentional

and unintentional (such as Pompeii), and those scheduled for retrieval on a certain date (often 10, 100, or 1000 years later), and those not.

The concept of time capsules is not recent. In the *Epic of Gilgamesh*, humanity's earliest literary work, it began with instructions on how to find a box of copper inside a foundation stone in the great walls of Uruk, and in the box was Gilgamesh's tale, written on lapis tablet. There were other time capsules 5000 years ago as vaults of artifacts hidden inside the walls of Mesopotamian cities.

In 1937, during preparations for the 1939 New York World's Fair, someone suggested burying a "time bomb" for 5000 years, a more discreet name of "time capsule" was suggested, and the name has stuck since. The 1939 New York World's Fair time capsule was created by Westinghouse as part of their exhibit. It measured 90", weighed 800 pounds, and had an interior diameter of 6.5 inches. Westinghouse named the nickel and silver alloy Cupaloy, claiming it was harder than steel.

The original capsule was followed in 1963 by a second capsule at the same site, but 10 feet to the north of the original. Both capsules are buried 50 feet below Flushing Meadows Park, site of the Fair. The first capsule contained everyday items such as a spool of thread and doll, but also a Book of Record, a vial of staple food crop seeds, and a microscope. Microfilm spools condensed the contents of a Sears Roebuck catalog, dictionary, almanac, and other texts. An RKO Pathe Pictures newsreel, 15 minutes in length, is also included.

### ***The International Time Capsule Society (ITCS)***

Reference 3 explains: "The International Time Capsule Society is an organization dedicated to tracking the world's time capsules to ensure that those that are created are not lost. Along with their database of time capsules, they have published a list of "most desired" time capsules that have been lost over the years, along with recommendations on how to build and seal a successful time capsule."

The ITCS is based at Oglethorpe University, home of the world's first successful time capsule, the Crypt of Civilization.

### ***Summary Comments***

A time capsule can have the following features:

- A time capsule can document the past or foretell the future.
- A time capsule can become lost.
- A time capsule can contain junk or decayed material.

### ***A Simple Example of a "Time Capsule"***

This brief section is an example (Ref 4) that suggests questions that should be addressed when a time capsule is being instigated. Although this is a sociological example, there is close affinity to the science, engineering, practice, and art of thermal spray.

- What do you want to tell people about yourself? What is important about your life and the times in which you live?
- What will be in the time capsule that will convey your image of your life and times? How large will it need to be?
- Will there be sculptures of humans? What size? What will they be wearing? What will they be doing?
- Will there be objects of some aspect of the culture, for ex-

ample, art, musical instruments, modes of transportation, implements of war, consumer items and job-related tools?

This example, and the many in the previous section, indicate that it is quite important to ask the right questions when it comes to planning and implementing a time capsule. Therefore, it would probably not be of lasting value to pack a few thermal spray devices (torches), books, photos, and electronic media into a chest that is then stored at some site.

### ***Educating Younger and Future Generations in Technology***

The fundamental purposes of a time capsule are (in the opinions of these authors) (a) to provide a historical framework for thermal spray and (b) to make some predictions about thermal spray for future generations.

Our audiences are several: (a) people who have made known, important contributions and who should be accorded some prominence and respect, (b) current generations who will be old-timers when the time capsule is opened, and (c) future generations, as yet unborn, who will inherit the legacies of the first two groups.

Within the framework as described above, it is pertinent to promote activities that will involve children and young adults: people less than 18 years in age. There are several websites (Ref 5) that describe how time capsules can be used as a tool to open up the awareness of school children. Thus, from the perspective of thermal spray, there are opportunities where the art and technology of thermal spray is used as a mechanism to educate children.

### ***They are the Big Names\*: An Oral History of Thermal Spraying***

In 2002, the authors of this article commenced a collaboration that intended to create a process that would allow an oral history of world famous sprayers to be collected. This is not a new idea; for example, "The Caltech Archives Oral History Project began in 1978 for the purpose of recording the personal memoirs of the distinguished scientists, teachers and administrators of the Institute. To date, approximately 170 interviews have been completed and most are open to readers in transcript form" (Ref 6). The "Oral Histories Online" project of Caltech commenced in Nov 2002 and brought selected interviews to the public in digital form.

Within the area of TS, there have been at least three documented interviews: with Ballard (Ref 7), with Meyer (Ref 8), and with Muehlberger (Ref 9). This section details a methodology whereby such oral histories would be systematically collected and stored. This is a component to the concept of a historical time capsule.

### ***Purpose***

The purpose of the interviews is:

- To establish an oral history of thermal spraying by collecting oral and possibly videotaped interviews of "Big Names" in thermal spraying
- To publish these interviews in the "gossip" pages of JTST under the label "They are the Big Names ... An oral history of thermal spraying"

---

\*The term "Big Names" is being used to denote "World Famous Sprayers."

- To use these resources in a Web-based training system on thermal spray science (*e-learning*)
- To publish these interviews completed by others of junior researchers and Ph.D. students in 2006 in a format to be defined, for example, in the ITSC2006 conference proceedings, in a special issue of JTST, in a specific book, etc.

### **Some Advice**

Oral history (Ref 10, 11) is an interview that records a person's recollection of experiences, thoughts, and feelings about a specific event or a period of time. Some requirements concerning the major step in interviewing a person, that is, planning the interview and conducting the interview, are discussed hereafter.

### **Planning the Interview**

- Write an introduction to your interview. Introduce yourself and recall the purpose of the interview.
- Write the questions related to the different categories depending on the information you collected. Use the resume of the person as well as your own knowledge and feeling.
- Write three warm-up questions.
- Confirm the date, hour, and place of the interview to the subject.

### **Conducting the Interview**

- Be on time and be prepared.
- Remind the subject that the interview will be recorded and/or videotaped.
- Provide time for the person to answer questions. Be patient when answers take a long time.
- Do not argue with or correct the subject.
- Begin the interview with the introduction you prepared.
- Develop your questions. If the subject strays from the topic, try to refocus by asking one of your prepared questions.

### **After the Interview**

- Send a thank you letter to the subject.
- Transcribe the interview tape extensively.
- Write an extended resume of the interview.

### **Interview Questions for Big Names**

#### *Warm-up questions:*

- When you were born?
- What is your actual occupation/position?
- Would you share with us your motto?

#### *Family background:*

- Could you tell us a little bit about your family background? In which family did you grow up?
- What is your educational background?

#### *Introduction to thermal spraying:*

- When were you involved for the first time in the field of thermal spraying?
- How were you involved?

- What aroused your interest most in this technique when discovering it?

#### *Your contribution:*

- In retrospect, what constitutes from your point of view your major contribution to the science and technology of thermal spraying?
- What is your major interest or quest today?

#### *Your vision:*

- Could you please describe the principle of thermal spraying in a few words?
- Could you please describe the structure of a thermal spray coating in a few words?
- Thermal spray coating and residual stresses: what is your vision?
- What are the three critical points that have to be managed and controlled in thermal spraying?

#### *Yesterday:*

- M.U. Schoop is the original inventor of thermal spraying in 1909 (i.e., use of an enthalpy of reaction for flame spraying) and 1911 (i.e., use of the electric power for arc spraying). Please quote what constitutes for you the two other major dates (and contributors) in the development of the technique?
- Thermal spraying finds applications in numerous industrial fields. What were from your point of view the two fields that gained most from thermal spray coatings?
- Numerous functionalities can be provided by thermal spray coatings. What were from your point of view the two major improvements provided by them?
- Multiple spray guns can be chosen to manufacture a thermal spray coating. What were from your point of view the two major developments of thermal spray tools?
- Reproducibility and robustness have always been elements of concern when considering thermal spray coatings. What has been from your point of view the development that permitted an increase in quality control of thermal spray coatings most?

#### *Today:*

- Thermal spray techniques come to maturity in years 2000. What are from your point of view the two major advantages provided today by thermal spray coatings, intrinsically and compared to other coatings manufactured via other routes?
- Thermal spray coatings cannot fulfill all the requirements. What are from your point of view the two major disadvantages provided by thermal spray coatings?
- Thermal spray science exhibits eminently a multidisciplinary character. Does the education of thermal spraying seem enough developed, especially in your country/area? If not, which specific points should be increased from your point of view?

#### *Tomorrow:*

- Thermal spray techniques have evolved since M.U. Schoop and will continue to evolve in the future. What will be from your point of view the perspectives over the next 10 years in terms of: (a) industrial applications, (b) process develop-

ments, (c) market developments, (d) research developments, and (e) education?

- Concerning thermal spray tools, what should be the major technical developments over the next 10 years, from your point of view?
- What should be the major new and innovative application(s) over the next 10 years, from your point of view?
- Which area(s) of the technique from your point of view will have to be drastically improved to fulfill new requirements (i.e., economical, technical, environmental, etc.)?
- What would constitute from your point of view THE major breakthrough of the technique?

*Last but not least:*

- Would you develop something specifically?

### Capturing the History and Future of Thermal Spray

The foregoing discussion suggests ways in which a “Thermal Spray Time Capsule” (aka “TSTC”) can be initiated. A multi-pronged approach would allow the TSTC to be developed over the coming decade.

The following components of the TSTC are proposed with participants from the TS community responsible for subtasks:

- Interview well-known personalities of TS, aka “the old timers,” while there is the opportunity. Honor these people in an appropriate fashion; for example, a special issue of JTST can be considered.
- Obtain their “recorded history” by interview through a standard set of question. The section “Some Advice” in this Commentary presents the start of “an interview manual” that can be compiled for these oral recordings to be obtained.
- Include the TSTC concept as the focus or theme for an ITSC of the future. The horizon time is of the order of 2010. The following activities could be planned under this theme:
  - ◆ Include a “Special Historical Session” at ITSC events that presents progress in materials, equipment, testing, and applications.
  - ◆ Create a special “museum of hardware” in a central location of the ITSC exhibition floor.
  - ◆ Compile a historical photo gallery of people in action throughout the ages.
  - ◆ Solicit presentations detailing company perspectives within the history of TS.
  - ◆ Include a session on TS that addresses “the future of TS.”
- Make up a classical time capsule of TS for insertion at ASM Headquarters, Materials Park, OH, for example. This major subtask would incorporate the contributions described previously. The major challenge that dictates the content of the TSTC is its physical form, dimensions, and construction material(s). The question concerning its physical location, record of its location, and the “dig up” or opening date are also a large subject for discussion.

### Summary and Concluding Remarks

Within this short commentary the authors have detailed the preservation of the historical base of thermal spray. The overarching intellectual framework is presented, as well examples of activities that can be trialed. The general areas of involvement are (a) a physical artifact that represents a time capsule for future generations of thermal spray technologists, (b) an oral history project concerning the detailed recording of people who have been associated with thermal spray, and (c) a special event, to be held in conjunction with an international thermal spray conference, that memorializes thermal spray history.

The aforementioned projects are collectively identified as the thermal spray time capsule, TSTC, and they have various time scales for implementation. These long-term initiatives are based on the good will of volunteer contributors who consider this project to be fundamental to the heritage of thermal spray so that future generations have a strong sense of identity. From this perspective, every contribution is considered to be important. The authors consider that the oral history project deserves some prominence since there is a time scale that is related to the ability to interview people who may be unavailable in the near future.

The TSTC project will need both strong engagement and leadership from the TS community so that the management, organization, and promotion of this activity can progress. This support from the TS community is fundamental and, with this in mind, the authors of this article welcome remarks, comments, and suggestions.

### References

1. T.H. Turner and N.F. Budgen, *Metal Spraying. The Origin, Development, and Applications of the Metal-Spray Process of Metallization*, 1st ed., Charles Griffin and Company Limited, London, 1926, 175 pages
2. [http://en.wikipedia.org/wiki/Time\\_capsule](http://en.wikipedia.org/wiki/Time_capsule)
3. [http://en.wikipedia.org/wiki/International\\_Time\\_Capsule\\_Society](http://en.wikipedia.org/wiki/International_Time_Capsule_Society)
4. <http://collaboratory.nunet.net/cps/tsteele/chinatimecapsule.html#finalquestion>
5. [http://www.eduplace.com/rdg/gen\\_act/growing/capsule.html](http://www.eduplace.com/rdg/gen_act/growing/capsule.html)
6. <http://oralhistories.library.caltech.edu/>
7. Interview, *J. Thermal Spray Technol.*, Vol 4 (No. 2), 1995, p 111-112
8. W.B. Meyer, A History of the Nooter Metallizing Department, St. Louis Metallizing Company, A JTST Historical Paper, *J. Thermal Spray Technol.*, Vol 5 (No. 2), 1996, p 215-221
9. Plasma Spraying as a By Product of the Gemini Space Capsule, *PMI J.*, Vol 23 (No. 6), 1991, p 363-365
10. [http://go.hrw.com/resources/go\\_ss/teacher99/toolkit/TOOLKT15.pdf](http://go.hrw.com/resources/go_ss/teacher99/toolkit/TOOLKT15.pdf)
11. <http://memory.loc.gov/ammem/ndlpedu/lessons/oralhist/ohguide.html>

**Christopher C. Berndt**  
James Cook University  
Townsville, Australia

**Ghislain Montavon**  
University of Limoges  
Limoges, France

### Permission to publish

C.C. Berndt and G. Montavon, "Thermal Spray: Preserving 100 Years Of Technology", *J. Thermal Spray Technology*, 15[1] (2006) 5-8.

With kind permission from Springer Science+Business Media. The complete article (text, figures, tables and references) have been kindly reproduced.



# Commentary

## The End of the Beginning; Now Let's Make a Real Effort!



**Christopher C. Berndt**

Colleagues and Friends:

I am honored to receive this award. I am grateful that the efforts of my students and thermal spray collaborators have been acknowledged.

I am the second person from the Southern Hemisphere to be so honored, and I am proud to say that the first person was my Ph.D. advisor.

I would like to leave you with three points:

- Thermal spray science and engineering provides all of us with a good life: a life that is exciting and fulfilling and of many dimensions.
- Thermal spray has come out of the closet and been recognized. We all need to rejoice in its rediscovered identity.
- The future of TS is held in the hands of all of us. We must all rise to this challenge and reap the rewards that we create.

Thank you.

And that was the end of my one-minute speech.

At a deep, personal level, it is humbling to receive unsolicited peer recognition. It came as a pleasant surprise to be invited to join a group of distinguished thermal spray luminaries. From an Australian cultural perspective, it seems somewhat peculiar to be rewarded for what I have enjoyed most; that is "Participation in the world of thermal spray is a reward within its own right." However, I temper this purist approach with the bona fide happiness and celebration in being acknowledged by the thermal spray community. Thanks!

So ... what was I really trying to say and what was the subtext of my acceptance message? Here comes a longer and more conversational version of my HoF one-minute speech.

In my particular case, I give thanks to a rigorous applied science education that paved the way to undertaking research and development in an engineering technology field. It would be negligent for me not to mention Stony Brook University, New York; where I grew under the tutelage of many colleagues. I am grateful for these opportunities.

Any individual award or honor relies on a team of people who all make important contributions. In my case I have had "a bunch" of students and Post-Doctoral Fellows who have challenged me as much as I have challenged them! They have all been demanding in some form or fashion, just as I have been of them with strange ideas and theories that they have tested. This mutual interaction has been a satisfying part of my professional and personal life. Students have turned into colleagues and become lifelong friends.

Then, in the last 30 seconds of my speech I talk about thermal spray; that is, it is exciting, it has a distinct identity, and it is has a future that is worthy of effort and resources. Thus, TS is not about the present and the capabilities of individuals, but it is about a healthy future that relies on new people stepping up and making contributions.

Consequently, we arrive at the title of this short commentary; "The End of the Beginning; Now Let's Make a Real Effort!" The prime message is that there is ample scope for major contributions to thermal spray from individuals. On the basis of prior knowledge and understanding, as imparted during an ITSC for example, we progress in a systematic fashion further up the evolutionary tree of science.

I urge everyone to contribute to thermal spray: you will not be disappointed!

**Christopher C. Berndt**, Ph.D., HoF, FASM, FIMMM, FIEAust, CPEng, CEng, CSci  
Prof. of Surface and Interface Engineering  
Department of Surface and Interface Engineering  
James Cook University  
Townsville, Queensland, Australia

The Thermal Spray Society; President, 2002–2004  
ASM International; Board of Trustees, 2005–2008  
Editor: *International Thermal Spray and Surface Engineering*  
Editor Emeritus: *The Journal of Thermal Spray Technology*  
Stony Brook University; Adjunct Professor, NY



# Commentary

## One Way to Pick “Low-Hanging Fruit” Is To Chop the Tree Down!



**Christopher C. Berndt**

There is a phrase that has entered “management jargon” that defies a rationale explanation: yes ... “low-hanging fruit.” I am wondering whether others may be confused—is it good or bad, or desirable or undesirable, to pick low-hanging fruit?

First let me explain how this phrase has been interpreted in two environments: (a) for the manufacturing sector the phrase implies that firms produce the least expensive units first, (b) for the political sector the phrase

clarifies that the election season is the time to count people, not convert them to your party. Thus, in very general terms, low-hanging fruit is defined as “The easiest task or the most readily achievable goal.” (<http://www.wordspy.com/words/low-hangingfruit.asp>) An example from the Web that might resonate with some of us concerns parking violations. The low-hanging fruit that the traffic wardens pick in this situation are (a) illegally parked cars in residential areas during early-morning hours on Sundays, (b) expired inspection stickers, (c) cars faced the wrong way on dead-end streets, etc. The low-hanging fruit represent easy revenue in terms of traffic fines.

How about for thermal sprayers and technologists; what are the low-hanging fruit? Here is a very short list: attend an ITSC! Then carry the analogy a bit further; actually participating in an ITSC by presenting a paper allows you to pick more fruit because you gain so much more knowledge and understanding.

So far the discussion has been oriented to the classical management-speak that we have become accustomed to. Let me now explain why some low-hanging fruit are *not* desirable. In my own world of research there are a lot of very bright and aggressive people picking low-hanging fruit, as well as the rest of the tree until it is bare! Then the tree is

chopped down and nothing remains. It appears as if the R&D becomes derivative in order to satisfy a program manager or funding agent because they want results, as measured in the currency of presentations, publications, higher degrees, awards, etc., and they want these NOW. And you may well say, “What’s the problem here? These are tangible results that indicate accountability for those people spending our tax dollars!”

Here is the *fundamental problem* behind this skewed logic. For there to be fruit there needs to be a tree, and this tree needs to be of a completely different variety so that breakthroughs in science and engineering evolve over a time frame that is often longer than the tenure of a 3-year grant. In plain language, the low-hanging fruit philosophy precludes long-term research that will advance true innovation. Low-hanging fruit rule out the adage that “a person’s reach should exceed their grasp.”

If you have a contrary viewpoint then contact me; I am more than happy to help you shake the bushes and see what falls out!

**Christopher C. Berndt**, Ph.D., HoF, FASM, FIMMM, FIEAust, CPEng, CEng, CSci  
Prof. of Surface and Interface Engineering  
Department of Surface and Interface Engineering  
James Cook University  
Townsville, QLD, Australia

The Thermal Spray Society; President, 2002-2004  
ASM International; Board of Trustees, 2005-2008  
Editor: *International Thermal Spray and Surface Engineering*  
Editor Emeritus: *The Journal of Thermal Spray Technology*  
Stony Brook University; Adjunct Professor, NY

### Permission to publish

C.C. Berndt, "One way to pick "Low-hanging fruit" is to chop the tree down!", *Journal of Thermal Spray Technology*, 16[4] (2007) p. 465. Also 385 AM&P (2007) 165[5] P70.

With kind permission from Springer Science+Business Media. The complete article (text, figures, tables and references) have been kindly reproduced.

## Appendix 7. List of Publications of Christopher C. Berndt

The known publications of the applicant are presented in tabular format in this appendix. The unique ID number is presented in reverse chronological order. The shaded cells are used to demark the last entry in any particular year.

ID	Reference
459	A.S.M. Ang and C.C. Berndt, "A review of testing methods for thermal spray coatings", J. International Materials Reviews, On line published in February 2014. DOI:10.1179/1743280414Y.0000000029]
458	M.F. Hasan, J. Wang and C.C. Berndt, "A Taguchi design study for optimisation of plasma sprayed hydroxyapatite coatings", Materials Science Forum Vols. 773-774 (2014) pp 590-601, doi:10.4028/www.scientific.net/MSF.773-774.590
457	M.R. Mansur, J. Wang and C.C. Berndt, "Hydroxyapatite and titanium composite coatings on austenitic stainless steel substrates using direct material deposition", p.602-615 of 15th International Conference on Advances in Materials and Processing Technologies, AMPT 2012, Vol. 773-774 (2014).
456	K. Mediaswanti, C. Wen, E.P. Ivanova, F. Malherbe, C.C. Berndt, V.T.H. Pham and J. Wang, "Biomimetic Creation of Surfaces on Porous Titanium for Biomedical Applications", Advanced Materials Research Vol. 896 (2014) pp 259-262, doi:10.4028/www.scientific.net/AMR.896.259
455	S. Minagar, C.C. Berndt, T. Gengenbach C. Wen, "Fabrication and characterization of TiO <sub>2</sub> -ZrO <sub>2</sub> - ZrTiO <sub>4</sub> nanotubes on TiZr alloy manufactured via anodization", Journal of Materials Chemistry B (2014) 2[1] p.71-83.
454	M.L. Sesso, C.C. Berndt, Y.C. Wong, "Topographical and Microstructural Property Evolution of Air Plasma-Sprayed Zirconia Thermal Barrier Coatings, J. American Ceramic Society, Article first published online: 4 FEB 2014, DOI: 10.1111/jace.12842
453	M. Vcelka, M. Dunn, Y. Durandet, C.C. Berndt and R. Dong, "Behavior of CFRC/Al foam composite sandwich beams under three-point bending", Advanced Engineering Materials, 16 [1] (2014) 9-14.
452	W. Xie, J. Wang and C.C. Berndt, "Analysis of EMAA splats on glass and mild steel substrates", Journal of Thermal Spray Technology, 23[3] (2014) p.317-324.
451	A.S.M. Ang, N. Sanpo N, M.L. Sesso, S.Y. Kim and C.C. Berndt, "Thermal Spray Maps: Material Genomics of Processing Technologies", J. Thermal Spray Tech., 22[7] (2013) p. 1170-1183. DOI: 10.1007/s11666-013-9970-3 Published: OCT 2013
450	T.A. Choudhury, C.C. Berndt and Z. Man, "An Extreme Learning Machine Algorithm to Predict the In-flight Particle Characteristics of an Atmospheric Plasma Spray Process", Plasma Chem. and Plasma Proc., 33[5] (2013) p. 993-1023. DOI: 10.1007/s11090-013-9466-4 Published: OCT 2013
449	J.A. Gan and C.C. Berndt, "Effects of standoff distance on porosity, phase distribution and mechanical properties of plasma sprayed Nd-Fe-B coatings", Surface & Coatings Tech., 216 (2013) p. 127-138. DOI: 10.1016/j.surfcoat.2012.11.040 Published: FEB 15 2013
448	J.A. Gan and C.C. Berndt, "Quantification and Taxonomy of Pores in Thermal Spray Coatings by Image Analysis and Stereology Approach", Metall. and Mater. Trans. A, 44A[10] (2013) p. 4844-4858. DOI: 10.1007/s11661-013-1818-4 Published: OCT 2013
447	J.A. Gan and C.C. Berndt, "Review on the Oxidation of Metallic Thermal Sprayed Coatings: A Case Study with Reference to Rare-Earth Permanent Magnetic Coatings",

ID	Reference
	J. Thermal Spray Tech., 22[7] (2013) p. 1069-1091. DOI: 10.1007/s11666-013-9955-2 Published: OCT 2013
446	J.A. Gan, C.C. Berndt, Y.C. Wong and J. Wang, "Void Formation and Spatial Distribution in Plasma Sprayed Nd-Fe-B Coatings", J. Thermal Spray Tech., 22[2-3] (2013) p. 337-344. DOI: 10.1007/s11666-012-9819-1 Published: MAR 2013
445	M.F. Hasan, J. Wang and C.C. Berndt, "Effect of power and stand-off distance on plasma sprayed hydroxyapatite coatings", Materials and Manufacturing Processes, 28[12] (2013) p.1279-1285.
444	M.R. Mansur, J. Wang and C.C. Berndt, "Microstructure, composition and hardness of laser-assisted hydroxyapatite and Ti-6Al-4V composite coatings", Surface and Coatings Technology, 232 (Oct 2013), p. 482-488.
443	K. Mediaswanti, C. Wen, E.P. Ivanova, C.C. Berndt and J. Wang, "Sputtered hydroxyapatite nanocoatings on novel titanium alloys for biomedical applications", P. 21-44 of "Titanium alloys: advances in properties control", (2013) J. Sieniawski and W. Ziaja (eds.), Chapter 2.
442	S. Minagar, J. Wang, C.C. Berndt, E.P. Ivanova and C. Wen, "Cell response of anodized nanotubes on titanium and titanium alloys", J. of Biomedical Mater. Research Part A, 101[9] p. 2726-2739. DOI: 10.1002/jbm.a.34575 Published: SEP 2013
441	N. Sanpo, C.C. Berndt, A.S.M. Ang and J. Wang, "Effect of the chelating agent contents on the topography, composition and phase of SPPS-deposited cobalt ferrite splats", Surface and Coatings Technology, 232 (2013) p.247-253.
440	N. Sanpo, J. Wang, A.S.M. Ang and C.C. Berndt, "Influence of the different organic chelating agents on the topography, physical properties and phase of SPPS-deposited spinel ferrite splats", Applied Surface Science, 284 (2013) p.171-178.
439	N. Sanpo, C.C. Berndt, C. Wen and J. Wang, "Transition metal-substituted cobalt ferrite nanoparticles for biomedical applications", Acta Biomaterialia, 9[3] (2013) p. 5830-5837. DOI: 10.1016/j.actbio.2012.10.037 Published: MAR 2013
438	N. Sanpo, J. Wang and C.C. Berndt, "Influence of Chelating Agents on the Microstructure and Antibacterial Property of Cobalt Ferrite Nanopowders", J. Australia Ceramic Soc., 49[1] (2013) p. 84-91.
437	N. Sanpo, J. Wang and C.C. Berndt, "Sol-Gel Synthesized Copper-Substituted Cobalt Ferrite Nanoparticles for Biomedical Applications", J. of Nano research, 22 (2013) p. 95-106. DOI: 10.4028/www.scientific.net/JNanoR.22.95 Published: 2013
436	M. Vcelka, Y. Durandet and C.C. Berndt, "Mechanical Response of Composite Sandwich Panels: Deformation and Energy Absorption", Key Engineering Materials Vols. 535-536 (2013) pp 409-412, doi:10.4028/www.scientific.net/KEM.535-536.409
435	A.S.M. Ang, C.C. Berndt, M. Dunn, M.L. Sesso, S.Y. Kim, "Modeling the Coverage of Splat Areas Arising from Thermal Spray Processes", J. Am. Ceramic Soc., 95[5] (2012) p. 1572-1580. DOI: 10.1111/j.1551-2916.2012.05113.x Published: MAY 2012.
434	T.A. Choudhury, N. Hosseinzadeh and C.C. Berndt, "Improving the Generalization Ability of an Artificial Neural Network in Predicting In-Flight Particle Characteristics of an Atmospheric Plasma Spray Process", J. Thermal Spray Tech., 21[5] (2012) p. 935-949. DOI: 10.1007/s11666-012-9775-9 Published: SEP 2012.
433	J.A. Gan, C.C. Berndt, Y.C. Wong and J. Wang, "Void Formation and Spatial Distribution in Plasma Sprayed Nd-Fe-B Coatings", p. 752-757 of Proceedings of the International Thermal Spray Conference 2012 – Air, Land, Water and the Human Body: Thermal Spray Science and Applications, Houston, TX, USA, R.S. Lima, A. Agarwal, M.M. Hyland, Y.C. Lau, C.J. Li, A. McDonald and F.L. Toma (Eds.), Pub.

ID	Reference
	(2012) ASM International, Materials Park, OH, USA.
432	S. Minagar, C. Wen, E.P. Ivanova, C.C. Berndt and J. Wang, "Powder metallurgy: a promising route for bone implants fabrication", p. 42-44 of Proceedings of the 4th High Temperature Processing Symposium (HTP 2012), Hawthorn, Victoria, Australia, 06-07 February 2012. Eds. M. Akbar Rhamdhani, G. Brooks, Md Saiful Islam and S. Sabah (eds.).
431	K. Mediaswant, C. Wen, E.P. Ivanova, C.C. Berndt, F. Malherbe and J. Wang, "Biological Performances of Titanium Scaffolds: A Review ", p. 1634-1637 of "Advanced Engineering Materials II", Pts 1-3 Book Series: Advanced Materials Research Volume: 535-537 Chunxiang Cui, Yali Li and Zhihao Yuan (Eds.). DOI:10.4028/www.scientific.net/AMR.535-537.1634 Published:2012 ; Editor(s): Cui, CX; Li, YL; Yuan, ZH
430	K. Mediaswanti, V.K. Truong, J. Hasan, E.P. Ivanova, F. Malherbe, C.C. Berndt, C. Wen and J. Wang, "Influence of Titanium Alloying Element Substrata on Bacterial Adhesion", p. 992-995 of "Advanced Engineering Materials II", (2012) Pts 1-3 Book Series: Advanced Materials Research Volume: 535-537 Chunxiang Cui, Yali Li and Zhihao Yuan (Eds.). DOI: 10.4028/www.scientific.net/AMR.535-537.992.
429	K. Mediaswanti, V.K. Truong, J. Hasan, Y. Li, C. Wen, E.P. Ivanova, C.C. Berndt, F. Malherbe and J. Wang, "Fabrication of Ti4Nb4Sn Alloys for Bone Tissue Engineering Applications"; (2012) Powder Metallurgy of Titanium: Powder Processing, Consolidation and metallurgy of Titanium, Book Series: Key Engineering Materials Volume: 520, p. 214-219. Ed. M. Qian. DOI:10.4028/www.scientific.net/KEM.520.214.
428	S. Minagar, C.C. Berndt, J. Wang, E.P. Ivanova and C. Wen, "A review of the application of anodization for the fabrication of nanotubes on metal implant surfaces", Acta Biomaterialia, 8[8] (2012) p. 2875-2888. DOI: 10.1016/j.actbio.2012.04.005 Published: AUG 2012.
427	N. Sanpo, A.S.M. Ang, Md. F. Hasan, J. Wang and C.C. Berndt, "Phases and microstructures of solution precursor plasma sprayed cobalt ferrite splats", p. 145-146 of ATSC2012, Proceedings of the 5th Asian Thermal Spray Conference, Nov. 26-28, Tsukuba, Japan, Pub. Japan Thermal Spray Society, 2012.
426	N. Sanpo, C.C. Berndt and J. Wang, "Microstructural and antibacterial properties of zinc-substituted cobalt ferrite nanopowders synthesized by sol-gel methods", J. Applied Physics, 112[8] (2012). Article Number: 084333 DOI: 10.1063/1.4761987 Published: OCT 15 2012.
425	N. Sanpo, J. Wang and C.C. Berndt, "Effect of Zinc Substitution on Microstructure and Antibacterial Properties of Cobalt Ferrite Nanopowders Synthesized by Sol-gel Methods", p. 436-439 of Advanced Engineering Materials II, Pts 1-3, (2012) Book Series: Advanced Materials Research Volume: 535-537. DOI: 10.4028/www.scientific.net/AMR.535-537.436.
424	Wei Xie, J. Wang and C.C. Berndt, "Spreading behavior and morphology of ethylene methacrylic acid (EMAA) deposits via the flame spray process", Coatings, 2[2] (2012), p. 76-93 .
423	K. Alamara, S. Saber-Samandari, P.R. Stoddart and C.C. Berndt, "Effect of substrate temperature on the splat formation of flame sprayed polypropylene", Surface and Coatings Tech., 206[6] (2011) p. 1180-1187. DOI: 10.1016/j.surfcoat.2011.08.020

ID	Reference
	Published: DEC 15 2011
422	K. Alamara, S. Saber-Samandari and C.C. Berndt, "Splat taxonomy of polymeric thermal spray coating", Surface and Coatings Tech., 205[21-22] (2011) p. 5028-5034. DOI: 10.1016/j.surfcoat.2011.05.002 Published: AUG 25 2011
421	A.S.M. Ang, C.C. Berndt and P. Cheang, "Deposition effects of WC particle size on cold sprayed WC-Co coatings", Surface and Coatings Tech., 205[10] (2011) p. 3260-3267. DOI: 10.1016/j.surfcoat.2010.11.045 Published: FEB 15 2011
420	T.A. Choudhury, N. Hosseinzadeh and C.C. Berndt, "Artificial Neural Network application for predicting in-flight particle characteristics of an atmospheric plasma spray process", Surface and Coatings Tech., 205[21-22] (2011) p. 4886-4895. DOI: 10.1016/j.surfcoat.2011.04.099 Published: AUG 25 2011
419	J.A. Gan and C.C. Berndt, "Microstructure of Plasma Sprayed Neodymium Iron Boron Magnetic Coatings", Proceedings of the 4th International Workshop on Plasma Application and Hybrid Functionally Materials, Melbourne, Australia, Institute of Applied Plasma Science, (2011) Osaka, Japan, p. 47-48.
418	J.A. Gan and C.C. Berndt, "Technical Note: Microstructure of Plasma Sprayed Neodymium Iron Boron Magnetic Coatings", Frontiers of Applied Plasma Technology, 4[2] (2011) p. 115-116.
417	J.A. Gan, C.C. Berndt and Y.C. Wong, "Effects of Standoff Distance on the Microstructure and Phase Distribution of Plasma Sprayed NdFeB Coatings", The 9th International Meeting of Pacific Rim Ceramic Societies (PACRIM 9), Cairns, Australia, 2011, The Australian Ceramic Society and Materials Australia.
416	J.A. Gan and C.C. Berndt, "Design and manufacture of Nd-Fe-B thick coatings by the thermal spray process", Surface and Coatings Tech., 205[19] (2011) p. 4697-4704. DOI: 10.1016/j.surfcoat.2011.04.034 Published: JUN 25 2011
415	E. Ivanova, J.Y. Wang, V.K. Truong, A. Kemp, C.C. Berndt and R.J. Crawford, "Bacterial Attachment onto the Surfaces of Sputter-prepared Ti and Ti-based Nanocoatings", p. 195-224 of "Advances in Nanotechnology. Volume 8", ED. Zacharie Bartul and Jérôme Trenor, (2011) Pub. Nova Science Publishers, Inc., NY-USA
414	A.F. Kanta, G. Montavon, C.C. Berndt, M.P. Planche and C. Coddet, "Intelligent system for prediction and control: Application in plasma spray process", Expert Systems with Applications, 38[1] (2011) p.260-271. DOI: 10.1016/j.eswa.2010.06.056 Published: JAN 2011
413	S. Saber-Samandari, C.C. Berndt and K. Gross, "Selection of the implant and coating materials for optimized performance by means of nanoindentation", Acta Biomaterialia, 7[2] (2011) p. 874-881. DOI: 10.1016/j.actbio.2010.09.023 Published: FEB 2011
412	J. Wang, J.A. Gan, Y.C. Wong and C.C. Berndt, "A Review of Preparation, Properties and Applications of Rare Earth Magnetic Thin Films, Magnetic Thin Films: Properties, Performance and Applications", J.P. Volkerts (Ed.), Materials Science and Technologies, Nova Publishers, Hauppauge, NY, USA, 2011, p. 1-69.
411	K. Alamara, S. Saber-Samandari and C.C. Berndt, "Splat formation of polypropylene flame sprayed onto a flat surface", Surface and Coatings Tech., 205[7] (2010) p. 2518-2524. DOI: 10.1016/j.surfcoat.2010.09.056 Published: DEC 25 2010
410	A.S.M. Ang, C.C. Berndt, P. Cheang and J. Wang, "Effects of WC Particle Size on Deposition of Cold Spray WC-Co Coatings", International Thermal Spray Conference & Exposition (ITSC 2010), Singapore, 3-5th, May, 2010.



ID	Reference
409	K. Bazaka, M.V. Jacob, V.K. Truong, F. Wang, W.A.A. Pushpamali, J.Y. Wang, A.V. Ellis, C.C. Berndt, R.J. Crawford and E.P. Ivanova, "Plasma-Enhanced Synthesis of Bioactive Polymeric Coatings from Monoterpene Alcohols: A Combined Experimental and Theoretical Study", <i>Biomacromolecules</i> , 11[8] (2010) p. 2016-2026. DOI:10.1021/bm100369n Published:AUG 2010
408	E.J. Teh, Y.K. Leong, Y. Liu, B.C. Ong, C.C. Berndt and S.B. Chen, "Yield stress and zeta potential of washed and highly spherical oxide dispersions: Critical zeta potential and Hamaker constant", <i>Powder Technology</i> , 198 (1), p.114-119, Feb 2010
407	E.P. Ivanova, V.K. Truong, J.Y. Wang, C.C. Berndt, R.T. Jones, I.I. Yusuf, I. Peake, H.W. Schmidt, C. Fluke, D. Barnes and R.J. Crawford, "Impact of Nanoscale Roughness of Titanium Thin film Surfaces on Bacterial Retention", <i>Langmuir</i> , 2010, 26 (3), 1973-1982.
406	M. Hanna and C.C. Berndt, "Corrosion and Oxidation Properties of NiCr Coatings Sprayed in presence of Gas Shroud", <i>Applied Surface Science</i> , 256[13] (2010) p. 4322-4327. Ms. Ref. No.: APSUSC-D-10-00098R1
405	M.F. Morks, C.C. Berndt, Y. Durandet, M. Brandt and J. Wang, "Microscopic observation of laser glazed yttria-stabilized zirconia coatings", <i>App. Surface Sci.</i> , 256[21] (2010) p.6213-6218. DOI:10.1016/j.apsusc.2010.03.143 Published:AUG 15 2010
404	M.F. Morks and C.C. Berndt, "Plasma Sprayed NiCr Coatings using a Gas Shroud System", <i>International Thermal Spray Conference &amp; Exposition (ITSC 2010)</i> , Singapore, 3-5th, May, 2010.
403	S. Saber-Samandari, C.C. Berndt, K.A. Gross and J. Wang, "A Morphological Study of Hydroxyapatite Splats Flame-sprayed onto Titanium", <i>International Thermal Spray Conference &amp; Exposition (ITSC 2010)</i> , Singapore, 3-5th, May, 2010.
402	U. Tietz, C.C. Berndt and K.-P. Schmitz, "Microstructural Modelling and Performance Simulation of Engineering Bio-Composites", <i>International Thermal Spray Conference &amp; Exposition (ITSC 2010)</i> , Singapore, 3-5th, May, 2010. paper 264. 6p.
401	V.K. Truong, J. Wang, W. Shurui, C.C. Berndt, F. Malherbe, R.J. Crawford and E.P. Ivanova, "Bacterial Attachment Response to Nanostructured Titanium Surfaces", <i>International Conference On Nanoscience and Nanotechnology (ICNN 2010)</i> , Sydney, 22-26th February 2010.
400	W. Xie, S. Saber-Samandari, J. Wang and C.C. Berndt, "The Effect of Standoff Distance on the Single Splat of EMAA on Glass and Mild Steel Substrates", <i>International Thermal Spray Conference &amp; Exposition (ITSC, 2010)</i> , Singapore, 3-5th May 2010.
399	V.F.C. Lins, J.R.T. Branco and C.C. Berndt, "Post-Consumer Pet and Post-Consumer Pet-Containing Materials for Flame Spray Coatings on Steel: Processing, Properties and Use", in <i>Surface Coatings</i> , M. Rizzo and G. Bruno (Eds), (2009) Pub Nova, Pages:237-257 ISBN: 978-1-60741-193-2
398	V.K. Truong, S. Rundell, R. Lapovok, Y. Estrin, J.Y. Wang, C.C. Berndt, D.G. Barnes, C.J. Fluke, R.J. Crawford and E.P. Ivanova, "Effect of Ultrafine-grained Titanium Surfaces on Adhesion of Bacteria", <i>Appl Microbiol Biotechnol.</i> , 83 (2009) p. 925-937.
397	C.C. Berndt, "Born again as a technologist", <i>Advanced Materials and Processes</i> , Vol. 166, no. 5 (May 2008), p. 68.
396	C.C. Berndt, "'At the end of the day': let-us all take on responsibility for thermal spray", <i>Advanced Materials &amp; Processes</i> , Vol. 166, no. 8 (Aug 2008), p. 58 .

ID	Reference
395	C.C. Berndt, "Editorial: will thermal spray ever be the basis for a Nobel Prize?", Advanced Materials & Processes, Vol. 166, no. 11 (Nov 2008), p. 66 .
394	D. Henderson, J. Ginger, C. Berndt and G.A. Kopp, "Fatigue failure of G550 steel building components during wind loading", Paper No. 043 of Australasian Structural Engineering Conference (ASEC), 26 – 27 June 2008, Melbourne Australia, ISBN 978 1 877040 70 2
393	A. Ibrahim, H. Salem and C.C. Berndt, "Characterization of nanostructured and conventional alumina-13wt.% titania coatings", (2008) p. 785-790 of "Thermal Spray 2008: Crossing Borders", Pub. ASM International, Materials Park, OH-USA.
392	A. Ibrahim and C.C. Berndt, "Effect of nanostructural thermal spray coatings on fatigue bahaviour of low carbon steel", Proceedings of the ASME 2nd International Multifunctional Nanocomposites and Nanomaterials Conference, Sharm El Sheikh, Egypt, 11-13 January 2008, pp. 187-191 .
391	M.V. Jacob, C.D. Easton, G.S. Woods and C.C. Berndt, "Fabrication of a novel organic polymer thin film", Thin Solid Films, 516[12] (2008) 3884-3887.
390	A.F. Kanta, G. Montavon, M. Vardelle, M.P. Planche, C.C. Berndt and C. Coddet, "Artificial Neural Networks vs. Fuzzy Logic: Simple tools to predict and control complex processes-application to plasma spray processes", J. Thermal Spray Technology, 17[3], (2008) 365-376.
389	A.-F. Kanta, M.-P. Planche, C. Coddet, G. Montavon, M. Vardelle and C.C. Berndt, "Atmospheric plasma spray process control", (2008) p. 1417-1423 of "Thermal Spray 2008: Crossing Borders", Pub. ASM International, Materials Park, OH-USA.
388	Y.K. Leong, M. Sganzerla, C.C. Berndt and G.R. Campbell, "Metal ions solubility in plant phosphoric acid-degree of ammonia neutralization and temperature effects", Industrial & Engineering Chemistry Research, 47[5] (2008) 1380-1385.
387	A. Scrivani, G. Rizzi and C.C. Berndt, "Enhanced thick thermal barrier coatings that exhibit varying porosity", MSEA, 476[1-2] (2008) p.1-7.
386	A. Scrivani, A. Lanzi, G. Rizzi, D. Russo, M. Spagnoli, C.C. Berndt and C. Giolli, "Development of Thick Thermal Barrier Coatings that Exhibit Varying Porosity", Metallurgia Italiana, Issue: 3 (2008) 27-32.
385	A. Scrivani, G. Rizzi and C.C. Berndt, "Enhanced thick thermal barrier coatings that exhibit varying porosity", MSEA, 476 [1-2] (2008) 1-7.
384	C.C. Berndt, "One way to pick "Low-hanging fruit" is to chop the tree down!", Journal of Thermal Spray Technology, 16[4] (2007) p. 465.
383	C.C. Berndt, K.J. Rankine and N. Sivakugan, "Materials properties of barricade bricks for mining applications", Geotechnical and Geological Engineering, 25[4] (2007) 449-471.
382	A. Hodzic, R.Coakley, R. Curro, C.C. Berndt and R.A. Shanks, "Design and optimisation of biopolyester bagasse fibre composites", J Biobased Materials and Bioenergy, 1 (2007) 1-10.
381	A. Ibrahim and C.C. Berndt, "Fatigue and deformation of HVOF sprayed WC–Co coatings and hard chrome plating", MSE-A 456 (2007) 114-119.
380	A. Ibrahim, R.S. Lima, C.C. Berndt and B.R. Marple, "Fatigue and Mechanical Properties of Nanostructured and Conventional Titania (TiO <sub>2</sub> ) thermal spray coatings", Surface Coatings and Tech., 201 (2007) 7589-7596.

ID	Reference
379	A. Ibrahim and C.C. Berndt, "Fatigue and deformation of HVOF sprayed WC–Co coatings and hard chrome plating", <i>Materials Science and Engineering A</i> , 456 [1-2] (2007) 114-119.
378	M.V. Jacob, C.D. Easton, G.S. Woods and C.C. Berndt, "Fabrication of a novel organic polymer thin film", <i>TSF</i> 516 [12] (2008) 3884-3887.
377	J.R.T. Branco, V.F. Lins, F.R.C. Diniz, J.C. Brogan and C.C. Berndt, "Erosion behavior of thermal sprayed, recycled polymer and ethylene-methacrylic acid composite coatings", <i>Wear</i> , 262 (2007) 274-281.
376	S. Bandyopadhyay, Q. Zeng, C.C. Berndt, S. Rizkalla, N. Gowripalan and J. Matisons, "ACUN-5 International Composites Conference; Developments in Composites: Advanced, Infrastructural, Natural & Nano-Composites", Pub. University of New South Wales, UNSW Sydney, 2052, Australia; 2006, 706 pages. ISBN: 0-7334-2363 9.
375	C.C. Berndt, K. Bobzin, C. Coddet, P. Fauchais, E. Lugscheider, K. Mohwald, L. Singheiser, and A. Vardelle, "Thermal Spraying Developments", <i>Advanced Engineering Materials</i> , 8 (7) (2006) 595-596.
374	C.C. Berndt and G. Montavon, "Thermal Spray: Preserving 100 Years Of Technology", <i>J. Thermal Spray Technology</i> , 15[1] (2006) 5-8.
373	G.R. Campbell, Y.K. Leong, C.C. Berndt and J.L. Liow, "Ammonium Phosphate Slurry Rheology and Particle Properties - The influence of Fe(III) and Al(III) impurities, solid concentration and degree of neutralization", <i>Chemical Engineering Science</i> , 61 [17] (2006) 5856-5866.
372	D.N. Guru, J.V.R. Heberlein, W. Mook, W.W. Gerberich and C.C. Berndt, "Nanostructured partially stabilized zirconia as an interlayer in a multi layered thermal barrier coating", 6 p, "Thermal Spray 2006: Science, Innovation and Application"; B.R. Marple, M.M. Hyland, Y-C. Lau, R.S. Lima and J. Voyer (Eds), Pub. ASM International, OH-USA, 2006.
371	A. Hodzic, R. Curro, P. Britton, L. Shu, C.C. Berndt and R A. Shanks, "Mechanical Properties of PHB-Bagasse Composites", An Overview of Applications", 11 Jul 2006 / 14 Jul 2006 - Australia, ACUN-5: International Composites Conference, Sydney, Developments in Composites: Advanced, Infrastructural, Natural and Nano-composites. pp. 156-161.
370	Li Shu, C.C. Berndt and A. Hodzic, "Sugar Cane Bagasse Fibre for Sustainable Manufacturing: An Overview of Applications", 11 Jul 2006 / 14 Jul 2006 - Australia. ACUN-5: International Composites Conference, Sydney, Developments in Composites: Advanced, Infrastructural, Natural and Nano-composites. pp. 248-253.
369	G. Mariaux, A. Vardelle, M. Vardelle and C.C. Berndt, "Time-dependent gas dynamics and gas-particle heat and mass transfer during Plasma Spray Deposition", <i>Proc. 13th International Heat Transfer Conference</i> , Sydney, Australia. 13-18 August, 2006. "Annals of the Assembly for International Heat Transfer Conference 13", 12 pages, DOI: 10.1615/IHTC13.p5.270.
368	P. Michlik and C.C. Berndt, "An Image-Based Extended Finite Element Modeling of Thermal Barrier Coatings", <i>Surface Coatings and Tech.</i> , 201 (2006) 2369-2380.
367	O. Racek, C.C. Berndt, D.N. Guru and J. Heberlein, "Nanostructured and conventional YSZ coatings deposited using APS and TTPR techniques", <i>Surface and Coatings Technology</i> , 201 (2006) 338-346.
366	K.A. Gross, F.Y. Yan, C.C. Berndt and G.P. Simon, "Repair of Multi-Layered, Polymer-Based Thermal Spray Coatings" Pages 74-79 of "Thermal Spray Connects:

ID	Reference
	Explore its Surfacing Potential!", Ed. E. Lugscheider, Pub. DVS - German Welding Society, Düsseldorf, 2005, ISBN 3-87155-793-5.
365	A. Ibrahim, R.S. Lima, B.R. Marple, and C.C. Berndt, "Fatigue and Mechanical Properties of Nanostructured vs. Conventional Titania (TiO <sub>2</sub> ) Coatings" Pages 855-859, of "Thermal Spray Connects: Explore its Surfacing Potential!", Ed. E. Lugscheider, Pub. DVS - German Welding Society, Düsseldorf, 2005, ISBN 3-87155-793-5.
364	L. Sun, C.C. Berndt and K.A. Gross, "Phase Formation Mechanisms in Plasma Sprayed Hydroxyapatite Coatings", Pages 563-568, of "Thermal Spray Connects: Explore its Surfacing Potential!", Ed. E. Lugscheider, Pub. DVS - German Welding Society, Düsseldorf, 2005, ISBN 3-87155-793-5.
363	P. Michlik, C.C. Berndt and O. Racek, "XFEM Modeling of Effective Thermal Properties and Fracture of Thermal Barrier Coatings", Pages 293-298, of "Thermal Spray Connects: Explore its Surfacing Potential!", Ed. E. Lugscheider, Pub. DVS - German Welding Society, Düsseldorf, 2005, ISBN 3-87155-793-5.
362	G. Montavon, C.C. Berndt, F.I. Trifa and S. Guessasma, "Correlating the Spray Pattern to the Coating Architecture: Exploring the Dominant Mechanisms and Process Parameters", Pages 798-809, of "Thermal Spray Connects: Explore its Surfacing Potential!", Ed. E. Lugscheider, Pub. DVS - German Welding Society, Düsseldorf, 2005, ISBN 3-87155-793-5
361	E. Palermo, M. Si, R. Occhiogrosso, C.C. Berndt, G. Rudomen and M. Rafailovich, "Effects of supercritical carbon dioxide on phase homogeneity, morphology and mechanical properties of poly(styrene-blend-ethylene-stat-vinyl acetate)", <i>Macromolecules</i> , 38[22] (2005) 9180-9186.
360	O. Racek, C.C. Berndt, D. Guru and J.V. Heberlein, "Microstructural Observation of the Sintering Behavior of Nanostructured Yttria Stabilized Zirconia", pages 505-511, of "Thermal Spray Connects: Explore its Surfacing Potential!", Ed. E. Lugscheider, Pub. DVS - German Welding Society, Düsseldorf, 2005, ISBN 3-87155-793-5
359	C.C. Berndt, "Thermal Spray Society: Opportunities For Your Company To Prosper", web news for the 39,000 members of ASM Int., January 27, 2004. <a href="http://www.asminternational.org/Content/NavigationMenu/Membership/A_Members_Voice/TSS.htm">http://www.asminternational.org/Content/NavigationMenu/Membership/A_Members_Voice/TSS.htm</a>
358	C.C. Berndt, "Feedstock Material Considerations", p.137-141 of "Handbook of Thermal Spray Technology", Ed. J.R. Davis, (2004) Pub. ASM International, Materials Park, OH-USA.
357	C.C. Berndt, "Introduction to Materials Production for Thermal Spray Processes", pp. 135-136 of "Handbook of Thermal Spray Technology", Ed. J.R. Davis, (2004) Pub. ASM International, Materials Park, OH-USA.
356	C.C. Berndt, "Material Categories for Thermal Sprayed Coatings", pp. 142-146 of "Handbook of Thermal Spray Technology", Ed. J.R. Davis, (2004) Pub. ASM International, Materials Park, OH-USA.
355	C.C. Berndt, "Particle Characterization", pp. 159-168 of "Handbook of Thermal Spray Technology", Ed. J.R. Davis, (2004) Pub. ASM International, Materials Park, OH-USA.
354	C.C. Berndt, "Materials Production For Thermal Spray Processes", in "Handbook of Thermal Spray Technology", Ed. J.R. Davis, Pub. ASM International, Materials Park, OH-USA, 2004. ISBN: 0-87170-795-0

ID	Reference
353	“TS Explorer CD-ROM”, C.C. Berndt, L. Sun and P. Michlik, ASM International, Materials Park, OH-USA, 2004. “The TS Explorer provides a quick, comprehensive reference to papers presented at the Thermal Spray conferences from 1980 – 2003.”
352	The Adhesion Of Flame And Plasma Sprayed Coatings, Ph.D. Thesis, 259 pages. Published as a digital historical CD by the University at Stony Brook, 2004. < <a href="https://dspace.sunyconnect.suny.edu/handle/1951/18847">https://dspace.sunyconnect.suny.edu/handle/1951/18847</a> >
351	J.R.T. Branco, R. Gansert, S. Sampath, C.C. Berndt and H. Herman, “ Solid particle erosion of plasma sprayed ceramic coatings”, Mat. Res., 7[1] (2004) 147-153.
350	D.N. Guru, M. Palacio, W. Mook, M. Chambers, J. Heberlein, W. Gerberich, O. Racek and C.C. Berndt, "Nanophase Partially Stabilized Zirconia Intermediate Layer for Strain Accommodation in a Multi-layer Thermal Barrier Coating", Proc. ITSC-2004 Osaka, Pub. Verlag fur Schweissen und verwantle Verfahren DVS-Verlag GmbH, Dusseldorf, Germany, 2004. ISBN 3-87155-792-7.
349	A. Ibrahim and C.C. Berndt, "Fatigue and Mechanical Properties of Nanostructured WC-Co Coatings", Thermal Spray 2004: Advances in Technology and Application , pp. 878-880.
348	P. Michlik, O. Racek and C.C. Berndt, "The Effect of YSZ Microstructure on Young's Modulus", Proc. ITSC-2004 Osaka, Pub. Verlag fur Schweissen und verwantle Verfahren DVS-Verlag GmbH, Dusseldorf, Germany, 2004. ISBN 3-87155-792-7.
347	F.Y. Yan, K.A. Gross, G.P. Simon and C.C. Berndt, “Mechanical And Erosion Properties Of Caco3-EMAA Thermal Sprayed Coatings”, Polymer Engineering And Science, 44 [8], (2004) 1448-1459.
346	M.L. Berndt and C.C. Berndt, “Thermal Spray Coatings For Corrosion Protection”, Invited Chapter for the ASM Corrosion Handbook, Volume 13A, Chapter 4d4: Principles of Metallic Corrosion, Corrosion Protection and Control, Eds. Stephen D. Cramer and Bernard S. Covino, Jr., Pub. ASM International, Materials Park, OH-USA, 2003. ISBN: 0-87170-705-5.
345	Materials Research Society Fall Meeting (2002) December, Boston. Reference: Nanomaterials for Structural Applications, C.C. Berndt, T.E. Fischer, I. Ovid’ko, G. Skandan and T. Tsakalakos (co-Editors), Volume 740 of the Materials Research Society Symposium Series, Pub. MRS, 2003. ISBN 1-55899-677-X.
344	H. Boukari, A. Allan, G. Long, J. Ilavsky, J. Wallace, C. Berndt and H. Herman, “Small-Angle Neutron Scattering Study Of The Role Of Feedstock Particle Size On The Microstructural Behavior Of Plasma-Sprayed YSZ Deposits”, JMRS, 18 (2003) 624-634.
343	M.S. Fofana, B. Zhang, C.C. Berndt and I.S. Jawahir, “Nanostructured Cutting Tools: Tool-Wear and Machining Stability”, Poster presentation at NSF-MIT workshop March 2003.
342	A. Ibrahim and C.C. Berndt, "Fatigue and Deformations of HVOF Sprayed WC-Co Coatings vs. Hard Chrome Plating", ITSC 2003: International Thermal Spray Conference 2003: Advancing the Science and Applying the Technology; Orlando, FL; USA; 5-8 May 2003. pp. 377-380.
341	L. Sun, C.C. Berndt and C.P. Grey, “Phase, Structural And Microstructural Investigations Of Plasma Sprayed Hydroxyapatite Coatings”, MSE-A, 360 (2003) 70-84.
340	L. Pawlowski and C.C. Berndt, “The Globalization of JTST: A Forum for a World Wide Network”, JTST, 12 (2003) 3-4.



ID	Reference
339	K. Remesh, S.C.M. Yu, H.W. Ng and C.C. Berndt, "Computational Study And Experimental Comparison Of The In-Flight Particle Behavior For An External Injection Plasma Spray Process", JTST, 12[4] (2003) 508-522.
338	F.Y. Yan, K.A. Gross, G.P. Simon and C.C. Berndt, "Peel-Strength Behaviour Of Bilayer Thermal Sprayed Polymer Coatings", J. Applied Polymer Science, 88 (2003) 214-226.
337	C.C. Berndt, "A Message from the President of the TSS – Join US in Orlando as we bring Thermal Spray into the 21st Century", JTST, 11 (2002) 431.
336	C.C. Berndt and R.H. Unger, "Applications Of Thermal Spray Coatings: A Technology With No Bounds", The Finishing Line, 18[2] (2002) online invited paper.
335	K.A. Gross and C.C. Berndt, pp. 631-672 of "Biomedical Application Of Apatites", in Reviews in Mineralogy and Geochemistry, Volume 48, 2002 on "PHOSPHATES: Geochemical, Geobiological and Materials Importance", Eds. Matthew L. Kohn, John Rakovan & John M. Hughes, Pub. Mineralogical Society of America, Washington, DC, USA. ISBN 0-939950-60-X.
334	S. Guessasma, G. Montavon, C. Coddet, C. Mancini and C.C. Berndt, "Fractal Dimension As An Indicator Of Thermal Spray Coatings Roughness", pp. 949-953 of International Thermal Spray Conference, Ed. E. Lugscheider and C.C. Berndt, Pub. DVS, Dusseldorf, Germany, 2002. ISBN 3-87155-783-8.
333	A. Kucuk, C.G. Dambra, C.C. Berndt, U. Senturk and R.S. Lima, "Cracking Behavior Of Nicalay/YSZ Thermal Barrier Coatings Under Four Point Bend Loads", pp. 177-186 of Functionally Graded Materials 2000, Eds. K. Trumble et al., Ceramic Transactions Volume 114, 2002.
332	R.S. Lima, A. Kucuk and C.C. Berndt, "Bimodal Distribution Of Mechanical Properties On Plasma Sprayed Nanostructured Partially Stabilized Zirconia", Mat. Sci. Eng. A, A327 (2002) 224-232.
331	R.S. Lima, A. Kucuk, C.C. Berndt, J. Karthikeyan, C. Kay and J. Lindemann, "Deposition Efficiency, Mechanical Properties And Coating Roughness In Cold-Sprayed Titanium", J. Materials Science Letters, 21 (2002) 1687-1689.
330	R.S. Lima, J. Karthikeyan, C.M. Kay, J. Lindemann and C.C. Berndt, "Microstructural Characteristics Of Cold-Sprayed Nanostructured WC-Co Coatings", J. Thin Solid Films, 416 (2002) 129-135.
329	L. Sun, C.C. Berndt and K.A. Gross, "Hydroxyapatite / Polymer Composite Flame Sprayed Coatings For Orthopedic Applications", J. Biomaterials Science, 13[9] (2002) 977-990.
328	L. Sun, C.C. Berndt, K.A. Khor, H.N. Cheang and K.A. Gross, "Surface Characteristics And Dissolution Behavior Of Plasma Sprayed Hydroxyapatite Coating", J. Biomedical Materials Research, 36 (2002) 228-236.
327	International Thermal Spray Conference, E. Lugscheider and C.C. Berndt (Eds.), Pub. Pub. DVS Deutscher Verband für Schweißen, Germany, 2002, 1061+ pages. ISBN 3-87155-783-8.
326	A.J. Allen, J. Ilavsky, G.G. Long, J.S. Wallace, C.C. Berndt and H. Herman, "Microstructural Characterization Of Yttria-Stabilized Zirconia Plasma-Sprayed Deposits Using Multiple Small-Angle Neutron Scattering", Acta Materialia, 49[9] (2001) 1661-1675.
325	C.C. Berndt, "Input Sought from Testers of Thermal Spray Coatings for Cohesion", JTST, 10[1] (2001) 13.

ID	Reference
324	C.C. Berndt, "How do we Market JTST", 10 (2001) 3-4.
323	C.C. Berndt, "Thermal Spray: A Case History For The Integration Of Materials Science And Thermo-Fluid Dynamics", 4 pages ASME invited paper, September 2001, New York.
322	C.C. Berndt, "The Origins of Thermal Spray Literature", 10 (2001) 199-204.
321	C.C. Berndt, "Thermal Spray Processing Of Nanoscale Materials II – Extended Abstracts", JTST, 10[1] (2001) 147-182.
320	C.C. Berndt, "The Origins Of Thermal Spray Literature", pp. 1351-1360 of Thermal Spray 2001: New Surfaces for a New Millennium, Eds. C.C.Berndt, K.A. Khor and E. Lugscheider, Pub. ASM International, Materials Park, OH-USA, 2001. ISBN 0-87170-737-3.
319	2nd International Thermal Spray Conference (2001) May, Singapore. Reference: Thermal Spray 2001: New Surfaces for a New Millennium, Eds. C.C.Berndt, K.A. Khor and E. Lugscheider, Pub. ASM International, Materials Park, OH-USA, 2001, 1400+ pages. . ISBN 0-87170-737-3.
318	M.R. Gold and C.C. Berndt, "Scratch Testing Of Alumina+13%Titania Zirconia", pp. 1105-1110 of Thermal Spray 2001: New Surfaces for a New Millennium, Eds. C.C.Berndt, K.A. Khor and E. Lugscheider, Pub. ASM International, Materials Park, OH-USA, 2001. ISBN 0-87170-737-3.
317	J. Karthikeyan, C.M. Kay, J. Lindemann, R.S. Lima and C.C. Berndt, "Cold Sprayed Nanostructured WC-Co", pp. 383-387 of Thermal Spray 2001: New Surfaces for a New Millennium, Eds. C.C.Berndt, K.A. Khor and E. Lugscheider, Pub. ASM International, Materials Park, OH-USA, 2001. ISBN 0-87170-737-3.
316	A. Kucuk, C.G. Dambra and C.C. Berndt, "Influence Of Plasma Spray Parameters On The Cracking Behavior Of Yttria Stabilized Zirconia Coatings", J. Practical Failure Analysis, 1[1] (2001) 55-64.
315	A. Kucuk, R.S. Lima and C.C. Berndt, "Influence Of Plasma Spray Parameters On Formation And Morphology Of ZrO <sub>2</sub> -8wt% Y <sub>2</sub> O <sub>3</sub> Deposits", J. Am. Ceram. Soc, 84[4] (2001) 693-700.
314	A. Kucuk, R.S. Lima and C.C. Berndt, "Influence Of Plasma Spray Parameters On In-Flight Characteristics Of ZrO <sub>2</sub> -8wt% Y <sub>2</sub> O <sub>3</sub> Ceramic Particles", J. Am. Ceram. Soc, 84[4] (2001) 685-92.
313	A. Kucuk, U. Senturk and C.C. Berndt, "Deformation Characteristics Of Plasma Sprayed YSZ Coatings Using Acoustic Emission" pp. 283-300 or Ceramic Transactions 2001; Vol. 122 on "Fractography of Glasses and Ceramics IV", Eds. J.R. Varner and G.D. Quinn, Pub. American Ceramic Society.
312	R.S. Lima, A. Kucuk and C.C. Berndt, "Integrity Of Nanostructured Partially Stabilized Zirconia After Plasma Spray Processing", Mat. Sci. Eng. A, A313 (2001) 75-82.
311	R.S. Lima, A. Kucuk and C.C. Berndt, "Evaluation Of Microhardness And Elastic Modulus Of Thermally Sprayed Nanostructured Zirconia Coatings", Surface and Coatings Technology, 135 (2001) 166-172.
310	R.S. Lima, A. Kucuk, U. Senturk and C.C. Berndt, "Properties and Microstructures of Nanostructured Alumina-13% Titania+ Zirconia Coatings", Journal of Thermal Spray Technology, 10[1] (2001) 179-180.

ID	Reference
309	R.S. Lima, A. Kucuk and C.C. Berndt, "In-Flight Particle Characteristics And Deposition Formation In PSZ", pp. >>-?? of Thermal Spray 2001: New Surfaces for a New Millennium, Eds. C.C.Berndt, K.A. Khor and E. Lugscheider, Pub. ASM International, Materials Park, OH-USA, 2001. ISBN 0-87170-737-3.
308	L. Sun, C.C. Berndt, K.A. Gross and A. Kucuk, "Material Fundamentals And Clinical Performance Of Plasma Sprayed Hydroxyapatite Coatings: A Review", J. Biomedical Materials Research, 58 [5] (2001) 570-592.
307	L. Sun, C.C. Berndt and K.A. Gross, "Characterization And Mechanical Properties Of Flame Sprayed Hydroxyapatite/Polymer Composite Coatings", pp. 321-326 of Thermal Spray 2001: New Surfaces for a New Millennium, Eds. C.C.Berndt, K.A. Khor and E. Lugscheider, Pub. ASM International, Materials Park, OH-USA, 2001. ISBN 0-87170-737-3.
306	C.E. Mancini, A. Kucuk and C.C. Berndt, "Porosity Determinations In Thermally Sprayed Hydroxyapatite Coatings", Mater. Sci. Letter, 36 [16] (2001) 3891-3896.
305	K. Remesh, S.C.M. Yu, H.W. Ng, Y.C. Lam and C.C. Berndt, "Effects of Carrier Gas Flow on Particle In-Flight Characteristics During the Plasma Spray Process with External Injection", Proceedings of the National Heat Transfer Conference 1 pp. 467-474.
304	K. Remesh, S.C.M. Yu, H.W. Ng, Y.C. Lam, A. Devasenpathi and C.C. Berndt, "Effects Of Carrier Gas Flow On Particle In-Flight Characteristics During The Plasma Spray Process With Internal Injection", Reviewed for ASME 35th National Heat Treat Conference, June 2001, CA-USA.
303	D.L. Vasquez, A. Kucuk, R.S. Lima, U. Senturk and C.C. Berndt, "Elastic Modulus Measurements Of Air Plasma Sprayed Yttria Partially Stabilized Zirconia Coatings Using Laser Ultrasonics And Indentation Techniques", pp. 1045-1050 of Thermal Spray 2001: New Surfaces for a New Millennium, Eds. C.C.Berndt, K.A. Khor and E. Lugscheider, Pub. ASM International, Materials Park, OH-USA, 2001. ISBN 0-87170-737-3.
302	C.C. Berndt, "Sensors And Controls For Thermal Spray: Is There A Need?", pp. 59-64 of "Thermal Spray Coatings Workshop: Sensors, Modeling and Control Strategies", F.S. Biancaniello and S.D. Ridder, Pub., NIST under Report Number NISTIR 6460, January 2000.
301	1st International Thermal Spray Conference (2000) May, Montreal (Canada). Reference: Thermal Spray: Surface Engineering via Applied Research, Ed. C.C.Berndt, Pub. ASM International, Materials Park, OH-USA, 2000, 1410+ pages.
300	T. Chraska, A.H. King and C.C. Berndt, "On The Size-Dependent Phase Transformation In Nanoparticulate Zirconia", Mat. Sci. Eng. A A286 (2000) 169-178.
299	A.Z. Ibrahim and C.C. Berndt, "The Effect Of HFPD Thermally Sprayed WC-Co Coatings On The Fatigue Behavior And Deformation Of Al 2024-T4", pp. 1297-1301 of "Thermal Spray: Surface Engineering via Applied Research", Ed. C.C. Berndt, ASM International, Materials Park, OH-USA. 2000
298	J. Karthikeyan, C.M. Kay, J. Lindeman, R.S. Lima and C.C. Berndt, "Cold Spray Processing Of Titanium Powder", pp. 255-262 of "Thermal Spray: Surface Engineering via Applied Research", Ed. C.C. Berndt, ASM International, Materials Park, OH-USA. 2000
297	A. Kucuk, C.C. Berndt, U. Senturk, R.S. Lima and C.R.C. Lima, "Influence Of Plasma Spray Parameters On The Mechanical Properties Of Yttria Stabilized Zirconia Coatings I: Four Point Bend Test", J. Materials Engineering and Science A, A284 (2000) 29-40.

ID	Reference
296	A. Kucuk, C.C. Berndt, U. Senturk, R.S. Lima and C.R.C. Lima, "Influence Of Plasma Spray Parameters On The Mechanical Properties Of Yttria Stabilized Zirconia Coatings II: Acoustic Emission Response", Materials Engineering and Science A, A284 (2000) 41-50.
295	A. Kucuk, R.S.Lima and C C. Berndt, "Composite Coatings Of Si3N4-Soda Lime Silica Produced By The Thermal Spray Process", J. Materials Engineering and Performance, 9[6] (2000) 603-608.
294	A. Kucuk, C.C. Berndt, U. Senturk, R.S.Lima and C.R.C. Lima, "Deformation Characteristics Of Plasma Sprayed Thermal Barrier Coatings", pp. 681-690 of Ceramic Engineering and Science Proceedings 2000, Volume 21, Part 4.
293	A. Kucuk, C.C. Berndt, U. Senturk and R.S. Lima, "Characterization Of The Mechanical Properties Of Tbc's Via A Taguchi Experimental Design". pp. 1211-1217 of "Thermal Spray: Surface Engineering via Applied Research", Ed. C.C. Berndt, ASM International, Materials Park, OH-USA. 2000
292	R.S. Lima, A. Kucuk and C.C. Berndt, "Correlation Between Deposition Efficiency, Hardness And Elastic Modulus For Thermally Sprayed Zirconia", pp. 1201-1205 of "Thermal Spray: Surface Engineering via Applied Research", Ed. C.C. Berndt, ASM International, Materials Park, OH-USA. 2000
291	C.R.C. Lima, U. Senturk, R.S. Lima and C.C. Berndt, "Thermal Conductivity Behavior Of Sol-Gel Post Treated Thermal Barrier Coatings". pp. 1057-1060 of "Thermal Spray: Surface Engineering via Applied Research", Ed. C.C. Berndt, ASM International, Materials Park, OH-USA. 2000.
290	L. Sun, C.C. Berndt, A. Kucuk, R.S. Lima and K.A. Khor, "Surface Characterization Of Plasma Sprayed Hydroxyapatite Coatings," pp. 251-258 of Ceramic Engineering and Science Proceedings 2000, Volume 21, Part 4.
289	L. Sun, C.C. Berndt, R.S. Lima, A. Kucuk and K.A. Khor, "Effects Of Spraying Parameters On Phase Formation And Distribution In Plasma Sprayed Hydroxyapatite Coatings," pp. 803-809 of "Thermal Spray: Surface Engineering via Applied Research", Ed. C.C. Berndt, ASM International, Materials Park, OH-USA. 2000
288	T. Nakamura, G. Qian and C.C. Berndt, "Effects Of Pores On Mechanical Properties Of Plasma Sprayed Ceramic Coatings", J. A. Cer. Soc., 83[3] (2000) 578-84.
287	U. Senturk, R.S. Lima, C.R.C. Lima and C.C. Berndt, "Deformation Of Plasma Sprayed Thermal Barrier Coatings", J. Engineering for Gas Turbines and Power, 122[July] (2000) 387-392.
286	A. Abbate, W. Russell, J. Goldman, P. Kotidis and C.C. Berndt, "Nondestructive Determination Of Thickness And Elastic Modulus Of Plasma Spray Coatings Using Laser Ultrasonics", Review of Progress in Quantitative Nondestructive Evaluation, Ed. Thompson and Chimenyi, Pub. Kluwer Academic/Plenum, Vol. 18 (2000) pp. 373-380.
285	A.J. Allen, G.G. Long, J. Wallace, J. Ilavsky and C.C. Berndt , "Microstructural Changes in YSZ Deposits During Annealing", UTSC '99: United Thermal Spray Conference; Dusseldorf; Germany; 17-19 Mar. 1999. pp. 228-233.
284	C.C.Berndt, "Thermal Spray Processing Of Nanoscale Materials", Defense Technical Information Center Document #ADA370846, December 11, 1999.
283	H. Boukari, A.J. Allen, G.G. Long, J. Ilavsky, J. Wallace, C.C. Berndt and H. Herman, "The Role Of Feedstock Particle Size On The Microstructure Behavior Of Plasma-Sprayed YSZ Deposits During Annealing", Conference Proceedings of the United Thermal Spray Conference, Ed. E. Lugscheider and P. A. Kammer, Verlag fur Schweissen und verwantle Verfahren DVS-Verlag GmbH, Dusseldorf, Germany, 1999,

ID	Reference
	p799-804.
282	P.J. Callus and C.C. Berndt, "Relationships Between Mode II Fracture Toughness And Microstructure Of Thermal Spray Coatings", Surface and Coatings Technology, 111 (1999) 114-128.
281	A Ibrahim, CC Berndt and U Senturk, "Cyclic deformation and fatigue damage of aluminum alloy and steel HVOF sprayed with WC-Co coating", UTSC '99: United Thermal Spray Conference; Dusseldorf; Germany; 17-19 Mar. 1999. pp. 479-482.
280	J. Ilavsky, G.G. Long, A.J. Allen and C.C. Berndt, "Evolution Of The Void Structure Of Plasma-Sprayed YSZ Deposits During Heating", J. Materials Engineering and Science A, A272 (1999) 215-221.
279	J. Ilavsky, A.J. Allen, G.G.Long, C.C. Berndt and H. Herman, "Microstructural Changes In Plasma-Sprayed Deposits During Annealing", Conference Proceedings of the United Thermal Spray Conference, Ed. E. Lugscheider and P. A. Kammer, Verlag fur Schweissen und verwantle Verfahren DVS-Verlag GmbH, Dusseldorf, Germany, 1999.
278	S-H. Leigh and C.C. Berndt, "Quantitative Evaluation Of Void Distributions Within A Plasma Sprayed Ceramic", J. Am. Ceramic Soc, 82[11] (1999) 17-21.
277	S-H. Leigh and C.C. Berndt, "Modelling Of Elastic Constants Of Plasma Sprayed Deposits With Ellipsoid-Shaped Voids", Acta Materialia, 47[5] (1999) 1575-1586.
276	R.S. Lima, U. Senturk, C.R.C. Lima and C.C. Berndt, "Spraying Characteristics Of Nanostructured Zirconia Particles", Conference Proceedings of the United Thermal Spray Conference, Ed. E. Lugscheider and P. A. Kammer, Verlag fur Schweissen und verwantle Verfahren DVS-Verlag GmbH, Dusseldorf, Germany, 1999.
275	L. Sun, C.C. Berndt and K.A. Khor, "Nanostructure In Plasma Sprayed Hydroxyapatite Coating," Extended Abstract, p.49-50 in Thermal Spray Processing of Nanoscale Materials II, Quebec City, Aug. 15-20, 1999. Ed. C.C. Berndt.
274	L. Sun and C.C. Berndt, "Microdiffraction Studies Of Plasma Sprayed Hydroxyapatite Coatings Using Synchrotron Radiation," 1999 National Synchrotron Light Source Activity Report, Brookhaven National Laboratory, Upton, NY.
273	C.K. Lin, U. Senturk, R.S. Lima, C.C. Berndt, J.C. Shieh and P.Y. Lee, "Investigations Of Thermal Barrier Coatings With Loading And Unloading To Various Stress Levels". Conference Proceedings of the United Thermal Spray Conference, Ed. E. Lugscheider and P. A. Kammer, Verlag fur Schweissen und verwantle Verfahren DVS-Verlag GmbH, Dusseldorf, Germany, 1999, p. 809-814.
272	R. Nachwalter, B.P. Meinhard, U. Senturk, J. Habrect and C.C. Berndt, "A Comparison Of Various Methods Of Fixation In Pauwels' III Femerol Neck Fractures", 66th Annual Meeting of the American Academy of Orthopaedic Surgeons, "Anaheim, CA, Feb. 1999.
271	R. Seals and C.C. Berndt, "Rationale for a JTST Award for the Best Scientific Paper", JTST, 8[1] (1999) 3-5.
270	U. Senturk, R.S.Lima, C.C. Berndt, C.K. Lin and C.R.C. Lima, "Processing And Mechanical Properties Of Plasma Sprayed Thermal Barrier Coatings". Conference Proceedings of the United Thermal Spray Conference, Ed. E. Lugscheider and P. A. Kammer, Verlag fur Schweissen und verwantle Verfahren DVS-Verlag GmbH, Dusseldorf, Germany, 1999, p. 815-819.



ID	Reference
269	A. Abbate, W. Russell, P. Kotidis and C.C. Berndt, "Nondestructive Characterization Of Plasma Spray Coatings - Some Recent Industry / University Work", JTST, 7[1] (1998) 25-27.
268	M.L. Allan, C.C. Berndt and D. Otterson, "Polymer Coatings For Corrosion Protection In Biochemical Treatment Of Geothermal Residues", Geothermal Resources Council Transactions, 22 (1998) 20-23.
267	M.L. Allan, D. Otterson and C.C. Berndt, "Plasma Sprayed Ni-Al Coatings For Safe Ending Heat Exchanger Tubes", Brookhaven National Laboratory Report 66149, 38 pages, 1998.
266	M.L. Allan, C.C. Berndt, J.A. Brogan and D. Otterson, "Thermal Sprayed Polymer Coatings For Corrosion Protection In A Biochemical Treatment Process", pp. 13-18 of Thermal Spray Meeting the Challenges of the 21st Century", Ed. C. Coddet, ASM International, Materials Park, OH-USA, 1998.
265	C.C. Berndt and E.J. Lavernia, "Thermal Spray Processing Of Nanoscale Materials - A Conference Report With Extended Abstracts", JTST, 7[3] (1998) 411-441.
264	C.C. Berndt, C.K. Lin and S-H. Leigh, "Characterization of Cracking within Thermal Spray Deposits by an Acoustic Emission Method - Extended abstract", JTST, 7[3] (1998) 334-336. Also in Proc. Int. Conf. On Composites Engineering, Hawaii, July 6-11, 1997. Pp. 1-2.
263	C.C. Berndt, J.A. Brogan, G. Montavon, A. Claudon and C. Coddet, "Mechanical Properties of Metal- and Ceramic-Polymer Composites Formed via Thermal Spray Consolidation - Extended Abstract", Journal of Thermal Spray Technology, 7[3] (1998) 337-339.
262	1st United Thermal Spray Conference (1997) 15-18 September, Indianapolis (IN). Reference: Thermal Spray: A United forum for Scientific and Technological Advances, Ed. C.C. Berndt, Pub. ASM International, Materials Park, OH-USA, 1998, 1020+ pages.
261	V.T. Breslin, U. Senturk and C.C. Berndt, "Long-Term Engineering Properties Of Recycled Plastic Lumber Used In Pier Construction", Resources, Conservation and Recycling, 23 (1998) 243-258..
260	J.A. Brogan, C.C. Berndt, G.P. Simon and D. Hewitt, "Physical And Relaxation Properties Of Flame-Sprayed Ethylene-Methacrylic Acid Copolymer", Polymer Engineering and Science, 38 [11] (1998) 1873-1881.
259	J.A. Brogan, C.C. Berndt, A. Claudon and C. Coddet, "Mechanical Properties Of Spray-Formed Polymer Composite Structures", pp. 1173-1178 of Thermal Spray Meeting the Challenges of the 21st Century", Ed. C. Coddet, ASM International, Materials Park, OH-USA, 1998.
258	T. Chraska, A.H. King and C.C. Berndt, "Self-Similarity And Lognormal Size Distributions In Coarsening Systems: The Case Of Nanocrystalline Zirconia", 3rd International Conference on Grain Growth, Pittsburgh, PA-USA, June 14-19, 1998.
257	K.A. Gross and C.C. Berndt, "Thermal Processing Of Hydroxyapatite For Coating Production", J. Biomedical Materials Research, 39 (1998) 580-587.
256	K.A. Gross, C.C. Berndt and H. Herman, "Amorphous Phase Formation In Plasma Sprayed Hydroxyapatite Coatings", J. Biomedical Materials Research, 39 (1998) 407-414.
255	K.A. Gross, C.C. Berndt and V.J. Iacono, "Variability Of Hydroxyapatite Coated Dental Implants", The International J. Oral & Maxillofacial Implants, 13 [5] (1998)

ID	Reference
	601-610..
254	K.A. Gross, C.C. Berndt, R. Dinnebier and P. Stephens, "Oxyapatite In Hydroxyapatite Coatings", J. Materials Science – Materials in Medicine, 33 (1998) 3985-3991.
253	K.A. Gross, V.Gross and C.C. Berndt, "Thermal Analysis Of Amorphous Phases In Hydroxyapatite Coatings", J. Am. Ceram. Soc., 81 [1] (1998) 106-112.
252	K.A. Gross, M. Phillips, B. Ben-Nissan and C.C. Berndt, "Identification Of The Amorphous Phase In Plasma Sprayed Apatite Coatings", pp. 177-180 of Bioceramics Volume 11, Ed. R. Z. LeGeros and J.P. LeGeros, Pub. World Scientific Publishing Co., New York, 1998.
251	A. Ibrahim and C.C. Berndt, "The Effect Of HVOF Thermally Sprayed WC-Co Coatings 3109-3114.
250	A. Ibrahim and C.C. Berndt, "Fatigue Behavior And Deformation Of Aluminum And Steel HVOF Sprayed With WC-Co Coatings", pp. 731-736 of "Thermal Spray: A United forum for Scientific and Technological Advances", C.C. Berndt (Ed.), ASM International, Materials Park, OH-USA, 1998.
249	J. Ilavsky and C.C. Berndt, "Thermal Expansion Properties Of Metallic And Cermet Coatings", J. Surf. Coat. Tech., 102 (1998) 19-24.
248	J. Ilavsky, G.G. Long, A.L. Allen, H. Herman and C.C. Berndt, "Use Of Small-Angle Neutron Scattering For The Characterization Of Anisotropic Structures Produced By Thermal Spraying, Ceramics – Silikáty, 42[3] (1998) 81-89.
247	J. Ilavsky, G.G. Long, A.J. Allen, C.C. Berndt and H. Herman, "Changes In The Microstructure Of Plasma-Sprayed Ytria-Stabilized Zirconia Deposits During Simulated Operating Conditions", pp. 697-702 of "Thermal Spray: A United forum for Scientific and Technological Advances", C.C. Berndt (Ed.), ASM International, Materials Park, OH-USA, 1998.
246	J. Karthikeyan, C.C. Berndt, S. Reddy, J.-Y. Wang, A.H. King and H. Herman, "Nanomaterial Deposits Formed By DC Plasma Spraying Of Liquid Feedstocks", J. Am. Ceram. Soc., 81[1] (1998) 121-28.
245	A.H. King, T. Chraska and C.C. Berndt, "Growth, Transformation and Agglomeration of Nanocrystalline Zirconia Particles Produced by Plasma Spraying of Liquid Feedstocks", American Physical Society, Annual March Meeting, March 16-20
244	S-H. Leigh, C.C. Berndt, M.K. Ferber and L. Riester, "Nanoindentation Study Of Thermal Spray Deposits", pp. 723-729. of "Thermal Spray: A United forum for Scientific and Technological Advances", C.C. Berndt (Ed.), ASM International, Materials Park, OH-USA, 1998.
243	S-H. Leigh, G-C. Lee and C.C. Berndt, "Modelling Of Elastic Constants Of Plasma Spray Deposits With Spheroid-Shaped Voids", pp. 587-592 of Thermal Spray Meeting the Challenges of the 21st Century", Ed. C. Coddet, ASM International, Materials Park, OH-USA, 1998.
242	G. Montavon, C. Coddet, C.C. Berndt and S.-H. Leigh, "Microstructural Index To Quantify Thermal Spray Deposit Microstructures Using Image Analysis", J. Thermal Spray Tech., 7[2] (1998) 229-241.
241	K. Murakami, C.-K. Lin, S.-H. Leigh, C.C. Berndt, S. Sampath, H. Herman, S. Sodeoka and H. Nakajima, "Porosity Measurement And Densification Of Plasma Sprayed Alumina-Titania Deposits", pp. 204-212 of Surface Modification

ID	Reference
	Technologies X1, Ed. T.S. Sudarshan, M. Jeandin and K.A. Khor, Pub. The institute of Materials, London, 1998
240	A. Newman, T. Jewett, S. Sampath, C.C. Berndt and H. Herman, "Indentation Response Of Molybdenum Disilicide", J. Materials Research, 13 [9] (1998), 2662-2671.
239	G. Qian, T. Nakamura and C.C. Berndt, "Effects Of Thermal Gradient And Residual Stresses On Thermal Barrier Coating Fracture", Mechanics of Materials, 27 (1998) 91-110.
238	A.J. Slifka, B.J. Filla, J.M. Phelps, G. Bancke and C.C. Berndt, "Thermal Conductivity Of A Zirconia Thermal Barrier Coating", JTST, 7[1] (1998) 43-46.
237	C.C. Berndt, C.K. Lin and S-H. Leigh, "Characterization Of Cracking Within Thermal Spray Deposits By And Acoustic Emission Method", Proc. Int. Conf. On Composites Engineering, Hawaii, July 6-11, 1997. Pp. 1-2
236	C.C. Berndt, J. Karthikeyan, T. Chraska and A.H. King, "Plasma Spray Synthesis Of Nanozirconia Powder", Proceedings of the Joint NSF-NIST Conference on Nanoparticles: Synthesis, Processing into Functional Nanostructures and Characterization, 12-13 May 1997, NSF Arlington, USA.
235	C.C. Berndt, J.A. Brogan, G. Montavon, A. Claudon and C. Coddet, "Mechanical Properties Of Metal- And Ceramic-Polymer Composites Formed Via Thermal Spray Consolidation", Proc. Int. Conf. On Composites Engineering, Hawaii, July 6-11, 1997. Pp. 185-186.
234	C.C. Berndt and S.A. Drotz, "Development of Recycled Polymer Blends for Thermal Spray Applications", NASA no. 19980041514.
233	J. Brogan, C.C. Berndt, G.P. Simon and D. Hewitt, "Oxidation Of Polyolefins During Flame Spraying", Fall'97 MRS meeting, Boston (MA-USA), 1-5 December 1997.
232	J.A. Brogan and C.C. Berndt, "The Coalescence Of Combustion Sprayed Ethylene-Methacrylic Acid Copolymer", J.Mater. Sci., 32 (1997) 2099-2106.
231	T. Chraska, A.H. King, C.C. Berndt and J. Karthikeyan, "Phase Transformation As A Function Of Particle Size In Nanocrystalline Zirconia", MRS Proceedings, Fall, 1997.
230	K.A. Gross, C.C. Berndt, D.E. Goldschlag and V. Iacono, "Location Of Amorphous Phases In Hydroxyapatite Coated Dental Implants", Proc. 12th Annual Meeting of the Academy of Osseointegration, San Francisco, CA, March 6-8 1997.
229	K.A. Gross, C.C. Berndt, D.D. Goldschlag and V.J. Iacono, "In Vitro Changes Of Hydroxyapatite Coatings", International J. Oral & Maxillofacial Implants, 12 (1997) 589-597.
228	J. Ilavsky, A.J. Allen, G.G. Long, H. Herman and C.C. Berndt, "Characterization Of The Closed Porosity In Plasma-Sprayed Alumina", J. Mat. Sci., 32 (1997) 3407-3410.
227	J. Ilavsky, A.J. Allen, G.G. Long, S. Krueger, C.C. Berndt and H. Herman, "Influence Of Spray Angle On The Porous Microstructure Of Plasma-Sprayed Ceramic Deposits", J. Am. Ceram. Soc., 80[3] (1997) 733-42.
226	J. Ilavsky, C.C. Berndt and J. Karthikeyan, "Mercury Intrusion Porosimetry Of Plasma-Sprayed Ceramic", J. Mater. Sci., 32 (1997) 3925-3932.
225	J. Ilavsky, C.C. Berndt, H. Herman, P. Chraska and J. Dubsky, "Alumina-Base Plasma-Sprayed Materials - Part II: Phase Transformations In Aluminas", JTST, 6[4] (1997) 439-444.

ID	Reference
224	J. Karthikeyan, C.C. Berndt, J. Tikkanen, J.-Y. Wang, A.H. King and H. Herman, "Nanomaterial Powders And Deposits Prepared By Flame Processing Of Liquid Precursors", Nanostructured Materials, 8[1] 1997 61-74.
223	J. Karthikeyan, C.C. Berndt, J. Tikkanen, J.Y. Wang, A.H. King and H. Herman, "Preparation Of Nanophase Materials By Thermal Spray Processing Of Liquid Precursors", Nanostructured Materials, 9 (1997) 137-140.
222	J. Karthikeyan, C.C. Berndt, J. Tikkanen, S. Reddy and H. Herman, "Plasma Spray Synthesis Of Nanomaterial Powders And Deposits", Materials Science and Engineering A, 238[2] (1997) 275-286.
221	S-H. Leigh and C.C. Berndt, "Evaluation Of Off-Angle Thermal Spray", J. Surf. Coat. Tech., 89 (1997) 213-224.
220	S-H. Leigh, C.K. Lin and C.C. Berndt, "Elastic Response Of Thermal Spray Deposits Under Indentation Tests", J. Am. Ceramic Soc., 80[8] (1997) 2093-2099.
219	C.-K. Lin and C.C. Berndt, "Acoustic Emission Studies On Thermal Spray Materials", J. Surface and Coatings Technology, 102 (1997) 1-7.
218	C.K. Lin, C.C. Berndt, S-H. Leigh and K. Murakami, "Acoustic Emission Studies Of Alumina-13% Titania Free Standing Forms During Four Point Bend Tests", J. Am. Ceramic Society, 80 [9] (1997) 2382-94.
217	C.K. Lin, S.-H. Leigh and C.C. Berndt, "Acoustic Emission Responses Of Plasma-Sprayed Alumina-3% Titania Deposits", Thin Solid Films, 310 [1/2] (1997) 108-115.
216	G. Montavon, C.C. Berndt, C. Coddet, S. Sampath and H. Herman, "Quality Control Of The Intrinsic Deposition Efficiency From Controls Of The Splat Morphologies And The Deposit Microstructure", JTST, 6[2] (1997) 152-166.
215	G. Montavon, S-H. Leigh, C.C. Berndt and C. Coddert, "Effect Of The Spray Angle On Splat Morphology During Thermal Spraying", J. Surf. Coat. Tech., 91[1-2] (1997) 107-115.
214	T. Nakamura, G. Qian and C.C. Berndt "Mechanical Properties Of Thermal Barrier Coatings: Effects Of Fracture, Residual Stresses And Void Distributions", Fall'97 MRS meeting, Boston (MA-USA), 1-5 December 1997.
213	G. Qian, C.C. Berndt, S-H. Leigh and T. Nakamura, "Tensile Toughness Test And High Temperature Fracture Analysis Of Thermal Barrier Coatings", Acta mater., 45[4] (1997) 1767-1784 .
212	J. Tikkanen, K.A. Gross, J. Karthikeyan, V. Pitkanen, J. Keskinen, S. Raghu, M. Rajala and C.C. Berndt, "Characteristics Of The Liquid Flame Spray Process", J. Surf. Coat. Tech., 90 (1997) 210-216.
211	S. Wuttiaphan, A. Pajares, B.R. Lawn and C.C. Berndt, "Effect Of Substrate And Bond Coat On Contact Damage In Zirconia-Based Plasma Sprayed Coatings", Thin Solid Films, 293 (1997) 251-260.
210	C.C. Berndt, "Standardize And Deliver", JTST, 5[1] (1996) 2-3.
209	C.C. Berndt, R.Zatorski, G.Bancke, J.A.Brogan, J. Karthikeyan, R.Benary, S. Sampath and H. Herman, pp. 970 of Thermal Spray: Practical Solutions for Engineering Problems, Ed. C.C. Berndt, Pub. ASM International, Materials Park, OH-USA, 1996.
208	C.C. Berndt, "Thermal Spraying In Japan", JTST, 5[3] (1996) 352-367.

ID	Reference
207	9th National Thermal Spray Conference (1996) 7-11 October, Cincinnati (OH). Reference: Thermal Spray: Practical Solutions for Engineering Problems, Ed. C.C.Berndt, Pub. ASM International, Materials Park, OH-USA, 1996, 992+ pages.
206	J.A. Brogan, C.C. Berndt, A. Claudon and C. Coddet, "The Mechanical Properties Of Combustion-Sprayed Polymers And Blends", pp. 221-226 of Thermal Spray: Practical Solutions for Engineering Problems, Ed. C.C. Berndt, Pub. ASM International, Materials Park, OH-USA, 1996.
205	K. Dopler, J.R.T. Branco, S. Sampath, C.C. Berndt, H. Herman and P.J. Chraska, "Iron-Based Deposits Produced By High-Throughput Water Stabilized Plasma," pp. 413-418 of Thermal Spray: Practical Solutions for Engineering Problems, Ed. C.C. Berndt, Pub. ASM International, Materials Park, OH-USA, 1996.
204	R. Gansert, S.-H. Leigh, C.-K. Lin, R. Purandare, S. Sampath, C.C. Berndt, H. Herman and S. Raghu, "Net Shape Manufacturing Engineering By Plasma Technology", pp. 375-376 of Proc. 1996 NSF Design and Manufacturing Grantees Conference, Albuquerque, NM, Pub. SME, 1996.
203	J. Ilavsky, G.G. Long, A.J. Allen, H. Herman and C.C. Berndt, "The Effect Of Spray Distance And Chemistry On Pore And Crack Development In Plasma Sprayed Ceramic Deposits", pp. 725-728 of Thermal Spray: Practical Solutions for Engineering Problems, Ed. C.C. Berndt, Pub. ASM International, Materials Park, OH-USA, 1996.
202	J. Karthikeyan, C.C. Berndt, A. Ristorucci and H. Herman, "Ceramic Impregnation Of Plasma Sprayed Thermal Barrier Coatings", pp. 477-482 of Thermal Spray: Practical Solutions for Engineering Problems, Ed. C.C. Berndt, Pub. ASM International, Materials Park, OH-USA, 1996.
201	J.C. Knowles, K. Gross, C.C. Berndt and W. Bonfield, "Structural Changes Of Thermal Sprayed Hydroxyapatite Investigated By Rietveld Analysis", Biomaterials, 17[6] (1996) 639-645..
200	W.Y. Lee, K.M. Cooley, C.C. Berndt, D.J. Joslin and D.P. Stinton, "High-Temperature Chemical Stability Of Plasma-Sprayed Ca <sub>0.5</sub> Sr <sub>0.5</sub> Zr <sub>4</sub> P <sub>6</sub> O <sub>24</sub> Coatings On Nicalon/Sic Ceramic Matrix Composite And Ni-Based Superalloy Substrates", J.Am. Ceram. Soc., 79[10] (1996) 2759-62.
199	W.Y. Lee, Y.W. Bae, C.C. Berndt, F. Erdogan, Y.-D. Lee and Z. Mutasim, "The Concept Of Functionally Graded Materials For Advanced Thermal Barrier Coating Applications: A Review", J.Am.Ceram.Soc, 79[12] (1996) 3003-3012.
198	A.C.Leger, M.Vardelle, A.Vardelle, P.Fauchais, S. Sampath, C.C. Berndt and H. Herman, "Plasma Sprayed Zirconia: Relationship Between Particle Parameters, Splat Formation And Deposit Generation -Part I: Impact And Solidification", pp. 623-628 of Thermal Spray: Practical Solutions for Engineering Problems, Ed. C.C. Berndt, Pub. ASM International, Materials Park, OH-USA, 1996.
197	S.-H. Leigh, S. Sampath, H. Herman and C.C. Berndt, "Evaluation Of Size-Shape Distribution Of Voids Within Plasma Spray-Formed Ceramics", For PacRim Meeting July, 1996. Aust. Ceramic Soc.
196	C.-K. Lin, S.-H. Leigh, R. Gansert, K. Murakami, S. Sampath, H. Herman and C.C. Berndt, Investigation Of Cracking Mechanisms Of Plasma Sprayed Alumina-13% Titania By Acoustic Emission, in Fracture - Instability Dynamics, Scaling and Ductile/Brittle Behavior, Eds. R.L. Blumberg Selinger, J.J.Mecholsky, A.E.Carlsson and E.R.Fuller, Jr., Mat. Res. Soc. Symp. Proc. Vol. 409 (1996) 261-266.
195	C.K. Lin, S-H. Leigh, C.C. Berndt, R.V. Gansert, S. Sampath and H. Herman, "Acoustic Emission Responses of Plasma Sprayed Ceramics during Four Point Bend



ID	Reference
	Tests". Ceramic Engineering and Science Proceedings 17 (3), pp. 44-50.
194	A. Pajares, L. Wei, B.R. Lawn and C.C. Berndt, "Contact Damage In Plasma-Sprayed Alumina-Based Coatings", J. Am. Ceram. Soc., 79[7] (1996) 1907-14.
193	A. Pajares, L. Wei, B.R.Lawn, N.P. Padture and C.C. Berndt, "Mechanical Characterization Of Plasma Sprayed Ceramic Coatings On Metal Substrates By Contact Testing", Materials Science and Engineering, A208 (1996) 158-165.
192	S. Sampath, J.Matejicek, C.C. Berndt, H. Herman, A.C.Leger, M.Vardelle, A.Vardelle and P.Fauchais, "Plasma Sprayed Zirconia: Relationship Between Particle Parameters, Splat Formation And Deposit Generation -Part II: Microstructure And Properties", pp. 629-636 of Thermal Spray: Practical Solutions for Engineering Problems, Ed. C.C. Berndt, Pub. ASM International, Materials Park, OH-USA, 1996.
191	W. Smith, T.J. Jewett, S. Sampath, C.C. Berndt, H. Herman, J. Fincke and R.N. Wright, "Plasma Processing Of Functionally Graded Materials: Diagnostics And Characterization", pp. 317-324 of Thermal Spray: Practical Solutions for Engineering Problems, Ed. C.C. Berndt, Pub. ASM International, Materials Park, OH-USA, 1996.
190	H.H. Tawfik, F. Zimmerman, H. Herman and C.C. Berndt, "Mathematical Modeling Of The High Velocity Oxy Fuel Systems To Optimize Their Thermally Sprayed Coatings", Technical papers of North American Manufacturing Research Institution of SME(NAMRC), Vol. XXIV, 1996, 6 pages.
189	R. Benary, R.V. Gansert, C.C. Berndt, S. Sampath, H. Herman and V. Hock, "Field Evaluation And Economic Impact Of An Automated Thermal Spray System (ATSS) For Infrastructure Rehabilitation", pp. 621-626 of 1995 Advances in Thermal Spray Science and Technology", Ed. C.C. Berndt and S.Sampath, ASM International, Materials Park, OH-USA, 1995.
188	C.C. Berndt, "Surface Modifications Technologies VII", Materials Characterization, 34 (1995) 2 pages.
187	C.C. Berndt, S. Reddy and M.L. Allan, "Thermal Spraying Of Zinc Onto Concrete", Proc. 4th World Congress on Coating Systems for Bridges and Steel Structures, 1-3 February, 1995, St. Louis, MO-USA. pp. 182.
186	C.C. Berndt, S. Reddy and M.L. Allan, "Optimization Of Thermal Spray Parameters For Cathodic Protection Of Reinforcement In Concrete", pp. 51-64 of Innovative Ideas for Controlling the Decaying Infrastructure, Ed. V.Chaker, Pub. NACE International, 1995.
185	8th National Thermal Spray Conference (1995) 11-15 September, Houston (TX). Reference: Thermal Spray Science & Technology, Eds. C.C.Berndt and S.Sampath, Pub. ASM International, Materials Park, OH-USA, 1995, 774+ pages.
184	J.A. Brogan, R. Lampo and C.C. Berndt, "Thermal Spraying Of Polymers", Proc. 4th World Congress on Coating Systems for Bridges and Steel Structures, 1-3 February, 1995, St. Louis, MO-USA. pp. 200-212.
183	J.A. Brogan, C.C. Berndt and W.C. Smith, "Real-Time Imaging Of The Plasma Spray Process - Work In Progress", J. Thermal Spray Tech., 4[4] (1995) 374-376.
182	J.A. Brogan, S. Sampath, H. Herman and C.C. Berndt, "Combustion Spraying Of Post-Consumer Commingled Polymer Blends", Abstract accepted for MRS 1995 Fall Meeting, Boston, 1995.
181	J.A. Brogan, J. Margolies, S. Sampath, H. Herman, C.C. Berndt and S. Drozd, "Adhesion Of Combustion-Sprayed Polymer Coatings", pp. 521-526 of 1995 Advances

ID	Reference
	in Thermal Spray Science and Technology”, Ed. C.C. Berndt and S.Sampath, ASM International, Materials Park, OH-USA, 1995.
180	R. Gansert, S. Sampath, C.C. Berndt, H. Herman and P. Chraska, "Free-Standing Ceramic Forms Fabricated By Plasma Technology", pp. 723-728 of 1995 Advances in Thermal Spray Science and Technology”, Ed. C.C. Berndt and S.Sampath, ASM International, Materials Park, OH-USA, 1995.
179	K.A. Gross, C.C. Berndt, P. Stephens and R. Dinnebier, "Analysis Of Oxyapatite In Plasma Sprayed Hydroxyapatite Coatings", Abstract accepted for MRS 1995 Fall Meeting, Boston, 1995.
178	K.A. Gross and C.C. Berndt, "The Amorphous Phase In Plasma Sprayed Hydroxyapatite Coatings", pp. 361-366 of Bioceramics Volume 8, Eds. L.L.Hench and J.Wilson, Pub. Elsevier, New York, 1995.
177	H. Herman and C.C. Berndt, "Plasma Spray Processing of TBC's", State Univ. of New York, Thermal Barrier Coating Workshop p 127-134 (SEE N96-24395 08-27).
176	H. Herman and C.C. Berndt, "Thermal Spray Processing (Abstract)", NASA. Lewis Research Center, Thermal Barrier Coating Workshop p 23 (SEE N95-26119 08-27); UNITED STATES; 1995
175	J. Ilavsky, A.J. Allen, G.G. Long, S. Krueger, H. Herman, C.C. Berndt and A.N. Goland, “Anistropy Of The Surfaces Of Pores In Plasma Sprayed Alumina Deposits”, pp. 483-488 of Thermal Spraying – Current Status and Future Trends, Pub. High Temperature Society of Japan, Osaka-Japan, 1995.
174	J. Karthikeyan, J. Chen, G.A. Bancke, H. Herman, C.C. Berndt and V.T. Breslin, "Thermal Spray Vitrification Process For The Removal Of Lead Oxide Contained In Organic Paints", pp. 599-604 of 1995 Advances in Thermal Spray Science and Technology”, Ed. C.C. Berndt and S.Sampath, ASM International, Materials Park, OH-USA, 1995.
173	J.C. Knowles, K. Gross, C.C. Berndt and W. Bonfield, "Structural Changes Induced During Thermal Spraying Of Hydroxyapatite. A Comparison Of Three Different Spraying Methods", pp. 311-316 of Bioceramics Volume 8, Eds. L.L.Hench and J.Wilson, Pub. Elsevier, New York, 1995.
172	S-H. Leigh, C.K. Lin, S. Sampath, H. Herman and C.C. Berndt, “An Elastic Response Method Of Testing Thermal Spray Deposits”, pp. 945-950 of Thermal Spraying – Current Status and Future Trends, Pub. High Temperature Society of Japan, Osaka-Japan, 1995.
171	S-H. Leigh, S. Sampath, H. Herman, C.C. Berndt, G. Montavon and C. Coddet, "Quantitative Analysis Of Thermal Spray Deposits Using Stereology", pp. 273-278 of 1995 Advances in Thermal Spray Science and Technology”, Ed. C.C. Berndt and S.Sampath, ASM International, Materials Park, OH-USA, 1995.
170	C.K. Lin and C.C. Berndt, "Statistical Analysis Of Microhardness Variations In Thermal Spray Coatings", J.Materials Science, 30 (1995) 111-117.
169	C.K. Lin, C.C. Lin and C.C. Berndt, “Simulation Of Hardness Testing On Plasma Sprayed Coatings”, J. Am. Ceramic Society, 78[5] (1995) 1406-10.
168	C.K. Lin, S-H. Leigh and C.C. Berndt, “Investigation Of Plasma Sprayed Materials By Vickers Indentation Tests”, pp. 903-908 of Thermal Spraying – Current Status and Future Trends, Pub. High Temperature Society of Japan, Osaka-Japan, 1995.
167	S.H. Maxian, M.C. Melican, K.A. Gross, C.C. Berndt and J.P. Zawadsky, “Effect Of Hydroxyapatite Crystallinity On Coating Dissolution And Bone Cell Behavior”

ID	Reference
	(reviewed abstract), 21st Annual Meeting of the Society for Biomaterials, March 18-22, 1995, San Francisco, CA-USA.
166	M. Melican, K. Gross, C.C. Berndt and S. Maxian, "Change in Hydroxyapatite Coating Crystallinity After Culture with Osteoblasts", Bioengineering, Proceedings of the Northeast Conference pp. 51-52.
165	G. Montavon, S. Sampath, C.C. Berndt, H. Herman and C. Coddet, "Effects Of Vacuum Plasma Spray Processing Parameters On Splat Morphology", JTST 4[1] (1995) 67-74.
164	G. Montavon, C. Coddet, S-H. Leigh, S. Sampath, H. Herman and C.C. Berndt, "Stereology Analysis Of Thermally Sprayed Deposits", Pp. 279-283 Of 1995 Advances In Thermal Spray Science And Technology", Ed. C.C. Berndt and S.Sampath, ASM International, Materials Park, OH-USA, 1995.
163	G. Montavon, S. Sampath, C.C. Berndt, H. Herman and C. Coddet, "Effects Of The Substrate Nature On The Splat Morphology Of Vacuum Plasma Sprayed Deposits", pp. 365-370 of Thermal Spraying – Current Status and Future Trends, Pub. High Temperature Society of Japan, Osaka-Japan, 1995.
162	S. Sampath, C.C. Berndt and H. Herman, "Thermal Sprayed Composites", Abstract accepted for MRS 1995 Fall Meeting, Boston, 1995.
161	T. Sugama, R. Kawase, C.C. Berndt and H. Herman, "An Evaluation Of Methacrylic Acid-Modified Polyethylene Coatings Applied By Flame-Spray Technology", Progress in Organic Coatings, 25[2] (1995) 205-216. Also BNL report BNL-49393.
160	W.M. Vetter, C.K. Lin, M. Dudley and C.C. Berndt, "Synchrotron X-Ray Topographic And Acoustic Emission Observations During Twin Boundary Movement In Lanthanum Aluminate", Abstract accepted for MRS 1995 Fall Meeting, Boston, 1995.
159	O. Yokota, J.Z. Chen, D. Bernard, S. Usmani, C.C. Berndt and H. Herman, "Thermal Shock Resistance Of Thermal Spray Coatings Produced From Mechanofused Powders", pp. 973-978 of Thermal Spraying – Current Status and Future Trends, Pub. High Temperature Society of Japan, Osaka-Japan, 1995.
158	D. Bernard, O. Yokota, A. Grimaud, P. Fauchais, S. Usmani, Z.J. Chen, C.C. Berndt and H. Herman, "Mechanofused Metal-Carbide-Oxide Cermet Powders For Thermal Spraying", pp. 171-178 of "1994 Thermal Spray Industrial Applications", Ed. C.C. Berndt and S.Sampath, Pub. ASM International, Cleveland, OH-US, 1994.
157	C.C. Berndt, "Who's Holding The Gun?", J. Thermal Spray Technology, 4[1] (1994) 331-332.
156	C.C. Berndt, H. Herman and S. Raghu, "Real-Time Imaging Of The Plasma-Spray Process", poster, 1994 NSF Design and Manufacturing Grantees Conference, January 5-7, 1994, Boston, MA.
155	7th National Thermal Spray Conference (1994) 20-24 June, Boston (MA). Reference: Thermal Spray Industrial Applications, Eds. C.C.Berndt and S.Sampath, Pub. ASM International, Materials Park, OH-USA, 1994, 800+ pages.
154	J.A. Brogan, K.A. Gross, Z. Chen, H. Herman and C.C. Berndt, "Investigation Of Combustion Sprayed Hydroxyapatite/Polymer Composite Coatings", pp. 159-164 of "1994 Thermal Spray Industrial Applications", Ed. C.C. Berndt and S.Sampath, Pub. ASM International, Cleveland, OH-US, 1994.
153	R.V. Gansert, R. Benary, C.C. Berndt and H. Herman, "Automated Thermal Spray System (ATSS) For Rehabilitation And Maintenance Of Infrastructure", pp. 445-450 of "1994 Thermal Spray Industrial Applications", Ed. C.C. Berndt and S.Sampath, Pub.

ID	Reference
	ASM International, Cleveland, OH-US, 1994.
152	D. Goldschlag, V. Iacono, K.A. Gross, C.C. Berndt, D. Chan and M. Wiener, "Effects Of Compressive Stresses On Hydroxyapatite (HA) Coatings Of Dental Implants", J. Dent. Res. Spec. Issue, 73:137, (1994) Abstract #284.
151	D. Goldschlag, V. Iacono, K.A. Gross, C.C. Berndt, D. Chan and M. Wiener, "Stress Mediated Phase Changes In Plasma Sprayed Hydroxyapatite (HA) Coatings", abstract, Proc. 9th Annual Meeting of the Academy of Osseointegration, 9 (1994) 110-111.
150	K.A. Gross and C.C. Berndt, "In Vitro Testing Of Thermally Sprayed Hydroxyapatite", J. Materials Science for Medicine, 5 (1994) 219-224.
149	K.A. Gross and C.C. Berndt, "Thermal Analysis Of The Amorphous Phase In Hydroxyapatite Coating", abstract, 7th International Symposium on Ceramics in Medicine, 28-30 July, 1994, Turku, Finland.
148	K.A. Gross, C.C. Berndt and P. Stephens, "Composition Variation With Thickness In Hydroxyapatite Coatings", abstract, The 20th Annual Meeting of the Society for Biomaterials, April 5-9, 1994, Boston, MA.
147	K.A. Gross and C.C. Berndt, "Structural Changes Of Plasma Sprayed Hydroxyapatite Coating During In-Vitro Testing", pages 124-139 of Characterization and Performance of Calcium Phosphate Coatings for Implants, Ed. E.Horowitz and J.E.Parr, Pub. ASTM, Philadelphia, 1994.
146	H. Herman, C.C. Berndt and S. Sampath, "Near-Net Shape Forming", poster, 1994 NSF Design and Manufacturing Grantees Conference, January 5-7, 1994, Boston, MA.
145	J.Ilavsky, H. Herman, C.C. Berndt, A.N. Goland, G.G. Long, S. Krueger and A.J. Allen, "Porosity In Plasma Sprayed Alumina Deposits", Pp. 709-714 Of "1994 Thermal Spray Industrial Applications", Ed. C.C. Berndt and S. Sampath, Pub. ASM International, Cleveland, OH-US, 1994.
144	S-H. Leigh and C.C. Berndt, "A Test For Coating Adhesion On Flat Substrates - A Technical Note", JTST 3[2] (1994) 184-190.
143	S-H. Leigh, C.C. Berndt, C.L. Wu and T. Nakamura, "Tensile Adhesion Testing Of Thermal Spray Coatings On Flat Substrates", pp. 655-662 of "1994 Thermal Spray Industrial Applications", Ed. C.C. Berndt and S. Sampath, Pub. ASM International, Cleveland, OH-US, 1994.
142	C.K. Lin and C.C. Berndt, "Measurement And Analysis Of Adhesion Strength For Thermally Sprayed Coatings", JTST, 3 [1] (1994) 75-104.
141	G. Montavon, C. Coddet, S. Sampath, H. Herman and C.C. Berndt, "Vacuum Plasma Spray Forming Of Astroloy: An Investigation Of Processing Parameters", pp. 469-475 of "1994 Thermal Spray Industrial Applications", Ed. C.C. Berndt and S.Sampath, Pub. ASM International, Cleveland, OH-US, 1994.
140	J. Rastegar, Y. Qin, C.C. Berndt, H. Herman, S. Sampath and Q. Tu, "On The Optimal Robot Manipulator Motion Planning For Solid Freeform Fabrication By Thermal Spraying", pp. 463-468 of "1994 Thermal Spray Industrial Applications", Ed. C.C. Berndt and S. Sampath, Pub. ASM International, Cleveland, OH-US, 1994.
139	W.M. Vetter, C.K. Lin, M. Dudley and C.C. Berndt, "Synchrotron X-Ray Topographic And Acoustic Emission Observations During Twin Boundary Movement In Lanthanum Aluminate" (reviewed abstract), MRS Symposium K on High-Temperature Superconductors - Material and Fabrication Issues for Applications, Boston, December, 1994.

ID	Reference
138	C.C. Berndt and H. Herman, "Thermal Spraying Helps Shore Up The Infrastructure", Advanced Materials & Processes, 143[1] (1993) 24-25.
137	C.C. Berndt, "Concise Encyclopedia Of Advanced Ceramic Materials", Book Review, Materials Science and Engineering, A160 (1993) 283-284.
136	C.C. Berndt and C.K. Lin, "Measurement Of Adhesion For Thermally Sprayed Materials", J. Adhesion Science & Technology, 7 [12] (1993) 1235-1264.
135	6th National Thermal Spray Conference (1993) 7-11 June, Anaheim (CA). Reference: Thermal Spray: Research, Design and Applications, Eds. C.C.Berndt and T.F.Bernecki, Pub. ASM International, Materials Park, OH-USA, 1993, 691+ pages.
134	J.A. Brogan, K.A. Gross, Z. Chen, H. Herman and C.C. Berndt, "Hydroxyapatite / Polymer Composite Materials For Biomaterial Applications", Poster, 6th International Symposium on Ceramics in Medicine", November 14-17, 1993, Philadelphia, PA.
133	K.A. Gross, C.C. Berndt, D. Goldschlag and V. Iacono, "Stability Of The Hydroxyapatite Under Compressive Stresses", abstract, Ceramics in Biomedical Applications Workshop, June 2-4, 1993, Rochester, NY.
132	K.A. Gross, C.C. Berndt, R. Cimdins and L. Berzina, "Characterization Of The Amorphous Phase In Hydroxyapatite Coatings", Poster, 6th International Symposium on Ceramics in Medicine", November 14-17, 1993, Philadelphia, PA.
131	H. Herman, C.C. Berndt and H. Wang, "Plasma Sprayed Ceramic Coatings", pp. 131-188 of Ceramic Films and Coatings, J.B.Wachtman and R.A.Haber (eds.), Noyes Publications, 1993.
130	J. Ilavsky and C.C. Berndt, "Protective Coating Processes 1990-1991", Book Review, JTST, 2[3] (1993), 226-227.
129	J. Ilavsky, C.C. Berndt, H. Herman and M.B. Beardsley, "Thermal Expansion Of Metallic And Cermet Coatings", pp. 601-606 of "Thermal Spray Coatings: Research, Design and Applications", C.C. Berndt and T.F.Bernecki (Editors), Pub. ASM International, Materials Park, OH, USA, 1993.
128	J. Ilavsky, J. Forman, J. Dubsky, P. Chraska, K. Neufuss, C.C. Berndt and H. Herman , "Analysis Of Porosity Of Free-Standing Ceramics Manufactured By Plasma Spraying", pp. 505-511 of "Thermal Spray Coatings: Research, Design and Applications", C.C. Berndt and T.F.Bernecki (Editors), Pub. ASM International, Materials Park, OH, USA, 1993.
127	C.K. Lin and C.C. Berndt, "Microhardness Variations In Thermally Sprayed Coatings", pp. 561-568 of "Thermal Spray Coatings: Research, Design and Applications", C.C. Berndt and T.F.Bernecki (Editors), Pub. ASM International, Materials Park, OH, USA, 1993.
126	P. Treadway and C.C. Berndt, "A Microstructural Index For Pores In Thermal Spray Coatings", pp. 513-517 of "Thermal Spray Coatings: Research, Design and Applications", C.C. Berndt and T.F.Bernecki (Editors), Pub. ASM International, Materials Park, OH, USA, 1993.
125	C.C. Berndt, "Introduction To Book", Thermal Spray: International Advances in Coatings Technology; C.C. Berndt (ed.), 1030 pages, Pub. ASM International, Materials Park, OH, USA, 1992.
124	C.C. Berndt and H. Herman, "Conference Report On Maintenance Of Steel And Reinforced Concrete", JTST, 1[4] (1992) 287.
123	C.C. Berndt, "Concise Encyclopedia Of Medical & Dental Applications", Book review, Materials Science and Engineering, 1992.



ID	Reference
122	C.C. Berndt, "Conference Report On Advances In Materials Processing", JTST, 1[4] (1992) 285-287.
121	C.C. Berndt, "Property Variations", Special report in Advanced Materials & Processes, 141[5] (1992) p. 24.
120	C.C. Berndt, "Thermal Spray Research And Applications", Book review, J. Thermal Spray Tech., 1[1] (1992) p. 17.
119	C.C. Berndt, W. Brindley, A.N. Goland, H. Herman, D.L. Houck, K. Jones, R.A. Miller, R. Neiser, W. Riggs, S. Sampath, M. Smith and P. Spanne, "Current Problems In Plasma Spray Processing", JTST 1[4] (1992) 1-16.
118	C.C. Berndt, "Preparation Of Thermal Spray Powders", Education module on thermal spray, Pub. ASM International, OH, Materials Park, USA, 1992.
117	C.C. Berndt and D. Wang, "Thermal Gravimetric Analysis Of Ceramic Coatings", pp. 799-805 of Thermal Spray: International Advances in Coatings Technology, Ed. C.C. Berndt, Pub. ASM International, OH, USA, 1992.
116	C.C. Berndt and K.A. Gross, "Characteristics Of Hydroxyapatite Bio-Coatings", pp. 465-471 of Thermal Spray: International Advances in Coatings Technology, Ed. C.C. Berndt, Pub. ASM International, OH, USA, 1992.
115	C.C. Berndt, J. Ilavsky and J. Karthikeyan, "Microhardness - Lifetime Correlations For Plasma Sprayed Thermal Barrier Coatings", pp. 941-947 of Thermal Spray: International Advances in Coatings Technology, Ed. C.C. Berndt, Pub. ASM International, OH, USA, 1992.
114	13th International Thermal Spray Conference (1992) (5th National Thermal Spray Conference - 1992) 28 May - 5 June, Orlando (FL). Reference: Thermal Spray: International Advances in Coatings Technology, Ed. C.C. Berndt, Pub. ASM International, Materials Park, OH-USA, 1992, 1044+ pages.
113	J.L. Gluck, H. Herman and C.C. Berndt, "Thermal Spray Optimization And Characterization Of Ultra High Molecular Weight Polyethylene", Abstract, The International Thermal Spraying Conference in Orlando, June, 1992.
112	R.H. Mair and C.C. Berndt, "Wear Of Coatings In Wool-Severing Applications", J. Materials Science, 27 (1992) 6687-6694.
111	R. Tiwari, C. Perdikaris, C.C. Berndt and H. Herman, "Oxidation Of Nickel-Based Bond Coat Materials", Proc. of the 1992 Coatings for Advanced Heat Engines Workshop, Monterey 1992, Pub. DOE.
110	C.C. Berndt, "Handbook Of Ceramics And Composites, Vol. 1: Synthesis And Properties", Book review, Materials Forum, 15[4] (1991) 388-389.
109	C.C. Berndt, "Surface Modifications Technologies IV", Materials and Processing Report, Book review, 6[6] (1991) 13-14.
108	C.C. Berndt, "Thermal And Mechanical Properties Of Thermal Barrier Coatings", Inter.J. Turbo and Jet Engines, 8[1&2] (1991) 75-82
107	C.C. Berndt, "Mechanical, Thermomechanical And Tribological Applications Of Ceramic Coatings", pp. 577-590 of High Performance Ceramic Films and Coatings, Ed. P.Vincenzini, Pub. Elsevier Science Publishers B.V., 1991.
106	C.C. Berndt, "Thermally Sprayed Coatings: Properties And Applications", pp. 193-213 of Surface Modification Technologies IV, Ed. T.S.Sudarshan, D.G.Bhat and M.Jeandin, Pub. TMS, 1991.

ID	Reference
105	C.C. Berndt, "Opportunities And Needs For Standardization Of Ceramic Coatings", The 7th. CIMTEC World Ceramics Congress, Montecatini Terme, Italy, 27-30 June, 1990. p. 3287-3200 of "Ceramics Today - Tomorrow's Ceramics", Ed. P. Vincenzini, Materials Science Monographs 66D, Pub. Elsevier, New York, 1991.
104	C.C. Berndt, "The Need For Standardization Of Testing Methods In The Thermal Spray Industry", pp. 325-330 of Thermal Spray Research and Applications, Ed. T.F.Bernecki, Pub. ASM International, OH, USA, 1991.
103	C.C. Berndt, J. Karthikeyan, R. Ratnaraj and Y.D. Jun, "Material Property Variations In Thermally Sprayed Coatings", pp. 199-204 of Thermal Spray Coatings: Properties, Processes and Applications, Ed. T.F.Bernecki, Pub. ASM International, OH, USA, 1991.
102	C.C. Berndt, "A Bibliography Focused On Thermal Spray Coatings, Volume 1, References". Privately published book, 246 pages. January 1991, Monash University, Melbourne, Australia.
101	C.C. Berndt, "A Bibliography Focused On Thermal Spray Coatings, Volume 2, Indices". Privately published book, 122 pages. January 1991, Monash University, Melbourne, Australia.
100	P.J. Callus and C.C. Berndt, "Analysis And Calibration Of A Shear Fracture Toughness Test For Thermally Sprayed Coatings", pp. 299-308 of High Performance Ceramic Films and Coatings, Ed. P.Vincenzini, Pub. Elsevier Science Publishers B.V., 1991.
99	K.A. Gross and C.C. Berndt, "Thermal Spraying of Hydroxyapatite for Bioceramic Applications", Key Engineering Materials 53-55 (1991) pp. 124-129
98	K.A. Gross and C.C. Berndt, "Optimization Of Spraying Parameters For Hydroxyapatite", pp. 159-170 of Volume 3 of 2nd. Plasma-Technik-Symposium, Ed. S.Blum-Sandmeier, H.Eschnauer, P.Huber and A.R.Nicoll, Pub. Plasma-Technik AG, 1991.
97	J. Karthikeyan, R. Ratnaraj, A.J. Hill, Y.C. Fayman and C.C. Berndt, "A Parametric Study In Plasma Spraying Of YBCO Powder", pp. 497-502 of Thermal Spray Coatings: Properties, Processes and Applications, Ed. T.F.Bernecki, Pub. ASM International, OH, USA, 1991.
96	R.H. Mair and C.C. Berndt, "Coatings For Sheep Shears", pp. 661-669 of High Performance Ceramic Films and Coatings, Ed. P.Vincenzini, Pub. Elsevier Science Publishers B.V., 1991.
95	D. Wang and C.C. Berndt, "Particle/Substrate Interactions During Thermal Spraying", Key Engineering Materials 53-55 pp. 499-504.
94	D. Wang and C.C. Berndt, "Anisotropic Thermal Expansion Behavior Of Thermally Sprayed Coatings", pp. 295-304 of Volume 2 of 2nd. Plasma-Technik-Symposium, Ed. S.Blum-Sandmeier, H.Eschnauer, P.Huber and A.R.Nicoll, Pub. Plasma-Technik AG, 1991.
93	J.H. Yi and C.C. Berndt, "An Electron Microscopic Examination Of Composite Coatings Produced By Thermal Spraying", pp. 299-310 of Surface Modification Technologies IV, Ed. T.S.Sudarshan, D.G.Bhat and M.Jeandin, Pub. TMS, 1991.
92	J.H. Yi and C.C. Berndt, "The Microstructure Of Fiber-Reinforced Plasma Sprayed Coatings", pp. 383-392 of Thermal Spray Research and Applications, Ed. T.F.Bernecki, Pub. ASM International, OH, USA, 1991.
91	C.C. Berndt, "Thermal Spray Technology: New Ideas And Processes", Book review, J. Advanced Materials and Processes, 1990.

ID	Reference
90	C.C. Berndt, D. Collinson and G. Roberts, "Mechanical Properties Of A Polyester-Collagen Vascular Prosthesis", pp. 481-486 of Clinical Implant Materials, Ed. G.Heimke, U.Soltesz and A.J.C.Lee, Pub. Elsevier, New York, 1990.
89	C.C. Berndt, "Tensile Adhesion Testing Methodology For Thermally Sprayed Coatings", ASM J.Mater.Eng., 12[2] (1990) 151-160.
88	C.C. Berndt, G.N. Haddad, A.J.D. Farmer and K.A. Gross "Review Article: Thermal Spraying For Bioceramic Applications", Materials Forum, 14 (1990) 161-173.
87	C.C. Berndt, G.N. Haddad and K.A. Gross, "Thermal Spraying For Bioceramic Applications", pp. 201-210 of Bioceramics, G.Heimke (ed.), Pub. German Ceramic Society, Cologne, 1990.
86	P.J. Callus and C.C. Berndt, "Mode II Fracture Toughness Test For Thermally Sprayed Coatings", Inter.J.Fracture, 43[4] (1990) R57-R60.
85	K.A. Gross, G.N. Haddad and C.C. Berndt, "Hydroxyapatite Coatings", Abstract, Biomaterials: Research in Australia, Kyneton, Victoria, 17th.-19th June, 1990.
84	A. Jones, C.C. Berndt and J.W. Adams, "Quality Control Of Pellets For Mouse Production", Poster, Australia Animal Technicians Conference, 20-22 June, 1990, Melbourne University, Australia.
83	K.A. Gross and C.C. Berndt, "Thermal Spraying Of Hydroxyapatite For Bioceramic Applications", AUSTCERAM-90, Pages 124-129.
82	D. Wang and C.C. Berndt, "Particle/Substrate Interactions During Thermal Spraying", AUSTCERAM-90.
81	C.C. Berndt, "Department Of Materials Engineering Biomaterials Capabilities", Abstract, Workshop on Abstract for Workshop on Materials for Medical Devices Biocompatibility, Leura, NSW, 14-16 May, 1989.
80	C.C. Berndt, "Metallurgical Coatings 1987: Volume IV", Book review, Mater.Sci.Engin., A114 (1989) 218.
79	C.C. Berndt, "Rapid Review Reports Current Developments In Materials Technology And Engineering", Book review, RACI Polymer Division News, 32[Nov] (1989) 33.
78	C.C. Berndt, D. Collinson, G. Edwards and G. Roberts, "The Tensile Properties Of Vascular Prostheses", pp. 52-55 of Advances in Biomedical Polymers Conf., Perth, 5-9 February, 1989.
77	C.C. Berndt, P.J. Callus and G. Jessup, "The Failure Analysis And Material Properties Of Sutures", pp. 110-113 of Advances in Biomedical Polymers Conf., Perth, 5-9 February, 1989.
76	C.C. Berndt, "Cracking Mechanisms Within Thermal Barrier Coatings And Their Implications For Material Property Measurements", The SAMPE-Australian Fracture Group Meeting, 12-13 October, 1989.
75	C.C. Berndt, D. Collinson and G. Roberts, "The Composite Nature Of Dacron Collagen Vascular Prostheses", Abstract, Workshop on Materials for Medical Devices Biocompatibility, Leura, NSW, 14-16 May, 1989.
74	C.C. Berndt, G.N. Haddad and K. Gross, "Bioceramic Coatings Formed By Thermal Spraying Processes", Abstract, Workshop on Materials for Medical Devices Biocompatibility, Leura, NSW, 14-16 May, 1989.
73	C.C. Berndt and J.H. Yi, "The Manufacture And Microstructure Of Fiber Reinforced Thermally Sprayed Coatings", J. Surf. Coat. Tech., 37 (1989) 89-110.

ID	Reference
72	C.C. Berndt, "Instrumented Tensile Adhesion Tests On Plasma Sprayed Thermal Barrier Coatings", ASM J.Mater.Eng., 11[4] (1989) 275-282.
71	C.C. Berndt and J.H. Yi, "Composite Plasma Sprayed Coatings", Paper 2, Volume 1 of The 12th. Inter. Thermal Spraying Conf., 4-9 June, 1989, London, Pub. The Welding Institute, Abington, UK.
70	C.C. Berndt and P.J. Callus, "A Shear Test For Thermally Sprayed Coatings", Paper 103 of The 12th. Inter. Thermal Spraying Conf., 4-9 June, 1989, London, Pub. The Welding Institute, Abington, UK.
69	A.B. Conn, C.C. Berndt, G.P. Simon, J. Palamara, W.A. Rachinger and P. Phakey, "Polymer Mineral Composites For Orthopaedic Applications", Abstract, Workshop on Materials for Medical Devices Biocompatibility, Leura, NSW, 14-16 May, 1989.
68	K.A. Gross, G.N. Haddad and C.C. Berndt, "Thermally Sprayed Coatings For Orthopaedic Applications", Paper 119 of The 12th. Inter. Thermal Spraying Conf., 4-9 June, 1989, London, Pub. The Welding Institute, Abington, UK.
67	B.W. Oakes and C.C. Berndt, "Design And Development Of A Prosthetic Human Cruciate Ligament", Abstract, Workshop on Materials for Medical Devices Biocompatibility, Leura, NSW, 14-16 May, 1989.
66	C.C. Berndt, "ATTAC-88: Thermal Spraying In Japan", Conference review, J.Metals, 40[12] (1988).
65	C.C. Berndt, "The 1987 National Thermal Spray Conference And Exhibition", Conference review, Materials Australasia, 20[1] (1988) 23.
64	C.C. Berndt and P. Callus, "Shear (Mode II) Tests On Thermally Sprayed Coatings", pp. 36-43 of Proc. of Fracture Mechanics in Engineering Practice, Melbourne, Australia, November 1988, Ed. N.E.Ryan, Aeronautical Research Laboratories, Melbourne, Australia, 1988.
63	C.C. Berndt and P.J. Callus, "Shear (Mode II) Tests On Thermally Sprayed Coatings", in "Fracture Mechanics in Engineering Practice", Ed. N.E.Ryan, ARL, Melbourne, November 1988.
62	C.C. Berndt and J.H. Yi, "Toughening Of Thermally Sprayed Coatings", Materials Science Forum, 34-36 (1988) 469-474.
61	C.C. Berndt, "Cracking Processes In Ceramic Coatings", Materials Science Forum, 34-36 (1988) 457-461.
60	C.C. Berndt, "Failure Processes Within Ceramic Coatings At High Temperatures", J.Mater.Sci., 24 (1989) 3511-3520.
59	C.C. Berndt, "Material Property Measurements On Thermal Barrier Coatings", Paper 88-GT277 of the Gas Turbine and Aeroengine Congress, Amsterdam, The Netherlands, 6-9 June, 1988, Pub. ASME, New York.
58	C.C. Berndt and J.H. Yi, "Strength Enhancement Of Plasma Sprayed Coatings", pp. 297-308 of Thermal Spray Advances in Coating Technology, Ed. D.L.Houck, Pub. ASM, 1988.
57	C.C. Berndt and P. Ostojic, "Strength Testing Of Plasma Sprayed Coatings", pp. 191-197 of the Inter. Symposium on Advanced Thermal Spraying Technology and Allied Coatings Conf., Osaka, Japan, 13-15 May, 1988, Pub. The High Temperature Society of Japan, Osaka, 1988.
56	P. Ostojic and C.C. Berndt, "The Variability In Strength Of Thermally Sprayed Coatings", pp. 175-180 of Thermal Spray Advances in Coating Technology, Ed. D.L.Houck, Pub. ASM, 1988.

ID	Reference
55	P. Ostojic and C.C. Berndt, "Variability In Strength Of Thermally Sprayed Coatings", J. Surf. Coat. Tech., 34 (1988) 43-50.
54	Anon. "How Strong Is It?", article in Advanced Materials and Processes, 132[12] (1987) 80, reporting the work of C.C. Berndt and P.Ostojic.
53	C.C. Berndt, "Ceramic Containing Systems Mechanical Aspects Of Interfaces And Surfaces", Book review, Mater.Sci.Eng., 96 (1987) 330-331.
52	C.C. Berndt, "Ceramic Heat Exchanger Concepts And Materials Technology", Book review, Materials Forum, 1987.
51	C.C. Berndt, "Materials Sciences And Implant Orthopedic Surgery", Book review, J.Aust.Ceram.Soc., 23[1] (1987) 52.
50	C.C. Berndt, "NTSC-87 Coating Characterization And Testing (A & B)", Invited Conf. Review, J.Metals, [12] (1987) 18.
49	C.C. Berndt, "Perspectives On Biomaterials", Book review, J.Aust.Ceram.Soc., 23[1] (1987) 51.
48	C.C. Berndt, "Polymeric Biomaterials", Book review, Polymer Division, Newsletter No. 27 (1987) 36-37. [short version of review appearing in Materials Forum, 10[4] (1987) 289.]
47	C.C. Berndt and R.A. Miller, Tables of "Mechanical Property Measurements", "Average Mechanical Properties" and "Chemical Compositions Of Materials Used For NiCrAlY and NiCrAlZr Bond Coatings With Y2O3-ZrO2 Overlays", extracted from Ceramic Source '87, Vol. 2 p.213, The Am. Ceram. Soc., 1986.
46	C.C. Berndt, "Defect Properties And Processing Of High Technology Non Metallic Materials", Book review, Metals Forum, 9[1&2] (1986).
45	C.C. Berndt and R. McPherson, "Failure Locus And Strength Correlations Of Plasma Sprayed Coatings", Materials Technology Congress, 19-21 May, 1986, Adelaide, Australia, Paper number 2A9.
44	C.C. Berndt, "Methods Of Acoustic Emission Analysis", Materials Technology Congress, 19-21 May, 1986, Adelaide, Australia, Paper number 3C1.
43	C.C. Berndt and R. McPherson, "Assessment Of The Adhesion Of Plasma Sprayed Coatings", Surf.J.Int., 1[2] (1986) 49-52.
42	C.C. Berndt, "Determination Of Material Properties Of Ceramic Coatings", pp. 149-158 of the 11th. Inter. Thermal Spraying Conf., 7-12 September, 1986, Montreal, Canada, Pub. The Welding Institute of Canada.
41	C.C. Berndt, "Discrimination Of Micro And Macrocracking Processes In Plasma Sprayed Ceramic Coatings", pp. 585-594 of the 11th. Inter. Thermal Spraying Conf., 7-12 September, 1986, Montreal, Canada, Pub. The Welding Institute of Canada.
40	C.C. Berndt and H. Herman, tables of "Phase Analysis Of YSZ Powders And Coatings" and "Thermal Expansion Properties Of YSZ Coatings" extracted from Ceramic Source '86, p.328, The Am. Ceram. Soc., 1985.
39	C.C. Berndt et al., contributor to chapter on "Coating Characteristics", pp. 29-49 of Thermal Spraying Practice, Theory and Application, Pub. The American Welding Society, 1985.
38	C.C. Berndt, "Crack Density Functions Of Plasma Sprayed Coatings", pp. 22-30 of the 1985 Symposium of the Australian Fracture Group, 28-29 November, Ed. B.L.Kaliharoo.



ID	Reference
37	C.C. Berndt and R. McPherson, "Electron Microscopic Studies Of Plasma Sprayed Coatings", Mater.Sci.Res., 19 (1985) 265-278.
36	C.C. Berndt, "Acoustic Emission Evaluation Of Plasma Sprayed Thermal Barrier Coatings", Trans.ASM Eng.Gas Turbines, 107 (1985) 142-146.
35	C.C. Berndt, "Examination Of Coating Failure By Acoustic Emission", pp. 127-137 of Thermal Barrier Coatings Workshop, May 21-22, 1985, Pub. Lewis Research Center, 1985.
34	C.C. Berndt and R.A. Miller, "Failure Analysis Of Plasma Sprayed Thermal Barrier Coatings", Thin Solid Films, 119 (1984) 173-184. [also in NASA Technical Memorandum 83777, April 1984].
33	C.C. Berndt and R.A. Miller, "Mechanical Property Measurements Of Plasma Sprayed Thermal Barrier Coatings Subjected To Oxidation", Ceram.Eng.Sci.Proc., 5[7-8] (1984) 479-490.
32	R.A. Miller and C.C. Berndt, "Performance Of Thermal Barrier Coatings In High Heat Flux Environments", Thin Solid Films, 119 (1984) 195-202. [also in NASA Technical Memorandum 83663, April 1984].
31	C.C. Berndt, "Behavior Of Plasma Sprayed Coatings", pp. 524-532 of Ultrastructure Processing of Ceramics, Glasses and Composites, Eds. L.L.Hench and D.R.Ulrich, Pub. J.Wiley and Sons, 1984.
30	C.C. Berndt, "Fracture Mechanics Tests On Plasma Sprayed Coatings", pp. 2545-2552, Vol. 4 of Advances in Fracture Research, Eds. S.R.Valluri et al., Pergamon Press, 1984.
29	C.C. Berndt, "Studies On Plasma Sprayed Thermal Barrier Coatings", pp. 546-560 of Surface Engineering, Eds. R.Kossowsky and S.C.Singhal, Pub. Martinus Nijhoff, Dordrecht, The Netherlands, 1984.
28	C.C. Berndt, "Tensile Adhesion Test Measurements Of Plasma Sprayed Coatings", pp. 2553-2559, Vol. 4 of Advances in Fracture Research, Eds. S.R.Valluri et al., Pergamon Press, 1984.
27	C.C. Berndt, W. Phucheroen and G. Chang, "The Mechanical Properties Of Thermal Barrier Coatings Used For Gas Turbine Blades", pp. 155-166 of Turbine Engine Hot Section Technology, 1984 Workshop, NASA CP2339, October 1984.
26	N.R. Shankar, H. Herman, S.P. Singhal and C.C. Berndt, "Neutron And X-Ray Diffraction Of Plasma Sprayed Zirconia-Yttria Thermal Barrier Coatings", Thin Solid Films, 119 (1984) 159-171.
25	C.C. Berndt and H. Herman, "Failure During Thermal Cycling Of Plasma-Sprayed Thermal Barrier Coatings", Thin Solid Films, 108[4] (1983) 427-437.
24	C.C. Berndt and R.A. Miller, "Adhesion Tests On Oxidized Plasma-Sprayed Coatings", Am. Ceramic Soc. Bull., 61[11] (1983) 1247-1247
23	C.C. Berndt and H. Herman, "Anisotropic Thermal Expansion Effects In Plasma Sprayed ZrO <sub>2</sub> -8wt% Y <sub>2</sub> O <sub>3</sub> Coatings", Ceram.Eng.Sci.Proc., 4[9-10] (1983) 792-801.
22	C.C. Berndt and H. Herman, "Properties And Phase Studies Of Plasma Sprayed Y Stabilized Zirconia Thermal Barrier Coatings", pp. 175-179 of The 10th. Inter. Thermal Spraying Conf., May 26, 1983, Essen, Germany, Pub. DVS (The German Welding Society).
21	C.C. Berndt, D. Robins, R. Zatorski and H. Herman, "Fire Barrier Coatings For Protection Of Aluminum Structures", pp. 182-186 of The 10th. Inter. Thermal Spraying Conf., May 26, 1983, Essen, Germany, Pub. DVS (The German Welding Society).

ID	Reference
20	N.R. Shankar, C.C. Berndt, H. Herman and S.Rangaswamy, "Acoustic Emission From Thermally Cycled Plasma Sprayed Oxides", Am.Ceram.Bull., 62[5] (1983) 614-619.
19	N.R. Shankar, C.C. Berndt and H. Herman, "Characterization Of The Mechanical Properties Of Plasma Sprayed Coatings", Mater.Sci.Res., 15 (1983) 473-490.
18	N.R. Shankar, C.C. Berndt and H. Herman, "Phase Analysis Of Plasma Sprayed Zro2-Y2O3 Coatings", Ceram.Eng.Sci. Proc., 4[9-10] (1983) 784-791.
17	N.R. Shankar, C.C. Berndt and H. Herman, "Structural Integrity Of Thermal Barrier Coatings By Acoustic Emission", pp. 41-45 of The 10th. Inter. Thermal Spraying Conf., May 26, 1983, Essen, Germany, Pub. DVS (The German Welding Society).
16	C.C. Berndt, R. Kolipara, R.A. Zatorski, H. Herman, A. Jonca, T. Templeton and R. MacCrone, "Characterization Of Imperfections In Plasma Sprayed Titania", Mater. Sci. Res., 15 (1983) 465-472. [also DOE/ER/10428T2, 1982].
15	N.R. Shankar, C.C. Berndt and H. Herman, "Failure And Acoustic Emission Response Of Plasma Sprayed Zro2-8wt.% Y2O3", Ceram.Eng.Sci.Proc., 3[9-10] (1982) 772-792.
14	C.C. Berndt and H. Herman, "Anisotropic Thermal Expansion Effects in Plasma Sprayed ZrO2-8 Wt-percent Y2O3 Coatings", Am. Ceramic Soc. Bull., 61[11] (1982) 1193.
13	C.C. Berndt and R. McPherson, "Fracture Mechanics And Fractography Of Plasma Sprayed Coatings", Poster Session of The 5th. Inter. Conf. on Fracture, 29 March - 3 April, 1981, Cannes, France.
12	C.C. Berndt and R. McPherson, "Adhesion Of Thermally Sprayed Coatings", Australian Welding Research, 11[December] (1981) 23-25.
11	C.C. Berndt and R. McPherson, "The Adhesion Of Plasma Sprayed Ceramic Coatings To Metals", Mater.Sci.Res., 14 (1981) 619-628.
10	C.C. Berndt, "The Adhesion Of Flame And Plasma Sprayed Coatings", Ph.D. Thesis, 259 pages. Submitted December 1980 and accepted 5 June, 1981, Monash University, Department of Materials Engineering, Melbourne, Australia.
9	R. McPherson and C.C. Berndt, "Mechanism Of Adhesion Of Plasma Sprayed Coatings", pp. 586-591 of Proc. 5th International Symposium on Plasma Chemistry, 10-14 August, 1981, Heriot-Watt University, Edinburgh, Scotland. Eds B.Waldie and G.A.Farnell.
8	C.C. Berndt and R. McPherson, "Determination Of The Adhesion Of Thermally Sprayed Ceramic Coatings To Metals Using Fracture Mechanics", pp. 74-81 of The 9th. Australian Ceramic Conf., 27-29 August, 1980, Sydney, Australia.
7	C.C. Berndt and R. McPherson, "Fracture Mechanics And Fractography Of Plasma Sprayed Coatings", pp. 100-105 of The Conf. of the Australian Fracture Group, 25 November, 1980, Melbourne, Australia.
6	C.C. Berndt and R. McPherson, "A Fracture Mechanics Approach To The Adhesion Of Flame And Plasma Sprayed Coatings", pp. 387-392 of The Inter. Conf. on Manufacturing Engineering, 25-27 August, 1980, Melbourne, Australia. [also in Trans. Inst. Engineers, Australia, ME6[1] (1981) 53-58].
5	C.C. Berndt and R. McPherson, "A Fracture Mechanics Approach To The Adhesion Of Plasma Sprayed Coatings", pp. 310-316 of The 9th. Inter. Thermal Spraying Conf., 19-23 May, 1980, The Hague, Netherlands. Published by Nederlands Instituut voor Lasteniek, 1980. Discussion on pp. 40-41 of Rapporteurs Volume.

ID	Reference
4	C.C. Berndt and R. McPherson, "The Adhesion Of Flame And Plasma Sprayed Coatings - A Review", Australian Welding Research, 6[Jan] (1979) 75-85.
3	C.C. Berndt and R. McPherson, "Plasma Sprayed Coatings", pp. 173-178 of Proc. of the 8th. Australian Ceramic Conf., 15-17 August, 1978, Melbourne, Australia, Pub. The Australian Ceramic Society.
2	C.C. Berndt, S.A. Cox and P.A. Slattery, "Environmental Cracking Of Magnesium Alloys", The 17th. Australian Corrosion Association Conf., 13-18 November, 1977, Newcastle, NSW, Australia.
1	C.C. Berndt, "The Stress Corrosion Cracking Of Magnesium-Aluminium Alloys", Graduate Diploma Thesis, 131 pages. Accepted November 1976, The South Australian Institute of Technology, School of Metallurgy, Adelaide, Australia.

Christopher C. BERNDT  
Professor of Surface Science and Interface Engineering  
Swinburne University of Technology, Faculty of Engineering  
John Street, H66  
Hawthorn, Victoria 3122  
AUSTRALIA



Chris Berndt graduated in 1977 with a B.App.Sc. in Metallurgy, from what is now called the University of South Australia. His Ph.D. was earned in the Materials Engineering Department of Monash University in mid-1981. He undertook several Fellowships in the USA in the early 1980's; which included a 2 year stint at NASA-Lewis Research Center in Cleveland (OH-USA) where he worked on aerospace hardware.

Chris was appointed a Senior Lecturer at Monash in 1985. He was invited to apply for a position at Stony Brook University, NY-USA in 1989. He was promoted to Full Professor with tenure in 1995 and appointed an Adjunct Professor in Orthopedics in 1996. Berndt was the Deputy Chairman of the Department of Materials Science and Engineering for 9-years and the Associate Dean of the Faculty for 4-years. He undertook training to become qualified as an ABET visitor for materials and engineering science programs. Berndt remains as an Adjunct Professor at Stony Brook University.

In early 2005 Berndt returned to Australia as the founding Professor of Surface and Interface Engineering, James Cook University, Queensland, Australia. He was the Chairman of the Townsville Division of Engineers Australia and Chaired the Regional Engineers Australia Conference in 2007. He moved to Swinburne University of Technology in late 2007 as the founding Professor of Surface Science and Interface Engineering. He was invited to become the Director of the Industrial Research Institute Swinburne (aka 'IRIS') in March 2008. He stepped down from that position in August 2011 when he assumed other responsibilities. Chris has served as a member of 4 Engineers Australia Accreditation Teams and Chaired one of these.

Berndt's professional interests gravitate around manufacturing; especially in the area of protective coatings. He was inducted into the Thermal Spray Hall of Fame in 2007. He was the President of Thermal Spray Society (an affiliate of ASM International) in 2002 through to 2004. He has been the Chair or Co-Chair of 5 International Conferences. He was appointed a Trustee (the Board of Directors) of ASM Int. (aka "the American Society of Materials") for 2005-2008. Chris became the Vice-President of ASM Int. and progressed to President in October 2011. Berndt was also the President of the Australian Ceramic Society from mid-2008 through to mid-2010.

Berndt is a Member of 10 professional societies in the materials, mechanical, manufacturing and bioengineering fields. He is a Fellow of the Australian Institution of Engineers, Fellow of ASM International, Fellow of the Institute of Materials, Minerals and Mining (UK), Fellow of the Australian Ceramic Society, Fellow of the American Ceramic Society (USA), and a Fellow of Alpha Sigma Mu (The Materials Engineering Honor Society). He was nominated by the student members of Stony Brook University to become a member of Tau Alpha Pi (the Engineering Technology Honor Society) as an "Eminent Engineer". He is also a Chartered Engineer (UK), a Chartered Professional Engineer (Australia), and a Member of the College of Bioengineers (Australia). Berndt has held guest positions as a Faculty Fellow of Oak Ridge National Laboratory and as a Guest Scientist of Brookhaven National Laboratory.

BERNDT has in excess of 450 publications. He is the Editor/Co-editor of 10 conference proceedings on thermal spray. Berndt has an 'h-index' of 44 and more than 6,900 citations to his work. He is especially proud of his students and post docs who have achieved professional prominence and earned good lives over the past 30 years.

March 2014.

## **READ ME FIRST: Commentary concerning the e-thesis.**

The Adobe Acrobat version (e-thesis) has several features. But an explanation is in order first.

The hardbound version of the thesis was created in MS Word. The twenty Adobe Acrobat files were trimmed of their white borders and then each page of the publication saved as a 600 dpi resolution image. The images were imported into the MS Word file so that there was consistency in presentation throughout the thesis. Thus, the images could be centered on each page, a formal header and footer applied and the general look of the thesis be controlled. A similar process was used for the creation of the Appendices.

The file sizes of the main body of the thesis and appendices were 246 GB and 44 GB, respectively. Conversion of the two MS Word files into Acrobat files was not realistic since the OCR transformation process was quite poor and error-ridden.

Thus, the Acrobat version of the thesis was created by combining the MS Word text files and Acrobat versions of the twenty manuscripts. The resulting pdf file is about 45 MB in size. This file is heavily bookmarked so that information can be readily located.

The e-thesis incorporates some features that are intended to enrich the content. These are:

1. Scanned images of the hard bound front cover and the thesis spine.
2. A copy of the “HD General Declaration” required for administrative purposes.
3. A scanned image of the Higher Doctorate Testamur.

The author has sought “reprint permissions” from the publishers of the articles that appear in this e-thesis. These 38 permissions have been forwarded to the institution that has this e-thesis available. The bookmarks in this permissions file correspond to the identification numbers (IDs) provided below.

Table 1 lists the 20 peer reviewed publications that constitute the body of the thesis. The ID of the far left column is keyed to the manuscript number that appears in the Table of Contents section of the thesis. The corresponding publisher of the journal in which the article appears is indicated in the column on the far right of Table 1.

Table 1. Identification of the publisher for the 20 prime peer-reviewed articles that constitute the body of this DEng thesis.

<b>ID</b>	<b>Publication title</b>	<b>Publisher</b>
1.	Characteristics of the Liquid Flame Spray Process’, Surf. Coat. Tech., 90 (1997) 210-216.	Elsevier
2.	Topographical and microstructural property evolution of air plasma-sprayed zirconia thermal barrier coatings, J. Am. Ceramic Soc., Article first published online: 4 FEB 2014, DOI: 10.1111/jace.12842.	Wiley
3.	Microstructural characteristics of cold-sprayed nanostructured WC-Co coatings, Thin Solid Films, 416 (2002) 129-135.	Elsevier
4.	Design and manufacture of Nd-Fe-B thick coatings by the thermal spray process, Surf. Coat. Tech., 205[19] (2011) p. 4697-4704.	Elsevier
5.	Effects of standoff distance on porosity, phase distribution and mechanical	Elsevier



ID	Publication title	Publisher
	properties of plasma sprayed Nd-Fe-B coatings, Surf. Coat. Tech., 216 (2013) p. 127-138. DOI: 10.1016/j.surfcoat.2012.11.040, Published: FEB 15 2013.	
6.	Quantification and taxonomy of pores in thermal spray coatings by image analysis and stereology approach, Metall. and Mater. Trans. A, 44A[10] (2013) p. 4844-4858.	Springer
7.	Measurement of adhesion for thermally sprayed material', J. Adhesion Science and Technology, 7 [12] (1993) 1235-1264.	Taylor and Francis
8.	Contact damage in plasma-sprayed alumina-based coatings, J. Am. Ceram. Soc., 79[7] (1996) 1907-14.	Wiley
9.	Influence of plasma spray parameters on the mechanical properties of yttria stabilized zirconia coatings I: Four point bend test, J. Mater. Sci. and Engin., A284 (2000) 29-40.	Elsevier
10.	Influence of plasma spray parameters on the mechanical properties of yttria stabilized zirconia coatings II: Acoustic emission response, J. Mater. Engin. and Sci., A284 (2000) 41-50.	Elsevier
11.	Evaluation of microhardness and elastic modulus of thermally sprayed nanostructured zirconia coatings, Surf. Coat. Tech., 135 (2001) 166-172.	Elsevier
12.	Evaluation of off-angle thermal spray, Surf. Coat. Tech., 89 (1997) 213-224.	Elsevier
13.	Modeling the coverage of splat areas arising from thermal spray processes, J. Am. Ceramic Soc., 95[5] (2012) p. 1572-1580.	Wiley
14.	Thermal spray maps: Material genomics of processing technologies, J. Thermal Spray Tech., 22[7] (2013) p. 1170-1183.	Springer
15.	Material fundamentals and clinical performance of plasma-sprayed hydroxyapatite coatings: A review, J. Biomedical Materials Research, 58 [5] (2001) 570-592.	Wiley
16.	Impact of nanoscale roughness of titanium thin film surfaces on bacterial retention, Langmuir, 2010, 26 (3), 1973-1982.	American Chemical Society
17.	Transition metal-substituted cobalt ferrite nanoparticles for biomedical applications, Acta Biomaterialia, 9[3] (2013) p. 5830-5837.	Elsevier
18.	Failure during thermal cycling of plasma-sprayed thermal barrier coatings, Thin Solid Films, 108[4] (1983) 427-437.	Elsevier
19.	Performance Of Thermal Barrier Coatings In High Heat Flux Environments, Thin Solid Films, 119 (1984) 195-202.	Elsevier
20.	A review of testing methods for thermal spray coatings, J. Inter. Materials Reviews, 2014, 45 pages, advance on-line article: <a href="http://dx.doi.org/10.1179/1743280414Y.0000000029">http://dx.doi.org/10.1179/1743280414Y.0000000029</a>	Maney

Table 2 lists the 17 lay articles that are included in the Appendices section of the thesis. The identification (ID) number of the far left column is keyed to the sequence of articles that appears in the Appendices. The corresponding publisher of the journal or magazine in which the article appears is indicated in the column on the far right of Table 1. The book marks in this PDF file correspond to the IDs provided below. Table 2 also lists Appendix 2 that appears in the thesis.

Table 2. Identification of the publisher for the 17 short-form contributions (editorials and commentaries) and Appendix 2 that appear in the Appendices of this DEng thesis.

<b>ID</b>	<b>Year</b>	<b>Title</b>	<b>Publisher</b>
1	1992	C.C. Berndt, "Editorial: 1st Issue of JTST", JTST, 1[1] (1992) 3.	Springer
2	1992	C.C. Berndt, "Editorial: Closure of 13th ITSC", JTST, 1[2] (1992) 99.	Springer
3	1994	C.C. Berndt, "The Significance of Thermal Spray Awards", JTST (1994) 3[3] 244.	Springer
4	1994	C.C. Berndt, "Who's Holding The Gun?", J. Thermal Spray Technology, 4[1] (1994) 331-332.	Springer
5	1996	C.C. Berndt, "Standardize And Deliver", JTST, 5[1] (1996) 2-3.	Springer
6	1999	R. Seals and C.C. Berndt, "Rationale for a JTST Award for the Best Scientific Paper", JTST, 8[1] (1999) 3-5.	Springer
7	2001	C.C. Berndt, "How do we Market JTST", JTST, 10 (2001) 3-4.	Springer
8	2003	L. Pawlowski and C.C. Berndt, "The Globalization of JTST: A Forum for a World Wide Network", JTST, 12 (2003) 3-4. (Note: The author is incorrectly identified in the permissions pdf.)	Springer
9	2006	C.C. Berndt, "State of the Society The Birth of Opportunity", Advanced Materials & Processes, (2006) 164[5] p94.	ASM Int.
10	2006	C.C. Berndt and G. Montavon, "Thermal Spray: Preserving 100 Years Of Technology", J. Thermal Spray Technology, 15[1] (2006) 5-8.	Springer
11	2007	C.C. Berndt, "Activism in Thermal Spray: A Call to Arms", Advanced Materials & Processes, 165[8] (2007) 72. Also in JTST, 16[2] (2007) 167.	Springer
12	2007	C.C. Berndt, "Commentary. The End of the Beginning; Now Let's Make a Real Effort!", JTST, 16[3] (1992) 320.	Springer
13	2007	C.C. Berndt, "One way to pick "Low-hanging fruit" is to chop the tree down!", Journal of Thermal Spray Technology, 16[4] (2007) p. 465. Also 385 AM&P (2007) 165[5] P70.	Springer
14	2007	C.C. Berndt, "Thermal Spray: The Best Thing Since Sliced Bread", Advanced Materials & Processes, 165[1] (2007) 100.	ASM Int.
15	2008	C.C. Berndt, "'At the end of the day': let-us all take on responsibility for thermal spray", Advanced Materials & Processes, Vol. 166, no. 8 (Aug 2008), p. 58 .	ASM Int.
16	2008	C.C. Berndt, "Born again as a technologist", Advanced Materials and Processes, Vol. 166, no. 5 (May 2008), p. 68.	ASM Int.
17	2008	C.C. Berndt, "Editorial: will thermal spray ever be the basis for a Nobel Prize?", Advanced Materials & Processes, Vol. 166, no. 11 (Nov 2008), p. 66.	ASM Int.
A2	2012	R. Knight, "Christopher C. Berndt 2011-2012 President of ASM International", Advanced Materials & Processes, Vol. 170, no. 1 (January 2012), p. 34-35.	ASM Int.

-- END --